

**Symposium on Interfacial Phenomena at Colloid and Electrode Interfaces,
Atlantic, City, N. J., September 1968**

Some Common Problems with the Double Layer and Ionic Solutions. An Introductory Paper B. E. Conway and L. G. M. Gordon	3523
Isotherms of Contact Adsorption in the Double Layer Halina Wroblowa and Klaus Müller	3528
A Theory of the Electrical Capacity of the Inner Region in the Absence of Ionic Adsorption at the Mercury-Water Interface S. Levine, G. M. Bell, and A. L. Smith	3534
Studies of the Double Layer at Oxide-Solution Interface Syed M. Ahmed	3546
Interactions of Silver Halides with Metal Chelates and Chelating Agents Egon Matijević, Nicholas Kolak, and David L. Catone	3556
The Nature of Fresh Metal Surfaces in Aqueous Solutions Terrell N. Andersen, Jeffrey L. Anderson, and Henry Eyring	3562
A Study of Anion Adsorption on Platinum by Ellipsometry Ying-Chech Chiu and M. A. Genshaw	3571
Adsorption Isotherms in Mixed Solvent Systems John Lawrence and Roger Parsons	3577
Some Aspects of the Adsorption of Nitrate and Phthalate Ions at the Mercury-Solution Interface B. V. K. S. R. A. Tilak and M. A. V. Devanathan	3582
The Compact Double Layer as a Function of Temperature and Pressure Graham Hills	3591
The Electrical Double Layer in Amide Solvents Richard Payne	3598
Entropy and Structural Effects in the Electrochemical Adsorption of Pyridine at Mercury B. E. Conway and L. G. M. Gordon	3609
Electrocapillary Studies in Aqueous Lithium Chloride Solutions R. G. Barradas and E. W. Hermann	3619
Structured Liquids near Platinum Electrodes Peter C. Owzarski and W. E. Ranz	3628
<hr/>	
The Thermodynamics of Electrolyte Equilibria in Media of Variable Water Concentration R. A. Matheson	3635
Proton Nuclear Magnetic Resonance Solvent Shifts in Aqueous Electrolyte Solutions. I. Behavior of Internal References John E. Gordon and Robert L. Thorne	3643
Proton Nuclear Magnetic Resonance Solvent Shifts in Aqueous Electrolyte Solutions. II. Mixtures of Two Salts. Additivity and Nonlinearity of Shifts John E. Gordon and Robert L. Thorne	3652
The Calculation of Madelung Potentials for Faujasite-Type Zeolites. I E. Dempsey	3660
Proton Spin Relaxation and Exchange Properties of Hydrated Chromic Ions in H ₂ O and H ₂ O-D ₂ O Mixtures B. F. Melton and V. L. Pollak	3669
Diffusion of Halogenated Hydrocarbons in Helium. The Effect of Structure on Collision Cross Sections Edward N. Fuller, Keith Ensley, and J. Calvin Giddings	3679
The Effect of Hydrogen Bonding upon the Autoxidation Kinetics of Tetrakis(dimethylamino)ethylene Aaron N. Fletcher	3686
Thermal Isomerization of the Maleate Ion in Potassium Halide Matrices I. C. Hisatsune, R. Passerini, R. Pichai, and V. Schettino	3690
Studies of Water Vapor Dissociated by Microwave Discharges at Low Flow Rates. I. Effect of Residence Time in the Traversed Volume on Product Yields at Liquid Air Temperature R. A. Jones, Walter Chan, and M. Venugopalan	3693
Dielectric Study of Esters in Benzene. Barrier to Internal Rotation and Molecular Configuration Bal Krishna, Bhartendu Prakash, and S. V. Mahadane	3697

The Unit Compressibility Law and Corresponding-States Behavior of Hydrogen Sulfide . . .	Eugene M. Holleran	3700
Radiation Chemistry of the Aqueous Nitrate System. II. Scavenging and pH Effects in the Cobalt-60 γ Radiolysis of Concentrated Sodium Nitrate Solutions	Malcolm Daniels and Eric E. Wigg	3703
Radiation Chemistry of the Aqueous Nitrate System. III. Pulse Electron Radiolysis of Concentrated Sodium Nitrate Solutions	Malcolm Daniels	3710
The Rates of Methanolysis of Several Organosilazanes	William L. Budde	3718
Three-Element Reaction Coordinates and Intramolecular Kinetic Isotope Effects	William J. Kass and Peter E. Yankwich	3722
Absorption Spectrum and Decay Kinetics of O_2^- and HO_2 in Aqueous Solutions by Pulse Radiolysis	Joseph Rabani and Sigurd O. Nielsen	3736
The Apparent Molal Volumes of the Lithium and Sodium Halides. Critical-Type Transitions in Aqueous Solution	Fred Vaslow	3745
Reactions of Shock-Heated Carbon Disulfide-Argon Mixtures. I. Light Emission	S. J. Arnold and G. H. Kimbell	3751
Hydrogen Atom Permeation through Solid Hydrocarbons at 77°K	J. M. Ditz, C. G. Hill, Jr., and R. C. Reid	3756
An Electron Spin Resonance Study of Copper(II) O-Alkyl-1-amidinourea Complexes. Properties of the CuN_4^{2-} Chromophore	John R. Wasson and Charles Trapp	3763
Hydrogenation of Ethylene by Zinc Oxide. I. Role of Slow Hydrogen Chemisorption	A. L. Dent and R. J. Kokes	3772
Hydrogenation of Ethylene by Zinc Oxide. II. Mechanism and Active Sites.	A. L. Dent and R. J. Kokes	3781
Catalysis of the Reduction of Supported Nickel Oxide	E. James Nowak	3790
Pulse Radiolysis Study of Alcohols in Aqueous Solution	M. Simic, P. Neta, and E. Hayon	3794
A Simple Differential Thermometric Technique for Measuring the Rates of Chemical Reactions in Solutions	Thelma Meites, Louis Meites, and Joginder N. Jaitly	3801
Differential Heat of Adsorption and Entropy of Water Adsorbed on Zinc Oxide Surface	Mahiko Nagao and Tetsuo Morimoto	3809
The Complexation Kinetics of Leucine with Nickel(II), Cobalt(II), and Copper(II)	R. F. Pasternack, E. Gibbs, and J. C. Cassatt	3814
Association of Methanol in Vapor and in <i>n</i> -Hexadecane. A Model for the Association of Alcohols	Edwin E. Tucker, Sutton B. Farnham, and Sherril D. Christian	3820
The Thermal Decomposition of Perfluorocyclobutane in a Single-Pulse Shock Tube	J. M. Simmie, W. J. Quiring, and E. Tschuikow-Roux	3830
Electron Spin Resonance of Transient Alkyl Radicals during Alkylolithium-Alkyl Halide Reactions	Hanns Fischer	3834
The Kinetics of Crystal Growth of Dicalcium Phosphate Dihydrate	Robert W. Marshall and George H. Nancollas	3838
Plane Specificity in the Reaction of Methanol and Ethanol Vapor with Clean Germanium	F. Meyer	3844
Concurrent Solution and Adsorption Phenomena in Chromatography. III. The Measurement of Formation Constants of H-Bonded Complexes in Solution	D. F. Cadogan and J. H. Purnell	3849
The Kinetics of the Reaction of Trifluoromethyl Radicals with Ammonia	Henry F. LeFevre and Richard B. Timmons	3854
Semiempirical Calculation of Molecular Polarizabilities and Diamagnetic Susceptibilities of Fluorocarbons, Substituted Fluorocarbons, Ethers, Esters, Ketones, and Aldehydes	J. A. Beran and L. Kevan	3860
Molecular Electron Ionization Cross Sections at 70 eV	J. A. Beran and L. Kevan	3866
Matrix Infrared Studies of OF Radical Systems	Alfred Arkell	3877
Ion-Solvent Interactions. Infrared Studies of Solvation of the Sodium Ion	E. G. Höhn, J. A. Olander, and M. C. Day	3880
The Radiation-Induced Isotopic Exchange in Gaseous Hydrogen-Deuterium Mixtures	T. Terao and R. A. Back	3884
Some Energetics and the Kassel Fit Parameter s_K in Unimolecular Reactions : : : : :	E. Tschuikow-Roux	3891
A Nuclear Magnetic Resonance Study of the Effect of Charge on Solvent Orientation of a Series of Chromium(III) Complexes	Lawrence S. Frankel	3897
Electron Paramagnetic Resonance Study of the Anion Radical of Phenyl Methyl Sulfone and of 4-Nitrophenyl Methyl Sulfone	Elizabeth Keller and Robert G. Hayes	3901

The Photochemistry of Methylamine at 1470 Å John J. Magenheimer, Robert E. Varnerin, and Richard B. Timmons	3904
Acid Dissociation in Acetone-Water Mixtures. An Anomalous Medium Effect When London Dispersion Forces Are Large Dodd-Wing Fong and Ernest Grunwald	3909
An Electron Impact Study of Ionization and Dissociation of Monosilane and Disilane P. Potzinger and F. W. Lampe	3912
A Kinetic Investigation of an Isomerization of Aqueous Lysozyme near Neutral pH Jeffrey D. Owen, Edward M. Eyring, and David L. Cole	3918
Infrared Spectra and Bonding in the Sodium Superoxide and Sodium Peroxide Molecules Lester Andrews	3922
Chemical Effects Following $N^{14}(n,p)C^{14}$ in Magnesium Nitride Ronald D. Finn, Hans J. Ache, and Alfred P. Wolf	3928
Solvation Enthalpies of Various Ions in Water, Propylene Carbonate, and Dimethyl Sulfoxide C. V. Krishnan and Harold L. Friedman	3934
Estimation of Activation Energies for Nitrous Oxide, Carbon Dioxide, Nitrogen Dioxide, Nitric Oxide, Oxygen, and Nitrogen Reactions by a Bond-Energy Method S. W. Mayer	3941
The Surface Hydroxylation of Silica C. G. Armistead, A. J. Tyler, F. H. Hambleton, S. A. Mitchell, and J. A. Hockey	3947
The Density Function for End-to-End Lengths of Self-Avoiding Random Walks on a Lattice Frederick T. Wall and Stuart G. Whittington	3953
Heats of Mixing Aqueous Electrolytes. VII. Calcium Chloride and Barium Chloride with Some Alkali Metal Chlorides R. H. Wood and M. Ghamkhar	3959
Equilibria in Propylene Carbonate. I. Viscosity and Conductance Studies of Some Lithium and Quaternary Ammonium Salts L. M. Mukherjee and David P. Boden	3965
The Electric Moments of the Halotrifluoroethylenes E. J. Gauss and Theodore S. Gilman	3969
Infrared Spectroscopic Study of Oxygen Species in Vanadium Pentoxide with Reference to Its Activity in Catalytic Oxidation Yoshiya Kera and Kozo Hirota	3973
Rate Constants for Quenching of Biacetyl Triplets in Benzene R. B. Cundall, G. B. Evans, and E. J. Land	3982
Transport Processes in Hydrogen Bonding Solvents. III. The Conductance of Large Bolaform Ions in Water at 10 and 25° T. L. Broadwater and D. Fennell Evans	3985
Cooperativity and Composition of the Linear Amylose-Iodine-Iodide Complex Charles L. Cronan and Friedemann W. Schneider	3990
The Hydration of Propionaldehyde, Isobutyraldehyde, and Pivalaldehyde. Thermodynamic Parameters, Buffer Catalysis, and Transition State Characterization Y. Pocker and D. G. Dickerson	4005

NOTES

A Dechlorination Reaction in the Radiolysis of Aqueous Monochloroacetic Acid Solutions in the Presence of Nitrous Oxide Akira Yokohata, Takuichi Ohmura, and Satoru Tsuda	4013
3d Transition Metal Complexes in Molten Potassium Thiocyanate Solution H. C. Egghart	4014
Electron Spin Resonance Studies on Trapped Electrons and Free Radicals in γ -Irradiated Isobutyl Vinyl Ether Glasses Kozo Tsuji and Ffrancon Williams	4017
Temperature-Dependence Nuclear Magnetic Resonance Studies of a Very Strongly Coupled Spin System. Ethylene Sulfite Harold Finegold	4020

COMMUNICATIONS TO THE EDITOR

Comments on the Paper "Activity Coefficients for Ionic Melts" David M. Moulton	4022
Reply to the Comments on the Paper "Activity Coefficients for Ionic Melts" R. Haase	4023
Electron Density and Electronegativity Effects in the Substitution for Hydrogen Atoms by Energetic Tritium Atoms from Nuclear Recoil F. S. Rowland, E. K. C. Lee, and Y.-N. Tang	4024
Effect of Water on the Kinetics of the Solid Lithium-Lithium Ion Reaction in Propylene Carbonate James N. Butler, David R. Cogley, and John C. Synnott	4026
Temperature Dependence of the Molar Absorptivity of the OH Stretching Vibration G. P. Hoover, E. A. Robinson, R. S. McQuate, H. D. Schreiber, and J. N. Spencer	4027
The Homoconjugation Constant of Picric Acid in Acetonitrile I. M. Kolthoff and M. K. Chantooni, Jr.	4029

AUTHOR INDEX

- Ache, H. J., 3928
 Ahmed, S. M., 3546
 Andersen, T. N., 3562
 Anderson, J. L., 3562
 Andrews, L., 3922
 Arkell, A., 3877
 Armistead, C. G., 3947
 Arnold, S. J., 3751

 Back, R. A., 3884
 Barradas, R. G., 3619
 Bell, G. M., 3534
 Beran, J. A., 3860, 3866
 Boden, D. P., 3965
 Broadwater, T. L., 3985
 Budde, W. L., 3718
 Butler, J. N., 4026

 Cadogan, D. F., 3849
 Cassatt, J. C., 3814
 Catone, D. L., 3556
 Chan, W., 3693
 Chantooni, M. K., Jr., 4029
 Chiu, Y.-C., 3571
 Christian, S. D., 3820
 Cogley, D. R., 4026
 Cole, D. L., 3918
 Conway, B. E., 3523, 3609
 Cronan, C. L., 3990
 Cundall, R. B., 3982

 Daniels, M., 3703, 3710
 Day, M. C., 3880
 Dempsey, E., 3660
 Dent, A. L., 3772, 3781
 Devanathan, M. A. V., 3582

 Dickerson, D. G., 4005
 Ditz, J. M., 3756

 Egghart, H. C., 4014
 Ensley, K., 3679
 Evans, D. F., 3985
 Evans, G. B., 3982
 Eyring, E. M., 3918
 Eyring, H., 3562

 Farnham, S. B., 3820
 Finegold, H., 4020
 Finn, R. D., 3928
 Fischer, H., 3834
 Fletcher, A. N., 3686
 Fong, D.-W., 3909
 Frankel, L. S., 3897
 Friedman, H. L., 3934
 Fuller, E. N., 3679

 Gauss, E. J., 3969
 Genshaw, M. A., 3571
 Ghamkar, M., 3959
 Gibbs, E., 3814
 Giddings, J. C., 3679
 Gilman, T. S., 3969
 Gordon, J. E., 3643, 3652
 Gordon, L. G. M., 3523, 3609
 Grunwald, E., 3909

 Haase, R., 4023
 Hambleton, F. H., 3947
 Hayes, R. G., 3901
 Hayon, E., 3794
 Hermann, E. W., 3619
 Hill, C. G., Jr., 3756
 Hills, G., 3591

 Hirota, K., 3973
 Hisatsune, I. C., 3690
 Hockey, J. A., 3947
 Höhn, E. G., 3880
 Holleran, E. M., 3700
 Hoover, G. P., 4027

 Jaitly, J. N., 3801
 Jones, R. A., 3693

 Kass, W. J., 3722
 Keller, E., 3901
 Kera, Y., 3973
 Kevan, L., 3860, 3866
 Kimbell, G. H., 3751
 Kokes, R. J., 3772, 3781
 Kolak, N., 3556
 Kolthoff, I. M., 4029
 Krishna, B., 3697
 Krishnan, C. V., 3934

 Lampe, F. W., 3912
 Land, E. J., 3982
 Lawrence, J., 3577
 Lee, E. K. C., 4024
 LeFevre, H. F., 3854
 Levine, S., 3534

 Magenheimer, J. J., 3904
 Mahadane, S. V., 3697
 Marshall, R. W., 3838
 Matheson, R. A., 3635
 Matijević, E., 3556
 Mayer, S. W., 3941
 McQuate, R. S., 4027
 Meites, L., 3801
 Meites, T., 3801
 Melton B. F., 3669

 Meyer, F., 3844
 Mitchell, S. A., 3947
 Morimoto, T., 3809
 Moulton, D. M., 4022
 Mukherjee, L. M., 3965
 Müller, K., 3528

 Nagao, M., 3809
 Nancollas, G. H., 3838
 Neta, P., 3794
 Nielsen, S. O., 3736
 Nowak, E. J., 3790

 Ohmura, T., 4013
 Olander, J. A., 3880
 Owen, J. D., 3918
 Owzarski, P. C., 3628

 Parsons, R., 3577
 Passerini, R., 3690
 Pasternack, R. F., 3814
 Payne, R., 3598
 Pichai, R., 3690
 Pocker, Y., 4005
 Pollak, V. L., 3669
 Potzinger, P., 3912
 Prakash, B., 3697
 Purnell, J. H., 3849

 Quiring, W. J., 3830

 Rabani, J., 3736
 Ranz, W. E., 3628
 Reid, R. C., 3756
 Robinson, E. A., 4027
 Rowland, F. S., 4024

 Schettino, V., 3690

 Schneider, F. W., 3990
 Schreiber, H. D., 4027
 Simic, M., 3794
 Simmie, J. M., 3830
 Smith, A. L., 3534
 Spencer, J. N., 4027
 Synnott, J. C., 4026

 Tang, Y. N., 4024
 Terao, T., 3884
 Thorne, R. L., 3643, 3652
 Timmons, R. B., 3854, 3904
 Tilak, B. V. K. S. R. A., 3582
 Owen, J. D., 3918
 Trapp, C., 3763
 Tschuikow-Roux, E., 3830, 3891
 Tsuda, S., 4013
 Tsuji, K., 4017
 Tucker, E. E., 3820
 Tyler, A. J., 3947

 Varnerin, R. E., 3904
 Vaslow, F., 3745
 Venugopalan, M., 3693

 Wall, F. T., 3953
 Wasson, J. R., 3763
 Whittington, S. G., 3953
 Wigg, E. E., 3703
 Williams, F., 4017
 Wolf, A. P., 3928
 Wood, R. H., 3959
 Wroblowa, H., 3528

 Yankwich, P. E., 3722
 Yokohata, A., 4013

Some Common Problems with the Double Layer and Ionic Solutions.

An Introductory Paper

by B. E. Conway¹ and L. G. M. Gordon¹

Department of Chemistry, University of Ottawa, Ottawa, Canada (Received January 7, 1969)

As an introduction to papers presented in a symposium, attention is directed to some problems arising in the treatment of the double layer which can usefully be considered in the light of similar or related problems with ionic solutions.

Introduction

Eighteen papers were presented (13 of which are published in the present issue) at the symposium, the theme of which was the problem of the constitution of the double layer at electrode interfaces and at colloids in relation to adsorption of ions and molecules from solution. The opening session was chaired by B. E. Conway (University of Ottawa) following introductory remarks by the Chairman of the Colloid Science Division, Dr. F. Fowkes (Lehigh University). Other session chairmen were C. Barlow, Jr. (Texas Instrument Corp.), R. G. Barradas (Carleton University), and L. G. M. Gordon (University of Ottawa). An introductory paper was presented by B. E. Conway, the text of which is given briefly below.

The behavior of electrolyte solutions is, on the whole, better understood quantitatively than is the "double layer" at electrodes and colloids or the behavior of ions, solvent, and other adsorbate molecules within it; a comparative discussion of the problems which are common in these fields may therefore help to indicate areas in the treatment of the double layer that may usefully be considered in the light of information on electrolyte solutions and thus provide in this introductory paper a framework for consideration of the various contributions presented at the symposium.

Electrolyte solutions necessarily have both a three-dimensional homogeneity and an overall isotropy

while the situation of ions and solvent molecules in the double layer at electrodes and colloidal particles is discontinuous and the interphasial region² locally anisotropic. Most of the problems which arise, *e.g.*, in electrostatic treatments of ionic solutions therefore become more complex^{3,4} owing to the presence of the metal or colloid-particle interface² and the local superimposition of the electrode field upon that due to ions in the interphasial region. Correspondingly, solvent molecules find themselves under either the conflicting or reinforcing influence of the fields arising both at the electrode interface and locally at ions in the double layer.

A basic aspect of the latter situation is the degree of hydration and extent of orientation of solvent molecules at ions in the double layer and at the electrode surface itself. Until the theory of Bockris, Devanathan, and Müller,⁵ little attention had been paid to the role of

(1) Organizing chairmen of a symposium on "Interfacial Phenomena at Colloid and Electrode Interfaces," sponsored by the Colloid Science Division of the American Chemical Society at the 156th National Meeting at Atlantic City, N. J., Sept 1968.

(2) The usages "interfacial" and "interphasial" are deliberately distinguished; the former refers to the two-dimensional "electronic" surface of the metal in contact with the solution and the latter to the thin but three-dimensional region which accommodates the local changes of concentration and other properties arising on account of adsorption.

(3) F. P. Buff and F. H. Stillinger, *J. Chem. Phys.*, **39**, 1911 (1963).

(4) S. Levine, G. M. Bell, and D. Calvert, *Can. J. Chem.*, **40**, 518 (1962); D. C. Grahame, *Z. Elektrochem.*, **62**, 264 (1958).

adsorption and orientation of solvent molecules in the treatment of the double layer, although the dipole potential and capacitance associated with adsorbed polar organic molecules had been treated by Devanathan⁶ in 1961. The adsorbed, partially oriented layer of solvent at a charged electrode interface is to be regarded as analogous to the primary hydration shell⁷ associated with small cations and anions in bulk aqueous electrolyte solutions. The fields developed in the inner layer, *e.g.*, at a mercury electrode at *ca.* 1.25 V E_H , are of the same order of magnitude as those at an ion of radius 1 Å in water.

In double-layer theory⁸ and in the treatment of ionic solutions,⁹ the question of local dielectric constant and electric saturation effects at high fields is important. At the short distances either from ions or from the electrode interface at which fields as high as 10^7 V cm^{-1} exist, it is doubtful if continuous dielectric theories even with allowance for saturation effects give more than a rough and nonspecific idea of the behavior of the solvent near electrodes or ions. In both cases, a more discrete molecular approach is preferable although continuous dielectric theory with allowance for saturation effects has provided, in the interim development of the subject, important guidelines for better estimates of the local fields and field effects on the solvent medium in such situations. A matter related to this question is the use of single and multiple (dielectric) imaging⁴ in the evaluation of interaction and adsorption effects in the double layer. Imaging in the metal seems to be an acceptable procedure since the polarizable interface on the metal side is composed of delocalized microscopic charges. Imaging in the water dielectric seems a procedure of more doubtful validity owing to the rather specific charge distributions already present in the water molecules, the finite size of the latter, and the significant local structure of the solvent in and near the interphase.

Electrostatic problems connected with dielectric saturation were presented in a paper by Barlow (not published) and the question of field-dependent orientation of water in the inner layer is discussed by Levine in relation to anomalies in the capacity behavior (capacity "hump"). Experimental aspects of this problem are treated in the papers of Hills, Hsieh, and Reeves (through capacity studies at high pressures) and of Payne (in relation to comparisons between the capacity hump behavior in amide solvents and in water). Structural effects in hydrogen-bonded liquids near platinum electrode interfaces are considered in the work presented by Ozwarski.

The presence of the oriented solvent "hydration layer" at a charged metal interface is of basic importance in regard to the nature of specific and nonspecific ionic adsorption. Bockris, Devanathan, and Müller⁵ (BDM, see below) have assumed that hydrated cations cannot share or penetrate the solvent layer at the

electrode interface. Their model thus puts the centers of nonspecifically adsorbed cations at a position approximately two water molecule diameters $2d_{\text{H}_2\text{O}}$ (plus the ionic radius r_i) away from the electronic surface of the metal while in the outer Helmholtz layer of Grahame,¹⁰ nonspecifically adsorbed hydrated cations reside at a distance $d_{\text{H}_2\text{O}} + r_i$ from the metal. The situation in these two cases is closely analogous to that in ion-pair formation where, depending on the charge and radius of the ions concerned and the polarity of the solvent, ion association can vary all the way from a hydrated ion pair (where both ions retain their primary hydration sheaths) to a contact ion pair^{11,12} (actual ions in contact with residual hydration of the pair dipole). Since the orientation of water at a cation is (along the line of centers of the ions) also a favorable orientation for the associated anion in the pair, optimum association with retention of some hydration by both ions will tend to arise if the ions *share* their hydrate shells. The situation in the double layer is analogous and the nature of specific adsorption of cations at a negatively charged electrode can be advantageously considered in relation to association between a cation and an anion (the latter being the analog of the negatively charged electrode) where solvent sharing can arise. The average position of cations in the double layer will then depend on (a) the electrode surface charge density and (b) the charge and radius of the cation in the double layer. These considerations suggest that the significant specificity which is observed in cation adsorption¹³ can be usefully considered in relation to analogous specificities in ion-pair formation and to the different types of pairs that can be formed with a given pair of ions, *e.g.*, as indicated in the relaxation experiments of Eigen and Tamm.¹⁴ The average location of adsorbed cations in the double layer at an electrode is of obvious importance in relation to the kinetics of discharge of cations (and anions¹³), *e.g.*, particularly of the proton which can penetrate¹⁵ to

(5) J. O'M. Bockris, M. A. V. Devanathan, and K. Müller, *Proc. Roy. Soc.*, **A274**, 55 (1963).

(6) M. A. V. Devanathan, *ibid.*, **A264**, 133 (1961).

(7) J. O'M. Bockris, *Quart. Rev. (London)*, **3**, 173 (1949).

(8) B. E. Conway, J. O'M. Bockris, and A. M. Azzam, *Trans. Faraday Soc.*, **47**, 756 (1951).

(9) F. Booth, *J. Chem. Phys.*, **19**, 1615 (1951).

(10) D. C. Grahame, *Chem. Rev.*, **41**, 441 (1947).

(11) S. Levine and H. E. Wrigley, *Discussions Faraday Soc.*, **24**, 43, 73 (1957); S. Levine and G. M. Bell in "Electrolytes," B. Pesce, Ed., Pergamon Press, London, 1957, p 77.

(12) R. M. Fuoss, *Trans. Faraday Soc.*, **30**, 967 (1934); *J. Amer. Chem. Soc.*, **81**, 2659 (1959).

(13) *E.g.*, A. N. Frumkin, *Trans. Faraday Soc.*, **55**, 156 (1959); see also A. N. Frumkin and B. Florianovich, *Dokl. Akad. Nauk SSSR*, **80**, 907 (1951).

(14) M. Eigen and K. Tamm, *Z. Elektrochem.*, **66**, 107 (1962).

(15) *Cf.* the treatment of J. O'M. Bockris and R. Parsons, *Trans. Faraday Soc.*, **47**, 914 (1951), and of B. E. Conway and J. O'M. Bockris, *Can. J. Chem.*, **35**, 1124 (1957).

the inner water layer in the BDM model by the usual mechanism¹⁶ of acid-base proton transfer and thence become discharged.^{15,17} Factors in specificity of adsorption of phthalate, acetate, and nitrate anions are discussed in the paper of Tilak and new optical and mechanical methods for studying adsorption of ions and the constitution of the double layer at metals are presented in the papers by Genshaw and Chiu, by Kuwana and Winograd (not published), and by Andersen, Anderson, and Eyring (potentials of zero charge).

At an ion or at a colloid particle, the charge is usually localized and in the latter case arises by specific ionic adsorption (hydrophobic colloids) or chemical ionization of acidic or basic groups on the interface of the colloid (hydrophilic colloids). At a metallic electrode, however, the surface charge is delocalized, and the field will hence be more homogeneous than that at the interface of a colloidal particle. The relation between measurements of charge developed on ionization at colloids and electrocapillary treatments of the double layer at Hg is discussed in the paper by Ahmed, and the role of adsorption of complex ions at colloids is treated by Matijevic and Stryker.

A feature of ionic aqueous solutions that requires consideration in the more complex case of the double layer is the structural change which most ions bring about over a distance of 2-3 d_{H_2O} from the ion.^{18,19} These effects are usually quite specific for the ion concerned, being dependent on its hydrophobicity, radius, and charge. The hydrophobic tetraalkylammonium cations, and cations derived from various organic bases, usually cause structure promotion in the water solvent^{20,21} as do small cations, but for other reasons. An inert metal surface at the potential of zero charge might be regarded as tending to have a structure-promoting effect on the neighboring solvent, but this effect will be replaced by an electrostrictive one²² as the numerical value of the surface charge increases at more cathodic or anodic rational¹⁰ potentials. Some aspects of these matters are considered in the papers by Oswarski and by Conway and Gordon.

At most potentials except those near (± 0.2 V) the potential of zero charge, the "two-dimensional" ionic concentration in the double layer is relatively high in comparison with the corresponding three-dimensional concentration of ions in what are conventionally called dilute solutions (*i.e.*, from the point of view of the Debye-Hückel theory). Thus a charge of $10 \mu\text{C cm}^{-2}$ of ions in the double layer corresponds to mean interionic distances of *ca.* 13 Å. In a three-dimensional solution, this is equivalent to an ionic concentration of approximately 0.75 g-ion l.⁻¹. At such concentrations of 1:1 salts, specific solvation, effects are known to have a major influence^{23,24} on the thermodynamic behavior of the ionic solution, and it is therefore likely that they cannot be ignored in the analogous two-

dimensional problem of isotherms and equations of state for specifically adsorbed ions in the double layer.

An important result of the structural effects which most solute ions and molecules have on the water solvent is a mutual salting-out or salting-in effect. Salting-out effects arise for electrostatic reasons with simple ions but with organic structure-breaking and structure-making ions, a nonelectrostatic effect can also become significant²⁵⁻²⁷ if one ion is causing a structural change either cooperatively with the first ion or antagonistically. Such structural effects at finite concentrations are equivalent, respectively, to negative or positive contributions to the nonideal free energy of the solution. Correspondingly, in the double layer, they will appear as apparent interaction effects and thus be one of the factors determining the form of the adsorption isotherm for the species involved. Bearing in mind that solvent structure changes (co-sphere effects¹⁹) may persist over at least 2 molecular diameters of water, the co-circle of influence between two hydrated ions say of 1.3-Å radius in water can evidently have a diameter of up to 13.6 Å, a figure quite comparable with the average interionic distance commonly encountered between adsorbate ions in the double layer. It is recognized, however, that quantitative representation of such nonelectrostatic effects is prohibitively difficult at the present time.

At infinite dilution (or zero coverage) such factors will also determine in part the initial heat of adsorption (and hence the "specificity" of adsorption²⁸) since the structure-promoting or structure-breaking influence of the metal surface itself will either act cooperatively or antagonistically with the structural influence of the adsorbate itself in the water phase at the surface of the electrode or colloid particle.

A number of other problems connected with solutions

(16) B. E. Conway, J. O'M. Bockris, and H. Linton, *J. Chem. Phys.*, **24**, 834 (1956).

(17) B. E. Conway and M. Salomon, *Discussions Faraday Soc.*, **39**, 266 (1965).

(18) H. S. Frank and W. Y. Wen, *ibid.*, **24**, 133 (1957).

(19) See ref 18 and also H. S. Frank and A. S. Quist, *J. Chem. Phys.*, **36**, 604 (1961).

(20) B. E. Conway and R. E. Verrall, *J. Phys. Chem.*, **73**, 3637, 3655 (1967); B. E. Conway and L. Laliberte, Proceedings of the Symposium on Equilibria and Kinetics in Hydrogen Bonded Systems, Newcastle, England, 1968, in press as "Hydrogen Bonded Solvent Systems," A. Covington and P. Jones, Ed.

(21) D. H. Everett, *Discussions Faraday Soc.*, **24**, 216 (1967).

(22) J. R. MacDonald, *J. Chem. Phys.*, **22**, 1859 (1954).

(23) R. H. Stokes and R. A. Robinson, *J. Amer. Chem. Soc.*, **70**, 1870 (1948).

(24) H. S. Frank and R. A. Robinson, *J. Chem. Phys.*, **8**, 933 (1940).

(25) J. E. Desnoyers, G. E. Pelletier, and C. Jolicœur, *Can. J. Chem.*, **43**, 3232 (1965).

(26) R. M. Diamond, *J. Phys. Chem.*, **67**, 2513 (1963).

(27) H. S. Frank in "Chemical Physics of Ionic Solutions," B. E. Conway and R. C. Barradas, Ed., John Wiley & Sons, Inc., New York, N. Y., 1966.

(28) T. N. Andersen and J. O'M. Bockris, *Electrochim. Acta*, **9**, 347 (1964).

arise in a related form when attempts are made to develop adsorption isotherms or equations of state for adsorbed layers at electrodes. The more important factors are summarized in Table I and analogous factors for colloid interfaces are recorded in Table II.

The significance of two-dimensional interaction effects in the double layer was treated in the papers of Wroblowa and of Milner and related data obtained for pyridine and acetophenone adsorption by a new electrocapillary technique are presented in the contribution of Conway and Gordon, who also evaluate

Table I: Problems with Isotherms

Mobile or immobile layer?
Relative size of adsorbate and solvent (Flory-Huggins isotherm— <i>cf.</i> solutions)
Evaluation of Γ_{\max} corresponding to $\theta = 1$
Finite area effect (Volmer)
Interaction (or heterogeneity, for solid metals) term (Frumkin type isotherm)?
Form of interaction term ($r\theta$, $r\theta^{1/2}$, $r\theta^{2/3}$, etc.)
Image potentials
Dependence of free energy of adsorption and interaction effects on potential or surface charge

Table II: Colloid Double Layers

{ Colloid charge by ion adsorption
{ Interaction effects by repulsion
{ Colloid charge by site ionization
{ Interaction effects by pK dependence on degree of ionization
Surface charge localized (at metal delocalized)
Solvation of surface more specific and more localized

the entropies and heats of adsorption under isosteric conditions of constant charge. Analogous temperature effects in ionic adsorption are treated in the paper by Barradas and Hermann.

Related to the structural effects is the relative size factor (determined by the ratio of volumes or molecular areas) which influences the thermodynamics of mixing. It is contained implicitly in Buff and Stillinger's cluster theory of the double layer³ and has been considered for three-dimensional solutions.²⁹ The analogous case for a two-dimensional interphase is treated in the paper by Lawrence and Parsons in terms of a Flory-Huggins type of isotherm (*cf.* ref 3) for adsorption from various solvents at the mercury electrode.

A final point may be made regarding the role of field-solvent quadrupole interactions. In the case of ionic solutions, it has been shown^{30,31} that the appreciable quadrupole moment of water can, by its interaction with the inhomogeneous field of cations and anions, lead to a substantial difference of hydration

energy of cations and anions of similar radii. The effect is a large one and can account, for example, for the differences deduced for hydration energies of K^+ and F^- by Verwey³² and by Latimer, Pitzer, and Slansky³³ (*cf.* Halliwell and Nyburg³¹). The field-dipole and field-quadrupole effects are additive at anions and subtractive at cations; hence, the higher relative solvation energy of the former. It is evident that similar effects might be expected to arise at electrode interfaces and give a higher energy of electrostatic adsorption of water at potentials negative to that of zero charge than at corresponding positive potentials where the charge density on the metal is positive. The effect will depend on the field *gradient* (constancy of field in the Helmholtz layer is only an idealization) and will add to any chemical effect connected with specific interaction of the O lone-pair electrons with the metal, *e.g.*, as indicated by surface conductivity measurements on thin metallic films.³⁴ The adsorption behavior observed experimentally, *e.g.*, for pyridine³⁵ and *n*-butyl alcohol⁵ appears, however, inconsistent with the role of quadrupole effects since maximum adsorption of neutral molecules occurs often at a small negative surface charge, *viz.* 2–3 $\mu C\ cm^{-2}$ which was attributed by Bockris, Devanathan, and Müller⁵ to the noncentral situation of the electric dipole in water. In fact, the adsorption of neutral molecules is usually less over a *range* of positive rational potentials than it is over a corresponding range of negative potentials,³⁶ so that it appears that this behavior cannot be attributed to the preferred electrostatic solvent adsorption at negative surface charge densities arising from the dipole and quadrupole field interactions which would be additive under such conditions. However, the appreciable magnitude of this effect in ionic hydration indicates that other effects which may mask its significance in electrochemical adsorption at charged interfaces should be considered. Most of the non-electrolytes which have been studied at the mercury electrode either hydrogen bond with the water solvent, *e.g.*, pyridine,³⁵ butanol,⁵ or interact specifically (*e.g.*, thiourea⁶) with the mercury surface. As the surface charge changes from positive to negative values, re-orientation of the adsorbate dipole tends to occur

(29) B. E. Conway and R. E. Verrall, *J. Phys. Chem.*, **70**, 1473 (1966).

(30) A. D. Buckingham, *Quart. Rev. (London)*, **13**, 183 (1959); *Discussions Faraday Soc.*, **24**, 151 (1957).

(31) H. F. Halliwell and S. C. Nyburg, *Trans. Faraday Soc.*, **59**, 1126 (1963).

(32) E. J. W. Verwey, *Rec. Trav. Chim. Pays Bas*, **60**, 887 (1941); **61**, 127 (1942).

(33) W. M. Latimer, K. F. Pitzer, and C. M. Slansky, *J. Chem. Phys.*, **7**, 108 (1939).

(34) R. E. Verrall, B.Sc. Hons. Thesis, Ottawa, 1962.

(35) B. E. Conway and R. G. Barradas, *Electrochim. Acta*, **5**, 319 (1961).

(36) This effect does not seem to be due entirely to competitive anion adsorption at positive surface charges since it is maintained in non-specifically adsorbed supporting electrolyte solutions.

Table III: Summary of Some Common Problems with Ionic Solutions and the Double Layer

Solutions	Double layer
1. Hydration and solvation	1. Nature of solvated ions near electrode interfaces: local structural effects
2. Solvent structure and ionic solution behavior	2. Constitution of solvent dipole layer at electrode surface in relation to ionic adsorption
3. Ionic interactions (long range)	3. Two-dimensional, transverse interactions between adsorbed ions
4. Ion-pair equilibria and solvation effects; types of ion pairs	4. Ion association (specific adsorption) with the electrode surface; Ion-pair formation at high fields in the double layer
5. Ion-solvent quadrupole effects in solvation	5. Electrode surface charge-quadrupole interactions in the double layer: asymmetry of adsorption of solvent and neutral molecules w.r.t. potentials of zero charge
6. Dielectric saturation at ions and molecular model calculations	6. Dielectric saturation in the double layer and molecular model calculations
7. Potential of mean force and mean electrostatic potential—Poisson-Boltzmann inconsistency	7. Poisson-Boltzmann inconsistency in diffuse layer theory
8. Thermodynamic theory of binary solutions	8. Isotherms for neutral molecules—substitutional adsorption in the interphase

with a resultant change of hydrogen bonding. This is sufficient, *e.g.*, in the case of pyridine,³⁵ to account for the asymmetry of adsorption at positive and negative charges. Table III contains a list of some of the problems associated with ionic solutions and the double layer.

The meeting concluded with papers on the use of potentiodynamic transient methods for the study of adsorbed species and the double-layer capacity at solid metals by Brummer (published elsewhere³⁷) and by Gilman who considered, in his paper (to be published elsewhere), the problem of evaluation of adsorption

information for mixed neutral and ionic species at Pt electrodes.

Acknowledgments. We take this opportunity of acknowledging the interest of Dr. F. Fowkes, Chairman of the Colloid Science Division, in this symposium and for his help in its organization. Thanks are also due to Mrs. A. Eriksen of the Department of Chemistry, University of Ottawa, for secretarial assistance in organizing the meeting, and to Dr. C. Barlow, Jr., for discussions on imaging.

(37) S. B. Brummer, *J. Phys. Chem.*, **71**, 2838 (1967); see also *J. Electroanal. Chem.*, **16**, 207 (1968).

Isotherms of Contact Adsorption in the Double Layer

by Halina Wroblowa¹ and Klaus Müller²

Electrochemistry Laboratory, University of Pennsylvania, Philadelphia, Pennsylvania 19104 (Received February 17, 1969)

Experimental data on the contact (specific) adsorption of ions, the Esin–Markov effect, and the humps on the capacity–metal charge curves for the Hg–solution interface are used to test theoretical treatments of the structure of the double layer given by two schools of authors. Comparison with experiment favors a model which implies single imaging in the metal plane rather than multiple imaging and confines the region of low dielectric constant to a monolayer of adsorbed water.

Introduction

The development of molecular theories of the electrical double layer remained from Stern's work in 1924³ until that of Grahame during the 1950's more or less unchanged. Grahame's extensive experimental determinations of the surface excesses, and in particular his methods of separation of these values into parts amenable to testing models, added a new dimension to the theoretical framework, and a fairly competent, though not absolutely thermodynamic, separation of diffuse layer contributions from those of the compact layer became possible.

Grahame did not stress the application of isotherms in his work, but his methods⁴ yield reliably the amount of ions adsorbed in contact with the electrode as a function of concentration and electric variable. This is the information required to advance molecular concepts concerning the forces involved, and thus to elucidate the vital aspects of the double-layer structure.

This analysis has been carried out in several different ways. One approach, which is empirical, consists in fitting the adsorption data to isotherms derived for adsorption from the gas phase. Certain parameters from this analysis can be interpreted in terms of, say, interactions between adsorbing particles, but there are large uncertainties. Firstly, it is often found that different isotherms give similar fit. Secondly, the parameters may be "lumped" values and cannot be assigned unambiguously.

Another approach combines a model for the double-layer structure (with parameters derived from independent experimental evidence) with a simple electrostatic description of the system.

A third approach emphasizes statistical methods in using certain approximations to the electrostatic situation (in terms of components of the potential at adsorption sites and of the potential generated by the adsorbing charge) and allows physical parameters to vary more widely.

Comparison of the two latter approaches with experiment appears particularly important now since Levine, *et al.*,^{5a} have shown their expressions and those of other authors in comparable forms. Up to now,

results of the third group have hardly been compared with experiment, or if so with a limited range of data. In order to partly fill this gap, we wish to single out two particular cases from groups 2 and 3 which from the discussion in the literature appear discrepant: the Levine–Bell–Calvert theory^{5b} (which claims some measure of identity with the Macdonald–Barlow results⁶ and that of the Bockris school.^{7,8} Using a consistent set of parameters, the coefficients for the modified⁸ isotherm of Bockris, Devanathan, and Müller (BDM) and for the isotherm of Levine, Bell, and Calvert⁵ (LBC) are calculated and compared with experimentally derived data.

The Modified Bockris–Devanathan–Müller and the Levine–Bell–Calvert Isotherms

The BDM isotherm⁷ can be presented in the form

$$\ln \frac{\theta}{1-\theta} = -\Delta G^\circ/RT + \ln \frac{a_{\pm}}{a_0} + Aq_M - B\theta^{3/2} \quad (1)$$

where θ is the fractional coverage of the electrode with the specifically adsorbed ion, ΔG° is the chemical standard free energy of adsorption, a_{\pm} and a_0 are activities in solution of the ion and water, respectively, $A = 4\pi e_0 h / \epsilon kT$, $h = 2r_{\text{H}_2\text{O}} - r_{\text{ion}}$, r denotes radius, ϵ is the dielectric constant in the layer immediately adjacent to the electrode, $B = M' e_0^{1/2} r_{\text{ion}}^2 Q_{\text{max}}^{3/2} / \epsilon kT$, $M' = M\pi^{3/2}/4$ for a square, and $M' = M \cdot 3^{3/4}/2^{1/2}$ for the hexagonal lattice. $M = 11.0$ is⁹ a two-dimensional

(1) Institute for Direct Energy Conversion, University of Pennsylvania, Philadelphia, Pa. 19104.

(2) American Cyanamid Co., Stamford, Conn. 06904.

(3) O. Stern, *Z. Elektrochem.*, **30**, 508 (1924).

(4) D. C. Grahame and B. A. Soderberg, *J. Chem. Phys.*, **22**, 449 (1954).

(5) (a) S. Levine, J. Mingins, and G. M. Bell, *J. Electroanal. Chem.*, **13**, 280 (1967); (b) S. Levine, G. M. Bell, and D. Calvert, *Can. J. Chem.*, **40**, 518 (1962).

(6) C. A. Barlow and J. R. Macdonald, *Advan. Electrochem. Electrochem. Eng.*, **6**, 1 (1967).

(7) J. O'M. Bockris, M. A. V. Devanathan, and K. Müller, *Proc. Roy. Soc.*, **A274**, 55 (1963).

(8) H. Wroblowa, Z. Kovač, and J. O'M. Bockris, *Trans. Faraday Soc.*, **61**, 1523 (1965).

(9) J. Topping, *Proc. Roy. Soc.*, **A114**, 67 (1927); I. Langmuir, *J. Amer. Chem. Soc.*, **54**, 1252, 2798 (1932).

⊖ A Anion
 ⊕ C Cation
 // M Metal
 ○ Water molecules

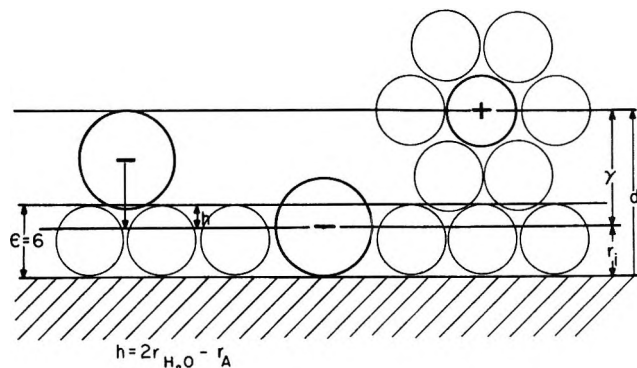


Figure 1. Model of the double layer.

analog of the Madelung constant, and Q_{max} is the maximum coverage (in units of charge).

The term $Aq_M kT$ represents the work of transfer of the center of the ionic charge through the region of low dielectric constant, which in the BDM model is thought to extend over the first monolayer of adsorbed oriented water dipoles^{7,8} (Figure 1). Beyond this monolayer the dielectric constant continuously increases, reaching the value of the bulk water beyond the outer Helmholtz plane (OHP). The term $B\theta^{3/2}kT$ represents the contribution to the free energy of adsorption arising from ion-ion interactions (Figure 2). The model for calculation of this term is indicated in Figure 2.

The isotherm derived by Levine, Bell, and Calvert⁵ on the basis of a cut-off disk model for the discrete charges, assuming multiple imaging between metal surface and OHP, and using Flory-Huggins statistics, can be presented in the form

$$\ln \frac{\theta}{(1 - \theta p)^p} = -\frac{\Delta G^\circ}{RT} + \ln \frac{a_{\pm}}{a_0} + (A')q_M - C\theta + \frac{\epsilon_0 \psi_{diff}}{kT} \quad (2)$$

where p is the ratio of the area occupied by an adsorbed ion to that of a water dipole, $A' = 4\pi\epsilon_0\gamma/\epsilon kT$, $\gamma \equiv d - r_{ion}$, d is the distance between the electrode and OHP, $C = 4\pi\gamma\epsilon_0 Q_{max}(1 - r_i/d)/\epsilon kT$, and ψ_{diff} is the mean potential at OHP.

The two isotherms differ considerably, reflecting the differences in the models used, as discussed in the following sections.

Imaging Conditions

(1) *Model.* The "lateral interaction terms" are proportional to $\theta^{3/2}$ and θ in the BDM and LBC isotherms, respectively. This arises, as pointed out by Levine, Bell, and Mingins^{5a} and Macdonald and Bar-

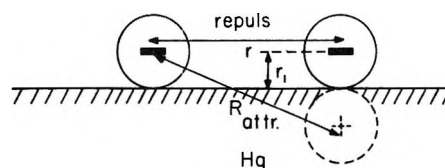


Figure 2. Lateral interactions in the double layer.

low,⁶ from the assumed (single or multiple) imaging conditions. Multiple imaging results in a higher screening effect, decreasing the lateral interaction energy which becomes approximately proportional to θ , instead of $\theta^{3/2}$ as found with single imaging in the metal only.

Single and infinite imaging are limiting cases of the complex situation in the double layer. Some partial imaging most probably takes place on the solution side. It is difficult to envisage that conductive imaging in the extremely poor conductor formed by the diffuse layer will occur to any significant extent. Dielectric imaging, on the other hand, requires the existence of a relatively well-defined plane of dielectric discontinuity between two layers of media with different dielectric constants. No sharp discontinuity exists at the OHP; the dielectric constant increases continuously as a complex function of distance from the plane located at the distance $2r_{H_2O}$ from the electrode to the bulk value. The sharpest discontinuity may be expected to exist at the $2r_{H_2O}$ plane (cf. Figure 1). It appears that this cannot serve as the imaging plane, however, since it passes through the adsorbed ions themselves. An estimate of the degree of partial imaging occurring therein is desirable but would require calculations which seem exceedingly difficult. The question remains, therefore, which of the two approximations—single or perfect multiple imaging—is closer to the physical situation, and at present this can best be done by comparison with experiment. This test can be carried out (i) by plotting $\log [a_{\pm}(1 - \theta)/\theta]_{qm}$ vs. $\theta^{3/2}$, and $\log [a_{\pm}(1 - p\theta)^p/\theta]_{qm}$ vs. θ (a) to examine the expected linearity or (b) to compare the experimental slopes with the theoretical values of B and C (cf. eq 1 and 2), respectively, and (ii) by examining the Esin-Markov effect.

(2) *Comparison with Experiment.* The plots of $\log [a_{\pm}(1 - \theta)/\theta]_{qm=0}$ vs. $\theta^{3/2}$ and θ are shown in Figures 3 and 4.^{9,10} It may be seen that the sensitivity of the plots to the respective powers on θ is insufficient to distinguish between single or multiple imaging as more or less valid conditions.

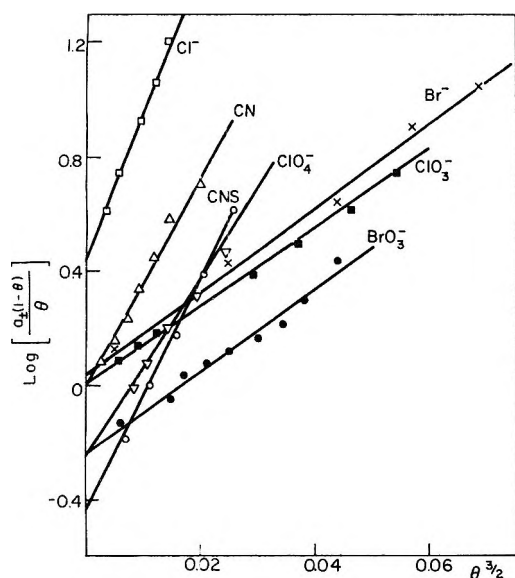
The values of the slopes B and C obtained experimentally are next compared to those predicted (eq 1 and 2) at $\theta^{3/2}$ and θ , respectively. The theoretical slopes were calculated using⁸ the crystallographic radii

(10) Z. Kovac, Thesis, University of Pennsylvania, Philadelphia, Pa., 1964.

Table I: Isotherm Parameters B and C (Eq 1 and 2)

Ion	Radius, r_i , Å	$B(\text{BDM})/2.3$		$C(\text{LBC})/2.3$			
		From expt ^{8,10}	Calcd	From expt ^{8,10}		Calcd, $\epsilon = 6$	Calcd, $\epsilon = 10$
				$p = 1$	$p = 3$		
Cl^-	1.81	52	45	17	13	149	89
Br^-	1.96	17	42	6	2	119	71
I^-	2.19	15	37 ^a	6	2	85	51
CN^-	1.96	36	42	12	8	119	71
CNS^-	1.60 ^b	34	50	18	14	207	124
BrO_3^-	1.60 ^b	15	14	7	3	88	54
ClO_3^-	1.50 ^b	14	13	6	2	93	55
ClO_4^-	2.54	36	32	9	5	52	31

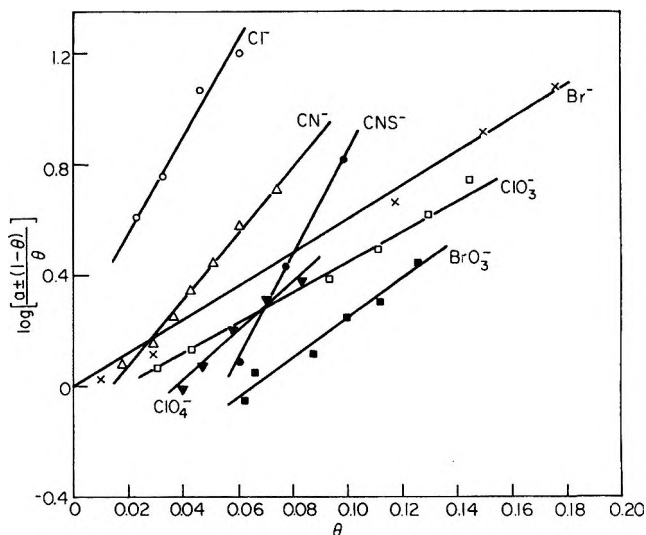
^a 13, if the center of charge is shifted by 0.5 Å toward the metal. ^b Effective radii, as outlined in text.

Figure 3. Test of the BDM isotherm at $q_M = 0$.

as r_{ion} of Cl^- , Br^- , I^- , CN^- , and ClO_4^- . The centers of charge of the ClO_3^- , BrO_3^- , and CNS^- ions were assumed to be situated in the center of the Cl, Br, and S atoms, which are taken to be directed toward the metal surface. For calculations of the Q_{max} term, crystal radii or radii obtained from models⁸ were used.

The value of the dielectric constant, $\epsilon = 6$,^{7,11-14} is used for calculating A , assuming that the major part of the work is that connected with transferring the ion across the region of the low dielectric constant, over the distance h (cf. Figure 1). The LBC model assumes this region to extend up to the OHP plane and then attributes to it the higher value of $\epsilon = 10$. Since the value $\epsilon = 6$ is relatively well established for the inner region, results are presented for both values. The values of $d = \gamma + r_{\text{ion}}$ are based on the double-layer model presented in Figure 1 (cf. ref 7 for justification of the model), wherefrom $d \approx 6.3$ Å and $\gamma = 6.3$ Å $- r_{\text{ion}}$.

The only other reasonable position of the OHP plane would be at a distance of ~ 3.7 Å from the

Figure 4. Test of the LBC isotherm at $q_M = 0$.

metal.¹⁴ However, for the purposes of the LBC model, the imaging plane would then, for all ions except Cl^- , pass through the ions themselves, which does not seem satisfactory. The experimentally obtained B and C values are compared in Table I with those derived theoretically.

The BDM model leads to an agreement between the theory and experiment within $\pm 17\%$, except for I^- , Br^- , and CNS^- ions, where discrepancies are larger. This may be connected with a wrong estimate of the distance between the metal and the center of the ionic charge for the highly adsorbable I^- and Br^- ions, as well as for the CNS^- ion.

The LBC model with $p = 1$ leads to values which even for $\epsilon_1 = 10$ exceed the experimental ones 4 to

(11) R. W. Rampolla, R. C. Miller, and C. P. Smyth, *J. Chem. Phys.*, **30**, 566 (1959); C. P. Smyth, "Dielectric Behavior and Molecular Structure," McGraw-Hill Book Co., Inc., New York, N. Y., 1955.

(12) R. Parsons, *Proc. Roy. Soc.*, **A261**, 79 (1961).

(13) J. R. Macdonald, *J. Chem. Phys.*, **22**, 1857 (1954); J. R. Macdonald and C. A. Barlow, *ibid.*, **36**, 3062 (1962).

(14) M. A. V. Devanathan, *Trans. Faraday Soc.*, **50**, 373 (1954).

12 times. The assumption of $p > 1$ leads to even larger discrepancies (increasing with p) between the theory and experiment. For $p = 3$, the theoretical slopes exceed 6–35 times those obtained experimentally.

Esin–Markov Effect

The Esin–Markov effect has been related by Parsons¹⁵ to the change at constant concentration of the specifically adsorbed charge, q^- , with the charge on the metal

$$\left(\frac{\partial E^+}{\partial \ln a_{\pm}}\right)_{q_M} \approx \frac{2RT}{F} \left(\frac{\partial q^-}{\partial q_M}\right)_{a_{\pm}} \quad (3)$$

valid for $q^- > 5 \mu\text{C}/\text{cm}^2$.

Thus for electrolytes leading to a linear change of electrode potential at constant q_M with activity, a basically linear q^- - q_M relation should be expected, and adsorption isotherms should also predict this behavior.

In order to examine whether the modified BDM and the LBC isotherms have this Esin–Markov effect built in, eq 1 and 2 rewritten in the form

$$Aq_M = \text{constant} + \ln\left(\frac{\theta}{1-\theta}\right) + B\theta^{1/2} \quad (1a)$$

$$A'q_M = \text{constant} + \ln\frac{\theta}{(1-p\theta)^p} + C\theta \quad (2a)$$

have been differentiated using the relation $dq = Q_{\text{max}}d\theta$.

From eq 1a

$$\left(\frac{\partial q^-}{\partial q_M}\right)_{a_{\pm}} = A Q_{\text{max}} \left[\frac{1}{\theta(1-\theta)} + 1.5B\theta^{1/2} \right]^{-1} \quad (4)$$

The plots of $1/\theta(1-\theta)$ and of $1.5B\theta^{1/2}$ against θ are shown in Figure 5, curves 1 and 2, for the value of B corresponding to $r_i = 1.8 \text{ \AA}$. The sum of these two terms is shown in Figure 5 as curve 3, and as curve 4 for $r_i = 2.6 \text{ \AA}$.

The two terms in brackets (eq 4) compensate each other in the range $0.04 < \theta < 0.17$ for smaller ions and in the range $0.09 < \theta < 0.2$ for larger ions (cf. Figure 5, curves 3 and 4), leading to almost constant $(\partial q^-/\partial q_M)_{a_{\pm}}$, and consequently (eq 3) constant $(\partial E^+/\partial \ln a_{\pm})_{q_M}$ values.

This constancy is clearly connected with the existence of the $\theta^{1/2}$ term, which in turn arises owing to the assumed single-imaging conditions.

For multiple imaging

$$\left(\frac{\partial q^-}{\partial q_M}\right)_{a_{\pm}} = A' Q_{\text{max}} \left[\frac{1}{\theta(1-\theta)} + C \right]^{-1} \quad (\text{with } p = 1) \quad (5a)$$

$$\left(\frac{\partial q^-}{\partial q_M}\right)_{a_{\pm}} = A' Q_{\text{max}} \left[\frac{1-p\theta+p^2\theta}{\theta(1-p\theta)} + C \right]^{-1} \quad (\text{with } p > 1) \quad (5b)$$

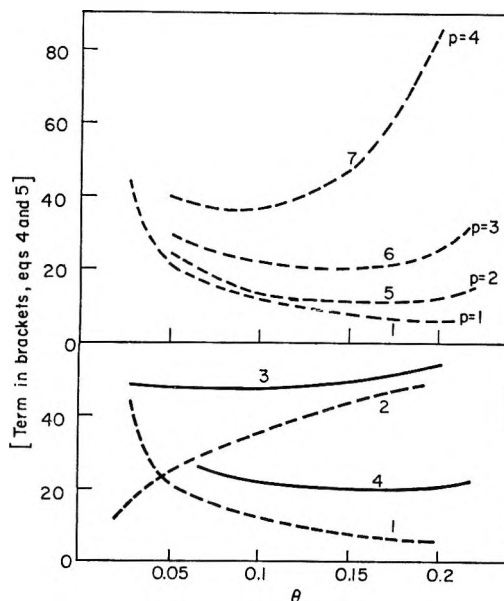


Figure 5. The change with coverage of the $(\partial q^-/\partial q_M)_{a_{\pm}}$ term: 1, $1/\theta(1-\theta)$ vs. θ ; 2, $1.5B\theta^{1/2}$ vs. θ ; 3, resulting change of the term in brackets (eq 4) with θ ($r_i \approx 2 \text{ \AA}$); 4, same as 3 for $r_i = 2.6 \text{ \AA}$; 5, change of the θ -dependent term in brackets (eq 5b) with θ for $p = 2$; 6, same as 5 for $p = 3$; 7, same as 5 for $p = 4$.

It can readily be seen from eq 5a that the change of the $1/\theta(1-\theta)$ term with θ (Figure 5, curve 1) is not compensated by another term and consequently (for $p = 1$) the constancy of $(\partial q^-/\partial q_M)_{a_{\pm}}$ at the coverages usually encountered in ionic adsorption could not be expected (unless $C \gg 1/\theta(1-\theta)$, which contradicts experiment).

For $p = 2$ or 3, fairly constant values of $(\partial q^-/\partial q_M)_{a_{\pm}}$ may be expected, according to Figure 5, although more detailed calculations by Levine, *et al.*,^{5a} show that the constancy is not good. With the value of $p = 4$, perhaps appropriate for large ions such as ClO_4^- , $(\partial q^-/\partial q_M)_{a_{\pm}}$ should strongly decrease with increasing θ . Some tendency in this direction is observed.¹⁶

Thus it may be concluded that it is the single-imaging model which leads to an isotherm resulting in the often observed relative constancy of the $(\partial \ln E^+/\partial \ln a_{\pm})_{q_M} = (\partial q^-/\partial q_M)_{a_{\pm}}$ expressions over the predicted range of coverages.

The actual values of the Esin–Markov effect calculated from eq 4 are given in Table II, along with the experimental values of $(\partial q^-/\partial q_M)_{a_{\pm}}$ and $2RT/F \cdot (\partial E^+/\partial \ln a_{\pm})$ obtained in previous work⁸ or by other authors.^{10, 15–19}

(15) R. Parsons, Proceedings of the Second International Congress of Surface Activity, Vol. III, Butterworth and Co., Ltd., London, 1957, p 38.

(16) R. Payne, *J. Phys. Chem.*, **70**, 204 (1966).

(17) T. Erdey-Gruz and P. Szarvas, *Z. Phys. Chem. (Leipzig)*, **A177**, 277 (1936).

Table II: Esin–Markov Effect

Ion	Radius, r_i , Å	Q_{\max} , $\mu\text{C}/\text{cm}^2$	Esin– Markov effect (theory)	Esin–Markov effect observed as			
				$\left(\frac{\partial q^-}{\partial q_M}\right)_{a_{\pm}}$	Ref	$\frac{F}{2RT} \left(\frac{\partial E_+}{\partial \ln a_{\pm}}\right)_{q_M}$	Ref
Cl ⁻	1.81	127	1.56	1.23–1.33	8, 18	1.22	15
Br ⁻	1.96	109	1.19	1.27–1.41	18, 19	1.35	15
I ⁻	2.19	87	0.73 ^a	1.29	23	1.36	15
CN ⁻	1.96	109	1.19	0.61	8	0.86–1.42	10, 17
CNS ⁻	1.60 ^b	162	2.19 ^c	1.12–1.26	8	1.31	10
BrO ₃ ⁻	1.60 ^b	70	2.17 ^d	0.87	8	0.83–1.31	10
ClO ₃ ⁻	1.50 ^b	70	2.52 ^e	0.92	8	1.23	10
ClO ₄ ⁻	2.54	64	0.25	0.28–0.5	16	0.29–0.46	10

^a 1.35, if the center of charge is shifted 0.5 Å toward the metal. ^b Effective radii, as outlined in text. ^c 1.32, if the center of charge is shifted 0.3 Å away from the metal. ^d 1.17, if the center of charge is shifted 0.35 Å away from the metal. ^e 1.09, if the center of charge is shifted 0.5 Å away from the metal.

The agreement is reasonable in the case of Cl⁻, Br⁻, and ClO₄⁻ ions. In the case of I⁻, CNS⁻, and oxy-ions the agreement with experiment is again achieved only if it is assumed that the center of the charge is shifted. Attempts to explain in a somewhat similar way the anomalies in the adsorption behavior of the iodide ion were already made previously.²⁰ The geometry of CNS⁻ and of the oxy-ions was taken from atomic models⁸ and the center of charge placed in the middle of the atom in contact with the electrode; however, as indicated for CNS⁻ by Parsons,²¹ this may be an unsatisfactory approximation, and the center of charge may be at a larger distance from the electrode.

In the case of CN⁻ ions the experimental $\partial q^-/\partial q_M$ slope is about half that of the calculated value, while the oxy-ions ClO₄⁻ and BrO₃⁻ have $(\partial q^-/\partial q_M)_{a_{\pm}}$ slopes changing with the charge on the metal,^{8,16} a feature not predicted by the BDM isotherm, and only in 1 *N* solutions is a better agreement between experiment and theory obtained. The structure of the double layer in the presence of these ions may not correspond to the model involved owing, *e.g.*, to structure-breaking properties affecting the value of the dielectric constant.

In summary, the single-imagining condition resulting in a $B\theta^{3/2}$ term in eq 1 leads to a constancy of the Esin–Markov coefficient and a fair agreement with the numerical values for simple ions.

The Capacitance Humps

The hump on the capacitance curve has been interpreted by several authors^{7,14,16,22,23} as due to the specific adsorption of ions. According to the BDM model the hump arises from the contribution of repulsive forces to the standard free energy of adsorption, which produces an inflection on the $q^- - q_M$ curve that coincides with the positions of the hump on the $C - q_M$ curves.

The charge on the metal at which the inflection occurs can be found by equating $(\partial^2 q^-/\partial q_M^2)_{a_{\pm}}$ to zero; the second derivatives can be obtained from eq 1a and 2a.

From eq 1a one obtains for the inflection point the condition

$$2 - 4q^- - \frac{3}{2}B(q^-)^{3/2} + \frac{9}{2}B(q^-)^{5/2} = 0$$

which when solved numerically yields the predicted values of q_M at which capacity humps should be observed. In Figure 19 of ref 8 a plot of these values against the experimental ones is shown, demonstrating a fairly good agreement between the position of the inflection in the $(\partial q^-/\partial q_M)_{a_{\pm}}$ curve and that of the capacity hump. (See Table III.)

Table III: Position of the Hump

Ion	Concn, <i>N</i>	θ_{hump} , exptl	θ_{hump} , calcd
Cl ⁻	1	0.09	0.1
CN ⁻	0.3	0.085	0.1
CNS ⁻	1	0.07	0.09
BrO ₃ ⁻	0.1	0.12	0.11
ClO ₃ ⁻	0.3	0.11	0.11
ClO ₄ ⁻	0.3	0.11	0.1

(18) M. A. V. Devanathan and B. V. K. S. R. A. Tilak, *Proc. Roy. Soc.*, **A290**, 527 (1966).

(19) J. Lawrence, R. Parsons, and R. Payne, *J. Electroanal. Chem.*, **16**, 193 (1968).

(20) D. C. Grahame and R. Parsons, *J. Amer. Chem. Soc.*, **83**, 1291 (1961).

(21) R. Parsons and P. C. Symons, *Trans. Faraday Soc.*, **64**, 1077 (1968).

(22) A. Watanabe, F. Tsuji, and S. Ueda, Proceedings of the Second International Congress of Surface Activity, Vol. III, Butterworth and Co., Ltd., London, 1957, p 94.

(23) S. Minc and J. Jastrzebska, *Rocz. Chem.*, **37**, 507 (1963); *Electrochim. Acta*, **9**, 533 (1964).

Table IV: Isotherm Parameter A

Ion	Radius, $r_i, \text{Å}$	$h, \text{Å}$	$\gamma, \text{Å}$	A/2.3, cm ² /μC, (calcd)			Exptl
				BDM	LBC ($\epsilon = 6$)	LBC ($\epsilon = 10$)	
Cl ⁻	1.81	1.01	4.49	0.32	1.43	0.86	0.15
Br ⁻	1.96	0.86	4.34	0.27	1.38	0.83	0.15
I ⁻	2.19	0.63	4.11	0.20	1.31	0.78	0.12
CN ⁻	1.96	0.86	4.34	0.27	1.38	0.83	0.21
CNS ⁻	1.60	1.22	4.70	0.39	1.49	0.89	0.11
BrO ₃ ⁻	1.60	1.22	4.70	0.39	1.49	0.89	0.08
ClO ₃ ⁻	1.50	1.32	4.80	0.42	1.53	0.92	0.06
ClO ₄ ⁻	2.54	0.28	3.76	0.09	1.20	0.72	0.09

At the same time, good agreement is found between the predicted and experimentally found θ values at which inflection occurs on the θ - q_M curve (Table IV). The data in Figure 19 (ref 8) and Table IV confirm the assumptions concerning the contribution of repulsive forces to the free energy of adsorption underlying the BDM model.

On the other hand, isotherms derived on the basis of multiple imaging models, *i.e.*, containing a term in θ and not $\theta^{3/2}$, predict (for $p = 1$), as shown below, the existence of the hump at $\theta = 0.5$, *i.e.*, at a coverage which is hardly ever reached in ionic adsorption.

Differentiating eq 2a twice, one obtains

$$\left(\frac{\partial^2 q^-}{\partial q_M^2}\right)_{a_{\pm}} = 0 \text{ when } \theta = \frac{\sqrt{p} - 1}{p^2 - p}$$

Thus the hump may be expected at $\theta = 0.5$ for $p = 1$, $\theta \simeq 0.2$ for $p = 2$, $\theta \simeq 0.12$ for $p = 3$, and $\theta \simeq 0.08$ for $p = 4$.

Generally the hump is observed at θ values close to 0.1 (*cf.* Table IV) which would be predicted by the LBC isotherm if $3 < p < 4$. However, this assumption results in experimental values of C which are still lower, and thus even more in disagreement with theoretical values than those at $p = 1$ (*cf.* Table I).

Ion-Field Interactions

A test of the isotherms with respect to the ion-field interactions can be carried out by comparing with experiment the values of $(\partial \ln a_{\pm} / \partial q_M)_{\theta}$ coefficients (*cf.* eq 1 and 2) calculated according to both models. In Table III the experimental values obtained in the previous work⁸ and from data of Lawrence, *et al.*,¹⁹ for Br⁻ as well as of Grahame²⁴ for I⁻ are compared with the calculated values of $A = 4\pi e_0 h / \epsilon k T$ (BDM) and $A' = 4\pi e_0 \gamma / \epsilon k T$ (LBC). In the latter case both $\epsilon = 6$ and $\epsilon = 10$ were assumed.

The calculated values of A are consistently higher than the experimental ones. Agreement within a factor of 2 is observed for simple ions and ClO₄⁻ in the case of the BDM isotherm. This discrepancy may be connected with the work expended in redistribution of charges already adsorbed upon adsorption

of an arriving ion, which has not been taken into account in the theoretical treatment.

The large discrepancies observed for the complex ions CNS⁻, ClO₃⁻, and BrO₃ seem to be connected, as previously, with the uncertainty met in arbitrarily assigning the center of the ionic charge to the center of S, Cl, or Br atoms (see above), which leads to overestimated values of h .

The disagreement between the LCB theory and experiment is much greater even in the case of simple ions and perchlorate, where no serious ambiguity as to the position of the center of the charge exists.

Concluding Remarks

The four tests in which theoretical conclusions are confronted with experiment are an attempt to improve our knowledge of double-layer structure, both in respect to parameters and in respect to assumptions concerning more complex physical features.

Since throughout the four tests the BDM model gives a more satisfactory qualitative and quantitative fit, it may be concluded that (i) the outer Helmholtz plane is not a good imaging plane, as compared to metal. In fact, Macdonald and Barlow⁶ report that even in the metal imaging at molecular distances is not perfect; one should think that in view of the short distances involved, of the thermal motions, and of the hydrogen bonding, dielectric imaging in the solution beyond the OHP is far from perfect, and that this is why single imaging conditions lead to better agreement with experiment. (ii) The region of low dielectric constant does not extend beyond the first water layer; thus the ions have their centers of charge approximately in the plane of dielectric discontinuity. (iii) The less favorable comparison of the LBC isotherm with experiment is not connected with the method of evaluation, but with the model of the double layer used and with the assumed perfect imaging. (iv) The elementary BDM model certainly requires further elaboration. The contribution of the potential of the OHP has been neglected as a small correction term;

(24) D. C. Grahame, *J. Amer. Chem. Soc.*, **80**, 4201 (1958); O. N. R. Technical Report, Second Series, No. 5 (1957).

however, at lower concentrations it should certainly be taken into account.

The electrical contribution to the free energy of adsorption of solvent dipoles has also been neglected, since the χ potential in aqueous solutions has been shown to change relatively little in the relevant regions of charge on the metal.⁷ However, experimental data obtained in other solvents, or at high anodic potentials, indicate that there the solvent dipoles should be taken

into account, particularly for the larger ions. Further, differences in adsorption of ions from pure and mixed solutions²⁵ are not explicable in terms of the present BDM model. All these effects, however, will require special experimental tests, since the general data do not appear accurate enough to go beyond the present conclusions.

(25) E. Dutkiewicz and R. Parsons, *J. Electroanal. Chem.*, **11**, 100 (1966).

A Theory of the Electrical Capacity of the Inner Region in the Absence of Ionic Adsorption at the Mercury–Water Interface

by S. Levine,

Department of Mathematics, University of Manchester, Manchester, England

G. M. Bell,

Department of Mathematics, Chelsea College of Science and Technology, University of London, London, England

and A. L. Smith

Department of Chemistry, Liverpool College of Technology, Liverpool, England (Received February 21, 1969)

We develop a statistical mechanical theory of the dielectric properties of the Stern inner region at the mercury–water interface in the absence of specific adsorption of ions. The model of the region is a plane monolayer of polarizable water (point) dipoles at fixed surface density. These are sandwiched *in vacuo* between two continuous media, the aqueous phase and the mercury phase which carries a surface charge. Two orientation states are assigned to the water dipoles, with the magnitudes of the dipole moment components perpendicular to the surface differing in the two states. Also different “residual” energies at the zero point of charge (zpc) are postulated for the two orientation states. We imagine a dipole situated at each site on a two-dimensional hexagonal lattice and assume random distribution over the sites, of dipoles in the two states. Dipole–dipole interactions and also dipole imaging due to the two continuous media are considered. The coordination number is 6 for nearest-neighbor interactions only in a plane hexagonal lattice, but because of the appreciable dipole–dipole interactions at larger than nearest-neighbor distances and also of imaging, the effective coordination number reaches a value of about 15. A consequence is that the mean dipole moment per molecule is very much reduced and there is no need to introduce an “effective dielectric constant” to diminish the potential drop across the dipole layer to a “reasonable value.” The integral and differential capacities of the inner region and the corresponding temperature coefficients are determined as functions of the surface charge. It is shown that with a residual energy at the zpc and unequal dipole moments normal to the surface in the two orientation states, it is possible for the maximum in the capacity to occur on the positive side of the zpc and yet the residual orientation of dipoles at the zpc is directed with the negative end toward the mercury phase. Reasonable values of capacities and their temperature coefficients are obtained in the neighborhood of the zpc. The general experimental trends of the capacities, and to a lesser extent of their temperature coefficients, are reproduced for negatively charged surfaces. The theory predicts somewhat different behavior of the capacities on the two sides of the zpc. However, if the monolayer density of water dipoles is assumed fixed, then the theory does not show any tendency for the capacities to remain approximately constant as the surface charge becomes more positive.

1. Introduction

A number of authors have proposed theories of the electrical capacity of the so-called inner region, at the mercury–aqueous electrolyte interface, which are based to varying degrees on a statistical mechanical

treatment of oriented water dipoles. We shall describe here further developments of these theories, making use in particular of the works by Watts-Tobin,¹ Mott and Watts-Tobin,² Macdonald and Barlow,^{3–8} and Bockris, *et al.*^{9,10} Usually, a two-state model of

dipole orientation is assumed for the water molecules in the inner region, although Macdonald and Barlow³ have also examined the possibility of all orientations of the water dipoles. One shortcoming in previous theories, however, is either the neglect¹⁻³ or the inadequate account⁴⁻¹⁰ of the lateral interaction of dipoles in the inner region. Another unsatisfactory feature is the use of the so-called effective dielectric constant ϵ_e . A familiar formula for the potential drop V_0 across a layer of oriented dipoles, each of moment p and in number N per unit area, is $V_0 = 4\pi Np/\epsilon_e$. In the absence of the reduction factor ϵ_e , V_0 is found to be too large and the usual justification for inserting ϵ_e is that it is due to the "nonpermanent" part of the dipoles. Using a method partly resembling that described in this paper, Bockris, Devanathan, and Müller⁹ choose, for example, $\epsilon_e = 6$. Macdonald and Barlow⁴ stress that a proper microscopic theory requires no such factor. Nevertheless, their statement is inconsistent with their use of the factor n^{-2} , where n is the optical refractive index, when they consider the orienting electric field acting on a water dipole. The theory of the dielectric behavior of the inner region developed in the present paper avoids the introduction *a priori* of an effective dielectric constant ϵ_e and in fact calculates ϵ_e from microscopic considerations.

The direction of residual orientation of the water dipoles at the zero point of charge (zpc) at the mercury-aqueous electrolyte interface has been a matter of controversy. Grahame¹¹ calculated the differential capacity of the inner region at the mercury-aqueous NaF interface for which specific adsorption of ions is presumed negligible and obtained a hump in this capacity at temperature $T = 25^\circ$ and slightly positive values of charge (surface charge density $\sigma \approx 4 \mu\text{C}/\text{cm}^2$) on the mercury. If this hump is interpreted as the position of zero net orientation of water dipoles in the inner region, then Grahame's results indicate a slight orientation of the water dipoles with the positive end (hydrogens) toward the mercury phase at the zpc. Various authors,^{9,12,13} however, have argued that the orientation is in the opposite direction at the zpc. Recently, Stillinger and Ben Naim¹⁴ have investigated the potential difference across the water vapor interface just below the critical temperature and predict the surface water dipoles to be oriented with the positive end away from the vapor phase. Their model of the water dipole is a rigid point dipole plus a rigid point quadrupole in a spherical enclosure, which is embedded in a continuous medium of slowly varying dielectric inhomogeneity, and they combine classical electrostatics with some statistical mechanics. It is questionable, however, whether their model is suitable for the much denser inner region at the mercury-water interface, where the potential drop due to oriented water dipoles at the zpc should be of the order of 100 mV, as compared with the few millivolts which

they calculate at the air-water interface. (Recently, Fletcher¹⁵ has proposed a potential drop of ~ 100 mV at the air-water interface with the positive end toward the vapor phase.) In this paper, we shall suggest one way of resolving the contradictory views on the water dipole orientation at the mercury-water interface.

On the basis of their measurements of surface excess entropy Γ_s and volume Γ_v at the mercury-0.1 M NaF aqueous interface at 25° , Hills and Payne¹⁶ have proposed a dielectric model of the inner region, which differs significantly from those of previous authors. Hills and Payne find an increase of 3.1×10^{-9} cal $\text{deg}^{-1} \text{cm}^{-2}$ in Γ_s from the far positive (anodic) side of the zpc (where $\sigma \approx 20 \mu\text{C}/\text{cm}^2$) to a negative value $\sigma \approx -10 \mu\text{C}/\text{cm}^2$ for the surface charge density where Γ_s has a maximum. The surface excess volume Γ_v shows a corresponding increase of $0.35 \times 10^{-8} \text{cm}^3 \text{cm}^{-2}$ over the same range in σ . They regard the surface excess entropy and volume as properties of the inner region of the double and suggest that the variations in these quantities are primarily due to adsorption of water molecules into the inner region. This implies an almost twofold increase in surface density of water over a range in σ of about $30 \mu\text{C}/\text{cm}^2$. These authors further propose that because of this adsorption, the thickness d of the inner region may increase as σ becomes more positive. They interpret the capacity hump at $\sigma \approx 4 \mu\text{C}/\text{cm}^2$ as a maximum in the ratio ϵ_i/d , where ϵ_i is the dielectric constant of the inner region. However, the value of ϵ_i at the hump is attributed to the induced polarization which increases with the surface concentration of water

- (1) R. J. Watts-Tobin, *Phil. Mag.*, **6**, 133 (1961).
- (2) N. F. Mott and R. J. Watts-Tobin, *Electrochim. Acta*, **4**, 79 (1961).
- (3) J. R. Macdonald and C. A. Barlow, *J. Chem. Phys.*, **36**, 3062 (1962).
- (4) J. R. Macdonald and C. A. Barlow, *ibid.*, **39**, 412 (1963).
- (5) J. R. Macdonald and C. A. Barlow, "Electrochemistry" (Proceedings of the 1st Australian Conference, 1963), J. A. Friend and F. Gutmann, Ed., Pergamon Press, London, 1964, pp 199-247.
- (6) J. R. Macdonald and C. A. Barlow, *J. Chem. Phys.*, **44**, 202 (1966).
- (7) J. R. Macdonald and C. A. Barlow, *Surface Sci.*, **4**, 381 (1966).
- (8) C. A. Barlow and J. R. Macdonald, *Advan. Electrochem. Electrochem. Eng.*, **6**, 1 (1967).
- (9) J. O'M. Bockris, M. A. V. Devanathan, and K. Müller, *Proc. Roy. Soc.*, **A274**, 55 (1963).
- (10) J. O'M. Bockris, M. Green, and D. A. J. Swinkels, *J. Electrochem. Soc.*, **111**, 743 (1964).
- (11) D. C. Grahame, *J. Amer. Chem. Soc.*, **76**, 4819 (1954); **79**, 2093 (1957).
- (12) A. N. Frumkin, Z. A. Iofa, and M. A. Gerovich, *Zh. Fiz. Khim.*, **30**, 1455 (1956).
- (13) R. Parsons and F. G. R. Zobel, *J. Electroanal. Chem.*, **9**, 333 (1965).
- (14) F. H. Stillinger and A. Ben Naim, *J. Chem. Phys.*, **47**, 4431 (1967).
- (15) N. H. Fletcher, *Phil. Mag.*, **18**, 1287 (1968).
- (16) G. J. Hills and R. Payne, *Trans. Faraday Soc.*, **61**, 326 (1965).

molecules, rather than to a dipole orientation effect. They also suggest that the mean orientation of the water dipoles is reversed not at $\sigma \approx 4$ but at $\sigma \approx -10 \mu\text{C}/\text{cm}^2$.

The numerical results obtained in section 4 indicate some merit in the suggestion by Hills and Payne that the adsorption of water molecules into the inner region is charge dependent. Nevertheless, there are difficulties in their interpretation of the experimental results. In their argument, they make the assumption that the surface entropy per water molecule is independent of the surface charge σ . This is contradictory, since according to them, the number of adsorbed molecules changes considerably with σ , so that the latter must have a powerful direct effect on the state of the water molecule in or near the inner layer. Another difficulty is that such a density change in the inner region is bound to alter the "structure" of the adjacent layers of water molecules and these would contribute to Γ_s and Γ_v . Indeed the following argument based on their measurements of Γ_v indicates that the density of molecules in the inner region will not double. Let us assume that the surface density of water dipoles equals 10^{15} molecules/cm² at the zpc, and that this increases to 1.6×10^{15} molecules/cm² at $\sigma = 20 \mu\text{C}/\text{cm}^2$. The volume contraction of 0.35×10^{-8} cm³/cm² over the range of $\sigma = 30 \mu\text{C}/\text{cm}^2$ is shared by the 1.6×10^{15} molecules, giving a volume reduction ~ 1.4 cm³/mol, equivalent to a compression of only 8%. If the surface density of molecules doubles, this suggests that the thickness of the inner region has increased by a factor rather less than 2 and as a further implication, that the second layer of water has the same Γ_s per mole as the first layer, which is unlikely. The interpretation of Γ_s and Γ_v in terms of molecular configurations seems much more difficult than that of the surface excess of ions Γ_i in terms of ionic configuration. In the latter case, Γ_i can be expressed, to a reasonable approximation, in terms of the potential distribution in the double layer. Other points which require substantiation in the model of Hills and Payne, are (i) their assumption that the distortional part of the total polarizability of the water molecule is responsible for the capacity hump at $\sigma = 4 \mu\text{C}/\text{cm}^2$ and (ii) the anisotropy in the water dipole orientations with respect to the charge density σ if the mean orientation were zero at $\sigma \approx -10 \mu\text{C}/\text{cm}^2$. The work of these authors has also been discussed by Parsons and Zobel¹³ and Bijsterbosch and Lyklema.¹⁷ An estimation of the magnitude of adsorption of water molecules into the inner region seems difficult and will not be attempted here.

One limitation of the theory described in this paper is that the layers of water immediately adjacent to the monolayer of the inner region have been treated as a continuum, with the same properties as bulk water. A more adequate theory would, perhaps,

embody some features of the statistical mechanical theory of the surface layers of a (nonpolar) liquid developed by various authors (see, for example, Defay, *et al.*,¹⁸ and Everett¹⁹), who introduce a series of parallel monomolecular layers, each having a different composition. Such a theory for a hydrogen-bonded polar liquid like water is a formidable task.

2. Discrete Two-State Orientation Model

Our model of the inner region is a plane monolayer of electrostatically interacting, polarizable water molecules situated *in vacuo* between two plane interfaces beyond which are continuous media representing the mercury and aqueous phases, respectively. We imagine the monolayer to be horizontal with the aqueous phase above the mercury phase. The charge distribution on each water molecule is approximated by a point dipole and each dipole is imagined as situated on one site of a two-dimensional hexagonal lattice, each site having $C (= 6)$ nearest neighbors. If N is the number of sites per unit area and d the distance between nearest neighbors, then $Nd^2 = 2/\sqrt{3}$; we assume that the thickness of the inner region $d_i = d$. If adsorption of water molecules into the inner region takes place with change in the charge density σ on the mercury surface, then N will be a function of σ . In these circumstances, d will probably also depend on σ , and we should not identify the inner region thickness with the nearest-neighbor lateral distance. These extensions of the theory will not be considered because the dependence of N and of inner region thickness on σ are unknown.

We shall be interested in the polarization of the monolayer in the normal direction and shall therefore only consider the normal component of the permanent water dipole moments, in the inner region. In the two-state model it is assumed that there are only two possible values for this component, and taking the downward direction as positive, these will be denoted by p^\dagger and $-p^\dagger$, corresponding to the "down" and "up" positions (positive pole, *i.e.*, the hydrogens, toward or away from the mercury phase). In the general form of the two-state model $p^\dagger \neq p^\ddagger$, and it is convenient to introduce the quantities p and δ , defined by

$$p = \frac{1}{2}(p^\dagger + p^\ddagger); \quad \delta = (p^\dagger - p^\ddagger)/2p \quad (2.1)$$

so that components p^\dagger and p^\ddagger can be written as

$$p^\dagger = p(1 - \delta); \quad p^\ddagger = p(1 + \delta) \quad (2.2)$$

If the permanent dipole is perpendicular to the interface in both states, then $p^\dagger = p^\ddagger = p = p_w$, where

(17) B. H. Bijsterbosch and L. Lyklema, *J. Colloid Interfac. Sci.*, **28**, 506 (1968).

(18) R. Defay, I. Prigogine, A. Bellemans, and D. H. Everett, "Surface Tension and Adsorption," Longmans, London, 1966.

(19) D. H. Everett, *Trans. Faraday Soc.*, **60**, 1803 (1964); **61**, 2478 (1965).

p_w is the magnitude of the permanent dipole moment. As will be seen below, the contradictory phenomena concerning the residual dipole orientation at the zpc, to which we referred in the Introduction, are explicable on the hypothesis that $p^{\downarrow} \neq p^{\uparrow}$ (i.e., $\delta \neq 0$). A possible explanation is that when the oxygen of the water molecule points toward the mercury the dipole is perpendicular but that when it points away the dipole is at angle $\theta \neq 0$ to the downward normal. This would involve different hydrogen bonding with the water in the second layer immediately adjacent to the inner region for the two orientation states. (Compare the difference between anions and cations as suggested by Verwey²⁰ in regard to the water molecules occupying the hydration shells of these ions.) It can be shown from (2.1) that if $p^{\downarrow} = p_w$, $p^{\uparrow} = p_w \cos \theta$, then

$$p = p_w \cos^2 \frac{1}{2}\theta; \delta = \tan^2 \frac{1}{2}\theta \quad (2.3)$$

The largest possible value of θ probably corresponds to an OH direction in the water molecule being perpendicular to the interface and then $\theta = 52.5^\circ$.

It will be assumed that every site of the hexagonal lattice is occupied so that if N^{\downarrow} and N^{\uparrow} denote the numbers of dipoles per unit area in the "down" and "up" positions, respectively, then

$$N^{\downarrow} + N^{\uparrow} = N \quad (2.4)$$

The mean dipole moment per site in the downward normal direction due to the permanent dipole moment is given by

$$m_p = (p^{\downarrow}N^{\downarrow} - p^{\uparrow}N^{\uparrow})/N = p(\lambda - \delta) \quad (2.5)$$

where we have substituted from (2.2) and introduced the variable

$$\lambda = (N^{\downarrow} - N^{\uparrow})/N = (2N^{\downarrow} - N)/N \quad (2.6)$$

which measures the extent to which the water dipole lies in one state rather than in the other. From (2.5) it can be seen that when $\delta \neq 0$, m_p is the sum of a "permanent" polarization term $-p\delta$ and a term $p\lambda$ due to preferential orientation. There will also be a mean induced dipole component m_i per molecule, measured in the downward direction.

We introduce the approximation of random distribution over the sites of dipoles in the two orientational states. This is equivalent to the molecular field method in magnetism or the method of Bragg and Williams in ordered alloys.²¹ Because the electrostatic interaction energy of a pair of dipoles depends on their mutual orientation, the state of a dipole on a given site will influence the probability of occurrence of the two states on neighboring sites, giving rise to "local order." Hence the mean field at a given site due to its neighbors depends on the orientational state of the dipole on the site. In the random approximation these local correlations are neglected, and the mean field is taken to be the same at all sites and is cal-

culated by assuming the same polarization for each monolayer molecule. When the water dipole is not perpendicular to the interface, there will be horizontal dipole components (parallel to the interface) in one or both of the two orientation states. However, in the absence of an external horizontal field it can be assumed that the mean horizontal dipole component at any site will be zero. In the random approximation, there is thus no resulting horizontal field, and any interaction energy due to the horizontal dipole components is neglected. In the normal direction, on the other hand, there is in general a mean external field $4\pi\sigma$ due to the charge density σ on the mercury. In addition there will be an effective "residual" electric field at the zpc, expressed in the form of residual energies E_r^{\downarrow} and E_r^{\uparrow} which will be different in the two orientational states and will contribute to the preferential orientation in the normal direction. The energies E_r^{\downarrow} and E_r^{\uparrow} describe the interaction with the interfaces of an individual water molecule in the two states. They include dipole-image terms (unequal in the two states if the magnitude of the cosine of the angle between the normal and the dipole axis is different), terms due to images of higher moments (in particular quadrupole images), hydrogen bonding with the second layer of water, as well as nonelectrostatic adsorption energies.

With the random approximation, we see from the preceding discussion that a downward polarization component $m_p + m_i$ is assumed for each site. The field acting at any site due to its neighbors must thus be proportional to $m_p + m_i$, and we can write

$$\varepsilon = 4\pi\sigma + \frac{C_e}{d^3}(m_p + m_i) \quad (2.7)$$

where ε is the total field in the upward direction at each site and C_e is an effective coordination number which we discuss below. The nature of the error arising from the random approximation becomes apparent if we observe that this approximation makes the field on a site due to its neighbors zero when $m_p + m_i = 0$, although there would in fact still be an appreciable field due to local order of the antiferroelectric type. The effect of the field on any site due to neighbors is to resist reorientation of the dipole at this site due to the external field $4\pi\sigma$. The random approximation is therefore likely to underestimate this reorientation at low σ when $|m_p + m_i|$ is small, and consequently the effective inner-layer dielectric constant will be overestimated.

It is now necessary to evaluate the coefficient C_e . If the hexagonal lattice of dipoles were situated *in vacuo* at a large distance from any dielectric interfaces, then

(20) E. J. W. Verwey, *Rec. Trav. Chim. Pays Bas.*, **61**, 127 (1942).

(21) R. H. Fowler and E. A. Guggenheim, "Statistical Thermodynamics," Cambridge University Press, Cambridge, 1949.

the field upward at a site due to each nearest neighbor would be $(m_p + m_i)/d^3$ and for nearest-neighbor interactions $C_e = 6$. However, Topping²² has shown that the electrostatic field at any site of a plane hexagonal lattice due to equal normal dipoles on all the other sites is given by putting $C_e \approx 11.0$. In our case, where the plane of lattice sites is situated between the mercury and aqueous phases, it is necessary to consider the field due not only to the dipole on a neighboring site, but also the field due to the infinite image system of this dipole in the two interfaces. These images are all parallel to the original dipole but are diminished in magnitude by multiples of $f = (\epsilon - 1)/(\epsilon + 1)$, where ϵ is the dielectric constant of bulk water. They therefore increase the field of the dipole at another site, making C_e larger than Topping's value. The coefficient C_e may be obtained from the work of Macdonald and Barlow,⁷ who find the electrostatic field due to a hexagonal array of dipoles *in vacuo*, at an arbitrary distance from the dipole plane, along the normal through a site. For simplicity, we suppose that the monolayer plane is midway between the mercury and water interfaces, at a distance $d/2$ from each. Then, retaining the first three plane arrays of images in each phase, we estimate that

$$C_e = 11.0[1 + 0.1612(1 + f) + 0.0522f + 0.0067f(1 + f) + \dots] \quad (2.8)$$

which gives $C_e = 15.2$ for $\epsilon = 78.3$ ($T = 25^\circ$).

In the random approximation the induced polarization on each site is given by

$$m_i = -\alpha\epsilon \quad (2.9)$$

where α is the (isotropic) polarizability of a water molecule. By combining (2.9) with (2.7) and making use of (2.7), we can eliminate m_i to obtain

$$\epsilon = \frac{4\pi\sigma + C_e m_p/d^3}{(1 + \alpha C_e/d^3)} = \frac{4\pi\sigma + C_e p(\lambda - \delta)/d^3}{(1 + \alpha C_e/d^3)} \quad (2.10)$$

We shall also find useful the relations

$$m_p + m_i = \frac{m_p - 4\pi\alpha\sigma}{(1 + \alpha C_e/d^3)} = \frac{p(\lambda - \delta) - 4\pi\alpha\sigma}{(1 + \alpha C_e/d^3)} \quad (2.11)$$

which follows from (2.9) and (2.10). We observe that at the zpc ($\sigma = 0$), the mean induced dipole moment is in the opposite direction to the mean "permanent" dipole moment. The denominator in (2.10) measures the extent to which the permanent moment m_p is reduced by the polarization effect at $\sigma = 0$, and may therefore be described as the "depolarizing" factor.

We shall now obtain the equilibrium values of m_p and λ in the random approximation by minimizing the free energy F per unit area of the monolayer of

interacting dipoles. The corresponding (internal) energy per unit area is

$$E = \frac{NC_e}{2d^3}(m_p + m_i)^2 + \frac{1}{2}N\alpha\epsilon^2 + 4\pi\sigma N(m_p + m_i) + N^l E_r^l + N^i E_r^i \quad (2.12)$$

The first term is the dipole-dipole (permanent plus induced) interaction energy, the second is the work of producing the induced dipoles against the internal forces within the monolayer molecules, the third is the energy of the water dipoles in the field of the mercury surface charge density σ , and the last two terms are due to the residual energies E_r^l and E_r^i . The van der Waals part of the interaction energy need not concern us if it is assumed independent of dipole orientation. Assuming random mixing of dipoles in the two states, the number g of configurations on the lattice sites, per unit area, is given by

$$\ln g = -N^l \ln(N^l/N) - N^i \ln(N^i/N) \quad (2.13)$$

The free energy per unit area of the inner region is

$$F = E - kT \ln g \quad (2.14)$$

where k is the Boltzmann constant. This must be stationary at constant σ and N , with respect to variations in N^l and N^i , or with respect to variation in λ . Writing $N^i = N - N^l$ and using (2.6) we have the equilibrium condition

$$0 = \left(\frac{\partial F}{\partial N^l}\right)_{N,\sigma} = \frac{2}{N} \left(\frac{\partial F}{\partial \lambda}\right)_{N,\sigma} = kT \ln(N^l/N^i) + 2p\epsilon + E_r^l - E_r^i \quad (2.15)$$

The right-hand number of these equations is obtained by substituting (2.13) into (2.14) and then making use of (2.9) and (2.10). An equivalent relation may be derived more directly by observing that in the upward field ϵ the energies of the dipoles in the "down" and "up" states, respectively, contain the terms $p(1 - \delta)\epsilon + E_r^l$ and $-p(1 + \delta)\epsilon + E_r^i$. Then we can write

$$\frac{N^l}{N^i} = \frac{\exp[-\{p(1 - \delta)\epsilon + E_r^l\}/kT]}{\exp[\{p(1 + \delta)\epsilon - E_r^i\}/kT]} \quad (2.16)$$

The induced polarization and van der Waals energy are assumed to be the same in the two states and therefore do not appear in relation 2.16. The condition of fully occupied states (2.4) must be regarded as equivalent to equating chemical potentials of the water molecule in the inner region and in the bulk water. Expressed differently, the condition of equal chemical potentials fixes the number N or the mean area per molecule in the inner region.

To put (2.15) or (2.16) into a more suitable form

(22) J. Topping, *Proc. Roy. Soc.*, A113, 67 (1927).

for calculation, it is convenient to define the dimensionless quantities

$$\Delta e_r = \frac{(E_r^{\downarrow} - E_r^{\uparrow})}{kT}; \quad e_w = \frac{C_e p^2}{d^3 kT} \frac{1}{(1 + \alpha C_e/d^3)} \quad (2.17)$$

These measure, in units of kT , respectively, the orientational anisotropy in the residual energy and the intensity of the dipole-dipole interactions, reduced by the depolarizing factor. We also introduce the parameter

$$\nu = 4\pi p / \{ (1 + \alpha C_e/d^3) kT \} \quad (2.18)$$

which has dimensions (surface charge density)⁻¹. Then (2.15) or (2.16) leads to

$$\ln \left(\frac{1 + \lambda}{1 - \lambda} \right) = -\Delta e_r - 2\nu\sigma + 2e_w(\delta - \lambda) \quad (2.19)$$

At the zpc, where $\sigma = 0$, we put $\lambda = \lambda_0$, given by

$$\ln \left(\frac{1 + \lambda_0}{1 - \lambda_0} \right) = -\Delta e_r + 2e_w(\delta - \lambda_0) \quad (2.19i)$$

Equation (2.19) yields σ as a function of λ . Alternatively, consider the plots of the two sides of (2.19) as functions of λ in the range $-1 < \lambda < 1$. The left-hand side is a monotonic increasing function varying from $-\infty$ to ∞ as λ increases from -1 to 1 , and passing through the origin. The right-hand side is a straight line of slope $-2e_w$, which meets the ordinate at $2e_w\delta - \Delta e_r - 2\nu\sigma$ and the λ axis is at $\lambda = \delta - (1/2\Delta e_r + \nu\sigma)/e_w$. It is seen that for each value of σ there is a unique solution for λ .

We first examine the above relations at the zpc. Choosing an area per lattice site $N^{-1} = 12.5 \text{ \AA}^2$ (so that $d = 3.80 \text{ \AA}$) and putting $p_w = 1.84 \text{ D}$, $\alpha = 1.5 \text{ \AA}^3$, $C_e = 15.2$, and $T = 25^\circ$, we have

$$1 + \alpha C_e/d^3 = 1.42; \quad e_w \sec^4 \frac{1}{2}\theta = C_e p_w^2 / \{ d^3 kT (1 + \alpha C_e/d^3) \} = 16.1$$

It is seen that e_w is likely to be large and since we can expect $|\Delta e_r|$ to be of order 1 or less, the value λ_0 satisfying (2.19) at $\sigma = 0$ will make $|\delta - \lambda_0|$ quite small. An expansion in powers of a variable proportional to $\lambda - \delta$ is indicated, and it proves convenient to define

$$S = (\lambda - \delta)/(1 - \delta^2); \quad S_0 = (\lambda_0 - \delta)/(1 - \delta^2) \quad (2.20)$$

Expansion of the left-hand side of (2.19i) in powers of S_0 yields

$$-\xi_0 = (1 + e_w')S_0 + \delta S_0^2 + \frac{1}{3}(1 + 3\delta^2)S_0^3 + \delta(1 + \delta^2)S_0^4 + \dots \quad (2.21)$$

where

$$e_w' = e_w(1 - \delta^2); \quad \xi_0 = \frac{1}{2} \left\{ \Delta e_r + \ln \left(\frac{1 + \delta}{1 - \delta} \right) \right\} \quad (2.22)$$

The series 2.21 can be inverted to yield S_0 as a power series in ξ_0 , namely

$$S_0 = S(\xi_0) = -\frac{\xi_0}{(1 + e_w')} \left[1 + \frac{\delta \xi_0}{(1 + e_w')^2} - \frac{\zeta \xi_0^2}{3(1 + e_w')^3} + \dots \right] \quad (2.23)$$

where $\zeta = 1 + 3\delta^2 - 6\delta^2/(1 + e_w')$.

In the special case of equal dipole moments in the two states, $\delta = 0$, $\xi_0 = \frac{1}{2}\Delta e_r$, $e_w' = e_w$, $S(\xi_0) = \lambda_0$, $\theta = 0$, and $\zeta = 1$. A good approximation to λ_0 is given simply by the first term in (2.23), namely $\lambda_0 = -\Delta e_r/34.2$. From (2.11), the mean dipole moment is $\lambda_0 p_w/1.42 \ll p_w$. Because of the strong dipole-dipole interactions at greater than nearest-neighbor distance and the imaging effects which produce a large value for C_e , the requirement of a minimum free energy produces a marked mutual compensation in dipole orientation so that λ_0 , and therefore the mean dipole moment per lattice site is very small. At the other extreme, if we put $\theta = 52.5^\circ$, then by (2.3) $\delta = 0.243$, $p = 0.804 p_w$ and by (2.17) $e_w = 10.4$. Choosing $\Delta e_r = 0$ for simplicity, the solution of (2.19) is found to be 0.221, making $\delta - \lambda_0 = 0.022$. In the series 2.23, $e_w' = 9.8$, $\xi_0 = \frac{1}{2} \ln [(1 + \delta)/(1 - \delta)] = 0.248$ and on using the first term only in (2.23), $\delta - \lambda_0 = -(1 - \delta^2)\xi_0/(1 + e_w') = 0.022$, accurate to at least two significant figures. Physically this small value of $\delta - \lambda_0$ means that the field due to the "permanent" polarization $-p\delta$ per site causes a preferential orientation which gives a polarization term $p\lambda_0$ largely compensating the permanent polarization. Again this is due to the strong dipole-dipole interaction.

From (2.19) it can be seen that when $\sigma \neq 0$, we need only replace ξ_0 on the left-hand side of (2.21) by

$$\xi = \frac{1}{2}\Delta e_r + \nu\sigma + \frac{1}{2} \ln \left(\frac{1 + \delta}{1 - \delta} \right) \quad (2.24)$$

and S_0 by S on the right-hand side of (2.21). Provided $\nu\sigma$ is not too large, an inversion similar to (2.23) is still possible. An alternative expansion is obtained by writing (2.19) in the form

$$\lambda = -\tanh [\frac{1}{2}\Delta e_r + \nu\sigma + e_w(\lambda - \delta)] \quad (2.25)$$

from which

$$\frac{1}{2}\Delta e_r + \nu\sigma + e_w(\lambda - \delta) = -\tanh^{-1} \lambda = -(\lambda + \frac{1}{3}\lambda^3 + \frac{1}{5}\lambda^5 + \dots) \quad (2.26)$$

Introducing

$$\eta = \frac{1}{2}\Delta e_r - \nu\sigma - \delta e_w \quad (2.27)$$

we can invert the series in (2.25) to obtain

$$\lambda = -\frac{\eta}{(1 + e_w)} \left[1 - \frac{\eta^2}{3(1 + e_w)^3} - \frac{(3e_w - 2)}{15(1 + e_w)^6} \eta^4 + \dots \right] \quad (2.28)$$

At the zpc, the first two terms on the right-hand sides of (2.23) and (2.28) give identical values for λ_0 if $\delta = 0$. If $\theta = 52.5^\circ$ and $\Delta e_r = 0$, then the first term in (2.28) gives $\lambda_0 = \delta e_w / (1 + e_w)$ so that $\delta - \lambda_0 = \delta / (1 + e_w)$, which again equals 0.022 for the particular parameter values chosen previously.

3. The Capacity of the Inner Region

We proceed to derive expressions for the capacity and effective dielectric constant of the inner region, based on the two-state orientation model described above. For this, it is necessary to consider the potential drop across the inner region, which we shall take in the sense mercury to water. We begin with the potential drop at the zpc which we denote by χ and which, by (2.11) and (2.20), can be written as

$$\chi = 4\pi N(m_p + m_i)_{\sigma=0} = \frac{4\pi N p (\lambda_0 - \delta)}{(1 + \alpha C_e / d^3)} = \frac{4\pi N p (1 - \delta^2) S_0}{(1 + \alpha C_e / d^3)} \quad (3.1)$$

If we approximate by using the first term only of the series (2.23), the last expression of (3.1) gives

$$\chi = - \frac{2\pi N p (1 - \delta^2) \left\{ \Delta e_r + \ln \left(\frac{1 + \delta}{1 - \delta} \right) \right\}}{(1 + \alpha C_e / d^3) \{ 1 + e_w (1 - \delta^2) \}} \quad (3.2i)$$

Alternatively, if the first term of (2.27) is used

$$\chi = - \frac{2\pi N p}{(1 + \alpha C_e / d^3)} \frac{(\Delta e_r + 2\delta)}{(1 + e_w)} \quad (3.2ii)$$

In the simple case of equal dipole moments in the two directions, $\theta = 0$, $\delta = 0$, the two formulas (3.2i) and (3.2ii) are identical and for the values of N , $p = p_w$, α , C_e , and d chosen in section 2, $\chi = -115\Delta e_r$ mV, which is of the right order of magnitude when $|\Delta e_r| \approx 1$. If $E_r^{\downarrow} < E_r^{\uparrow}$, then $\Delta e_r < 0$ and so we have $\chi > 0$, $\lambda_0 > 0$; there are more water dipoles in the "down" state with the positive end toward the mercury than in the "up" state, and this produces a positive potential across the inner layer. This situation can be altered if $\delta \neq 0$. Taking the case of the previous section with $\delta = 0.243$ and using (3.2i) and the corresponding first term of series 2.21, we have

$$\chi = -182(\Delta e_r + 0.496) \text{ mV} \\ \lambda_0 = \delta - 0.0436(\Delta e_r + 0.496)$$

If $-0.496 < \Delta e_r < 0$, we have $\chi < 0$ but $0.243 > \lambda_0 > 0.221$ and the dipoles are still preferentially in the "down" state. From (3.1) it can be seen that this preferential orientation still makes positive contribution to χ , but that this is now more than counteracted by the negative contribution due to the permanent upward polarization $p\delta$ per molecule, due to fact that $p^{\downarrow} > p^{\uparrow}$. Referring back to the first members of (2.5) and (2.11) we can say that $\chi < 0$ because $p^{\downarrow} N^{\downarrow} > p^{\uparrow} N^{\uparrow}$ in spite of the fact that $N^{\downarrow} < N^{\uparrow}$. Very

similar results are obtained with (3.2ii) and the first term of series 2.27.

When $\sigma \neq 0$, the potential drop V across the inner region is given by

$$V = 4\pi \{ \sigma d + (m_p + m_i) N \} = 4\pi \sigma d + 4\pi N \frac{p(\lambda - \delta) - 4\pi \alpha \sigma}{1 + \alpha C_e / d^3} \quad (3.3)$$

where we have substituted from (2.11). The inner region integral capacity $K_i(\sigma)$ and dielectric constant $\epsilon_i(\sigma)$ are defined by

$$V = \chi + \frac{\sigma}{K_i(\sigma)} = \chi + \frac{4\pi \sigma d}{\epsilon_i(\sigma)} \quad (3.4)$$

and substitution from (3.1) and (3.3) yields

$$\frac{1}{\epsilon_i(\sigma)} = 1 - \frac{4\pi \alpha N}{d(1 + \alpha C_e / d^3)} + \frac{Np}{d(1 + \alpha C_e / d^3)} \frac{(\lambda - \lambda_0)}{\sigma} \quad (3.5)$$

Because we are considering $\sigma \neq 0$, in eq 2.23 S_0 is replaced by S and ξ_0 by ξ , which we defined by (2.24). We now expand the two sides of (2.23) as power series in σ and equate coefficients of σ . If the left-hand side of (2.23) is written as

$$S = S_0 + S_0' \sigma + \frac{1}{2} S_0'' \sigma^2 + \frac{1}{6} S_0''' \sigma^3 + \dots \quad (3.6)$$

where the primes denote differentiation with respect to σ , this yields

$$S_0' = - \frac{\nu}{(1 + e_w')} \left[1 + \frac{2\delta \xi_0}{(1 + e_w')^2} - \frac{\xi \xi_0^2}{(1 + e_w')^3} + \dots \right] \quad (3.7)$$

$$S_0'' = \frac{2\nu^2}{(1 + e_w')^3} \left[-\delta + \frac{\xi \xi_0}{(1 + e_w')} + \dots \right] \quad (3.8)$$

$$S_0''' = \frac{2\nu^3 \xi}{(1 + e_w')^4} + \dots \quad (3.9)$$

Substitution of (3.6) into (3.5) yields an expansion of $1/\epsilon_i(\sigma)$ in powers of σ , namely

$$\frac{1}{\epsilon_i(\sigma)} = \frac{1}{\epsilon_i(0)} + \frac{Np(1 - \delta^2)}{2d(1 + \alpha C_e / d^3)} \times [S_0'' \sigma + \frac{1}{3} S_0''' \sigma^2 + \dots] \quad (3.10)$$

where

$$\frac{1}{\epsilon_i(0)} = 1 - \frac{4\pi N \alpha}{d(1 + \alpha C_e / d^3)} + \frac{Np(1 - \delta^2) S_0'}{d(1 + \alpha C_e / d^3)} \quad (3.11)$$

First considering the case $\delta = 0$, where $\xi_0 = 1/2$, Δe_r , $\theta = 0$, and $e_w' = e_w$, it follows from (3.11) and (3.7) that for the parameter values chosen above

$$1/\epsilon_i(0) = 0.0858 + 3.2 \times 10^{-5} (\Delta e_r)^2$$

We observe that $\epsilon_i(0)$ and hence $K_i(0) = \epsilon_i(0)/4\pi d$ are practically independent of Δe_r , unless the latter is considerably greater than 1. For $\Delta e_r = 0$, $\epsilon_i(0) = 11.8$, and we obtain the reasonable value $K_i(0) = 27.4 \mu\text{F}/\text{cm}^2$ for the integral capacity of the inner region at the zpc. Changes in d have a considerable effect upon $K_i(0)$. For example, if the area per monolayer molecule is $N^{-1} = \sqrt{3d^2/2} = 10 \text{ \AA}^2$, then $d = 3.40 \text{ \AA}$, $1 + \alpha C_e/d^3 = 1.58$, and for $\delta = 0$ ($\theta = 0$), $e_w = 20.2$, and $\Delta e_r = 0$, $\epsilon_i(0) = 13.5$, and $K_i(0) = 35.2 \mu\text{F}/\text{cm}^2$. If we consider the case $\delta = 0.243$ discussed above, then from (3.7)

$$1/\epsilon_i(0) = 0.108 - 1.3 \times 10^{-3}(\Delta e_r + 0.496)$$

As can be seen from (3.7), a first-order term in ξ_0 appears when $\delta \neq 0$ and we have retained this term, which in fact leaves $\epsilon_i(0)$ still practically independent of Δe_r unless the latter is much greater than 1. If we put $\Delta e_r + 0.496 = 0$, then $K_i(0) = 21 \mu\text{F}/\text{cm}^2$. Although changes in Δe_r make little difference to $K_i(0)$, we see that changes in δ (*i.e.*, in θ) are more significant.

We have already mentioned the apparent contradiction between a maximum in the capacity of the inner region at positive σ and the hypothesis of a residual orientation at the zpc of water dipoles with positive end away from the mercury (*i.e.*, with downward polarization and hence the potential χ negative). We shall now show that by choosing $\delta \neq 0$, and small negative Δe_r , the occurrence of a maximum in $K_i(\sigma)$ at positive σ is compatible with a negative value for χ at the zpc. From (3.4) and (3.5)

$$\frac{d}{d\sigma} \left(\frac{1}{\epsilon_i(\sigma)} \right) = \frac{1}{4\pi d} \frac{d}{d\sigma} \left(\frac{1}{K_i(\sigma)} \right) = \frac{Np}{d(1 + \alpha C_e/d^3)\sigma} \left(\frac{d\lambda}{d\sigma} - \frac{\lambda - \lambda_0}{\sigma} \right) \quad (3.12)$$

Making use of the fundamental equilibrium relation in the form (2.19), the condition for the occurrence of a stationary point in $K_i(\sigma)$ at $\sigma = \sigma_1$ where $\lambda = \lambda_1$ say is

$$0 = \frac{\sigma_1}{(\lambda - \lambda_1)} - \left(\frac{d\sigma}{d\lambda} \right)_1 = \frac{1}{2\nu} \left[\frac{2}{(1 - \lambda_1^2)} - \frac{1}{(\lambda_0 - \lambda_1)} \ln \left\{ \frac{(1 + \lambda_0)(1 - \lambda_1)}{(1 - \lambda_0)(1 + \lambda_1)} \right\} \right]$$

which can be expressed as

$$0 = \frac{1}{\nu} \left[\frac{1}{(1 - \lambda_1^2)} - \frac{1}{(\lambda_0 - \lambda_1)} \int_{\lambda_1}^{\lambda_0} \frac{d\lambda}{(1 - \lambda^2)} \right] = f(\lambda_1, \lambda_0) \quad (3.13)$$

When $0 < \lambda_0 < \lambda_1 < 1$ or $-1 < \lambda_1 < -\lambda_0 < 0$, then $(1 - \lambda_1^2)^{-1}$ is the largest value of the integrand in (3.13) and so $f(\lambda_1, \lambda_0) > 0$. On the other hand, when $0 < \lambda_1 < \lambda_0$, then $(1 - \lambda_1^2)^{-1}$ is the smallest value of the integrand and $f(\lambda_1, \lambda_0) < 0$. Hence, there must be a

zero of $f(\lambda_1, \lambda_0)$ in the range $(-\lambda_0, 0)$ for λ_1 , and it is not difficult to show that the right-hand side of (3.12) changes from negative to positive at this point so that it represents a minimum in $1/\epsilon_i(\sigma)$ and a maximum in $\epsilon_i(\sigma)$ and $K_i(\sigma)$. Near $\sigma = 0$ it can be seen from (3.10) that $d(1/\epsilon_i(\sigma))/d\sigma$ remains negative.

To obtain an estimate of λ_1 for a given value of λ_0 we expand $f(\lambda_1, \lambda_0)$ in series and (3.13) is then equivalent to

$$0 = \sum_{n=1}^{\infty} \left[\lambda_1^{2n} - \frac{(\lambda_0^{2n+1} - \lambda_1^{2n+1})}{(2n+1)(\lambda_0 - \lambda_1)} \right] = \frac{1}{3}(2\lambda_1^2 - \lambda_1\lambda_0 - \lambda_0^2) + \frac{1}{5}(4\lambda_1^4 - \lambda_1^3\lambda_0 - \lambda_1^2\lambda_0^2 - \lambda_1\lambda_0^3 - \lambda_0^4) + \dots \quad (3.14)$$

If λ_0 is small compared with 1, the value $\lambda_1 = -1/2\lambda_0$, obtained from the terms of degree 2, is a good approximation. For $\delta = 0.243$ and $\Delta e_r = 0$ we have found $\lambda_0 = 0.221$, making $\lambda_1 = -0.111$. It can be shown that in this case the correction due to terms of degree 4 in (3.14) is less than 0.001. The charge density $\sigma = \sigma_1$ at which the maximum in K_i occurs can then be obtained from (2.19) which, with $\Delta e_r = 0$ and $\lambda = \lambda_1$, gives $\nu\sigma_1 = 3.80$. From (2.18) and the assumed values of the parameters, $\nu^{-1} = 0.246 \times 10^4 \text{ esu}/\text{cm}^2$, so that $\sigma_1 = 0.935 \times 10^4 \text{ esu}/\text{cm}^2 = 3.12 \mu\text{C}/\text{cm}^2$. It can be seen from the above analysis that the combination $\chi < 0$, $\sigma_1 < 0$ can only be obtained if $\delta \neq 0$. If $\delta = 0$, then by (3.1) $\chi < 0$ only if $\lambda_0 < 0$. Then $\lambda_1 \approx -1/2\lambda_0 > 0$ and since σ is a decreasing function of λ , this implies $\sigma_1 < 0$.

From (3.3), the differential capacity of the inner region is given by

$$\frac{1}{C_i(\sigma)} = \frac{dV}{d\sigma} = 4\pi d \left[1 - \frac{4\pi N\alpha}{d(1 + \alpha C_e/d^3)} \right] + \frac{4\pi Np}{(1 + \alpha C_e/d^3)} \frac{d\lambda}{d\sigma} \quad (3.15)$$

where by (2.19)

$$\frac{d\lambda}{d\sigma} = - \frac{\nu(1 - \lambda^2)}{1 + (1 - \lambda^2)e_w} \quad (3.16)$$

From (3.4), (3.5), (3.15), and (3.16), it is easily seen that $C_i(0) = K_i(0)$.

Because the temperature coefficient of capacity is a sensitive test of any theory of the inner region, an examination of $(\partial K_i/\partial T)_\sigma$ and $(\partial C_i/\partial T)_\sigma$ is of considerable interest. It will be assumed that the asymmetry parameter δ , the thickness d , and the density of molecules N are all independent of temperature T . Noting that Δe_r , e_w , and ν are all proportional to T^{-1} , we derive from (2.19)–(2.19i)

$$\left[\frac{\partial(\lambda - \lambda_0)}{\partial T} \right]_\sigma = - \frac{1}{2T} \left[\frac{(1 - \lambda^2)}{\{1 + (1 - \lambda^2)e_w\}} \times \ln \left(\frac{1 + \lambda}{1 - \lambda} \right) - \frac{(1 - \lambda_0^2)}{\{1 + (1 - \lambda_0^2)e_w\}} \ln \left(\frac{1 + \lambda_0}{1 - \lambda_0} \right) \right] \quad (3.17)$$

Then, by (3.4)–(3.5)

$$\left(\frac{\partial K_i}{\partial T}\right)_\sigma = -\frac{Np\epsilon_i^2(\sigma)}{4\pi d^2(1 + \alpha C_e/d^3)\sigma} \left[\frac{\partial(\lambda - \lambda_0)}{\partial T}\right]_\sigma \quad (3.18)$$

We wish to investigate whether the maximum in the magnitude of the temperature coefficient (3.18) occurs at positive or negative σ . Equations 2.19–2.19i provide an expansion for λ in powers of σ , equivalent to (2.28), namely

$$\lambda = \lambda_0 - \frac{\nu(1 - \lambda_0^2)\sigma}{\{1 + (1 - \lambda_0^2)e_w\}} - \frac{\nu^2\lambda_0(1 - \lambda_0^2)\sigma^2}{\{1 + (1 - \lambda_0^2)e_w\}^3} + \dots \quad (3.19)$$

Making use of (3.17) and (3.19) and introducing

$$g(\lambda_0) = 1 - \frac{\lambda_0}{\{1 + (1 - \lambda_0^2)e_w\}} \ln\left(\frac{1 + \lambda_0}{1 - \lambda_0}\right) \quad (3.20)$$

we can write (3.18) at $\sigma = 0$ as

$$\left(\frac{\partial K_i}{\partial T}\right)_{\sigma=0} = -\frac{Np\nu\epsilon_i^2(0)(1 - \lambda_0^2)g(\lambda_0)}{4\pi d^2T(1 + \alpha C_e/d^3)\{1 + (1 - \lambda_0^2)e_w\}^2} \quad (3.21)$$

which is negative. Provided $|(\partial K_i/\partial T)_\sigma|$ has a single maximum near $\sigma = 0$, we can expect this to occur at $\sigma \geq 0$, according as the slope $(\partial^2 K_i/\partial\sigma\partial T)_{\sigma=0} \leq 0$.

We find that this slope is proportional to $a_1 + a_2 + a_3$, where

$$a_1 = -\frac{4Np\nu\epsilon_i(0)(1 - \lambda_0^2)g(\lambda_0)}{d\{1 + \alpha C_e/d^3\}\{1 + (1 - \lambda_0^2)e_w\}} \quad (3.22)$$

$$a_2 = 2\lambda_0\{1 - \lambda_0^2\}e_w - 2$$

$$a_3 = -\frac{1}{\lambda_0}\{1 - g(\lambda_0)\} \times [1 - 3\lambda_0^2 + e_w(1 - \lambda_0^2)(1 + 3\lambda_0^2)]$$

From (3.15), the temperature coefficient of $C_i(\sigma)$ is

$$\left(\frac{\partial C_i}{\partial T}\right)_{\sigma=0} = -\frac{4\pi Np\nu C_i^2(\sigma)(1 - \lambda^2)g(\lambda)}{(1 + \alpha C_e/d^3)T\{1 + (1 - \lambda^2)e_w\}^2} \quad (3.23)$$

which again is negative at $\sigma = 0$. The slope $(\partial^2 C_i/\partial\sigma\partial T)_{\sigma=0}$ is also proportional to $a_1 + a_2 + a_3$.

4. Numerical Results and Discussion

Figures 1–4 show plots of the integral and differential capacities $K_i(\sigma)$ and $C_i(\sigma)$ and also of the temperature coefficients $(\partial K_i/\partial T)_\sigma$ and $(\partial C_i/\partial T)_\sigma$ over a range of σ from -20 to $+20 \mu\text{C}/\text{cm}^2$. We have assumed two fixed surface densities of dipoles, corresponding to areas of 10 and 12.5 \AA^2 per water molecule. In Figures 1 and 2, $\theta = 0$, $p^i = p_i = p_w = 1.84 \text{ D}$

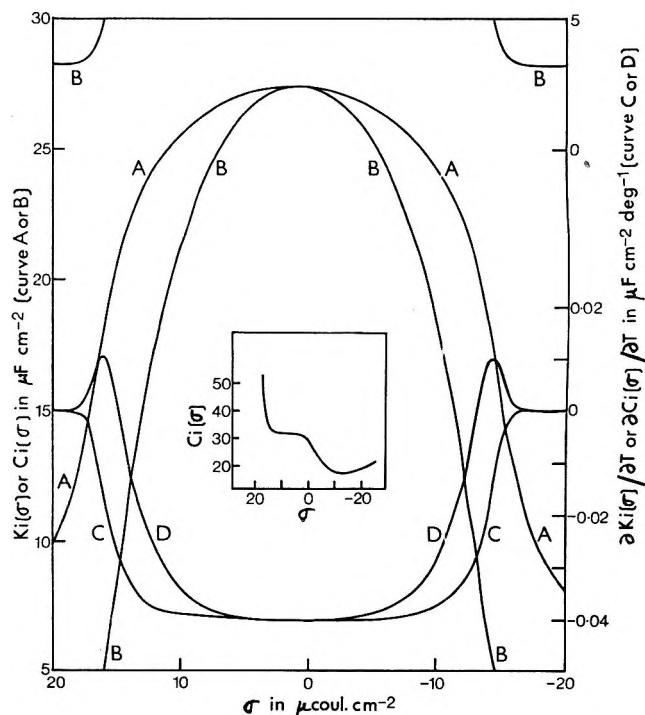


Figure 1. Plots of integral and differential capacities of the inner region and of their temperature coefficients as functions of surface charge density, for $p^i = p^l = p_w$, $\Delta\epsilon_r = -2$, and $N^{-1} = 12.5 \text{ \AA}^2$. Curve A, $K_i(\sigma)$ vs. σ ; curve B, $C_i(\sigma)$ vs. σ . Continuations of curve B at capacities $< 5 \mu\text{F cm}^{-2}$ are shown in upper right-hand and left-hand corners. Curve C, $(\partial K_i/\partial T)_\sigma$ vs. σ ; curve D, $(\partial C_i/\partial T)_\sigma$ vs. σ . Inset: experimental $C_i(\sigma)$ vs. σ , from Delahay.²³

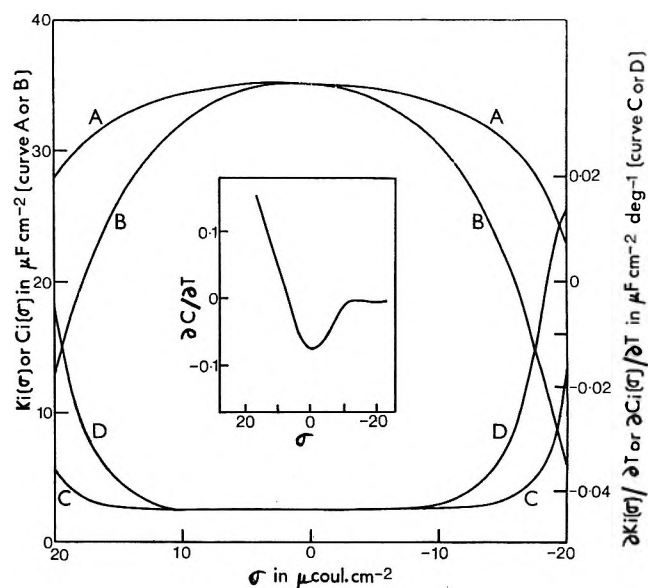


Figure 2. Plots similar to those in Figure 1, for $p^i = p^l = p_w$, $\Delta\epsilon_r = -2$, and $N^{-1} = 10 \text{ \AA}^2$. Inset: experimental $(\partial C/\partial T)_\sigma$ vs. σ , where C is the differential capacity of the whole double layer, from Hills and Payne.¹⁶

and $\Delta\epsilon_r = -2$. In Figures 3 and 4, $\theta = 52.5^\circ$, $p^i = p_w$, $p^l = p_w \cos 53.5^\circ = 0.804p_w$ and $\Delta\epsilon_r = -0.4$. Other relevant parameters are $T = 25^\circ$, $\epsilon = 78.3$,

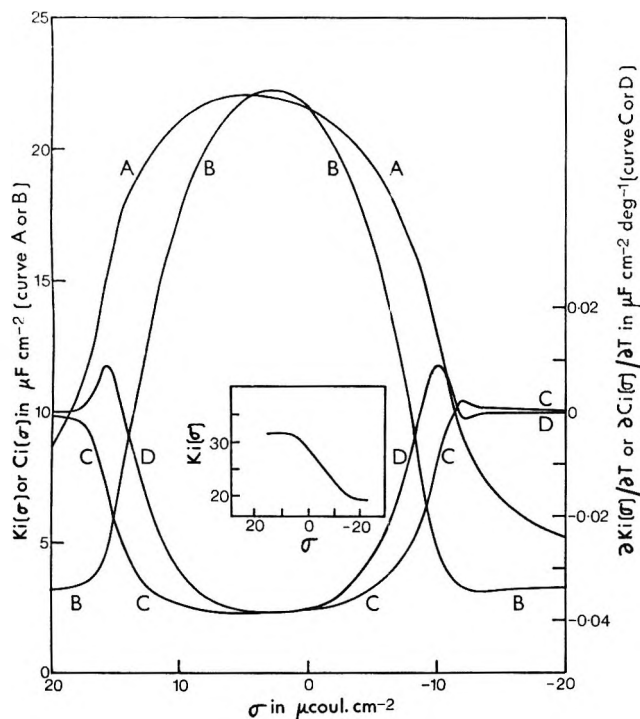


Figure 3. Plots similar to those in Figure 1 for $p^1 = p_w$, $p^1 = 0.804p_w$, $\Delta e_r = -0.4$, and $N^{-1} = 12.5 \text{ \AA}^2$. Inset: experimental $K_i(\sigma)$ vs. σ from Hills and Payne.¹⁶

$\alpha = 1.5 \text{ \AA}^3$, and $C_e = 15.2$. In the figure insets 1a-4a, corresponding experimental plots are shown for the system mercury-NaF aqueous solution at 25° . Figure 1a is taken from Delahay,²³ who calculated the curve from data by Grahame¹¹ for 0.916 M NaF , and Figures 2a-4a, which pertain to 0.1 M NaF , are taken from Hills and Payne.¹⁶ The latter authors determine the temperature coefficients of the integral and differential capacities of the whole double layer, so that the curves in Figures 2a and 4a are not strictly comparable with our corresponding theoretical plots. Further numerical results, in particular the positions of the maxima in $K_i(\sigma)$ and $C_i(\sigma)$ and also in $|\partial K_i/\partial T|$ and $|\partial C_i/\partial T|$, are presented in Tables I-III. These are calculated not only for the cases plotted in Figures 1-4, but also for other values of Δe_r and N .

Our theoretical results for $K_i(\sigma)$ and $C_i(\sigma)$ show the same general trend as the experimental data for negatively charged surfaces, except for the observed increase in $C_i(\sigma)$ at large negative σ . A certain degree of asymmetry with respect to the sign of the charge density σ is achieved by choosing either $E_r^1 \neq E_r^2$ or $p^1 \neq p^2$. If $E_r^1 > E_r^2$ or $p^1 > p^2$, then the inner region capacities $K_i(\sigma)$ and $C_i(\sigma)$ tend to be larger on the positive side of σ , where they also show maxima. The difference between positive and negative σ of course increases with $E_r^1 - E_r^2$. However, if the density of water molecules in the inner region is assumed to be constant, then our theory does not predict the experimental observations that the inner

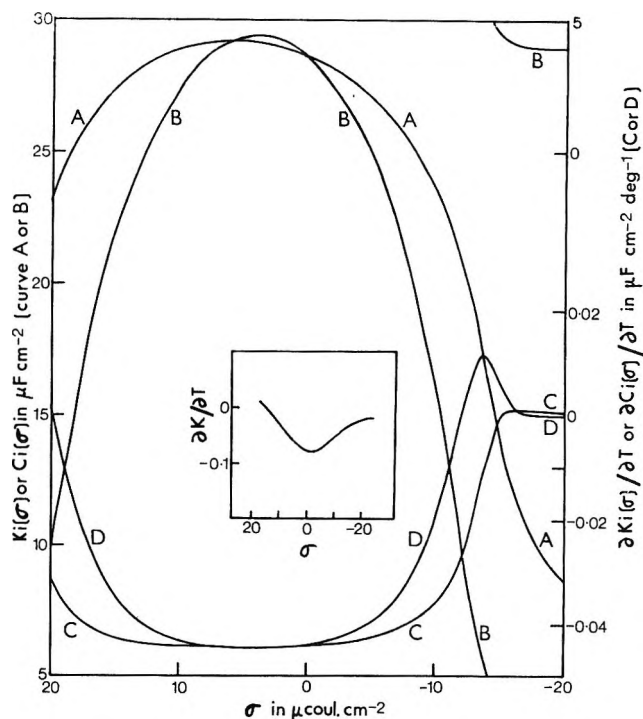


Figure 4. Plots similar to those in Figure 3 for $p^1 = p_w$, $p^1 = 0.804p_w$, $\Delta e_r = -0.4$, and $N^{-1} = 10 \text{ \AA}^2$. Continuation of curve B at capacities $< 5 \mu\text{F cm}^{-2}$ is shown in upper right-hand corner. Inset: experimental $(\partial K/\partial T)_\sigma$ vs. σ , where K is the integral capacity of the whole double layer, from Hills and Payne.¹⁶

region remains approximately constant or even increases as the surface charge becomes highly positive. From a comparison at different N of our plots, or of our results in the tables, it is seen that such a behavior can be obtained if we permit N to increase with σ . For example, in the particular examples of Table III, a variation in N^{-1} from 12.5 to 10 \AA^2 as σ changes from 0 to $20 \mu\text{C/cm}^2$ would cause $K_i(\sigma)$ to alter from 21.6 to $23.2 \mu\text{F/cm}^2$, although $C_i(\sigma)$ drops from 21.6 to $9.9 \mu\text{F/cm}^2$. However, $C_i(\sigma)$ shows such a strong dependence on N at $\sigma = 20 \mu\text{C/cm}^2$ that a change in N^{-1} from 12.5 to 8.33 \AA^2 (a 50% increase in N) causes $C_i(\sigma)$ to increase from 21.6 to $27.1 \mu\text{F/cm}^2$ in the range 0 - $20 \mu\text{C/cm}^2$ for σ . Unless some process of ion adsorption is operating it is difficult to understand the observed steep rise in $C_i(\sigma)$ at large σ which is shown in Figure 1a. Consequently, in the opinion of the authors, any such marked rise in $C_i(\sigma)$ with σ should be ruled out in a theory of the inner region in the absence of adsorbed ions. It would appear that the suggestion by Hills and Payne that N varies with σ has some merit, although the present calculations and our discussion in the Introduction indicate that they have overestimated the magnitude of this variation in N . A theoretical relation between N and

(23) P. Delahay, "Double Layer and Electrode Kinetics," Interscience Publishers, New York, N. Y., 1965.

Table I: Characteristics of Capacity-Surface Charge Plots ($T = 25^\circ$; $\epsilon = 78.3$; $N^{-1} = 10 \text{ \AA}^2$; $d = 3.04 \text{ \AA}$; $p^l = p^l = p_w = 1.84 \text{ D}$; $K_i = K_i(\sigma)$ and $C_i = C_i(\sigma)$ in $\mu\text{F}/\text{cm}^2$; $(\partial K_i/\partial T)_\sigma$ and $(\partial C_i/\partial T)_\sigma$ in $\mu\text{F}/\text{cm}^2 \text{ deg}$; χ in mV; σ in $\mu\text{C}/\text{cm}^2$)At Maximum Capacity $K_i \approx C_i = 35.2$; $\epsilon_i \approx 13.5$, All Δe_r

Δe_r	K_i σ at max	C_i σ at max	$\sigma = 20$			$\sigma = -20$			χ	$\sigma = 0$	
			K_i	C_i	ϵ_i	K_i	C_i	ϵ_i		$K_i = C_i$	ϵ_i
0	0	0	25.8	9.9	9.2	25.8	9.2	9.9	0	35.2	13.5
-0.4	0.3	≈ 0.2	26.3	10.1	9.9	25.3	8.5	9.7	41	35.2	13.5
-2	1.4	1.0	28.0	12.8	10.7	22.9	6.1	8.8	207	35.2	13.5
-4	2.8	1.9	29.5	16.2	11.3	19.4	4.5	7.5	415	35.1	13.5
-6	4.2	2.8	30.7	19.2	11.8	16.3	4.1	6.3	622	34.9	13.4

Maximum in Temperature Coefficients of Capacity at $-0.0436 \mu\text{F}/\text{cm}^2 \text{ deg}$; Minimum at -0.0434 , All Δe_r

Δe_r	$ (\partial K_i/\partial T)_\sigma $			$ (\partial C_i/\partial T)_\sigma $			Expressions 3.23			sum
	σ at max	σ at min	σ at max	σ at max	σ at min	σ at max	a_1	a_2	a_3	
0	9	0	-9	6	0	-6	0	0	0	0
-0.4	10	0.2	-9	7	0.3	-6	-0.3	0.3	-0.02	0.03
-2	10	1	-8	7	1	-6	-1.5	1.7	-0.1	0.15
-4	11	2	-7	8	2	-5	-2.9	3.4	-0.2	0.27
-6	13	3	-6	9	3	-4	-4.4	5.0	-0.4	0.36

Table II: Characteristics of Capacity-Surface Charge Plots ($N^{-1} = 12.5 \text{ \AA}^2$; $d = 3.80 \text{ \AA}$. Other Parameters and Units as in Table I)At Maximum Capacity $K_i \approx C_i \approx 27.4$; $\epsilon_i \approx 11.8$, All Δe_r ; At $\sigma = \pm 20$, $C_i \approx 3.2$, All Δe_r

Δe_r	K_i σ at max	C_i σ at max	$\sigma = 20$		$\sigma = -20$		χ	$\sigma = 0$	
			K_i	ϵ_i	K_i	ϵ_i		$K_i = C_i$	ϵ_i
0	0	0	8.8	3.8	8.8	3.8	0	27.4	11.8
-0.4	0.3	≈ 0.2	9.0	3.9	8.7	3.7	46	27.4	11.8
-2	1.3	0.8	9.8	4.2	8.0	3.4	229	27.4	11.8
-4	2.4	1.7	11.1	4.8	7.3	3.2	458	27.3	11.7
-6	3.7	2.5	12.7	5.4	6.8	2.9	687	27.1	11.6

Maximum in Temperature Coefficients of Capacity

 $|(\partial K_i/\partial T)_\sigma|, |(\partial C_i/\partial T)_\sigma| = 0.0403$, All Δe_r

Δe_r	$ (\partial K_i/\partial T)_\sigma $		$ (\partial C_i/\partial T)_\sigma $		Expressions 3.23			Sum
	σ at max	σ at min	σ at max	σ at min	a_1	a_2	a_3	
0	0	0	0	0	0	0	0	0
-0.04	0.8	0.2	0.3	0.3	-0.4	0.3	-0.02	-0.04
-2	1.3	0.8	0.8	0.8	-1.7	1.6	-0.1	-0.22
-4	2.5	1.7	1.7	1.7	-3.4	3.2	-0.2	-0.47
-6	3.8	2.5	2.5	2.5	-5.1	4.8	-0.4	-0.76

Table III: Characteristics of Capacity-Surface Charge Plots ($p^l = p_w = 1.84 \text{ D}$; $p^l = p_w \cos 52.5^\circ = 0.804 p_w$; $\Delta e_r = -0.4$. T , ϵ and Units as in Table I)

N^{-1} , \AA^2	d , \AA	Maximum in K_i			Maximum in C_i			$\sigma = 20$			$\sigma = -20$			χ
		K_i	σ	ϵ_i	C_i	σ	ϵ_i	K_i	C_i	ϵ_i	K_i	C_i	ϵ_i	
8.3	3.10	36.1	8	12.7	36.3	5	12.6	34.0	27.1	11.9	16.3	4.8	5.7	-11
10.0	3.40	29.2	6	11.2	29.4	4	11.2	23.2	9.9	8.9	8.7	4.0	3.3	-12
12.5	3.80	22.2	4	9.5	22.3	3	9.5	8.8	3.2	3.8	5.3	3.2	2.3	-13

N^{-1} , \AA^2	d , \AA	$\sigma = 0$		Maximum in $ (\partial K_i/\partial T)_\sigma $		Maximum in $ (\partial C_i/\partial T)_\sigma $		Expressions 3.23			Sum
		$C_i = K_i$	ϵ_i	$(\partial K_i/\partial T)_\sigma$	σ	$(\partial C_i/\partial T)_\sigma$	σ	a_1	a_2	a_3	
8.3	3.10	35.5	12.4	-0.0482	8	-0.0482	5	-6.0	6.0	-0.6	-0.6
10.0	3.40	28.7	11.0	-0.0445	6	-0.0446	4	-5.9	4.9	-0.6	-1.5
12.5	3.80	21.6	9.3	-0.0384	4	-0.0386	3	-5.4	3.7	-0.6	-2.2

σ would require the adsorption isotherm for the water molecules in the inner region, a problem considerably more difficult than that considered in this paper. As already discussed briefly in the Introduction, this would involve, for example, some model of the second and higher layers of water molecules at the interface.

In the present simplified model, we have equated the inner region thickness d_i to the nearest-neighbor lateral separation d between the water dipoles. Consequently, d_i is proportional to $N^{-1/2}$; *i.e.*, d_i decreases as the density N increases, whereas Hills and Payne suggest the opposite behavior. Our expression (3.3) for the potential drop V across the inner region, and therefore the integral and differential capacities $K_i(\sigma)$ and $C_i(\sigma)$, depend on d_i through the electrostatic imaging, *i.e.*, through the effective coordination number C_e . If now d_i does not decrease as rapidly as $N^{-1/2}$, or if it even increases with N , then C_e will decrease as N increases, although for a hexagonal lattice C_e cannot be less than 11.0. A smaller C_e implies a larger mean dipole moment per lattice site. We may expect V , and hence $K_i(\sigma)$, to decrease less rapidly as N increases, for a decreasing C_e than for a fixed C_e . However, if we bear in mind that a changing N will also affect the residual energies E_r^+ and E_r^- , there seems little point in examining more closely the effect of a varying C_e with the present model of the inner region. It should be stressed that our theory gives directly the integral capacity $K_i(\sigma)$ in terms of a molecular model and that we *define* the dielectric constant $\epsilon_i(\sigma)$ as $4\pi d_i K_i(\sigma)$. Furthermore, because C_e must exceed 11.0, a change in the thickness of the inner region should not alter greatly the value of $K_i(\sigma)$.

Our calculated temperature coefficients show much too broad a maximum in their magnitudes. Indeed, as illustrated in Table I, at $N^{-1} = 10 \text{ \AA}^2$ we find two maxima, one at positive, the other at negative σ , with a very shallow intervening minimum. For the smaller surface density $N^{-1} = 12.5 \text{ \AA}^2$ both the capacities and their temperature coefficients have their maxima at positive σ and at the zpc, χ is correspondingly positive, indicating a net orientation of water dipoles toward the mercury. We have already explained that by choosing $p^+ \neq p^-$ it is possible for the maxima in $K_i(\sigma)$ and $C_i(\sigma)$ to occur at positive σ and nevertheless for $\chi < 0$ at the zpc. In the example of Table III,

where this is illustrated, we observe that the maxima in the capacity temperature coefficients also occur at positive σ . One strong piece of evidence that $\chi < 0$, however, is that these temperature coefficients have their maxima at negative σ , as suggested by the plots in Figures 2a and 4a. A study of the three terms a_1 , a_2 , and a_3 in the tables shows that a_1 and a_2 are of the same order but opposite in sign and also are much larger than a_3 . This suggests that a small alteration in the model of the inner region may change the sign of their sum, thereby shifting the maximum in the temperature coefficient of the capacity from positive to negative σ . As expected, our calculations are less successful with the temperature coefficients of the capacities than with the capacities themselves. It appears that we require a more elaborate treatment to reproduce the experimental variation of these coefficients with surface charge σ .

The theory of a monolayer of oriented dipoles developed in this paper can be adapted to polar solvents other than water. Each solvent will probably have a characteristic distribution of dipole orientations, depending on its molecular structure. It is possible that our theory will be more suitable to high dielectric constant aprotic solvents in which the hydrogen bonding is absent. For a number of polar nonaqueous solvents,²⁴⁻³⁰ experimental studies of the double-layer capacities as functions of potential have revealed characteristic humps away from the zpc. Maxima in the inner-layer capacity have been calculated on the anodic side of the zpc in the cases of dimethyl sulfoxide²⁷ and sulfolane²⁸ and on the cathodic side in the case of formamide.^{26,28} Inner-layer properties of the other solvents remain to be investigated in more detail.

(24) S. Minc, J. Jastrzebska, and M. Brzostowska, *J. Electrochem. Soc.*, **108**, 1161 (1961).

(25) B. B. Damaskin and Yu. M. Povarov, *Dokl. Akad. Nauk SSSR*; **140**, 394 (1961).

(26) R. Payne, *J. Chem. Phys.*, **42**, 3371 (1965).

(27) R. Payne, *J. Amer. Chem. Soc.*, **89**, 489 (1967).

(28) E. Dutkiewicz and R. Parsons, *J. Electroanal. Chem.*, **11**, 196 (1966).

(29) R. Payne, *J. Phys. Chem.*, **71**, 1548 (1967).

(30) J. Lawrence and R. Parsons, *Trans. Faraday Soc.*, **64**, 751 (1968).

Studies of the Double Layer at Oxide-Solution Interface

by Syed M. Ahmed

*Mineral Sciences Division, Mines Branch, Department of Energy, Mines and Resources, Ottawa, Canada
(Received January 28, 1969)*

Data have been obtained on the following double-layer characteristics of Al_2O_3 , ZrO_2 , and ThO_2 by measuring the equilibrium distribution of the potential-determining ions (H^+ , OH^-) at the oxide-solution interface as a function of pH, and of the ionic strength of the solution: (a) the zero point of charge, (b) the surface-charge densities, q^\pm , of Al_2O_3 in KNO_3 , KCl , and NaClO_4 solutions and q^+ of ZrO_2 and ThO_2 in KCl and NaClO_4 solutions, (c) the differential capacity of the double layer on Al_2O_3 , and (d) the change in the interfacial energy resulting from ionic adsorption. Results of the present work and of the previous work on other oxides (SiO_2 , ZrO_2 , ThO_2 , Fe_2O_3 , Fe_3O_4 , SnO_2 , and TiO_2) have been correlated to elucidate the general mechanisms of surface-charge formation and of ionic adsorption on oxides. The anions or cations may be specifically adsorbed on oxides through a basic or an acidic dissociation of the surface hydroxyl groups, respectively. An isotherm has been derived for the specific adsorption of K^+ on the cathodic surfaces of oxides and the $\Delta G^\circ_{\text{K}^+}$ has been calculated from this isotherm for different oxides. The variation of $\Delta G^\circ_{\text{K}^+}$ with pH, with a_{KNO_3} , and with surface coverage and also the relationship of $\Delta G^\circ_{\text{K}^+}$ with the ζ potentials of oxides has been discussed.

Introduction

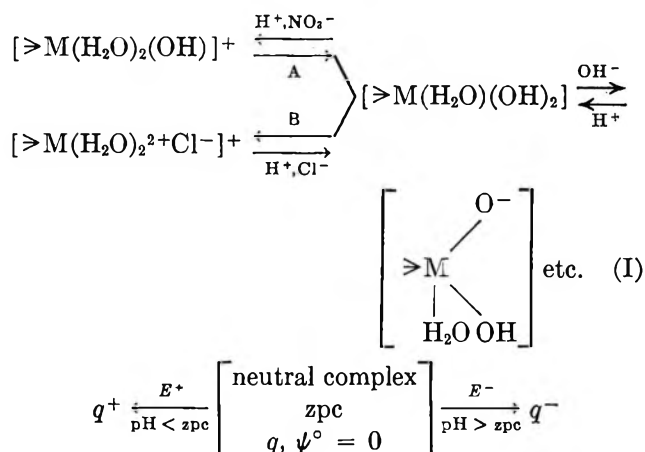
A number of studies have been made of the double layer on oxides¹⁻⁵ by measuring the equilibrium distribution of the potential-determining ions (H^+ , OH^-) at the oxide-solution interface, as a function of their electrochemical potential (pH) and of the ionic strength of the solution. This paper reports studies of the double layer on Al_2O_3 , ZrO_2 , and ThO_2 . These studies are a continuation of previous work on a series of oxides (SiO_2 , ZrO_2 , ThO_2 ,³ Fe_2O_3 , Fe_3O_4 ,⁶ SnO_2 , and TiO_2)⁷ reported earlier from this laboratory. The general properties of the oxide-solution interface have also been examined in this paper by correlating the results obtained on the above series of oxides.^{3,6,7} An attempt is also made to obtain the charge densities and the standard free energies, for the specific adsorption of K^+ on some of the above oxides.

The present work on oxides is based on the same well-established principles as those employed for studying the AgI ⁸⁻¹⁰ and the Ag_2S ^{11,12} systems. However, as the oxide-solution system is much more complex than the AgI and the Ag_2S systems, modified experimental techniques have had to be used in the present work. Hence the theory and assumptions involved in this work with oxides will be outlined first.

Theory

The occurrence of neutral and charged (\pm) surfaces at the oxide-solution interface has been attributed^{6,7} to the formation of metal aquo complexes, as shown schematically in (I).

The negative surface charge originates from acidic dissociation of the surface hydroxyl groups (at $\text{pH} > \text{zpc}$) and increases with increasing pH and also with increasing cation concentration. The cations (K^+ , in the present work) may be adsorbed on the oxide layer



either in a hydrated form or in a form dehydrated in the direction normal to the surface. The adsorption of K^+ in the dehydrated form on oxides is comparable to the well-known specific adsorption described in double-layer theories.¹³⁻¹⁵

- (1) G. A. Parks and P. L. De Bruyn, *J. Phys. Chem.*, **66**, 967 (1962)
- (2) J. Lyklema, *J. Electroanal. Chem.*, **18**, 341 (1968).
- (3) S. M. Ahmed, *Can. J. Chem.*, **44**, 1663, 2769 (1966).
- (4) G. Y. Onoda, Jr., and P. L. De Bruyn, *Surface Sci.*, **4**, 48 (1966).
- (5) S. M. Ahmed and D. Maksimov, Mines Branch, Research Report R 196, Department of Energy, Mines and Resources, Ottawa, 1968.
- (6) S. M. Ahmed and D. Maksimov, *Can. J. Chem.*, **46**, 3841 (1968).
- (7) S. M. Ahmed and D. Maksimov, *J. Colloid Interfac. Sci.*, **29**, 97 (1969).
- (8) E. L. Mackor, *Rec. Trav. Chim.*, **70**, 663, 747, 763 (1951).
- (9) J. Lyklema and J. Th. G. Overbeek, *J. Colloid Sci.*, **16**, 595 (1961).
- (10) B. H. Bijsterbosch and J. Lyklema, *ibid.*, **20**, 665 (1965).
- (11) W. L. Freyberger and P. L. De Bruyn, *J. Phys. Chem.*, **61**, 586 (1957).
- (12) I. Iwasaki and P. L. De Bruyn, *ibid.*, **62**, 594 (1958).
- (13) D. C. Grahame, *Chem. Rev.*, **41**, 441 (1947).
- (14) P. Delahay, "Double Layer and Electrode Kinetics," Interscience Publishers, Inc., New York, N. Y., 1965, pp 17-80.

The behavior of oxide surfaces on the anodic side of the zpc is best explained on the basis of proton addition to the neutral aquo complex, together with or without the replacement of the surface hydroxyl groups by the anions present. Thus in mechanism A, the anions do not replace the surface hydroxyl groups and stay as counterions outside the primary hydration shell of the surface. The oxide electrode^{16,17} is then reversible to H^+ and the positive-surface-charge densities (q^+) depend primarily on a_{H^+} and not on the anion concentration as such. However, on increasing the anion concentration, at a given pH, any increase in q^+ will be determined solely by the effect of the increased ionic strength on the structure of the diffuse double layer, and on a_{H^+} itself. From the theory of the diffuse double layer,¹³⁻¹⁵ the increase in q^+ values on increasing the ionic strength of the solution from 0.001 *M* to 1 *M* of a 1:1 salt is only 1-2 $\mu\text{C}/\text{cm}^2$ for a double-layer potential of about 100 mV.¹⁸ As this variation in q^+ is within the present experimental error ($\pm 1 \mu\text{C}$), the q^+ values will depend solely on a_{H^+} .

In mechanism B, in addition to the chemisorption of H^+ on the neutral, aquo complex, the anions replace the surface hydroxyl groups through a basic dissociation and are themselves chemisorbed on the metal atoms of the surface. This process, in the acid-base titrations (see Experimental Section), would liberate more OH^- from the surface and result in higher (apparent) q^+ values in comparison to those in mechanism A. These apparent q^+ values depend not only on a_{H^+} but also markedly on the anion concentration. The above behavior appears to be characteristic of all the transition metal oxides. For other oxides, such as quartz,³ neither the complex formation with H^+ nor the basic dissociation of the surface hydroxyl groups may occur. Hence, no excess of positive surface charge would result on such oxides. All the above possibilities have been encountered in the series of oxides investigated in this work.

Thermodynamics

If the surface structure at the zpc is taken as the reference plane, then $(\Gamma_{H^+} - \Gamma_{\text{OH}^-})_{zpc} = 0$, where Γ_{H^+} or Γ_{OH^-} is the surface excess, in mol/cm², of the potential-determining ion adsorbed on the surface. At any other pH the effective or excess surface charge is

$$q^\pm = F(\Gamma_{H^+} - \Gamma_{\text{OH}^-}) \quad (1)$$

Thus q is positive or negative depending on whether $\Gamma_{H^+} >$ or $<$ Γ_{OH^-} . At a given pH, the potential, E , of the double layer on oxides relative to the zpc (the reference plane) is calculated from the Nernst equation

$$E = -0.059(\text{pH} - \text{pH}_{zpc}) \text{ at } 25.0^\circ \quad (2)$$

The Gibbs adsorption equation, applied to the above

system in presence of 1:1 potassium salts, at constant temperature and pressure, is written as

$$d\gamma = -(\Gamma_{\text{OH}^-} - \Gamma_{H^+})d\bar{\mu}_{HX} - (\Gamma_{K^+} \cdot d\bar{\mu}_{KX}) - (\Gamma_{X^-} \cdot d\bar{\mu}_{KX}) \quad (3)$$

where X is an anion and other terms have their usual meaning. From the above equation, the following standard relationships for the differential capacity, $C(\pm)$, of the double layer and for the change in the interfacial energy (γ) have been derived.^{1,3,8,9,12,13}

$$d\gamma = -(q \cdot dE)\bar{\mu}_{KX} \quad (4)$$

hence

$$\left(\frac{\partial^2 \gamma}{\partial E^2}\right)_{\mu_{KX}} = \left(\frac{\partial q}{\partial E}\right)_{\mu_{KX}} = C(\pm) \quad (5)$$

and

$$\gamma - \gamma_0 = \left(\int_{E_{zpc}}^E q \cdot dE\right)_{\mu_{KX} = -\infty} - \left(\int_{-\infty}^{\mu} \Gamma_{K^+, X^-} \cdot d\mu_{KX}\right)_E \quad (6)$$

where γ_0 is the interfacial energy at the reference plane (zpc). The significance of these parameters will be discussed later in relation to the present work. At constant pH or half-cell potential, E_\pm

$$-\left(\frac{\partial \gamma}{\partial \mu_{KX}}\right)_{E^-} = \Gamma_{K^+}; \left(\frac{\partial q^-}{\partial \mu_{KX}}\right)_{E^-} = \left(\frac{\partial \Gamma_{K^+}}{\partial E^-}\right)_\mu \quad (7)$$

at the cathodic surfaces and

$$-\left(\frac{\partial \gamma}{\partial \mu_{KX}}\right)_{E^+} = \Gamma_{X^-}; \left(\frac{\partial q^+}{\partial \mu_{KX}}\right)_{E^+} = \left(\frac{\partial \Gamma_{X^-}}{\partial E^+}\right)_\mu \quad (8)$$

at the anodic surfaces.

The excess surface charge, q^+ or q^- , is obtained directly from the present experiments, so that, from the principle of electroneutrality

$$q^\pm = -F(\Gamma^i + \Gamma^d) \quad (9)$$

where Γ^i and Γ^d refer to the relative, ionic ($z = 1$) excess in the inner and in the diffuse double layers, respectively. As evidence for the validity of the above relationship, the q^- values for quartz obtained in this work³ by potentiometric titrations, and the Γ_{Na^+} on quartz, obtained by Li and de Bruyn¹⁹ using ²²Na as a tracer, are in good agreement ($\sim 9 \mu\text{C}/\text{cm}^2$, at pH 10 in 0.001 *M* KNO_3 or NaCl). The double-layer charge due

(15) M. A. V. Devanathan and B. V. K. S. R. A. Tilak, *Chem. Rev.*, **65**, 635 (1965).

(16) G. Kortüm and J. O'M. Bockris, "Textbook of Electrochemistry," Vol. I, Elsevier Publishing Co., London, 1951, p 293.

(17) J. T. Stock, W. C. Purdy, and L. M. Garcia, *Chem. Rev.*, **58**, 611 (1958).

(18) C. D. Russel, *J. Electroanal. Chem.*, **6**, 486 (1963).

(19) H. C. Li and P. L. De Bruyn, *Surface Sci.*, **5**, 203 (1966).

to Ca^{2+} adsorption on quartz²⁰ obtained by using ^{45}Ca as a tracer is also found to agree closely with the q^- values of quartz³. Hence, if Γ^d is known experimentally, or calculated from the diffuse double-layer theory, the density of the specifically adsorbed ions as a function of pH and the activity a_{KX} may be obtained by difference using eq 9. From the adsorption data, it is then possible to obtain the standard free energy (ΔG°) for the specific adsorption of ions on oxides using a suitable adsorption isotherm.^{14,21} These ΔG° values (apparent), for a given composition of the solution, represent the work done in transferring the ion from the bulk solution to the interface and, therefore, also provide information on the effective potential of the compact layer (relative to the bulk solution) that the adsorbate ion encounters as it approaches the adsorption site. Hence, these standard free energy values are expected to be closely related to the ζ potentials of oxides. A study of the variation of ΔG° with pH, with electrolyte concentration, and with surface coverage would be particularly helpful in understanding the oxide-solution equilibria and also in comparing the reactivity of different oxides. The use of Langmuir adsorption isotherm in calculating ΔG° for the adsorption of K^+ on oxides will be considered in the last section.

Experimental Section

Materials. Crystalline $\alpha\text{-Al}_2\text{O}_3$ in a powder form and ZrO_2 and ThO_2 in fused forms were supplied by the Aluminum Co. of Canada and the Norton Co., Chipawa, Ont., respectively. These oxides in $-100 + 150$ mesh size were passed through a Franz magnetic separator to remove any magnetic impurities and were subsequently leached with hot 20% HNO_3 in an all-glass Soxhlet. The resultant material was washed free of excess acid, deslimed,³ and stored in degassed conductivity water that was replaced frequently. From spectrographic analysis, the Al_2O_3 and ThO_2 were found to be 99.9% pure, while the ZrO_2 contained 0.5% trace impurities whose interference was assumed to be negligible. From X-ray diffraction analysis, ZrO_2 and ThO_2 were found to be single-phase baddelyite (monoclinic) and thorianite (cubic), respectively. $\alpha\text{-Al}_2\text{O}_3$ may be considered either as rhombohedral or hexagonal in structure, where each Al is surrounded by six oxygen atoms arranged octahedrally. Recrystallized AR grade KNO_3 , KCl , or NaClO_4 were used to adjust the ionic strength of the solution while the pH was adjusted, as required, using CO_2 -free KOH , HNO_3 , HCl , or HClO_4 depending on the salt used. The electrolyte solutions were freshly prepared before each set of experiments using degassed conductivity water and were kept under an argon atmosphere before use. Any dissolved oxides of nitrogen in the HNO_3 were removed by bubbling argon through a hot solution of the acid that was subsequently preserved in a dark bottle at low temperatures.

Method. The adsorption studies were carried out in a small Pyrex glass cell that was provided with a water jacket for maintaining constant temperature (25.0°) and with two side tubes for circulating argon during the experiment. The cell was also closed to the air by a flexible covering. The pH of the solution was measured with a Beckman Research Model pH meter using a small glass electrode and a saturated calomel reference electrode. The pH meter was enclosed in a constant-humidity (50%) box, leaving the electrodes outside, and could be read with a relative accuracy of 0.002 pH unit. Beckman buffers, prepared according to the NBS standards,²² were used for standardizing the pH meter. The pH is henceforth referred to as pH_s . The calomel electrode was separated from the KNO_3 solution using a KNO_3 -saturated solution bridge with a fiber junction. When using NaClO_4 solutions, a solution bridge containing KNO_3 and NaNO_3 in the molar ratio of 1:7 was used.⁸ The liquid-junction potentials in both these cases are small. The calibration of pH_s against molar concentrations of KOH , HNO_3 , HCl , or HClO_4 was carried out separately in 0.001, 0.1, and 1 *M* solutions of the respective potassium salts (NaClO_4 used for HClO_4 and KNO_3 for KOH). These calibration curves were used later in calculating the charge densities. As these curves were obtained under constant conditions of electrode combinations, small shifts may arise in the potential scale on increasing the ionic strength of the solution, but the calculations of the charge densities should remain unaffected. The total shifts in the half-cell potentials, as measured by the glass electrode, on increasing the ionic strength from 0.001 to 0.1 and 1 *M* were also determined and taken into account where necessary.

The stored oxide samples were taken directly out of water, rewashed, and almost all the excess water filtered out under suction in an atmosphere of argon. The resultant moist material (water content $\sim 2.5\%$ by wt of oxide) was used for further work. A 10-ml sample of the electrolyte solution was placed in the reaction vessel and any dissolved CO_2 was expelled by rapid stirring in a current of argon and the variation of pH_s on stirring the blank solution was then followed at intervals of 2 min. After the solution attained a steady pH_s , an oxide sample (2–3 g), prepared as above, was added to the solution, and the variation of pH_s with time was again followed, normally at intervals of 2 min but at intervals of 1 min near the zpc. From kinetic studies of the oxide-solution interface, it has been shown⁶ that almost all the change in pH_s occurs during the first 2–6 min after adding the oxide to the

(20) S. M. Ahmed and A. B. Van Cleave, *Can. J. Chem. Eng.*, **43**, 23 (1965).

(21) E. Blomgren and J. O'M. Bockris, *J. Phys. Chem.*, **63**, 1475 (1959).

(22) R. G. Bates, *J. Res. Nat. Bur. Stand.*, **A66**, 179 (1962)

solution. This initial change was followed by a slow variation in pH_s that was attributed to the solubility of the oxide and to slime formation. The rapid change in pH_s occurring in the first few minutes after addition of the oxide to the solution has been attributed^{6,7} to the reaction of the oxide surfaces with the electrolyte. The amount of oxide dissolved in solution during the course of each experiment (2–6 min) was found to be below detection limits using colorimetric methods (sensitivity $1 \mu\text{mol/l}$). It should be emphasized, however, that although the amount of oxide in solution at any given time during the experiment may be very small because of the low solubility product of the metal hydroxides, the total pH_s changes due to the cumulative solubility effects (such as dissolution, dissociation, and reprecipitation) could be far beyond this limit and such as to mask the primary surface effects. In order to avoid the above solubility effects, fresh samples of oxides (coarse and crystalline) and of solutions were used for each of the charge-density values obtained, so that the oxides were not allowed to contact the test solution for more than 2–6 min. This procedure is comparable to using fresh surfaces of mercury in electrocapillary work.

The surface areas of the oxides were determined by the krypton gas adsorption method²³ and were $4414 \text{ cm}^2/\text{g}$ for Al_2O_3 , $1438 \text{ cm}^2/\text{g}$ for ZrO_2 , and $192 \text{ cm}^2/\text{g}$ for ThO_2 . These areas were determined on oxides which had first been given a blank stirring treatment in water under the same conditions as used in the adsorption experiments.

Results

The addition of oxides to the electrolyte solutions resulted in a decrease or an increase in pH_s depending on whether the initial pH_s of the solution was greater than or less than the zpc of the oxides. Thus, the oxides acquire a negative or a positive surface charge in solutions whose pH_s is greater than or less than the pH_s of the zpc, respectively, according to mechanisms already discussed. In order to calculate the surface-charge densities, the initial and final values of a_{H^+} (below pH_s 7) or a_{OH^-} (above pH_s 7) were corrected for the pH_s variations of the blank and for the solubility effects. The a_{H^+} and a_{OH^-} values were converted into concentration terms (C_{H^+} and C_{OH^-}) using the corresponding calibration curves. From these concentration values, $(\Delta C_{H^+}$ or $\Delta C_{OH^-})/10 \text{ ml/cm}^2$ of oxide and hence the surface-charge densities, q^\pm , were calculated. The results of q^\pm for Al_2O_3 in 0.001, 0.1, and 1 M KNO_3 , KCl , and NaClO_4 solutions are shown plotted against the final pH_s and the potential relative to the zpc in Figure 1. Similar results of q^+ for ZrO_2 and ThO_2 in KCl and NaClO_4 solutions are shown in Figures 2 and 3, respectively. The results of q^\pm for the same ZrO_2 and ThO_2 samples in KNO_3 solutions have also been reported earlier.³

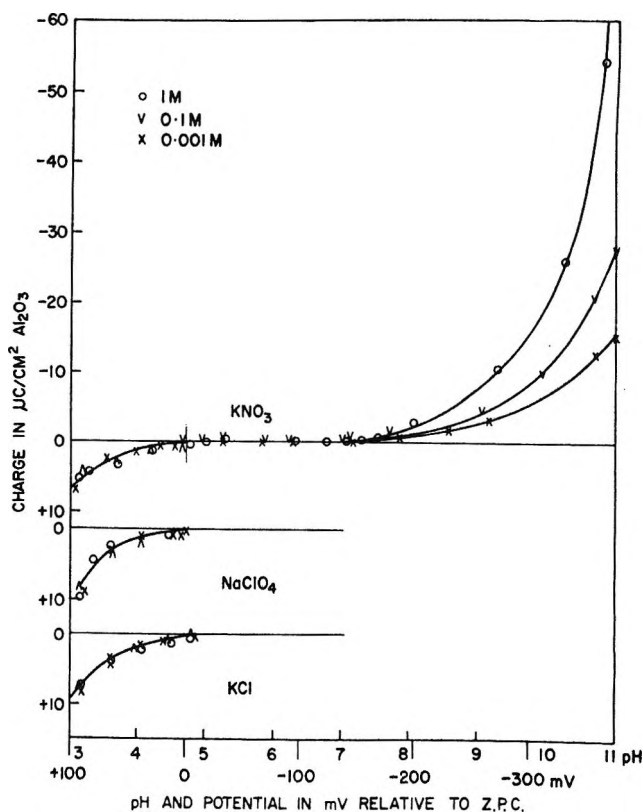


Figure 1. Variation in charge density (q^\pm) on Al_2O_3 with final pH_s and potential difference relative to the zpc in KNO_3 , NaClO_4 , and KCl solutions.

Table I: Zpc of Oxides in KNO_3 Solutions

Oxide	KNO_3 , concn, M	pH_s of zpc	
Quartz	Dry samples	1	3.6 ± 0.05
ZrO_2	Dry samples	0.001	5.5 ± 0.05
ZrO_2	Dry samples	1	6.2 ± 0.05
ThO_2	Dry samples	0.001	5.9 ± 0.05
ThO_2	Dry samples	1	6.8 ± 0.05
Fe_2O_3	Specular hematite, moist	0.001	5.3 ± 0.05
Fe_2O_3	Specular hematite, moist	0.1	5.4 ± 0.05
Fe_2O_3	Specular hematite, moist	1	5.7 ± 0.1
Fe_3O_4	Magnetite, moist	0.001	6.4 ± 0.1
SnO_2	Cassiterite, moist	0.001	5.5 ± 0.1
SnO_2	Cassiterite, moist	0.1, 1	5.4 ± 0.1
TiO_2	Rutile, moist	0.001	5.3 ± 0.05
TiO_2	Rutile, moist	0.1	5.0 ± 0.05
TiO_2	Rutile, moist	1	4.8 ± 0.1
$\alpha\text{-Al}_2\text{O}_3$	Moist	0.001	4.7 ± 0.1
$\alpha\text{-Al}_2\text{O}_3$	Moist	0.1	4.8 ± 0.1
$\alpha\text{-Al}_2\text{O}_3$	Moist	1	5.0 ± 0.1

The differential capacity, $C(\pm)$, of the double layer was obtained by the graphical differentiation of the

(23) S. M. Ahmed, Mines Branch Technical Bulletin TB 84, Department of Energy, Mines and Resources, Ottawa, 1966.

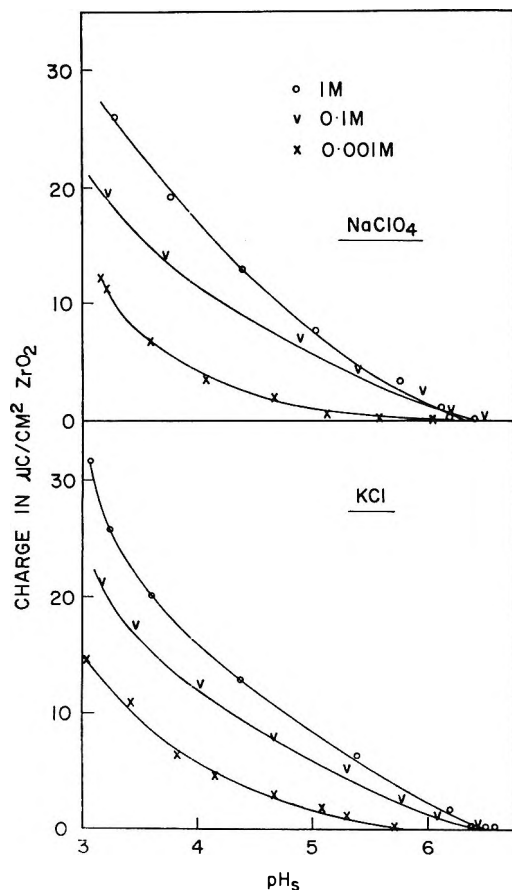


Figure 2. Variation in charge density (q^+) on ZrO_2 with final pH_s in $NaClO_4$ and KCl solutions.

smoothed charge-density plots and these results for Al_2O_3 , and also for SnO_2 and TiO_2 (from previous work⁷), are shown in Figure 4. The $(\gamma - \gamma_0)$ values for Al_2O_3 were obtained by graphical integration of the charge-density plots and are shown in Figure 5.

Discussion

The Zero Point of Charge. The pH_s values obtained in this work^{3,5-7} for the zpc of various oxides are summarized in Table I. These zpc values were obtained for the primary equilibrium (2-6 min) between the oxide surfaces and their potential-determining ions in electrolyte solutions that were practically free of their dissolved metal complexes.

The values listed in Table I for the zpc of oxides, as shown previously,^{6,7} are in close agreement with the pH of the zero streaming potentials (ζ potentials) for the same oxides where fresh solutions, free of dissolved metal complexes, are brought into contact with the oxides. The zpc of oxides obtained during prolonged oxide-solution equilibria (~ 15 hr or more) are, however, different from the above values and are reported to be identical with the isoelectric points of the dissolved metal complexes. Further problems concerning the zpc of oxides have been discussed in detail elsewhere.⁵⁻⁷

On increasing the KNO_3 concentration from 0.001 to 1 M in a blank experiment, the half-cell potential was found to shift to a lower pH_s by 0.3 ± 0.05 pH_s unit near the zpc. In order to compensate for the above shift in the half-cell potential, a corresponding shift in the zpc of oxides to a higher pH_s is expected. Such a shift in the zpc of Al_2O_3 and Fe_2O_3 to a higher pH_s may be seen in Table I and this shift does not indicate any specific adsorption of K^+ or NO_3^- on these two oxides at the zpc. However, similar shifts in the zpc of ZrO_2 and ThO_2 to a higher pH_s (exceeding 0.3 pH_s unit) and in the zpc of SnO_2 and TiO_2 to a lower pH_s indicate specific adsorption of NO_3^- on ZrO_2 and ThO_2 and of K^+ on SnO_2 and TiO_2 . Further evidence of the above effects is available from the charge-density and differential-capacity values, as shown in the next section.

The Positive Surface Charge Densities. The positive surface charge densities of the following oxides have been found to be practically independent ($\pm 1 \mu C$) of the concentration of anions under investigation: Al_2O_3 (Figure 1) and TiO_2 ⁷ in NO_3^- , Cl^- and ClO_4^- , and SnO_2 ⁷ and Fe_2O_3 ⁶ in NO_3^- and ClO_4^- solutions. Hence, in the anodic region, the behavior of these oxides follows mechanism A (see Introduction) where H^+ are chemisorbed on the neutral surface giving rise to a positively charged surface, and the anions stay as counterions outside the primary hydration shell of the surface.^{23a} In terms of double-layer theories,¹³⁻¹⁵ the anions in the above cases may be said to be nonspecifically adsorbed on the metal atoms of the surface. Although the q^+ values, at a given pH_s , may differ from one oxide to another in the above cases, depending on the nature of the coordination of the surface complexes, the increase in the q^+ values with the increasing anion concentration at a given pH_s (cf. eq 8) will, however, be determined by the diffuse double-layer theory. The behavior of the semiconductor and magnetic oxides in the q^+ region was, however, found to be exceptional. Thus, although the q^+ values of specular hematite (Fe_2O_3 , an n-type semiconductor) in NO_3^- and ClO_4^- solutions⁶ were found to be independent of the NO_3^- and ClO_4^- concentrations, these q^+ values were much higher ($\sim 30 \mu C/cm^2$ 130 mV) than the q^+ values for other oxides. These high values of q^+ indicate a much closer packing of anions (NO_3^- and ClO_4^-) on the Fe_2O_3 than for other oxides. The behavior of magnetite⁶ (an n-type semiconductor, and also highly magnetic) in the q^+ region was also found to be inconsistent with the general behavior of the other oxides. Hence the semiconductor and magnetic oxides require

(23a) NOTE ADDED IN PROOF. Recent investigations of $Al(OH_2)_6^{3+}$ complexes by nmr spectroscopy have shown that this complex is stable in Cl^- , NO_3^- , or ClO_4^- solutions with no detectable replacement of H_2O by Cl^- and that proton exchange reactions are predominant between the complexes and the acid solutions (D. W. Fong and E. Grunwald, *J. Amer. Chem. Soc.*, **91**, 2413 (1969)).

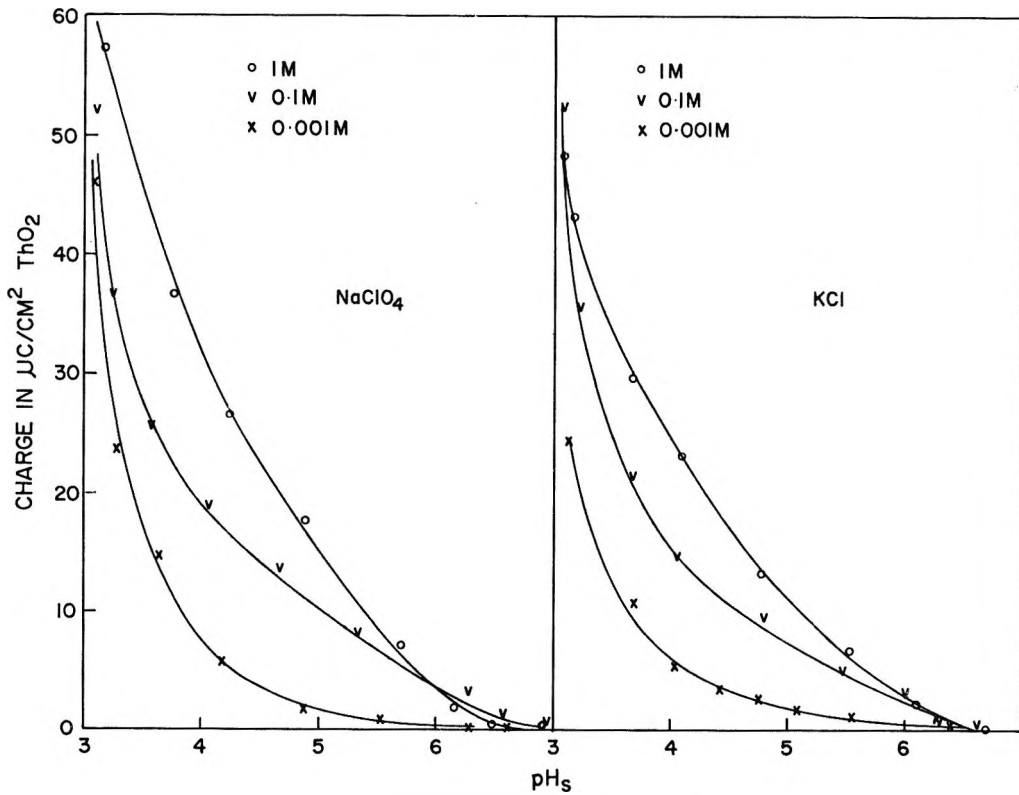


Figure 3. Variation in charge density (q^+) on ThO_2 with final pH_s in NaClO_4 and KCl solutions.

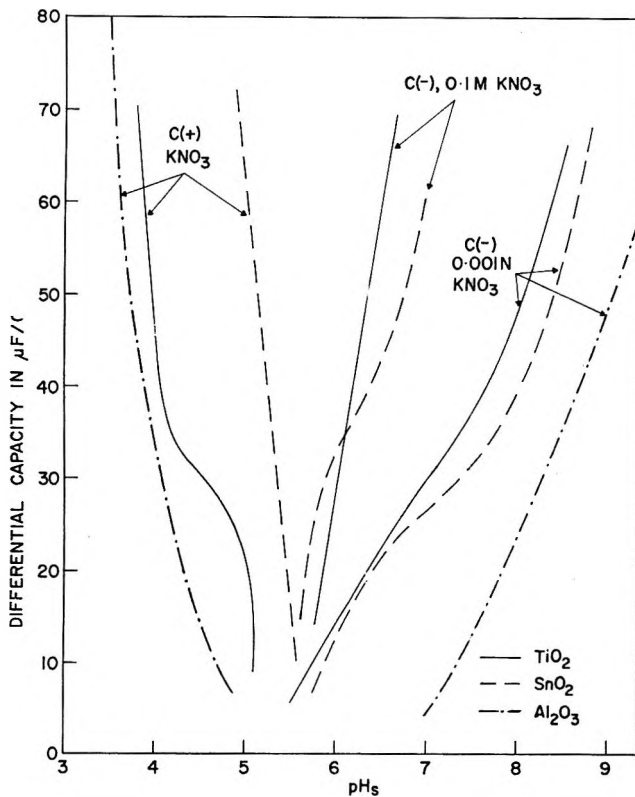


Figure 4. Variation in the differential capacity, $C(\pm)$, of the double layer on Al_2O_3 , SnO_2 , and TiO_2 in KNO_3 with final pH_s .

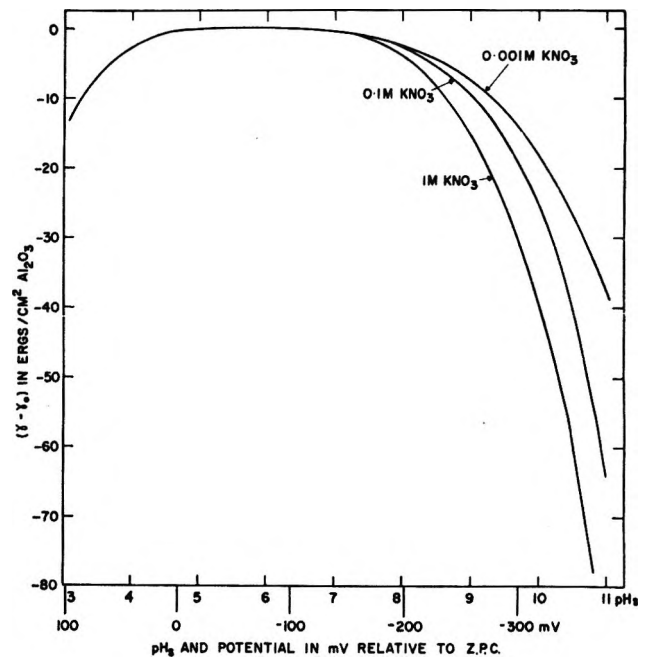


Figure 5. Variation in $(\gamma - \gamma_0)$ at the Al_2O_3 -solution interface with final pH_s and potential difference relative to the zpc.

a more detailed study, particularly with reference to the space-charge region inside these solids.

The q^+ values of ZrO_2 and ThO_2 in ClO_4^- , Cl^-

(Figures 2 and 3) and in NO_3^- solutions, and the q^+ values of Fe_2O_3^6 and SnO_2^7 in Cl^- solutions have been found to increase not only with a_{H^+} but also markedly with the particular anion concentration. Thus the slopes, $(\partial q^+ / \partial \mu_{\text{KNO}_3})_{E^+}$, as given by eq 8, were found

to be much higher than expected from diffuse double-layer theory for the nonspecific adsorption of ions on solid surfaces. Hence, in all the above cases the increase in q^+ with increase in the salt concentration is due to the specific adsorption of the given anions on the metal atoms of the surface through basic dissociation of the surface hydroxyl groups. The type of anionic adsorption (specific or nonspecific) on different oxides is summarized in Table II. As an

Table II: Nature of Anion Adsorption on Oxides

Oxide	Anions nonspecifically adsorbed	Anions specifically adsorbed
SiO ₂ (quartz) ³	NO ₃ ⁻ , Cl ⁻ , ClO ₄ ⁻	...
ZrO ₂ ³	...	NO ₃ ⁻ , Cl ⁻ , ClO ₄ ⁻
ThO ₂ ³	...	NO ₃ ⁻ , Cl ⁻ , ClO ₄ ⁻
TiO ₂ ⁷	NO ₃ ⁻ , Cl ⁻ , ClO ₄ ⁻	...
Al ₂ O ₃	NO ₃ ⁻ , Cl ⁻ , ClO ₄ ⁻	...
SnO ₂ ⁷	NO ₃ ⁻ , ClO ₄ ⁻	Cl ⁻
Fe ₂ O ₃ ⁶	NO ₃ ⁻ , ClO ₄ ⁻	Cl ⁻

extreme case, however, if the specific interaction of anions with the surface-metal atoms is very strong, then a saturation limit in anionic adsorption may be reached at a low anionic concentration, so that a further increase in the anion concentration would show little increase in the q^+ values, e.g., Cl⁻ on SnO₂⁷.

The Negative Surface Charge Densities. The negative surface charge on oxides, as discussed earlier, originates from the acidic dissociation of the surface hydroxyl groups and leads, subsequently, to the adsorption of K⁺ on oxides. The q^- values of Al₂O₃ (Figure 1) and hence the adsorption of K⁺ on this oxide (and on other oxides^{3,5-7} in general) increase with the increasing pH_s, as well as with increase in the K⁺ concentration in solution. The relative surface excess, $\Gamma_{K^+}^i$, due to the specific adsorption (as defined in the Introduction) of K⁺ on oxides was obtained for various oxides by subtracting the values of $\Gamma_{K^+}^d$ (the cation excess in the diffuse double layer) from the q^- values. These $\Gamma_{K^+}^i$ values are shown plotted against the activity a_{KNO_3} in Figures 6 and 7. The $\Gamma_{K^+}^d$ values were calculated¹⁸ from the theory of the diffuse double layer^{13,14} knowing the oxide-electrode potentials relative to the zpc and the ionic strength of the solution. This procedure may not be precise but the error involved is less than the experimental errors usually encountered in this type of work. These adsorption isotherms for K⁺ on oxides (Figures 6 and 7) are comparable in shape and magnitude to the isotherms for the specific adsorption of anions²⁴⁻²⁷ and of Tl⁺²⁸ on Hg.

ΔG° for the Specific Adsorption of K⁺ on Oxides. As the pH_s of the solution is increased relative to the zero point of charge of the oxide (cathodic side), the OH⁻

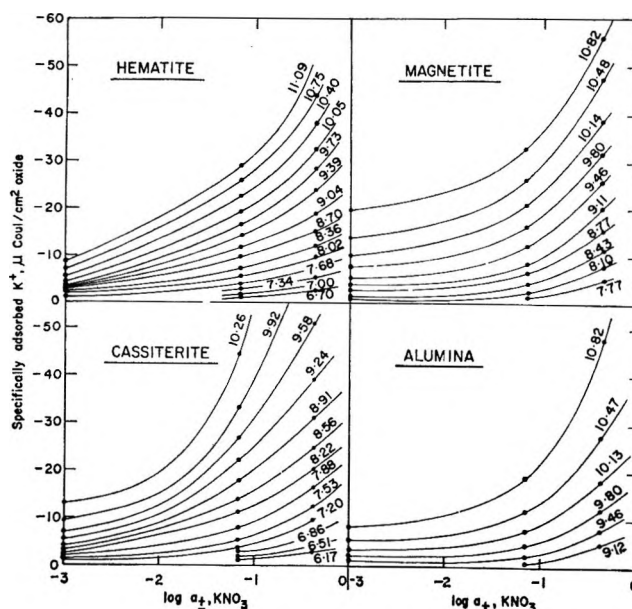


Figure 6. Variation in the specific adsorption of K⁺ on Fe₂O₃, Fe₃O₄, SnO₂, and Al₂O₃ with the log of the mean activity of KNO₃, at different pH_s.

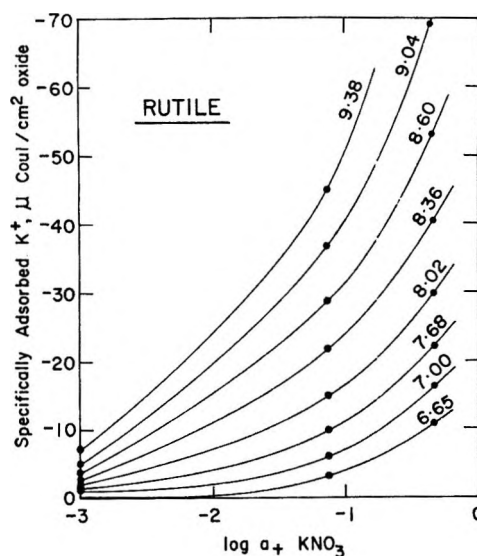


Figure 7. Variation in the specific adsorption of K⁺ on TiO₂ with the log of the mean activity of KNO₃, at different pH_s.

ions from the solution may be considered, as a first step, to neutralize the surface H⁺ ions to form water molecules which are initially adsorbed on the oxide surface. The K⁺ from solution subsequently replace the water molecules and are specifically adsorbed on

(24) D. C. Grahame and R. Parsons, *J. Amer. Chem. Soc.*, **83**, 1291 (1961).

(25) D. C. Grahame, *ibid.*, **80**, 4201 (1958).

(26) J. Lawrence, R. Parsons, and R. Payne, *J. Electroanal. Chem.*, **16**, 193 (1968).

(27) H. Wroblowa, Z. Kovac, and J. O'M. Bockris, *Trans. Faraday Soc.*, **61**, 1523 (1965).

(28) G. G. Susbilles, P. Delahay, and E. Solon, *J. Phys. Chem.*, **70**, 2601 (1966).

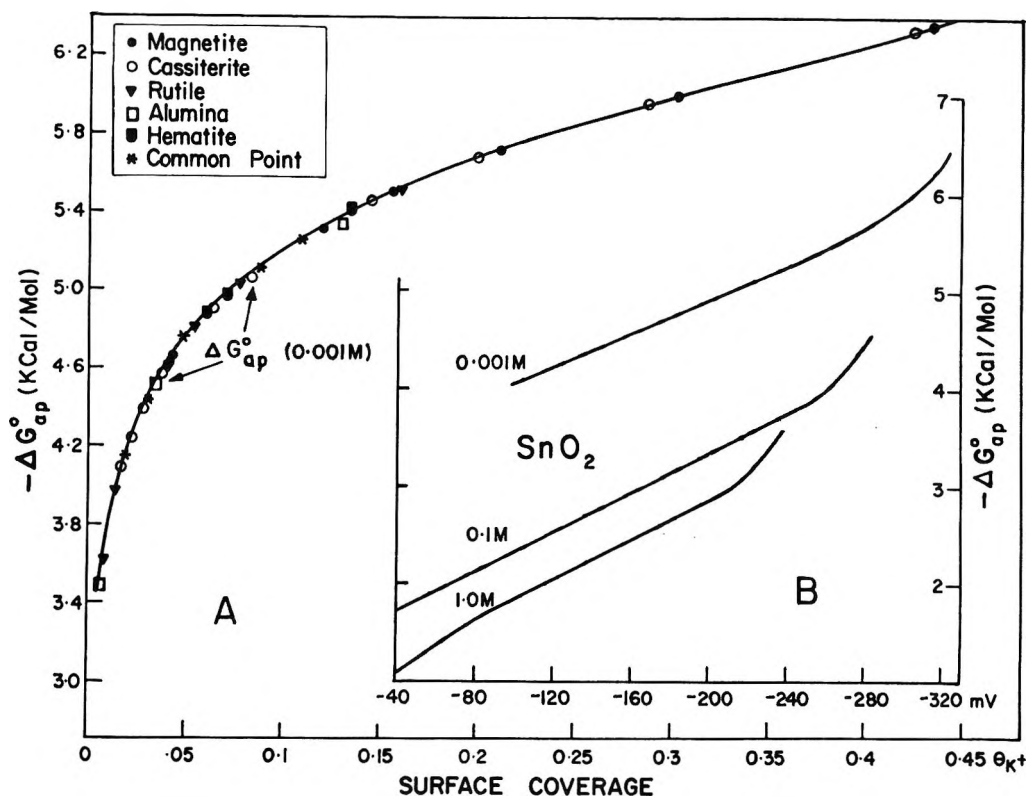


Figure 8. Variation in the ΔG_{ap}° for the specific adsorption of K^{+} on the cathodic surfaces of oxides: (A) with surface coverage $\theta_{K^{+}}$; (B) with potential (relative to zpc) and with KNO_3 concentration, for SnO_2 .

the oxide. The apparent ΔG° for the K^{+} replacing the water molecules, at a given pH_s and a_{KNO_3} , is given²¹ by

$$-G_{ap}^{\circ} = 2.303RT \left[\log \frac{\theta}{1 - \theta} \frac{55.5}{a_{KNO_3}} \right] \quad (10)$$

where θ is the fractional surface coverage due to the specific adsorption of K^{+} on oxide and a_{KNO_3} is the mean activity of the salt in the bulk solution. For calculating θ , a surface charge of $65 \mu C/cm^2$ is assumed to correspond to an effective saturation coverage. The apparent free energy values, as obtained from eq 10, for the adsorption of K^{+} on oxides vary systematically with pH_s (or potential relative to zpc) as well as with a_{KNO_3} , as shown in Figures 8A and 8B. These variations will be discussed shortly. One interesting observation from Figure 8A is that the ΔG_{ap}° values (for a given a_{KNO_3}) of different oxides fall on the same line. This indicates that the differences in the free energy values of different oxides are not revealed from a physical parameter such as surface coverage. Instead, the differences in the free energies of different oxides appear in their $\theta_{K^{+}}$ values being different for different oxides for a given composition of the solution (Figures 6 and 7).

The increase in $-\Delta G_{ap}^{\circ}$ with increasing pH_s for cassiterite (Figure 8B) is typical of the oxides investigated and is obviously due to the ionization of the surface hydroxyl groups which increases the po-

tential difference between the oxide surface and the bulk solution. However, this pH_s dependence of the ΔG_{ap}° may be incorporated in the adsorption isotherm by taking into account the equivalent change in the electrochemical free energy, of the oxide-solution half-cell, that occurs during the neutralization of the surfacebound H^{+} ions by OH^{-} (first step, see above). This change in the free energy of the half cell is given by

$$-\Delta G_{H^{+}}^{\circ} = RT \ln \frac{(a_{H^{+}})^i}{(a_{H^{+}})^f} = 2.303RT(pH_f - pH_i) \quad (11)$$

where i and f refer to the initial and final values of $a_{H^{+}}$ or pH_s during adsorption. By combining eq 10 and 11

$$-\Delta G_{K^{+}}^{\circ} = 2.303RT \times \left[\log \frac{\theta}{1 - \theta} \frac{55.5}{a_{KNO_3}} + (pH_f - pH_i) \right] \quad (12)$$

(Alternatively, ΔG° in terms of a_{KNO_3} and $a_{H_3O^{+}}$ may be obtained by considering replacement of H_3O^{+} from the surface by K^{+} and by equating their electrochemical potentials in the adsorbed layer and in the bulk solution.²¹ Then, by substituting $C_{H_3O^{+}} \cdot a_{H^{+}}$ for $a_{H_3O^{+}}$ and including further changes in $a_{H^{+}}$ during adsorption, the isotherm obtained is identical with eq 12.)

In Figure 9A, the $\Delta G_{K^{+}}^{\circ}$ for hematite and cassiterite, as obtained from eq 12, for the three a_{KNO_3} ,

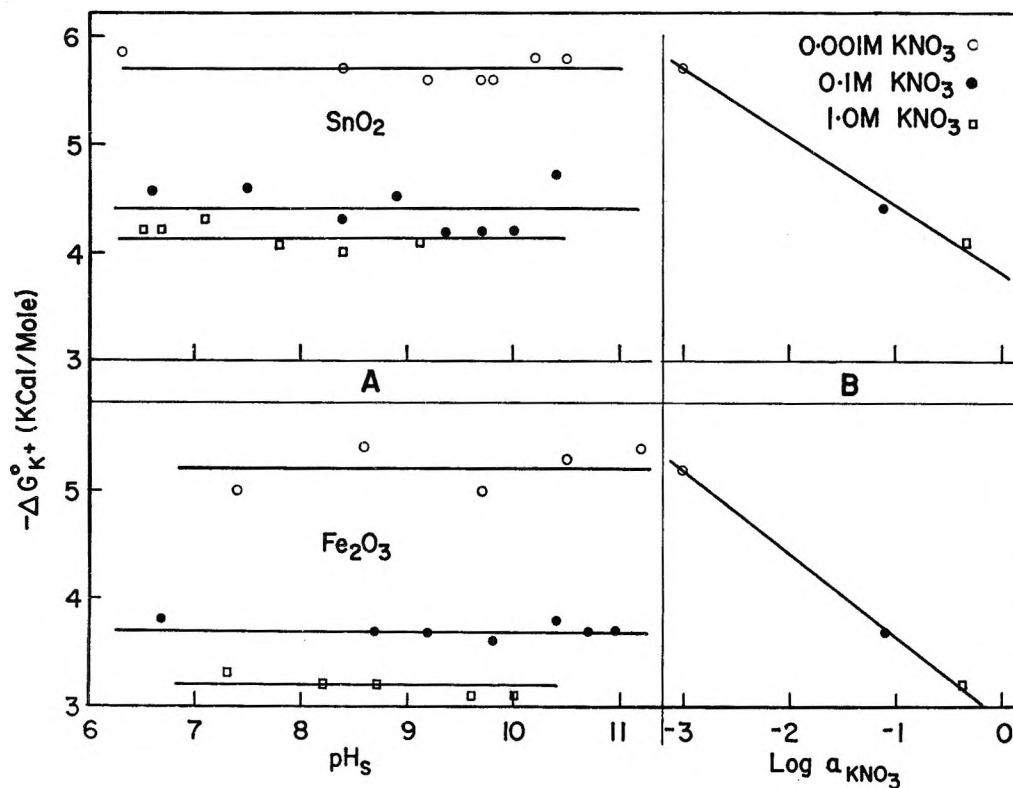


Figure 9. Variation of $\Delta G^{\circ}_{K^+}$ for Fe_2O_3 and SnO_2 : (A) with pH_s at different a_{KNO_3} ; (B) with $\text{log } a_{\text{KNO}_3}$.

values, are shown to be independent of pH_s within $\pm 2\%$ error. This deviation was somewhat larger ($\pm 5\%$) at extreme values of pH_s because of higher experimental error at these pH_s values and because the solubility corrections in pH_i and pH_f were also neglected. In Figure 9B, it is further seen that these $-\Delta G^{\circ}_{K^+}$ values decrease linearly (*i.e.*, adsorption of K^+ becomes increasingly difficult) with increasing values of $\text{log } a_{\text{KNO}_3}$. The slope of these plots in Figure 9B and the extrapolated values of $\Delta G^{\circ}_{K^+}$ to unit salt activity appear to be characteristic of each oxide and represent their reactivity for ionic adsorption. Hence, the $\Delta G^{\circ}_{K^+}$ at unit salt activity (-2.9 , -3.8 , and -5.7 kcal/mol for hematite, cassiterite, and rutile, respectively) may be taken as a standard value for comparing different oxides. A comparative study of the oxides in this way is being carried out.

The $\Delta G^{\circ}_{K^+}$ values for each oxide are seen (Figure 9A and 9B) to vary by about 2 kcal during adsorption. Thus, the variation in $\Delta G^{\circ}_{K^+}$ for hematite from 5 to 3 kcal/mol, corresponds to a variation from 200 to 100 mV on the potential scale. These values in mV, say ψ_{K^+} , represent the effective potential (of the plane of K^+ adsorption, relative to bulk solution) that a K^+ ion would encounter as it approaches the surface for adsorption from bulk solution. The variation of $\Delta G^{\circ}_{\text{ap}}$ and $\Delta G^{\circ}_{K^+}$ (or the ψ_{K^+} values) (Figures 8 and 9) and of the ζ potentials of oxides^{19,29} with pH_s and a_{\pm} (salt) are qualitatively similar. The ψ_{K^+} and the ζ potentials of oxides are also of the same order of

magnitude, which provides some evidence for the validity of assumptions made in deriving the adsorption isotherm. For a strict comparison between the ζ potentials of oxides and the present ψ_{K^+} values, the ζ potentials of the particular samples used in this investigation would have to be determined. However, the ζ potentials of oxides in general (~ -120 and -200 mV_{max} for quartz¹⁹ and SnO_2 ,²⁹ respectively) appear to be somewhat lower than the ψ_{K^+} values, for a given composition of the solution. This difference is in qualitative agreement with the general assumption that the slipping plane⁹ in electrokinetic measurements lies somewhat farther from the compact layer. It is hoped to examine this subject further by parallel measurements of the ζ potentials.

The Differential Capacity and the $(\gamma - \gamma_0)$ Curves. The differential capacities, $C(\pm)$, of the double layer on Al_2O_3 , SnO_2 ,⁷ and TiO_2 ,⁷ are shown plotted against the final pH_s in Figure 4. The data in Figure 4 and the previous plots^{3,6} of C against pH_s exhibit three main features that may be interpreted on the basis of the mechanisms involved. First, the increase in $C(+)$ values with decreasing pH_s (Figure 4) on the anodic side of the zpc is attributed to the chemisorption of H^+ on the surfaces. A similar increase in the differential capacity of Sn electrodes with decreasing pH has also been observed recently from direct

(29) D. J. O'Connor and A. S. Buchannan, *Aust. J. Chem.*, **6**, 278 (1953).

capacitance measurements.³⁰ Second, in the cathodic region, a plateau-like break occurs in the $C(-)$ against pH_s plots of many oxides at $C \sim 30\text{--}40 \mu\text{F}/\text{cm}^2$, and is followed by a steep rise in $C(-)$ due to the increasing specific adsorption of K^+ on the oxide layer. The plateau probably corresponds to the smoothed-out "hump" that usually occurs in the double-layer capacitance of Hg, if the specific adsorption of counterions is not intense.¹³⁻¹⁵ These plateaus were found to be particularly prominent in the capacity plots of quartz³ and Fe_2O_3 ⁶ and to disappear for ThO_2 ³ and Al_2O_3 (Figure 4) which is attributed to the intense specific adsorption of K^+ on the latter two oxides. The third noteworthy characteristic is the occurrence of broad and flat minima in the differential-capacity curves of some oxides (quartz,³ Fe_2O_3 ,⁶ and Al_2O_3 (Figure 4)) at the cathodic side of their zpc. The occurrence of such flat minima in the double-layer capacity of certain metals, notably Zn,³¹ has also been observed by direct capacitance measurements. In the present case of Al_2O_3 , for example, the broad minima in the $C(-)$ values (Figure 4) have resulted from the flat portions in the q^- against pH_s plots of Figure 1. This indicates that a considerable potential drop occurs across the hydration layer of the oxide (~ 130 mV for Al_2O_3) before proton dissociation occurs from the surface hydroxyl groups. In electrocapillarity, such a potential drop across the hydration layer of solid surfaces is known as the χ potential. This effect is most pronounced for oxide surfaces that are strongly hydrated, e.g., quartz,³ Fe_2O_3 ,⁶ and Al_2O_3 (Figure 4), and does not arise in the anodic region of Fe_2O_3 or Al_2O_3 , because the surface charge (+) on oxides in this region originates from proton adsorption instead of from proton dissociation.

The $(\gamma - \gamma_0)$ against pH_s plots of Al_2O_3 (Figure 5) and other oxides^{3,5} are similar in shape to the electrocapillary curves but have a different meaning. These $(\gamma - \gamma_0)$ values represent the integral values of the electrochemical work done in transferring the adsorbed ions from the bulk of the solution to the interface. Except for a small correction for the contribution of the diffuse double layer, in general the $(\gamma - \gamma_0)$ values of the oxides examined are of the

same order of magnitude and have the same meaning as the "equivalent, effective surface pressure" calculated by Parsons and others³²⁻³⁴ for the specific adsorption of anions on Hg. The single anodic branch of the $(\gamma - \gamma_0)$ against pH_s plots represents non-specific adsorption of anions on the metal atoms of the oxide surfaces and in this respect resembles the cathodic branch of the electrocapillary curves of Hg, where the cations remain nonspecifically adsorbed.

Conclusions

As a result of some inherent uncertainties arising from factors such as pH_s , the absolute values of surface areas and the solubility effects, this work is not sufficiently precise to investigate the properties of the diffuse double layer on oxides. However, it is evident from the present investigation that several major effects and the general trends in the properties of the oxide-solution interface can be studied using the present techniques, provided that the solubility effects are prevented from interfering with the surface effects. The usefulness of this work could be further enhanced by performing simultaneous adsorption studies using radioactive tracers and streaming potential studies on the same material. Some of the properties of the oxide-solution interface considered in this paper are expected to be helpful in the future theoretical development of the subject. The applications of this work in practical fields have already been discussed elsewhere.^{3,5}

Acknowledgments. The assistance of D. Maksimov (Visiting Scientist, Skochinski Mining Institute, Moscow, U.S.S.R.) in the work⁵ on Al_2O_3 , ZrO_2 , and ThO_2 , and helpful discussions with Professor B. E. Conway, University of Ottawa, and Dr. H. P. Dibbs, Mineral Sciences Division, are gratefully acknowledged.

(30) N. A. Hampson and D. Larkin, *J. Electrochem. Soc.*, **115**, 612 (1968).

(31) D. S. Brown, J. P. G. Farr, N. A. Hampson, D. Larkin, and C. Lewis, *J. Electroanal. Chem.*, **17**, 421 (1968).

(32) J. M. Parry and R. Parsons, *Trans. Faraday Soc.*, **59**, 241 (1963).

(33) R. Payne, *J. Chem. Phys.*, **42**, 3371 (1965).

(34) R. Payne, *J. Electrochem. Soc.*, **113**, 999 (1966).

Interactions of Silver Halides with Metal Chelates and Chelating Agents^{1,2}

by Egon Matijević, Nicholas Kolak,³ and David L. Catone⁴

Institute of Colloid and Surface Science and Department of Chemistry, Clarkson College of Technology, Postdam, New York 13676 (Received February 18, 1969)

It is shown that the chelating agents ethylenediamine (en), 2,2'-dipyridyl (dipy), and 1,10-phenanthroline (phen) can coagulate and reverse the charge of a silver bromide sol, the order of efficiency being phen > dipy > en. With increasing pH the critical coagulation concentration (ccc) and the critical stabilization concentration (csc) increase for en and decrease for dipy and phen. Apparently two different mechanisms apply to interactions of en and of dipy and phen with silver halide sols. These are discussed in light of the composition of the solute species along the ccc and csc boundaries. The addition of a small amount of dipy (in concentrations considerably less than the ccc of dipy) strikingly sensitizes the sol toward Ni²⁺, the ccc of the latter being lowered by more than four orders of magnitude. If the ratio of the added [Ni²⁺] to [dipy] is kept constant (1:3), the charge of the sol can be reversed. The ir spectra show that the Ni(dipy)²⁺ complex is formed at the interface. On the other hand, when the concentration of dipy is constant and [Ni²⁺] is varied, the charge reversal does not occur, yet the sol is stable again at higher nickel concentration. In this case the sol mobility goes through a minimum, which coincides with the coagulation maximum.

Introduction

In a recent publication,⁵ it was shown that certain metal chelates exhibit striking effects upon the stability of lyophobic colloids. These complexes coagulate at extremely low concentrations, and they also act as powerful reversal of charge agents. For example, for a silver bromide sol the critical coagulation concentration (ccc) of the trisphenanthroline nickel ion, Ni(phen)₃²⁺, is $7 \times 10^{-8} M$ and the critical stabilization concentration due to charge reversal (csc) is $4 \times 10^{-7} M$. In contrast, noncomplexed Ni²⁺ ion coagulates at $\sim 1 \times 10^{-3} M$ and cannot reverse the charge at all.

In addition, it was found that the enhanced coagulation and reversal of charge ability of metal chelates (as compared to noncomplexed metal ions) takes place over a broad pH range. This observation is surprising as the stability of some of these complexes in solution depends strongly on the pH. The purpose of this investigation is to examine the reasons for such a behavior of metal chelates. To this end the interactions of several chelating agents (ethylenediamine, 2,2'-dipyridyl, and 1,10-phenanthroline) with a silver bromide sol in the absence and in the presence of metal ions have been studied. Also, the adsorption of the complex chelates and the chelating agents on silver halides has been followed by infrared spectroscopy.

These results should contribute toward a better understanding of coagulation processes which are caused by charge neutralization owing to the chemisorption of counterions. They should also indicate the ways for modifications of lyophobic interfaces, particularly when charge reversal is desired. Finally, the investigated systems can serve as models for processes of interfacial conversion, such as adhesion, polymer-solid interactions, etc.

Experimental Section

A. Materials. Ethylenediamine, 2,2'-dipyridyl, and 1,10-phenanthroline were commercially available chemicals, which were purified before use. The trisdipyridyl nickel(II) chloride, [Ni(dipy)₃]Cl₂, was prepared following the procedure by Morgan and Burstall.⁶ All other chemicals were of the highest purity grade available and were used without further purification. All solutions were prepared at 25° using doubly distilled water from an all-glass still. In order to prevent aging of the solutions upon standing, fresh solutions were prepared every few days. A Millipore filter with a pore size of 0.22 μ was used to remove any foreign particles from the stock solutions.

B. Methods. The critical coagulation concentration (ccc) and the critical stabilization concentration (csc) due to charge reversal were determined by following the changes in light scattering of a silver bromide sol *in statu nascendi* according to a procedure described earlier.^{7,8} Scattering intensities were measured with a Brice-Phoenix Model D-M light-scattering photometer and were expressed in terms of Rayleigh ratios (RR).⁵

Mobilities of silver bromide particles were deter-

(1) Supported by the Federal Water Pollution Control Administration, Grant WP-00815.

(2) Presented at the 156th National Meeting of the American Chemical Society, Atlantic City, N. J., Sept 8-13, 1968.

(3) Part of an M.S. thesis by N. Kolak.

(4) Part of a Ph.D. thesis by D. L. Catone.

(5) E. Matijević and N. Kolak, *J. Colloid Interfac. Sci.*, **24**, 411 (1967).

(6) J. T. Morgan and F. H. Burstall, *J. Chem. Soc.*, 2213 (1931).

(7) E. Matijević and M. Kerker, *J. Phys. Chem.*, **62**, 1271 (1958).

(8) B. Težak, E. Matijević, and K. Schulz, *ibid.*, **55**, 1557 (1951).

mined in a microelectrophoresis cell of the Mattson type.^{9,10}

A Beckman Model G pH meter with glass electrodes was used for pH measurements. The instrument was regularly standardized using appropriate buffer solutions.

The infrared spectra of the adsorbed species on silver bromide particles were obtained with a Beckman IR-12 spectrophotometer. This instrument has a wave number reproducibility of 0.1 cm^{-1} , a wave number accuracy of $\pm 0.2 \text{ cm}^{-1}$ at 740 cm^{-1} , and a resolution of 0.25 cm^{-1} at 923 cm^{-1} . The solutions containing the species to be adsorbed were stirred for about 5 days with a silver bromide sol. The mixture was then filtered, washed three times with 5-ml aliquots of doubly distilled water, and the solids were dried under vacuum at 25° for at least 4 days. The samples were then pressed into pellets. No additional support material needed to be added because silver bromide is a suitable medium itself.

Results

The interactions of a silver bromide sol with three chelating agents have been studied in detail. These are ethylenediamine (en), 2,2'-dipyridyl (dipy), and 1,10-phenanthroline (phen).

In Figure 1 are given several coagulation curves in which the Rayleigh ratio (RR) is plotted against the concentration of ethylenediamine. Each curve is for a different but narrow pH range. High and low RR represent coagulated and stable sols, respectively. The critical coagulation concentration (ccc) is obtained by

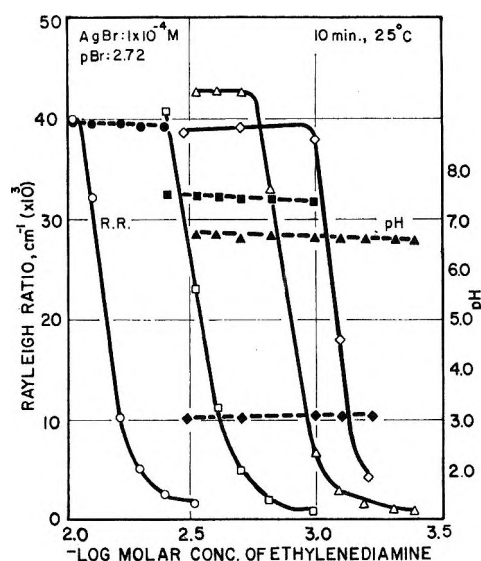


Figure 1. Coagulation curves (solid lines, open symbols) for a silver bromide sol *in statu nascendi* in the presence of ethylenediamine at various pH values (dashed lines, blackened symbols). High and low Rayleigh ratios (RR) designate coagulated and stable sols, respectively. Concentrations: AgBr, $1.0 \times 10^{-4} M$; excess Br^- , $1.9 \times 10^{-3} M$. RR measured 10 min after mixing the reacting components.

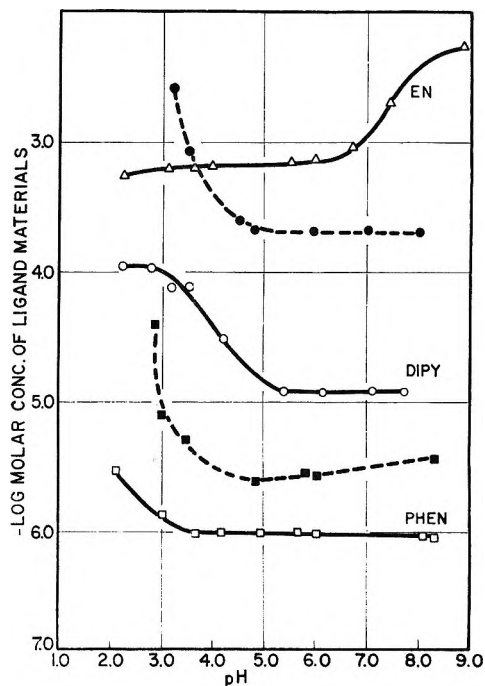


Figure 2. Plot of the critical coagulation concentrations (ccc, solid lines) and of the critical stabilization concentrations (csc, dashed lines) of a silver bromide sol *in statu nascendi* as a function of pH for ethylenediamine (en, Δ), 2,2'-dipyridyl (dipy, \circ), and 1,10-phenanthroline (phen, \square). AgBr, $1.0 \times 10^{-4} M$; excess Br^- , $1.9 \times 10^{-3} M$.

extrapolation of the steepest part of a coagulation curve to zero RR. Similar experiments were carried out with dipy and phen. With these substances the coagulation curves showed a maximum in RR. (One example of such a curve can be seen in Figure 6.)

Figure 2 gives a summary of the results as obtained with the three chelating agents. Above the solid lines the sols are coagulated and above the dashed lines they are restabilized. Thus, with dipy and phen the coagulation occurs only between the corresponding solid and dashed boundaries.

The results of electrophoretic measurements on a silver bromide sol in the presence of the three chelating agents are given in Figure 3. Each system was studied at two different pH values. The mobilities show that all three substances can reverse the charge of the sol, with the order of efficiency being phen > dipy > en. This would explain the restabilization phenomenon of phen and dipy as observed by light scattering (Figure 2).

The experiments described give evidence that the chelating agents interact with silver halide sols even when they are not complexed with a metal ion. In order to see whether the presence of the metal ion has any effect upon the behavior of the chelating agents, coagulation and mobility studies were carried out with

(9) S. Mattson, *J. Phys. Chem.*, **37**, 223 (1933); **32**, 1532 (1928).

(10) E. Matijević, K. G. Mathai, R. H. Ottewill, and M. Kerker, *ibid.*, **65**, 826 (1961).

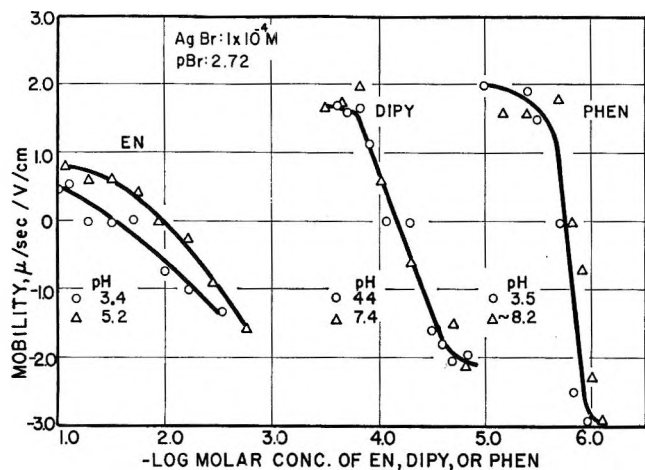


Figure 3. Electrophoretic mobilities of a silver bromide sol *in statu nascendi* (AgBr , $1.0 \times 10^{-4} M$; excess Br^- , $1.9 \times 10^{-3} M$) as a function of varying concentrations of ethylenediamine (en), 2,2'-dipyridyl (dipy), and 1,10-phenanthroline (phen) at pH values as indicated in the diagram.

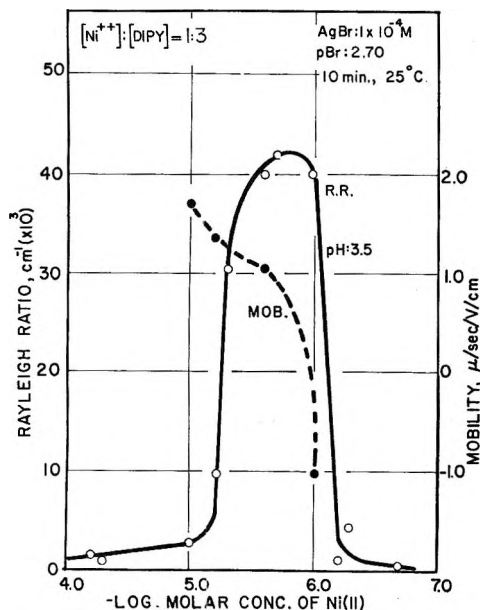


Figure 4. Coagulation curve (solid line) of a silver bromide sol *in statu nascendi*. (AgBr , $1.0 \times 10^{-4} M$; excess Br^- , $1.9 \times 10^{-3} M$) as a function of $\text{Ni}(\text{NO}_3)_2$ at pH 3.5 in the presence of 2,2'-dipyridyl (dipy). The concentration of dipy in each system was equal to $3 \times$ the concentration of Ni^{2+} ions. Dashed line gives the corresponding electrophoretic mobilities.

silver bromide sols to which the chelating agent and the metal ion were simultaneously added. In Figure 4 a coagulation curve is given as a function of the nickel nitrate concentration. Each system contained dipy in amounts sufficient to maintain a constant ratio $[\text{Ni}^{2+}]:[\text{dipy}] = 1:3$. The ccc and the csc of the nickel ion are approximately the same as when the complex $\text{Ni}(\text{dipy})_3^{2+}$ is added to the sol. The mobility measurements (dashed line) indicate strong charge reversal.

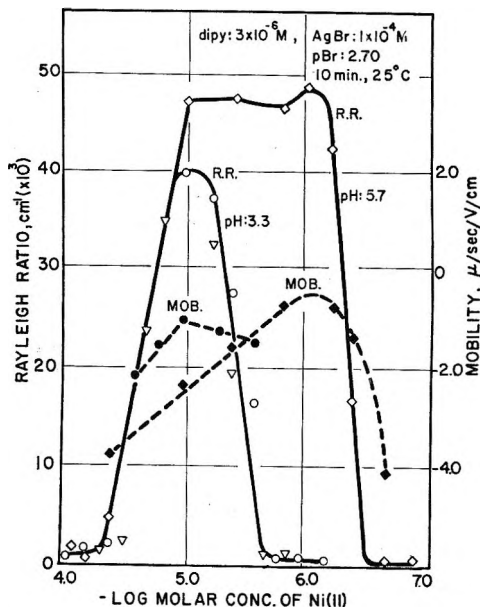


Figure 5. Coagulation curves of a silver bromide sol (AgBr , $1.0 \times 10^{-4} M$; excess Br^- , $1.9 \times 10^{-3} M$) as a function of $\text{Ni}(\text{NO}_3)_2$ in the presence of a constant amount of 2,2'-dipyridyl ($3.0 \times 10^{-6} M$) at two different pH (O, ∇ , 3.3; \diamond , 5.7). Dashed lines give the corresponding mobilities. Circles and diamonds represent a sol *in statu nascendi*, whereas triangles are for a sol aged for 30 min before addition of $\text{Ni}(\text{NO}_3)_2$.

An unexpected result was obtained when the 2,2'-dipyridyl was added to the silver bromide sol in constant concentration, whereas the concentration of $\text{Ni}(\text{NO}_3)_2$ was systematically varied. This is shown in Figure 5 in which the two systems are for different pH values. Again coagulation maxima appear but the stability at higher concentrations of the nickel salt is not due to charge reversal. The corresponding curves for the electrophoretic mobilities show that the sols remain negatively charged over the entire salt concentration range. A minimum in the mobility coincides with a maximum in turbidity. It should be noted that the amount of dipyridyl added is considerably below the ccc of this compound for the same sol. Most surprisingly, the amount of nickel salt needed to coagulate the silver bromide is at least three orders of magnitude lower in the presence of the very small amount of dipyridyl than in the absence of it.

Discussion

1. *Stability Effects by Chelating Agents.* Since all of the three chelating agents used in this work can coagulate the negatively charged silver bromide sols and reverse their charge, one would expect them to be present in aqueous solutions in the form of cationic species. It is known that en, dipy, and phen behave as organic bases which may undergo protonation in aqueous solutions. The corresponding stability constants are given in Table I.

Table I: Stability Constants for Metal Chelates and Chelating Agents^a

	Log K_1	Log K_2	Log K_3
$\text{en} + x\text{H}^+ \rightleftharpoons \text{enH}_x^{2+}$	10.17	7.44	
$\text{dipy} + x\text{H}^+ \rightleftharpoons \text{dipyH}_x^{2+}$	4.44	0.52	
$\text{phen} + x\text{H}^+ \rightleftharpoons \text{phenH}_x^{2+}$	4.86	0.70	
$\text{Ni}^{2+} + x\text{en} \rightleftharpoons \text{Ni}(\text{en})_x^{2+}$	7.51	6.35	4.42
$\text{Ni}^{2+} + x\text{dipy} \rightleftharpoons \text{Ni}(\text{dipy})_x^{2+}$	6.80	6.46	5.20
$\text{Ni}^{2+} + x\text{phen} \rightleftharpoons \text{Ni}(\text{phen})_x^{2+}$	8.60	8.10	7.55

^a The values have been selected from "Stability Constants of Metal-Ion Complexes," compiled by L. G. Sillén and A. E. Martell, The Chemical Society, London, 1964, and "Dissociation Constants of Organic Bases in Aqueous Solution," compiled by D. D. Perrin, Butterworth and Co. Ltd., London, 1965.

The coagulation effects of ethylenediamine can be explained in terms of protonation. In Table II the composition of the en solutions for various ccc is given as a function of the corresponding pH. In all cases the concentration of the doubly protonated species enH_2^{2+} is reasonably constant. The average value of $6.4 \pm 0.6 \times 10^{-4} M$ is what one would expect for counterions of 2+ charge for the silver bromide sol used. The ccc is somewhat lower than for simple divalent counterions for the same sol,¹¹ but this is to be expected since enH_2^{2+} is a larger species. The concentration of the monoprotonated ion becomes larger with increasing pH, but even at pH 8.0 this is much too low for a monovalent counterion to affect the rate of coagulation; hence the ccc will not be influenced by enH^+ . It appears, then, that the amount of en needed to coagulate the sol is such to produce at a pH the sufficient concentration of the coagulating species, which is in this case enH_2^{2+} .

Electrophoretic measurements (Figure 3) indicate that the adsorption of en is negligible over the ccc range, which explains why the enH_2^{2+} counterion obeys the Schulze-Hardy rule.¹²

The stability effects of dipy and phen are considerably more involved. The following experimental observations should be considered. Both substances coagulate and also reverse the charge of the silver bromide sol. The ccc and the csc decrease with increasing pH until above a given pH these values remain constant. The composition of the solutions along the coagulation boundary and the limit marking the restabilization due to charge reversal (Figure 2) are given in Table II. The concentration of protonated species decreases rapidly as the pH becomes higher. Thus, the protonated species cannot be responsible for charge reversal and may adsorb less strongly than the unprotonated chelating agents. This is corroborated by the mobility measurements which indicate strong charge reversal even at pH 7-8 (Figure 3) at which condition there are no protonated species present in the solution.

Infrared adsorption studies confirm that the uncharged species adsorb on silver bromide sol particles. Table III gives the characteristic frequencies of dipy and the protonated dipy ($\text{dipy} \cdot \text{HClO}_4$) in the absence of silver bromide. The same frequencies of the most intense bands for unprotonated dipy are observed for the species adsorbed on silver bromide for samples equilibrated over the pH range 3-7. The peaks become more intense with increasing pH. All of this indicates that the uncharged dipy adsorbs and causes coagulation and charge reversal, which at first would seem to be a rather unusual result. The following mechanism is suggested by way of explanation of these effects. The neutral dipy molecules adsorb by an ion-exchange mechanism in which they substitute the potential determining bromide ions. In doing so they may form a chelate with the silver ion at the silver bromide-solution interface. The removal of bromide ions at first destabilizes the particles due to charge neutralization and then restabilizes the sol when more bromide ions than necessary to establish the point of zero charge are exchanged. The silver-dipyridyl chelate is rather stable¹³ and will not easily desorb. The formation of the Ag-dipy ions at the interface cannot be distinguished by ir because the characteristic peaks due to this chelate are identical with those of 2,2'-dipyridyl alone. The suggested mechanism certainly would explain the inapplicability of the Schulze-Hardy rule to this case.

It is noteworthy that at the csc the concentration of the unprotonated dipy (L) remains constant over the entire pH range (Table II). The same is true for the ccc except at pH <2.0. At this high acidity, hydrogen ions are present in sufficient concentrations to influence the coagulation rate.

The difference in hydration may explain the reason why the positively charged protonated chelating agent does not adsorb strongly on negative silver bromide particles whereas the neutral species do adsorb. The protonated molecules will be more strongly hydrated and consequently "repelled" by the lyophobic sol particles. On the other hand, the neutral molecules with little or no bound water of hydration will adsorb. As it was recently shown, the counterion charge plays no detectable role in its adsorptivity on lyophobic particles.¹⁴

The difference in the degree of hydration may also be responsible for the somewhat different behavior of dipy and phen.

2. Stability Effects of Metal Chelates. In the first

(11) E. Matijević, D. Broadhurst, and M. Kerker, *J. Phys. Chem.*, **63**, 1552 (1959).

(12) E. Matijević and L. H. Allen, *Envir. Sci. Technol.*, **3**, 264 (1969).

(13) S. Canani and E. Scroco, *J. Inorg. Nucl. Chem.*, **8**, 332 (1958).

(14) L. J. Stryker and E. Matijević, *Advances in Chemistry Series*, No. 79, American Chemical Society, Washington, D. C., 1968, p 44; *J. Colloid Interfac. Sci.*, in press.

Table II

Species	Concn., M	pH	Free meta ¹		ML ₁		ML ₂		ML ₃		L		LH		LH ₂ ²	
			M	%	M	%	M	%	M	%	M	%	M	%	M	%
Ethylene diamine (en)	6.0 × 10 ⁻⁴	2.0														
	6.0 × 10 ⁻⁴	4.0														
	6.0 × 10 ⁻⁴	6.0														
	1.0 × 10 ⁻³	7.0														
[Ni(en) ₃] ²⁺	3.6 × 10 ⁻³	8.0														
	1.7 × 10 ⁻⁴	3.0	1.7 × 10 ⁻⁴	100.0												
	2.3 × 10 ⁻⁴	5.0	2.3 × 10 ⁻⁴	100.0	1.6 × 10 ⁻⁷											
	1.2 × 10 ⁻⁴	7.0	3.7 × 10 ⁻⁶	32.4	6.9 × 10 ⁻⁶	60.4	8.2 × 10 ⁻⁶	7.1	1.5 × 10 ⁻⁸							
2,2'-Dipyridyl (dipy)	1.0 × 10 ⁻⁴	2.0														
	4.0 × 10 ⁻⁶	4.0														
	1.5 × 10 ⁻⁶	5.0														
	1.2 × 10 ⁻⁶	6.0														
2,2'-Dipyridyl (dipy)	1.2 × 10 ⁻⁶	8.0														
	2.6 × 10 ⁻³	3.3														
	2.0 × 10 ⁻⁴	5.0														
	2.0 × 10 ⁻⁴	7.0														
[Ni(dipy) ₃] ²⁺	6.6 × 10 ⁻⁷	3.0	4.5 × 10 ⁻⁷	68.2	1.7 × 10 ⁻⁷	25.8	3.1 × 10 ⁻⁶	4.7	2.9 × 10 ⁻¹⁰							
	4.0 × 10 ⁻⁷	5.0	4.6 × 10 ⁻⁸	11.5	1.4 × 10 ⁻⁷	35.0	2.0 × 10 ⁻⁷	50.0	1.5 × 10 ⁻⁸							
	4.0 × 10 ⁻⁷	7.0	3.5 × 10 ⁻⁸	8.8	1.3 × 10 ⁻⁷	32.5	2.2 × 10 ⁻⁷	55.0	1.9 × 10 ⁻⁸							
	1.0 × 10 ⁻⁶	3.0	1.0 × 10 ⁻⁶	10.0	3.4 × 10 ⁻⁶	34.0	5.1 × 10 ⁻⁶	51.0	4.2 × 10 ⁻⁷							
[Ni(dipy) ₃] ²⁺	4.5 × 10 ⁻⁶	4.0	9.8 × 10 ⁻⁸	2.2	8.0 × 10 ⁻⁷	17.8	3.0 × 10 ⁻⁶	66.7	6.1 × 10 ⁻⁷							
	4.5 × 10 ⁻⁶	5.0	2.0 × 10 ⁻⁸	0.4	3.5 × 10 ⁻⁷	7.8	2.9 × 10 ⁻⁶	64.4	1.3 × 10 ⁻⁶							
	4.8 × 10 ⁻⁶	6.0	1.3 × 10 ⁻⁸	0.3	2.9 × 10 ⁻⁷	6.0	2.9 × 10 ⁻⁶	60.4	1.6 × 10 ⁻⁶							
	6.5 × 10 ⁻⁶	7.0	1.1 × 10 ⁻⁸	0.2	3.0 × 10 ⁻⁷	4.6	3.7 × 10 ⁻⁶	56.9	2.5 × 10 ⁻⁶							
1,10-Phenanthroline (phen)	3.0 × 10 ⁻⁶	2.0														
	1.5 × 10 ⁻⁶	3.0														
	1.0 × 10 ⁻⁶	4.0														
	1.0 × 10 ⁻⁶	6.0														
1,10-Phenanthroline (phen)	1.0 × 10 ⁻⁶	8.0														
	8.0 × 10 ⁻⁶	3.0														
	3.1 × 10 ⁻⁶	4.0														
	2.5 × 10 ⁻⁶	5.0														
[Ni(phen) ₃] ²⁺	3.1 × 10 ⁻⁶	7.0														
	6.0 × 10 ⁻⁸	3.0	3.2 × 10 ⁻⁸	53.3	2.2 × 10 ⁻⁸	36.7	5.5 × 10 ⁻⁹	9.2	3.9 × 10 ⁻¹⁰							
	1.0 × 10 ⁻⁷	5.0	7.4 × 10 ⁻¹⁰	0.7	9.0 × 10 ⁻⁹	9.0	4.0 × 10 ⁻⁸	40.0	5.0 × 10 ⁻⁸							
	1.0 × 10 ⁻⁷	7.0	3.5 × 10 ⁻¹⁰	0.4	5.8 × 10 ⁻⁹	5.8	3.5 × 10 ⁻⁸	35.0	5.9 × 10 ⁻⁸							
[Ni(phen) ₃] ²⁺	4.0 × 10 ⁻⁷	3.0	5.2 × 10 ⁻⁸	13.0	1.5 × 10 ⁻⁷	35.5	1.5 × 10 ⁻⁷	37.5	4.5 × 10 ⁻⁸							
	4.8 × 10 ⁻⁷	6.0			7.8 × 10 ⁻⁹	1.6	1.0 × 10 ⁻⁷	20.8	3.7 × 10 ⁻⁷							
	5.8 × 10 ⁻⁷	8.0			7.5 × 10 ⁻⁹	1.3	1.1 × 10 ⁻⁷	19.0	4.6 × 10 ⁻⁷							
	6.0 × 10 ⁻⁷	3.5	2.7 × 10 ⁻⁷	45.0	2.4 × 10 ⁻⁷	40.0	9.6 × 10 ⁻⁸	16.0	2.1 × 10 ⁻⁹							
Ni ²⁺ (in the presence of dipy) ^{max}	1.5 × 10 ⁻⁶	3.5	3.4 × 10 ⁻⁷	22.7	6.2 × 10 ⁻⁷	41.3	5.1 × 10 ⁻⁷	34.0	2.3 × 10 ⁻⁸							
	1.0 × 10 ⁻⁶	3.5	2.7 × 10 ⁻⁷	2.7	2.0 × 10 ⁻⁶	20.0	6.6 × 10 ⁻⁶	66.0	1.2 × 10 ⁻⁶							
	1.0 × 10 ⁻⁶	3.5	2.7 × 10 ⁻⁷	2.7	2.0 × 10 ⁻⁶	20.0	6.6 × 10 ⁻⁶	66.0	1.2 × 10 ⁻⁶							
	[Ni]:[dipy] = 1.3															

Table III: Infrared Frequencies from 700 to 800 cm^{-1} of 2,2'-Dipyridyl (dipy), Its Monoperchlorate, and Two of Its Metal Complexes as KBr Pellets

Species	Frequency, cm^{-1}			
	In the absence of $\text{AgBr}-\text{Br}^-$		In the presence of $\text{AgBr}-\text{Br}^-$	
dipy	741	757 ^a	739	758 ^a
dipy \cdot HClO_4	725	768 ^a		
$[\text{Ag}(\text{dipy})_2]^+$	741	757 ^a		
$[\text{Ni}(\text{dipy})_3]^{2+}$	730	779 ^a	738	778 ^a
$[\text{Ni}^{2+}] + [\text{dipy}] = 1:3$			738	778 ^a

^a Indicates the more intense band.

communication on this topic⁵ only the approximate calculations of the composition of the electrolyte environment were made. Particularly, the pH effect upon the protonation of the chelating agents was disregarded. Here, a rigorous analysis has been carried out and presented.

Table II shows that in the case of $\text{Ni}(\text{en})_3^{2+}$ the chelate is completely decomposed up to $\text{pH} \sim 5$ in concentrations corresponding to the ccc. The concentration of the free doubly protonated chelating species, enH_2^{2+} , equals the ccc of ethylenediamine when the latter is used alone. Thus under these conditions it is this species which coagulates the sol. At higher pH values there are two coagulating counterions, i.e., enH_2^{2+} and $\text{Ni}(\text{en})_3^{2+}$. The chelate must be a somewhat more efficient coagulant since the sum of the concentrations of the two species is less than the ccc of enH_2^{2+} alone.

Ni-dipyridyl and Ni-phenanthroline complexes represent a different case. These ions are only partly decomposed and the data in Table II would indicate that there is too little of the free ligand material to affect the sol stability. Ni-phen species coagulate apparently in the form of bis- and tris-complex ions, whereas the Ni-dipy complexes are predominantly in the form of mono- and bis-ions at the ccc. It is interesting that the sum of the concentrations of the coagulating counterions is reasonably constant over the pH range reported. The ccc is somewhat higher for the nickel-dipyridyl complex, but this is to be expected as the $\text{Ni}(\text{dipy})_2^{2+}$ ions adsorb less strongly on silver bromide particles (Figure 3). The reason that the Schulze-Hardy rule does not hold in these cases is explained by the exceptional adsorptivity of the coagulating complexes.¹⁴

The results presented in Figures 4 and 5 are of special interest. The addition of a very small amount of dipy

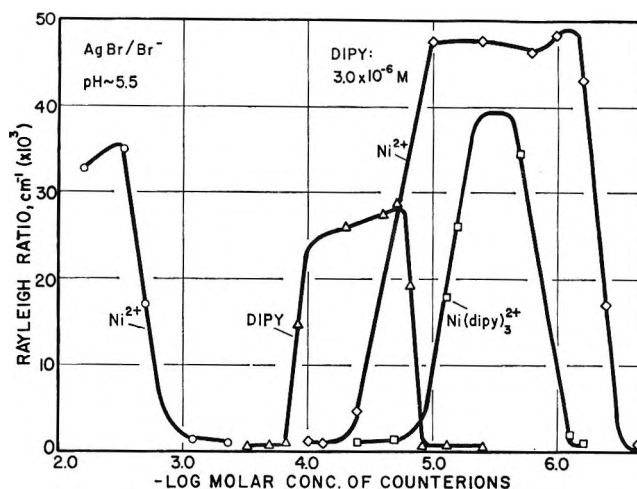


Figure 6. A comparison of coagulation curves for a silver bromide sol *in statu nascendi* (AgBr , $1.0 \times 10^{-4} M$; excess Br^- , $1.9 \times 10^{-3} M$) in the presence of $\text{Ni}(\text{NO}_3)_2$ (O), 2,2'-dipyridyl (Δ), $\text{Ni}(\text{dipy})_2^{2+}$ (\square), and $\text{Ni}(\text{NO}_3)_2$ at constant addition of 2,2'-dipyridyl ($3.0 \times 10^{-6} M$) (\diamond).

dramatically sensitizes the sol toward the Ni^{2+} ion. When the $[\text{Ni}^{2+}]:[\text{dipy}] = 1:3$ the sol behaves essentially as if the chelate were added directly. The restabilization is due to charge reversal. The last set of numbers in Table II indicates that the composition of the solution at the ccc and the csc indeed corresponds to the systems in which the nickel chelate is added to the silver bromide sol at the similar pH. Ir spectra show characteristic peaks of $\text{Ni}(\text{dipy})_2^{2+}$ for the absorbed species over the pH range 3-7 (Table III). These peaks become more intense as the pH rises. Thus the chelation has occurred at the interface and is responsible for the stability effects. Apparently, dipy adsorbs first and the complexation with Ni^{2+} follows.

When the concentration of dipy is held constant and the concentration of Ni^{2+} systematically changed, the unexpected minimum in electrophoretic mobility is found and no charge reversal takes place. It would seem that there is a competition for the dipy between the silver halide interface and the nickel ions in solution so that at higher nickel nitrate concentrations dipy adsorbs less strongly. At the moment it is not possible to say more about the mechanism of the effects involved in this case.

Figure 6 gives a summary of the results with Ni^{2+} , dipy, and the chelate at a constant pH. It is seen that the presence of the metal ion and the chelating agent exercises a considerably greater effect than when either of the components is alone in the system.

The Nature of Fresh Metal Surfaces in Aqueous Solutions

by Terrell N. Andersen, Jeffrey L. Anderson, and Henry Eyring

Institute for the Study of Rate Processes, University of Utah, Salt Lake City, Utah 84112 (Received February 21, 1969)

The surfaces of 24 different elemental metal electrodes were removed by scraping up to 500 times/sec and the fresh surface potentials were recorded. From the scrape potentials obtained in the solutions of varying pH and anion type and from the nature of the potential decays at the cessation of scraping it was concluded that the scrape potentials fit into one of two categories: (1) faradaic reactions charged the freshly formed surface so slowly that the scrape potential yielded the potential of zero charge; or (2) faradaic reactions occurred so rapidly on the fresh surface that the scrape potential was shifted, in some cases positively and sometimes negatively, away from the zero charge potential. On several of the electrodes the faradaic reactions were found to establish the potential faster than would have been predicted from kinetic data. The use of dimethyl sulfoxide instead of water apparently diminished but did not eliminate the rapid oxidation of the reactive metals by the solvent. For the nonreactive metals the pzc was used to deduce the relative adsorbabilities of halide ions on the various metals. These adsorbabilities showed no simple relationship to the covalent metal-halogen bond strengths.

I. Introduction

If a bare metal surface could be instantaneously exposed to an electrolyte, the open circuit metal *vs.* solution potential would be expected to change from zero with electrical double-layer formation and faradaic reactions. The potential change of such a system with time would be indicative of the relative relaxation times for the various charge-separation processes. In practice a finite time is required to renew an electrode surface, and hence the observed potential during such surface renewal is indicative of which relaxation processes are faster than surface renewal. That is to say, if the rate of double-layer formation is rapid and the rates of charge-transfer reactions are slow enough, then at surface renewal times between the relaxation times of the above processes, the potential of the renewed surface will be the potential of zero charge. Mercury streaming through a capillary into a nitrogen-saturated solution containing common salts such as NaCl or KI exemplifies this case. When surface renewal is discontinued, the potential shifts following the fastest faradaic reaction and finally comes to a steady state at an equilibrium or mixed potential (for example, the mercury electrode potential in chloride solutions is often found to come to a steady state near the mercury-calomel potential).

When the electrode-solution system contains substances which are oxidized or reduced faster than the surface can be renewed, the potentials observed during surface renewal do not represent "double-layer-controlled" potentials but are shifted from the potential of zero charge (pzc) according to the kinetics of the reactions. Thus the potential of the streaming mercury electrode in solutions containing MnO_4^- ions is positive of the pzc and is near the Hg-HgO potential.

In the present work the surfaces of solid metal electrodes were mechanically removed by scraping in various N_2 -saturated electrolyte solutions and the

potentials during and after such surface renewal were measured. Previous work¹⁻⁴ with several metals has shown that the potentials of the freshly produced surfaces correspond to the pzc for some metals over at least part of the pH range while for other metals the experimental rates of surface renewal were not great enough to outrun faradaic reactions. The present study includes many common metals not previously studied. Its purpose, therefore, is to compare all the present and past results in order (1) to establish the criteria for obtaining the pzc by the present surface renewal method and thus to be able to find the limitations of the method; (2) to obtain zero charge potentials for solid metals which have heretofore not been available and thus to provide preliminary information regarding specific adsorption of ions onto solid metal electrodes; and (3) to find from the scrape potentials and the potential decays after scraping which reactions are fastest on the more active metals; this information is relevant to the structure of the double layer as well as informative in relationship to the mechanism of metal oxidation.

II. Experimental Section

The metal surface along with its accompanying charge and double layer was removed by cutting (or scraping) with a sapphire or carborundum bit which was rotated in a dental handpiece. A wire was fitted into a Teflon sleeve with only its cross-sectional end exposed to the (N_2 -saturated) solution. This electrode surface, while submerged in the electrolyte, was re-

(1) T. N. Andersen, R. S. Perkins, and H. Eyring, *J. Amer. Chem. Soc.*, **86**, 4496 (1964).

(2) D. D. Bodé, Jr., T. N. Andersen, and H. Eyring, *J. Phys. Chem.*, **71**, 792 (1967); D. D. Bodé, Jr., Ph.D. Thesis, University of Utah, 1966.

(3) T. N. Andersen, J. L. Anderson, D. D. Bodé, Jr., and H. Eyring, *J. Res. Inst. Catalysis Hokkaido Univ.*, **16**, 449 (1968).

(4) R. S. Perkins, Ph.D. Thesis, University of Utah, 1967.

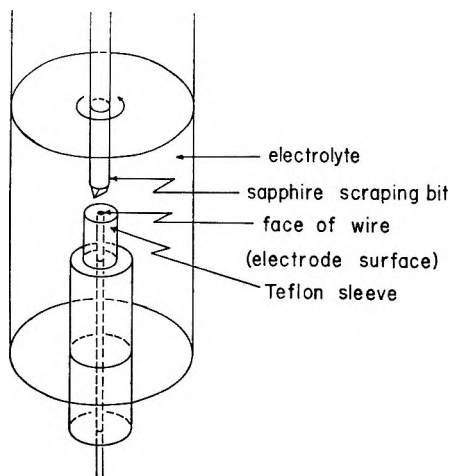


Figure 1. Schematic cell assembly showing wire electrode in Teflon sleeve and its positioning for cutting off the electrode surface.

moved completely by the rotating bit (see Figure 1) at speeds of up to 400 rps.^{5a,b} Thus the maximum rate of surface renewal should be twice per revolution of the bit (see Figure 1). The effectiveness of the scraper in removing the entire surface was shown by the fact that the wire was consumed (shortened) at rates of the order of 1 mm/sec (the exact value depended on the hardness of the metal, the scraper speed, and the pressure of the scraper on the wire surface). The effectiveness in cleanly cutting off the surface was also shown by the fact that the scraped metal was disintegrated into tiny chips or powder in the solution. In previous work,² the effective rate of surface removal was shown to be approximately that expected from the speed of the cutter by comparing the potential change due to a fast reaction (H_3O^+ reduction on silver) with that expected on the basis of the reaction rate, electrode capacity, and scraping speed measured with a strobe light.

The electrode potential during and after scraping was measured with respect to a saturated calomel electrode which contacted a side compartment of the cell through an agar-saturated KCl salt bridge. This side compartment of the cell contacted the experimental compartment through a stopcock, the results not seeming to matter whether the latter was open or closed, since the voltage measuring instrument had an input impedance of 10^9 ohms and since the experiments were not of long enough duration for a significant amount of chloride ions to diffuse to the main cell compartment. Either an amplifier-recorder assembly of balance time $1/120$ sec or an oscilloscope was used to record the potential-time transients, so the relative decay rates could readily be determined. The measured potentials are recorded relative to the normal hydrogen electrode (nhe) without any correction for liquid junction potentials. The latter are presumed small compared to the precision of the results. The temperature was 25° for all the

experiments. The metals were generally of the highest purity obtainable which was 99.99% or 99.999% pure for the noble and the softer, less-noble metals (e.g., In, Ga, Tl, etc.). For a few cases (e.g., Bi, Pt, and Au) metals of lower purity (99.9%) were also studied and yielded the same results as did the high-purity material. For some of the active metals (e.g., Ti, Fe, V) the purity was only $\sim 99.9\%$. The carbon electrode consisted of a pyrolytic graphic rod. Aqueous solutions were prepared from reagent grade chemicals and water bidistilled from a basic permanganate solution. For the nonaqueous solutions either dimethyl sulfoxide (DMSO) containing less than 0.03% water or absolute ethanol was used without further purification.

III. Experimental Results and Discussion

A. *General.* The general appearance of the data is shown by the particular potential vs. time transients shown in Figure 2. When the electrode was scraped the rest potential abruptly shifted negatively to a plateau or series of plateaus (the scrape potential or V_{sc}). This shift in potential follows the replacement of the initial surface, with its accompanying charge and double layer, by the fresh surface with its different charge and double layer. A very few scrapes undoubtedly effect this change such that in the potential recording of Figure 2 the change appears as discontinuous. A minor fraction of the peaks, which resulted from incomplete scraping of the surface, were less

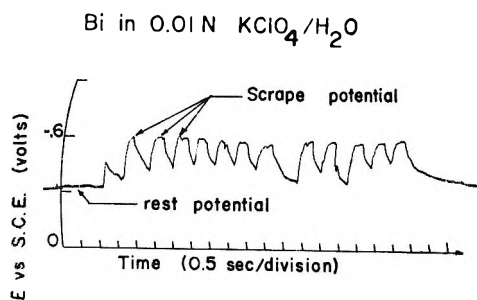


Figure 2. Recorder trace of scrape transients.

(5) (a) Antimony was only available in lump form and therefore the experimental setup was different for it than for the other metals. The Sb was covered with a film of epoxy cement and the scrape potential was measured as scraping first occurred through this film. The presence of epoxy cement next to a scraped electrode has been shown to alter the results on Pt but not on Au. Since Sb is not a highly surface-active, catalytic metal, it was presumed that the epoxy did not seriously affect the scrape potential. (b) The rapidly moving electrolyte is thought to adequately maintain the temperature of the electrode surface within a few degrees of the temperature of the bulk solution during scraping. There are several evidences for this conclusion. (i) Ga metal shows no evidence of melting near the bit when scraped in a solution at $T = 25^\circ$ (the mp of Ga is 29.8°). (ii) The pzc of Ga obtained in this work is almost identical with those precise values obtained by static methods. (iii) When the scraping bit is removed from the electrode, no abrupt change in potential is noted as might be expected if a hot surface were quickly cooled by the solution. Rather the potential changes in accordance with the expected reaction rates, as much of this paper points out. (iv) Estimates of the surface temperature made through friction calculations (R. S. Perkins, personal communication) indicate that very small changes (the order of a few degrees) would be expected to accompany the scraping.

negative than the true fresh-surface potential, but these erroneous potentials could readily be discovered. At the cessation of scraping the potential decayed positive to a steady-state value. The impurity O_2 in the cell (the cell was closed and saturated with 99.996% pure N_2) seemed to be responsible for the slow decays observed for many of the systems. The oxygen was not present in high enough concentration to affect the scrape potential as could be shown both experimentally (by making small variations in P_{O_2}) and theoretically through calculations of the limiting current of O_2 . When water or H_3O^+ ions underwent rapid reduction at V_{sc} , the observed decays were more rapid. In some cases no significant decays were observed due to the rapid dissolution of the metal causing a reversible potential (*i.e.*, $M-M^{+n}$) to be established at some local concentration of metal ions. The nature of the decays and the rest potential were thus of use in the interpretation of the scrape potentials.

From double-layer studies on other metals the time for solvent-dipole orientation and the specific adsorption of ions (from solutions of the concentrations considered here) is expected to be very rapid compared to the present rate of surface renewal; *i.e.*, the time for water dipole relaxation is the order of 10^{-8} sec for Hg and 10^{-7} sec for Cu.⁶ Specific adsorption of common ions is found to reach equilibrium in less than 10^{-5} sec on Hg⁷ and to be diffusion-controlled on smooth Pt.⁸ In consideration of these findings and the present electrolyte concentrations and stirring rates, the present scrape potentials are expected to be controlled solely by equilibrium adsorption and/or by faradaic reactions. The scrape potentials obtained in all the solutions studied as well as the potential decay data are consistent with this conclusion (*i.e.*, even for metals on which the reactions and corresponding decay were very slow, such as gold, the decay was never negative indicating an increase in anion adsorption with time). From the above evidence we conclude that the scrape potential is the potential of zero charge, if the rate of removing the surface is fast enough to suppress the effects of double-layer charging by faradaic reactions. If faradaic reactions cannot be outrun, the scrape potential may be a Nernst potential, a mixed potential, or a potential between the pzc and a steady-state potential, depending on the rates of the electron-transfer reactions. A decision as to which case prevails rests with the deduction of which reactions (if any) can determine the results. If no known or conceivable reactions can account for the results, but if the scrape potentials are in accordance with the expected potential of zero charge, then one is compelled to identify the fresh surface potentials or V_{sc} with the pzc. The interpretation of the results is best demonstrated by the consideration of the specific results for several systems.

B. Phenomenology of Results for Several Metals. Indium. Figure 3 shows the scrape potentials as a

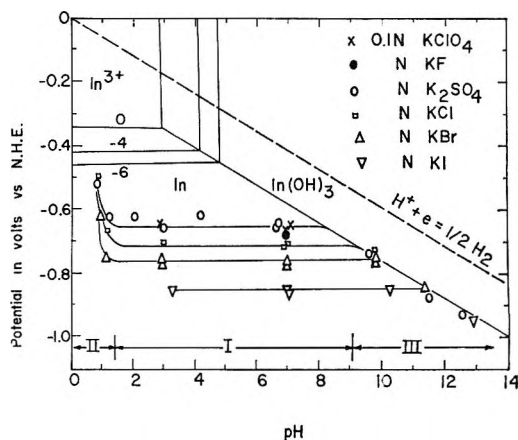


Figure 3. Scrape potential (points) of In in various aqueous salt solutions to which NaOH or H_2SO_4 was added to adjust the pH. Superimposed are equilibrium potential *vs.* pH diagrams for $In-In^{3+}$, $In-In(OH)_3$ and $H^+ + e = 1/2 H_2$ couples. Potential control: region I, pzc; regions II and III, reactions (see text).

function of pH for indium in various solutions. Superimposed on the experimental points are the equilibrium potential *vs.* pH lines for various reactions which may possibly occur and help to determine the potential. The scrape potentials may be classified into three pH regions: (I) from $pH \approx 1$ to 8–12 (depending on the anion present) V_{sc} is found to be independent of pH but to increase negatively with a change in anion in the order $F^- = SO_4^{2-} = ClO_4^- < Cl^- < Br^- < I^-$; (II) in the acidic range ($pH < 1$), V_{sc} increases positively with an increase in H_3O^+ ion concentration, and (III) in the basic pH region V_{sc} is found to follow the $In-In(OH)_3$ line, independent of the anion present. The following observations lead to the conclusion that the intermediate pH values (region I) of V_{sc} correspond to the pzc: (a) V_{sc} is independent of scraping speed and the potential decays very slowly to steady-state values near -0.44 V (reduction of impurity O_2 and oxidation of the In seemed responsible for the decay and steady-state potential); (b) the V_{sc} values are independent of pH and dependent on the anion in the manner expected for the pzc; (c) there are no Nernst potentials or mixed potentials close enough to V_{sc} to reasonably control this potential; *i.e.*, for V_{sc} to equal E° for the $In-In^{3+}$ couple would require In^{3+} ion concentrations of less than 10^{-14} M. It is highly unlikely that the exchange current is great enough that a redox couple at such low activities could outrun the scraping speed (which can outrun reactions of the order of 10^{-4} A/cm²). It would also not appear likely that a couple involving a lower

(6) J. O'M. Bockris and B. E. Conway, *J. Chem. Phys.*, **28**, 707 (1958).

(7) V. I. Melik-Gaikazyan, *Zh. Fiz. Khim.*, **26**, 560 (1952); A. N. Frumkin and V. I. Melik-Gaikazyan, *Dokl. Akad. Nauk SSSR*, **77**, 855 (1951).

(8) S. Gilman, *J. Phys. Chem.*, **68**, 2098, 2112 (1964).

oxidation state of indium could be responsible for V_{sc} since the couple $\text{In}-\text{In}^+$ has an equilibrium potential of -0.16 V ,⁹ a value more positive than that for $\text{In}-\text{In}^{3+}$; (d) the present scrape results give very reasonable values for the pzc based on electrocapillary studies of In in molten salts as well as on the electronic work function of In and the pzc vs. work function relationship.¹⁰ From the present work the potential of zero charge of In is thus found to be -0.65 , -0.71 , -0.76 , and -0.85 V (nhe) for 1 N K_2SO_4 , KCl , KBr , and KI , respectively.

In region II of Figure 3 the positive decay becomes extremely rapid as the pH is lowered, and the observed scrape potentials are positive of the pzc because H_3O^+ ion reduction consumes electrons, leaving the electrode charge, q_m , positive at the measured scrape potentials. These scrape potentials in acid solutions decay only a few tens of mV—to values near -0.42 ; the latter steady-state values can be rationalized by the simultaneous oxidation of In and reduction of H_3O^+ ions (or the simultaneous reduction of local In^{3+} ions).

As the pH of the solution becomes great enough that the pzc intersects the $\text{In}-\text{In}(\text{OH})_3$ line, the oxidation of In occurs so rapidly that the Nernst potential is established faster than the surface can be renewed. The potential decay is slow for region III and appears to be due to the reduction of impurity O_2 . This decay must be made possible by the passivation of the surface as the oxide thickens, such that the $\text{In} \rightarrow \text{In}(\text{OH})_3$ reaction slows down.

Bismuth. Figure 4 shows the scrape potentials for Bi in various solutions as a function of pH. Superimposed on this figure are the potential vs. pH values for several relevant redox couples.¹¹ The scrape potentials show the same characteristics as those for In and we accordingly interpret the V_{sc} values from pH 2 to 12 as the pzc, while for $\text{pH} < 2$ the reduction of H_3O^+ ions occurs so rapidly that it shifts V_{sc} positive of the pzc. The very rapid potential decays in the latter region substantiate this interpretation. The pzc intersects the bismuth oxide lines only at $\text{pH} > 12$ and hence the pzc is observed over a very long pH range. Higher oxides of bismuth (*e.g.*, Bi_2O_7 , Bi_2O_4 , and Bi_2O_5) are stable only at potentials very positive of the $\text{Bi}-\text{Bi}_2\text{O}_3$ line¹¹ and are hence not shown in Figure 4. Also the standard potentials for the $\text{Bi}-\text{Bi}^{3+}$ and $\text{Bi}-\text{BiO}^+$ or $\text{Bi}-\text{BiOH}^{2+}$ couples would seem to be too positive (E_0 for $\text{Bi}-\text{Bi}^{3+} = +0.215\text{ V}$)¹¹ to play any part in determining V_{sc} , and are likewise not shown in Figure 4. The values of the pzc found here for Bi are -0.35 , -0.42 , -0.48 , and -0.64 V (nhe) for 1 N K_2SO_4 , KCl , KBr , and KI , respectively. Our value for the pzc in solutions of little specific adsorption are in agreement with values found from the immersion (-0.36 V)¹² and capacitance (-0.4 V)¹³ methods.

Cadmium. In the case of many of the metals studied it appears that various reactions determine the potential

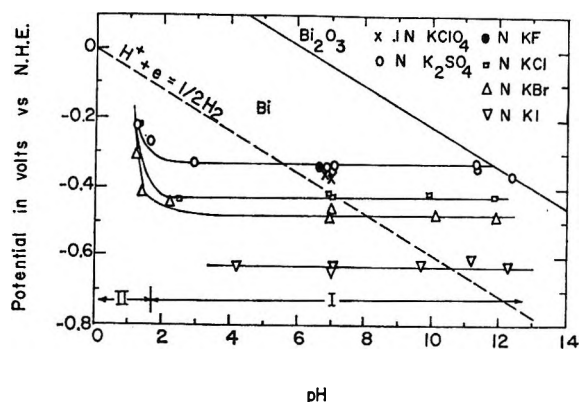


Figure 4. Scrape potential (points) vs. pH for Bi in aqueous salt solutions shown. pH was adjusted by addition of NaOH or H_2SO_4 . Superimposed are equilibrium potential vs. pH lines for H^+-H_2 and $\text{Bi}-\text{Bi}_2\text{O}_3$. Potential control: region I, pzc; II, reactions.

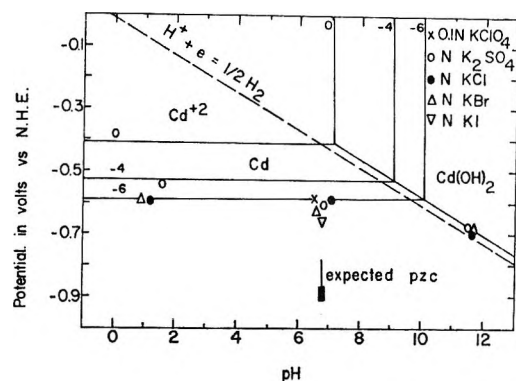


Figure 5. Scrape potential (points) of Cd in aqueous solutions listed. Also shown are equilibrium potential vs. pH lines for redox couples. The range of pzc values obtained by independent methods¹⁴⁻¹⁶ is shown as vertical line.

and the pzc is not obtained over any of the pH range. Such behavior is demonstrated by cadmium, the results being shown in Figure 5. Although the values of V_{sc} are relatively insensitive to pH in the acidic and neutral range, they are also independent of the anion type. Furthermore, there is no potential decay in acidic solutions and only a short (less than 100 mV) one in neutral and basic solutions. Thus the scrape potential and steady-state potential in acid and neutral solutions are both controlled by the $\text{Cd}-\text{Cd}^{2+}$ couple, the local concentration of the Cd^{2+} ions being approximately 10^{-6} M . In basic solutions for which the $\text{Cd}-\text{Cd}^{2+}$ line intersects the $\text{Cd}-\text{Cd}(\text{OH})_2$ line, the $\text{Cd}-\text{Cd}(\text{OH})_2$

(9) B. Miller and R. S. Visco, *J. Electrochem. Soc.*, **115**, 251 (1968).

(10) A. N. Frumkin, *Svensk Kemisk Tidskrift*, **77**, 300 (1965).

(11) J. van Muylder and M. Pourbaix, CEBELCOR, Rappt. Tech. No. 48, 1, (1957); International Committee for Electrochemical Thermodynamics and Kinetics, Vol. 9, 1957, pp 49, 50.

(12) B. Jakuszewski and Z. Kozłowski, *Rocz. Chem.*, **36**, 1873 (1962).

(13) U. Palm, V. Past, and R. Pullerits, *Elektrokhimiya*, **2**, 604 (1966).

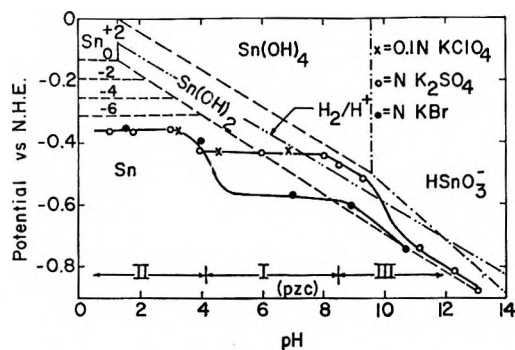


Figure 6. Scrape potential (points) vs. pH for Sn in aqueous solutions shown. pH was adjusted by addition of NaOH or H₂SO₄. Superimposed are equilibrium potential vs. pH lines for various redox couples.^{16b} Potential control: region I, pzc; II and III, reactions (see text).

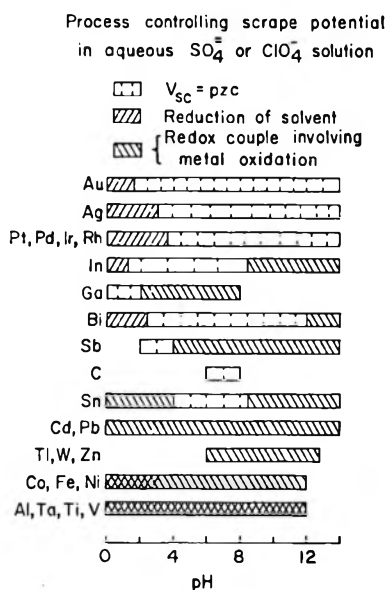


Figure 7. Factors controlling scrape potential as a function of pH for metals studied.

potential is established. It is also noted that the reported values of the pzc^{14-16a} obtained by the capacity method (see Figure 5 for values) are significantly negative of the presently obtained values of V_{sc} .

Tin. Figure 6 shows the scrape potentials for tin, superimposed on several potential vs. pH equilibrium lines.^{16b} The results for tin are similar to those for In and Bi except that in the acid region the scrape values do not shift sharply positive with an increase in H₃O⁺ ion concentration. In this region there is little or no decay and no dependence of V_{sc} on the anion present, so the potentials are reaction rate controlled but the reduction of H₃O⁺ ions is not one of the fast reactions. The pzc for Sn obtained in neutral solutions is -0.44 V for 1 N K₂SO₄ and -0.58 V for 1 N KBr. In the literature the values reported are -0.38 V (from the immersion method¹²), -0.24 V (from electrode deformation¹⁷), and -0.43 V (from the capacity method¹⁸).

C. Summary of Results for All Metals Studied. The fresh surface potentials for the various metals are categorized in Figure 7 according to which factors control the observed scrape values. "Solvent reduction" is only listed for those metals on which an active production of hydrogen is obvious, i.e., for the cases in which (a) a very rapid positive decay occurs following the scraping, or (b) V_{sc} is significantly positive of the standard reversible metal-metal ion potential (the local concentration of metal ions cannot be many times greater than 1 M), or (c) V_{sc} increases with an increase in concentration of H₃O⁺ ions. In other cases, however, a very rapid reduction of the solvent appears to help establish the double layer and the initial concentration of metal ions outside the metal, although hy-

Table I: Scrape Potentials, V_{sc} , of Various Metals in 1 N NaClO₄ or K₂SO₄ Solutions at Various pH's. Values Interpreted as the Pzc are Italicized

Metal	pH ≈ 1	pH ≈ 7	pH ≈ 11
Ag	-0.60	-0.64	-0.64
	(pH = 1.7)		
Al	-1.24	-1.56	-1.58
Au	0.13	0.12	0.05
Bi	-0.15	-0.34	-0.34
C		-0.26	
Cd	-0.56	-0.59	-0.68
Co	-0.26	-0.42	-0.47
	(pH = 1.8)		
Fe	-0.31	-0.64	-0.65
Ga	-0.63	-0.86 ^a	
In	-0.60	-0.65	-0.83
Ir	0.21	-0.04	-0.17
Ni	-0.10	-0.34	-0.46
Pb	-0.30	-0.37	-0.40
Pd		0.00	
Pt	0.24	0.02	-0.30
Rh	0.17	-0.02	-0.36
Sb	-0.11	-0.28	-0.50
Sn	-0.36	-0.43	-0.79
Ta	-0.48	-0.78	-1.10
Ti	-0.93	-1.19	-1.19
Tl		-0.56	-0.56
V	-0.59	-0.98	-1.07
	(pH 1.8)		
W		-0.47	
Zn		-0.92	

^a Value from G. J. Clark, University of Utah, unpublished results.

(14) T. I. Borisova and B. V. Ershler, *Zh. Fiz. Khim.*, **24**, 337 (1950).

(15) V. L. Kheffets and B. S. Krasikov, *Dokl. Akad. Nauk SSSR*, **109**, 586 (1956); *Zh. Fiz. Khim.*, **31**, 1992 (1957).

(16) (a) N. A. Hampson and D. Larkin, *J. Electrochem. Soc.*, **114**, 933 (1967); (b) P. Delahay, M. Pourbaix, and P. van Rysselberghe, *International Committee for Electrochemical Thermodynamics and Kinetics*, Vol. 3, 1952.

(17) E. K. Venstrum and P. A. Rebinder, *Zh. Fiz. Khim.*, **26**, 1847 (1952).

(18) N. A. Hampson and D. Larkin, *J. Electrochem. Soc.*, **115**, 612 (1968).

drogen does not appear to be liberated at V_{sc} . Table I lists the scrape potentials for the various metals in normal potassium sulfate or perchlorate solutions at pH values which are acidic ($\text{pH} \approx 1$), neutral, and basic ($\text{pH} \approx 11$). (To present the complete V_{sc} vs. pH profiles would be very cumbersome; some complete V_{sc} vs. pH profiles may be found in ref 2 and 3). The values of V_{sc} which are considered to be the pzc are italicized.

The boundary (pH value) between pzc values and reaction-controlled values varies with the type of anion studied as is demonstrated in Figures 3 and 4. Therefore Figure 7 corresponds to 1 N KClO_4 or K_2SO_4 solutions.

Certain of the electrodes were not studied over the entire pH range as shown by incomplete data representation. In the cases of Tl, W, and Zn the V_{sc} values in the acidic range are expected to be controlled by metal oxidation with perhaps some solvent reduction. The studies on carbon were limited to neutral solutions because of time and technical difficulties in obtaining data; however, it is felt that these measurements could profitably be extended to acidic and basic solutions.

These results of Figure 7 were deduced from a detailed comparison of the scrape potentials in solutions of varying pH and anion type with potential vs. pH diagrams (of the type shown in Figures 3-6) and from the nature of the decays. In most cases the interpretation of V_{sc} could be readily made on the basis of each of the following criteria: comparison with equilibrium potentials, anion effects, potential decays, and comparison with expected potentials of zero charge. Thus, the values which yield zero charge potentials (*cf.* Figure 6 and Table I) are typified by the following five effects. (1) The potential decay is slow enough that it does not change significantly in the time of the fresh surface exposure and yet decays far enough (*e.g.* $\gtrsim 200$ mV) that V_{sc} does not appear to be due to a steady-state mixed potential. (2) A definite negative shift of V_{sc} occurs with more adsorbable anions. (3) An independence of pH is observed through some intermediate pH range. It should be noted that even when metal oxidation is very slow, hydroxide ion adsorption is found to shift the pzc negative depending on the metal and the OH^- ion concentration. (4) The scrape potentials yield values which cannot be reasonably rationalized by Nernst potentials (at some local concentration of ions at values greater than *ca.* 10^{-8} M) or mixed potentials. (5) The scrape potentials of the pzc agree with the literature values obtained by other means. References 10 and 19 record these values.

When V_{sc} does not equal the zero charge potential, it is because of rapid metal oxidation or of solvent reduction or of both. When only solvent reduction outruns surface renewal, the scrape potential shifts positive with an increase in acidity. This is indicated in Figure 7 by shading having a positive slope. Decay is very

rapid in most of these cases (*i.e.*, for Au, Ag, Bi, In) showing that H_2 is evolved. For the Pt metals, however, the potential decays are very slow, indicating that the equilibrium ($\text{H}^+ + e \rightleftharpoons \text{H}_{ads}$) is established rapidly while the desorption of H_2 is slow compared to the scrape time.

For all the fresh surfaces involving rapid metal oxidation, the scrape potential coincides with the metal-metal hydroxide couple, the metal-metal ion (with $C_{M^{+n} \text{ ion}} = 10^{-3}$ to 10^{-7} M) couple, or with a mixed potential lying between the metal oxidation and the H_3O^+ ion reduction couples. These values were usually outside the potential range expected for the pzc, although for a few metals such as Co and W this was not so. If the values of V_{sc} left doubt as to whether they were the potentials of zero charge, the anion effects resolved this question. For all the systems involving rapid metal oxidation the scrape potential was practically independent of the type of anion involved. The diagonal shading in Figure 7 having a negative slope is used to indicate this case. The rates of decay of V_{sc} are not shown but they also helped in identifying the electrode mechanisms; *i.e.*, several of the metals show little (< 100 mV) or no decay of potential. Examples of this are Fe, Ni, Sn, Pb, and Cd in acid solutions. This indicated that scraping was too slow to upset the dynamic steady-state making up the mixed potential. The small decay that was observed probably represented a readjustment of local concentrations of ions with changes in the stirring rate since the stirring was slower after discontinuing scraping. On the other hand, rapid decay was observed for the very negative scrape potentials of Al, Ti, Ta, and V in both acidic and neutral solutions. This indicates that the rapid reduction of H_3O^+ or H_2O continues even after the self-protective oxide films have reformed, slowing down the formation of metal ions. For a large number of the systems (*e.g.*, Ni, Co, W, and Tl in nonacidic solutions, and Ti in basic solutions) the decay was slow as observed earlier in the case of metals yielding the pzc in nonacidic solutions. Although these slow decays were of no particular diagnostic value in identifying V_{sc} , they do exemplify the fact that metal oxidation decelerates markedly as the oxide thickens. This allows the potential to be shifted positively by the reduction of O_2 .

IV. Discussion of Results

A. *Condition for Obtaining Pzc as Scrape Potential.* One of the purposes of this study was to establish a method of predicting from known kinetic information whether or not the pzc could be obtained for any given metal by the scrape method. The last section indicated that the only reactions of significance at the

(19) R. S. Perkins and T. N. Andersen in "Modern Aspects of Electrochemistry," Vol. 5, J. O'M. Bockris and B. E. Conway, Ed., Plenum Press, 1969.

potentials in question are the reduction of H_3O^+ ions or H_2O and the oxidation of the metal. If these reactions are measured to be slower than approximately 10^{-4} A/cm² (which velocity can change the potential of an electrode of capacity = $30 \mu\text{F}/\text{cm}^2$ by only a few millivolts in the scrape time) at the pzc, one would expect V_{sc} to equal the pzc.

For those cases in which the zero charge potential is obtained as V_{sc} the reactions in question are predicted from kinetic data to be slower than 10^{-4} A/cm²; *i.e.*, the metal oxidation line is so far positive of the pzc that the rate of metal oxidation is inhibited by the negative potential at the pzc, even if the standard rate constant is substantial (*e.g.*, 1 A/cm²). Likewise, the rate of hydrogen evolution is reported to be very low at the potentials presently obtained as the pzc.^{20,21}

On the metals for which scraping does not yield potentials of zero charge there are some anomalies to classical kinetics, however. For example, the rates of dissolution for Fe, Ni, and Co are measured by polarization curves to be slow ($i^\circ \simeq 10^{-8}$ A/cm²),^{22,23} and yet the reversible metal-metal ion couples are established in less than the scrape time in our work; the actual rates must accordingly be many orders of magnitude greater than 10^{-8} A/cm². This suggests that there are inhibiting films or layers of molecules on these (and probably other) active metals such that the slow step in metal oxidation is not the transfer of an ion to the solution from a bare metal. Another anomaly concerns the fact that the predicted pzc on Tl, Cd, Sn (in acid), and Pb are very negative of the reversible metal-metal ion potentials while the measured rate of H_3O^+ ion or H_2O reduction is slow—yet $V_{\text{sc}} \neq \text{pzc}$. For all the other metals on which V_{sc} corresponds to reaction control, the pzc is positive of the observed potential. Thus the manner of double-layer establishment on all the active metals except the above 4 is understandable on the basis of the bare metal (at zero charge) rapidly oxidizing, and giving ions to the solution; this causes the charge and potential to shift negatively until the rate of metal oxidation is balanced by the rate of metal ion reduction plus hydrogen atom production (when possible). On Cd, Pb, Tl, and Sn an initial reduction process is necessary to charge the double layer from the pzc to the more positive reversible potential observed at V_{sc} . Thus we conclude that H atoms must be discharged on these metals very rapidly in order to bring V_{sc} from the pzc positive to the metal-metal ion potential and also in order to counteract the negative charge produced by the production of the local concentration of metal ions. Calculations show that this latter quantity of charge is very small. Since kinetic measurements show the rate of H_3O^+ ion reduction to be very small ($<10^{-4}$ A/cm²) at the overvoltages corresponding to the pzc, we conclude that there must be active sites on these fresh, bare metal surfaces at which H may be taken up very rapidly and irreversibly (since

there is no evidence from capacity measurements of a fast, reversible reaction at these potentials). The current for anodic stripping of such a small amount of H ($<10 \mu\text{C}/\text{cm}^2$) would be masked by oxidation of the metal itself. The possibility of the adsorption of H^+ ions on the hydrated metal surface (analogous to that on metal oxides) also should not be ruled out, since the scrape potentials are somewhat more positive in acidic than in neutral solutions for Cd, Pb, and Sn. This same H^+ ion adsorption may well occur on other metals also (such as Fe, Co, and Ni) but its effect on V_{sc} is not outstanding since other fast reactions also occur.

B. Attempts to Outrun Oxidation Reaction. It would be desirable to expand the list of metals for which the pzc was obtained by scraping. The natural direction to go, attempting this, would be to increase the rate of surface renewal. This was attempted with a faster handpiece (rated speed of 300,000 rpm). Preliminary studies on some of the active metals have shown no difference in the results obtained with the two drills. This may be due to the interfering reactions being significantly faster than the new, faster surface renewal times. There are, however, mechanical problems associated with the faster drill such as a slowing down (loss of speed) when contact is made with the electrode, and bubble formation on the electrode at the higher speeds. More meaningful attempts than these are the work of Hagyard and coworkers^{24,25} in which some plastic-coated metals have been scratched with a ruby wedge in times of the order of microseconds. In the case of aluminum the above workers²⁴ obtained potentials of -1.6 V (nhe) and apparently outran the hydrogen evolution reaction, but not the aluminum oxidation equilibrium. In their scratching of cadmium,²⁵ they obtained values equal to ours. We attempted to perform experiments similar to the above ones of Hagyard and coworkers using a lead electrode (we did not measure the actual time of surface renewal, however). Our scratch potentials agreed with our former scrape potentials. Photographic work by the above workers indicated that the slow step in the process was apparently the coating of the fresh surface with solution. These results indicate that the rates at which metal ions jump into the solution are so great that the presently available mechanical attempts to outrun many of such reactions are futile.

(20) K. J. Vetter, "Electrochemical Kinetics," Academic Press, New York, N. Y., 1967, Chapter 4.

(21) A. N. Frumkin, *Advan. Electrochem. Electrochem. Eng.*, **3**, 287 (1963).

(22) J. O'M. Bockris, "Modern Aspects of Electrochemistry," Vol. 1, J. O'M. Bockris and B. E. Conway, Ed., Butterworth and Co., Ltd., London, 1954, Chapter 4.

(23) R. Piontelli, "International Committee for Electrochemical Thermodynamics and Kinetics," Vol. 2, 1950, p 136.

(24) T. Hagyard and J. B. Williams, *Trans. Faraday Soc.*, **57**, 2288 (1961).

(25) T. Hagyard and K. M. Chapman, *J. Electrochem. Soc.*, **113**, 961 (1966).

A second attempt to outrun faradaic reactions consisted of scraping of the electrodes in dimethyl sulfoxide (DMSO) and absolute ethanol solutions, our hope being that these solvents (or at least DMSO) would not deprotonate and hence would not accept metal ions as rapidly as water. The scrape potentials in these solvents (in solutions of potassium perchlorate) are compared to those in water in Figure 8. Also shown are the pzc of the streaming Hg electrode in aqueous and DMSO solutions. The latter value is taken from the work of Payne.²⁶ Potassium perchlorate was chosen as the solute in all cases in order to minimize ionic specific adsorption. The results in ethanol are similar to those in water, as one might expect. In DMSO one notes two general features of the scrape potentials: (1) the order of V_{sc} with respect to the metal is similar to that in water except for a few inactive metals, and (2) for most metals V_{sc} in DMSO is approximately 100 to 200 mV more negative than V_{sc} in water. Since the order of V_{sc} with respect to the metal does not change in the case of active metals, we can presume that these metals still oxidize in the DMSO (*i.e.*, if the reactions had been completely outrun one might expect some of the metals to change their order from the values in H_2O). That the values in DMSO are negative of those in H_2O is in accord with the fact that DMSO is less reactive than water and does not give up its hydrogen as easily. Thus the potentials in DMSO correspond to less metal ions in solution than do those in water. On the noble metals the differences in potential in the two solvents would seem to reflect the different relative orientation of the two solvent molecules on the metals (coupled with the fact that the dipole moment is larger for DMSO than for H_2O). Also some hydrogen may go into some of the noble metals at the pzc in water, causing an additional positive shift of potential.

C. Estimation of Relative Specific Adsorption of Halide Ions on Various Metals. The shift of the zero charge potential in various solutions of adsorbable ions can be used to estimate the amount of ionic adsorption. On Hg in aqueous solutions this shift of the pzc, ΔE_z , can be correlated with the amount of adsorption of the halides through the expression (*e.g.*, see ref 19)

$$\Delta E_z = E_{z,ads} - E_{z,0} = \frac{4\pi q_1 d_{1-2}}{\epsilon_{1-2}} + \Delta\phi_{diffuse} \quad (1)$$

or if we can neglect $\Delta\phi_{diffuse}$ because of high electrolyte concentration

$$\Delta E_z \text{ (volts)} = \frac{0.113 q_1 (\mu C \text{ cm}^{-2}) d_{1-2} (\text{\AA})}{\epsilon_{1-2}} \quad (2)$$

Here q_1 is the amount of specifically adsorbed charge, d_{1-2} is the distance between the inner and outer Helmholtz planes, and ϵ_{1-2} is the dielectric constant in the region between the Helmholtz planes. If d_{1-2} is taken

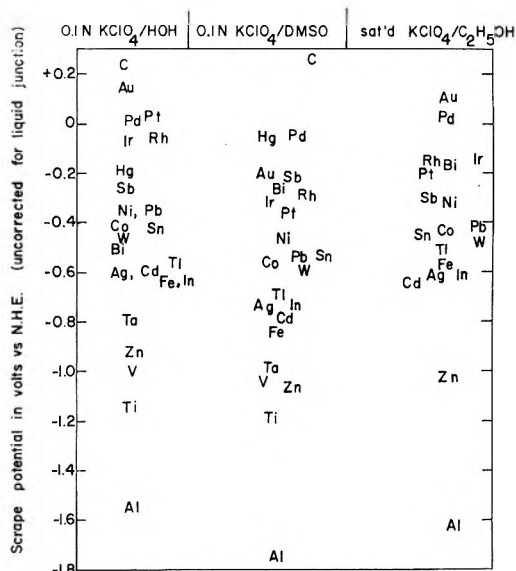


Figure 8. Scrape potential for various metals in solutions of $KClO_4$ in water, dimethyl sulfoxide (DMSO), and ethanol. Also shown are potential of streaming mercury electrode in H_2O and DMSO.²⁶

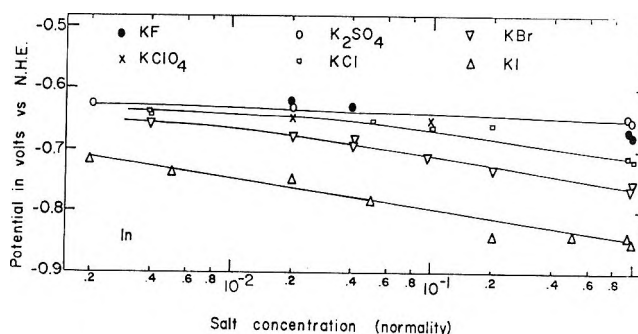


Figure 9. Scrape potential of In in aqueous salt solutions of varying concentrations.

as $4 \text{ \AA} - r_1$ (r_1 = the radius of the adsorbed ion), the appropriate value of ϵ_{1-2} is approximately 10.

In this work we have considered the shift of the pzc caused by 1 *N* concentrations of Cl^- , Br^- , and I^- ions. The shift of the zero charge potential is taken as the difference between the pzc in the given solution and that in dilute ($\sim 10^{-3}$ *N*) sulfate or perchlorate solutions. Figures 9 and 10 show that the change of pzc (scrape potential) with salt concentration for In and Bi is very slight for SO_4^{2-} and ClO_4^- solutions such that these ions appear to be only slightly adsorbed. For other metals the same observation is made (for some metals ClO_4^- is somewhat adsorbed).

The shift of the pzc due to 1 *N* halide solutions is shown in Figure 11 for various metals. The data were taken from the work of other investigators for Cu,²⁷ Tl,²⁸ and Hg.²⁹

(26) R. Payne, *J. Amer. Chem. Soc.*, **89**, 489 (1967).

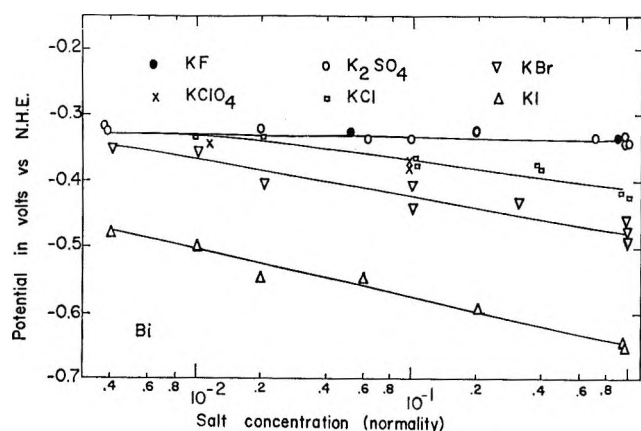


Figure 10. Scrape potential of Bi in aqueous salt solutions of varying concentrations.

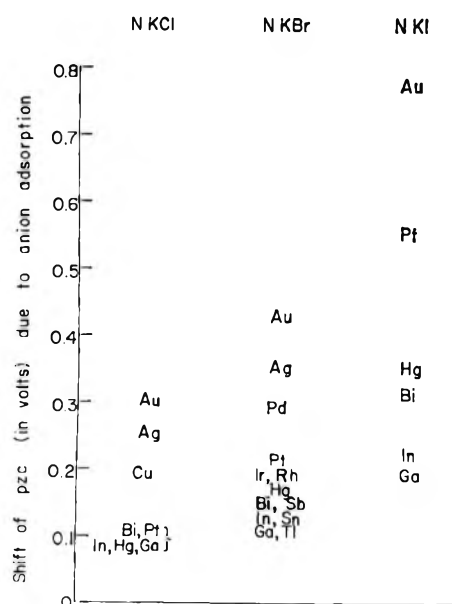
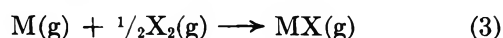


Figure 11. Magnitude of negative shift of potential of zero charge due to anion specific adsorption in 1 N KCl, KBr, and KI aqueous solutions. Data for scrape potentials except for Cu,²⁷ Tl,²⁸ and Hg.²⁹

From calculations using eq 2 and consideration of the size of the halide ions, the amount of ionic adsorption represented by ΔE_x in Figure 11 varies from only slight electrode coverage in the case of Cl^- on In to just less than one-half monolayer in the case of I^- on Au. There is an apparent increase in adsorbability with chemical family in the order $\text{Ga}, \text{In}, \text{Tl} < \text{Bi}, \text{Sb} < \text{Hg} < \text{Pt}$ metals $< \text{Cu}, \text{Ag}, \text{Au}$. To gain some insight into the nature of the adsorption bond between the various metals and the halide ions or water, an attempt was made to correlate the adsorbability with the strength of a covalent M-X bond. The relative value of the latter bonds was taken as proportional to the standard free energy change for the reaction



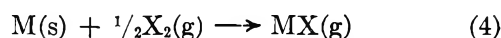
These values are shown in Table II^{30,31} for the metals for which the necessary data could be found.

Table II: Free Energy (in kcal/mol) for the Reaction $\text{M}(\text{g}) + \frac{1}{2}\text{X}_2(\text{g}) \rightarrow \text{MX}(\text{g})$ at 25° and 1 Atm. Values Taken from Latimer³⁰ Except as Noted

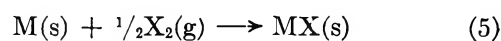
Metal	Cl	Br	I
Sb	-80.6 ^a		
Tl	-57.2	-49.2	-39.2
In	-72.6	-48.6	-40.6
Ga	-57.0	-42.4 ^a	
Cu	-47	-44	-22
Ag	-43.0	-42.8	
Au	-55 ^a		
Bi	-35.2	-36.6	-29.4
Hg	-6.4	10.4	+15.4
Sn	-57.6 ^a	-49.3 ^a	

^a Calculated from dissociation energy, D^0 , of MX (values from Herzberg³¹) and other thermal data from Latimer.³⁰

It is seen that the order of bond strength does not correspond to the order of adsorbability. If we assume the reactions



or



instead of that given by eq 3, we are still unable to explain the observed order of adsorbability. We thus conclude that the differences in adsorption energy of H_2O on the metals is greater and therefore overrides the differences in bond energy. This indicates that the bonds formed are not the covalent bonds present in the corresponding salts but presumably arise from dispersion and image forces. Since mercury appears to be the only metal for which independent values are available for the energy of adsorption of water and of adsorbed ions, additional measurements are needed for the other metals before the observed order of potentials shown in Figure 11 can be interpreted with certainty in terms of adsorbed water and adsorbed ions.

Acknowledgment. The authors gratefully acknowledge financial support of this project from the Army Research Office (Durham) under Contract No. DA-31-124-ARO-D-408 Mod. #1.

(27) B. Jakuszewski and Z. Kozlowski, *Lodz. Towarz. Nauk, Wydział III, Acta Chim.*, **9**, 25 (1964).

(28) E. K. Venstrem and P. A. Rebinder, *Dokl. Akad. Nauk SSSR*, **68**, 329 (1949).

(29) M. A. V. Devanathan and P. Peries, *Trans. Faraday Soc.*, **50**, 1236 (1954).

(30) W. M. Latimer, "Oxidation Potentials," 2nd ed, Prentice-Hall, Inc., Englewood Cliffs, N. J., 1952.

(31) G. Herzberg, "Molecular Spectra and Molecular Structure," D. van Nostrand Co., Inc., New York, N. Y., 1950.

A Study of Anion Adsorption on Platinum by Ellipsometry¹

by Ying-Cheh Chiu and M. A. Genshaw

The Electrochemistry Laboratory, The University of Pennsylvania, Philadelphia, Pennsylvania (Received February 21, 1969)

Anion adsorption at platinum was determined using an optical technique, ellipsometry. The following ions (in order of increasing adsorption) were found to adsorb: SO_4^{2-} , Cl^- , Br^- , I^- . The adsorption of ClO_4^- and F^- was found to be less than the limit of detection ($\theta = 0.01$).

I. Introduction

The interfacial region between a metal and electrolyte is very important (in electrochemistry), as all electrochemical reactions occur in this region. The study of adsorption of ions at electrodes provides some insight into the structure of this region. At mercury the method of electrocapillary thermodynamics has provided a basis for speculation on the structure of the double layer. At solid metals, a comparable method does not exist.

Adsorption of anions on platinum has previously been studied by a variety of techniques. These methods include: (1) observation of the effect of anion adsorption on hydrogen deposition;² (2) measurement of the shift in electrode potential resulting on addition of the adsorbable ion to a solution of sulfuric or perchloric acid;^{3,4} (3) measurement of the pH or conductivity change of a relatively small volume of liquid, caused by displacement of hydrogen ions from the ionic double layer by anions;⁵ (4) direct determination by quantitative analysis of anions lost from solution;⁶ (5) direct determination of anion surface concentration by means of radioactive tracers;⁷⁻⁹ (6) capacity measurement;¹⁰ (7) measurement of adsorption of electroactive species in a thin layer cell;¹¹ (8) by chronopotentiometry¹² or (9) chronocoulometry;¹³ and (10) measurements by inference from effects on the kinetics of oxygen deposition^{14,15} or other reactions.¹⁶

The development of a general method for the study of ion adsorption is highly desirable. For this reason, the application of ellipsometry to the study of ion adsorption was developed. (An ellipsometer measures the change in relative phase, Δ , and amplitude ratio, $\tan \psi$, of the parallel and normal components of a beam of polarized light upon reflection from a test surface.) Ellipsometry has proved a very useful technique for making *in situ* determinations of the thickness of very thin films. The technique has been shown to be applicable to the adsorption of molecules from the gas phase¹⁷ as well as from solution.^{18,19} Since it has a resolution of the order of ~ 0.01 monolayer of oxide or adsorbed layers, it seemed an appropriate technique for the determination of the adsorption of ions. The results obtained by this method at mercury have been

compared with the electrocapillary measurements made on a mercury surface.²⁰ The good agreement obtained for these two methods indicates that the measurement made by ellipsometry is reliable. In this paper, the method was applied to the study of anion adsorption on platinum surfaces.

II. Experimental Section

The experimental method used for the study of anion adsorption on platinum is very similar to that described for the mercury system.²⁰

To obtain the maximum resolution of the ellipsometer, two modifications to the basic technique were made. As a light source, a 2-W tungsten arc lamp was used with a well filtered constant current supply to minimize intensity fluctuations usually observed with arc lamps.

In addition, to avoid the use of the calibrated scales

- (1) This paper was presented at the 156th National Meeting of the American Chemical Society, Atlantic City, N. J., Sept. 9-13, 1968.
- (2) B. Ershler, *Acta Physicochim.*, **7**, 327 (1937).
- (3) A. D. Obrucheveva, *Zh. Fiz. Khim.*, **32**, 2155 (1958).
- (4) (a) A. D. Obrucheveva, *Dokl. Akad. Nauk SSSR*, **141**, 1413 (1961); (b) A. D. Obrucheveva, *ibid.*, **142**, 859 (1962).
- (5) A. Slygin, A. Frumkin, and W. Medwedowsky, *Acta Physicochim.*, **4**, 911 (1936).
- (6) I. M. Kolthoff and T. Fameda, *J. Amer. Chem. Soc.*, **51**, 2888 (1929).
- (7) N. A. Balaschova, *Electrochim. Acta*, **7**, 559 (1962).
- (8) N. A. Balaschova, *Z. Phys. Chem. (Leipzig)*, **207**, 340 (1957).
- (9) K. Schwabe, *Electrochim. Acta*, **6**, 223 (1962).
- (10) P. V. Popat and N. Hackerman, *J. Phys. Chem.*, **62**, 1198 (1958).
- (11) A. T. Hubbard and F. C. Anson, *J. Electroanal. Chem.*, **9**, 163 (1965).
- (12) R. A. Osteryoung, *Anal. Chem.*, **35**, 1100 (1963).
- (13) F. C. Anson, *J. Phys. Chem.*, **72**, 727 (1968).
- (14) S. Gilman, *ibid.*, **68**, 2093 (1964).
- (15) S. Gilman, *ibid.*, **68**, 2112 (1964).
- (16) M. W. Breiter, *Electrochim. Acta*, **9**, 827 (1964).
- (17) F. Meyer and G. P. Botsma, "Conference on Recent Developments in Ellipsometry," Lincoln, Neb., Aug. 7-9, 1968.
- (18) R. R. Stromberg, E. Passaglia, and P. J. Tutas, "Ellipsometry in the Measurement of Surfaces and Thin Films," E. Passaglia, R. R. Stromberg, and J. Kruger, Eds., National Bureau of Standards Miscellaneous Publication 256, Washington, D. C., 1964, p 281.
- (19) R. J. Ruch and L. S. Partell, *J. Phys. Chem.*, **64**, 513 (1960).
- (20) Y. C. Chiu and M. A. Genshaw, *ibid.*, **72**, 4325 (1968).

(calibrated to 0.01°), the intensity of the light at 4° from extinction was monitored. Since²¹

$$I \propto \sin^2(A - A_0) + \sin 2A_0 \sin 2A \sin^2(P - P_0)$$

where I is the intensity, A is the analyzer setting, A_0 is the extinction analyzer setting, P is the polarizer setting, and P_0 is the extinction polarizer setting, with $A = A_0$ the intensity is

$$I \propto \sin^2(P - P_0)$$

For small values of θ , $\sin^2 \theta \simeq \theta^2$, therefore for small changes in P or P_0

$$I \propto [(P - P_0) + \delta(P - P_0)]^2$$

$$I \propto (P - P_0)^2 + 2(P - P_0) \times \delta(P - P_0)$$

The intensity is linearly dependent on small changes of either P or P_0 . Also

$$\Delta = 90 + 2P_0$$

so that the intensity is linearly dependent on Δ . A calibration is readily made by determining the intensity- P relation. Interpolation between the calibrated intensity points is then possible. Due to the noise caused by randomness of photoemission, it proved necessary to limit the bandpass of the ammeter measuring the photomultiplier current to less than 1 Hz. Then a resolution of 0.002 – 0.005° in P_0 was possible.

An all-Teflon cell was used for this study. The detailed construction of the cell is shown in Figure 1. The cell was made air-tight by the use of Beckman fittings and O-rings. Homosil clear fused-quartz windows were mounted into the Teflon to permit the transmission of light. A Beckman sodium ion glass electrode (No. 39278, Beckman Instruments, Inc.) was used as the reference electrode for most of the experiments. A saturated calomel electrode was employed occasionally when the effect of the chloride ion leaking from the electrode was small, *e.g.*, for halides at high concentrations. The construction of the counter electrode is shown in Figure 2. A difficult part of the cell was the design to keep the reflecting surface in position with a good electrical contact with the outside while an airtight condition was maintained. This was done by careful matching of a Teflon holder, as shown in Figure 3. The platinum surface was made by sputtering of platinum on a microscope glass slide (3×1 in.). The thickness of the platinum film was estimated to be 5000 \AA as calculated from the measured resistance.

The ellipsometer used was the Gaertner Model L119 (Gaertner Optical Instrumentation) which was designed to study reflection from a vertical surface. The quarter wave plate was set at 45° and the angle of incidence was 72.53° . The wavelength used was 5500 \AA with a band width of 50 \AA .

In performing an experiment, the platinum surface was initially washed with nitric acid or sulfuric acid

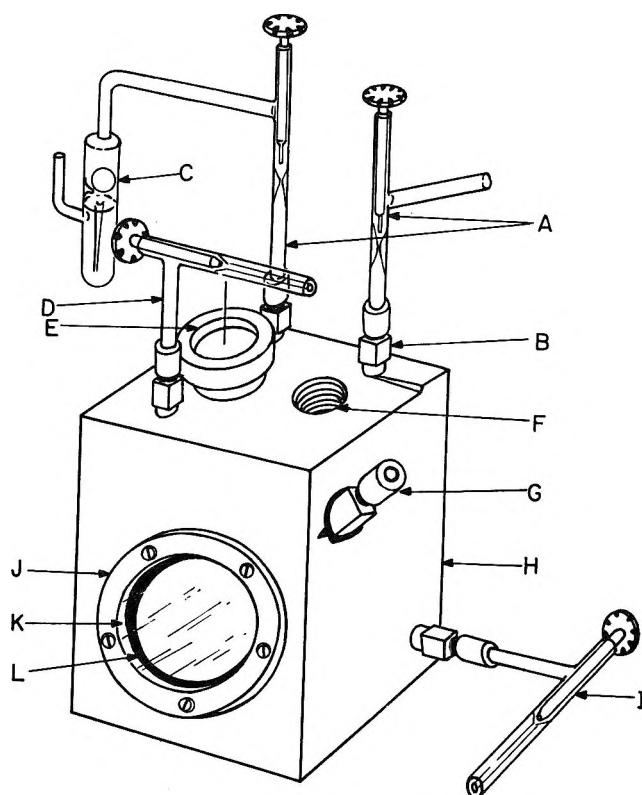


Figure 1. Cell for the adsorption study: A, needle valve for gas inlet and outlet; B, Beckman fitting; C, check valve; D, quick opening valve for solution inlet; E, Teflon holder for reflecting surface; F, for reference electrode; G, for counter electrode; H, Teflon wall; I, quick opening valve for solution outlet; J, Teflon holder; K, quartz window; L, O-ring.

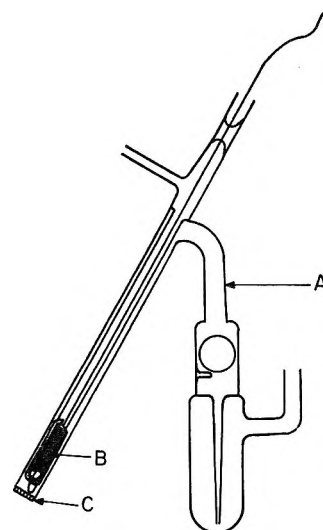


Figure 2. The counter electrode: A, check valve; B, platinum sheet; C, fritted glass.

solution (about 1:5 acid-water ratio), distilled water, and conductivity water. The solution was bubbled with purified nitrogen all the time except at the time of measurement. After the cell was assembled, a set of

(21) K. H. Zaininger and A. G. Revesz, *R.C.A. Rev.*, 25, 85 (1964).

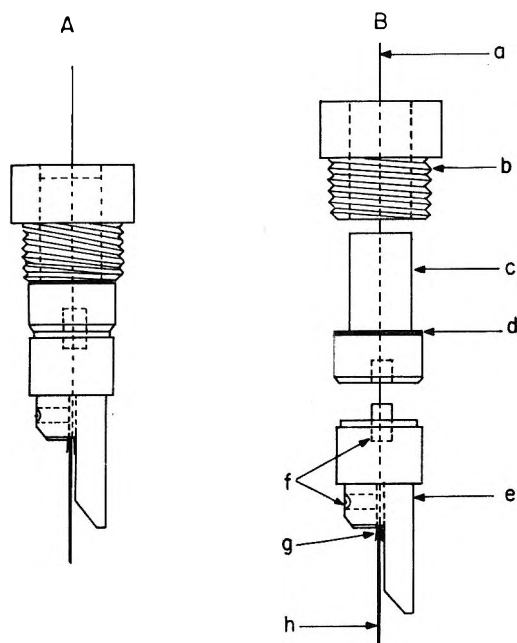


Figure 3. Teflon holder for reflecting surface: A, the unit as a whole; B, the detailed assembly; a, gold wire; b, Teflon screw; c,e, Teflon block; d, O-ring; f, Teflon screw; g, gold foil; h, reflecting surface.

extinction readings of the optical components was first obtained by the swing method.²¹ The surface was then reduced to about 200 mV vs. the reversible hydrogen electrode scale (rhe) in an electrolyte solution of 0.032 *N* sodium fluoride. All the potentials in this paper will be referred to the rhe scale. The potential was then changed to 800 mV and the surface was swept between 200 and 800 mV for three cycles (the potential was changed by manual adjustment of a potentiometer dial at ~ 20 mV/sec). The surface was again kept at 200 mV for about 1 min and was then potentiostated at 400 mV. Another set of extinction readings of the optical components was obtained. The adsorption on the surface was registered by the intensity change of the light with the analyzer set at the null setting and the polarizer set 4° from null. The potential was changed in steps of 0.1 V with the intensity measured after 2 min.

On the platinum surface, some complication arises in the hydrogen and oxygen regions of the potential range. One has to be very careful in changing the potential in these regions. The adsorption of ions usually changed the potential of the hydrogen region to a more negative value and the oxygen region to a more positive value.^{7,22} These regions were first studied in solutions of the least adsorbing species. The result was used as a guide for the other systems. The oxygen interference can be avoided by not going into the oxygen region. It is somewhat difficult to avoid going into the hydrogen region since the method depends on the relative change of adsorption with potential. The zero adsorption potential usually lies in the hydrogen region for ions

having strong adsorption. As the hydrogen began to adsorb, it caused either an intensity change or a change in Δ , which produces a change in intensity, or both. The change continued with time and distinguished itself from the changes produced by ionic adsorption, which took place in a shorter time. The change in intensity due to the hydrogen adsorption could be corrected by recording the change on both sides of the extinction point of the polarizer. A criterion for taking the zero adsorption potential when the adsorptions begin in the hydrogen region was the current reading of the potentiostat. It was taken at the potential when the cathodic current density was increased to 0.01 mA/cm² (at higher currents hydrogen bubbles would form).

All the solutions used were prepared from the sodium salts of the anions (Baker Analyzed Reagents for all the salts except sodium perchlorate, which was produced by Fisher Scientific Co.). The halide solutions were all made up in 0.032 *N* NaF to provide ionic conductivity.

III. Calculation of the Coverage

To analyze the experimental data, a model must be taken for the optical behavior of a submonolayer. A number of methods of calculation have been suggested^{23,24} on the basis that a submonolayer either acts as a film with averaged properties or that the adsorbed species act as scattering centers. The model used in this work is to assume that a layer of ions and water molecules of a thickness equal to the length of the ion is always present at the surface. The refractive index of this layer is assumed to be a linear combination of the refractive index of the ion and water

$$n_{\text{film}} = n_{\text{H}_2\text{O}}(1 - \theta) + n_{\text{ion}}\theta$$

where $n_{\text{H}_2\text{O}} = 1.33$ and θ is the surface coverage of ion.

The refractive index of the ion was calculated from the Lorentz-Lorenz equation²⁵

$$R = V_m \frac{n^2 - 1}{n^2 + 2}$$

where R is the molar refractivity, V_m is the molar volume, and n is the refractive index.

The Δ and ψ values were calculated for different refractive indices of the film by using the exact ellipsometry equations by an electronic computer. The calculated change of Δ at different θ values was plotted as a calibration curve. The experimental values of the

(22) M. Breiter, *Electrochim. Acta*, **8**, 925 (1963).

(23) R. J. Archer in "Ellipsometry in the Measurement of Surfaces and Thin Films," E. Passaglia, R. R. Stromberg, and J. Kruger, Ed., National Bureau of Standards Miscellaneous Publication 256, Washington, D. C., 1964, p 255.

(24) G. A. Bootsma and F. Meyer, "Conference on Recent Developments in Ellipsometry," Lincoln, Neb., Aug. 7-9, 1968.

(25) E. A. Moelwyn-Hughes, "Physical Chemistry," 2nd ed, Pergamon Press, Inc., New York, N. Y., 1961, p 382.

change of Δ were then applied to these calibration curves and the θ values were directly obtained.

Results

The optical constant of the platinum surface was measured in a 0.032 *N* sodium fluoride solution at a potential of 400 mV where no adsorption of ion was detected. The constant obtained was $n_{Pt}^* = 1.90 - 3.99i$, which is close to the values reported in the literature for the bulk metal (2.06 - 4.26*i*,²⁶ 2.04 - 3.00*i*,²⁷ 2.629 - 3.536*i*,²⁸ and 1.76 - 4.33*i*²⁹).

Six different anions have been studied: fluoride, chloride, bromide, iodide, sulfate, and perchlorate. The results will be given as a function of potential and concentration in the order of the adsorbability of the ions.

Fluoride. Sodium fluoride solutions of concentrations of 0.032, 0.1, and 0.64 *M* were studied. The change in Δ for the 0.032 and 0.1 *M* solutions in the potential range of 800-200 mV was less than 0.005°, which is within the experimental error. In 0.64 *M* solution, a similar change in Δ was found in the potential range of 360-860 mV. Greater changes in Δ were observed at 960 mV and more anodic potentials, presumably due to the oxide formation.³⁰ It was concluded from these measurements that fluoride was not adsorbed at the potentials and concentrations studied.

Perchlorate. Sodium perchlorate solutions of concentrations of 0.015, 0.1, and 1 *M* were studied. The change in Δ was found to be less than 0.005° in the potential range of 800-200 mV for the 0.015 *M* solution. In the 0.1 *M* solution, the change in Δ was found to be less than 0.005° in the potential range of 1 V to 200 mV. In 1 *M* solution, the change in Δ was less than 0.005° in the potential range of 940-40 mV. A change of 0.03° in Δ was observed at 1040 mV, presumably due to oxide formation. It was concluded from these measurements that perchlorate was not adsorbed at the potentials and concentrations studied.

Sulfate. Sodium sulfate solutions of 0.01, 0.1, 0.5, and 1 *M* were studied. The change in Δ was found to be less than 0.005° in the 0.01 *M* solution in the potential range of 1 V to 300 mV. Considerable changes in Δ were observed for the other solutions. The refractive index of the sulfate was calculated from the Lorentz-Lorenz equation using the values in Table I. The surface coverages of sulfate as a function of concentration and potential are shown in Figure 4. A hysteresis was observed, showing the irreversibility of the process. An average value of the adsorption and desorption processes was then plotted in Figure 4 as a best approximation to equilibrium. The adsorbability of sulfate was actually quite small in the potential range studied, as can be seen from the figures. However, the changes in Δ were clearly detected. This is probably due to the high refractive index of the ion

Table I: Equations and Parameters Used in the Calculation of θ^a

Ion	V^{22}	R^{21}	r^{24}	n
Cl ⁻	18.0	8.22	1.806	1.88
Br ⁻	25.0	11.60	1.951	1.90
I ⁻	36.6	17.53	2.168	1.94
SO ₄ ²⁻	15.0	13.36	2.23 ^b	5.08

^a R = molar refractivity, cc/g-ion; V = partial molar volume, cc/g-ion; n = refractive index; r = ionic radius, Å. ^b The ionic radius of sulfate was estimated from the bond distance. The average value of S-O distances within the sulfate ion is 1.49 Å. Since sulfate is a tetrahedral ion, it is reasonable to take the ionic radius as the S-O distance plus the covalent radius of the oxygen atom which was given as 0.74 Å. The ionic radius used in the calculation was therefore 2.23 Å.

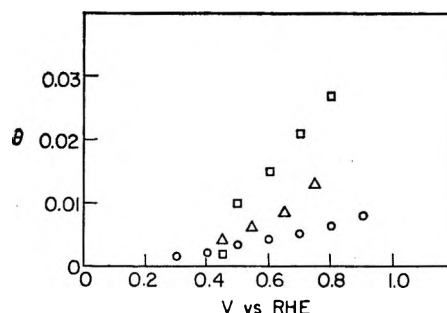


Figure 4. Dependence of coverage on potential for SO₄²⁻ at platinum at pH 4.4: □, 1 *M*; △, 0.5 *M*; ○, 0.1 *M* Na₂SO₄.

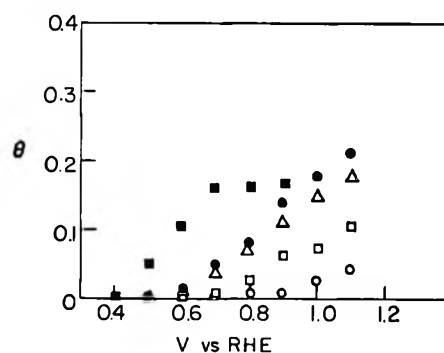


Figure 5. Dependence of coverage on potential for Cl⁻ at platinum at pH 6.5: ○, 3 × 10⁻⁴ *M*; □, 1 × 10⁻³ *M*; △, 5 × 10⁻³ *M*; ●, 1 × 10⁻² *M*; ■, 2 × 10⁻¹ *M* NaCl.

which greatly distinguishes itself from the water molecules.

(26) P. Drude, "The Theory of Optics," Dover Publications, New York, N. Y., 1959, p 366.

(27) B. Pogany, *Ann. Phys.*, **49**, 531 (1916).

(28) W. Meier, *ibid.*, **31**, 1017 (1910).

(29) W. H. M. Visscher, Thesis, Tech. Hogeschool Eindhoven, The Netherlands, 1967, p 82.

(30) A. K. N. Reddy, M. A. Genshaw, and J. O'M. Bockris, *J. Chem. Phys.*, **48**, 671 (1968).

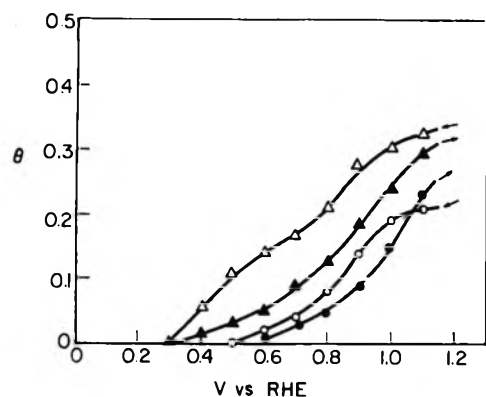


Figure 6. Hysteresis in measured coverage of Br^- at platinum at pH 6.5: \circ , $10^{-3} M$; Δ , $5 \times 10^{-3} M$ NaBr.

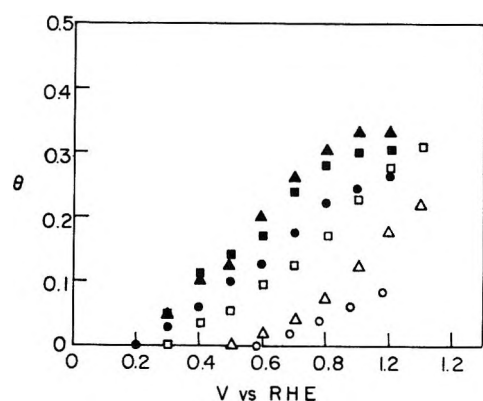


Figure 7. Dependence of coverage on potential for Br^- at platinum at pH 6.5: \circ , $10^{-4} M$; Δ , $10^{-3} M$; \square , $5 \times 10^{-3} M$; \bullet , $10^{-2} M$; \blacktriangle , $3 \times 10^{-2} M$; \blacksquare , $9 \times 10^{-2} M$ NaBr.

Chloride. Adsorption of chloride ion was made with sodium chloride solutions in the concentration range of 10^{-4} to $10^{-1} M$. Figure 5 shows the average values of adsorption and desorption measurements.

Bromide. Adsorption of bromide ion was made with sodium bromide solutions in the concentration range of 10^{-4} to $10^{-1} M$. Figure 6 shows the hysteresis found in the adsorption and desorption processes. Figure 7 shows the average values of these processes.

Iodide. The adsorption of iodide ion was studied in 10^{-5} to $10^{-3} M$ sodium iodide solutions. The results are shown in Figure 8, which gives the average value for the adsorption and desorption processes. A hysteresis similar to that of the bromide ion was also found for the iodide adsorption. The study of the iodide adsorption was further complicated by the iodine formation on the counter electrode. At concentrations of iodide less than $10^{-3} M$, the iodine formed on the counter electrode was confined by the fritted glass of the counter-electrode compartment without much effect on the solution outside. At higher concentrations of iodide, the iodine leaked through the fritted glass and contaminated the solution. Therefore, the study of iodide adsorption was only made to a concentration of

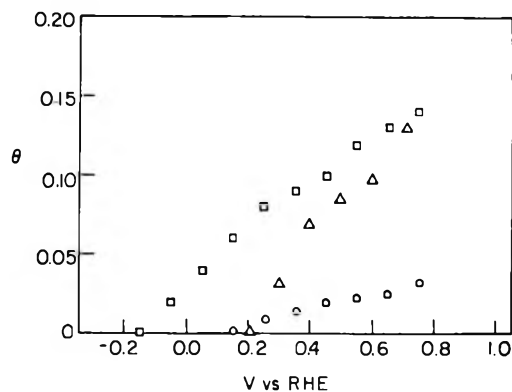


Figure 8. Dependence of coverage on potential for I^- at platinum at pH 6.5: \circ , $10^{-3} M$; Δ , $1.4 \times 10^{-4} M$; \square , $10^{-3} M$ NaI.

$10^{-3} M$. As iodide adsorbs very strongly, the adsorption begins below the reversible hydrogen potential.

IV. Comparison of Results Obtained by Different Workers

There are only a very few measurements of ion adsorption on platinum in the current literature. The values measured by different methods are compared in Tables II, III, and IV. The comparison is rather

Table II: Comparison of Chloride Adsorption by Various Techniques

Potential, V vs. rhe	Radio-tracer ^{a, 31}	Coverage Electro-chemical ¹⁶	Ellip-sometric
0.177	0.000		
0.377	0.018	0.27	0.00
0.577	0.07	0.35	0.01
0.777	0.101	0.50	0.05
0.977	0.12		0.11

^a $\theta = 4.6 \times 10^8 \Gamma$.

Table III: Comparison of Radiotracer and Ellipsometric Adsorption of $10^{-3} M$ Br^-

Potential, V vs. rhe	Radiotracer ^{a, 31}	Ellipsometry
0.177	0	
0.377	0.106	0
0.518	0.138	0.01
0.577	0.143	0.03
0.777	0.170	0.075
0.977	0.184	0.175

^a $\theta = 4.6 \times 10^8 \Gamma$.

rough, as it involves the assumptions of roughness factor in the radiotracer measurements³¹ and the mono-

(31) N. A. Balashava and V. E. Kazarinov, *Elektrokhimiya*, 1, 512 (1965).

Table IV: Comparison of Radiotracer and Ellipsometric Adsorption of $10^{-3} M I^-$

Potential, V vs. r.h.e.	Radiotracer ³¹	Ellipsometry	Ellipsometric with correction
-0.023	0.069		0.09
0.177	0.092	0.05	0.14
0.377	0.144	0.07	0.16
0.518	0.230	0.11	0.20
0.577	0.258	0.13	0.22
0.677	0.310	0.14	0.23

layer coverage of hydrogen in converting one result to the other. For the chloride ion adsorption, the agreement between the radiotracer and ellipsometry is not bad and improves with increasing coverage. However, the electrochemical result of Gilman¹⁵ is much higher. In the bromide ion adsorption, the ellipsometry data agree well with the radiotracer³¹ results at higher coverages. The differences resulting from these two methods could be due to two factors. (1) The radiotracer method involves making correction for the adhering solution and the potential of the electrode is not controlled during removal from solution. (2) Ellipsometric method is subject to the problem of determining the zero point of adsorption. The changes are determined as relative values to a certain potential. Errors could be introduced in this way. One way of correcting the ellipsometry error of the zero determination is the determination of the change in Δ at a constant potential in the presence and absence of adsorbing species.

The results obtained for iodide adsorption are compared with the radiotracer³¹ data in Table IV. The radiotracer method gives higher values than the single reflection ellipsometry. If one applies a zero correction of 0.09 in θ for $10^{-3} M NaI$ obtained by making measurements at constant potential with varying concentration, one obtains the values in the last column. The zero correction in the iodide system is appreciable, due to the adsorption of iodide beginning at a potential cathodic to the reversible hydrogen potential. In order to avoid the interference of hydrogen, ellipsometry data were taken at a higher potential which resulted in a higher zero correction.

The θ values obtained from ellipsometry for sulfate adsorption were also compared with the radiotracer data.³¹ The radiotracer method shows sulfate adsorption at the concentration of $10^{-3} M$ with a maximum surface coverage of 0.04 at 0.6 V (nhe). The ellipsometry method did not see any adsorbed sulfate until the concentration was increased to 0.1 M. The θ values obtained for the higher concentrations are also small, in agreement with the radiotracer results.

Trends in Adsorption at Platinum. The adsorption of anions begins well before the reversible potential of the formation of platinum halide complexes is reached

(0.75 V (nhe) for $PtCl_4^{2-}$, 0.67 V (nhe) for $PtBr_4^{2-}$, and 0.40 V (nhe) for PtI_4^{2-}).³² All measurements were conducted in the region cathodic to the complex formation.

The potential at which adsorption begins from solutions of the same concentration became more anodic in the order $I^- < Br^- < Cl^- < SO_4^{2-} < ClO_4^-$, F^- . Also, at a given potential and concentration, the relative surface coverage was in the order $I^- > Br^- > Cl^- > SO_4^{2-} > ClO_4^-$, F^- . A tendency also existed for a decrease in $d\theta/dV$ at more anodic potentials. Also, $d\theta/dV$ seemed to increase with increasing concentration.

Similar trends in adsorption have been reported by Schwabe⁹ ($CN^- > HS^- > I^- > Cl^- > SO_4^{2-} > ClO_4^-$), Balashova and Kazarinov³¹ ($I^- > Br^- > Cl^- > SO_4^{2-} > F^-$), Popat and Hackerman¹⁰ ($I^- > Br^- > Cl^- > SO_4^{2-} > F^-$, NO_3^-), and Sasaki, *et al.*,³³ ($SCN^- > I^- > Fe(CN)_6^{4-} > Br^- > NO_3^- > AcO^- > Cl^-$).

A Comparison of Adsorption on Platinum with Mercury. The trend of adsorption at mercury was the same as on platinum except that perchlorate adsorbed³⁴ and sulfate did not. At mercury³⁴ $d\theta/dV$ for chloride and bromide increased with concentration as it did at platinum but $d\theta/dV$ increased with increasing potential, which was opposite to the trend observed at platinum. The adsorption occurred near the potential of zero charge for both metals and if the coverage at the potential corresponding to the potential of zero charge in the absence of specific adsorption were compared (Table V),

Table V: Comparison of Adsorption on Mercury and Platinum at 200 mV above pzc of the Metals^a

	Concn., M	θ (Hg)	θ (Pt) Ellipsometry
Cl ⁻	10^{-2}	0.04	0.06
Br ⁻	10^{-2}	0.09	0.20
I ⁻	10^{-3}	No data	0.21

^a pzc of mercury is taken as -0.19 V (nhe);³⁴ pzc of platinum is taken as 0.20 V (nhe) (S. Agrade, Thesis, University of Pennsylvania, 1968, p 295).

the coverages were not very different. A hysteresis in adsorption at platinum was found in this work which was not observed in measurements at mercury.

Future Prospects for the Use of Ellipsometry in Adsorption Studies. A number of restrictions to the application of ellipsometry will limit its applicability. At anodic potentials metals dissolve or form oxide films which are seen by the ellipsometer and prevent the determination of adsorption. On the cathodic side,

(32) R. N. Goldberg and L. G. Hepler, *Chem. Rev.*, **68**, 229 (1968).

(33) K. Sasaki, I. Izumi, K. Onashi, T. Verjura, and S. Nagura, *Nippon Kagaku Zasshi*, **87**, 918 (1966).

(34) H. Wroblowa, Z. Kovac, and J. O'M. Bockris, *Trans. Faraday Soc.*, **61**, 1523 (1965).

hydrogen adsorption or hydrogen evolution producing gas bubbles limits the optical technique. Thus only ions adsorbing in the region between the anodic and cathodic processes may be determined. Also, the method can only be applied to ions which have refractive indices significantly different from that of the solution.

On the favorable side, the sensitivity of the method can probably still be improved somewhat, probably to a resolution of 0.001° . For ions such as iodide, which do not desorb before hydrogen evolution, measurements may be conducted at constant potential with a vari-

ation of concentration to obtain the isotherms. Improvements in the calculation of θ from changes in Δ can probably be made as more results on the submonolayer region in gas phase are obtained.²⁴ A separation of the contributions of the diffuse and compact layers may result from the application of double-layer theory with double film computations.

Acknowledgment. We wish to thank the National Aeronautics and Space Administration for their financial support of this work and Professor J. O'M. Bockris for the suggestion of the topic and encouragement in this work.

Adsorption Isotherms in Mixed Solvent Systems^{1a}

by John Lawrence^{1b} and Roger Parsons

School of Chemistry, University of Bristol, Bristol 8, England (Received February 21, 1969)

Previously published experimental results of the electrical double layer at a mercury electrode in contact with sulfolane and water, methanol and water, and formic acid and water have been analyzed in terms of the adsorption of the nonaqueous component of the mixtures. Each of the three systems obeys a Flory-Huggins type of isotherm which has been modified to account for long-range particle-particle interactions. The isotherm best described the results if the parameter Γ was estimated assuming the solvent water to exist on the electrode surface as monomer units rather than clusters. The standard free energy of adsorption has been calculated and for each of the systems it showed a quadratic dependence on electrode charge. The interaction parameter of the isotherms is discussed in terms of preferred orientation of the adsorbed species and its dependence on electrical charge.

Introduction

Most of the early work on electrochemical adsorption of ions and neutral molecules was carried out in aqueous solutions, considering the solvent water as a continuum. More recently, however, adsorption from nonaqueous solvents has been receiving increasing attention²⁻⁸ and it must be concluded from this work that the solvent plays an important role in interfacial adsorption processes. In fact, adsorption should always be considered as a competitive process between the adsorbate and solvent since for an adsorbate molecule to move to a surface site, a certain number of solvent molecules must first be removed. In order to clarify this competitive effect of the solvent, the present study was undertaken of the adsorption of nonaqueous solvents from water over the entire composition range from pure nonaqueous solvent to pure water.

The systems analyzed here are sulfolane-water at 30° , formic acid-water at 25° , and methanol-water at 25° , since experimental data are available.^{5,6,9} The results for the first two systems were obtained using differential

capacity and electrocapillary measurements, while results for the third system were obtained by electrocapillary measurements alone. It is unfortunate that in these two experimental techniques it is necessary to have an electrolyte present because activity coefficients are not known for electrolytes in most solvent-water mixtures and consequently it is not possible to keep the electrolyte activity constant throughout the solvent

(1) (a) For a recent tabulation of the numerous systems see R. Parsons, *Rev. Pure Appl. Chem.*, **18**, 91 (1968). (b) Address correspondence to this author at the Department of Chemistry, University of Ottawa, Ottawa 2, Ont., Canada.

(2) R. Payne, *J. Chem. Phys.*, **42**, 3371 (1965).

(3) J. D. Garnish and R. Parsons, *Trans. Faraday Soc.*, **63**, 1754 (1967).

(4) R. Payne, *J. Amer. Chem. Soc.*, **89**, 489 (1967).

(5) J. Lawrence and R. Parsons, *Trans. Faraday Soc.*, **64**, 751 (1968).

(6) J. Lawrence and R. Parsons, *ibid.*, **64**, 1656 (1968).

(7) B. B. Damaskin and R. V. Ivanova, *Zh. Fiz. Khim.*, **38**, 92 (1964).

(8) R. Payne, *Advan. Electrochem. Electrochem. Eng.*, in press.

(9) R. Parsons and M. A. V. Devanathan, *Trans. Faraday Soc.*, **49**, 673 (1953).

composition range. However, as Parsons and Devanathan showed for the aqueous methanol system,⁹ by using a constant, dilute concentration of a nonadsorbed electrolyte, the effect on solvent adsorption can be minimized. The electrolytes chosen were 0.1 *M* potassium hexafluorophosphate for the sulfolane system, 0.01 *M* hydrogen chloride for the methanol system, and 0.1 *M* sodium formate for the formic acid system. The potentials were measured against electrodes reversible to one of the ions in the respective solutions and to eliminate liquid junction potentials the electrodes were prepared in the aqueous-solvent mixture. Potassium amalgam, hydrogen, and mercury-mercurous formate electrodes were employed for the sulfolane, methanol, and formic acid systems, respectively. The activities of the nonaqueous components in the aqueous mixtures were calculated from vapor pressure measurements recorded in the literature.¹⁰⁻¹² At this stage it had to be assumed that the presence of the low concentrations of electrolyte had no appreciable effect on the activity of the solvent components.

Calculation of Amounts Adsorbed and Analysis of the Adsorption Isotherm

Surface excesses (Γ_i) of the nonaqueous component in each mixture were calculated from the equation

$$(\partial\xi/\partial\mu)_{q, \mu_{\text{salt}}} = -\Gamma_i$$

where $\xi = \gamma + qE_{\pm}$, γ is the interfacial tension, q is the charge on the electrode, and E_{\pm} the potential of the mercury electrode with respect to an electrode reversible to the cation (methanol and sulfolane mixtures) or anion (formic acid mixtures). $d\mu$ is put equal to $RT \ln a$ where a is the activity of the nonaqueous component in the mixture. The condition of constant salt chemical potential was shown previously⁹ to be approximately satisfied if a dilute solution of a nonspecifically adsorbed electrolyte is used.

Adsorption was considered at constant charge rather than at constant potential throughout this work. There has been some controversy recently¹³⁻¹⁷ about the validity of this condition in the consideration of non-electrolyte adsorption. The arguments in favor of the constant potential condition have been applied to systems of aqueous solutions which are dilute in the nonaqueous component. The application of such a condition to a system studied over the complete range of mixtures from one pure solvent to the other is difficult, if not impossible. In contrast, the constant charge condition can be applied exactly without any difficulties of principle.

The surface excess of nonaqueous component with respect to water, defined as

$$\Gamma_{i(2)} = \left(\Gamma_i - \Gamma_w \frac{x_i}{x_w} \right)$$

could not be approximated to surface concentrations

since it is only in dilute solutions of the adsorbing species that the second term can be safely neglected. At high nonaqueous concentrations, the second term actually exceeds the first. The true surface concentrations were calculated from the surface excesses using the following relationship,⁸ which assumed adsorption in a monolayer

$$\Gamma_{i(2)} = \frac{N_s \theta_i}{r} - \frac{x_i N_s}{x_s} + \frac{x_i}{x_s} N_s \theta_i$$

This can be rearranged to give

$$\theta_i = \left(\frac{\Gamma_{i(2)}/N_s + x_i/x_s}{(1/r + x_i/x_s)} \right)$$

where N_s represents the number of solvent sites on the surface and is equal to the reciprocal of the area of the solvent unit multiplied by a geometrical packing factor, r is the number of solvent molecule units desorbed when one adsorbed molecule moves on to a surface site, and x_i and x_s are the bulk mole fractions of the adsorbing species and solvent, respectively. It has been suggested earlier^{18,19} that water molecules are adsorbed at electrode interfaces in clusters of 5 or 6 with each cluster occupying an area of surface of 30–40 Å². However, it will be shown here that these results do not support this suggestion and consequently the water molecules have been considered as monomer units in a close-packed hexagonal lattice. If the area occupied by each water molecule is 12.3 Å², the resulting number of adsorption sites is $0.813 \times 10^{15} \text{ cm}^{-2}$.

The most likely isotherm to be obeyed by mixed systems such as these is the Flory-Huggins isotherm,¹⁹ which was derived originally by Zhukovitskii.²⁰ This is based on a model in which the adsorbed species form a monolayer at the electrode interface with each molecule replacing r solvent molecules. The basic isotherm can be written as

$$\frac{\theta}{r(1-\theta)^r} = \beta a$$

but this has since been modified to allow for interactions between the adsorbed species by the addition of an exponential term in θ ,¹⁷ *i.e.*

- (10) C. H. Langford, private communication.
- (11) A. N. Campbell and A. J. R. Campbell, *Trans. Faraday Soc.*, **30**, 1109 (1934).
- (12) J. A. V. Butler, D. W. Thomson, and W. H. Maclennan, *J. Chem. Soc.*, 674 (1933).
- (13) R. Parsons, *J. Electroanal. Chem.*, **7**, 136 (1964).
- (14) R. Payne, *J. Phys. Chem.*, **69**, 4113 (1965).
- (15) E. Dutkiewicz, J. D. Garnish, and R. Parsons, *J. Electroanal. Chem. Interfac. Electrochem.*, **16**, 505 (1968).
- (16) A. N. Frumkin, *Z. Phys.*, **35**, 792 (1926).
- (17) A. N. Frumkin, B. B. Damaskin, and A. A. Survita, *J. Electroanal. Interfac. Electrochem.*, **16**, 493 (1968).
- (18) J. M. Parry and R. Parsons, *J. Electrochem. Soc.*, **113**, 992 (1966).
- (19) R. Parsons, *J. Electroanal. Chem.*, **8**, 93 (1964).
- (20) A. A. Zhukovitskii, *Acta Physicochim. U.R.S.S.*, **19**, 176 (1944).

$$\frac{\theta}{r(1-\theta)^r} e^{A\theta} = \beta a$$

The adsorbed species are considered as a thermally disordered, two-dimensional gas or liquid and A can be related to a two-dimensional second virial coefficient at low values of θ , a is the activity of the adsorbing species in the bulk, and $RT \ln \beta = -\Delta G^\circ$ is the standard free energy of adsorption. The standard states are unit mole fraction activity of pure nonaqueous component in the bulk and θ^* on the surface where $\theta^* = r(1-\theta^*)^r e^{-A\theta^*}$, while the reference states are infinite dilution for both the bulk and surface phases.

The isotherm can be rearranged to give

$$\log \frac{a(1-\theta)^r}{\theta} = \frac{A}{2.303} \times \theta - \log \beta r$$

and consequently plots of $\log (a(1-\theta)^r/\theta)$ against θ at constant charge should yield a series of straight lines of slope $A/2.303$ and intercepts $-\log \beta r$. These plots are shown for the sulfolane and water system in Figure 1. The projected area occupied by a sulfolane molecule was estimated from both "Courtauld's" atomic models and van der Waals crystal radii calculations as 28.6 \AA^2 . This leads to a value of r of 2.27. It was found that variations in the values of r and N_s of up to 15% had only a small effect on the overall shape of the curves. It is unfortunate that there is no independent method for calculating a reliable value for r . It has been shown¹⁹ that $\partial\theta/\partial \ln \beta$ for this isotherm has a maximum when $\theta = (1 + \sqrt{r})^{-1}$ but for systems such as these where the standard free energy of adsorption is normally a quadratic function of electrode charge there is no direct way of relating $\partial\theta/\partial \ln \beta$ to experimental results. However, if r was taken as unity or less, which is necessary for the cluster theory to apply, then the points became just a scattered array. The figure shows that, assuming monomer solvent units, good linearity is obtained for θ less than 0.9. For θ greater than 0.9, marked deviations occur due probably to the approximate nature of the isotherm. Even on the imperfect gas model higher terms in θ would be expected in the exponential term corresponding to interaction between more than two particles. The vertical scale of this graph has been compressed to allow all the lines to be shown. However, this does not conceal any curvature since with a tenfold magnification of this scale, the lines remain linear. The lines are all parallel with a slope of -0.94 corresponding to a small attractive force between the molecules. The values of $\log \beta$ obtained from the intercepts follow, within the limits of error, a quadratic dependence on the electrode charge with a maximum value ($\log \beta^{\max}$) of 1.39 occurring at a charge q^{\max} of $-5.4 \mu\text{C cm}^{-2}$. The total dependence of $\log \beta$ on q^M can be expressed as

$$\log \beta = 1.39 - 0.0072\delta^2$$

where $\delta = (q^{\max} - q)$.

Figure 2 shows the corresponding isotherm plots for the aqueous methanol system. The same value of N_s was used as for the previous system and the total area occupied by a methanol molecule was taken as 18.6 \AA^2 . This leads to a value of r of 1.51. Again it was found that if r was made less than or equal to unity corresponding to the existence of solvent clusters, then the points became scattered. This figure shows a similar behavior to the sulfolane system except that the slopes are not independent of electrode charge. The slight increase in scatter of the points is mainly a consequence of the increase in error in the original values of Γ . The lines all have a negative slope with A varying from -2.42 at $q^M = 0$ to -0.30 at $q^M = -5$ to -1.89 at $q^M = -8 \mu\text{C cm}^{-2}$, corresponding to an attraction between the molecules which is a minimum at $q^M = -5 \mu\text{C cm}^{-2}$. The values of $\log \beta$ from the intercepts again show a quadratic dependence on q^M with q^{\max} occurring at the same charge as the minimum particle-particle attraction. $\log \beta^{\max}$ for this system is equal to 0.886 and the charge dependence can be written as

$$\log \beta = 0.886 - 0.0399\delta^2$$

Figure 3 shows the isotherms for the aqueous formic acid system with the total area occupied by a formic

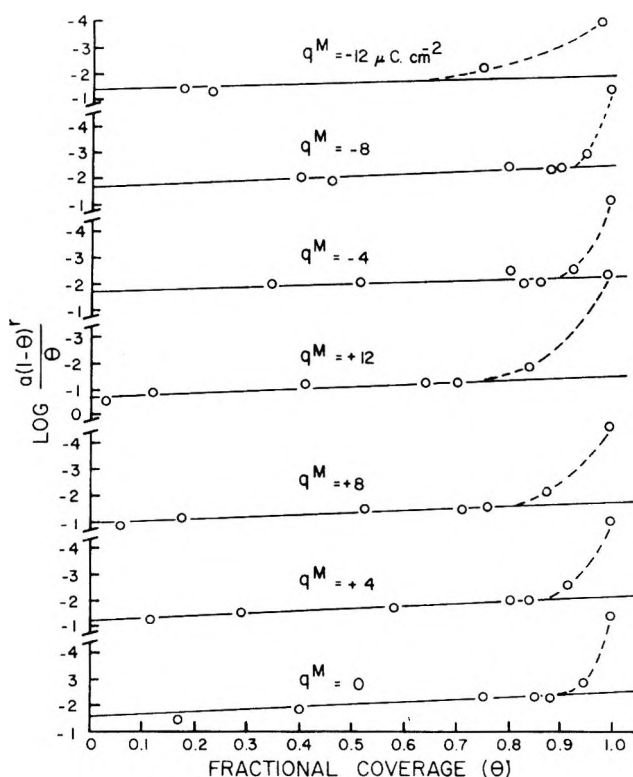


Figure 1. Modified Flory-Huggins isotherm for adsorption of sulfolane from sulfolane-water mixtures at constant electrode charge, q^M .

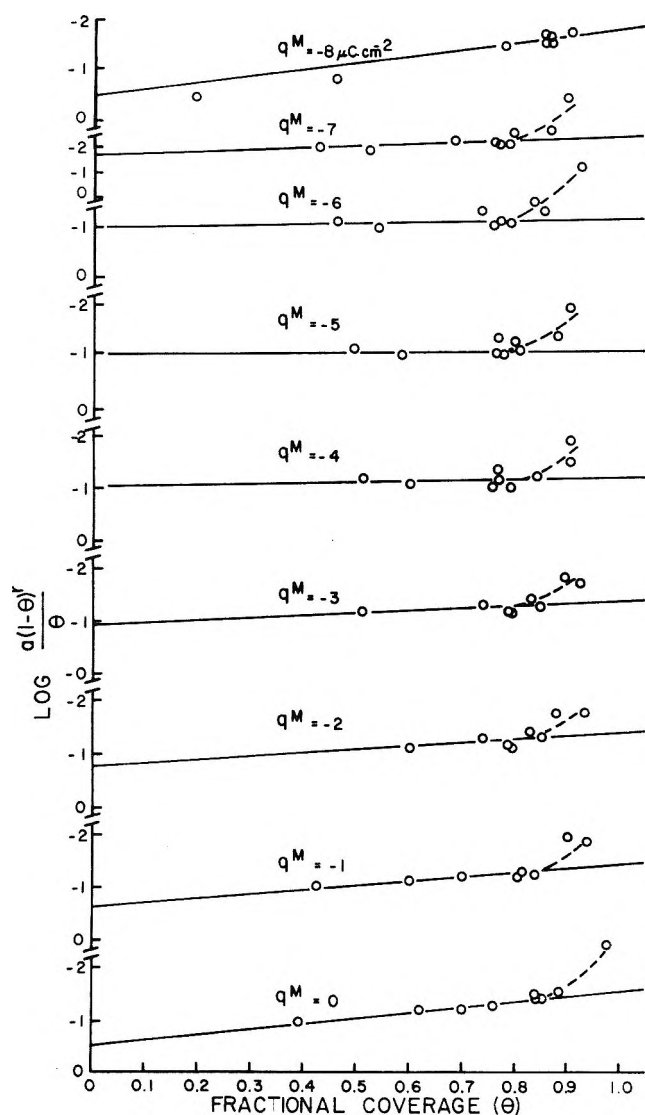


Figure 2. Modified Flory-Huggins isotherm for adsorption of methanol from methanol-water mixtures at constant electrode charge, q^M .

acid molecule taken as 18.85 \AA^2 . This gives r a value of 1.53. As a further test of the cluster theory, a value of approximately 0.5 was substituted for r (assuming the area of a water unit to be $35\text{--}40 \text{ \AA}^2$), and a corresponding change made in the value of N_s . However, the curve obtained had zero slope at $\theta = 0$ and 1 and a positive slope of up to 9.7 at intermediate coverages. Hence it must be concluded that this and the two previous systems support the argument that the solvent water exists as monomer units and not as clusters. The linearity is again satisfactory for coverages of less than about 0.7 but marked deviations occur above 0.7 probably again because higher terms in θ have been omitted from the exponential. The positive slopes correspond to intermolecular repulsion and there is a slight increase at negative charges, A at $q^M = 0$ is $+2.97$. The variation of $\log \beta$ with electrode charge is less than 4% over the charge range

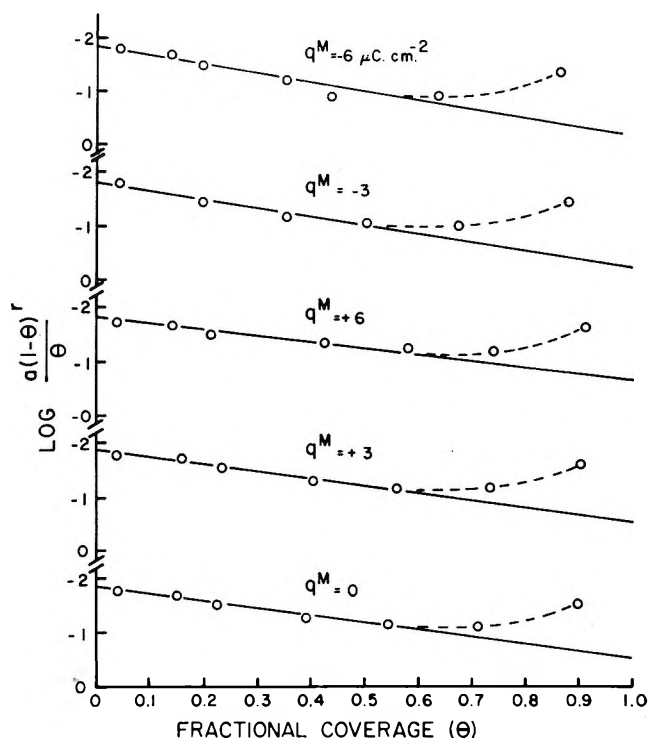


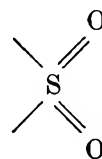
Figure 3. Modified Flory-Huggins isotherm for adsorption of formic acid from formic acid-water mixtures at constant electrode charge, q^M .

studied and since this is approaching the limits of the error no attempt has been made to determine the dependence. $\log \beta$ at $q^M = 0$ is 1.67.

Discussion

It is evident from the preceding section that the Flory-Huggins isotherm modified to a first approximation to account for long-range interparticle interactions closely describes the adsorption behavior of the three systems. Since the isotherm is an approximate form which does not allow for interactions between more than two particles, it is not surprising that deviations occur at high coverages.

It has been suggested in a previous publication⁵ that sulfolane is preferentially adsorbed at the mercury interface with the hydrocarbon ring in contact with the metal and the polar



group directed toward the solution. This suggestion is further substantiated by the fact that $\log \beta^{\max}$ occurs at $q^M = -5.4 \mu\text{C cm}^{-2}$ corresponding to ΔG° , the standard free energy of adsorption having a maximum negative value at that charge. The negative value of A is also consistent with this preferred orientation since the repulsion between the oriented dipolar

groups, which must be at least 4.5 Å from the surface and consequently in a region of relatively high dielectric constant, is likely to be more than compensated for by the attraction between the hydrocarbon rings which are close to the electrode surface and therefore in a region of relatively low dielectric constant.

The observed dependence of A on the electrode charge for the aqueous methanol system tends to suggest that the molecules have only a small preferential orientation with the $-OH$ group directed toward the solution. It is then reasonable to suppose that the main interaction would be attractive with only a small repulsive contribution from the oriented dipoles. This repulsive term would increase to a maximum at $q^M = q^{max}$ as a result of an increase in orientation leading to an overall minimum in the attraction at that charge.

The repulsion between the adsorbed formic acid molecules, which increases slightly at negative charges, can be attributed to the interaction of the partially oriented, polar carboxyl groups. Previously published results on the preferred orientation of formic acid at the mercury interface⁶ suggested that the negative end of the dipole was directed toward the metal and consequently a repulsive interaction is only to be expected. The relatively large value of $\log \beta^{max}$

for this system undoubtedly arises from the strong interaction of the lone pairs of electrons on the two carboxyl oxygen atoms with the mercury. In the other two systems, the preferred orientation is such that any lone pairs of electrons are directed toward the solution phase and hence $\log \beta^{max}$ is relatively smaller.

It should be noted that the interpretation of the A values given above is only qualitative. This parameter can be interpreted for the adsorption of a simple species at low densities as a two-dimensional second virial coefficient and under these circumstances it gives direct information about the forces between the adsorbed particles. However, in mixed solvent system its significance is less clear-cut since its value must depend not only on the solute-solute interactions but also on solute-solvent and solvent-solvent interactions. Nevertheless the interpretation of the sign of A given above in terms of net attraction or repulsion seems likely to be meaningful.

Acknowledgment. We are grateful to General Electric Company (Schenectady) and Texas Instruments Incorporated (Dallas) for maintenance awards to J. L. during 1965-1966 and 1966-1967, respectively.

Some Aspects of the Adsorption of Nitrate and Phthalate Ions at the Mercury-Solution Interface

by B. V. K. S. R. A. Tilak^{1a} and M. A. V. Devanathan^{1b}

Central Electrochemical Research Institute, Karaikudi-3, India (Received March 5, 1969)

Differential capacity and electrocapillary measurements were made on a mercury electrode at 25° in the presence of phthalate and nitrate ions. The components of charge were evaluated thermodynamically. The differential capacity curves in the presence of phthalate ions show (i) the presence of cathodic humps even in dilute solutions and (ii) concentration independence of the potential of the ecm measured with respect to the potential of a saturated KCl calomel electrode. Phthalate ions appear to reach saturation adsorption even at the ecm, a situation which results in the capacitance descending on the anodic side from the humps to values of $\sim 16 \mu\text{F}/\text{cm}^2$. Further, the second carboxylic acid group of the phthalate ion seems to be ionized due to the intense electric field at the interface. Nitrate ions from ammonium nitrate solutions appear to be adsorbed at the Hg-solution interface with their hydration shell intact. However, the number of water molecules surrounding the nitrate ion decreases as the bulk concentration of NH_4NO_3 is increased. The heights of the capacity humps increase with increasing concentration up to $\sim 0.6 M$. As the concentration is further increased, the height of the hump decreases and its width increases. Analysis of the inner-layer capacitance data in terms of changes in dq_1/dq_M shows that it is necessary to consider the hydration structure of the adsorbed ion in any examination of the fine structure of the electrical double layer. Some evidence is presented which indicates that present models are inadequate as a basis for explanation of the experimental observations.

Introduction

Despite the fact that many experimental and theoretical investigations have been made, no finally definitive picture has yet emerged on the fine structure of the electrical double layer. A critical appraisal of previous work carried out shows that basic problems such as (i) the structure of the layer of adsorbed water dipoles at the Hg-solution interface and (ii) the nature of the capacitance humps still remain to be better understood (but see other papers in this Symposium). The two opposite viewpoints²⁻⁴ on the structure of electrical double layer in the absence of specific adsorption have to be resolved at the outset since the model chosen influences to a large extent interpretations of kinetic studies and explanations of adsorption of organic substances.⁴ For the purpose of obtaining diagnostic information concerning previously treated models, the nitrate and phthalate ions were chosen for a further study of the structure of the electrical double layer (edl) in aqueous media. The phthalate ion is large and consequently the influence of this factor on its adsorbability could throw some light on the nature of the hump. Nitrate ion is a bulky, hydrated ion and its salts are very soluble; hence an attempt at an understanding of the structure of edl in concentrated solutions can be made.

Experimental Section

(a) *Procedure.* Differential capacity measurements were made at Hg drops using the transformer bridge described elsewhere.⁵ The bridge was balanced toward the end of the life of each drop. Measurements

of capacitance were made at a frequency of 10^3 Hz and had an accuracy of $\pm 0.2\%$ at the extreme cathodic region and $\pm 0.4\%$ at the extreme anodic region.

The solutions were deaerated with purified hydrogen. The potential of the dropping mercury electrode was measured with respect to a saturated calomel electrode by means of a vernier potentiometer (Cambridge Instruments Co. Ltd., England) together with a Multiflex galvanometer (Brune Lange Type MG2 SI No. 193859) having an input resistance of 1300Ω and a sensitivity of $4 \times 10^{-9} \text{ A/division}$.

Electrocapillary measurements were performed using the capillary electrometer described previously.⁶ The reproducibility of the interfacial tension was $\pm 0.2 \text{ dyn cm}^{-1}$. All the measurements were made at $25 \pm 0.1^\circ$ in an air thermostat.

(b) *Reagents.* AnalaR grade mercury was purified electrolytically and then distilled in an all-glass Hulett still. A second distillation was carried out under reduced pressure before use in the dropping mercury electrode and capillary electrometer. Doubly dis-

(1) (a) Department of Chemistry, University of Ottawa, Ottawa, Ont., Canada. (b) Ceylon Institute of Scientific and Industrial Research, Colombo, Ceylon.

(2) (a) R. Parsons, *Rev. Pure Appl. Chem.*, **18**, 91 (1968); (b) M. A. V. Devanathan and B. V. K. S. R. A. Tilak, *Chem. Rev.*, **65**, 635 (1965).

(3) K. Müller, *J. Res. Inst. Catal., Hokkaido Univ.*, **14**, 224 (1966).

(4) J. O'M. Bockris, M. A. V. Devanathan, and K. Müller, *Proc. Roy. Soc.*, **A274**, 55 (1963).

(5) M. A. V. Devanathan and B. V. K. S. R. A. Tilak, unpublished work.

(6) M. A. V. Devanathan and P. Peries, *Trans. Faraday Soc.*, **50**, 1236 (1959).

tiled conductivity water was used for preparing the solutions. AnalaR grade potassium hydrogen phthalate was recrystallized twice in conductivity water and carefully dried before use. Since NH_4NO_3 is deliquescent, saturated solutions were prepared immediately after recrystallization and kept at 25° . Aliquot quantities of the saturated solution were taken for making up solutions having the required concentrations.

Traces of impurities were removed during the first recrystallization by means of a treatment with activated charcoal. The purity of the solutions was judged by the constancy of the series resistance obtained in the impedance measurements.

Results and Discussion

The ecm (electrocapillary maximum) potentials were obtained from the electrocapillary measurements by Paschen's method.⁷⁻⁹ Numerical integration of the capacity values was carried out once, at 20-mV intervals, to evaluate q_M and twice, at the same interval, to obtain γ as a function of potential E . A comparison of the potential values (at integral values of q_M) between the numerically integrated and computer integrated data showed the difference between the data obtained by the two methods to be less than 1 mV.

Surface excesses of the two anions were evaluated by graphical differentiation of the derived curves for γ as a function of $E_{\text{satd. cal}}$ obtained for the respective salt solutions at a constant reference electrode potential.¹⁰ The following equation was employed.

$$\left(\frac{\partial \gamma}{\partial \mu}\right)_{E, \text{ satd. cal.}} = -1/2(\Gamma_+ + \Gamma_-) + \Gamma_{\text{H}_2\text{O}} \left(\frac{x_{\text{salt}}}{x_{\text{H}_2\text{O}}}\right) \quad (1)$$

Since the last term is negligible and $-q_M$ values give the difference between Γ_+ and Γ_- , the surface excesses of the anion and cation can be calculated from eq 1. Activity coefficients for NH_4NO_3 solutions were taken from the compilation of Robinson and Stokes¹¹ and mean activity coefficients for potassium hydrogen phthalate solutions were calculated from the Debye-Hückel equation

$$-\log f_{\pm} = \frac{A\sqrt{\mu'}}{1 + 3.76 B\sqrt{\mu'}} \quad (2)$$

where A is a constant equal to 0.5085 (for 1:1 electrolytes), B is another constant equal to 0.3281, and μ' is the ionic strength of the solution. It is assumed that potassium hydrogen phthalate is a 1:1 electrolyte because (a) of the small ionization constant of the second carboxylic acid group and (b) the calculation of Hamer, *et al.*,¹² show that the extent of ionization to diphtalate ion is very small. From Γ_+ and Γ_- , q_1 (specifically adsorbed charge), q_d (dif-

fuse layer charge) and ϕ^{M-2} values were calculated using standard procedures wherein it is assumed that the cations only populate the diffuse layer. Figures 1 and 2 and Tables I and II refer to potassium acid phthalate and NH_4NO_3 , respectively.¹³

Table I: Coordinates of Electrocapillary Maximum for the System Hg-Potassium Hydrogen Phthalate (Aqueous)

Concn, M	$-E_{\text{ecm}}$, V	γ_{ecm} , ergs/cm ²
0.05	0.6662	408.4
0.075	0.6662	406.4
0.1	0.6662	404.0
0.15	0.6662	401.1
0.2	0.6662	399.4
0.3	0.6662	396.6
0.4	0.6662	393.6

Table II: Coordinates of Electrocapillary Maximum for the System Hg-Ammonium Nitrate (Aqueous)

Concn, M	$-E_{\text{ecm}}$, V	γ_{ecm} , ergs/cm ²
0.05	0.4585	424.3
0.10	0.4680	423.9
0.30	0.4858	423.3
0.60	0.5005	421.9
1.00	0.5140	420.9
2.00	0.5370	418.7
3.00	0.5519	417.2
5.00	0.5730	415.3
7.00	0.5905	413.7
9.00	0.6038	412.3
11.23	0.6190	411.0

Adsorption of Phthalate Ions. The differential capacity curves for phthalate ion show very interesting features such as the presence of humps on the cathodic side of the ecm. (These curves could not, however, be traced on the extreme cathodic side due to interference in the measurements by H_2 evolution.) The constancy of the potential of the ecm (measured with respect to the saturated KCl calomel electrode) with concentration suggests, according to the equation

$$\left(\frac{dE_{\text{satd. cal.}}}{d \ln a_{\pm}^2}\right) = \frac{RT}{F} \left[\frac{dq_1}{dq_M} + \frac{1}{2}\right] \quad (3)$$

(7) B. V. K. S. R. A. Tilak, Ph.D. Thesis, Banaras Hindu University, 1966.

(8) K. Muller, Ph.D. Thesis, University of Pennsylvania, 1965.

(9) J. O'M. Bockris, K. Müller, H. Wroblowa, and Z. Kovac, *J. Electroanal. Chem.*, **10**, 416 (1965).

(10) A. N. Frumkin, *Zh. Fiz. Khim.*, **30**, 2066 (1956).

(11) R. A. Robinson and R. H. Stokes, "Electrolyte Solutions," Butterworth and Co., Ltd., London, 1959.

(12) W. J. Hamer, G. D. Pinching, and S. F. Acree, *J. Res. Nat. Bur. Stand.*, **36**, 47 (1946).

(13) W. J. Hamer and S. F. Acree, *ibid.*, **35**, 381 (1945).

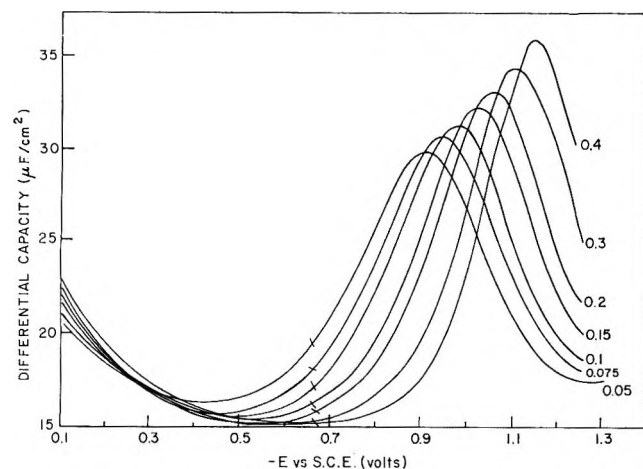


Figure 1. Differential capacity curves at the interface Hg-potassium hydrogen phthalate (aq) at 25°; \leftarrow refer to the potential of zero charge and the numbers on the curve to the concentration of the solution.

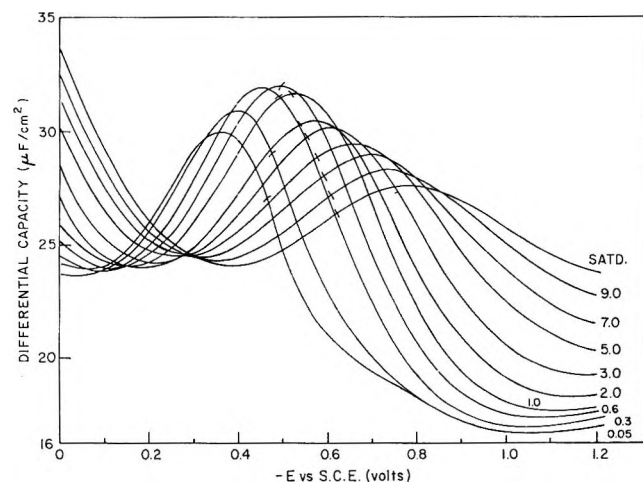


Figure 2. Differential capacitance curves at the interface Hg-NH₄NO₃ (aq) at 25°; \leftarrow refer to the potential of zero charge and the numbers on the curve to the concentration of the solution.

and because $(d\gamma/d\mu)$ reaches a constant value at high salt concentrations, that saturation adsorption is attained at the ecm. This conclusion is also suggested from the variation of specifically adsorbed charge (see Figure 3) with q_M at different concentrations.

In order to gain further insight into the mode of adsorption, the q_1 values were evaluated in the first instance by the model method of Devanathan.¹⁴ The model (see Figure 4) assumed here is that the COO⁻ group is adsorbed with the oxygen and toward the metal and with the benzene ring parallel to the metal surface. In this configuration, the benzene ring is separated from the metal by one layer of water molecules, which means that the benzene ring is between the inner Helmholtz plane and the outer Helmholtz plane. It is assumed here that this orientation does

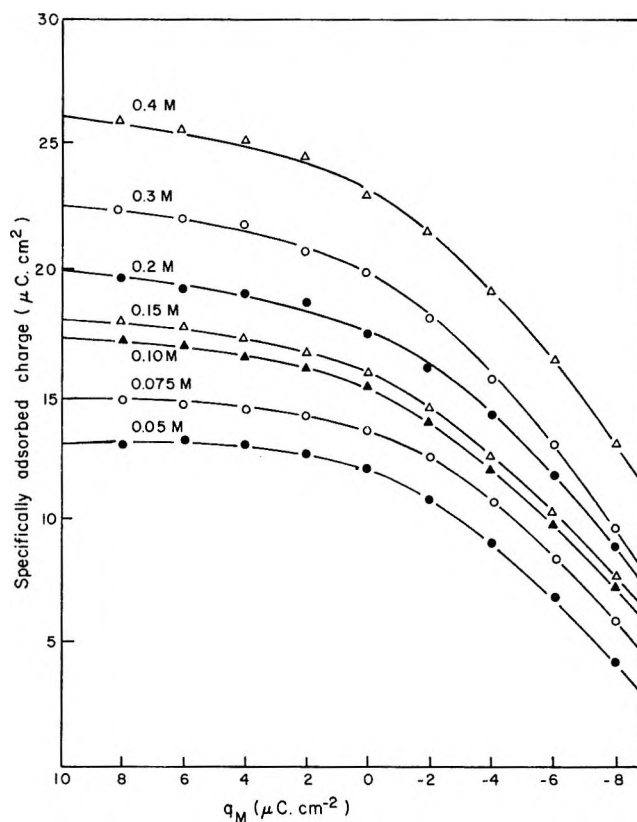


Figure 3. Variation of specifically adsorbed charge (q_1) with q_M for the adsorption of phthalate ions on Hg.

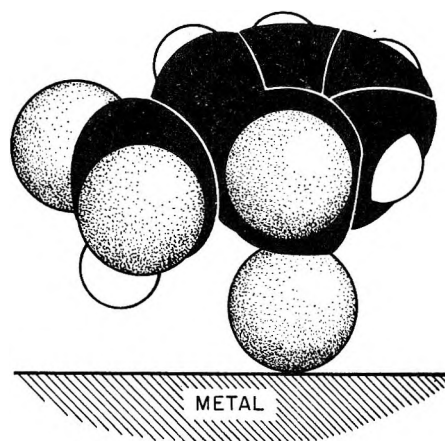


Figure 4. Model for the adsorption of potassium hydrogen phthalate ion on mercury (not drawn to scale).

not alter the dielectric constant in the region between the IHP and OHP from the value¹⁴ $\epsilon = 7.2$.

The tabulated^{15,16} length of the C=O group is 1.37 Å. Since the O=C-O angle is *ca.* 120°, the vertical distance from the line of centers between the carbon and

(14) M. A. V. Devanathan, *Trans. Faraday Soc.*, **50**, 373 (1954).

(15) "Tables of Interatomic Distances and Configuration in Molecules and Ions," Special Publication No. 11, The Chemical Society, London, 1958.

(16) R. W. G. Wykoff, "Crystal Structure," Interscience Publishers, New York, N. Y., 1948.

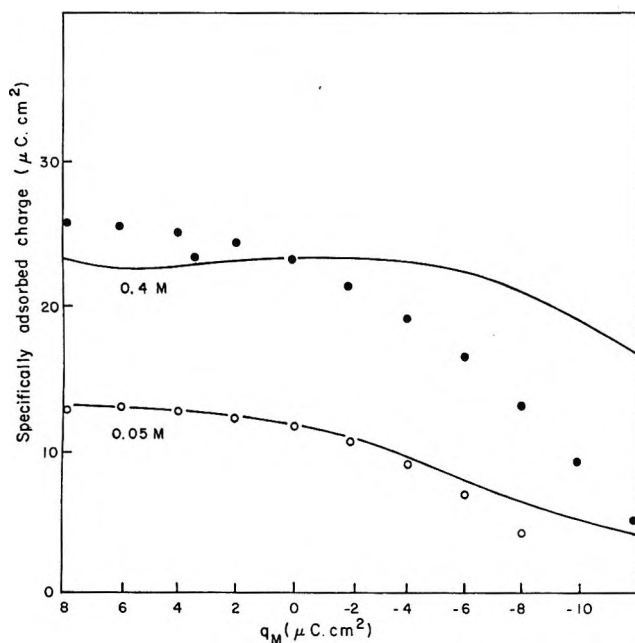


Figure 5. Comparison of q_1 values obtained thermodynamically with the q_1 values calculated (—) using Devanathan's model (for phthalate ion adsorption).

oxygen atoms is 0.685 \AA . Hence the distance from the metal to the IHP is 0.685 \AA plus the radius of the oxygen atom (taken from Catalin models), *i.e.*, 1.82 \AA . Hence K_{m-1} and K_{m-2} are 34.9 and 33.3 \mu F , respectively. For calculation of q_1 from the model, the q_1 value at any q_M should be known in advance. Previously,¹⁴ it was assumed, based on thermodynamic data, that q_1 approaches zero at $q_M = -12$ to $-13 \text{ \mu C cm}^{-2}$. Since, for the case of phthalate ion investigated in the present work, the differential capacity curves could not be traced on the extreme cathodic side, the q_1 value (obtained by the usual thermodynamic methods) at the ecm is chosen as the starting point for the integration. A comparison (see Figure 5) with the q_1 values obtained thermodynamically shows that for 0.05 N solutions the agreement is satisfactory but, at high concentrations, the model method fails because of factors to be discussed below.

Since the differential capacitance curve at constant concentration can be described¹⁴ by the equation

$$\frac{1}{C} = \frac{1}{K_{m-1}} + \frac{1}{K_{1-2}} \frac{dq_d}{dq_M} \quad (4a)$$

$$\frac{dq_d}{dq_M} = \left(1 - \frac{dq_1}{dq_M} \right) \quad (4b)$$

where subscripts 1 and 2 refer to the regions between the metal and inner and outer Helmholtz planes, respectively. The present discussion will be directed toward understanding the nature of the (dq_1/dq_M) term and its role in determining the form of the differential capacitance curves.

From the isotherm derived elsewhere,¹⁷ $(dq_1/dq_M)_{a_{\pm}}$ is given (after taking into account the $(1 - \theta)$ term) by

$$\left(\frac{dq_1}{dq_M} \right)_{a_{\pm}} = \frac{1}{R^* + \frac{1}{Bq_1(1 - \theta)}} \quad (5)$$

Since the area of the phthalate ion (calculated from Catalin models) is *ca.* 65.6 \AA^2 , q_s would be $12.2 \text{ \mu C cm}^{-2}$. The calculated values of dq_1/dq_M are compared (see Figure 6) with those evaluated by differentiation of the q_1 vs. q_M curves obtained by thermodynamic methods. The marked disagreement can be attributed to two factors. The first is that q_s is changing from $12.2 \text{ \mu C cm}^{-2}$ to $24.4 \text{ \mu C cm}^{-2}$ because the area available for each ion is becoming reduced from its co-area of 131.2 \AA^2 to its actual area of 65.6 \AA^2 . This explanation can be understood by postulating that the type of adsorption is changing from mobile to localized. The supposition that the latter mode of adsorption can arise on a liquid surface is, however, probably not justifiable. An alternative explanation is based on the assumption that carboxylic acid group of the potassium hydrogen phthalate ion is being ionized by the intense electric field at the interface. This assumption allows the model based on a mobile mode of adsorption to be retained because the value of q_s for a given area of one ion, *viz.*, 131.2 \AA^2 changes from $12.2 \text{ \mu C cm}^{-2}$ to $24.4 \text{ \mu C cm}^{-2}$ (when phthalate is completely ionized). This behavior of field-induced ionization¹⁸ can be expected in view of the expectation that a change of $2.303RT \text{ pK V}$, *i.e.*, 0.306 V (where pK is the ionization constant of the second COOH group), would be sufficient to facilitate surface ionization of the COOH group and such electrolytes are known to exhibit the dissociation field effect. Thus, considering the re-

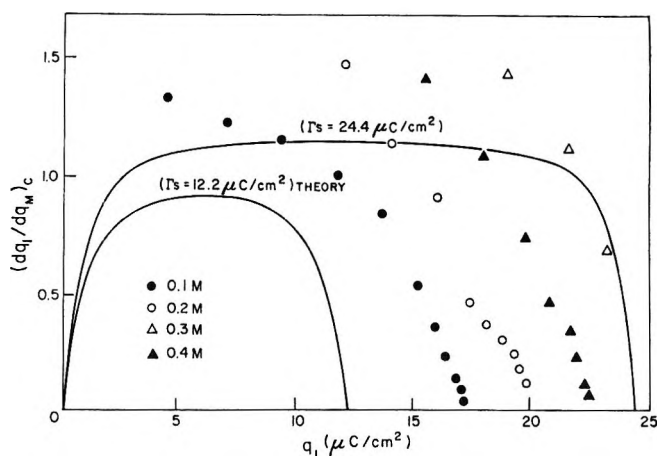


Figure 6. Test of eq 5 for the adsorption of phthalate ions on mercury.

(17) M. A. V. Devanathan and B. V. K. S. R. A. Tilak, *Proc. Roy. Soc.*, **A290**, 527 (1966).

(18) L. Onsager, *J. Chem. Phys.*, **2**, 599 (1934).

Table III: (dq_1/dq_M)₂ Values for Nitrate Adsorption on Mercury Obtained by Graphical Differentiation of q_1 vs. q_M Curves

q_M , $\mu\text{C}/\text{cm}^2$	Concn							
	0.1 M	0.3 M	1 M	3 M	5 M	7 M	9 M	
12	0.81	0.81	0.59	1.55	1.27	1.92	1.12	
10	0.85	0.89	0.73	1.25	1.31	1.64	1.40	
8	0.98	0.95	0.88	1.07	1.39	1.46	1.60	
6	1.04	0.99	0.93	1.31	1.36	1.52	1.80	
4	0.97	1.00	0.98	1.45	1.40	1.68	1.77	
2	0.85	0.88	1.17	1.59	1.63	1.74	1.97	
0	0.75	0.78	1.22	1.65	1.79	1.93	2.13	
-2	0.61	0.68	1.29	1.72	2.07	2.07	2.19	
-4	0.39	0.60	1.10	2.02	2.19	2.26	2.46	
-6	...	0.41	1.03	2.13	2.33	2.62	2.62	
-8	0.84	2.29	2.75	

sulting ions to be divalent, dq_1/dq_M values can be calculated and compared with experiment (see Figure 6). The experimental values lie between the dq_1/dq_M values calculated on the basis of unit charge per ion and two unit charges per ion, and hence suggest that surface ionization may be responsible for the variations of q_s . It is not possible, with the data at present available, to distinguish between surface ionization and transition of the adsorption behavior from nonlocalized to localized, but the latter situation is unlikely.

Adsorption of Nitrate Ions. It is well known that nitrates and perchlorates of Na^+ and NH_4^+ are extensively hydrated. The specific adsorption of these ions presents unusual features compared to that of halides or large anions. (This is to be expected because a hydrated ion may not possess a permanent dipole moment since the disposition of water molecules in the hydration sheath is usually symmetrical. However, when the adsorbed ion is partially hydrated in the adsorbed position, a residual permanent electric moment may be set up.) These features are the following.

(i) The dq_1/dq_M values (see Table III) range from 0.8 for 0.1 N solution to 2.0 for saturated solutions (see Figure 7). These figures agree well with values of dq_1/dq_M obtained from the slope of the plot of $E_{\text{satd. cal.}}$ against $\log a_{\pm}$ at constant q_M .

(ii) The inner layer capacity curves show (Figure 8) that the hump height decreases with increasing concentration (see also ref 19 and 20). This behavior is different for potassium hydrogen phthalate adsorption (see Figure 9) wherein, as for halides, C_1 increases with increasing concentration.

(iii) The variation of q_1 with q_M for these ions suggests that there exists a saturation value of q_s for each concentration and this value of q_s is a function of concentration. If this idea is accepted, then the q_s values vary, as the bulk concentration is varied, from $12 \mu\text{C cm}^{-2}$ (0.1 M) to ca. $44 \mu\text{C cm}^{-2}$ for saturated solutions.

It should be mentioned here that Payne¹⁹ studied adsorption of nitrate ion from nitrate-fluoride mix-

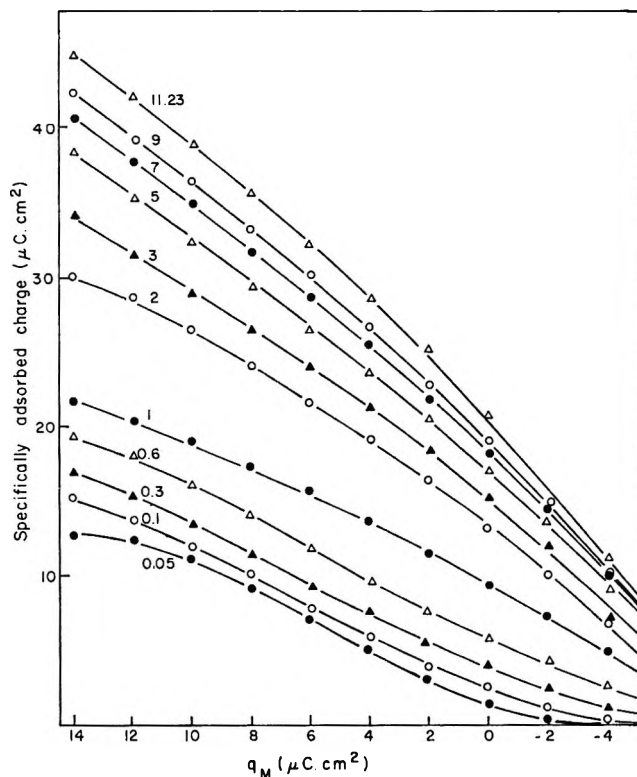


Figure 7. Variation of q_1 with q_M at different bulk concentrations (shown as numbers on each curve) for the adsorption of nitrate ions on mercury.

tures over the concentration range 0 to 1 M in aqueous solutions and reported low dq/dq_M values of the order of 0.5 for dilute solutions.

The variation of q_s with concentration is unexpected in these systems. It is necessary to postulate a model within the framework of which at least the extreme variations can be accounted for. The model assumed here is that nitrate ion is adsorbed "flat" with the plane passing through all the four atoms parallel to the mercury surface. The "flat" orientation for the adsorption

(19) R. Payne, *J. Phys. Chem.*, **69**, 4113 (1965).

(20) R. Payne, *ibid.*, **70**, 204 (1966).

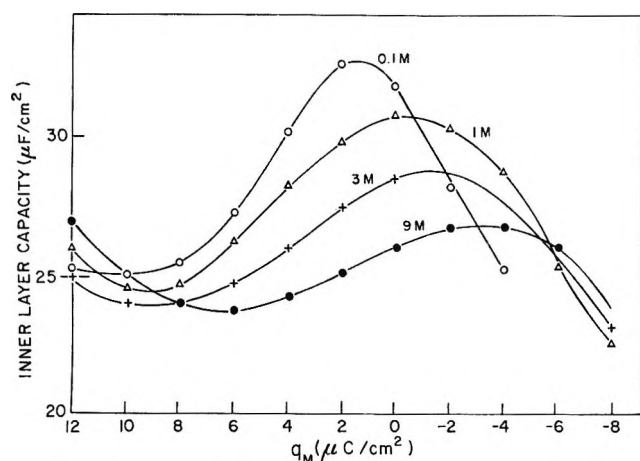


Figure 8. Inner layer capacitance of the interface Hg-NH₄NO₃ (aq) (the concentrations are shown on each curve).

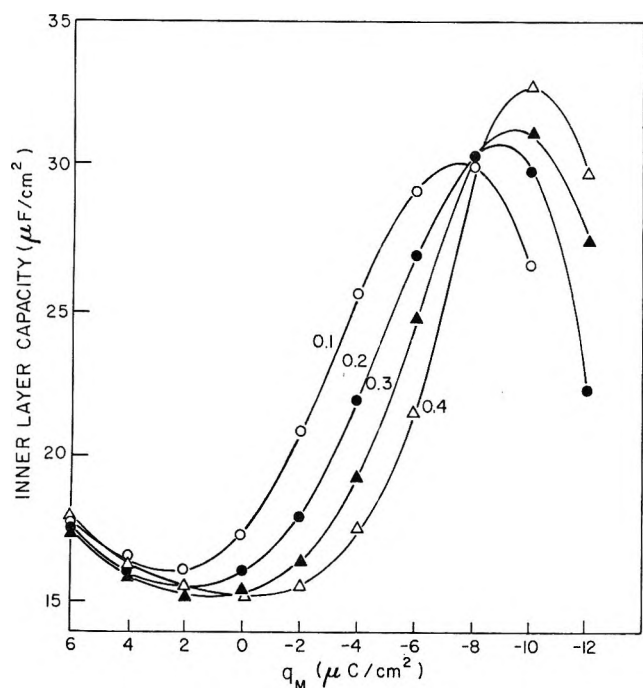


Figure 9. Inner-layer capacitance at the interface Hg-potassium hydrogen phthalate (aq) (the numbers refer to the concentration of ion in the solution).

of nitrate ions was also proposed earlier by Payne.¹⁹ Since the area of nitrate ion in this configuration is ca. 21.2 Å², a maximum q_1 of 37.7 μC cm⁻² should be expected and compares well with the experimental value of 42 μC cm⁻². For setting up a lower limit of q_s , let it be assumed that the ion is hydrated and that the area of the hydrated ion is equal to the sum of its area and the area of the total number of water molecules attached to it (which lie in the same plane on the Hg surface); then it can be seen that the number of water molecules attached to each ion varies from 5 (in dilute solutions corresponding to a q_s of 15 μC cm⁻²) to 0 (in concentrated solutions). Thus it ap-

pears that there may be variation in the hydration of the adsorbed ions as the solution concentration is changed.

Effect of χ . As pointed out earlier, C_i decreases with increasing concentration contrary to the following equation²¹ for C_i

$$\frac{1}{C_i} = \left(\frac{\partial \phi^{M-2}}{\partial q_M} \right) + \left(\frac{\partial \phi^{M-2}}{\partial q_1} \right) \frac{dq_1}{dq_M} \quad (6)$$

according to which C_i is dependent directly on dq_1/dq_M . When dq_1/dq_M is small, C_i should be small, but this is contrary to the experimental observations which show that when dq_1/dq_M is small, C_i is high and *vice versa*. Hence it appears that a possible potential contribution (χ) from the water dipoles which form part of the adsorbed species is omitted in the model of the electrical double layer. This extra χ contribution from the adsorbed dipoles around the specifically adsorbed anions to the potential of the inner Helmholtz plane can be empirically evaluated (in the first instance) in the following way.

When water dipoles contribute χ to the measured potential, ϕ^{M-2} is given by

$$\phi^{M-2} = \frac{q_M}{K_s} - \frac{|q_1|}{K_{1-2}} - \chi \quad (7)$$

Hence ϕ_1 (potential of the IHP) is equal to

$$\phi_1 = \frac{q_M}{K_{1-2}} - \frac{|q_1|}{K_{1-2}} - \chi \quad (8)$$

and ϕ_a , the adsorption potential, is given, following an earlier treatment,¹⁷ by

$$\phi_a = \frac{q_M}{K_{1-2}} - \frac{|q_1|R^*}{K_{1-2}} - \chi \quad (9)$$

where R^* is a factor introduced to allow for discreteness-of-charge effects. By substituting ϕ_a into the isotherm derived earlier, and differentiating at constant μ , it follows that

$$\left(\frac{dq_1}{dq_M} \right)_\mu = B \left(\frac{q_s}{q_1(q_s - q_1)} + BR^* + \frac{\chi'e_0}{kT} \right)^{-1} \quad (10)$$

where $\chi'e_0/kT$ is equal to $(d\chi/dq_1)(e_0/kT)$. The factor $(\chi'e_0/kT)$ is only a correction factor to eq 5 for evaluating from the experimental (dq_1/dq_M) values the nature and extent of the potential contribution arising from adsorbed ion-bound water. Various values of $\chi'e_0/kT$ were used and it was found that for a 0.1 *N* solution, reasonable agreement with experiment (see Figure 10) could be obtained with a value of $q_s = 15$ μC cm⁻² and $\chi'e_0/kT = 0$ while for 9 *M* solution agreement arose when $q_s = 37.7$ μC cm⁻² and $\chi'e_0/kT = -0.492$.

(21) R. Parsons, *Trans. Faraday Soc.*, **55**, 999 (1959).

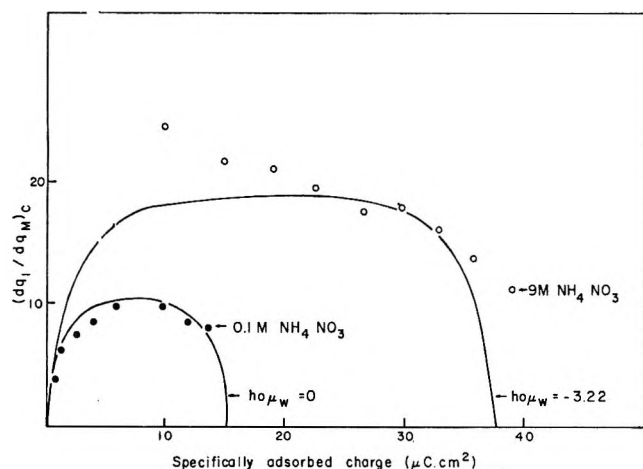


Figure 10. Comparison of experimental $(dq_1/dq_M)_c$ values with theory (for nitrate ion adsorption).

Rigid Hydration Model. Various models have been formulated for evaluation of χ . They are as follows.

(i) "Up and Down Water" Model. Here it is assumed that water dipoles are oriented in "up" and "down" directions with respect to the Hg surface around the specifically adsorbed ion, *i.e.*, in a way similar to the orientation of water molecules adsorbed on the electrode surface envisaged by Watts-Tobin,²² but around the ion. These dipoles are supposed to respond to the field due to q_M only and thereby contribute an extra capacity.

(ii) "Exponential Field Response" Model. The dipoles are assumed to respond to the field through an exponential relationship.

(iii) "Polarizability" Model. The χ contribution in this model is assumed to be given by $4\pi N\bar{\mu}/\epsilon$ where $\bar{\mu}$ is equal to αF ; α is equal to the sum of the polarizability of the ion (α_i) and the number of water dipoles (h_0) around each ion and is given by

$$\alpha = \alpha_i + \frac{q_1 h_0}{e_0} \alpha_w \quad (11)$$

None of these models is able to provide an adequate description of the experimental situation; hence the following representation, which will be termed the "rigid hydration model," is proposed. (Here it is necessary to distinguish this model from that suggested by Payne¹⁹ according to which there is a potential contribution from the dipole moment of the displaced water molecules to ϕ^{M-2} . While this may be true for adsorption of organic substances, it seems to be an unlikely factor in ionic adsorption since no peculiarities were observed in investigations on the adsorption of ions such as *m*-benzenedisulfonate²³ or *p*-toluenesulfonate²⁴ which can displace a selectively large number of water dipoles from the interface.) According to this model, the adsorbed ion has a certain configuration of adsorbed water molecules. (This configuration of

adsorbed water dipoles is characteristic of the structure of the adsorbed ion.) The whole assembly gives rise to a dipole potential of χ , which is expressed, for convenience, in terms of a multiple of the elementary moment of water (μ_w) and the effective number h_0 of water molecules around the adsorbed ion by writing

$$\chi = 4\pi q_1 h_0 \mu_w / \epsilon \quad (12)$$

In this equation $h_0 \mu_w$ represents the average moment contributed by the adsorbed ion-bound water dipoles. It is at present difficult to break this quantity down into individual contributions. However, we can assume $\mu_w = 1.84$ D and calculate h_0 to get some idea of the extent of the number of water molecules associated with each ion in the double layer. It follows from eq 7 that

$$\frac{1}{C_i} = \frac{1}{K_s} - \frac{1}{K_{1-2}} \frac{dq_1}{dq_M} - \frac{4\pi h_0 \mu_w}{\epsilon e_0} \frac{dq_1}{dq_M} \quad (13)$$

and

$$\frac{dq_1}{dq_M} = B \left[\frac{q_s}{q_1(q_s - q_1)} + BR^* + \frac{4\pi h_0 \mu_w}{\epsilon e_0 kT} \right]^{-1} \quad (14)$$

A calculation of h_0 from the previously evaluated $\chi' e_0 / kT$ values shows that h_0 varies from 0 (at 0.1 M) to -1.7 or -2 in concentrated solutions. This approach appears to be simple and perhaps more meaningful than that in the first three models studied. The above values can be understood if it is proposed that when nitrate ion is adsorbed, water molecules are oriented around the ion toward the oxygen end of NO_3^- (see Figure 11). It can be seen from the Figure 11 that the total moment due to the three water molecules around the ion is 4.38 D. There is a possibility that the water dipole is interacting on the top of an oxygen atom of the NO_3^- ion. In this configuration, the dipole contribution due to one water molecule is 1.51 – 1.51

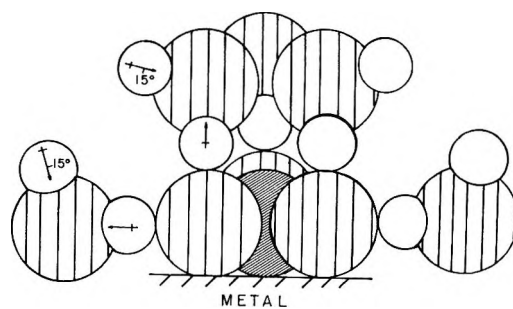


Figure 11. Model for the adsorption of nitrate ion on mercury (not drawn to scale) (The orientation of water molecules on the third oxygen atom is not shown in the figure).

(22) R. J. Watts-Tobin, *Phil. Mag.*, **6**, 133 (1961).

(23) J. M. Parry and R. Parsons, *Trans. Faraday Soc.*, **59**, 241 (1963).

(24) J. M. Parry and R. Parsons, *J. Electrochem. Soc.*, **113**, 992 (1966).

$\cos 75$, which is equal to 1.12 D. Since there is one water molecule on each of the three oxygen atoms of the nitrate ion, the net moment would be -3.36 D and act in opposition to the moment of 4.38 D generated by the three water dipoles around the ion. Hence the net moment is 1.02 D. As the solution becomes more concentrated, there is a progressive diminution of water molecules adsorbed on the Hg surface and hence around the adsorbed ions, and this contributes to an apparent increase in area of the adsorbed ion. When there are limitingly no dipoles laterally adjacent to the ion in the interphase, there is a net moment of -3.36 D normal to the surface. These extreme values of 1.02 and -3.36 D appear to compare roughly, though not exactly, with the previously calculated value. It should be kept in mind that there is considerable uncertainty in the orientation of adsorbed molecules on the surface due to thermal agitation and the trend calculated above must be considered satisfactory. Thus it appears that it may be necessary to consider the fine structure of the adsorbed ion, especially its hydration structure at the IHP, since it is not a requirement that the ion be completely dehydrated for adsorption to occur at the Hg-solution interface and indeed such a situation would be energetically improbable. It may be noted here that the humps tend to become broader with increasing concentration. This appears to be a consequence of the widening of the double layer, but this conclusion has to be verified with other systems at high concentrations.

Inner-Layer Capacity in the Absence of Specific Adsorption. There are essentially two models so far proposed (see ref 2 and 3) for the structure of the inner layer in the absence of specific adsorption. According to the dielectric model,²⁵ the adsorbed dipoles on the electrode contribute a potential to the measured voltage difference by orientation in the direction of the field due to the charge q_M . Although such behavior is theoretically expected,²⁶ certain experimental evidence, however, does not unequivocally lead us in that direction. Thus: (i) While NaOH,²⁷ and NaF²⁸ meet all the criteria for nonspecific adsorption, the C_i curves are quite different.

(ii) When the reciprocal of $(\partial\phi^{M-2}/\partial q_M)_{q_1 \rightarrow 0}$ is evaluated at different charge densities on the metal and compared with the inner layer capacitance curve in the presence of NaF, it is found^{29,30} that the curves are very similar.

This agreement gave support to the notion that the NaF curve is representative of the ideal case of nonspecifically adsorbed anions and is characteristic only of the solvent. However, when values of $(\partial\phi^{M-2}/\partial q_M)^{-1}_{q_1 \rightarrow 0}$ are calculated for a large number of ions including the ions studied in the present work (see Figures 12 and 13) and the quantities are compared (Figure 14) as integral capacities with the data for inner layer capacitance obtained by Payne³¹ for

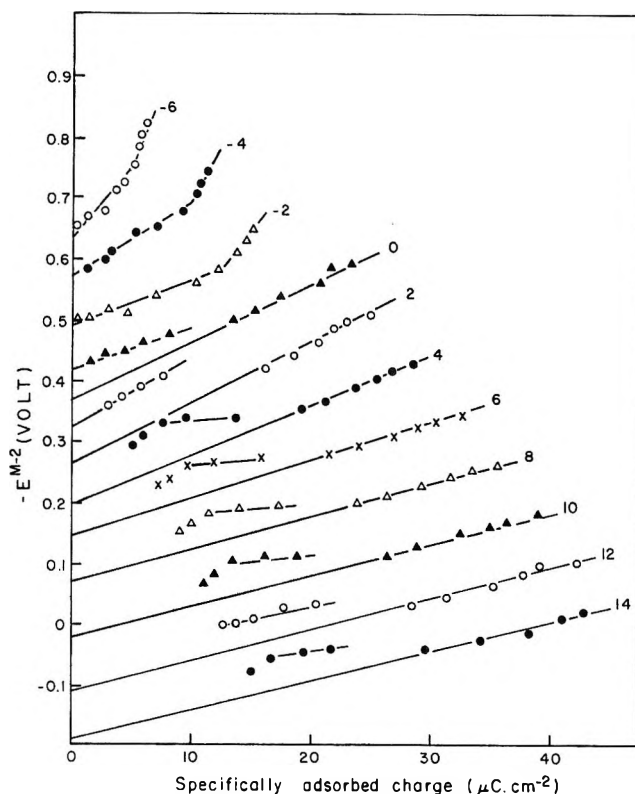


Figure 12. Plots of E^{M-2} with q_1 at constant q_M for the adsorption of nitrate ions on mercury (The values of q_M are given on each curve).

1.0 N NH_4F solutions, it is found that no definite conclusion can be reached about the solvent capacitance behavior. In the above comparison, the data of Wroblowa, *et al.*,³² were taken and plots of ϕ^{M-2} vs. q were made for CN^- , CNS^- , BrO_3^- , ClO_3^- , and ClO_4^- . For *m*-benzenedisulfonate,³³ chloride,²⁹ iodide,³⁰ Ti^{+34} values were taken from the data quoted in the literature. For Br^- ion, plots were made from the data in ref 35. The capacitance curve evaluated by the above method is dependent on the specific adsorption characteristics of the anions.

(iii) If $\chi_{\text{H}_2\text{O}}$ is large, its effects will be quite pronounced in organic adsorption behavior, which is one

(25) R. Parsons, *Chem. Soc. (Ann. Reports)*, **56**, 80 (1964).

(26) J. R. Macdonald and C. A. Barlow, Jr., *Proceedings of the First Australian Conference on Electrochemistry*, Pergamon Press, London, 1964, p 199.

(27) R. Payne, *J. Electroanal. Chem.*, **7**, 343 (1964).

(28) D. C. Grahame, *Chem. Rev.*, **41**, 441 (1947).

(29) D. C. Grahame and R. Parsons, *J. Amer. Chem. Soc.*, **83**, 1291 (1961).

(30) D. C. Grahame, *ibid.*, **80**, 4201 (1958).

(31) R. Payne, personal communication.

(32) H. Wroblowa, Z. Kovac, and J. O'M. Bockris, *Trans. Faraday Soc.*, **61**, 1523 (1965).

(33) J. M. Parry and R. Parsons, *ibid.*, **59**, 241 (1963).

(34) P. Delahay and G. G. Susbielles, *J. Phys. Chem.*, **70**, 647 (1966).

(35) P. Peries, Thesis University of Ceylon, 1954.

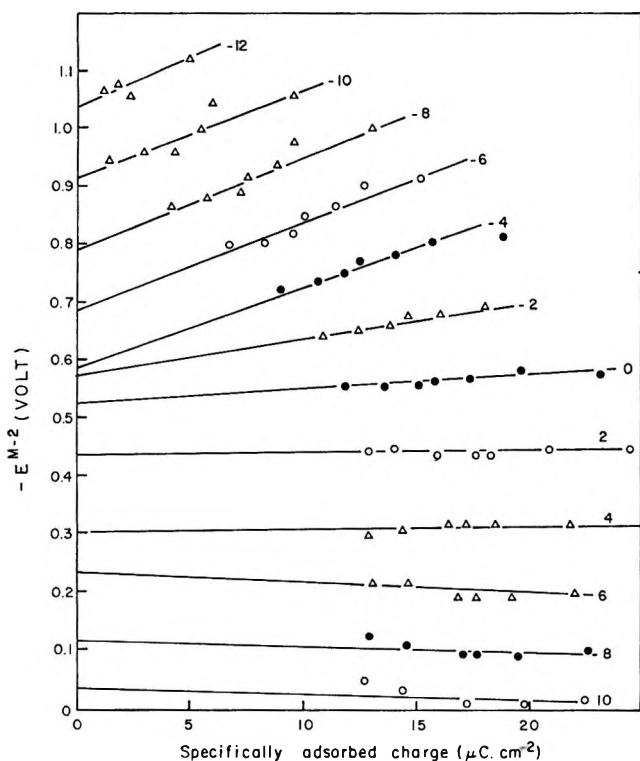


Figure 13. Plots of E^{M-2} with q_1 at constant q_M for the adsorption of phthalate ions on mercury (the values of q_M are given on each curve).

of competition for sites at the interface between the solvent and the organic species, and also in kinetic studies,⁴ but no specific χ_{H_2O} effects appear to have been observed so far.³⁶

(iv) By definition³⁷

$$C = \frac{\partial \Gamma_+}{\partial E} + \frac{\partial \Gamma_-}{\partial E} \quad (15)$$

and in the hump region

$$\frac{\partial C}{\partial E} = 0 \text{ or } \left(\frac{\partial^2 \Gamma_+}{\partial E^2} \right) \text{ and } \left(\frac{\partial^2 \Gamma_-}{\partial E^2} \right)$$

should be either equal in magnitude or zero. Hence it appears reasonable to ascribe hump properties to changes brought about by anions or cations rather than to variations, *e.g.*, solvent orientation, which are independent of Γ_+ or Γ_- .

Since the BDM model⁴ could explain some of the above points, one may regard it as a better description of the electrical double layer than the dielectric model. However, it is difficult to explain the equilibrium properties of the Hg-solution interface in the presence of NaF and NaOH solutions which, according to many tests for nonspecific adsorption, show that these ions are indeed not specifically adsorbed. This means that either the tests are not sensitive enough to distinguish weak adsorption or the basic model which involves assignment of two different planes, *viz.*, the IHP for anions and the OHP for cations is not always correct,

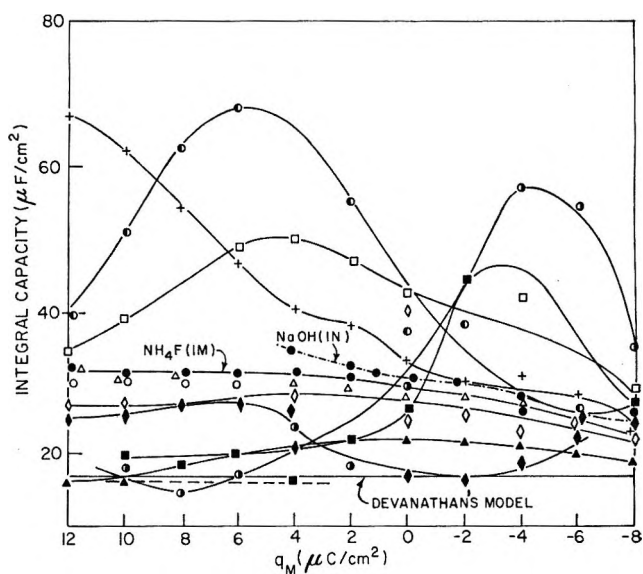


Figure 14. Inner-layer capacitance curves (plotted as integral capacity) in the absence of specific adsorption: ---, Tl^+ ; \circ , Cl^- (KCl); Δ , I^- (KI); \blacktriangle , *m*-benzenedisulfonate; \bullet , ClO_3^- (NaClO₃); \ominus , CN^- (NaCN); \times , ClO_4^- (NaClO₄); \square , BrO_3^- (NaBrO₃); \blacksquare , phthalate; \diamond , acetate (sodium acetate); \blacklozenge , NO_3^- (NH₄NO₃); - - - - - , NaOH (1 M).

particularly for the larger ions. Further, according to this model, the hump is solely ascribed to changes in dq_1/dq_M . While this is true for some ions such as benzenesulfonate or phthalate, it does not appear to be the case for hydrated anions like NO_3^- , etc. (see Table IV).

Table IV: Hump Properties in the Presence of Nitrate Ion

Concn. M	C_{hump} $\mu\text{F}/\text{cm}^2$	E vs. sce (hump), V	q_M , hump, $\mu\text{C}/\text{cm}^2$	$-q_1$, hump, $\mu\text{C}/\text{cm}^2$
0.05	30.00	-0.36	2.7	3.8
0.1	30.95	-0.40	2.0	4.2
0.3	31.95	-0.45	1.1	4.9
0.6	32.02	-0.50	0	6.0
1.0	31.78	-0.53	-0.6	8.8
2.0	30.60	-0.57	-1.1	11.7
3.0	30.15	-0.60	-1.5	12.6
5.0	29.45	-0.65	-2.3	13.0
7.0	28.95	-0.70	-3.1	12.2
9.0	28.27	-0.75	-4.1	10.2
11.23	27.60	-0.80	-4.9	8.9

Thus it appears that these two approaches do not lead to a better understanding of the structure of the electrical double layer and deeper insight can be gained, it seems, by consideration of the hydration structure of the adsorbed ion. This approach could possibly provide a bridge between the two opposite viewpoints (further

(36) R. Payne, *J. Electroanal. Chem.*, **19**, 1 (1968).

(37) D. C. Grahame and B. A. Soderberg, *J. Chem. Phys.*, **22**, 449 (1954).

details will be published in a later communication) referred to earlier,^{2b} unless the basic model of Grahame is itself not applicable, so that one has to think in terms of *three* planes of closest approach, one corresponding to the anions (as in Grahame's model), the other cations "adsorbed on anions" probably as ion pairs,^{38,39} and the third for the remaining cations (as in Grahame's model).

Acknowledgments. The authors wish to thank the Director, Central Electrochemical Research Institute,

Karaikudi-3 (India), for providing the facilities which enabled these investigations to be carried out and Dr. Richard Payne for sending us the data quoted in ref 31 and the computer program. Our thanks are due to Professor B. E. Conway for reading the manuscript and giving many valuable suggestions.

(38) S. K. Rangarajan, private communication, 1967.

(39) A. Jenard and H. D. Hurwitz, *J. Electroanal. Chem.*, **19**, 441 (1968).

The Compact Double Layer as a Function of Temperature and Pressure

by Graham Hills

Chemistry Department, University of Southampton, Highfield, Southampton, England (Received February 24, 1969)

Consideration is given to the temperature and pressure coefficients of interfacial properties such as surface tension and electrical capacity. The thermodynamic excess entropy and the thermodynamic excess volume are expressed in terms of the composition of the interphase. Observed values of Γ_s and Γ_v are related to the properties of the solvent in the interface and to the adsorption of ions. Particular attention is directed to the temperature-invariant point of common intersection of the inner-layer capacitance-potential curves. This is also explained in terms of competitive adsorption between anions and solvent molecules and in terms of the influence of the adsorbed ions on the properties of the solvent.

Virtually all the studies of the double-layer at polarizable metal-solution interfaces have been concerned with varying the chemical composition of the system. The use of a variety of amalgams, solutes, and solvents has produced a large body of thermodynamic data consistent with elementary theories of electrostatics and adsorption. Attempts to relate these data to molecular models of the interphase have been largely frustrated by the inadequacies of the statistical mechanics of condensed phases and there remain even qualitative uncertainties regarding, for example, the nature of the inner or compact part of the double layer. Somewhat surprisingly, there has been little effort to involve the other thermodynamic variables, namely temperature and pressure, in spite of the large changes they are known to produce. Necessarily, the interpretation of derived entropies and volumes is also limited by our ignorance of microscopic properties of near-neighbor interactions, etc., but these thermodynamic quantities can be directly and usefully related to the inner layer in a way which emphasizes the importance of competitive adsorption into the interface.

This paper deals in turn with (1) the thermodynamic significance of temperature and pressure coefficients, (2) their experimental investigation, and (3) some spec-

ulations on the gross features of the inner-layer capacitance for aqueous systems.

Thermodynamic Relationships

Temperature and pressure are equivalent variables and an almost identical set of relations can be used to describe the entropy or the volume functions of the interface. The resultant quantities of course differ significantly in their interpretability. Over the range of pressures usually involved (1-5 kbars), individual molecules are incompressible and only changes in the free or excess volume of the solvent are sensed. Temperature coefficients, on the other hand, may be sensitive to intramolecular as well as to intermolecular entropy factors and are therefore likely to be less easy to interpret.

A number of basic equations relating to interfacial properties are given by Guggenheim,¹ some of them necessarily complex. The free energy of an interphase between two liquids is given by

$$dG^\sigma = V^\sigma dP - S^\sigma dT + \gamma dA + \sum_i \mu_i^\sigma dm_i^\sigma \quad (1)$$

from which it follows that

(1) E. A. Guggenheim, "Thermodynamics," North Holland Publishing Co., Amsterdam, 1949.

$$\left(\frac{\partial G^\sigma}{\partial A}\right)_{T,P,m_i} = \gamma \quad (2)$$

$$\left(\frac{\partial G^\sigma}{\partial P}\right)_{T,A,m_i} = V^\sigma \quad (3)$$

$$\left(\frac{\partial^2 G^\sigma}{\partial P \partial A}\right)_{T,m_i} = \left(\frac{\partial V^\sigma}{\partial A}\right)_{T,P,m_i} = \left(\frac{\partial \gamma}{\partial P}\right)_{T,A,m_i} \quad (4)$$

V^σ is the arbitrary volume of the interphase (which is as yet unbounded) whereas $(\partial V^\sigma / \partial A^\sigma)_{T,P,m_i}$, the change in volume of the interphase per unit increment of area, is a definite quantity operationally defined by $(\partial \gamma / \partial P)_{T,A,m_i}$ and equal to the volume of formation of the interphase, *i.e.*

$$\left(\frac{\partial \gamma}{\partial P}\right)_{T,A,m_i} = V^\sigma - \sum_\alpha m^\alpha \bar{V}^\alpha - \sum_\beta m^\beta \bar{V}^\beta \quad (5)$$

The variation of interfacial tension with pressure is neither easily nor accurately observed and a better source of experimental information for metal-solution interfaces is to be found in the measurement of interfacial electrical capacities. The system under consideration is invariably Hg-solvent, salt, and control of the electrical variable, surface charge density, or electrode potentials involves a reference electrode and *inter alia* the chemical potential of the dissolved salt.

In this case, the appropriate form of the Gibbs-Duhem relation (for an aqueous system) is

$$S^\sigma dT - V^\sigma dP + Ad\gamma + m_{\text{Hg}}^\sigma d\mu_{\text{Hg}} + m_{\text{H}_2\text{O}}^\sigma d\mu_{\text{H}_2\text{O}} + m_{\text{salt}}^\sigma d\mu_{\text{salt}} + qd\epsilon_\pm = 0 \quad (6)$$

from which it is usual to eliminate *one* of the component variables from each of the bulk phases (α and β) in terms of the Gibbs-Duhem relation for that phase. Thus, in terms of volume changes only (*i.e.*, at constant temperature) we can write

$$m_{\text{Hg}}^\beta \bar{V}_{\text{Hg}}^\beta dP - m_{\text{Hg}}^\beta d\mu_{\text{Hg}} = 0 \quad (7)$$

$$(m_{\text{H}_2\text{O}}^\alpha \bar{V}_{\text{H}_2\text{O}}^\alpha + m_{\text{salt}}^\alpha \bar{V}_{\text{salt}}^\alpha) dP - m_{\text{H}_2\text{O}}^\alpha d\mu_{\text{H}_2\text{O}}^\alpha - m_{\text{salt}}^\alpha d\mu_{\text{salt}}^\alpha = 0 \quad (8)$$

Remembering that both bulk phases are in equilibrium with the interphase, the chemical potentials of the various components are equal. We can thus equate and eliminate the $d\mu_{\text{Hg}}$ terms and the $d\mu_{\text{H}_2\text{O}}$ terms to give

$$\begin{aligned} -Ad\gamma = & - \left(V^\sigma - m_{\text{Hg}}^\sigma \bar{V}_{\text{Hg}}^\beta - m_{\text{H}_2\text{O}}^\sigma \bar{V}_{\text{H}_2\text{O}}^\alpha - m_{\text{H}_2\text{O}}^\sigma \frac{m_{\text{salt}}^\alpha}{m_{\text{H}_2\text{O}}^\alpha} \bar{V}_{\text{salt}}^\alpha \right) dP \\ & + \left[\left(\frac{\partial \gamma}{\partial P} \right)_{T,A,\mu_{\text{salt}},\epsilon_\pm} = \Gamma_v \right] d\mu_{\text{salt}} + qd\epsilon_\pm \\ & + \left[- \left(\frac{\partial \gamma}{\partial \mu_{\text{salt}}} \right)_{P,T,A,\epsilon_\pm} = \Gamma_\pm \right] \left[- \left(\frac{\partial \gamma}{\partial \epsilon_\pm} \right)_{P,T,A,\mu_{\text{salt}}} = q \right] \end{aligned} \quad (9)$$

The full equation allowing also for variations in temperature is

$$-Ad\gamma = \Gamma_s dT - \Gamma_v dP + \Gamma_\pm d\mu_{\text{salt}} + qd\epsilon_\pm \quad (10)$$

where Γ_\pm represents an *ionic* surface excess (which ionic excess depends on the reference electrode) and where Γ_s is given by

$$\Gamma_s = - \left(\frac{\partial \gamma}{\partial T} \right)_{T,A,\mu_{\text{salt}},\epsilon_\pm} = \left(S^\sigma - m_{\text{Hg}}^\sigma \bar{S}_{\text{Hg}}^\beta - m_{\text{H}_2\text{O}}^\sigma \bar{S}_{\text{H}_2\text{O}}^\alpha - m_{\text{salt}}^\sigma \frac{m_{\text{salt}}^\alpha}{m_{\text{H}_2\text{O}}^\alpha} \bar{S}_{\text{salt}}^\alpha \right) \quad (11)$$

The advantage of these surface excesses is that they can be derived from measurements of interfacial capacity which are normally of high precision. Thus if, following Parsons,² we define the alternative variable ξ_\pm as

$$\xi_\pm = \gamma + q\epsilon_\pm \quad (12)$$

then eq 10 can be rewritten (per unit area) as

$$-d\xi_\pm = \Gamma_s dT - \Gamma_v dP + \Gamma_\pm d\mu_{\text{salt}} - \epsilon_\pm dq \quad (13)$$

cross-differentiation of which gives ($\mu = \mu_{\text{salt}}$)

$$\left(\frac{\partial \Gamma_v}{\partial q} \right)_{T,P,\mu} = \left(\frac{\partial \epsilon_\pm}{\partial P} \right)_{T,q,\mu} \quad (14)$$

or

$$\left(\frac{\partial \Gamma_s}{\partial q} \right)_{T,P,\mu} = - \left(\frac{\partial \epsilon_\pm}{\partial T} \right)_{q,P,\mu} \quad (15)$$

If the reference electrode is a mercury-mercurous salt electrode reversible to the anion, A^- , in question

$$\left(\frac{\partial \epsilon_\pm}{\partial P} \right)_{T,q,\mu} = \left(\frac{\partial E_-}{P} \right)_{T,q} + \frac{1/2 V_{\text{Hg}_2\text{A}_2} - V_{\text{Hg}}}{F} \quad (16)$$

where E_- is the observed emf of the cell Hg | C₊A⁻(aq) | Hg₂A₂ | Hg in which the capacitance is determined and $V_{\text{Hg}_2\text{A}_2}$ and V_{Hg} are the molar volumes of the phases concerned. Furthermore, in general terms

$$\left(\frac{\partial E_\pm}{\partial P} \right)_{T,q,\mu} = \left(\frac{\partial E_\pm}{\partial P} \right)_{T,q,c} + \left(\frac{\partial E_\pm}{\partial \mu} \right)_{T,q} \left(\frac{\partial \mu}{\partial P} \right)_{T,c} \quad (17)$$

where the subscript *c* here signifies restriction to constant composition. The second factor of the last term

is the partial molar volume of the salt in solution. Finally, since

$$\left(\frac{\partial \frac{1}{c}}{\partial P}\right)_{T,q,c} = \frac{\partial}{\partial P} \left(\frac{\partial E_{\pm}}{\partial q}\right)_{T,P,c} = \frac{\partial}{\partial q} \left(\frac{\partial E_{\pm}}{\partial P}\right)_{T,q,c} \quad (18)$$

it follows that

$$\left(\frac{\partial E_{\pm}}{\partial P}\right)_{T,q,c} = \int \left(\frac{\partial \frac{1}{c}}{\partial P}\right)_{T,q,c} dq \quad (19)$$

By incorporating the correction terms in eq 16 and 17, Γ_v is finally obtained as

$$\Gamma_v = \int \left(\frac{\partial \epsilon_{\pm}}{\partial P}\right)_{T,q,\mu} dq \quad (20)$$

The first integration constant is easily obtained from the value of $\partial E_{\pm}/\partial P$ at $q = 0$. The second integration constant requires a knowledge of $(\partial \gamma/\partial P)_{T,q}$ at $q = 0$. This has yet to be determined and only relative Γ_v values have been recorded.³ The variation of interfacial tension with temperature has been determined⁴ for several systems so that the integration constant $(\partial \gamma/\partial T)_{P,q,\mu}$ and hence absolute values of Γ_s can be found.

Experimental Results

There have been very few systematic studies of the temperature and pressure coefficients of interfacial tension, charge, or capacity. The temperature coefficients are not difficult to determine, although their subsequent analysis often calls for more supporting information (partial molar heat capacities, reversible electrode potentials, etc.) than is currently available. Similar limitations are placed on the analysis of the pressure coefficients and here there are additional experimental problems. The most comprehensive study was that of Payne³ and some of his results are illustrated in Figures 1, 2, and 3, which show the charge dependence of observed values of $[\partial(1/c)/\partial P]_{T,q,c}$, of derived relative values of Γ_v and of derived absolute values of Γ_s for several aqueous systems. In this work and in all the subsequent discussion we shall be concerned with studies of systems involving relatively concentrated aqueous solutions in which the observed capacities are overwhelmingly those of the inner or compact double layer.

All of these surface excesses are operationally defined, as in eq 9 and 11; their interpretation rests on how they can be related to the known bulk properties of the various components. The surface excess volume is not the volume of formation of the interphase (as suggested previously³), which following eq 4 and 5 is

$$\bar{V}^{\sigma} = \left(\frac{\partial \gamma}{\partial P}\right)_{T,A,m_i,\epsilon_{\pm}} = V^{\sigma} - m_{H_2O}^{\sigma} \bar{V}_{H_2O}^{\beta} - m_{H_2O}^{\sigma} \bar{V}_{H_2O}^{\alpha} - m_{C^{+}}^{\sigma} \bar{V}_{C^{+}}^{\alpha} - m_{A^{-}}^{\sigma} \bar{V}_{A^{-}}^{\alpha} \quad (21)$$

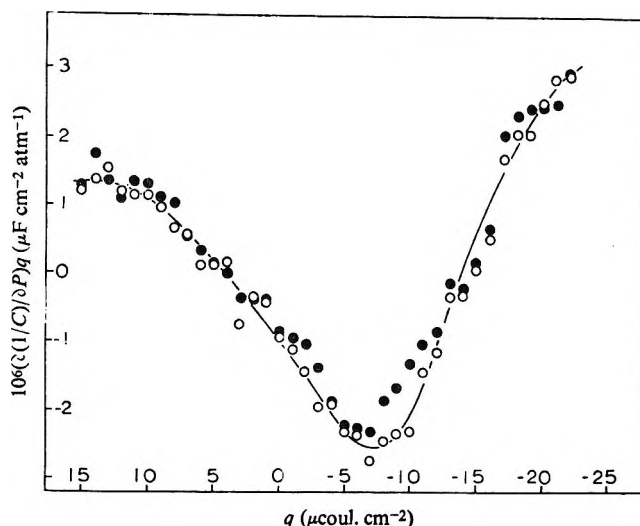


Figure 1. Variation of $[\partial(1/c)/\partial P]_q$ with charge for 0.1 *N* aqueous sodium fluoride at 25° and 1 atm; O, $[\partial(1/c)/\partial P]_q$; ●, $1/C^2(\partial C/\partial P)_q$.

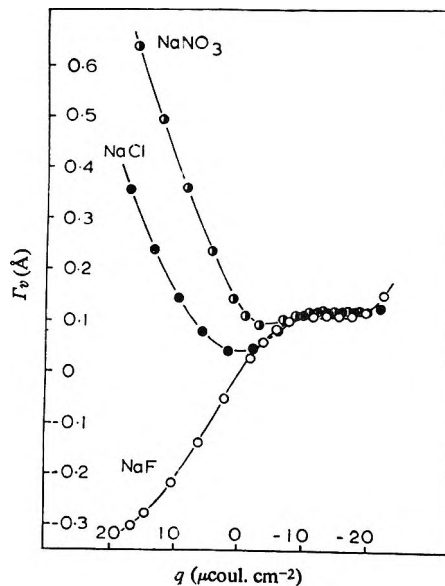


Figure 2. Surface excess volume as a function of charge for 0.1 *N* solutions of the salts at 25° and 1 atm. Values are relative to the arbitrarily chosen zero at $q = 0$ for the NaF system.

A comparison of eq 21 and the appropriate part of eq 9 gives the difference between Γ_v and \bar{V}^{σ} as

$$\Gamma_v - \bar{V}^{\sigma} = m_{C^{+}}^{\sigma} \bar{V}_{C^{+}}^{\alpha} + m_{A^{-}}^{\sigma} \bar{V}_{A^{-}}^{\alpha} - m_{H_2O}^{\sigma} \frac{m_{salt}^{\alpha}}{m_{H_2O}^{\alpha}} \bar{V}_{salt}^{\alpha} \quad (22)$$

For a completely dissociated salt, \bar{V}_{salt}^{α} must equal the sum of the corresponding ionic volumes, but only in the

(2) R. Parsons, *Trans. Faraday Soc.*, **51**, 1518 (1955).

(3) G. J. Hills and R. Payne, *ibid.*, **61**, 326 (1965).

(4) G. Gouy, *Ann. Chim. Phys.*, **9**, 75 (1906).

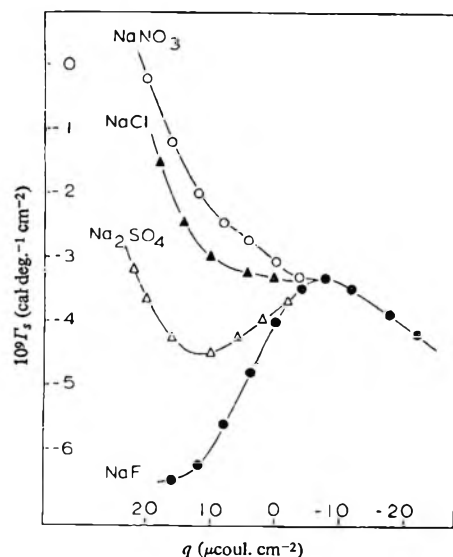


Figure 3. Surface excess entropy as a function of charge for 0.1 *N* solutions of the salts at 25° and 1 atm.

absence of specific adsorption *and* of any ionic excess will the difference between Γ_v and \bar{V}^σ be zero.

If now we consider mean values for the partial molar volumes of the components of the interphase, $\bar{V}_{H_2O}^\sigma$ etc., then

$$V^\sigma = m_{H_2O}^\sigma \bar{V}_{H_2O}^\sigma + m_{H_2O}^\sigma \bar{V}_{H_2O}^\sigma + m_{C^{+\sigma}} \bar{V}_{C^{+\sigma}} + m_{A^{-\sigma}} \bar{V}_{A^{-\sigma}} \quad (23)$$

and the surface excess volume is

$$\Gamma_v = m_{H_2O}^\sigma (\bar{V}_{H_2O}^\sigma - \bar{V}_{H_2O}^\alpha) + m_{H_2O}^\sigma (\bar{V}_{H_2O}^\sigma - \bar{V}_{H_2O}^\alpha) + m_{C^{+\sigma}} \bar{V}_{C^{+\sigma}} + m_{A^{-\sigma}} \bar{V}_{A^{-\sigma}} - m_{H_2O}^\sigma \frac{m_{salt}^\alpha}{m_{H_2O}^\alpha} \bar{V}_{salt}^\alpha \quad (24)$$

This type of formulation restates the obvious fact that the volume (or entropy) changes can arise either from variations of the corresponding intensive properties or from variations of extensive quantities such as $m_{C^{+\sigma}}$ and $m_{A^{-\sigma}}$. We might intuitively expect that the largest contributions will arise from $(\bar{V}_{H_2O}^\sigma - \bar{V}_{H_2O}^\alpha)$ and from the two terms relating to the adsorption of anions, *i.e.*

$$m_{A^{-\sigma}} \bar{V}_{A^{-\sigma}} - m_{H_2O}^\sigma \frac{m_{salt}^\alpha}{m_{H_2O}^\alpha} \bar{V}_{A^{-\sigma}}$$

In Figures 2 and 3, the principal changes in Γ_v and Γ_s occur on anodic polarization, *i.e.*, at positive values of q where anion adsorption occurs. No distinction has been made in this analysis between the different types of adsorption which may occur (*e.g.*, specific or non-specific as defined by other measurements), although we shall expect to see these differences reflected in the experimental values of Γ_v and Γ_s and in their interpretation *via* eq 24. At cathodic polarizations where specific

adsorption of alkali metal cations is usually negligible, Γ_v values, in particular, are insensitive to q which suggests that $m_{H_2O}^\sigma$ is not varying significantly from $q = -5$ to $q = -20 \mu C cm^{-2}$ and that the contribution to Γ_v from $m_{C^{+\sigma}} \bar{V}_{C^{+\sigma}}$ is small. In these terms Γ_q for the NaF system might be expected to be constant for the range of q values involved here, because the fluoride ion is also not specifically adsorbed. However, this is not the case and from $q = -5$ to $q = +15 \mu C cm^{-2}$ a marked decrease in Γ_v is observed. Some of this decrease could be associated with the relatively negative partial molar volume of the fluoride ion, but it is much more likely to arise from reorganization of the water in the interphase, *i.e.*, from a change of density and polarizability following the reversal of the direction of preferred orientation. A similar variation is observed in the entropy data. In the presence of specific adsorption, an entirely different trend in Γ_v and Γ_s values is seen and the incorporation of anions into the inner layer is, as might be expected, accompanied by relatively large increments of volume. Similar increments in entropy are also observed, the relative magnitudes of which (per mole of adsorbed ions) are close to the relative partial molar ionic entropies.

The Capacitance Hump

To extract more certain inferences from these meagre data is not easy and a more extended range of temperatures *and* pressures will be required to complete this type of thermodynamic framework. Such a study is in hand. Even so the data give little support to the proposed reorientation of water at $\sim +5 \mu C cm^{-2}$ which is often held to account for the capacitance hump observed with many aqueous systems.⁵

For all common anions, with the possible exception of fluoride ions, this region of charge sees the onset of marked anion adsorption. Since the magnitude and the exact location of the hump varies considerably with ion type, it might reasonably be supposed that it is related to competition between anions and water for adsorption sites on the metal surface. That solvent orientation is not the sole cause of the hump is further evident from those polar nonaqueous systems in which no hump is observed and from the observation that in at least one nonaqueous system *two* humps are seen.⁶ Finally, it can be argued that even if solvent reorientation were to give rise to a maximum in local permittivity, it would do so for aqueous solutions on the *cathodic* side on the electrocapillary maximum.

These and other aspects of the problem were discussed in detail in a previous paper³ and here consideration is given to another aspect of the temperature dependence, namely the temperature-invariant point of common intersection of the capacitance-charge relation over a

(5) N. F. Mott and R. J. Watts-Tobin, *Electrochim. Acta*, **4**, 79 (1961).

(6) R. Payne, *J. Phys. Chem.*, **73**, 3598 (1969).

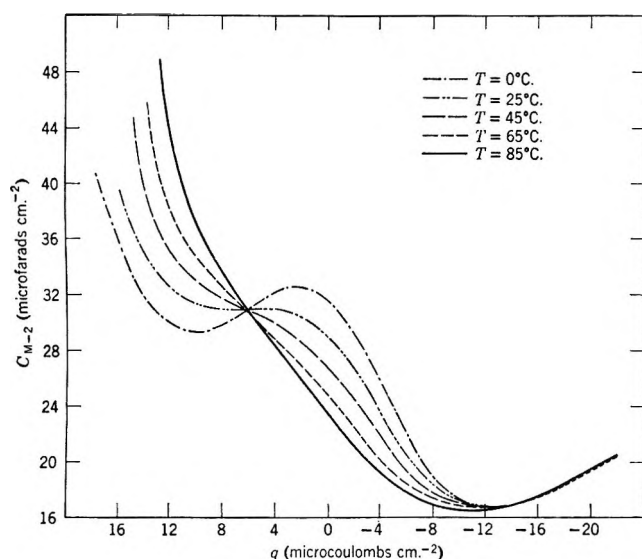


Figure 4. Calculated values of C_1 , the differential capacity of the inner part of the double layer, between mercury and aqueous solutions of sodium fluoride at several temperatures. Calculations made from data obtained with 0.8 *N* solutions by Grahame.

wide temperature range. Grahame's results for fluoride solutions are well known⁷ and are shown again for reference purposes in Figure 4. The point of common intersection is precisely defined and similar points have been observed with other systems (KCl:⁸ aqueous HCl has recently been examined from 25 to 150° by Conning⁹). It is therefore unlikely to be an artifact and it is surprising that such a distinctive feature has not received more attention.

Similar concentration-invariant points occur commonly in spectroscopic analysis as isosbestic points and are a necessary consequence of the intersection of two Gaussian curves, the exponential terms of which are related. Thus, the overlapping spectra of two absorbing components A and B in equilibrium with each other such that $dn_A = -dn_B$ and having closely similar extinction coefficients will intersect at a common point which is independent of the relative concentrations of A and B. It is interesting to speculate to what extent a similar argument could explain the common point of intersection of the capacitance curves and, *inter alia*, the nature of the hump.

First it is worth restating that the temperature coefficient of capacity is opposite in sign on either side of the intersection point. The decrease with temperature on the cathodic side is in keeping with the idea that in this region, the capacitance results from one or more adsorption processes. The fact that it is a feature of fluoride systems as well as of those in which specific adsorption takes place is strong evidence that in this range of potential the solvent is either involved in or strongly affected by this process of adsorption. It can be argued that the inner layer polarizability is intensified by the

field-neutralizing effect of the adsorbed ions whether they are at the inner or outer Helmholtz planes, although their influence is evidently much stronger at the former. Similar considerations are to be found in the papers by Bockris, Devanathan, and Müller¹⁰ and by Shvarts, Damaskin, and Frumkin.⁸ In other words, the electrostrictive effect of the metal-solution potential difference which must ordinarily reduce the total polarizability of the solvent is offset by the opposing field of the adsorbed ions. There may be other contributory facts such as the compression of the inner layer,¹¹ but all involve the solvent and the adsorbing ions and there have been a number of detailed and extended treatments of this and other aspects of the problem.^{5,10,11} However, it is not the purpose of the present paper to argue the pro's and con's of these theories or to reiterate that the experimental evidence is as yet inconclusive, but rather to note it is usual to invoke some form of competitive adsorption between ions and solvent molecules.

The next question that arises is whether this interpretation of inner layer polarizability can be increased indefinitely by continued anodic polarization. The maximum in differential capacity suggests that it rapidly reaches a maximum value and thereafter declines to a low value. The capacity of a complete monolayer of chlorine atoms or ions on mercury approaches low values.⁹ For the sake of argument this decline is shown hypothetically as the dotted line in Figure 5.

If this is the case, then there remains to explain the steep rise in differential capacity that is observed at potentials anodic to the hump. This steep rise is related to the faradaic process where by the anions in question are ultimately discharged at the mercury surface (see Armstrong, *et al.*,¹² for a recent discussion of the facts). It is always asymptotic to the corresponding reversible potential and with rising temperature it progressively overshadows the other features of the capacitance-potential relationship.⁹ However, at potentials not too far removed from that of the temperature-invariant point, it is not a faradaic pseudocapacitance. There is no observed frequency dependence or dc component and the large anodic capacities are attributed to adsorption effects. The existence of large, frequency-independent adsorption capacities is well known and several of these are evidently associated with a corresponding faradaic process and symmetrically disposed

(7) D. C. Grahame, *J. Amer. Chem. Soc.*, **79**, 2093 (1967).

(8) E. Shvarts, B. B. Damaskin, and A. N. Frumkin, *Russ. J. Phys. Chem.*, **11**, 1311 (1962).

(9) D. G. Conning, Thesis, Southampton, 1968.

(10) J. O'M. Bockris, M. A. V. Devanathan, and K. Müller, *Proc. Roy. Soc.*, **A274**, 55 (1963).

(11) McDonald and C. A. Barlow, *Advances in Electrochemistry and Electrochemical Engineering*, Vol. VI, P. Delahay and C. W. Tobias, Ed., Interscience Publishers Inc., New York, N.Y.

(12) R. D. Armstrong, W. P. Race, and H. R. Thirsk, *J. Electroanal. Chem.*, **14**, 143 (1967).

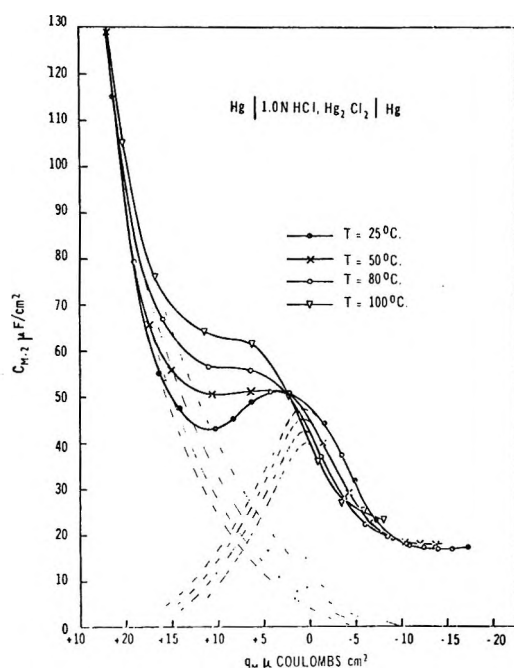


Figure 5. Calculated values of C_1 . The inner layer part of the double layer differential capacity of C_1 between mercury and aqueous HCl at several temperatures. Calculation made on data obtained with 1.0 N solutions.

about the reversible potential.^{13,14} They are superimposed on the faradaic pseudocapacity but can be resolved from it in terms of the usual network analysis provided the faradaic process is fast (*cf.* the Tl-Tl⁺ system in H₂O¹⁴ and the Br-Br⁻ system in molten nitrates¹⁵). Timmer, Sluyters-Rehbach, and Sluyters¹⁶ have related this additional, adsorption capacitance (K in their terminology) to the equilibrium bulk concentration (in this case of oxidant) c_0^* and to a potential term $\phi = nF(E - E_{rev})/RT$, *i.e.*

$$K = \frac{Kc_0^*n^2F^2 \exp \phi}{RT(1 + \exp \phi)^2} \quad (25)$$

where k is the assumedly linear adsorption isotherm constant ($\Gamma_0 = kc_0^*$) and other terms have their usual significance.

The important factor to note in this context is the dependence of K on E and T . The dependence is not a simple one for K itself is also likely to be temperature dependent. The simple assumption made here is that K exhibits the *same* temperature dependence as the solvent capacitance term discussed above since both stem from the same process, namely the adsorption of anions. Their dependence on potential is also likely to follow the same form but, it must be noted, the two effects will be *opposite* in sign, since we suppose one exponentially to approach E_{rev} and the other E_{max} (the potential of the hump). If therefore we denote the two capacities as C_A and C_S and their potential-temperature dependences within this range of potential as $C_A = f(E/T)$

and $C_S = f(-E/T)$, then the apparent isosbestic point follows at once.

This simple proposition is further illustrated in Figure 5 where the supposed individual contributions to the two adsorption capacitances have been sketched onto the observed curves for the charge dependence of the capacity of the inner layer for 1.0 M HCl. There is no theoretical justification for the particular dotted lines as shown except that they approximately synthesize the observed relationships and the apparent "isosbestic" point. It is not difficult to resolve the observed curves for the other systems into two overlapping (Gaussian) curves which satisfy to within a few per cent the requirements that these two separate and parallel contributions sum to the observed total capacity. The maxima and minima in the capacitance-potential curves and their characteristic temperature dependence are thus seen to follow inevitably from the competitive adsorption of two polarizable components. The exact nature of the two adsorption capacitances is not clear but they are certainly different since the *ion*-adsorption coefficient (*e.g.*, in $\mu\text{F cm mol}^{-1}$ is normally many orders of magnitude greater than that of the corresponding solvent term.¹⁵

Whether maxima and minima of this kind are to be found in other (nonaqueous) systems is a matter for further conjecture. Humps have been detected in many other systems, and in various mixtures of dimethyl sulfoxide and H₂O (but at constant ionic composition) humps appear and disappear as the solvent composition is changed from one pure solvent to the other.¹⁷ The possibility that some of these humps may be the result of solvent reorientation is not precluded. Humps are usually (but not invariably) found on the anodic side of the potential of zero charge. In aqueous systems this is likely to be the consequence of two factors: (1) the smaller tendency for cations to be specifically adsorbed, and (2) the probability that it is not easy to polarize so far beyond the potential of solvent reorganization and therefore to influence its degree of electrostriction.

Conclusion

The purpose of this paper was to examine in somewhat greater detail than usual the temperature (and pressure) coefficients of the double-layer capacity, especially that of the inner or compact layer. The interpretation of the coefficients and the derived thermodynamic functions is not easy because the macroscopic properties we observe are not readily related to the microscopic properties of any likely model system.

(13) B. Timmer, M. Sluyters-Rehbach, and J. H. Sluyters, *J. Electroanal. Chem.*, **15**, 343 (1967).

(14) P. Delahay and G. Susbielles, *J. Phys. Chem.*, **70**, 3150 (1966).

(15) G. J. Hills and P. D. Power, *Trans. Faraday Soc.*, **64**, 1629 (1968).

(16) B. Timmer, M. Sluyters-Rehbach, and J. H. Sluyters, *J. Electroanal. Chem.*, **18**, 93 (1968).

(17) R. Payne, *J. Amer. Chem. Soc.*, **89**, 489 (1967).

There is a further complication in that the differential capacities on which much of the discussion has been based are peculiarly sensitive to the way in which charge and coverage are related. Thus the inner layer capacity, here designated C_i , can be resolved into two contributions, *i.e.*

$$\frac{1}{C_i} = \frac{d\phi^{M-2}}{dq} = \left(\frac{\partial\phi^{M-2}}{\partial q}\right)_{q'} + \left(\frac{\partial\phi^{M-2}}{\partial q'}\right)_q \frac{dq'}{dq} \quad (26)$$

where q' is the charge of specifically adsorbed ions. It can be argued that many eccentricities in C_i might be expected from the second term on the right-hand side which may be comparable in magnitude with the first and also of opposite sign. Under these conditions, C_i could assume large values. On the other hand, the virtual constancy of $(\partial\phi^{M-2}/\partial q)_{q'}$ is strong evidence of the specific effect of anions (as opposed to charge) on the polarizability of the interphase. The fact that $(\partial\phi^{M-2}/\partial q)_{q'}$ is not very dependent on the nature of the anion¹⁸ is less easily accommodated by the present speculation and it may well be as Shvarts, *et al.*,⁸ have stressed that these questions will not be resolved to general satisfaction until many more data (including data of a different kind) are available.

Acknowledgment. The author wishes to thank Dr. John Lane (C.S.I.R.O., Sydney) and Dr. David Schriffrin (Southampton University) for helpful discussions.

Appendix. Symbols Not Defined in the Text

A	Electrode area, cm ²
c	Concentration, mol l. ⁻¹
C	Interfacial capacity, $\mu\text{F cm}^{-2}$
C_i	Interfacial capacity of the inner, compact double layer, $\mu\text{F cm}^{-2}$
E	Emf, V
E^-	Emf of the cell Hg-solution-anion reversible electrode
F	Faraday, C mol ⁻¹
G	Molar free energy
m_i	Concentration, units unspecified, of component i
n	Number of electrons defined by the relation $\text{O} + ne \rightleftharpoons \text{R}$
P	Pressure
q	Charge on the metallic side of the interface, $\mu\text{C cm}^{-2}$
q'	Charge on the solution side of the interface due to specifically adsorbed ions, $\mu\text{C cm}^{-2}$
R	Gas constant
S	Molar entropy
\bar{S}	Partial molar entropy
T	Temperature
V	Volume
\bar{V}	Partial molar volume
α	Superscript denoting solution phase
β	Superscript denoting metallic phase
γ	Surface tension, ergs cm ⁻²
Γ	Thermodynamic surface excess
ϵ_{\pm}	Electrochemical potential, V
ϕ	Potential, V
μ	Chemical potential, cal mol ⁻¹
σ	Superscript denoting interphase

(18) R. Parsons, *Trans. Faraday Soc.*, **55**, 999 (1959).

The Electrical Double Layer in Amide Solvents

by Richard Payne

*Air Force Cambridge Research Laboratories, L. G. Hanscom Field, Bedford, Massachusetts
(Received February 21, 1969)*

Double-layer measurements are reported for a mercury electrode in the solvents N-ethylformamide (NEF), N-*t*-butylformamide (NBF), N-methylacetamide (NMA), N-ethylacetamide (NEA), N-*n*-butylacetamide (NBA), dimethylacetamide (DMA), and N-methylpropionamide (NMP). The behavior of NEF resembles that of the previously studied formamide and N-methylformamide (NMF) systems; a broad capacity hump appears on the cathodic branch of the capacity-potential curve. This hump, however, is absent in NBF. For KPF₆ solutions in the N-monoalkylacetamides and NMP two capacity humps occur on opposite sides of the point of zero charge (pzc). The cathodic hump resembles the formamide hump and is a property of the solvent. Study of the anodic hump is complicated by specific adsorption of PF₆⁻ ions. This hump is probably also a solvent property but may be due to specific adsorption. The capacity generally decreases with increasing molecular weight of the solvent but is not directly dependent on the macroscopic dielectric constant. The interfacial tension at the electrocapillary maximum in the high dielectric constant solvents NMA, NEA, and NEF is close to 380 ergs/cm² and is not significantly temperature dependent.

Introduction

The physical properties and electrochemistry of the aliphatic amide solvents have been described in a recent comprehensive review.¹ A large number of these solvents exist, many of them liquid at ambient temperatures, but the properties of only a few have been investigated. Double-layer studies reported for formamide and its N-methyl derivatives can be summarized as follows.² The form of the capacity potential curve is related to the structural properties of the solvent; capacity humps occur in the high dielectric constant solvents, formamide, and N-methylformamide but not in dimethylformamide where the dielectric constant is relatively low. Specific adsorption of anions is inversely proportional to the ability of the solvent to solvate anions through N-hydrogen bonding. It is the object of the present work to test the general validity of these broad conclusions by extending the measurements to a number of related solvents.

In most investigations of the influence of the solvent on the properties of the double layer undue emphasis has been placed on the significance of the macroscopic dielectric constant of the solvent. However, as Frumkin's experimental work³ of 1923 showed, the double-layer capacity is not directly related to the macroscopic dielectric constant nor is such a relationship to be expected on theoretical grounds. However, there is no doubt that the unusual structural properties of high dielectric constant solvents are also reflected in the double-layer properties of these solvents. Probably more important factors which have received little attention are the specific chemical interactions of the solvent molecules with both the ions and the electrode, and the effect of the size of the solvent molecule on the mean thickness of the inner region of the double layer. The relative importance of the effective dielectric

constant and thickness of the inner region is at the heart of the current controversy^{4,5} concerning the choice of electrical variable in adsorption studies. In this work the significance of the thickness factor is emphasized for solvents ranging in molecular weight from 45 (formamide) to 115 (N-*n*-butylacetamide). Measurements are described for seven new solvent systems in addition to new measurements in formamide, N-methylformamide, and dimethylformamide.

Experimental Section

The capacity of the electrical double layer at a growing mercury drop was measured by the ac bridge technique described previously.⁶ Measurements were normally conducted at a single frequency of 1 kHz, but in solutions of low conductance a frequency of 400 Hz was used. Electrocapillary measurements were made in a simple version of the Lippman capillary electrometer also described previously⁶ but modified by the use of a water thermostat bath controlled to $\pm 0.01^\circ$. In all the measurements described the reference electrode used was a normal calomel electrode isolated from the nonaqueous solution by a long electrolyte path and a solution-sealed stopcock.

Solvents supplied by Eastman Organic Chemicals were normally purified by repeated distillation through a 40-cm column packed with glass helices under reduced pressure. No chemical or other pretreatment

(1) D. S. Reid and C. A. Vincent, *J. Electroanal. Chem.*, **18**, 427 (1968).

(2) R. Payne, *Advan. Electrochem. Electrochem. Eng.*, in press.

(3) A. N. Frumkin, *Z. Phys. Chem.*, **103**, 43 (1923).

(4) A. N. Frumkin, B. B. Damaskin, and A. A. Survila, *J. Electroanal. Chem.*, **16**, 493 (1968).

(5) E. Dutkiewicz, J. D. Garnish, and R. Parsons, *ibid.*, **16**, 505 (1968).

(6) R. Payne, *J. Amer. Chem. Soc.*, **89**, 489 (1967).

was used. Solvents prepared in this way had the following typical specific conductances: N-methylacetamide, 1.5×10^{-7} ohm $^{-1}$ cm $^{-1}$; N-ethylacetamide, 2.6×10^{-6} ohm $^{-1}$ cm $^{-1}$; N-ethylformamide, 5×10^{-4} ohm $^{-1}$ cm $^{-1}$; N-methylpropionamide, 1×10^{-7} ohm $^{-1}$ cm $^{-1}$; N,N-dimethylacetamide, 5.5×10^{-8} ohm $^{-1}$ cm $^{-1}$; N-*t*-butylformamide, 1.4×10^{-4} ohm $^{-1}$ cm $^{-1}$; and N-*n*-butylacetamide, 1.3×10^{-7} ohm $^{-1}$ cm $^{-1}$. These values are similar to previously reported values for NMA, DMA, and NMP. There appear to be no published data for NEA, NBA, NEF, and NBF. The high conductance of NEF and NBF is typical of formamide and the N-alkyl formamides and is probably due to ionization of a volatile trace impurity (*e.g.*, formic acid or ammonia) which is not completely removed by distillation under these conditions. This impurity had no noticeable effect on the measurements. However, extreme care is necessary in assessing the effect of such impurities on capacity measurements, as shown by the behavior of formamide. The residual high conductance of formamide distilled from CaO or other alkali is due to the presence of traces of ammonia, which are evidently almost impossible to remove by distillation. This was attempted in the present work by distillation of formamide through a 50 plate column under carefully controlled conditions. The lowest conductance obtained was 1.0×10^{-5} ohm $^{-1}$ cm $^{-1}$ under the following conditions: column head pressure 0.5mm, temperature 64°, reflux ratio 1, distillation rate 6-7 ml/hr. This product gave the capacity curve shown in Figure 1. The small peak at $E = -0.15$ V is due to a pseudocapacitance associated with anodic discharge of traces of ammonia as was shown by adding more ammonia. In previously reported measurements for KF solutions in formamide^{7,8} anodic polarization beyond 0.2 V was evidently not possible because of discharge of ammonia introduced in substantial concentrations by treatment of the solvent with alkali in the purification procedure. This clearly illustrates the danger of chemical pretreatment of solvents which may increase rather than decrease the impurity level as stressed recently by Butler.⁹

Solutions were made up gravimetrically using ACS Grade salts, in general, dried at 150° for 24 hr without further purification. Practical Grade KPF₆ supplied by Matheson Coleman and Bell was recrystallized from water and vacuum dried before use. Tetra-*n*-propylammonium bromide and tetraethylammonium perchlorate (Eastman) and LiClO₄ (Alfa Inorganics) were used as received. Cyclohexane and isooctane (Fisher Spectranalyzed) and *n*-heptane (Eastman) were distilled at atmospheric pressure before use.

Results

1. *N*-Methylacetamide. Capacity measurements are reported for 0.1 M solutions of KPF₆, LiClO₄, LiBF₄, KNO₃, CsI, NH₄Cl, NEt₄ClO₄, and NPr₄Br at 30°. Further capacity measurements were obtained for 1 M

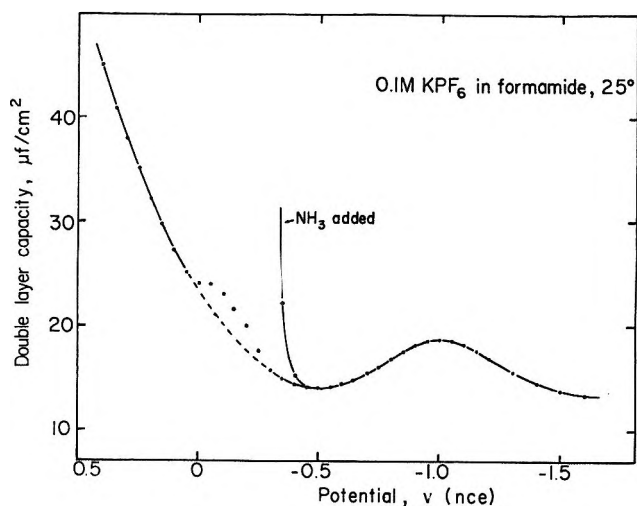


Figure 1. Double-layer capacity for 0.1 M KPF₆ in formamide showing pseudocapacity peak at -0.15 V due to discharge of traces of ammonia.

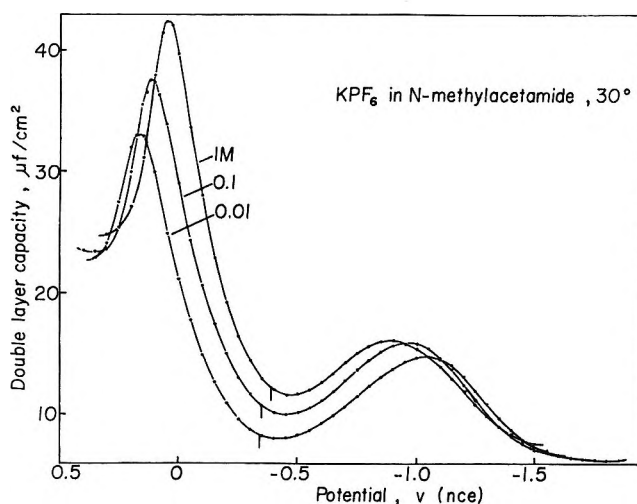


Figure 2. Double-layer capacity for KPF₆ solutions of indicated concentration in N-methylacetamide at 30°. Vertical lines indicate potential of zero charge.

KPF₆ (30 and 50°), 0.01 M KPF₆ (30°), 0.1 M KPF₆ in mixtures of NMA with water (25°) and 0.1 M KPF₆ is NMA containing cyclohexane, *n*-heptane, and isooctane (30°). Electrocapillary curves were obtained for 0.5 and 1 M KPF₆ (30°), 0.1 M KPF₆ (30 and 40°) and 0.1 M CsI (30°).

Two capacity humps on opposite sides of the pzc occur in NMA solutions of KPF₆, LiBF₄, LiClO₄, and NEt₄ClO₄. This has not been observed previously in a two-component solution of an inorganic electrolyte. Curves for three concentrations of KPF₆ are shown in Figure 2. The cathodic hump is typical of the hump

(7) B. B. Damaskin, R. V. Ivanova, and A. A. Survilla, *Elektrokhimiya*, **1**, 767 (1965).

(8) E. Dutkiewicz and R. Parsons, *J. Electroanal. Chem.*, **11**, 196 (1966).

(9) J. N. Butler, *Advan. Electrochem. Electrochem. Eng.*, in press.

found in other amide solvents whereas the anodic hump is more pronounced (as in aqueous solutions). The capacity at both humps decreases with increasing temperature as usual.² The effect is larger at the anodic hump. In 1 M KPF₆ the temperature coefficient is $-0.19 \mu\text{F}/\text{cm}^2 \text{ deg}$ for the anodic hump compared with $-0.04 \mu\text{F}/\text{cm}^2 \text{ deg}$ for the cathodic hump. The latter agrees precisely with the formamide value.² The frequency dependence of the capacity for the 1 M KPF₆ solution was investigated carefully in the range 0.5–4 kHz. The capacity showed a small but significant frequency dependence at both humps. At the cathodic hump the capacity was 0.4% higher (compared with the 1 kHz value) at 0.5 kHz and 2.1% lower at 4 kHz. At the anodic hump the capacity was 1.8% higher at 0.5 kHz and 2.4% lower at 4 kHz. The cathodic hump therefore is essentially independent of frequency below 1 kHz whereas the anodic hump remains somewhat frequency dependent even at 0.5 kHz. The dispersion of $\sim 2\%$ between 1 and 4 kHz is somewhat larger than the effect normally found in aqueous and other solutions of comparable conductance, but can probably be attributed, as in these other solutions, to imperfect geometry of the electrodes and electrolyte penetration effects.¹⁰

Strong specific adsorption of anions from NMA is suggested by the capacity curves shown in Figure 3. The anodic hump appears in LiBF₄, LiClO₄, and NEt₄ClO₄ but is absent in other solutions. The effect of

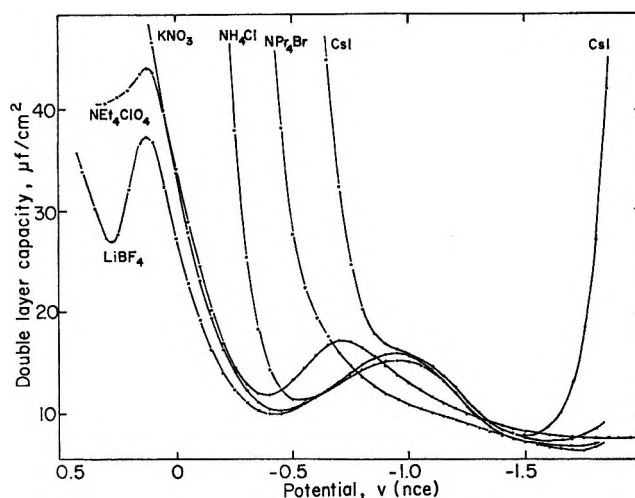


Figure 3. Double-layer capacity for 0.1 M solutions in N-methylacetamide at 30°.

anion adsorption is reflected in the negative shift of the pzc (Table I). The order of specific adsorption of anions is evidently $\text{I}^- > \text{Br}^- > \text{Cl}^- > \text{PF}_6^- > \text{ClO}_4^-$, NO_3^- , BF_4^- . The negative shift of the pzc with increasing concentration of KPF₆ is consistent with specific adsorption of PF₆⁻ ions. This is not, however, confirmed by the electrocapillary measurements which show an increase of γ_s with concentration.

The cathodic hump depends only slightly on the electrolyte for inorganic salts. The capacity is $\sim 0.4\%$ lower in 0.1 M LiClO₄ compared with KPF₆. Tetraalkylammonium ions, however, change the shape of the hump and shift it to more anodic potentials probably due to specific adsorption of the cation, which, however, appears to be much weaker than in water.¹¹ No significant shift of the pzc attributable to specific adsorption of NEt₄⁺ or NPr₄⁺ could be detected. Specific adsorption of Cs⁺ and NH₄⁺ cations on the far cathodic side is indicated by the sharp rise of the capacity (Figure 4). This is confirmed for the Cs⁺ ion by a marked lowering of the interfacial tension (Figure 5).

NMA is strongly adsorbed from aqueous solution (Figure 6). Partial desorption occurs on the far cathodic side in dilute solutions. There is no indication of desorption on the anodic side, however, suggesting that the NMA molecule is most strongly adsorbed on a positively charged electrode. The NMA anodic capacity hump is absent for concentrations $\lesssim 50 \text{ mol } \%$.

The electrocapillary measurements in NMA solutions at 30° were marked by unusual experimental difficulties which may be of interest to other workers in this area. The meniscus could normally be set to the required mark (0.9 mm from the capillary tip) without difficulty, but would quickly become unstable and move

Table I: Interfacial Tension (γ_s) and Potential (E_s) at the Electrocapillary Maximum for Various Solutions

Solvent	Solute	Temp. °C	γ_s , ergs/cm ²	E_s , V
NMA	0.01 M KPF ₆	30		-0.333
NMA	0.1 M KPF ₆	30	378.2	-0.345
NMA	0.1 M KPF ₆	40	377.8	
NMA	1 M KPF ₆	30	383.4	-0.383
NMA	0.1 M LiClO ₄	30		-0.335
NMA	0.1 M LiClO ₄	40	377.8	
NMA	0.1 M LiClO ₄	45	377.5	
NMA	0.1 M LiBF ₄	30		-0.320
NMA	0.1 M CsI	30	369.8	-0.635
NMA	0.1 M KNO ₃	30		-0.332
NMA	0.1 M NH ₄ Cl	30		-0.374
NMA	0.1 M NEt ₄ ClO ₄	30		-0.340
NMA	0.1 M NPr ₄ Br	30		-0.465
NEA	0.1 M KPF ₆	25		-0.33
NEA	0.1 M CsI	25		-0.649
NBA	0.1 M KPF ₆	25		-0.310
DMA	0.01 M KPF ₆	25		-0.20
DMA	0.1 M KPF ₆	25		-0.25
DMA	Satd. KPF ₆	25		-0.32
NEF	0.1 M KPF ₆	25		-0.36
NEF	0.1 M CsI	25	369.7	-0.643
NEF	0.1 M LiClO ₄	25	378.8	-0.349
NEF	0.1 M LiClO ₄	35	378.8	
NBF	0.1 M KPF ₆	25		-0.313
NMP	0.1 M KPF ₆	25		-0.342

(10) R. De Levie, *J. Electroanal. Chem.*, **9**, 117 (1965).

(11) A. N. Frumkin and B. B. Damaskin, "Modern Aspects of Electrochemistry," Vol. 3, J. O'M. Bockris, and B. E. Conway, Ed., Butterworth Inc., Washington, D. C., 1964, p 149.

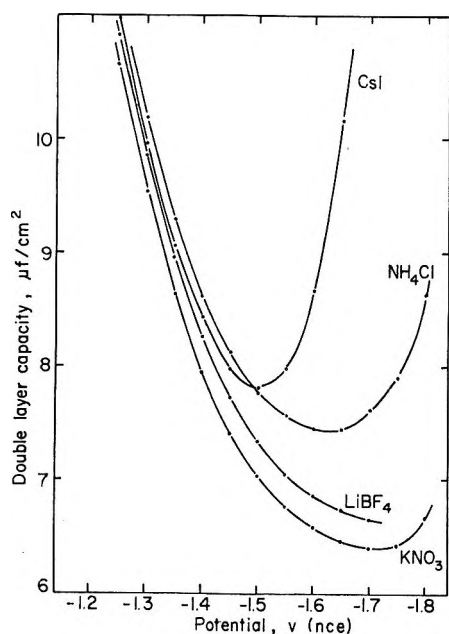


Figure 4. Cathodic branch of the capacity-potential curve for 0.1 M solutions in N-methylacetamide at 30°.

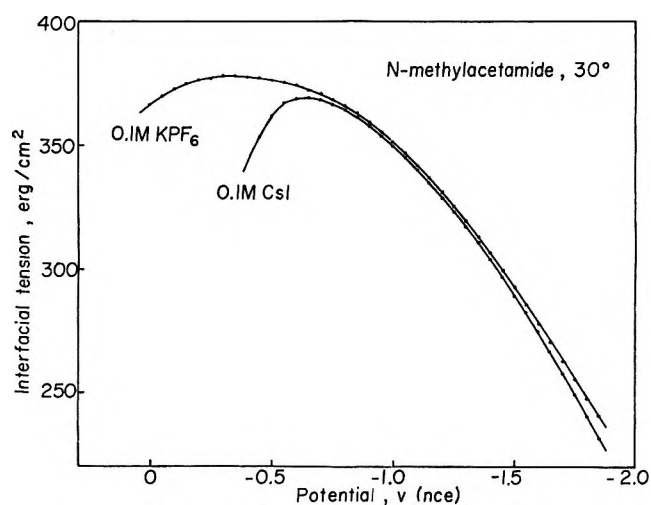


Figure 5. Electrocapillary curves in N-methylacetamide at 30°.

rapidly up or down the capillary. The instability was usually accompanied by formation of an occlusion in the mercury column a few tenths of a millimeter above the meniscus which would eventually break the thread. The occluded material appeared to be solution but proved to be a gas bubble. The problem disappeared in 0.1 M LiClO_4 raised to 40° but reappeared in a severe form on lowering the temperature to 35°. It was attributed to supersaturation of the solution with nitrogen (used for deaeration) which tends to form gas bubbles in the annular film of solution in the capillary.

2. *N-Ethylacetamide and N-n-Butylacetamide.* Capacity curves for 0.1 M KPF_6 and 0.1 M CsI in NEA and 0.1 M KPF_6 in NBA at 25° are shown in Figure 7. The behavior in both solvents is similar to the NMA system

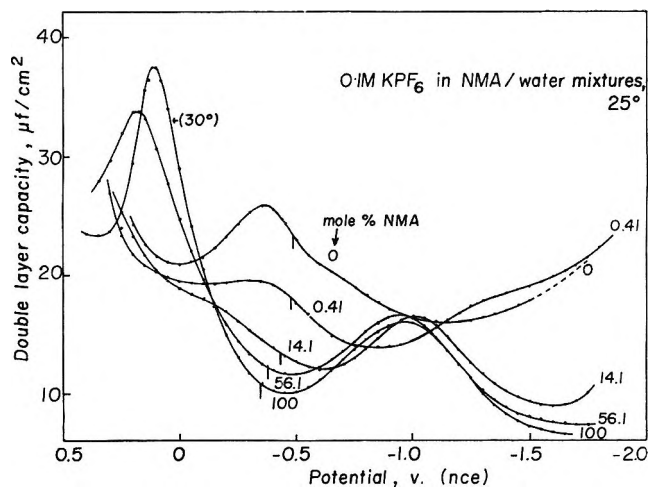


Figure 6. Capacity curves for 0.1 M KPF_6 solutions in mixtures of N-methylacetamide and water at 25°. Vertical lines indicate potential of zero charge.

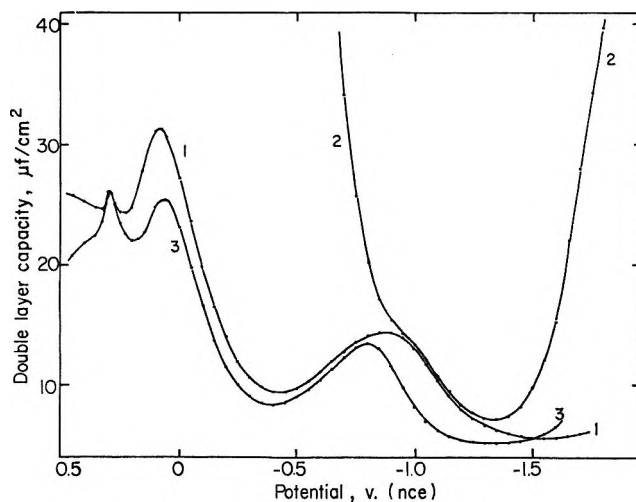


Figure 7. Double-layer capacity for 0.1 M solutions of (1) KPF_6 and (2) CsI in N-ethylacetamide and (3) KPF_6 in N-n-butylacetamide at 25°.

but the capacities are somewhat lower. Double humps are found for KPF_6 solutions in both NEA and NBA as in NMA. The cathodic hump becomes sharper and shifts in the anodic direction in the series NMA, NEA, NBA. The anodic hump decreases in size in the same order. In NEA and NBA a small peak occurs at ~ 0.3 V which is absent from the NMA system. The origin of this is unknown. It is not accompanied by significant direct current or polarization resistance and is presumably therefore a double-layer effect rather than a pseudocapacity peak due to adsorption or discharge of an impurity.

Strong specific adsorption of both I^- and Cs^+ ions is indicated as in NMA by the negative shift of the pzc (I^- adsorption) and sharp increase of capacity at the extremes of polarization. The cathodic rise shows an inflection at -1.7 V which is unusual.

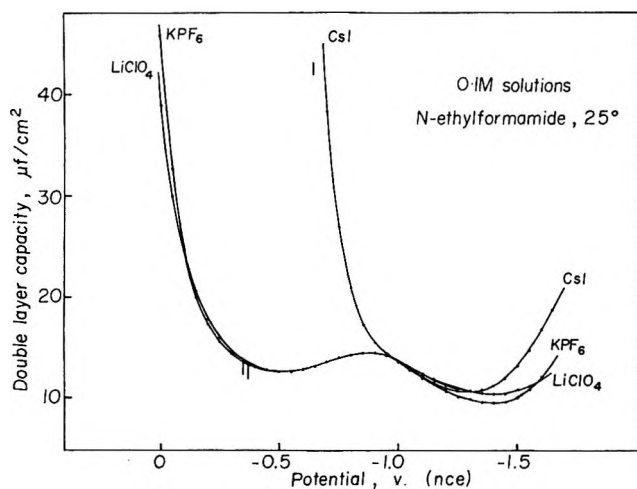


Figure 8. Double-layer capacity for 0.1 *M* solutions of KPF_6 , LiClO_4 , and CsI in *N*-ethylformamide at 25°. Vertical lines indicate potential of zero charge.

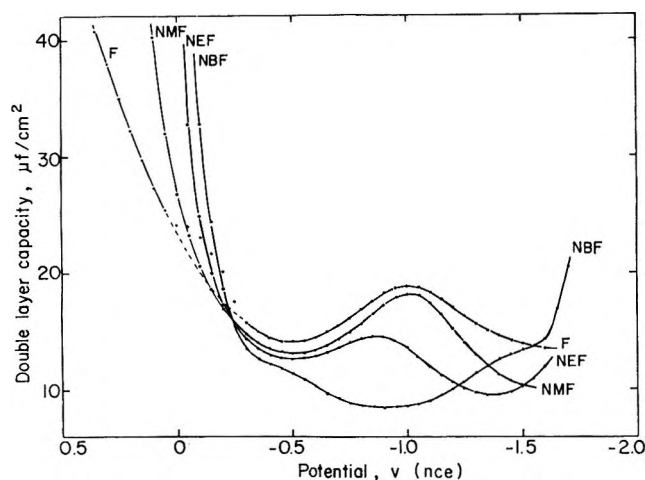


Figure 9. Double-layer capacity for 0.1 *M* KPF_6 solutions in formamide, *N*-methylformamide, *N*-ethylformamide, and *N*-*t*-butylformamide at 25°.

Satisfactory electrocapillary curves in NEA could not be obtained owing to sticking of the meniscus in the capillary and the instability problem described for NMA. The interfacial tension at the ecm for 0.1 *M* KPF_6 in NEA at 25° is ~ 378 ergs/cm².

3. *N*-Ethylformamide and *N*-*t*-Butylformamide. The capacity was measured for 0.1 *M* solutions of KPF_6 , LiClO_4 , and CsI in NEF (Figure 8) and 0.1 *M* KPF_6 in NBF at 25° (Figure 9). NEF resembles formamide and NMF insofar as a single capacity hump occurs on the cathodic side. However, the hump occurs at a less negative potential and is flatter. In NBF the characteristic hump disappears and is replaced by a trough. The depression close to the pzc may be due to the effect of the diffuse layer capacity although this seems unlikely in view of the high dielectric constant (102 at 25°¹²). From the trend of the curves in the series NMF, NEF, NBF this effect seems more probably due to the

residue of the cathodic hump centered at -0.5 V (Figure 9). The similar effect on the far cathodic side at ~ 1.4 V and the sharp rise of the capacity at -1.6 V are hard to explain.

The KPF_6 and LiClO_4 in NEF curves are almost superimposable except at far cathodic potentials where the KPF_6 curve is somewhat lower as usually found in nonaqueous solutions.² Strong specific adsorption of I^- ions is evident but Cs^+ is apparently less strongly adsorbed from NEF than from NMA and NEA.

The interfacial tension for 0.1 *M* LiClO_4 in NEF (378.8 ergs/cm²) is close to the value for the same solution in NMA (377.8 ergs/cm² at 40°) and as in NMA is almost independent of the temperature. In contrast to the extreme instability of the electrometer measurements in the acetamides, the behavior of NEF was unusually good and excellent electrocapillary curves were obtained.

4. *Dimethylacetamide*. Capacity curves for three concentrations of KPF_6 in DMA at 25° are shown in Figure 10. As in DMF the cathodic hump is absent but there is a hump on the anodic side of the pzc. The capacity at the hump is somewhat dependent on frequency (+1.9% at 0.5 kHz and -5.9% at 4 kHz referred to the 1 kHz value) as in NMA. Most of this is believed due to solution penetration in the capillary because of the high mobility of DMA. At potentials far cathodic of the pzc a stable dropping mercury electrode in DMA solution could be maintained only with difficulty owing to the solution penetration problem. No increase in the series resistance or direct current was found in the region of the capacity hump.

The dielectric constant of DMA is relatively low (37.8 at 25°¹³). Consequently, the effect of the min-

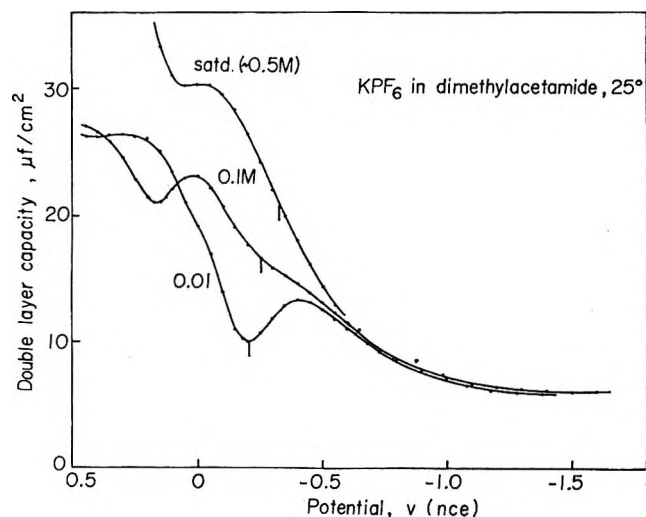


Figure 10. Double-layer capacity for KPF_6 solutions in dimethylacetamide at 25°. Vertical lines show potential of zero charge.

(12) R. Payne and I. E. Theodorou, unpublished data.

Table II: Physical Properties and Double-Layer Capacity in Amide Solvents at 25°

Solvent	C_{\min}^a $\mu\text{F}/\text{cm}^2$	Ref	Mol wt	Length of ^b molecule, Å	Dielectric constant
Formamide	12.5 (0.1 M KCl)	7	45	5.6	109.5
N-Methylformamide	8.5 (0.1 M KCl)	25	59	6.4	182.4
Dimethylformamide	6.8	This work	73	6.7	36.7
N-Methylacetamide	6.7 (30°)	This work	73	6.8	178.9
N-Ethylformamide	9.5	This work	73	7.7	
Dimethylacetamide	6.0	This work	87	6.9	37.8
N-Methylpropionamide	5.6	This work	87	7.8	172.2
N-Ethylacetamide	5.6	This work	87	7.7	129.9
N- <i>t</i> -Butylformamide	8.4	This work	101	7.5	
N- <i>n</i> -Butylacetamide	5.2	This work	115	9.6 or 7.0 ^c	101.7

^a C_{\min} is measured at the minimum on the cathodic branch of the capacity-potential curve for 0.1 M KPF₆ solutions except where otherwise stated. ^b Measured along axis of the dipole assuming a planar molecule (R. J. Kurland and E. B. Wilson, *J. Chem. Phys.*, **27**, 585 (1957)). ^c *n*-Butyl group and oxygen atom in *cis* (7.0 Å) or *trans* (9.6 Å) configuration.

imum in the diffuse layer capacity is clearly visible in the 0.01 M solution (Figure 10). The marked concentration dependence of the capacity and corresponding negative shift of the pzc suggests substantial specific adsorption of PF₆⁻ ions. Satisfactory electrocapillary measurements in DMA could not be made. However, γ_z is close to 372.4 ergs/cm² for 0.01 M KPF₆ at 25°.

Discussion

1. *Solvent Dependence of Double-Layer Properties in the Absence of Specific Adsorption of Ions.* The effect of the solvent on the capacity is summarized in Table II. The cathodic capacity hump is present only in solvents with unsubstituted N-hydrogen. Anodic capacity humps occur in DMA solutions of KPF₆ whereas the N-monoalkylacetamides and NMP show both anodic and cathodic humps. The capacity at the minimum on the far cathodic side generally decreases with increasing solvent molecular weight. NEF and NBF, however, are exceptions. Close agreement of the capacity is found between the structural isomers DMF, NMA and DMA, NMP, NEA. It should be noted that NEF is also isomeric with DMF and NMA.

The macroscopic dielectric constant varies by a factor of 5 within this group of solvents and bears no direct relationship to the capacity. This further confirms Frumkin's early work³ and is to be expected since the unusual structural effects responsible for the high dielectric constants of solvents like water and formamide are presumably absent in the adsorbed state. The behavior of such solvents in the double layer should resemble that of normal polar solvents (*i.e.*, nonassociated) with possible complications due to lateral interaction, and interaction with solvent in the diffuse layer. The effective dielectric constant of even normal polar solvents in the double layer is impossible to predict. It seems reasonable to assume that for strong electrode polarization the dipoles are permanently aligned in the field and that the effective dielectric constant of the

layer will be close to the high-frequency value. According to measurements on bulk liquids this does not vary much among solvents of similar chemical type and is therefore unlikely to exert an important effect on the double-layer capacity.

A factor which seems potentially more important and which is usually neglected is the effect of the size of the solvent molecule on the thickness of the inner region. According to Table II the capacity generally decreases with increasing size of the solvent molecule as would be expected. Similar correlations are found for other series of solvents.² However, the selection of the minimum capacity on the cathodic side of the curve as the reference point is arbitrary although the correlation of capacity with solvent molecular weight seems fairly general over the whole curve. If it is assumed that reorientation of solvent dipoles occurs as the applied potential is varied, then variation of the capacity could be attributed to variation of the thickness since the solvent molecule is generally nonspherical. Variation of the thickness of the inner layer would seem to be at least as important as variation of the dielectric constant, a possibility which has often been ignored in the interpretation of adsorption from aqueous solution.

The cathodic capacity decreases in the alkali metal cation series in the order Li⁺ < Na⁺ < K⁺ in the amides as in all other nonaqueous solvents. This is opposite to the order found in aqueous solutions.¹⁴ The smallness of the effect in all solvents is difficult to understand. Many factors enter into the discussion including ionic solvation and structure, compressibility, and polarizability of the adsorbed solvent. Since little is known of any of these factors, discussion of the minor variations of the capacity seems pointless. However, it can be noted that the trend in the capacity in nonaqueous so-

(13) G. R. Leader and J. F. Gormley, *J. Amer. Chem. Soc.*, **73**, 5731 (1951).

(14) D. C. Grahame, *J. Electrochem. Soc.*, **98**, 343 (1951).

Table III: Lowering of the Interfacial Tension at the Electrocapillary Maximum for 0.1 *N* Solutions in the Amides and Water at 25°

Salt	$\Delta\gamma_{25}$, erg/cm ²					
	DMF ^a	NMF ^b	Formamide ^c	Water ^d	NMA ^e	NEF ^e
LiCl	7.3	0	0.2 (KCl)	1.5 (NaCl, 18°)		
LiBr	9.5			3.4 (CaBr ₂ , 18°)		
CsI	15	7.5			8.9 (30°)	9.1
KI	14.6		3.9	12.2 (18°)		

^a Data of Bezuglyi and Korshikov (*Elektrokhimiya*, 1, 1422 (1965); 3, 390 (1967)) relative to 0.1 *N* LiClO₄. ^b Data of Damaskin and Ivanova (*Zh. Fiz. Khim.*, 38, 176 (1964)) relative to 0.1 *N* Cs₂CO₃. ^c Data of Payne (unpublished) relative to 0.01 *N* KCl. ^d Data of Gouy (*Ann. Chim. Phys.*, 29, 145 (1903)) relative to pure solvent. ^e This work.

lutions is generally consistent with the trend in the crystallographic radii of cations, but not the Stokes radii (obtained from conductance data), whereas in aqueous solutions the opposite is true. The significance of these observations is obscure.

2. Specific Adsorption of Ions. According to current ideas on ionic solvation,¹⁵ anions are strongly solvated by solvents like water and formamide which are capable of forming a hydrogen bond with the ion. Specific adsorption of anions from such solvents should therefore be relatively weak. This is confirmed for halide anions in the formamides where, according to Table III, the strength of adsorption increases in the order formamide < NMF < DMF. In DMF and in other aprotic solvents (dimethyl sulfoxide for example) adsorption of simple anions is unusually strong,² consistent with weak solvation indicated by other measurements. Adsorption of halide ions from water is weaker than from DMF but appreciably stronger than from NMF and formamide. This is consistent with the observation^{16,17} that heats of solution of alkali metal halides in NMF and formamide are generally much larger than in water. However, cation adsorption is generally stronger in the formamides than in water. Damaskin, *et al.*,⁷ have suggested therefore that the more negative heats of solution in the formamides is due entirely to enhanced solvation of anions.

Polyatomic anions like ClO₄⁻, PF₆⁻, NO₃⁻, and SCN⁻ are by contrast considerably more strongly adsorbed from water than from the amides including DMF.² According to Bezuglyi and Korshikov,¹⁸ the interfacial tension at the ecm actually increases with concentration for LiClO₄ and LiNO₃ in DMF. The surface activity of SCN⁻ was likewise shown to be much smaller in DMF than in water. This was attributed to strong solvation in DMF, which however is not supported by the conductance data.¹⁹ Adsorption of polyatomic anions from formamide (PF₆⁻, NO₃⁻²⁰), NMA (NO₃⁻, ClO₄⁻, PF₆⁻, BF₄⁻), NEA (PF₆⁻), and NEF (ClO₄⁻, PF₆⁻) also appears to be generally weak. It seems likely that coadsorption of the solvent and possibly two-dimensional solvation of adsorbed ions are important factors.

Specific adsorption of alkali metal cations in the order K⁺ < Rb⁺ < Cs⁺ is evident from the capacity and electrocapillary data in all of the systems studied. In the formamides the order of increasing adsorption is evidently formamide < NEF < NMF < DMF. In DMF published capacity curves²¹ for CsCl solutions show a sharp, concentration-dependent rise on the cathodic side indicating strong specific adsorption of Cs ions, which is confirmed by the corresponding depression of the interfacial tension (10 ergs/cm² at -1.8 V against sce for 0.1 *M* CsCl). Adsorption of Cs⁺ ions from formamide although evident from the capacity curves of Damaskin, Ivanova, and Survila⁷ is weak. The observation by these workers and also by Nancollas, Reid, and Vincent²² that K⁺ ions are strongly specifically adsorbed from formamide does not seem consistent with the experimental results. Thus Damaskin, *et al.*, observed deviations from diffuse-layer behavior (for a nonspecifically adsorbed electrolyte) on the far cathodic side and concluded therefore that Na⁺ and Cs⁺ ions are both specifically adsorbed to an equal and appreciable extent. However, their capacity curves for NaCl and KCl (Figure 2 of ref 7) are almost superimposable and show no evidence of specific adsorption of cations. In any case it seems extremely unlikely that Na⁺ and Cs⁺ ions would be specifically adsorbed to the same degree. Nancollas, *et al.*, reported even larger deviations from diffuse layer behavior for 0.1 *M* KCl in formamide. Positive adsorption of the anion over the whole range of potential was reported amounting to

(15) See, for example, A. J. Parker, *Quart. Rev.* (London), 16, 163 (1962).

(16) R. P. Held and C. M. Criss, *J. Phys. Chem.*, 69, 2611 (1965).

(17) Yu. M. Povarov, Yu. M. Kessler, A. I. Gorbanev, and I. V. Safonova, *Dokl. Akad. Nauk SSSR*, 155, 1411 (1964).

(18) V. D. Bezuglyi and L. A. Korshikov, *Elektrokhimiya*, 3, 390 (1967).

(19) J. E. Prue and P. J. Sherrington, *Trans. Faraday Soc.*, 57, 1795 (1961).

(20) R. Payne, unpublished data.

(21) S. Mine, J. Jastrzebska, and M. Brzostowska, *J. Electrochem. Soc.*, 108, 1160 (1961).

(22) G. H. Nancollas, D. S. Reid, and C. A. Vincent, *J. Phys. Chem.*, 70, 3300 (1966).

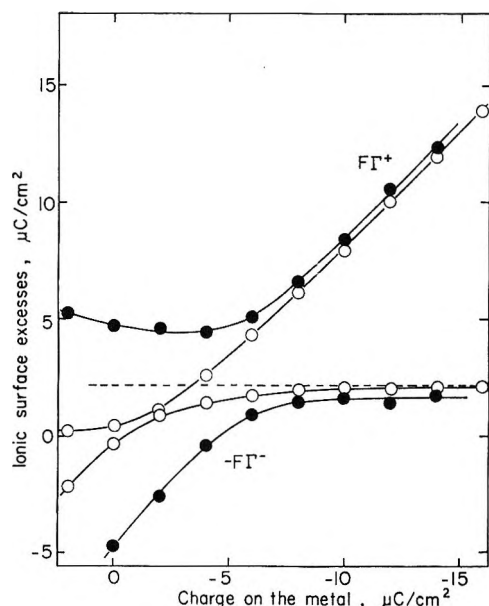


Figure 11. Ionic surface excesses for 0.09 M solutions of KI (closed circles) and KCl (open circles) in formamide at 25°. Broken line indicates limiting repulsion of anions ($2.1 \mu\text{C}/\text{cm}^2$) calculated from diffuse-layer theory for a nonadsorbed electrolyte.

$\sim 4 \mu\text{C}/\text{cm}^2$ at the extreme of cathodic polarization (Figure 5 of ref 22). If this were assumed wholly present in the diffuse layer (*i.e.*, no specific adsorption of Cl^- ions) the cation would have to be specifically adsorbed to the extent of no less than $20 \mu\text{C}/\text{cm}^2$. Capacity and electrocapillary measurements reported elsewhere²³ for KI solutions in formamide are consistent with the absence of specific adsorption of K^+ ions even at concentrations approaching $1 M$. This is confirmed by similar measurements²⁰ for KCl and KNO_3 solutions which are also in good agreement with the predictions of diffuse layer theory for a nonadsorbed electrolyte at charges up to $-16 \mu\text{C}/\text{cm}^2$ (Figure 11). Esin and Markov plots (which are independent of electrocapillary measurements) are shown to have zero slope at all concentrations confirming the conclusions reached from the surface excesses. The results for the KCl system, which are typical, are shown in Figure 12. Since the slope of the E and M plot is related to the charge dependence of the surface excess of anions through the well-known relationship

$$\frac{F}{RT} \left(\frac{\partial E^+}{\partial \ln a_{\pm}} \right)_q = F \left(\frac{\partial \Gamma^-}{\partial q} \right)_\mu \quad (1)$$

it follows from the constancy of the slope at sufficiently negative values of q that Γ^- has reached a constant value, which as shown by the curves in Figure 11 is close to the diffuse layer limiting value. Finally it should be noted that Nancollas, *et al.*, find $\sim 4 \mu\text{C}/\text{cm}^2$ of neutral KCl adsorbed at the ecm from $0.1 M$ KCl in formamide compared with the reported value²⁴ for aqueous $0.1 M$ KCl of only $1.2 \mu\text{C}/\text{cm}^2$. This is in direct disagree-

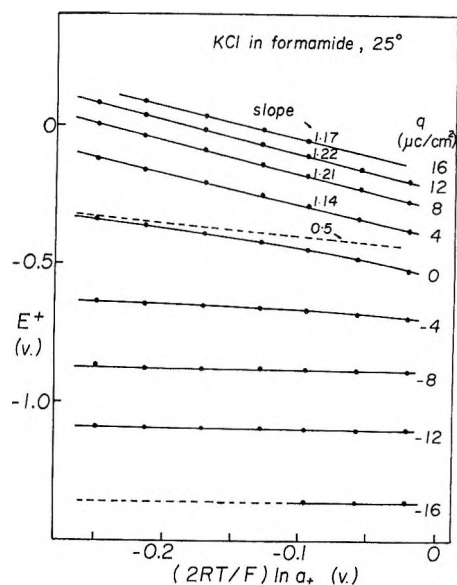


Figure 12. Esin and Markov plots for KCl solutions in formamide at 25°. Broken line of slope 0.5 is predicted by diffuse layer theory for a nonadsorbed electrolyte at the potential of zero charge.

ment both with the results in Figure 11 and those of Damaskin, *et al.* (who report $0.6 \mu\text{C}/\text{cm}^2$ for $0.1 M$ NaCl), and is also in conflict with the generally lower level of specific adsorption of anions in formamide compared with water (Table III). It seems reasonable to conclude therefore that no significant specific adsorption of alkali metal cations other than Cs^+ occurs from formamide.

Specific adsorption of Cs^+ , Rb^+ , and possibly K^+ ions from NMF,²⁵ Cs^+ , NH_4^+ and K^+ from NMA (Figure 4) and Cs^+ from NEF (Figure 8), NEA (Figure 7) and DMF,²¹ however, is clearly evident from the capacity curves in these systems. Specific adsorption of tetraalkylammonium cations from amide solvents (NBu_4^+ from NMF,²⁵ NEt_4^+ , and NPr_4^+ from NMA) seems to be considerably weaker than from aqueous solutions probably due to stronger interaction of these ions with the organic solvent.

3. *Nature of the Capacity Humps.* The origin of the capacity humps in aqueous and nonaqueous solutions of inorganic ions is probably the most controversial aspect of double-layer theory. It has been variously suggested that the aqueous solution hump is due to reorientation of solvent dipoles, specific adsorption of anions, interaction of adsorbed solvent, and anions and competitive adsorption of solvent anions. While there is evidence to suggest that all of these effects play a part in different systems the fact remains that the capacity hump occurs in the absence of specific adsorption of

(23) R. Payne, *J. Chem. Phys.*, **42**, 3371 (1965).

(24) D. C. Grahame and R. Parsons, *J. Amer. Chem. Soc.*, **83**, 1291 (1961).

(25) B. B. Damaskin and Yu. M. Pavarov, *Dokl. Akad. Nauk SSSR*, **140**, 394 (1961).

anions (or when the effects of such adsorption have been taken into account). It must be concluded therefore that the hump is either a property of the solvent alone or the solvent and nonspecifically adsorbed (*i.e.*, diffuse layer) ions. This conclusion is reinforced by the occurrence of humps on the cathodic side of the pzc in solvents like formamide and NMF in a potential region where specific adsorption of ions can certainly be discounted. Since these humps are also virtually independent of the identity of the cation (except for specifically adsorbed tetraalkylammonium ions) it can be further concluded that if ions are involved at all they are involved in a nonspecific way.

The most widely accepted interpretation of the hump is the solvent dipole reorientation theory of Watts-Tobin²⁶ and Macdonald and Barlow,²⁷ according to which the permanent dipoles of the adsorbed solvent layer are able to rotate in the potential region of the hump, but become permanently oriented in the applied field at more positive or negative potentials. Since the hump is rarely found at the potential of zero charge the dipoles evidently possess a preferred orientation, *i.e.*, positive (toward the metal) for solvents like water and DMSO (anodic hump) and negative for solvents like formamide and NMF (cathodic hump). For solvents exhibiting anodic humps (*e.g.*, DMSO, butyrolactone) the preferred orientation (as inferred from the shift of the pzc relative to water) appears to be positive as predicted by the theory, but independent evidence suggests that the orientation of the water dipole itself is small and negative.²⁸ The potential of zero charge in formamide (measured against aqueous nce) is close to that of water,^{6,7} indicating little or no preferential orientation of the dipole, while NMF shows a positive shift^{6,25} consistent with positive orientation. In both formamide and NMF the hump occurs at ~ -0.5 V with respect to the pzc; a strong negative preferred orientation of the dipole is therefore predicted by the theory. The occurrence of two humps in some systems raises a more serious question since it does not at first seem possible to explain both humps in terms of solvent dipole reorientation. However, it has not yet been established that both humps arise from the same cause. It is reasonable to assume that the cathodic hump in NMA for example, is like the characteristic formamide hump (which it closely resembles). The anodic hump however could be due to specific adsorption of anions.

The specific adsorption of PF_6^- ions in NMA was therefore investigated using standard methods. The negative shift of the ecm with increasing concentration (Table I) suggests appreciable adsorption of anions, which, however, is not confirmed by the electrocapillary measurements (Figure 13). γ_2 actually increases with concentration indicating a surface deficiency of electrolyte at the ecm. However, as noted earlier, the electrocapillary measurements are not very reliable especially on the anodic branch of the curve. Comparison with

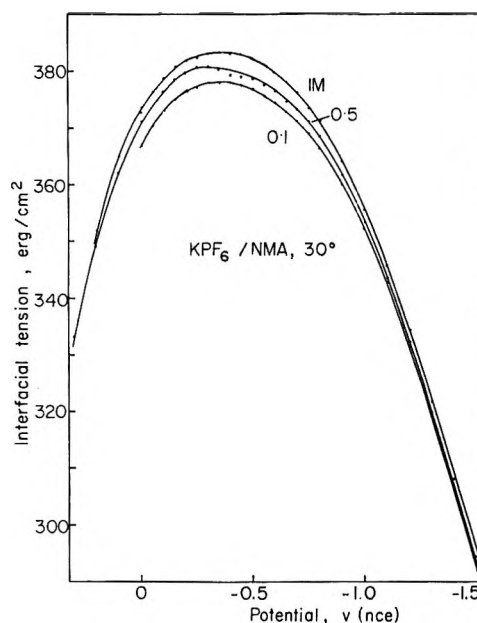


Figure 13. Electrocapillary curves for KPF_6 solutions in N-methylacetamide at 30° .

the doubly integrated capacity curves revealed discrepancies of up to 3 ergs/cm² on the anodic side in the 0.1 M KPF_6 solution. Discrepancies on both sides of the ecm in the 1 M KPF_6 solution were consistent with a small liquid junction potential difference between the two sets of measurements. However, both sets of data, although not entirely independent, were in reasonable agreement showing evidence of some specific adsorption of PF_6^- on the far anodic side.

As a further test for anion adsorption the capacity of the inner layer (C_i) was calculated, assuming the absence of specific adsorption, using the series capacitor formula of Grahame.²⁹

$$\frac{1}{C} = \frac{1}{C_i} + \frac{1}{C_d} \quad (2)$$

The diffuse layer capacity (C_d) was calculated from the relationship

$$C_d = 19.14(314.8c + q^2)^{1/2} \quad (3)$$

which is appropriate for a solvent of dielectric constant 178.9 at 30° .³⁰ The results of this calculation are shown in Figure 14. C_i depends strongly on the concentration for $q \gtrsim 6 \mu\text{C}/\text{cm}^2$ indicating the breakdown of the assumption of no specific adsorption. It is not possible to determine the amounts adsorbed in the

(26) R. J. Watts-Tobin, *Phil. Mag.*, **6**, 133 (1961).

(27) J. R. Macdonald and C. A. Barlow, *J. Chem. Phys.*, **36**, 3062 (1962).

(28) R. Parsons, *Ann. Rep. Chem. Soc.*, **61**, 80 (1964).

(29) D. C. Grahame, *Chem. Rev.*, **41**, 441 (1947).

(30) S. J. Bass, W. I. Nathan, R. M. Meighan, and R. H. Cole, *J. Phys. Chem.*, **68**, 509 (1964).

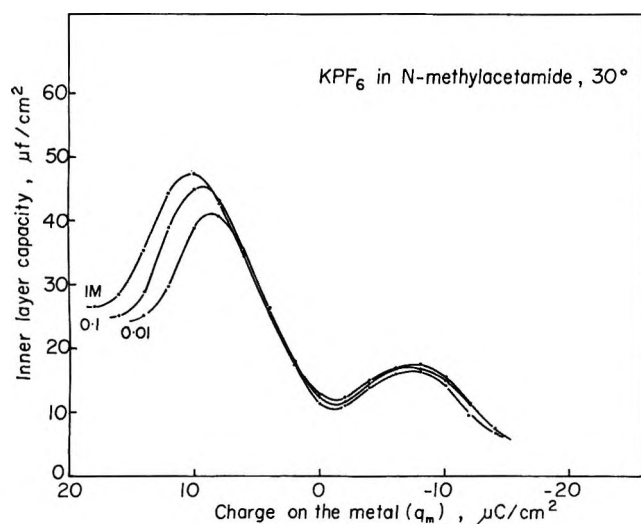


Figure 14. Capacity of the inner region of the double layer for KPF_6 solutions in *N*-methylacetamide at 30° calculated from eq 2.

absence of thermodynamic data. The electrocapillary measurements, however, suggest that it will be small.

As a direct test of the dipole reorientation theory an idea originally due to Bockris, Devanathan, and Müller³¹ was employed. According to Bockris, *et al.*, the solvent dipole should be least strongly adsorbed on the electrode at the potential of reorientation, *i.e.*, in the vicinity of the hump. This test was recently applied by Dutkiewicz and Parsons⁸ to the formamide system in which diethyl ether was adsorbed from a solution of KF . Maximum lowering of the capacity (and hence maximum adsorption) occurred at the hump, from which the correctness of the dipole reorientation interpretation was inferred. Since the ether itself is polar, however, some ambiguity is introduced. For this reason a search for a nonpolar adsorbate was made. Aliphatic hydrocarbons are appreciably soluble in NMA and seemed suitable, but unfortunately are not strongly adsorbed. Capacity measurements were obtained for $0.1 M$ KPF_6 solutions with added cyclohexane, *n*-heptane, and isooctane at $\sim 1 M$ concentration. Isooctane and *n*-heptane produced no significant effect on the cathodic hump but cyclohexane lowered the capacity in this region (Figure 15). This confirms Dutkiewicz and Parsons' findings for the formamide system. The effect on the anodic hump in all cases was to increase the capacity; the cyclohexane curve in Figure 15 is typical. This can be interpreted as enhanced specific adsorption of PF_6^- ions due to a reverse of the salting-out effect, *i.e.*, increase in the activity of the electrolyte due to the added hydrocarbon. However, changes in the shape of the hump are evidence of some adsorption of the hydrocarbon so that no clear interpretation can be made. The test seems to confirm the validity of the dipole reorientation interpretation of the cathodic hump whereas the origin

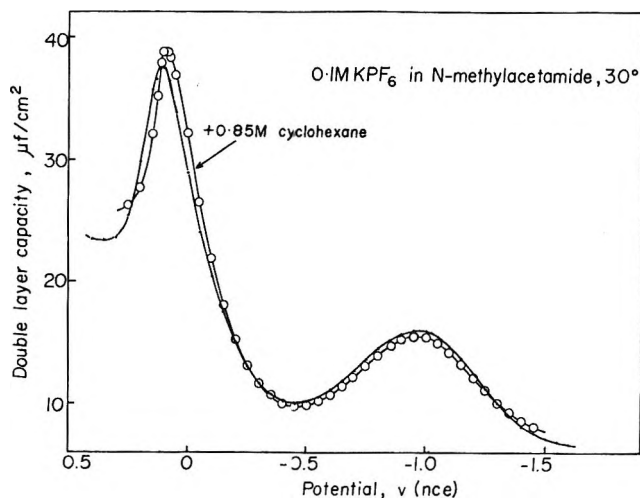


Figure 15. Effect of added cyclohexane on the capacity for $0.1 M$ KPF_6 solution in *N*-methylacetamide at 30° .

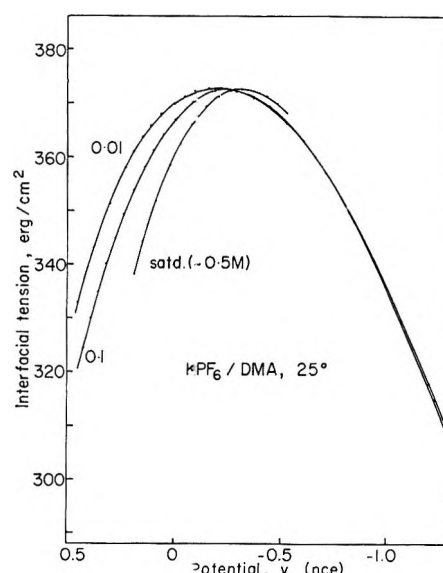


Figure 16. Electrocapillary curves for KPF_6 solutions in dimethylacetamide at 25° calculated by double integration of the capacity curves of Figure 10. γ_z is arbitrarily taken as 372.4 ergs/cm^2 independent of concentration.

of the anodic hump is still uncertain. All the tests applied indicate some specific adsorption of PF_6^- . However, it seems unlikely that this is sufficiently extensive to be wholly responsible for the hump although it undoubtedly has some effect.

The anodic hump in the DMA system is accompanied by much more substantial specific adsorption of PF_6^- ions according to the electrocapillary curves in Figure 16. An adsorption hump is therefore a stronger possibility in this system. Comparison of the DMA curve with a two-hump system (*e.g.*, NMP) shows that the anodic hump in the two systems (and also in NMA,

(31) J. O'M. Bockris, M. A. V. Devanathan, and K. Müller, *Proc. Roy. Soc.*, **A274**, 55 (1963).

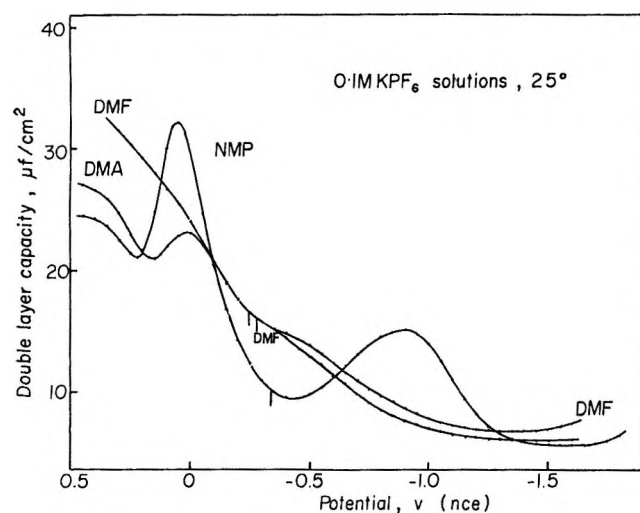


Figure 17. Capacity curves for 0.1 M KPF_6 solutions in dimethylformamide, dimethylacetamide, and N-methylpropionamide at 25°. Vertical lines show potential of zero charge.

NEA, and NBA) occur at the same potential and are generally similar, suggesting a common origin. A marked inflection in the KPF_6 -DMF system reported previously³² also coincides with the anodic hump in the other systems (Figure 17). The question of whether the hump is a property of the solvent or the result of anion adsorption must therefore remain open.

In theoretical treatments of the interaction of the solvent molecule with the electrode it is usually assumed implicitly that the dipole will be preferentially oriented on an uncharged electrode with at least a component of the dipole moment normal to the interface. Such preferential orientation has been attributed somewhat vaguely to the effect of a "natural" field arising from overlap of electronic wave functions and other factors.²⁷ The weakness of this approach is that it is purely electrostatic and takes no account of the specific chemical properties of the solvent molecule which are often a far more important factor than the dipole moment. This is shown rather clearly in the amides where the double-layer properties are related to the physical and chemical properties of the solvent rather than the dipole moment which is almost independent of the solvent. The preferred orientation of solvent molecules on an uncharged mercury electrode is therefore more probably due to specific chemical interaction of one or more sites in the molecule with the mercury.

Furthermore, such "specifically adsorbed" solvent molecules would not necessarily be oriented with a component of the dipole moment normal to the interface, although this would generally be the case. Reorientation of a dipolar molecule would normally be expected to occur at sufficiently high applied field strengths except where the strength of the chemical binding is unusually large (e.g., for the thiourea molecule³³).

This concept removes at least one serious difficulty of the reorientation theory, namely the anomalous orientation of dipoles at the pzc. The small surface potential generated by formamide on mercury can be attributed to parallel orientation of the dipole which is adsorbed by specific chemical interaction with the mercury. That such chemical interaction occurs is suggested by the unusually large work of adhesion of formamide on mercury,² which also explains why such a large polarization (~ 0.5 V) is required to reorientate the molecule (at the hump). The positive shift of the pzc in NMF can be likewise be seen as the incidental consequence of a preferred orientation of the dipole dictated by "chemical" rather than electrostatic forces. The existence of double humps in some solvent systems also follows naturally since the molecule can realign with the dipole oriented positively or negatively according to the polarity of the applied field.

The nature of the strong interaction of molecules like formamide with mercury is not obvious in the way that the interaction of thiourea, for example, is. The unexpectedly small temperature dependence of the interfacial tension in NMA and NEF may be significant in this respect (the temperature dependence in formamide itself has unfortunately not been measured). This suggests that the surface excess entropy in these solvents is small whereas in water it is large and positive.³⁴ This has been attributed to disruption of the solvent structure when the solvent molecules become adsorbed, an effect which should be even more drastic for highly structural solvents like formamide and NMA. It must be assumed, therefore, that the adsorbed molecules are also in a highly ordered state which implies two-dimensional association. This may be related to the extraordinary stability of these solvents on mercury and their unusual double-layer properties.

(32) R. Payne, *J. Phys. Chem.*, **71**, 1548 (1967).

(33) R. Parsons, *Proc. Roy. Soc.*, **A261**, 79 (1961).

(34) G. J. Hills and R. Payne, *Trans. Faraday Soc.*, **61**, 326 (1965).

Entropy and Structural Effects in the Electrochemical

Adsorption of Pyridine at Mercury

by B. E. Conway and L. G. M. Gordon

Department of Chemistry, University of Ottawa, Ottawa, Ontario, Canada (Received February 25, 1969)

Previous studies on electrochemical adsorption of pyridine at the mercury electrode-water interface have indicated the role of orientation and interaction effects. Work is reported on the evaluation of free energies, entropies, and heats of electrochemical adsorption of pyridine in 0.03 *N* aqueous NaClO₄ solutions from electrocapillary measurements over a range of temperatures. Comparative measurements were made with acetophenone. A new electrocapillary technique is described. The entropy effects are shown to be an important factor in determining the free energy of adsorption and depend appreciably on electrode surface charge. Substantial compensation between the heat and entropy of adsorption is shown to arise. The entropies of adsorption are examined in the light of calculations on the configurational and librational entropy of electrostatically adsorbed solvent molecules. The results of such calculations indicate that the experimental results are to be interpreted in terms of structure-breaking effects in the inner water layer adsorbed at the electrode. The calculated thermodynamic results depend on the type of isotherm assumed; selected data have been treated in terms of a Flory-Huggins type of equation for various ratios of the areas of the adsorbate and solvent molecules.

Introduction

In previous papers,¹⁻³ we have studied the electrochemical adsorption of pyridine in neutral and ionic form in relation to orientation effects, the role of ionization, and the effect of the molecule on the components of charge in the double layer in aqueous KCl solutions. Analogous work in regard to orientation of reactive functional groups was carried out with acetophenone in relation to the reduction kinetics.⁴ In the earlier work,¹ KCl was used as the supporting electrolyte for neutral pyridine solutions but ionization studies showed² the role of specific adsorption of the chloride ion in comparison with that of ClO₄⁻. Here perchlorate supporting electrolytes were used to minimize coadsorption of anions.

In the work reported at this symposium, we have studied the electrochemical adsorption of pyridine at mercury over a range of temperatures in order to establish the relation between entropy of adsorption and the apparent^{1,3} interaction effects; the corresponding heats and standard free energies of adsorption were, of course, also evaluated. Few temperature studies exist in the literature: Anderson and Parsons⁵ have studied KI solutions where the combined adsorption of the ion in the inner Helmholtz layer and in the diffuse layer adds complications in the thermodynamic interpretation of the data. The study of neutral molecules offers some advantages in this respect. Hills and Payne⁶ have made a detailed study of the adsorption of several salts at mercury through capacity measurements over a range of temperatures and pressures and evaluated the excess volumes and entropies of the interphase as a function of surface charge; the potentials of zero charge at mercury in various solutions as a function of

temperature have also been measured.⁷ The behavior of acetophenone was also examined both for direct comparative purposes and in relation to our previous work⁴ on the kinetics of reduction of this ketone. In the case of pyridine, the dipole is integrally within the whole molecule, while in acetophenone it is within a structurally independent functional group which is, however, involved in some conjugation with the ring.

Experimental Section

1. *New Electrocapillary Technique.* The evaluation of thermodynamic quantities for adsorption at the mercury electrode by electrocapillary measurements demands the execution of a large number of measurements both at closely spaced intervals of potentials and with a variety of solution concentrations if satisfactory accuracy in the derived thermodynamic quantities is to be attained.

Previously,⁸ we have published details of (a) a new

- (1) B. E. Conway and R. G. Barradas, *Electrochim. Acta*, **5**, 319, 349 (1961).
- (2) B. E. Conway, R. G. Barradas, P. G. Hamilton, and J. M. Parry, *J. Electroanal. Chem.*, **10**, 485 (1965).
- (3) R. G. Barradas, P. G. Hamilton, and B. E. Conway, *Collect. Czech. Chem. Commun.*, **32**, 1790 (1967).
- (4) B. E. Conway, L. G. M. Gordon, and E. Rudd, *Discussions Faraday Soc.*, **45**, 84 (1968).
- (5) W. Anderson and R. Parsons, Second International Congress on Surface Activity, Vol. III, J. H. Schulman, Ed., Butterworth and Co. Ltd., London, 1957, pp 45-52.
- (6) G. J. Hills and R. Payne, *Trans. Faraday Soc.*, **61**, 326 (1965); cf. D. C. Grahame, *J. Amer. Chem. Soc.*, **79**, 2093 (1957); *J. Chem. Phys.*, **16**, 1117 (1948).
- (7) W. Paik, T. N. Andersen, and H. Eyring, *J. Phys. Chem.*, **71**, 1891 (1967).
- (8) B. E. Conway and L. G. M. Gordon, *J. Electroanal. Chem.*, **15**, 7 (1967).

electrical method for locating the meniscus in the fine capillary and (b) a new method for measurement of the excess pressure by means of an electrically indicating micrometer-manometer. Both of these modifications to the conventional technique give improved accuracy and diminish tedium in the measurements.

In the present work, we have developed a further improvement in technique which again increases accuracy and greatly facilitates the measurements. The mercury capillary is strongly illuminated from the side and a television microscope is focussed on the capillary. The image from the television camera is fed to an 18-in. screen television monitor and the end of the capillary can be seen directly at a high magnification. The fine end of the capillary appears as an image about 25 cm wide on the screen and the mercury can be seen as a dark (or bright, depending on the illumination) thread moving down the capillary and having a width on the screen of about 1 cm. A fiducial mark can be introduced on the outside of the capillary itself (*e.g.*, by means of a fine wire⁸) or by marking the television screen with a transparent scale fixed at some point of reference with respect to the lower end of the capillary image. The capillary image was in fact projected horizontally by 90° rotation of the scanning system of the camera; this was found to give a sharper focus on the monitor screen. The microscope used was one side of the binocular zoom instrument used previously;^{1,2} the other optical path of the binocular eyepiece enabled the apparatus to be lined up and properly focussed by eye. The apparatus is shown in Figure 1.

2. *Cell.* The cell was similar to that described previously⁸ and was comprised of three compartments; the center one contained a detachable capillary end-piece⁸ for the Hg thread and was provided with an annular jacket for thermostating. The Hg reservoir and the reference electrode were also thermostated at the same temperature. A 0.03 *N* NaCl-calomel reference electrode was employed in a separate compartment; the NaCl solution used was chosen to give a minimum liquid junction potential with respect to 0.03 *N* NaClO₄ used as the supporting electrolyte. The reference electrode solution, together with Hg and Hg₂Cl₂, was contained in a separate tube closed with a small wetted 7-mm ground-glass joint and kept in the reference electrode compartment of the cell (see Figure 1); the latter compartment was filled with the experimental supporting electrolyte solution (0.03 *N* NaClO₄) and could be varied in temperature by circulation of controlled-temperature water through an annular jacket. In the experiments with acetophenone, a Pt-H₂ electrode was used in methanolic H₂SO₄ solution and no liquid junction was present.

3. *Solutions.* Solutions of redistilled pyridine were made up in aqueous 0.03 *N* NaClO₄. Acetophenone solutions were made up in purified methanol containing H₂SO₄, these and other conditions being chosen to be

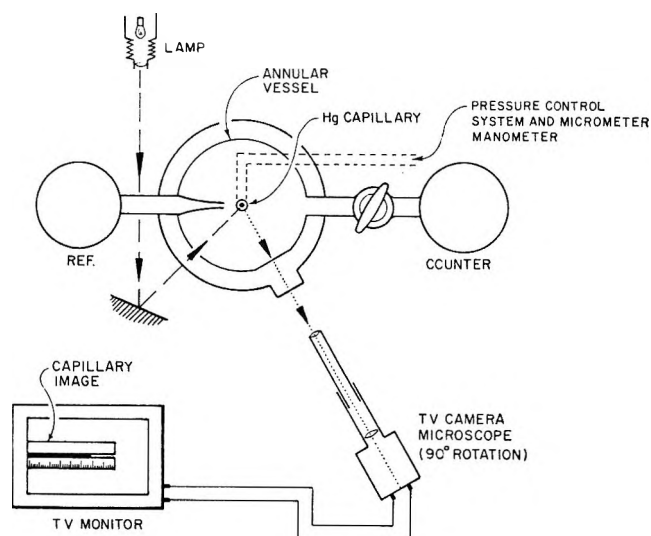


Figure 1. Schematic drawing of television microscope and illumination arrangement for electrocapillary measurements by the method of determining excess pressures.

similar to those employed in previous kinetic studies⁴ on acetophenone reduction at Hg carried out in this laboratory. A dilute perchlorate solution was used in the pyridine work as the supporting electrolyte in order to minimize complications due to specific anion adsorption (*cf.* ref 2) and to provide a basis for comparison with results obtained earlier in chloride solutions.¹

4. *Significance of Measurements over a Range of Temperatures.* Studies of adsorption over a range of temperatures normally lead to the evaluation of the heat and standard entropy of adsorption if constant, or "isosteric," conditions of coverage are specified. A number of types of heats and corresponding entropies of adsorption can in fact be specified depending on the conditions.^{5,9} Care must therefore be exercised, particularly in electrochemical adsorption studies carried out over a range of temperature, in defining the quantities evaluated.

Under Langmuir conditions, it is convenient to take a standard state of half-coverage and this can be also taken as the isosteric condition enabling the standard heats of adsorption to be evaluated from the standard free energies of adsorption ΔG° . When interaction effects are involved and can be expressed in terms of a Frumkin type isotherm, the results may be examined in terms of the relation

$$\frac{\theta}{1-\theta} C \exp r\theta = K \quad (1)$$

where $K = \exp -\Delta G^\circ/RT$, C is the bulk adsorbate concentration, and r is an interaction parameter containing the factor $1/RT$ and determining the magnitude of an interaction term linear in θ ; the question of evalu-

(9) D. H. Everett, *Trans. Faraday Soc.*, **46**, 453, 942, 957 (1951).

ation of $\Delta G^\circ_{\text{ads}}$ is then more complex; $\exp r\theta$ can be regarded as an activity coefficient term f so that

$$\frac{f\theta}{1-\theta} = C \exp[-\Delta G^\circ/RT] \quad (2)$$

As in the electrolyte solution case, where unit activity is taken as the standard state, here it becomes convenient to evaluate $\Delta G^\circ_{\text{ads}}$ for $f\theta/(1-\theta) = 1$, i.e., at $\theta = 1/(1+f)$. Usually f is not directly known, so an apparent value of ΔG° is evaluated from eq 1 and extrapolated w.r.t. θ to $\theta = 0$ thus eliminating f . Evaluation of an apparent ΔG° at a constant finite coverage, say $\theta = 0.5$, from eq 1 at various temperatures will include a varying interaction energy, since at $\theta = 0.5$

$$-\Delta G^\circ = 0.5rRT - RT \ln C_{0.5} \quad (3)$$

where $C_{0.5}$ is the bulk concentration required to give $\theta = 0.5$ at the given temperature.

In electrochemical measurements, the question of electrode potential E or surface charge q also becomes involved. For various reasons,¹⁰ it seems desirable to evaluate the thermodynamic quantities derived from surface tension or capacitance at constant q rather than at constant E . In the case of measurements at various temperatures, this has the added advantage that the changing absolute potential difference at the reference electrode interface does not directly complicate the evaluation of the thermodynamic quantities as it would with measurements at constant measured potential. However, even if ΔH° and ΔS° were derived at constant measured E , some correction could be made to constant metal-solution potential difference at the reference electrode since only the temperature coefficients of emf are required (in this respect, allowing the reference electrode to vary with temperature may be preferable to maintaining it at room temperature and suffering the uncertainty of a thermal junction potential difference) and for the hydrogen electrode for example, this quantity can be calculated to $\pm 0.025 \text{ mV } (^\circ\text{C})^{-1}$, i.e., to 10% since the single standard partial ionic entropy of H^+ is known as -5 eu to an accuracy of $\pm 0.5 \text{ eu}$. A procedure which enables these effects to be allowed for in a rigorous manner has been described.⁶

In the present discussion, the results will be evaluated in terms of ΔG° , ΔH° , and ΔS° derived for isosteric conditions at constant q (and constant supporting electrolyte activity) using the ξ function employed in various publications of Parsons¹⁰ and others.^{2,6} The Gibbs equation also gives the excess entropy Γ_s associated with the interphase from

$$d\gamma = -\Gamma_s dT - \Gamma_i d\mu_i - qdE \quad (4)$$

for components i in the solution and in the interphase. It is evident (cf. ref 6) that $-d\gamma/dT$ does not simply give Γ_s unless the chemical potential(s) of the components i in solution are kept constant at constant E . In practice, this is difficult to achieve and implies, for

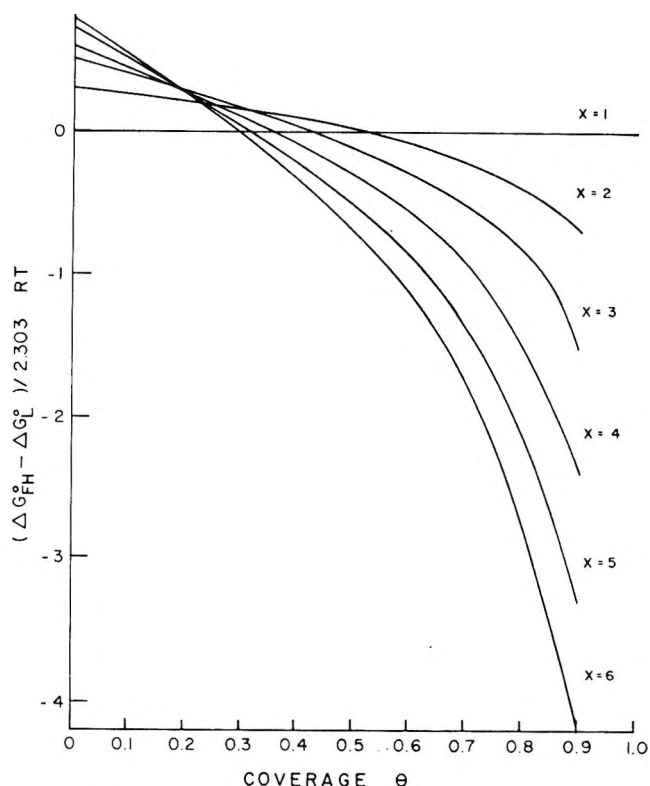


Figure 2. Values of the difference of ΔG° for an adsorption process as calculated in terms of a Flory-Huggins and a Langmuir adsorption isotherm for a given value of coverage θ of an adsorbate in equilibrium with the adsorbate in solution at a fixed concentration.

example, that for a neutral adsorbate such as pyridine, the partial vapor pressure at various temperatures must be kept constant by adjustments of the concentration or by appropriate interpolations. Alternatively, if $d\mu_i/dT$ is known (it is the partial molar entropy of the adsorbate in solution), Γ_s can be evaluated.⁶ In fact Γ_s will be a complex quantity related to the temperature dependence of the free energy of solute and solvent species, and their interactions, in the interphase. It is for this reason that the entropy (and heat) of the substitutional adsorption process directly evaluated from ΔG° , calculated for various temperatures, is the quantity to which preferred attention is given in the present paper.

Results and Discussion

1. *Isotherms and the Free Energies of Adsorption.* As in previous work,^{1,11} it is convenient to evaluate the quantity ΔG° , the apparent standard free energy of adsorption in an isotherm $F(\Gamma)$ where

$$\ln F(\Gamma) = -\frac{\Delta G^\circ}{RT} + \ln C \quad (5)$$

(10) R. Parsons, *Trans. Faraday Soc.*, **51**, 1518 (1955).

(11) E. Blomgren and J. O'M. Bockris, *J. Phys. Chem.*, **63**, 1475 (1959).

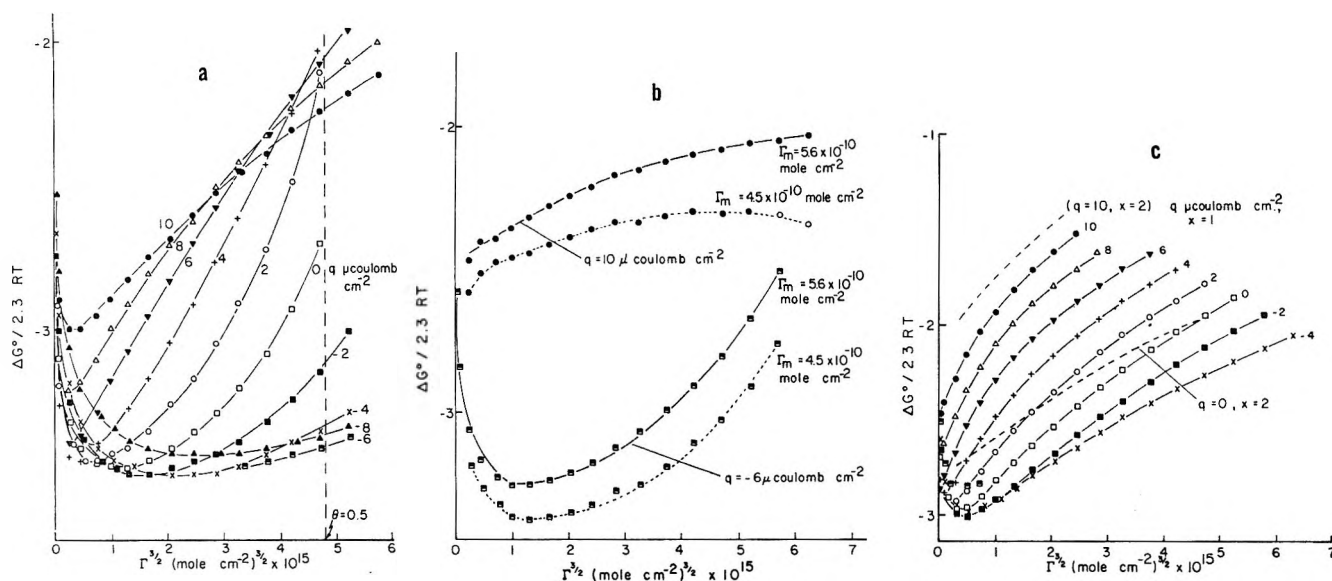


Figure 3. Evaluation of apparent ΔG° values as a function of $\Gamma^{3/2}$ for pyridine adsorption at mercury at various values of q or E^- , and at several temperatures: (a) 280.5°K; (b) 313°K; (c) 353°K. [In (b), the ΔG° data were evaluated for two values of the saturation coverage Γ_m .]

and Γ is the surface excess evaluated preferably for constant charge q and for various values of concentration C . When interaction effects are significant, the apparent¹² standard free energy value ΔG° varies with Γ but a value ΔG°_0 referring to the adsorption process in the absence of interactions or equivalent structural effects may be obtained¹¹ by extrapolation to $\Gamma = 0$. Generally such values and corresponding ΔS°_0 and ΔH°_0 quantities will not be so accurate as the actual values evaluated at finite Γ . Following the procedures adopted in earlier publications, *e.g.*,^{1,11} we assume

$$F(\Gamma) = \frac{\Gamma}{\Gamma_m} \left/ \left(1 - \frac{\Gamma}{\Gamma_m} \right) \right. \quad (6)$$

where Γ_m is the saturation surface coverage ($\theta = 1$), and obtain ΔG° as a function of Γ which may be plotted, *e.g.*, with respect to $\Gamma^{3/2}$ or $\theta^{3/2}$ if dipole repulsion effects dominate the nonideality of the surface layer.¹ "Langmuir" substitutional adsorption¹³ will give ΔG° values independent of θ , a result rarely found in adsorption at mercury. In cases where the ratio of areas of adsorbate and solvent molecules is appreciable, the relative area factor may be as significant as the interaction effect and $F(\Gamma)$ will then be (*cf.* ref 4) of the Flory-Huggins form $(\Gamma/\Gamma_m)/x(1 - \Gamma/\Gamma_m)^2$ as examined in the paper by Lawrence and Parsons presented at this symposium. However, for a given value of x applicable to the substitutional adsorption, variation of the apparent ΔG° , calculated from eq 7, with Γ will still properly characterize the interaction or other equivalent effects (see below). In the above case, it is of interest to compare the results for ΔG° or K which would be derived from the Langmuir (L) and Flory-Huggins (FH) type isotherms for a given determined coverage in equilib-

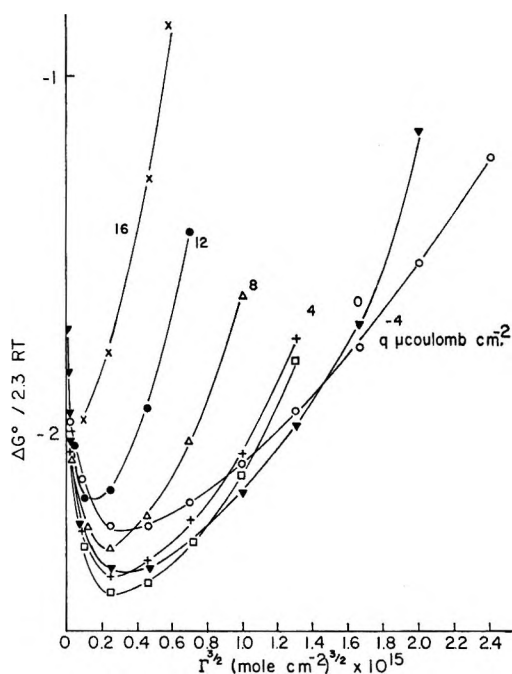


Figure 4. Evaluation of apparent ΔG° values for acetophenone adsorption at mercury from methanolic 1 *N* H_2SO_4 solutions at 293°K.

rium with adsorbate at a fixed bulk concentration C in the solution. Writing the FH isotherm as a function of θ in the form

$$\frac{\theta}{x(1 - \theta)^2} = K_{FH}C \quad (7)$$

(12) E. Gileadi and B. E. Conway, "Modern Aspects of Electrochemistry," Vol. III, J. O'M. Bockris and B. E. Conway, Ed., Butterworth and Co. Ltd., London, 1964, Chapter V.

(13) R. Parsons, *J. Electroanal. Chem.*, **7**, 136 (1964); *cf.* A. N. Frumkin, *ibid.*, **7**, 152 (1964).

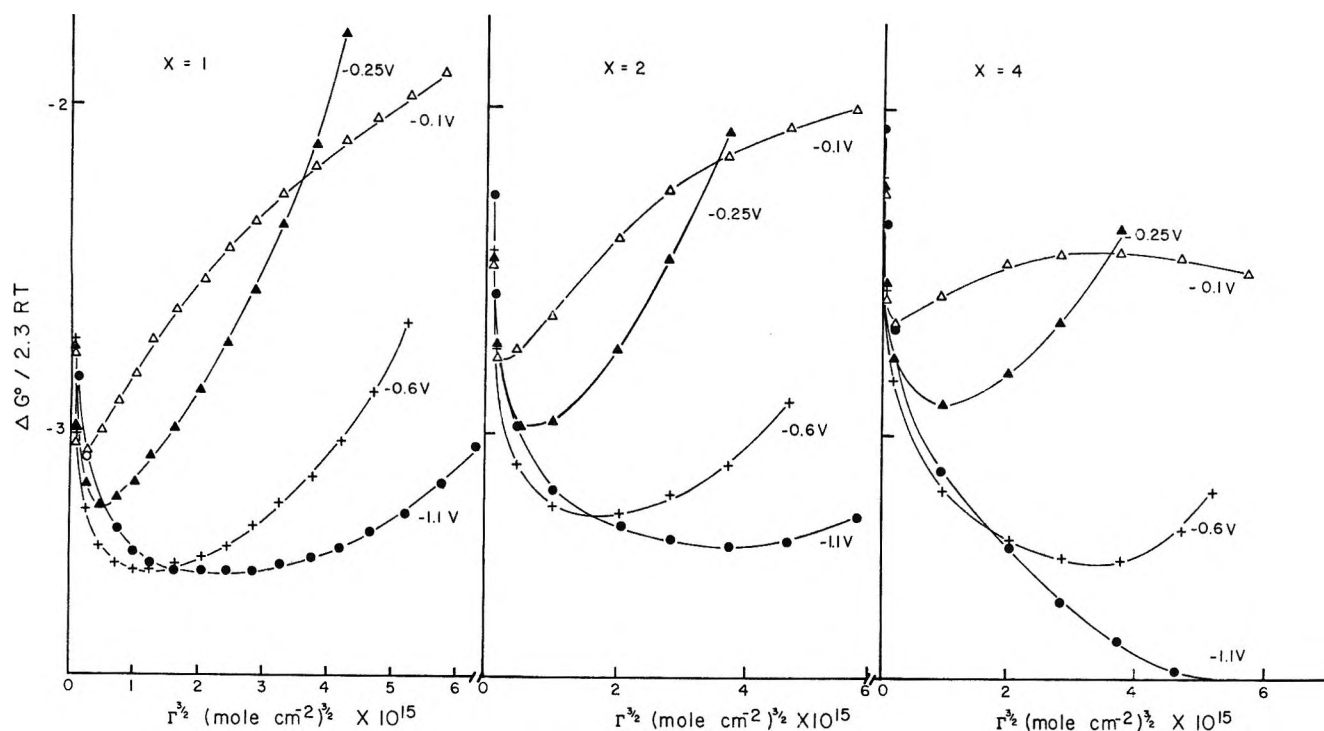


Figure 5. Calculations of ΔG° from the experimental results on the basis of the Flory-Huggins isotherm with various x values (eq 7).

we see immediately that

$$K_L/K_{FH} = x(1 - \theta)^{x-1} \quad (8)$$

or

$$\frac{1}{RT}(\Delta G^\circ_{FH} - \Delta G^\circ_L) = \ln x + (x - 1) \ln(1 - \theta) \quad (9)$$

where x is the molecular size ratio of adsorbate and adsorbed solvent. $(\Delta G^\circ_{FH} - \Delta G^\circ_L)/2.303RT$ is shown as a function of θ in Figure 2 for various values of x from 1 (Langmuir case) to 6, *i.e.*, over the range applicable to pyridine in water ($x = 3-4$). It is evident that at appreciable coverages ($\theta > 0.5-0.7$) the relative area factor can introduce changes in the evaluated ΔG° quantity which are comparable with the magnitudes of ΔG° commonly obtained (*ca.* -2 to -6 kcal mol $^{-1}$) for substitutional molecular adsorption at Hg. However, at $\theta = 0.25$ the ΔG° values derived from both isotherms are almost identical. Also, the choice of the correct value for Γ_m is critical.

Plots of ΔG° on the basis of eq 6 (used for evaluation purposes only) are shown in Figure 3a-c for various temperatures and at various q values. At $T = 280.5^\circ\text{K}$ for example, ΔG° initially becomes more negative with coverage (plotted as $\Gamma^{1/2}$) but eventually becomes less negative, the effect increasing as q becomes more positive. Similar effects are maintained, for example, at 353°K but the variation of ΔG° to less negative values with increasing Γ is more marked and the minima occur correspondingly at lower Γ . That this behavior is not peculiar to pyridine is shown in Figure 4 where typical

results are shown for methanolic solutions of acetophenone (in which the essential dipole is in an orientable functional group [$\mu_{CO} = 2.9$ D] rather than in the "whole molecule" as it is in pyridine). The results obtained in dilute (0.03 N) NaClO_4 may be assumed to refer to pyridine molecule adsorption (hydrolysis effects are negligible¹⁴) in the absence of significant specific adsorption of anions. It is for this reason that they probably differ from the previous results¹ obtained for pyridine adsorption at 298°K which were based on experiments in 1 N KCl. The results in that supporting electrolyte were interpreted¹⁻³ in terms of relatively sudden orientation of pyridine at a critical Γ dependent on electrode potential, and the behavior was shown² to be dependent on the Cl^- adsorption. It is evident that the present results in the presence of ClO_4^- anions are rather different although formally, over much of the $\Delta G^\circ - \Gamma^{1/2}$ curves, ΔG° is numerically decreasing, corresponding to repulsion or other nonideality effects, but the apparent repulsion effects are evidently least at the most negative q values.

The extent to which the variations of ΔG° calculated from the experimental observations depend on the choice of x in eq 7 is shown in Figure 5 for $x = 1, 2$, and 4. Space-filling models indicate x will be between 2 and 4, depending on the rotational freedom. Increasing x has the effect of lowering the ΔG° values calculated for the larger coverages.

A variation of ΔG° with Γ need not, of course, be

(14) B. E. Conway and R. G. Barradas, *J. Electroanal. Chem.*, 6, 314 (1963).

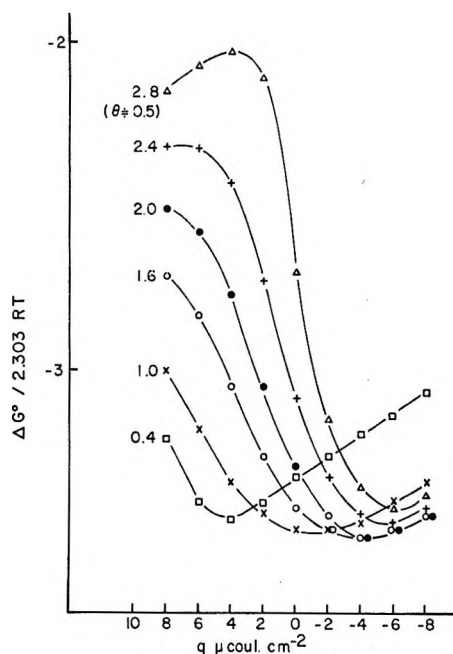


Figure 6. Variation of ΔG° calculated for various Γ values as a function of surface charge q (for $\alpha = 1$).

ascribed only to repulsion effects, although this was^{1,2} and is a reasonable interpretation of the results obtained previously^{1,2} in chloride solutions. The role of solvent structural effects in relation to the adsorbate(solute)-solvent interaction in the ad-layer, similar to those which occur in aqueous solutions of soluble organic molecules,^{15,16} must be considered. It is in regard to such effects that the studies over a range of temperatures are particularly informative insofar as entropies of substitutional adsorption can be evaluated for appropriate isosteric and constant charge conditions. Before referring to such results, however, it is of interest to illustrate how ΔG° evaluated for various constant Γ values is dependent on q (Figure 6).

Basically, ΔG° has maximum values of *ca.* -4.5 kcal mol⁻¹ for various Γ and these maxima occur at q values which become more negative with increasing Γ . ΔG° for neutral molecules usually¹⁷ has a parabolic form with respect to q (except at high $\pm q$ where orientation saturation polarization becomes dominant). There is evidently (Figure 6) a shift of the ΔG° - q relationship toward higher q values as Γ increases so that at given q values, ΔG° tends to become less negative with increasing Γ except where the curves cross over toward the more negative q values. Over most of the curves, a higher negative value of q is required for ΔG° to attain a given value as Γ increases; we suggest this reflects (a) the competition arising from orientation polarization of water dipoles and pyridine molecules in the interphase, and the resulting hydrogen bonding which can arise at the N-center when it is oriented away from the electrode at more negative q ; (b) the change in two-dimensional structure breaking in the water ad-

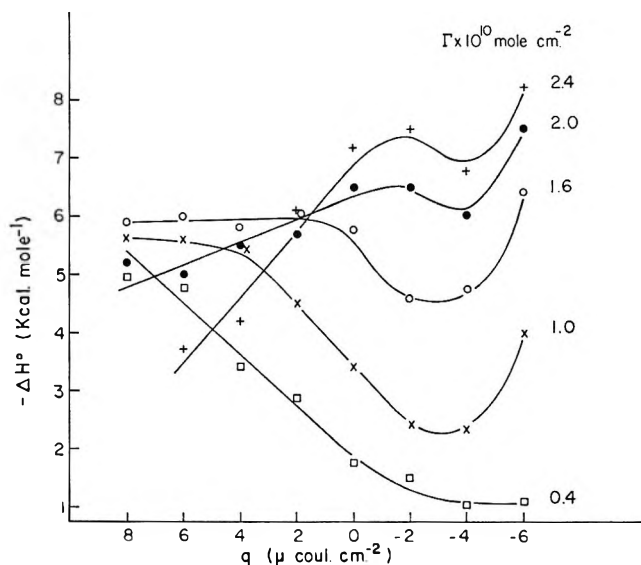


Figure 7. Isosteric heats of adsorption of pyridine plotted as a function of charge q for various coverages.

layer comprising the interphase as the surface excess of pyridine is increased; and (c) the displacement of anions as q is made more negative, an effect which we have shown previously to depend on the pyridine adsorption² insofar as at higher pyridine coverage the anion specific adsorption (Cl^- in that case) is enhanced at a given potential.

2. *The Heats and Entropies of Adsorption.* Here isosteric entropies of adsorption were evaluated at constant charge from plots of ΔG° vs. T and ΔH° was obtained from ΔG° with the derived values of ΔS° . Previously, for ions,⁵ *isotensile* thermodynamic functions for adsorption were evaluated but the isosteric quantities will reflect better any effects of changing interaction effects with charge at given degrees of coverage. The standard heats and entropies of adsorption are shown in Figures 7 and 8 as a function of q . The striking feature of these results is that ΔS° for give Γ values increases toward a maximum *positive* value (*cf.* ref 14) as q varies from $+48$ to *ca.* $-\mu\text{C cm}^{-2}$ and then tends to decrease while ΔH° has a corresponding variation with q . Similarly, the isotensile entropy of adsorption of I^- is largest near $q = 0$.⁶ Behavior related to these effects is more difficult to discern in the ΔG° plots and indeed there is a substantial compensation between ΔH° and ΔS° or $T\Delta S^\circ$ tending to make ΔG° a function rather less sensitive to

(15) B. E. Conway and L. Laliberté, "Hydrogen Bonded Solvent Systems" (Proceedings of the Symposium on Equilibria and Kinetics in Hydrogen Bonded Systems, Newcastle, 1958), Taylor and Francis, London, 1968, p 139; see also *J. Phys. Chem.*, **72**, 4317 (1968).

(16) R. M. Diamond, *ibid.*, **67**, 2513 (1963); W. Y. Wen and S. Saito, *ibid.*, **69**, 3589 (1965); H. S. Frank, *Z. Phys. Chem. (Leipzig)*, **228**, 364 (1965).

(17) R. Parsons, *J. Electroanal. Chem.*, **5**, 397 (1963); *cf.* A. N. Frumkin, *Z. Phys.*, **35**, 792 (1926), and I. Zhukovitskii, *Acta Physicochim. U.R.S.S.*, **19**, 176 (1944), for relative area effects.

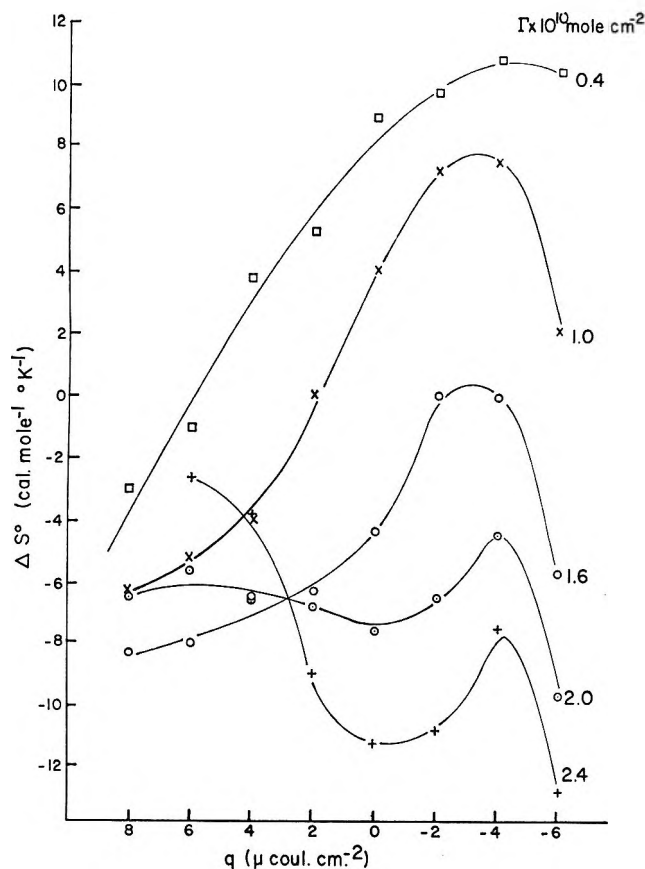


Figure 8. Isosteric standard entropies of adsorption of pyridine plotted as a function of charge for various coverages.

q (cf. the analogous case of ionization constants in relation to structure of organic acids and bases). This type of compensation is familiar in ionic solutions^{18,19} and has recently been demonstrated²⁰ in the thermodynamics of binding of acetylcholine competitors at the enzyme acetylcholinesterase. The compensation plot relating ΔH° and ΔS° for pyridine adsorption at Hg is shown in Figure 9 and covers a wide range of ΔS° values (for various Γ and q values) with a slope of ca. 300°K close to the value obtained for binding of various competitors at the enzyme mentioned above²⁰ and for hydration of ions.¹⁹ At high values of Γ and for the more positive values of q , the degree of compensation is less (Figure 8) and the relation has a slope of ca. 200°K . This is probably connected with the reversal of orientation of pyridine together with the presence of ClO_4^- ions in the ad-layer which enhance structure-breaking effects in the interphase. In general, as is shown below, the best compensation between entropy and energy terms is achieved when interaction-dependent librations are involved. Configurational entropy changes are usually insufficient²¹ to account for the large changes of entropy often associated with substantial energies of interaction (cf. the case of ionic solutions¹⁹).

Although pyridine is more strongly adsorbed at a given concentration of the negative branch of the

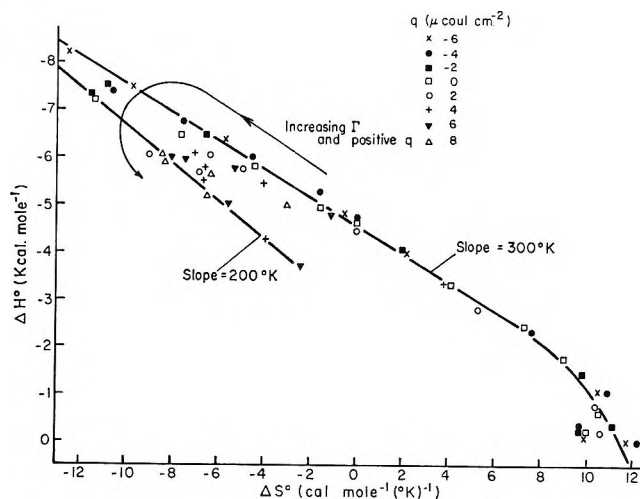


Figure 9. Compensation effect between heat and standard entropy of adsorption of pyridine at mercury for various q and Γ values.

electrocapillary curve so that ΔG° values are relatively more negative at the negative q values, ΔH° in fact tends to become less negative as $-q$ increases except at higher Γ values where it tends to remain more constant (Figure 7). The unfavorable trend in ΔH° is compensated by an opposite trend in $-T\Delta S^\circ$. At low coverage, the positive ΔS° reflects, we believe, release of structured, low-entropy water at the surface with a consequent net positive entropy change in the adsorption process, an effect which we have observed previously¹⁴ at solid electrodes. This implies that the water layer at Hg tends to be most structured in the region of $q = -3$ to $-6 \mu\text{C cm}^{-2}$ (Figure 8). This may not seem consistent with the maximum observed⁶ in the derived excess entropy Γ_s of the interphase in NaF solution at ca. $q = -8 \mu\text{C cm}^{-2}$, but Γ_s is a complex quantity involving both the electrostatically adsorbed ions, their hydration shells, and the water itself in the interphase, and cannot be directly related to the entropy of the water layer or to the entropies of adsorption calculated here.²⁴

That the water in the interphase may be maximally structured near the potential of zero charge might be inferred by analogy with the effect of large organic hydrophobic groups in promoting structure in water solutions.²² Mercury probably has little specific interaction with water molecules²³ (except perhaps residually

(18) K. J. Laidler, *Trans. Faraday Soc.*, **55**, 1725 (1959); cf. P. Ruetschi, *Z. Phys. Chem.*, **14**, 277 (1958).

(19) D. D. Eley and M. G. Evans, *Trans. Faraday Soc.*, **34**, 1093 (1938).

(20) B. Belleau and J. L. Lavoie, *Can. J. Biochem.*, **46**, 1397 (1968).

(21) T. L. Hill, "Introduction to Statistical Thermodynamics," Addison-Wesley Publ. Co., Reading, Mass., 1960, pp 380, 381.

(22) G. Nemethy and H. A. Scheraga, *J. Chem. Phys.*, **36**, 3401 (1962); cf. A. Ben Naim, *J. Phys. Chem.*, **69**, 1922 (1965).

(23) R. Parsons, *Proc. Roy. Soc.*, **A261**, 79 (1961).

(24) R. Parsons, *Can. J. Chem.*, **37**, 308 (1959).

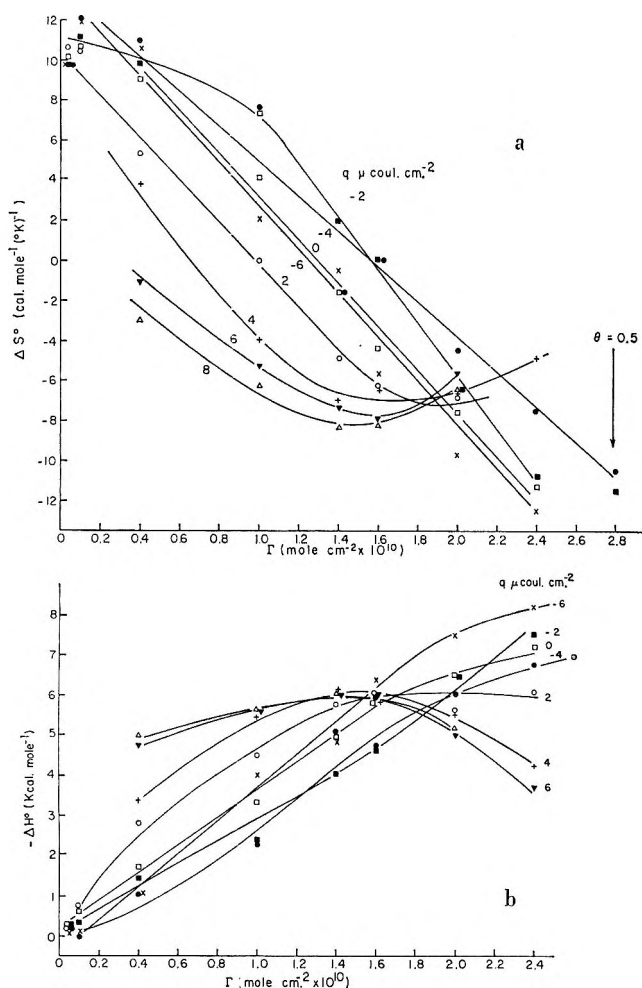


Figure 10. (a) Dependence of ΔS° on coverage Γ ; (b) dependence of ΔH° on coverage Γ .

at positive q with the lone pair electrons on oxygen; cf. the weak Hg(II) complex with dioxane), but its metallic nature will allow an effective continuation of the dipole (hydrogen bond) interactions among the water molecules "through" the interface on account of the dipole images and their interactions with the parent charge distributions on the solution side.

As in the ΔG° plots (Figure 3), ΔS° depends appreciably on the coverage, becoming less positive for ΔS° values calculated for higher Γ values (Figure 10a). This suggests that at the higher Γ values in Figure 10, the water layer is already disorganized so that less entropy is released per mole of pyridine adsorbed under such conditions and the apparent standard entropy of adsorption, like the corresponding ΔG° , varies with the equilibrium Γ value from which the ΔG° , and hence the ΔS° value, has been calculated. The dependence of ΔH° on coverage is shown in Figure 10b.

At higher negative or positive q values, the ΔS° values decrease presumably due to (a) the field effect on water orientation leading to structure-breaking effects analogous to those associated with electrostriction which arise at small ions, so that substitutional adsorption no

longer leads to anomalous positive entropy changes, and (b) orientation of the pyridine itself (cf. ref 1, 2) at high fields. At positive q values, the tendency for ClO_4^- ions increasingly to enter the interphase may assist the structure-breaking effect of the electrode field itself and enhance the tendency for ΔS° to become more negative.

3. *Components of the Entropy of the Water Layer.* It is of interest to examine to what extent the electrostatic and configurational entropy of water in the interphase could vary with electrode surface charge and then to examine if such solvent adsorption effects could account for part of the substitutional entropy changes found in the present thermodynamic study of pyridine adsorption.

(a) *Configurational Effects.* Solvent dipole orientation can be considered in terms of the model of Bockris, Devanathan, and Müller²⁵ in which dipoles are regarded as being in an up (\uparrow) and down (\downarrow) direction with respect to the surface. This will give rise to a molar configurational entropy of mixing S_c of the two orientational states

$$S_c = -R[\theta\downarrow \ln \theta\downarrow + \theta\uparrow \ln \theta\uparrow] \quad (10)$$

where the θ terms are the surface fractions (and hence relative coverages) of dipoles oriented in \uparrow or \downarrow directions. In eq 10, interaction effects (see below) have not been considered. The orientation of dipoles will be determined by their interaction with the electrode field E and by their mutual interactions.²⁵ The resulting distribution function²⁶ for interacting dipoles is given²⁵ by

$$\frac{N\uparrow - N\downarrow}{N_T} = \tanh \left[-\frac{Uz}{kT} \left(\frac{N\uparrow - N\downarrow}{N_T} \right) + \frac{\mu E}{kT} \right] \quad (11)$$

where U is the interaction energy per pair of dipoles in a configuration with coordination number z and $N\uparrow$, $N\downarrow$ are the numbers of dipoles in \uparrow and \downarrow orientations, respectively, and $N_T = N\uparrow + N\downarrow$. In terms of the relative coverages θ

$$(2\theta\downarrow) - 1 = \tanh \left[-\frac{Uz}{kT} (2\theta\uparrow - 1) + \frac{\mu E}{kT} \right] \quad (12)$$

which is evaluated below for various values of the interaction factor $f_i = Uz/kT$ and the electrostatic field-dipole interaction term $\mu E/kT$. The configurational entropy of the layer of molecules with mixed orientations then follows from eq 10. $\theta\uparrow$ and $\theta\downarrow$ may be related to q through²⁷ E given by $E \doteq -4\pi q/\epsilon$ where

(25) J. O'M. Bockris, M. A. V. Devanathan, and K. Müller, *Proc. Roy. Soc.*, A274, 55 (1963).

(26) B. E. Conway, "Theory and Principles of Electrode Processes," Ronald Press Co., New York, N. Y., 1964.

(27) R. Parsons, "Modern Aspects of Electrochemistry," Vol. I., J. O'M. Bockris and B. E. Conway, Ed., Butterworth and Co., Ltd., London, 1954, Chapter 3.

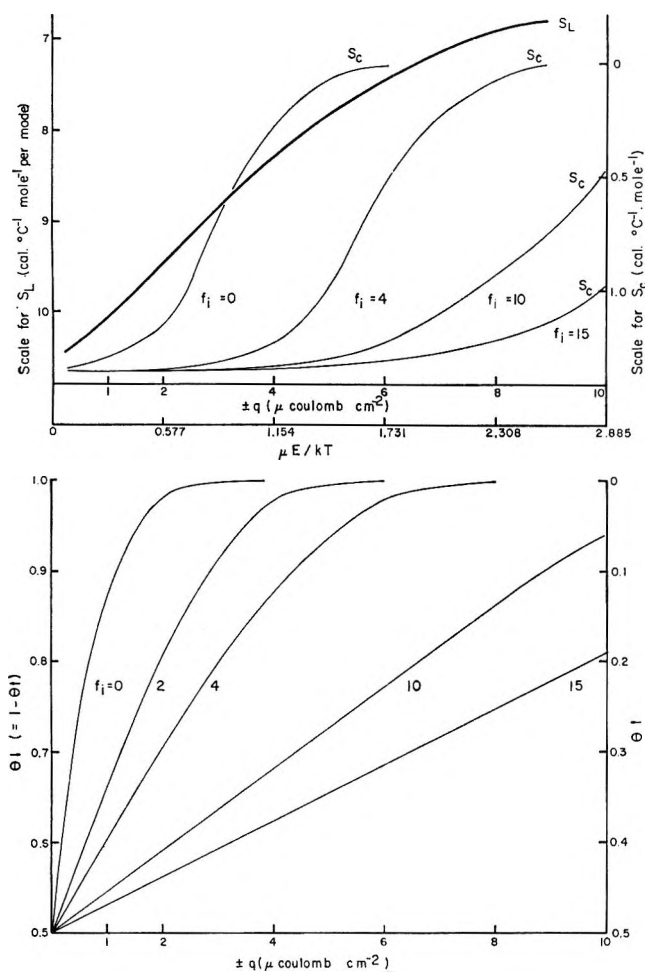


Figure 11. Configurational and librational entropy of oriented water molecules in the electrode interphase in relation to the orientation distribution function (lower figure) plotted in terms of the orienting field E and corresponding charge $\pm q$.

ϵ , the effective dielectric constant of the surface layer, may be taken as *ca.* $6^{28,29}$ (actually ϵ will be $f(q)$ at low values of q but we take the reasonable value of 6 discussed previously). The results are shown in Figure 11.

The problem considered here is seen to be closely related to that involved in the calculation of magnetization in a lattice of magnetic dipoles. While interaction effects have been included here in the orientation distribution function, we have followed the usual Bragg-Williams approximation in assuming that the interactions do not appreciably influence the configurational entropy. This is not an entirely satisfactory assumption in any problem in lattice statistics (except in the quasi-ideal case of regular solutions) but corrections for nonrandom mixing²³ when interaction effects are significant are in fact relatively small and to a first-order approximation, are of the order

$$-R \frac{(\theta \uparrow \theta \downarrow)^2}{4z} \left(\frac{zU}{kT} \right)^2 \quad (13)$$

i.e., the nonrandomness introduced by interaction contributes, as expected, a negative term in the entropy of

mixing. For $\theta \uparrow = \theta \downarrow$ near $q = 0$, the maximum value of this entropy correction amounts to only -0.5 eu for $2U/kT = 5$ say.

(b) *Librational Entropy.* In an electric field, a dipole tends to become oriented but this orientation is rarely complete and the degree of orientation is determined by the field-dipole interaction energy factor $\mu E/kT$. The dipole executes librative motion in the field and the partition function for the libration mode is^{19,30}

$$f_L = \frac{8\pi^2(8\pi^3 I_1 I_2 I_3 k^3 T^3)^{1/2} \sinh [U_e/kT]}{\sigma h^3 U_e/kT} \quad (14)$$

where U_e is the electrostatic field-dipole interaction energy and I 's are the principal moments of inertia of the water dipole. The entropy associated with the librational energy states in the field is then

$$\frac{S_L}{R} = \ln \frac{8\pi^2(8\pi^3 I_1 I_2 I_3 k^3 T^3)^{1/2}}{\sigma h^3} - \ln U_e/kT + \ln \sinh [U_e/kT] - \frac{U_e}{kT} \coth \left[\frac{U_e}{kT} \right] + 5/2 \quad (15)$$

S_L was evaluated for various values of the inner Helmholtz field $E = -4\pi q/\epsilon$ with μ_{H_2O} taken as 1.87 D (a larger value could be taken corresponding to the water molecule associated in the water structure; this would result in given S_L values arising at somewhat lower values of field E or charge q). S_L as a function of $\pm q$ is shown in Figure 11 for one librational mode. The variation of entropy with q is appreciable and larger than that of S_C with q . It is also approximately linear with U_e thus providing a basis for compensation between energy and entropy terms.

(c) *Vibrations.* It can generally be assumed that the internal vibrations of H_2O molecules are little affected by the field except indirectly by hydrogen bond bending or breaking effects. In any case, the internal vibrational entropy will be small at room temperatures since the bend and stretch vibrational quanta are between 8 and $16kT$. However, near the electrode surface, water dipoles will tend to execute vibrations normal to the surface, as at ions.¹⁹ This effect is difficult to evaluate in terms of the associated entropy but for appreciable q ($\approx 20 \mu C cm^{-2}$) the magnitude of S_{vib} may be assumed to be similar to that at an ion where the field is of similar magnitude to that at the interface. *E.g.*, for the F^- ion (4 coordinated) S_{vib} of water in the hydration shell is *ca.* $2.05 \text{ cal mol}^{-1} (\text{ }^\circ\text{C})^{-1}$, while for the I^- ion (6 coordinated) S_{vib} is *ca.* $3.0 \text{ cal mol}^{-1} (\text{ }^\circ\text{C})^{-1}$.¹⁹

(28) B. E. Conway, J. O'M. Bockris, and I. A. Ammar, *Trans. Faraday Soc.*, **47**, 756 (1951).

(29) R. W. Rampolla, R. C. Miller, and C. P. Smyth, *J. Chem. Phys.*, **30**, 566 (1959); (*cf. ref 25*).

(30) E. A. Moelwyn-Hughes, "Physical Chemistry," Pergamon Press, Ltd., London, 1957; see also R. H. Fowler, "Statistical Mechanics," Cambridge University Press, 1936, and ref 19.

(d) *Translational Effects and Entropy of Water in the Bulk.* According to the calculations of Eley and Evans,¹⁹ the components of the entropy of water at 25° in the bulk are

$$S_{\text{vib}} = 5.3; S_{\text{lib}} = 6.7; S_{\text{trans}} = 12.8 \text{ cal mol}^{-1} (\text{°C})^{-1}$$

per pair of water molecules. We can assume that the translational entropy of water in the interphase is *ca.* $\frac{2}{3}$ of the value in the bulk and will be almost independent of field except insofar as the free area in the interphase may diminish due to electrostriction (*cf.* ref 6).

4. *Relation to Pyridine Adsorption.* The curves of Figure 8 indicate appreciable positive entropy changes for low coverages and the lower q values. At higher coverages, the entropy changes are negative but exhibit a reproducible maximum around $q = -3$ to $-6 \mu\text{C cm}^{-2}$. The magnitudes of ΔS° for various conditions reflect (i) the entropy of adsorption of pyridine itself and (ii) the entropy associated with displacements of x water molecules (*cf.* eq 7) previously adsorbed where x will be between 2 and 4 based on inspection of space-filling models.

The entropies of adsorption and their variation with q or Γ are seen to be quite large in comparison with the calculated librational entropy of water in the interphase or in relation to the known entropy of fusion of water (*ca.* 6 eu). If allowance is made, however, for the fact that substitutional adsorption will involve displacement of several water molecules ($x = 2$ to 4) per pyridine molecule, the observed values of ΔS° seem plausible. They can be accounted for qualitatively in terms of structural effects to be discussed below.

We have seen above that electrostatic effects in the interphase would tend to give rise to both diminishing configurational and librational entropy contributions as $\pm q$ increases. In point of fact, the librational freedom of solvent water may be less on the negative branch than on the positive, by analogy with the lower entropy of hydrate water at anions in comparison with that at cations. It is now seen (*cf.* Figure 10a) that the observed entropy change for low coverage conditions ($\Gamma = 0.4$ and $1.0 \times 10^{-10} \text{ mol cm}^{-2}$) is the opposite of what might be expected in terms of the electrostatic entropy of water in the interphase as a function of q (Figure 11). It is for this reason that it becomes necessary to suppose that the Hg interface has a structure-promoting effect which minimizes the entropy of water in the interphase near the potential of zero charge. This effect may be enhanced by the dipole image interaction which in effect preserves the local structure "across" the interface and indeed the surface excess volume Γ_v tends toward a maximum value near the potential of zero charge.⁶

At positive q the ΔS° values tend to be more negative than at corresponding negative charges. It seems likely that this could be due to the different orientation which pyridine can take up in the interphase, since on

the positive branch the N center will be oriented away from the solvent with which it tends to hydrogen bond, and thus tend to be more specifically associated with the electron-deficient metal surface. In this connection, it is interesting to note that the excess partial molal entropy of pyridine³¹ in aqueous solution calculated limitingly for infinite dilution is $-12 \text{ cal } (\text{°C})^{-1} \text{ mol}^{-1}$, an unusually low value reflecting presumably strong association with water molecules (*cf.* the case of ionic solutions¹⁹). Loss of some of this associated water upon adsorption would cause release of positive entropy. The observation that entropies of adsorption at positive q are in fact the most negative (at low Γ) seems to indicate retention of some of the hydrogen bonding to water so that a "flat" orientation (rather than one in which the pyridine dipole is oriented toward the metal surface) may be preferred in order to minimize "dehydration."

At higher coverages, structure-breaking by the pyridine itself¹⁵ may become significant, so that the entropy of displacement of water is a less positive quantity and the librational effects calculated above may become more representative of the experimental situation, *e.g.*, for $\Gamma = 2.4 \times 10^{-10} \text{ mol cm}^{-2}$. Corresponding variations of enthalpy can arise in a similar way: at appreciable coverage, water in the interphase will be less hydrogen bonded and more easily displaced, so that the process of displacement can become relatively more exothermic; this effect will be enhanced by increasing pyridine-pyridine interactions which can contribute approximately $1.47 \text{ kcal mol}^{-1}$ per pair as may be estimated from the known heat of vaporization of pure pyridine ($8.8 \text{ kcal mol}^{-1}$) assuming 12-coordination in a close-packed liquid lattice.

Analogously, with regard to the variation of the heats of adsorption at low Γ with charge, ΔH tends to become (Figure 7) appreciably less negative with decreasing q ; this effect could also be interpreted in terms of increasing difficulty of substitutional adsorption requiring H-bond breaking in the structured and H-bonded water layer as q decreases since the electrostatic energy difference of pyridine and water dipoles, due to field-dipole interactions, can only amount to *ca.* 1 kcal over this range of q (see below). At higher Γ values, an opposite trend is seen and ΔH° becomes more exothermic with decreasing q ; with a sufficient population of the ad-layer with pyridine, the structural effects associated with the water layer will be less important so that the pyridine reorientation effect can become dominant; *i.e.*, the tendency for the adsorption energy of the N center to be smaller at positive than at negative q owing to the diminution of H bonding which the N center would suffer if oriented away from the solvent must be considered. Contrary to earlier expectations,¹ the ΔH° is quite negative at the most positive q values

(31) R. J. L. Andon, J. D. Cox, and E. F. G. Herington, *Trans. Faraday Soc.*, **53**, 410 (1957); *J. Chem. Soc.*, 3188 (1954).

where the N center of pyridine is presumably oriented more toward the mercury and is thus less H bonded. The disadvantage with respect to H bonding which the molecule would experience when in this orientation may be compensated by electron overlap (specific adsorption) with the positive Hg surface under these conditions (*cf.* the stability of thiourea at Hg,²³ the existence of ammonia, amine, and amide complexes with Hg(II) and the π -orbital interaction of pyridine with positive surfaces¹). On the other hand, at appreciable q values (4 and 6 $\mu\text{C cm}^{-2}$), ΔH° changes relatively little with Γ ; this may indicate that pyridine is oriented in a "flat" manner at the electrode and carries with it locally at least one H₂O molecule which at the same time is able to interact with the charged metal surface. This is consistent with the argument made above regarding ΔS° and "dehydration" effects.

Electrostatic calculations (*cf.* ref 1) of the energy of polarization of pyridine (dipole-field and electronic

polarization energy) at various fields in comparison with that of 2 or 3 water molecules which it would replace indicate that water would tend to remain preferentially adsorbed even up to high $\pm q$. Again, a purely electrostatic treatment of the problem seems qualitatively inadequate so that structural effects involving hydrogen bonding may be as important in the enthalpies of adsorption as in the entropies. The close compensation between the entropy and enthalpy terms lends confirmation to the supposition that the adsorption characteristics of pyridine at mercury are closely and specifically connected with the behavior of water adsorbed in the interphase.

Acknowledgments. We are indebted to the National Research Council, Canada, for support of this work. L. G. M. G. acknowledges the award of a fellowship from the Sprague Electric Company, which also provided some financial assistance with the research project.

Electrocapillary Studies in Aqueous Lithium Chloride Solutions¹

by R. G. Barradas and E. W. Hermann

Department of Chemistry, Carleton University, Ottawa 1, Ontario, Canada (Received February 21, 1969)

A modified Lippmann electrocapillometer for the direct determination of interfacial tension as a function of variation in applied electrode potential, aqueous lithium chloride solution activity, and temperature is described. Measurements of electrocapillary curves for LiCl from 10^{-3} to 3.19 *m* were investigated over a temperature range of 1–45°. Derived results comprised of total charge on the electrode, ionic components of charge in the inner and diffuse double layer, Esin and Markov coefficients at constant charge are presented and discussed. All calculations were carried out by digital computer methods. The significance of certain peculiar charge effects is explained in terms of ion-water interactions, and the importance of the role of adsorbed water in the double layer is emphasized. Some preliminary data on entropies of adsorption are presented.

Introduction

Adsorption on mercury from lithium chloride solutions has been determined by the electrocapillary method² and by capacity measurements³ at 25°. In general there is a relative scarcity of temperature dependent double-layer studies, but a few noteworthy papers have been reported in the literature.^{4–9} There are two apparent shortcomings in most of the work cited, namely the small number of temperature intervals studied and/or the lack of simultaneous variation of solution activities in the bulk phase.

Experimental Section

Lippmann Capillary Electrometer. Improvement in electrometer design has been stated as one of several

possible ways of overcoming some of the experimental problems associated with double-layer studies¹⁰ and

(1) Presented as an invited paper at the Symposium on Interfacial Phenomena at Electrodes, 156th National Meeting of the American Chemical Society, Atlantic City, N. J., Sept 1968.

(2) H. Wroblowa, Z. Kovac, and J. O'M. Bockris, *Trans. Faraday Soc.*, **61**, 1523 (1965).

(3) D. C. Grahame, E. M. Coffin, J. I. Cummings, and M. A. Poth, *J. Amer. Chem. Soc.*, **74**, 1207 (1952); D. C. Grahame, *J. Electrochem. Soc.*, **98**, 343 (1951).

(4) J. E. B. Randles and K. S. Whiteley, *Trans. Faraday Soc.*, **52**, 1509 (1956).

(5) W. Anderson and R. Parsons, *Proceedings of the 2nd International Congress of Surface Activity*, Butterworth and Co., Ltd., London, p 45.

(6) G. J. Hills and R. Payne, *Trans. Faraday Soc.*, **61**, 326 (1965).

(7) J. M. Parry and R. Parsons, *J. Electrochem. Soc.*, **113**, 992 (1966).

(8) J. N. Butler, *J. Phys. Chem.*, **70**, 2312, (1966).

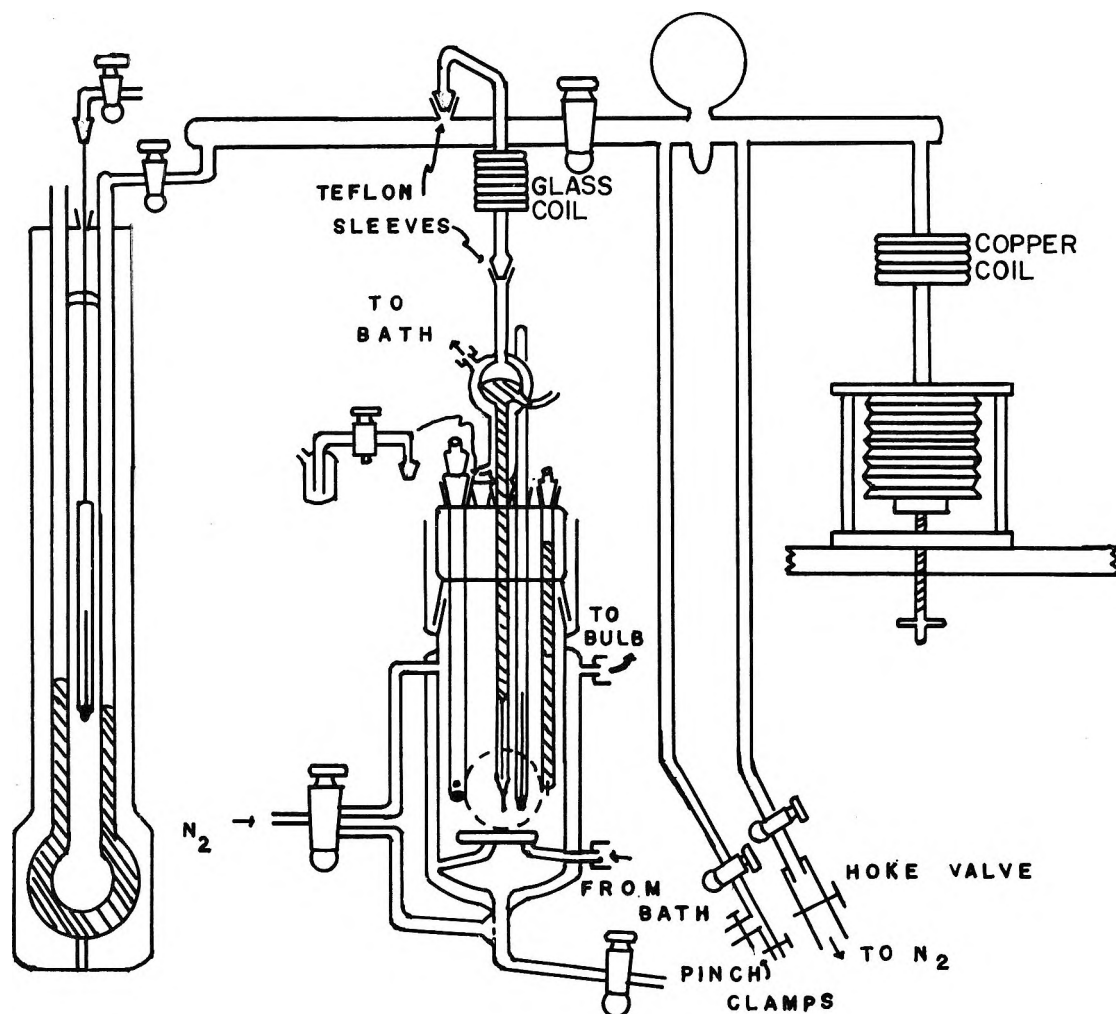


Figure 1. Schematic diagram of electrocapillary assembly.

during the course of this work a novel technique in this direction has been published.¹¹ The apparatus used in the present work is shown schematically in Figure 1 and it does not differ too substantially from those previously described (see, *e.g.*, ref 12). Basically, it is comprised of a one-compartment cell which houses a thermometer and working, counter, and reference electrodes of conventional design. However, appropriate changes were made to the cell and ancillary equipment to allow for more dependable electrocapillary measurements over a wider temperature range. The temperatures examined were $1^\circ (\pm 0.05^\circ)$ and from 10 to 45° at 5° intervals (within the limits of $\pm 0.02^\circ$ for each step). The cell and mercury reservoir were both thermostated by surrounding condenser jackets attached together in series. In addition, the thermostating solution was allowed to circulate through a glass coil within the base of the cell (see Figure 2). The thermostating solution consisted of a dilute solution of about $10^{-3} M$ sodium chromate which helped to prevent the buildup of impurities on the glass walls and yet served to avoid undesirable electrical phenomena

resulting from external ac circuitry, for example, from the wires of the Neslab heating and cooling unit.¹³

Twin optical flats of 7.5 cm diameter separated by a distance of about 4 cm were built in the mercury meniscus viewing area of the electrometer. The volume between the two parallel optical flats was evacuated and glass sealed in the construction of the cell. It is to be noted that the thermostating solution was not passed between the optical flats. The advantage of this design is to prevent "fogging" at low temperatures and to minimize heat conduction. Interfacial tension (γ) measurements were made from 0 to -1200 mV with respect to an internal calomel reference electrode (rce)¹² at 50-mV intervals, except for a range

(9) W. Paik, T. N. Andersen, and H. Eyring, *J. Phys. Chem.*, **71**, 1891 (1967).

(10) R. Parsons, *Rev. Pure Appl. Chem.*, **18**, 91 (1968).

(11) B. E. Conway and L. G. M. Gordon, *J. Electroanal. Chem. Interfac. Chem.*, **15**, 7 (1967).

(12) R. G. Barradas and P. G. Hamilton, *Can. J. Chem.*, **43**, 2468 (1965).

(13) L. Meites, "Polarographic Techniques," 2nd ed, Interscience Publishers, New York, N. Y., 1965, p 65.

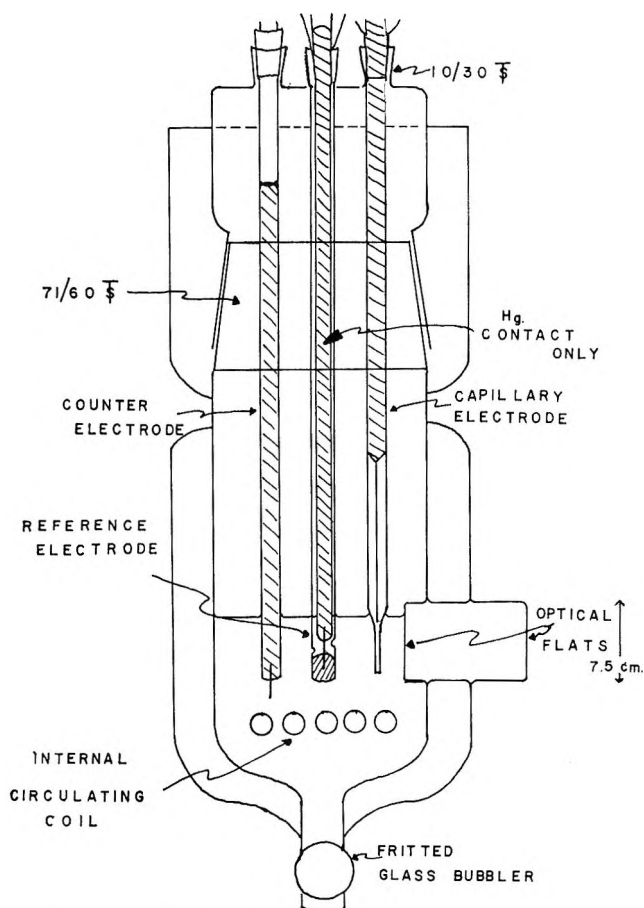


Figure 2. Thermostatted glass electrocapillometer cell: \\\, mercury; ///, calomel *in situ* reference electrode.

of ± 60 mV around the electrocapillary maximum (ecm) where readings were taken at 20-mV intervals instead. The usual method¹² of returning the mercury in the capillary to a reference mark using N_2 gas, followed by pressure readings as registered in a 1-in. bore manometer, was employed. Replicate points were determined at each potential to ensure maximum experimental accuracy. All measurements were taken at atmospheric pressure conditions.

Reagents. Mercury and conductivity water were purified as described before.¹² Commercially available lithium chloride of the highest analytical purity was used directly from sealed bottles. Recrystallization procedures did not seem to improve its quality in any significant manner. The concentration of all aqueous solutions examined (10^{-3} to 3.19 *m*) was regularly checked by standard Volhard titrimetry due to the highly hygroscopic nature of the LiCl solutions.

Results and Discussion

(a) **Electrocapillary Curves.** A total of 117 electrocapillary curves were obtained, being a representation of investigating 13 concentrations of LiCl at nine different temperatures. The full numerical data are recorded elsewhere,¹⁴ but exemplary primary results

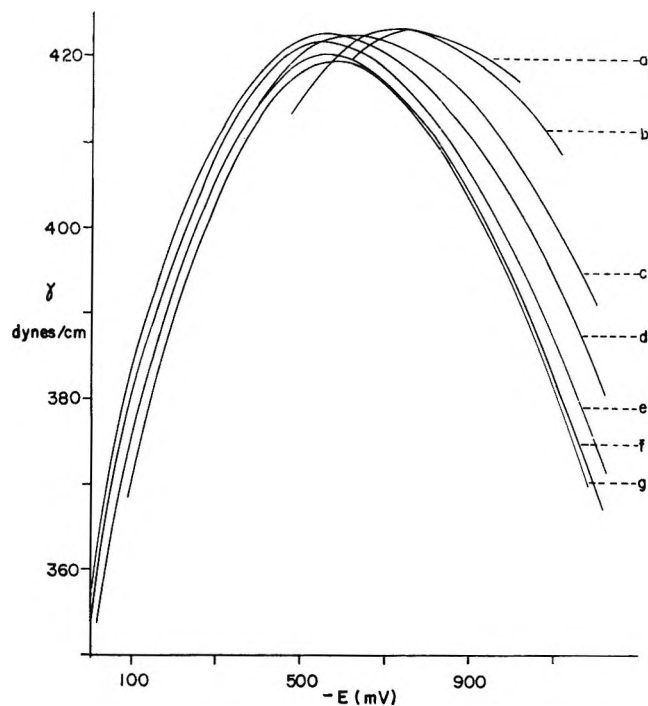


Figure 3. Electrocapillary curves determined in LiCl solutions at 45.0°: (a) 0.001 *m*; (b) 0.002 *m*; (c) 0.02 *m*; (d) 0.10 *m*; (e) 0.51 *m*; (f) 1.55 *m*; (g) 3.19 *m*.

and other relevant derived information will be presented here.

A typical family of electrocapillary curves is depicted in Figure 3. Although this group represents those measured at 45° there are several general features common in all those studied at lower temperatures. Complete curves over the whole potential range could not in general be obtained for concentrations below 0.1 *m*. However, for the same concentration a proportionately wider range of results of γ vs. potential (E) could be obtained as the temperature was increased from 1 to 45°. Up to a concentration of 0.2 *m* the trend of the ecm shifts progressively to more anodic potentials relative to the rce but at concentrations greater than 0.2 *m* the trend of the ecm shift is reversed. The inability to obtain complete electrocapillary curves in dilute solutions may very likely be due to the extremely slow approach to equilibrium of adsorbable species, resulting in a slow response of the mercury in the capillary electrode to changes in applied N_2 pressure. No sticking of the meniscus was observed when viewed by means of a 10 \times microscope, even at concentrations as low as 10^{-3} *m* in LiCl.

(b) **Calculation of Derived Quantities.** Derived results were calculated using an IBM 7094 and/or G.E. 410 digital computer with FORTRAN IV and programs based on those published earlier.¹⁴⁻¹⁸ Because of the

(14) E. W. Hermann, M.Sc. thesis, University of Toronto, 1967.

(15) R. G. Barradas and F. M. Kimmerle, *Can. J. Chem.*, **45**, 109 (1967).

Table I: Mean Molal Activity Coefficients for Aqueous LiCl

Molality, m	Temp., °C								
	1.0	10	15	20	25	30	35	40	45
1.0×10^{-3}	0.9641	0.9637	0.9635	0.9633	0.9630	0.9627	0.9624	0.9621	0.9618
2.0×10^{-3}	0.9503	0.9495	0.9490	0.9485	0.9480	0.9475	0.9470	0.9464	0.9459
5.0×10^{-3}	0.9234	0.9226	0.9221	0.9215	0.9210	0.9204	0.9198	0.9192	0.9186
1.0×10^{-2}	0.8982	0.8971	0.8964	0.8957	0.8950	0.8942	0.8934	0.8926	0.8917
2.0×10^{-2}	0.8694	0.8678	0.8669	0.8660	0.8650	0.8639	0.8628	0.8617	0.8606
5.0×10^{-2}	0.8253	0.8231	0.8218	0.8204	0.8189	0.8175	0.8159	0.8142	0.8126
1.0×10^{-1}	0.7900	0.7873	0.7856	0.7838	0.7820	0.7800	0.7780	0.7758	0.7737
2.0×10^{-1}	0.7684	0.7649	0.7627	0.7604	0.7579	0.7554	0.7527	0.7499	0.7470
5.2×10^{-1}	0.755	0.750	0.747	0.744	0.740	0.736	0.732	0.728	0.724
1.02	0.799	0.792	0.787	0.782	0.777	0.771	0.765	0.759	0.753
1.55	0.872	0.863	0.857	0.851	0.844	0.837	0.829	0.822	0.814
2.08	0.975	0.961	0.952	0.943	0.933	0.922	0.912	0.901	0.890
3.19	1.30	1.27	1.25	1.23	1.21	1.19	1.17	1.15	1.13

implicit nature of the work, solution concentrations must be expressed in terms of molalities and mean molal activities (a_{\pm}). Values of a_{\pm} for LiCl are available for 25° only.^{19,20} Vapor pressure and emf measurements were not carried out because of the additional difficulty and tedium involved. Accordingly, the procedure recommended by Robinson and Harned²¹ was used to estimate the necessary a_{\pm} values through the equation

$$\log a_{\pm} = \log a_{\pm}^R + \frac{\bar{L}_2^R - \bar{J}_2^R T^R}{2.303RT} - \frac{\bar{J}_2^R}{\nu R} \log T - I' \quad (1)$$

with the realization that this equation assumes that the relative partial molal heat capacity is approximately constant over a limited range of temperatures, T , around T^R (25°). The calculations were facilitated by means of a simple computer program, and the values obtained are listed in Table I.

Three polynomial fitting techniques^{14,17,18} were used on the experimental data to facilitate the calculation of the charge densities, q_m and q_s , on the metal and solution side of the interface, respectively, where

$$-q_s = q_m = -(\partial\gamma/\partial E_-)_{T,P,\mu_{\text{LiCl}}} \quad (2)$$

The first designated as Method A¹⁴ chose the coefficients of a least-squares fifth-order (≤ 20 experimental points) or seventh-order (> 20 points) polynomial of the form

$$\gamma = a_0 + a_1 E_- + a_2 E_-^2 + \dots \quad (3)$$

The best fit of the experimental points [*i.e.*, the smallest standard deviation of $(\gamma_{\text{calcd}} - \gamma_{\text{exptl}})^2$] was consistently obtained, if the coordinate axis was shifted to correspond to the potential where the maximum surface tension was measured (a first approximation to the ecm). In this way the coefficients of the even powers of E_- were found to predominate over the odd ones (a_1, a_3 etc.) and as such is a better approximation to the correct

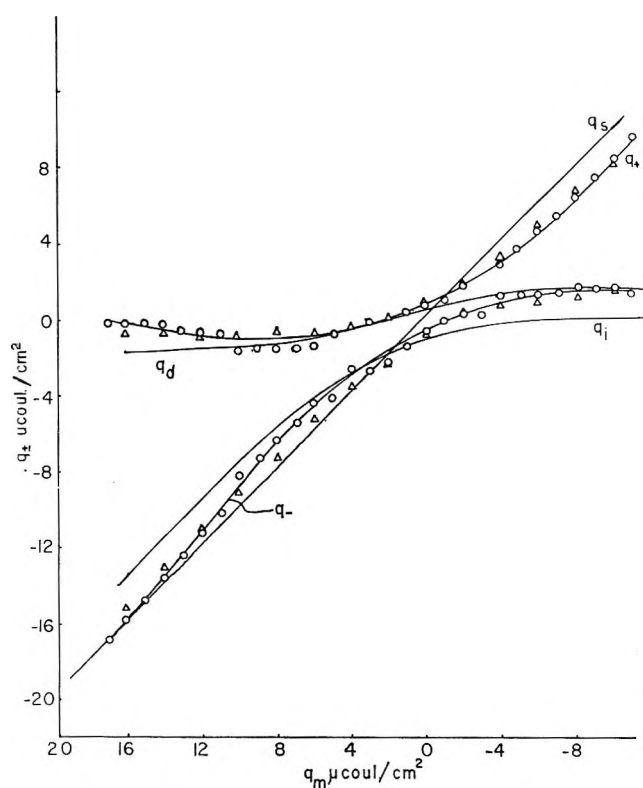


Figure 4. The charge dependence of the ionic components of charge (q_+ , q_-) and the charge distribution in the diffuse (q_d) and inner (q_i) double layer for 0.1 m LiCl at 25°; Δ represents values obtained using Method A, \circ values using Method B.

shape of an electrocapillary curve. q_m was then obtained by analytic differentiation of the polynomial.

(16) R. G. Barradas, F. M. Kimmerle, and E. M. L. Valeriotte, *J. Polarog. Soc.*, **13**, 30 (1967).

(17) D. M. Mohilner and P. R. Mohilner, *J. Electrochem. Soc.*, **115**, 261 (1968).

(18) W. R. Fawcett, private communication, University of Guelph.

(19) B. E. Conway, "Electrochemical Data," Elsevier Publishing Co., Amsterdam, 1952.

(20) R. Parsons, "Handbook of Electrochemical Constants," Butterworth and Co., Ltd., London, 1959.

(21) R. A. Robinson and H. S. Harned, *Chem. Rev.*, **28**, 419 (1941).

Table II: Comparison of Surface Tension, γ , and Electrode Charge, q_m , for 0.1 *m* LiCl at 25°^a

$-E_-, \text{mV}$ (vs. rce)	Grahame ²³ q_m	Wroblowa		Method A		Method B	
		γ ²⁴	q_m ²²	γ	q_m	γ	q_m
100	18.28	385.7	19.6	387.3	18.8	386.8	20.1
200	13.61	402.5	14.1	402.9	13.1	402.8	13.8
250	11.60	409.0	11.7	409.0	11.2	409.1	11.7
300	9.70	414.3	9.5	414.2	9.5	414.4	9.6
350	7.77	418.6	7.4	418.5	7.7	418.7	7.7
400	5.79	421.8	5.5	421.9	5.9	422.0	5.8
450	3.81	424.1	3.7	424.4	4.0	424.4	4.0
500	1.92	425.6	2.1	425.9	2.1	425.9	2.1
550	0.26	426.2	0.5	426.5	0.4
600	-1.15	426.1	-0.8	426.3	-1.2	426.3	-1.2
650	-2.36	425.3	-2.1	425.4	-2.5
700	-3.46	424.0	-3.3	423.8	-3.7	423.8	-3.4
800	-5.44	419.5	-5.4	419.2	-5.4	419.4	-5.3
900	-7.24	413.1	-7.3	413.1	-6.9	413.1	-7.2
1000	-8.92	405.0	-8.9	405.2	-8.9	405.0	-8.9
1100	-10.51	395.4	-10.4	395.2	-10.9	395.3	-10.6

^a All q_m values have the units of $\mu\text{C}/\text{cm}^2$. All γ values have the units of dyn/cm .

The second approach, Method B,¹⁸ employed a moving second-order polynomial which fit the data five points at a time. The charge on the metal was then calculated by analytic differentiation at the central point only. A value for q_m at each experimental potential was obtained by systematically dropping the first point in the set of five and adding a new point at the end of the previous potential interval. The third approach, Method C,¹⁷ is identical with Method B except that only three points are used to determine the three quadratic coefficients. Upon double differentiation, this last method gave the most erratic differential capacity curves, and for this reason it was eliminated from further consideration.

Methods A and B provided smoothed surface tension values whose deviations from the experimental values were well within the accuracy of the electrocapillometer [$\leq 0.2 \text{ dyn}/\text{cm}$],²² and on the basis of comparison with results previously obtained,^{2,23,24} as shown in Table II, both methods of calculation appear to be of comparable merit. It is worthwhile noting that Method A exhibits slightly less random deviation from experimental values and has a tendency to overfit the most cathodic three or four points on the electrocapillary curve. This overfitting is presumably due to the large value of E_- used in eq 3 at these very negative potentials. It also may slightly alter the shape of the curve, if there is a large difference (five or six points) in the number of experimental points recorded on either side of the ecm. Method B, on the other hand, faithfully reproduces the experimental values, except for the first and last two points, where this five-point method must be slightly altered.¹⁸ Further derived data, however, exhibit a proportionately larger scatter than the same data obtained using smoothed values of γ obtained *via* Method A.

For calculations of relative positive surface excess

$$\Gamma_+ = -(\partial\gamma/\partial\mu)_{T,P,E_-} \quad (4)$$

and the Esin and Markov coefficient

$$-(\partial E_-/\partial\mu)_{T,P,q_m} \quad (5)$$

either Method A, when using a third-order polynomial, or Method B was equally well suited.

(c) *The Chemical Nature of Li⁺ in the Double Layer and its Effect on the Ionic Components of Charge in Solution.* Figure 4 gives detailed information on the total charge in the solution (q_s) as a function of q_m for one concentration of LiCl at 25°. The figure includes q_d , the total negative charge in the diffuse double layer, q_i , the total negative charge in the inner double layer, and q_+ and q_- , which are, respectively, the total cationic and anionic components of q_s . All the charge terms illustrated in Figure 4 have been calculated according to the conventional theoretical equations^{25,26} used for specifically adsorbed electrolytes. The morphology of the curves obtained at other temperatures is essentially similar. Below 25°, the absolute values increase linearly with temperature, and above 25° the values decrease in the same manner. These observations are expected from thermal agitation changes of the ionic species in solution. Figure 5 shows a plot of q_+ vs. q_m for various concentrations of LiCl at 25°. The

(22) J. O'M. Bockris, K. Mueller, H. Wroblowa, and Z. Kovac, *J. Electroanal. Chem.*, **15**, 101 (1967).

(23) D. C. Grahame, *J. Electrochem. Soc.*, **98**, 343 (1951).

(24) H. Wroblowa, private communication, University of Pennsylvania.

(25) P. Delahay, "Double Layer and Electrode Kinetics," Interscience Publishers, New York, N. Y., 1965.

(26) D. M. Mohilner, "Electroanalytical Chemistry," Vol. I, A. J. Bard, Ed., Marcel Dekker Inc., New York, N. Y., 1966, p 241 ff.

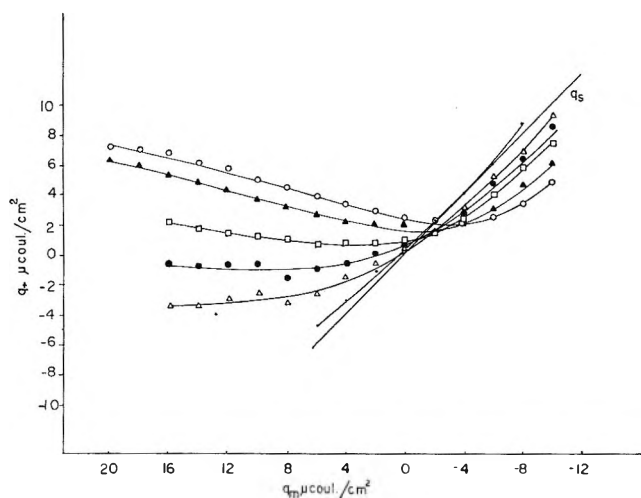


Figure 5. Charge dependence of the cationic component of the double layer charge, q_+ , for LiCl solutions at 25°C: O, 1.02 m ; \blacktriangle , 0.50 m ; \square , 0.20 m ; \bullet , 0.10 m ; \triangle , 0.05 m ; and \cdot , 0.002 m .

object in presenting this figure is to demonstrate that for concentrations below 0.1 m , values of q_+ obtained are less than those expected by the limit of the Gouy-Chapman theory.²⁶

The excellent agreement between the primary results obtained in this laboratory and those cited elsewhere^{2,24} support the validity of Figures 4 and 5. From experience obtained with other alkali metal chlorides, where q_+ remains positive for all values of q_m due to super-equivalent adsorption of chloride, one might tend to be somewhat surprised at negative values of q_+ in LiCl solutions more dilute than 0.1 m . At first sight these results seem to imply that a fundamental change in the conventional model of the double-layer structure is necessary and that the general applicability of the Gouy-Chapman theory is questionable. However, it is our contention that the results do not contravene published notions of the double-layer structure but they do offer further evidence of some ambiguities in the Gouy-Chapman theory.²⁵⁻²⁷

The commonly accepted structure of the double layer²⁶ consists of a compact region and a diffuse region, whose detailed natures depend on the chemical properties of the ions in solution, the potential on the metal, ϕ_m , and the potentials at the inner (IHP) and outer (OHP) Helmholtz planes, ϕ_1 and ϕ_2 , respectively. Certain ions (notably the halides) are thought to approach and make contact with the metal surface and thus reside in the inner double layer, while others (notably the alkali metal ions, with the possible exception of Cs^+) do not enter the inner layer. Figure 4 does indicate that Cl^- alone (*cf.* q_i) enters the inner layer and is present there even for values of $q_m < 0$. At the potentials studied Li^+ does not appear to populate the inner layer, *i.e.*, q_i is never greater than zero. The only difference in the LiCl behavior from the other

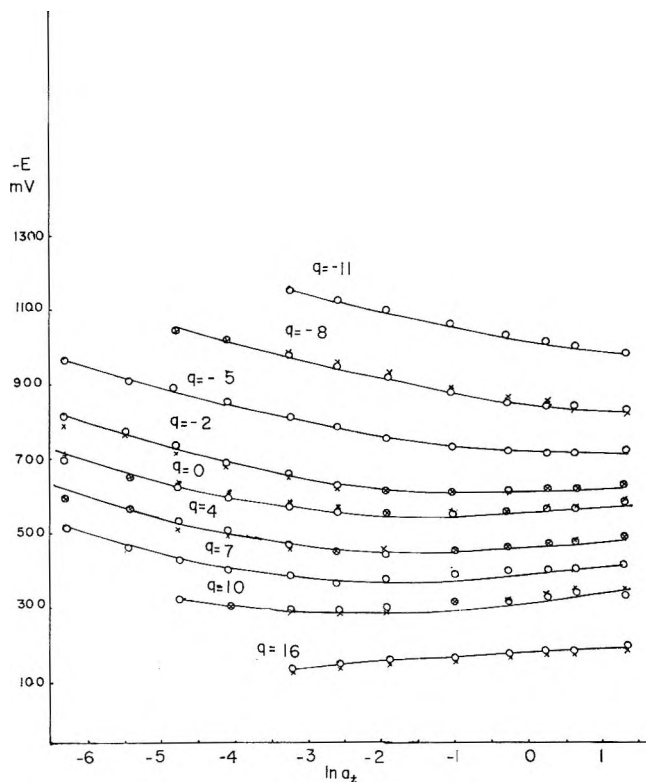


Figure 6. Concentration dependence ($\ln a_{\pm}$) of the applied potential at constant electrode charge (Esin and Markov plot) for LiCl at 25°C; \times represents potentials obtained by interpolating between q_m values obtained *via* Method A; O, those values obtained from Method B.

alkali halides is that in dilute solutions, the amount of Cl^- in the double layer does not reach super-equivalent proportions; *i.e.*, q_+ may be less than zero. The term super-equivalent used here describes ionic concentrations which are greater than those attainable solely by electrostatic considerations.

Whether this unusual behavior can be attributed to the specific adsorption of Li^+ ions or not depends on the choice of one's definition of specific adsorption. (All definitions discussed hereunder have been taken from ref 26, p 331 ff.) One definition is possible in terms of the structural model of Grahame: specific adsorption occurs when (i) ions can interact so strongly with the metal that they lose their solvation, at least in the direction toward the metal; (ii) penetrate into the inner layer; and (iii) become fixed to the metal with their electrical centers at the IHP. In this sense Figure 4 indicates that Cl^- is specifically adsorbed, but certainly not Li^+ ($q_i \leq 0$ for all q_m). Another definition termed "phenomenological" is best given in three parts: (a) if, for $q_m = 0$, the relative surface excess of any ionic species is positive; (b) if, for $q_m > 0$, the relative surface excess of any cation is positive; or (c) if, for $q_m < 0$, the

(27) R. Parsons in "Modern Aspects of Electrochemistry," Vol. I, J. O'M. Bockris, Ed., Butterworth and Co. Ltd., London, 1954, p 103 ff.

relative surface excess of any anion is positive (*i.e.*, $q_- = -F\Gamma_- < 0$), then there is specific adsorption. This kind of definition is more general and offers greater flexibility in assessing which ion is specifically adsorbed. For $2 > q_m > -2$, Figure 4 indicates that either Cl^- or Li^+ or both are specifically adsorbed. Finally, a "quasi-phenomenological" definition has been given. According to this, it is said there is specific adsorption, if the experimental data cannot be explained by the theory of the diffuse layer. Figure 5 shows that in this sense Li^+ is definitely specifically adsorbed, since q_+ is more negative than is theoretically possible according to the Gouy-Chapman theory, where

$$q_+ = A \left[\exp\left(\frac{-zF\phi_2}{2RT}\right) - 1 \right] \quad (6)$$

and²⁶

$$\lim_{\phi_2 \rightarrow +\infty} q_+ = -A \quad (7)$$

Although the last definition may appear less satisfying in view of the defects in double-layer theory,²⁶ it is in fact the most important. The pure model definition according to Grahame is nonoperational and therefore cannot provide an experimental criterion for specific adsorption in terms of a molecular model. The quasi-phenomenological definition does lead to interpretation based on models and is referred to by Mohilner²⁶ as the one most widely used in practice.

Parsons²⁷ has pointed out that a major weakness in the Gouy-Chapman theory is its dependence on a solution for the Poisson equation (eq 64, p 145, ref 27) based solely on the valency and not on the nature of the particular ions forming the double layer. In our opinion, it is the distinct chemical nature of the Li^+ ion which results in the apparently anomalous q_+ values reported here. Our most plausible suggestion is that Li^+ , a well-known structure maker,²⁸⁻³¹ influences the role of water in the double layer by preferential orientation of the water dipoles and bulk structural enhancement (*cf.* especially ref 31). Both considerations are important, because equilibrium measurements done in electrocapillary work require electrical neutrality in the double layer as well as thermodynamic equilibrium with respect to temperature, pressure, and electrochemical potential over the total system.

A given charge, q_m , (*e.g.*, greater than zero) may be balanced on the solution side of the interface by a local increase of negative ions, by a local shortage of positive ions and/or by a net effective charge due to the dipole of the solvent. Ions undoubtedly play an important role, but the solvent dipoles may be forced into an average attractive or repulsive configuration by an ion and as such contribute a significant part in determining the concentration of species in the double layer. In addition, the structure making or breaking characteristics of a particular ion may make it energetically more or

less favorable for the ion to remain in bulk solution configurations, relative to any possible double-layer configuration. This latter effect may manifest itself more obviously in dilute solutions, where relatively fewer ions are available to satisfy hydration equilibria. Possibly the structure making nature of Li^+ limits the number of positive ions entering the double layer and, consequently, the number of Cl^- as well. While this phenomenon would occur at all concentrations, it becomes pronounced only in solutions where the Cl^- concentration is less than superequivalent as is the case in dilute solutions. This behavior does not eliminate the entrance of Cl^- into the inner layer, but rather it limits the total number of Cl^- ions that are admitted. Hence a competitive equilibrium exists between the structural enhancement of the Li^+ ion with respect to water molecules and the specific interaction of Cl^- with the charged mercury surface. This explanation implicitly assumes that the electrocapillary equation

$$-d\gamma = qdE_- + \Gamma_+dT + \Gamma_+d\mu \quad (8)$$

holds for Grahame's model of the double layer and neglects any complications arising from the calculated cationic surface excesses (eq 4) which only have meaning relative to a plane where $\Gamma_{\text{H}_2\text{O}} = 0$,²⁶ *i.e.*

$$\Gamma_+(\text{measured}) = \Gamma_+(\text{real}) - \frac{X_{\text{Li}^+}}{X_{\text{H}_2\text{O}}} \Gamma_{\text{H}_2\text{O}} \quad (9)$$

The position of the plane where $\Gamma_{\text{H}_2\text{O}} = 0$ is not independent of solution concentration. By this argument the values of q_+ as depicted in Figure 5 cannot be interpreted in terms of a strict molecular model of the double layer. Hills and Payne⁶ inferred that the $\Gamma_{\text{H}_2\text{O}} = 0$ plane may change its position relative to the metal surface by their suggestion that water plays a more important role in the structure of the double layer than had hitherto been credited. In essence their contention regarding water is not in conflict with our emphasis on the special chemical role of lithium ions in influencing the double layer. There is some evidence^{2,32} that cations of different identity correspondingly affect the components of charge in the double layer. This is exemplified by the fact that positive surface excess (Γ_+) at constant charge decreases in the following order: $\text{CsCl} > \text{RbCl} > \text{KCl} > \text{NaCl} > \text{LiCl}$.² A clearer resolution and understanding of the special role of each of the alkali metal ions would be possible if experimental

(28) H. S. Frank in "Chemical Physics of Ionic Solutions," B. E. Conway and R. G. Barradas, Ed., John Wiley & Sons, New York, N. Y., 1966.

(29) O. Ya. Samoilov, *Discussions Faraday Soc.*, **24**, 141 (1957).

(30) O. Ya. Samoilov, "Structure of Aqueous Electrolyte Solutions," Consultants Bureau, Plenum Press, New York, N. Y., 1965.

(31) J. E. Desnoyers and C. Jolicoeur, in "Modern Aspects in Electrochemistry," Vol. 5, J. O'M. Bockris, Ed., Butterworth and Co. Ltd., London, 1968, p 1.

(32) M. A. V. Devanathan and B. V. K. S. R. A. Tilak, *Chem. Rev.* **65**, 635 (1965).

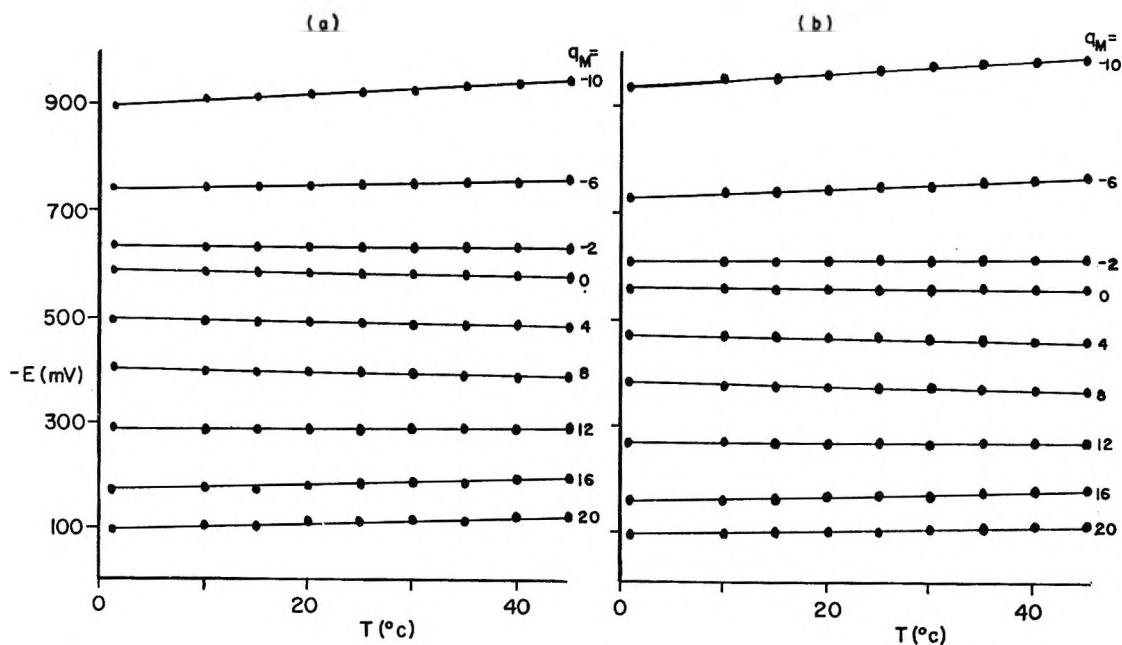


Figure 7. The temperature dependence of the applied electrode potential at constant electrode charge for (a) 3.19 *m* LiCl and (b) 1.02 *m* LiCl solutions.

results were available for the bromide, iodide, and fluoride salts of these cations.

(d) *Esin and Markov Effect.* Figure 6 demonstrates a generalized Esin and Markov plot²⁵ of E_- vs. $\ln a_{\pm}$ at constant charge for measurements made at 25°. Other Esin and Markov plots at different temperatures show the same characteristics. The importance of Figure 6 is that, while the curves are not exactly linear (as might be expected from similar plots for the potassium halide salts, *e.g.*, see Figure 4-2 in ref 25), their shapes are theoretically predictable.

One of the relationships (ref 25 p 28, and ref 26) obtained from the differential electrocapillary equation (eq 8) is

$$-(\partial E_- / \partial \mu)_{q, T, P} = \left(\frac{\partial q_+}{\partial q} \right)_{\mu, T, P} \quad (10)$$

where the left-hand side is the Esin and Markov coefficient (eq 5) and the right-hand side is the slope of curves like those presented in Figures 4 and 5. For our purposes, the mathematical implications of eq 10 are twofold. (a) If the q_+ vs. q_m curves have a minimum or maximum for a certain solution concentration, the Esin and Markov curve obtained for the value of q_m at which it occurs must exhibit a corresponding maximum or minimum. (b) If the extremum point in the q_+ vs. q_m curve occurs at different values of q_m depending on solution concentration, the Esin and Markov curves will exhibit an extremum at different values of $\ln a_{\pm}$ depending on what constant value of q_m is chosen. Figures 5 and 6 display this stated behavior for LiCl solutions.

There is ample evidence in the literature^{2,32} that there

is a minimum in the q_+ vs. q_m curves for most other halide solutions and that the value of q_m at which this minimum occurs is a function of solution concentration, moving to more cathodic charges with increased concentration. Consequently, we should expect an Esin and Markov plot similar to that shown in Figure 6 for most halides, although it should be realized that measurements (although experimentally difficult to obtain) in concentrations below 10^{-3} *m* may be necessary for this to be apparent. For example, Figure 4-2 in ref 25 exhibits almost strict linearity for KI, but not for KCl especially near $q_m = 0$. Unfortunately, plots for all values of q_m are not included in Figure 4-2 (ref 25).

One interpretation of the Esin and Markov behavior attributes a shift in the ecm potential toward increasingly negative potentials for predominant anion specific adsorption, and toward positive potentials for predominant cation adsorption. Further, when both anions and cations are strongly adsorbed, the sign of the shift of potential may be reversed as the concentration changes. This interpretation may be extended to all values of q_m ; however, its implication must be limited because the Esin and Markov coefficient reflects only what species determine the double-layer structure. Inspection of Figure 6 shows that the positions of the minima are also dependent on electrode charge and chemical potential. This complex behavior points again to the uniqueness of Li^+ in affecting the configuration of the double layer.

(e) *Entropies of Adsorption.* Although our discussion thus far has concentrated on the constant temperature behavior of LiCl, a large range of temperatures, as stated in the Experimental Section, has been systematically studied as well. Figures 7 and 8 illustrate the

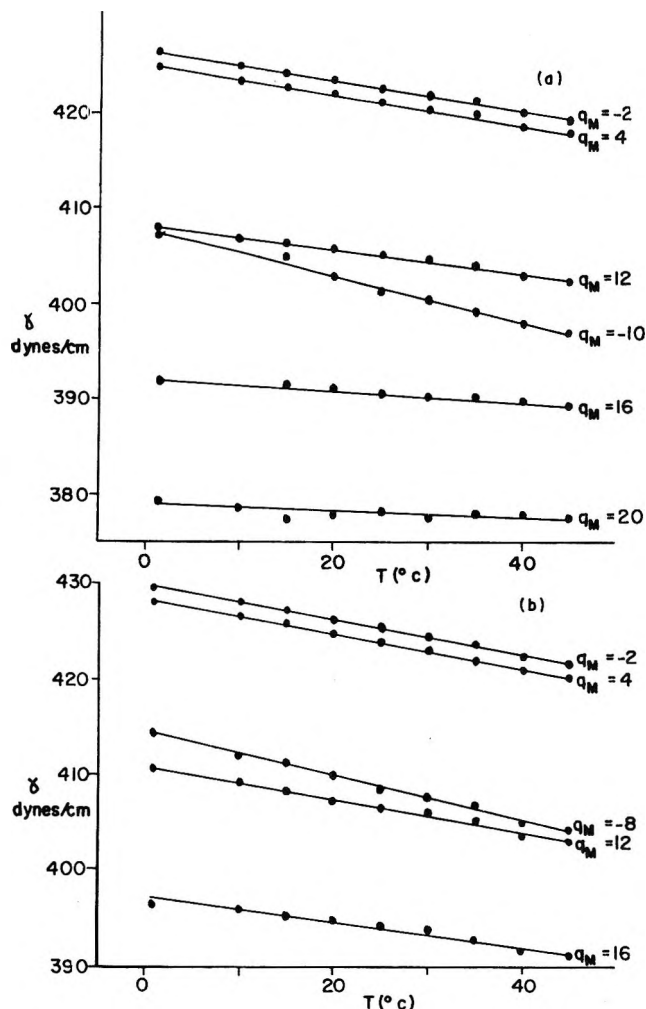
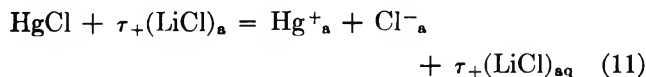


Figure 8. Temperature dependence of the interfacial tension at constant charge in LiCl solutions: (a) 2.08 m; (b) 0.20 m.

temperature dependence at constant q_m of the electrode potential and the surface tension, respectively. Of particular interest is the linearity of each curve at all values of q_m between -10 and $20 \mu\text{C}/\text{cm}^2$. While only two concentrations are shown, linear plots were observed in all other solutions studied. The slopes of these straight lines may be used to define entropies of adsorption.

$(\partial E^-/\partial T)_{q,\mu,P}$ has been interpreted by Grahame³³ and Randles and Whitely⁴ as an entropy of adsorption term (ΔS) for the reaction



where the symbol τ_+ is the transference number of the cation in the double layer and the subscript "a" represents the species in the "adsorbed" state. Figure 9 shows that this entropy is a function of both electrode charge and solution composition. The electrocapillary equation (eq 8), on the other hand, allows the evaluation of a surface excess entropy of adsorption,²⁶ Γ_s , from the

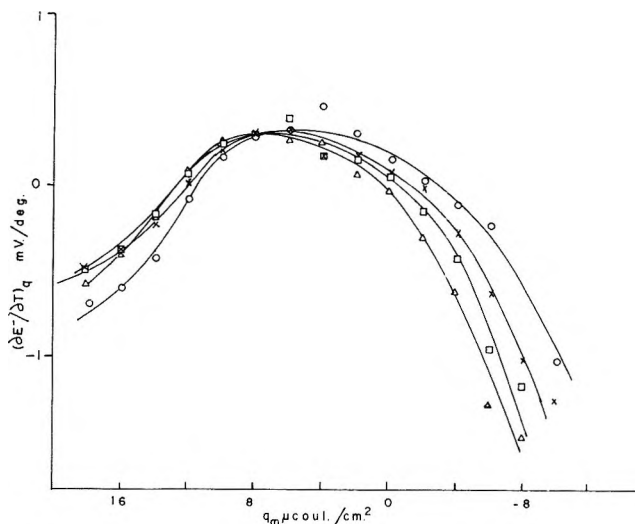


Figure 9. The charge dependence of the temperature coefficient of the applied electrode potential $(\partial E^-/\partial T)_q$ for LiCl solutions: O, 3.19 m; X, 2.08 m; □, 1.02 m; and Δ, 0.20 m.

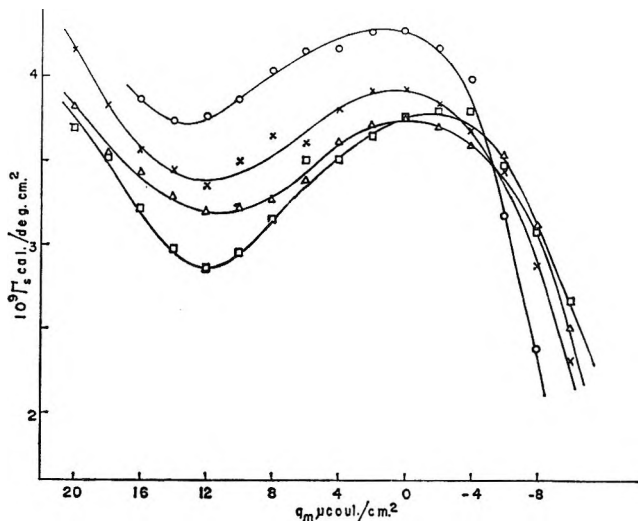


Figure 10. Surface excess entropy as a function of charge for LiCl solutions: O, 0.10 m; X, 0.51 m; Δ, 1.55 m; and □, 3.19 m.

coefficient $(\partial \gamma/\partial T)_{E,P,\mu}$, which may be contrasted with ΔS through the usage of Parsons' auxiliary function

$$\xi_+ = \gamma + q_m E_- \quad (12)$$

to define the equivalent (eq 52b in ref 26) excess entropy at constant charge

$$-(\partial \xi_+/\partial T)_{q,P,\mu} = \Gamma_s \quad (13)$$

Figure 10 illustrates that this too is a function of surface charge and solution concentration.

Unfortunately, the interpretation of these entropy terms, as well as other thermodynamic properties of adsorption not presented here, e.g., free energies and

(33) D. C. Grahame, *J. Chem. Phys.*, **16**, 1117 (1948).

heats of adsorption, are very complex.³⁴ Consequently, we will only point out that Figures 9 and 10 have the same shape as comparable plots for 0.1 *m* NaCl presented by Hills and Payne (Figures 6 and 10 in ref 6), but that the Grahame entropy values ($\partial E/\partial T$) are smaller for LiCl than for NaCl, while the Γ_s values are much larger. ΔS^{32} is not surprisingly smaller for LiCl than for NaCl aqueous solutions because Li^+ is a stronger structure maker than Na^+ .³¹ This is inherent in the way through which ΔS has been defined. By eq 11 we may infer that Li^+ ions are transported from a more strongly hydrated and restricted state than Na^+ to another restricted adsorbed state at the mercury-solution interface. We are inclined to prefer Γ_s as a better parameter for representing the entropy of adsorption not only because it can be calculated directly from interfacial data as shown in eq 13, but also because Γ_s includes in an intrinsic way the charging of the double layer.⁶ The reverse trend in Γ_s for LiCl and NaCl indicates that the overall double-layer environment

(particularly the effect of charging the double layers) is more restrictive in lithium chloride solution. These observations are perhaps not inconsistent with the complex Esin and Markov effect and the apparently unusual q_+ results for dilute solutions presented earlier in this paper. Further investigations with other lithium halide salts are in progress³⁵ which may eventually help to further clarify the unique chemical nature of Li^+ ions in the electrical double layer.

Acknowledgments. E. W. H. is indebted to Carleton University for the award of an Open Fellowship. Financial support by the National Research Council of Canada is gratefully acknowledged. We are also indebted to Professor M. C. Giordano for helpful experimental assistance and valuable discussions.

(34) R. Parsons, *Can. J. Chem.*, **37**, 308 (1959).

(35) E. W. Hermann, M. C. Giordano, and R. G. Barradas, unpublished results.

Structured Liquids near Platinum Electrodes¹

by Peter C. Owzarski² and W. E. Ranz

Department of Chemical Engineering, University of Minnesota, Minneapolis, Minnesota 55455
(Received February 21, 1969)

A voltage-step method was used to measure the diffusion coefficient of I_2 near platinum microelectrodes in primary normal aliphatic alcohols containing 0.5 *N* LiCl. Diffusivities observed were lower than bulk-phase liquid diffusivities. This indicates the presence of liquid structures different from bulk phase liquid. Irregular transients obtained in the solvents 1-hexanol, 1-heptanol, and 1-octanol could be described by an analytical solution of the diffusion equation using first-order electrode kinetics and a spacial step change in diffusivity at a distance δ from the electrode. Diffusivity ratios, $D(\text{bulk})/D(\delta \text{ region})$, were 80 in 1-heptanol, 15 in 1-hexanol, and 2 in 1-octanol. Corresponding step-function thicknesses were 200, 400, and 4000 Å, respectively, at 25°. Regular transients observed in solvents methanol through 1-pentanol gave apparent diffusivities close to predicted bulk liquid values. However, first-order rate constants for the latter were attenuated as solvent molecular weight increased. This may be attributed to a rigid region whose penetration time is less than the double-layer charging times. Estimates of such a δ for solvents methanol through 1-pentanol agree with the trend established from anomalous transients in 1-hexanol, 1-heptanol, and 1-octanol. These results indicate that multi-layer solvent orientation increases as the aliphatic chain length increases, but the diffusivities near the surface are less different from the bulk-phase diffusivities for larger chain lengths.

Introduction

The significance of the third dimension in liquids near phase interfaces is being realized.³⁻⁶ That liquids may have structures and hence properties different from bulk phase in the interfacial region has significance in many chemical and biological processes. In this work an experimental technique is described for detecting the extent and diffusivity of the "structured" region in polar

liquid electrolyte solutions. A transient diffusional electrolytic process, the voltage step, is analyzed with an

(1) This research was supported by N.D.E.A., N.A.S.A., and Fridley Foundation fellowships.

(2) Battelle Memorial Institute, Pacific Northwest Laboratory, Richland, Wash. 99352.

(3) J. C. Henniker, *Rev. Mod. Phys.*, **21**, 322 (1949).

(4) B. V. Deryagin, Ed., "Research in Surface Forces," Vol. 1, Consultants Bureau, New York, N. Y., 1963.

analytical solution to continuum diffusion equations for a spacial step change in diffusivity in the liquid near the interface. From this, an effective thickness, δ , and diffusivity of the structured region can be calculated.

Iodine reduction at platinum microelectrodes after a voltage step in anhydrous primary normal alcohols, methanol through 1-octanol, 0.5 *N* LiCl, was carried out at 25°. For large voltage steps, -0.07 to -0.5 V, and low iodine concentration, 0.005-0.02 *M*, relaxation curves were analyzed. A positive time shift in relaxation due to double-layer charging was quantitatively analyzed and corrected.

Results are tabulated in terms of "structured" liquid zone thicknesses and diffusivities estimated from irregular relaxation curves and from kinetic rate constants that were attenuated as solvent molecular weight increased.

Theory and Models

For a simple first-order electrode reaction, $O + ne^- \rightleftharpoons R$, involving electron exchange without phase change, adsorption, or other complications, the net faradaic current can be written

$$\frac{i_F}{nFA} = k_O c_O - k_R c_R \quad (1)$$

The first-order rate constant (cm/sec) is basically an exponential function of faradaic overpotential η .

$$k_i = k_i^\circ \exp(-\alpha n' F \eta / RT) \quad (2)$$

where

$$\eta = \Delta V + i_T R_T \quad (3)$$

for a voltage step ΔV and circuit voltage drop $i_T R_T$.⁷ Usually $|\eta| < 2-5$ mV, so the exponent can be expanded and only linear i_F terms kept. With this approximation, the diffusion equation can be solved analytically.

It is now proposed that an analytical solution for $k_O \ll k_R$ or $k_O \gg k_R$, that is for large η (\pm), is applicable for times of relaxation greater than the characteristic double-layer charging time, τ . The total cell current is a sum of double-layer and faradaic currents $i_T = i_F + i_{DL}$ where

$$i_{DL} = \frac{\Delta V}{R_T} \exp(-t/\tau) \quad (4)$$

when $\Delta V/R_T \gg i_F$ (max). Then after a large cathodic step

$$\frac{i_F}{nFA} = k_O c_O^B \exp\left(\frac{k_O t'}{D_O}\right) \operatorname{erfc}\left(\frac{k_O t'^{1/2}}{D_O^{1/2}}\right) \quad (5)$$

$$k_O = k_O^\circ \exp(-\alpha n' \bar{\eta} F / RT) \quad (6)$$

$$t' = t - \tau \quad (7)$$

$$\bar{\eta}(\tau < t' < \bar{l}) = \Delta V + R_T \frac{i_F(\text{max}) + i_F(\bar{l})}{2} \quad (8)$$

when $t' = t - \tau > 5\tau$ and ΔV is an order of magnitude larger than $R_T i_F$.

Equation 5 is a solution to (with no field gradient)

$$\frac{\partial c_O}{\partial t} = D_O \frac{\partial^2 c_O}{\partial x^2} \quad (9)$$

for initial and boundary conditions

$$c_O = c_O^B \text{ at } t' = 0, c_O \rightarrow c_O^B \text{ as } x \rightarrow \infty$$

$$c_R^B = 0$$

$$k_O c_O = D_O \frac{\partial c_O}{\partial x} \gg k_R c_R \text{ at } x = 0$$

The time shift is apparent in a finite difference solution of eq 9 where the latter boundary condition becomes ($i_F R_T \ll \Delta V$)

$$D_O \frac{\partial c_O}{\partial x} = c_O k_O^\circ \exp\left\{\frac{-\alpha n' F}{RT} \times [\Delta V(1 - \exp - t/\tau) + i_F R_T]\right\} \quad (10)$$

Figure 1 shows c_O/c_O^B vs. t at $x = 0$ for various τ (cf. along the broken line) with $k_O^2/D = 3.3 \times 10^4 \text{ sec}^{-1}$.

The positive shift in time is nearly exactly τ , and the concentration profiles of $c_O = c_O(x, t')$ agree within 0.1% deviation. Therefore, this is an improvement over an earlier empirical correction for double-layer charging.⁸

As indicated in eq 8, the influence of a variable $i_F R_T$ can be averaged with an estimated per cent confidence in kinetic and diffusion parameters. This is done by error plotting $\log k$ vs. $\bar{\eta}$.

To get D_O , a preferred method is to obtain the derivative $\partial i_F / \partial t$ at some time, t' , and apply the method of Oldham and Osteryoung.⁹ This method employs a dimensionless plot of $(\partial i_F / \partial t') t' / i_F$ vs. $kt'^{1/2} / D_O$. With a plot of $i_F / i_F(t' = 0) = \operatorname{erfc}(kt'^{1/2} / D_O^{1/2}) \exp(k^2 t' / D_O)$, k and D_O are obtained knowing that $k = i_F(t' = 0) / nF c_O^B$ where $\tau = C_{DL} R_T A$, $R_T = \rho / 2\pi a + R_e$ and where a , A , and ρ are electrode radius, area, and electrolyte resistivity, respectively, and R_e is other circuit resistance.

Detection of Unusual Diffusivities. Liquid surface structures manifested as diffusivities different from bulk diffusivities are detectable in a transient response to a voltage step if the diffusion penetration time is greater than the double-layer charging time. Such transients are not described by eq 5.

(5) B. V. Deryagin, Ed., "Research in Surface Forces," Vol. 2, Consultants Bureau, New York, N. Y., 1966.

(6) K. J. Mysels, Abstracts, 154th National Meeting of the American Chemical Society, Chicago, Ill., Sept 1967.

(7) J. P. Elder, "Electrode Kinetics," Argonne National Laboratory Bulletin ANL-7072, 1965.

(8) H. A. Laitinen, R. P. Tischer, and D. K. Roe, *J. Electrochem. Soc.*, **107**, 546 (1960).

(9) K. B. Oldham and R. A. Osteryoung, *J. Electroanal. Chem.*, **11**, 397 (1966).

To explain possible anomalous transients, the diffusion equation was solved for a spacial step change in diffusivity at some distance δ from the electrode surface. In a semiinfinite medium in the absence of a field gradient

$$\frac{\partial c_1}{\partial t} = D_1 \frac{\partial^2 c_1}{\partial x^2} \quad (0 \leq x < \delta) \quad (11a)$$

$$\frac{\partial c_2}{\partial t} = D_2 \frac{\partial^2 c_2}{\partial x^2} \quad (\delta < x < \infty) \quad (11b)$$

with the boundary conditions

$$D_1 \frac{\partial c_1}{\partial x} = kc_1 \quad (\text{at } x = 0)$$

$$c_1 = c_2$$

$$D_1 \frac{\partial c_1}{\partial x} = D_2 \frac{\partial c_2}{\partial x} \quad \text{at } x = \delta$$

$$c_2 \rightarrow c^B \quad (\text{as } x \rightarrow \infty)$$

and initial condition

$$c_1 = c_2 = c^B \quad (\text{at } t = 0 \text{ (all } x))$$

The solution of the above for dimensionless flux at $x = 0$, $c_1/c^B = c^*$, is composed of two parts: one converges rapidly for small values (eq 12) of the dimensionless time $t^* = k^2t/D_1$, and one converges for large values (eq 13).¹⁰

$$c^* = \sum_{n=0}^{\infty} (-1)^n \left[\frac{2kt^{1/2}}{D_1^{1/2}} \right]^n \sum_{r=0}^n \frac{n!}{r!(n-r)!} \sum_{p=0}^{\infty} \times \frac{(n+p-1)!}{(n-1)!p!} \gamma^{p+r} i^n \operatorname{erfc} \left(\frac{(p+r)\delta}{(D_1 t)^{1/2}} \right) \quad (12)$$

$$c^* = \operatorname{erfc} (kt^{1/2}/D_1^{1/2}) \exp(k^2t/D_1) + \sum_{n=0}^{\infty} (-1)^n \times \left(\frac{D_1^{1/2}}{2kt^{1/2}} \right)^{n+1} \frac{2}{\sqrt{\pi}} \sum_{r=0}^{n+1} \frac{(n+1)!}{r!(n-r+1)!} \sum_{p=0}^{\infty} \times \frac{(n+p)!}{n!p!} (-\gamma)^{p+r} \exp[-(p+r)^2\delta^2/D_1 t] \times H_n[(p+r)\delta D_1^{1/2}t^{1/2}] \quad (13)$$

Figure 2 is a parametric plot of c^* vs. $t^{*1/2}$ for $D_1 < D_2$. Of importance in the c^* vs. $t^{*1/2}$ plots is that the primary first derivative inflection point occurs at $D_1 t/\delta^2 = 1$ for both $D_1 < D_2$ and $D_1 > D_2$. This fact provides the needed clue for parameter estimates. When known dimensionless parameters $c^* = i_F(t)/nFAKc^B$ and $kt^{1/2}/D_2^{1/2}$ at this inflection are plotted with unknown D_1/D_2 as parameters, inflection point data give immediately D_1/D_2 and $\delta = \sqrt{D_1 t}$. This was the analysis scheme used to analyze anomalous transients. Figure 3 is a working plot of c^* vs. $kt^{1/2}/D_2^{1/2}$ at $D_1 t^{1/2}/\delta = 1.0$.

When $\tau > \delta^2/D_1$, a structured zone will not be evident in the transient response, but identical resistance to

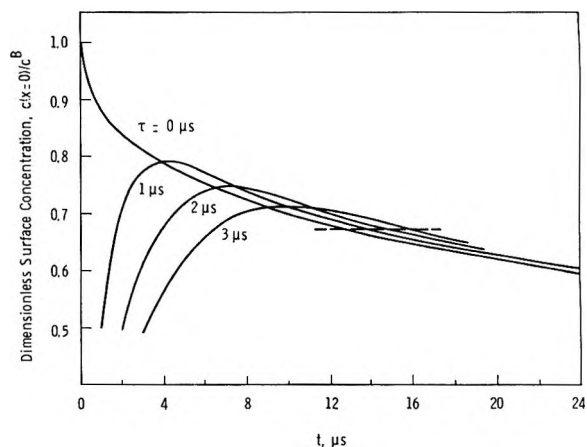


Figure 1. Effect of double-layer rise time (τ) on faradaic current or electrode surface concentration.

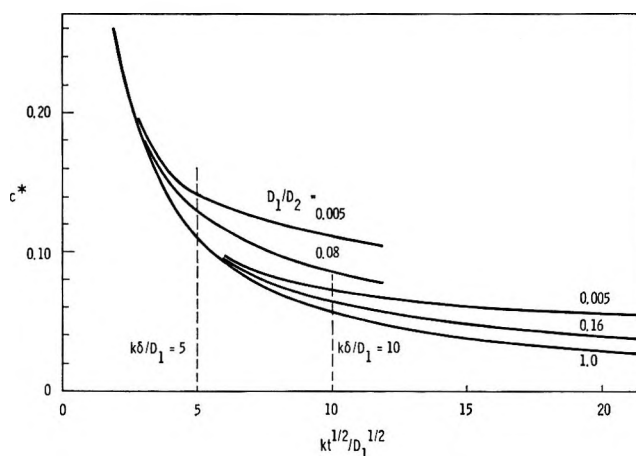


Figure 2. Dimensionless flux or surface concentration, c^* , vs. large $t^{*1/2}$ from eq 13. Vertical broken lines are at $D_1 t/\delta^2 = 1.0$.

mass transport may appear in the apparent first-order rate constant. This constant k' would be

$$k' = k(1 + k\delta/D_2) \quad (\text{for } D_1 \gg D_2) \quad (14)$$

and

$$k' = k/(1 + k\delta/D_2) \quad (\text{for } D_1 \ll D_2) \quad (15)$$

In the latter case, the rate constant will be attenuated by the presence of a more viscous than bulk liquid region near the electrode and the plot of $\log k'$ vs. $-\bar{\eta}$ would not be linear for a cathodic voltage step. Instead

$$\frac{d \ln k'}{d(-\bar{\eta})} \rightarrow 0 \quad (\text{as } -\bar{\eta} \rightarrow \infty)$$

This comprises an argument used to explain some of the experimental results.

(10) P. C. Owzarski, Ph.D. Thesis, University of Minnesota, Minneapolis, Minn., 1967.

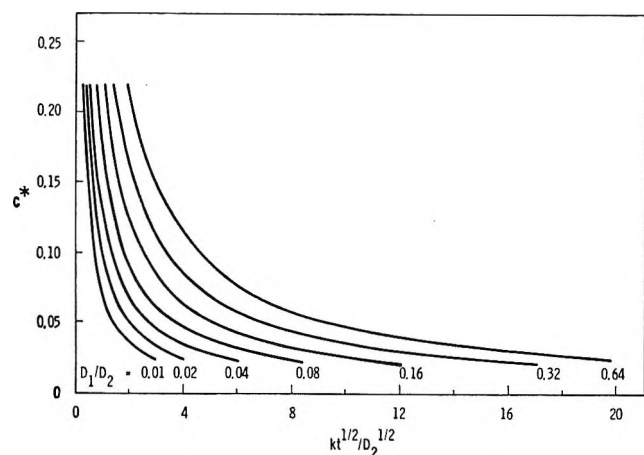


Figure 3. Surface concentration vs. $(t^* D_1/D_2)^{1/2}$ from step-function model analysis with D_1/D_2 as a parameter at $D_1 t/\delta^2 = 1.0$.

Experimental Section

Cells and Electrodes. Two cells made up the working system. Both cells had a pair of platinum electrodes where the anode was 10^6 larger in area than the microelectrode where I_2 reduction occurred. Cell A contained only 0.5 N LiCl and cell B contained 0.005 or 0.01 M I_2 as well as 0.5 N LiCl. When they were pulsed in parallel, the double-layer current from A could be electronically subtracted from B.

Microelectrodes were prepared by setting 0.5-mil Pt wires in soft glass and preparing the final polished surface on the wire cross section ($1.27 \times 10^{-6} \text{ cm}^2$) with 0.05- μ alumina-water on a microcloth wheel followed by rinsing with AR methanol. Electrodes were then carefully inspected with a $500\times$ metallurgical microscope.

Cell containers were 250-ml glass Berzelius beakers. A Teflon stopper held the N_2 tube inlet, thermometer, and coaxial BNC connectors attached to the electrodes. Both cell and thermometer were surrounded with a grounded shield. Both cells were contained in a box whose atmosphere was maintained at the desired temperature to $\pm 0.1^\circ$.

Circuit and Instruments. The voltage-step circuit was a low resistance (relative to the cells) voltage divider. A ΔV having a rise time less than $0.2 \mu\text{sec}$ was obtained by closing a Potter and Brumfield JML 1260 81 mercury-wetted contact relay. Current was measured as voltage drop across a precision resistor in series with the cells.

To prevent distortion of faradaic transient responses, oscilloscope input probes of 10 megohm input resistance and 11-pF input capacitance were used. This would distort double-layer charging traces somewhat, but not faradaic responses which had much larger time constants. Double-layer parameters were obtained separately on 10-mil diameter electrodes.

Chemicals. The following were used without further purification: LiCl, anhydrous (Mallinckrodt AR); I_2

(Merck Reagent); methanol, anhydrous (Mallinckrodt 3016 AR); absolute ethanol (bp 78.5°); 1-propanol, anhydrous (Baker No. 414 AR); 1-butanol (Eastman No. 50 Reagent); 1-pentanol (Eastman No. 568); 1-hexanol (Eastman No. P825 Practical); 1-heptanol (Eastman No. 381 Reagent); and 1-octanol (Eastman No. 871, Reagent). Iodine-alcohol solutions were prepared and used within 24 hr since the solutions slowly deteriorated when exposed to light.

Procedure. A 50-ml aliquot was placed in each cell, the electrodes were immersed, the temperature was adjusted, and about 2 l. of N_2 was slowly bubbled through the cells for about 30 min (less N_2 for the more volatile alcohols). Data were taken from 2 to 6 hr after electrode immersion. Data from longer times differed from data from the 2-6-hr period. Double-layer charging data (Cell A), as well as the faradaic relaxation traces, were recorded photographically using a Tektronix 551 oscilloscope.

Results

To use an analytical solution of the diffusion equation, it was necessary to find a range of I_2 concentrations and voltage steps that would give apparent first-order kinetics for I_2 reduction. Large voltage steps -0.07 to -0.5 V and concentrations of 0.005-0.01 M I_2 in 0.5 N LiCl gave the desired result. At 0.5-mil electrodes the faradaic current was low such that $i_F R_T < 0.1 \Delta V$. This enabled eq 5-8 to govern relaxation curves in the one to five carbon alcohols. For iodine reduction in this range $n = 2/3$ which means the apparent overall reaction at the surface was $3I_2 + 2e^- \rightarrow 2I_3^-$ where the reaction $I_2 + I^- \rightarrow I_3^-$ was very rapid and not rate controlling. For times greater than $0.05 D/(2a)^2$, the influence of the radial dimension (electrode edge) became important. This is shown in the regular responses plotted in Figures 4 and 5. The dotted line represents equation 5.

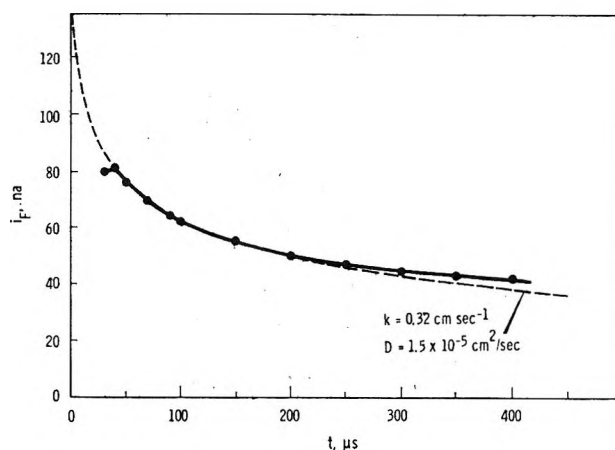


Figure 4. Voltage-step faradaic relaxation curve at a 0.5-mil Pt circle in half space; 0.5 N LiCl and 0.005 M I_2 in methanol at 25.0° ; $R_T = 69.3 \text{ k}\Omega$, $C_{DL} = 9.5 \mu\text{F}/\text{cm}^2$, $\tau = 0.2 \mu\text{sec}$, and $\bar{\eta} = -0.261 \pm 0.002 \text{ V}$. Dotted line is eq 5.

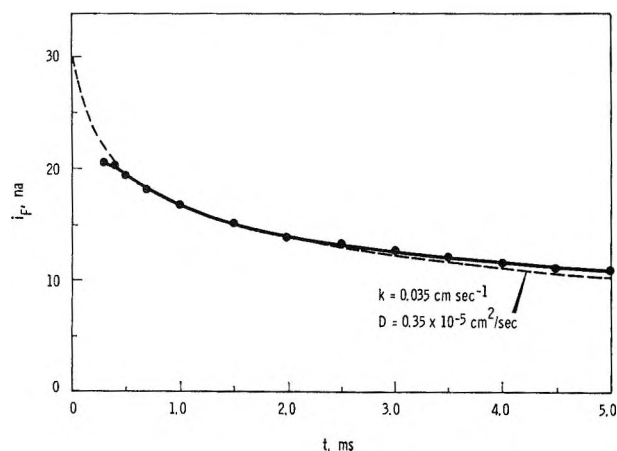


Figure 5. Voltage-step faradaic relaxation curve at a 0.5-mil Pt circle in half space; 0.48 *N* LiCl and 0.01 *M* I₂ in 1-pentanol at 25.0°; *R*_T = 1.27 MΩ, *C*_{DL} = 14 μF/cm², τ = 17 μsec, and $\bar{\eta} = -0.43 \pm 0.01$ V. Dotted line in eq 5.

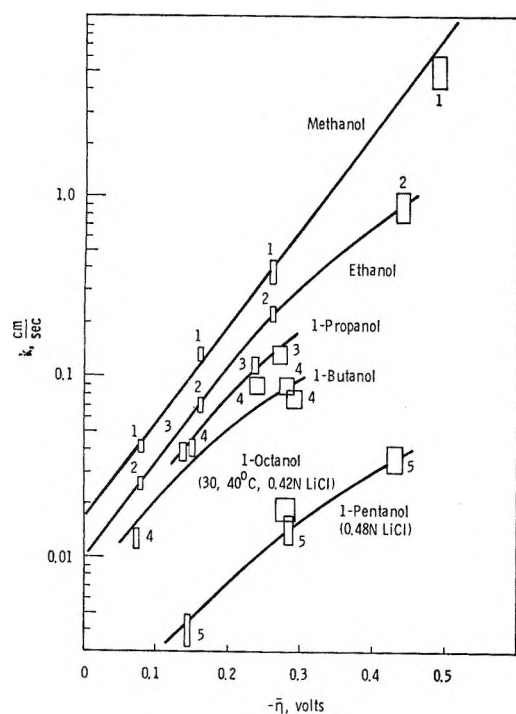


Figure 6. First-order rate constants vs. charge-transfer overpotential for I₂ (0.005–0.02 *M*) reduction at 25.0°, 0.5 *N* LiCl in indicated solvents.

Double-layer capacity and cell resistance were calculated to determine corrections for time displacements ($R_T C_{DL} A$) and estimates of $\bar{\eta}$. Double-layer capacity as calculated from eq 4 was usually about 10 μF/cm².

First-order rate constants are plotted in Figure 6 vs. charge-transfer overpotential. Confidence limits are represented by the size of the rectangle for each datum. This reflects absolute errors in current measurements which were $\pm 5\%$ of full scale of the oscilloscope. Little error was generated by calculation techniques, so bulk phase diffusivities and rate constants should have about

a 90% confidence level. The slope of the linear regions for both ethanol and methanol is

$$\Delta \ln k / (-\Delta F \bar{\eta} / RT) = 0.315$$

Slopes decrease rapidly at large $-\bar{\eta}$ for the higher molecular weight alcohols.

Diffusivities calculated from the transient responses are compared with literature values calculated with Wilke's equation (eq 16) using measured viscosities in Table I.¹¹ Measured values agree with predicted values when the actual 0.5 *N* LiCl solution viscosity (μ_B) is used (cf. in Table I).

$$D_{AB} = 7.4 \times 10^{-8} \frac{(\psi_B M_B)^{1/2} T}{\mu_B \bar{V}_A^{0.6}} \quad (16)$$

Here ψ_B is an association parameter and \bar{V}_A is the molar volume (cm³/mole) of *A* as liquid at its normal boiling point.

Irregular Transients. Faradaic currents in 1-hexanol, 1-heptanol, and 1-octanol did not follow the regular transient response (cf. Figure 7). However, their responses behaved as though the diffusion wave \sqrt{Dt} , as it moved away from the electrode, passed from a region of low to high diffusivity. Rapid current attenuation followed by a plateau is characteristic of this response. The mathematical model of eq 13 was applied to these cases.

The following parameters were calculated from inflection points in $di_F/d(t^{1/2})$ curves (e.g., Figure 7 for 1-heptanol). They appear to be independent of applied potential. They are also nearly independent of the rate constant *k* due to the near hyperbolic shape of contours of Figure 3 used in the calculations.

1-Hexanol. *t'* (at inflection) = 137 μsec, 25.0°

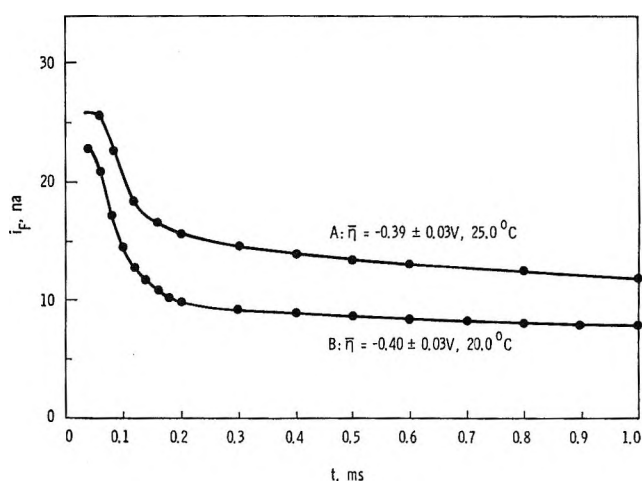


Figure 7. Voltage-step faradaic relaxation curve at a 0.5-mil Pt circle in half space; 0.42 *N* LiCl and 0.01 *M* I₂ in 1-heptanol. *R*_T = 3.3 MΩ, *C*_{DL} = 7.5 μF/cm², and τ = 32 μsec.

(11) C. R. Wilke and P. Chang, *A.I.Ch.E. J.*, 1, 264 (1955).

Table I: Bulk-Phase Transport Coefficients

Solvent, T°C	Electrolyte ^a	Viscosity, μ (CP) or μ_0	μ/μ_0^b	$D_{I_1}^c$	$D_{I_2}^d$	$D_{I_2}^e$	ψ_B
Methanol, 25°		0.547 ^a		1.95 ^o	2.42 ^o		1.9
	0.500 N LiCl	0.7678	1.404		1.72-1.39	1.0-1.5	
Ethanol, 25°		1.096 ^a		1.316	1.32		1.5
	0.500 N LiCl	1.7497	1.596		0.83	0.75	
1-Propanol, 25°		1.95 ^a			0.80		1.4'
	0.500 N LiCl	3.410	1.75		0.46	0.38	
1-Butanol, 25°		2.60 ^a			0.64		1.3'
	0.500 N LiCl	4.62	1.78		0.36	0.35	
1-Pentanol, 25°		3.50 ^a			0.50		1.2'
	0.480 N LiCl	6.76	1.93		0.26	0.35	
1-Hexanol, 25°		4.37 ^a			0.41		1.1'
	0.525 N LiCl	9.763	2.23		0.185		
1-Heptanol, 25°		5.68 ^a			0.33		1.0'
	0.420 N LiCl	10.92	1.925		0.17		
20°	0.420 N LiCl	13.13	1.873		0.14	0.10	
1-Octanol, 25°		7.21 ^a			0.27		1.0'
	0.420 N LiCl	15.2	2.106		0.13		
30°	0.420 N LiCl					0.10	
40°	0.420 N LiCl					0.18	

^a Values or interpolations from "Handbook of Chemistry and Physics," 39th ed, Chemical Rubber Publishing Co., Cleveland, Ohio, 1957, and "International Critical Tables." ^b Measured in Ostwald; pipet μ_0 is the pure solvent viscosity. ^c "International Critical Tables" and C. R. Wilke and P. Chang, *A.I.Ch.E. J.*, 1, 264 (1955). ^d Calculated with Wilke's formula (eq 16). ^e Experimental values from voltage step. ^f Estimates from methanol to ethanol trend. ^o Diffusivities are 10^6 cm²/sec.

(0.525 N LiCl); $D_2 = 0.185 \times 10^{-5}$ cm²/sec; $D_2/D_1 = 80$, $D_1 = 0.23 \times 10^{-7}$ cm²/sec; $\delta = D_1 t' = 180$ Å.

1-Heptanol. t' (at inflection) = 120 μ sec, 25° (0.42 N LiCl); $D_2 = 0.167 \times 10^{-5}$; $D_2/D_1 = 15$; $D_1 = 0.109 \times 10^{-5}$; $\delta = 360$ Å. $t' = 170$ μ sec, 20° (0.42 N LiCl); $D_2 = 0.136 \times 10^{-5}$; $D_2/D_1 = 25$; $D_1 = 0.0544 \times 10^{-5}$; $\delta = 310$ Å.

1-Octanol. $t' = 320$ μ sec, 25.0° (0.42 N LiCl); $D_2 = 0.128 \times 10^{-5}$; $D_1/D_2 = 0.466$; $D_1 = 0.6 \times 10^{-5}$; $\delta = 4000$ Å.

Two other experimental observations are worth noting. First, raising the 1-octanol solution to 30 and 40° eliminated any apparent transient anomaly. Second, a 0.105 N LiCl in 1-hexanol solution had too high a resistance to obtain the complete transient for small t' , but nearly the same current level at large t as in 0.525 N LiCl indicated that the rigid region still existed.

For ethanol to 1-pentanol the rate constants were used to obtain an estimate of variations in rigid surface zone thickness by assuming a diffusivity, D_1 , and δ (methanol) = 0 so that $k(\bar{\eta})$ for methanol is the true electron exchange parameter. Using eq 14 and $\bar{\eta} = 0.28$ V, Table II was constructed and compared with results for 1-hexanol to 1-octanol. This table suggests a pattern of increasing surface zone thickness for the one to five carbon alcohols which matches results for the six to eight carbon alcohols.

The above argument is limited by lack of knowledge of the true standard potential between solvents. However, a small horizontal shift in the $\ln k$ vs. $\bar{\eta}$ curves (Figure 6) would not likely invalidate the trend dis-

Table II: "Structured" Zone Thickness δ , Å

Solvent, T°C	If $D_1 = 1 \times 10^{-8}$ cm ² /sec	If $D_1 = 2 \times 10^{-8}$	If $D_1 = 10 \times 10^{-8}$
0.5 N LiCl, ethanol, 25.0°	2	4	20
0.5 N LiCl, 1-propanol, 25.0°	5	10	50
0.5 N LiCl, 1-butanol, 25.0°	20	40	200
0.48 N LiCl, 1-pentanol, 25.0°	60	120	600
0.42 N LiCl, 1-octanol, 30 and 40°	50	100	500
Compared with			
0.52 N LiCl, 1-hexanol, 25°	$\delta = 180$	$D_1 = 2 \times 10^{-8}$	cm ² sec ⁻¹
0.42 N LiCl, 1-heptanol, 20°	$\delta = 310$	$D_1 = 5 \times 10^{-8}$	
0.42 N LiCl, 1-heptanol, 25°	$\delta = 360$	$D_1 = 10 \times 10^{-8}$	
0.42 N LiCl, 1-octanol, 25°	$\delta = 4000$	$D_1 = 60 \times 10^{-8}$	

covered here. The two 1-octanol data points that appear between the C₄ and C₅ curves substantiate this.

Iodine adsorption was detected after 6 hr of electrode immersion. These data did not fit the models discussed. The 2-6-hr results for the one to five carbon alcohols fit the homogeneous diffusion coefficient model as well as 1-octanol at high temperatures. This seems to indicate that adsorption problems were minimized by

keeping to a rigid experimental time schedule. Since the faradaic current was an order of magnitude less than the peak double-layer current, little influence of triiodide ion on the double layer was suspected during a transient response. This might not have been true after 6 hr, and then the parallel cells could not be used.

Discussion

It has been demonstrated that the voltage-step method can be used for large voltage steps. Kinetic and diffusion parameters can be obtained if the particular couple at the microelectrode has a faradaic current an order of magnitude less than the maximum double-layer current. Here the positive time shift in faradaic relaxation is equal to the characteristic double-layer charging time.

An analytical solution to the diffusion equation has been used to describe unusual relaxation curves in terms of a spacial step change in the diffusion coefficient of the electrode reactant. This model indicates the existence of low diffusivities of I_2 near platinum microelectrodes. Several trends in surface anomalies are apparent in the primary normal aliphatic alcohols. These trends are the following. (1) At the same temperature there is an increase in depth of a "structured" zone of solvent molecules as the aliphatic chain length of the solvent is increased. (2) The diffusion coefficient in the structured regions increases as chain length increases. This may be due to the greater flexibility of the longer chains which give a less rigid, less-ordered structure. As a result, the net interfacial resistance to mass transfer may be less in a longer chain solvent even if the structured zone is more extensive. (3) Lowering the temperature markedly increases interfacial resistance to mass transfer.

The nature of forces causing the rigid region near the electrode is not certain. The classical Debye radius at 25° of systems studied here ranges from 6 Å in 0.5 *N* LiCl-methanol to 80 Å in 0.42 *N* LiCl-1-octanol. This may preclude electrostatic forces such as those that cause the double layer. However, there is recent evidence that attractive van der Waals forces exist at interfaces and that the range of attraction often exceeds 100 Å.⁶

Appendix. Notation

A	Electrode area
a	Electrode radius
C	Capacitance
C_{DL}	Double-layer capacity, $\mu\text{F}/\text{cm}^2$
c	Concentration
c^*	Dimensionless concentration
c^B	Bulk-phase concentration
c_i	Concentration of component i
D	Two component—Fick's law with concentration gradient diffusivity
D_1	Two-component diffusivity in "structured" region near electrode boundary
D_2	Two-component diffusivity in bulk phase
E	Electrode potential vs. a standard electrode
e^-	Electron
F	Faraday's constant
H_n	n th Hermite polynomial
$i^n \text{erfc } x$	n th integral error function
i	Current
i_T	Total current
i_{DL}	Double-layer current
i_F	Faradaic current
k, k_i	First-order rate constant (component i)
k_i^0	First-order rate constant at a reference potential
k'	First-order rate constant affected by "structured" layer near electrode
l	Length
n	Overall number of electrons exchanged
n'	Number of electrons in the transfer step
R	Gas constant
R	Resistance (Ω)
R_T	Total circuit resistance
T	Absolute temperature
t	Time ($t = 0 =$ voltage-step starting point)
t_c	Characteristic double-layer charging time
$t' = t - t_c$	Corrected time
t^*	Dimensionless time
$V, \Delta V$	Potential, potential difference
\bar{V}_B	Molar volume of B as liquid at nbp
x	Distance from electrode
γ	Dimensionless diffusivity parameter, $\{[(D_1/D_2)^{1/2} - 1]/[(D_1/D_2)^{1/2} + 1]\}$
η	Charge-transfer overpotential
$\bar{\eta}$	An average charge-transfer overpotential
μ	Viscosity
μ_0	Pure liquid viscosity
ρ	Resistivity
ψ_B	Association parameter

The Thermodynamics of Electrolyte Equilibria in Media of Variable Water Concentration

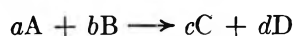
by R. A. Matheson¹

Chemistry Department, Victoria University of Wellington, Wellington, New Zealand (Received October 7, 1968)

The standard states commonly used for electrolyte solutions are discussed with particular reference to the implications of these standard states in regard to the effects of pressure and solvent changes upon the standard chemical potentials of both ions and neutral solutes. Consideration is given to both normal standard chemical potentials and those which result when aqueous solutions are considered to consist of hydrated solutes and free water molecules. The equations obtained for the variation of conventional equilibrium constants and solubility products with pressure are found not to justify a previous proposal for the formulation of pressure-independent complete equilibrium constants and complete solubility products. The thermodynamics of solutions of electrolytes in mixed solvents consisting of water and a second component which does not solvate ions are considered. Experimental data for solutions of hydrochloric acid in dioxane-water mixtures and of acetic acid in the same solvent mixtures are shown to be inconsistent with the assumption that the standard chemical potentials of the relevant hydrated solutes are independent of solvent composition. The variation of conventional equilibrium constants with solvent composition and a previous proposal for the formulation of a complete equilibrium constant supposed to be independent of solvent composition are discussed.

Introduction

At constant temperature the equilibrium condition for the chemical reaction



is

$$a\mu_A + b\mu_B = c\mu_C + d\mu_D \quad (1)$$

μ_i , the chemical potential of the species i , is a state function which depends on temperature, pressure and, in the case of a dissolved substance, solution composition. Commonly a particular state is chosen as standard state and the chemical potential of any other state related to the chemical potential of the standard state (μ_i^0) by means of the equation

$$\mu_i = \mu_i^0 + RT \ln a_i \quad (2)$$

where a_i is the activity of i in the state for which the chemical potential of this substance is μ_i . By definition $a_i = 1$ in the standard state. From eq 1 and 2 one obtains the equilibrium condition

$$c\mu_C^0 + d\mu_D^0 - a\mu_A^0 - b\mu_B^0 = -RT \ln \frac{a_C^c a_D^d}{a_A^a a_B^b} \quad (3)$$

In the case of a gaseous equilibrium it is customary to choose standard states such that each of the standard chemical potentials is a function of temperature only² and the equilibrium constant $(a_C)^c (a_D)^d / (a_A)^a (a_B)^b$ is strictly constant under isothermal conditions. However, the position is less simple when nongaseous substances are involved. For an equilibrium in solution, the determination of the equilibrium constant normally involves the study of a series of solutions in which the

concentrations of A, B, C, and D in a given solvent are varied while the temperature and pressure are held constant. Standard states are chosen so that, *under these conditions*, the various standard chemical potentials and the equilibrium constant are constant. However, a change in conditions may alter the values of the standard chemical potentials and cause the equilibrium constant to vary. It is usually understood that all quantities in eq 2 must refer to the same temperature and that standard chemical potentials are temperature dependent. However, for liquids and solids two conventions³ are in use in regard to pressure. These may be illustrated by considering possible standard states for a liquid. First, we may choose, for any pressure, the pure liquid *at that pressure* as the standard state so that the activity of the pure liquid is unity at all pressures. Since the chemical potential of a liquid is a function of pressure, this procedure implies a pressure-dependent standard chemical potential and, if eq 2 is used, both μ_i and μ_i^0 must refer to the same pressure. Alternatively, the pure liquid at 1 atm may be chosen as the standard state so that the standard chemical potential is independent of pressure. However, the activity of the pure liquid is not now unity at pressures other than 1 atm. Obviously the differences between the two conventions are important in high pressure studies.

For dissolved substances one may choose the pure

(1) Send correspondence to author at the Chemistry Department, Otago University, Dunedin, New Zealand.

(2) See, e.g., J. G. Kirkwood and I. Oppenheim, "Chemical Thermodynamics," McGraw-Hill Book Co., Inc., New York, N. Y., 1961, p 104.

(3) See, e.g., K. G. Denbigh, "Principles of Chemical Equilibrium," 2nd ed, Cambridge University Press, Cambridge, 1966, p 287.

liquid form of the substance as the standard state and thus obtain a standard chemical potential which is not altered when the solvent is changed. However, the standard state is sometimes specified by requiring that the activity coefficient of the substance shall approach unity as its concentration tends to zero. This second procedure gives a standard chemical potential the value of which varies from solvent to solvent.⁴

It is clear from the foregoing that, for reactions involving nongaseous substances, the equilibrium constant is not necessarily a function of temperature only. Depending on the standard states chosen for the various substances, the equilibrium constant may or may not be pressure dependent or solvent dependent.

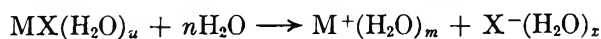
A further point to be considered is the possibility that the solvent may be involved in the equilibrium. Commonly the dissociation of an aqueous electrolyte MX is represented thus



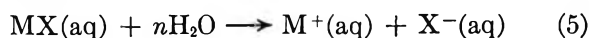
so that at equilibrium

$$\mu^0_{\text{M}^+} + \mu^0_{\text{X}^-} - \mu^0_{\text{MX}} = -RT \ln K \quad (4)$$

where the quantity K , which we shall call the conventional equilibrium constant, equals $a_{\text{M}^+} a_{\text{X}^-} / a_{\text{MX}}$. However if the species M^+ , X^- , and MX are hydrated, the dissociation presumably takes place thus



For brevity we shall represent this reaction as



where $i(\text{aq})$ refers to the hydrated species i , *e.g.*, $\text{M}^+(\text{aq})$ refers to $\text{M}^+(\text{H}_2\text{O})_m$, and $n = m + x - u$ is the change in hydration number for the reaction.

At equilibrium

$$\mu^0_{\text{M}^+(\text{aq})} + \mu^0_{\text{X}^-(\text{aq})} - n\mu^0_{\text{H}_2\text{O}} - \mu^0_{\text{MX}(\text{aq})} = -RT \ln K^0 \quad (6)$$

where

$$K^0 = \frac{a_{\text{M}^+(\text{aq})} a_{\text{X}^-(\text{aq})}}{a_{\text{MX}(\text{aq})} (a_{\text{H}_2\text{O}})^n} \quad (7)$$

Following Quist and Marshall^{5a} we shall call K^0 the complete equilibrium constant.

For dilute solutions in pure water at a fixed pressure, $a_{\text{H}_2\text{O}}$ is virtually constant and the distinction between the two equilibrium constants unimportant. Indeed if pure water at the pressure in question is taken as the standard state for H_2O , they are equal. However, when $a_{\text{H}_2\text{O}}$ is not constant it is important to distinguish between the two equilibrium constants, a point which has been stressed by Quist and Marshall in their study of the changes in conventional equilibrium constants brought about by the pressurization of aqueous electrolyte solutions or by the addition to such solutions of an "inert"

solvent (one which does not solvate the substances involved in the equilibrium). They propose^{5b} "That the activity (or concentration) of solvent molecules indeed be included, in molar concentration units, as very important *variables* in the complete equilibrium constant K^0 " and add that "when this is done it is found that the isothermal K^0 for a particular equilibrium is independent of changes in dielectric constant, whether these are made by varying the density of the solution by pressurization or by adding an 'inert' solvent." Subsequently⁶ they remark that "This K^0 is independent of density (pressure) at constant temperature, and therefore meets one of the requirements of a true thermodynamic equilibrium constant." Elsewhere⁷ they say that "The complete equilibrium in ion-pair formation thus includes solvation of ions and ion pairs, as well as the interaction between the solvated ions to form the solvated ion pair. With this concept the correct constant for the equilibrium should indeed be a constant (at constant temperature) and would correspond to the K^0 in (their) equation (1) where $(C_{\text{H}_2\text{O}})^n$ could be replaced by C^n (reactive solvent) for some other reactive solvent."

Their eq 1 is

$$K^0 = K / (C_{\text{H}_2\text{O}})^n \quad (8)$$

This equation follows from eq 7 if it is assumed that the activity of water is equal to its molar concentration ($C_{\text{H}_2\text{O}}$) and if $a_{\text{M}^+(\text{aq})} a_{\text{X}^-(\text{aq})} / a_{\text{MX}(\text{aq})}$ is equated to the conventional equilibrium constant K . From eq 8

$$\log K = \log K^0 + n \log C_{\text{H}_2\text{O}}$$

Quist and Marshall quote numerous instances where a linear relation between $\log K$ and $\log C_{\text{H}_2\text{O}}$ is found. These examples include cases where $C_{\text{H}_2\text{O}}$ is varied by applying pressure to the solution as well as those where the variation is effected by the addition of an inert solvent. However, they do not give a detailed thermodynamic proof that either eq 8 or its antecedent $K^0 = K / (a_{\text{H}_2\text{O}})^n$ correctly relate the hydration number change and the conventional equilibrium constant for the reaction to a complete equilibrium constant K^0 which is a function of temperature only.

We believe that an examination of the possibility of such a proof is required in order to elucidate the following matters.

(1) The status of the hydration number changes calculated from variations of K with $C_{\text{H}_2\text{O}}$.⁸ While the

(4) See *e.g.*, K. G. Denbigh "Principles of Chemical Equilibrium," 2nd ed, Cambridge University Press, Cambridge, 1966, Chapter 9, especially eq 9.5. K_1 in 9.5 is solvent dependent.

(5) (a) A. S. Quist and W. L. Marshall, *J. Phys. Chem.*, **72**, 1536 (1968); (b) *ibid.*, see p 1537.

(6) Reference 5a, p 1538.

(7) W. L. Marshall and A. S. Quist, *Proc. Nat. Acad. Sci. U. S.*, **58**, 902 (1967).

(8) Reference 5a, Tables I and II.

previously mentioned linear relation between $\log K$ and $\log C_{\text{H}_2\text{O}}$ shows that a number x can be found such that $K/(C_{\text{H}_2\text{O}})^x$ is constant under isothermal conditions, it does not prove this number to be the hydration number change for the reaction in question.

(2) The correct formulation of "true isothermal equilibrium constants" (equilibrium constants which are a function of temperature only) for reactions in electrolyte solutions.

(3) Whether the linear relation between $\log K$ and $\log C_{\text{H}_2\text{O}}$ is in any fundamental sense an explanation of the changes in conventional equilibrium constants brought about by the application of pressure or by the addition of an "inert" solvent.

Equations 6 and 7 follow directly from the application of the general equilibrium condition, eq 1, to the reaction represented by eq 5. However, if K^0 is to be a "true isothermal equilibrium constant," standard states must be chosen so that $(\mu^0_{\text{M}^+(\text{aq})} + \mu^0_{\text{X}^-(\text{aq})} - n^0_{\text{H}_2\text{O}} - \mu^0_{\text{MX}(\text{aq})})$ is a function of temperature only. While this requirement can be met, at least in principle, it is not obvious that it is satisfied by the choice of standard states upon which conventional equilibrium constants are based, or by the standard state for water implicit in the relation $a_{\text{H}_2\text{O}} = C_{\text{H}_2\text{O}}$. We therefore present a discussion of common standard states for electrolyte solutions with a view to establishing the behavior of the corresponding standard chemical potentials when the solvent or the pressure is changed, a point which is of considerable significance in view of the current interest in studying the properties of electrolyte solutions over extended ranges of pressure. We shall discuss both the thermodynamic functions for solute and solvent as commonly obtained and those which result when one makes explicit recognition of the phenomenon of hydration.

Thermodynamic Functions for Hydrated Solutes⁹

Consider a solution prepared from n_w moles of water and n_s moles of some anhydrous salt, each molecule of which ionizes to form n_1 cations and n_2 anions. Ordinarily no attention is paid to the possibility that in solution the ions of the salt may be hydrated, and any extensive thermodynamic property X of the solution is related to the corresponding partial molar properties of salt and water (\bar{X}_s and \bar{X}_w) by the equations

$$X = n_s \bar{X}_s + n_w \bar{X}_w$$

$$\bar{X}_s = \left(\frac{\partial X}{\partial n_s} \right)_{T,P,n_w} ; \bar{X}_w = \left(\frac{\partial X}{\partial n_w} \right)_{T,P,n_s} \quad (9)$$

However, explicit recognition of hydration can be made by considering the solution to consist of n_s' moles of hydrated salt (*i.e.*, $n_1 n_s'$ moles of hydrated cations and $n_2 n_s'$ moles of hydrated anions) and n_w' moles of free water (water not hydrated to any ion). Then

$$X = n_s' \bar{X}_s' + n_w' \bar{X}_w'$$

$$\bar{X}_s' = \left(\frac{\partial X}{\partial n_s'} \right)_{T,P,n_w'} ; \bar{X}_w' = \left(\frac{\partial X}{\partial n_w'} \right)_{T,P,n_s'} \quad (10)$$

where \bar{X}_s' refers to the hydrated salt and \bar{X}_w' refers to free water. Assuming that there is sufficient water to hydrate all the ions present and that a fixed number of molecules of water (h) are required to hydrate n_1 cations and n_2 anions, assumptions which we shall make throughout this paper

$$n_s = n_s'$$

$$n_w' = n_w - hn_s$$

Now the addition of dn moles of water to the solution will increase the number of moles of free water by dn and leave the number of moles of hydrated salt unchanged. Thus

$$\bar{X}_w = \bar{X}_w' \quad (11)$$

and since the value of X is independent of any assumption made about the molecular state of the constituents

$$\bar{X}_s' = \bar{X}_s + h\bar{X}_w \quad (12)$$

It follows from eq 11 that, at least when the pure liquid is chosen as standard state for water, the standard chemical potential and the activity of free water are the same as the ordinary standard chemical potential and activity of water, respectively. In contrast (*cf.* eq 12) the standard chemical potential, activity and activity coefficient of a hydrated salt differ from the ordinary values of the standard chemical potential, activity, and activity coefficient of the salt, *i.e.*, the values of these quantities which are obtained when the components of the solution are considered to be unhydrated salt and water. However, examination of Robinson and Stokes, discussion of activity coefficients¹⁰ shows that in the case of the activity and activity coefficient the difference is very small when the solute is sufficiently dilute for hn_s to be small compared with n_w and the water activity to be close to unity.

Standard States for Electrolyte Solutions

The standard states for the ions M^+ and X^- are specified by stipulating that, at any temperature and pressure, the activity coefficients of these species shall tend to unity as infinite dilution is approached. The standard state thus defined is a hypothetical solution in which the concentrations and activity coefficients¹¹ of these ions are unity and in which, by virtue of the above mentioned stipulation, there are no interactions between solute particles. However, since solute-solvent interactions do not vanish at infinite dilution, any

(9) The following discussion owes much to the arguments of R. A. Robinson and R. H. Stokes, "Electrolyte Solutions," 2nd ed (revised), Butterworth and Co. Ltd., London, 1965, pp 238-241.

(10) R. A. Robinson and R. H. Stokes, "Electrolyte Solutions," 2nd ed (revised), Butterworth and Co. Ltd., London, 1965, p 240.

(11) Mean concentration and mean activity coefficient should the electrolyte be unsymmetrical.

solute-solvent interactions present in real dilute solutions will persist in the standard state. Thus, when a standard state of this type is chosen in each of several solvents by specifying that, in each solvent, the activity coefficient of the solute shall be unity at infinite dilution, the standard chemical potential of the solute cannot be expected to be the same in all solvents.

The standard chemical potential of the ions on the molal concentration scale is given by

$$(\mu^0_{M^+} + \mu^0_{X^-})_{(m)} = \lim_{m \rightarrow 0} (\mu_{M^+} + \mu_{X^-} - RT \ln m^2) \quad (13)$$

and on the molar concentration scale by

$$(\mu^0_{M^+} + \mu^0_{X^-})_{(c)} = \lim_{c \rightarrow 0} (\mu_{M^+} + \mu_{X^-} - RT \ln c^2) \quad (14)$$

where m denotes the molality of the ions and c the molarity. Relations between these two quantities and between the molar (y) and molal (γ) activity coefficients are given by Robinson and Stokes.¹² It follows from these that, when the density of the solvent is not 1 g ml⁻¹, the two standard chemical potentials differ as also do the molar and molal activities and molar and molal activity coefficients. While the difference between the two activity coefficients is always negligible for dilute solutions, the two activities are related thus

$$\frac{a_{\pm(m)}}{a_{\pm(c)}} = \frac{m\gamma_{\pm}}{cy_{\pm}} = \frac{1}{d_0}$$

and so differ appreciably when the density of the pure solvent (d_0) is not unity.

For a solution of components, 1, 2, . . . i

$$\left(\frac{\partial \mu_i}{\partial P}\right)_{T, n_1, n_2, \dots, n_i} = \bar{V}_i$$

or, since both μ and \bar{V} are intensive properties

$$\left(\frac{\partial \mu_i}{\partial P}\right)_{T, x_1, x_2, \dots, x_i} = \bar{V}_i$$

where x_i and \bar{V}_i are, respectively, the mole fraction and partial molar volume of the species i . Since a solution of fixed mole fraction has a fixed molality, differentiation of eq 13 gives

$$\frac{\partial}{\partial P} (\mu^0_{M^+} + \mu^0_{X^-})_{(m)} = \bar{V}^0_{M^+} + \bar{V}^0_{X^-} \quad (15)$$

where $\bar{V}^0_i = \lim_{m \rightarrow 0} \bar{V}_i$. Since for a solution of fixed mole fraction

$$\frac{\partial \ln c}{\partial P} = -\frac{1}{V} \frac{\partial V}{\partial P}$$

differentiation of eq 14 gives

$$\frac{\partial}{\partial P} (\mu^0_{M^+} + \mu^0_{X^-})_{(c)} = \bar{V}^0_{M^+} + \bar{V}^0_{X^-} - 2RT\kappa \quad (16)$$

where κ is the compressibility of pure water.

When, as is common, the standard state for the species MX is chosen by specifying that its activity coefficient shall tend to unity as its concentration tends to zero, the standard chemical potential of this species may depend on the solvent and, in any given solvent, will vary with pressure thus

$$\frac{\partial}{\partial P} (\mu^0_{MX})_{(m)} = \bar{V}^0_{MX} \quad (17)$$

if the molal concentration scale is used. When the molar concentration scale is employed

$$\frac{\partial}{\partial P} (\mu^0_{MX})_{(c)} = \bar{V}^0_{MX} - RT\kappa \quad (18)$$

When the solution is considered to be made up of hydrated solutes and free water, it is again specified that the solute activity coefficients shall become unity at infinite dilution so the standard states for the solutes are once more hypothetical solutions in which there may be solute-solvent interactions, but not solute-solute interactions. However, the solvent molecules most affected by the (bare) ions are now regarded as part of the hydration sheath of the (hydrated) ions and therefore as part of the solute. The interaction between the hydrated ions and the free solvent will thus be smaller than the total interaction between bare ions and solvent. Nevertheless, because the hydrated ions are charged particles they will interact to some extent with the dipoles of nearby *free* solvent molecules. Consequently, when one is considering solutions of an electrolyte in a series of solvents containing variable proportions of water and an "inert" solvent, one cannot exclude the possibility of some variation of the standard chemical potentials of the *hydrated* ions with solvent composition if it is specified that, in any solvent mixture, the activity coefficient of the electrolyte shall be unity at infinite dilution.

From eq 12, 13, and 14

$$\mu^0_{M^+(aq)} + \mu^0_{X^-(aq)} = \mu^0_{M^+} + \mu^0_{X^-} + h\mu^0_{H_2O}$$

where $(\mu^0_{M^+(aq)} + \mu^0_{X^-(aq)})$ is the standard chemical potential of the hydrated ions, $\mu^0_{M^+} + \mu^0_{X^-}$ the standard chemical potential of the ions as ordinarily obtained without considering hydration, and $\mu^0_{H_2O}$ is the chemical potential of pure water at the temperature and pressure in question. The pressure coefficients of $(\mu^0_{M^+(aq)} + \mu^0_{X^-(aq)})_{(m)}$ and $(\mu^0_{M^+(aq)} + \mu^0_{X^-(aq)})_{(c)}$ are obtained by replacing $\bar{V}^0_{M^+} + \bar{V}^0_{X^-}$ in eq 15 and 16 by $\bar{V}^0_{M^+(aq)} + \bar{V}^0_{X^-(aq)}$, *i.e.*, by $\bar{V}^0_{M^+} + \bar{V}^0_{X^-} + h\bar{V}^0_{H_2O}$. There is no reason to believe that either of these pressure coefficients is generally zero.

If pure water at the temperature and pressure in question is chosen as the standard state for water

(12) Reference 9, p 30 ff.

$$\frac{\partial \mu_{\text{H}_2\text{O}}^0}{\partial P} = V_{\text{H}_2\text{O}}^0$$

where $V_{\text{H}_2\text{O}}^0$, the molar volume of pure water, is identical with the limiting partial molar volume of water, $\bar{V}_{\text{H}_2\text{O}}^0$. Suppose, however, we specify that, for any solution in which the properties of the water do not differ significantly from those of the pure liquid at the same temperature and pressure, $a_{\text{H}_2\text{O}} = C_{\text{H}_2\text{O}}$. This implies a standard chemical potential $\mu_{\text{H}_2\text{O}(c)}^0$ such that

$$\mu_{\text{H}_2\text{O}} = (\mu_{\text{H}_2\text{O}(c)}^0) + RT \ln C_{\text{H}_2\text{O}}$$

When this equation is applied to pure water, it follows that

$$\frac{\partial}{\partial P} (\mu_{\text{H}_2\text{O}(c)}^0) = V_{\text{H}_2\text{O}}^0 - RT\kappa_{\text{H}_2\text{O}}$$

The right-hand side of this equation is not generally zero, *e.g.*, at 25° for pressures near 1 atm $\kappa_{\text{H}_2\text{O}} = 4.6 \times 10^{-5} \text{ atm}^{-1}$ while $V_{\text{H}_2\text{O}}^0/RT = 7.3 \times 10^{-4} \text{ atm}^{-1}$.

Pressure Dependence of Equilibrium Constants

When calculating conventional equilibrium constants from experimental data it is common to choose standard states for M^+ , X^- and MX by requiring that, at any pressure, the activity coefficients of each shall become unity at infinite dilution.¹³

Thus (eq 4, 15, and 17)

$$-RT \frac{\partial \ln K_{(m)}}{\partial P} = \Delta V^0$$

where $K_{(m)}$ is the conventional equilibrium constant expressed in terms of molal concentration scale activities and $\Delta V^0 = \bar{V}_{M^+}^0 + \bar{V}_{X^-}^0 - \bar{V}_{MX}^0$. The corresponding expression for the molar scale is (eq 4, 16, and 18)

$$-RT \frac{\partial \ln K_{(c)}}{\partial P} = \Delta V^0 - RT\kappa \quad (19)$$

It follows from our discussion of standard states that the complete equilibrium constant

$$K^0 = \frac{a_{M^+(aq)} a_{X^-(aq)}}{a_{MX(aq)} (a_{\text{H}_2\text{O}})^n}$$

is not necessarily independent of pressure and that its pressure coefficient will depend on the standard states upon which the various activities are based. Since for dilute solutions the activity of a hydrated solute and the corresponding ordinary solute activity are the same, the activity quotient $a_{M^+(aq)} a_{X^-(aq)} / a_{MX(aq)}$ may be replaced by the conventional equilibrium constant so that (*cf.* eq 6)

$$\mu_{M^+(aq)}^0 + \mu_{X^-(aq)}^0 - \mu_{MX(aq)}^0 - n\mu_{\text{H}_2\text{O}}^0 = -RT \ln \frac{K}{(a_{\text{H}_2\text{O}})^n} \quad (20)$$

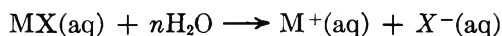
It must be emphasized that this step implies, in the case

of the hydrated solutes, the choice of a standard state of the type discussed in the previous section of the paper so that each of the terms $\mu_{M^+(aq)}^0$, $\mu_{X^-(aq)}^0$ and $\mu_{MX(aq)}^0$ is, in general, pressure dependent. If either of the more usual standard states are chosen for water, $K/(a_{\text{H}_2\text{O}})^n$ is pressure dependent. The choice of pure water at the pressure in question as the standard state for water gives $a_{\text{H}_2\text{O}} = 1$ at all pressures so that $K/(a_{\text{H}_2\text{O}})^n$ reduces to K , a quantity which is, in general, pressure dependent. If pure water at 1 atm is chosen as the standard state, $\mu_{\text{H}_2\text{O}}^0$ is independent of pressure. This does not make $K/(a_{\text{H}_2\text{O}})^n$ independent of pressure unless $\bar{V}_{M^+(aq)}^0 + \bar{V}_{X^-(aq)}^0 = \bar{V}_{MX(aq)}^0$ (assuming molal concentration scale activities for the solutes) or $\bar{V}_{M^+(aq)}^0 + \bar{V}_{X^-(aq)}^0 = \bar{V}_{MX(aq)}^0 + RT\kappa$ (assuming molar concentration scale solute activities). We can see no reason why either of these equations should necessarily hold.

However, as mentioned earlier it has been proposed that the quantity $K_{(c)}/(C_{\text{H}_2\text{O}})^n$ is a complete equilibrium constant which is independent of pressure. For the following reasons we believe that this approach to the formulation of a pressure-independent complete equilibrium constant is questionable. It follows from our discussion that the conventional equilibrium constant is based on standard states such that *each* of the standard chemical potentials in eq 20 is pressure dependent. Putting $a_{\text{H}_2\text{O}} = C_{\text{H}_2\text{O}}$ instead of $a_{\text{H}_2\text{O}} = 1$ changes the standard state for water but does not alter the standard states for the other substances. Moreover, the relationship $a_{\text{H}_2\text{O}} = C_{\text{H}_2\text{O}}$ implies a standard chemical potential $(\mu_{\text{H}_2\text{O}(c)}^0)$ which is pressure dependent. Thus each of the terms on the left-hand side of eq 20 remains pressure dependent and

$$-RT \frac{\partial}{\partial P} \ln \frac{K_{(c)}}{(C_{\text{H}_2\text{O}})^n} = \Delta V^0 + (n-1)RT\kappa \quad (21)$$

Were the various participants in the equilibrium to behave as ideal gases, the molar volume of each would be RT/P so that the right-hand side of this equation would vanish and $K/(C_{\text{H}_2\text{O}})^n$ would be independent of pressure. However, we can see no reason why $\Delta V^0 + (n-1)RT\kappa$ should necessarily be zero for a reaction in aqueous solution and therefore conclude that the application of thermodynamics to the reaction



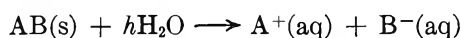
does not lead to the result that the quantity $K/(C_{\text{H}_2\text{O}})^n$ is necessarily independent of pressure. It follows that the quantity x which makes $K/(C_{\text{H}_2\text{O}})^x$ independent of pressure is not necessarily the hydration number change for the reaction in question. This view is reinforced by the rather large values of x which have been reported for

(13) This requirement is explicit when $a_{M^+} a_{X^-} / a_{MX}$ is equated to the infinite dilution limit of the corresponding concentration quotient. It is implicit when it is assumed that, in dilute solution, the activity coefficient of MX is unity and the activity coefficients of M^+ and X^- are given by the Debye-Hückel theory.

the ionization of water ($x = 20$),¹⁴ ammonia ($x = 28$), methylamine ($x = 25$), and the bisulfate ion ($x = 20$). We do not believe that these figures are in fact hydration number changes and therefore reject the explanation of the original authors that "these large hydration changes may possibly be related to the "extra" mobility of the hydrogen and hydroxide ions, the structure of water at room temperature, and their changes when solvent concentrations are varied by pressure alone."

Pressure Dependence of Solubility Products

Presuming the dissolved ions to be hydrated, the equilibrium between the solid salt AB and the saturated solution of its ions is



Thus

$$\begin{aligned} \mu^0_{A^+(aq)} + \mu^0_{B^-(aq)} - \mu^0_{AB(s)} - h\mu^0_{H_2O} = \\ -RT \ln \frac{a_{A^+(aq)} a_{B^-(aq)}}{a_{AB(s)} (a_{H_2O})^h} \end{aligned}$$

If one chooses the respective pure phases at the pressure in question as standard states for water and the solid AB, then $a_{AB(s)}$ is unity at any pressure and $a_{H_2O} = 1$ in sufficiently dilute solutions regardless of pressure. Thus with the usual choice of standard states for the ions

$$\mu^0_{A^+(aq)} + \mu^0_{B^-(aq)} - \mu^0_{AB(s)} - h\mu^0_{H_2O} = -RT \ln K_s$$

where K_s is the solubility product $a_{A^+} a_{B^-}$. Each of the terms on the left is, in general, pressure dependent. Hence where the ionic activities are on the molal concentration scale

$$-RT \frac{\partial}{\partial P} \ln K_{s(m)} = \Delta V^0$$

and where they are on the molar concentration scale

$$-RT \frac{\partial}{\partial P} \ln K_{s(c)} = \Delta V^0 - 2RT\kappa$$

$$\begin{aligned} \Delta V^0 &= \bar{V}^0_{A^+(aq)} + \bar{V}^0_{B^-(aq)} - \bar{V}^0_{AB(s)} - h\bar{V}^0_{H_2O} \\ &= \bar{V}^0_{A^+} + \bar{V}^0_{B^-} - \bar{V}^0_{AB(s)} \end{aligned}$$

$\bar{V}^0_{A^+} + \bar{V}^0_{B^-}$ is the limiting partial molar volume of the salt as ordinarily calculated.

If a complete solubility product K_s^0 is formulated thus

$$K_s^0 = \frac{K_{s(c)}}{(C_{H_2O})^h}$$

then

$$- \frac{\partial}{\partial P} K_s^0 = \frac{\Delta V^0}{RT} + (h - 2)\kappa$$

There appears to be no reason why the right-hand side of this equation should necessarily vanish or why the quantity q which makes $-\Delta V^0/RT = (q - 2)\kappa$ and which makes $K_{s(c)}/(C_{H_2O})^q$ independent of pressure

should necessarily be the hydration number for the salt in question. For a number of salts we have calculated q using figures for ΔV^0 derived from the appropriate partial molar ionic volumes¹⁵ and solid-salt densities.¹⁶ We obtained the following: $MgSO_4$ $q = 47.8$, $CaSO_4$ $q = 45.5$ (solid phase natural anhydrite) or 51.0 (soluble anhydrite), $BaSO_4$ $q = 45.9$, $MgCO_3$ $q = 48.9$, $CaCO_3$ $q = 51.2$ (solid phase aragonite) or 53.5 (calcite), $BaCO_3$ $q = 55.5$, $AgCl$ $q = 9.7$, $AgBr$ $q = 6.4$, AgI $q = 7.0$ (α form of the solid) or 5.0 (β form), $LiCl$ $q = 5.0$, $NaCl$ $q = 11.3$, KCl $q = 11.5$, $RbCl$ $q = 12.1$ and $CsCl$ $q = 4.7$ (all data refer to 25°). The very large values for the alkaline earth carbonates and sulfates strongly suggest that for these salts q is *not* the hydration number. On electrostatic grounds it would be expected that the lithium ion would be the most strongly hydrated of the alkali ions yet the value of q for $LiCl$ is much less than for $NaCl$, KCl , and $RbCl$. Moreover, where the solid can exist in two crystalline forms which have different densities, two different values of ΔV^0 (and therefore two different values of q) result. However, once in solution ions from the two different forms of the solid are indistinguishable and must have the same hydration numbers. We are therefore inclined to the view that q is not the hydration number for the salt in question. "Hydration numbers" have also been derived¹⁷ from plots of $\log s$ ($s =$ molar solubility) *vs.* $\log C_{H_2O}$; *e.g.*, a value of 28 for $CaSO_4$ at 250° was obtained in this way using solubility data for pressurized aqueous solutions. Presuming the pressure coefficient of the relevant activity coefficients to be negligible, such "hydration numbers" are identical with the corresponding values of q and in our view equally deserving of suspicion.

Equilibria in Mixed Solvents

If it is specified that, *in any solvent*, the activity coefficient of a solute shall become unity at infinite dilution, the standard chemical potential of that solute can be expected to vary from solvent to solvent. While such variation is well known in the case of ordinary standard chemical potentials (those which result when one makes no specific recognition of hydration), the position is less clear in the case of the standard chemical potential of a solute which is specifically considered to be hydrated. However, we suggested earlier that, given the choice of standard state under discussion, the standard chemical potentials of hydrated ions in a mixed solvent consisting of water and an "inert" component might vary with solvent composition. We now proceed to confirm this suggestion by showing that a satisfactory

(14) Reference 5a, Tables I and II. The "net changes in water of hydration" which appear in these tables are identical with the quantity z defined above.

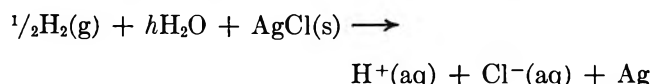
(15) B. B. Owen and S. T. Brinkley, *Chem. Rev.*, 29, 46 (1941).

(16) "Handbook of Chemistry and Physics," 47th ed, The Chemical Rubber Publishing Co., Cleveland, Ohio, 1966.

(17) Reference 5a, pp 1541, 1542.

interpretation of the thermodynamic properties of certain electrolytes in such a solvent system is impossible if one assumes the standard chemical potentials of the hydrated ions to be independent of solvent composition. We choose for the solvent system dioxane-water since nmr studies¹³ indicate no solvation of ions by dioxane in 50% (v/v) dioxane-water. The emf of the cell

Pt, H₂(g, *p* = 1 atm)|HCl(in dioxane-water)|AgCl(s)|Ag has been studied at several solvent compositions. Having regard to hydration, the cell reaction is



The emf is given by

$$-FE = \mu_{\text{H}^+(\text{aq})} + \mu_{\text{Cl}^-(\text{aq})} + \mu_{\text{Ag}} - \frac{1}{2}\mu_{\text{H}_2(\text{g})} - h\mu_{\text{H}_2\text{O}} - \mu_{\text{AgCl}(\text{s})}$$

For each solvent mixture the standard potential E° was calculated on the basis that $\gamma \rightarrow 1$ as $m \rightarrow 0$ in that solvent mixture. Thus $E^{\circ(x)}$, the standard potential for any particular solvent mixture of composition x , is related to the standard chemical potentials of the hydrated solutes in this solvent mixture by the equation

$$-FE^{\circ(x)} = (\mu_{\text{H}^+(\text{aq})}^0 + \mu_{\text{Cl}^-(\text{aq})}^0)^{(x)} + \mu_{\text{Ag}} - \frac{1}{2}\mu_{\text{H}_2(\text{g})}^0 - \mu_{\text{AgCl}(\text{s})} - h\mu_{\text{H}_2\text{O}}^{(x)}$$

where $\mu_{\text{H}_2\text{O}}^{(x)}$ is the chemical potential of water in this solvent mixture when m (the molality of hydrochloric acid) $\rightarrow 0$. Choosing pure liquid water as the standard state for H₂O

$$\mu_{\text{H}_2\text{O}}^{(x)} = \mu_{\text{H}_2\text{O}}^0 + RT \ln a_{\text{H}_2\text{O}}^{(x)}$$

where $\mu_{\text{H}_2\text{O}}^0$ is the chemical potential of pure liquid water and $a_{\text{H}_2\text{O}}^{(x)}$ is the water activity in the mixed solvent. Thus, if the standard chemical potentials of the ions are independent of solvent composition

$$F(E^{\circ(x)} - E^{\circ(w)}) = hRT \ln a_{\text{H}_2\text{O}}^{(x)}$$

where $E^{\circ(w)}$ is the standard potential of the cell when pure water is the solvent. In order that this equation be consistent with the relevant experimental data¹⁹ one has to assume the following rather large values of h : 18.4 ($x = 20\%$ w/w dioxane-water), 17.9 ($x = 45\%$), 27.6 ($x = 70\%$), and 41.2 ($x = 82\%$).

For the dissociation of MX(aq) (cf. eq 5)

$$-RT \ln K^{(x)} = (\mu_{\text{M}^+(\text{aq})}^0 + \mu_{\text{X}^-(\text{aq})}^0)^{(x)} - (\mu_{\text{MX}(\text{aq})}^0)^{(x)} - n\mu_{\text{H}_2\text{O}}^{(x)} \quad (22)$$

where $K^{(x)}$ is the conventional dissociation constant in the solvent mixture x . Both this quantity and the standard chemical potentials of the hydrated solutes are based on the choice of solute standard states discussed at the beginning of this section. $\mu_{\text{H}_2\text{O}}^{(x)}$ is again the chemical potential of water in the solvent mixture x .

Assuming the standard chemical potentials of the hydrated solutes to be independent of solvent composition and again choosing pure liquid water as the standard state for H₂O

$$\ln \frac{K^{(x)}}{K^{(w)}} = n \ln a_{\text{H}_2\text{O}}^{(x)} \quad (23)$$

where $K^{(w)}$ is the conventional dissociation constant in pure water and $a_{\text{H}_2\text{O}}^{(x)}$ is the activity of water in the solvent mixture x . We have analyzed the dissociation constants of a number of electrolytes in dioxane-water mixtures and find that the following values of n are required if eq 23 is to be consistent with the experimental data:²⁰ MnSO₄, $n = 40$; MgSO₄, 37; manganese *m*-benzene disulfonate, 46; LaFe(CN)₆, 50; and acetic acid, 30 to 50 depending on solvent composition. These "hydration number changes" are even more unsatisfactory than the "hydration numbers" previously calculated for hydrochloric acid. Since several of these excessively large values of n and h were obtained from data for solvents of lower dioxane content than the one for which nmr studies indicated ionic solvation by water only, we attribute the unreasonable magnitude of these "hydration" parameters to failure of the assumption that the standard chemical potentials of the hydrated solutes are independent of solvent composition. We do not, however, rule out the possibility of some solvation by dioxane in media of sufficiently high dioxane content.

Examination of eq 22 shows that in a mixed solvent system such as dioxane-water there are two factors involved in the variation of conventional equilibrium constants with solvent composition. First, because of the standard states upon which conventional equilibrium constants are based, the standard chemical potentials on the right-hand side of eq 22 vary with solvent composition. Second, because the water activity is not included in the conventional equilibrium constant, the chemical potential of water in the mixed solvent appears on the right, rather than a standard chemical potential of water which is independent of solvent composition. While theories which attempt to relate changes in conventional equilibrium constant with the dielectric constant of the solvent mixture may possibly deal with the first factor in a satisfactory fashion, they ignore the second completely. On the other hand, recent treatments which seek a correlation between the variation in equilibrium constant and the solvent activity disregard the first factor which we have already seen to be significant. Since

(18) A. Fratiello and D. C. Douglass, *J. Chem. Phys.*, **39**, 2017 (1963).

(19) Standard potentials from Table 8.2 in ref 9. Water activities interpolated graphically from the data of J. R. Goates and R. J. Sullivan, *J. Phys. Chem.*, **62**, 188 (1958).

(20) Dissociation constants from sources cited in ref 4, p 1539. Water activities as in ref 19.

$$-RT \ln \frac{K^{(z)}}{(a_{\text{H}_2\text{O}}^{(z)})^n} = (\mu_{\text{M}^{+(\text{aq})}}^0 + \mu_{\text{X}^{-(\text{aq})}}^{(z)}) - (\mu_{\text{MX}^{(\text{aq})}}^0)^{(z)} - n\mu_{\text{H}_2\text{O}}^0$$

and since only the last of the terms on the right is independent of solvent composition, we can see no reason to believe that the "complete equilibrium constant" $K^{(z)}/(a_{\text{H}_2\text{O}}^{(z)})^n$ is independent of solvent composition. While it may sometimes be possible to find a number p such that $K^{(z)}/(a_{\text{H}_2\text{O}}^{(z)})^p$ is independent of solvent composition, there is no reason to believe that this number is the hydration number change for the reaction in question. Indeed p is identical with the "hydration number changes" which we calculated from eq 23 and which we have seen to be absurdly large. It has been proposed²¹ that the conventional equilibrium constant, the hydration number change, and the molar concentration of water in the mixed solvent are related by the equation $K^0 = K/(C_{\text{H}_2\text{O}})^n$ where K^0 is a complete equilibrium constant assumed independent of $C_{\text{H}_2\text{O}}$. It follows from eq 22 that

$$-RT \ln K^{(z)}/(C_{\text{H}_2\text{O}}^{(z)})^n = (\mu_{\text{M}^{+(\text{aq})}}^0 + \mu_{\text{X}^{-(\text{aq})}}^{(z)}) - \mu_{\text{MX}^{(\text{aq})}}^0)^{(z)} - n(\mu_{\text{H}_2\text{O}}^{(z)} - RT \ln C_{\text{H}_2\text{O}}^{(z)})$$

At least in the case of the dioxane-water system it is easy to show that $(\mu_{\text{H}_2\text{O}}^{(z)} - RT \ln C_{\text{H}_2\text{O}}^{(z)})$ depends on the solvent composition.²² Thus in dioxane-water each of the terms on the right can be expected to vary with solvent composition. As there appears to be no reason why the right-hand side as a whole need be constant we conclude that $K/(C_{\text{H}_2\text{O}})^n$ is not necessarily independent of solvent composition. While it is apparently possible to find a number z such that $K/(C_{\text{H}_2\text{O}})^z$ is independent of solvent composition (the slopes of the linear plots of $\log K$ vs. $\log C_{\text{H}_2\text{O}}$ reported by Quist and Marshall are such numbers) we can see no reason why this number is necessarily equal to the hydration number change for the reaction in question.

Since the standard chemical potentials of hydrated ions appear to vary significantly with solvent composition, a calculation of this variation is desirable. The charged sphere-dielectric continuum model of the electrostatic interactions between ion and solvent is known to be unsatisfactory in the case of the total interaction between bare ions and the solvent. If the main trouble here is the inappropriateness of this model in the case of the water molecules immediately adjacent to the bare ions, it might be expected that, since these water molecules presumably form part of the hydrated ions, the deficiencies of the model would be less serious when one is considering the electrostatic interactions between *hydrated* ions and *free* solvent molecules. Assuming that the variation of the standard chemical potentials of the

hydrated ions with solvent composition is entirely due to electrostatic interactions between hydrated ions and solvent, the model under discussion leads to the result that

$$\Delta\mu_{\text{M}^{+(\text{aq})}}^0 + \Delta\mu_{\text{X}^{-(\text{aq})}}^0 = \frac{Ne^2}{r_m} \left(\frac{1}{D^{(z)}} - \frac{1}{D^{(w)}} \right)$$

where $\Delta\mu_{i^{(\text{aq})}}^0 = \mu_{i^{(\text{aq})}}^{(z)} - \mu_{i^{(\text{aq})}}^{(w)}$, $D^{(z)}$ and $D^{(w)}$ are, respectively, the dielectric constants of the mixed solvent and water, N is Avogadro's number, e is the electronic charge, and r_+ and r_- are the radii of the hydrated ions, with $2/r_m = 1/r_+ + 1/r_-$.

Applying this equation to the hydrated hydrogen and chloride ions, one obtains for the standard potentials of the cell discussed previously the result

$$F(E^{\circ(z)} - E^{\circ(w)}) = hRT \ln a_{\text{H}_2\text{O}}^{(z)} - \frac{Ne^2}{r_m} \left(\frac{1}{D^{(z)}} - \frac{1}{D^{(w)}} \right)$$

When the right-hand side is calculated it is found that, for any reasonable values of h and r_m , the result is greatly in excess of the experimental quantity $F(E^{\circ(z)} - E^{\circ(w)})$. We suspect that the failure of this equation is at least in part due to our assumption that the standard chemical potentials of hydrated species would be independent of solvent composition in the absence of electrostatic interactions between these species and the solvent.

Conclusion

Our analysis gives us no reason to dispute the view that solute-solvent interactions are a factor which must be considered in any attempt to account for the variations in conventional equilibrium constants which are brought about by the pressurization of aqueous solutions or by the addition to such solutions of an inert solvent. However, the proper formulation of the effect of such interactions upon the equilibrium constant and other thermodynamic properties is found to be less simple than has sometimes been supposed. In particular, even if it is assumed that solute-solvent interactions lead to the formation of hydrated solute species each containing a fixed number of water molecules, thermodynamic arguments give one no reason to suppose that for a reaction in which the hydration number change is n either of the quantities $K/(a_{\text{H}_2\text{O}})^n$ or $K/(C_{\text{H}_2\text{O}})^n$ is necessarily a function of temperature only.

(21) W. L. Marshall and A. S. Quist, *Proc. Nat. Acad. Sci. U. S.*, **58**, 901 (1967).

(22) Consideration of the equilibrium between the mixed solvent and its vapor shows that this term is not constant unless $P_{\text{H}_2\text{O}}/C_{\text{H}_2\text{O}}$ is constant ($P_{\text{H}_2\text{O}}$ = partial pressure of water above a mixed solvent containing $C_{\text{H}_2\text{O}}$ mol l.⁻¹ of water). The data of A. L. Vierk (*Z. Anorg. Allgem. Chem.*, **261**, 283 (1950)) show that $P_{\text{H}_2\text{O}}/C_{\text{H}_2\text{O}}$ is far from constant in the dioxane-water system.

Proton Nuclear Magnetic Resonance Solvent Shifts in Aqueous Electrolyte

Solutions. I. Behavior of Internal References^{1a}

by John E. Gordon^{1b} and Robert L. Thorne

Woods Hole Oceanographic Institution, Woods Hole, Massachusetts 02543 and Department of Chemistry, Kent State University, Kent, Ohio 44240 (Received December 3, 1968)

Water line shifts in solutions of nine salts were measured relative to four internal references as a function of salt molality, m_s , and the results were fitted to the equation $\delta = am_s + bm_s^2$. The a and b values for a given salt are systematically dependent upon the reference, a result of simultaneous salt effects upon the water and reference proton resonances. The values of a and b in solutions of the alkali halides and their mixtures can be predicted by empirical equations of the form $a = r_a + R_a S$ where r and R are parameters characteristic of the reference and S is characteristic of the salt. The salt shifts of 18 more internal references of widely varied structure were determined in a single salt solution. The manner in which these reference line shifts due to 1:1 inorganic electrolytes depend upon the structure of the reference compound is not easily accounted for on the basis of direct ion-molecule interactions alone; indirect effects of ions on the water structure are believed to be important. Direct interactions do occur in solutions containing $C_6H_5SO_3^-$, $C_3F_7CO_2^-$, Li^+ , and Ca^{2+} . The implications of these results for internal referencing of aqueous salt solutions are discussed.

Accurate referencing of pmr chemical shifts in aqueous solutions is a continuing problem. Polar, water-soluble substances may serve as internal references, but their chemical shifts depend on identity and concentration of dissolved salts. External referencing with correction for bulk susceptibility differences is subject to limitations of accuracy and availability of susceptibility data. Measurements on aqueous electrolytes have employed *t*-butanol,^{2,3} acetone,³ and tetra-*n*-alkylammonium ions² as internal standards. In one study⁴ of aqueous solutions of nonelectrolytes, acetonitrile was found to be the best-behaved reference.

We have now studied the use of a battery of several internal references⁵ in aqueous salt solutions. In this paper we report measurements of water chemical shifts in solutions of 11 salts (0–5 *m*) using internal acetonitrile (AN), dimethyl sulfoxide (DMSO), *t*-butanol (TBUOH), and tetramethylammonium bromide (TMAB), all $\leq 0.04 M$, as well as external cyclohexane as references. Measurements at a single salt concentration are reported for 18 additional internal references. We will show that a striking regularity of salt-induced reference shifts exists, against which eccentric reference behavior can be recognized.

Experimental Section

Inorganic salts were of reagent or analytical reagent quality. The quaternary ammonium salts were those used previously.⁶ Potassium heptafluorobutyrate was prepared by neutralizing heptafluorobutyric acid (Columbia Organic Chemicals) with potassium hydroxide, evaporating, and recrystallizing twice from ethanol-toluene. The salt was analyzed by passage through an ion-exchange resin column in the hydrogen form, and titration of the effluent with standard alkali:

equiv wt calcd, 252.1; found, 250.1. Sodium benzenesulfonate was Eastman White Label material, recrystallized twice from 90–95% ethanol and analyzed as above: equiv wt calcd, 180.2; found, 180.6. Inorganic salts were dried at 125°, organic salts at 0.01 Torr and 40°. Laboratory distilled water was treated as previously described.⁶ Organic liquids were Fisher Certified reagents or spectrograde materials, used without purification.

Solutions were prepared directly by weight except in the case of calcium chloride, weighed aliquots of whose solutions were analyzed by Mohr titration. The medium with which all solutions were prepared was water 0.04 *M* in AN, 0.02 *M* in DMSO, 0.013 *M* in TBUOH, and 0.02 *M* in TMAB.

Measurements were made at 41.0° and 60 MHz using a Varian A-60A spectrometer. The probe temperature was measured periodically using a thermistor calibrated against an NBS thermometer. Long-term temperature fluctuation was $\leq \pm 0.5^\circ$; variation during a single series of measurements was not detectable. Line separations were measured by the audio sideband method. A Hewlett-Packard 521 C frequency

(1) (a) Contribution No. 2355 from the Woods Hole Oceanographic Institution; supported in part by National Science Foundation Grants GP-5110 and GA-1261; (b) Department of Chemistry, Kent State University, Kent, Ohio 44240.

(2) H. G. Hertz and W. Spalthoff, *Z. Elektrochem.*, **63**, 1096 (1959).

(3) R. E. Glick, W. E. Stewart, and K. C. Tewari, *J. Chem. Phys.*, **45**, 4049 (1966).

(4) R. A. Y. Jones, A. R. Katritzky, J. N. Murrell, and N. Sheppard, *J. Chem. Soc.*, 2576 (1962).

(5) Such a multiple-referencing technique has recently been recommended for organic solvents: P. Laszlo, A. Speert, R. Ottinger, and J. Reisse, *J. Chem. Phys.*, **48**, 1732 (1968).

(6) J. E. Gordon and R. L. Thorne, *J. Phys. Chem.*, **71**, 4390 (1967).

Table I: Values of a Observed in Eq 1 and Predicted by Eq 5

Key	Salt	n^c	a^a, b					
			vs. CH ₃ CN	vs. DMSO	vs. <i>t</i> -BuOH	vs. Me ₄ N ⁺	vs. ext. C ₆ H ₁₂	
1	NaCl	16	obsd	-5.40 ± 0.04	-5.21 ± 0.03	-4.61 ± 0.02	-5.28 ± 0.05	-3.83 ± 0.02
			calcd	-5.40	-5.25	-4.65	-5.26	-3.90
2	NaBr	10	obsd	-7.62 ± 0.04	-7.50 ± 0.04	-6.70 ± 0.04	-7.75 ± 0.08	-5.55 ± 0.04
			calcd	-7.63	-7.51	-6.78	-7.65	-5.56
3	LiCl	9	obsd	-1.32 ± 0.02	-1.33 ± 0.01	-0.69 ± 0.03	-1.24 ± 0.03	
			calcd	-1.32	-1.11	-0.75	-0.88	
4	KBr	10	obsd	-7.76 ± 0.05	-7.59 ± 0.04	-6.86 ± 0.03	-7.76 ± 0.08	-5.82 ± 0.02
			calcd	-7.77	-7.65	-6.90	-7.80	-5.66
5	KI	9	obsd	-10.35 ± 0.05	-10.39 ± 0.09	-9.36 ± 0.06	-10.76 ± 0.17	-7.51 ± 0.07
			calcd	-10.34	-10.25	-9.38	-10.56	-7.59
6	Na ₂ SO ₄	9	obsd	-3.04 ± 0.18	-2.47 ± 0.19	-1.74 ± 0.18	-2.43 ± 0.23	
			calcd	-3.04	-2.85	-2.39	-2.72	
7	CaCl ₂	10	obsd	-1.13 ± 0.07	-1.13 ± 0.22	$+0.30 \pm 0.09$	-0.76 ± 0.08	
			calcd	-1.12	-0.91	-0.56	-0.66	
8	Me ₄ NBr	18	obsd	-4.60 ± 0.05	-4.38 ± 0.06	-3.69 ± 0.04	-4.93 ± 0.10	
			calcd	-4.59	-4.43	-3.88	-4.39	
9	Bu ₄ NBr	9 ^d	obsd	-6.38 ± 0.12	-4.87 ± 0.17	-5.02 ± 0.08	-6.50 ± 0.09	
			calcd	-6.37	-6.24	-5.58	-6.31	
10	C ₆ H ₅ SO ₃ Na	9	obsd	$+1.24 \pm 0.12$	$+2.75 \pm 0.15$	-1.82 ± 0.21	$+11.74 \pm 0.59$	
11	LiCl-NaCl	9	obsd	-3.46 ± 0.02	-3.35 ± 0.02	-2.78 ± 0.03	-3.22 ± 0.04	
			calcd	-3.45	-3.27	-2.79	-3.17	
12	LiCl-KBr	8	obsd	-4.51 ± 0.02	-4.43 ± 0.02	-3.82 ± 0.02	-4.43 ± 0.06	
			calcd	-4.51	-4.35	-3.80	-4.31	
13	NaCl-NaBr	9	obsd	-6.47 ± 0.02	-6.30 ± 0.02	-5.68 ± 0.03	-6.30 ± 0.05	
			calcd	-6.47	-6.34	-5.68	-6.42	
14	NaCl-KBr	9	obsd	-6.54 ± 0.03	-6.36 ± 0.04	-5.75 ± 0.02	-6.40 ± 0.08	
			calcd	-6.54	-6.41	-5.74	-6.49	
15	NaCl-KI	7	obsd	-7.82 ± 0.03	-7.76 ± 0.04	-6.97 ± 0.01	-7.83 ± 0.10	
			calcd	-7.83	-7.72	-6.97	-7.87	
16	NaCl-Na ₂ SO ₄	10	obsd	-4.50 ± 0.10	-4.10 ± 0.08	-3.32 ± 0.10	-4.17 ± 0.11	
			calcd	-4.50	-4.34	-3.79	-4.29	
17	NaCl-CaCl ₂	10	obsd	-3.24 ± 0.06	-3.16 ± 0.07	-2.06 ± 0.07	-2.94 ± 0.09	
			calcd	-3.24	-3.06	-2.58	-2.94	
18	NaCl-Me ₄ NBr	9	obsd	-4.98 ± 0.04	-4.88 ± 0.04	-4.17 ± 0.04	-5.37 ± 0.09	
			calcd	-4.98	-4.83	-4.25	-4.81	
19	NaCl-Bu ₄ NBr	9	obsd	-6.02 ± 0.10	-5.15 ± 0.06	-4.95 ± 0.06	-5.83 ± 0.07	
			calcd	-6.02	-5.88	-5.24	-5.93	
20	NaBr-KBr	10	obsd	-7.65 ± 0.05	-7.49 ± 0.05	-6.79 ± 0.03	-7.58 ± 0.09	
			calcd	-7.65	-7.54	-6.80	-7.68	
21	KBr-Me ₄ NBr	6	obsd	-6.18 ± 0.08	-6.01 ± 0.10	-5.24 ± 0.07	-6.45 ± 0.14	
			calcd	-6.17	-6.04	-5.39	-6.09	
22	KBr-Bu ₄ NBr	9	obsd	-7.11 ± 0.12	-6.02 ± 0.24	-6.04 ± 0.10	-7.18 ± 0.06	
			calcd	-7.11	-6.99	-6.29	-7.10	
23	KBr-KI	9	obsd	-8.97 ± 0.07	-8.89 ± 0.07	-8.07 ± 0.05	-9.03 ± 0.13	
			calcd	-8.97	-8.87	-8.06	-9.10	

^a Precision measure is standard deviation. ^b Calculated a values *via* eq 5, which applies strictly only to salts 1, 2, 4, 5, 11, 12, 13, 14, 15, 20, and 23. Calculated a values of other salts are included only for identification of specific effects by comparison. S values for these salts are not in Table III, but are given by $(a_{AN} + 0.17)/1.34$ ^c Number of observations. ^d 0-1.42 *m*; see ref 11.

Table II: Values of b Observed in Eq 1 and Predicted by Eq 5

Key Salt	n^c	b^a, b					
		vs. MeCN	vs. DMSO	vs. <i>t</i> -BuOH	vs. Me ₄ N ⁺	vs. ext. C ₆ H ₁₂	
1 NaCl	16	obsd	0.216 ± 0.011	0.221 ± 0.008	0.178 ± 0.006	0.274 ± 0.012	0.166 ± 0.005
		calcd	0.203	0.211	0.171	0.242	0.169
2 NaBr	10	obsd	0.306 ± 0.010	0.318 ± 0.012	0.262 ± 0.010	0.408 ± 0.021	0.208 ± 0.010
		calcd	0.311	0.325	0.275	0.370	0.222
3 LiCl	9	obsd	-0.006 ± 0.006	0.003 ± 0.003	-0.035 ± 0.007	0.053 ± 0.006	
		calcd	0.005	0.002	-0.020	0.007	
4 KBr	10	obsd	0.331 ± 0.010	0.341 ± 0.008	0.289 ± 0.007	0.390 ± 0.016	0.243 ± 0.004
		calcd	0.317	0.331	0.281	0.378	0.225
5 KI	9	obsd	0.459 ± 0.010	0.485 ± 0.019	0.414 ± 0.013	0.563 ± 0.035	0.282 ± 0.018
		calcd	0.443	0.464	0.403	0.527	0.286
6 Na ₂ SO ₄	9	obsd	0.255 ± 0.119	0.188 ± 0.130	0.186 ± 0.122	0.386 ± 0.156	
		calcd	0.088	0.090	0.061	0.104	
7 CaCl ₂	10	obsd	-0.213 ± 0.043	-0.104 ± 0.059	-0.266 ± 0.053	0.052 ± 0.047	
		calcd	-0.005	-0.008	-0.029	-0.005	
8 Me ₄ NBr	18	obsd	0.290 ± 0.012	0.323 ± 0.015	0.269 ± 0.010	0.370 ± 0.024	
		calcd	0.163	0.170	0.133	0.195	
9 Bu ₄ NBr	9 ^d	obsd	-0.528 ± 0.088	-0.590 ± 0.121	-0.309 ± 0.131	-0.233 ± 0.064	
		calcd	0.250	0.261	0.217	0.298	
10 C ₆ H ₅ SO ₃ Na	9	obsd	0.447 ± 0.11	-0.354 ± 0.14	0.447 ± 0.20	-3.80 ± 0.54	
11 LiCl-NaCl	9	obsd	0.133 ± 0.003	0.133 ± 0.003	0.104 ± 0.004	0.155 ± 0.006	
		calcd	0.108	0.111	0.080	0.129	
12 LiCl-KBr	8	obsd	0.196 ± 0.026	0.198 ± 0.003	0.171 ± 0.003	0.230 ± 0.002	
		calcd	0.159	0.166	0.130	0.190	
13 NaCl-NaBr	9	obsd	0.252 ± 0.003	0.256 ± 0.002	0.224 ± 0.005	0.282 ± 0.007	
		calcd	0.255	0.266	0.221	0.304	
14 NaCl-KBr	9	obsd	0.258 ± 0.005	0.264 ± 0.006	0.231 ± 0.003	0.290 ± 0.012	
		calcd	0.258	0.269	0.224	0.307	
15 NaCl-KI	7	obsd	0.296 ± 0.004	0.306 ± 0.006	0.267 ± 0.001	0.333 ± 0.014	
		calcd	0.320	0.334	0.285	0.381	
16 NaCl-Na ₂ SO ₄	10	obsd	0.356 ± 0.049	0.326 ± 0.038	0.226 ± 0.047	0.459 ± 0.052	
		calcd	0.159	0.164	0.129	0.189	
17 NaCl-CaCl ₂	10	obsd	0.100 ± 0.019	0.133 ± 0.022	0.029 ± 0.020	0.210 ± 0.027	
		calcd	0.098	0.100	0.070	0.116	
18 NaCl-Me ₄ NBr	9	obsd	0.222 ± 0.016	0.276 ± 0.016	0.203 ± 0.017	0.401 ± 0.041	
		calcd	0.182	0.190	0.152	0.217	
19 NaCl-Bu ₄ NBr	9	obsd	0.166 ± 0.034	0.099 ± 0.021	0.178 ± 0.022	0.183 ± 0.025	
		calcd	0.233	0.242	0.200	0.277	
20 NaBr-KBr	10	obsd	0.301 ± 0.007	0.306 ± 0.007	0.270 ± 0.005	0.340 ± 0.014	
		calcd	0.311	0.326	0.277	0.372	
21 KBr-Me ₄ NBr	6	obsd	0.298 ± 0.021	0.320 ± 0.026	0.257 ± 0.017	0.383 ± 0.037	
		calcd	0.240	0.251	0.207	0.287	
22 KBr-Bu ₄ NBr	9	obsd	0.256 ± 0.042	0.145 ± 0.083	0.272 ± 0.035	0.336 ± 0.021	
		calcd	0.286	0.299	0.249	0.341	
23 KBr-KI	9	obsd	0.361 ± 0.010	0.367 ± 0.010	0.327 ± 0.008	0.405 ± 0.019	
		calcd	0.375	0.393	0.338	0.447	

^a Precision measure is standard deviation. ^b See footnote b, Table I. ^c Number of observations. ^d 0-1.42 m; see ref 11.

counter was used to determine the side-band frequency, ten 10-sec counts being averaged during each two replicate recordings of the lines; results of four such recordings were averaged for each solution measured. Correction was made for nonlinearity ($\sim 0.6\%$) in the spectrometer's recorder. Externally referenced measurements were made relative to cyclohexane, using a Wilmad precision coaxial cell.

Susceptibility corrections⁷ were applied to the externally referenced data using the molar susceptibility values of Myers⁸ and solution densities from "International Critical Tables."

Results and Discussion

Nature of the Internally Referenced Results. The data for sodium chloride afford the typical plot of water line chemical shift, δ , vs. salt molality shown in Figure 1. Qualitatively similar results were obtained for eight other salts, which are listed in Tables I and II. Downfield shifts are positive. These data conform accurately to eq 1, as has been observed by others.⁹

$$\delta = am_s + bm_s^2 \quad (1)$$

The coefficients a and b were determined by the method of least squares. These and their standard errors are given in Table I. Associated with the 44 regressions which Tables I and II present are the following mean standard errors of estimate of δ (Hz at 60 MHz): vs. AN, 0.06; vs. DMSO, 0.07; vs. TBUOH, 0.06; vs. TMAB, 0.11; vs. external C_6H_{12} , 0.04. These may be compared with the estimated precision of a single determination of δ , 0.06 Hz. Only for the measurement vs. internal TMAB do small systematic deviations from eq 1 appear to exist.

The first remarkable feature of these results is the large difference between the shifts measured vs. the four internal references, and between these and the externally referenced shifts. Glick, Stewart, and Tewari³ have recently observed similar differences at a single salt concentration, using acetone and TBUOH as internal references.

The second remarkable feature is that the shapes of these curves, and the order in which they fall in Figure 1, are almost completely independent of the salt for the alkali halides and some of the organic salts. The a coefficients vs. one reference are accurately linear functions of those vs. any other reference. The salts studied divide themselves into two groups with respect to these correlations. The alkali halides and their mixtures (excluding LiCl) obey eq 2 with high precision while the

$$a_1 = \alpha + \beta a_2 \quad (2)$$

remaining salts show characteristic and consistent deviations. Consequently, the former group was employed to establish the ten possible regressions interrelating the a values vs. the five references; correlation coefficients for the seven internal-internal regressions

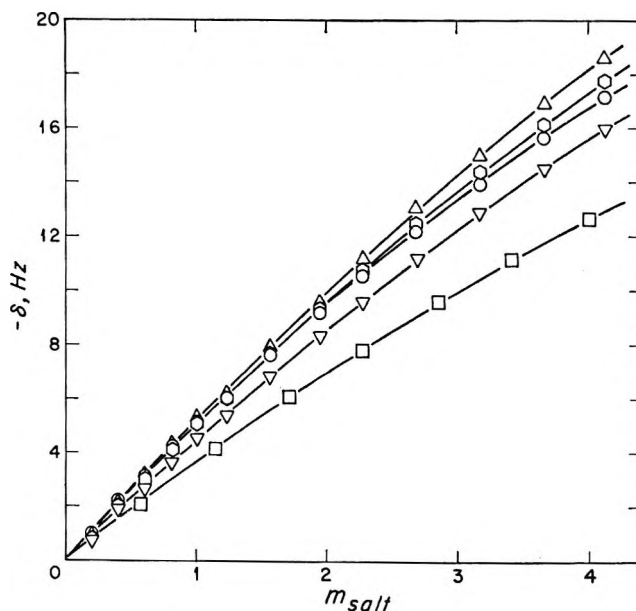


Figure 1. Upfield water line shifts due to added sodium chloride plotted against salt molality: \square , vs. external cyclohexane; ∇ , vs. *t*-butanol; \circ , vs. $(CH_3)_4N^+$; \circ , vs. dimethyl sulfoxide; \triangle , vs. CH_3CN .

are all ≥ 0.999 ; those involving the external reference are ≥ 0.995 . An analogous set of correlations exists for the b values (eq 3), with mean correlation coefficients

$$b_1 = \alpha' + \beta' b_2 \quad (3)$$

of 0.988 (internal-internal) and 0.962 (internal-external).^{10,11} Further examination shows that, for each reference, a and b are strongly correlated (correlation coefficient = 0.999) according to eq 4

for AN, DMSO, TBUOH

$$b = -(0.067 \pm 0.011) - (0.052 \pm 0.002)a \quad (4)$$

for TMAB

$$b = -(0.011 \pm 0.008) - (0.053 \pm 0.001)a$$

These correlations imply that the a and b values should be representable by eq 5, where S is a parameter characteristic only of the salt, and r_a , r_b , R_a , and R_b

$$\begin{aligned} a &= r_a + R_a S \\ b &= r_b + R_b S \end{aligned} \quad (5)$$

are characteristic of the reference. The values of these parameters listed in Table III are based on $r_a = 0$, $R_a = 1$ and $r_b = 0.046$, $R_b = -0.0316$ for the externally ref-

(7) J. A. Pople, W. G. Schneider, and H. J. Bernstein, "High-resolution Nuclear Magnetic Resonance," McGraw-Hill Book Co., Inc., New York, N. Y., 1959, p 80.

(8) W. R. Myers, *Rev. Mod. Phys.*, **24**, 15 (1952).

(9) J. C. Hindman, *J. Chem. Phys.*, **36**, 1000 (1962).

(10) Contrary to previous practice,⁹ we attribute physical significance to the quadratic term (see the following paper¹¹).

(11) J. E. Gordon and R. L. Thorne, *J. Phys. Chem.*, **73**, 3652 (1969).

Table III: Parameters for Calculation of a and b by Eq 5

Reference	r_a	R_a	Std error in a		r_b	R_b	Std error in b	
			calcd, ^a eq 5	obsd ^b			calcd, ^c eq 5	obsd ^b
AN	-0.17	1.34	...	0.04	-0.051	-0.0650	0.019	0.009
DMSO	0.056	1.36	0.06	0.04	-0.057	-0.0686	0.020	0.008
TBUOH	0.35	1.28	0.03	0.03	-0.074	-0.0629	0.018	0.006
TMAB	0.36	1.44	0.09	0.08	-0.060	-0.0774	0.035	0.015

Salt ^e	S	Salt ^e	S	Salt ^e	S
LiCl-NaCl	-2.45	NaCl-KBr	-4.75	NaCl-KI	-5.71
LiCl-KBr	-3.24	NaBr	-5.56	KBr-KI	-6.56
NaCl	-3.90	NaBr-KBr	-5.58	KI	-7.59
NaCl-NaBr	-4.70	KBr	-5.66		

^a $(\sum(a_{\text{calcd}} - a_{\text{obsd}})^2/10)^{1/2}$ for the above 11 salts. ^b Mean of 11 standard deviations in a or b from fitting of observed shifts to eq 1 (Tables I and II). ^c $(\sum(b_{\text{calcd}} - b_{\text{obsd}})^2/10)^{1/2}$ for the above 11 salts. ^d AN values were used to establish the S scale. ^e Salt mixtures are equimolar.¹¹

erenced data. They yield the calculated values of a and b in Tables I and II; these values are given for all of the salts to facilitate comparison of the behavior of the "irregular" salts with that of the alkali halides. For the alkali halides and their mixtures the mean errors of estimate of a and b by eq 5 are compared with the mean experimental uncertainties in Table III. Equations 5 predict 44 values of a and of b within an average of 1.2 and 2.5 standard deviations, respectively.

We attribute the failure of the lines for the internal references in Figure 1 to superimpose on one another and on the externally referenced line to different salt effects on the chemical shifts of the various references.¹² We shall call these shifts *reference salt shifts* (RSS). They are given by $\delta_{\text{ext}}^{\text{H}_2\text{O}} - \delta_{\text{int}}^{\text{H}_2\text{O}}$. Three types of dependence of the RSS on salt and reference structure are observed. First there is the systematic dependence accurately described by eq 5 for the salts listed in Table III. We consider the physical significance of this in the next paragraph. Second, there is an erratic variation superimposed on that of eq 5, observed for LiCl, CaCl₂, Na₂SO₄, Me₄NBr, and Bu₄NBr, which will not be discussed further. Third, there are two salts for which specific solute-solute interactions are demonstrable; these are discussed in the next to last section.

Equations 5 are interpreted as containing two terms analogous to Bothner-By's¹³ expression (eq 6) for the downfield shift accompanying transfer from gas to solution phase. Here x_i is characteristic only of the solute proton, i , and y_j only of the solvent, j . This sug-

$$-\beta_i^j = x_i y_j \quad (6)$$

gests, in other words, that the form of eq 5 is that of eq 7 where the second salt parameter, s , happens to be

$$a = r_a s + R_a S \quad (7)$$

relatively insensitive to salt identity. The implication is that (to borrow a name from the literature of linear

free-energy relationships) at least two salt-reference interaction mechanisms exist. The principal evidence for this comes from the structure dependence of the RSS, which we shall discuss next, not from the form of eq 7. For simplicity we will assume that the same two interaction mechanisms determine a and b .¹⁴

Dependence on Reference Structure. In hope of identifying the interaction mechanisms producing the RSS, 17 more substances, representing a great variety of structural types, were measured in a single salt solution. Table IV summarizes these results. These shifts are in reasonable agreement with reported³ values for acetone (1.9 Hz) and *t*-butanol (1.4 Hz). Fratiello and Douglass¹⁵ report zero salt shift for dioxane in a variety of aqueous salt solutions; accordingly we find a very small though measurable shift for dioxane.

Models for the Reference Salt Shifts Obeying Eq 2-5. The data of Table IV serve to test two hypotheses about the origin of the RSS. The first is that reference proton shieldings are altered due to polarization by the field of the added ions, in analogy with the equivalent explanation^{9,16} of the downfield component of the water salt shift. This should depend on two factors: the mean ion-reference distance and the shielding change provoked by the ion at this distance. Our test involves the first factor. If electrostatic forces only are con-

(12) The presence of one reference was shown not to affect the chemical shift of another or that of the water.

(13) A. A. Bothner-By, *J. Mol. Spectrosc.*, **5**, 52 (1960).

(14) This is not necessarily so, because a single salt parameter, say S , could easily be proportional to two physically distinct interaction variables (e.g., hydrated cation size and acidity of cation-bound water) which are closely correlated throughout the limited class of salts involved here. Although the water line shifts are also given by eq 5 ($r_a = 0$, $R_a = 1$; $r_b = 0.046$, $R_b = -0.0316$) it is for the same reason unnecessary that the same interaction mechanisms operate for the water and the reference salt shifts.

(15) A. Fratiello and D. C. Douglass, *J. Chem. Phys.*, **39**, 2017 (1963).

(16) J. N. Shoolery and B. J. Alder, *ibid.*, **23**, 805 (1955).

Table IV: Reference Salt Shifts for Various Internal References Produced by 1.00 *m* Potassium Iodide

Substance	$\delta_{\text{ext}}^{\text{H}_2\text{O}} - \delta_{\text{int}}^{\text{H}_2\text{O}}$	Substance	$\delta_{\text{ext}}^{\text{H}_2\text{O}} - \delta_{\text{int}}^{\text{H}_2\text{O}}$
$(\text{CH}_3\text{CH}_2)_3\text{N}$	3.42	THF, $\alpha\text{-H}^a$	1.72
$(\text{CH}_3)_4\text{N}^+$	3.08	THF, $\beta\text{-H}^a$	1.58 \pm 0.02 ^b
CH_3SOCH_3	2.82 \pm 0.08 ^p	$\text{CH}_3\text{CH}_2\text{NO}_2$	1.58
C_6H_6	2.31	$\text{HCON}(\text{CH}_3)_2$	1.48
CH_3CN	2.25 \pm 0.06	$\text{CH}_3\text{CH}_2\text{OH}$	1.48
$\text{CH}_3\text{CON}(\text{CH}_3)_2$	2.16	$\text{CH}_3(\text{CH}_2)_2\text{CN}$	1.42
CH_3COCH_3	2.14	CH_3OH	1.41
HCONH_2	2.13	$\text{CH}_3(\text{CH}_2)_2\text{OH}$	1.32
CH_3SO_3^-	2.10	$\text{CH}_3(\text{CH}_2)_3\text{OH}$	1.32
$(\text{CH}_2\text{OH})_2$	1.96	Dioxane	0.53
$(\text{CH}_3)_3\text{COH}$	1.79 \pm 0.04		

^a THF = tetrahydrofuran. ^b Mean of values observed in solutions containing various combinations of these references.

sidered, nonelectrolytes are distributed in the field of aqueous ions according to their dielectric constants; the more polar the molecule, the shorter the mean ion-molecule distance.¹⁷ Alternatively, the empirical order of solvation of alkali, alkaline earth, and aluminum halides by polar nonelectrolytes parallels the basicity of the nonelectrolytes.¹⁸⁻²² However, examination of Table IV reveals no correlation of the RSS with either dielectric constant or $\text{p}K_a$ of the reference (note especially the position of benzene). Also, Glick, Stewart, and Tewari³ find the RSS of acetone and TBUOH to be cation independent (for Li^+ , Na^+ , K^+ , Rb^+ , though not for Cs^+) and strongly anion dependent, whereas it is known that the dipolar aprotic nonelectrolytes of Table IV interact more strongly with cations than with anions.²³⁻²⁵ Finally, we employed an electrostatic model due to Basolo and Pearson²⁶ (based upon earlier calculations by Garrick²⁷) to estimate the interaction enthalpies for $\text{K}^+\cdot\text{CH}_3\text{OH}$ vs. $\text{K}^+\cdot\text{N}(\text{C}_2\text{H}_5)_3$ as -13 and -6 kcal mol⁻¹ of ligand. Since the CH_3OH protons are one bond closer to the ion than the $(\text{CH}_3\text{-CH}_2)_3\text{N}$ protons measured, on all counts we would expect the salt shift for CH_3OH to be the larger, contrary to the values of Table IV.

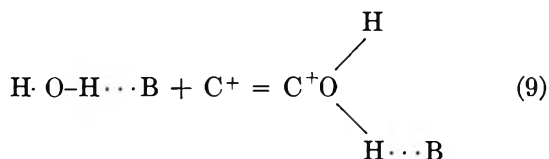
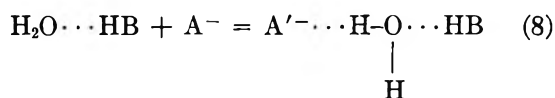
The second hypothesis was offered by Glick, Stewart, and Tewari,³ (GST hereafter) as an explanation of the RSS, and of the downfield component of the water salt shifts as well. The effect is attributed wholly to interaction with the anions of the added salt, by way of charge overlap of reference C-H bonds with these centers of enhanced polarizability. The RSS of acetone and TBUOH³ correlate with anion polarizability as required by the model, and they parallel the analogous salt effects on the Raman intensities of certain water vibrations in aqueous salt solutions. Ta-

ble IV affords some simple tests in which the mean anion-(reference molecule) distance in the solutions is varied. (1) The anion-(reference molecule) distribution function should differ drastically for uncharged, cationic, and anionic references; the order of reference line shifts should be cationic > neutral > anionic reference. However, the observed RSS for the cation $(\text{CH}_3)_4\text{N}^+$ and that for the anion CH_3SO_3^- are similar and both are mingled among the upper half of the neutral reference values. (2) The RSS do not correlate with reference dielectric constant (see above). (3) The RSS should increase with increased anionic charge in the salt, especially when the reference itself is a cation. However, the values of $\delta_{\text{ext}}^{\text{H}_2\text{O}} - \delta_{\text{int}}^{\text{H}_2\text{O}}$ for 1.00 *m* NaCl, Na_2SO_4 , and CaCl_2 solutions vs. $(\text{CH}_3)_4\text{N}^+$ reference are 1.34, 0.81, and 2.63 Hz. (4) Nonelectrolytes capable of specifically solvating anions,²⁸ e.g. HCONH_2 and the ROH of Table IV, should suffer greater shifts than non-H-bonding molecules, but no evidence of such an effect is observed;²⁹ the RSS for ROH are among the smallest rather than the largest observed. (5) The RSS might be expected to be linear in salt concentration. The Raman intensities which form the principal analogy for the GST hypothesis are linear in salt molarity.³⁰ GST measured RSS only at single salt concentrations. We have therefore obtained the RSS as a function of salt molarity for NaCl, KBr, and KI, each vs. the four standard internal references. In each case a significant curvature is observed, e.g., for KBr vs. DMSO: $\delta_{\text{int}}^{\text{H}_2\text{O}} - \delta_{\text{ext}}^{\text{H}_2\text{O}} = (-1.77 \pm 0.04)m_{\text{salt}} + (0.098 \pm 0.009) \cdot m_{\text{salt}}^2$. This is also true when the data are refitted on a molarity scale.

In summary, the GST model accounts for the limited information available on variation of salt structure, but not that for reference structure. We conclude that neither of the above hypotheses explains the reference salt shifts.

- (17) P. Debye, *J. Phys. Chem.*, **130**, 56 (1927).
 (18) A. Fratiello and D. P. Miller, *Mol. Phys.*, **11**, 37 (1966).
 (19) A. Fratiello, R. E. Lee, D. P. Miller, and V. M. Nishida, *ibid.*, **13**, 349 (1967).
 (20) A. Fratiello, R. E. Lee, V. M. Nishida, and R. F. Schuster, *J. Chem. Phys.*, **47**, 4951 (1967).
 (21) L. L. Chan and J. Smid, *J. Amer. Chem. Soc.*, **90**, 4654 (1968).
 (22) A. Yingst and D. H. McDaniel, *Inorg. Chem.*, **6**, 1067 (1967).
 (23) A. J. Parker, *Quart. Rev. (London)*, **16**, 163 (1962).
 (24) E. M. Arnett and D. R. McKelvey, *J. Amer. Chem. Soc.*, **88**, 2598 (1966).
 (25) J. F. Coetzee and J. J. Campion, *ibid.*, **89**, 2513 (1967).
 (26) F. Basolo and R. G. Pearson, "Mechanisms of Inorganic Reactions," John Wiley & Sons, Inc., New York, N. Y., 1967, p 63.
 (27) F. J. Garrick, *Phil. Mag.*, **9**, 131 (1930); **10**, 76 (1930).
 (28) A. Allerhand and P. von R. Schleyer, *J. Amer. Chem. Soc.*, **85**, 1233 (1963).
 (29) We have shown this to be true also for 1.00 *m* $(\text{CH}_3)_4\text{NBr}$ where interactions with the cation are unlikely to interfere: vs. AN, -4.31 ; vs. DMSO, -4.06 ; vs. TBUOH, -3.42 ; vs. CH_3OH , -3.21 ; vs. $(\text{CH}_2\text{OH})_2$, -3.31 ; vs. TMAB, -4.56 Hz.
 (30) G. E. Walrafen, *J. Chem. Phys.*, **36**, 1035 (1962).

An alternative explanation is that the nonelectrolyte shifts proceed by way of salt effects on the properties of the water—on the internal pressure;³¹ on the fractions of nonbonded, singly H-bonded etc. water; on the stability of clathrate structures; and on the water's acid-base properties.³² At least two salt-reference interaction mechanisms could reasonably derive from these effects of the salt: (1) polarization of coordinated water enhances its H-bonding ability. This shifts the H-bonding equilibria (eq 8 and 9) of references possessing basic and acidic groups, which results in



shifts in the resonances of neighboring CH_3 groups. These shifts can be appreciable,³³ and they can presumably be propagated through several water molecules.³⁴ (2) Alteration of the internal pressure³⁵ and the intricate local structure of the water influences the physical nature of the cavities accommodating reference molecules and changes the magnetic shielding of exposed protons. Such shifts are analogous to the gas \rightarrow solution shifts treated by Bothner-By,¹³ who considered the following mechanisms: (a) shielding-desielding by oriented, diamagnetically anisotropic solvent molecules, and (b) change in shielding due to the mean square electric fields arising from London interactions with, and permanent electric dipoles in, solvent molecules. These interactions can produce shifts of 5–30 Hz at 60 MHz for the change from gas to solution.

This model can presently be subjected to only rather superficial tests. First, it explains the large contribution of anions and of Cs^+ to the RSS, since these are the strong water structure breaking ions. Second, it makes the correlation of both reference and water shifts by the same set of salt parameters, S , rational rather than accidental.¹⁴ Third, it predicts that the reference parameters r and R should depend on several of the following variables: basicity, polarizability, molecular shape⁶ and volume, dipole moment, accessibility of ^1H nuclei at the molecular periphery, and susceptibility to salt-induced conformational changes.³⁶ Thus the dependence on reference structure should be complex, as observed. Fourth, when the water chemical shift is measured relative to the four internal standards and to external cyclohexane as a function of temperature (2–62°), the five sets of data are expressible as $\delta_{i^0} = \delta_0^0 + ut + vt^2$, and $v = 0.0016 \pm 0.0002$ for all references. The values of u vary from

-5.83 ± 0.03 for the external reference to -6.34 ± 0.02 for internal AN. These shifts are almost certainly due to changes in water structure-dependent solute-solvent interactions^{13,37} rather than to native temperature variation of solute chemical shifts³⁸ or shifts of the primary H-bonding equilibria $\text{B}\cdots\text{HOH} = \text{B} + \text{H}_2\text{O}$ (B = reference), which would give $u_{\text{internal}} - u_{\text{external}}$ values of the wrong sign. Fifth, addition of dioxane (0.0–5 m) to water plus the five references also gives five curves, representable by eq 1 with m_a = dioxane molality. The observed parameters vary from $a = -1.00 \pm 0.04$, $b = -0.066 \pm 0.008$ for the external reference to $a = -1.47 \pm 0.03$, $b = -0.030 \pm 0.006$ for internal AN. This is interpreted in the same way as the variable temperature experiment, but one must bear in mind the possibility of contributions from direct dioxane-reference interactions.

Direct Reference-Salt Interactions. Sodium benzenesulfonate produces the interesting shifts shown in Figure 2 and summarized in Tables I and II. The results *vs.* AN and DMSO stand in the "normal" (*i.e.*, that observed for the alkali halides) relation to one another. They reflect predominantly the water line behavior, a net downfield shift. TBUOH and TMAB, which deviate from this behavior, are capable, respectively, of H-bonding and ion-pair interaction with the magnetically anisotropic $\text{C}_6\text{H}_5\text{SO}_3^-$ ion. The anomalous upfield shift observed *vs.* TBUOH reflects a large downfield shift of the reference methyl lines. This indicates association with the SO_3^- group in such a way as to place the methyls in the equatorial belt of the ring.³⁹ The shifts *vs.* TMAB imply a large upfield shift of the reference's CH_3 resonance. This implies interaction between $(\text{CH}_3)_4\text{N}^+$ and $\text{C}_6\text{H}_5\text{SO}_3^-$ which on a time average keeps the methyl protons predominantly over the ring.³⁹ Some additional force beyond electrostatic attraction to the $-\text{SO}_3^-$ group appears to be involved.

The shifts due to potassium heptafluorobutyrate

(31) W. F. McDevit and F. A. Long, *J. Amer. Chem. Soc.*, **74**, 1773 (1952).

(32) (a) F. A. Long and R. L. Bergen, Jr., *J. Phys. Chem.*, **58**, 166 (1954); (b) F. A. Long and W. F. McDevit, *Chem. Rev.*, **51**, 119 (1952).

(33) Equimolar methanol produces downfield shifts of 2.19 Hz for DMSO protons and 1.02 Hz for AN protons (0.4 M solutions in CCl_4).

(34) R. A. Robinson and H. S. Harned, *Chem. Rev.*, **28**, 419 (1941).

(35) Salt effects on the internal pressure of water vary from a central value by only $\pm 10\%$ for the alkali halides (excluding F^-).^{32b} Hence this interaction mechanism is consistent with the apparent constancy of s in eq 7. It is interesting that the coefficients τ_a and τ_b are monotonically and nearly linearly related to the molar volumes for AN, DMSO, and TBUOH.³¹

(36) J. B. Hyne, *J. Amer. Chem. Soc.*, **85**, 304 (1963).

(37) F. H. A. Rummens, W. T. Raynes, and H. J. Bernstein, *J. Phys. Chem.*, **72**, 2111 (1968).

(38) L. Petrakis and C. H. Sederholm, *J. Chem. Phys.*, **35**, 1174 (1961).

(39) J. W. Emsley, J. Feeney, and L. H. Sutcliffe, "High Resolution Nuclear Magnetic Resonance Spectroscopy," Pergamon Press, Oxford, 1965, p 851; ref 7, p 424.

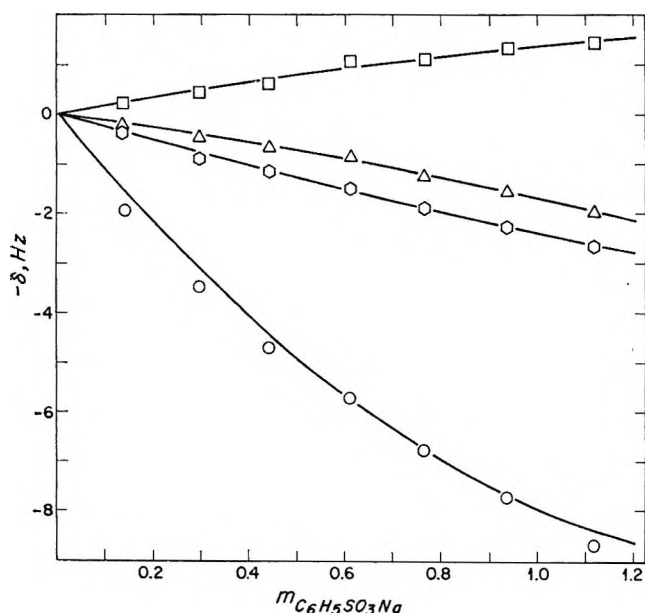


Figure 2. Water line shifts produced by added sodium benzenesulfonate, plotted vs. salt molality and measured relative to $(\text{CH}_3)_4\text{N}^+$, \circ ; $(\text{CH}_3)_2\text{SO}$, \circ ; CH_3CN , Δ ; and $t\text{-C}_4\text{H}_9\text{OH}$, \square .

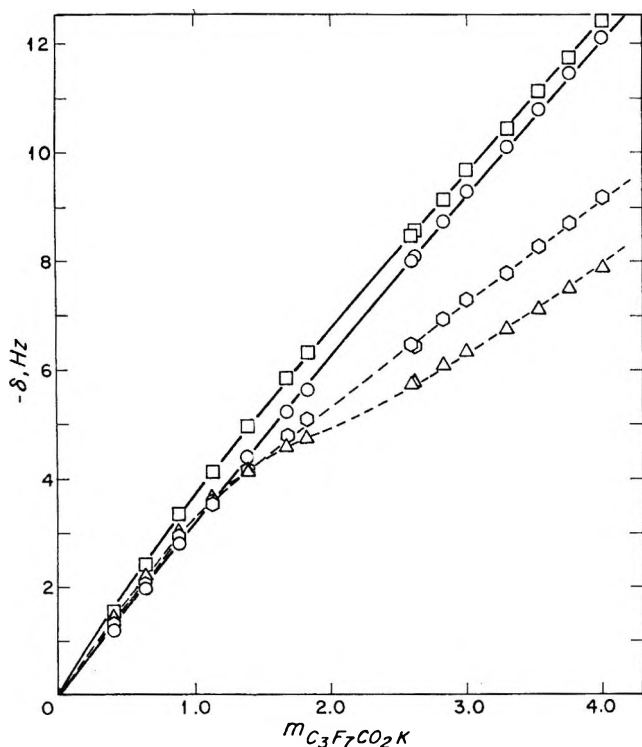


Figure 3. Water line shifts produced by added potassium heptafluorobutyrate, plotted as in Figure 2.

shown in Figure 3 reflect anion-anion association. Again, AN and DMSO should interact least with the electrolyte and their behavior appears "normal," except that the water shifts vs. these references no longer approximate eq 1 closely. A break occurs near 0.8 m salt. The diminished slope on the high-salt side of

the break is consistent with onset of aggregation at this point.⁴⁰ Klevens and Raison⁴¹ report critical micelle concentrations (cmc) for $\text{C}_3\text{F}_7\text{CO}_2\text{H} = 0.71 M$ (surface tension) and $0.42 M$ (conductance). Substitution of K^+ for H^+ as the counterion in a higher homolog increases the cmc by ca. 50%. Thus the breaks in Figure 3 are identifiable with the cmc. The shifts vs. TBUOH and TMAB evidently reflect association with $\text{C}_3\text{F}_7\text{CO}_2^-$ over the entire concentration range.

Conclusions on Internal Referencing in Aqueous Electrolyte Solutions. (1) The separation of two reference lines is a function of electrolyte identity and concentration, given for simple 1:1 salts by eq 10. This sys-

$$\delta^1 - \delta^2 = [r_a^1 - r_a^2 + S(R_a^1 - R_a^2)]m_s + [r_b^1 - r_b^2 + S(R_b^1 - R_b^2)]m_s^2 \quad (10)$$

tematic dependence of reference line positions can be approximately eliminated by using eq 5 to estimate externally referenced line positions. For example, measurement of a and b for a new electrolyte vs. one of the standard internal references allows computation of the salt parameter S ; the externally referenced shifts are then approximated by eq 11. We have employed this method in the evaluation of measured shifts

$$\delta_{\text{ext}}^{\text{H}_2\text{O}} = Sm_s + (0.046 - 0.0316S)m_s^2 \quad (11)$$

for aqueous mixtures of 1:1 electrolytes.¹¹

(2) The four references studied vary in their reliability in the correlations underlying eq 5 in a rather consistent way. The sum of the correlation coefficients for the a -value correlations involving each reference according to eq 2 and the similar sums for eq 3 (b values) decrease in the order $\text{DMSO} \sim \text{AN} > \text{TBUOH} > \text{TMAB}$. Thus, AN and DMSO obey the correlations better than TBUOH and TMAB.

(3) Deviations from the systematic behavior of the alkali halides and their mixtures are most pronounced for TBUOH in solutions containing Li^+ or divalent ion salts. Bergqvist and Forslund presented evidence that implies large TBUOH shifts in the presence of Rb^+ and Cs^+ .⁴²

(4) Water shifts vs. internal TMAB display small but significant deviations from eq 1.

(5) In view of the above points AN and DMSO are preferred to TBUOH and TMAB for aqueous electrolyte solutions. Acetone and AN are recommended for aqueous nonelectrolyte solutions.⁴ The relative behavior of AN and DMSO is retained even in structurally complex organic salt solutions. Such par-

(40) J. Clifford and B. A. Pethica, *Trans. Faraday Soc.*, **60**, 1483 (1964).

(41) H. B. Klevens and M. Raison, *J. Chim. Phys. (Paris)*, **51**, 1 (1954).

(42) M. S. Bergqvist and E. Forslund, *Acta Chem. Scand.*, **16**, 2069 (1962).

Table V: Salt Shifts vs. DSS as Internal Reference, Fitted to Eq 1

	NaCl		KI	
	a	b	a	b
DSS, 0.0133 M	-4.57 ± 0.08^a	0.169 ± 0.018^a	-9.50 ± 0.07^a	0.412 ± 0.015^a
DSS, 0.25 M			-9.49 ± 0.05	0.536 ± 0.013

^a Standard deviation.

allelism is thought to be some guarantee of the absence of shifts due to specific interactions.

(6) We have made a few measurements employing sodium 4,4-dimethyl-4-silapentane-1-sulfonate, DSS, which has been recommended⁴³ as an internal reference for aqueous solutions. Water shifts in aqueous KI and NaCl solutions measured relative to 0.0133 M and 0.25 M DSS as internal reference were compared with our standard battery of references. Least-squares coefficients are listed in Table V. The lower concentration matches that (0.12 M protons) of the other four substances and lies well below the reported⁴⁴ critical micelle concentration (cmc, 0.22 M) of DSS; the higher concentration is above the cmc. The behavior of DSS is unexceptional. The shifts vs. DSS at the two concentrations bracket the line for TBUOH in Figure 1. From the KI and NaCl results we have

estimated the parameters r_a , R_a , r_b , and R_b to be 0.64, 1.34, -0.089 , and -0.066 .

DSS appears to obey eq 1 as accurately as AN and DMSO. The DSS line is shifted by salt to an extent about midway between the extremes of Table IV. Whether its behavior in alkali halide solutions is as regular, according to eq 5, as that of AN and DMSO, and how its specific interactions outside the alkali halides compare is not yet known. Except for its line position, it would appear to offer no advantages over AN or DMSO.

Acknowledgment. Financial support by the National Science Foundation is gratefully acknowledged.

(43) G. V. D. Tiers and R. I. Coon, *J. Org. Chem.*, **26**, 2097 (1961).

(44) B. R. Donaldson and J. C. P. Schwarz, *J. Chem. Soc., B*, 395 (1968).

Proton Nuclear Magnetic Resonance Solvent Shifts in Aqueous

Electrolyte Solutions. II. Mixtures of Two Salts.

Additivity and Nonlinearity of Shifts^{1a}

by John E. Gordon^{1b} and Robert L. Thorne

Woods Hole Oceanographic Institution, Woods Hole, Massachusetts 02543 and
Department of Chemistry, Kent State University, Kent, Ohio 44240 (Received December 3, 1968)

Water line shifts were measured in solutions of 15 equimolar mixtures of two salts as a function of the total salt molality, m_t . Several additivity rules were examined; the following predicts with reasonable accuracy the observed shifts for the alkali halides and $(\text{CH}_3)_4\text{NBr}$: $\delta_{\text{mixt}} = 1/2(a_1 + a_2)m_t + 1/2(b_1 + b_2)m_t^2$. Here a_1, b_1 , etc., are parameters obtained from corresponding measurements on the pure salts, which take the form $\delta = am_s + bm_s^2$ (m_s = salt molality). Two models of the origin of the quadratic term in this expression were investigated. In one model, due principally to Hindman, interaction of electrostrictive ion hydration with water structure-making or breaking produces a quadratic term. In the other, polarization of water molecules by more than one ion, a suggestion originally made by Shoolery and Alder and revived in the light of later measurements, is the cause. The shifts observed in salt mixtures, and various other results, were employed to test the two models. Information presently available does not allow a choice between the two. Shifts in salt mixtures involving $(n\text{-C}_4\text{H}_9)_4\text{NBr}$ were not well accounted for by either model. The discrepancy may be related to strong $\text{R}_4\text{N}^+ - \text{R}_4\text{N}^+$ interactions in these solutions.

The shifts of the ^1H resonance of water produced by added single salts have been the subject of several well-known studies.²⁻⁷ The present work extends these measurements to solutions of two salts. Given the nonlinear δ vs. m dependence observed in solutions of single salts, it is unlikely that simple additivity of pure salt contributions to δ in the salt mixtures will result. We have therefore investigated the source of the nonlinearity in the process of attempting to account for the water shifts in the salt mixtures.

Hertz and Spalthoff³ considered their results (measured to ca. ± 0.5 –1 Hz) linear to 3–4 m . Similarly, Fabricand and Goldberg⁴ reported linearity to $\geq 2.2 M$. Bergqvist and Forslind⁵ found nonlinearity apparent at 1–2 m . Our data are inconsistent with any linear range.

The sources of nonlinearity considered by Shoolery and Alder² and by Hindman⁶ are: (1) polarization of water molecules beyond the first hydration shell of the ions, so that some waters are polarized by two ions simultaneously; (2) decrease in the upfield shift accompanying hydrogen-bond breaking by added salt due to exhaustion of bulk water above ca. 4 M ;² (3) ion association; (4) nonlinear polarizability of water at high field strengths in concentrated solutions. Shoolery and Alder² believed their measurements (± 1 Hz at 30 MHz, externally referenced and uncorrected for bulk susceptibility differences) to be linear in M out to 1–4 M salt; hence they concluded that no water molecules are polarized by more than one ion and that item (1) is inoperative. Hindman⁶

interpreted some measurements of alkali metal and halide ion resonances as indicating only small degrees ($< 5\%$) of ion association in the concentrated aqueous solutions; he did not attribute any substantive component of the water shifts to item (3). Hindman⁶ concluded from the near-linear shifts due to 0–6.6 m LiCl (which he considered most prone of the alkali halides to give linear behavior on all other criteria) that competition for water molecules, item (2), is not important. Hindman divides bond breaking into that necessary to form the first hydration spheres of the added ions and any additional making or breaking of hydrogen bonds, due to the effect of the salt on the water structure, which he calls the structural contribution to the water shift. The structural contribution is considered to be linear in salt molality. Hindman then shows that the existence of a structural contribution implies nonlinearity of the bond-breaking term.

Experimental Section

Techniques of measurement, instrumentation, and

(1) (a) Contribution No. 2356 from the Woods Hole Oceanographic Institution. Supported by National Science Foundation Grants GP-5110 and GA-1261. (b) Department of Chemistry, Kent State University, Kent, Ohio 44240.

(2) J. N. Shoolery and B. J. Alder, *J. Chem. Phys.*, **23**, 805 (1955).

(3) H. G. Hertz and W. Spalthoff, *Z. Elektrochem.*, **63**, 1096 (1959).

(4) B. P. Fabricand and S. Goldberg, *J. Chem. Phys.*, **34**, 1624 (1961).

(5) M. S. Bergqvist and E. Forslind, *Acta Chem. Scand.*, **16**, 2069 (1962).

(6) J. C. Hindman, *J. Chem. Phys.*, **36**, 1000 (1962).

(7) R. E. Glick, W. E. Stewart, and K. C. Tewari, *ibid.*, **45**, 4049 (1966).

materials were those described in the preceding paper.⁸ In the mixed salt solutions the mole fraction of each salt was 0.500 ± 0.001 except in the case of Na/Cl, SO₄ where $X_{\text{NaCl}} = 0.5034$.

Results

Some representative water line shifts, from pure water as zero, for equimolar aqueous solutions of two salts are plotted against the total salt molality, m_t , in Figures 1-3. Corresponding data for the individual salts were presented in the preceding paper.⁸ Up-field shifts are negative. The fourfold internal referencing system (*vs.* CH₃CN, (CH₃)₂SO, *t*-C₄H₉OH, and (CH₃)₄N⁺) employed was that previously used and evaluated.⁸ The data were fitted to the following equation by the method of least squares; four sets

$$\delta_{\text{H}_2\text{O}} = am_t + bm_t^2 \quad (1)$$

of the coefficients a and b were thus obtained for each salt mixture. The mean standard errors of estimate

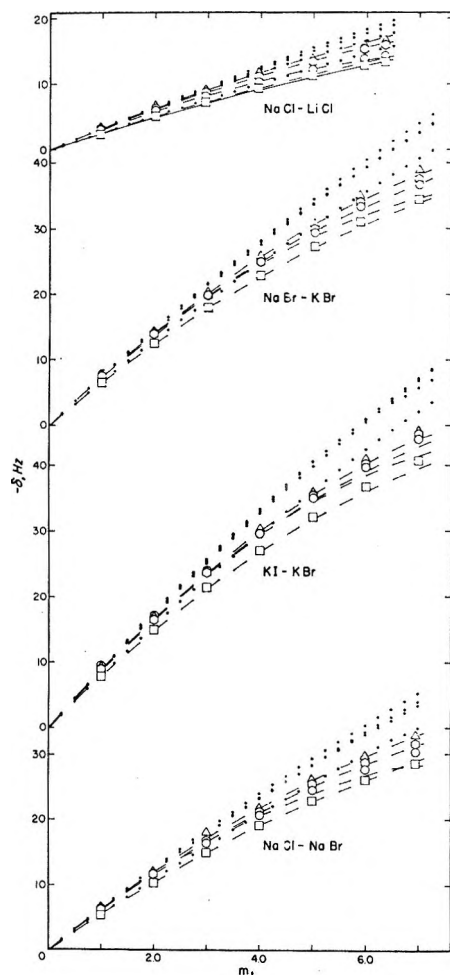


Figure 1. Water resonance shifts *vs.* total salt molality for equimolar mixtures of two salts with common ion, measured *vs.* four internal references: Δ , *vs.* CH₃CN; \circ , *vs.* (CH₃)₂SO; \circ , *vs.* (CH₃)₄N⁺; \square , *vs.* *t*-C₄H₉OH. Dotted lines: predicted shifts *via* eq 2. Dashed lines: predicted shifts *via* eq 3a. Solid line: predicted shift *via* Model II (*vs.* *t*-C₄H₉OH).

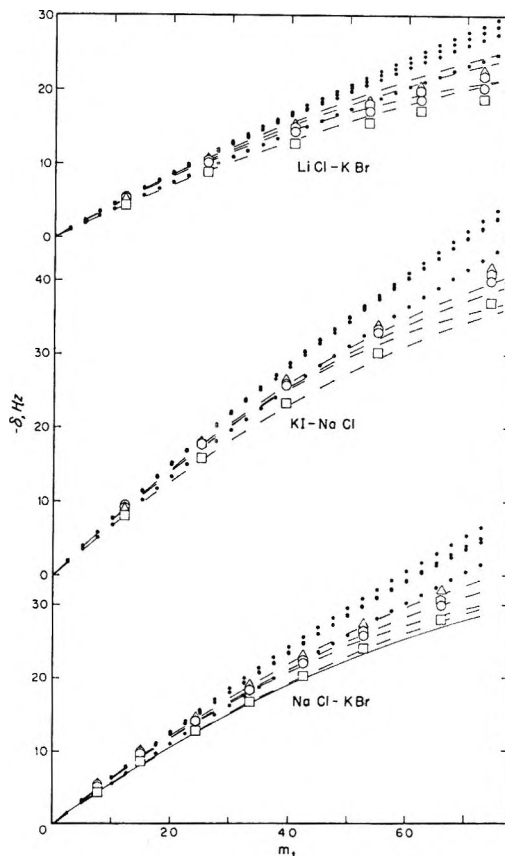


Figure 2. Water resonance shifts *vs.* total salt molality for equimolar mixtures of two salts without common ion, plotted as in Figure 1.

of δ were 0.07 (*vs.* CH₃CN), 0.08 (*vs.* (CH₃)₂SO), 0.06 (*vs.* *t*-C₄H₉OH), and 0.12 Hz (*vs.* (CH₃)₄N⁺), compared with an estimated precision of 0.06 Hz in a single measurement of δ . As with the pure salts, eq 1 is thus a very satisfactory representation of the data relative to the nonelectrolyte references, but noticeably less so with respect to (CH₃)₄N⁺ as internal reference.

Additivity Rules. The simplest possible additivity rule is eq 2, which combines contributions from the pure salt components evaluated at their individual concentrations in the mixture, $1/2m_t$, where m_t is the total molality. Shifts for the salt mixtures calculated

$$\delta_{\text{H}_2\text{O}} = 1/2(a_1 + a_2)m_t + 1/4(b_1 + b_2)m_t^2 \quad (2)$$

using eq 2 are shown as dotted lines in Figures 1 and 2.

A second approach⁹ evaluates pure salt contributions, per mole, at a total ionic concentration equal to that of the mixture. For an equimolar mixture of 1:1 electrolytes this leads to eq 3a, and for equimolar mixtures of 1:1 with 1:2 or 2:1 electrolytes, to eq 3b. Shifts for the mixtures of two 1:1 salts calculated using eq 3a

(8) J. E. Gordon and R. L. Thorne, *J. Phys. Chem.*, **73**, 3643 (1969).

(9) R. A. Robinson and V. E. Bower, *J. Res. Nat. Bur. Stand.*, **A**, 69, 365 (1965).

$$\delta_{\text{H}_2\text{O}} = 1/2(a_1 + a_2)m_t + 1/2(b_1 + b_2)m_t^2 \quad (3a)$$

$$\delta_{\text{H}_2\text{O}} = 1/2(a_{1.1} + a_{1.2})m_t + (5/8b_{1.1} + 5/12b_{1.2})m_t^2 \quad (3b)$$

are shown as dashed lines in Figures 1 and 2. Shifts for the 1:1-1:2 and 1:1-2:1 mixtures studied, calculated according to eq 3b, are shown in Figure 3.

Finally, the individual contributions to the mixture shift can be evaluated at an ionic strength equal to that of the mixture.⁹ This additivity rule again produces eq 3a for 1:1 electrolyte mixtures, but leads to eq 4 for equimolar 1:1-1:2 and 1:1-2:1 electrolyte mixtures.

$$\delta_{\text{H}_2\text{O}} = 1/2(a_{1.1} + a_{1.2})m_t + (b_{1.1} + 1/3b_{1.2})m_t^2 \quad (4)$$

All of the 1:1-1:1 electrolyte mixture shifts, excluding $(n\text{-C}_4\text{H}_9)_4\text{NBr}$ which we will consider later, are reasonably well accounted for by the total ionic concentration or ionic strength rule, eq 3a, but not by eq 2, which also gives a poor account of the 1:1-1:2 and 1:1-2:1 systems. In these cases the total ionic concentration (eq 3b) and ionic strength (eq 4) rules predict rather different behavior. The former is in better overall agreement with the observations (Figure 3 and Table IV).

The observed and calculated (eq 3a, 3b, 4) values of a and b are summarized in Tables I-IV. The reliability⁸ of the referencing system can be specifically demonstrated for the comparison of observed shifts for salt mixtures with those predicted from eq 2-4.

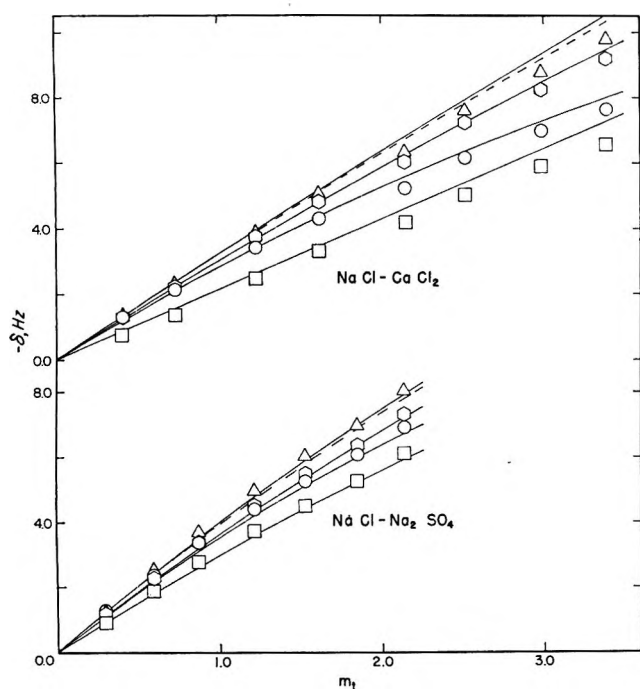


Figure 3. Water resonance shifts vs. total salt molality for mixtures involving divalent ions, measured vs. four internal references: Δ , vs. CH_3CN ; \circ , vs. $(\text{CH}_3)_2\text{SO}$; \circ , vs. $(\text{CH}_3)_4\text{N}^+$; \square , vs. $t\text{-C}_4\text{H}_9\text{OH}$. Solid lines: predicted shifts via eq 3b. Dashed lines: Predicted shifts via Model II.

First, the values of $b_{\text{calcd}} - b_{\text{obsd}}$ in Tables II-IV are generally identical, within experimental error, for each of the nonelectrolyte references.¹⁰ Second, we can use the correlations of the preceding paper⁸ to estimate the observed and calculated b values relative to external cyclohexane. For example, $b_{\text{calcd}} - b_{\text{obsd}}$ for NaCl-KBr becomes $0.197 - 0.189 = 0.008$ as compared with 0.011, the average vs. the three internal references.

Source of the Quadratic Term. Observation of a nonlinear δ -vs. m relation at low salt concentrations invalidates the original basis on which Shoolery and Alder discounted polarization of water molecules by more than one ion. We are thus obliged to develop the consequences of assuming that overlapping regions of influence of more than one ion are the source of the quadratic term in eq 1. In addition, conductance and other results now consistently point to ion association, to the extent of ca. 1% at 0.1 M , for alkali halides in water.¹¹⁻¹³ Using association constants from an extended conductance equation treating data up to 0.1 M , Chiu and Fuoss¹⁴ obtained ion pair contact distances near 6 Å for NaCl and KCl, indicating solvent separated ion pairs, $\text{C}^+\text{OH}_2\text{A}^-$. Assuming that the only water molecules appreciably influenced by the ion association are the ion-separating ones and those freed by desolvation, the effects of ion association will be included in and accounted for by any theory which accounts for the shifts of water molecules in the field of two ions.

The various sources of the quadratic term thus boil down to two: overlapping spheres of influence of two ions, including formation of solvent-separated ion pairs (Model I), and interaction between ion hydration and structure-breaking (Model II).¹⁵ We next compare the salt mixture data with the predictions of Models I and II.

Model I. The observed shifts in salt mixtures can be shown to be in agreement with Model I by showing the latter to correspond to additivity rule 3a (1:1-1:1 systems). If appropriate boundary conditions are used to divide the water molecules in a solution of salt C^+A^- into the classes bulk H_2O , H_2O in the field of C^+ only, H_2O in the field of A^- only, H_2O in the field of C^+ and A^- , etc., then the chemical shift of the water

(10) This is not so for solutions containing $\text{C}_6\text{H}_5\text{SO}_3^-$, in which case specific salt-reference interactions are present.⁸ The ionic reference $(\text{CH}_3)_4\text{N}^+$ has proved less reliable than the three nonelectrolyte references, and shifts measured relative to it are excluded from interpretations of the results.

(11) R. L. Kay, *J. Amer. Chem. Soc.*, **82**, 2099 (1960).

(12) R. M. Fuoss and K.-L. Hsia, *Proc. Natl. Acad. Sci.*, **57**, 1550 (1967); *J. Amer. Chem. Soc.*, **90**, 3055 (1968).

(13) E. Andalaft, R. P. T. Tomkins, and G. J. Janz, *Can. J. Chem.*, **46**, 2959 (1968).

(14) Y.-C. Chiu and R. M. Fuoss, *J. Phys. Chem.*, **72**, 4123 (1968).

(15) The nonlinear polarizability effect² can be operative only for molecules in the field of more than one ion; it is thus also subsumed in Model I.

Table I: Calculated^a and Observed Values of a for Salt Mixtures

Mixture	a			
	vs. CH ₃ CN	vs. (CH ₃) ₂ SO	vs. <i>t</i> -C ₄ H ₉ OH	vs. (CH ₃) ₄ N ⁺
NaCl-KBr				
a_{calcd}	-6.58 ± 0.03 ^b	-6.40 ± 0.02 ^b	-5.73 ± 0.02 ^b	-6.52 ± 0.05 ^b
a_{obsd}	-6.54 ± 0.03	-6.36 ± 0.04	-5.75 ± 0.02	-6.40 ± 0.08
NaCl-KI				
a_{calcd}	-7.87 ± 0.03	-7.80 ± 0.05	-6.98 ± 0.03	-8.02 ± 0.09
a_{obsd}	-7.82 ± 0.03	-7.76 ± 0.04	-6.97 ± 0.01	-7.83 ± 0.10
NaCl-NaBr				
a_{calcd}	-6.51 ± 0.03	-6.35 ± 0.03	-5.66 ± 0.02	-6.51 ± 0.05
a_{obsd}	-6.47 ± 0.02	-6.30 ± 0.02	-5.68 ± 0.03	-6.30 ± 0.05
LiCl-NaCl				
a_{calcd}	-3.36 ± 0.02	-3.27 ± 0.02	-2.65 ± 0.02	-3.26 ± 0.03
a_{obsd}	-3.46 ± 0.02	-3.35 ± 0.02	-2.78 ± 0.03	-3.22 ± 0.04
LiCl-KBr				
a_{calcd}	-4.54 ± 0.03	-4.46 ± 0.02	-3.78 ± 0.02	-4.50 ± 0.04
a_{obsd}	-4.51 ± 0.02	-4.43 ± 0.02	-3.82 ± 0.02	-4.43 ± 0.05
NaBr-KBr				
a_{calcd}	-7.69 ± 0.03	-7.54 ± 0.03	-6.78 ± 0.03	-7.75 ± 0.06
a_{obsd}	-7.65 ± 0.05	-7.49 ± 0.05	-6.79 ± 0.03	-7.58 ± 0.09
KBr-KI				
a_{calcd}	-9.05 ± 0.04	-8.99 ± 0.05	-8.11 ± 0.04	-9.26 ± 0.09
a_{obsd}	-8.97 ± 0.07	-8.89 ± 0.07	-8.07 ± 0.05	-9.03 ± 0.13
NaCl-CaCl ₂				
a_{calcd}	-3.26 ± 0.04	-3.17 ± 0.05	-2.15 ± 0.05	-3.02 ± 0.05
a_{obsd}	-3.24 ± 0.06	-3.16 ± 0.07	-2.06 ± 0.07	-2.94 ± 0.09
NaCl-Na ₂ SO ₄				
a_{calcd}	-4.23 ± 0.09	-3.85 ± 0.10	-3.18 ± 0.09	-3.86 ± 0.12
a_{obsd}	-4.50 ± 0.10	-4.10 ± 0.08	-3.32 ± 0.10	-4.17 ± 0.11
NaCl-Me ₄ NBr				
a_{calcd}	-5.00 ± 0.03	-4.80 ± 0.03	-4.15 ± 0.02	-5.10 ± 0.05
a_{obsd}	-4.98 ± 0.04	-4.88 ± 0.04	-4.17 ± 0.04	-5.37 ± 0.09
NaCl-Bu ₄ NBr				
a_{calcd}	-5.89 ± 0.06	-5.05 ± 0.08	-4.82 ± 0.04	-5.89 ± 0.05
a_{obsd}	-6.02 ± 0.10	-5.15 ± 0.06	-4.95 ± 0.06	-5.83 ± 0.07
KBr-Me ₄ NBr				
a_{calcd}	-6.18 ± 0.04	-5.99 ± 0.04	-5.27 ± 0.03	-6.34 ± 0.06
a_{obsd}	-6.18 ± 0.08	-6.01 ± 0.10	-5.24 ± 0.07	-6.45 ± 0.14
KBr-Bu ₄ NBr				
a_{calcd}	-7.07 ± 0.07	-6.24 ± 0.09	-5.94 ± 0.04	-7.13 ± 0.06
a_{obsd}	-7.11 ± 0.12	-6.02 ± 0.24	-6.04 ± 0.10	-7.18 ± 0.06
NaCl-C ₆ H ₅ SO ₃ Na				
a_{calcd}	-2.08 ± 0.06	-1.23 ± 0.08	-3.22 ± 0.11	+3.22 ± 0.30
a_{obsd}	-2.10 ± 0.09	-1.24 ± 0.08	-3.20 ± 0.08	+2.36 ± 0.23
Me ₄ NBr-C ₆ H ₅ SO ₃ Na				
a_{calcd}	-1.68 ± 0.07	-0.82 ± 0.08	-2.76 ± 0.11	+3.38 ± 0.30
a_{obsd}	-2.11 ± 0.05	-1.44 ± 0.03	-2.96 ± 0.04	+1.33 ± 0.18

^a Equations 2, 3a, 3b or 4: $a_{\text{calcd}} = 1/2(a_1 + a_2)$. ^b Precision measure is standard deviation.

relative to pure (bulk) water can be represented by

$$\delta_{\text{H}_2\text{O}}^{\text{C}^+\text{A}^-}_{\text{obsd}} = (t^{\text{C}^+} + t^{\text{A}^-})m_s + (t^{\text{C}^+\text{A}^-} + t^{\text{C}^+\text{C}^+} + t^{\text{A}^-\text{A}^-})m_s^2 \quad (5)$$

In eq 5, the first term on the right-hand side,

$t^{\text{C}^+\text{A}^-}m_s^2$, for example, has the form $\sum_i \delta_{\text{H}_2\text{O}_i}^{\text{C}^+\text{A}^-} \cdot X_{\text{H}_2\text{O}_i} = \sum_i \delta_{\text{H}_2\text{O}_i}^{\text{C}^+\text{A}^-} \cdot k_i \cdot m_s^2$ representing the product of chemical shift and water mole fraction summed over all configurations for waters interacting with one C⁺ and

Table II: Calculated^a and Observed Values of *b* for Mixtures of 1:1 Electrolytes with Common Ion

Salts	Reference	<i>b</i> _{obsd}	<i>b</i> _{calcd}	<i>b</i> _{calcd} - <i>b</i> _{obsd}
NaCl-NaBr	CH ₃ CN	0.252 ± 0.003 ^b	0.261 ± 0.007 ^b	0.009 ± 0.008 ^b
	(CH ₃) ₂ SO	0.256 ± 0.002	0.269 ± 0.007	0.014 ± 0.007
	<i>t</i> -C ₄ H ₉ OH	0.224 ± 0.005	0.220 ± 0.006	-0.004 ± 0.008
	(CH ₃) ₄ N ⁺	0.282 ± 0.007	0.341 ± 0.012	0.059 ± 0.014
KBr-KI	CH ₃ CN	0.361 ± 0.010	0.395 ± 0.007	0.034 ± 0.012
	(CH ₃) ₂ SO	0.367 ± 0.010	0.413 ± 0.010	0.047 ± 0.015
	<i>t</i> -C ₄ H ₉ OH	0.327 ± 0.008	0.352 ± 0.007	0.025 ± 0.011
	(CH ₃) ₄ N ⁺	0.405 ± 0.019	0.477 ± 0.019	0.072 ± 0.027
NaBr-KBr	CH ₃ CN	0.301 ± 0.007	0.318 ± 0.007	0.017 ± 0.010
	(CH ₃) ₂ SO	0.306 ± 0.007	0.330 ± 0.007	0.024 ± 0.010
	<i>t</i> -C ₄ H ₉ OH	0.270 ± 0.005	0.275 ± 0.006	0.005 ± 0.008
	(CH ₃) ₄ N ⁺	0.340 ± 0.014	0.399 ± 0.013	0.059 ± 0.019
NaCl-LiCl	CH ₃ CN	0.133 ± 0.003	0.105 ± 0.006	-0.028 ± 0.007
	(CH ₃) ₂ SO	0.133 ± 0.003	0.112 ± 0.004	-0.021 ± 0.005
	<i>t</i> -C ₄ H ₉ OH	0.104 ± 0.004	0.072 ± 0.005	-0.033 ± 0.006
	(CH ₃) ₄ N ⁺	0.155 ± 0.006	0.164 ± 0.007	0.008 ± 0.009
(CH ₃) ₄ NBr-KBr	CH ₃ CN	0.298 ± 0.021	0.310 ± 0.008	0.012 ± 0.022
	(CH ₃) ₂ SO	0.320 ± 0.026	0.322 ± 0.009	0.012 ± 0.027
	<i>t</i> -C ₄ H ₉ OH	0.257 ± 0.017	0.279 ± 0.006	0.022 ± 0.018
	(CH ₃) ₄ N ⁺	0.383 ± 0.037	0.380 ± 0.014	-0.003 ± 0.039
(C ₄ H ₉) ₄ NBr-KBr	CH ₃ CN	0.256 ± 0.042	-0.098 ± 0.044	-0.354 ± 0.061
	(CH ₃) ₂ SO	0.145 ± 0.083	-0.124 ± 0.061	-0.269 ± 0.103
	<i>t</i> -C ₄ H ₉ OH	0.272 ± 0.035	-0.050 ± 0.028	-0.322 ± 0.045
	(CH ₃) ₄ N ⁺	0.336 ± 0.021	0.079 ± 0.033	-0.257 ± 0.039
NaCl-C ₆ H ₅ SO ₃ Na	CH ₃ CN	0.532 ± 0.040	0.331 ± 0.056	-0.201 ± 0.069
	(CH ₃) ₂ SO	0.300 ± 0.035	-0.066 ± 0.068	-0.366 ± 0.077
	<i>t</i> -C ₄ H ₉ OH	0.499 ± 0.034	0.312 ± 0.098	-0.187 ± 0.103
	(CH ₃) ₄ N ⁺	-0.310 ± 0.101	-1.760 ± 0.270	-1.450 ± 0.288

^a From eq 3a. ^b Precision measure is the standard deviation.

one A⁻. Higher terms are neglected. The expression for a mixture of C⁺A₁⁻ and C⁺A₂⁻, each salt at concentration 1/2*m*_t (*m*_t = total salt molality), is eq 6. Application of additivity rule 3a to eq 5 written for C⁺A₁⁻ and for C⁺A₂⁻ gives eq 7

$$\delta_{\text{H}_2\text{O}}^{\text{mixt, obsd}} = 1/2(2t^{C^+} + t^{A_1^-} + t^{A_2^-})m_t + t^{C^+C^+}m_t^2 + 1/2(t^{C^+A_1^-} + t^{C^+A_2^-} + t^{A_1^-A_2^-})m_t^2 + 1/4(t^{A_1^-A_1^-} + t^{A_2^-A_2^-})m_t^2 \quad (6)$$

$$\delta_{\text{H}_2\text{O}}^{\text{mixt, calcd}} = 1/2(2t^{C^+} + t^{A_1^-} + t^{A_2^-})m_t + 1/2(t^{C^+A_1^-} + t^{C^+A_2^-} + 2t^{C^+C^+} + t^{A_1^-A_1^-} + t^{A_2^-A_2^-})m_t^2 \quad (7)$$

which becomes identical with eq 6 when

$$t^{A_1^-A_1^-} + t^{A_2^-A_2^-} = 2t^{A_1^-A_2^-} \quad (8)$$

Similarly, expressions for common-anion and reciprocal (C₁,C₂/A₁,A₂) systems can be obtained. For the latter, additivity rule 3a accounts for the terms in the salt mixture equation exactly if eq 9 holds in addition to eq 8 and its common-anion analog.

$$t^{C_1^+A_1^-} + t^{C_2^+A_2^-} = t^{C_1^+A_2^-} + t^{C_2^+A_1^-} \quad (9)$$

These approximations should be good ones if only electrostatic interactions are operating. In any case, the homoionic terms $t^{A_1^-A_2^-}$, $t^{C^+C^+}$, etc., should be small relative to the heteroionic ones, $t^{C^+A_1^-}$, etc., due to the greater anion-anion and cation-cation *vs.* cation-anion distances, so that eq 6 and 7 should approach identity even when (8) is imperfectly satisfied.

The agreement of the salt mixture shifts with Model I is thus represented to a good approximation by the dashed lines of Figures 1 and 2. Observed and calculated (eq 3a) *b* values agree within 0.01-0.04 (Tables II and III), excluding for the moment the systems involving (C₄H₉)₄N⁺. The largest deviation corresponds to the system with the greatest discrepancy in ion sizes, and the only systems with negative deviations are those involving Li⁺, the only ion studied which produces a net downfield shift.⁶ The observed deviations are reasonably identified with deviations from eq 8 and 9.

This means of testing Model I fails for mixtures involving 2:1 or 1:2 electrolytes, since a number of terms fail to cancel for equimolar mixtures, and no simple relationship analogous to eq 8 and 9 results.

Model II. Rearrangement of Hindman's expression⁶

Table III: Calculated^a and Observed Values of *b* for Mixtures of 1:1 Electrolytes without Common Ion

Salts	Reference	<i>b</i> _{obsd}	<i>b</i> _{calcd}	<i>b</i> _{calcd} - <i>b</i> _{obsd}
NaCl-KBr	CH ₃ CN	0.258 ± 0.005 ^b	0.273 ± 0.007 ^c	0.015 ± 0.009 ^b
	(CH ₃) ₂ SO	0.264 ± 0.006	0.281 ± 0.006	0.017 ± 0.009
	<i>t</i> -C ₄ H ₉ OH	0.231 ± 0.003	0.234 ± 0.005	0.002 ± 0.006
	(CH ₃) ₄ N ⁺	0.290 ± 0.012	0.332 ± 0.010	0.042 ± 0.016
NaCl-KI	CH ₃ CN	0.296 ± 0.004	0.337 ± 0.008	0.041 ± 0.009
	(CH ₃) ₂ SO	0.306 ± 0.006	0.353 ± 0.010	0.047 ± 0.012
	<i>t</i> -C ₄ H ₉ OH	0.267 ± 0.001	0.296 ± 0.007	0.029 ± 0.007
	(CH ₃) ₄ N ⁺	0.333 ± 0.014	0.419 ± 0.018	0.086 ± 0.023
LiCl-KBr	CH ₃ CN	0.196 ± 0.026	0.162 ± 0.006	-0.034 ± 0.027
	(CH ₃) ₂ SO	0.198 ± 0.003	0.172 ± 0.004	-0.026 ± 0.005
	<i>t</i> -C ₄ H ₉ OH	0.171 ± 0.003	0.127 ± 0.005	-0.044 ± 0.006
	(CH ₃) ₄ N ⁺	0.230 ± 0.008	0.222 ± 0.006	-0.008 ± 0.012
NaCl-(CH ₃) ₄ NBr	CH ₃ CN	0.222 ± 0.016	0.253 ± 0.008	0.031 ± 0.018
	(CH ₃) ₂ SO	0.276 ± 0.016	0.272 ± 0.008	-0.004 ± 0.018
	<i>t</i> -C ₄ H ₉ OH	0.203 ± 0.017	0.223 ± 0.006	0.021 ± 0.018
	(CH ₃) ₄ N ⁺	0.401 ± 0.041	0.322 ± 0.015	-0.079 ± 0.044
NaCl-(C ₄ H ₉) ₄ NBr	CH ₃ CN	0.166 ± 0.034	-0.156 ± 0.044	-0.322 ± 0.056
	(CH ₃) ₂ SO	0.099 ± 0.021	-0.185 ± 0.061	-0.284 ± 0.064
	<i>t</i> -C ₄ H ₉ OH	0.178 ± 0.022	-0.106 ± 0.028	-0.284 ± 0.035
	(CH ₃) ₄ N ⁺	0.183 ± 0.025	0.021 ± 0.035	-0.163 ± 0.041
(CH ₃) ₄ NBr-C ₆ H ₅ SO ₃ Na	CH ₃ CN	0.045 ± 0.018	0.368 ± 0.056	0.324 ± 0.059
	(CH ₃) ₂ SO	-0.071 ± 0.012	-0.014 ± 0.066	0.057 ± 0.070
	<i>t</i> -C ₄ H ₉ OH	0.175 ± 0.014	0.357 ± 0.097	0.182 ± 0.098
	(CH ₃) ₄ N ⁺	-0.626 ± 0.069	-1.708 ± 0.266	-1.082 ± 0.278

^a Equation 3a. ^b Precision measure is standard deviation.

Table IV: Calculated and Observed Values of *b* for Mixtures Involving Divalent Salts

Salts	Reference	<i>b</i> _{obsd}	<i>b</i> _{calcd} (eq 3b)	<i>s</i> ^a (eq 3b)	<i>b</i> _{calcd} (eq 4)	<i>s</i> ^a (eq 4)
NaCl-Na ₂ SO ₄	CH ₃ CN	0.356 ± 0.049 ^b	0.241	0.15	0.301	0.28
	(CH ₃) ₂ SO	0.326 ± 0.038	0.216	0.14	0.284	0.29
	<i>t</i> -C ₄ H ₉ OH	0.226 ± 0.047	0.189	0.13	0.240	0.26
	(CH ₃) ₄ N ⁺	0.459 ± 0.052	0.332	0.17	0.403	0.33
NaCl-CaCl ₂	CH ₃ CN	0.100 ± 0.019	0.046	0.46	0.144	0.24
	(CH ₃) ₂ SO	0.133 ± 0.022	0.095	0.17	0.186	0.47
	<i>t</i> -C ₄ H ₉ OH	0.029 ± 0.020	0.001	0.41	0.090	0.22
	(CH ₃) ₄ N ⁺	0.210 ± 0.027	0.193	0.31	0.292	0.38
			Σ = 1.94			Σ = 2.47

^a Divergence of the calculated line from the least-squares line through the observed points, expressed as standard deviation. ^b Standard deviation.

for the bond-breaking component of the shift gives eq 10 for the quadratic coefficient, *b*, in solutions of pure and mixed salts, where the shift is in ppm. In this equation, *n_i* is the structure-making or structure-

$$b = -4.05 \times 10^{-4} (\sum_i n_i) (\sum_i s_i) \quad (10)$$

breaking factor expressed as the number of moles of hydrogen bonds created per mole of salt, and the summation is over all ions. The ion solvation factor, *s_i* (= Hindman's *h_i/b_i*), is the moles of hydrogen bonds broken by ion hydration per mole of added salt. For

equimolar mixtures of two 1:1 electrolytes, C₁⁺, C₂⁺, A₁⁻, A₂⁻, the expression for the mixture shift according to Model II is eq 11 (tested in the followin

$$b^{\text{mixt}} = -\frac{4.05 \times 10^{-4}}{4} (n_{C_1} + n_{A_1} + n_{C_2} + n_{A_2}) \times (s_{C_1} + s_{A_1} + s_{C_2} + s_{A_2}) \quad (11)$$

way). Hindman's values of *s* were used in eq 11, together with observed *b* values, to compute $\sum n_i$ for each pure salt. The $\sum n_i$ values were used to compute

Table V: Shifts for Equimolar Salt Mixtures, Estimated According to Model II

Salt	Contributions to δ_{calcd}		Polarization	δ_{calcd}	δ_{obsd}
	Bond breaking due to hydration	Structure making			
NaCl ^a	-7.41 m + 0.178 m ²	-6.37 m	9.17 m	-4.61 m + 0.178 m ²	same
KBr ^a	-5.02 m + 0.289 m ²	-15.28 m	13.44 m	-6.86 m + 0.289 m ²	same
NaCl-KBr ^a	-6.12 m + 0.253 m ²	-10.83 m	11.30 m	-5.74 m + 0.253 m ²	-5.75 m + 0.231 m ²
LiCl ^a	-9.56 m - 0.035 m ²	+0.972 m	7.90 m	-0.69 m - 0.035 m ²	same
NaCl-LiCl ^a	-8.48 m + 0.086 m ²	-2.70 m	8.53 m	-2.65 m + 0.086 m ²	-2.78 m + 0.104 m ²
KI ^a	-5.02 m + 0.414 m ²	-21.90 m	17.56 m	-9.36 m + 0.414 m ²	same
KBr-KI ^a	-5.02 m + 0.351 m ²	-18.59 m	15.50 m	-8.11 m + 0.351 m ²	-8.07 m + 0.327 m ²
CaCl ₂ ^b	-12.66 m - 0.213 m ²	+4.47 m	7.07 m	-1.13 m - 0.213 m ²	same
CaCl ₂ -NaCl ^b	-10.04 m + 0.062 m ²	-1.64 m	8.41 m	-3.26 m + 0.062 m ²	-3.24 m + 0.100 m ²
Na ₂ SO ₄ ^b	-17.20 m + 0.255 m ²	+3.93 m	18.09 m	-3.04 m + 0.255 m ²	same
Na ₂ SO ₄ -NaCl ^b	-12.30 m + 0.271 m ²	-5.84 m	13.92 m	-4.22 m + 0.271 m ²	-4.50 m + 0.356 m ²
Bu ₄ NBr ^{a,c}	-2.15 m - 0.389 m ²	+48.03 m	-50.90 m	-5.02 m - 0.309 m ²	same
Bu ₄ NBr-NaCl ^{a,c}	-4.78 m - 0.375 m ²	20.83 m	-20.86 m	-4.81 m - 0.362 m ²	-4.95 m + 0.178 m ²

^a Internal reference: *t*-C₄H₉OH. ^b Internal reference: CH₃CN. ^c Hydration number = 0.9 (ref 16).

the contributions of the structure-breaking and ion solvation terms to the linear concentration term coefficient, *a*, using the expressions of Hindman. The polarization contribution to *a* was then determined by difference to make $a_{\text{calcd}} = a_{\text{obsd}}$ for each pure salt. The parameters thus chosen to reproduce the pure salt data exactly were then used in eq 11, and the appropriate expression for *a*, to predict the mixture shifts. The results of such calculations for six systems are shown in Table V. Very similar results are obtained if *s* values are taken from Glueckauf's¹⁶ hydration numbers rather than Hindman's. The calculated curves are shown as solid lines in Figures 1 and 2 for the systems LiCl-NaCl and NaCl-KBr. The computed curve for KBr-KI coincides with that of Model I, shown as a dashed line in Figure 1. All of these calculations are for shifts vs. *t*-butanol. Figure 3 shows the calculated curves for NaCl-CaCl₂ and NaCl-Na₂SO₄ as dashed lines (reference: CH₃CN).

Discussion

Comparison of the Models. Of the five systems compared, two sets of observations are better accounted for by Model I and two sets by Model II, while I and II give identical results for the fifth. The following further evaluations can be made.

Though Model I predicts reasonably well the relation of the salt mixture shifts to those of the pure salts, we cannot compute any of the terms in eq 6 or 7.

Model I corresponds to a reasonable physical picture. At ~1 M salt numerous C+H₂OH₂OH₂OA⁻ and C+H₂OH₂OA⁻¹⁷ and some C+H₂OA⁻¹⁴ structural situations are present. While the literature is divided on the extent of polarization of waters beyond the first hydration shell,¹⁸⁻²¹ the electrostatic influence of an ion thus needs to extend only barely beyond the first hydrate water to produce a quadratic contribution to $\delta_{\text{H}_2\text{O}}$. Furthermore, the enhanced acidity of the first

shell waters about the cation and the enhanced basicity of the first-shell waters about the anion²²⁻²⁴ result in enhanced hydrogen bonding capabilities²⁵ for these water molecules. Due to the cooperative nature of hydrogen-bond stabilization in such a chain,²⁶ the entire structure C+OH₂···OH₂···OH₂···A⁻ is stabilized relative to alternative H-bonding arrangements for these waters. There will be an extra downfield contribution to the chemical shift of the central water(s) which depends on both ions simultaneously and which is independent of whether or not this water is experiencing an appreciable electric field due to C⁺ and A⁻. The hydrogen bonding and field effects reinforce one another if both are present. On this basis, the heteroionic term, $t^{\text{C}^+\text{A}^-}$, in eq 5 will make a positive contribution to *b*. If the water structure in the instantaneous direction of neighboring counterions is thus enhanced, the structure-broken B region of Frank and Wen²⁷ must be concentrated in the instantaneous direction of the co-ions and/or in directions in which all ions are remote. The former is consistent with the fact that the hydrogen bridging roles of the terminal waters in

(16) E. Glueckauf, *Trans. Faraday Soc.*, **51**, 1235 (1955).

(17) R. M. Lawrence and R. F. Kruh, *J. Chem. Phys.*, **47**, 4758 (1967).

(18) R. A. Robinson and R. H. Stokes, "Electrolyte Solutions," Butterworth and Co., Ltd., London, 1965, p 20.

(19) J. L. Kavanau, "Water and Solute-Water Interactions," Holden-Day, Inc., San Francisco, 1964, p 30.

(20) H. S. Frank and M. W. Evans, *J. Chem. Phys.*, **13**, 507 (1945).

(21) J. A. Schellman, *ibid.*, **26**, 1225 (1957).

(22) R. A. Robinson and H. S. Harned, *Chem. Rev.*, **28**, 419 (1949).

(23) R. M. Diamond, *J. Amer. Chem. Soc.*, **80**, 4808 (1958).

(24) F. A. Long and R. L. Bergen, Jr., *J. Phys. Chem.*, **58**, 166 (1954);

F. A. Long and W. F. McDevit, *Chem. Rev.*, **51**, 119 (1952).

(25) J. E. Gordon, *J. Org. Chem.*, **26**, 738 (1961).

(26) H. S. Frank, *Proc. Roy. Soc.*, **247A**, 481 (1958).

(27) H. S. Frank and W.-Y. Wen, *Discussions Faraday Soc.*, **24**, 133 (1957).

$C^+H_2O(H_2O)_nH_2OC^+$ and $A^-H_2O(H_2O)_nH_2OA^-$ are opposed, *i.e.*, both enhanced as donors or as acceptors, thus destabilizing the water chain. One would thus expect the homo-ionic terms, $t^{C^+C^+}$ and $t^{A^-A^-}$, to have the same sign as t^{C^+} and t^{A^-} with a probable extra upfield (negative) contribution due to impoverishment of structure relative to pure water. Since the a values show $t^{C^+} + t^{A^-}$ to possess a net negative value, $t^{C^+C^+} + t^{A^-A^-}$ should be a negative contribution to b . Since the mean anion-anion and cation-cation distances are greater than the anion-cation distance, the hetero-ionic term, $t^{C^+A^-}$, should predominate, and b should be positive for most salts according to Model I. With the exception of $CaCl_2$ and Bu_4NBr , this is the experimental finding.

Model II does provide an explicit calculation of b for the salt mixtures, but the input data are presently so flexible that this is not a stringent test. For example, estimates of the fractions of non-, singly-, etc., H-bonded water molecules in pure water cover a very wide range.^{28,29} The assignments on which the only results³⁰ of this type for salt solutions are based have been questioned.³¹ The structural effects required to account for the observed quadratic terms are large. Table VI compares the values of Σn_i required to produce the observed values of b with some values estimated by Hindman⁶ and those calculated from the measurements of Choppin and Buijs.³⁰ Furthermore, the linear dependence of structure breaking on salt concentration assumed in the derivation of eq 7 cannot be tested at this time.

Table VI: Structure Alteration Parameters for Eq 10

Salt	Σn_i required in eq 10	Σn_i (ref 6)	Σn_i (ref 30)
LiCl	-0.64	+0.5	-0.36
NaCl	-2.20	-0.6	-1.92
NaBr	-2.76	-1.2	
KBr	-4.76	-1.2	-2.64
KI	-5.53	-1.5	-3.48

Model II, as applied to the calculation of b above, yields downfield polarization contributions which increase with increasing ion size (Table V) contrary to expectation.

Model II does give a qualitative physical explanation of the negative b observed^{6,8} for Mg^{2+} and Ca^{2+} salts and the near-zero values of b observed^{6,8} for some Li^+ and F^- salts *vs.* the positive values for the remaining alkali halides. This follows from eq 10 where Σn_i is negative for net structure-breaking and positive for net structure-making salts. Thus the strong structure-making Mg^{2+} and Ca^{2+} salts should have negative values of b , and a crossover region of $\Sigma n_i = b = 0$ should be observed with salts composed of a weakly

structure-making (Li^+ or F^-) and a structure-breaking (Cl^- or K^+) ion. Indeed, there should be a general tendency of b to become more positive with increased structure-breaking character of the salt, and the observed order⁸ corresponds fairly well to this expectation: $Bu_4NBr < CaCl_2 < LiCl < NaCl < Na_2SO_4 < Me_4NBr < NaBr < KBr < KI$.

Behavior of the Quaternary Ammonium Salts. Both models substantially overestimate the shifts for mixtures involving $(C_4H_9)_4NBr$ (Tables II and III). The deviations from Model I are an order of magnitude greater than those for any other mixtures studied. On the other hand, the corresponding systems involving $(CH_3)_4NBr$ are quite as accurately accounted for as any of the alkali halide mixtures. This divergence of solution behavior for these R_4N^+ salts shows up in many properties,^{32,33} including the water shifts observed in solutions of the pure R_4NBr . While the $(CH_3)_4NBr$ shifts have the form of the alkali halide shifts, those for $(C_4H_9)_4NBr$ display a large negative value of b at lower concentrations and an inflection between 1 and 1.5 *m* salt.⁸ This inflection may be connected with a minimum in the partial molal volume of the salt observed by Wen and Saito³³ near 0.85 and 0.9 *m* at 25 and 35°. The region below the minimum is believed³³ to correspond to packing of ions together in clathrate hydrate-like cages. Wen and Nara,³⁴ by applying Friedman's ionic solution theory to measurements of the volume change on mixing $(C_4H_9)_4NBr$ and KBr solutions, were able to show that strong, volume-reducing $(C_4H_9)_4N^+ \cdots (C_4H_9)_4N^+$ interactions are involved in the low concentration range.

The large negative value of b for pure $(C_4H_9)_4NBr$ suggests identification with the term $t^{C^+C^+}$ in eq 5. If nonelectrostatic forces, *e.g.*, hydration of the second kind,³⁵ make $t^{Bu_4N^+Bu_4N^+}$ large and negative, it is likely that $t^{Bu_4N^+Bu_4N^+} + t^{K^+K^+} < 2t^{Bu_4N^+K^+}$ so that b_{obsd} would be more positive than b_{calcd} (common-cation analogs of eq 6 and 7) as observed in Table V. The unusually large upfield shift for water in the situation $Bu_4N^+ \cdots (H_2O)_n \cdots Bu_4N^+$ (large negative $t^{C^+C^+}$) is analogous to that for $Bu_4N^+ \cdots H_2O$, *i.e.*, large negative t^{C^+} leading to large negative a for pure $(C_4H_9)_4NBr$. These upfield shifts are in the direction of hydrogen-bond breaking and are puzzling because thermodynamic evidence and relaxation times, on the other hand, indicate increased water structure surrounding R_4N^+ .³⁶

(28) D. P. Stevenson, *J. Phys. Chem.*, **69**, 2145 (1965).

(29) Z. Luz and C. Yagil, *ibid.*, **70**, 554 (1966).

(30) G. R. Choppin and K. Buijs, *J. Chem. Phys.*, **39**, 2042 (1963).

(31) D. F. Hornig, *ibid.*, **40**, 3119 (1964).

(32) R. L. Kay and D. F. Evans, *J. Phys. Chem.*, **70**, 2325 (1966).

(33) W.-Y. Wen and S. Saito, *ibid.*, **68**, 2639 (1964).

(34) W.-Y. Wen and K. Nara, *ibid.*, **71**, 3907 (1967).

(35) H. G. Hertz, *Ber. Bunsenges. Phys. Chem.*, **68**, 907 (1964).

(36) H. S. Frank, *Federation Proc.*, **24**, S-1 (1965).

Hertz's³⁵ conclusion is that the structure increase corresponds to a sharpening of maxima in orientational distribution functions which is consistent with simultaneous breaking of hydrogen bridges. Frank³⁶ suspects that the correlation of downfield pmr shift with hydrogen-bond formation may not be indiscriminately applicable in aqueous solutions—that a net upfield shift may occur despite concomitant increase in hydrogen bonding, due to intrusion of other, yet unknown effects on the shielding. Table V shows what the magnitude of these effects would have to be if Model II applies.

The residual contribution to $\delta_{\text{H}_2\text{O}}$, after accounting for bond breaking to hydrate Br^- with $0.9 \text{ H}_2\text{O}^{16}$ and structure making (determined from *b*) is -69.41 m Hz (upfield). This would include any downfield (positive) contribution from polarization by Br^- and the upfield shift of unknown origin. Clearly, the latter would be an extremely large effect.

Acknowledgments. Financial support from the National Science Foundation is gratefully acknowledged. The authors thank Dr. James C. Hindman for helpful comments on this work.

The Calculation of Madelung Potentials for Faujasite-Type Zeolites. I

by E. Dempsey

Mobil Research and Development Corporation, Research Department, Central Research Division, Princeton, New Jersey 08540 (Received December 13, 1968)

Using the assumption of complete ionicity, Madelung potentials for the ions in ordered models of X and Y faujasites have been calculated for various cation sizes, valencies, and distributions. For monovalent zeolites the results of the calculations agree well with ionic distributions found from X-ray studies. For divalent zeolites divergences between the results of the calculations and ionic distributions derived from crystallographic studies are explained on the basis that the materials used for the X-ray diffraction work retained a small amount of water.

Introduction

In recent years there has been a great deal of effort directed toward acquiring an understanding of the structure, nature, and properties of zeolites. It has been suggested that cations that are accessible to molecules entering the rather open structure of many zeolites may play a direct or indirect role in the catalytic behavior of the materials, and there has been considerable speculation about this.¹⁻³

Calculations have shown that, for divalent cations in zeolites having the faujasite structure, there are correlations between field strengths in the vicinity of exchangeable cations in exposed sites and absorption energies for various molecules.⁴ These field strengths are sufficiently high (that is, the cations are sufficiently unshielded by the surrounding crystal) that changes in the ionic distributions should not have very large effects upon the magnitudes of the fields. On the other hand, for detailed comparisons of the relative behaviors of different zeolites, it is important to base the calculations upon models that are as reliable in their details as possible.

Unfortunately, a great deal of doubt remains about even the nature of the distribution of ions in zeolites.

In many cases the relative distributions of the silicon and aluminum ions in the regular framework structure of the zeolites is not known, nor do we have a clear idea of the extent to which the bonding in zeolites is ionic. Recent work on faujasite materials^{5,6} does suggest that these materials have a tendency to adopt different forms of ordering depending on their Si:Al ratio; because some aspects of this ordering may be predicted from ionic models of the materials, this latter work also gives justification for emphasizing the ionicity of zeolites.

In any case, the importance of the assumption of ionic bonding can be minimized; so long as we make comparisons between zeolites having the same general structure, with only the silicon:aluminum ratio or

- (1) P. E. Pickert, J. A. Rabo, E. Dempsey, and V. Schomaker, *Actes Congr. Intern. Catalyse, 3^e, Amsterdam, 1964*, 714 (1965).
- (2) P. B. Venuto and P. S. Landis, *Advan. Catal.*, **18**, 259 (1968).
- (3) J. W. Ward, *J. Catal.*, **10**, 34 (1968).
- (4) E. Dempsey in "Molecular Sieves," Society of Chemical Industry, London, 1968, p 293.
- (5) E. Dempsey, G. H. Kuehl, and D. H. Olson, *J. Phys. Chem.*, **73**, 387 (1969).
- (6) D. H. Olson and E. Dempsey, *J. Catal.*, **13**, 221 (1969).

the cation type (excluding hydrogen) varying, we may assume that all faujasites, say, have the same degree of covalency in their bonding and that the behavior of one crystal relative to others may be correctly inferred from ionic models.

Similarly, we may, if necessary, minimize the importance of the assumption of silicon-aluminum ion order in zeolites. In the first place, since the silicon and aluminum ions are different, there must be a tendency for the ions to order at least in a short-range way (indeed, Lowenstein's rule precludes two Al ions being near neighbors separated by only one oxygen ion). In the calculation of fields in zeolites the relatively near vicinity of a given cation gives the major field contributions, and summations over greater distances from the cation in question should be served equally well by assuming ordered or disordered models. Secondly, calculations on faujasite materials have shown that, for a given silicon:aluminum ratio, variations in the nature of the assumed order of silicon and aluminum ions make only small differences to the fields near relatively unshielded cations.

Of greater concern, from the point of view of setting up theoretical models of zeolites, is any inadequacy in our knowledge of the distribution of exchangeable cations in zeolites and of the effect on this distribution of the presence of residual water in the materials. X-Ray structural investigations have already given a considerable amount of information on zeolitic cation distributions^{7,8} and should be very fruitful as larger synthetic zeolite crystals become available.⁹ Other techniques (electron paramagnetic resonance¹⁰ and infrared¹¹ and optical spectroscopy) are also proving to be valuable supplementary tools for structural and bonding investigations on zeolites.

In the hope of shedding further light on the possibilities for cation distributions in zeolites, calculations of "Madelung constants," or reduced ionic potentials,¹² in a range of faujasite materials, have been made. Although these relate to idealized models and have neglected dipole effects (which have been shown⁴ to be important), the calculations should be useful as a basis for the discussion of real faujasites.

Models. The structure of faujasite-type zeolites is well known and has often been described. Essentially, the structure, like that of all zeolites, is built of tetrahedrally arranged groups of four oxygen ions about silicon or aluminum ions. Each oxygen ion is shared by two positive ions, which may be silicon or aluminum, with the proviso that no two aluminum ions should be near neighbors separated by only one oxygen ion. The silicon and aluminum tetrahedra build, for the faujasite structure, into so-called sodalite units; these contain 24 tetrahedra each, and stack together tetrahedrally to form an f.c.c diamond lattice, with each carbon site occupied by a sodalite unit. Between

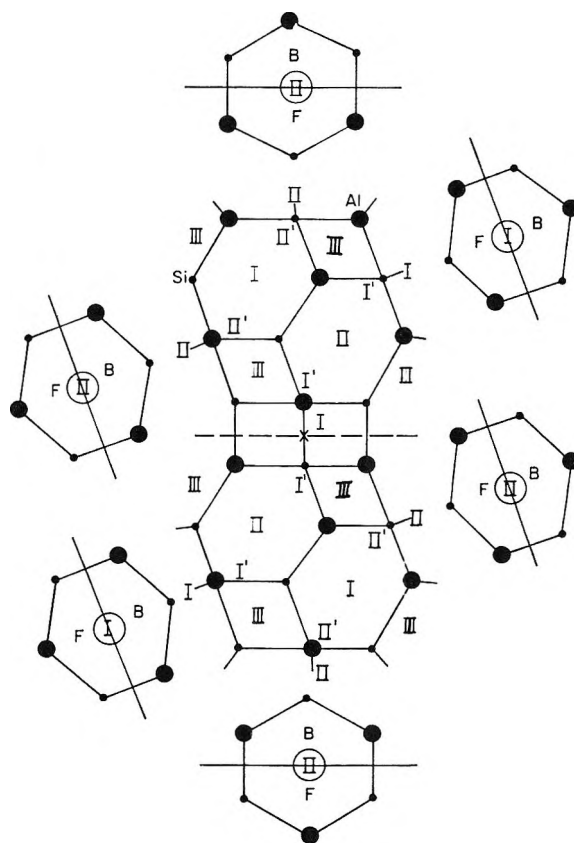


Figure 1. Exchangeable cation sites in a faujasite double sodalite unit. Site I lies at centers of hexagonal prisms, site II on outsides of free hexagonal faces, sites I' and II' opposite sites I and II through relevant hexagonal faces, within sodalite cages, site III on outer sites of square faces. All sites other than sites III lie on nominally three-fold axes.

each pair of sodalite units is a hexagonal prism (see Figure 1).

Associated with each AlO_2 group there is a net negative charge of unity (in units of electronic charge, e). These negative charges are compensated in the structure by the exchangeable cations, which take up positions in the structure dependent on the Si:Al ratio, the state of hydration of the zeolite, and the size and valence of the ions.

When this work was begun, relatively little information was available on the distribution of cations in faujasite structures, and none at all was available on the possible ordering of the silicon and aluminum ions relative to each other. In order to set up models suitable for calculation it was necessary to make up

(7) G. R. Eulenberger, D. P. Shoemaker, and J. G. Keil, *J. Phys. Chem.*, **71**, 1812 (1967).

(8) D. H. Olson, *ibid.*, **72**, 1400 (1968).

(9) J. Ciric, *Science*, **155**, 689 (1967).

(10) T. I. Barry and L. A. Lay, *J. Phys. Chem. Solids*, **29**, 1395 (1968).

(11) For a brief review: D. J. C. Yates, *Catal. Rev.*, **2**, 113 (1968).

(12) "Reduced" in that the potentials are calculated in units in which electronic charge and the crystal lattice parameter are unity.

this lack of information. The way in which this was done is described in ref 4. Essentially, it was arranged that the zeolite should be built of identical pairs of sodalite units (with the silicon and aluminum ions ordered relative to each other) placed at the points of an f.c.c. lattice, and that these units should have zero net charge and dipole moment. These criteria, along with the requirement of nonadjacent aluminum tetrahedra and minimum total electrostatic energy, were adequate to define all of the models used in ref 4 and in this paper.

As a basis for the calculations the X-ray coordinates found by R. P. Dodge¹³ for natural crystals of faujasite containing either sodium or calcium ions were used. Dodge's results and those of Olson indicate that, for site II ions (see Figure 1), the sum of the Pauling radii for the cations and the adjacent oxygen ions is close to the observed ion separation. This justified our placing larger cations in the zeolites by geometry using Pauling radii for the cations. Thus Dodge's coordinates were used mainly to determine the positions of the framework Al, Si, and O ions.

Figure 1 illustrates the cation site designation. This represents a projection onto a plane of the ions in an idealized double sodalite unit (having Si:Al = 1:1), with a center of symmetry at X. Oxygen ions are not shown; these lie near the centers of lines joining adjacent large and small dark points (representing aluminum and silicon ions, respectively). Sites I and II hexagonal rings, seen edge-on in the main figure, are also shown projected from the main figure; in these, B and F denote back and front, respectively. Site I is at the center of a hexagonal prism at a position of inversion symmetry. Site I' is on the inside of the sodalite cage opposite site I. Site II is on the large cavity side of the free hexagonal faces of the sodalite unit, while site II' is within the sodalite cage opposite site II. All of these sites lie on nominally threefold symmetry axes. For the monovalent zeolites the above sites are not sufficient to accommodate all of the cations necessary for charge balance; the remaining cations are placed in sites III on the outsides of the square faces of sodalite cages.

Form of the Calculations. The calculation of potentials in ionic crystals is not straightforward. Not only does the simple form

$$\varphi = \sum_i \frac{q_i}{r_i} \quad (1)$$

(q_i = charge on ion i distance r_i from potential point) converge very slowly, it has the more serious drawback of being only conditionally convergent. In the literature various transformations may be found which, applied to eq 1, produce equivalent absolutely convergent series that converge rapidly. For the calculations given below we have used the method of Ewald.

Since Ewald's method has been adequately described elsewhere,^{14,15} we give merely the final equation in the form in which we have applied the method to zeolite calculations

$$\varphi_T = \frac{4\pi}{\Delta} \sum_{\vec{G}} S(\vec{G}) G^{-2} e^{i\vec{G} \cdot \vec{r} - G^2/4\eta} + \sum_t \sum_l \frac{q_t}{r_{t,l}} F(\eta^{1/2} r_{t,l}) - 2q_T \left(\frac{\eta}{\pi}\right)^{1/2} \quad (2)$$

where

$$S(G) = \sum_t q_t e^{-i\vec{G} \cdot \vec{r}_t}; F(x) = \int_x^\infty e^{-s^2} ds \quad (3)$$

Here φ_T is the potential required at ion T in the basis at the origin of coordinates. The first summation for φ_T is in reciprocal space, \vec{G} being a reciprocal lattice vector times 2π . \vec{r} is the vector from the origin to ion T and η is a parameter by means of which the rates of convergence of the two series may be adjusted: η arises from the method of setting up the problem; physically, it represents the width parameter of a variable Gaussian charge distribution. The second summation is taken over real space. q_t is the charge on ion t in the crystallographic basis placed at the lattice point l , distance $r_{t,l}$ from the origin. F is the error-function complement and $S(\vec{G})$ is related to the X-ray structure factor. Δ is a volume element in the crystal.

At this point it is well to remember the complex nature of zeolite crystals compared to the simpler ionic structures to which eq 2 is more usually applied. The zeolites under discussion, for instance, contain between 600 and 700 ions in their unit cells, the unit cells being close to 25 Å on a cell edge. In the calculations described below, every ion in the structure is taken into account and is given its full ionic charge (Al⁺³, Si⁺⁴, O²⁻, Na⁺, etc.). Since the calculations involved varying the size, number, and positions of exchangeable cations in the structure, it was important to write our computer programs in a way that would facilitate modifications of this nature as well as variations in the silicon:aluminum ratio. This is described briefly in the next section.

Form of the Computer Programs. In ref 4 it is described how a particular silicon-aluminum ion distribution for the 2:1 faujasite was determined as being the most probable one of the alternatives available. For all of our calculations, this ratio and the idealized 1:1 ratio were taken to be basic; the first data card read informs the computer that a monovalent or di-

(13) R. P. Dodge, private communication. See also P. H. Kasai, *J. Chem. Phys.*, **43**, 3322 (1965).

(14) P. P. Ewald, *Ann. Phys.*, **64**, 253 (1921).

(15) C. Kittel, "Introduction to Solid State Physics," John Wiley & Sons, Inc., New York, N. Y., 1956, p 571.

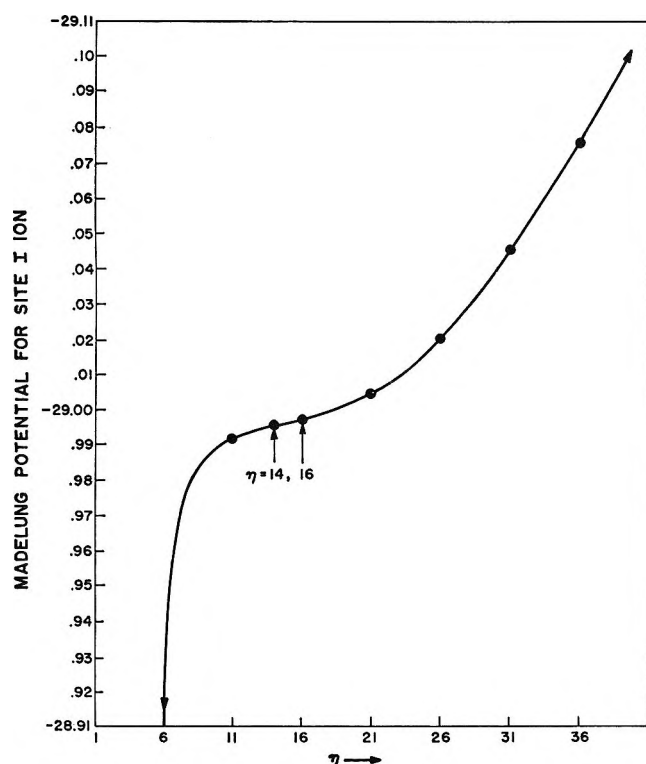


Figure 2. Variation of potential at site I as function of Gaussian width parameter η , in eq 2.

valent zeolite¹⁶ is to be set up having either the standard 1:1 or 2:1 Si:Al ratio. Using this information, the symmetry operations for the structure, and the appropriate X-ray coordinates for the silicon, aluminum, and oxygen ions, the computer sets up a full crystallographic basis (excluding the cations); this involves labeling and assigning coordinates and charges for 144 ions. Subsequently, the computer will modify the charges on ions specified, according to the next data card read, in order to move away from the 1:1 or 2:1 ratio if this is required. The computer next reads the valence and size of the cation to be placed in the zeolite and generates the coordinates for this ion in sites I, I', II, II', and III, as appropriate. It then places the correct number of cations in standard site positions in the basis using the crystal symmetry operations. Finally, the ion positions can be modified by reading additional data cards.

At this point, having set up a basis defining the zeolite, the master program directs the computer into the calculation of fields, Madelung potentials, potentials for points not occupied by ions, dipole moments, field gradients, etc., as required. In each calculation, the basis described above is placed at each lattice point included in the summations.

Calculations and Results

To test the program, Madelung constants were calculated for structures having f.c.c. lattices. This involved replacing the part of the computer program

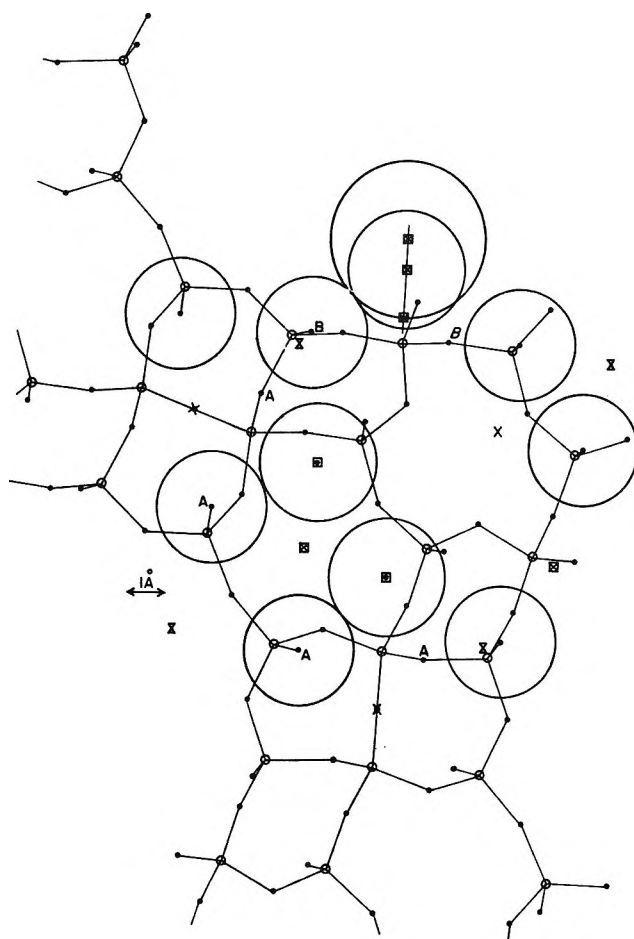


Figure 3. Zeolite structure drawn from X-ray coordinates. X, site I; \square , site I'; \square , site II; \square , site III; O, Al or Si; \bullet , oxygen. Large circles represent cations of radius 1.5 and 2.0 Å sitting on appropriate oxygen ions, A or B, in sites I' and II for the 1.5 Å cation, and in site II for the 2.0 Å cation. Seven oxygen ions in the plane of the cations are also shown as circles—radius 1.4 Å.

that set up the zeolite basis by alternative programs that set up, instead, various forms of the bases for NaCl and CsCl. It was found that the program calculated the Madelung constants for these crystals to any accuracy required, depending upon the value of η —which was left variable in the program.

In order to find the optimum value of η for the zeolite calculations, the Madelung potential for an ion in site I in Ca 1:1 was computed for a range of η values, with the series in eq 2 terminated at appropriate points, as shown in Figure 2. From this figure it is clear that a value for η of about 14 optimizes the convergence of the calculation.¹⁷ This value was used in all of the work described in the sequel.

(16) Zeolites containing monovalent and divalent cations will be referred to as monovalent and divalent zeolites, respectively.

(17) At the extremes of the curve, one or the other of the series of eq 2 converges badly: at the turning point both series converge well. In general the series were terminated so as to give at least 0.5% reliability in potential values.

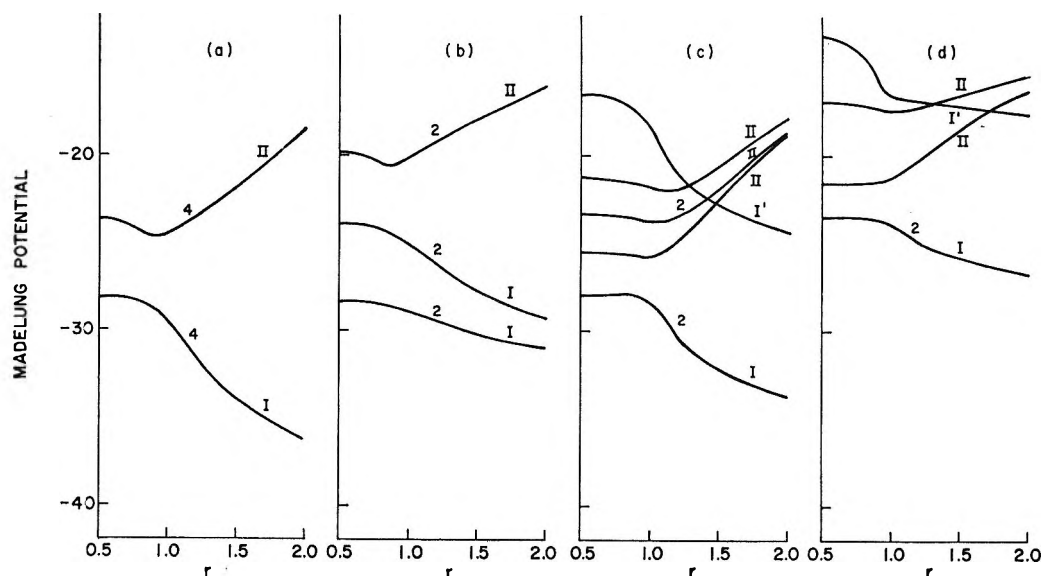


Figure 4. Potential curves for (a) divalent X (1:1) zeolite as functions of cation size. Sites I and II 100% occupied; (b) divalent Y (2:1) zeolite: sites I—100%, sites II—50% occupied; (c) divalent X (1:1) zeolite: sites I—50%, sites II—100%, sites I'—25% occupied; (d) divalent Y (1:1) zeolite: sites I—50%, sites II—50%, sites I'—25% occupied. r is cation radius in Å.

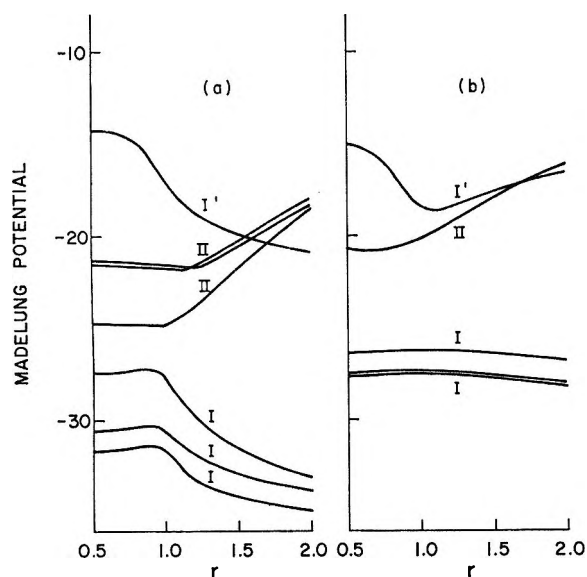


Figure 5. Potential curves for (a) divalent X (1.18:1) zeolite: sites I—75%, sites II—75%, sites I'—25% occupied; (b) divalent Y (2.43:1) zeolite: sites I—75%, sites II—25%, sites I'—25% occupied. r is cation radius in Å.

The main sequence of results is shown in Figures 4–7. In these the Madelung potentials for distinct ions in one sodalite cage are shown as functions of the cation radius. Roman numerals on the curves indicate the site labeling: arabic numerals indicate the number of equivalent sites represented by each curve: curves with no arabic numeral represent only one ion site each. Since the models deal only with spherically symmetrical ions, the size of the ion in site I is irrelevant; this ion always lies with its center at the inversion center of the hexagonal prism regardless

of its size.^{18,19} In cases where the radius of the cation appears to exceed the available space within the hexagonal prism, we may assume, without loss of generality, that the ion in site I is smaller than the ions placed at positions having symmetry lower than that of site I.

Figure 3 illustrates the fact that our procedure of placing ions in site I' by setting them on the oxygen ions labeled A does not interfere with other oxygen ions or cations in the sodalite cage: the ions shown in the sodalite cage have a radius of 1.5 Å. Oxygen ions in a [110] plane through the center of a sodalite cage are shown with radii of 1.4 Å.

The basic set of four graphs—Figures 4a,b; 6a, b—gives plots of the variation of Madelung potential *vs.* cation radius, r , for our standard divalent and monovalent 1:1 and 2:1 models. In these the site filling goes as follows: site I is filled first, to 100% occupancy; site II is filled next, to the extent that ions are available—this depends upon the silicon:aluminum ratio. Any (monovalent) ions remaining are then placed in sites III. It should be noted here that in our models there are always just as many square faces carrying two Al ions in the sodalite units as there are monovalent ions to be accommodated in sites III.

The next set of six graphs, *i.e.*, Figures 4c,d; 5 and 6c,d, illustrates the effect on the Madelung potentials, for the ions associated with a sodalite cage,

(18) More recent X-ray data of Olson¹⁹ have shown that the zeolite framework structure adjusts to accommodate ions of different sizes; the ions of the hexagonal prisms and site II six-rings move together to hold small cations. In particular, as is also clear from an electrostatic argument, cations never lie in the same plane as their three nearest-neighbor oxygen ions, although it is sometimes necessary to assume this for lack of better framework parameters.

(19) D. H. Olson, *J. Phys. Chem.*, **72**, 4366 (1968).

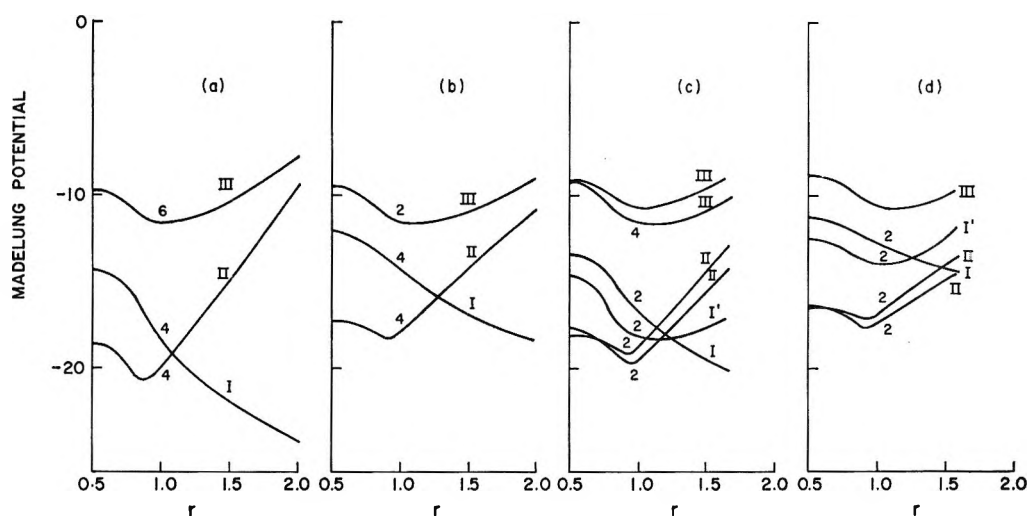


Figure 6. Potential curves for (a) monovalent X (1:1) zeolite: sites I, II, III—100% occupied; (b) monovalent Y (2:1) zeolite: sites I, II—100%, sites III—33.3% occupied; (c) monovalent X (1:1) zeolite: sites I, I'—50%, sites II—100%, sites III—83.3% occupied; (d) monovalent Y (2:1) zeolite: sites I, I'—50%, sites II—100%, sites III—16.7% occupied. r is cation radius in Å.

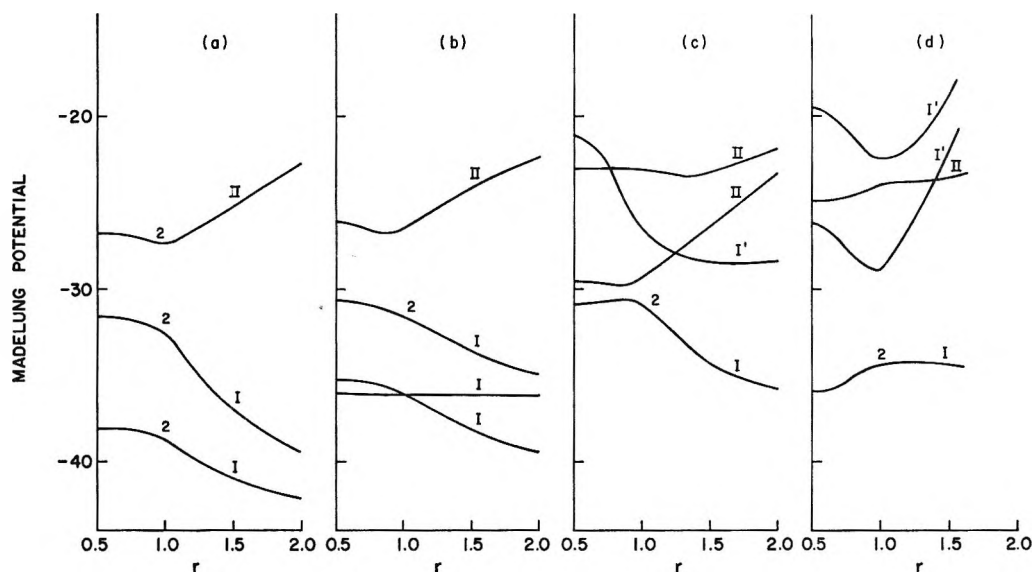


Figure 7. Potential curves for (a) trivalent X (1:1) zeolite: sites I—100%, sites II—50% occupied; (b) trivalent X (1.67:1) zeolite: sites I—100%, sites II—25% occupied; (c) trivalent X (1:1) zeolite: sites I, II—50%, sites I'—25% occupied; (d) trivalent X (1:1) zeolite: sites I, I'—50%, sites II—25% occupied. r is cation radius in Å.

of moving some of the ions to positions within the sodalite cage, and, more particularly, of moving them into site I' positions. In order to limit the number of computations to be carried out, we view the transfer of ions into sites I' as follows, starting from the standard distributions for which Figures 4a,b; 6a,b were calculated. We assume that adjacent sites I and I' cannot simultaneously be occupied, so that a site I' is occupied partially at the expense of its adjacent site I. Formally, for monovalent zeolites, since each site I is shared by two sodalite cages, we move the four halves of two site I ions into their four adjacent site I' positions (Figure 1). For each sodalite cage we then use one site III ion, split into two, to make

up the full ions in the two occupied sites I' per sodalite cage—(Figures 6c,d). Site III ions are used because these have the highest potential energy in the standard configurations corresponding to Figures 6a and 6b.

For divalent zeolites we fill one site I' per sodalite cage, at the expense of the adjacent, and one other, site I, to produce Figures 4c,d. Alternatively, we may occupy one site I' per sodalite cage, emptying the adjacent site I. This is most conveniently done for zeolites having Si:Al ratios of 1.18 and 2.43 rather than 1:1 and 2:1. These ratios have, respectively, 11 and 7 positive charges per sodalite cage, which permits us to fill three sites I, one site I', and three and one sites II, respectively; the odd numbers of

Table I: Total Cation E.S. Energy per Sodalite Cage for Various Cation Arrangements^a (Reduced Units)

Cation radius, Å	Me ⁺				Me ²⁺			
	X-6a	X-6c	Y-6b	Y-6d	X-4a	X-4c	Y-4b	Y-4d
0.5	-162	-160	-112	-111	-151	-139	-92	-75
1.0	-186	-186	-123	-120	-157	-142	-94	-79
1.5	-168	-166	-112	-107	-155	-141	-94	-78
2.0	-133	...	-98	...	-148	-132	-92	-76

^a Columns are labeled to correspond to the figures in the text.

charges per sodalite cage are important here. The results for these models are shown in Figure 5.

Finally, Figures 7a,b,c,d give results for zeolites containing trivalent ions. Figures 7a and 7b are for standard configurations with all sites I filled, accounting for two ions or a total charge of +6 per sodalite cage. For 1:1 zeolites (Figure 7a), two more ions per sodalite cage have to be accommodated, and these have been put into sites II. For the 1.67:1 case (Figure 7b) one more ion has to be placed, and this also goes into a site II. For comparison with Figure 7a, Figures 7c and 7d give the reduced potentials for 1:1 zeolites for situations with first one and then two ions removed from site I, and from sites I and II, and placed in site I'.

Discussion

A problem that presents itself in the discussion of curves relating crystal energies to changing physical conditions within a crystal (changing ionic content, or position, for instance) is that the whole energetic situation (involving all ions) changes when small changes are made in the circumstances of a few ions. As an aid to discussing the overall situation in the crystals represented by Figures 4-7 we look for similarities between different sets of curves; that is, we look for relationships that persist as the physical situation changes.

The simplest set of curves is that for faujasites containing divalent cations (Figures 4 and 5). In these we see that the general behavior of the fully symmetrical divalent X material, with all cations in sites I or II (Figure 4a), carries over qualitatively into the other cases; cations in sites I are more strongly held than are cations in sites II; and the stability of the site I cations relative to that of the site II cations increases as the size of the cation increases. The divalent Y case (Figure 4b) shows a splitting of the curves²⁰ due to the reduced symmetry of this model, but the qualitative behavior remains unaltered.

The behavior of the curves is more or less as one would expect: as the centers of charge for the site II ions move toward the centers of the large zeolite cavities the binding of these ions to the crystal clearly must diminish, and as the site II ions move in this

direction they move away from the site I ions, which consequently sink lower into their potential holes.

On varying the silicon:aluminum ratio slightly, in order to introduce 25% occupancy of site I' into the divalent faujasites (Figures 4c, 4d, and 5), the general trends of the site I and II potential curves do not change, although for the 2.43:1 model (Figure 5b) we see that the slopes of both the site I and site II curves are greatly reduced. Again, in Figures 5a and 5b, the degeneracies of the curves are resolved, completely now, because of the loss of symmetry associated with the ionic arrangements.

The positions of the site I' potential curves relative to the sites I and II curves are roughly similar in Figures 4c, 4d, and 5. Because they derive from the replacing of an ion formerly in site I, it is clear that the overall electrostatic energy of the exchangeable cation system is increased by the replacement of the ion. This is also clear from Table I, which gives the total cation e.s. energy for mono and divalent 1:1 and 2:1 zeolites: the various columns are labeled to correspond to the relevant figures.

In general we can infer from the curves that divalent zeolites having the faujasite structure should have sites I fully occupied, the remaining ions going into sites II unless the ionic radius exceeds about 1.3 Å. Initially, this appeared to conflict with ion-exchange data²¹ and with preliminary X-ray data²² on nominally dehydrated zeolites, for which it was found that the calcined calcium X material has a distribution of ions between sites I and I'. To resolve the conflict, it was proposed that the discrepancy between the results derived from a lack of correspondence between the physical situation in the nominally dehydrated zeolites and the situation assumed in the models—in particular that a small amount of residual water in the real material might hold a few cations in sites I'. On continuing the refinement of the X-ray data, evidence was indeed found for water retention in the

(20) In other words the ordering of the Si and Al ions, and of the cations, forces the four nominally equivalent sites I to split into two non-equivalent groups of two each. Similar effects occur in most of the other models also.

(21) D. H. Olson, private communication.

(22) H. S. Sherry, private communication.

sodalite cages;⁸ thermogravimetric analysis of divalent zeolites previously subjected to a standard calcination treatment²³ gave further evidence for water retention of from one to two water molecules per sodalite cage.

Looking now at the potential curves for monovalent faujasites (Figure 6), we see again that they have common features. So far as the curves for sites I and II are concerned, these resemble the corresponding curves for divalent faujasites except that the curves are now displaced so far toward each other that they cross over; for small ions (radius less than 1–1.3 Å) the curves for site II ions lie below those for site I ions. The curves for site III ions always lie at quite high energies, indicating that these ions are loosely held. This agrees with the results of field calculations (see ref 4), where it was shown that the fields near site III ions are rather high, and that the field variation on varying the silicon:aluminum ratio was not very pronounced—all indicating that these ions are not well shielded by the surrounding crystal.

Moving ions from sites I into sites I' in models of monovalent faujasites has interesting consequences (Figures 6c and 6d). First of all, we note that the site I' potential curves for monovalent zeolites are quite unlike those for divalent zeolites. We see also that for small cations the site I' curves lie below, but relatively close to, those for site I ions.

Taking advantage of the similarities between the various figures we can adopt something like a rigid energy band point of view (in which the energy curves are fixed as the zeolite cation content is varied) and can draw the following conclusions from the curves for water-free monovalent faujasites. Since for small ions (radius up to about 1–1.5 Å) the site II curve consistently lies lowest in the energy diagrams, this site should be fully occupied. Furthermore, the relative positions of the site I and site I' curves suggest that for small cations (again up to 1–1.3 Å), there may be a distribution of cations between sites I and I', even in the absence of residual water in the materials. This is also clear from Table I: the total monovalent cation energy is little changed on moving cations into sites I'. As the cation size increases, a tendency for higher occupancy of site I should be observed. Again, it must be borne in mind that we do not permit adjacent sites I and I' to be occupied simultaneously.

The X-ray data of Eulenberger, Shoemaker, and Keil⁷ do show site II to be highly occupied and show a distribution of ions between sites I and I' in nominally dehydrated X zeolites (*i.e.*, following something like the standard calcination treatment). A tendency for larger cations to prefer site I (giving higher occupancy of this site) is also evident in ref 7. The results given in ref 7 also indicate that it is possible for adjacent sites I and I' to be occupied simultaneously, to some extent, by monovalent cations, a situation that has been excluded from the present work. However, it may be

that it is more favorable, energetically, for some simultaneous occupancy of sites I and I' to occur, than for cations to occupy sites III: the relative positions of the curves in Figures 6c and 6d would support this. Additional calculations are required to investigate this point, however, and it remains to be seen how sensitive the sites I and I' curves will be to some degree of simultaneous occupancy of adjacent sites.

The results agree also with Dodge's unpublished data¹³ on sodium-exchanged crystals of natural faujasite. Dodge found site II to be 100% occupied, site I about 75% occupied, and site I' about 25% occupied, following vacuum calcination at 350°.

On looking for residual water, using thermogravimetric analysis, in the materials in the manner described above, a water content of only 0.1–0.4 molecule per sodalite cage was found. The standard calcination treatment is thus adequate to dehydrate faujasites containing cations of radius equal to or greater than that of sodium cations—in contrast to the situation described above for divalent cation materials.

Figure 7 gives potential calculations for zeolites containing trivalent ions. For the standard situation with site I fully occupied in a 1:1 zeolite (Figure 7a), the curves show the behavior that we have seen for monovalent and divalent zeolites; for increasing ion size, the site I curves move to lower energies while the site II curves move to higher energies. In all figures the site I curves lie below the site II curves. Since site II is only half occupied even in the 1:1 case, the symmetry of the zeolite is low and, for nominally equivalent sites, the curves split into branches.

On moving first one site I ion (Figure 7c) and then a site I and a site II ion (Figure 7d) into site I' positions, the resulting potential curves show radical changes; in general, however, it appears that an overall loss of stability results. Evidently trivalent ions in dry faujasite materials should prefer to occupy sites I and II rather than sites I'. On the other hand, it is known that in zeolites containing trivalent ions, the ions are held in the sodalite cages by residual water oxygens.²⁴

The need to postulate the existence of residual water in *divalent* cation zeolites to reconcile calculations on model zeolites with observations on real ones leads one to speculate on the role of residual water in the materials. The results suggest that a few water molecules per sodalite cage may be held with increasing tenacity as we increase the valency of the cation. It seems reasonable to suggest that the size of the cation and its nature

(23) Standard calcination treatment refers to calcination of the zeolite specimens at 500° for some hours under a helium or air atmosphere. In the tests zeolite samples were held, generally overnight, in helium on a thermogravimetric balance. Once an equilibrium weight had been reached at this temperature, the sample temperature was raised at 30° deg/min to about 1000°. Loss of weight between 500 and 1000° was attributed to the loss of residual water.

(24) D. H. Olson, G. T. Kokotailo, and J. F. Charnell, *J. Colloid Interfac. Sci.*, **28**, 305 (1968).

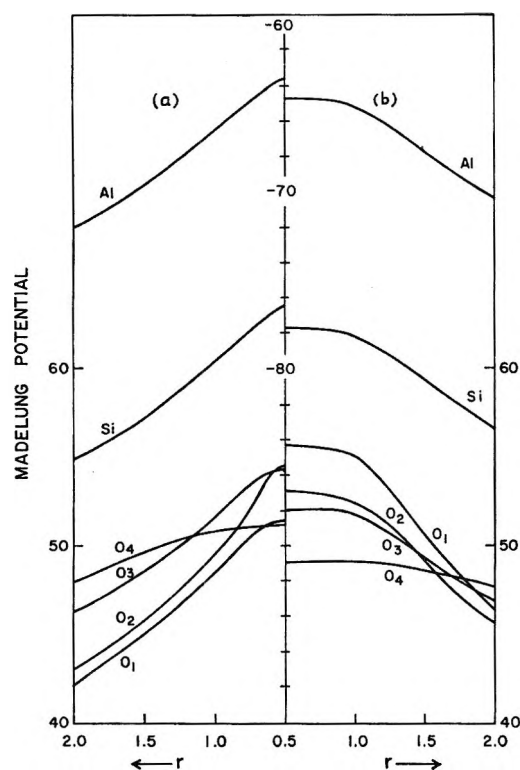


Figure 8. Potential curves for oxygen, silicon, and aluminum ions in (a) monovalent X (1:1) zeolite, (b) divalent X (1:1) zeolite as functions of cation size. Outer axes relate to the oxygen ions, central axis to the Al and Si ions. r is cation radius in Å.

(transition metal or not) will also play a role. If we then assume (in order to distribute the available positive charge of the zeolite) that dissociation of the residual water takes place, a situation arises in which, for given calcination conditions, the specific number of Bronsted sites in the zeolite may be a function of the field near the cation. This would support the point of view of Hirschler and of Plank given in the discussion to ref 1 and the recent results and discussions of Ward³ on the formation of pyridinium ions in divalent Y faujasites.²⁵ In other words, an apparent direct connection between catalytic activity and cation field may really be an indirect connection involving the dissociation of residual water.

Figure 7b gives the results for the only run carried out on a trivalent cation zeolite with Si:Al > 1. The figure relates to a 1.67:1 trivalent Y material having the standard cation configuration (site I fully occupied, the remaining cations going into a site II position).

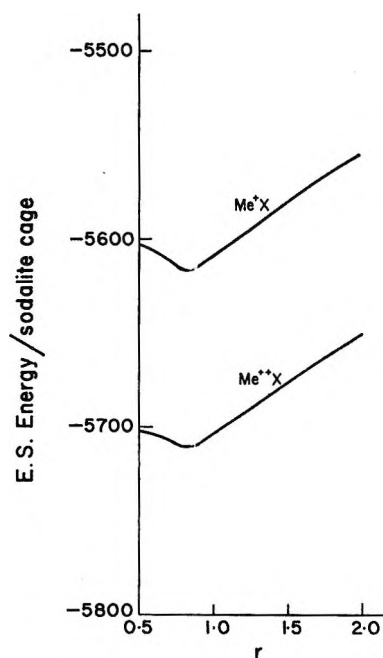


Figure 9. Electrostatic energy per sodalite cage in reduced units for monovalent and divalent ion X zeolite as function of cation size. r is cation radius in Å.

The results are in line with those that have gone before: the site I curves fall and the site II curve rises, with increasing cation size.

For completeness, Figures 8a and 8b show variation in Madelung potential for the framework ions (Si, Al, O₁, O₂, O₃, O₄) for monovalent and divalent X models as the cation radius increases. Using the data in these figures and the data of Figures 4a and 6a, Figure 9 was produced. This gives the electrostatic energy in arbitrary units (electronic charge = 1; lattice parameter = 1) for a sodalite cage of X material containing mono- and divalent cations, respectively, as a function of cation radius. Since the difference between the repulsive energies for the two models should be small, the curves indicate that dehydrated divalent cation zeolites are more stable than those containing monovalent cations.

Acknowledgments. Thanks are due to G. T. Kerr for carrying out the thermogravimetric analyses on sodium and calcium X and Y zeolites, and to D. H. Olson for many valuable discussions.

(25) See also Venuto and Landis, ref 2, p 283.

Proton Spin Relaxation and Exchange Properties of

Hydrated Chromic Ions in H₂O and H₂O-D₂O Mixtures^{1a}by B. F. Melton^{1b}*Department of Physics, Oklahoma State University, Stillwater, Oklahoma 74074*and V. L. Pollak^{1c}*Department of Physics, Case Western Reserve University, Cleveland, Ohio, 44106*
(Received December 26, 1968)

Experimental results are presented on proton spin relaxation in Cr(III) solutions of H₂O and mixtures of H₂O and D₂O, in fields from 1.1 G to 14 kG, and at temperatures from 0 to 99°. Water solutions containing 0.10 M HClO₄ give results which reflect the relaxation and exchange properties of Cr(H₂O)₆³⁺ alone, uncomplicated by the effects of hydrolysis products or polymers which cause thermal hysteresis or by acid-catalyzed proton exchange which is present in solutions of high acidity. Measurements on weakly acidified solutions confirm that Cr(H₂O)₆³⁺ is a more strongly relaxing species than Cr(H₂O)₅OH²⁺, but the latter undergoes more rapid proton exchange with the solvent water. A homogeneous (local) proton exchange mechanism involving the coordinated OH⁻ ion is proposed to account for this result. Measurements on 0.10 M HClO₄ solutions containing varying mole fractions of H₂O and D₂O indicate that the principal effect of deuteration at low temperatures is an increase in the lifetime of protons in the primary hydration sphere of Cr³⁺, resulting from the greater basicity of H₂O as compared to D₂O. At high temperatures T_2 remains constant, whereas T_1 decreases with deuteration due to slower rotational motion of the hydrated complex. The latter is correlated with the marked increase in viscosity which occurs in going from H₂O to D₂O.

Introduction

Although the basic mechanism for proton spin relaxation in aqueous chromium(III) solutions is well understood,² relaxation times reported by different observers for apparently identical systems do not agree.³⁻⁸ Thermal hysteresis,^{4,7} solution aging,³ specific anion effects,⁸ and pH dependence^{9,10} have all been noted. Some of these effects appear to be a result of the unusual features of chromium(III) chemistry. In aqueous solution Cr³⁺ hydrolyzes readily, forming CrOH²⁺ and higher hydrolysis products, which have been shown⁹ to have a pronounced effect on proton relaxation times in the solution. Chromium(III) also forms stable coordination compounds with a large number of other ligands, and at high temperatures long-lasting hydrolytic polymers are easily formed.¹¹ Once formed, these polymers break down very slowly, even in highly acid media, giving rise to the thermal hysteresis effects which have been reported.⁷

Chromium is one among several paramagnetic ions in which the lifetime for protons in the primary hydration sphere at low temperatures is relatively long, so that the observed relaxation rate of the solution is limited by the rate of proton exchange between the hydration sphere of the ion and the bulk water. At high temperatures exchange is fast and the solution relaxation rate is limited by the rate of relaxation in the ion hydration sphere. The observed proton relaxation time in a solution containing only Cr(H₂O)₆³⁺ is given by the expression¹²

$$(T_1^{\text{obs}})^{-1} = (T_{1w}^0)^{-1} + (T_{1w}^s)^{-1} + p(T_{1x} + \tau_{xw})^{-1} \quad (1)$$

where the subscripts x and w refer to water of hydration in Cr(H₂O)₆³⁺ and bulk water, respectively. The quantity T_{1w}^s is the proton relaxation time in the bulk water due to dipolar interaction with the Cr³⁺ spins, and T_{1w}^0 is the relaxation time due to other mechanisms in the solvent. The latter quantity can be equated to the relaxation time in the solvent not containing paramagnetic ions, but otherwise under conditions identical with those of the studied solution. The time τ_{xw} is

(1) (a) This work was supported in part by the U. S. Army Research Office (Durham). (b) NASA Trainee 1966-1969. To whom all correspondence should be addressed. (c) On leave from Oklahoma State University, 1967-1968. Now at Department of Physics, University of North Carolina, Charlotte, N. C. 28205.

(2) N. Bloembergen and L. O. Morgan, *J. Chem. Phys.*, **34**, 842 (1961).

(3) G. Laukien and J. Schlüter, *Z. Phys.*, **146**, 113 (1956).

(4) R. Hausser and G. Laukien, *Arch. Sci. (Geneva)*, **11**, 252 (1958).

(5) R. Hausser and G. Laukien, *Z. Phys.*, **153**, 394 (1959).

(6) L. O. Morgan and A. W. Nolle, *J. Chem. Phys.*, **31**, 365 (1959).

(7) T. H. Brown, R. A. Bernheim, and H. S. Gutowsky, *ibid.*, **33**, 1593 (1960).

(8) R. Hausser and F. Noack, *Z. Phys.*, **182**, 93 (1964).

(9) C. E. Manley and V. L. Pollak, *J. Chem. Phys.*, **46**, 2106 (1967).

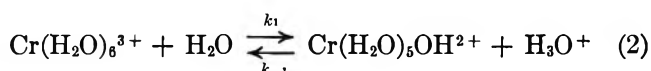
(10) T. J. Swift and T. A. Stephenson, *Inorg. Chem.*, **5**, 1100 (1966); T. J. Swift, T. A. Stephenson, and G. R. Stein, *J. Amer. Chem. Soc.*, **89**, 1611 (1967).

(11) J. A. Laswick and R. A. Plane, *ibid.*, **81**, 3564 (1959).

(12) A more general expression for T_1^{obs} , valid for solutions containing Cr(H₂O)₅OH²⁺ in addition to Cr(H₂O)₆³⁺, is given in the Appendix. Also reproduced there are theoretical expressions for T_{1x} and T_{1w}^p which will be used later in interpreting the experimental data.

the average lifetime of a proton in the hydration sphere of $\text{Cr}(\text{H}_2\text{O})_6^{3+}$, and p is the probability of finding a particular proton in $\text{Cr}(\text{H}_2\text{O})_6^{3+}$. We assume a relation similar to eq 1 holds for T_2^{obs} , although in general there will also be transverse relaxation by the so-called " $\Delta\omega$ effect."¹³ However, on the basis of the parameters derived herein, one can show that this relaxation mechanism is negligible in the case of $\text{Cr}(\text{H}_2\text{O})_6^{3+}$ solutions up to 14 kG, which was the highest field studied.

Protons in $\text{Cr}(\text{H}_2\text{O})_6^{3+}$ are known to exchange with the bulk water by transfer across hydrogen bonds rather than by exchange of whole water molecules. The latter have hydration lifetimes of the order of hours.¹⁴ In intermediate acid concentrations the dominant exchange mechanism is believed to be the first acid hydrolysis reaction^{9,15}

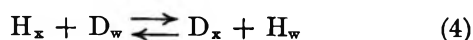


In highly acidified solutions there is an additional acid-catalyzed proton exchange mechanism,¹⁰ but its effect is negligible in the range of acid concentrations studied herein. In weakly acidified or nonacidified solutions complications arise due to the formation of $\text{Cr}(\text{H}_2\text{O})_5\text{OH}^{2+}$, which is believed to have a pronounced effect on the observed relaxation rate due to its rapid rate of proton exchange with the bulk water.⁹

The effects of isotopic substitution of deuterons on the proton relaxation times in aqueous solutions of $\text{Cr}(\text{NO}_3)_3$ have been studied by Mazitov.¹⁶ The observed increase in the proton relaxation times with deuteration was interpreted on the basis of an increase in the lifetime of protons in the primary hydration sphere of Cr^{3+} . It has been recently suggested that changes in proton relaxation times as the solvent is changed from H_2O to D_2O can also be expected on the basis of a change in the probability of finding a proton in the ion hydration sphere.¹⁷ This arises due to the difference in vibrational zero-point energies of protons and deuterons, which can give rise to a proton fraction in the hydration sphere which differs from that in the bulk. In this case the observed relaxation time would be given by the equation

$$(T_1^{\text{obs}})^{-1} = (T_{1w}^0)^{-1} + (T_{1w}^s)^{-1} + p(T_{1x} + \tau_{xw})^{-1}[(1 - K)\beta + K]^{-1} \quad (3)$$

where β is the fraction of protons in the solution. The constant K is the equilibrium constant for the exchange reaction



where K is assumed to be independent of β .¹⁸ Its temperature dependence is given by the relation $K = \exp(\Delta S^\circ/R) \exp(-\Delta H^\circ/RT)$, where ΔS° and ΔH° are the differences in entropy and enthalpy between the products and reactants in their standard states. This

theory was in partial agreement with published experimental results, but definitive conclusions were not possible on the basis of available data.

In the present study, measurements of the field and temperature dependence of proton spin relaxation times were undertaken on a 0.10 *M* HClO_4 solution of $\text{Cr}(\text{NO}_3)_3$ for the purpose of determining the rate constants of reaction 2 and the relaxation parameters of the hexaquo species $\text{Cr}(\text{H}_2\text{O})_6^{3+}$. Measurements were made as a function of mole fraction of D_2O to determine the quantity K in eq 3 and to study the effect of deuteration on the other parameters influencing proton spin relaxation. Measurements were also made on weakly acidified solutions of H_2O which contained appreciable quantities of the first hydrolysis product $\text{Cr}(\text{H}_2\text{O})_5\text{OH}^{2+}$. Its relaxation and exchange properties were examined and compared with those for $\text{Cr}(\text{H}_2\text{O})_6^{3+}$.

Experimental Section

Measurements of proton T_1 in the range from 1.0 to 520 G were made using the earth's field free precession technique.^{19,20} In fields between 1 and approximately 250 G the method is as follows: The sample, approximately 400 ml in volume, is placed inside a coil whose axis is oriented perpendicular to the earth's magnetic field, B_e . At time $t = 0$ the current is turned on through the coil, establishing a polarizing field B_p of the order of 500 G along the axis of the coil. The magnetization within the sample grows exponentially toward its equilibrium value with a time constant T_{1p} , the spin-lattice relaxation time in B_p . After a time $t = t_p$ long compared to T_{1p} , the polarizing field is reduced to some intermediate value B_i . At time $t = t_p + t_i$ the intermediate field is reduced suddenly to zero, leaving the magnetization at right angles to the earth's magnetic field. The initial amplitude of the ensuing free precession signal is a measure of the amount of relaxation that took place in the interval t_i . Variation of t_i in successive measurements allows calculation of the relaxation time T_{1i} in the intermediate field. To measure T_1 in the field B_p , the magnetic field is reduced to zero at time $t = t_p$ —i.e., $t_i = 0$. By varying t_p

(13) T. J. Swift and R. E. Connick, *J. Chem. Phys.*, **37**, 307 (1962).

(14) J. P. Hunt and R. A. Plane, *J. Amer. Chem. Soc.*, **76**, 5960 (1954).

(15) R. G. Pearson, J. Palmer, M. M. Anderson, and A. L. Allred, *Z. Elektrochem.*, **64**, 110 (1960).

(16) R. K. Mazitov, *Dokl. Akad. Nauk SSSR*, **156**, 135 (1964).

(17) V. L. Pollak and R. R. Slater, *Z. Naturforsch.*, **A**, **22**, 2110 (1967).

(18) Although not stated explicitly in the derivation in ref 17, eq 3 holds only if the concentrations of the species $\text{AH}_m\text{D}_{n-m}$, where $m = 0, 1, \dots, n$, are related to one another by statistical factors alone [see A. E. Brodsky, *Trans. Faraday Soc.*, **33**, 1180 (1937)]. This is a very good approximation for solvent water and should be expected to hold for coordinated water as well.

(19) M. Packard and R. Varian, *Phys. Rev.*, **93**, 941 (1954).

(20) A. Abragam, "The Principles of Nuclear Magnetism," Oxford University Press, London, 1961, p 64.

the relaxation time T_{1p} can be determined. Measurements at 14 kG (60 MHz) were made using standard spin-echo nmr techniques.²¹

The sample temperature was controlled, in the earth's field technique, by pumping heated or cooled water around the sealed glass sample bottle. The tempering liquid was doped with Mn²⁺ ions so as to suppress its contribution to the nmr signal. At 14 kG the sample temperature was controlled by a regulated gas flow cryostat. Temperature stability was approximately $\pm 0.5^\circ$ with both systems.

The chromium solutions were prepared from reagent grade Cr(NO₃)₃ and were acidified with HClO₄. All were prepared by dilution of the same master solution, which was 0.10 M in HClO₄. No measurable change could be detected between a freshly prepared master solution and one stored for over a year at room temperature.

Values of the viscosity of H₂O used in calculating rotational correlation times were taken from standard tables;²² those for D₂O were calculated from $\eta(\text{D}_2\text{O})/\eta(\text{H}_2\text{O})$ ratios taken from the data of Hardy and Cottington²³ and Lewis and McDonald.²⁴ Viscosities for mixtures of H₂O and D₂O were estimated by assuming a linear variation of viscosity with proton fraction.²⁴ For the calculation of T_{1w}^0 , self-diffusion coefficients for H₂O were taken from the data of Simpson and Carr.²⁵ Self-diffusion coefficients for Cr³⁺ do not appear to have been measured and were approximated by the values for La³⁺, which were calculated from conductivity data using the Nernst equation.²⁶ Errors introduced by this approximation are not serious since diffusion coefficients for the ions are less than 25% of those for water, and only the sum appears in the calculations. Self-diffusion coefficients for protons in mixtures of H₂O and D₂O have been measured by Douglass and McCall²⁷ at 25°. Values at other temperatures were calculated using the Stokes–Einstein equation

$$D(\beta, T) = kT/6\pi r(\beta)\eta(\beta, T)$$

Values of $\eta(\beta, T)$ were known experimentally, and the β dependence of the Stokes–Einstein radius r could be calculated from the known variation of D and η with proton fraction at 25°. Self-diffusion coefficients for Cr³⁺ in deuterated solutions were calculated from the Stokes–Einstein equation by assuming that the ratios $r(\beta)/r(\beta = 1)$ were the same for Cr³⁺ as for H₂O.

Results and Discussion

Solutions of Moderate Acidity. The experimental field and temperature results for chromic ions in 0.10 M perchloric acid solution of water are shown in Figures 1–3. The observed proton relaxation times in the solution have been corrected for relaxation in water not containing paramagnetic ions using the relation

$$(T_1^{\text{cor}})^{-1} \equiv (T_1^{\text{obs}})^{-1} - (T_{1w}^0)^{-1} \quad (5)$$

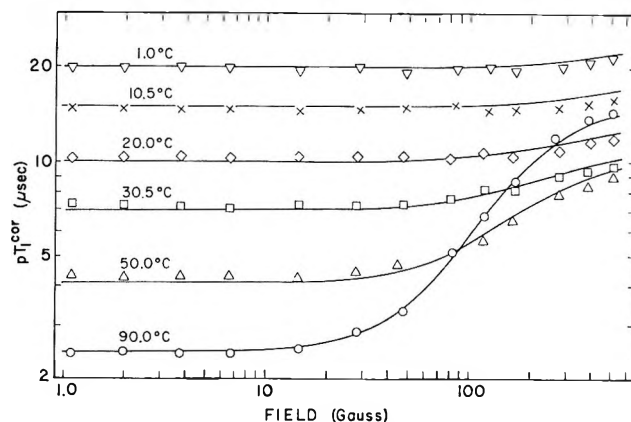


Figure 1. Field dependence of proton relaxation times at different temperatures in a $3.0 \times 10^{-4} M$ Cr(NO₃)₃ solution of 0.10 M HClO₄. Observed values have been corrected for relaxation in water using eq 5 and normalized by multiplying by the probability of finding a proton in the hydration sphere of a paramagnetic ion. The pT_1^{cor} values were independent of the concentration of paramagnetic ions. The solid lines are least-squares fits to the experimental data using the equations given in the text.

with a similar definition for T_2^{cor} . According to eq 1, pT_1^{cor} should be independent of the concentration of paramagnetic ions, which was indeed found to be the case.

The experimental curves can be accounted for satisfactorily by using eq 1 along with the standard theoretical expressions for T_{1x} and T_{1w}^0 which are given in the Appendix. In all, the equations contain five unknown quantities which are to be determined by fitting the theoretical expressions to the experimental data. They are the proton lifetime τ_{xw} , the rotational correlation time τ_r of the Cr(H₂O)₆³⁺ complex, the correlation time for electron relaxation τ_ν , the scalar coupling constant A , and the constant C appearing in the Bloembergen–Morgan equation for τ_{1s} , which is related to the asymmetry of the crystalline field around a Cr³⁺ ion. For the ion–proton distance in Cr(H₂O)₆³⁺ we used the value $r = 2.74 \text{ \AA}$ obtained by Hausser and Noack.⁸ We used the same value for the closest distance of approach of a proton in the bulk to the ion spin since larger values gave slightly poorer fits to the data.

According to the Debye model,²⁸ the temperature

(21) H. Y. Carr and E. M. Purcell, *Phys. Rev.*, **94**, 630 (1954); S. Meiboom and D. Gill, *Rev. Sci. Instr.*, **29**, 688 (1958).

(22) "International Critical Tables," Vol. V, E. W. Washburn, Ed., McGraw-Hill Book Co., Inc., New York, N. Y., 1926, p 10.

(23) R. C. Hardy and R. L. Cottington, *J. Chem. Phys.*, **17**, 509 (1949).

(24) G. N. Lewis and R. T. McDonald, *J. Amer. Chem. Soc.*, **55**, 4730 (1933).

(25) J. H. Simpson and H. Y. Carr, *Phys. Rev.*, **111**, 1201 (1958).

(26) B. Ottar, "Self-Diffusion and Fluidity in Liquids," Oslo University Press, Oslo, 1958, p 118.

(27) D. C. Douglass and D. W. McCall, *J. Chem. Phys.*, **31**, 569 (1959).

(28) N. Bloembergen, E. M. Purcell, and R. V. Pound, *Phys. Rev.*, **73**, 679 (1948).

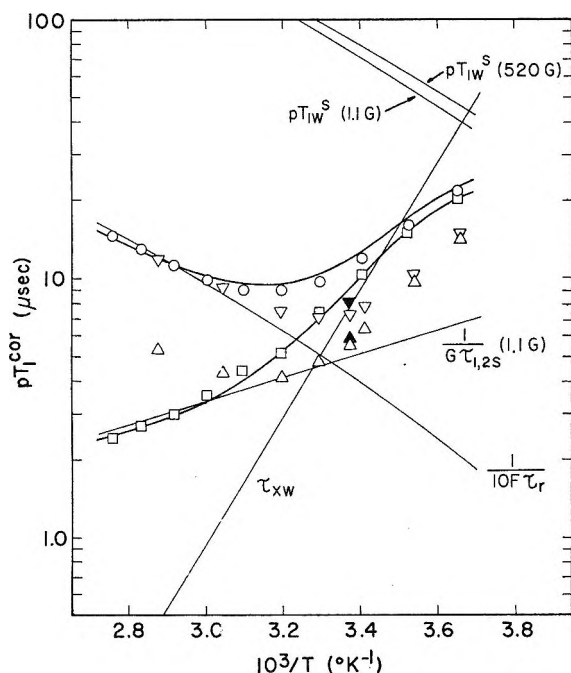


Figure 2. Temperature dependence of pT_1^{cor} for $\text{Cr}(\text{NO}_3)_3$ solutions at various fields and acid concentrations. For solutions containing 0.10 M HClO_4 , pT_1^{cor} values are denoted by \circ at 520 G and by \square at 1.1 G. The solid lines result from the least-squares fit to the experimental data and also indicate the temperature dependences of the proton relaxation time T_{1w}^s in the bulk water due to dipolar interaction with the ion spins, the proton lifetime τ_{xw} , the electron relaxation times $\tau_{1,2s}$, and the rotational correlation time τ_r for $\text{Cr}(\text{H}_2\text{O})_6^{3+}$. The constants F and G are given by $F = 4/30 S(S+1) \gamma_I^2 \gamma_S^2 \hbar^2 \tau^{-6}$ and $G = 2/3 S(S+1)(A/\hbar)^2$ (see eq A2 of the Appendix). For a 0.001 M HClO_4 solution of $3.0 \times 10^{-4} M$ $\text{Cr}(\text{NO}_3)_3$, the pT_1^{cor} values are denoted by ∇ at 410 G and by Δ at 1.1 G. This solution exhibited thermal hysteresis, as shown by the values \blacktriangledown and \blacktriangle , which were measured at room temperature after the sample had been heated to 75° . The pT_1^{cor} values for this solution were dependent on the concentration of paramagnetic ions due to the shift in equilibrium of reaction 2 to the right with decreasing metal ion concentration.

dependence of the rotational correlation time can be computed from the expression

$$\tau_r = 4\pi\eta a^3/3kT \quad (6)$$

where η is the bulk viscosity of the solution at temperature T , and a is the radius of the coordinated paramagnetic ion. For τ_{xw} and τ_v we assume exponential temperature dependences of the forms $\tau_{xw} = \tau_{xw}^0 \exp(-V_{xw}/RT)$ and $\tau_v = \tau_v^0 \exp(-V_v/RT)$. The solid curves through the data points in Figures 1–3 represent least-squares fits of the theoretical equations to the experimental data, using as adjustable parameters the unknown quantities τ_{xw}^0 , V_{xw} , τ_v^0 , V_v , a , C , and A . All are determined unambiguously from the combination of field and temperature results and are presented in Table I. The remaining curves in Figures 2 and 3

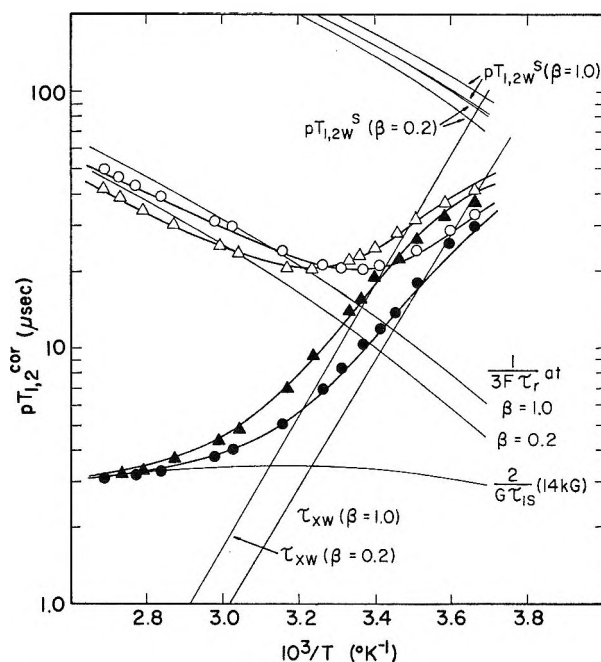


Figure 3. Temperature dependence of $pT_{1,2}^{\text{cor}}$ at 14 kG for 0.10 M HClO_4 solutions of $\text{Cr}(\text{NO}_3)_3$. Values for a solution containing 100% H_2O ($\beta = 1.0$) are denoted by \circ and \bullet . Those for a 80% D_2O –20% H_2O solution ($\beta = 0.2$) are denoted by Δ and \blacktriangle . The solid lines result from the least-squares fits to the experimental data. Those for the $\beta = 0.2$ solution were calculated assuming only changes in rotational correlation times and in the activation energy for proton exchange in going from H_2O to a mixture of H_2O and D_2O . The notation is the same as that in Figure 2.

Table I: Parameters Obtained from the Least-Squares Fit of the Equations in the Text to Proton Relaxation Data on Cr^{3+} Solutions of H_2O

$$\begin{aligned} \tau_{xw} &= 4.1 \times 10^{-14} \exp(11.2/RT) \\ \tau_v &= 9.3 \times 10^{-14} \exp(2.1/RT) \\ a &= 4.4 \text{ \AA} \\ C &= 1.3 \times 10^{20} \text{ sec}^{-2} \\ A/h &= 2.1 \text{ MHz} \end{aligned}$$

result from the least-squares curve fits and may be used to synthesize all the experimental data.

At low fields where $\omega_s^2 \tau_v^2 \ll 1$, we expect $\tau_{1s}^{-1} = \tau_{2s}^{-1} = 5C\tau_v$ from eq A5 of the Appendix. The slope of the line $(G\tau_{1,2s})^{-1}$ in Figure 2 gives an activation energy for τ_v of 2.1 kcal/mol. This compares favorably with the 2.4 kcal/mol from the esr data of Hayes.²⁹ Using the parameters in Table I we calculate $\tau_{1,2s} = 4.3 \times 10^{-10}$ sec in low fields and at 17.5° , which agrees within the experimental error with the value $\tau_{2s} = 4.7 \times 10^{-10}$ sec obtained from esr data by Sancier and Mills³⁰ at 15 – 20° and $\text{pH} = 1$. In high fields where $\omega_s^2 \tau_v^2 \gtrsim 1$, τ_{1s} increases above its low field value, which

(29) R. G. Hayes, Lawrence Radiation Laboratory Report UCRL-9873, Sept 29, 1961.

(30) K. M. Sancier and J. S. Mills, *J. Phys. Chem.*, **67**, 1438 (1963).

causes a decrease in T_{2x} with increasing field. The quantity $2(G\tau_{1s})^{-1}$ at 14 kG is plotted in Figure 3 for comparison with the low-field values of $(G\tau_{1,2s})^{-1}$ in Figure 2. At 25° we find $\tau_v = 3.3 \times 10^{-12}$ sec, as compared with 6.2×10^{-12} sec obtained by Hausser and Noack.⁸ Their values may be systematically too high since they also report $\tau_v = 5.3 \times 10^{-12}$ sec for Mn²⁺, as compared with $\tau_v = 2.4 \times 10^{-12}$ sec reported by Bloembergen and Morgan.² The value of the scalar coupling constant $A/h = 2.1$ MHz is only slightly larger than the 2.0 MHz obtained by Luz and Shulman³¹ from measurements of proton chemical shift and by Bloembergen and Morgan² from proton relaxation data. The value $a = 4.4$ Å for the radius of the coordinated Cr³⁺ ion compares favorably with a Stokes radius of 4.1 Å obtained by Nightingale.³² The Debye formula gives $\tau_r = 7.7 \times 10^{-11}$ sec at 25°, which agrees with the 8×10^{-11} sec obtained by Bloembergen and Morgan.² As is seen by the goodness of fit of the T_1^{cor} curve at 14 kG and at high temperature (Figure 3), the Debye formula predicts quite well the temperature dependence of the rotational correlation time τ_r . An exponential temperature dependence $\tau_r = \tau_r^0 \exp(V_r/RT)$ could have been assumed (which gives $V_r = 4.2$ kcal/mol), but the Debye formula gives an equally good fit with one less adjustable parameter.

The slope of the line τ_{xw} in Figure 3 gives the activation energy for proton exchange $V_{xw} = 11.2$ kcal/mol. This is greater than the 10 kcal/mol reported earlier^{2,16} since previous authors have neglected the contribution of T_{1w}^0 to the observed proton relaxation time. This error is particularly serious at 0° and in low fields where the contributions to proton relaxation in the primary hydration sphere of Cr³⁺ and in the bulk are approximately equal. The curves in Figure 3 are remarkably similar to those for VO²⁺,³³ in which it is also necessary to take into account relaxation outside the first hydration shell.

At 25° the lifetime τ_{xw} for proton exchange leads to a forward rate constant for reaction 2 of $k_1 = 12/\tau_{xw} = 1.7 \times 10^6$ sec⁻¹. Using this value and the value $K_1 = k_1/k_{-1} = 1.4 \times 10^{-4}$ for the equilibrium constant of reaction 2,³⁴ we calculate for the reverse rate constant $k_{-1} = 1.2 \times 10^{10}$ mol⁻¹ sec⁻¹. The change in enthalpy for reaction 2 has been measured by Postmus and King³⁴ who report a value of 9.4 ± 0.4 kcal/mol for ΔH° . Thus we find for the activation energy of the reverse rate constant $V_{-1} = 11.2 - 9.4 = 1.8$ kcal/mol. Both the magnitude of k_{-1} and its activation energy are consistent with a diffusion-limited recombination process.³⁵

Solutions of Low Acidity. Also shown in Figure 2 are results on a weakly acidified solution of Cr(NO₃)₃, which contains, in addition to the hexahydrate Cr(H₂O)₆³⁺, some of the first hydrolysis product Cr(H₂O)₅OH²⁺. At low temperatures and low field (1.1 G) the effect of CrOH²⁺ is to shorten the observed

relaxation time,⁹ whereas at high temperatures the formation of CrOH²⁺ lengthens T_1^{obs} . At these high temperatures the proton lifetimes in both species are sufficiently short that the conditions $\tau_{xw} \ll T_{1x}$ and $\tau_{yw} \ll T_{1y}$ are fulfilled. Here the subscript y refers to the species Cr(H₂O)₅OH²⁺. Under these conditions the general expression for proton relaxation in the solution (see eq A1 of the Appendix) reduces to

$$(T_1^{\text{obs}})^{-1} = (T_{1w}^0)^{-1} + (T_{1w}^0)^{-1} + (12x/2w)(T_{1x})^{-1} + (11y/2w)(T_{1y})^{-1} \quad (7)$$

where x and y are the molar concentrations of Cr³⁺ and CrOH²⁺ in the solution and w is the molar concentration of solvent water. In this simple case the relaxation rate in the solution is the weighted average of the relaxation rates in the separate environments.

The fact that the presence of CrOH²⁺ at high temperatures lengthens T_1^{obs} at 1.1 G, whereas in fields greater than approximately 400 G there is almost no effect at all, suggests that the dipolar contribution to T_1 is approximately the same for both species, but the scalar contribution is much less in CrOH²⁺ than in Cr³⁺ due to a shorter electron relaxation time $\tau_{1,2s}$, a smaller scalar coupling constant A , or both.³⁶ A precise quantitative study is difficult since this solution exhibited thermal hysteresis effects similar to those observed by Brown, *et al.*⁷ These effects occur at high temperatures and are attributed to the formation of polynuclear species which decompose very slowly when the sample is returned to room temperature.¹¹ However, the effect of polymerization on T_1 was small compared to the effect of the presence of CrOH²⁺, and the qualitative conclusions reached above remain unaltered.

The experimental data reported earlier⁹ for $(T_1^{\text{obs}})^{-1} - (T_{1w}^0)^{-1}$ at 0.5° as a function of acidity of solutions of Cr(NO₃)₃ have been refitted using eq A1 of the Appendix. In the previous paper⁹ the contribution of the quantity $(T_{1w}^0)^{-1}$ to the observed relaxation rate was neglected, which leads to considerable errors in the resulting parameters. If we use the values $(T_{1w}^0)^{-1} = 0.74$ sec⁻¹,³⁷ $T_{1x} = 3.7$ μsec, and $\tau_{xw} = 39$ μsec, which were obtained in the present study at 380 G and 0.5°, then a least-squares fit of the data of Manley and Pollak⁹ using

(31) Z. Luz and R. G. Shulman, *J. Chem. Phys.*, **43**, 3750 (1965).

(32) E. R. Nightingale, Jr., *J. Phys. Chem.*, **63**, 1381 (1959).

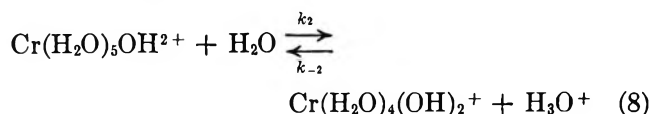
(33) K. Wüthrich and R. E. Connick, *Inorg. Chem.*, **7**, 1377 (1968).

(34) C. Postmus and E. L. King, *J. Phys. Chem.*, **59**, 1208 (1955).

(35) See, *e.g.*, the chapter by M. Eigen, W. Kruse, G. Maass, and L. DeMaeyer in *Progr. Reaction Kinetics*, **II**, 285 (1964).

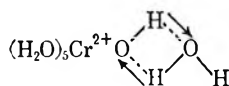
(36) In the 0.001 M HClO₄ solution of 3.0×10^{-4} M Cr(NO₃)₃ we estimate a value $x/y = 0.46$ at 75°, using the value $K_1 = 2.6 \times 10^{-3}$ for the equilibrium constant of reaction 2. This value is for an ionic strength of 2.4×10^{-3} mol l.⁻¹ and was calculated from the experimental data of ref 34 at $I = 0.034$ mol l.⁻¹, using activity coefficients calculated from the Davies equation. By using $T_{1x} = 2.4$ μsec and assuming that T_{1y} is identical with the dipolar contribution to T_{1x} , which is 12.2 μsec at 75° (Figure 2), we calculate $pT_1^{\text{cor}} = 5.5$ μsec at 1.1 G and 75°. This agrees well with the experimental value of 5.3 μsec.

τ_{yw} and T_{1y} as adjustable parameters yields the values $T_{1y} = 7 \mu\text{sec}$ ³⁸ and $\tau_{yw} = 1.3 \mu\text{sec}$. If we assume that species *y* exchanges protons with the bulk water *via* the second hydrolysis reaction



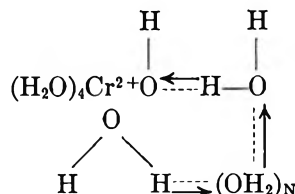
then $k_2 = 10/\tau_{yw} = 7.7 \times 10^6 \text{ sec}^{-1}$. Using the value $K_2 = 2.5 \times 10^{-7}$ for the equilibrium constant of reaction 8 at 0°,³⁹ we calculate $k_{-2} = k_2/K_2 = 3.1 \times 10^{13} \text{ sec}^{-1}$, which is about 300 times greater than the diffusion-limited recombination of H^+ and OH^- .³⁵ Such a rate constant for diffusional encounter is impossibly high; hence, we conclude the proton exchange must occur by some additional reaction. A mechanism involving a collision between $\text{Cr}(\text{H}_2\text{O})_5\text{OH}^{2+}$ and OH^- may be ruled out since it would also require an impossibly large reaction rate. An exchange reaction between H^+ and coordinated water in $\text{Cr}(\text{H}_2\text{O})_5\text{OH}^{2+}$ would require a rate constant of the order of $10^{10} \text{ mol}^{-1} \text{ sec}^{-1}$ at $10^{-3} M \text{ H}^+$, which is not impossibly large. But rate constants for such acid-catalyzed proton exchange mechanisms are typically $10^6 \text{ mol}^{-1} \text{ sec}^{-1}$ or less.¹⁰ Furthermore, such a mechanism would give a τ_{yw} which varied with solution acidity, contrary to what is observed. The short proton lifetimes cannot be due to rapid exchange of whole water molecules in $\text{Cr}(\text{H}_2\text{O})_5\text{OH}^{2+}$ since reaction 2 would provide a fast bridge for water molecules in $\text{Cr}(\text{H}_2\text{O})_6^{3+}$ to enter the water system. In 1.0 *M* acid solutions at 0° lifetimes of water molecules in $\text{Cr}(\text{H}_2\text{O})_6^{3+}$ would be of the order of milliseconds rather than days as experimentally observed.¹⁴ It follows that the rapid proton exchange of $\text{Cr}(\text{H}_2\text{O})_5\text{OH}^{2+}$ occurs *via* some mechanism involving proton jumps across hydrogen bonds to solvent water molecules.

It could be suggested that the rapid rate of proton exchange of CrOH^{2+} compared to Cr^{3+} is due to a mechanism involving the coordinated OH^- alone. A possibility would be a four-center concerted proton transfer involving a jump of the two protons in the directions shown



Similar four-center proton transfers have been postulated previously.⁴⁰ But such a mechanism would allow only one of the eleven protons in $\text{Cr}(\text{H}_2\text{O})_5\text{OH}^{2+}$ to be exchangeable with the bulk, and the increase in proton relaxation rate with the formation of CrOH^{2+} could only be accounted for if CrOH^{2+} were a more strongly relaxing species than Cr^{3+} , which has been shown not to be the case. Four-center proton transfer involving coordinated water molecules is not important for Cr

$(\text{H}_2\text{O})_6^{3+}$, and there is no reason to assume that it would be an effective mechanism for $\text{Cr}(\text{H}_2\text{O})_5\text{OH}^{2+}$ either. The most logical mechanism seems to be a concerted proton transfer reaction of the form



in which a coordinated water molecule is connected via a Grotthuss chain to the coordinated OH^- ion. The water molecules at the ends of the chain act as either acid or base catalysts, and transfer occurs *via* a counter-clockwise jump of the protons through the chain in the directions indicated. The OH^- "diffuses" throughout the hydration sphere, which ensures that all 11 protons are exchangeable with the bulk. Similar mechanisms have been proposed⁴¹ to account for the rapid rates of other reactions, *e.g.*, the mutarotation of glucose, which are both acid and base catalyzed. Such concerted mechanisms are not diffusion limited and are favored since they avoid the solvation and desolvation of any charged intermediates.

Isotope Effects. Measurements at 14 kG on $\text{Cr}(\text{NO}_2)_3$ samples of varying volume fractions of H_2O and D_2O are presented in Figure 4. The temperature dependence of proton T_1 and T_2 for a 20% H_2O –80% D_2O sample ($\beta = 0.2$) are given in Figure 3 along with the results for a sample containing only H_2O . All the samples were uniformly made 0.10 *M* in HClO_4 . An interesting empirical result from Figure 3 is that the proton relaxation measurements at $\beta = 1.0$ and $\beta = 0.2$ can be made to coincide by a shift in the temperature scale by an amount of $10^3/T = 0.12^\circ \text{K}^{-1}$, which corresponds to a temperature shift of approximately 11° near room temperature. This fact suggests that the water structure around Cr^{3+} , and therefore the structure difference between H_2O and D_2O , remains constant over an extended range of temperature. A similar

(37) We assume $(T_{1w})^{-1}$ to be independent of the relative concentrations of Cr^{3+} and CrOH^{2+} in the solution. Actually $(T_{1w})^{-1}$ could decrease slightly as the equilibrium shifts to the right in reaction 2, due to a shorter electron relaxation time for CrOH^{2+} . However, this effect is masked by the increase in the third term of eq A1 which accompanies the formation of CrOH^{2+} at 0°.

(38) A shorter electron relaxation time for CrOH^{2+} could make $T_{1y} > T_{1x}$ at 0° and 380 G since at low temperatures τ_{1s} competes with τ_r for the correlation time of the dipolar interaction. At high temperatures $\tau_r \ll \tau_{1s}$ for both Cr^{3+} and CrOH^{2+} , which makes $T_{1y} \approx T_{1x}$ in high fields, since τ_r is expected to be approximately the same for both species.

(39) N. Bjerrum, *Z. Phys. Chem. (Leipzig)*, **73**, 724 (1910).

(40) H. Kwart, L. P. Kuhn, and E. L. Bannister, *J. Amer. Chem. Soc.*, **76**, 5998 (1954); J. Hine, "Physical Organic Chemistry," McGraw-Hill Book Co., Inc., New York, N. Y., 1962, p 112.

(41) C. G. Swain and J. F. Brown, *J. Amer. Chem. Soc.*, **74**, 2534 (1952); E. S. Gould, "Mechanism and Structure in Organic Chemistry," Holt-Dryden, New York, N. Y., 1959, p 542.

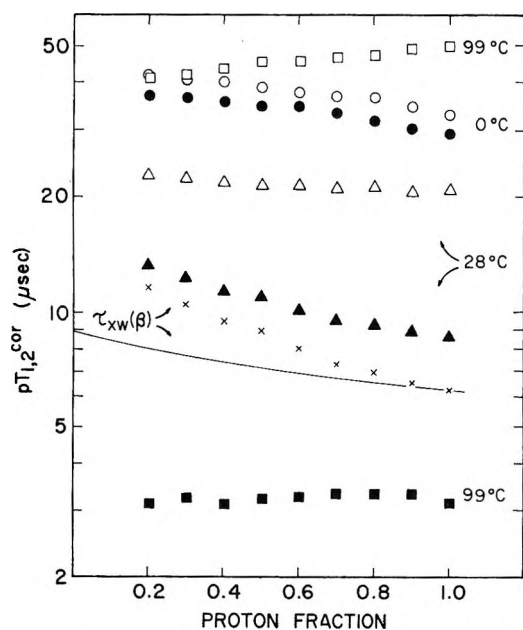


Figure 4. Proton relaxation at 14 kG in 0.10 *M* HClO₄ solutions of Cr(NO₃)₃ of varying proton fraction β . Values of $pT_{1,2}^{\text{cor}}$ at 0° are denoted by ○ and ●; by Δ and ▲ at 28°; and by □ and ■ at 99°. The values denoted by × represent the β dependence of the proton lifetime in the hydration sphere of Cr³⁺ at 28°. The solid curve was calculated using the $\tau(\beta)/\tau(\beta = 1)$ ratios from the theory of Bunton and Shiner and the value $\tau(\beta = 1) = 6.3 \mu\text{sec}$.

result was noted by Baker,⁴² who observed that the viscosity of heavy water equals that of light water at a temperature 8.5° less, from 15° to the highest temperature studied, 35°.

At low temperatures where $\tau_{\text{xw}} \gg T_{1x}, T_{2x}$, both pT_1^{cor} and pT_2^{cor} increase with decreasing proton fraction β . From eq 3 this could be due either to an increase in the term in brackets with decreasing β (*i.e.*, $K > 1$), an increase in τ_{xw} , or both. The relaxation time T_{1w} contributes significantly to T_1^{cor} at 0°, but it gives an isotope effect in the opposite direction due to the decrease in self-diffusion coefficients of the solvent protons with partial deuteration. Near 100° where $\tau_{\text{xw}} \ll T_{2x}$, T_2^{cor} is independent of proton fraction to within $\pm 3\%$. This requires $K = 1.00 \pm 0.03$. Using this value and the equation $K = \exp(-\Delta G^\circ/RT)$, we obtain $\Delta G^\circ = \Delta H^\circ - T\Delta S^\circ = 0 \pm 22 \text{ cal/mol}$ at 100°. If, as is usually the case,⁴³ the main cause of any deviation from $K = 1$ in reaction 4 is a difference in vibrational zero-point energies between the products and the reactants, then $\Delta G^\circ \approx \Delta H^\circ$, and we calculate $K = 1.00 \pm 0.04$ at 0°. Thus we expect that most of the isotope effect near 0° must be due to a change in τ_{xw} with changing proton fraction. In any case, the data cannot be fitted satisfactorily by assuming deviations from $K = 1$ are alone responsible for the isotope effect at 0°, regardless of what assumptions are made regarding the relative magnitudes of ΔH° and ΔS° for reaction 4.

The linear decrease in T_1^{cor} at high temperatures with decreasing β correlates qualitatively with the linear increase in viscosity as the solvent is changed from H₂O to D₂O.²⁴ This gives rise to a longer rotational correlation time in deuterated solutions and a decrease in T_{1x} . The absence of an isotope effect for T_{2x} implies that the correlation time τ_v for electron relaxation does not change with proton fraction, and is further evidence that electron relaxation is not related to rotation of the hydrated Cr³⁺ complex.² By linear extrapolation of the T_1^{cor} curve at 99° in Figure 4 to $\beta = 0$, we find that the rotational correlation time increases by approximately 28% in going from H₂O to D₂O, whereas the solvent viscosity increases by only 16%.²³ In terms of the Debye model this would imply that deuteration is accompanied by an increase in the radius of the Cr³⁺ complex ion. The increase in τ_r with decreasing proton fraction for Cr³⁺ is in marked contrast to Mn²⁺ ions, which have a rotational correlation time that is independent of the proton fraction, except near 0° where the difference in viscosities of H₂O and D₂O is a maximum.⁴⁴ This is almost certainly linked to the stronger interaction of Cr³⁺ ions with the solvent as compared with Mn²⁺. Lifetimes of water molecules in the primary hydration sphere of Cr³⁺ are of the order of hours¹⁴ as compared with approximately 10⁻⁸ sec for water molecules in Mn(H₂O)₆²⁺.¹³ Evidence for strong hydrogen bonds between Cr(H₂O)₆³⁺ and a secondary hydration sphere has been provided by measurements on transverse relaxation times of the fluorine nuclei in PF₆⁻ in aqueous solutions of Cr(H₂O)₆³⁺. Despite its high positive charge, Cr(H₂O)₆³⁺ showed only a small tendency to form secondary coordination sphere complexes with PF₆⁻.⁴⁵ Furthermore, in spite of the smaller ionic radius of Cr³⁺, its rotational correlation time in H₂O at 25° is 8×10^{-11} sec as compared with 3×10^{-11} sec for Mn²⁺ at the same temperature.² The "structure-making" property of Cr³⁺ gives rise to this long rotational correlation time since additional water molecules (the secondary coordination sphere) rotate with the Cr(H₂O)₆³⁺ ion. Due to the large volume of the rotating complex, it is not surprising that the Debye formula, which was derived for rotation of macroscopic particles, holds much better for Cr³⁺ than for other ions not having a well-defined secondary coordination sphere.⁴⁶ These considerations also provide the rationale for allowing for a larger Debye radius in the more strongly hydrogen-bonded deuterated solutions. The present situation is in accord with that in pure liquids, where rotational correlation times are

(42) W. N. Baker, *J. Chem. Phys.*, **4**, 294 (1936).

(43) See, *e.g.*, Chapter XI, "Isotope Effects in Acid-Base Reactions," in R. P. Bell, "The Proton in Chemistry," Cornell University Press, Ithaca, N. Y., 1959.

(44) H. Sprinz, *Z. Naturforsch.*, **A**, **19**, 1243 (1964).

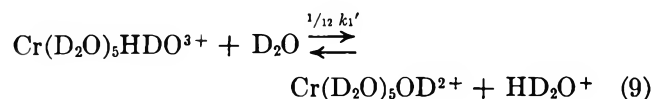
(45) T. R. Stengle and C. H. Langford, *J. Phys. Chem.*, **69**, 3299 (1965).

satisfactorily accounted for by the Debye formula only in the case of liquids which are highly associated.

The solid curve in Figure 3 for $\beta = 0.2$ represents a least-squares fit to the experimental data using as adjustable parameters the Debye radius a and the activation energy V_{xw} for proton exchange. The constant K was assumed identical with unity over the whole temperature range, and the remaining parameters were assumed to be the same as those found from fitting the $\beta = 1.0$ data (Table I). We found $a = 4.5 \text{ \AA}$ and $V_{xw} = 11.6 \text{ kcal/mol}$ at $\beta = 0.2$. The assumption of a constant τ_{xw}^0 is in accord with the model which will be introduced later to account for the isotope effect. However, an equally satisfactory fit can be obtained by making the opposite assumption of a constant activation energy and variable preexponential factor. The experimental data offers little information on this point due to the limited temperature range over which τ_{xw} is the dominant factor influencing relaxation.

Finally there remains to be discussed the β dependence of τ_{xw} . At 28° the normalized relaxation time pT_2^{cor} is determined mainly by the rate of proton exchange between the primary hydration sphere of Cr^{3+} and the bulk water (Figure 3). Furthermore, since T_{2x} is almost independent of β and pT_{2w}^s varies only slightly with β , the β dependence of pT_2^{cor} at 28° in Figure 4 reflects primarily the β dependence of τ_{xw} . Semiexperimental values of τ_{xw} vs. β at 28° have been extracted from the pT_2^{cor} data by using the T_2 analogs of eq 1 and 5 along with the values $T_{2x} = 2.8 \text{ \mu sec}$ and $pT_{2w}^s = 170 \text{ \mu sec}$. The calculated τ_{xw} values are given in Figure 4. Extrapolation to $\beta = 0$ shows that the proton lifetime increases by approximately a factor of 2.3 as the solvent is changed from H_2O to D_2O .

Changes in proton lifetimes in the hydration sphere of Cr^{3+} with partial deuteration could be due to a difference between the rate constant k_1 of reaction 2 and the rate constants of reactions such as

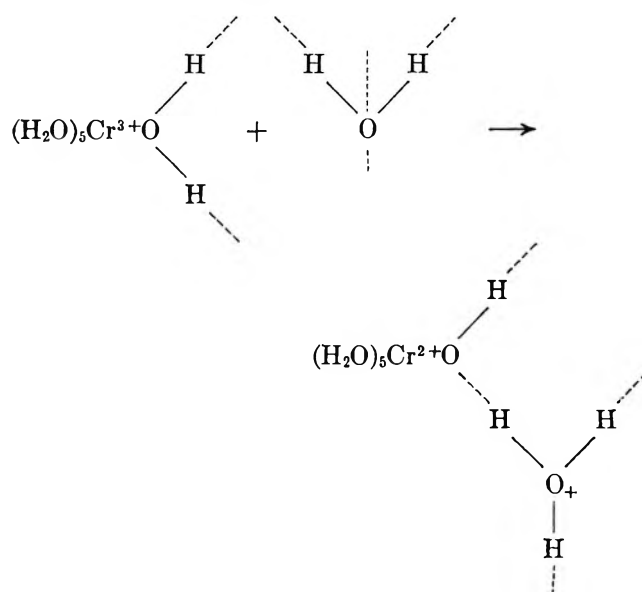


In almost pure D_2O proton exchange with the bulk water occurs mainly by reaction 9, whereas in pure H_2O the exchange is by reaction 2. The ratio of the proton lifetimes in the two solvents is given by $\tau(\text{D}_2\text{O})/\tau(\text{H}_2\text{O}) = k_1/k_1'$. Differences between the rate constants k_1 and k_1' (secondary isotope effects) can occur if the binding at proton sites other than the one being transferred changes in going from the initial to the transition state. Bunton and Shiner^{47b} have proposed a model for calculating secondary isotope effects which assumes that they arise mainly from the changes in zero-point energy, associated in turn principally with changes in hydrogen bond stretching frequencies in going from the initial to the transition state. In their model the ratio of the rates in H_2O and D_2O is given by

$$\frac{k_1}{k_1'} = \exp\left(\frac{\sum \nu_{\text{H}} - \sum \nu_{\text{H}}^\ddagger}{5.44T}\right) \quad (10)$$

where $\sum \nu_{\text{H}}$ and $\sum \nu_{\text{H}}^\ddagger$ are the sums of the hydrogen stretching frequencies (cm^{-1}) in the initial and transition states, respectively. The sum extends over all the isotopically substituted sites in the molecules.

Application of this theory requires assumptions concerning the nature of the transition state. We assume for reaction 2 the model



where the dotted lines represent hydrogen bonds to solvent water molecules. The transition state consists of a hydronium ion hydrogen-bonded to a coordinated OH^- ion. This is the most reasonable assumption since the position of the proton in the state of highest potential energy, the transition state, should be nearer to the weaker base, and the coordinated OH^- ion is a much stronger base than a bulk water molecule. For the stretching frequencies of hydrogen-bonded water and hydronium ions we use the frequencies 3400 and 2900 cm^{-1} , respectively. The stretching frequencies of protons bound to coordinated water molecules in $\text{Cr}(\text{H}_2\text{O})_6^{3+}$ are not known, so we follow the suggestion of Bunton and Shiner^{47a} and estimate these frequencies using the equation

(46) If, as suggested, there is a secondary coordination sphere which rotates with the $\text{Cr}(\text{H}_2\text{O})_6^{3+}$ ion and exchanges protons rapidly with the bulk water, then eq 1 should contain an additional term $p'(T_{1x}')^{-1}$, where p' is the probability of finding a proton in the secondary coordination shell and T_{1x}' is the proton relaxation time in that environment. The correlation time for T_{1x}' is the rotational correlation time τ_r , which is related to the bulk viscosity of the solvent by the Debye formula. The quantity T_{1w}^s then becomes the relaxation time for protons outside the secondary coordination shell. Such a model introduces two additional unknown quantities, since the number of water molecules in the secondary coordination shell and the ion-proton distance are not known. In the present treatment $p'(T_{1x}')^{-1}$ has been lumped in with $(T_{1w}^s)^{-1}$ since this procedure gives a satisfactory fit to the data with fewer adjustable parameters.

(47) (a) C. A. Bunton and V. J. Shiner, Jr., *J. Amer. Chem. Soc.*, **83**, 42 (1961); (b) *ibid.*, **83**, 3207 (1961); (c) *ibid.*, **83**, 3214 (1961).

$$\nu(\text{cm}^{-1}) = 2937 + 28.8pK_a \quad (11)$$

where K_a is the acid dissociation constant per proton of $\text{Cr}(\text{H}_2\text{O})_6^{3+}$. Using the value $K_a = 1.4 \times 10^{-4}/12$ at 25°, ³⁴ we calculate from eq 11 a value $\nu = 3080 \text{ cm}^{-1}$. For the stretching frequency of the proton on the coordinated OH^- ion in the transition state, we assume a value of 3500 cm^{-1} , which is intermediate between the 3600-cm^{-1} frequency of free OH^- and the 3400-cm^{-1} frequency of free water. Thus, summing over all the protons except the one being transferred, we obtain

$$\sum \nu_{\text{H}} = 3080 + 4(3400) = 16,680 \text{ cm}^{-1} \quad (12a)$$

$$\sum \nu_{\text{H}}^{\ddagger} = 3500 + 2(2900) + 2(3400) = 16,100 \text{ cm}^{-1} \quad (12b)$$

The two 3400-cm^{-1} frequencies are included in $\sum \nu_{\text{H}}^{\ddagger}$ because two of the hydrogen bonds which were accepted by water molecules in the initial state are assumed to be accepted by solvent water molecules in the transition state (see rule e of ref 47a). Using eq 12a and 12b in eq 10 we obtain $\tau(\text{D}_2\text{O})/\tau(\text{H}_2\text{O}) = 1.4$ at 25°, as compared with an observed value of approximately 2.3 (Figure 4). In the summations of eq 12a and 12b we have neglected the stretching frequencies of the protons on the five-coordinated water molecules in the initial and transition states. Actually one should expect a slight increase in stretching frequency according to eq 11 due to a larger pK_a of CrOH^{2+} , which would lower $\tau(\text{D}_2\text{O})/\tau(\text{H}_2\text{O})$. However, the increase in stretching frequency is small and is probably offset by a decrease in librational frequencies of the water molecules of similar magnitude, so we have neglected their effects altogether.

In the range $0 < \beta < 1$ other reactions besides 2 and 9 must be considered in calculating proton lifetimes. Examples are proton jumps from $\text{Cr}(\text{H}_2\text{O})_6^{3+}$ to HDO or D₂O molecules. By performing a calculation similar to that above for all possible such reactions and weighting each reaction rate by its probability of occurrence at a given value of β , we calculated $\tau(\beta)/\tau(\beta = 1)$ ratios at several values of β . The results are given in Figure 4, where we have used the reference value $\tau(\beta = 1) = 6.3 \mu\text{sec}$ at 28°. The calculated $\tau(\beta)$ curve is concave upward, in agreement with the curvature of the "experimental" τ_{xw} values at 28°.

Isotope effects on reaction rates can also occur due to the change in librational frequencies of adjacent solvent molecules in going from the initial to the transition state (solvent isotope effect). Reactions of solute molecules which are "structure making" in the initial state (high solvent librational frequency), but "structure breaking" in the transition state (low solvent librational frequency) can be expected to proceed more rapidly in H₂O than in D₂O.⁴⁸ Owing to the strong "structure-making" character of Cr^{3+} we thus expect

the proton transfer rate constants to decrease as the solvent is changed from H₂O to D₂O which would serve to improve the agreement between the experimental and calculated isotope effects. The low frequency librations of the solvent have been shown to be responsible for the difference in solubilities of salts in H₂O and D₂O.⁴⁸ The effects are small compared to isotope effects on dissociations of oxygen acids and bases, however, so we have neglected the solvent isotope effect altogether.

Equation 10 can also be used to calculate the difference between the proton and deuteron lifetimes, or primary isotope effect, in the same solvent.^{47c} In this case the summations include only the proton being transferred. If we assume that the proton-stretching frequency in the transition state is the same as that on a hydronium ion hydrogen-bonded to water, then $\sum \nu_{\text{H}} - \sum \nu_{\text{H}}^{\ddagger} = 3080 - 2900 = 180 \text{ cm}^{-1}$, and using eq 10 we obtain $\tau^{\text{D}}/\tau^{\text{H}} = 1.1$. Deuteron lifetimes in the hydration sphere of Cr^{3+} have not been experimentally measured, but in solutions of vanadyl a ratio $\tau^{\text{D}}/\tau^{\text{H}} = 1.3$ has been reported,⁴⁹ and one should expect a similar result for chromic solutions.

The agreement between the predicted and measured isotope effects is about as close as can be expected owing to the approximations involved in the derivation of eq 10 and our neglect of all but the stretching frequencies in the summations, as well as the uncertainties in estimating the stretching frequencies from eq 11. The presence of large secondary and small primary isotope effects in the proton exchange is, however, correctly predicted by the theory, which lends support to our proposed model for the transition state.

Conclusions

The experimental proton spin relaxation results reported herein for moderately acidified solutions of $\text{Cr}(\text{NO}_3)_3$ reflect the relaxation and exchange properties of $\text{Cr}(\text{H}_2\text{O})_6^{3+}$ alone, free from the effects of hydrolysis products or polymers which cause thermal hysteresis. At low temperatures the relaxation times are determined by the proton exchange rate and by the magnetic dipole interaction between the ion spin and protons outside the first hydration shell. The results on weakly acidified solutions confirm that $\text{Cr}(\text{H}_2\text{O})_6^{3+}$ is a more strongly relaxing species than $\text{Cr}(\text{H}_2\text{O})_5\text{OH}^{2+}$ and that the latter undergoes much more rapid proton exchange with the bulk water. The rapid exchange is explained satisfactorily by assuming a homogeneous proton exchange mechanism involving the coordinated OH^- ion. A similar mechanism can be expected for the hydroxides of other metal ions, although it is uncertain

(48) C. G. Swain and R. F. Bader, *Tetrahedron*, **10**, 182 (1960); C. G. Swain, R. F. Bader, and E. R. Thornton, *ibid.*, **10**, 200 (1960).

(49) R. K. Mazitov and A. I. Rivkind, *Dokl. Akad. Nauk SSSR*, **166**, 654 (1966).

whether favorable cases could be found to demonstrate its effectiveness.

The increase in proton relaxation times with partial deuteration is due primarily to an increase in the lifetime of protons in the hydration sphere of Cr^{3+} , which is caused in turn by the greater basicity of H_2O as compared to D_2O . This result is in accord with other cases reported in the literature^{47b} and may be explained on the basis of the theory of Bunton and Shiner.

Acknowledgments. The authors are indebted to Dr. Eli Namanworth of the Chemistry Department of Case Western Reserve University for allowing them to use his 60-MHz pulsed nmr spectrometer. They wish to thank Mr. Israel Mayk, Summer NSF Undergraduate Research Participant at CWRU, for his assistance in carrying out the high-frequency measurements. Acknowledgment is made to the donors of the Petroleum Research Fund, administered by the American Chemical Society, for partial support of this research.

Appendix

It has been recently shown⁹ that in chromic solutions in the range of pH where the system is adequately described by the single equilibrium constant $K_1 = k_1/k_{-1}$ of reaction 2,⁵⁰ the observed relaxation time is given by

$$\frac{1}{T_1^{\text{obs}}} = \frac{1}{T_{1w}^0} + \frac{1}{T_{1w}^s} + (12x/2w) \left\{ \frac{1}{12} \tau_{yw} + (11\tau_{yw}/12\tau_{xw})T_{1x} + [1 + (x/y)(\tau_{yw}/\tau_{xw})]T_{1y} \right\} + (11y/2w) \left(T_{1x} + \frac{1}{12} \tau_{xw} \right) \frac{(T_{1x} + \frac{1}{12} \tau_{xw})(T_{1y} + \tau_{yw}) + (x/y)(\tau_{yw}/\tau_{xw})(T_{1x} + \tau_{xw})T_{1y}}{(A1)}$$

where the subscripts x , y , and w refer to the species $\text{Cr}(\text{H}_2\text{O})_6^{3+}$, $\text{Cr}(\text{H}_2\text{O})_5\text{OH}^{2+}$, and the bulk water, respectively. The quantities x , y , and w are the molar concentrations of the various species in the solution; τ_{yw} is the average lifetime of a proton in the species j before transfer to the bulk water; and T_{1j} is the proton relaxation time in environment j . The quantity $(T_{1w}^s)^{-1}$ is the relaxation rate in the bulk water due to dipolar interaction with the spins S and is proportional to the number of ion spins per unit volume; $(T_{1w}^0)^{-1}$ is the relaxation rate due to other mechanisms in the bulk water and can be equated to the relaxation rate in the solvent not containing paramagnetic ions, but otherwise under conditions identical with those of the studied solution. The proton lifetime τ_{xw} is related to the forward rate constant of reaction 2 by the equation $\tau_{xw} = 12/k_1$.⁵⁰ The quantity τ_{yw} is included to allow for transfer of protons from the species $y = \text{Cr}(\text{H}_2\text{O})_5\text{OH}^{2+}$ to the water system. Such transfer is assumed

to occur without the formation of appreciable quantities of other species in solution. As the solution acidity is increased y approaches zero, and x approaches m , the total analytical concentration of chromium in the solution. Equation A1 then reduces to eq 1 of the text, where $p = 12m/2w$ is the probability of finding a proton in the hydration sphere of Cr^{3+} .

The relaxation times T_{1x} and T_{2x} of protons in $\text{Cr}(\text{H}_2\text{O})_6^{3+}$ are given to a good approximation by the equations²

$$\frac{1}{T_{1x}} = \frac{4}{30} \frac{S(S+1)\gamma_I^2\gamma_S^2\hbar^2}{r^6} \left[3\tau_c + \frac{7\tau_c}{1 + \omega_s^2\tau_c^2} \right] + \frac{2}{3} \frac{S(S+1)A^2}{\hbar^2} \left[\frac{\tau_{2s}}{1 + \omega_s^2\tau_{2s}^2} \right] \quad (A2)$$

and

$$\frac{1}{T_{2x}} = \frac{4}{60} \frac{S(S+1)\gamma_I^2\gamma_S^2\hbar^2}{r^6} \left[7\tau_c + \frac{13\tau_c}{1 + \omega_s^2\tau_c^2} \right] + \frac{1}{3} \frac{S(S+1)A^2}{\hbar^2} \left[\tau_{1s} + \frac{\tau_{2s}}{1 + \omega_s^2\tau_{2s}^2} \right] \quad (A3)$$

where

$$\tau_c^{-1} = \tau_r^{-1} + \tau_{1s}^{-1} \quad (A4)$$

In the above equations I and S refer to proton and electron spins respectively, ω_s is the electron precession frequency; γ_I and γ_S , the proton and electron gyromagnetic ratios; r , the ion-proton internuclear distance; A , the scalar coupling constant; τ_r , the rotational correlation time; and τ_{1s} and τ_{2s} , the longitudinal and transverse electron relaxation times. Bloembergen and Morgan² have derived an approximate equation for τ_{1s} based on the assumption that relaxation occurs by modulation of the quadratic crystalline field splitting by collisions with water molecules outside the complex. The resulting equation was

$$\frac{1}{\tau_{1s}} = C \left[\frac{\tau_v}{1 + \omega_s^2\tau_v^2} + \frac{4\tau_v}{1 + 4\omega_s^2\tau_v^2} \right] \quad (A5)$$

where τ_v is the characteristic correlation time for the relaxation, and C is a constant for the hydrated complex. In high fields where $\omega_s^2\tau_v^2 \gtrsim 1$ we expect $\tau_{2s} < \tau_{1s}$, but in such high fields the terms involving τ_{2s} in eq A2 and A3 are negligible.

Theoretical equations for $T_{1,2w}$ ⁹ have been derived by Pfeifer.⁵¹ His model includes modulation of the dipolar interaction by translational diffusion as well as by relaxation of the ion spin. With the usual approxi-

(50) Note that the rate constant k_1 of this paper corresponds to k_{1w} of ref 9.

(51) H. Pfeifer, *Ann. Phys.*, **7**, 1 (1961).

mations $\omega_I \ll \omega_s$ and $\omega_I^2 \tau_{1s}^2 \ll 1$, these equations reduce to

$$\frac{1}{T_{1w}^s} = \frac{\gamma_I^2 \gamma_S^2 \hbar^2 S(S+1)}{2} [3J(0) + 7J(\omega_s)] \quad (\text{A6})$$

and

$$\frac{1}{T_{2w}^s} = \frac{\gamma_I^2 \gamma_S^2 \hbar^2 S(S+1)}{4} [7J(0) + 13J(\omega_s)] \quad (\text{A7})$$

The term $J(\omega)$ is the spectral density function at the frequency ω and is given by the integral

$$J(\omega) = \frac{16\pi N \tau_{1s}}{15d^3} \int_0^\infty B_{3/2}^2(\rho d) \times \frac{1 + D\rho^2 \tau_{1s}}{(1 + D\rho^2 \tau_{1s})^2 + \omega^2 \tau_{1s}^2} \frac{d\rho}{\rho} \quad (\text{A8})$$

where N is the number of paramagnetic ions per unit volume; d is the average closest distance of approach between a proton in the bulk and spin S ; $B_{3/2}$, the Bessel function of order 3/2; and $D = D_I + D_S$, the self-diffusion coefficient of the bulk protons plus that of the spins S . Equation A8 can be integrated in closed form. The result, given by eq 33 of Pfeifer's paper,⁵¹ was used to calculate T_{1w}^s and T_{2w}^s .

Diffusion of Halogenated Hydrocarbons in Helium.

The Effect of Structure on Collision Cross Sections

by Edward N. Fuller, Keith Ensley, and J. Calvin Giddings

Department of Chemistry, University of Utah, Salt Lake City, Utah 84112 (Received December 27, 1968)

Experimental binary gas-phase diffusion coefficients for some halogenated hydrocarbon compounds diffusing into helium have been determined utilizing the gas chromatography (GC) peak-broadening technique. Certain modifications are described which have improved the speed and accuracy of the technique. A critical discussion of the validity of the method is given. Based mainly on the acquired data, additional parameters have been determined for use in connection with the Fuller-Schettler-Giddings diffusion volume method for estimating binary diffusion coefficients. The relationship between effective collision cross sections and various molecular shape and structural features is discussed.

Widespread efforts to characterize numerous diffusion processes more exactly have resulted in an increased need for accurate diffusion data and improved methodology. Gradually more diffusion data are being published, but very little data are presently available for most organic vapors. The major objectives of this investigation were to develop improved experimental apparatus and techniques, to generate reliable data for new systems, and to study the dependence of collision cross sections on complex molecular structure. In contrast to simple systems where temperature variations are of utmost importance, the present complex systems yield more information when studied as a function of structural features such as chain length and substituent position.

Experimental binary diffusion coefficients were determined for thirty-one halogenated hydrocarbons diffusing into helium. From these data additional "atomic diffusion volume" parameters were obtained

for use with the method developed by Fuller, Schettler, and Giddings¹ for predicting diffusion coefficients. With the exception of two confirmatory determinations, all diffusion coefficients reported here are for systems not previously investigated.

A limited amount of related diffusion data have been reported in the literature. Relatively recent work includes studies reported by Trautz and Ries² for $\text{H}_2\text{-CCl}_4$; Trautz and Mueller³ for $\text{O}_2\text{-CCl}_4$; Gilliland⁴ for air-chlorobenzene; Klotz and Miller⁵ for air-CNCl, air-COCl₂ and air-CCl₃NO₂; Lee and Wilke⁶ for Freon-

- (1) E. N. Fuller, P. D. Schettler, and J. C. Giddings, *Ind. Eng. Chem.*, **58**, 18 (1966).
- (2) M. Trautz and W. Ries, *Ann. Phys.*, **8**, 163 (1931).
- (3) M. Trautz and W. Mueller, *ibid.*, **22**, 353 (1935).
- (4) E. R. Gilliland, *Ind. Eng. Chem.*, **26**, 681 (1934).
- (5) I. M. Klotz and D. K. Miller, *J. Amer. Chem. Soc.*, **69**, 2557 (1947).
- (6) C. Y. Lee and C. R. Wilke, *Ind. Eng. Chem.*, **46**, 2381 (1954).

12-water, Freon-12-benzene and Freon-12-ethanol; Bose and Chakraborty⁷ for O₂-CCl₄, N₂-CCl₄ and air-CCl₄; and Mueller and Cahill⁸ for CH₄-CF₄. Since this work was completed, Byrne, Maguire, and Clarke⁹ reported values for four halogenated hydrocarbons in N₂, H₂, and Ar. Earlier work is summarized in the International Critical Tables.¹⁰

Experimental diffusion coefficients were determined using the gas chromatography (GC) peak-broadening technique first developed by Giddings and Seager.^{11,12} With this technique which employs the experimental sequence of gas chromatography, a narrow pulse of a trace component is introduced into a carrier gas which is flowing at a constant rate down an empty tube of uniform circular cross section. As the trace component is swept down the diffusion tube, diffusion and non-equilibrium processes cause axial broadening of the sample peak. At the far end of the tube, sample passes through a detector producing a proportional electrical signal. A strip-chart recorder traces out the resulting Gaussian shaped concentration profile. From the observed peak width the binary diffusion coefficient can be deduced.^{11,12} The method is much like that proposed by Taylor^{13,14} and applied to liquid systems; his equations are not valid in our flow range, but correspond to the high-velocity limit mentioned below.

The diffusion coefficient is rather arbitrarily expressed here in terms of the experimentally determined "plate height," the quantity used in gas chromatography to characterize peak dispersion, by the theoretical expression

$$D_{AB} = \left(\frac{\bar{v}}{4}\right)(H + \sqrt{H^2 - r_0^2/3}) \quad (1)$$

where \bar{v} is the gas velocity averaged over the tube cross section, r_0 the tube radius, H the plate height determined as $L\tau^2/t^2$, L the tube length, τ^2 the peak variance in time units and t the tube residence time. The positive root of eq 1 is valid up to a certain critical velocity, \bar{v}_c , given by¹²

$$\bar{v}_c = 4\sqrt{3} D_{AB}/r_0 \quad (2)$$

At velocities greater than \bar{v}_c the negative root becomes valid. When $\bar{v} \gg \bar{v}_c$ the Taylor limit becomes valid.

In practice the proper choice of roots poses no serious problem since one can make a reasonable estimate of \bar{v}_c beforehand or, alternately, make diffusion runs at several velocities, the data from which specify \bar{v}_c .

Experimental Section

Apparatus. A diffusion apparatus with improved characteristics was constructed. The basic components are shown schematically in Figure 1.

Previously, using commercial GC apparatus with excessive dead volume, it was necessary to obtain rather complete data from a short correction tube for subtraction from the principal data in order to compensate

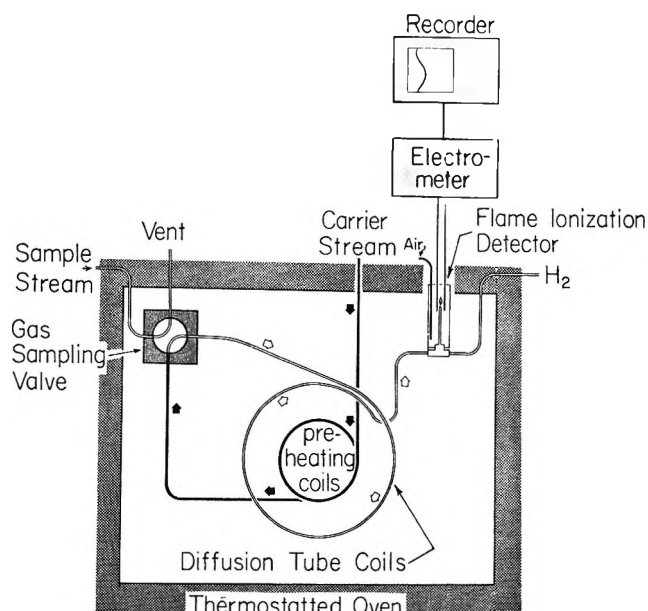


Figure 1. GC broadening apparatus for diffusion measurements.

for end effects. The latter originate mainly in dead volumes associated with sampling and detection devices. The need for this cumbersome two-column procedure has been eliminated through direct on-column sample introduction and a rigorous reduction of detector dead volume. In addition oven dimensions were increased to accommodate the diffusion tube without tight coils and bends which tend to distort tube cross sections and otherwise alter peak dispersion.

Temperature in the electrically heated oven was controlled by a Sim-Ply-Trol pyrometer manufactured by Assembly Products, Inc. During any one run temperature was controlled within about $\pm 0.2^\circ$; for any repeating set of runs used for a given diffusion coefficient, the control level was about $\pm 0.4^\circ$. This temperature regulation is adequate within the limits set by the experimental precision of the present technique.

A nominal 50-ft by $1/4$ -in. o.d. stainless steel beverage tube with a bright interior finish was obtained from Superior Tube Co. The length of the coiled tube was determined by taping a wire to the tube's side midway between the inside and outside radius. Laid flat on the floor, the length of wire (tube) was measured as 1521 cm. The volume of the diffusion tube was determined

(7) N. K. Bose and B. N. Chakraborty, *Trans. Ind. Inst. Chem. Eng.*, **8**, 67 (1955-56).

(8) C. R. Mueller and R. W. Cahill, *J. Chem. Phys.*, **40**, 651 (1964).

(9) J. J. Byrne, D. Maguire, and J. K. A. Clark, *J. Phys. Chem.*, **71**, 3051 (1967).

(10) "International Critical Tables," Vol. 5, McGraw-Hill Book Co., Inc., New York, N. Y., 1926, p 62.

(11) J. C. Giddings and S. L. Seager, *J. Chem. Phys.*, **35**, 2242 (1958).

(12) J. C. Giddings and S. L. Seager, *I. and E. C. Fund.*, **1**, 277 (1962).

(13) G. I. Taylor, *Proc. Roy. Soc.*, **A219**, 186 (1953).

(14) G. I. Taylor, *ibid.*, **A255**, 473 (1954).

from the weight of water required to fill it, giving 343.7 cm³. From these data the average tube radius was estimated to be 0.2682 cm (or 0.1056 in.). This agrees well with the value 0.210 ± 0.004 in. i.d. specified by the vendor. The lead connecting the sampling valve to the diffusion tube, made from the same size tubing, was considered part of the diffusion tube making a total length of 1536 cm.

A stainless steel gas-sampling valve obtained from Wahl-Henius Institute was used for sample introduction. Carrier gas and sample stream may be passed continuously through two loops, each of about 0.5 cm³ volume, attached to a plate at the back of the valve. By rotating the back plate and interchanging carrier and sample loops, sample is introduced directly on the diffusion column as a narrow plug.

Connected to the opposite end of the diffusion tube is the base of the hydrogen flame ionization detector with internal mixing volume of 0.38 cm³. The electrical signal from the flame ionization detector was fed to an electrometer whose sensitivity could be varied widely by selecting input resistances of 10¹⁰, 10⁹, 10⁸ or 10⁷ ohms. The amplified signal was fed to a Fisher Laboratory Recorder Model PWF, manufactured by Texas Instruments, Inc., with 0.5 sec full-scale response time, adjustable damping and gain, and variable chart speeds up to 8 in./min.

Procedure. Gas samples were introduced slowly into the sample stream. Since 0.5 cm³ of pure gas would yield a signal much too large, and the approach to "infinite dilution" is theoretically desirable, the sample stream was greatly diluted with carrier gas through a "T" joint. The ratio of carrier gas to sample was adjusted until peaks of convenient size were obtained.

Vapor samples were introduced into the sample stream by slowly bubbling carrier gas through a test tube of the liquid inside a cylindrical steel chamber. The resulting gas mixture passed out the side of the chamber into the sample stream. When necessary the mixture was diluted as described above.

A small pressure drop across the flame ionization detector was determined using a mercury manometer in the hydrogen stream. To specify correctly the experimental pressure this small correction (usually 30–40 mm) was added to the observed laboratory pressure. The pressure drop through the diffusion tube was negligible.

The plate height, H , was determined by measuring the width of the recorder peaks at half height, measured from outside the line of the leading edge to inside of the trailing edge. The peak width at half height (in time units) multiplied by the factor $1/(2\sqrt{2\ln 2})$ gives τ for Gaussian peaks. The diffusion coefficient was calculated according to eq 1.

Gases and Vapors. Helium and nitrogen were employed as the carrier gases. Grade A helium with

stated purity 99.995% was obtained from the U. S. Bureau of Mines. Whitmore Oxygen Co. supplied the nitrogen, stated purity 99.989%, and hydrogen for the detector, stated purity 99.98%. The gases and vapors used as trace components were obtained from a variety of sources and were in the range 95–99+ % purity.

Analysis of Accuracy. The largest single source of experimental error associated with the GC peak dispersion technique appears to be the measurement of τ . This presently can be determined to about ±1%. This gives, since H depends on the square of τ , an experimental uncertainty of roughly 2% in H and D_{AB} .

The magnitude of other possible sources of experimental error can be estimated and shown to be generally small in comparison.

The effect of finite sample size can be calculated approximately by assuming that the sample is introduced as a plug of concentration c_0 . The initial sample variance will be given by

$$\sigma_0^2 = \frac{\int_{-x_0/2}^{x_0/2} c_0 x^2 dx}{\int_{-x_0/2}^{x_0/2} c_0 dx} = \frac{x_0^2}{12} \quad (3)$$

where x_0 is the length of the sample plug in the tube. The standard 0.5 cm³ sample will occupy 2.26 cm of tube length, *i.e.*, $x_0 = 2.26$ cm and $\sigma_0^2 = 0.425$ cm². Experimentally observed σ^2 's were in the range 250–200 cm²; thus finite sample size represents a contribution of about 0.1–0.2%.

Using chromatographic theory derived by Giddings,¹⁵ spurious plate height contributions arising from the detector volume, stagnant pockets, and from tube coiling can be estimated. The plate-height contribution due to detector volume will be given by the expression.

$$H_d = \frac{L}{N_d} \left(\frac{V_d}{V_t} \right)^2 \quad (4)$$

where V_d is the detector volume, in our case ~0.38 cm³, V_t the diffusion tube volume, ~350 cm³, and N_d the number of theoretical plates ascribable to the detector alone, ~10–20. For these dimensions we have $H_d \sim 1.3 \times 10^{-4}$ cm. Since observed plate heights were usually about 0.2 cm, the error contribution from this source is ~0.1%.

Small pockets at various connections are perhaps unavoidable. The contribution to H from stagnant pockets can be approximated by the relation

$$H_p \sim \frac{\bar{v}^2 \delta^4}{64 D_{AB}^2 L} \sim 4 \times 10^{-6} \text{ cm} \quad (5)$$

where δ is the depth of the stagnant pocket. It is assumed here that $\bar{v} \sim 10$ cm/sec, $D_{AB} \sim 0.5$ cm²/sec

(15) J. C. Giddings, *J. Gas Chromatog.*, **1**, 12 (1963).

Table I: Experimental Results for N₂-Ethane and N₂-Butane Compared with Literature Values^a

System	No. of Runs	T, °K	D _{AB} ± std dev, cm ² /sec	Lit. values and ref (corrected to exptl temp)
N ₂ -ethene	10	302.6	0.170 ± 0.0034	0.174 (0.163 at 291.2°K) ¹⁶ 0.174 (0.170 at 298.2°K) ⁸ 0.167 (0.163 at 298.0°K) ¹⁹
N ₂ -butane	10	302.4	0.100 ± 0.0015	0.0985 (0.0960 at 298.0°K) ¹⁹ 0.1006 (0.0930 at 293.2°K) ²⁰

^a Reduced to 1 atm pressure.

and $\delta \sim 1$ mm. The effect of two or three such pockets would be entirely negligible.

Another spurious contribution to H comes from the coiled configuration of the diffusion tube. The effect arises in the unequal path lengths and pressure gradients along "inside" and "outside" streampaths. The contribution from this effect can be approximated by¹⁵

$$H_c \sim \frac{0.12\bar{v}r_0^4}{D_{AB}R_0^2} \sim 1.4 \times 10^{-5} \text{ cm} \quad (6)$$

where R_0 is the coil radius ~ 30 cm, with \bar{v} and D_{AB} as above. This contribution to H is presently negligible but could become important for diffusion tubes with tighter coils and larger cross sections.

Coiling also leads to secondary flows,¹⁶ which may be important in extreme circumstances. However, in the vicinity of velocity \bar{v}_c (our velocity was generally $< \bar{v}_c$), a displacement across the tube radius occurs about equally fast by diffusion and by the primary flow.¹⁷ Secondary flows are, of course, of much smaller magnitude. No effect was observed in earlier work¹² at velocities up to nearly $3\bar{v}_c$ using a tighter coil; we therefore assume the effect to be negligible here.

Experimental Results

The accuracy of the present results was checked using nitrogen-ethene and nitrogen-butane systems since consistent literature values^{8,18-20} were available. Both the experimental and literature values, reduced to one atmosphere pressure, are shown in Table I. The latter were corrected over short temperature ranges to our experimental temperature assuming a $T^{1.76}$ dependence.¹ The comparison shows that present results differ, in each case, from the average literature value by less than 1.5% and fall between extreme values.

Results of binary gas-phase diffusion measurements for thirty-one helium-halogenated hydrocarbon systems are shown in Table II. All results have been reduced to one atmosphere pressure assuming a p^{-1} dependence. Each diffusion coefficient represents the average value from at least five diffusion runs made at two or more different gas-flow velocities. Precision is indicated by the standard deviation of the individual determinations, in most cases about 2% of the observed diffusion coefficient.

Table II: Experimental Diffusion Coefficients for Some He-Halogenated Hydrocarbon Systems^a

System	No. of Runs	T, °K	D _{AB} ± std dev, cm ² /sec
He-difluoromethane	5	430.8	0.874 ± 0.030
He-1,1-difluoroethane	9	429.6	0.754 ± 0.015
He-1-fluorohexane	10	431.6	0.492 ± 0.006
He-fluorobenzene	8	429.7	0.566 ± 0.008
He-hexafluorobenzene	11	428.7	0.453 ± 0.008
He-4-fluorotoluene	10	431.6	0.508 ± 0.006
He-dichloromethane	10	427.5	0.750 ± 0.009
He-trichloromethane	8	429.1	0.624 ± 0.012
He-1,2-dichloroethane	8	427.1	0.683 ± 0.006
He-1-chloropropane	11	427.5	0.631 ± 0.009
He-1-chlorobutane	12	429.2	0.555 ± 0.010
He-2-chlorobutane	9	429.1	0.561 ± 0.008
He-1-chloropentane	8	428.2	0.518 ± 0.004
He-chlorobenzene	10	430.9	0.542 ± 0.006
He-dibromomethane	8	427.7	0.665 ± 0.007
He-bromoethane	15	427.7	0.740 ± 0.011
He-1-bromopropane	20	428.2	0.592 ± 0.009
He-2-bromopropane	10	428.0	0.606 ± 0.012
He-1-bromobutane	11	426.6	0.545 ± 0.006
He-2-bromobutane	7	427.2	0.553 ± 0.013
He-1-bromohexane	6	427.5	0.461 ± 0.008
He-2-bromohexane	7	427.9	0.470 ± 0.012
He-3-bromohexane	8	428.5	0.469 ± 0.004
He-bromobenzene	9	427.1	0.543 ± 0.010
He-2-bromo-1-chloropropane	6	427.2	0.570 ± 0.016
He-iodomethane	7	431.2	0.783 ± 0.016
He-iodoethane	9	428.4	0.648 ± 0.013
He-1-iodopropane	10	430.0	0.579 ± 0.007
He-2-iodopropane	11	430.2	0.579 ± 0.012
He-1-iodobutane	8	428.1	0.524 ± 0.007
He-2-iodobutane	6	427.1	0.545 ± 0.013

^a Reduced to 1 atm pressure.

(16) R. J. Adler and J. A. Koutsky, *Can. J. Chem. Eng.*, **42**, 239 (1964).

(17) J. C. Giddings, "Dynamics of Chromatography, Part I. Principles and Theory," Marcel Dekker, Inc., New York, N. Y., 1965.

(18) J. H. Knox and L. McLaren, *Anal. Chem.*, **36**, 1477 (1964).

(19) C. A. Boyd, N. Stein, V. Steingrimsson, and W. F. Rumpel, *J. Chem. Phys.*, **19**, 548 (1951).

(20) L. McLaren, Ph.D. Thesis, University of Edinburgh, Edinburgh, 1965.

Atomic Diffusion Volumes

The preceding data have been used to determine previously unavailable parameters for use in predicting binary diffusion coefficients in the absence of experimental data.

Fuller, Schettler, and Giddings have developed a correlation equation based on special *atomic diffusion volumes*.¹ The equation is

$$D_{AB} = \frac{1.00 \times 10^{-3} T^{1.75} (1/M_A + 1/M_B)^{1/2}}{p \{ (\sum_A v_i)^{1/3} + (\sum_B v_i)^{1/3} \}^2} \quad (7)$$

where T is the temperature, °K; M_A, M_B the molecular weight, g/mol; p the pressure, atm; and the v_i 's are the atomic diffusion volumes, cm³, to be summed over the atoms, groups, and structural features of each diffusing species. Numerous v_i 's and the 1.75 exponent to T were determined from a nonlinear least-squares analysis of over 300 experimental points. At that time the necessary data were lacking for -F, -Br, and -I, but values can now be established. More generally the data listed in Table I and II and additional points from the literature (references 8, 20, 21-32) were used to expand our data collection to 512 points. (Some points from a few references were not included in order to keep the quantity of data within reasonable limits.) Another least-squares analysis was carried out as before. The resulting optimized values of the atomic diffusion volumes are listed in Table III in comparison with the previous values. The list includes parameters for those halogen substituents not previously determined and gives improved values for the others.

The diffusion volumes in Table III were obtained excluding three data points for freon-12 systems

determined by Lee and Wilke.⁶ If these points are included, the parameters are -F = 11.9, -Cl = 22.5, -Br = 21.8 and -I = 29.8 cm³. Since it seems unreasonable that addition of -Cl should increase the collision cross section more than the addition of -Br, the listed values were for the present assumed more reliable.

In the latest least-squares analysis the temperature exponent was found to be 1.776. For simplicity it was decided to retain the previously determined 1.75. The diffusion volumes of Table III were obtained with the temperature exponent fixed at this value. (Average absolute error at the least-squares minimum 4.1%; at the constrained minimum = 4.2%.) The resulting increase in average error is insignificant.

Effective Collision Cross Sections of Complex Molecules

The nature and magnitude of collision cross sections are of considerable importance in the study of transport and rate phenomena.³³ Efforts have naturally focused on simple geometrical models ("hard" and "soft" spheres, spherocylinders, etc.). Relatively little work has been directed at the study of collision cross sections for complex molecules and the effect of chemical and structural parameters. This neglect has been reinforced by the long recognized difficulty in extending rigorous theory beyond models of utmost simplicity. As Watson and Goldberger point out, the collision of bound systems is an aspect of the intractable many-body problem.³⁴ Understanding is further complicated by the uncertain statistical populations of rotamers in gas-phase, flexible-chain molecules.

Transport coefficients, particularly viscosity and more recently crossed molecular beam scattering measurements have provided cross sectional data for many systems.³⁵ Hirschfelder, Curtiss, and Bird point out

Table III: Special Atomic Diffusion Volumes (cm³)^a

A. Atomic and structural diffusion volume increments, v_i 's					
C	15.9	[16.5]	(F)	14.7	...
H	2.31	[1.98]	(Cl)	21.0	[19.5]
O	6.11	[5.48]	(Br)	21.9	...
(N)	4.54	[5.69]	(I)	29.8	...
(S)	22.9	[17.0]	Aromatic or Heterocyclic Ring - 18.3 [-20.2]		
B. Diffusion volumes of atom and simple molecules, Σv_i 's					
He	2.67	[2.88]	CO	18.0	[18.9]
Ne	5.98	[5.59]	CO ₂	26.7	[26.9]
Ar	16.2	[16.1]	N ₂ O	35.9	[35.9]
Kr	24.5	[22.8]	NH ₃	20.7	[14.9]
Xe	32.7	[37.9]	H ₂ O	13.1	[12.7]
H ₂	6.12	[7.07]	SF ₆	71.3	[69.7]
D ₂	6.84	[6.70]	(Cl ₂)	38.4	[37.7]
N ₂	18.5	[17.9]	(Br ₂)	69.0	[67.2]
O ₂	16.3	[16.6]	(SO ₂)	41.8	[41.1]
Air	19.7	[20.1]			

^a Note: () indicates the listed value is based on only a few data points. [] indicates previous values, ref 1.

- (21) R. E. Bunde, University of Wisconsin Naval Research Laboratory Report CM 850, 1955.
 (22) J. P. Kohn and N. Romero, *J. Chem. Eng. Data*, **10**, 125 (1965).
 (23) A. P. Malinauskas, *J. Chem. Phys.*, **42**, 156 (1965).
 (24) R. Paul and I. B. Srivastava, *ibid.*, **35**, 1621 (1961).
 (25) R. Paul and I. B. Srivastava, *Ind. J. Phys.*, **35**, 465 (1961).
 (26) R. Paul and I. B. Srivastava, *ibid.*, **35**, 523 (1961).
 (27) W. F. Rumpel, University of Wisconsin Naval Research Laboratory Report CM 851, 1955.
 (28) S. C. Saxena and E. A. Mason, *Mol. Phys.*, **2**, 379 (1959).
 (29) K. P. Srivastava, *Physica*, **25**, 571 (1959).
 (30) R. E. Walker and A. A. Westenberg, *J. Chem. Phys.*, **32**, 436 (1960).
 (31) A. A. Westenberg and G. Frazier, *ibid.*, **36**, 3499 (1962).
 (32) S. Weissman, S. C. Saxena, and E. A. Mason, *Phys. Fluids*, **4**, 643 (1961).
 (33) J. O. Hirschfelder, C. F. Curtiss, and R. B. Bird, "Molecular Theory of Gases and Liquids," John Wiley & Sons, Inc., New York, N. Y., 1954.
 (34) M. L. Goldberger and K. M. Watson, "Collision Theory," John Wiley & Sons, Inc., New York, N. Y., 1964, Chapter 11.
 (35) E. W. Rothe and R. B. Bernstein, *J. Chem. Phys.*, **31**, 1619 (1959); R. W. Landorf and C. R. Mueller, *ibid.*, **45**, 240 (1966).

the advantage of binary diffusion, as opposed to viscosity and thermal conductivity, in that it reflects directly the interaction between dissimilar molecules.³³ Adding to this advantage, the GC peak broadening method, with the extreme sensitivity of existing GC detectors, can be used for components in exceedingly small concentrations (*e.g.*, 10^{-9} mole ratio). Hence large and complex molecules, which may decompose before reaching their boiling point, can be studied at high vapor dilutions well below this temperature. Gas chromatography itself has been applied to high boiling compounds 200–250° below their boiling points;³⁶ such species would be difficult to study by viscosity, molecular beam or most diffusion techniques.

The statistics of collisions between like molecules become exceedingly complicated if the molecules are complex and especially if they are flexible. By our approach the cross sectional probe is a helium atom or other inert species. This "atomic probe" has the advantage of simple geometry, low mass, smallness, and inertness. It is little affected by attractive forces, thus yielding an approximation to the repulsive shell independent of dipole and chemical factors. By virtue of its small size and low mass, D_{AB} will reflect a degree of structural fine graining.

For simple systems, temperature is a key variable, providing evidence on the depth and shape of the potential well. For complex systems, particularly where one is probing for the relatively hard shell of repulsion, chemical structure is presently a more relevant parameter. The fine nuances of temperature variability, complicated by structural change, would, to be useful, require theoretical elaboration much beyond present knowledge. This explains our present emphasis on structural factors.

Liquid droplet models. Eq 7 has its roots in hard-sphere kinetic theory. The denominator is essentially a replacement for $p(\sigma_A + \sigma_B)^2$, where σ 's are collision diameters. Arnold replaced the σ 's by the sum of the atomic LeBas volumes raised to the $-1/3$ power.³⁷ This has proven an effective way for estimating the cross sections of complex molecules using bulk volumetric data. Equation 7 relates to the Arnold approach except that the cross sections are provided by the diffusion data themselves. Therefore eq 7, with allied atomic diffusion volume parameters, provide an approximate measure of relative collision cross sections.

The above are essentially "liquid droplet" models, in which the group volumes add together and somehow assume spherical shape. The success of these approaches is somewhat surprising; one would expect shape (nonsphericity) factors to have more influence on cross section. There is presently no tractable theoretical approach to this question for truly complex molecules, although significant advances have been made in basic theory.³⁸ Some semiquantitative considerations are given below based on collision "shielding."

Groups within complex molecules are partially shielded from collision by other groups which exempt certain collision paths. When a group is completely shielded it contributes nothing to the cross section of the target molecule. Extended molecules, with exposed (minimally shielded) groups, have relatively large total cross sections.

The contribution of group i to cross section may be written as $a_i = a_{i0} (1 - S_i)$ where S_i is the shielding probability. If other groups were positioned randomly around group i we would have

$$S_i = 1 - \prod_{j \neq i} (1 - s_{ij}) \quad (8)$$

where s_{ij} is the probability that group j intercepts the collision path. However the structural correlation introduced by fixed bond lengths, angles and, for rigid molecules, rotational states, will alter the result somewhat.

The effect of molecular dimensions can be shown by assuming a probe molecule of diameter σ_p and a shielding group of diameter σ_j at distance d_{ij} from group i . Providing d_{ij} is large compared to the σ 's, orientation averaging yields

$$s_{ij} = \left(\frac{\sigma_p + \sigma_j}{4d_{ij}} \right)^2 \quad (9)$$

i.e., the shielding probability falls off with the inverse square of group separation distance. One would therefore expect larger s_{ij} 's and smaller cross sections for molecules in a droplet form than in an extended chain configuration. The contradiction of this with the widespread success of the "liquid droplet" model invites closer scrutiny.

Experimental Evidence. The experimental data in Table II show that smaller diffusion coefficients are associated with halogens in the 1-position than in the 2- or 3-position on a straight chain. The latter are presumably more globular. The helium-1-iodopropane and helium-2-iodopropane systems, with nearly equal diffusion coefficients, were the only exceptions. Statistical tests³⁹ indicate that these small differences are significant; for 1-bromohexane and 2-bromohexane at the 75% confidence level and for the other pairs at the 95% level.

Early diffusion data for halogenated hydrocarbons diffusing in air, summarized in the International Critical Tables,¹⁰ show the same effect. Similar results for isomeric butanols diffusing in air have been observed by

(36) B. L. Karger and W. D. Cooke in "Advances in Chromatography," Vol. 1, J. C. Giddings and R. A. Keller, Marcel Dekker, Inc., New York, Ed., N. Y., 1965, Chapter 9.

(37) J. H. Arnold, *Ind. Eng. Chem.*, **22**, 1091 (1930).

(38) C. F. Curtiss and J. S. Dahler, *J. Chem. Phys.*, **28**, 2352 (1963).

(39) C. A. Bennett and N. L. Franklin, "Statistical Analysis in Chemistry and the Chemical Industry," John Wiley & Sons, Inc., New York, N. Y., 1954.

Gilliland⁴ and for propanols in helium by Seager, Geertson, and Giddings.⁴⁰

While many data for unsubstituted hydrocarbons show a similar trend, diffusion coefficients for branched hydrocarbons are often equal or less than values for the straight chain compounds.^{19,20,41} Such results have been used to infer a crumpled form for straight-chain paraffins.⁴¹

Additional evidence comes from the comparison of diffusion volumes (added from Table III) with LeBas boiling points volumes ($-C = 14.8$ and $-H = 3.7$ cm³) for straight-chain hydrocarbons. With increasing carbon number beginning at C₁ the ratio is 0.848, 0.883, 0.896, 0.901, 0.906, 0.908 0.923; the latter being the limiting long-chain value. It appears that the diffusion data may have "distorted" the carbon-hydrogen diffusion volume ratio (responsible for the above variation) so that slightly reduced diffusion among long chains is obtained. This broad trend reflects results with over one hundred binary pairs. Some contradictions arise among aromatic compounds; *e.g.*, benzene, compact in structure, has a ratio of 0.948. This may result from incorrectly lumping heterocyclic and other aromatic rings into a single parameter.

We conclude that the liquid-droplet model works surprisingly well, which may relate to the following considerations. Few chain compounds are expected to actually assume near-spherical configurations. However cross sections, when averaged over all external rotations, apparently have roughly similar asymmetric contributions. (The abnormal sphericity of methane is allowed for in the adjustable C-H volume ratio; also the calculated cross sections are usually too high.) The long-chain molecules, whose deviations alone

could be extreme, may have rotational-isomer populations weighted toward intramolecular associated forms. This would contrast with liquid-state, and especially solid-state, populations where the *trans-trans* conformation about each single bond is favored by roughly 500 cal.⁴² However the net attractive interactions between segments in solvent-free (*i.e.*, gas-phase) long-chain molecules may decrease mean dimensions. This is not unlike Langmuir's arguments for coiling due to excess surface energy in unlike media, and has been confirmed at intervals for gas-phase paraffins based on transport cross sections.^{41,43} The effect would likely increase with chain length, but increasing nonvolatility hinders investigation. Perhaps the present technique, applicable at high dilutions, could produce cross section data bearing on the matter.

More theoretical work is needed with these complex systems in order to ascertain the effects of rotameric and external-rotation averaging, increasingly important secondary collisions (successive collisions of the "probe" with the same "target" molecule) and realistic intergroup and intermolecular potentials.

Acknowledgment. This investigation was supported by Public Health Service Research Grant GM 10851-12 from the National Institutes of Health.

(40) S. L. Seager, L. R. Geertson, and J. C. Giddings, *J. Chem. Eng. Data*, **8**, 168 (1963).

(41) G. A. McD. Cummings and A. R. Ubbelohde, *J. Chem. Soc.*, 3751 (1953).

(42) R. A. Scott and H. A. Scheraga, *J. Chem. Phys.*, **44**, 3054 (1966); S. Mizushima, "Structure of Molecules and Internal Rotation," Academic Press, New York, N. Y., 1954.

(43) R. M. Melavin and E. Mack, *J. Amer. Chem. Soc.*, **54**, 888 (1932); J. C. McCoubrey, J. N. McCrea, and A. R. Ubbelohde, *J. Chem. Soc.*, 1961 (1951).

The Effect of Hydrogen Bonding upon the Autoxidation Kinetics of Tetrakis(dimethylamino)ethylene

by Aaron N. Fletcher

Chemistry Division, Research Department, Naval Weapons Center, China Lake, California 93555 (Received January 2, 1969)

The autoxidation of tetrakis(dimethylamino)ethylene has an apparent negative, zero, or positive Arrhenius activation energy depending upon the concentration of the hydrogen bonding catalyst, 1-octanol. The kinetics are both first and fourth order with respect to the 1-octanol monomer concentration. When the concentrations of the alcohol self-association species are considered, it is found possible to explain these results by a zero Arrhenius activation energy for both the acyclic self-association tetramer and the monomer. These results suggest that the acidity of the acyclic self-association species may be the important parameter in high-order alcoholysis rather than "solvation" of the reaction intermediate.

Introduction

Conflicting interpretations¹⁻⁸ of kinetics and mechanism usually result when alcohols serve as chemical reactants. For example, Fagley, *et al.*,³ interpret the alcoholysis of acid chlorides as being second order with a push-pull⁵ mechanism. Hudson and Loveday,² on the other hand, interpret the same reaction as being first, second, and third order with different alcohol self-association species serving as the reactants. Furthermore, Hudson and Loveday found second order only over a very limited concentration range.

This writer wishes to report results on the autoxidation of tetrakis(dimethylamino)ethylene (TMAE), where similar high-order alcohol kinetics have been observed⁹ (and with similar conflicts with respect to the kinetics and mechanism).^{10,11} It will be shown that the effect of the alcohol, 1-octanol, can be explained solely on the basis of the acidity of the alcohol self-association species without having to consider that the high kinetic order is due to solvation of the reaction intermediate as reported earlier.⁹

Experimental Results

The experimental techniques have been previously described.⁹ A new automated system was constructed around a Turner 210 spectrofluorometer.¹² The solvent was *n*-decane.

The rates of reaction at 1-octanol concentrations below $10^{-2} M$ were found to be sensitive to the degree of agitation of the solution (Figure 1). This is attributed to catalysis by O-H groups attached to the glass walls of the reaction vessel and will be designated the wall effect, W .

The kinetic parameters were related by⁹

$$-\frac{d(\text{TMAE})}{dt} = (\text{TMAE}) \times O_2 \times F(A) \quad (1)$$

where O_2 represents the partial pressure of oxygen in

Torr and $F(A)$ represents some function of the alcohol concentration. An iterative procedure⁹ was used to determine constants, C_i in the expression

$$F(A) = W + C_1A_1 + C_2A_1^2 + C_4A_1^4 \quad (2)$$

where A_1 is the concentration of the 1-octanol monomer calculated from the equilibrium quotients reported by Fletcher and Heller.¹³ Values for W were determined with no added alcohol; values for C_1 (Figure 2) were determined at very low alcohol concentrations; values for C_4 were determined at very high alcohol concentrations; both C_1 and C_4 were corrected for the effect of each other.

It was not found possible to determine a reasonable value for C_2 (consistent with subsequent activation energies and enthalpy changes for hydrogen-bond formation). The values for W (static), C_1 , and C_4 are shown in Table I. Plots of the data at the two extremes of temperature, 5 and 45°, are shown in Figure 3. As indicated by Figure 1 and Table I, an average value for C_1 was taken from the results of all four temperatures.

Discussion

The Effect of Alcohol Self-Association. With in-

- (1) R. F. Hudson, *J. Chem. Soc.*, 761 (1966).
- (2) R. F. Hudson and G. W. Loveday, *ibid.*, 766 (1966).
- (3) T. F. Fagley, G. A. von Bodungen, J. J. Rathmell, and J. D. Hutchinson, *J. Phys. Chem.*, **71**, 1374 (1967).
- (4) A. E. Oberth and R. S. Bruenner, *ibid.*, **72**, 845 (1968).
- (5) C. G. Swain, *J. Amer. Chem. Soc.*, **70**, 1119 (1948).
- (6) E. D. Hughes, C. K. Ingold, S. F. Mok, and Y. Pocker, *J. Chem. Soc.*, 1238 (1957).
- (7) E. A. Cavell and J. A. Speed, *ibid.*, 226 (1961).
- (8) A. J. Parker, *Quart. Rev.* (London), **16**, 163 (1962).
- (9) A. N. Fletcher and C. A. Heller, *J. Catal.*, **6**, 263 (1966).
- (10) A. N. Fletcher and C. A. Heller, *J. Phys. Chem.*, **71**, 1507 (1967).
- (11) J. P. Paris, *Photochem. Photobiol.*, **4**, 1059 (1965).
- (12) G. K. Turner, *Science*, **146**, 183 (1964).
- (13) A. N. Fletcher and C. A. Heller, *J. Phys. Chem.*, **71**, 3742 (1967).

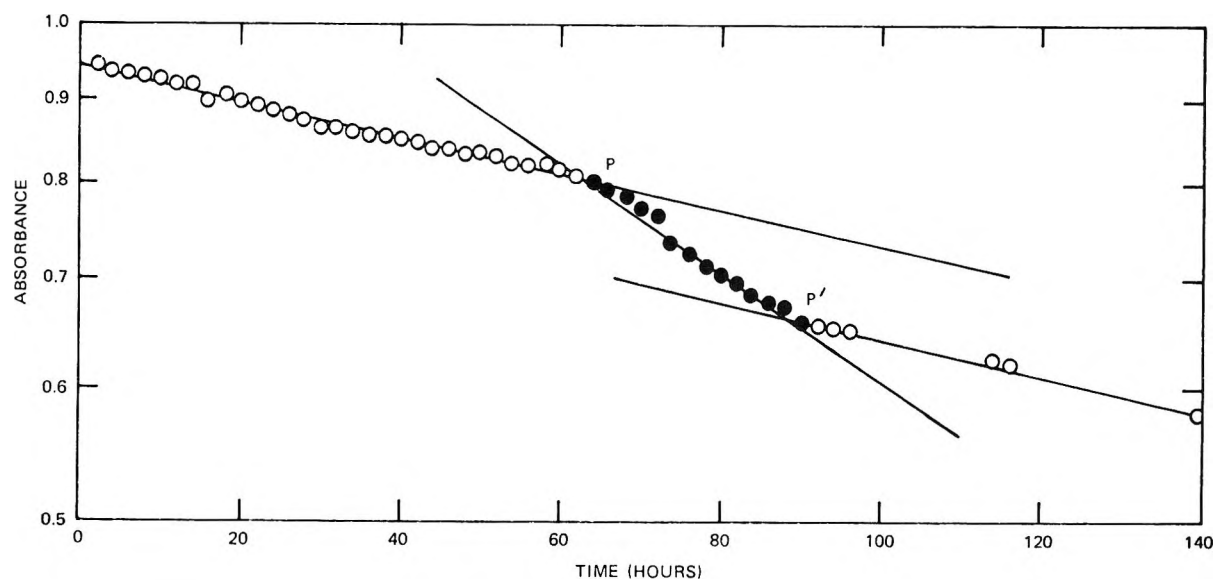


Figure 1. Reaction kinetics under quiescent and agitated conditions. Agitation was performed from P to P'. Experimental conditions: 1200 Torr of O_2 ; 5° temperature; zero added 1-octanol; absorbance measurements were performed at 350 nm.

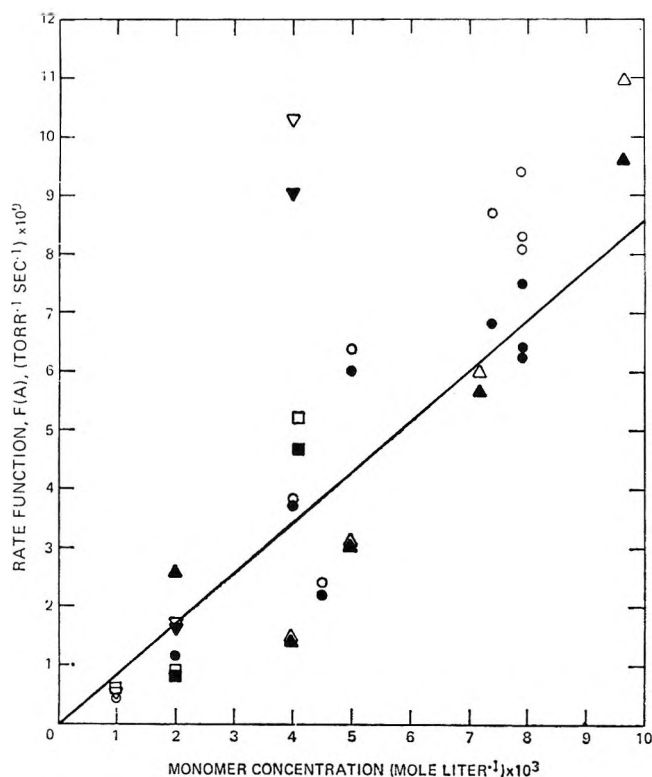


Figure 2. Determination of specific rate function for the monomer. All points corrected for wall effect, W . Solid points show tetramer correction in contrast to measured open points: Δ , 45°; \circ , 30°; \square , 15°; ∇ , 5°. Solid line is average of all four temperatures for solid points.

creasing alcohol concentration, the observed rate of autoxidation is found to be independent of temperature, to decrease with increasing temperature, and then to increase with increasing temperature (Figures 2 and 3). This type of anomalous behavior can be readily explained by the variation in the concentrations of the

Table I: Average Values for the Terms in $F(a)$ at Various Temperatures

Temp, °C	$W \times 10^3$, Torr ⁻¹ sec ⁻¹	$C_1 \times 10^6$, mol ⁻¹ Torr ⁻¹ sec ⁻¹	C_4 , mol ⁻⁴ Torr ⁻¹ sec ⁻¹
5	0.82	0.85	4.75
15	0.92	0.85	1.82
30	1.02	0.85	0.485
45	2.48	0.85	0.134

monomer and the acyclic tetramer (Figure 4). The concentrations of the acyclic tetramer at 5 and 45° undergo a reversal in their relative amounts in the same manner as the over-all reaction rate function, $F(A)$.

Using the data of Table I, specific rate constants, $k(A_i)$ can be calculated for one of the two tetramer species if the remaining species has a negligible kinetic effect. The rate constants also can be calculated as if both species had the same effect

$$k(A_i) = [F(A) - W - k(A_1)]/A_i \quad (3)$$

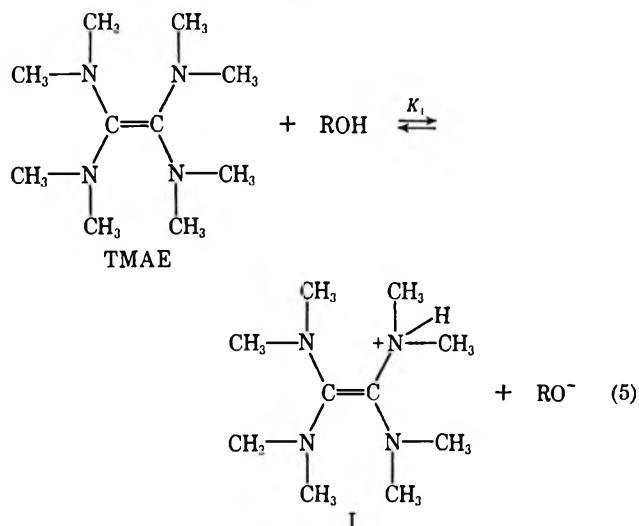
where A_i may be the concentration of the acyclic tetramer, A_{4a} , the cyclic tetramer, A_{4c} , or their sum, A_4 . Figure 5 shows the results of these calculations in an Arrhenius plot. Either the acyclic or the cyclic tetramer give a linear Arrhenius plot leading to activation energies of 0.0 and 3.8 kcal/mol, respectively. An averaging of both acyclic and cyclic species leads to a non-linear plot (Figure 5). It would be unreasonable for the monomer to have a zero activation energy while the cyclic tetramer had a thousandfold larger specific rate constant with a positive activation energy. It appears far more likely that the acyclic species, with its avail-

able O-H and zero activation energy, is the reactive tetramer. Thus it is possible to write

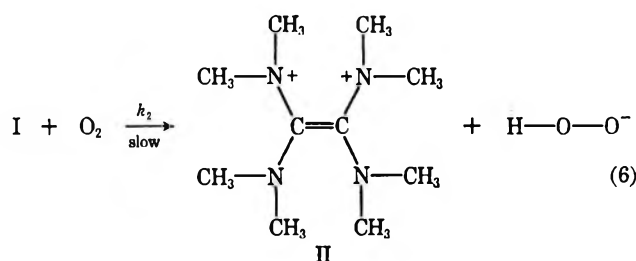
$$F(A) = W + 0.85 A_1 + 10^{-6} + 2.9 A_{4a} \times 10^{-3} \quad (4)$$

which is valid from 5 to 45°.

The Reaction Mechanism. Fletcher and Heller considered that the initial step in the autoxidation of TMAE was the formation of a contact donor-acceptor complex between TMAE and oxygen.⁹ The donor-acceptor complex in turn was considered to react with each alcohol species. Their mechanism,^{9,10} however, does not account for the markedly different rates of reaction observed between the monomer and the polymeric forms. The initial step proposed by Urry and Sheeto¹⁴ would be preferable



followed by



since a steady-state treatment⁹ leads to

$$-\frac{d(\text{TMAE})}{dt} = K_1 k_2 (\text{ROH})(\text{TMAE})(\text{O}_2) \quad (7)$$

where the differing acidity of the alcohol species, ROH, is reflected in the value of the equilibrium constant, K_1 . The subsequent kinetic steps are identical with those previously described.¹⁰ In eq 5 and 7, R represents either an aliphatic or an alcohol self-association acyclic chain. Since the "free" end of acyclic self-association polymeric species should be more acidic than the monomer,¹⁵ this mechanism can account for the reaction rate constants having the relationship

$$\text{acyclic tetramer} > \text{monomer} \gg \text{cyclic tetramer} \quad (8)$$

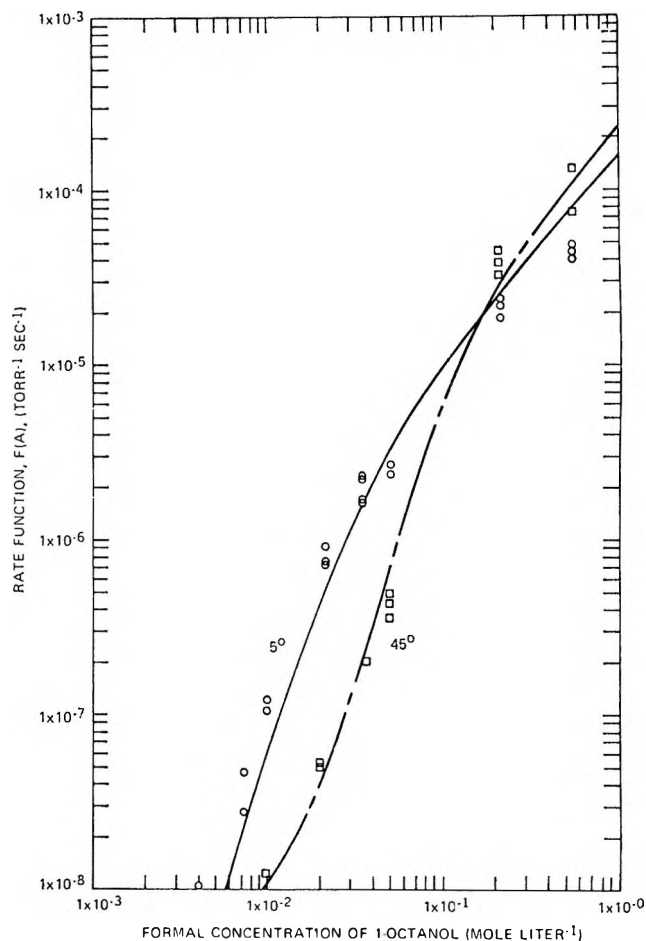


Figure 3. Determination of specific rate constant for the tetramer. Lines are calculated from eq 4.

Thus it is not necessary to assume that the solvation of the reaction intermediate by alcohol is the cause of the observed high order kinetics. If the cyclic tetramer is completely nonreactive, then "solvation" of the reaction intermediate by the catalyst is a very unlikely argument in the autoxidation of TMAE.

Conflicts in the Kinetic Order of Alcohol Reactions. A primary cause for conflicting results for reactions involving alcohol has been the practice^{3-7,16} of using the formal "added" alcohol concentration as if it was the molar concentration of the monomer. Since nonsterically hindered alcohols self-associate, the formal concentration is approximately equal to the molar concentration only at low concentrations in a nonreactive solvent—and even carbon tetrachloride can serve as an acceptor for hydrogen bond formation.¹⁷ How low a concentration depends primarily upon the solvent and the temperature (different nonhindered alcohols appear

(14) W. H. Urry and J. Sheeto, *Photochem. Photobiol.*, **4**, 1067 (1965).

(15) L. J. Bellamy and R. J. Pace, *Spectrochim. Acta*, **22**, 525 (1966).

(16) F. W. Balfour and T. F. Fagley, *J. Phys. Chem.*, **72**, 1300 (1968).

(17) A. N. Fletcher, *ibid.*, **73**, 2217 (1969).

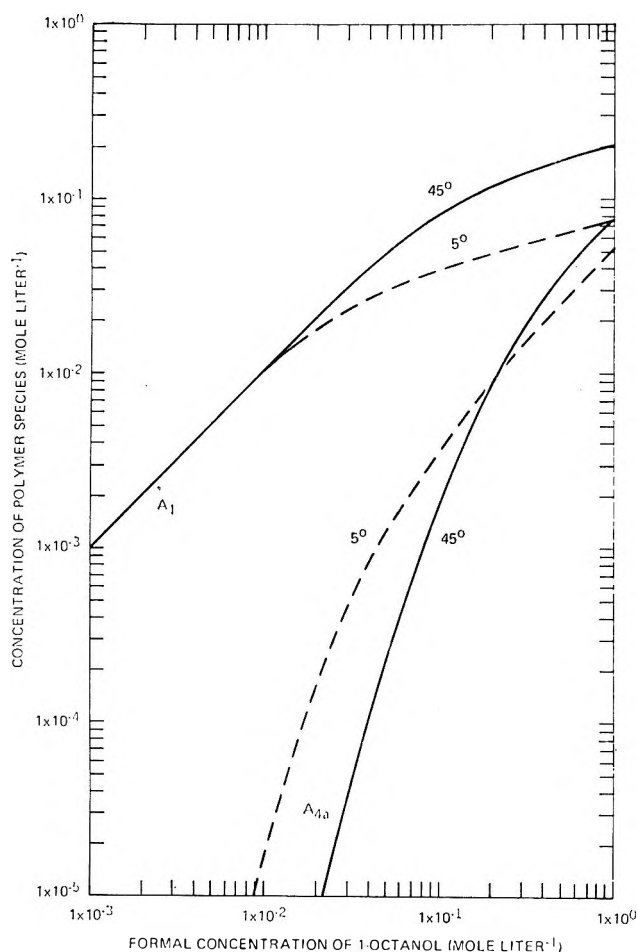


Figure 4. Calculated concentration of 1-octanol monomer, and A_1 , acyclic tetramer, A_{4a} , at 5 and 45°.

to self-associate to about the same degree.¹⁷) An example of the effect of plotting formal concentrations can be seen in the work of Fletcher and Heller⁹ where they found that the autoxidation of TMAE gave a very reasonable third order in formal "added" 1-octanol over a tenfold range (up to 0.1 F), whereas the order became fourth from the same data when the molar concentration of the monomer was plotted.

Any overestimation of the monomer concentration in effect causes a reduction of the apparent kinetic order in alcohol. This is a particular problem for high order reactions where the limited range of concentrations (either due to the speed of the reaction or else due to the possibility of reaching concentrations greater than

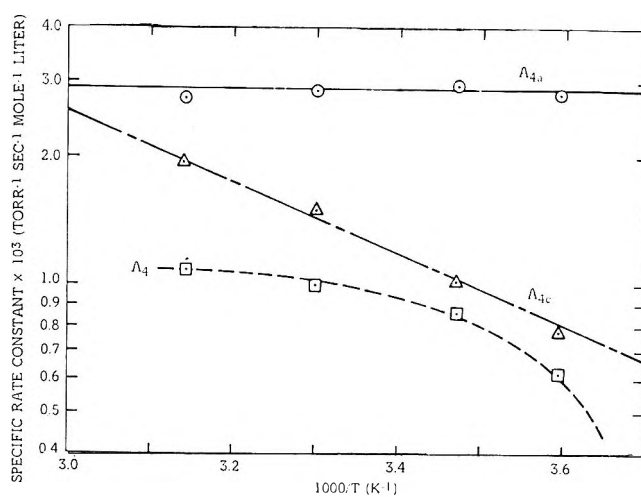


Figure 5. Determination of Arrhenius activation energies for a specific polymer species. Acyclic tetramer, A_{4a} ; cyclic tetramer, A_{4c} ; total tetramer, A_4 .

that of neat alcohol) prevent the observation of rate constants over a range of values that is large enough to truly distinguish a third order from a fourth. Since the only *positive*¹⁸⁻²⁰ evidence for particular self-association polymeric species of alcohols are those for dimers^{21,22} and tetramers,¹³ with only the tetramer being found in high concentrations of nonhindered alcohols,²² true evidence for a reaction being third order in alcohol monomer over a large concentration range is probably an indication of an increased complication of the mechanism rather than a simple reaction with an alcohol trimer.

(18) By positive, I eliminate evidence from two-parameter power series that have been fit to experimental evidence. It has been demonstrated^{13,19} that numerous different models of self-association can be fit to these equations. Only very small differences in error functions (which very often have not been properly "weighted")²⁰ must be used as evidence of one model in preference to another. These power series are useful only after the correct model has been determined by positive evidence for the existence of the species used in the mathematical relationship. The most positive evidence of which I know is the variation of the 2.86- μm band with the second power of the monomer band at 1.41 μm as evidence for the dimer^{21,22} and the variation of the 1.43-1.65- μm region to the fourth power of the 1.41- μm monomer band as evidence for the tetramer.¹³

(19) H. Dunken and H. Fritzsche, *Spectrochim. Acta*, **20**, 785 (1964).

(20) W. E. Denning, "Statistical Adjustment of Data," John Wiley and Sons, Inc., New York, N. Y., 1943.

(21) R. M. Hammaker, R. M. Clegg, L. K. Patterson, P. E. Rider, and S. L. Rock, *J. Phys. Chem.*, **72**, 1837 (1968).

(22) A. N. Fletcher and C. A. Heller, *ibid.*, **72**, 1839 (1968).

Thermal Isomerization of the Maleate Ion in Potassium Halide Matrices¹

by I. C. Hisatsune,² R. Passerini, R. Pichai, and V. Schettino

Department of Chemistry, Whitmore Laboratory, The Pennsylvania State University, University Park, Pennsylvania 16802 and Molecular Spectroscopy Laboratory, Institute of Organic Chemistry, University of Florence, Florence, Italy (Received January 9, 1969)

The thermal isomerization of the maleate ion to the fumarate has been studied in KCl, KBr, and KI matrices by infrared spectroscopy. In the temperature range of 240–300°, the reaction proceeds essentially quantitatively by first-order kinetics with a negligible decomposition of the maleate or the fumarate ion. When crystalline, hydrated, disodium maleate was used as the solute, the same rate constant of $2.6 \times 10^{16} \exp[(-47,000 \pm 5000)/RT] \text{ sec}^{-1}$ was obtained from KCl and KBr matrices while the rate constants were lower in the KI matrix by a factor of about 3 but with the same activation energy. With anhydrous disodium maleate as the solute, the rate constant was $5.3 \times 10^8 \exp[(-30,000 \pm 5000)/RT] \text{ sec}^{-1}$ in KCl while those from KBr and KI matrices had the same activation energy but were both lower by a factor of about 3. It is suggested that this variation in the reaction activation energy arises from the changes in the structure of the maleate ion according to the method of dehydration of the crystalline hydrated disodium maleate.

Introduction

The transformation of the maleate ion to the fumarate by the rotation about a double bond appears to be the simplest isomerization reaction that one can study in the solid state.³ Although the usual experimental procedure of thermogravimetric analysis (tga) is not applicable to the study of this reaction, the infrared method utilizing pressed alkali halide matrices is. We have shown earlier that the latter experimental technique is a convenient way of studying solid state thermal decomposition reactions and, where comparisons can be made, gives results similar to those from tga.⁴ In this paper we report an infrared study of the thermal isomerization of the maleate ion isolated in KCl, KBr, and KI matrices.

Experimental Section

Hydrated disodium maleate was a reagent grade chemical from Fluka AG, while the potassium halides were optical grade salts from the Harshaw Chemical Co. The technique of fabricating pressed disks and using them in kinetic studies has been described before.⁴ Ovens used to maintain the disks at appropriate reaction temperatures were electrically heated aluminum blocks in which small holes were drilled into their sides for sample compartments. The sample compartments were kept dark while the disks were being heated, and temperatures were controlled to within 2°. The infrared spectra of the disks were recorded with a Perkin-Elmer Model 421 (Florence) and Model 521 (Penn. State) spectrometers.

Results

The infrared spectrum of crystalline, hydrated disodium maleate dispersed in KCl, KBr, and KI matrices was essentially the same as the one reported in the literature.⁵ Heating of a disk at 120° for about 10 hr caused a complete dehydration of the solute, and this

was accompanied by the disappearance of the broad and intense hydroxyl group infrared band system near 3500 cm^{-1} and of other absorption band fine structures characteristic of the crystalline solute. Further heating at 120° for a 24-hr period led to no additional changes in the infrared spectrum of the disk. At temperatures above about 240°, the isomerization reaction occurred at a measurable rate, and new infrared bands due to the fumarate ion appeared. After completion of the reaction, the infrared spectrum of the disk showed, in addition to the absorption bands of the fumarate ion,⁵ weak bands due to the formate^{6a} and monomeric bicarbonate^{6b} ions. The latter ions are formed by the solute decomposition which becomes appreciable at temperatures above 300°.

The isomerization rate of the maleate ion in a KBr disk was followed by observing the intensity changes of the maleate infrared band at 1308 cm^{-1} and the fumarate band at 807 cm^{-1} . Both of these bands are sharp, relatively intense, and nearly free from overlap with other bands of the reactant and product. In the temperature range of 210–300°, the decay of the 1308- cm^{-1} band and the growth of the 807- cm^{-1} band followed first-order kinetics over about 80–90% of the reaction, and rate constants from these bands were the

(1) Supported by the Air Force Office of Scientific Research (SRC) Grant AFOSR-907-67, by the Public Health Service National Center for Radiological Health Grant RH-433, and by the Italian National Research Council.

(2) To whom correspondence should be addressed at the Pennsylvania State University.

(3) R. B. Cundall, *Progr. Reaction Kinetics*, **2**, 165 (1964).

(4) F. E. Freeberg, K. O. Hartman, I. C. Hisatsune, and J. M. Schempf, *J. Phys. Chem.*, **71**, 397 (1967).

(5) M. K. Hargreaves and E. A. Stevinson, *Spectrochim. Acta*, **20**, 317 (1964).

(6) (a) K. O. Hartman and I. C. Hisatsune, *J. Phys. Chem.*, **70**, 1281 (1966); (b) D. L. Bernitt, K. O. Hartman, and I. C. Hisatsune, *J. Chem. Phys.*, **42**, 3553 (1965).

same within the limits of experimental errors. However, since there was some dependence of the rate constants on the initial solute concentrations as shown in Table I, in our kinetic runs the solute concentrations

Table I: Concentration Dependence of the Isomerization Rate Constant in a KBr Matrix at 277° (Initial Solute: Hydrated Disodium Maleate)

$k \times 10^4 \text{ sec}^{-1}$		Initial concn, mg/g				
		0.20	0.60	1.2	1.8	2.4
	From maleate	8.9	8.8	9.3	4.6	2.2
	From fumarate	9.2	8.8	8.8	5.0	2.1

were kept below about 1.5 mg/g (1.5 mg of hydrated disodium maleate crystal/g of potassium halide matrix).

Since the hydrated disodium maleate crystal can be dehydrated just as well outside of the halide matrix as within, we also prepared disks in which the anhydrous disodium maleate powder was used as the initial solute. These disks showed infrared spectra which were indistinguishable from those obtained with samples containing hydrated crystals as initial solutes, but their kinetics were different. Thus, we made two sets of kinetic runs using as solutes the maleate ion in two different crystal forms. Isomerization rate constants obtained from these runs in various matrices are summarized in Figures 1 and 2. In these figures, the experimental uncertain-

Table II: Arrhenius Parameters for the Isomerization Reaction of the Maleate Ion

Matrix	Temp range, °C	Frequency factor, sec ⁻¹	Activation energy, kcal/mol
Series I. Initial Solute = Hydrated Disodium Maleate Crystal (Figure 1)			
KCl	244-307	2.6×10^{15}	47 ± 5
KBr	210-299	2.6×10^{15}	47 ± 5
KI	258-300	8.0×10^{14}	47 ± 5
Series II. Initial Solute = Anhydrous Disodium Maleate Powder (Figure 2)			
KCl	251-300	5.3×10^8	30 ± 5
KBr	265-295	1.7×10^8	30 ± 5
KI	255-299	1.7×10^8	30 ± 5

ties are the greatest for the rate constants obtained near 300° since shorter heating times (5 min) were required and fewer concentration determinations were possible in such runs. Because of the scatter in the experimental points, the Arrhenius activation energies from the three matrices are considered to be the same for each kind of solute. These activation energies and the frequency factors are listed in Table II.

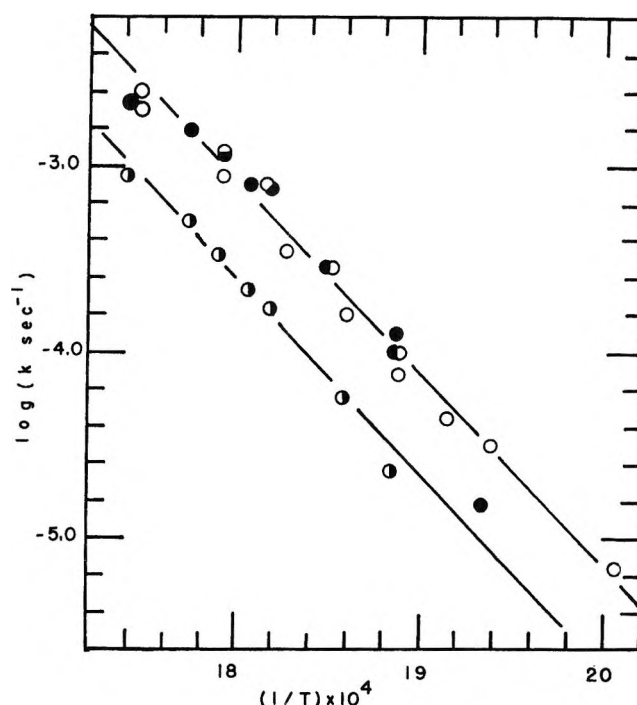


Figure 1. Series I isomerization rate constants for the maleate ion in potassium halide matrices: ●, KCl; ○, KBr; ◐, KI.

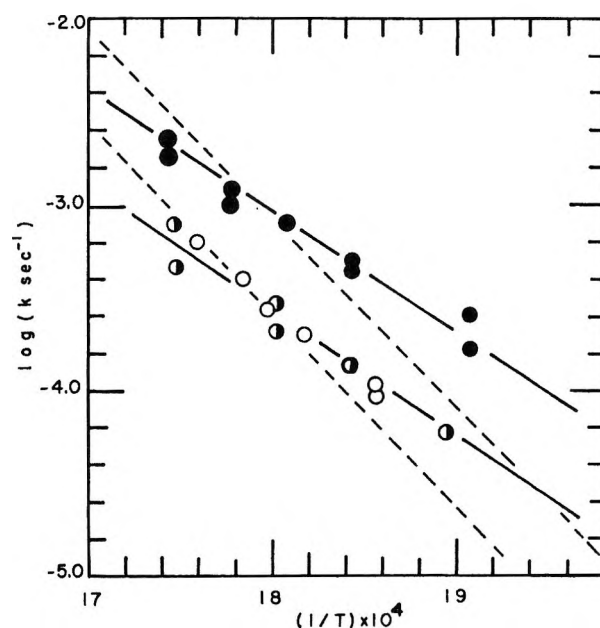


Figure 2. Series II isomerization rate constants for the maleate ion in potassium halide matrices: ●, KCl; ○, KBr; ◐, KI. The dotted lines are the slopes from Figure 1.

Discussion

The variations in the rate constant with different host matrix observed in the present study are comparable in magnitude, although not necessarily in the same order, to those found in earlier studies of the thermal decomposition of the formate^{6a} and the oxalate⁴ ions. Since such a dependence on the host matrix suggests a good

dispersion of the solute ions, it is surprising that two sets of kinetic results were obtained from the maleate ion in each matrix. Evidently, dehydration of a crystalline hydrated disodium maleate in a potassium halide matrix gives an ion which is different from the maleate ion present in anhydrous disodium maleate powder. The similarity of the infrared spectra of these two kinds of maleate suggests that a difference in the orientations of the carboxyl groups in the molecule may be the cause of the observed kinetic behavior. One notes in Figure 2 that at higher reaction temperatures, the difference between the results of series I and II runs for KCl and KI matrices are not great and may even be within the experimental error limit. However, at lower temperatures the series II rates in these matrices are about a factor of 3 faster than those of series I. On the other hand, the isomerization rates in KBr for series I

and II show a clear difference over the entire temperature range.

The Arrhenius activation energies obtained in the present study may be compared to 36 and 25 kcal/mol reported for the isomerization of dimethyl maleate in the gas phase⁷ and in the pure liquid phase,³ respectively.

Acknowledgments. I. C. Hisatsune is most grateful to the Italian National Research Council for the Visiting Professorship and to Professor Salvatore Califano for the hospitality at the University of Florence. V. Schettino wishes to thank the U. S. Fulbright-Hays Program Committee for a travel grant to the United States.

(7) W. W. Kwie and W. C. Gardiner, Jr., *Tetrahedron Lett.*, **6**, 405 (1963).

Studies of Water Vapor Dissociated by Microwave Discharges at Low Flow Rates.

I. Effect of Residence Time in the Traversed Volume

on Product Yields at Liquid Air Temperature^{1a}

by R. A. Jones, Walter Chan, and M. Venugopalan^{1b}

Department of Chemistry, Royal Military College of Canada, Kingston, Ontario, Canada (Received January 13, 1969)

Yields of hydrogen peroxide and evolved oxygen from the products trapped at liquid air temperature from water vapor dissociated by a low pressure microwave discharge at low flow rates were determined as functions of the time elapsing between the dissociation of the vapor and trapping of the dissociated products, using different traversed volumes and inlet pressures. For very small traversed volumes the yields of both H₂O₂ and evolved O₂ were negligible at all discharge powers studied, suggesting that either OH was not present in the gases passing out of the discharge or that, at least when H is present, OH radicals do not dimerize in a liquid air-cooled trap to form H₂O₂, but react with H to form H₂O. Both yields increased to a maximum and decreased thereafter with increasing traversed volume (at constant pressure) and increasing discharge pressure (at constant traversed volume), but were not affected markedly by increasing the discharge power. In any case, the maxima did not coincide and the evolved oxygen to peroxide ratio varied with traversed volume and pressure. However, the ratio was independent of the discharge power at all traversed volumes, thus indicating that the oxygen evolution is not due to decomposition of H₂O₂ by impurities carried over from the discharge. Finally, material balances showed that O₂ passed through the cold trap only at pressures and traversed volumes higher than those at which the peroxide yield was a maximum, suggesting that O₂ is one of the precursors involved in the formation of H₂O₂ and evolved O₂.

I. Introduction

The influence of residence time of dissociated water vapor in the discharge zone^{2,3} and in the reaction volume between the discharge exit and the cold trap⁴⁻⁶ on the yield of hydrogen peroxide has been investigated using different types of discharges and varying either the flow rate, the input pressure, or the volume traversed by the dissociated vapor before trapping. In general, the results of experiments^{2,3} in which the residence time was varied in the discharge zone by varying the flow rate showed that increasing the residence time increased the H₂O₂ yield to some extent, the curves showing a maximum. Experiments⁴⁻⁶ in which the traversed volume was varied also showed that the yield of hydrogen peroxide was represented by curves having distinct maxima. In particular, the latter work showed that at very low flow rates of water vapor the yield of H₂O₂ was negligible at small traversed volumes and that it increased with traversed volume to a maximum and then decreased.

Another significant product in this system is the oxygen evolved on warming the condensed products. Only in the traversed volume work⁴⁻⁶ were the yields of evolved O₂ measured as a function of residence time. In discharges using internal electrodes⁴ no correspondence was found between evolved O₂ and H₂O₂ yields for traversed volumes up to 100 ml, but beyond this value the yield of evolved O₂ followed the H₂O₂ yield curve. In electrodeless discharges^{5,6} driven by a

Tesla coil the evolved O₂ yield was independent of the traversed volume. It was, therefore, desirable to reinvestigate the product yields as a function of the residence time of the dissociated vapor in the traversed volume.

The present paper describes the results of experiments in which the residence time of water vapor dissociated at low flow rates in a microwave discharge was varied by varying either the traversed volume or the pressure, the latter under conditions when the product yield was independent of the discharge power.

II. Apparatus and Procedure

The apparatus consisted essentially of a conventional flow system and is shown semidiagrammatically in Figure 1. Two different discharge tubes made of quartz tubing of internal diameters 1.9 cm (D₁) and 2.7 cm

(1) (a) The research for this paper was supported by the Defence Research Board of Canada, Grant Number 9530-42. (b) To whom all correspondence should be addressed at the Department of Chemistry, Western Illinois University, Macomb, Ill. 61455.

(2) S. Takahashi, *Nippon Kagaku Zasshi*, **81**, 36 (1960).

(3) L. I. Nekrasov, N. I. Kobozev, and E. N. Eremin, *Vestn. Mosk. Univ., Ser II, Khim.*, **15**, 12 (1960); **18**, 7 (1963).

(4) R. A. Jones and D. J. McKenney, unpublished work referred to in M. Venugopalan and R. A. Jones, *Chem. Rev.*, **66**, 135 (1966). See also M. Venugopalan and R. A. Jones, *Chemistry of Dissociated Water Vapor and Related Systems*, Interscience Publishers, New York, N. Y., 1968, Chapter 3, pp 89-90.

(5) S. S. Barton and R. A. Jones, *Chem. Commun.*, 406 (1965).

(6) S. S. Barton, F. Groch, S. E. Lipin, and D. Brittain, *J. Chem. Soc. A*, 689 (1968).

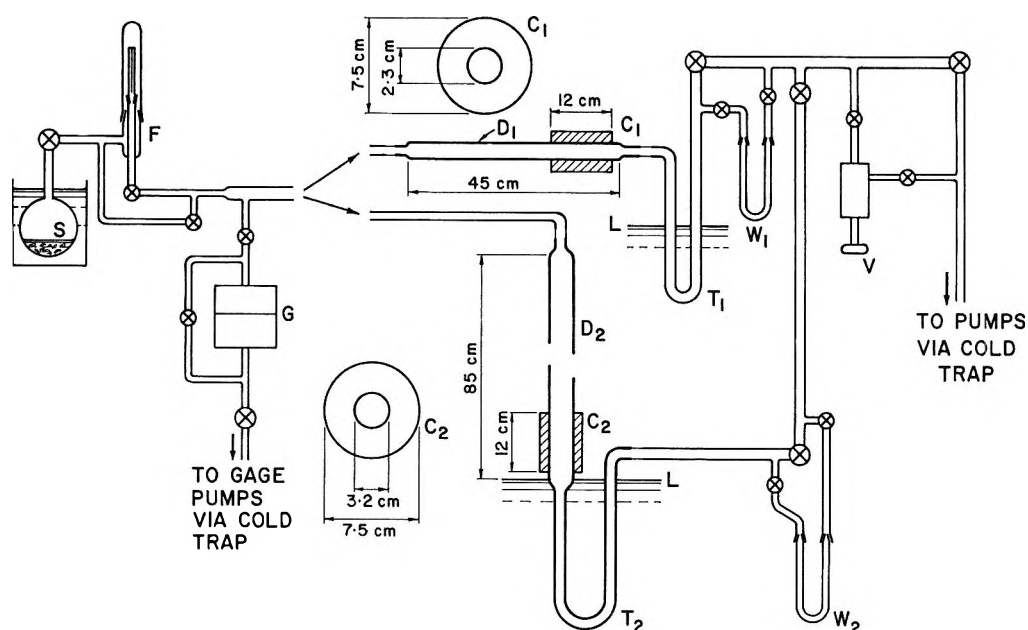


Figure 1. Apparatus for the study of reactions in dissociated water vapor by the discharge-flow method.

(D_2) were used. The discharge tubes terminated in U-tubes (both 1.7 cm i.d.) made of Pyrex (T_1) or quartz (T_2) which were used as cold traps for collecting condensable products, and were pumped by a high-speed mercury diffusion pump. An all-brass cylindrical cavity (C_1 or C_2 , for dimensions see Figure 1), through which passed the discharge tube, was used together with the Raytheon Microtherm Model CMD-5 (2450 Mc) for exciting the discharge. Pressure in the discharge tube was controlled by the throttling valve V in the by-pass to the pumps and was measured using a Consolidated Engineering Corporation Model 23-105 micromanometer, the gauge G of which was kept at 32° .

Previously deaerated distilled water contained in bulb S was first frozen and then kept immersed in a dewar filled with crushed ice and water. The rate of flow of water vapor into the discharge tube was varied by changing the length and/or diameter of capillary F; for each capillary the water vapor flow rate per hour was measured by weighing the water that was condensed in T_1 or T_2 cooled with liquid air.

In general, water vapor was first allowed to diffuse through the capillary flowmeter into the discharge tube with only the by-pass to the pumps kept open. The selected microwave power was then applied to the discharge cavity and the discharge initiated using a Tesla coil. Once a steady discharge was obtained, the product trap was cooled with liquid air, its level being kept constant during the course of a run. At the end of an experiment, the water vapor flow and the microwave power supply into the discharge tube were turned off in sequence, the liquid air level raised a few centimeters and the system evacuated. The condensed products in the cold trap were then warmed to ice-water

temperature and the oxygen evolved was measured. The remaining condensed products were distilled into the smaller weighing trap (W_1 or W_2) which could be detached from the system and weighed. The amount of H_2O_2 was determined by titration with ceric sulfate and the amount of water by difference. The weight of water determined by this procedure was only about 10–15 mg and therefore the reported water yields must be of low precision.

III. Results

(1) *Experiments Using Discharge Tube D_1 .* Two different series of experiments were carried out using a flow rate of 1.9 mmol H_2O /hr and a traversed volume of 182 cm^3 .

(a) At a constant water vapor pressure of 0.12 mm Hg, the yields of H_2O_2 (0.45 mmol/hr) and evolved O_2 (0.05 mmol/hr) were, within experimental error, not affected by varying the input power in the range 25–75 W. This showed that in the present system the composition of the gas entering the cold trap was independent of the discharge power.

(b) At a constant power input of 62.5 W, an increase in discharge pressure increased the yields of H_2O_2 and evolved O_2 initially by very small amounts to maximum values and afterwards decreased first rapidly and then slowly. A close examination of Figure 2 indicates that the maxima do not coincide and that there is a scatter of points in the falling regions of the curves. Minor changes in pressure (which was controlled during the course of a run at a pre-selected value by the manually operated throttling valve) and flow conditions may have contributed to the scatter of points. Figure 2 also shows that the experimental water yields decreased with the initial increase in pressure to a minimum value

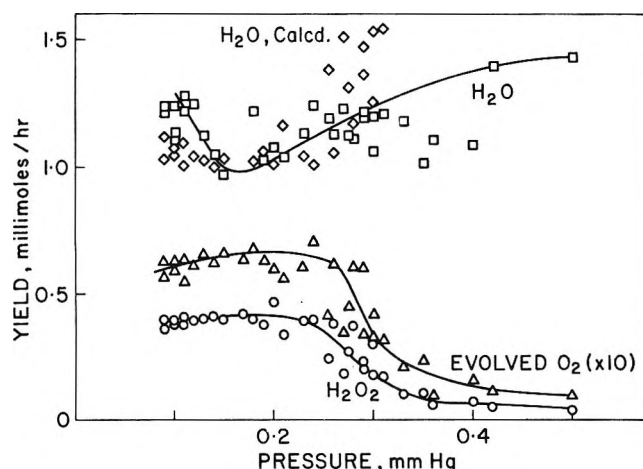


Figure 2. Yields of H_2O_2 , evolved O_2 , and H_2O at liquid air temperature as functions of water vapor pressure.

at a pressure (≈ 0.17 mm Hg) at which the peroxide yield was a maximum and thereafter increased with increasing pressure. Since material balances indicated that significant oxygen loss from the system occurred only after the maximum in the peroxide yield was attained, theoretical H_2O yields were calculated assuming no oxygen loss. The calculated yields (also shown in Figure 2) indicated that oxygen loss beyond the H_2O_2 maximum increased with increasing pressure more or less corresponding with the decreasing peroxide yield.

(2) *Experiments Using Discharge Tube D₂*. Two series of experiments were done at discharge powers of 62.5 W and 100 W, respectively, keeping the input pressure constant at 0.25 mm Hg and using a flow rate of 0.92 mmol H_2O /hr. The results are shown in Figure 3.

At traversed volumes less than 5 ml, the yields of H_2O_2 and evolved O_2 were negligible, most of the input water was collected in the cold trap, and small amounts of hard gas (mostly H_2) passed through the trap. It was concluded that either OH was not present in the gases passing out of the discharge zone or that, at least when H is present, OH radicals do not dimerize in a liquid air-cooled trap to form H_2O_2 .

Although the product yields were slightly dependent on the discharge power used, the nature of their variation with traversed volume was similar at both discharge powers studied (see Figure 3)—with increasing traversed volume the yields of H_2O_2 and evolved O_2 increased first slowly and then rapidly from negligible to maximum values, and thereafter decreased. For both discharge powers, the maximum yields of evolved O_2 were obtained at the same traversed volume which was much smaller than the traversed volume at which peroxide yields were maximum. Water yields decreased with traversed volume to minimum values at or very near the traversed volume for which H_2O_2 yields were maximum and then increased. The measured water yields were higher than those expected assuming no oxygen loss (see Figure 3). Nevertheless within

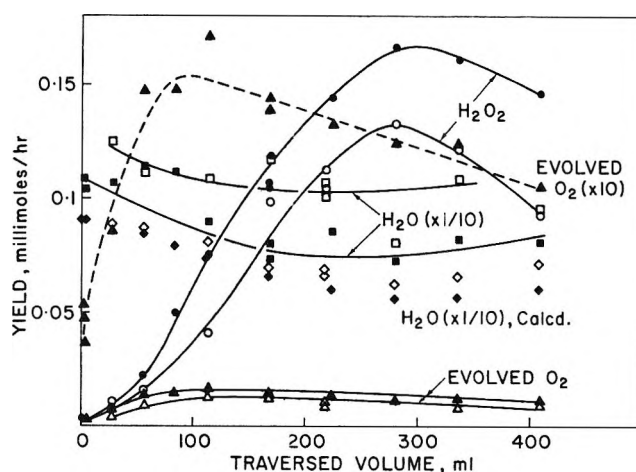
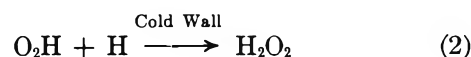
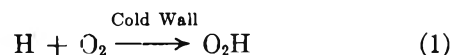


Figure 3. Yields of H_2O_2 , evolved O_2 , and H_2O at liquid air temperature as functions of the traversed volume. Open and shaded points for data at 62.5 and 100 W, respectively.

allowable error, the material balances indicated that oxygen loss from the system as O_2 occurred only after the maximum H_2O_2 yield was attained.

IV. Discussion

The results from the pressure and traversed volume experiments at 62.5 W interpreted in terms of the residence time⁷ of the gas in the traversed volume are shown in Figure 4. Other conditions remaining unchanged, with increasing residence time the yields of H_2O_2 and evolved O_2 (both open points, taken from the traversed volume work at constant pressure) increased gradually to maximum values and then decreased slowly. This behavior is consistent with a gradual decrease in the concentration of any one or all of the active species in the traversed volume as the residence time is increased, provided the variations in peroxide and evolved O_2 yields can be accounted for by an increase with residence time in the concentrations of O_2 and H_2 , *i.e.*, a decrease in the concentrations of O and H. Based on this view, the Geib and Harteck⁸ mechanism for peroxide formation



(7) For the calculation of the residence times, the molar rate of flow through the traversed volume was assumed to vary between the two limits possible: (a) if the gas in the traversed volume was composed of O and H only, the molar rate of flow would have been three times the molar rate of input of water vapor while (b) if the gas was composed of H_2O molecules only, the molar rate of flow would have been equal to the molar rate of input of water vapor. If the vapor in the traversed volume was composed of H atoms and OH radicals only, naturally the molar rate of flow would have been midway between the above two limits, *viz.*, twice the molar rate of input of water vapor. From these two limiting values of the molar flow rate and the values of the input pressures or traversed volumes, the residence times were calculated. These residence times are, of course, only approximate, but are useful for relative comparisons.

(8) K. H. Geib and P. Harteck, *Ber.*, **B65**, 1551 (1932). See also K. H. Geib, *J. Chem. Phys.*, **4**, 391 (1936).

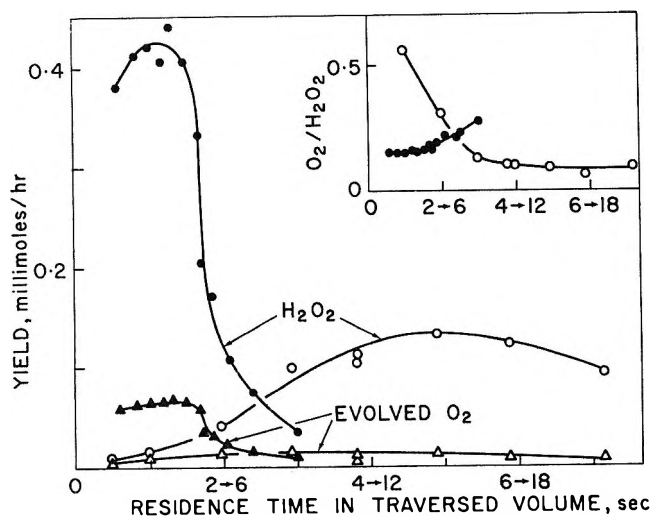
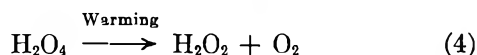
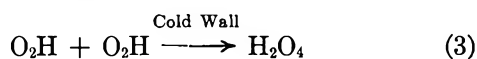
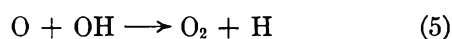


Figure 4. Yields of H_2O_2 and evolved O_2 and evolved $\text{O}_2/\text{H}_2\text{O}_2$ ratio (inset) as functions of the two possible limits of residence time in traversed volume. Open and shaded points taken from traversed volume and pressure data for 62.5 W given in Figures 3 and 2, respectively.

together with Ohara's mechanism⁹ for evolved O_2



can explain the present results. That is, the initial increase in H_2O_2 and evolved O_2 yields with residence time is due to an increase in the concentration of O_2 and the subsequent decrease in yields at longer durations is due to a gradual decrease in H concentration caused by its recombination in the traversed volume to yield H_2 or by the reaction with OH to form H_2O . It must be noted that the well-known fast reaction¹⁰



will certainly contribute to the formation of O_2 in the traversed volume.

On the other hand, the data from pressure work (shaded points in Figure 4) showed that the yield of H_2O_2 increased rapidly to a maximum value by a small increase in residence time, but fell abruptly thereafter. This was, however, not the case with evolved O_2 yields which increased with increasing residence time gradually to a maximum and then fell abruptly to one-half the maximum yield at a residence time at which the peroxide yield was already less than half its maximum value. It must be noted that an increase in discharge pressure in these experiments increased both the residence time and collision frequency of the particles in the system. If it is assumed that H_2O was completely dissociated in the discharge¹¹ at all pressures (~ 0.1 – 0.5 mm Hg) studied, then the variation in inlet pressure affected only the processes occurring in the traversed volume. Undoubtedly, both the collision frequency

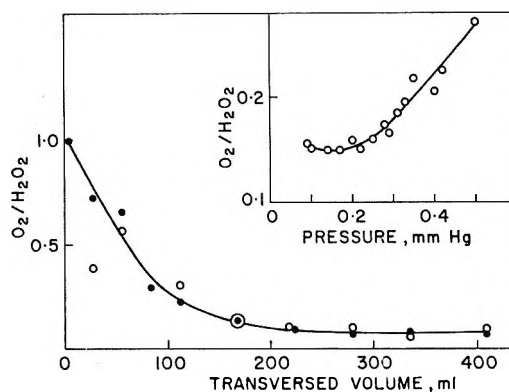


Figure 5. Variation of evolved $\text{O}_2/\text{H}_2\text{O}_2$ ratio with traversed volume and pressure. Open and shaded points for data at 62.5 and 100 W, taken from Figures 2 and 3, respectively.

and residence time of the species in the traversed volume will be increased; an increase in collision frequency naturally increases the recombination rate of the species in the traversed volume. The observed abrupt decrease in H_2O_2 and evolved O_2 yields by a small increase in residence time brought about by increasing pressure seems to be explicable on this basis.

Evolved Oxygen to Hydrogen Peroxide Ratio. $\text{O}_2/\text{H}_2\text{O}_2$ ratios are meaningful only if the mechanism of the evolution of oxygen is associated with the mechanism of either the formation of (residual) H_2O_2 by decomposition of hydrogen superoxides or the decomposition of H_2O_2 itself. The variation of the evolved O_2 to peroxide ratios are shown as functions of the traversed volume (Figure 5), pressure (inset, Figure 5), and calculated residence times in the traversed volume (inset, Figure 4). The ratios were independent of the discharge power (see Figure 5, and also section III (1a)), suggesting that the evolved oxygen cannot be accounted for by the decomposition of H_2O_2 by impurities carried over from the discharge tube into the cold trap.¹² Neither can impurities originating in the traversed volume be responsible since $\text{O}_2/\text{H}_2\text{O}_2$ ratios *decrease* rather than increase with traversed volume. On the other hand, the decreasing ratios with increasing residence time in the traversed volume and the increasing ratios with increasing collision frequency are explicable on the basis of Ohara's mechanism⁹ (reactions 3 and 4). However, the existence of this compound is hitherto unconfirmed by direct means.¹³ Other mechanisms for evolved O_2 such as occlusion,

(9) E. Ohara, *J. Chem. Soc. Jap.*, 61, 569, 657 (1940).

(10) F. Kaufman, *Progr. Reaction Kinetics*, 1, 1 (1961).

(11) E. A. Secco, *J. Chem. Phys.*, 23, 1734 (1955).

(12) P. A. Giguère, *ICSU (Intern. Council Sci. Unions) Rev.*, 4, 172 (1962); *J. Chem. Phys.*, 42, 2989 (1965). See also N. Hatta and P. A. Giguère, *Can. J. Chem.*, 44, 869 (1966); R. A. Jones and M. Venugopalan, *Can. J. Chem.*, 45, 2452 (1967).

(13) K. Herman and P. A. Giguère, *Can. J. Chem.*, 46, 2649 (1968). For a review of earlier work, see ref. (4).

trapping, and the formation of "complexes" of oxygen¹⁴ with H₂O₂ and/or H₂O when codeposited at low temperature from the gas phase are essentially based on evidence from experiments done at liquid-helium temperature (bp 4.2°K), at which temperature O₂ readily condenses. The likelihood of these mechanisms operat-

ing at liquid air temperature (bp 81°K) at which the present experiments were done is remote indeed.¹⁵

(14) R. A. Ruehrwein, J. S. Hashman, and J. W. Edwards, *J. Phys. Chem.*, **64**, 1317 (1960).

(15) J. W. Edwards, "Chemical and Physical Studies of Trapped Radicals," in "Formation and Trapping of Free Radicals," A. M. Bass and H. P. Broida, Ed., Academic Press, New York, N. Y., 1960, p 291.

Dielectric Study of Esters in Benzene. Barrier to Internal Rotation and Molecular Configuration

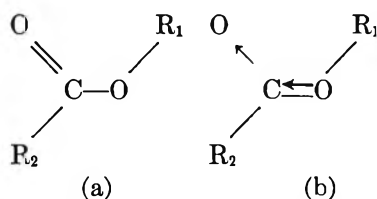
by Bal Krishna, Bhartendu Prakash,¹ and S. V. Mahadane

Department of Chemistry, University of Allahabad, Allahabad, India (Received January 17, 1969)

Electric dipole moment values at a frequency of 1 Mc/sec and relaxation time values at a frequency of 9.79 kMc/sec for methyl-*p*-nitrobenzoate, methyl-*m*-nitrobenzoate, ethyl-*m*-nitrobenzoate, ethyl-*o*-nitrobenzoate, methyl-*o*-aminobenzoate, glycerol triacetate, and glycerol tributyrates have been determined in benzene at 30°. The comparison of the observed and theoretically calculated moment values indicates the absence of intramolecular rotation in these esters except for methyl and ethyl-*m*-nitrobenzoate molecules. The relaxation time values for these rigid, transplanar esters are expected to be due to the overall rotation of the molecules in the solvent. Discussing the thermodynamic quantities (ΔF^* and ΔH^*), a high negative value for the entropy of activation (ΔS^*) has been suggested so that the molecules during activation, are in a state of better order than the initial state. In the case of methyl-*o*-aminobenzoate, possibility of hydrogen bond formation between the two *ortho*-substituted groups is expected to give this molecule a rigid planar configuration.

Introduction

Most of the esters derived from a saturated monohydric alcohol and a saturated carboxylic acid, possess a *trans*-planar configuration,² and a resonance occurs between the classical (a) and excited (b) structures giving considerable double-bond character to the C-O bond



and, hence, inhibiting free rotation of O-R₁ bond around it.^{3,4} The electric dipole moments of esters have been found to be independent of temperature⁵ over a large range of temperature. The exceptions are methyl and ethyl chloroformates⁶ and carbonates,⁷ where a free rotation or restricted rotation of O-R₁ bond around C-O bond has been suggested. The dipole moment values for some esters in benzene, reported earlier by the authors,⁸ showed that these molecules may possess a configuration in which C-O-C plane lies considerably

out of the *trans* plane. A coplanar configuration is expected for the molecules containing the carboxylic group in addition to the general conjugated systems.⁹ The insertion of an -NO₂ group, a highly polar one, in the benzene ring, which is symmetric and nonpolar in itself, gives rise to a high value of the electric dipole moment for a nitrobenzene molecule.

In the light of above facts, the alkylnitrobenzoate molecules are expected to possess high dipole moments and a rigid planar configuration. The esters derived

(1) To whom correspondence is to be addressed at the Department of Chemistry, Indian Institute of Technology, Kanpur, India.

(2) A. Eucken and L. Meyer, *Phys. Z.*, **30**, 397 (1929).

(3) R. J. B. Marsden and L. E. Sutton, *J. Chem. Soc.*, 1383 (1936).

(4) J. M. O'Gorman, W. Shand, and V. Schomaker, *J. Amer. Chem. Soc.*, **72**, 4222 (1950).

(5) C. T. Zahn, *Phys. Z.*, **33**, 730 (1932).

(6) S. Mizushima and M. Kubo, *Bull. Chem. Soc. Jap.*, **13**, 174 (1938).

(7) M. Yasumi, *J. Chem. Soc. Jap.*, **60**, 1208 (1939).

(8) B. Krishna, S. C. Srivastava, and S. V. Mahadane, *Tetrahedron*, **23**, 4801 (1967).

(9) G. W. Wheland, "Theory of Resonance," John Wiley & Sons, Inc., New York, N. Y., 1945, p 92.

Table I: Electric Dipole Moment, Relaxation Time and Thermodynamic Quantities (ΔF^* and ΔH^*) for Esters in Benzene (30°)

Compound	Slopes, ^a	μ , D, obsd ^a	μ , D, calcd	τ , μsec^a	ΔF^* , kcal/mol	ΔH^* , kcal/mol
Methyl- <i>p</i> -nitrobenzoate	$\alpha = 8.24$ $\beta = -0.41$	3.73	3.67 ^b	10.9	2.6	2.3
Methyl- <i>m</i> -nitrobenzoate	$\alpha = 7.94$ $\beta = -0.38$	3.67	2.85 ^b	10.6	2.5	2.2
Ethyl- <i>m</i> -nitrobenzoate	$\alpha = 8.05$ $\beta = -0.36$	3.82 3.74 ^d	2.85 ^b	14.0	2.7	2.4
Ethyl- <i>o</i> -nitrobenzoate	$\alpha = 8.22$ $\beta = -0.35$	3.88 3.94 ^d	4.02 ^b	7.0	2.3	2.0
Methyl- <i>o</i> -aminobenzoate	$\alpha = 1.25$ $\beta = -0.28$	1.30	1.11 ^b	10.6	2.5	2.2
Glycerol triacetate	$\alpha = 9.49$ $\beta = -0.65$	2.73 ^e	5.35 ^c	6.7	2.3	2.0
Glycerol tributyrate	$\alpha = 2.36$ $\beta = -0.19$	2.68	5.35 ^c	8.7	2.4	2.1

^a The uncertainties in the determination of α , β , μ , and τ are 1%, 1%, 1%, and 8%, respectively. ^b Moments calculated by assuming a *trans*-planar configuration. ^c Moments calculated by assuming free intramolecular rotation (as given by Smyth for glycerol tribromohydrin).¹⁷ ^d See ref 18. ^e See ref 8.

from the glycerol molecule, due to the presence of three $-\text{OOC}\cdot\text{R}$ linkages, are of much interest from the viewpoint of intramolecular rotation; a possibility of the presence of hydrogen bonding at the *ortho* position of methyl-*o*-aminobenzoate is also expected to give this molecule a rigid *trans*-planar structure. The present investigations have been carried out to ascertain these views.

Experimental Section

Details of the techniques for measuring the static dielectric constants and densities of the solutions of esters in benzene have already been reported.¹⁰⁻¹² The microwave measurements were made at a frequency of 9.79 kMc/sec (wavelength, 3.06 cm). The details of the X-band setup have been described elsewhere.¹³ A slight alteration has been made for the solution measurements. The Halverstadt and Kumler method¹⁴ for calculation of electric dipole moments (μ) in the static frequency region and Gopalakrishna's method¹⁵ for the computation of relaxation time (τ) in the microwave region, were employed. The electronic polarization has been taken to be equal to the molecular refraction values for sodium D line. The correction for the atomic polarization was not made.

Benzene (S. Merck, guaranteed reagent) was distilled in a quick-fit (ground-glass joint) apparatus. The fraction boiling between 78.5 and 79.5° was collected and kept overnight in a dessicator before use. The fresh sealed samples of pure quality of methyl-*p*-nitrobenzoate, methyl-*m*-nitrobenzoate, ethyl-*m*-nitrobenzoate, ethyl-*o*-nitrobenzoate (all from Fluka A.G., Switzerland), methyl-*o*-aminobenzoate (B.D.H., England), glyceroltriacetate, and glyceroltributyrate (B.D.H., England) were used without further purification.

Results and Discussion

The experimental results for the esters under study have been summarized in Table I.^{17,18} Theoretical calculations of the molecular moments have been made on the lines suggested by Smyth assuming rigid *trans*-planar models¹⁶ for the first five esters and free internal rotation of the three $-\text{OOC}\cdot\text{R}$ groups¹⁷ for the remaining two esters. The values have been reported in Table I and the possible structures are given in Figure 1, the diagrams being self-explanatory.

In the methyl-*p*-nitrobenzoate molecule, mesomeric effect is expected and the inhibition is supposed to be minimum since the molecules of this type can best be represented by the quinonoid structure¹⁹ possessing high polarity. Thus, the higher observed moment value than the calculated one in this case may be attributed to mesomeric effect. Similar increase has been observed in *p*-substituted diethylanilines, which cannot be accounted for only by inductive effects.²⁰ The observed moment values for the methyl- and ethyl-*m*-nitrobenzoate molecules are higher than the calculated values.

(10) B. Krishna, B. B. L. Saxena, and S. C. Srivastava, *Tetrahedron*, **22**, 1597 (1966).

(11) B. Krishna and K. K. Srivastava, *J. Chem. Phys.*, **27**, 835 (1957).

(12) B. Krishna and K. K. Srivastava, *ibid.*, **32**, 663 (1960).

(13) Krishnaji and A. Mansingh, *ibid.*, **41**, 827 (1964).

(14) I. F. Halverstadt and W. D. Kumler, *J. Amer. Chem. Soc.*, **64**, 2988 (1942).

(15) K. V. Gopalakrishna, *Trans. Faraday Soc.*, **53**, 767 (1957).

(16) C. P. Smyth, "Dielectric Behavior and Structure," McGraw-Hill, New York, N. Y., 1955, pp 306-307.

(17) C. P. Smyth, ref 16, p 368.

(18) A. E. Lutskii, V. T. Alekseeva, and B. P. Kondratendo, *Zh. Fiz. Khim.*, **35**, 1706 (1961).

(19) C. P. Smyth, ref 16, p 324.

(20) C. P. Smyth, ref 16, p 327.

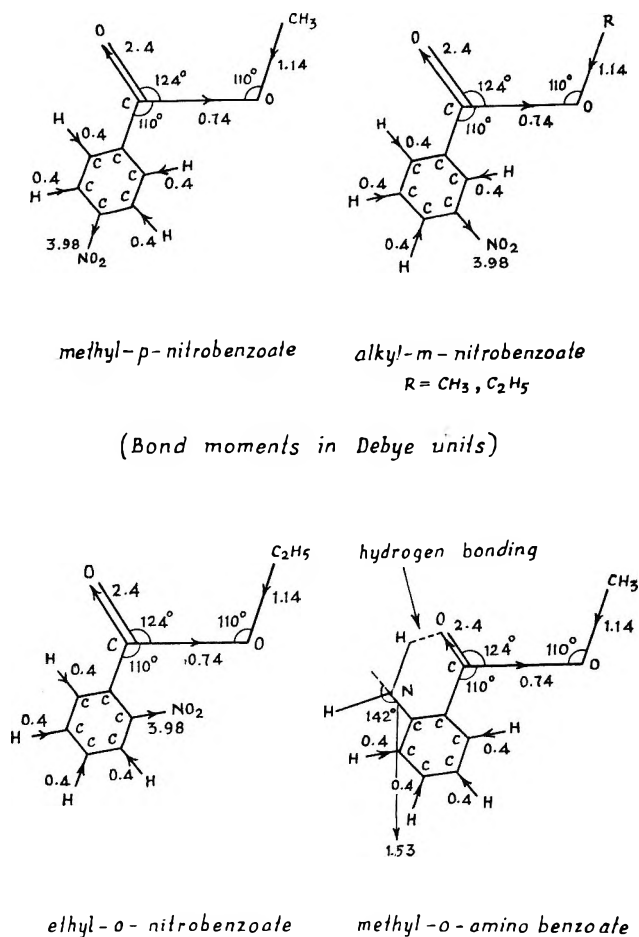


Figure 1.

This is surprising as the quinonoid structure cannot be written for these molecules. Smyth pointed out that such an abnormal difference in moments may be due to intramolecular rotation,²¹ but relaxation time values observed by us (Table I) do not support relaxation by internal mechanism. However, definite conclusions about internal rotation cannot be drawn from single frequency measurements. The calculated and the observed moments for ethyl-*o*-nitrobenzoate do not show a large difference and this slight variation may be due to the *ortho* effect, which generally results in widening of the angle between two dipole axes and the resulting mutual induction decreases the actual moment value.²² The observed moment is close to the value (3.94 D) reported earlier by Lutskii, *et al.*¹⁸

Methyl-*o*-aminobenzoate has a higher observed moment (1.30 D) than the calculated one (1.11 D) owing probably to hydrogen bonding between one of the hydrogen atom of -NH₂ group and the oxygen atom

of the carboxylic group (Figure 1). The formation of hydrogen bond, as shown by the infrared studies of Hambly and O'Grady,²³ increases the possibility for this molecule to have a rigid planar structure. The observed values of electric dipole moments for glycerol triacetate and glycerol tributryrate are much less than the theoretically calculated values for these esters assuming a free rotation of the three -OOC·R groups. This indicates the absence of such a free rotation in these esters.

Eyring's equation^{24,25} has been used to calculate the free energy of activation (ΔF^*) from the relaxation time (τ) values. Employing Higasi's assumption ($\Delta S^* = -1$ eu), the values of the heat of activation; *i.e.*, the height of the potential energy barrier (ΔH^*) has been calculated for the ester molecules (Table I).

The dipole moment values for all the esters studied except methyl- and ethyl-*m*-nitrobenzoate suggest the absence of intramolecular rotation. Thus, the relaxation time in these esters is due to overall rotation of the molecule in the solvent. The barrier heights calculated here point to the resistance offered by the medium surrounding the solute molecule which, generally, does not exceed ~ 0.5 kcal/mol in the benzene like solvents. Interpreting it in another way, if we assume the entropy of activation (ΔS^*) to be highly negative say between -6 and -7 eu, the heat of activation (ΔH^*) comes out to be ~ 0.5 kcal/mol, which is sufficient to overcome the viscosity or solute-solvent interaction barrier. A high negative entropy of activation would imply that the molecules, during activation, are in a highly organized state.²⁶ No doubt the overall rotation will be determined by the overall resultant dipole vector of the molecule, but during activation at least individual bonds tend to be displaced in such a way that the molecule attains a rigid configuration resulting in the decrease of entropy of activation.

Acknowledgment. The authors are thankful to Professor Krishnaji of the Physics Department for the use of the X-band setup in his microwave laboratory and to the University Grants Commission (New Delhi) for the financial assistance to B. P.

(21) C. P. Smyth, ref 16, p 254.

(22) C. P. Smyth and S. O. Morgan, *J. Amer. Chem. Soc.*, **49**, 1030 (1927).(23) A. N. Hambly and B. V. O'Grady, *Aust. J. Chem.*, **16**, 459 (1963).(24) H. Eyring, *J. Chem. Phys.*, **4**, 283 (1936).

(25) K. Higasi, "Dielectric Relaxation and Molecular Structure," 1961, Chapters 1 and 2.

(26) E. Bauer, "Dielectrics," General Discussion, The Faraday Society, 1946, p 162.

The Unit Compressibility Law and Corresponding-States

Behavior of Hydrogen Sulfide

by Eugene M. Holleran

Department of Chemistry, St. John's University, Jamaica, New York 11432 (Received January 31, 1969)

Recent literature pressure–volume–temperature data are used to demonstrate that H₂S follows the unit compressibility law and the related three-constant system of corresponding states. This is significant as the first reliable example of a moderately polar substance to be included in this correlation. The three characteristic constants of H₂S as derived from the data are used to evaluate the three parameters of several common intermolecular potentials.

Introduction

The Unit Compressibility Law (UCL). The UCL¹ is a linear relationship among the temperatures, T , and the densities, d , at which the compressibility factor, $Z = P/dRT$, has the value unity

$$T/T_B + d/d_0 = 1, \quad (1)$$

where d_0 and the Boyle temperature T_B are characteristic constants for each fluid. This relation appears to hold within experimental error for the twelve pure gases for which appropriate data have been found,^{1a} with the exception of hydrogen at low temperatures. How this simple equation, relating the states of a fluid in which the effects on Z of intermolecular attractions and repulsions are somehow balanced, might follow from the laws of classical mechanics is not known. It is interesting to note in this connection that the UCL can be obeyed accurately by mixtures, as illustrated recently by the CH₄–CF₄ system,² so that the presence of three different binary interaction potentials, A–A, A–B, and B–B, need not interfere with the relation beyond changing the two constants.

An indirect theoretical derivation of the UCL at low densities is provided by the virial coefficients calculated from assumed intermolecular potentials.^{2,3} The virial equation of state of the Lennard-Jones 12–6 potential obeys eq 1 accurately over the density range in which the five known virial coefficients are sufficient. The Stockmayer potential, designed to represent polar gases, also appears to conform, although its coefficients are known only through the third.

Most experimental measurements for polar substances are for $Z < 1$. The reason for this is that polar gases have high Boyle temperatures, so that compressibility measurements at ordinary temperatures usually do not extend to high enough densities to include the unit- Z line for these gases. Only one slightly polar substance, CO, is included among those for which the UCL constants have been determined. Recent measurements for H₂O by Burnham, Holloway, and Davis⁴ confirm

earlier data by Maier and Franck⁵ in showing a marked curvature in the unit- Z line at low reduced temperatures.⁶ Perhaps the most important outstanding question concerning the unit compressibility law is therefore whether or not it can hold for real gases of any considerable polarity.

Lewis and Fredericks⁷ have recently published compressibility measurements for hydrogen sulfide in a high density region (8 to 23 mol l.⁻¹) which fortunately includes $Z = 1$. This gas has a dipole moment of 0.92 D (compared to 0.10 D for CO, and 1.08 D for HCl, for example), and so should provide a fair test of the UCL for moderately polar gases.

The Three-Constant System of Corresponding States. Based on the unit compressibility law, a three-constant system of corresponding states has recently been proposed.^{8–10} The two constants of the UCL are used to define a reduced temperature, $\Theta = T/T_B$, and a reduced density, $\delta = d/d_0$. The system then assumes that the compressibility factor is given by

$$Z = 1 + k_B Y(\Theta, \delta) \quad (2)$$

where $Y(\Theta, \delta)$ is a universal function of Θ and δ , and k_B is the third characteristic constant. This constant can be found⁹ as $k_B = d_0 V_B = d_0^2 C_B = V_B^2 / C_B$, where C_B is the third virial coefficient at T_B , V_B is (TdB/dT)

(1) (a) E. M. Holleran, *J. Chem. Phys.*, **47**, 5318 (1967); (b) T. E. Morsy, Dissertation, Tech. Hoch. Karlsruhe, 1963; (c) E. H. Amagat, *Ann. Chim. Phys.*, **VI**, 29 (1893).

(2) E. M. Holleran and G. J. Gerardi, *J. Phys. Chem.*, **73**, 525 (1969).

(3) E. M. Holleran, *J. Chem. Phys.*, **49**, 39 (1968).

(4) C. W. Burnham, J. R. Holloway, and N. F. Davis, *Amer. J. Sci.*, **267-A**, 70 (1969).

(5) V. S. Maier and E. U. Franck, *Ber. Bunsenges. Phys. Chem.*, **70**, 639 (1966).

(6) Unpublished calculations.

(7) L. C. Lewis and W. J. Fredericks, *J. Chem. and Eng. Data*, **13**, 482 (1968).

(8) E. M. Holleran and G. J. Gerardi, *J. Phys. Chem.*, **72**, 3559 (1968).

(9) E. M. Holleran, *ibid.*, **73**, 167 (1969).

(10) E. M. Holleran and G. J. Gerardi, *ibid.*, **73**, 528 (1969).

Table I: Isotherm Coefficients for $Z = \Sigma C_n d^n$

$T, ^\circ\text{C}$	C_0	C_1	$10C_2$	10^2C_3	10^4C_4	10^6C_5	10^7C_6	Std dev
100	-1.2539	.360318	-.289773	.076515	0	0	0	0.003
120	5.5711	-2.15183	3.68610	-3.32265	1.64259	-4.21583	4.46336	0.003
140	2.5718	-0.76584	1.18244	-0.99771	4.67437	-1.12848	1.15239	0.003
160	3.8366	-1.25464	1.94343	-1.56822	6.78384	-1.45386	1.23194	0.004
180	2.6389	-0.88187	1.62140	-1.59872	8.62789	-2.37586	2.66598	0.004
200	4.1464	-1.45288	2.47668	-2.21699	10.8321	-2.70247	2.73693	0.005
220	8.7302	-3.50024	6.20240	-5.71720	28.7873	-7.47746	7.88829	0.008

at T_B , and B is the second virial coefficient. Relative values of k_B for two gases can be found from their relative deviations from ideality, *i.e.* $(Z - 1)$, at equal Θ and δ . This system of corresponding states has proved very accurate for the substances so far investigated;^{8,10} it holds for mixtures as well as pure gases;¹⁰ and it has the advantage of an analytic dependence of Z on the third factor, so that the same graph or tabulation of $Y(\Theta, \delta)$ can be used for substances having different k_B values. In this way, and also because the constant k_B is more distinctive than other third factors,⁹ this system appears to have an advantage over earlier systems. In addition, the correspondence of $(Z - 1)/k_B$ at equal Θ and δ implies the correspondence of G^*/k_B , where G^* is any reduced residual thermodynamic property,⁸ and of B/V_B and C/C_B at equal Θ , results which appear to be confirmed experimentally and by the predictions of various intermolecular potentials.⁹ Finally, the three constants are directly related to the intermolecular potential. If the potential is characterized by a temperature, ϵ/k ; a molecular volume, b_0 , and a third parameter, p_3 , then p_3 is fixed by k_B , ϵ/k equals T_B/T_B^* , and b_0 equals d_0^*/d_0 , where T_B^* and d_0^* are known constants of the potential.

As in the case of the UCL, an important question concerning this promising system of corresponding states is whether it can be applied without modification to moderately polar gases. The recent H_2S data provide an excellent opportunity to investigate this question.

Hydrogen Sulfide

The Unit Compressibility Law. Inspection of the tabulated compressibilities of Lewis and Fredericks⁷ shows that Z passes through unity on each of the seven experimental isotherms extending at 20° intervals from 100 to 220° . The density at which $Z = 1$ at each of these temperatures can be found by interpolation. This is best accomplished by means of an empirical polynomial representation of the data. Least-squares coefficients¹¹ for the isothermal sixth-degree equations (third at 100°) are given in Table I. The standard deviations listed in the table indicate that the third decimal place in Z is not reliable.

The unit compressibility densities resulting from

these empirical equations are listed as $d(\text{exptl})$ in Table II together with the isotherm temperatures. The linear relation of T and d is evident by inspection. Minimizing the sum of squares of $(\Theta + \delta - 1)$ yields

Table II: The Unit Compressibility Law for H_2S

$T, ^\circ\text{C}$	$d(\text{exptl}), \text{mol l.}^{-1}$	$d(\text{calcd}) \text{mol l.}^{-1}$	$10^4(\Theta + \delta - 1)$
100	22.94	22.96	-4
120	22.16	22.14	+5
140	21.35	21.33	+5
160	20.49	20.52	-7
180	19.70	19.70	-1
200	18.90	18.89	+3
220	18.07	18.07	-1

the most probable values of the constants: $T_B = 937.5^\circ\text{K}$, and $d_0 = 38.14 \text{ mol/l}$. Because of the sensitivity of the constants to small experimental errors, these values must be considered uncertain by at least 1%. The values of d calculated from eq 1 with these constants are listed in Table II as $d(\text{calcd})$. The deviations, $(\Theta + \delta - 1)$, are small and not systematic. The differences in Z given by the empirical isotherms at $d(\text{exptl})$ and at $d(\text{calcd})$ are well within the standard deviations of these polynomials from the experimental compressibilities. We therefore conclude that hydrogen sulfide obeys the unit compressibility law within the experimental error.

Corresponding States. With known values of the constants T_B and d_0 , it is then possible to determine whether H_2S fits into the new system of corresponding states. One way to do this is by comparing the compressibility factor at equal Θ 's and δ 's with that of a gas which is known to conform. Argon was chosen for this purpose because its constants are fairly well known and its data are accurate and cover the necessary corresponding region of temperature and density. Isotherms of Michels, Levelt, and DeGraaff¹² at five

(11) Polynomial coefficients are given in ref 7 but one term seems to have been omitted and the remainder are not adequate.

(12) A. Michels, J. M. Levelt, and W. DeGraaff, *Physica*, **24**, 659 (1958).

Table III: Correspondence of H₂S and Argon: $Z(\text{H}_2\text{S})$ and $10^3[Z(\text{exptl}) - Z(\text{caled})]$

$T, ^\circ\text{C}$	Density, mol l. ⁻¹															
	8	9	10	11	12	13	14	15	16	17	18	19	20	21	22	23
100							0.211	0.213	0.227	0.256	0.306	0.380	0.483	0.620	0.795	1.014
							10	10	9	7	7	8	10	10	8	1
120	0.399	0.365	0.344	0.329	0.317	0.309	0.308	0.318	0.341	0.382	0.443	0.528	0.640	0.783	0.966	1.199
	-31	-27	-17	-7	-1	0	-1	-1	-2	-1	0	2	3	0	-2	-1
140	0.479	0.445	0.422	0.406	0.397	0.396	0.404	0.424	0.457	0.507	0.577	0.670	0.790	0.940	1.125	1.352
	-13	-15	-12	-9	-7	-5	-3	-2	0	1	3	5	5	2	-4	-13
160	0.543	0.512	0.495	0.487	0.485	0.488	0.500	0.523	0.560	0.616	0.694	0.796	0.926	1.083	1.269	1.483
	-5	-9	-5	0	4	4	2	1	-2	-1	2	5	8	6	-4	-29
180	0.601	0.580	0.566	0.556	0.554	0.560	0.578	0.609	0.657	0.723	0.808	0.913	1.041	1.195	1.379	1.603
	3	4	5	3	0	-1	-2	-2	0	4	8	7	3	-7	-22	-41
200	0.646	0.626	0.618	0.616	0.620	0.632	0.654	0.688	0.739	0.809	0.899	1.012	1.148	1.308	1.494	1.708
	2	0	2	3	2	1	-2	-5	-5	-2	0	3	2	-7	-24	-55
220	0.699	0.680	0.678	0.683	0.691	0.704	0.727	0.764	0.819	0.895	0.992	1.110	1.249	1.407	1.590	1.807
	14	8	12	15	14	8	2	-3	-4	-1	4	6	4	-10	-34	-64

temperatures from -110 to -50° were used. Their sixth-power polynomial representations were evaluated for Z at the 16 densities corresponding to the experimental H₂S densities: $d(\text{Ar}) = d(\text{H}_2\text{S}) \cdot d_0(\text{Ar})/d_0(\text{H}_2\text{S})$. At each density the resulting compressibility factors were then fit by least squares to a polynomial in $1/T$, of second or third degree as necessary, and these isochores were solved for Z at the seven temperatures corresponding to the experimental H₂S temperatures: $T(\text{Ar}) = T(\text{H}_2\text{S}) \cdot T_B(\text{Ar})/T_B(\text{H}_2\text{S})$. The argon constants used were those given in ref 1: $T_B = 408.3^\circ\text{K}$, and $d_0 = 1047$ amagats = 46.75 mol/l. Z for H₂S was then calculated from this Ar Z as

$$Z(\text{H}_2\text{S}) = kZ(\text{Ar}) + (1 - k) \quad (3)$$

where k is $k_B(\text{H}_2\text{S})/k_B(\text{Ar})$ according to eq 2. The value of k chosen to give the best overall correspondence is 1.24.

Table III lists the experimental values of Z for H₂S as calculated from the empirical isotherms. Also listed are the differences between these compressibilities and those calculated from argon by eq 3. In general the correspondence is seen to be good except for the two corners of the table at low T and d and at high T and d . These regions represent the extreme limiting conditions of the experimental H₂S measurements, and discrepancies here are probably not significant. For example, in the low T and d region errors of several percent are unavoidable because the experimental pressures are of the order of 100 atm and, as the authors point out, the pressure can be read only to an accuracy of 3 atm. With the exception of about ten points in these extreme regions, the compressibilities calculated from argon fit the H₂S isotherm polynomials better than do the experimental H₂S points themselves. The main body of the H₂S data therefore conforms within experimental error to the corresponding states system.

Discussion

The importance of these results is that they provide the first reliable example of a moderately polar substance adhering to the unit compressibility law and the related system of corresponding states. This addition of a polar gas to the nonpolar gases, mixtures, and even the quantum fluid hydrogen at high reduced temperatures, extends the range of validity of the UCL and emphasizes the desirability of a simple theoretical explanation for this simple experimental relation. In this case at least, a polar gas need not be treated differently from nonpolar ones. Differences in their compressibility behavior are apparently accounted for, at least in this experimental range, by differences in the three characteristic constants. This expanding generality of the three constant corresponding states system increases interest in finding the three-parameter equation of state whose existence it implies.

Of more immediate utility is the possibility, inherent in any system of corresponding states, of extrapolating measurements beyond the experimental range. For polar gases in particular this means extrapolation to high temperatures. For example, 200° for argon corresponds to over 800° for H₂S.

In spite of the success of the above correlation for H₂S, however, caution must be observed in extending or generalizing this result, for two reasons. First, the range of reduced temperature covered by these measurements is relatively short, and second, H₂O provides a counter example. Of course, water is an exceptional substance, and the curvature of its unit- Z line may also be an exceptional case. It could be due to the increased structuring of the fluid at lower temperatures which converts previously available volume into inaccessible interstitial spaces, resulting in a lower density than the UCL would predict.

The results presented here for H₂S also provide a good illustration of the identification of possible intermo-

lecular potentials, and evaluation of the potential parameters by the three characteristic constants. The value of k_B for H_2S is found to be 2.31 from our k of 1.24 and argon's k_B of 1.86. Because of the uncertainties in T_B and d_0 for H_2S , this value of k_B may be in error by as much as 2 or 3%. Even so, we can draw several definite conclusions concerning the potentials in common use. The Lennard-Jones 12-6 potential, for example, with its k_B of 1.944, cannot represent H_2S . Similarly, the Stockmayer potential, which has a dipole superimposed on a 12-6 potential, has a maximum k_B of 1.944 and therefore cannot represent this polar gas. As discussed in ref 9, this potential could be modified to provide larger k_B values by adding a Kihara-type core or using a base potential with a repulsive index greater than 12. Among the potentials that can provide the proper k_B for H_2S are the square-well, the exp-6, and the Kihara potentials. Taking 2.31 tentatively as the exact k_B , the values of the three parameters for each of

these potentials, as found from k_B , T_B , d_0 and the tables of ref 9, are given in Table IV. This selection of possible three-parameter potentials for a gas from its PVT data was previously impossible. Perhaps other properties will allow a choice to be made among these possibilities.

Table IV: Parameter Values for H_2S Intermolecular Potentials

Potential	$\epsilon/k(^{\circ}\text{K})$	$b_0(\text{cc/mole})$	p_3^a
Square-Well	195	54.6	1.75
Exp-6	350	68.3	18.1
Kihara	351	67.9	0.15

^a For the square-well, p_3 is g , the ratio of outer to inner well diameters; for the exp-6, p_3 is γ , a measure of the steepness of the repulsive core; for the Kihara, p_3 is a^* , a measure of the inner hard core.

Radiation Chemistry of the Aqueous Nitrate System.¹ II. Scavenging and pH Effects in the Cobalt-60 γ Radiolysis of Concentrated Sodium Nitrate Solutions

by Malcolm Daniels and Eric E. Wigg²

Chemistry Department and Radiation Center, Oregon State University, Corvallis, Oregon 97331 (Received February 3, 1969)

Scavenging studies with H_2 , 1-propanol, nitrite, and iodide ions at neutral pH indicate that H_2 and 1-propanol react only with available OH radicals; $g(\text{OH})$ decreases with increasing nitrate concentration. Nitrite scavenging shows only minor amounts of O atom, and I^- interferes in the "direct" process. At alkaline pH, changes in yields are consistent with (a) the dilute solution mechanism involving H_2O_2 and (b) an effect of pH on the "direct" process. Scavenging studies at pH 9 (H_2 , and NO_2^-) and pH 12 (1-propanol) show yields of OH and O unchanged from neutral solution. A mechanism is proposed for the direct radiolysis, $\text{NO}_3^- \xrightarrow{\gamma} (\text{NO}_2 + \text{O} + e)_{\text{org}, \text{sur}}$; $\text{O} + \text{NO}_3^- \rightarrow \text{O}_2 + \text{NO}_2^-$, and is discussed in relation to pulse radiolysis and uv photolysis studies.

Introduction

In part I,³ data were presented for the Co^{60} γ radiolysis of sodium nitrate solutions as a function of nitrate concentration from 10^{-4} to 6 M , and a mechanism was established which satisfactorily accounted for the results up to about 5×10^{-2} M ; this will now be regarded as the "indirect effect." Above this concentration, $G(\text{NO}_2^-)$ increases by a factor of ~ 3.5 in neutral solution and this has been attributed to the "direct effect."⁴ The "direct effect" is not so clearly defined as the "indirect effect." In this paper we shall con-

sider it to be the chemical transformation in a solute due to energy deposition caused by the solute. Although we as yet know little about the mechanisms of the "direct effect," such a definition is mechanistically distinct from the effects of "subexcitation electrons"⁵

(1) This work was supported by U. S. A.E.C. and constitutes Report No. RC-2014-2

(2) Esso Research & Engineering Co., Linden, N. J. 07036.

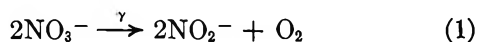
(3) M. Daniels and E. E. Wigg, *J. Phys. Chem.*, **71**, 1024 (1967).

(4) H. A. Mahlman, *ibid.*, **67**, 1466 (1963).

or of energy transfer from possible excited states of water.⁸ This definition is also operational and leads to a means of characterizing and quantitatively evaluating the efficiency of radiolysis due to the "direct effect," as follows. In concentrated solutions the major part of the energy deposition still will be due to the water component, the "indirect effect." Assuming as a working approximation that these modes of radiolysis are independent, then the overall decomposition may be described by the linear relation

$$G(\text{NO}_2^-) = G(\text{NO}_2^-)_{\text{H}_2\text{O}} f_{\text{H}_2\text{O}} + G(\text{NO}_2^-)_{\text{NO}_3^-} f_{\text{NO}_3^-} \quad (\text{I})$$

where $G(\text{NO}_2^-)_{\text{H}_2\text{O}}$ signifies the coefficient of net nitrate formation by the "indirect effect" (the yield in dilute solution when $f_{\text{H}_2\text{O}} = 1.00$) and $G(\text{NO}_2^-)_{\text{NO}_3^-}$ the coefficient for nitrite formation from nitrate by the "direct effect." Estimating the fractional energy absorptions $f_{\text{H}_2\text{O}}$ and $f_{\text{NO}_3^-}$ from the electron densities of the components and the concentrations of the solutions, it has been shown⁷ that $G(\text{NO}_2^-)$ and $G(\text{O}_2)$ fit relation (I), allowing $G(\text{NO}_2^-)_{\text{NO}_3^-} = 4.0$ and $G(\text{O}_2)_{\text{NO}_3^-} = 2.0$ to be deduced; this clearly is good stoichiometry for describing the "direct effect" simply as



It is the purpose of this paper to present further results bearing on the relative roles of "indirect effect" and "direct effect" in the high concentration range and to investigate the mechanism of the "direct effect." Studies of (a) the scavenging by hydrogen, 1-propanol, nitrite, and iodide in 2.2, 4.0, and 6.0 *M* sodium nitrate solutions (neutral pH), (b) the effect of pH in concentrated solutions, and (c) scavenging at various alkaline pH's are reported. They are discussed in conjunction with the previously reported³ values for $G(\text{NO}_2^-)$ and $G(\text{H}_2\text{C}_2)$, the $G(\text{H}_2)$ and $G(\text{O}_2)$ values of Mahlman,⁸ and recent studies of the uv photolysis⁹ and pulse radiolysis¹⁰ of concentrated nitrate solutions.

Experimental Section

The techniques and analytical procedures have been described previously.³ A slight dependence on nitrate concentration was found in the method used for the analysis of nitrite. This amounted to 4% in ϵ at a final nitrate concentration of 2.5 *M*. No effect of nitrate was found in the hydrogen peroxide analysis. G values are calculated on the basis of total energy absorption. Energy deposition in concentrated solutions was calculated from Fricke dosimetry assuming proportionality with electron density.

Varying the temperature of 3.0 *M* NO_3^- from 27 to 65° resulted in a 2% decrease in $G(\text{NO}_2^-)$, an insignificant effect probably attributable to expansion of the solution.

Results and Discussion

A. Neutral Solutions. (1) *Scavenging by H₂ and 1-Propanol; Determination of g(OH).* With the "direct

effect" separable according to (I) and established by its stoichiometry, scavenging experiments have been carried out to attempt the independent determination of the extent of the "indirect effect."

For concentrated solutions, we write (for any nitrate concentration) the nitrite yield in the absence of scavenger as

$$G(\text{NO}_2^-)_0 = G(d) + \frac{1}{2}[g(r) - g(\text{OH})] + \Delta g\text{H}_2 \quad (\text{II})$$

where $G(d)$ symbolizes the direct effect, $g(r)$ the primary yield of reducing species from water, $g(\text{OH})$ that of oxidizing species from water, and $\Delta g\text{H}_2$ the difference between the molecular yield H_2 expected at this particular concentration and that measured. It was shown in part I⁸ that, under suitable conditions, hydrogen gas can successfully compete with the radiolysis product NO_2^- for OH radicals, and for complete radical scavenging, the nitrite yield can then be written as

$$G(\text{NO}_2^-)_{\text{H}_2} = G(d) + \frac{1}{2}[g(r) + g(\text{OH})] + \Delta g\text{H}_2 \quad (\text{III})$$

if H_2 does not interfere with the mechanism of direct radiolysis.

Hydrogen-saturated solutions of nitrate (4.0 *M*) have been irradiated to low total doses ($\sim 2 \times 10^{18}$ eV/l.) and $G(\text{NO}_2^-)$ determined. As the buildup of even submicromolar nitrite concentrations caused a significant lowering of $G(\text{NO}_2^-)$, due to the reaction



it was necessary to extrapolate G values determined at various average nitrite concentrations to zero nitrite. In this way, a value $G(\text{NO}_2^-)_{\text{H}_2} = 3.4$ was obtained, 1.9 greater than $G(\text{NO}_2^-)$ found for an identical helium-swept solution. From eq II and III, this difference is $g(\text{OH})$ for 4 *M* NaNO_3^- . It is also found to be equal to the yield expected from the water fraction; *i.e.*, $g(\text{OH})_{\text{H}_2\text{O}}$, taking $g(\text{OH})_{\text{H}_2\text{O}} = 2.5$, as found in dilute solution.³ This suggests that the assumption concerning the role of H_2 is valid and indicates that OH radicals are not involved in the direct process.

Because of difficulties in working with the H_2 system to ensure complete radical scavenging, more extensive experiments have been carried out with 1-propanol, known to be an effective OH radical scavenger [$k(\text{OH} + \text{C}_3\text{H}_7\text{OH}) = 1.5 \times 10^9 \text{ M}^{-1} \text{ sec}^{-1}$],¹¹ over the range

(5) (a) J. Weiss, *Nature*, **174**, 78 (1954); (b) R. L. Platzmann, *Radiat. Res.*, **1**, 558 (1954).

(6) J. Bednar, *Collect. Czech. Chem. Commun.*, **27**, 2204 (1962).

(7) M. Daniels, *Advances in Chemistry Series*, No. 81, R. F. Gould, Ed., American Chemical Society, Washington, D. C., 1968, p 158.

(8) H. A. Mahlman, *J. Chem. Phys.*, **35**, 936 (1961).

(9) M. Daniels, R. V. Meyers, and E. V. Belardo, *J. Phys. Chem.*, **72**, 389 (1968).

(10) (a) M. Daniels, *ibid.*, **70**, 3022 (1966); (b) *ibid.*, **73**, 3710 (1969).

(11) G. E. Adams, J. W. Boag, J. Curren, and B. D. Michael in "Pulse Radiolysis," M. Ebert, J. P. Keene, A. J. Swallow, and J. H. Baxendale, Ed., Academic Press, London, 1965, p 131.

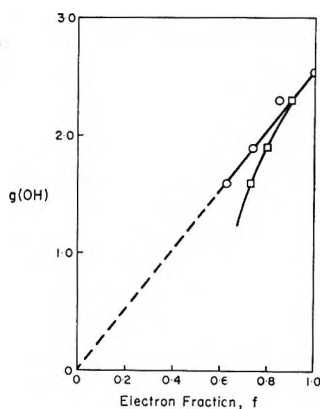
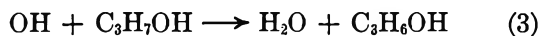


Figure 1. $g(\text{OH})$ values as a function of electron fraction: \circ , $f_{\text{H}_2\text{O}}$; \square , $f_{\text{H}_2\text{O}} + f_{\text{Na}^+}$. $g(\text{OH})$ determined from limits of propanol scavenging in He-swept neutral NaNO_3 solutions.

0.1–10 mM. The scavenging limit is almost identical with that found using H_2 ,⁷ and stoichiometry indicates that the radical formed in the scavenging process



causes further reduction, as reported by others.¹² This behavior substantiates the above interpretations and conclusions drawn from the H_2 scavenging work. Results from He-swept 2, 4, and 6 M NaNO_3 solutions, are collected in Table I. Over this wide range of nitrate concentration $g(\text{OH})$ is found to be linearly related to the fractional energy deposition due to water, but when the fractional energy deposition due to the cation is included steady deviation is observed (Figure 1). These results indicate that the cation Na^+ does not contribute to net water radiolysis, but leave unanswered its role in the direct radiolysis of nitrate. This aspect is presently under investigation. However, it seems clear that freely diffusing OH radicals originate only from water in an amount proportional to the fractional energy deposition due to water and take no part in the processes of direct radiolysis at low intensities. A similar decrease in $g(\text{OH})$ at high solute concentrations has been reported for the aqueous perchlorate system.¹³

Table I

	NO_3^- concn, M		
	2	4	6
$G(\text{NO}_2^-)_{\text{H}_2\text{O}}$	1.3	1.53	1.8
$G(\text{NO}_2^-)_{n\text{-prop}}$	3.6	3.4	3.3
$g(\text{OH})$	2.3	1.9	1.5
$g(\text{OH})_{\text{H}_2\text{O}}/f_{\text{H}_2\text{O}}$	2.2	1.9	1.6

where $g(\text{OH})_{\text{H}_2\text{O}} = 2.53$

(2) *Effect of Iodide Ion.* In view of the preceding results it was clearly desirable to attempt an independent determination of $g(r)$. In part I³ it was found

that iodide scavenging gave results which could be accounted for directly in terms of $g(r)$ and the consumption of molecular yield hydrogen ($\Delta g\text{H}_2$). If I^- does not interfere in the direct processes, $G(\text{NO}_2^-)_{\text{I}^-}$ should be accountable as

$$G(\text{NO}_2^-)_{\text{I}^-} = G(d) + g(r) + 2\Delta g(\text{H}_2) \quad (\text{IV})$$

Thus, for 4.0 M NO_3^- , we may anticipate from known values of $G(d)$, $g(r)$, and $G(\text{H}_2)$ that $G(\text{NO}_2^-)_{\text{I}^-} \simeq 4.0$. Experimentally, using 1 and 5 mM I^- (in oxygen-free solution), we find $G(\text{NO}_2^-)_{\text{I}^-} = 5.1$; the corresponding oxidation yield is $G\Sigma(\text{I}_2 + \text{H}_2\text{O}_2) = 3.55$, 0.60 greater than anticipated from the water fraction. So the assumption that I^- does not interfere in the direct process is invalid. To determine the extent of interference, the above procedure may be reversed to calculate $G(d)$ from the experimental determination of $G(\text{NO}_2^-)_{\text{I}^-}$. This gives $G(d)_{\text{I}^-} \simeq 1.9$, about double that in the absence of iodide.

Results including the 2.0 and 6.0 M nitrate are summarized in Table II where experimental values for $G(\text{NO}_2^-)_{\text{I}^-}$ and $G\Sigma(\text{I}_2 + \text{H}_2\text{O}_2)$ are compared with values calculated from the water fraction. It may be seen that in all cases the yield of nitrite from the direct effect is doubled in the presence of I^- (row 7), and that the ratio "direct effect nitrite"/iodide oxidized is approximately 3 (row 8). These conclusions are further discussed below in connection with the mechanism of the direct effect.

Table II: Nitrite and I_2 Yields with I^- as Scavenger

	NO_3^- concn, M		
	2.0	4.0	6.0
$G(\text{NO}_2^-)_{\text{I}^-}^a$	4.80	5.00	4.93
$G(\text{NO}_2^-)_{\text{H}_2\text{O}}^b$	3.65	3.15	2.70
$\Delta G(\text{NO}_2^-)_{\text{I}^-}^c$	1.15	1.85	2.23
$G\Sigma(\text{I}_2 + \text{H}_2\text{O}_2)^d$	3.92	3.55	3.33
$G_{\text{H}_2\text{O}}\Sigma(\text{I}_2 + \text{H}_2\text{O}_2)^e$	3.47	2.94	2.51
$\Delta G\Sigma(\text{I}_2 + \text{H}_2\text{O}_2)^f$	0.45	0.61	0.82
$\Delta G(\text{NO}_2^-)_{\text{I}^-}/G(d)$	1.92	2.10	2.05
$\Delta G(\text{NO}_2^-)_{\text{I}^-}/\Delta G\Sigma(\text{I}_2 + \text{H}_2\text{O}_2)$	2.56	3.03	2.72

^a Experimental values. ^b Calculated values for effect of I^- on water radiolysis. ^c Direct effect in presence of I^- , $G(\text{NO}_2^-)_{\text{I}^-} - G(\text{NO}_2^-)_{\text{H}_2\text{O}}$. ^d Experimental values. ^e Calculated values for water radiolysis. ^f Oxidation of iodide caused by direct processes, $G\Sigma(\text{I}_2 + \text{H}_2\text{O}_2) - G_{\text{H}_2\text{O}}\Sigma(\text{I}_2 + \text{H}_2\text{O}_2)$.

Comparison of these results may be made with the work of Hyder¹⁴ who, for 4 M NO_3^- , finds $G(\text{NO}_2^-)_{\text{I}^-} \sim 4.8$ –4.9, and for 2 M, ~ 5.1 (interpolated). These results must be considered to be in substantial agree-

(12) (a) J. T. Allen, *J. Phys. Chem.*, **68**, 2967 (1964); (b) E. Hayon, *Trans. Faraday Soc.*, **61**, 734 (1965).

(13) D. Katakis and J. Konstantos, *J. Phys. Chem.*, **72**, 2054 (1968).

(14) M. L. Hyder, *ibid.*, **64**, 1858 (1965).

Table III: Results of NO_2^- Scavenging

4.0 M NaNO_3 , pH 5.5			6.6 M NaNO_3 , pH 5.5			4.0 M NaNO_3 , pH 9.0		
$[\text{NO}_2^-]_0$, μM	$G(\text{NO}_2^-)$	$\Delta G(\text{NO}_2)$	$[\text{NO}_2^-]_0$, μM	$G(\text{NO}_2^-)$	$\Delta G(\text{NO}_2^-)$	$[\text{NO}_2^-]_0$, μM	$G(\text{NO}_2^-)$	$\Delta G(\text{NO}_2^-)$
0	1.53		0	1.72		0	2.16	
100	1.42	0.11	270	1.56	0.16	50	1.90	0.26
200	1.36	0.17				170	1.94	0.22
290	1.33	0.20				260	1.87	0.29

ment with those reported here. However in the absence of I^- , Hyder's values for 2 and 4 M NO_3^- are equal at $G(\text{NO}_2^-)_0 \approx 2.8$ and are approximately twice as large as those reported here. The reason for this difference is not known.

(3) *Nitrite Scavenging and the Role of O Atoms.* Considerable interest attaches to the possible role of O atoms in the mechanism of the "direct effect" and a major role has been assigned¹⁵ to it, despite the paucity of evidence requiring its participation. Recent work on the photolysis of nitrate solution has changed this situation. Experimentally, two phenomena are found in the near-uv photolysis⁹ of nitrate solutions which are attributed to ground state O atom reactions; (a) a marked increase in rate of photolysis in weakly alkaline solution, with an apparent pK of 8.8 in 1 M NO_3^- and 8.4 in 3 M NO_3^- , (b) strong inhibition of photolysis by nitrite in neutral solution, described by simple homogeneous competition ($\text{O} + \text{NO}_3^- \rightarrow \text{O}_2 + \text{NO}_2$, $\text{O} + \text{NO}_2^- \rightarrow \text{NO}_3^-$) and rate constant ratio $k(\text{O} + \text{NO}_2^-)/k(\text{O} + \text{NO}_3^-) \sim 2 \times 10^4$. Accordingly, if freely diffusing O atoms participate in the "direct effect," inhibition by nitrite should be apparent.

Solutions of sodium nitrate (4.0 and 6.6 M) were irradiated in the absence of oxygen, with initial nitrite concentrations ranging from zero to $\sim 300 \mu\text{M}$. The results are shown in Table III and are to be contrasted with the much greater effects observed in the photolysis. The magnitude of the decrease, coupled with the uncertainty due to analytical limitations at high NO_2^- concentrations, prevents detailed analysis but some important conclusions can be drawn. From the rate constant ratio $k(\text{O} + \text{NO}_2^-)/k(\text{O} + \text{NO}_3^-)$, the optimum conditions used correspond to 74% scavenging for 4 M NO_3^- and 62% for 6 M NO_3^- . From the simple scavenging mechanism, $G(\text{O})$ is given by $1/2 \Delta G(\text{NO}_2^-)/\text{fractional scavenging efficiency}$, and we estimate $G(\text{O}) \approx 0.14$ for 4 M NO_3^- and 0.12 for 6.6 M NO_3^- . The O atom yield does not show a strong dependence on nitrate concentration as would be expected for a scavengeable "direct effect" intermediate. Rather we draw attention to a correlation with the suggestion made in part I, that O atoms may be formed in water radiolysis with a $G(\text{O}) \approx 0.2$. A fractional energy correction to this value; *i.e.*, $G(\text{O})_{f_{\text{H}_2\text{O}}}$, leads to values of 0.15 and 0.12 for 4 and 6.6 M nitrate, respectively. Hence we conclude that the freely

diffusing O atom is not a major intermediate in the "direct effect" at these low intensities and suggest that the observed effects may be understood in terms of a small amount formed from the radiolysis of water.

B. Alkaline Solutions. (1) *General Characteristics; H_2 and Nitrite Scavenging at pH 9.* Change of pH in the alkaline region has been found to have a marked effect on the radiolysis of nitrate in dilute solution³ and on the photolysis in concentrated solution.⁹ Insofar as the pH behavior may be characteristic of the species involved, it has been investigated here as an aid in identifying these species.

$G(\text{NO}_2^-)$ and $G(\text{H}_2\text{O}_2)$ for 2.2 M NO_3^- are presented as a function of pH in Figure 2. Characteristic features are the consumption of molecular yield hydrogen peroxide and the increase in nitrite formation. Indeed the hydrogen peroxide curve is almost identical with that found in dilute solution. However, the nitrite curve exhibits two inflections, the first at pH 7-9, when little attack has occurred on the H_2O_2 consumption. The total increase in $G(\text{NO}_2^-)$ is not equivalent to the decrease in $G(\text{H}_2\text{O}_2)$, as was the case for dilute solutions, but is $\sim 50\%$ greater, and this suggests that two distinct processes are occurring in alkaline solution.

To separate these processes we suppose that the reactions of dilute solution described in part I, which consume H_2O_2 and lead to nitrite, are also operative here. Curve C is then obtained by subtracting from curve A the stoichiometric equivalent of the change in curve E with pH. As curve C was not observed in dilute solution, it must be attributed either to the "direct effect" or to an effect of high nitrate concentration on the OH radical reactions of dilute solutions. To determine if indeed OH radicals were being consumed, H_2 scavenging experiments were carried out at pH 9.4 in 4.0 M NO_3^- . Corrected for nitrite buildup, $G(\text{NO}_2^-)_{\text{pH 9}}$ was determined as 4.4 ± 0.2 . This is within the limits of the value obtained by adding $g(\text{OH})_{\text{H}_2\text{O}/\text{H}_2\text{O}}$ (≈ 1.9) to $G(\text{NO}_2^-)$ for He-swept 4.0 M NO_3^- (2.25). Similarly, scavenging experiments with nitrite have been carried out, and results are presented in Table III. No change is observed from neutral solution, and the major feature of those scavenging studies is that the

(15) J. Bednar and S. Lukac, *Collect. Czech. Chem. Commun.*, **24**, 341 (1964).

yield of scavengeable O and OH are essentially unchanged from pH 5.5 to pH 9.4. Consequently, the increase in $G(\text{NO}_2^-)$ with pH (curve C) is attributed to the direct process; as such $\Delta G(\text{NO}_2^-)/f_{\text{NO}_3^-}$ should be constant for different nitrate concentrations. Values of 4.1 and 4.2 were obtained both for 2.2 M NO_3^- and 4.0 M NO_3^- , supporting the assignment (Table IV). We have already found⁵ that the direct effect in neutral solution can be ascribed a G of 4.0; hence we conclude that in slightly alkaline solution the mechanism of the "direct effect" changes so as to double the net yield.

Table IV: pH Effects on the Direct Action Nitrite Yields

$[\text{NO}_3^-], M$	$\Delta G(\text{NO}_2^-)^a$	$f_{\text{NO}_3^-}$	$\Delta G(\text{NO}_2^-)/f_{\text{NO}_3^-}$
2.2	0.45	0.110	4.1
4.0	0.82	0.197	4.2

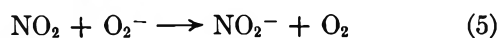
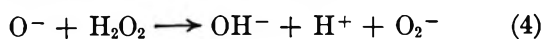
^a $G(\text{NO}_2^-)_{\text{pH}9} - G(\text{NO}_2^-)_{\text{pH}6}$.

Comparison with the results of Hyder shows only qualitative agreement, in that $G(\text{NO}_2^-)$ increases with pH; numerical disagreement is considerable, e.g., for oxygen-free 1 M NaNO_3 Hyder reports $G(\text{NO}_2^-) \simeq 2.3$ at neutral pH, increasing to ~ 4.6 at pH 13, whereas we find for 2 M NaNO_3 $G(\text{NO}_2^-)$ increases from 1.3 to 2.3 (Figure 2).

(2) *Effect of Oxygen.* Determination of the pH dependence of $G(\text{NO}_2^-)$ for air-equilibrated solutions (Figure 2, curve B) shows that 250 $\mu\text{M O}_2$ decreases the yield in alkaline solution by an amount which is approximately constant above pH 9. A similar effect of oxygen in alkaline solution was found in dilute solution,³ where it protected the molecular hydrogen peroxide. In the present work, no change is observed in $G(\text{H}_2\text{O}_2)$, indicating that the effect of O_2 may be on the direct process.

This effect of oxygen is qualitatively similar to that reported by Hyder, but again is much smaller in magnitude; e.g., at pH 13 Hyder finds $G(\text{NO}_2^-)$ for 1-2 M NaNO_3 decreases from a 4.8 to ~ 1.8 in the presence of O_2 , whereas our values decrease from 2.3 to 2.1.

(3) *Scavenging by 1-Propanol at pH 12.* It was suggested above that the effects observed from pH 9-13 are probably those of the indirect effect already investigated in part I. In this process H_2O_2 is consumed by O^- (or HO_2^- by OH) to give O_2^- , which then reduces NO_2 (or an equivalent form) to nitrite



Accordingly the increase in $G(\text{NO}_2^-)$ from pH 9 to pH 12 should be equivalent to the consumption of

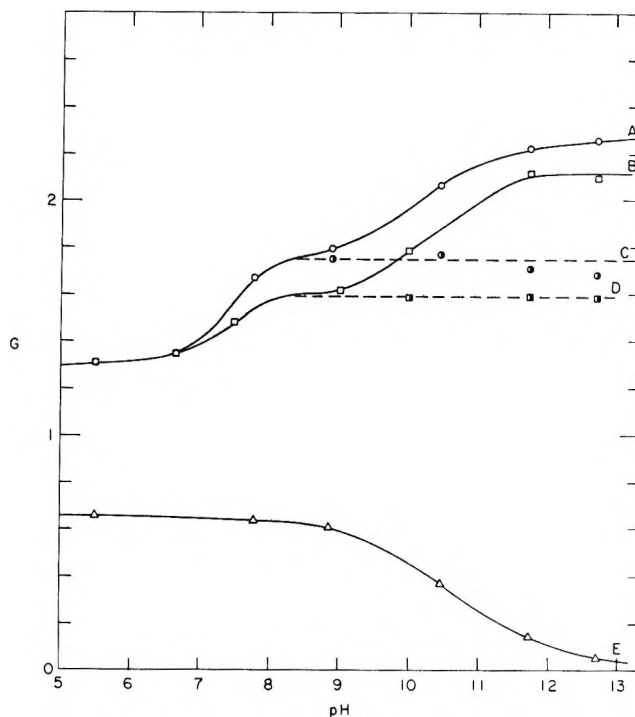


Figure 2. $G(\text{NO}_2^-)$ and $G(\text{H}_2\text{O}_2)$ as function of pH for 2.2 M NaNO_3 . A: $G(\text{NO}_2^-)$, oxygen-free; B: $G(\text{NO}_2^-)$, air-equilibrated; E: $G(\text{H}_2\text{O}_2)$, oxygen-free; C: curve A - [decrease in $G(\text{H}_2\text{O}_2)$ with pH]; D: curve B - [decrease in $G(\text{H}_2\text{O}_2)$ with pH].

H_2O_2 over this range. Results presented in Table V show that this is so for both 2.2 and 4.0 M solutions. Further, addition of an OH scavenger prior to irradiation should bring this process to a limit at which each OH contributes to the reduction. For 4 M NO_3^- the scavenging limit for 1-propanol is 4.1. The increased yield of nitrite (~ 1.9) for the 1-propanol case is nicely accounted for as $g(\text{OH})_{\text{H}_2\text{O}}/f_{\text{H}_2\text{O}}$.

Table V: Relation between Nitrite Formation and H_2O_2 Consumption at pH 12

$[\text{NO}_3^-], M$	$G(\text{NO}_2^-)_{\text{pH}9}$	$\Delta G(\text{H}_2\text{O}_2)^a$	Σ^b	$G(\text{NO}_2^-)_{\text{pH}12}$
2.2	1.80	0.50	2.30	2.20
4.0	2.25	0.50	2.75	2.80

^a $G(\text{H}_2\text{O}_2)_{\text{pH}9} - G(\text{H}_2\text{O}_2)_{\text{pH}12}$. ^b Sum of columns 2 and 3. ^c Experimentally determined.

C. Separation of Indirect and Direct Effects. (1) A significant conclusion from the foregoing results is that the effects of (1) hydrogen gas, 1-propanol, iodide ion, and nitrite in neutral solution, (2) pH, (3) hydrogen gas and nitrite at pH 9, and (4) 1-propanol at pH 12 can quantitatively and self-consistently be accounted for on the basis of separability of the initiation of direct and indirect processes, radical yields for the indirect process being calculable as electron fractions

of the dilute solution values. The success of this approach may be judged from Table VI. The important corollary to such a simple interpretation is that we find no evidence requiring the postulate of energy transfer from "excited water" or "subexcitation electrons" to nitrate.

Table VI: Relations Accounting for G Values Observed under Various Conditions of pH and Scavenging in 4 M NaNO_3

Quantity measured	Proposed relation	$G(\text{NO}_2^-)$	
		Calcd	Exptl
$G(\text{NO}_2^-)_{0^{\text{pH}}}^{\text{a}}$	$G(d) + \frac{1}{2}(gr - g\text{OH}) + \Delta g\text{H}_2$	1.54	1.53
$G(\text{NO}_2^-)_{\text{H}_2^{\text{pH}}}^{\text{b}}$	$G(d) + \frac{1}{2}(gr + g\text{OH}) + \Delta g\text{H}_2$	3.44	3.4
$G(\text{NO}_2^-)_{\text{I}^-^{\text{pH}}}^{\text{c}}$	$2G(d) + gr + 2g\text{H}_2$	5.0	5.1
$G(\text{NO}_2^-)_{0^{\text{pH}}}^{\text{a}}$	$2G(d) + \frac{1}{2}(gr - g\text{OH}) + \Delta g\text{H}_2$	2.35	2.35
$G(\text{NO}_2^-)_{\text{H}_2^{\text{pH}}}^{\text{b}}$	$2G(d) + \frac{1}{2}(gr + g\text{OH}) + \Delta g\text{H}_2$	4.25	4.3

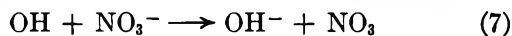
^a Total G for nitrite formation, in absence of additive.

(2) *Mechanism of Direct Process.* Nitrite formation by the direct process can be considerably affected by some scavengers. Thus iodide and change of pH both effectively double the $G(\text{NO}_2^-)_{\text{NO}_3^-}$.

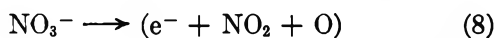
A satisfactory account of the mechanisms involved can be based on results of pulse radiolysis¹⁰ and uv photolysis⁹ of concentrated nitrate solutions. At high intensities NO_3 has been found to be a transient species characteristic of the "direct effect." It is not an immediate species, but builds up rapidly after the pulse, and hence is not formed only by (6), but has a precursor.



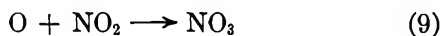
Scavenging studies indicate that this precursor is not the OH radical, and hence NO_3 is also not formed by



and it is suggested that a significant "primary process" may be represented as the dissociative ionization

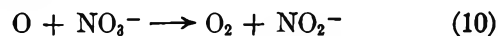


At such high nitrate concentrations as are involved here, e^- will be rapidly scavenged by nitrate ion. NO_3 may then be formed by



which may occur either within a "cage" and be indistinguishable from (6), or following diffusive processes, within a "spur." This accords with the intensity dependence of NO_3 formation.^{10b} Similarly the work of Pikaev, *et al.*,¹⁶ indicating that $G(\text{NO}_2^-)_{\text{NO}_3^-}$ decreases with intensity at very high intensities, and

our own result that $G(\text{NO}_2^-)_{\text{NO}_3^-}$ is independent of intensity at low intensities, suggests that the fate of the O atoms formed in reaction 8 is to react further with nitrate, rather than undergo self-recombination.



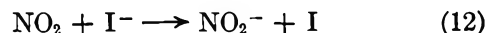
This behavior is also found in the uv photolysis.⁹ Definitive evidence concerning the fate of the O atoms both in radiolysis and photolysis can probably be obtained by suitable O^{18} experiments, which are presently being undertaken.

The state of the O atom is unknown, but if it were ^1D then hydrogen peroxide would be expected to be a product of the direct process by reaction of O with water¹⁷



Our hydrogen peroxide results⁷ discount this as a major process. Hence we suggest the overall process at these low intensities is described by reactions 8 and 10, followed by reaction of NO_2 as investigated in dilute solution.

The effect of iodide on the nitrite yield may be understood in terms of reactions 12 and 10. It was found in part I that I^- , in addition to being a scavenger of OH radicals, reacts efficiently with NO_2



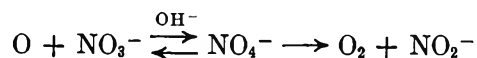
The increased yield of nitrite in the presence of I^- over that expected from the indirect effect may thus be ascribed to reaction of iodide with the NO_2 originating in the direct process. Evidence of NO_2 as a transient of the "direct effect" is presented in the following paper. Stoichiometry then indicates that $G(\text{NO}_2^-)_{\text{I}^-}/G(\text{I}_2)$ should be 3.¹⁸ Experimental results approach this (Table II). If the effect of I^- were simply to change the mechanism, the $G(\text{NO}_2^-)_{\text{I}^-}/G(d)_0$ should be 1.5. Experimentally the ratio is 2.0, suggesting that I^- is also scavenging in the primary recombination following reaction 8. This suggestion is consistent with the interpretation of the pH effect below.

The effect of pH on the "direct process" is very similar to that observed in the uv photolysis.⁹ There it was shown that nitrate at pH 10 behaved as a "cage" scavenger, according to reaction 10. The same effect may be occurring here, that is, that reaction 10 may compete with primary recombination (reversal of reaction 8), reaching the same limit as the iodide scavenging. The rationalization offered in eq 7 was in terms of a pH dependent reversibility of reaction 10

(16) A. K. Pikaev, P. Ya. Glazunov, and A. A. Yakubovich, *Kinet. Katal.*, **4**, 735 (1963).

(17) (a) H. Taube, *Trans. Faraday Soc.*, **53**, 656 (1957); (b) W. D. McGrath and R. G. W. Norrish, *Nature*, **182**, 235 (1958).

(18) The net effect of eq 8 and 10, together with capture of the electron by NO_3^- to give NO_2 , is $2\text{NO}_2 + 1\text{NO}_2^-$; on reaction with I^- (eq 12), the NO_2^- yield will be 3 and the I_2 yield will be 1.



and this should also be applicable here.

We are thus led to the idea that most of the overall chemistry in concentrated solution occurs within the so-called spur. This is the logical extension of the concept of spur scavenging of water primary products by solutes, to the case where the solute now acts as scavenger for the primary products of its own radiolysis. This would explain why scavenging with low nitrite concentrations failed to detect O atoms.

Comparing nitrite scavenging results for γ radiolysis and uv photolysis, the immediate conclusion is that a smaller fraction of O atoms escape primary recombination in the γ radiolysis, but such a simple approach is not satisfactory because of the different physical situation in the two cases. In the photochemical case, when a reactive species escapes primary recombination within the "cage," then it behaves essentially as a free agent and as a consequence of the random nature of the uv photon absorption process, it exhibits little correlation with species escaping other cages. In the radiolysis case, when a species escapes its immediate "cage," it still finds itself in a "spur" and its behavior in space and time must be correlated within the "spur" with similar species from other "cages;" extensive secondary recombination may occur by diffusion within the "spur" (e.g., our proposal for NO_3 formation), and the yield of easily scavengeable species will be low. Considerations such as these, which raise

the question of the microstructure of "spurs," point a way whereby our conceptual picture of radiation chemical primary processes may be refined, both experimentally and theoretically.

(3) *Energy Distribution Coefficients, $f_{\text{H}_2\text{O}}$, $f_{\text{NO}_3^-}$, f_{Na^+} .* The present quantitative treatment of results through the use of eq I relies on the values assigned to the coefficients $f_{\text{H}_2\text{O}}$, $f_{\text{NO}_3^-}$, f_{Na^+} , which represent the partitioning of absorbed energy among the chemical components of the system. Although the total energy deposition from the beam, due mainly to Compton processes, can adequately be calculated from electron densities, there seems to be no practical procedure by which the f 's can be calculated from theoretical principles. Accordingly, we have had to assume that, in this particular system, all electrons are equally effective in leading to net decomposition and that the radiation chemical primary yield in a component is proportional to the fraction of electrons which it contributes to the medium. The *post-priori* success of this approach would seem to imply that the integrated "excitation spectra" (in the usage of Platzmann¹⁹) of water and NO_3^- are very similar. Experimental verification of this will be difficult, but work in progress on the role of different cations may contribute to our further understanding of energy-partitioning effects in concentrated solutions.

(19) R. L. Platzmann in "Radiation Research 1966," G. Silini, Ed., North-Holland Publishing Co., Amsterdam, 1967, p 20.

Radiation Chemistry of the Aqueous Nitrate System.¹ III. Pulse Electron Radiolysis of Concentrated Sodium Nitrate Solutions

by Malcolm Daniels

Chemistry Department and Radiation Center, Oregon State University, Corvallis, Oregon 97331 (Received February 3, 1969)

Optical absorption spectra and reaction kinetics of transient species in concentrated sodium nitrate and nitric acid solutions have been investigated for 0.5–6 M NaNO₃ and 6 × 10⁻² to 9 M HNO₃. NO₃ has been identified as a transient in concentrated neutral nitrate solutions and is shown to be characteristic of the "direct effect." Yield of NO₃ is constant from pH 4 to 11; it decays by first-order kinetics strongly dependent on pH. In neutral solution NO₂ is identified; it decays by second-order kinetics with 2k/ε = 1.4 × 10⁵. NO₂ is also produced by the "direct" effect, and as the yield of NO₃ is intensity-dependent, a mechanism of formation is probably O + NO₂ → NO₃. In acid solutions, NO₃ is also formed by an "indirect effect" with a rate constant first order in NO₃⁻ and H⁺. The reaction is probably OH + NO₃⁻ + H⁺ → H₂O + NO₃. The yield of NO₃ increases fourfold between pH 1 and 0, and the direct process may be pH dependent. In strongly acid solutions decay of NO₃ becomes second order with 2k/ε = 2.8 × 10⁶. ε(NO₃)/ε(NO₂) = 0.5 at 400 nm and ε(NO₃)₆₇₀/ε(NO₃)₄₀₀ = 2.9. NO₂ is not observed in acid solutions.

Previous papers in this series have investigated the low-intensity Co⁶⁰ γ radiolysis of dilute² and concentrated³ sodium nitrate solutions, primarily by "scavenger" techniques. For the dilute solution case, sufficient information concerning the absolute rate constants of primary species such as e_{aq}⁻ and OH with NO₃⁻ and NO₂⁻ was already available, so that a satisfactory mechanistic interpretation could be made (although it should be noted that identification of the transient products is still needed). However, for concentrated solutions in which the "direct effect" is important, no such corresponding information existed. Hence this present work was carried out with the aims of (a) searching for and identifying transient species in concentrated solutions, (b) determining the kinetics and mechanisms of their transformations. In a preliminary account⁴ of this work the identification of NO₃ in both neutral and acid solution was reported, and Broskiewicz⁵ has since presented his results on NO₃ in acid solutions. The only other work on pulse radiolysis of nitrate is that of Pikaev, *et al.*,⁶ who investigated product yields; their results are thus complementary to those now reported here in full.

Experimental Section

All experiments were carried out using analytical grade materials in triply distilled water; recrystallization of NaNO₃, which had a significant effect on the γ-radiolysis results, was found to be unnecessary at high intensities.

Radiolyses were carried out on two machines, the 13.5-MeV Linac at Argonne National Laboratory and the 2-MeV Van de Graaff of the Chemistry Department, Brookhaven National Laboratory. On the Linac, beam currents up to 180 mA were available at pulse

lengths from 0.4 to 1.0 μsec. The sample was contained in a 4-cm cell, and a multiple reflection system allowed the use of path lengths up to 64 cm.⁷ For determination of spectra, a split-beam method was used, one beam being monitored at 670 nm while the other was scanned over the required wavelengths. In all cases a stabilized beam was obtained from a 450-W xenon lamp, analyzed by Bausch and Lomb high-intensity grating monochromators (with appropriate secondary filtration) and detected by a photomultiplier (RCA 1P 28 or 7102)/oscilloscope (Tektronix 555) combination. Dosimetry was carried out using the 10⁻² M FeSO₄ (oxygen-saturated, chloride-free) system. With the 2-MeV Van de Graaff accelerator a 10-mA beam current was obtained at a 10-μsec pulse length. The optical arrangement allowed a path length of 6.1 cm, and dosimetry was carried out using the absorption at 500 nm of the (SCN)₂⁻ radical in 10⁻³ M NaSCN, assuming ε(SCN)₂⁻ = 7.1 × 10³ and g(OH) = 2.5.

Results

(1) *Transient Absorption Spectra and Kinetics in Neutral Solution.* In NaNO₃ solutions more concentrated than 0.5 M a transient is observed, absorbing

(1) This work was supported by U.S.A.E.C. and constitutes Report No. RC-2014-6.

(2) M. Daniels and E. E. Wigg, *J. Phys. Chem.*, **71**, 1024 (1967).

(3) M. Daniels and E. E. Wigg, *ibid.*, **73**, 3703 (1969).

(4) M. Daniels, *ibid.*, **70**, 3022 (1966).

(5) R. K. Broskiewicz, *Int. J. Appl. Radiat. Isotopes*, **18**, 25 (1967).

(6) A. K. Pikaev, P. Ya. Glazunov, and A. A. Yakubovich, *Kinet. Katal.*, **4**, 835 (1963); *Kinet. Catal. (USSR)*, **4**, 735 (1963).

(7) (a) E. J. Hart, S. Gordon, and J. K. Thomas, *J. Phys. Chem.*, **68**, 1271 (1964); (b) J. Rabani, W. A. Mulac, and M. S. Matheson, *ibid.*, **69**, 53 (1965).

Table I: Rate Constants for Decay of NO_3 in Neutral Solution

	$[\text{NaNO}_3]$	Pulse, $\mu\text{sec}/160 \text{ mA}$	Rate constant, $\text{sec}^{-1} \times 10^{-4}$	Conditions, nm
1	3.0	0.4	2.4	670
2		0.4	1.9	660
3		0.4	2.5	620
4		0.4	1.9	540
5	4.0	0.4	2.2	670
6	6.0	0.4	2.4	540
7	6.0	0.4	1.8	670
8		0.4	2.9	670 2nd pulse
9		0.4	6.1	670 After 5 pulses
10	1.0	1.0	3.4	670
11	2.0	1.0	3.1	670
12		1.0	4.2	670 2nd pulse
13		1.0	3.3	545
14		1.0	3.4	500
15	4.0	1.0	3.0	670
16		1.0	4.6	670 2nd pulse
17	6.0	1.0	3.0	670
18	8.0	1.0	2.8	670

weakly (path lengths commonly used were 32 cm and 48 cm) in the red region. In view of the high nitrate concentration and the large rate constant for the capture of hydrated electrons by nitrate, $k(e^- + \text{NO}_3^-) = 2 \times 10^{10} \text{ M}^{-1} \text{ sec}^{-1}$, this species cannot be the hydrated electron. From the similarity of its absorption spectrum⁴ to the species produced by flash photolysis of ceric nitrate solutions and by the gas-phase reaction of NO_2 with ozone, it has been identified as the NO_3 radical.

Over the wavelength range 680 to 550 nm, the absorption decays to zero by first-order kinetics, followed over 2–3 half-lives, with a rate constant independent of wavelength (Table I). The decay constant is sensibly independent of nitrate concentration, but increases considerably with both pulse duration and pulse repetition. Thus for 0.4- μsec pulses the average decay constant over all wavelengths and nitrate concentrations is $(2.2 \pm 0.3)10^4 \text{ sec}^{-1}$, whereas for 1.0- μsec pulses it increases to $(3.1 \pm 0.3)10^4 \text{ sec}^{-1}$. Similarly, the rate constant following a second pulse is $\sim 30\text{--}50\%$ greater than the first pulse. Accordingly, except where noted, all rate constants reported here are for first pulse on fresh solutions.

Below 550 nm the total absorption does not decay away with a single rate constant but rather a second component is left after the decay of the rapid NO_3 component. The decay of the second component is so slow (see below) that it can be treated as constant during the decay of the NO_3 , and it is then found that the NO_3 decays at the same rate as at other wavelengths. Separating out the slow component in this way gives the absorption spectrum shown in Figure 1 (as a consequence of the high NO_3^- concentration and the long path lengths used, it was not possible in these experiments to go below 400 nm). The decay of the

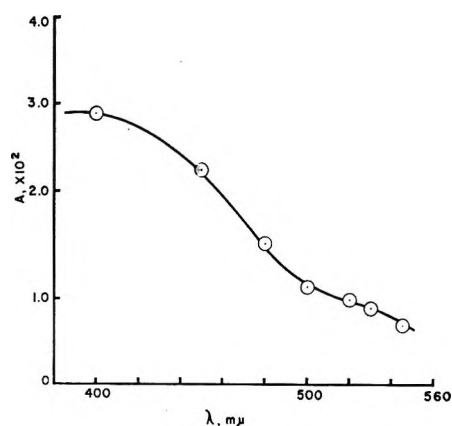


Figure 1. Spectrum of NO_2 from 2.0 M NaNO_3 , 1 $\mu\text{sec}/160 \text{ mA}$, $l = 48 \text{ cm}$.

slow component occurs in the millisecond range and follows clean second-order kinetics over at least 80% of its decay, with $(2k/\epsilon)_{400} = 1.44 \times 10^5$. On the basis of its close similarity with the gas-phase spectrum,⁸ this species is suggested to be NO_2 .

(2) *Effect of NO_3^- Concentration.* In the absence of any direct determination of the extinction coefficient of NO_3 (but see below) the effect of nitrate concentration on NO_3 yield has been expressed as absorbance at 670 nm, $A(\text{NO}_3)/\text{pulse}$, with the results (corrected for varying energy absorption with increasing nitrate concentration) presented previously.⁴ Although this could be due to NO_3 being formed by a reaction of OH with NO_3^- with a low rate constant, other results do not support this supposition.

In the work of Anbar and Thomas on the formation of Cl_2^- from concentrated neutral chloride solutions,⁹

(8) T. C. Hall and F. E. Blacet, *J. Chem. Phys.*, **20** 1765 (1952).

(9) M. Anbar and J. K. Thomas, *J. Phys. Chem.*, **68**, 1363 (1964).

it was found that the Cl_2^- yield was a linear function of the cube root of the chloride concentration and it was suggested that Cl_2^- was produced in "spur regions." The present results show no fit to a cube-root relation. An alternative interpretation is that NO_3^- (and possibly Cl_2^-) is a result of, and characteristic of, the "direct effect" and it was shown in the preliminary report⁴ that this approach leads to an expression to which the results can quantitatively be fitted. The same approach is used successfully in treating the results from low intensity γ radiolysis (part II).³

With the assignment of NO_3^- as a "direct effect" transient, considerable interest attaches to the origin of the NO_2 transient. It is known from low-intensity γ radiolysis² that NO_2 should be an important transient due to reactions of radicals originating in the radiolysis of water but there is little (direct) evidence concerning its role in the "direct effect" radiolysis. At 400 nm both NO_3^- and NO_2 can be observed, and results obtained with 1–6 M NaNO_3 solutions using a 10- μsec pulse of 1.9-MeV electrons are shown in Figure 2a. Qualitatively this again indicates the NO_3^- to be the result of "direct effect," but the NO_2 is different. If NO_2 were produced solely by water radiolysis, then the yield would be expected to decrease with increasing nitrate concentration. The results of Figure 2a indicate such a decrease is compensated by other means, and we suggest that NO_2 is a transient of the "direct effect" radiolysis of NO_3^- . The quantitative evaluation of the yields (corrected to constant (water) dose) in terms of energy fractionation between nitrate and water is shown in Figure 2b. Under the conditions of this experiment $A(\text{NO}_2)_{\text{H}_2\text{O}} \approx 0.58 \times 10^{-2}$, $A(\text{NO}_2)_{\text{NO}_3^-} \approx 0.45 \times 10^{-2}$, and $A(\text{NO}_3)_{\text{NO}_3^-} \approx 2.0 \times 10^{-2}$.

(3) *Effect of Intensity.* During the initial search for the NO_3^- species, the beam current was increased stepwise at constant pulse duration (0.4 μsec) for a given (3.0 M) nitrate concentration. The amount of transient formed was noticed to be a nonlinear function of beam intensity (Figure 3a) and examination of the data shows the dependence to be second-power (Figure 3b).

(4) *Effect of pH.* At pH 11, the decay of the transient at 670 nm is initially very rapid, and is succeeded by a slower component. As in the case of the two components in neutral solution, the decays can be separated, the rapid one being first order, $k = 5.3 \times 10^6 \text{ sec}^{-1}$ and the slower, second order, $(2k/\epsilon)_{670} = 4.8 \times 10^7$. At pH 13, no transients are seen at this wavelength, and at pH 8.8 only a rapid first-order decay to zero is found.

The slowly decaying absorption at pH 11 might be the tail of either the ozonide ion O_3^- or the carbonate radical CO_3^- . To distinguish these, the absorption spectrum was determined, 20 μsec after the pulse, in air-equilibrated and oxygen-saturated solutions.

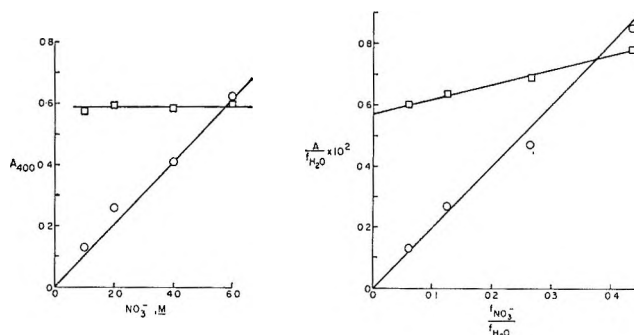


Figure 2. (a) Yield of NO_2 and NO_3 at 400 nm from NaNO_3 ; 10- μsec , 10-mA pulse of 1.9-MeV electrons, $l = 6$ cm. (b) Yields as function of $f_{\text{H}_2\text{O}}$ and $f_{\text{NO}_3^-}$: \circ , NO_2 ; \square , NO_3 .

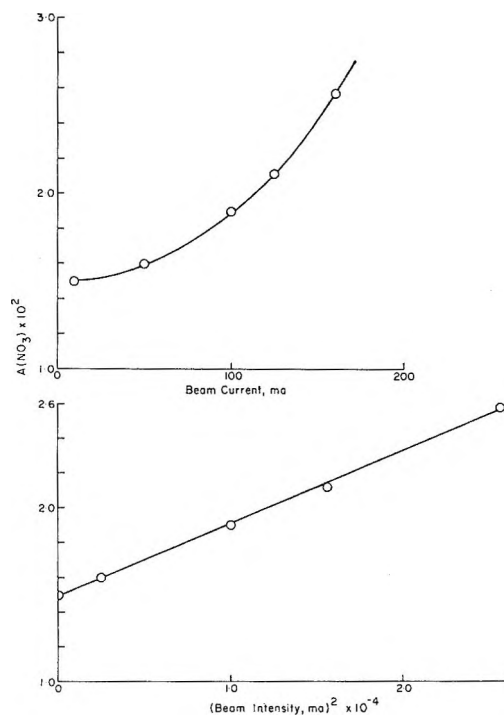


Figure 3. Intensity dependence of $A(\text{NO}_3)_{670}$ from 3.0 M NaNO_3 ; 0.4- μsec pulse.

The amount of transient is dependent on the concentration of oxygen and with $\lambda_{\text{max}} = 425$ nm closely resembles the spectra reported¹⁰ for O_3^- produced by pulse radiolysis of aqueous solution and by flash photolysis of persulfate, whereas the CO_3^- radical has λ_{max} at 600 nm. There is considerable unresolved complexity in the decay of O_3^- in alkaline solution,¹⁰ and it is sufficient to note that, estimating $\epsilon(\text{O}_3^-)_{670}$ as $\sim 10^2$ (from Czapski and Dorfman^{9a}) we then find $2k \approx 5 \times 10^7 \text{ M}^{-1} \text{ sec}^{-1}$.

It is to be noted that the yield of NO_3^- /pulse is the same at pH 11 as in neutral solution and is independent of the formation of O_3^- , indicating that reactions of O^- (hence OH^-) are not responsible for NO_3^- formation.

(10) (a) G. Czapski and L. M. Dorfman, *J. Phys. Chem.*, **68**, 1164 (1964); (b) E. Hayon and J. J. McGarvey, *ibid.*, **71**, 1472 (1967).

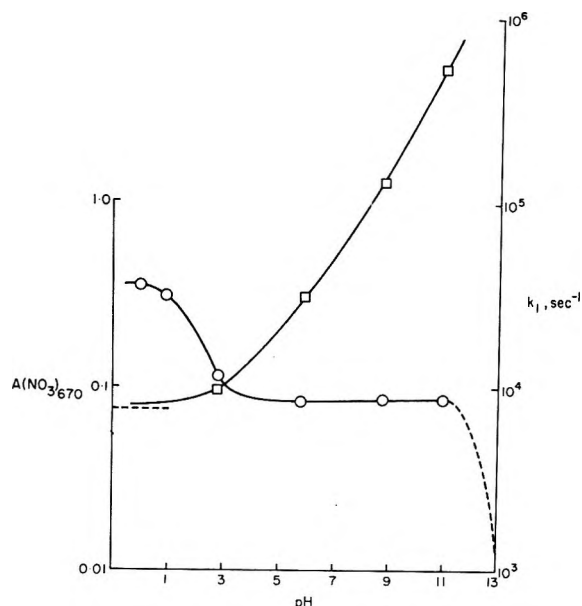


Figure 4. \circ , Yield of NO_3 , $A(\text{NO}_3)_{670}$ /pulse for 4.0 M NaNO_3 as function of pH; \square , first-order decay constant k_1 as function of pH for 4 M NaNO_3 ; $1\ \mu\text{sec}/160\ \text{mA}$, $l = 48\ \text{cm}$.

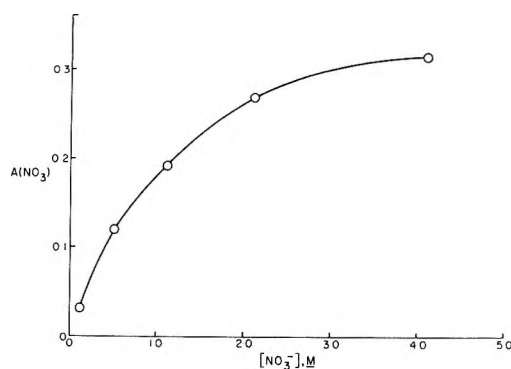


Figure 5. Formation of NO_3 in 0.12 M H^+ , as function of nitrate concentration; $1\text{-}\mu\text{sec}/100\ \text{mA}$ pulse, $l = 48\ \text{cm}$.

During experiments in which the NO_3 was detected in pulse-radiolyzed solutions of nitric acid⁴ it was noted that for a given pulse, much more NO_3 transient was formed in the acid than in neutral solution. At the same time Broskiewicz⁵ could detect NO_3 in nitric acid solution but not in neutral solution. These observations suggested that acidity might play an important role in the radiolysis of nitrate, and this has been investigated for solutions 4.0 M in NO_3^- and of varying acidity (pH 2.8, 0.12 M H^+ , and 1.0 M HNO_3).

The yield of NO_3 /pulse increases considerably in dilute acid solutions between pH 3 and pH 1 and reaches a value at $\sim 1\text{ M H}^+$ which is approximately a fourfold increase on neutral solution (Figure 4).

At constant acidity (0.12 M H^+), the yield of NO_3 increases nonlinearly with nitrate concentration (Figure 5) and appears to be reaching a limit. These results do not fit an energy fractionation function as

do those for neutral solution, but rather fit a scavenging type function

$$A = A_\infty \left[\frac{k_1[\text{NO}_3^-]}{k_1[\text{NO}_3^-] + k_2} \right]$$

as shown in Figure 6, with $k_2/k_1 = 1.25$.

The decay kinetics of NO_3 have been determined under the above sets of conditions. For 4.0 M NO_3^- at pH 2.8 the decay is mixed first and second order. On increasing the acidity, the decay becomes cleanly second order to over 80% reaction. For solutions of constant acidity (0.12 M H^+) the decay is first order (over 3 half-lives) at low nitrate concentration, is mixed first and second order in 1.12 M NO_3^- and 2.12 M NO_3^- , and is pure second order in 4.12 M NO_3^- (Table II).

A somewhat similar trend is found for nitric acid solutions; at the lowest concentration (0.12 M) decay is first order, becoming mixed first and second order for 0.6 and 1.2 M , predominantly second order for 3.0 M , and pure second order for 4.5 and 6.0 M (Table II).

(5) *Rise Times*. The formation of NO_3 does not entirely occur during the pulse; following a $0.4\text{-}\mu\text{sec}$ pulse buildup of NO_3 can easily be seen in mildly acid solutions. In all cases first-order kinetics is observed, and results for a variety of conditions are gathered in Table III. At constant acidity (0.12 M H^+) the rate constant varies with nitrate concentration as shown in Figure 7. Broskiewicz⁵ reports values for 0.1 M HNO_3 ($1.5 \times 10^5\ \text{sec}^{-1}$) and 0.4 M HNO_3 ($4.2 \times 10^5\ \text{sec}^{-1}$) in good agreement with those found here, but at 1.0 M HNO_3 ($4.2 \times 10^5\ \text{sec}^{-1}$) there is a discrepancy.

There are indications that NO_3 also builds up after the pulse in neutral solution, more rapidly than in acid (rise time $< 1\ \mu\text{sec}$). Due to the small yields and poor signal to noise ratio this behavior could not be thoroughly studied, but rise times appeared to be the same in 2 and 6 M NO_3^- .

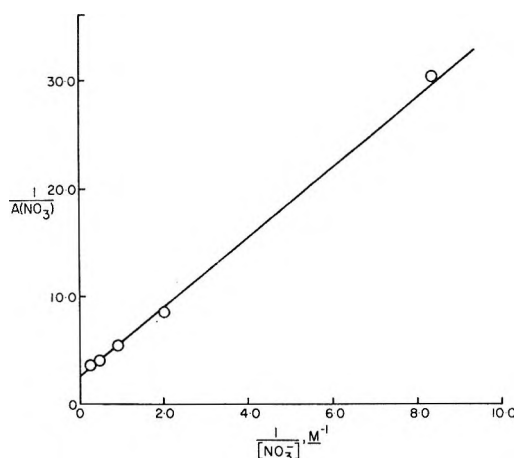


Figure 6. Competition relation.

Table II: Decay Kinetics of NO_3 in Nitric Acid and in Acid Solutions of Sodium Nitrate

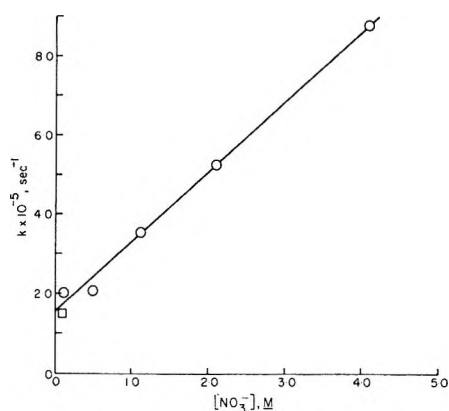
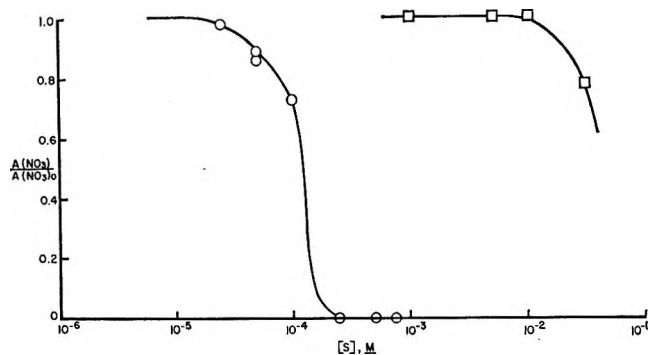
Constitution of solution		k_1, sec^{-1}	$2k_2/\epsilon$	Pulse, $\mu\text{sec}/\text{mA}$
NaNO_3, M	HNO_3, M			
4.0	10^{-3} (pH 2.8)	9.7×10^3	12×10^6	1/160
4.0	0.12		3.3×10^6	1/160
4.0	1.0		2.4×10^6	1/160
2.00	0.12	2.47×10^3	1.78×10^6	1/160
1.00	0.12	3.5×10^3	1.16×10^6	1/160
0.38	0.12	2.5×10^3		1/160
	0.1	3.45×10^3		1/50
	0.12	6.0×10^3		1/160
	0.60	1.13×10^3	1.27×10^6	1/50 ^a
		0.9×10^3	2.6×10^6	0.3/100
	1.20	1.75×10^3	2.23×10^6	1/50
	3.0		2.64×10^6	1/50
	4.5		2.92×10^6	1/50
	6.0	1.1×10^3	1.27×10^6	1/50
			3.3×10^6	1/
			4.1×10^6	1/160
	9.0	1.6×10^3	1.6×10^6	1/50

^a 630 nm.**Table III:** Rate Constants for Formation of NO_3 in Acid Nitrate and Nitric Acid Solutions

$[\text{H}^+]$	$[\text{NO}_3^-]$	$k \times 10^{-4}, \text{sec}^{-1}$
0.12	0.50	2.07
0.12	1.12	3.56
0.12	2.12	5.25
0.12	4.12	8.8
0.12	0.12	2.0
0.6	0.6	5.4
1.2	1.2	12.2

(6) *Scavenging Studies.* In view of the inference from intensity dependence and rise time kinetics that NO_3 is not an immediate product of energy dissipation but originates from reactive precursors, scavenging studies have been carried out to obtain information on the nature and reactivity of such precursors.

The effect of repeated pulsing on NO_3 yield and decay characteristics suggested the use of nitrite ion. NO_3 is found to react rapidly with NO_2^- in neutral solution. First-order rate constants are linear in nitrite concentration and lead to $k(\text{NO}_3 + \text{NO}_2^-) = 1.2 \times 10^9 M^{-1} \text{sec}^{-1}$. Methanol is much less reactive, $k(\text{NO}_3 + \text{MeOH}) = 1.6 \times 10^6 M^{-1} \text{sec}^{-1}$. The effect of these scavengers is also to decrease the initial yield of NO_3 (Figure 8). Although the rate constant for NO_2^- reacting with NO_3 is high, it does not seem that this can quite account for the scavenging effect on the yield, e.g., at $100 \mu M \text{NO}_2^-$, the half-life for NO_3 reacting with NO_2^- is $6 \mu\text{sec}$; during a $1\text{-}\mu\text{sec}$ pulse this cannot account for the 25% loss in absorbance. Similarly, for $250 \mu M \text{NO}_2^-$, $t_{1/2} \sim 2.3 \mu\text{sec}$, and absorbance should be detectable on a $1\text{-}\mu\text{sec}/\text{cm}$ sweep following a $1\text{-}\mu\text{sec}$ pulse, but none is seen. It is con-

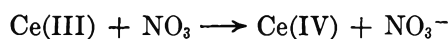
Figure 7. Rate of formation of NO_3 at $0.12 M \text{H}^+$. \square , Broskiewicz data.Figure 8. Maximum yield of NO_3 at 670 nm as a function of $[S]$, $4.0 M \text{NaNO}_3$, $1 \mu\text{sec}/160 \text{mA}$ pulse, $l = 48 \text{cm}$: \circ , NO_2^- ; \square , methanol.

cluded that nitrite scavenges the precursors of NO_3 as well as reacting with it. Similar considerations apply to methanol. From Figure 8 the relative rate

constants for nitrite and methanol reacting with the NO₃ precursor, X, can be estimated as $k(\text{NO}_2^- + \text{X})/k(\text{MeOH} + \text{X}) \sim 400$. This clearly eliminates the possibility that X might be the OH radical for which $k(\text{OH} + \text{NO}_2^-)/k(\text{OH} + \text{MeOH}) \sim 4$. Double-beam experiments carried out using SCN⁻ as scavenger strengthen this conclusion. For 6.0 M NaNO₃ it is found that the yield of NO₃ and its decay rate are unaffected by the presence of 10⁻²M NaSCN. The yield of transient derived from thiocyanate, the (SCN)₂⁻ radical, decreases with nitrate concentration, and at constant nitrate concentration (6.0 M) the yield of (SCN)₂⁻ is constant from 10⁻⁴ M SCN⁻ to 10⁻² M SCN⁻.

Discussion

(1) *Spectra and Extinction Coefficients of NO₃ and NO₂*. Despite a number of reports concerning NO₃ both in the gas phase and in solution,¹¹ no extinction coefficients are available. However, from the published results and mechanism of Martin, *et al.*,^{11c} a value for $\epsilon(\text{NO}_3)_{635\text{nm}}$ may be deduced as follows: the NO₃ produced by flash photolysis of Ce(IV) in 6 M HNO₃ decays by a pseudo-first-order reaction with excess Ce(III)

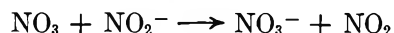


for which $k(\text{NO}_3 + \text{Ce(III)}) = 1.7 \times 10^6 \text{ M}^{-1} \text{ sec}^{-1}$. In the absence of excess Ce(III), the decay (presumably still by the above mechanism) becomes second order, with $(k/\epsilon)_{635} = 1.7 \times 10^4 \text{ cm sec}^{-1}$. This leads to $\epsilon(\text{NO}_3)_{635} \simeq 100$. More recent work (T. W. Martin, personal communication) indicates $\epsilon(\text{NO}_3)_{635} = 220 \text{ M}^{-1} \text{ cm}^{-1}$, and for reasons of internal conformity a value of 300 is used here. The true value must obviously be regarded as somewhat uncertain until the qualitative discrepancy between the published results^{10c,10d} is clearly resolved and the equilibrium of the species NO₃/HNO₃⁺ is clearly defined.

Comparisons of NO₃ spectra under different conditions show reasonable agreement between various workers (Table IV) and it may be concluded that the structure of NO₃ is the same in all conditions or that the absorption spectrum of [HNO₃]⁺ closely resembles that of NO₃.

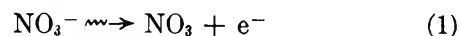
The situation concerning the extinction coefficient of NO₂ is equally unsatisfactory. A gas-phase extinc-

tion coefficient may be estimated⁸ as $\epsilon(\text{NO}_2)_{400} \sim 100 \text{ M}^{-1} \text{ cm}^{-1}$. Ottolenghi and Rabani, who attempted to generate NO₂ *in situ* by flash photolysis of ferrocyanide and scavenging the hydrated electron with NO₃⁻, obtained¹² $\epsilon(\text{NO}_2)_{400} = 130 \pm 70$, relative to $\epsilon = 1000$ for ferricyanide. However, a spectrum attributable to NO₂ was barely discernable. Recent pulse radiolysis work by J. Rabani, S.O. Nielson, P. Pagsberg, and H. Christenson (J. Rabani, personal communication) uses $\epsilon(\text{NO}_2)_{400} = 208$, also relative to ferricyanide. This latter value is selected here. In the present work we find that NO₃ reacts rapidly with NO₂⁻ to produce an increase in the slowly decaying absorption at 400 nm, which is attributed to NO₂. The reaction occurring is most probably

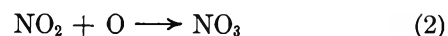


Comparative measurements in the presence and absence of NO₂⁻ allow the ratio of the extinction coefficients of NO₃ and NO₂ to be estimated and we find $\epsilon(\text{NO}_3)_{400}/\epsilon(\text{NO}_2)_{400} = 0.5$. This ratio is compatible with $\epsilon(\text{NO}_3)_{675} \simeq 300$ and $\epsilon(\text{NO}_2)_{400} \simeq 208$ and the observed spectrum of NO₃.^{4,11d}

(2) *Mechanism of NO₃ Formation in Neutral Solution; Radiation Yields*. Examination of the results shows that NO₃ formation is most simply accounted for in terms of a "direct effect," *i.e.*, as a result of energy absorption in the nitrate ion, and not as a result of energy absorption in water. However, NO₃ is not entirely formed by an immediate process such as



because it has scavengeable precursors, and the extent of its formation depends on intensity. Accordingly it is suggested that NO₃ is formed by



a reaction for which the rate constant has been determined in the gas phase¹³ as $k(\text{O} + \text{NO}_2) = 9.6 \times 10^9 \text{ M}^{-1} \text{ sec}^{-1}$. This proposal immediately raises the question of the origin of the precursors, NO₂ and O. Scavenging evidence has been presented previously (part II of this series) for NO₂ being an intermediate characteristic of the "direct effect" and this is further reinforced in the present pulse work. Together with the conclusion that OH (O⁻) is not produced by the "direct effect" (for example by a reaction such as $\text{NO}_3^- \rightarrow \text{NO}_2 + \text{O}^-$), this leads us to describe the overall primary process in the direct radiolysis by the equation

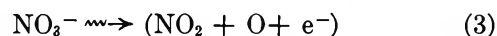


Table IV: Comparison of NO₃ Spectra

$\epsilon(670)/\epsilon(635)$	Conditions	Reference
0.83	6 M HNO ₃ ; photolysis	Martin ^{11c}
0.79	6 M HNO ₃ ; pulse radiolysis	Daniels ⁴
0.86	1 M HNO ₃ ; pulse radiolysis	Broskiewicz ⁵
0.85	pH 0.65; flash photolysis	Hayon ^{11d}
0.82	4 M NaNO ₃ ; pulse radiolysis	Daniels ⁴

(11) (a) G. Schott and N. Davidson, *J. Amer. Chem. Soc.*, **80**, 1841 (1958); (b) D. A. Ramsey, *Proc. Colloq. Spectrosc., Intern. 10th Univ. Maryland 1962*, 583 (1963); (c) T. W. Martin A. Henshall, and R. C. Gross, *J. Amer. Chem. Soc.*, **85**, 113 (1963); **86**, 2595 (1964); (d) L. Dogliotti and E. Hayon, *J. Phys. Chem.*, **71**, 2511 (1967).

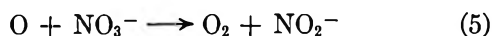
(12) M. Ottolenghi and J. Rabani, *ibid.*, **72**, 593 (1968).

(13) F. S. Klein and J. T. Herron, *J. Chem. Phys.*, **41**, 1285 (1964).

Subsequent events will be determined by competition of various processes. The concurrently produced electron is very likely converted into NO_3^{2-} at such high nitrate concentrations as are involved here. If rapid protonation reaction converts NO_3^{2-} to NO_2



then NO_3 formed within the molecular cage by recombination may be manifest, as the reaction of NO_3 with NO_2 is known to be slow, $k = 2.5 \times 10^5 \text{ M}^{-1} \text{ sec}^{-1}$.^{11a} If either O or NO_2 should escape the "cage" then the subsequent formation of NO_3 will be in competition with the reaction of O atom with NO_3^-



and this competition will be intensity dependent. Indeed reaction 5 is considered³ to be the major fate of O atoms under low-intensity γ radiolysis, and at high intensity NO_3 formation is found (see Results) to be proportional to I^2 . The yields of the transients under various conditions are of interest. With the lower intensity ($1 \times 10^{25} \text{ eV l.}^{-1} \text{ sec}^{-1}$), 10- μsec pulse of the B.N.L. accelerator and using the method of data treatment outlined in Results, we obtain $G(\text{NO}_2)_{\text{H}_2\text{O}} \cdot \epsilon(\text{NO}_2)_{400} = 6.0 \times 10^2$. Choosing $\epsilon(\text{NO}_2)_{400} = 208$ (Rabani) gives $G(\text{NO}_2)_{\text{H}_2\text{O}} = 2.9 \sim g(e^-)_{\text{aq}}$. This is the value to be anticipated from Pikaev's work on product yield at high intensities⁶ and γ -radiolysis work on dilute solutions (part I).² The corresponding value for the direct radiolysis, expressed as $G(\text{NO}_2)_{\text{NO}_3^-}$ is 2.25. The yield of NO_3 , under these conditions, is much different. Identifying the rapidly decaying absorbance at 400 nm as to NO_3 , and using $\epsilon(\text{NO}_3)_{400} = 104$, then $G(\text{NO}_3)_{\text{NO}_3^-} = 20$. A significantly different result is obtained using the shorter, more intense pulses of the A.N.L. accelerator; $G(\text{NO}_3)_{\text{NO}_3^-} = 8.3$ for 1- μsec pulses at the highest intensity ($1.65 \times 10^{26} \text{ eV l.}^{-1} \text{ sec}^{-1}$), using $\epsilon(\text{NO}_3)_{670} \approx 300$ based on $\epsilon(\text{NO}_3)_{400}$ and spectra of NO_3 .^{4,11d} It seems that prolonging the pulse leads to conditions favoring NO_3 formation. This is not unreasonable on the mechanism presented here.

In view of the dependence of G values on parameters such as "intensity" and pulse length, the data available for the pulse intensity dependence at the shortest pulse length (0.4 μsec) becomes significant. The results of Figure 3, extrapolated to zero intensity, give $G(\text{NO}_3)_{\text{NO}_3^-} = 4.8$, which must be interpreted as the sum of (a) direct ionization by reaction 1, (b) intracage recombination, and (c) geminate recombination. As $G(\text{NO}_3)_{\text{NO}_3^-}$ can increase with intensity to ~ 8 , without saturating, it may be concluded that at least half the originally formed O atoms escape cage and geminate recombination.

A simplified treatment of the intensity-dependent yield of NO_3 , assuming $k_5[\text{NO}_3^-] > k_2g(\text{NO}_2)It$, gives

$$[\text{NO}_3] \simeq \frac{k_2 g(\text{O})g(\text{NO}_2)t^2I^2}{k_5 [\text{NO}_3^-]}$$

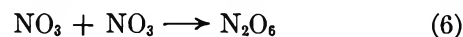
where $g(\text{O})$ and $g(\text{NO}_2)$ signify the yields of species escaping geminate recombination. The slope of Figure 3 then gives

$$\frac{k_2}{k_5}g(\text{O})g(\text{NO}_2) = 1.8 \times 10^4$$

and if $g(\text{NO}_2) \sim g(\text{O}) \sim 4$ (magnitude of intensity-dependent increase), k_5 may be roughly estimated as $5 \times 10^6 \text{ M}^{-1} \text{ sec}^{-1}$, based on $k_2 = 5 \times 10^9 \text{ M}^{-1} \text{ sec}^{-1}$. These numbers, consistent with the initial assumption, seem to validate the general model, although they can be no more than an indication of order of magnitude. It is to be noted that $k(\text{O} + \text{NO}_3^-) \sim 5 \times 10^6$ is not inconsistent with the previously derived ratio¹⁴ $k(\text{O} + \text{NO}_2^-)/k(\text{O} + \text{NO}_3^-) \sim 10^4$ and suggests that the reaction $\text{O} + \text{NO}_2^- \rightarrow \text{NO}_3^-$ may be diffusion-controlled.

(3) *Decay Kinetics of NO_3 and NO_2* . First-order decay of NO_3 is observed over a wide pH range. In acid solution the rate constant appears to be approaching that observed by Broskiewicz, which he found to be independent of HNO_3 concentration. However, the consistency of these results may be more apparent than real in view of the variation of k with dose (Table I) and with concentration of NO_3^- and H^+ (Table II). The dependence on dose suggests that NO_3 may be reacting with other radiolysis products, as well as undergoing pseudo-first-order reaction with solvent. The needed extension of these experiments to low doses will be difficult in view of the low extinction coefficient of NO_3 .

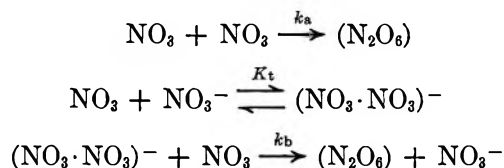
Under otherwise constant conditions, as the acidity is increased the rate constant of first-order decay decreases and second-order kinetics appear. At constant NO_3^- concentration, the second-order constant decreases with acidity (Table II, no. 1, 2, and 3), and at constant acidity it increases with nitrate concentration (Table II, no. 5, 4, and 2). However, at sufficiently high concentrations of both H^+ and NO_3^- (HNO_3 solutions) the rate of decay is reasonably constant at $(2k/\epsilon)_{670} = 2.8 \pm 0.5 \times 10^6$, giving with the previously chosen extinction coefficient, $k = 4.2 \times 10^8 \text{ M}^{-1} \text{ sec}^{-1}$. A recent report¹⁵ on the decay of NO_3 produced by the flash photolysis of Ce(IV) in HNO_3 quotes $k = 8 \times 10^8 \text{ M}^{-1} \text{ sec}^{-1}$ based on $\epsilon(\text{NO}_3)_{635} = 220$, but it is not clear how this is obtained and a consideration of the discrepancy must await full publication. The general reaction is probably



(14) M. Daniels, R. V. Meyers, and E. V. Belardo, *J. Phys. Chem.*, **72**, 389 (1968).

(15) R. W. Glass and T. W. Martin, Abstracts, 156th National Meeting of the American Chemical Society, Sept 1968, Phys-049.

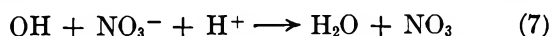
and the effect of NO₃⁻ and H⁺ on the rate can easily be rationalized in terms of complexes such as (NO₃·NO₃)⁻ and (HNO₃)⁺. Thus the present data (for solutions of constant acidity = 0.12 M H⁺) fit the following mechanism



and we evaluate $k_a = 6.8 \times 10^7 \text{ M}^{-1} \text{ sec}^{-1}$ and $k_b K_t (\text{NO}_3^-) = 1.1 \times 10^8$. However, the dependence on [H⁺], for 4 M NO₃, indicates that at [H⁺] $\gtrsim 0.1 \text{ M}$, the NO₃ may be largely protonated and be reacting (more slowly) as [HNO₃]⁺. Now that the general demarcations of behavior have been established, a more detailed kinetic study would appear to be called for.

For the NO₂ species the second-order decay constant can be estimated as $1.5 \times 10^7 \text{ M}^{-1} \text{ sec}^{-1}$ (using $\epsilon(\text{NO}_2)_{400} \sim 208$), and is to be compared with $3.8 \times 10^7 \text{ M}^{-1} \text{ sec}^{-1}$ recently deduced by Ottolenghi and Rabani.¹² The difference (a factor of 4 in k/ϵ) is not due to uncertainties in $\epsilon(\text{NO}_2)$ but comes directly from experimental observations; in the present work the decay occurs over ~ 30 msec, while that observed by Ottolenghi and Rabani is complete in ~ 2.5 msec. Subsequent pulse radiolysis work (J. Rabani, personal communication) indicates the decay of NO₂ may not follow simple second-order kinetics, and impurity effects may be important in dilute solution. On the other hand, in the present work the high nitrate concentration may be affecting the reaction rate, perhaps by complexing, similarly to the NO₃ above. Further work is needed before the simple second-order decay observed here may be simply interpreted.

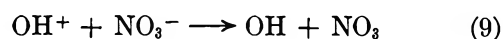
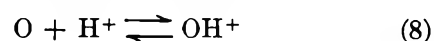
(4) *Acid Solutions.* Although in neutral nitrate NO₃ can only be detected in concentrated solutions, when H⁺ is present it can be detected in solutions commonly considered dilute. In the present work, NO₃ is very weak but detectable in $6 \times 10^{-2} \text{ M HNO}_3$, and is quite clear in 10^{-1} M HNO_3 . These results, which are in agreement with Broskiewicz,⁵ are a strong indication that NO₃ can be formed by an indirect effect, *i.e.*, a water-radical reaction which is most likely



At appropriate concentrations of NO₃⁻ and H⁺ the rate of formation of NO₃ has been measured. At constant H⁺, the rate constant is first order with respect to NO₃⁻ (Figure 7). The order with respect to H⁺ is not completely established by the present data, but results for 0.5 and 0.6 M NO₃⁻ are concordant

with Broskiewicz for 0.4 M and indicate first-order dependence on [H⁺].

The dependence of the yield of NO₃ on [H⁺] for 4 M NO₃⁻ shows it reaches a limit and is constant to 4.0 M H⁺. The same limit is reached when [NO₃⁻] is varied at constant [H⁺]. Examination of the maximum yield in acid solutions in terms of the above mechanism shows it to be inadequate, for at constant nitrate concentration the ratio of the yield in acid to that in neutral would be $1 + g(\text{OH})_{\text{H}_2\text{O}/\text{H}_2\text{O}}/G(\text{NO}_3)_{\text{NO}_3^-} f_{\text{NO}_3^-}$. With $g(\text{OH}) = 2.5$ and $G(\text{NO}_3)_{\text{NO}_3^-} = 8.3$, this ratio equals 2.4, to be compared with an experimental value ~ 4 . The experimental ratio may be closely approached if the mechanism of NO₃ formation, as a result of nitrate radiolysis, is dependent on acidity, and the following reactions are suggested



The ratio of the acid yield to the neutral then becomes

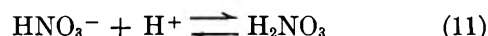
$$\begin{aligned} \frac{2G(\text{NO}_3)_{\text{NO}_3^-} f_{\text{NO}_3^-} + g(\text{OH})_{\text{H}_2\text{O}/\text{H}_2\text{O}}}{G(\text{NO}_3)_{\text{NO}_3^-} f_{\text{NO}_3^-}} = \\ 2 + \frac{g(\text{OH})_{\text{H}_2\text{O}/\text{H}_2\text{O}}}{G(\text{NO}_3)_{\text{NO}_3^-} f_{\text{NO}_3^-}} \simeq 3.4 \end{aligned}$$

Further support for such a mechanism comes from considerations of intensity dependence. If the mechanism suggested by reactions 8 and 9 predominates over (2) then the yield of NO₃ should be linear in intensity. No intensity dependence was observed for 4 M HNO₃ when the beam current was varied by a factor of 3 (0.4- μ sec pulses).

One other feature of acid solutions must be noted, namely, there is no evidence in the spectra or decay kinetics for the presence of NO₂. Similarly, Broskiewicz found an absorption minimum at 400 nm in 1.0 M HNO₃. A tentative explanation might be that species HNO₃⁻ (formed either by protonation of the electron product NO₃²⁻, or by H atom capture by NO₃⁻) which would normally give rise to NO₂ by the reaction



may be protonated and stabilized in strongly acid media



Acknowledgments. Thanks are due to Dr. E. J. Hart of A. N. L., and Dr. A. O. Allen of B. N. L. for facilitating the arrangements which made this work possible. Arne Straube, of the Royal Technical Institute, Stockholm, gave much appreciated assistance during midnight hours at A. N. L.

The Rates of Methanolysis of Several Organosilazanes

by William L. Budde

Midwest Research Institute, Kansas City, Missouri (Received February 13, 1969)

The kinetics of the methanolysis of three silazanes: hexamethyldisilazane, tris(trimethylsilyl)amine, and *N,N'*-bis(trimethylsilyl)tetramethylcyclodisilazane were studied to determine whether the differences in their reactivities could be correlated easily with differences in $p\pi-d\pi$ bonding. Although some effects of $p\pi-d\pi$ bonding were observed, this factor is not a dominant one in controlling the solvolysis reactivities of these compounds.

A large number of compounds with silicon to nitrogen bonds have been synthesized and their properties studied in the last ten years.¹ The interest in these compounds developed naturally from the extensive research on and commercial exploitation of the family of compounds having silicon to oxygen bonds. Early observations of compounds with silicon to nitrogen bonds suggested the generalization that Si-N bonds are very susceptible to solvolysis in hydroxylic solvents.² Only a few compounds were investigated which apparently were resistant to solvolysis in two-phase mixtures or homogeneous solutions. However, no quantitative measurements were made which permit comparisons of the reactivity of a series of these compounds under similar conditions. With the accumulation of physical evidence that silicon to nitrogen sigma bonds in some compounds are fortified by a $p\pi-d\pi$ interaction,³ some adopted the attitude that $p\pi-d\pi$ bonding was the source of the apparent hydrolytic stability of some compounds.⁶ Without denying the $p\pi-d\pi$ interaction and its probable influence over some properties of these molecules, it is questioned whether $p\pi-d\pi$ bonding is the dominant factor affecting the hydrolytic stability of silicon to nitrogen bonds. Indeed Breed and Elliott⁷ pointed out that the per cent of ammonia or amine which is evolved in a given time from a cyclodisilazane or bis(alkylamino)diorganosilane in aqueous methanol-toluene solution may be controlled by steric factors.

This research was undertaken to obtain some quantitative data about the differences in solvolytic stability within a series of compounds having silicon to nitrogen bonds and to determine whether these differences can be readily traced to differences in $p\pi-d\pi$ bonding. This paper presents the first set of data which has been obtained in pursuit of these goals.

Experimental Section

Materials. Commercial hexamethyldisilazane was distilled before use, bp 123–124°, $n_D^{20} = 1.4089$ (reported⁸ $n_D^{20} = 1.4078$). Tris(trimethylsilyl)amine was prepared by a published method,⁹ bp 85–86° (14 mm).

The synthesis of *N,N'*-bis(trimethylsilyl)tetramethylcyclodisilazane was published previously.¹⁰

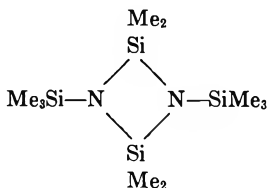
Methanol, carbon tetrachloride and cyclohexane were reagent grade commercial materials which were used without further treatment.

Methoxytrimethylsilane and dimethoxydimethylsilane were synthesized by the method of Langer, Connell, and Wender.¹¹ The former was purified by distillation bp 55–56°, $n_D^{20} = 1.3680$ (reported¹¹ $n_D^{20} = 1.3675$); the latter distilled at 81–82°, $n_D^{20} = 1.3707$ (reported¹² bp 81–82°).

Reaction Kinetics. Approximately 0.5 ml of a 0.2 *M* solution of the substrate in 50 volume per cent methanol, 46 volume per cent carbon tetrachloride, and 4 volume per cent cyclohexane was placed in a standard 5 mm o.d. nmr tube. The sample tubes which were used in the reactions run at 30° or lower were sealed with a simple plastic cap and quickly placed into the variable temperature probe of a Varian Associates HA-100 nmr spectrometer. The temperature of the probe had been adjusted to the desired operating temperature

- (1) For a fairly recent review, see U. Wannagat in "Advances in Inorganic Chemistry and Radiochemistry," Vol. 6, H. J. Emeleus and A. G. Sharpe, Ed., Academic Press, New York, N. Y., 1964, p 225.
- (2) C. Eaborn, "Organosilicon Compounds," Butterworth and Co. Ltd., London, 1960, p 345.
- (3) The original basis of this concept is the electron diffraction study of the structure of trisilylamine, $(H_3Si)_3N$, by Hedberg.⁴ The molecule was found to be planar (average $\langle SiNSi \rangle$ of $119.6 \pm 0.5^\circ$) with a silicon-nitrogen distance of $1.738 \pm 0.02 \text{ \AA}$ compared to the 1.80–1.87 \AA distance expected from atomic radii. In an authoritative paper Craig, Maccoll, Nyholm, Orgel, and Sutton⁵ pointed out this evidence and the possibility of extensive π bonding in trisilylamine.
- (4) K. Hedberg, *J. Amer. Chem. Soc.*, **77**, 6491 (1955).
- (5) D. P. Craig, A. Maccoll, R. S. Nyholm, L. E. Orgel, and L. E. Sutton, *J. Chem. Soc.*, 332 (1954).
- (6) See reference 1, p 232 or J. F. Klebe, H. Finkbeine, and D. M. White, *J. Amer. Chem. Soc.*, **88**, 3390 (1966).
- (7) L. W. Breed and R. L. Elliott, *Inorg. Chem.*, **3**, 1622 (1964).
- (8) E. G. Rochow, "Chemistry of the Silicones," 2nd ed, John Wiley and Sons, Inc., New York, N. Y., 1951.
- (9) W. L. Lehn, *J. Amer. Chem. Soc.*, **86**, 305 (1964).
- (10) L. W. Breed, W. L. Budde, and R. L. Elliott, *J. Organometal. Chem.*, **6**, 676 (1966).
- (11) S. H. Langer, S. Connell, and I. Wender, *J. Org. Chem.*, **23**, 50 (1958).
- (12) D. Seyferth and E. G. Rochow, *J. Org. Chem.*, **20**, 250 (1955).

Table I: Observed First-Order Rate Constants, Enthalpies of Activation, and Entropies of Activation for the Methanolysis of Organosilazanes 1, 2, and 3 in 50% Methanol

Compound	T, °K	$10^6 k_1^a$, sec ⁻¹	ΔH^* , kcal mol ⁻¹	ΔS_{298}^* , e. u.
(Me ₃ Si) ₂ NH	273	870	15 ± 1	-19 ± 3
	288	5,400		
	303	14,000		
(Me ₃ Si) ₃ N	303	0.77	17 ± 1	-30 ± 3
	323	3.7		
	333	10		
	{ 303 323 333 }	24	13 ± 1	-38 ± 3
		70		
		170		

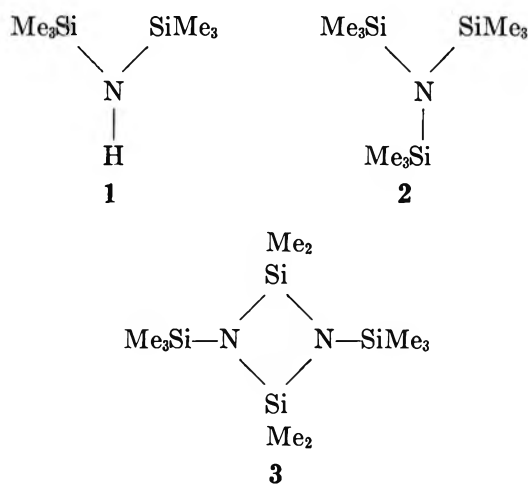
^a The measured rate constants were reproducible to ±7.5%.

prior to preparing the solutions and thermal equilibrium was assumed to be established within a few minutes. The solvents which were used in reactions conducted below 30° were equilibrated at the reaction temperature before the solutions were prepared at the same temperature. The samples which were used in reactions run at elevated temperatures were promptly frozen in liquid nitrogen and the nmr tubes were sealed either under reduced pressure or nitrogen. The sample was either placed in the heated probe and its nmr spectrum monitored periodically or—as in very slow reactions—placed in an external heated bath and periodically withdrawn for observation of its nmr spectrum. The temperature of the sample in the probe was controlled to ±0.3° and the temperature of the external bath was known to ±0.05°.

The nmr signal from either the methyl group or the hydroxyl group of methanol was used to provide a lock signal for the HA-100 internal lock field-frequency control system. The reaction progress was followed by periodically recording all the signals and electronically integrating the intensities from all the reactants and products. The chemical shifts of the reactants and products were measured from the cyclohexane signal. The per cent reaction and the per cent unchanged reactant were calculated from the intensities of the nmr absorption signals. The rate constants were calculated from the least-square slopes of standard first-order rate equation plots.

Results

The observed first-order rate constants for the methanolysis of three compounds, hexamethyldisilazane (1), tris(trimethylsilyl)amine (2), and N,N'-bis(trimethylsilyl)tetramethylcyclodisilazane (3), and the derived enthalpies and entropies of activation are given in Table I.



Discussion

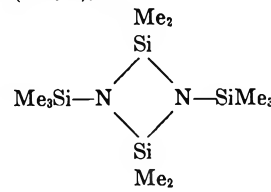
Methanolysis Products. Methoxytrimethylsilane and ammonia are the products of the methanolysis of hexamethyldisilazane (1) and tris(trimethylsilyl)amine (2). The former is undoubtedly an intermediate in the methanolysis of the latter, but 1 is not observed under the conditions of solvolysis of 2 because of its substantially greater reactivity (a factor of 20,000 at 30°). Similarly the unknown and surely extremely reactive compound aminotrimethylsilane (4), Me₃SiNH₂, is a probable but unobserved intermediate in the methanolysis of 1.

The methanolysis of 3 was studied by Breed and Elliott¹³ who isolated bis(methoxydimethylsilyl)tris(trimethylsilyl)amine (5) in 38% yield.

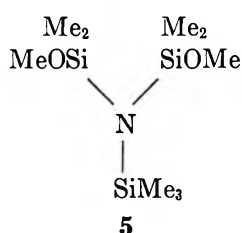
They found that the Si-Me hydrogens of the trimethylsilyl and the methoxydimethylsilyl groups had identical nmr chemical shifts at 60 MHz. At 100 MHz these absorptions are resolved (Table II). In addition to 5

(13) L. W. Breed and R. L. Elliott, *J. Organometal. Chem.*, **11**, 447 (1968).

Table II: Proton Magnetic Resonance Peak Positions of the Si-Me Hydrogens of the Silazanes and their Methanolysis Products^a

Reactant	$\delta_{\text{Si-Me}}$, Hz	Product	$\delta_{\text{Si-Me}}$, Hz
$(\text{Me}_3\text{Si})_2\text{NH}$	138.5	Me_3SiOMe	133.3
$(\text{Me}_3\text{Si})_3\text{N}$	124.6	Me_3SiOMe	133.3
	119.5 (intensity = 2)	Me_3SiOMe	133.5
	142.6 (intensity = 3)	$\text{Me}_2\text{Si}(\text{OMe})_2$	134.3
		$\text{Me}_3\text{SiN}(\text{SiMe}_2\text{OMe})_2$	125.0 (intensity = 4) 126.0 (intensity = 3)

^a Chemical shifts were measured from internal cyclohexane and are precise to at least ± 0.2 Hz.



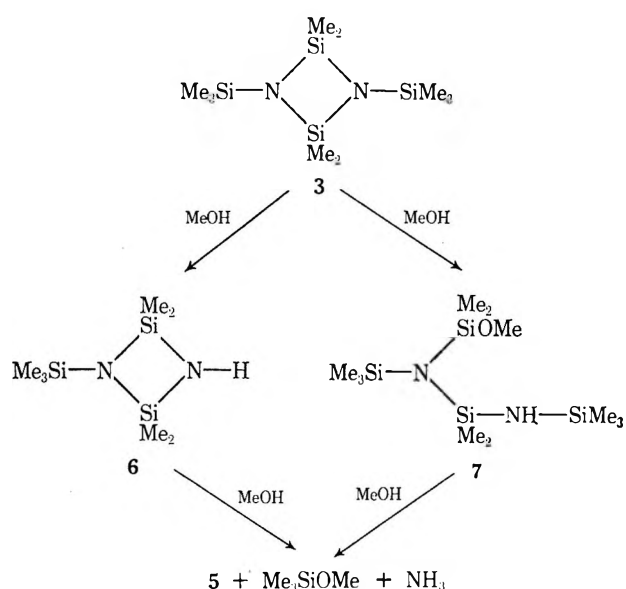
two other products are observed. The expected methoxytrimethylsilane was formed along with some dimethoxydimethylsilane from further methanolysis of **5**. These were identified by their nmr chemical shifts (Table II).

The accumulation of **5** in the methanolysis of **3** is not unexpected since **5** is a trisilylamine derivative and should behave similarly to **2** which is more resistant to methanolysis than **3** by a factor of 31 at 30°.

The precise course of the methanolysis of **3** is unknown. The cleavage of one of the trimethylsilyl groups would give the cyclosilazane **6**; solvolytic ring opening of **3** would give the open chain compound **7**. Since both **6** and **7** are disilazane derivatives, both are expected to cleave rapidly to bis(methoxydimethylsilyl)(trimethylsilyl)amine (**5**), methoxytrimethylsilane, and ammonia. The current experimental data do not allow these paths to be distinguished unequivocally.

Kinetics. The first order rate equation plots for the methanolysis of the three silazanes **1**, **2**, and **3** were generally linear to at least 70% of reaction. Several reactions were measured to 90% completion with excellent linearity indicating that the accumulation of the base ammonia in the reaction media does not exert any inhibiting or catalytic effects on the reactions.

Hexamethyldisilazane (**1**) and tris(trimethylsilyl)amine (**2**) differ in their rates of methanolysis in 50% methanol-carbon tetrachloride by a factor of about 20,000 at 30° (Table I). This difference, equivalent to a half-life at 30° of the order of a few minutes for **1**



but about 10.5 days for **2**, might be attributed to more extensive delocalization of the unshared electron pair on nitrogen in **2** compared to **1**. Support for this type of argument is found in the previously alluded to structural study of trisilylamine,^{3,4} in studies of the donor properties of **1**, **2**, and other silazanes,¹⁴ in a recent study of the electronic absorption spectra of **1**, **2**, and other silazanes,¹⁵ and in the studies of the equilibrations of 1,1- and 1,2-bis(trialkylsilyl)hydrazines.¹⁶

(14) E. W. Abel, D. A. Armitage, and G. R. Willey, *Trans. Faraday Soc.*, **60**, 1257 (1964), found that **1** is a very weak donor and that **2** has essentially no donor properties as measured by the shift in the C-D stretching frequency of DCCl_3 when it is mixed with a 10-mol excess of the silazane. This loss of donor properties is attributed to $p\pi-d\pi$ bonding in the silicon to nitrogen bond.

(15) C. G. Pitt and M. S. Fowler, *J. Amer. Chem. Soc.*, **89**, 6792 (1967), observed a progressive hypsochromic shift of the electronic absorption maxima of a series of silazanes resulting from the stepwise silylation of ammonia. They interpreted this shift in terms of increasing delocalization with increasing silylation of the nitrogen atom.

However, it is clear that the inertness of **2** compared to **1** could also be caused by the substantially greater physical shielding of the Si to N bond in **2** which renders the bond relatively inaccessible to attack by the solvent. This idea is supported by the measured activation parameters ΔH^* and ΔS^* (Table I). The enthalpies of activation for methanolysis of **1** and **2** are within 2 kcal of one another; however, the entropy of activation of **2** is about 11 e.u. more unfavorable than ΔS^* of **1**. This unfavorable term, where the effects of steric strain on rate are expected to be manifested, accounts for about 70% of the difference in the reactivities of **1** and **2**.

It is concluded that the differences in solvolytic reactivity of the Si to N bonds in **1** and **2** can be correlated with steric effects as convincingly as with bonding effects. The assumption of this argument is that the molecularity with respect to the solvent-reactant is the same in the solvolyses of **1** and **2**. If the molecularity with respect to methanol were known, and the correct solvent independent higher order rate constant were obtained, ΔS^* would be more negative, and a standard state would be chosen for the reaction; however, the relative values of ΔS^* for the solvolyses of **1** and **2** would remain unchanged and the interpretation unaffected.

The structure of N,N'-bis(trimethylsilyl)tetramethylcyclodisilazane (**3**) in the crystalline state has been established by X-ray diffraction.¹⁷ All silicon and nitrogen atoms are in one plane. The silicon to nitrogen bonds average 1.719 ± 0.04 Å and there is no significant difference in the lengths of the ring and exocyclic silicon to nitrogen bonds.

Within the limits of experimental precision, the silicon to nitrogen bond distances in **3** are the same as in trisilylamine, $(\text{H}_3\text{Si})_3\text{N}$.^{3,4} It is concluded that the extent of $p\pi-d\pi$ interaction in **3** is at least similar to the interaction in trisilylamine, and possibly more extensive because of delocalized π molecular orbitals. If it is assumed that the $p\pi-d\pi$ interaction in tris(trimethylsilyl)amine (**2**) is analogous to trisilylamine, and if the resistance of **2** to methanolysis is at least partly due to the $p\pi-d\pi$ interaction, then it is reasonable to

conclude that **3** should be at least as resistant to methanolysis as **2**.

In fact **3** is 31 times more reactive in the methanolysis reaction than **2**. More significantly **3** requires 4 kcal/mol less bond-breaking energy (ΔH^*) than **2** which implies that the $p\pi-d\pi$ bonding contributes even less to its solvolytic stability than to hexamethyldisilazane (**1**). The inertness of **3** is largely due to its very much more unfavorable entropy of activation.

The large negative entropies of activation for the methanolyses of **1**, **2**, and **3** are suggestive of (a) polar transition states and the requirement for substantial ordering of molecules of solvation; and/or (b) the requirement for substantial ordering of substituent groups in the transition state. It is probable that these factors are responsible for the inertness of **2** and **3** to methanolysis. The ground state of solvation of **1** decreases the extent to which new solvent molecules need to be accumulated and ordered to solvate the polar transition state. Similarly there is less strain involved in the ordering of the substituent groups of **1** compared to **2** and **3**.

Acknowledgment. The author wishes to thank Mr. L. W. Breed for pointing out some aspects of this problem and for several useful suggestions. Appreciation is due to Mr. J. E. Miller of the Midwest Research Institute computation center for help in processing the rate data, and to Professor Richard Schowen for his valuable comments. This research was supported in part by the United States Air Force under Contract AF 33(615)-3126 and was monitored by the Air Force Materials Laboratory, Research and Technology Division, Air Force Systems Command.

(16) R. West, M. Ishikawa, and R. E. Bailey, *J. Amer. Chem. Soc.*, **89**, 4068 (1967), investigated the fast, base-catalyzed transfer of trimethylsilyl and dimethylethylsilyl groups between the nitrogens of hydrazine. In general, the equilibrium composition of position isomers for a bis(trialkylsilyl)hydrazine consisted of nearly equal amounts of the 1,1- and 1,2-bis(trialkylsilyl)hydrazine. They suggested that the surprising thermodynamic stability of the 1,1-isomer was caused by a gain in delocalization energy through Si-N $p\pi-d\pi$ bonding which nearly compensated for the strain energy of this crowded molecule. A number of other chemical results have been interpreted in terms of $p\pi-d\pi$ bonding in silicon to nitrogen bonds.

(17) P. J. Wheatley, *J. Chem. Soc.*, 1721 (1962).

Three-Element Reaction Coordinates and Intramolecular Kinetic Isotope Effects

by William J. Kass and Peter E. Yankwich

Noyes Laboratory of Chemistry, University of Illinois, Urbana, Illinois 61801 (Received February 17, 1969)

A convenient form is developed for expressing the limitations upon the relative contributions to a reaction coordinate of three internal coordinate displacements imposed by the condition that there be a single zero (and no negative) vibrational eigenvalue at the transition state. The method is applied to exploration of the consequences of reaction coordinate "composition" variations for values of the temperature-dependent (TDF) and temperature-independent (TIF) factors in an intramolecular kinetic isotope effect. The related influences of changes in temperature, shifts in force constant values, etc., are studied also. For most reaction coordinates (but for none at high temperature), the contributions of TIF to the isotope effect are small in comparison with those of TDF. For both TIF and TDF, changes in the relative *signs* of given component displacements in the reaction coordinate yield effects which can be large compared with those arising in (a) displacement relative *magnitude* shifts of 10–30%; (b) temperature changes of several hundred degrees; or (c) alterations of 25–100% in values of diagonal force constants of "isotopic" internal coordinates. Some problems associated with the occurrence of multiple nonpositive eigenvalues are examined briefly.

Introduction

General methods have been developed¹ for forcing some arbitrary vibration of an activated complex to be a normal mode with preselected frequency; application of the methods to calculation of kinetic isotope effects is particularly straightforward when this frequency, $\nu_k = \nu_1$, is zero. In a previous publication,² reaction coordinates were surveyed which consisted of up to four internal coordinate displacements; the model system was the intramolecular carbon isotope effect in the decarboxylation of oxalic acid.

When the number of nonzero elements in the reaction coordinate is three or more, it is difficult to restrict to *one* the number of nonpositive eigenvalues, but a technique was developed² which guaranteed this situation though limiting, by rule, the *composition* of the reaction coordinate (*i.e.*, the relative signs and magnitudes of the nonzero eigenvector elements). This paper reports development of methods of general applicability in which the limitations on reaction coordinate composition are only those necessary to prevent the generation of a second zero frequency in the transition state.

Theory and Representation of Limits

Knowledge or assumption of a structure and force field for a given chemical species provides the information required for computation of the elements of the G and F matrices described by Wilson.³

The Potential Function, Reaction Coordinate, and Associated Frequency ν_1 . We solve the vibrational secular equation in the form

$$|\mathbf{GF} - \mathbf{EA}| = 0 \quad (1)$$

where \mathbf{E} is the identity matrix and the Λ are eigenvalues. Where \mathbf{S} is a column of the internal displacement coordinates and \mathbf{Q} a column of the normal coordinates, we have for the eigenvectors \mathbf{L} the relation

$$\mathbf{GFL} = \mathbf{LA} \quad (2)$$

Here

$$\mathbf{S} = \mathbf{LQ} \quad (3)$$

or

$$S_i = \sum_k L_{ik} Q_k \quad (4)$$

If we follow the convention that for the reaction coordinate $k = 1$, solution of the secular equation at the transition state yields

$$\mathbf{GFL}_{i1} = \mathbf{L}_{i1}\Lambda_1 \quad (5)$$

Equation 5 embodies the restrictions imposed on the solution *via* eq 2 of the problem of calculation of kinetic isotope effects given a transition state structure, \mathbf{G} , a description of the reaction coordinate, \mathbf{L}_{i1} , and a zero or imaginary value for the vibration frequency, ν_1 ($\Lambda_1 = 0$ or $-$), associated with the reaction coordinate. To "see" the character of Q_1 , we isolate its effects on the S_i by applying the constraints $Q_k \neq 1 = 0$; subject to these constraints, eq 3 becomes

$$\mathbf{S} = \mathbf{L}_{i1}Q_1 \quad (6)$$

To put this information in convenient form, we write the equation

$$X_1 = \sum_i L_{i1} S_i \quad (7)$$

and we say that X_1 is the description of the motion in normal coordinate 1; but, X_1 is not Q_1 , and $X_1 \neq Q_1$.

Similarly, we can obtain the eigenvalues, λ_k , and the

(1) W. E. Buddenbaum and P. E. Yankwich, *J. Phys. Chem.*, **71**, 3136 (1967).

(2) T. T.-S. Huang, W. J. Kass, W. E. Buddenbaum, and P. E. Yankwich, *ibid.*, **72**, 4431 (1968).

(3) E. B. Wilson, Jr., J. C. Decius, and P. C. Cross, "Molecular Vibrations," McGraw-Hill Book Co., Inc., New York, N. Y., 1955.

eigenvectors, \mathbf{A} , of the force field \mathbf{F} . The signs of the individual λ_k and Λ_k are the same. However, in the special case that $\nu_1 = 0$ ($\lambda_1 = \Lambda_1 = 0$), \mathbf{A}_{i1} is an eigenvector of both \mathbf{F} and \mathbf{GF} ; that is

$$\mathbf{A}_{i1} = c\mathbf{L}_{i1} \quad (8)$$

where c is a constant, when

$$\mathbf{FA}_{i1} = \mathbf{0} \quad (9)$$

Conditions for a Zero Frequency. This investigation is limited to reaction coordinates of up to three elements: $t = i, j, k$. Extension to four or more elements is reasonably straightforward, but is complicated by the fact that the number of off-diagonal force constants, F_{ij} , employed to generate a zero frequency may exceed the number of elements of \mathbf{A}_{i1} ; some of these F_{ij} are therefore parameters along with the diagonal force constants, F_{ii} .

For convenience, we define two quantities connecting diagonal and off-diagonal force constants

$$(F_{ij})_0 = |\sqrt{F_{ii}F_{jj}}| \quad (10)$$

and

$$\alpha_{ij} = F_{ij}/(F_{ij})_0 \quad (11)$$

and a third connecting diagonal force constants and the elements of \mathbf{A}_{i1}

$$P_i = cA_{i1}|\sqrt{F_{ii}}| \quad (12)$$

where c is a constant for a given triad (P_i, P_j, P_k). Expansion of the secular determinant of \mathbf{F}

$$|\mathbf{F} - E\lambda| = 0 \quad (13)$$

with the F_{ij} substituted by eq 10 and 11 yields

$$\lambda^3 - \mathbf{a}\lambda^2 + \mathbf{b}\lambda - \mathbf{c} = 0 \quad (14)$$

where

$$\mathbf{a} = F_{ii} + F_{jj} + F_{kk} \quad (15a)$$

$$\mathbf{b} = [F_{ii}F_{jj}(1 - \alpha_{ij}^2) + F_{ii}F_{kk}(1 - \alpha_{ik}^2) + F_{jj}F_{kk}(1 - \alpha_{jk}^2)] \quad (15b)$$

$$\mathbf{c} = F_{ii}F_{jj}F_{kk}(1 + 2\alpha_{ij}\alpha_{ik}\alpha_{jk} - \alpha_{ij}^2 - \alpha_{ik}^2 - \alpha_{jk}^2) \quad (15c)$$

The condition for $\lambda_1 = 0$ is that $\mathbf{c} = 0$; since we deal only with positive values of the F_{ii} , the second factor on the right of eq 15c must be zero. Rearranged, this factor yields three relations among the α_{ij} of the form

$$\alpha_{ij} = \alpha_{ik}\alpha_{jk} \pm \sqrt{(1 - \alpha_{ik}^2)(1 - \alpha_{jk}^2)} \quad (16)$$

Substitution of eq 11 and 12 into eq 9 and solution of the latter gives

$$\alpha_{ij} = \frac{(-P_i^2 - P_j^2 + P_k^2)}{2P_iP_j} \quad (17)$$

Re-resolution after introduction of eq 16 gives

$$\frac{P_j}{P_i} = \pm \sqrt{\frac{(1 - \alpha_{ik}^2)}{(1 - \alpha_{jk}^2)}} \quad (18)$$

Conditions for One Zero Frequency. When $\lambda_1 = 0$, we have the additional relations

$$\lambda_2 + \lambda_3 = \mathbf{a} \quad (19)$$

$$\lambda_2\lambda_3 = \mathbf{b} \quad (20)$$

Since \mathbf{a} is always positive, one of the three eigenvalues controlled by the three α_{ij} will always be positive; let it be λ_3 ; then λ_2 may be positive, zero, or negative. The case of interest here is λ_2 positive; examination of eq 16, 19, and 20 shows that this situation obtains in two circumstances

$$\alpha_{ij}^2 < 1; \alpha_{jk}^2 < 1; \alpha_{ik}^2 < 1 \quad (21a)$$

and

$$\alpha_{ij}^2 = 1; \alpha_{ik}^2 = \alpha_{jk}^2 < 1 \quad (21b)$$

It is apparent from eq 15b and 20 that a second zero eigenvalue is obtained when

$$\alpha_{ij}^2 = \alpha_{ik}^2 = \alpha_{jk}^2 = 1 \quad (22)$$

and this equation represents the limits of situations of chemical interest. When $\alpha_{ij} = \pm 1$, eq 17 can be rearranged to

$$\frac{P_k}{P_i} = \pm \left(\frac{P_j}{P_i} \pm 1 \right) \quad (23)$$

Representation in Terms of P Ratios. Within regions defined by parallel pairs of the four lines represented by eq 23, λ_2 is positive and we have an ordinary transition state; outside these regions λ_2 is negative, and the complex possesses both a zero and an imaginary vibration frequency. On the lines, λ_2 is zero and the complex has two zero frequencies of vibration; the compositions of these motions are different, though both conform to the same selection of sign in eq 23. The limits defined by eq 23 (and some other curves of interest) are shown in Figure 1. For convenience to the discussion, Table I contains a summary of the types of calculation described in the previous publication.²

The lines separating the space of Figure 1 into regions are those along which $\lambda_2 = 0$; the regions marked α are those where λ_2 is positive, and in them a three-element reaction coordinate calculation (Type III) is "permitted." The circle and the two pairs of hyperbolae are trajectories along which one of the α_{ij} is zero. According to eq 15c, the sum of the squares of the other two is unity; therefore, these curves represent calculations of Type IV. At the four points A, B, C, and D, and at the two composite points (G,G',J,J') and (H,H',M,M'), one of the α_{ij} is ± 1 and the other two are zero; thus, these points represent the six possible calculations of Type II for a given triad of coordinates (i, j, k). At the points (N,S), (R,T), and W, only $\lambda_1 = 0$,

Table I: Types of Kinetic Isotope Effect Calculation²

Type	To make $\lambda_1 = 0$	Reaction coordinate	
		A basis	Normalized P basis
I	$F_{ii} = 0$	$A_{i1} \neq 0$	$ P_i = 1$
II	$F_{ij} = \pm (F_{ij})_0$	$A_{i1}, A_{j1} \neq 0$	$ P_i = P_j = 0.5$
III	$F_{ij}, F_{ik}, F_{jk} \neq 0$	$A_{i1}, A_{j1}, A_{k1} \neq 0$	$ P_i + P_j + P_k = 1$
IV	$F_{ij}, F_{ik} = 0$; and $\alpha_{ij}^2 + \alpha_{ik}^2 = 1$	$A_{i1}, A_{j1}, A_{k1} \neq 0$	$ P_j = \frac{(1 - 2 P_k)}{2(1 - P_k)}$

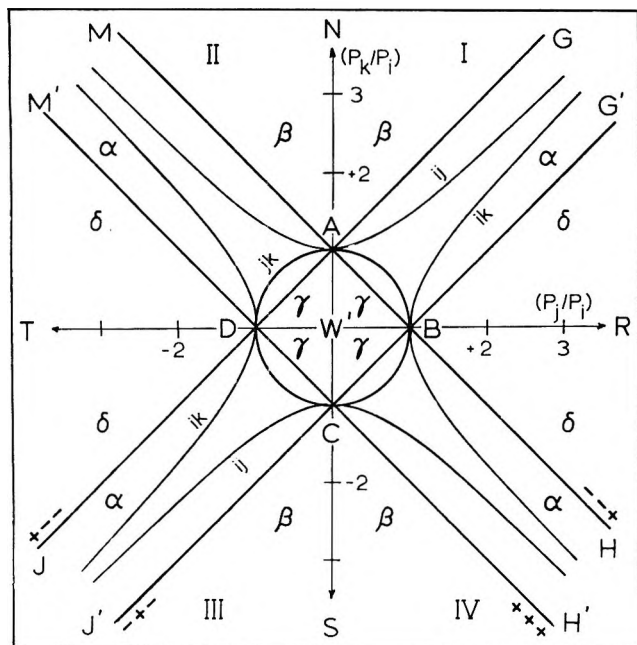


Figure 1. Permitted and forbidden regions in the P -ratio plane, one zero eigenvalue in the transition state: $\lambda_1 = 0$, and $\lambda_3 = +$, everywhere. The light lines NS and RT are the axes of the coordinate system of the figure; their intersection is the origin, which is occupied also by the coincident points W and W'. The actual points N, R, S, and T are located at infinity. The heavy lines are region boundaries for calculations of Type III ($\lambda_2 = 0$); on them all three α_{ij} are unity with signs as shown by the triads in the sequence ij, ik, jk (e.g. $- + +$: $\alpha_{ij} = \alpha_{ik} = -1, \alpha_{jk} = +1$). Like N, R, etc., the actual points G, G', H, H', J, J', M, and M' are located at infinity. There each primed and unprimed pair (e.g., M and M') are coincident, forming what is termed "a composite point.") The several areas within each quadrant are labeled according to the sign of λ_2 within them. For example, in quadrant I λ_2 is positive in the region GABG', which is labeled " α " accordingly; λ_2 is negative in regions GAN (" β "), AWB (" γ "), and G'BR (" δ "). The curves represent calculations of Type IV, the letter pair indicating which of the α_{ij} is zero in each case.

and only $A_{i1} \neq 0$, and the results appear to be of Type I; however, here this situation is achieved with infinite values of off-diagonal force constants rather than with some one $F_{ii} = 0$, and the isotope effects are very different in magnitude from those of Type I.

This representation in terms of P ratios is convenient for planning calculations along some line in the field; but, because the α -regions extend to infinity, it is very

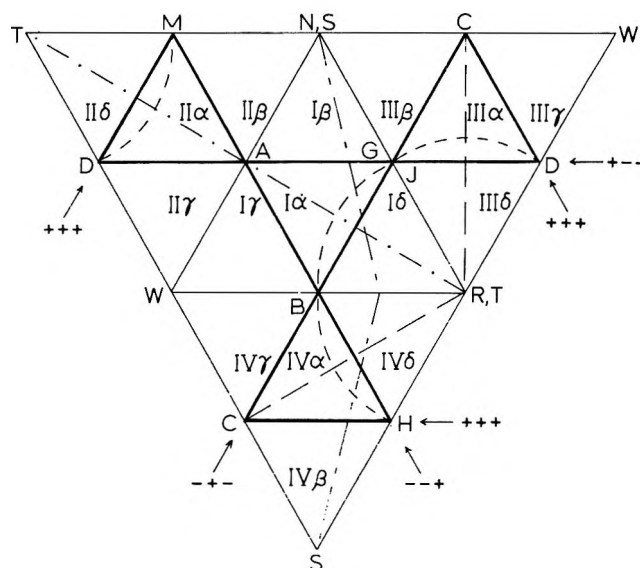


Figure 2. Permitted (α) and forbidden (β, γ, δ) regions in the triangular (P_i, P_j, P_k) space. Points and regions are labeled as in Figure 1. The defining (extremal) points are $P_i, W(+1)$ and $W'(-1)$; $P_j, R(+1)$ and $T(-1)$; $P_k, N(+1)$ and $S(-1)$. Broken lines represent certain linear trajectories in Figure 1: $-\cdot-\cdot-$, $(P_k/P_i) = +1$; $-\cdot-\cdot-$, $(P_k/P_i) = -1$; $-\cdot-\cdot-$, $(P_j/P_i) = +2.5$. The curve $-\cdot-\cdot-$ represents the Type IV calculation $\alpha_{ik} = 0$, shown as the left- and right-facing hyperbolae in Figure 1; the segments of this curve are not circular arcs. On the heavy lines, all three $|\alpha_{ij}| = 1$; the signs are given by the triads, the sequence being ij, ik, jk . In the quadrants of this space, the relative signs of P_i, P_j , and P_k are I(N, R, W), $+++$; II(N, T, W), $+ - +$; III(N, R, W'), $+ - -$; IV(R, S, W), $+ + -$.

inconvenient when one wishes to carry out or display the results of a systematic survey of the isotope effects arising in reaction coordinates describable in terms of a given triad of internal coordinates.

Representation in Terms of Normalized P Values. Equation 23 can be rearranged to

$$P_i \pm P_j \pm P_k = 0 \quad (24)$$

in which we adopt the convention that P_i is always positive. Since only two of the terms in eq 24 are independent, it occurred to us that the use of normalized values of the P_i , the constant c in eq 12 being selected so that

$$|P_i| + |P_j| + |P_k| = 1 \quad (25)$$

would permit planning of the calculations and display

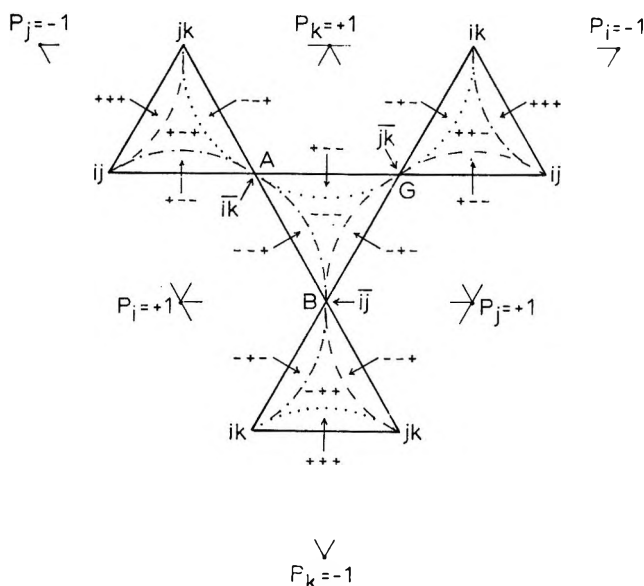


Figure 3. Permitted regions in the (P_i, P_j, P_k) space. (Orientation same as Figure 2.) Peripheral defining points, $P_i = \pm 1$, are shown. At $\bar{i}\bar{j}$, $\alpha_{ij} = +1$; at $\bar{j}\bar{j}$, $\alpha_{ij} = -1$; at both, $\alpha_{ik} = \alpha_{jk} = 0$. At $\bar{i}\bar{j}$ and $\bar{j}\bar{j}$, $P_k = 0$, and the calculations are of Type II. Along the curves, $\alpha_{ij} = 0$ and $\alpha_{ik}^2 + \alpha_{jk}^2 = 1$, and the calculations are of Type IV: \cdots , $\alpha_{ij} = 0$; $---$, $\alpha_{ik} = 0$; $-\cdots-$, $\alpha_{jk} = 0$. Within the subregions defined by the curves $\alpha_{ij} = 0$, the three α_{ij} (in the sequence $\bar{i}\bar{j}$, $\bar{i}\bar{k}$, $\bar{j}\bar{k}$) have the signs shown by the triads. Quadrant III (upper right) is placed correctly with respect to the others, but the convention $P_i = +$ requires that the signs of the three P_i be regarded as reverse of those shown.

of results in an equilateral triangular space finite in extent.⁴ The transcription to this space of Figure 1 is shown in Figure 2. Note that the α regions are defined by the lines $|P_i| = 0.5$.

At the points A, B, C, D, (G, J), and (H, M), one of the $|\alpha_{ij}|$ is unity and the other two are zero or unity. In the former situation, λ_2 is positive, the calculation is permitted and, because it lies also on the trajectories of two Type IV calculations, may be regarded as belonging to both of the adjacent permitted α -regions. The latter situation can come about in three different ways. Of these, two represent forbidden calculations because each such point lies in two of the defining lines and $\lambda_2 = 0$. The third case is also forbidden, but because the signs of the three unitary α_{ij} are those shown in the central area of each quadrant and with these $c \neq 0$ (eq 15c).

The permitted regions are shown separately from the forbidden in Figure 3, in which the signs of the three α_{ij} in various areas are given. The variations of a given α_{ij} over both the permitted and forbidden regions of a quadrant are displayed in Figure 4. Rotation by $\pm 120^\circ$ converts these contours to those for α_{ik} and α_{jk} .

Representation in Terms of Normalized A_{ii} -Values. Reaction coordinates of different compositions can, of course, be represented in terms of some normalized set of the elements A_{ii} ; and, it may be argued that such a

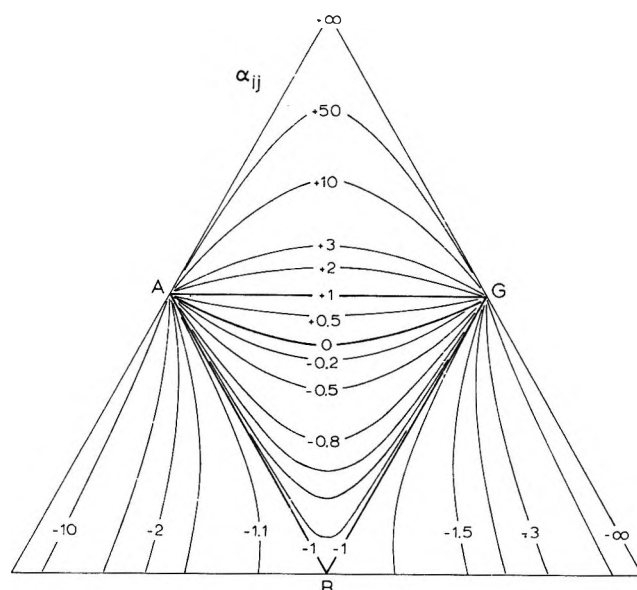


Figure 4. Contours of the variable α_{ij} in quadrant I, region α . The unmarked curves within the triangle ABG are for $\alpha_{ij} = -0.9, -0.95, \text{ and } -0.99$. The rotation $G \rightarrow A$ yields the α_{jk} surface, while $B \rightarrow A$ yields that for α_{ik} . Sign reversal may be required when the graphs are transposed to other quadrants. For example, in quadrant II, application to α_{ij} and α_{jk} requires that their signs be reversed.

set is a more faithful description of the motion than is the corresponding set of normalized P_i . However, the ruling of the P_i surface is independent of the relative values of the diagonal force constants, while that of the A_{ii} surface is not. That is, the eigenvalues Λ_1, Λ_2 , and Λ_3 have given signs at a given point on *any* P_i plane. An example of the superposition of a normalized A_{ii} surface onto the normalized P_i surface is shown in Figure 5. The reciprocal relations between the P_i and the A_i are

$$P_i = \frac{A_{ii}|\sqrt{F_{ii}}|}{\sum(A_{ii}|\sqrt{F_{ii}}|)} \text{ and } A_{ii} = \frac{(P_i/|\sqrt{F_{ii}}|)}{\sum(P_i/|\sqrt{F_{ii}}|)} \quad (26)$$

At the points A, G, and B, pairs of lines $|P_i| = 0.5$ meet; at the points a, g, and b, pairs of lines $|A_{ii}| = 0.5$ meet. These triads of points (and the rulings of the two surfaces) correspond only when $F_{ii} = F_{jj} = F_{kk}$.

Application

Other features of this method and certain properties of the results are best presented in terms of a specific reaction and model. For convenience, we extend here the discussion in a previous publication² of the intra-

(4) The normalization $P_i^2 + P_j^2 + P_k^2 = 1$, which retains the notion of direction cosines, can be employed if it is desired to plot results on four surface octants of a sphere. This approach was found to compress interesting detail toward edges, so we elected not to employ it for graphing in a plane triangle. Since we have knowledge only of relative signs of coordinate displacements, pairs of octants (*i.e.*, pairs of sign triads for P_i, P_j , and P_k) are redundant. Hereinafter, consistent with the sign convention $P_i = +$, we shall refer to the graphable space as comprising a set of *quadrants*, or similar subunits thereof.

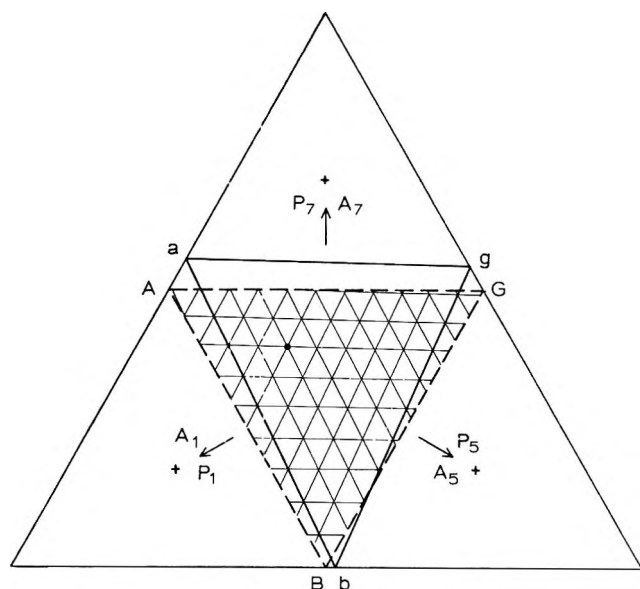
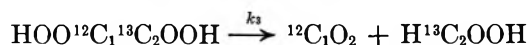
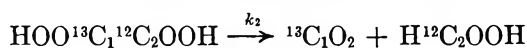


Figure 5. Superposition in quadrant I of the surfaces (P_1 , P_5 , P_7) and (A_{11} , A_{51} , A_{71}); $F_{11} = 4.5$, $F_{55} = 5.0$, and $F_{77} = 7.0$ mdyn/Å. The lines AG, GB, and BA are those along which the several P_i are individually 0.5; along the lines ag, gb, and ba the A_{ii} are individually 0.5. The ruling shown in the region of permitted calculations is that of the A_{ii} surface. The coordinates of the dot are: $A_1 = 0.40$, $A_5 = 0.25$, $A_7 = 0.35$; or, $P_1 = 0.3636$, $P_5 = 0.2396$, $P_6 = 0.3968$.

molecular carbon isotope effect in the decomposition of oxalic acid- ^{13}C , limiting ourselves to reaction coordinates composed from three bond-stretching internal coordinates.

The System. The intramolecular case is k_2/k_3 in the notation of Lindsay, McElcheran, and Thode⁵



We write

$$L(k_2/k_3) = L(\text{TIF}) + L(\text{TDF}) = L(k/k')$$

where $L(x) = 100 \ln x$. The temperature-independent factor (TIF) arises in the reaction coordinate motion, is (ν_1/ν_1') when only λ_1 is zero, and is the $T = \infty$ limit of k_2/k_3 . The temperature dependent factor (TDF) arises in the genuine vibrations of the isotopic pair of activated complexes.

The Model. The molecule is assumed planar with carbonyl groups *trans*; hydroxyl hydrogens are in juxtaposition with opposite carbonyl oxygens. Bond lengths, bond angles, and force constants were assigned the values shown in Table II, and were obtained or adjusted from a number of sources.² The analogous force field employed in an earlier publication from this laboratory (S field) was diagonal; redundancies were employed in nonstretching coordinates to achieve a match of calculated vibrational frequencies with those which seemed reasonable.

Table II: Values of Input Parameters^{a,b}

Coordinate	No., i	F_{ii} ^c
C ₁ —C ₂	1	4.5
C=O	2, 3	12.0
C—O	4, 5	5.0
O—H	6, 7	7.0
O=C—C	8, 9	1.79
O—C—C	10, 11	1.85
C—O—H	12, 13	0.70
		$F_{8,10} = F_{9,11} = 1.08$

^a Masses are in atomic mass units. ^b Bond distances (Å): C—C, 1.54; C—O, 1.37; C=O, 1.22; O—H, 0.96. Bond angles (degrees): O=C—O, 125; O=C—C, 122; C—O—H, 108. ^c Stretching force constants are in mdyn/Å; bending and bend-bend interaction force constants in mdyn Å.

A given internal coordinate may not be included in the reaction coordinate if it is a member of a redundant set. Because we wished later to investigate reaction coordinates involving bending and torsional motions, yet retain comparability of results to those already obtained, a nonredundant set of internal coordinates was employed in this investigation. Small interaction force constants were used to maintain correspondence of calculated eigenvalues between the two sets of coordinates.

The internal coordinates selected for inclusion in reaction coordinates were $S_i = S_1$, C₁—C₂ stretch; $S_j = S_5$, C₁—O₁ stretch; and $S_k = S_7$, O₁—H stretch. Because these S_i lie in the plane of the molecule, computer time was conserved by carrying out calculations with aplanar coordinates undefined.

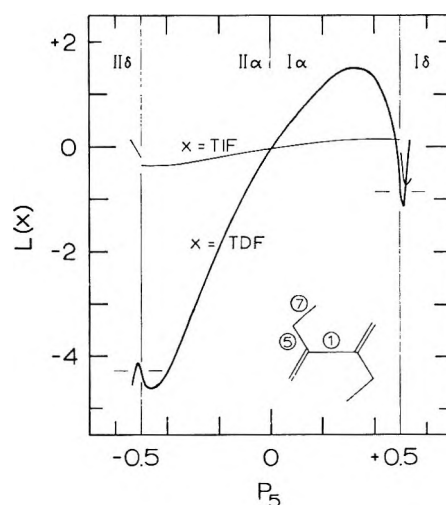


Figure 6. $L(\text{TIF})$ and $L(\text{TDF})$, the latter at $1000/T^\circ\text{K} = \theta = 5$, as functions of P_5 along the trajectory: $P_1 = P_7 = (1 - |P_5|)/2$. The light horizontal lines indicate the values of $L(\text{TDF})_{\theta=5}$ at the permitted-region edges, $P_5 = \pm 0.5$. This trajectory is shown as - - - - in Figure 2.

(5) J. G. Lindsay, D. E. McElcheran, and H. G. Thode, *J. Chem. Phys.*, 17, 589 (1949).

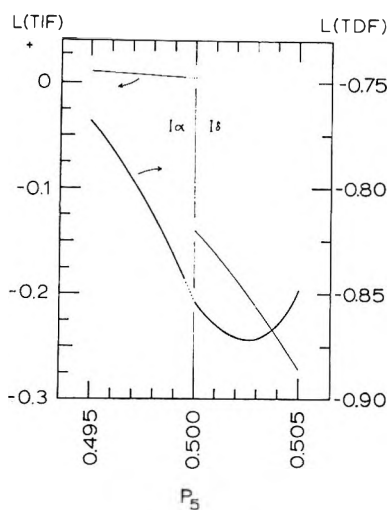


Figure 7. $L(\text{TIF})$ and $L(\text{TDF})_{\theta=5}$ near the $I\alpha$ (permitted)- $I\delta$ (forbidden) boundary, along the trajectory $P_7 = 0.4$. Note the different ordinate scales for the two L functions.

Calculations. The normal mode vibrational frequencies were calculated *via* Wilson's FG matrix method³ on an IBM 360-75 digital computer; Schachtschneider's original programs⁶ were modified extensively for this application.

Simple Trajectories. Consideration of results obtained by varying the P_i (or P_j) along simple trajectories provides useful indications of the influences of displacements in the individual internal coordinates. The intramolecular isotope effect originates in eigenvalue differences between a pair of isotopic isomeric activated complexes; in the latter, S_1 is isotopic in both, S_5 in one, and S_7 in neither. We would expect that P_1 and P_7 variations might sometimes have similar effects, and that these might be small in certain circumstances. On the other hand, variations in P_5 would be expected to have significant effects on calculated values of $L(\text{TIF})$ and $L(\text{TDF})$ in most situations.

Figure 6 displays results for reaction coordinates in which the relative values of P_1 and P_7 are equal while that of P_5 varies from the negative to the positive extremum. This corresponds to equal relative displacements in S_1 and S_7 being maintained while that in S_5 varies from an antisymmetric maximum, through zero, and to a symmetric maximum; results are shown also for short excursions into the forbidden regions beyond $|P_5| = 0.5$. Clearly, $L(\text{TIF})$ and $L(\text{TDF})_{\theta=5}$ are not simply related (and would not be expected to be at any other temperature), though here their general trends are similar between $P_5 = -0.4$ and $+0.3$. None of the special features of $L(\text{TDF})$ occur at the two Type IV points ($\alpha_{17} = 0$; $|P_5| = \sqrt{2} - 1$) in the permitted regions ($II\alpha$ and $I\alpha$). The changes in sign of the two L -functions as that of P_5 changes (though the three shifts are not exactly coincident) arise in the adjacency of coordinates S_1 and S_5 .²

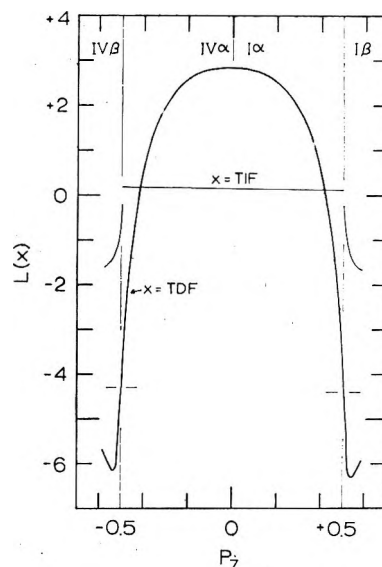


Figure 8. $L(\text{TIF})$ and $L(\text{TDF})_{\theta=5}$ as functions of P_7 along the trajectory $P_1 = P_5 = (1 - |P_7|)/2$. The light horizontal lines indicate the values of $L(\text{TDF})$ at the edges of the permitted region, $P_7 = \pm 0.5$.

An especially important feature of these graphs is the difference in behavior of $L(\text{TIF})$ and $L(\text{TDF})$ in the vicinity of $|P_5| = 0.5$. As the α -region boundary is approached from within and passed, $L(\text{TIF})$ appears to be discontinuous in both value and slope, while $L(\text{TDF})$ appears continuous in value but not in slope. That is, the values of these functions on the lines $P_5 = \pm 0.5$ are extrapolations of permitted-region values in the case of $L(\text{TDF})$ but not for $L(\text{TIF})$. These differences are observed generally, for any triad of coordinates (i, j, k) and at any temperature; and, as will be seen below, these properties confer important characteristics upon the two L - P_i surfaces in the permitted α regions.

The $P_5 = 0.5$ edge region of quadrant $I\alpha$ is shown in somewhat greater detail in Figure 7 along the trajectory $P_7 = 0.4$. $L(\text{TIF})$ does not seem often if ever to change slope in the neighborhood of the edge as precipitously as does $L(\text{TDF})$ at least some of the time. Therefore, one can obtain the limiting value at the edge for $L(\text{TIF})$ with considerable accuracy by extrapolation from the permitted region; the value of $L(\text{TDF})$ at the edge is obtained most conveniently by direct calculation for some case $\Lambda_1 = \Lambda_2 = 0$.

Results are shown in Figure 8 for the trajectory $P_1 = P_5$. The symmetry of $L(\text{TDF})_5$ about $P_7 = 0$ is due to the fact that S_7 is not an isotopic coordinate, while the failure of $L(\text{TIF})$ to exhibit similar symmetry is a second-order effect;² the nature of S_7 is also responsible for the mesa in $L(\text{TDF})$ for $|P_7| = 0 - 0.2$. We do not yet have an explanation for the drastic influence of increase in the motion in S_7 beyond $|P_7| = 0.2$.

(6) J. H. Schachtschneider and R. G. Snyder, *Spectrochim. Acta*, **19**, 117 (1965).

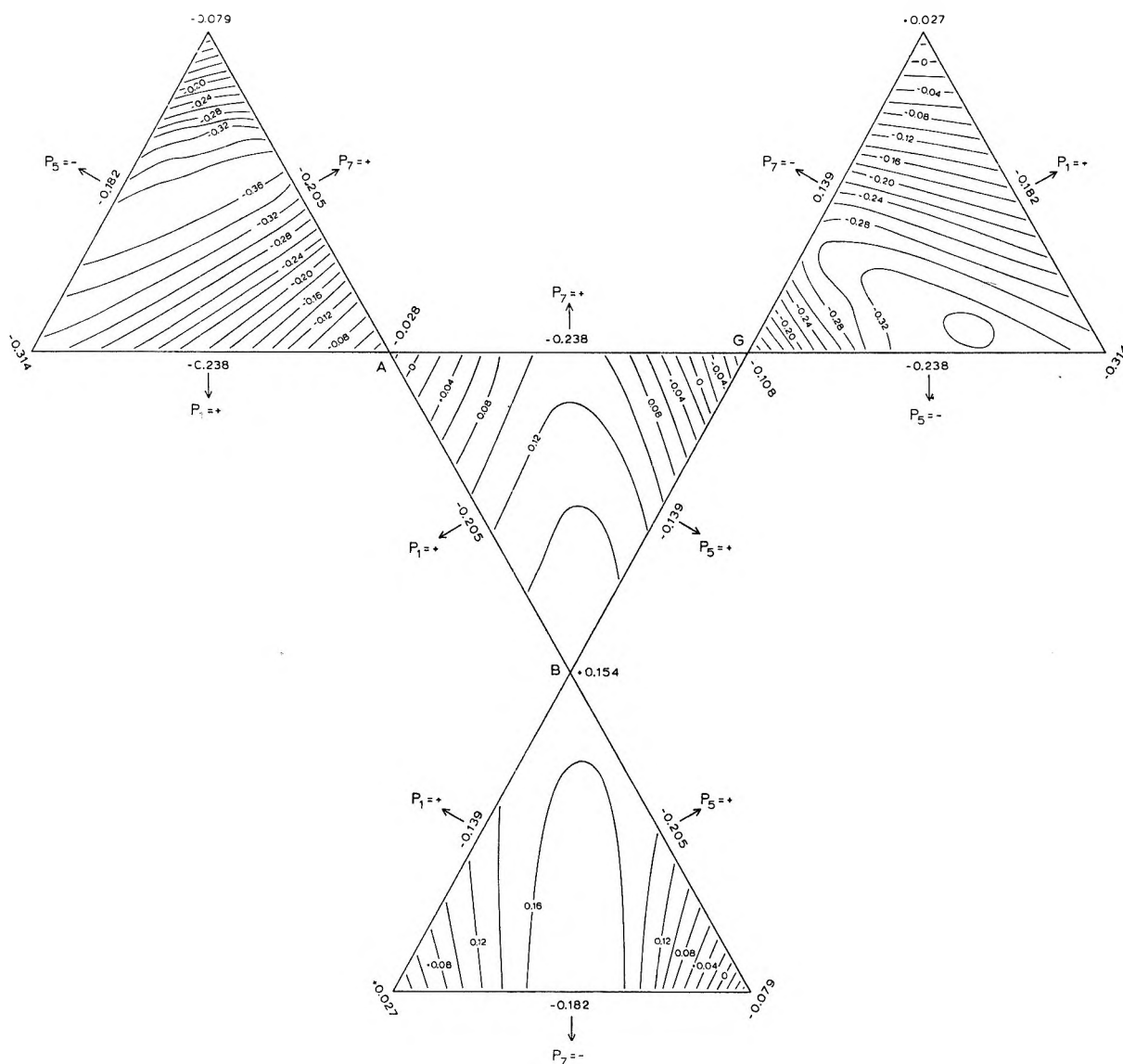


Figure 9. Map of the $L(\text{TIF})-(P_1, P_5, P_7)$ surface in the permitted α regions. At each vertex, one P_i is zero and the other two are ± 0.5 ; the directions of increase of each $|P_i|$ are shown. The isotif interval is $0.02 L$ unit.

Such a marked change in the directive power of a given P_i is commonplace, but it is not a general phenomenon.

The $L(\text{TIF})-P_i$ Surface. Figure 9 is a map of the $L(\text{TIF})-(P_1, P_5, P_7)$ surface in the permitted α regions; the curves are *isotifs*' with a contour interval of $0.02 L$ unit. The six different Type II calculation values at the vertices are continuous with those in the permitted fields; clearly, this situation does not obtain along the four lines $P_i = \pm 0.5$ (see Figure 2) which define the α -regions. Along those lines and everywhere in the (forbidden) regions β , γ , and δ

$$(\text{TIF}) = (\nu_1/\nu_1')(\nu_2/\nu_2') \quad (27)$$

That is

$$L(\text{TIF}) = L(\text{tif})_1 + L(\text{tif})_2 \quad (28)$$

with $L(\text{tif})_2 = 0$ within any α region. The degeneracy of ν_1 and ν_2 at each of the four defining lines results in L -

(TIF) being a constant along each one; thus there $L(\text{tif})_1$ and $L(\text{tif})_2$ are complementary to each other. Over the whole $L(\text{TIF})-P_i$ surface, $L(\text{tif})_1$ appears to be continuous, but neither $L(\text{tif})_2$ nor $L(\text{TIF})$ can be; this situation is examined in Figure 10.

Part a of Figure 10 shows $L(\text{TIF})$ and its components for reaction coordinates along the trajectory of the motion related to ν_1 employed for Figure 7. The vibration which will yield the second zero eigenvalue at $(P_5)_1 = 0.5$ was identified and $L(\text{tif})_2$, which is $L(\nu_2/\nu_2')$ in region α , plotted separately. The composition of that vibration is shown in its own $(P_i)_2$ space in part b of the figure. (For plotting purposes, small nonzero values of P_i 's other than P_1, P_5 , and P_7 were ignored.) It is interesting to note that the trajectory of this

(7) P. E. Yankwich and R. M. Ikeda, *J. Amer. Chem. Soc.*, **81**, 1532 (1959).

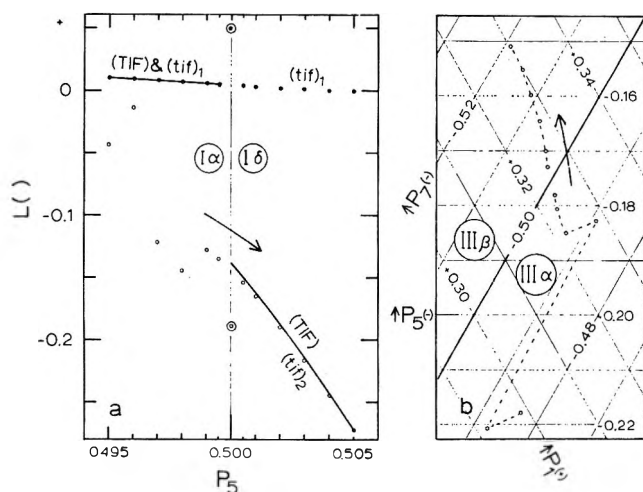


Figure 10. (a) $L(tif)_1$, \circ , $L(tif)_2$, \bullet , and their sum, $L(TIF)$, —, along the trajectory $(P_7)_1 = 0.40$ near the $I\alpha$ - $I\beta$ boundary line, $(P_5)_1 = 0.5$. $L(tif)_2$ is undefined in region $I\alpha$; there, the points are $L(\nu_2/\nu_2')$ and the frequencies are real. At the boundary the points are circled; in spite of their wide separation (arising in interaction of two nearly zero eigenvalues), their sum lies on $L(TIF)$. (b) The trajectory of ν_2 in Quadrant III; (P_5) is the independent variable.

second vibration crosses the same defining line as does the first eigenvalue when $(P_5)_1 = 0.5$, but it lies in quadrant III instead of in I; further, its zero eigenvalue occurs for $(P_7)_2 = 0.5$ instead of $(P_5)_2 = 0.5$ as might be expected.⁸ When both ν_1 and ν_2 are zero there is a conjugate relationship between their eigenvectors. Let the subscripts a and b designate different calculations at appropriate limits $|P_i| = 0.5$, both lying on the same α -region defining line (e.g., CBGC, Figure 2, for the calculations of Figure 10). In the first (employing the notation of eq 7), X_{1a} implies X_{2a} ; in the second, X_{1b} implies X_{2b} . Then if X_{1b} is taken as X_{2a} , it is observed that the motion X_{2b} is the same as X_{1a} .

The $L(TDF)$ - P_i Surface. Without regard at this point for the physical implications of a situation in which more than one normal mode of the activated complexes has an associated vibrational frequency which is zero or imaginary, the general formulation of the isotopic rate constant ratio in an intramolecular isotope effect is

$$(k/k') = \prod_{k=1}^j \left(\frac{\nu_k}{\nu_k'} \right) \cdot \prod_{k=j+1}^{3N-6} \frac{(u_k') \sinh(u_k/2)}{(u_k) \sinh(u_k'/2)} \quad (29)$$

where $u = (h\nu/kT)$; or, in logarithmic form

$$L(k/k') = \sum_{k=1}^j L(tif)_k + \sum_{k=j+1}^{3N-6} L(tdf)_k \quad (30)$$

As any ν_k approaches zero, so does the corresponding $L(tdf)_k$; when ν_k is zero or imaginary, j in eq 29 and 30 is increased by one, $L(tdf)_k$ is removed from the second summation and $L(tif)_k$ added to the first. In analogy with eq 28, we write for TDF

$$L(TDF) = L(tdf)_2 + \sum_{k=3}^{3N-6} L(tdf)_k \quad (31)$$

with $L(TDF) = 0$ outside any α region. The removal of $L(tdf)_2$ from the summation in eq 31 as ν_2 changes from positive to zero or imaginary accounts for the discontinuity in slope but not value of $L(TDF)$ vs P_i as $|P_i|$ passes through 0.5 (see Figures 6-8).

This property of the function $L(TDF)$ accounts for the most characteristic feature of the $L(TDF)$ - P_i surface (see Figure 11): that the limiting value of $L(TDF)$ as any $|P_i|$ approaches 0.5 from within an α region is equal to that on the appropriate defining line, where both ν_1 and ν_2 are zero. Figure 11 is based on calculations for $L(TDF)_{\theta=5}$; the curves are contours of constant $L(TDF)$ and are called *isotdfs* (pronunciation conjectural). As the surface passes through a vertex (i.e., through a Type II point) it becomes vertical (though the vertex itself is a singular point) and the values of $L(TDF)$ at the vertex and on the lines which define it determine which isotdfs run through it and how, as well as the gradients of the surface near the edges.

The situations at the six different vertices in Figure 11 are shown schematically in Figure 12. The $L(TDF)$ surface is seen to be two-sided in the cases of B, C, A, and D, but single-sided in the cases of G and H. For example, at vertex B one side of the vertical surface contains isotdfs between -0.85 and $+2.84$, while the other contains those between -1.02 and $+2.84$; that is, the isotdfs between -0.85 and $+2.84$ run through the vertex from two sides of an α region but those between -1.02 and -0.85 run through from only one. At a single-sided vertex like G, all isotdfs between the edge values run through once.

The cross-sections of the $L(TDF)$ - P_i surface near a given vertex along trajectories parallel to the opposite edge (i.e., P_i constant) have very similar shapes if plotted for corresponding points between the edges, as shown in Table III. One might say that third coordinate "concentration" effects are small at low third coordinate concentrations. The very steep gradients near edges DA and DC and those of quadrants I and IV show that major-coordinate effects near limiting P_i values can be large. Such high sensitivity of $L(TDF)$ to small variations in the P_i lowers the accuracy with which one can attribute an observed isotope effect to a particular reaction coordinate motion (a set of P_i) by matching results calculated at some point in the P_i plane to those observed experimentally.

Unfortunately, the set of four edge and six vertex values for $L(TDF)$ at a given temperature provide only general clues to the features of the α regions; even these clues vanish for the most part in the case of $L(TIF)$.

(8) The trajectory of the eigenvector of ν_2 is erratic near $(P_7)_2 = 0.48$ - 0.49 because of interaction in that region with a bending vibration of frequency ca. 225 cm^{-1} .

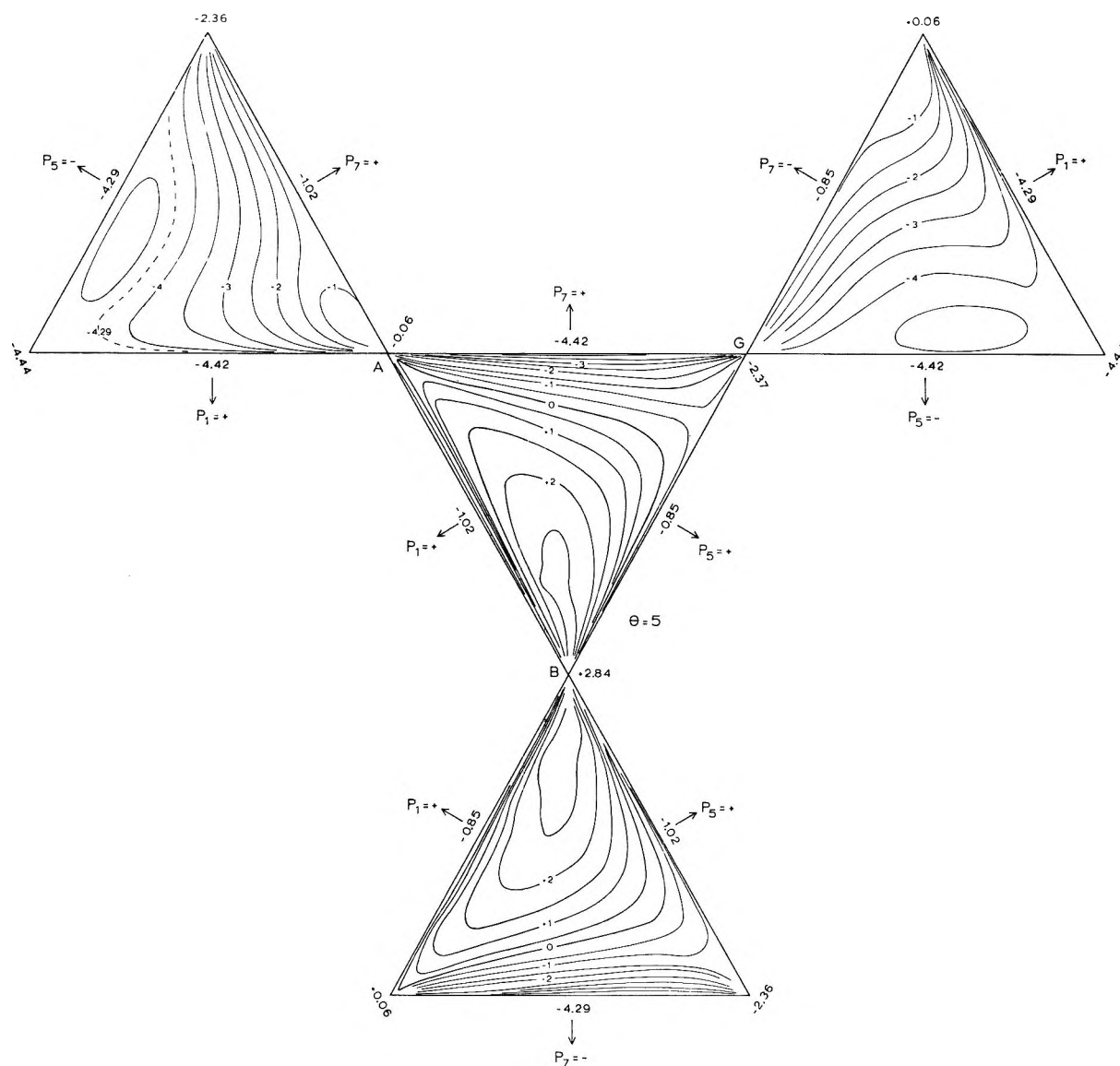


Figure 11. Map of the $L(\text{TDF})-(P_1, P_5, P_7)$ surface in the permitted α -regions at the temperature $\theta = 5$. The isotdf interval is $0.5 L$ unit. The orientation of the figure is the same as that of Figure 9.

For example, the closed isotdf for $L(\text{TDF}) = -4.50$ in quadrants $\text{II}\alpha$ and $\text{III}\alpha$ of Figure 11 could not have been predicted from the edge and vertex values of the function.

Effects of Temperature on $L(\text{TDF})$. The features of the $L(\text{TDF})-P_i$ surface and their dependence on temperature and on the input parameters for the calculations of the factors of (k/k') will depend on the triad of P_i selected for the reaction coordinate and their relative signs. As an example of temperature dependence, the surface in quadrant $\text{I}\alpha$ (P_1, P_5 , and P_7 all +) is shown in Figure 13 at integer values of θ from 1 to 5. At first glance, it appears that the general character of the surface is not altered by changes in θ ; but, closer examination shows this conclusion to be invalid with respect to a limited region near the edge BG .

The last part of Figure 13 is a superposition of the

isotdfs from the five preceding parts at $L(\text{TDF}) = 0$. These isotdfs divide quadrant $\text{I}\alpha$ into negative (at the top and a very narrow strip along AB) and positive domains. Near the edge AB and well into the mid-region of the quadrant, the isotdfs zero are essentially superimposable; (k/k') is independent of temperature and equal to TIF . But, as P_5 increases beyond 0.36, the position of the domain boundary becomes sensitive to temperature for $\theta = 1-3$. (The isotdf $L(\text{TDF}) = 0$ for $\theta = 0.5$ lies very close to that for $\theta = 1$.) Outside this range the sensitivity to temperature is almost negligible. At the higher values of θ , the zero isotdfs are again virtually superimposed for $P_7 \leq 0.3$. Thus, adjacent to the edge BG and in a roughly triangular area whose interior vertex is at $P_i = 0.23, P_5 = 0.36$, there is a region of *crossovers* in $L(\text{TDF})$; that is, an area in which the sign of $L(\text{TDF})$ is a function of θ .

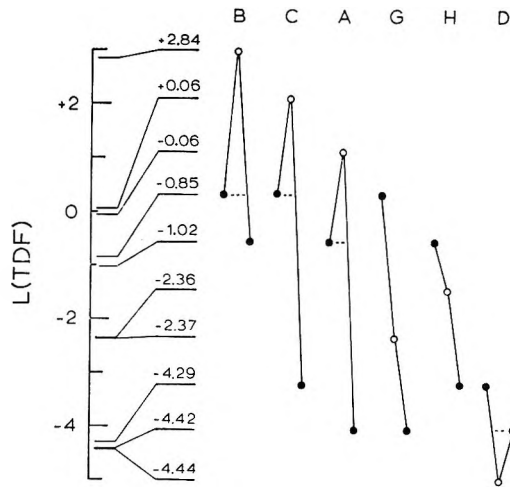


Figure 12. Characteristics of the $L(TDF)-(P_1, P_5, P_7)$ surface near the vertices of the α -regions at the temperature $\theta = 5$. (Schematic except for $L(TDF)$ scale and values.) \bullet are edge and \circ are vertex values of $L(TDF)$. The surface near B, C, A, and D is two-sided, that near G and H single-sided.

In the area, the temperature at which crossover occurs seems most sensitive to exchange in magnitude between P_1 and P_7 ; in the strip along edge AB the crossover tem-

perature is essentially independent of the value of P_1 . Elsewhere in the P_i plane $L(TDF)$ appears to be a monotonic function of temperature whose values and slopes vary with the composition of the reaction coordinate.

The $L(k/k')-P_i$ Surface. The general characteristics of the $L(TIF)-P_i$ and $L(TDF)-P_i$ surfaces are quite different in the example chosen for discussion, although certain of their symmetries are similar. A cursory examination of surfaces for some other P_i triads suggests that both the differences and the similarities are general in occurrence. Experimentally, it is $L(k/k')$ which is accessible, except in shock-tube or other very high temperature studies, and the $L(k/k')-P_i$ surfaces are those of greatest practical interest. Except at very high temperatures, the magnitude of $L(TDF)$ is much greater than that of $L(TIF)$ and one would expect the appearance of an $L(k/k')$ surface to be much like that of the corresponding $L(TDF)$ surface; however, as temperature increases, anything derived from $L(k/k')$ is increasingly reflective of $L(TIF)$.

The central portion of Figure 14 is the $L(k/k')-(P_1, P_5, P_7)$ surface in quadrant I_α at the high temperature $\theta = 1$. (The curves are contours of constant $L(k/k')$ and are called *isokrats*) Comparison of the central

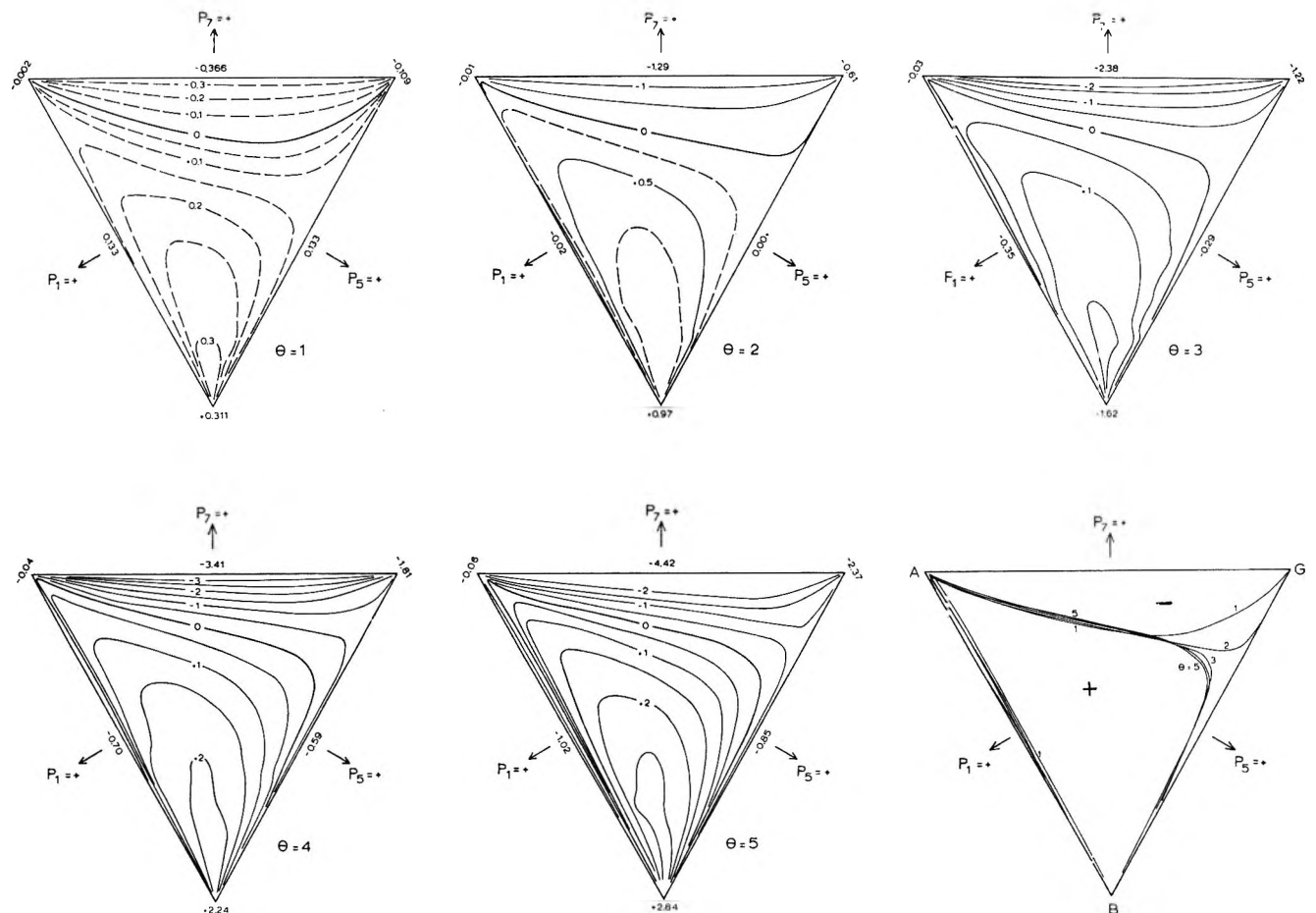


Figure 13. Effects of temperature on the $L(TDF)-(P_1, P_5, P_7)$ surface in the I_α quadrant (all $P_i = +$). Solid curves are isodfs at intervals of 0.5 L -units; dashed curves are at smaller intervals. The last part of the figure (lower right) is a superposition of the five zero isodfs from the preceding parts; all the graphs are oriented as shown for the last.

Table III: Values of $L(\text{TDF})_{\theta=5}$ in Quadrant $I\alpha$ at Corresponding Points along Several Trajectories with P_i Constant Near Vertices B and G

Near vertex B; $P_7 = \text{constant}$							
$P_7 = 0.05$		$P_7 = 0.02$		$P_7 = 0.01$		$P_7 = 0.005$	
P_5	$L(\text{TDF})$	P_5	$L(\text{TDF})$	P_5	$L(\text{TDF})$	P_5	$L(\text{TDF})$
0.45	-1.025	0.480	-1.025	0.490	-1.025	0.495	-1.025
0.46	2.008	0.484	1.968	0.492	1.954	0.496	1.947
0.47	2.768	0.488	2.761	0.494	2.757	0.497	2.755
0.48	2.693	0.492	2.729	0.496	2.739	0.498	2.743
0.49	1.846	0.496	1.904	0.498	1.921	0.499	1.929
0.50	-0.854	0.500	-0.854	0.500	-0.854	0.500	-0.854

Near vertex G; $P_1 = \text{constant}$							
$P_1 = 0.05$		$P_1 = 0.02$		$P_1 = 0.01$		$P_1 = 0.005$	
P_5	$L(\text{TDF})$	P_5	$L(\text{TDF})$	P_5	$L(\text{TDF})$	P_5	$L(\text{TDF})$
0.45	-4.423	0.480	-4.423	0.490	-4.423	0.495	-4.423
0.46	-3.126	0.484	-3.312	0.492	-3.370	0.496	-3.397
0.47	-2.296	0.488	-2.545	0.494	-2.622	0.497	-2.659
0.48	-1.668	0.492	-1.911	0.496	-1.986	0.498	-2.022
0.49	-1.177	0.496	-1.351	0.498	-1.405	0.499	-1.430
0.50	-0.854	0.500	-0.854	0.500	-0.854	0.500	-0.854

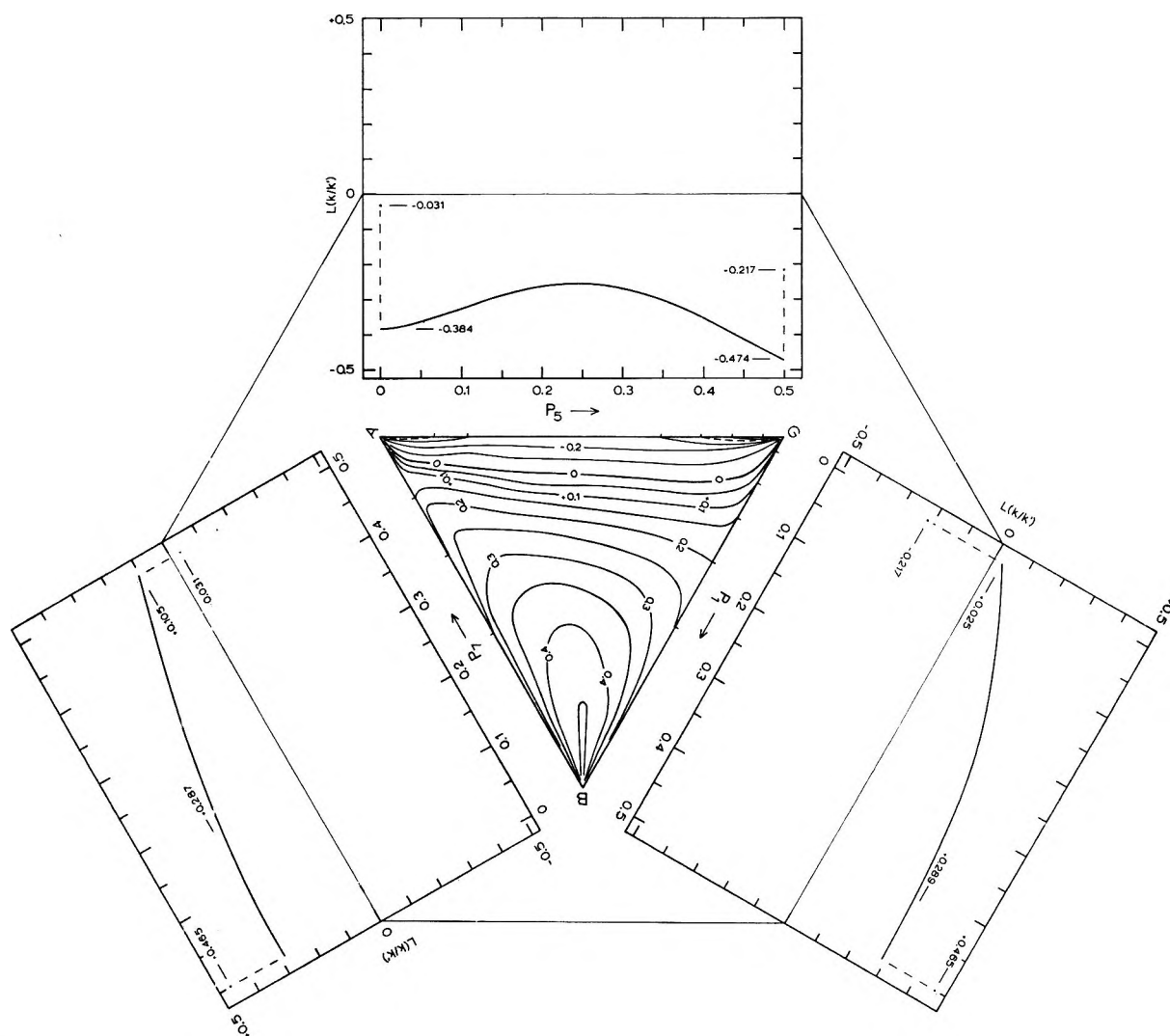


Figure 14. Map of the $L(k/k')-(P_1, P_5, P_7)$ surface in quadrant $I\alpha$ at the temperature $\theta = 1$. The isokrat interval is $0.1 L$ unit for negative values, $0.05 L$ unit for positive values; a dashed isokrat indicates placement at half the normal interval. The figure is in the same orientation as Figures 2 and 3, but the P_i scales are indicated along the edges instead of perpendicular to them. Each of the three surrounding graphs is of $L(k/k')_{\text{limit}}$ along that edge, the $P_i = 0$ and 0.5 values being shown. Dots at the ends of dashed vertical lines are Type II calculation values of $L(k/k')$ at the extremal points.

part of this figure with the $\theta = 1$ part of Figure 13 shows the significance to the former of the different gradient patterns of $L(\text{TIF})$ and $L(\text{TDF})$; the importance of $L(\text{TIF})$ wanes as θ increases.

Surrounding the central triangle in Figure 14 are plots of $L(k/k')_{\text{limit}}$ along each of its edges. At any point on the perimeter of AGB (excepting the vertices themselves), $L(k/k')_{\text{limit}}$ is the sum of the edge value of $L(\text{TDF})$ and that of $L(\text{TIF})$ obtained by extrapolation from the α region. (Because $L(\text{TDF})$ is constant along an edge, the $L(k/k')$ and $L(\text{TIF})_{\text{extrapolated}}$ curves have the same shape.) The Type II point values of $L(k/k')$ are indicated by dots connected by light dashed lines to the curves at the extremal values of the P_i . These curves and the Type II points permit ready determination of certain characteristics of the α region immediately adjacent to an edge.

As an example, consider the edge AG. In Figure 14 short ticks are placed on AG where it is crossed by the isokrats -0.35 , -0.30 , -0.30 , -0.35 , -0.40 , and -0.45 (reading left to right). One sees, then, that the isokrats between -0.031 and -0.384 run through A, those between -0.271 and -0.474 run through G, and that any isokrat equivalent to a point on the $L(k/k')_{\text{limit}}$ curve will cross the edge AG. The situations at the other edges can be handled similarly. When information from intersecting edges is combined, the properties of the surface near a vertex are completely defined; for example, isokrats between $+0.105$ and -0.384 run through A, while those between -0.474 and $+0.025$ run through G, the surface near both these vertices being single-sided. The surface is two-sided near vertex B: the isokrats between $+0.465$ and $+0.289$ pass through B twice, while those between $+0.289$ and $+0.287$ pass through it once and intersect BG.

In spite of the fact that $L(\text{TIF})$ is usually small with respect to $L(\text{TDF})$ at ordinary experimental temperatures, it seems obvious that in a given small region of P_i the $L(\text{TDF})$ and $L(k/k')$ surfaces will differ significantly in detail. As a practical matter one should probably not bother plotting the component surfaces but use those for $L(k/k')$ directly.

Effects of Force Constant Changes. Isotope effects are more sensitive to small variations in the ground state and transition state force fields than to similarly small alterations of the related geometric parameters of the models. As a consequence, force field changes are often tried first when one is attempting to bring calculated results into correspondence with experimental data.

Masses and geometries remaining unchanged, TIF will depend upon the motion selected for the reaction coordinate, here some (P_i, P_j, P_k) or (A_{i1}, A_{j1}, A_{k1}) ; it can be altered in a direct calculation by a shift in the value of any force constant F_{i1} or F_{im} provided i denotes an internal coordinate displacement which contributes to the reaction coordinate motion. TDF may be affected

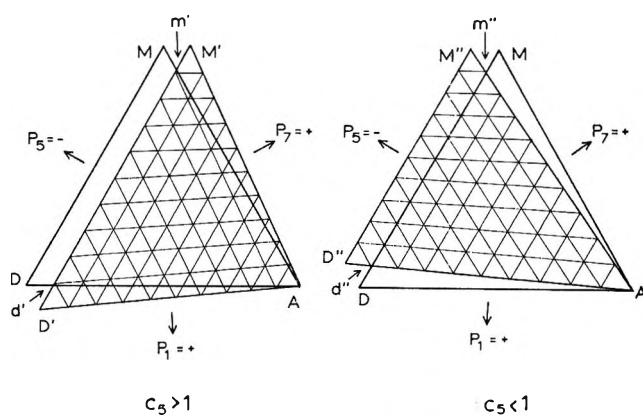


Figure 15. The transformation of the P_i plane arising from a change in the value of one diagonal force constant under conditions of invariance in the true relative motion in the reaction coordinate (A_{i1}, A_{j1}, A_{k1}) . Here, F_{55} changes and the surface is shown for region II α . The rulings are of the transformed regions $M'D'A'$ (F_{55} increased) and $M''D''A''$ (F_{55} decreased).

by a change in any F_{i1} or F_{im} , though its sensitivity to such shifts is greatest for force constants associated with internal coordinates which are isotopic between the two activated complexes, and where such effects are not internally compensated (as they are here in S_1 , for example).

Consider first the influence on the triad of P_i of changes in the diagonal force constants associated with S_i , S_j , and S_k , the internal coordinates which make up the reaction coordinate, under conditions such that the true relative motion in the reaction coordinate is unaffected. That is, we seek the transformation from the P_i associated with a given triad of F_{i1} to the P_i' associated with some $F_{i'1}$, with the A_{i1} remaining fixed. Let

$$|\sqrt{F_{i'1}}| = c_i |\sqrt{F_{i1}}| \quad (32)$$

Then

$$P_i' = \frac{c_i P_i}{(1 + \sum (c_i - 1) P_i)} \quad (33)$$

We show in Figure 15 the transcription from P_i to P_i' in the α region of quadrant II for the cases $c_5 > 1$ and $c_5 < 1$. In the case $c_5 > 1$, the original region of permitted calculations is bounded by MDA, while the increase in F_{55} yields the new permitted region $M'D'A'$; but, the actual motion in the reaction coordinate is invariant at every point in the plane. Thus, when this one force constant is raised, some reaction coordinate motions which were permitted originally become forbidden (area $MDd'm'$), while some which were forbidden turn out to be permitted (areas $AD'd'$ and $AM'm'$). The consequences are similar when $c_5 < 1$.

Direct calculation values of $L(\text{TIF})$ and $L(\text{TDF})_{\theta=5}$ in region II α are shown in the two parts of Figure 16 with the C_1 -O stretching force constant at $7.5 F_{55}'$ instead of 5.0 mdyn/\AA (F_{55}). The graphs are to be

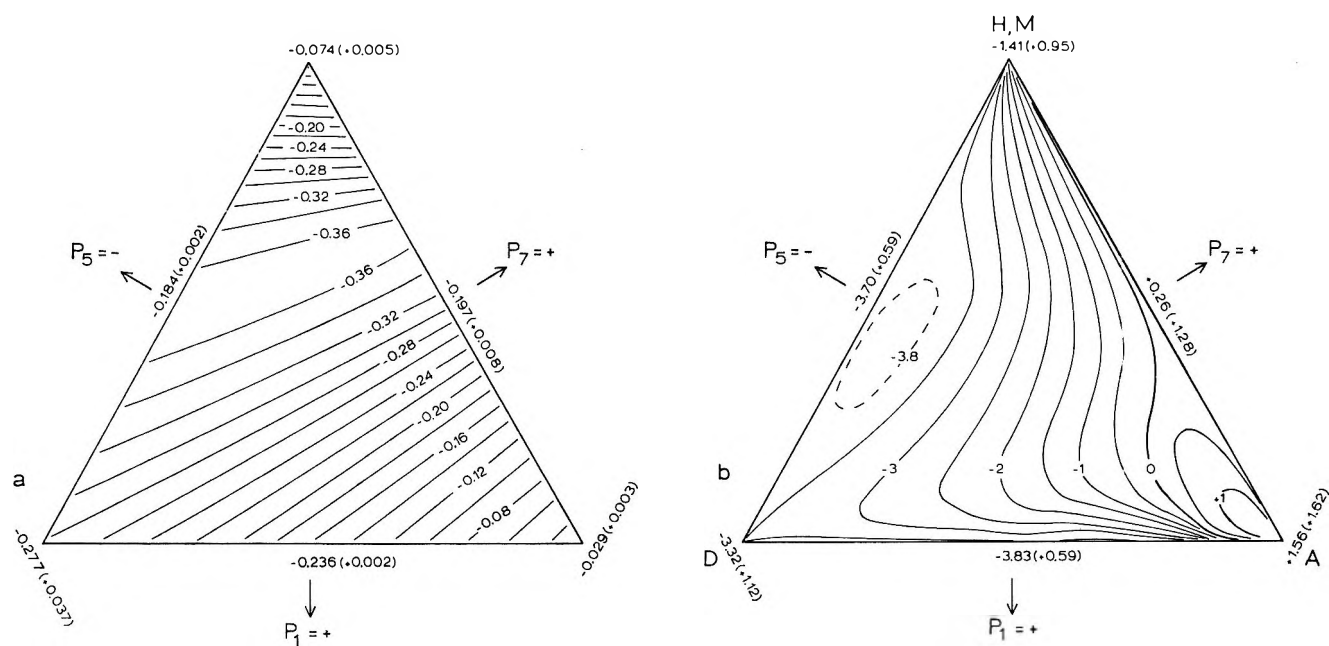


Figure 16. (a) $L(\text{TIF})$ and (b) $L(\text{TDF})$ in the α region of quadrant II, with the $C_1\text{-O}$ stretching force constant increased from 5.0 mdyne/Å to 7.5. (b) is plotted at the temperature $\theta = 5$. The figures in parentheses are the increases in vertex and edge values from those in quadrant II α of Figures 9 and 11, respectively; the isotif interval is 0.02 L unit, and the isotdf interval 0.5 L unit.

compared with corresponding areas in Figures 9 and 11, respectively. The valley in $L(\text{TIF})$ appears to be shifted towards M by the increase in F_{55} . But, application of the transformation of eq 33 to quadrant II α and its environs in Figure 9 results in part a of Figure 16. That is, the shift of the valley is real in a P_i space, which changes its relation to true relative motion as F_{it} are varied, but does not occur in an A_{it} space. $L(\text{TIF})$ depends only upon the true relative motions in the components of the reaction coordinate and not upon the force field which generates those motions.

The situation is quite different for $L(\text{TDF})$. Remarkably, though the $L\text{-}P_i$ and $L\text{-}P_i'$ surfaces differ in gradients, no major feature of the surfaces is shifted substantially in position between them. Clearly, part b of Figure 16 would not be obtained were the transformation of eq 33 applied to quadrant II α in Figure 11; among other things, that would result in the edges DA and MA being moved into the permitted region by rotation about A. Furthermore, the transformation does not affect the value of $L(\text{TDF})$ for a given (A_{i1}, A_{j1}, A_{k1}) , while it is apparent that every nonzero value of the function is affected by the shift in F_{55} . In this regard it is interesting to note that the nodal isotdf here appears to be nearly fixed on the $L\text{-}P_i$ surface, while it is movable on the $L\text{-}A_i$ surface.

Given a particular triad (i, j, k) of internal coordinates, with which to form reaction coordinates, variations in the composition of the latter determine the character of the $L(\text{TDF})\text{-}P_i$ surface much as they do the character and elevations of the $L(\text{TIF})\text{-}A_i$ surface. The elevations and gradients on the $L(\text{TDF})\text{-}P_i$ surface depend primarily on the values of

force constants associated with isotopic coordinates, but not insignificantly on the force constant of a nonisotopic or isotopically symmetric S_i which is part of the reaction coordinate.

Multiple Nonpositive Eigenvalues

The occurrence of more than one nonpositive vibrational eigenvalue at the transition state presents troublesome problems, both practical and conceptual. Formally, intersection of a pair of reaction-coordinate-like trajectories at a point on the potential energy surface implies existence of a "monkey saddle"⁹⁻¹³—in fact, one for a beast of the bicaudate type. Here, we have the situation that on a defining line there is a conjugate pair of degenerate zero frequencies; a little distance away from the line the degeneracy disappears while orthogonality and conjugacy remain. Clearly, to the degree that orthogonality obtains and the normal mode formalism is valid, the tail of one path is not accessible from the leg of the other (and vice versa). That is, this circumstance does not comprise a model for competing reaction pathways.

Aside from this not very satisfying point, one must naturally express concern in such a situation for the postulates of the transition-state theory itself. Physically, a related problem arises when force field manip-

(9) E. Kreysig, "Differential Geometry," University of Toronto Press, Toronto, 1959; pp 136-138.

(10) And, only formally, because a true monkey saddle cannot exist on a quadratic surface,¹¹ barring accommodation to genetic¹² or surgical caudia.

(11) Marcus¹³ mentions a type of exception inapplicable here: a triangular activated complex for the reaction $A + A_2 \rightarrow A_2 + A$.

(12) T. von Katz, *Ann. Mus. Felis*, 78, 122 (1801).

(13) R. A. Marcus, *J. Chem. Phys.*, 41, 610 (1964).

ulations yield an acceptable transition state (one zero or negative eigenvalue) one or more of whose genuine vibrations are very low in frequency and composed of displacements which could lead to chemical change.

One can side-step these conceptual problems and solve the practical one in the present examination of three-element reaction coordinates simply by establishing an *avoidance zone* near the edges of the α regions and of such width that a motion, X_2 , conjugate to that in the assumed reaction coordinate, X_1 , has a frequency ν_2 which is not the lowest among the set of real frequencies. In the example chosen for discussion in this paper, oxalic acid decomposing *via* $X_1 = (P_1, P_5, P_7)_1$, and at the level of force constant ratios displayed in Table II, this avoidance zone would be about 0.02 P unit wide. This would not impose a very severe limitation on one's exploration of the effects of reaction coordinate variations. Happily, adoption of this side-step eliminates from consideration the troublesome extreme gradient areas on the $L(\text{TDF})-P_i$ surface (see Figure 11) found near the edges of the α regions. The conceptual problems are worthy of more detailed consideration than they seem to have received.

Conclusion

This research has explored the effects of variations in

the composition of three-element reaction coordinates on the values of the temperature-dependent and temperature-independent factors in intramolecular rate constant ratios. Limitations on the contribution of any of the three component internal coordinate displacements have been established so that there is but one zero eigenvalue (and none negative) in the transition state. In turn, symmetrizing of these limitations permits the results of calculations on models to be displayed in a form convenient for guiding such studies. As in a previous report,² effects of force constant and temperature variations were investigated also and found to be something less than straightforward.

Intermolecular isotope effects may be expected to have properties different from those of intramolecular isotope effects, and these remain to be attacked, as do bending motion and bending force constant effects, selection of imaginary (instead of zero) frequencies for the reaction coordinate motion, etc. Although the task of exploring the isotope effects of even a simple reaction appears to be immense, this research has demonstrated a number of approaches which can simplify systematic inquiry considerably.

Acknowledgment. This research was supported by the U. S. Atomic Energy Commission, COO-1142-80.

Absorption Spectrum and Decay Kinetics of O_2^- and HO_2 in Aqueous Solutions by Pulse Radiolysis¹

by Joseph Rabani

Department of Physical Chemistry, The Hebrew University, Jerusalem, Israel

and Sigurd O. Nielsen

*Department of Chemistry, Danish Atomic Energy Commission, Research Establishment, Risø, Denmark
(Received February 18, 1969)*

The absorption spectrum and decay kinetics of O_2^- radical ions have been investigated in H_2O_2 and $H_2 + O_2$ solutions by the method of pulse radiolysis. The peak absorption at 2400–2450 Å has an extinction coefficient of $1970 M^{-1} cm^{-1}$. In the pH range ~5 to 9.7, optical absorption assigned to O_2^- was observed. The decay of O_2^- absorption is consistent with $k_{(HO_2+O_2^-)} = 7.9 \times 10^7 M^{-1} sec^{-1}$, and $k_{(O_2^-+O_2^-)} < 10^5 M^{-1} sec^{-1}$. In the pH range below 5, absorption due to HO_2 was also observed. The extinction coefficient of HO_2 at 2400 Å was measured and equals $1150 M^{-1} cm^{-1}$. Using both our own data and those of Bielski and Schwarz recently reported results, we could account for both sets of data with $k_{(HO_2+HO_2)} = 6.7 \times 10^5 M^{-1} sec^{-1}$. Both kinetic and spectroscopic results indicate that the pK of HO_2 radicals may be slightly higher than the previously reported value of 4.5, namely 4.8.

Introduction

The absorption spectra and decay kinetics of HO_2 and O_2^- have been investigated previously. Czapski and Dorfman² reported optical absorptions due to HO_2 and O_2^- , in pulse radiolysis of acid and near neutral solutions, respectively. In alkaline solutions they reported a relatively long-living optical absorption with a spectrum indistinguishable from O_2^- but with lifetimes and decay kinetics that were different from those expected for O_2^- . This absorption was attributed to O_4^{2-} or O_2^{2-} . Adams, Boag, and Michael³ supported the suggestion made before by Baxendale⁴ that O_2^- decays away by the reaction with HO_2 , except at relatively low or relatively high pH's, where radicals of the same type interact. (HO_2 with HO_2 or O_2^- with O_2^- at low and high pH's, respectively.) Gordon, Hart, and Thomas⁵ investigated the optical absorption of HO_2 and the rate of formation of HO_2 from hydrogen atoms and O_2 . Bielski and Schwarz⁶ investigated the decay of HO_2 and O_2^- in the acid pH range.

Despite the extensive work done on HO_2 and O_2^- , many features of the system remain unsolved. There is no agreement between different authors concerning rate constants, extinction coefficients, and ratios of rate constants to extinction coefficients in either acid or neutral pH ranges. The situation is even more complex in the alkaline pH range, where new intermediates have been invoked to explain the system.²

The main purpose of this work was to investigate the spectrum and decay kinetics of O_2^- , particularly in near neutral and slightly alkaline solutions. We used solutions of H_2 and O_2 , to convert all the radical species obtained in the pulse-irradiated solutions into

HO_2 and O_2^- within a few microseconds. Our system has the advantage of being relatively simple, because reactions due to OH, O^- or to intermediates formed from OH and O^- (other than HO_2 or O_2^-) can be neglected. Possible complications due to such reactions are thus avoided. In some experiments H_2O_2 solutions were used as a source of O_2^- radical ions. The spectrum of O_2^- in such solutions was identical with the spectrum obtained in the $H_2 + O_2$ solutions, as will be shown later. This spectrum, together with revised extinction coefficients of O_2^- and our new kinetic data have made it possible for us to present a reaction mechanism which accounts for our observations in the whole pH range studied from 2.0 to 9.7, without the need to invoke other light-absorbing species other than HO_2 and O_2^- .

Experimental Section

The linear accelerator at Risø was used as an electron pulse source. The pulsing technique, syringe filling, pulsed Xe lamp, the optical and electronic detection system, and pressure cell were described previously.⁷ A 7.1 cm long cell was used for all the H_2

(1) The experimental part of this work was carried out at Risø under the auspices of the Danish Atomic Energy Commission and the Danish-Swedish pulse radiolysis project operated jointly with AB Atomenergi, Sweden.

(2) G. Czapski and L. M. Dorfman, *J. Phys. Chem.*, **68**, 1169 (1964).

(3) G. E. Adams, J. W. Boag, and B. D. Michael, *Proc. Roy. Soc.*, **A289**, 321 (1965).

(4) J. H. Baxendale, *Radiat. Res.*, **17**, 312 (1962).

(5) S. Gordon, E. J. Hart, and J. K. Thomas, *J. Phys. Chem.*, **68**, 1262 (1964).

(6) B. H. J. Bielski and H. A. Schwarz, *ibid.*, **72**, 3836 (1968).

+ O_2 experiments. A 2.54 cm long cell with an optical path of 5.08 cm was used for the experiments with H_2O_2 solutions.

H_2 was purified as described before.⁷ The solution was introduced into the cell under an O_2 atmosphere, using a continuous flow of O_2 through the cell. Special precautions were taken while adding the high-pressure H_2 (up to 50 atm) to avoid compression of more O_2 from the filling system. This was done by pumping the filling system before the H_2 was added. The actual pressure of O_2 in the pressure cell after equilibration with 50 atm of H_2 was 1 atm.

H_2O_2 , Analar grade, was used without further purification. In some experiments, H_2O_2 was prepared by pulsing a neutral solution saturated with N_2O ⁸ in the absence of an irradiated gas phase to avoid contamination from possible radiation products in the gas phase. For this purpose, syringes containing water were saturated with N_2O . After removing the gas phase, the solutions were cooled to about 0° in order to increase gas solubility and prevent irradiation gas products from escaping out of the solution. Electron pulses were given, until the total irradiation dose was about 1 Mrad. During the irradiation, the electron beam was scanned so that all the volume of the syringes was homogeneously irradiated. After the end of the irradiation, we usually found one small bubble of 1–2 mm diam in each syringe due to gaseous products formed by the irradiation (H_2 , O_2 , and N_2). These bubbles were probably not present during the irradiation, but were slowly formed and increased with post-irradiation time. Except for gaseous products which can easily be removed, our "self-made" H_2O_2 solutions should be of extremely high purity. The pulse radiolytic results obtained in these solutions were identical with those obtained in solutions of Analar grade H_2O_2 . The concentration of H_2O_2 obtained using a total dose of about 1 Mrad was about 1 mM. Oxygen, 99.7% pure, was normally used after passing through an NaOH solution and through triply distilled water. In some cases, O_2 was prepared by the reaction of Ce^{4+} with H_2O_2 . All other chemicals used were of analytical grade and used without further purification. Stock solutions of 20 M NaOH were used for the preparation of alkaline solutions. The temperature was about 24° in all the experiments.

All the solutions containing H_2O_2 were analyzed to determine the exact concentration of H_2O_2 at the time of the pulse. Occasional measurements of optical transmission were made at 4300 \AA , especially at pH 13, in order to find the fraction of oxidizing radicals which reacted with O_2 (formed by the decomposition of H_2O_2) rather than with H_2O_2 . The method for analysis of H_2O_2 and of correcting for O_3^- formation were described previously.⁹

Since the method used for pressure cell filling is time consuming, we used to irradiate each pressurized solu-

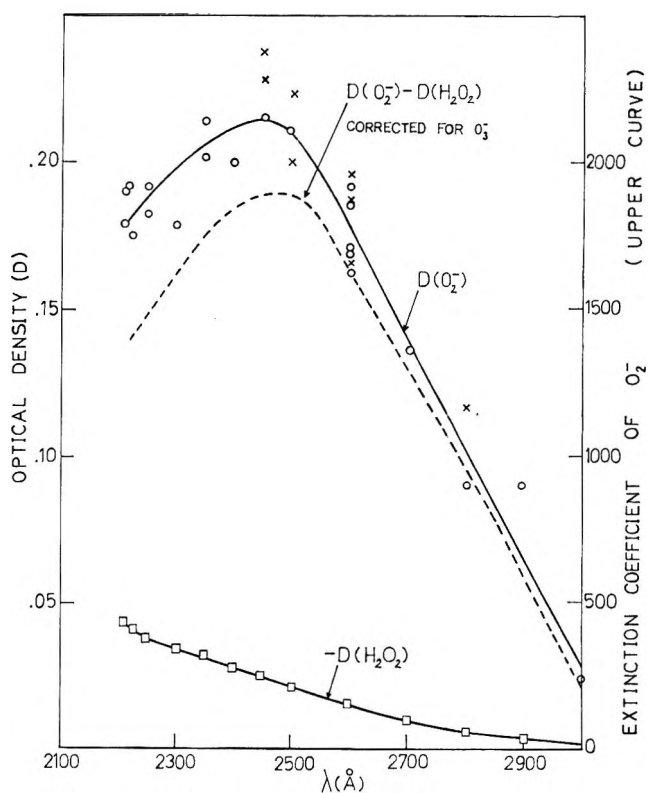


Figure 1. Spectrum of O_2^- in N_2O -saturated H_2O_2 solutions, 40 μ sec after the electron pulse: \circ , \square , pH 12.98 [H_2O_2] = $3 \times 10^{-4} M$, made by irradiation of N_2O solutions; pulse duration, 1 μ sec; total ($[OH] + [O^-]$) formed by the electron pulse was $2.20 \times 10^{-6} M$; dotted line, experimental optical density corrected for a small amount (less than 10%) of O^- and OH which reacted with O_2 and formed O_3^- . The O_3^- absorption was disregarded. \square , calculated absorption decreased due to H_2O_2 disappearance; $G(-H_2O_2) = 4.5$ was used; \circ , corrected spectrum of O_2^- . Use the scale to the right that represents the extinction coefficient of O_2^- , taking $G(O_2^-) = 5.4$. \times , corrected spectrum of O_2^- (use scale to the left) at pH 12.98, using [H_2O_2] = $8.3 \times 10^{-4} M$ (Analar grade), saturated N_2O , at 1 atm, ($[OH] + [O^-]$) = $4.04 \times 10^{-6} M$. D values multiplied by 4.65. Pulse duration was 0.7 μ sec. The electron beam was scattered by a thin aluminum plate. The normalization factor of 4.65 is somewhat lower than the dose factor of 5. This agrees with $G(O_2^-) = 5.8$ in these solutions compared with $G(O_2^-) = 5.4$ estimated for the results with $3 \times 10^{-4} M H_2O_2$. See further explanation in the text.

tion with several electron pulses (up to 25 pulses of 1- μ sec duration or their equivalent). Each solution was checked for the effect of accumulated radiation products by comparison of the kinetics and initial absorptions of the first and last pulses. No radiation product effect could ever be detected, and the last

(7) (a) P. Pagsberg, H. Christensen, J. Rabani, G. Nilsson, J. Fenger, and S. O. Nielsen, *J. Phys. Chem.*, **73**, 1029 (1969); (b) H. Christensen, G. Nilsson, P. Pagsberg, and S. O. Nielsen, *Rev. Sci. Instrum.*, **40**, 786 (1969).

(8) We wish to thank Mr. P. Pagsberg for suggesting this method for the preparation of H_2O_2 solutions.

(9) J. Rabani, *Advances in Chemistry Series*, No. 81, American Chemical Society, Washington, D. C., 1968, p 131.

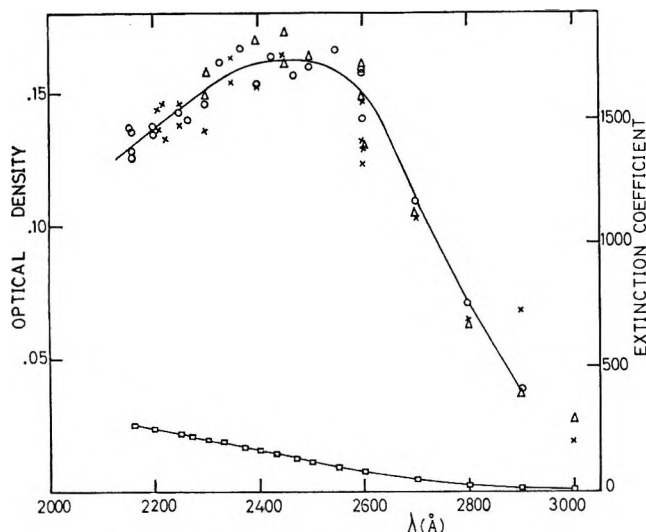


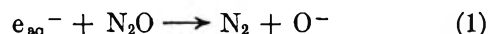
Figure 2. Spectrum of O_2^- in N_2O -saturated H_2O_2 solutions: \circ , corrected spectrum of O_2^- . (Use scale to the right); $1\text{-}\mu\text{sec}$ pulse with a dose of 2.38×10^{20} eV/l. per pulse. $[H_2O_2] = 6.4 \times 10^{-4} M$. (H_2O_2 made by irradiation of N_2O solutions); pH 11.50. \square , calculated decrease of absorption due to H_2O_2 disappearance. ($G(-H_2O_2) = 4.52$ was used); pH 11.50. Δ , corrected spectrum of O_2^- , (use scale to the left), using $8.3 \times 10^{-4} M$ H_2O_2 (Analar grade), $0.7 \mu\text{sec}$ pulses, with an intensity of 4.75×10^{19} eV/l. per pulse (with scatter plate); pH 11.48, calculated D values multiplied by 4.13. The normalization factor, 4.13, was used instead of the dose factor of 5 due to differences in $G(O_2^-)$ values. See text for further explanation. \times , corrected spectrum of O_2^- (use scale to the left), at pH 13 taken from Figure 1. The corrected D values were multiplied by 0.76. The factor of 0.76 is due in part to differences in $G(O_2^-)$. There is also probably an insignificant difference of about 10% in the absorption of O_2^- which is higher at pH 13 than at pH 11.5. Note: the scales on the right of Figures 1 and 2 give the extinction coefficient for the corrected O_2^- spectrum.

pulse always gave results identical with the first pulse within experimental error.

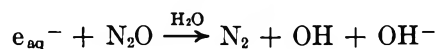
Results

(a) *The Absorption Spectrum of O_2^- Radical Ions in H_2O_2 Solutions.* In Figures 1 and 2 we present the optical absorption obtained in H_2O_2 solutions, saturated with 1 atm of N_2O , at pH 11.50 and 12.98. The same results were obtained no matter whether H_2O_2 self-prepared by irradiation or Analar grade H_2O_2 was used.

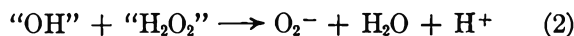
Under our conditions, reaction 1



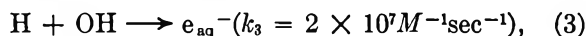
or



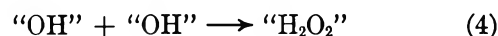
suggested first by Dainton and Peterson,¹⁰ leads to the formation of OH or O^- in much less than $1 \mu\text{sec}$. The evidence for the quick formation of OH (or O^-) is summarized in a previous paper.¹¹ OH (or O^-) radicals react quickly with hydrogen peroxide and form O_2^- radical ions by reaction 2.



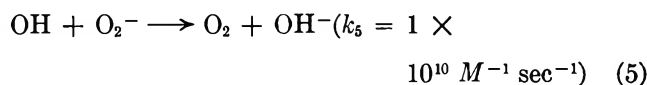
We use the quotation notation to indicate that the reaction may involve species equivalent to OH (*i.e.*, O^-) and H_2O_2 (*i.e.*, HO_2^-). At pH 13, H atoms are quickly converted to e_{aq}^- according to reaction 3.¹²



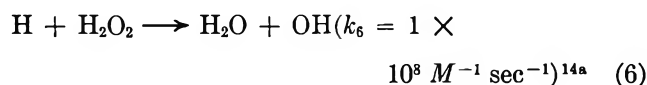
Therefore, at pH 13, if no radical radical reactions (" OH " + " OH " and " OH " + O_2^-) were involved, $G(O_2^-) = G_e + G_H + G_{OH} = 5.8$, and $G(-H_2O_2) = G_e + G_H + G_{OH} - G_{H_2O_2} = 5.1$. These conditions are valid for the experiments described in Figure 1 (crosses). Other experiments represented in Figure 1 were carried out with a relatively low H_2O_2 concentration and a higher ($\times 5$) pulse intensity. Under such conditions we expect some radical-radical reactions to take place, especially reaction 4 ($2k_4/2$ is of the order of $10^9 M^{-1} \text{sec}^{-1}$ at pH 13¹³).



For these experiments with low H_2O_2 concentration and high pulse intensity, $G(O_2^-) = 5.4$ and $G(-H_2O_2) = 4.6$ were estimated 40 μsec after the pulse. The excellent agreement (shown in Figure 1) between both sets of results at pH 13 obtained, at two pulse intensities differing by a factor of 5, justifies the neglect of radical-radical reactions other than reaction 4 such as



At pH 11.5 corrections for competing reactions are more important. Using the set of low-intensity experiments (Figure 2, triangles), we estimated $G(O_2^-) = 5.6$ and $G(-H_2O_2) = 5.5$. The relatively high $G(-H_2O_2)$ is due to the reaction of H atoms with H_2O_2 according to reaction 6.



For the set of data with higher intensities (Figure 2), $G(O_2^-) = 4.62$ and $G(-H_2O_2) = 4.52$ were computed, using the above given mechanism, and the following additional reactions and rate constants: $k_{("OH" + "H_2O_2")}^{19} = 2.2 \times 10^9$, $2k_{(H+H)} = 1.6 \times 10^{10}$,^{14b} $2k_{("OH" + "OH")}^{13} = 1.1 \times 10^{10}$, $k_{(H+OH)}^{14c} = 2 \times 10^{10} M^{-1} \text{sec}^{-1}$.

(10) F. S. Dainton and D. B. Peterson, *Nature*, **186**, 878 (1960).

(11) J. Rabani, "Radiation Chemistry of Aqueous Systems," Stein, Ed., The Weizmann Science Press of Israel, Jerusalem, 1968, p 229.

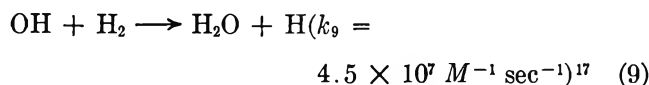
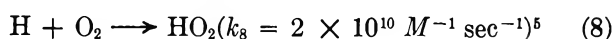
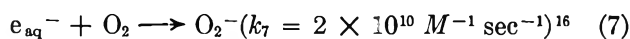
(12) (a) J. Rabani, *Advances in Chemistry Series*, No. 50, American Chemical Society, Washington, D. C., 1965, p 242; (b) G. Stein, "Hydrogen-Bonded Solvent Systems," A. K. Covington and P. Jones, Ed., Taylor and Francis Ltd., London, 1968, p 87.

(13) J. Rabani and M. S. Matheson, *J. Phys. Chem.*, **70**, 761 (1966).

(14) (a) J. P. Sweet and J. K. Thomas, *ibid.*, **68**, 1363 (1964); (b) S. O. Nielsen, P. Pagsberg, J. Rabani, H. Christensen, and G. Nilsson, *Chem. Commun.*, 1523, (1968); (c) H. A. Schwarz, *Radiat. Res. Suppl.*, **4**, 89 (1964).

Since the radical combination was relatively small, the error in the computed $G(\text{O}_2^-)$ value is not large, perhaps not more than 5%. The extinction coefficient of O₂⁻, $\epsilon_{\text{O}_2^-}$, was obtained with the aid of the ferrocyanide dosimeter ($10^{-3} M$ ferrocyanide, N₂O saturated, irradiated at the same pulse intensities and pH's as the H₂O₂ solutions; initial D values were taken for the dosimetry and were assumed not to be affected by reduction of ferricyanide by H). We can assume that the primary yields in the H₂O₂ solutions and dosimeter solutions were equal. The absolute values of the yields are not important for the evaluation of $\epsilon_{\text{O}_2^-}$, because only the ratios of G values in H₂O₂ and in the dosimeter solutions were used.

(b) *The Absorption Spectrum of O₂⁻ in H₂ + O₂ Solutions.* When appropriate concentrations of H₂ and O₂ together are present in an aqueous solution, H atoms and e_{aq}⁻ react with O₂ to form HO₂ and O₂⁻, respectively, and OH radicals react with H₂ to form H. The relative concentrations of HO₂ and O₂⁻ are determined by the pH of the solutions, the pK of HO₂ reported as 4.5.¹⁵⁻¹⁸



Under our conditions, using one atmosphere of O₂ and 45 atm of H₂, reactions 7, 8, and 9 are practically the only reactions by which the radical species OH, H, and e_{aq}⁻ disappear. The result of reactions 7, 8, and 9 is the conversion of all the radicals formed by the radiation into O₂⁻ and HO₂. $G(\text{O}_2^- + \text{HO}_2) = G_{\text{H}} + G_{\text{e}} + G_{\text{OH}}$. The optical density (D) scale in Figure 3 can be easily converted into an extinction coefficient scale. This is done by dividing D of Figure 3, curve a, with $C \times l = 8.2 \times 10^{-6} \times 7.1 = 5.8 \times 10^{-5}$ (for pH 9.7) and dividing D of Figure 3, curve c, with $C \times l = 6.8 \times 10^{-6} \times 7.1 = 4.8 \times 10^{-5}$. Calculated extinction coefficients of O₂⁻ at 2400, 2450 (the peak), and 2600 Å are given in Table I.

Table I: Extinction Coefficients of O₂⁻ at 2400, 2450, and 2600 Å

pH	System	Extinction coefficients at ^a		
		2400 Å	2450 Å	2600 Å
Near neutral ^b	H ₂ + O ₂	1860	1860	1550
Near neutral ^c	H ₂ + O ₂	1990	2020	1760
7.12 (phosphate)	H ₂ + O ₂	1930	1930	1650
9.7 (NaOH)	H ₂ + O ₂	2000	2000	1720
11.5 (NaOH)	H ₂ O ₂	1710	1720	1600
13 (NaOH)	H ₂ O ₂	2120	2150	1760

^a In units of $M^{-1} \text{cm}^{-1}$. ^b Taking $\text{p}K_{\text{HO}_2} = 4.45$. ^c Taking $\text{p}K_{\text{HO}_2} = 4.80$.

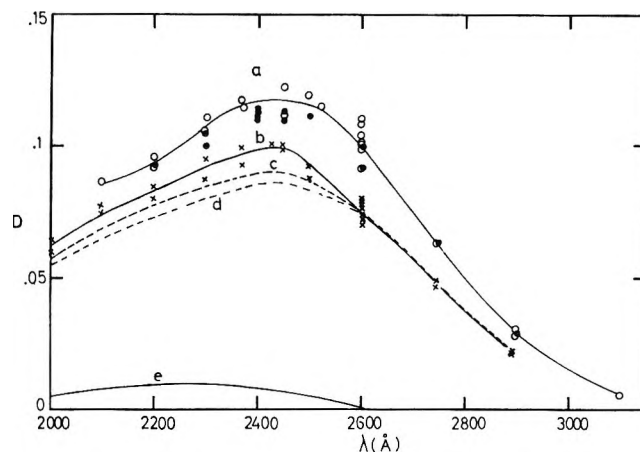


Figure 3. Spectrum of O₂⁻ obtained in H₂ + O₂ solutions, 10 μsec after the electron pulse; 1 atm of O₂ and 45 atm of H₂; light path, 7.1 cm; total ([HO₂] + [O₂⁻]) = $8.2 \times 10^{-6} M$ based on initial $G(\text{ferrocyanide}) = 5.8$ in neutral, N₂O saturated (at 1 atm) $10^{-3} M$ ferrocyanide, and $G([\text{HO}_2] + [\text{O}_2^-]) = 5.8$ in the H₂ + O₂ systems; curves b, c, and d coincide above 2600 Å. (a) Spectrum of O₂⁻ at pH 9.7 and pH 7.13 (pH is before the 1-μsec pulse). The result at 2100 Å was corrected for disappearance of OH⁻ (D was raised by 0.007 unit); O, pH 9.7; ●, pH 7.13, phosphate buffer (see Table II). (b) Spectrum at near neutral conditions of the equilibrium mixture of O₂⁻ and HO₂ (was neutral before the electron pulse). If $\text{p}K_{\text{HO}_2} = 4.45$, the pH of this solution is 5.17, [O₂⁻] = $6.8 \times 10^{-6} M$ and [HO₂] = $1.4 \times 10^{-6} M$. If $\text{p}K_{\text{HO}_2} = 4.80$, [O₂⁻] = $6.0 \times 10^{-6} M$ and [HO₂] = $2.2 \times 10^{-6} M$. (c) Spectrum of $6.8 \times 10^{-6} M$ O₂⁻ at pH 5.17 obtained from (b) by subtracting the absorption of HO₂. (d) Spectrum of $6.0 \times 10^{-6} M$ O₂⁻ at pH 5.22 obtained using the results of (b) taking $\text{p}K_{\text{HO}_2} = 4.8$. (e) The absorption of $1.4 \times 10^{-6} M$ HO₂.^{7a} This absorption was subtracted from curve b to give curve c.

(c) *Kinetics between pH 2 and pH 9.7.* A typical oscilloscope trace, showing the formation and decay of O₂⁻ is shown in Figure 4. In the upper trace (fast sweep) we observe the increase of optical density with a half-life of about 1 μsec. This is longer than the half-life of about 0.5 μsec expected for reaction 9 under our conditions. We suppose that this observation is due to the dissociation of HO₂ to give O₂⁻. O₂⁻ has a greater absorption than has HO₂ at 2400 Å (see below). The half-life of the spontaneous ionization of HO₂ may well be about 1 μsec. At pH 2, under similar conditions to Figure 4, the building up of optical density is very fast and is lacking the tail at the end with $t_{1/2} \cong 1 \mu\text{sec}$ which we see in Figure 4. This is expected below the pK of HO₂. As no appreciable dissociation of HO₂ to form O₂⁻ takes place at pH 2, no tail is observed in the buildup of optical density. Experiments at other

(15) K. Sehested, O. L. Rasmussen, and H. Fricke, *J. Phys. Chem.*, **72**, 626 (1968).

(16) S. Gordon, E. J. Hart, M. S. Matheson, J. Rabani, and J. K. Thomas, *J. Amer. Chem. Soc.*, **85**, 1375 (1963).

(17) H. A. Schwarz, *J. Phys. Chem.*, **66**, 255 (1962).

(18) J. Rabani, W. A. Mulac, and M. S. Matheson, *ibid.*, **69**, 53 (1965).

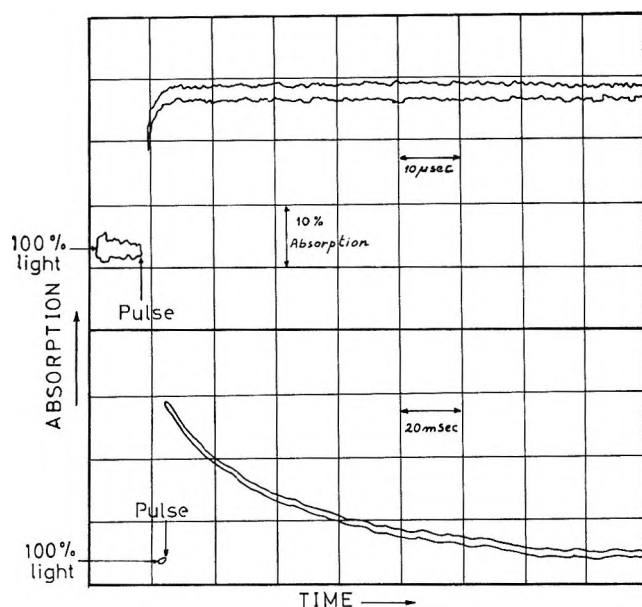


Figure 4. Formation and decay of O_2^- at 2400 \AA . Both traces were recorded with the same $1\text{-}\mu\text{sec}$ pulse; 42 atm of H_2 and 1 atm of O_2 ; pH (before pulse) = 6.65 ($3 \times 10^{-4} M$ NaH_2PO_4 and $1 \times 10^{-4} M$ Na_2HPO_4); light path, 7.1 cm .

pH values than 2 and 6.5, using various buffers, $HClO_4$, and $NaOH$ for the control of pH are in agreement with above considerations.

The decay of optical density was always observed to be much slower than its formation and could easily be separated from the formation and analyzed. A plateau is observed in Figure 4, upper trace, after about $5 \mu\text{sec}$ or more. In all the kinetic work described here, the plateau optical densities of the traces taken with $10 \mu\text{sec}/\text{div}$ sweep rates were equal to the initial optical densities of the decay traces recorded in the milliseconds to seconds time ranges (e.g., Figure 4, lower trace). In addition, the optical absorption appeared to decay away to zero in one stage. We conclude that one reaction or several reactions occurring simultaneously are responsible for the decay of the optical density. No conversion of the initially formed equilibrium mixture of O_2^- and HO_2 into other intermediates could be observed by means of the time dependency of the optical density. These comments and conclusions are valid for the entire pH ranges investigated (pH 2–9.7). The same features were found for other wavelengths in the range $2100\text{--}3000 \text{ \AA}$, whenever a full spectrum has been taken. At 2000 \AA we observed sometimes different kinetics in the $10 \mu\text{sec}/\text{div}$ pictures. This could be explained by the optical absorption of OH^- , but a detailed investigation of this observation is beyond the scope of this paper.

The features described above and demonstrated by Figure 4 are valid for all the experiments in which decay kinetics were observed, irrespective of whether the decay was first or second order, and independent of the pulse intensity. The decay kinetics were usually

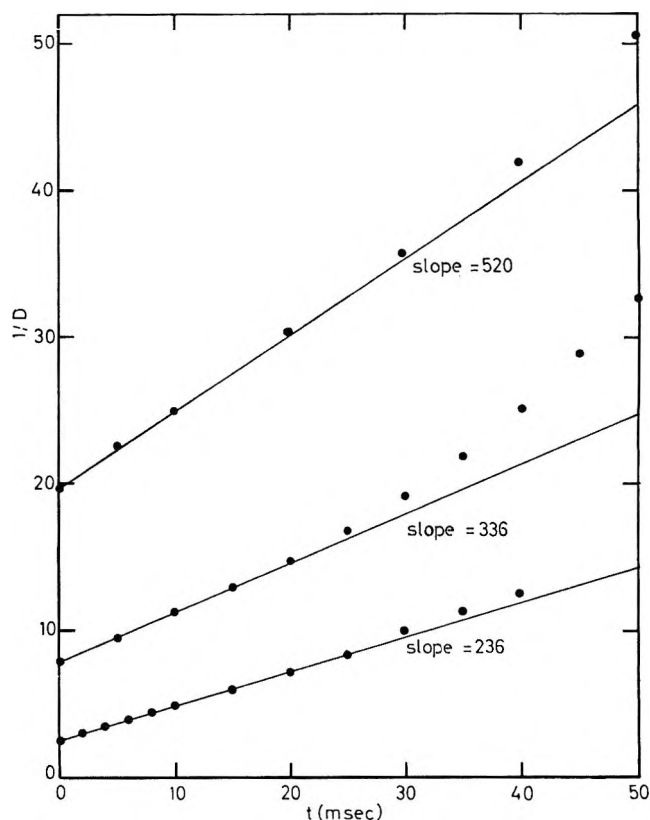


Figure 5. Second-order test of the decay of O_2^- . Conditions as in Figure 4. Intensity varied by changing the pulse duration from ~ 0.5 to $\sim 3 \mu\text{sec}$.

intermediate between second and first order. Three different pulse intensities were always used. The relative contribution of the first order component decreased with increasing dose per pulse. Typical second-order plots, i.e., $1/D$ vs. t plots, are shown in Figure 5. The pulse intensities used in Figure 4 are also typical for all other pH 's used. It can be seen that deviations from a straight line occur more rapidly at lower pulse intensities. In addition, the initial slopes of the $1/D$ vs. t curves decrease with increasing intensity. However, by varying the pulse intensity almost tenfold, the initial slope varied by only a factor of about 2. This dependency on pulse intensity is typical for the case when both first- and second-order reactions take place simultaneously. The relative contribution of the first-order reaction depended not only on the pulse intensity but also on pH . Thus, sometimes a tenfold change in intensity gave up to about fourfold change in initial $d(1/D)/dt$. In general, the higher the pH , the greater was the relative contribution of the first-order component.

With a single solution or with identical solutions irradiated on the same day, the reproducibility was excellent. However, sometimes a solution known to give mainly second-order kinetics showed first-order kinetics. Whenever this happened, the first-order decay was much faster than the mixed second- and

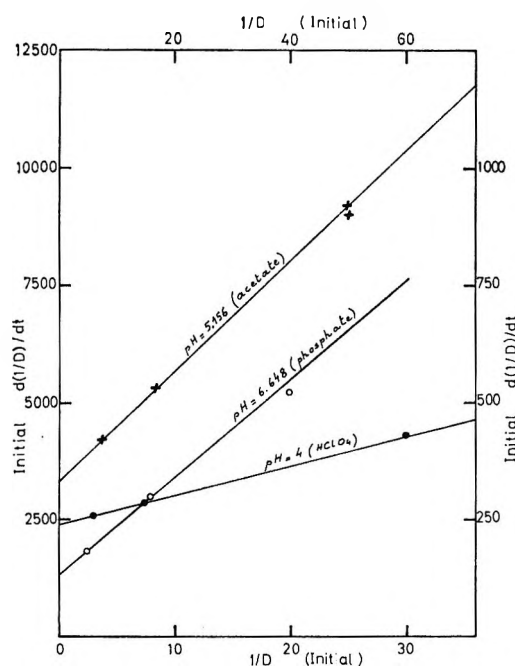


Figure 6. Demonstration of the separation into second- and first-order components (see text): \times , lower and left scales; \bullet , upper and left scales; \circ , lower and right scales.

first-order decays. We have found that by cleaning the valves in the pressurized H_2 system from traces of brass powder, slowing down the rate of H_2 flow through the molecular sieve, and extracting the membrane filter with water, the decay of optical density slowed down and was found to possess the relatively small first-order component mentioned above. The cleaning of O_2 did not have any effect on the results. The same results were obtained with O_2 taken directly from the gas cylinder as with O_2 that had first passed through a bubbler containing $NaOH$ and then through water, or with O_2 made in a glass container from solutions of Ce^{4+} and H_2O_2 . On the basis of these results, indicating that impurities were responsible for the first-order reactions, we have disregarded all the experiments in which the decay of D was only first order with no second-order component.

It can be shown that when second-order and first-order reactions take place simultaneously, *e.g.*



and when only A absorbs light, eq 12 describes the dependency of the slopes of $1/D$ vs. t curves on D .

$$d(1/D)/dt = 2k_{(A+A)}/(\epsilon_A \times l) + k_{(A \rightarrow p)}/D \quad (12)$$

D is the optical density of the species A . $k_{(A+A)}$ is the reaction rate constant of the bimolecular reaction. $k_{(A \rightarrow p)}$ is the reaction rate constant of the unimolecular (or pseudo-first-order) reaction in sec^{-1} . ϵ_A is the extinction coefficient of A .

In order to determine $2k_{(A+A)}$ and $k_{(A \rightarrow p)}$, we plotted the initial slopes of the $1/D$ vs. t curves against the initial $1/D$. At almost all pH's we had three points lying exactly on one straight line. When the three points were not exactly on a straight line, we used the two points which correspond to the higher intensities. These points are more reliable for the evaluation of the second-order component. In Figure 6 we demonstrate the use of the above method for the calculation of $2k_{(A+A)}$ and $k_{(A \rightarrow p)}$ in the O_2^- systems. The examples chosen for Figure 6 are typical, although in a few experiments the three points deviated appreciably from a straight line.

The initial $d(1/D)/dt$ values at the medium and highest pulse intensities have been corrected for changes in pH induced by the electron pulse. The method used for these corrections will be described later. The corrected $k_{(A+A)}$ and $k_{(A \rightarrow p)}$ are presented in Table II. It was shown by computation that they could account reasonably well for the experimental points in Figure 5.

The change of pH induced by the electron pulse was taken into account in the data treatment demonstrated in Figure 6. The change was calculated for each experiment from the pK of the acid used for the buffer, the buffer concentration, and the optical absorption after the pulse. For each O_2^- ion present, there is an H^+ ion formed. Thus, the initial values of $1/D$, from which $(^{\cdot}HO_2 + ^{\cdot}HO_2)$ was calculated, were measured at pH values smaller than those indicated in Figure 6 and Table II. All the results of figures such as 5 were normalized as explained below to the pH before the pulse. The calculations show that experiments with the lowest pulse intensities needed no correction. With respect to the medium pulse intensities ($8-9 \times 10^{19}$ eV l^{-1} per pulse), the changes in pH's 9.7, 8.12, 7.60, 7.12, 6.65, 6.12, 5.16, 4.61, 4.52, 4.00, and 2.00 were 0.07, 0.03, 0.05, 0.06-0.08, 0.05, 0.03-0.05, 0.08, 0.06, 0.05, 0.00, and 0.00, respectively. For the highest pulse intensities the pH decreased by 0.21, 0.115, 0.16, 0.21-0.24, 0.20, 0.13-0.15, 0.16, 0.17, 0.15, 0.0, and 0.00, respectively, for the same pH's. The corrections were done by making appropriate changes in the experimental initial $d(1/D)/dt$ measured from plots similar to those given in Figure 5 before using it for plots of the type given in Figure 6. At pH 2 and 4, the change in pH by the electron pulse was neglected and therefore no corrections were made. In the pH range above 6, $k_{(^{\cdot}HO_2 + ^{\cdot}HO_2)}$ is proportional to $[H^+]$. At the higher pulse intensities we have found that the initial $d(1/D)/dt$ values were also roughly proportional to $[H^+]$ and this relation was used for the pH corrections in this pH range. At pH 4.6 to 5.2, $k_{(^{\cdot}HO_2 + ^{\cdot}HO_2)}$ (and initial $d(1/D)/dt$ values) were found to be practically independent of pH, and hence no pH correction was applied for the results at pH 5.16 (see Table II). At pH near 4.5, $d(1/D)/dt$ increases with pH but the

Table II: Second- and First-Order Components as a Function of pH^a

pH ^b = - log [H ⁺]	Buffer	$k_{("HO_2" + "HO_2")}$, $M^{-1} \text{ sec}^{-1}$	$k_{("HO_2" \rightarrow p)}$, ^c sec^{-1}	$\epsilon \times l$, M^{-1}	Total dose $\text{eV} \times l^{-1} \text{ per pulse}$ $\times 10^{-10}$ ^e
2.00	$10^{-2} M \text{ HClO}_4$	8.1×10^5	3-8	8,200 ^f	0.34-2.8
4.00	$10^{-4} M \text{ HClO}_4$	1.05×10^7	30-45	8,900	0.23-2.9
4.52	$3 \times 10^{-5} M \text{ HClO}_4$	2.0×10^7	60	9,950	1.0-2.3
4.61	$2 \times 10^{-4} M \text{ CH}_3\text{CO}_2\text{H} +$ $1 \times 10^{-4} M \text{ CH}_3\text{CO}_2\text{Na}$	1.9×10^7	23	9,950	0.23-2.8
5.16	$1 \times 10^{-4} M \text{ CH}_3\text{CO}_2\text{H} +$ $2 \times 10^{-4} M \text{ CH}_3\text{CO}_2\text{Na}$	1.83×10^7	90-230	11,700	0.35-2.8
6.12	$1 \times 10^{-3} M \text{ NaH}_2\text{PO}_4 +$ $1 \times 10^{-4} M \text{ Na}_2\text{HPO}_4$	3.0×10^6	40-90	14,000	0.22-3.2
6.65	$3 \times 10^{-4} M \text{ NaH}_2\text{PO}_4 +$ $1 \times 10^{-4} M \text{ Na}_2\text{HPO}_4$	9.5×10^5	20	14,000	0.35-3.0
7.12	$1 \times 10^{-4} M \text{ NaH}_2\text{PO}_4 +$ $1 \times 10^{-4} M \text{ Na}_2\text{HPO}_4$	2.1×10^5	11	14,000	0.17-2.9
7.60	$1 \times 10^{-4} M \text{ NaH}_2\text{PO}_4 +$ $3 \times 10^{-4} M \text{ Na}_2\text{HPO}_4$	1.2×10^5	3.6	14,000	0.37-3.7
8.12	$1 \times 10^{-4} M \text{ NaH}_2\text{PO}_4 +$ $1 \times 10^{-3} M \text{ Na}_2\text{HPO}_4$	4.2×10^4	4	14,000	0.77-2.6
9.7	$5.0 \times 10^{-5} M \text{ NaOH}$	1.1×10^3	2×10^{-3}	14,000	2.1-3.5

^a Most of the three sets of pulse intensities presented in this table at each pH were duplicated. Only average values are given here. Whenever two duplicate sets gave different values of $k_{("HO_2" \rightarrow p)}$, both values were included. Values of $k_{("HO_2" + "HO_2")}$ from different experiments were the same for a given pH, within experimental error, and only average values were included in the table. ^b pH before the pulse, calculated from the buffer concentrations using pK values tabulated in the "Handbook of Chemistry and Physics," 43rd ed, 1961-62. ^c The quotation marks were used to emphasize that the appropriate reactions may involve species equivalent to HO_2 (e.g., O_2^-) and not necessarily HO_2 radicals as such. $k_{("HO_2" + "HO_2")}$ is obtained from figures similar to Figure 6, multiplying each intercept by the appropriate $\epsilon \times l/2$. ^d The extinction coefficients used here were calculated from experimental values of D obtained at the various pH's, by comparison with the optical densities at pH > 6 obtained with the same pulse intensities. The wavelength was 2400 Å. $\epsilon_{O_2^-} = 1970 M^{-1} \text{ cm}^{-1}$ at 2400 Å. $l = 7.1 \text{ cm}$ for all the experiments. $G_{(HO_2 + O_2^-)} = 5.8$ was used for the entire pH range 4 to 9.7. ^e ~ 0.25 , ~ 1 , and ~ 3 - μsec pulses have been used with $\sim 250 \text{ mA}$ peak current. ^f $G(HO_2) = 6.2$ was used at pH 2.

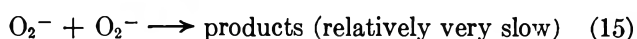
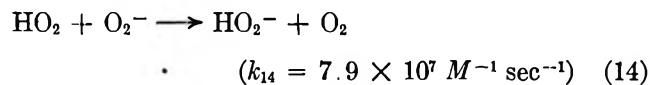
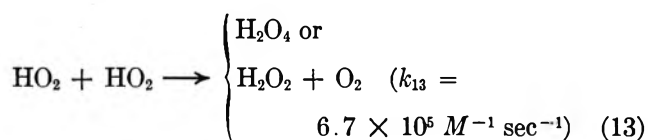
increase in $d(1/D)/dt$ is smaller than the change in $[H^+]$. Corrections were made by extrapolation making use of the experiments at pH 4.

Discussion

(a) *The Absorption Spectrum of O_2^- .* We found the same absorption spectrum in near neutral, (pH 7.12, phosphate buffer) and slightly alkaline (pH 9.7, NaOH) solutions of $H_2 + O_2$. This spectrum is identical with that we observed in N_2O saturated H_2O_2 solutions at pH 11.5 and 13. We attribute this absorption as being due to O_2^- radical ions as such. In Table I, we summarize some extinction coefficients for direct comparison. Our results disagree with a previous suggestion⁹ that " O_2^- " produced by the reaction of e_{aq}^- (and H) with O_2 differs in alkaline solutions from " O_2^- " produced by the oxidation of hydrogen peroxide by hydroxyl radicals. We have no explanation for the differences between our $\epsilon_{O_2^-}$ and values reported previously.^{2,6,9} Each experiment in Table I represents an average of several independent experiments and independent dosimetry has been carried out at most pH's. In addition, in our experiments there were relatively slow changes of optical density with time, once OH and H radicals had reacted and equilibrium between HO_2 and O_2^- had been obtained. This is an advantage

compared with some of the previous work where extrapolation to zero time was made from fast decays.

(b) *Kinetics.* We propose the following mechanism to account for the effect of pH on the decay of O_2^- and HO_2



This mechanism leads to the expression

$$k_{("HO_2" + "HO_2")} = k_{(HO_2 + HO_2)} \times 1/(1 + K/[H^+])^2 + k_{(HO_2 + O_2^-)} \times (1/(1 + K/[H^+]))(1/(1 + [H^+]/K)) \quad (16)$$

where $k_{("HO_2" + "HO_2")}$ is the apparent rate constant for the decay of the equilibrium mixture of HO_2 and O_2^- and K is the dissociation constant of HO_2 defined as $[H^+][O_2^-]/[HO_2] = K$.

Taking $pK_{HO_2} = -\log K = 4.80$ and $k_{(HO_2 + HO_2)} =$

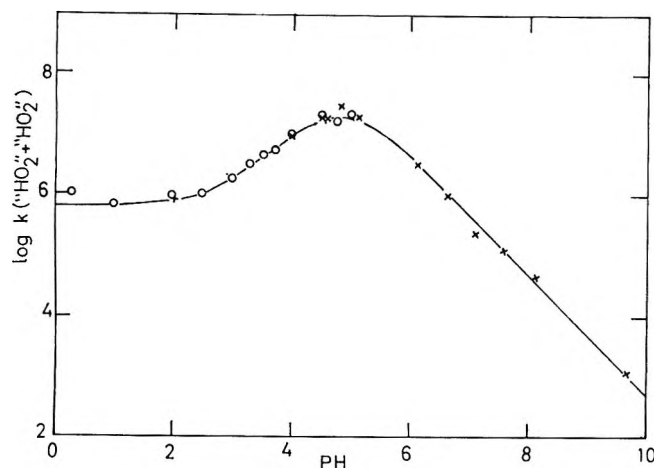


Figure 7. Test of the mechanism for the decay of O_2^- absorption. The line was calculated using $pK_{HO_2} = 4.80$, $k_{(HO_2 + HO_2)} = 6.7 \times 10^5$ and $k_{(HO_2 + O_2^-)} = 7.9 \times 10^7 M^{-1} sec^{-1}$; X, results of this paper; O, results of Bielski and Schwarz⁶ recalculated using $\epsilon_{HO_2} = 1150$ and $\epsilon_{O_2^-} = 1970 M^{-1} cm^{-1}$.

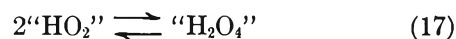
$6.7 \times 10^5 M^{-1} sec^{-1}$, the value for $k_{(HO_2+O_2^-)} = (7.7 \pm 0.4) \times 10^7 M^{-1} sec^{-1}$ could be calculated as an average from the results of Table II (with a maximum deviation $4.4 \times 10^7 M^{-1} sec^{-1}$ and a standard deviation of $0.4 \times 10^7 M^{-1} sec^{-1}$). The value of $k_{(HO_2+O_2^-)}$ so obtained depends very little on the value taken for $k_{(HO_2+HO_2)}$ because reaction 13 is not important in most of the pH range that we investigated. If $pK_{HO_2} = 4.45$, $k_{(HO_2+O_2^-)} = 1.3 \times 10^8 M^{-1} sec^{-1}$ results. However, the deviation of $k_{(HO_2+O_2^-)}$ values, found at different pH values, is much larger if $pK = 4.45$ is chosen, especially in the pH range 4–5. If the results of Bielski and Schwarz⁶ (recalculated using our ϵ_{HO_2} and $\epsilon_{O_2^-}$) are treated similarly, the best fit to their data is obtained with $k_{(HO_2+HO_2)} = 6.7 \times 10^5 M^{-1} sec^{-1}$ and $k_{(HO_2+O_2^-)} = (8.0 \pm 0.3) \times 10^7 M^{-1} sec^{-1}$ (maximum deviation $2.9 \times 10^7 M^{-1} sec^{-1}$), taking again $pK_{HO_2} = 4.80$. If $k_{(HO_2+HO_2)} = 8.4 \times 10^5 M^{-1} sec^{-1}$ is chosen, an average value of $k_{(HO_2+O_2^-)} = 7.4 \times 10^7 M^{-1} sec^{-1}$ results, but with a greater deviation. In Figure 7, the pH dependency of $k_{(HO_2+HO_2)}$ is presented. The curve to fit the experimental points was calculated, taking $pK = 4.80$, $k_{(HO_2+HO_2)} = 6.7 \times 10^5$ and $k_{(HO_2+O_2^-)} = 7.9 \times 10^7 M^{-1} sec^{-1}$. It can be seen that both Bielski and Schwarz's⁶ results, as well as our own, lie on the same calculated curve. It should be noted that if $pK_{HO_2} = 4.45$ had been chosen for HO_2 , we would have been unable to fit Bielski and Schwarz's⁶ results together with ours, using only one set of parameters, $k_{(HO_2+HO_2)}$ and $k_{(O_2^-+HO_2)}$.

(c) *Reaction Mechanisms.* Bielski and Schwarz⁶ assumed that reaction 15, $O_2^- + O_2^- \xrightarrow{2H^+} H_2O_2 + O_2$, proceeds with a rate constant of $1.2 \times 10^7 M^{-1} sec^{-1}$. We have shown that Bielski and Schwarz's results can be interpreted without assuming reaction 15. From

our own data, $k_{15} < 10^5 M^{-1} sec^{-1}$ results. It is probable that k_{15} is even smaller than $10^3 M^{-1} sec^{-1}$ but a value of $1.1 \times 10^3 M^{-1} sec^{-1}$ for $k_{(HO_2+HO_2)}$ (at pH 9.7) was obtained only in one set of experiments. (Other sets gave faster and first-order decays at pH 9.7). Therefore we hesitate to rely on the results obtained at pH 9.7.

Czapski and Dorfman² suggested O_2^{2-} or O_4^{2-} formed by disproportionation or combination of two O_2^- radical ions, respectively, in order to account for the first-order rate law observed by them in alkaline solutions. Our results indicate that the system is very sensitive to impurities, and that the first-order decay observed by Czapski and Dorfman² may perhaps be due to impurity catalysis of the decay of O_2^- . These authors have also shown that the results in the alkaline pH range were not very reproducible.

The mechanism proposed, reactions 13–15, accounts for our kinetic results. In reaction 13 H_2O_2 and O_2 may be formed by direct H transfer or *via* H_2O_4 as an intermediate. Although the O–O bond energy in H_2O_2 is reported to be 45–50 kcal/mol,¹⁹ it is not certain whether H_2O_4 is stable with respect to dissociation into two HO_2 radicals.²⁰ In analogy with H_2O_3 ,⁶ H_2O_4 may be expected to have only a weak absorptivity in the far-ultraviolet region, and its presence should not affect the present spectrophotometric determinations of HO_2 . In reaction 14 HO_2^- and O_2 may be formed by direct electron transfer from O_2^- to HO_2 , or hydrogen peroxide and oxygen may be formed *via* a HO_4^- intermediate that, if this were the case, either did not show strong light absorptivity or was present in only small concentrations relative to "HO₂." This conclusion follows from the observed, approximate second-order kinetics of decay of "HO₂" to zero concentration which, furthermore, rules out the situation where reaction 16 is in rapid equilibrium



maintaining $["HO_2"] / ["H_2O_4"] \approx 1$. Reaction 15 was found to be relatively slow. The reason for the low reactivity of $O_2^- + O_2^-$ may be connected with the difficulty of forming the double-charged O_2^{2-} ion in electron transfer, with the instability of O_4^{2-} with respect to dissociation into two O_2^- radical ions and with the inability of O_4^{2-} to transform into O_2 and hydrogen peroxide. Such a transformation should involve an unlikely intramolecular electron transfer to an O atom which is bound to a negatively charged O atom in the

(19) V. I. Vedeneyev, L. V. Gurvich, V. N. Kondrat'yev, V. A. Medvedev, and Ye. L. Frankevich, "Bond Energies, Ionization Potentials and Electron Affinities," Edward Arnold Ltd., 1966, p 76.

(20) (a) I. I. Skorokhodov, L. I. Nekrasov, L. A. Reznitskii, K. G. Khomyakov, and N. I. Kobozev, *Zh. Fiz. Khim.*, **33**, 2090 (1959); (b) S. W. Benson, *J. Chem. Phys.*, **33**, 306 (1960); (c) D. A. Csejka, F. Martinez, J. A. Wojtowicz, and J. A. Zaslowsky, *J. Phys. Chem.*, **68**, 3878 (1964); (d) M. Venugopalan and R. A. Jones, "Chemistry of Dissociated Water Vapor and Related Systems," Interscience Publishers Inc., New York, N. Y., 1968, p 418.

O_4^{2-} ion. The high value of k_{14} relative to k_{13} and k_{15} is in agreement with both inter- and the intramolecular electron transfer mechanisms for reaction 14. In the second case, HO_4^- is formed at equilibrium with O_2^- and HO_2 . The negative charge is transferred to the H-O-O part of the HO_4^- ion before it breaks into HO_2^- and O_2 .

(d) *pK of HO_2* . Our results show a better fit using $pK_{HO_2} = 4.80$ rather than the previously published value 4.45. In order to check this point further, we used optical density data in the pH range 4-5 and cal-

culated the *pK* of HO_2 in a way similar to that described by Czapski and Dorfman.² This involved the comparison of optical densities obtained after 10 μ sec in the $H_2 + O_2$ systems using constant pulse intensities and varying the pH. The effect of HO_2 dissociation on the pH was taken into account. Using $\epsilon_{O_2^-} = 1970 M^{-1} cm^{-1}$ and $\epsilon_{HO_2} = 1150 M^{-1} cm^{-1}$, both at 2400 \AA , we obtained the results presented in Table III.

The average pK_{HO_2} resulting from Table III is 4.78 ± 0.20 ; 0.20 is the estimated standard error. This value is not beyond the error limits of previously reported values. It has the advantage that it fits our kinetic data. Since the previous value of 4.4-4.5 was found by four independent groups, further work needs to be done to find pK_{HO_2} with higher precision.

Acknowledgment. We wish to thank the Risø Linac group for careful operation of the linear accelerator, and Mrs. J. Eriksen and Messrs. P. Genske and F. Said for invaluable technical assistance. The authors are indebted to Dr. H. A. Schwarz of Brookhaven National Laboratory and Professors G. Czapski and G. Stein for valuable comments.²¹

(21) NOTE ADDED IN PROOF. After this paper was submitted, further work on HO_2 and O_2^- was carried out at the Hebrew University of Jerusalem by D. Behar, G. Czapski, L. M. Dorfman, J. Rabani, and H. A. Schwarz. Pulse radiolysis of the formate oxygen aqueous system (no other buffers) confirmed our results showing similar kinetics and pH effects. The *pK* of HO_2 in the formate system was found to be 4.88 ± 0.10 at 27.5°. Careful experiments in oxygenated water gave $pK_{HO_2} = 4.8$.

Table III: Evaluation of pK_{HO_2} by the "Titration" Method

pH ^a	$D/D_{(O_2^-)}$ ^b	pK_{HO_2}
3.90	0.62	4.82
4.00	0.65	4.70
4.38	0.71	4.73
4.44	0.70	4.82
4.47	0.71	4.82
4.55	0.76	4.67
4.98	0.81	4.87
5.00	0.83	4.83
5.07	0.81	4.98
5.07	0.90	4.57
		Average 4.78

^a After the 1- μ sec electron pulse; 7.1-cm light path. ^b 10 μ sec after the electron pulse. We used the average optical density (0.140) at pH 6-9.7 for $D_{(O_2^-)}$.

The Apparent Molal Volumes of the Lithium and Sodium Halides.

Critical-Type Transitions in Aqueous Solution

by Fred Vaslow

Chemistry Division, Oak Ridge National Laboratory,¹ Oak Ridge, Tennessee 37830 (Received February 19, 1969)

Measurements of the apparent molal volumes of LiCl, LiBr, LiI, NaCl, NaBr, and NaI have been made with primary emphasis on obtaining precise values of $\Delta\phi_v/\Delta\sqrt{c}$ at small intervals. Most results were at 25°, a few at 5°, and one at 35°. For LiBr, LiI, NaBr, and NaI, the curves of $\Delta\phi_v/\Delta\sqrt{c}$ vs. \sqrt{c} appear to be discontinuous in a form suggesting a λ -shaped region for the integral curve or inverted for NaBr. Different series of measurements with LiI gave the apparent discontinuity at different concentrations and one of the four LiI runs did not show the apparent discontinuity. For NaCl the existence of a singularity is not definite and LiCl showed no sign of a singularity. It is suggested that these singularities are due to a new kind of transition of the critical type in the solution. Two possible sources of the transition are either in a change of solution structure as previously suggested or in a change in form of the ion radial distribution function as found by Kirkwood.

Introduction

In previous work^{2,3} the apparent molal volumes of the alkali chlorides were studied in order to test whether seemingly abrupt transitions in the slopes of the apparent molal volume (ϕ_v) vs. (\sqrt{c}) curves could be confirmed and related to physically significant transitions of the solutions. In ref 2 (I) a mathematical description of the curves for LiCl and NaCl in terms of two segments and a transition region appeared to have tentative validity but definitive proof could not be obtained. In ref 3 (II) more precise data on LiCl were obtained and confirmed that mathematically the two segment description was definitely valid but the existence of a physical transition was not necessarily proven.

The present paper is a continuation of the earlier work in which as in II, emphasis is placed on the highest possible relative precision of the measurements with somewhat relaxed requirements on the absolute precision. Mainly, this implies a somewhat greater uncertainty in the absolute concentration of the solutions than previously obtained.

The salts studied were the chlorides, bromides, and iodides of Li and Na at 25° with a few results at 5° and one at 35°.

Experimental Section

The apparatus and technique were essentially the same as previously described,^{2,3} *i.e.*, a differential density balance with 450-cc fused quartz floats is used. The principal change is that the loose fitting teflon covers for the solution and reference containers were replaced by all-glass ground joint covers with a one-mm diameter hole for the support wire as the only unsealed opening. A substantially improved control of dust and evaporation was obtained.

In view of the high precision claimed, some further details of the technique should be given. Freshly boiled

triply distilled water from the same container is used to fill the reference and solution containers and to prepare the stock solutions. After adding water to the containers, the liquid surface of each is swept with the tip of a pipet, taking up about 20 cc and removing dust and surface-active material. The process is repeated just before measurements are to begin, and also the surface of the stock solution is swept before use.

Samples of stock solution are added with Carlsberg constriction type pipets. For concentrations above 0.1 *N* the size generally used was 17 cc and held 20 to 25 gm of stock solution, the weights before and after addition being recorded to 0.1 mg. A number of precautions were taken to prevent evaporation from the various containers during transfer operations.

After additions of stock solution, the containers were stirred for 15 min and then readings taken for 50 min before more stock was added. The balance readings generally remained constant after 30 min.

The balance (Ainsworth type TY) with floats in place had a sensitivity of 4 to 6 divisions per mg and the reproducibility was 0.5 division or better. Readings were taken by allowing the balance to come to rest from 0 and repeating the measurement with the rest point on the other side of 0 by adding or subtracting 0.4 or 0.5 mg. The needle generally came to rest within 5 min. Rest points were recorded to 0.1 division and weights calculated to 0.01 mg \pm 0.03 below 0.1 *N* and to 0.1 mg above. Weights of the individual supports and floats as well as the zero point with both floats were checked in each series of measurements.

Except for the NaI, the chemicals were prepared from reagent grade carbonates by adding the appropri-

(1) Research sponsored by the U. S. Atomic Energy Commission under contract with Union Carbide Corporation.

(2) F. Vaslow, *J. Phys. Chem.*, **70**, 2286 (1966).

(3) F. Vaslow, *ibid.*, **71**, 4585 (1967).

ate acid and recrystallizing. Purity was checked by flame-photometer analysis and less than 0.1% total alkaline earths and foreign alkali were found for any salt. The NaI was commercial reagent grade and assayed about 99.9% by comparison with single-crystal KI using differential potentiometric titrations. Li solutions were analyzed by titration only, with Na salts being analyzed by evaporation and weighing as well. Satisfactory titrations for iodides could be obtained by raising the final temperature to about 90°.

Errors in ϕ_v have been considered as in I following the equation of Redlich and Bigeleisen⁴

$$\delta\phi_v = -\frac{1000 \delta d}{d^{\circ}c} + \frac{1000(d - d^{\circ})\delta c}{c}$$

where $\delta\phi_v$, δd , and δc are the uncertainties in volume, density and concentration, d° the density of pure water, d the solution density and c the concentration. The uncertainty in ϕ_v (i.e., $\delta\phi_v$) for $\delta c/c = 10^{-4}$ is about 0.007, 0.01, 0.006, and 0.008 cc for NaBr, NaI, LiBr, and LiI, respectively, with an uncertainty in the absolute value of c of about $\pm 0.05\%$. The uncertainty in density is taken as ± 0.1 mg on the balance corresponding to $\delta\phi_d = \pm 0.0002$ cc at 1 N and varying as $1/c$. In the present work, analyses were made after the first or second addition of stock solution and every 10 additions thereafter. The concentrations for all points of the run were calculated from the first analyses and subsequent additions and removals of solution. The agreements of calculated concentrations with the results of later analyses were within 0.02%.

Errors in the $\Delta\phi_v/\Delta\sqrt{c}$ curves depend only in a minor way on the absolute values of c but do depend on the relative precision of the points and on the size of the $\Delta\sqrt{c}$ interval. The error in $\Delta\sqrt{c}$ is essentially negligible and the main uncertainty is in $\Delta\phi_v$. For most runs c was varied by about 0.1 unit at a time and $\Delta\sqrt{c}$ varied approximately as $1/\sqrt{c}$. Since most of the interest of the curves centers about $c = 1$, the explicit calculation of uncertainties will be given for this concentration where $\Delta\sqrt{c}$ is about 0.05. While the full and empty weights of the stock solution pipet are recorded to 0.1 mg, a somewhat larger uncertainty seems reasonable and ± 0.3 mg is taken as the uncertainty in the weight of a single addition of stock solution. Since the error in $\Delta\phi_v$ depends on two successive additions or $\sqrt{2} \delta c$, a relative error in weight of about ± 0.5 mg can be considered. This uncertainty in weight corresponds to 1 part in 40,000 for the amount of stock solution added and since at 1 N the addition is about one tenth of the total salt, a relative uncertainty of about 1 part in 400,000 for the total concentration. The corresponding concentration dependent uncertainties in $\Delta\phi_v/\Delta\sqrt{c}$ are ± 0.002 , 0.005, 0.006, 0.004, 0.006, and 0.008 slope units for LiCl, LiBr, LiI, NaCl, NaBr, and NaI, respectively.

The relative uncertainty in the density measurement

for two successive measurements is about $\pm 0.1 \sqrt{2}$ mg on the balance corresponding for all salts to about ± 0.006 in $\Delta\phi_v/\Delta\sqrt{c}$ at 1 N and for NaI the combined uncertainty $\sqrt{\delta\phi_v^2 + \delta\phi_d^2}$ is about ± 0.01 . Examination of the $\Delta\phi_v/\Delta\sqrt{c}$ curves given in the next section indicates that the above estimate of uncertainty is reasonably consistent with the average deviation of the points from a smooth curve. At lower concentrations, the density error causes the uncertainty in ϕ_v to increase as $1/c$ and as 0.1 N is approached it becomes difficult to obtain coherent curves for $\Delta\phi_v/\Delta\sqrt{c}$. Above 1 N the computed errors are about the size of the symbols on the figures and not specifically indicated. Below 1 N the computed error at the anomaly is indicated by a vertical bar through one of the adjacent points.

For low and moderate concentrations, the differential method minimizes the effect of temperature fluctuations and at 25° they are apparently not serious. At other temperatures, temperature control is a serious problem, and this as well as mechanical difficulties with condensation and evaporation make satisfactory results much more difficult to obtain. In particular, satisfactory results for NaCl at 35° could not be obtained probably due to the large temperature coefficient of ϕ_v for NaCl.

Results

A summary of the results for ϕ_v as a function of rounded values of m are given in Table I. These values were obtained by interpolation on large scale graphs using french curves to draw smooth lines through the points.⁵ The values for \bar{V}_0 are obtained by integration of the slope curves between $\sqrt{c} = 0.25$ and 0 and subtracting the integral from the value of ϕ_v at $\sqrt{c} = 0.25$. A smooth curve was drawn between the lowest measured point for the slope and the theoretical limiting values.⁶ As noted before, the major uncertainty in ϕ_v and \bar{V}_0 is in the uncertainty in the absolute value of the concentration.

The results for NaBr may be compared with the precise data of Geffken and Price⁷ using the magnetic float and of Geffken, Kruijs, and Solana⁸ using the dilatometer. Above about 0.25 N there is precise agreement of results; below, however, there is a progressive discrepancy reaching a maximum at $c = 0$ of about 0.09 cc, the present results being larger. The nature and size of the discrepancy is very similar to that previously reported² for KCl where the measure-

(4) O. Redlich and J. Bigeleisen, *J. Amer. Chem. Soc.*, **64**, 758 (1942).

(5) Complete tables of m and Δp for each series of measurements have been deposited with National Auxiliary Publications Service Order NAPS Document 00499 from ASIS National Auxiliary Publications Service, c/o CCM Information Corp., 909 3rd Ave., New York, New York 10001, remitting \$1.00 for microfiche or \$3.00 for photocopies.

(6) O. Redlich and D. M. Meyer, *Chem. Rev.*, **64**, 221 (1964).

(7) N. Geffken and D. Price, *Z. Phys. Chem.*, **B26**, 81 (1934).

(8) W. Geffken, A. Kruijs, and L. Solana, *ibid.*, **B35**, 317 (1937).

Table I: The Apparent Molal Volumes of Alkali Halide

m	5°	25°	5°	25°	\bar{V}_0	35°	5°	25°	25°
	LiCl	LiBr	NaCl	LiI		LiCl	LiI	NaBI	NaI
	16.09	23.80	14.02	35.37		16.95	33.39	23.57	34.98
0.05	16.42		14.40				33.69	23.95	35.35
0.1	16.57	24.29	14.58	35.82	17.57	33.81	24.11	35.55	
0.2	16.77	24.46	14.86	35.96	17.78	33.96	24.32	35.68	
0.3	16.93	24.58	15.09	36.06	17.92	34.06	24.48	35.82	
0.4	17.06	24.67	15.30	36.13	18.04	34.16	24.61	35.93	
0.5	17.18	24.76	15.48	36.20	18.14	34.24	24.73	36.03	
0.6	17.29	24.84	15.65	36.25	18.24	34.31	24.84	36.12	
0.7	17.39	24.91	15.82	36.29	18.32	34.38	24.95	36.20	
0.8	17.49	24.97	15.97	36.33	18.40	34.45	25.04	36.28	
0.9	17.58	25.03	16.13	36.37	18.47	34.51	25.13	36.35	
1.0	17.67	25.09	16.27	36.40	18.54	34.55	25.21	36.42	
1.2	17.83	25.20	16.53	36.46	18.67	34.65	25.38	36.54	
1.4	17.99	25.29	16.80	36.52	18.79	34.73	25.53	36.65	
1.6	18.13	25.38	17.03	36.56	18.90	34.81	25.67	36.75	
1.8	18.26	25.46	17.27	36.60	19.00	34.88	25.80	36.85	
2.0	18.39	25.54	17.47	36.63	19.12	34.94			
2.5	18.68		17.95		19.32				
3.0	18.94		18.39						
3.5	(19.15)		18.76						

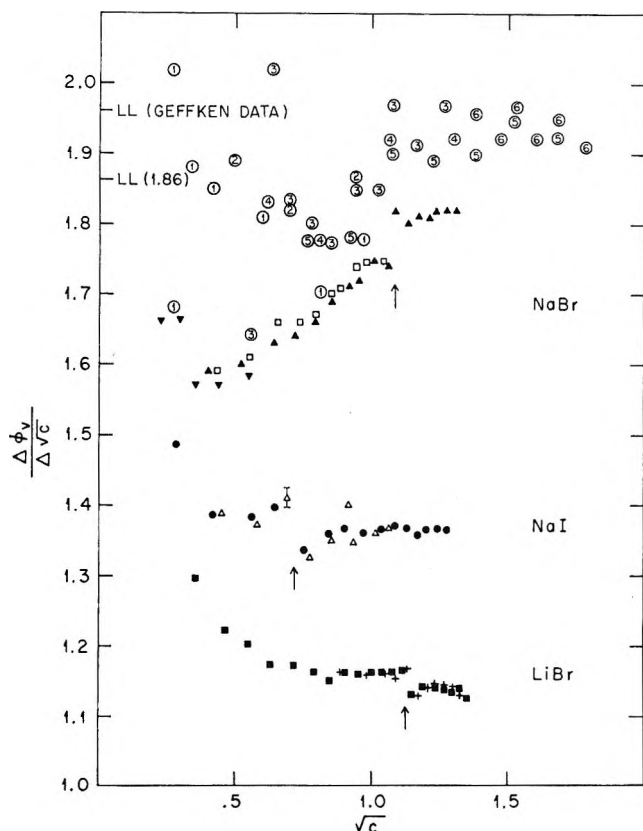


Figure 1. $\Delta\phi_v/\Delta\sqrt{c}$ at 25°. LiBr, ■ and +; NaI, Δ and ●; NaBr (this work), ∇ , \blacktriangle and \square ; NaBr (Geffken and Price,⁷ magnetic float), \odot , NaBr (Geffken, Kruis, and Solana,⁸ dilatometer), \circledast , \circledcirc , \circledR , \circledS and \circledT . The magnetic float and dilatometer results are displaced upward 0.1 unit on the scale. The theoretical limiting value of the slope is shown by LL,⁶ and a vertical arrow on each curve indicates where an anomaly may be present.

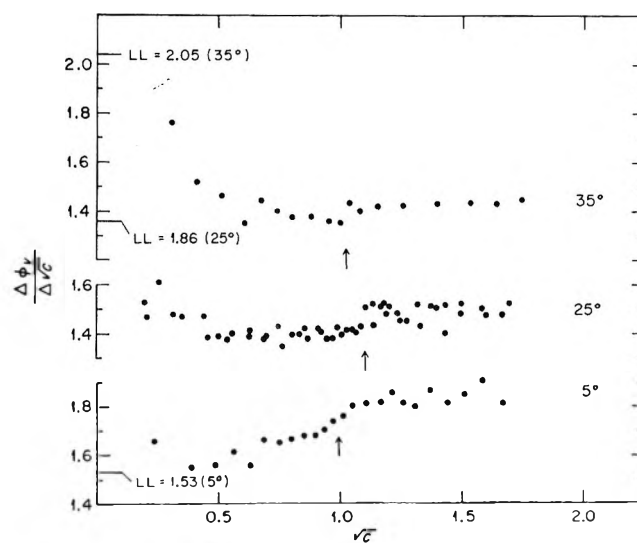


Figure 2. $\Delta\phi_v/\Delta\sqrt{c}$ for LiCl at 5, 25, and 35°.

ments reported from each laboratory were made with the same equipment used for the NaBr results, and it appears that the source of the discrepancy may be in the different types of equipment used although the actual cause is unknown. The value of \bar{V}_0 for NaCl at 5° of 14.02 cc can be compared with the value 14.15 given by Franks and Smith,⁹ and 14.018 by Dunn.¹⁰

Values of the common ion difference in \bar{V}_0 are as follows: LiBr–LiCl, 6.81 cc; LiI–LiCl, 18.38; LiCl–NaCl, 0.36; LiI–LiBr, 11.57; LiBr–NaBr, 0.25; LiI–

(9) F. Franks and H. T. Smith, *Trans. Faraday Soc.*, **63**, 2586 (1967).

(10) L. A. Dunn, *ibid.*, **64**, 2951 (1968).

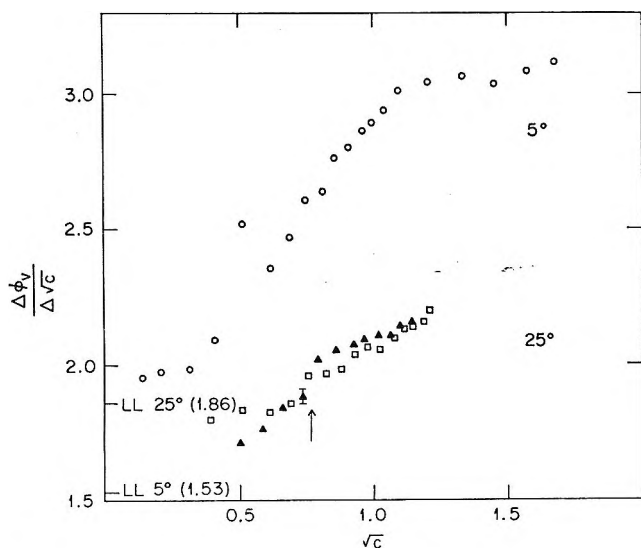


Figure 3. $\Delta\phi_v/\Delta\sqrt{c}$ for LiCl at 5 and 25°.

NaI, 0.39; NaBr–NaCl, 6.92; NaI–NaCl, 18.38; and NaI–NaBr, 11.43. These may be compared with Dunn's¹¹ values of 6.94 cc, 11.46 and 18.40 for Br–Cl, I–Br and I–Cl, respectively. Except for values involving LiBr in the present results, the internal and external agreement is satisfactory. The LiBr results here are about 0.1 cc lower and parallel to those given by Baxter and Wallace¹² and extrapolate into the theoretical slope. It is probable that the concentration of standard AgNO₃ solution in these runs was a few tenths per cent in error and the values of ϕ_v about 0.1 cc low, but since this will have only a slight effect on the slope curve the results have not been rechecked.

The graphs of $\Delta\phi_v/\Delta\sqrt{c}$ are shown in Figure 1 for LiBr, NaI, and NaBr. Also, in Figure 1 for NaBr are values calculated from ref 7 and 8 with individual series being indicated by numbers and these results being displaced 0.1 cc upward on the scale. For accuracy in obtaining $\partial\phi_v/\partial\sqrt{c}$ a chord area plot¹³ is necessary; however, placing the $\Delta\phi_v/\Delta\sqrt{c}$ points at the center of the $\Delta\sqrt{c}$ chords is sufficiently accurate for the present.

Figure 2 shows the results for LiCl at 5, 25, and 35°. Figure 3 gives the results for NaCl at 5 and 25° and Figure 4 gives results for LiI at 5 and 25°. The lowest concentrations measured here are still relatively high, and for several of the curves the last slope points are still far from the theoretical limiting values.⁶ Nevertheless, in each case there is a definite approach to the limiting value and at each temperature the results are consistent with the theoretical values.

At higher concentrations, the LiBr, NaI and NaBr curves appear to have discontinuities at $\sqrt{c} = 1.14$, 0.72 and 1.07, respectively. The forms of the derivative curves determine for the integral curves, forms very similar to the λ -shaped areas observed in specific heat measurements, (inverted for NaBr). The magnitude

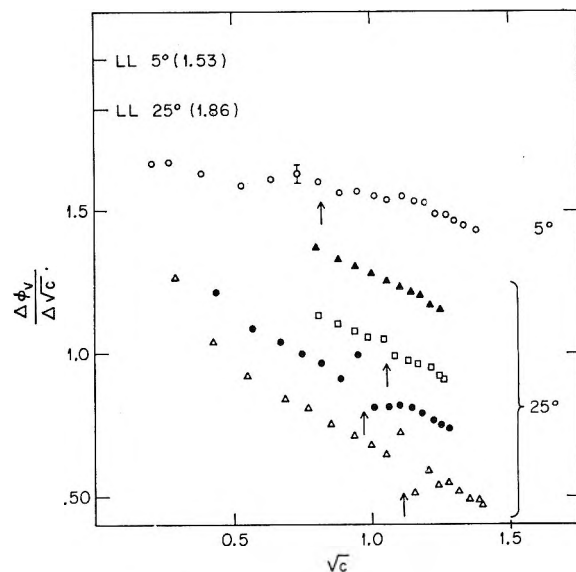


Figure 4. $\Delta\phi_v/\Delta\sqrt{c}$ for LiI at 5 and 25°. Data at 5° displaced upward 0.5 unit from scale. Each 25° run displaced upward 0.2 unit from one below.

of the singularity is sufficiently small however that it is almost unnoticeable on a normal sized plot of ϕ_v .

For NaCl at 25° the curves suggest a singularity at about $\sqrt{c} = 0.75$; however, the scatter of data is large enough that it is not definite. The 5° curve for NaCl has no definite indication of a singularity. Each of the four LiI curves at 25° are different; the three showing the singularity have it at $\sqrt{c} = 1.12$, 0.97, and 1.06 with differences in the size of the break and one curve does not show a singularity at all. At present there is no adequate explanation although a different batch of LiI salt was used in each run and the series not showing the break was about 0.1 lower in ϕ_v than the other three. At 5° the LiI seems to show a diffuse transition centering about $\sqrt{c} = 0.8$. The 5 and 25° LiCl curves also show a diffuse transition with the 35° curve possibly showing a small λ type effect.

Comparing the Geffken data^{6,7} on $\Delta\phi_v/\Delta\sqrt{c}$ for NaBr solutions with the present work, it is found that as with the ϕ_v curve, there is a divergence below $\sqrt{c} = 0.7$; however, the present data are within the scatter envelope of the earlier work. Although the scatter of the earlier work is relatively large, there is again very good agreement above about 0.6 N. In particular, there is detailed agreement in the flat or dropping region above $\sqrt{c} = 1.08$, the very sharp rise just before 1.08 and series 3 of the Geffken work may show the flat region before the rise, and finally an estimate of $\sqrt{c} = 1.05$ could be given for the center of the transition in the Geffken work compared to 1.07 obtained here.

(11) L. A. Dunn, *Trans. Faraday Soc.*, **64**, 1898 (1968).

(12) G. P. Baxter and C. C. Wallace, *J. Amer. Chem. Soc.*, **38**, 70 (1916).

(13) T. F. Young and O. G. Vogel, *ibid.*, **54**, 3030 (1932).

There is little or no data available for precise comparisons with other salts. Accurate and sufficiently detailed data are available for NaCl¹⁴ but only up to $\sqrt{c} = 0.8$ or just about the transition point. The curve based on composite data shown in Figure 1 of ref 7 does, however, show a knee at $\sqrt{c} = 0.8$ in approximate agreement with the derivative having a jump at a slightly lower point. Similarly the data of I which were independent of the present work also seem to have a rise at $\sqrt{c} = 0.8$ as may be seen in Figure 2 of I. Thus, the available data on NaCl do indicate an anomaly although no curve is definite.

No directly applicable data are available for the iodides; however, some data on alkaline earth iodides may be pertinent to LiI chemistry. The available data¹⁵ lack detail and perhaps accuracy, but curves of ϕ_v calculated from the original data for BaI₂, CaI₂, and MgI₂ show unusual features broadly similar to the curves for LiI.

Discussion

In analyzing the significance of the results, the question of whether the observed anomalies could be the result of experimental error rather than a physical transition must be considered. In the LiI solutions, the observed variations in the concentration where the effect occurred and in the magnitude of the effect are not normally expected in an equilibrium thermodynamic system. Secondly, the values of $\Delta\phi_v/\Delta\sqrt{c}$ are obtained by subtracting each value of ϕ_v from its following value. Consequently, a noncumulative error in a single value of ϕ_v will result in a high and low (or reverse), pair of values for $\Delta\phi_v/\Delta\sqrt{c}$, suggestive of the form of the observed anomalies. Finally, there are a few points (included in the curves) which deviate from smooth curves by amounts comparable to those in the anomalies but which have not been considered as significant. Most of these, however, are at relatively low concentrations or in older work such as the LiCl curves and the NaI point at $\sqrt{c} = 0.91$ is probably the only significant one.

Of the curves showing apparent discontinuities, the LiI anomalies are the ones that could most probably be ascribed to error both because of the variability and also because in the two lower curves of Figure 4, the point on the low-concentration side is not part of a reasonable sequence of points but is isolated and could be due to a single error.

While basic doubts as to the nature of the LiI curves cannot be removed, there are valid reasons for believing that the effects are physical rather than random errors. First, the effects are well outside the random scatter of points for any of the curves and are probably not part of the normal error population, *i.e.*, they are single "catastrophic" events. For the three LiI curves and also for the LiBr and probably the NaI curves each event occurs only once in any curve and always with the same sign, although as shown by the NaBr and pos-

sibly the NaCl curves, events of the opposite sign can occur. For the two lower curves and probably the third, there is a small but definite upward displacement of the curve on the high concentration side of the anomaly. Thus, a small inflection must occur and the effects of the transition do affect a relatively large number of points. Although error cannot be excluded as the source of the effects, the combined probability of obtaining these particular results is certainly very low.

It is proposed later in the paper that the effects are a form of critical phenomenon; if this is true, the variability may not be unexpected. Such transitions often are sensitive to minor changes in conditions or impurities and show hysteresis effects. For LiI solutions the overall displacement and change in curvature between the segments of the curve is the smallest for any of the salts studied, and it is possible that the driving force is exceedingly low, leading to erratic behavior.

For the LiBr and NaI systems there are two independent curves for each salt showing rather precise agreement for the anomaly. Also for these curves, the points both above and below the jump are ends of a reasonable sequence of points and are not disconnected. The $\sqrt{c} = 0.91$ point of NaI has not been confirmed in a second run, does not form part of a logical sequence, and therefore has been rejected. Since no more than one (excluding the NaI $\sqrt{c} = 0.91$ point) of the presumed error events is shown by any curve, the probability of it occurring must be quite low and the probability of a second event at the same concentration must be substantially lower. That a second system would now show the identical behavior would be highly improbable if error is the cause.

In the NaBr solutions, the presumed error is of opposite sign to those in the previous curves and has been accurately duplicated on the lower concentration side of the anomaly where the second series ended. However, each of the three Geffken series covering this concentration region confirms the upper part of the curve, and again it is improbable that random errors could cause the combined events.

The other systems studied such as NaCl and LiCl and the systems at other temperatures do not in general justify any strong conclusions. LiCl solutions may have an apparent discontinuity and this cannot be excluded, but there is no definite evidence for it. The nature of diffuse transitions such as those in LiCl solutions has been extensively discussed earlier.^{2,3}

Since each point of the curves represents a chord of finite length, it is obvious that the existence of a mathematical discontinuity cannot be proven. The situation is the same in the λ points of specific heats and is not a problem in the interpretation.

While the effects reported here are consistent and

(14) A. Kruis, *Z. Phys. Chem.*, **134**, 1 (1936).

(15) A. Heydweiller, *Ann. Phys. (Leipzig)*, [4] **30**, 873 (1909).

substantial in size, they are nevertheless based on the creditability of extremely delicate measurements. Consequently, until independent measurements of other properties are available, the nature of the anomalies will be in some doubt. Nevertheless, it is believed that the data presented do justify the remainder of the discussion.

With the very limited thermodynamic data available, the nature of the transition is very unclear. However, several reasons can be advanced for believing that it is of the critical type.¹⁶ First, the shape of the ϕ_c curve is very suggestive of the λ -point type of transition in specific heats. Second, a very analogous situation can be thought of in the order-disorder transitions of alloys, in that at constant temperature it is possible to go through the Curie point by varying the composition. It might be expected that the volume-composition curve would show an anomaly which might be similar to that observed here. Finally, the very general nature of critical-point type transitions,¹⁶ e.g., liquid-gas critical points, consolute points, order-disorder transitions, magnetic transitions and others, suggest that the present phenomena may be fitted within the framework already developed.

The theory of critical phenomena is very general and consequently it is necessary to further specify the nature of the transition. Any detailed mechanism of the transition would be highly speculative but one mechanism discussed earlier^{2,3} may involve a transformation from a structure determined mainly by the forces operative in pure water to a structure determined by solute forces in the concentrated region.¹⁷ Samoilov¹⁷ does in fact suggest the possibility of a critical-like transition for this transformation, although it is probable that a somewhat higher concentration than reported here was being considered. A question that arises is that water does not show any long-range order,¹⁸ but does a structure transition imply long-range order? In this connection the Ising model¹⁶ for critical point phenomena requires only nearest-neighbor cell interaction and not long-range forces or order.

While there are questions as to how the Ising model could be applied to solutions of electrolytes, if the model is applicable, there is no need for postulating long range order.

In addition to a mechanism involving changes in water structure, another possibility is one involving the electrostatic interactions among the ions. From a statistical mechanical treatment of ionic solutions, Kirkwood¹⁹ obtained an integral equation from which radial distribution functions for the ions could be calculated. At $\kappa a = 1.03$ (κ is the Debye-Hückel reciprocal length and a the ion-size parameter) or between about 0.5 and 1 N for the various salts concerned, the distribution function goes from an exponential to an oscillatory and presumably quasi-lattice form. The calculations have been improved by Kirkwood and Poirer²⁰ and Stillinger and Lovett,²¹ and Berlin and Montroll²² have obtained similar results, each using different types of treatments.

It is not known whether this transformation of the distribution function can give rise to critical-like phenomena and also other types of calculations and experiments have indicated that the lattice-like state of the ions might begin at a much lower concentration. None of the findings is conclusive; however, the concentration predicted by the Kirkwood theory is of the right magnitude, and there is simply not enough known to decide whether the theory is applicable or not.

(16) J. V. Sengers and A. L. Sengers, *Chem. Eng. News*, **46**, 104 (1968).

(17) O. Ya. Samoilov, "The Structure of Aqueous Solutions and the Hydration of Ions," English Translation, Consultant Bureau, New York, N. Y., 1965, p 141.

(18) A. M. Levelut and A. Guinier, *Bull. Soc. Fr. Mineral. Cristallogr.*, **90**, 445 (1967).

(19) J. G. Kirkwood, *Chem. Rev.*, **19**, 275 (1936).

(20) J. G. Kirkwood and J. C. Poirer, *J. Phys. Chem.*, **58**, 591 (1954).

(21) F. H. Stillinger, Jr., and R. Lovett, *J. Chem. Phys.*, **48**, 3858 (1968).

(22) T. H. Berlin and E. W. Montroll, *ibid.*, **20**, 75 (1952).

Reactions of Shock-Heated Carbon Disulfide-Argon Mixtures.

I. Light Emission

by S. J. Arnold and G. H. Kimbell

Canadian Armament Research and Development Establishment, and Centre de Recherches sur les Atomes et Molécules, P.O. Box 1427, Québec, P.Q., Canada (Received February 24, 1969)

The light emission from shock-heated CS₂-Ar mixtures varying in composition from 1 to 100% CS₂ has been measured as a function of wavelength in the range 3750-8250 Å. Measurements of the Arrhenius activation energy indicate that the molecule is excited to the ³Σ_g⁺ state. It was not possible to distinguish between a single-step excitation process and a more complex mechanism involving vibrational excitation of the ground state.

Introduction

When a CS₂-Ar mixture, varying in composition from 1 to 100% CS₂, is shock-heated, visible light is emitted.¹ Previous studies on the decomposition of CS₂^{2,3} indicated that the reaction was unimolecular and that the primary step was the collision-induced transition of the CS₂ molecule from the ground (¹Σ_g⁺) state to a ³A₂ state. A similar mechanism has been postulated for the CO₂ molecule.⁴ Preliminary results of a study of light emission by shock-heated CS₂-Ar mixtures indicated that the intensity was first order in CS₂ and zero order in Ar.¹ A further study of the light emission in the range 3750-8250 Å has been carried out. The activation energy for the primary step, which has been calculated as a function of wavelength, appears to be consistent with shock excitation of CS₂ to one of the predicted upper electronic states.

Experimental Section

The shock tube was constructed of chromium-plated steel and is 12 ft in length from diaphragm to observation station and 14 in.² in cross-sectional area. The shocks were generated by 1-10 atmospheres of helium in a 3-ft long driver section. All observations were made in the primary shock. Thin-film platinum-resistance detectors were used to measure the speed of all shocks fired. In the first experiments, the signals from the velocity gauges were recorded by photographing an oscilloscope sweep. In later experiments a microsecond counter was used to measure the time required for the shock to travel between two detectors located on either side of the observation window. Quartz windows, flush-mounted with the inner wall, enabled spectroscopic and spectrophotometric measurements to be made.

A Hilger-Watts F/4 quartz-prism spectrograph was used for the spectroscopic experiments and a McPherson Model 235 monochromator for the spectrophotometric experiments. In both cases the instruments were placed close to the quartz window; no lens was used.

For spectrophotometric measurements in the range 3750-6000 Å the monochromator was equipped with a 600L/mm grating having a reciprocal dispersion of 34 Å/mm. The entrance slit was set at 2 mm allowing a nominal band pass of 68 Å. The detector used was an EMI 9514SA photomultiplier which has an "S" type response. For similar measurements in the range 6000-8250 Å the monochromator was equipped with a 300L/mm grating having a reciprocal dispersion of 68 Å/mm. The entrance slit was reduced to 1 mm thus allowing the same nominal band pass. The detector used in this range was an EMI 9558QB photomultiplier which has an "S-20" response. The photomultiplier output was recorded by photographing a single sweep from a Tektronix 555 oscilloscope triggered by a velocity-gauge signal. A relative calibration of the system was carried out using a tungsten source at a color temperature of 2420°K. For both detection systems the intensity data was normalized to the intensity at 5000 Å.

The combined geometric and electronic rise time of the system was 2-3 μsec. This depended only on the time taken for the shock to pass the viewed region and on the resistance loading of the photomultiplier.

Prior to the firing of each shock, the tube and the ancillary filling system were evacuated to less than 10⁻² mm. The CS₂ used was Anachemia Reagent Grade which had been dried over "Drierite" and further purified by trap to trap distillation. The argon, of "ultra high purity" grade, containing less than 10 ppm of impurities, was supplied by Matheson.

The temperature, pressure, and density of the shocked gas were calculated from the measured shock

(1) S. J. Arnold, W. G. Brownlee, and G. H. Kimbell, *J. Phys. Chem.*, **72**, 4344 (1968).

(2) A. G. Gaydon, H. B. Palmer, and G. H. Kimbell, *Proc. Roy. Soc.*, **A279**, 313 (1964).

(3) H. A. Olschewski, J. Troe, and H. G. Wagner, *Z. Phys. Chem. (Frankfurt)*, **45**, 329 (1965).

(4) T. A. Brabbs, F. E. Belles, S. A. Zlatarich, *J. Chem. Phys.*, **38**, 1939 (1963).

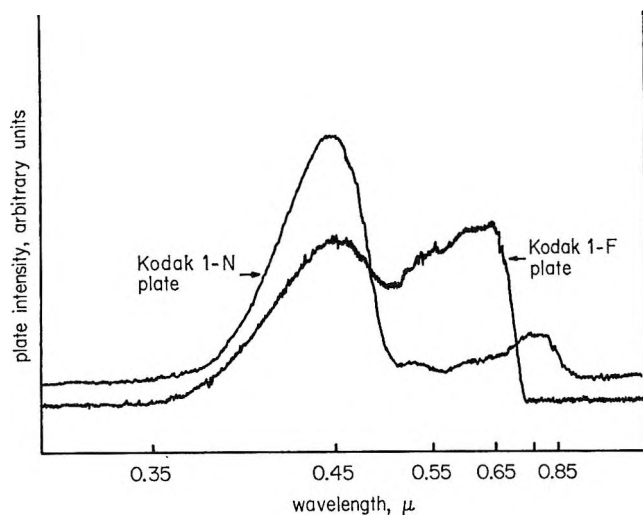


Figure 1. Microdensitometer traces of the emission obtained from a 20% mixture of CS_2 in argon shock-heated to 2000°K .

velocity. The high temperature enthalpy data was obtained from the JANAF Thermochemical Tables; solutions to the hydrodynamic equations were obtained using the CARDE Sigma 7 computer.

Results and Conclusions

Spectral Distribution of the Emission. A Hilger-Watts F/4 quartz prism spectrograph was used to photograph the emission from a 20% CS_2 -Ar mixture, shock-heated to 2000°K . Figure 1 shows microdensitometer tracings of the emission obtained on Kodak 1-F and 1-N spectroscopic plates. In the case of the 1-F plate, it was necessary to superimpose the radiation from 10 successive shocks, while for the 1-N plate, 30 successive shocks were required. The emission extends from 3600 \AA in the near ultraviolet to about 9000 \AA in the near infrared and appears to be continuous throughout the whole range. No structure was detectable with a slit width of 0.25 mm . The existence of the two maxima indicated on the 1-N plate appeared to be confirmed by an analysis of the photometric data.

Pressure Dependence of the Intensity. The peak radiation intensity was measured at 250-\AA intervals over the range $3750\text{--}8250 \text{ \AA}$ as a function of the temperature and pressure and the initial mole fraction of CS_2 . Values of the temperature and the pressure for typical shock data, calculated assuming frozen chemistry, are shown in Table I. At 4500 \AA plots of the logarithm of the peak intensity per unit concentration of frozen mixture vs. $10^4/T$ were linear for mixtures with initial mole fractions of 0.05, 0.10, 0.20, and 1.00 and yielded parallel straight lines. Consequently, over the temperature range $1500\text{--}3500^\circ\text{K}$, the intensity per unit gas concentration is proportional to the initial mole fraction of CS_2 . When the initial mole fraction was used to scale the ordinate value to the logarithm of the peak intensity per unit concentration of CS_2 , all these data could be correlated with a

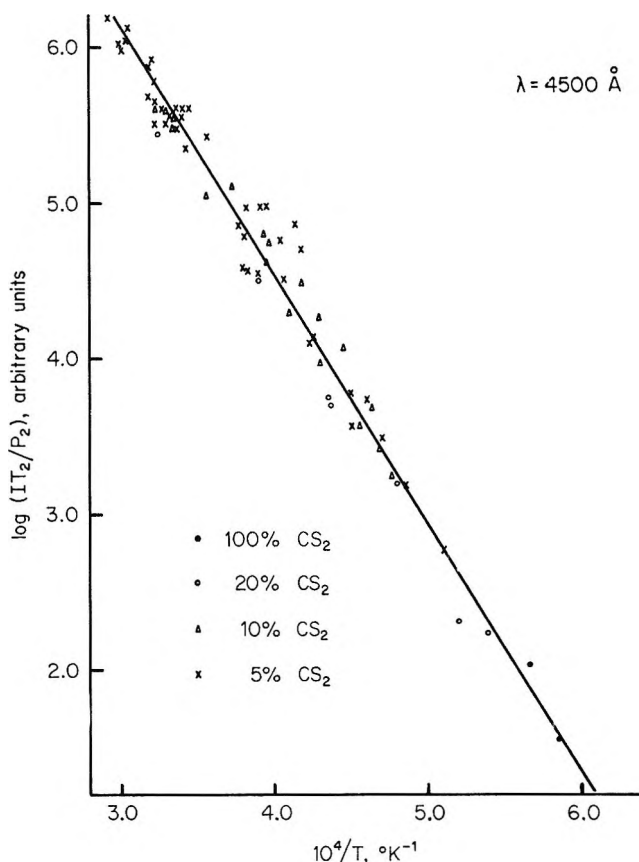
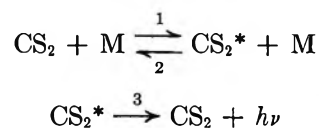


Figure 2. Plot of the logarithm of the emission intensity per unit concentration of CS_2 vs. $10^4/T$.

single straight line. Figure 2 shows the resulting plot obtained for the 4500-\AA data. Similar plots were obtained at all other wavelengths measured, although in most cases only mixtures with initial mole fractions of 0.05 and 0.10 were used. The intensity, therefore, is proportional to the concentration of CS_2 and independent of the concentration of argon.

Kinetics of Excitation. Since the emission intensity is a maximum at the shock front and decays to an equilibrium value (see Figure 3), the emission must result from excitation of ground state CS_2 and not from recombination of its dissociation products CS and S .

(a) *The Single-Step Mechanism.* The simplest kinetic scheme which will explain the observed first-order dependence on CS_2 and zero-order dependence on argon is one consisting of collisional excitation and quenching in which the electronic transition occurs in a single step during collision



where * represents the electronically excited molecule.

If a quasi-stationary state is assumed to exist immediately behind the front with respect to the electronic

Table I: Sample Calculations of Shock Parameters

Mole fraction CS ₂	Velocity, cm/sec × 10 ⁶	P _{initial} , mm	P _{final} , mm	Density ratio (Frozen chemistry)	T ₂ , °K	log ₁₀ (I ₂ /P ₂)
0.10	1.81	3.0	136	4.47	3033	5.59
0.10	1.56	11.0	370	4.31	2326	3.98
0.10	1.48	8.0	244	4.25	2137	3.42
0.10	1.50	14.5	456	4.27	2197	3.57
0.05	1.49	14.5	416	3.88	2201	3.57
0.05	1.65	10.4	368	3.99	2649	4.85
0.05	1.61	8.4	284	3.96	2543	4.57
0.05	1.64	5.0	175	3.98	2624	4.97
0.05	1.87	3.0	137	4.09	3320	5.98
0.05	1.86	1.0	45	4.08	3284	6.05

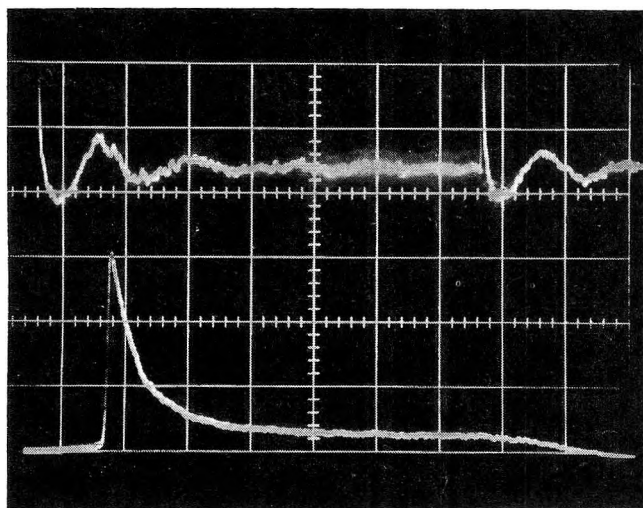


Figure 3. Oscilloscope trace showing the velocity-gauge signals (upper trace) and the intensity profile (photomultiplier output, lower trace) characteristic of a higher temperature shock. $T_2 = 3136^\circ\text{K}$, $P_2 = 128$ mmHg, velocity = 1.8×10^6 cm sec⁻¹.

excitation process, then the peak intensity at the front is given by

$$I \propto k_3[\text{CS}_2^*] = \frac{k_1 k_3 [\text{CS}_2]}{k_2 \left(1 + \frac{k_3}{k_2 [\text{M}]}\right)} \quad (\text{a})$$

In order to simplify the denominator further $k_3/(k_2[\text{M}])$ must be much less than 1. Under our experimental conditions $[\text{M}] \simeq 10^{-6}$ mol cm⁻³. The rate constant k_2 is equal to $P_2 Z$ where P_2 is the fraction of collisions effective in quenching ($P_2 \leq 1$) and Z , the collision rate, is equal to 10^{14} cm³ mol⁻¹ sec⁻¹. The rate constant k_3 for a forbidden transition is $\leq 10^6$ sec⁻¹. The inequality $k_3/(k_2[\text{M}]) < 1$ can, therefore, only be fulfilled if P_2 is in the interval $0.1 < P_2 < 1$ which infers that the primary quenching mode is with CS₂ acting as M (P_2 for argon should be approximately 10^{-3}). Therefore eq a reduces to

$$I \propto \frac{k_1 k_3 [\text{CS}_2]}{k_2} \sim C e^{-(E_a/RT)} [\text{CS}_2] \quad (\text{a}')$$

where E_a is the Arrhenius activation energy. More rigorously, k_1 and k_2 should be expressed in terms of the third body M resulting in

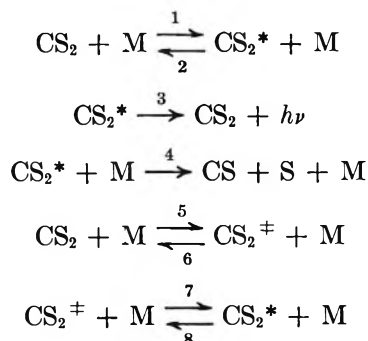
$$I = k_a \left[\frac{m k_1^{\text{CS}_2} + (1-m) k_1^{\text{Ar}}}{m k_2^{\text{CS}_2} + (1-m) k_2^{\text{Ar}}} \right] [\text{CS}_2]$$

where m is the mole fraction of CS₂. Figure 2 indicates that at any given temperature the intensity per unit concentration of CS₂ is essentially independent of m . This infers, therefore, (i) the derivative of the square-bracketed term with respect to m in the above equation equals zero and thus

$$\left(\frac{k_1}{k_2}\right)_{\text{Ar}} = \left(\frac{k_1}{k_2}\right)_{\text{CS}_2}$$

(ii) the expression will also be essentially independent of m if $k_1^{\text{Ar}} \ll k_1^{\text{CS}_2}$ and $k_2^{\text{Ar}} \ll k_2^{\text{CS}_2}$ without the relation in (i) being satisfied, for example, with $k_1^{\text{CS}_2} = 1000 k_1^{\text{Ar}}$ and $k_2^{\text{CS}_2} = 500 k_2^{\text{Ar}}$, the square-bracketed term varies by less than 5% for $0.05 \leq m \leq 1$. Although it is well known that argon is very inefficient in both activation and quenching, the present experiments do not allow differentiation between cases i and ii.

(b) *Multistep Mechanisms.* An alternative means of excitation is one in which the CS₂ molecule can be first excited to a high vibrational level of the ground state from where it is then excited to the electronically excited state in a second collision. The overall mechanism for this multistep excitation process which includes reactions 1 and 2 is



where * represents the electronically excited molecule and † represents the vibrationally excited molecule. If a quasi-stationary state is assumed to exist for CS_2^\ddagger and CS_2^*

$$I \propto k_3[\text{CS}_2^*] = \left\{ \frac{k_1 k_3 + \left(\frac{k_3 k_5 k_7}{k_6 + k_7} \right)}{k_2 + k_4 + \frac{k_3}{[\text{M}]} + \left(\frac{k_6 k_8}{k_6 + k_7} \right)} \right\} [\text{CS}_2] \quad (\text{b})$$

which on assuming $k_3/[\text{M}] \ll (k_2 + k_4)$ and upon eliminating all second order terms reduces to

$$I \propto \left(\frac{k_1 k_3}{k_2 + k_4} \right) [\text{CS}_2] \sim C' e^{-(E_a/RT)} [\text{CS}_2] \quad (\text{b}')$$

If CS_2^* is considered to be formed exclusively through a ladder-climbing mechanism, thus eliminating the possibility of direct excitation (eq 1)

$$I \propto k_3[\text{CS}_2^*] = \left(\frac{k_3 k_5 k_7}{(k_6 + k_7)(k_2 + k_4 + k_3/[\text{M}]) + k_6 k_8} \right) [\text{CS}_2] \quad (\text{c})$$

Assuming that $k_3/[\text{M}] \ll (k_2 + k_4)$ and representing k_5 in its Arrhenius form $e^{-(E_{a_1}/RT)}$ and k_7 in its Arrhenius form $e^{-(E_{a_2}/RT)}$ where E_{a_1} is the activation energy required for vibrational excitation and E_{a_2} is the activation energy required for excitation from the vibrational levels of the ground state to the electronically excited state, one obtains

$$I \propto k_3[\text{CS}_2^*] = \left\{ \frac{k_3 e^{-(E_{a_1} + E_{a_2})/RT}}{k_2 k_6 + k_4 k_6 + k_6 k_8 + k_2 k_7 + k_4 k_7} \right\} [\text{CS}_2] \quad (\text{c}')$$

$$\sim C'' e^{-(E_a/RT)} [\text{CS}_2]$$

since the sum of the activation energies for the two-step process is the same as the activation energy for a single-step process. Equations a', b' and c' have the same exponential factor in the numerator and thus all three mechanisms yield expressions which are essentially similar. If reaction 4 (representing the collision-induced dissociation of the CS_2^* molecule) were an important process, *i.e.*, $k_4 \sim k_2$, eq b' would be of the form

$$I \propto \frac{k_3 P_1 e^{-E_1/RT} [\text{CS}_2]}{P_2 + 1/2 P_4 [(E_D - E_1)/RT]^2} e^{-(E_D - E_1)/RT} \quad (\text{d})$$

where

$$k_1 = P_1 Z_1 e^{-E_1/RT}$$

$$k_2 = P_2 Z_1$$

$$k_4 = 1/2 P_4 Z_1 [(E_D - E_1)/RT]^2 e^{-(E_D - E_1)/RT}$$

and $(E_D - E_1)$ is the dissociation energy of the CS_2^* molecule. Equation d will give a curved Arrhenius

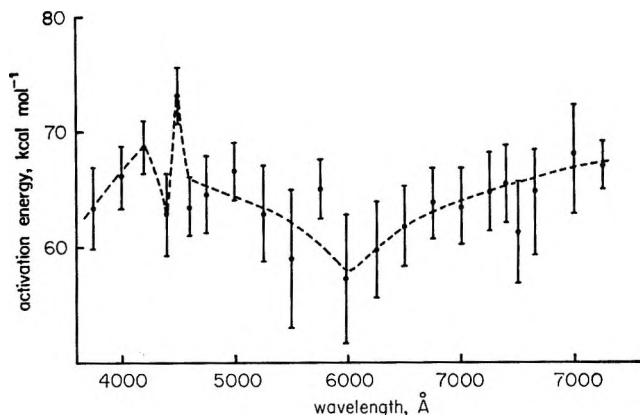


Figure 4. Plot of the Arrhenius activation energy (E_a) as a function of wavelength. Error bars indicate the range of E_a for a 95% confidence interval.

plot if the terms in the denominator are of similar magnitude. Figure 2, therefore, should then exhibit curvature. Inspection shows that no pronounced curvature does in fact exist. Thus, in order to determine a measure of the extent of curvature present, if any, in the Arrhenius plots, the data were arbitrarily divided into two sets; those points obtained at temperatures above 2500°K and those obtained at temperatures below 2500°K. The lower temperature points exhibited a higher activation energy than the higher temperature points thus indicating some curvature in the Arrhenius plots. From the data obtained in these experiments it was not possible to distinguish between the simple single-step mechanism and a mechanism involving an initial vibrational excitation of the CS_2 molecule.

Figure 4 shows a plot of E_a as a function of wavelength for the values shown in Table II. The vertical bars indicate the range of E_a for a 95% confidence interval. This plot is far from simple, exhibiting several pronounced irregularities, the most noticeable of which is the sharp spike at 4500 Å. At each wavelength the measured value of E_a has been found to have a range of less than 12 kcal mol⁻¹ for a 95% confidence interval with the majority of the values having a range of less than 8 kcal mol⁻¹. For most wavelengths 15 data points were sufficient to determine E_a ; the addition of more points did not alter E_a appreciably but simply reduced the range of E_a for the 95% confidence interval. Consequently, it is felt that the irregularities exhibited in the plot are real and are not due to the use of insufficient data points to give an accurate value of E_a . The E_a vs. wavelength plot obtained using either just the low-temperature data or just the high-temperature data exhibited the same irregularities shown in Figure 4.

The Electronic States of CS₂. Table III shows the expected low-lying electronic states of CS_2 as given by Douglas.⁵ Absorption studies^{6,7} have indicated the

Table II: Activation Energy E_a as a Function of Wavelength λ

(λ), Å	No. of points	E_a , kcal mol ⁻¹	95% confidence interval, kcal mol ⁻¹
3750	29	63.4	3.6
4000	28	66.2	2.8
4200	31	68.7	2.3
4400	37	62.9	3.6
4500	73	73.1	2.5
4600	36	63.6	2.6
4750	34	64.6	3.4
5000	30	66.6	2.5
5250	24	63.0	4.2
5500	17	59.0	6.0
5750	22	65.0	2.6
5990	16	57.3	5.6
6250	14	59.8	4.2
6500	20	61.8	3.5
6750	21	63.8	3.0
7000	17	63.4	3.3
7250	18	64.8	3.4
7400	18	65.5	3.4
7500	15	61.3	4.5
7650	17	64.9	3.6
8000	14	68.1	5.2
8250	22	67.0	2.1

existence of two band systems, a relatively strong system in the region 2200–1500 Å and a weaker system in the region 4300–2900 Å. Kleman⁶ has made a rotational analysis of some of the bands in the near-uv system and has obtained a ν_{000} of 26,187 cm⁻¹ or 74.9 kcal mol⁻¹. Douglas has identified the upper state as a bent ³A₂ state which correlates with the ³Δ_u of the linear configuration. This is the lowest excited state which has been observed for the CS₂ molecule. As predicted by Mulliken⁸ for the case of CO₂, a ³Σ_u⁺ state could exist approximately 0.8 eV lower in energy. This would place the value of ν_{000} at approximately 57 kcal mol⁻¹.

The Arrhenius activation energy must be greater or equal to ν_{000} , in order to populate an upper state, unless the rate of dissociation of the upper state is

Table III: Electronic States of CS₂

Electron configuration	Linear molecule	C _{2v} molecule	C _{2v} case C
(π _g) ³ σ _g	$\left\{ \begin{array}{l} {}^1\pi_g \\ {}^3\pi_g \end{array} \right.$	¹ A ₂ ¹ , B ₂	A ₂ , B ₂
		³ A ₂ ³ , B ₂	A ₁ , B ₁ , B ₂ , A ₁ , A ₂ , B ₁
(π _g) ³ π _u	$\left\{ \begin{array}{l} {}^1\Sigma_u^+ \\ {}^1\Delta_u \\ {}^3\Sigma_u^- \\ {}^3\Sigma_u^- \\ {}^3\Delta_u \\ {}^3\Sigma_u^+ \end{array} \right.$	¹ B ₂	B ₂
		¹ A ₂ ¹ , B ₂	A ₂ , B ₂
		³ A ₂	A ₁ , B ₁ , B ₂
		¹ A ₂	A ₂
		³ B ₂ , ³ A ₂	A ₁ , A ₂ , B ₁ , A ₁ , B ₁ , B ₂
		³ B ₂	A ₁ , A ₂ , B ₁
(π _g) ⁴	¹ Σ _g ⁺	¹ A ₁	A ₁

strongly temperature dependent. This temperature dependence would be exhibited by a curvature in the Arrhenius plot. In fact only a very slight curvature is noted. In no case is the measured E_a greater than or equal to 74.9 kcal mol⁻¹. Even with the slightly higher values of E_a obtained using the lower temperature set of data points, only at 4500 Å does the value of E_a reach 74.9 kcal mol⁻¹. Thus it does not appear that the electronically excited state responsible for the emission is the same state observed in absorption by Kleman. The measured E_a is, however, sufficient to populate the lower state if its assumed value of $\nu_{000} = 57$ kcal mol⁻¹ is correct.

If it is assumed that only one low-lying electronic state is appreciably populated, *e.g.*, the ³Σ_u⁺, the main features of the E_a vs. λ and the intensity vs. λ curves can be discussed.

The distribution of molecules in the upper state will be determined by the Boltzmann equation with the majority of molecules occurring in the lowest vibrational levels. The intensity curve will rise from some long wavelength cutoff to a maximum and then fall off in an exponential fashion to a short wavelength cutoff with the locations of the intensity maxima being primarily determined by the appropriate Franck-Condon factors.

The smallest measured value of E_a will occur at a wavelength whose energy equals the minimum energy difference between the potential surfaces, *e.g.* where $\nu_{000} = E_\lambda$, the energy of the photon emitted at wavelength λ . At longer wavelengths where $E_\lambda < \nu_{000}$ the bulk of the emission must arise from higher vibrational levels in the upper state, resulting in increasing values of E_a . Similarly, at shorter values where $E_\lambda > \nu_{000}$, the emission must again arise from higher vibrational levels of the upper state, resulting in increasing values of E_a . The E_a vs. λ curve, shown in Figure 4, does exhibit these general features although several exceptions to this simplified scheme appear. The most notable of these is the pronounced drop at 4400 Å followed by the sharp rise at 4500 Å which statistically appears to be real. In the spectral region less than 4500 Å an anomalous situation arises where $E_a < E_\lambda$. This anomaly is resolved by consideration of the curvature resulting from reaction 4. Values of E_a obtained from data where $T < 2500^\circ\text{K}$ are then consistent with $E_a \geq E_\lambda$.

Summary

The light emission from shock-heated CS₂-Ar mixtures has been measured in the region 3750–8250 Å and has been found to be proportional to the CS₂ concentration and independent of the Ar concentration.

- (5) A. E. Douglas and E. R. V. Milton, *J. Chem. Phys.*, **41**, 357 (1964).
- (6) B. Kleman, *Can. J. Phys.*, **41**, 2034 (1963).
- (7) W. C. Price and D. M. Simpson, *Proc. Roy. Soc.*, **A165**, 272 (1938).
- (8) R. S. Mulliken, *Can. J. Chem.*, **36**, 10 (1958).

The Arrhenius activation energy has been determined as a function of the wavelength and an attempt has been made to correlate the measured values of E_a with the known potential energy levels of CS_2 . The values of E_a could not be explained on the basis of populating the lowest previously observed electronic

state, $^3\Delta_u$, and it was necessary to invoke the existence of a lower $^3\Sigma_u^+$ state. It was not possible to determine from this data if the excitation of CS_2^* occurred via a single collision or if it was a multistep process involving vibrational excitation of the ground state molecule.

Hydrogen Atom Permeation through Solid Hydrocarbons at 77°K

by J. M. Ditz, C. G. Hill, Jr., and R. C. Reid

Department of Chemical Engineering, Massachusetts Institute of Technology, Cambridge, Massachusetts
(Received March 6, 1969)

The permeation rate of hydrogen atoms through thin films of solid hydrocarbons was measured at 77°K. Rates were determined by monitoring the color change in a MoO_3 film on the underside of the hydrocarbon film. Hydrogen atoms readily permeate propane and *n*-butane films but not 3-methylpentane films. The technique of depositing thin MoO_3 films is discussed.

In the past ten years, there have been a number of papers dealing with the reaction of thermalized hydrogen atoms with condensed olefin films at 77°K.¹⁻¹⁴ The reaction sequence is now reasonably well established in most cases, but there are a number of vexing questions still remaining. For example, it is not at all clear where the reactions take place. Do hydrogen atoms dissolve in the film and diffuse into the interior to react with the olefin or does the olefin diffuse to the surface and react with gas phase hydrogen atoms? In the latter case the product hydrocarbon radicals would diffuse back into the bulk of the film where the combination and disproportionation reactions occur. Both of these models have been proposed,^{1,6} and there exist data to support both models. Certainly it is obvious that some radical mobility is necessary if the postulated bimolecular chemical steps do occur. Also, esr studies of these systems have not indicated the presence of hydrocarbon radicals; thus, one may hypothesize that radical mobility and reactivity are sufficiently high to prevent the accumulation of even small concentrations of radicals. Other evidence also favors the concept of olefin and radical mobility. The interested reader is referred to the excellent research papers of Klein and Scheer referenced earlier.

One of the major questions one should ask in attempting to differentiate between these models is whether or not hydrogen atoms can penetrate and diffuse through solid hydrocarbon films. The purpose of this paper is to show that such penetration can indeed occur. Use was made of the fact that MoO_3 is

rapidly reduced by hydrogen atoms and that the degree of reaction can be followed quantitatively by noting the change in color from an initial pale yellow to a deep blue. When MoO_3 films covered by a solid hydrocarbon layer are exposed to a source of hydrogen atoms, they will suffer a color change if hydrogen atoms are capable of permeating this layer.

Apparatus and Procedure

The reactor used is shown in Figure 1. The upper section was removable so that the MoO_3 layer could be deposited before a hydrogen permeation run. The de-

- (1) R. Klein and M. D. Scheer, *J. Phys. Chem.*, **62**, 1011 (1958).
- (2) R. Klein and M. D. Scheer, *J. Chem. Phys.*, **31**, 278 (1959).
- (3) R. Klein, M. D. Scheer, and J. G. Waller, *J. Phys. Chem.*, **64**, 1247 (1960).
- (4) R. Klein and M. D. Scheer, *ibid.*, **65**, 324 (1961).
- (5) R. Klein and M. D. Scheer, Fifth International Symposium on Free Radicals, Uppsala, 1961.
- (6) R. Klein and M. D. Scheer, *J. Phys. Chem.*, **66**, 2677 (1962).
- (7) R. Klein, National Bureau of Standards Monograph No. 12, U. S. Government Printing Office, Washington D. C., 1960 p 34.
- (8) M. D. Scheer and R. Klein, *J. Phys. Chem.*, **63**, 1517 (1959).
- (9) M. D. Scheer and R. Klein, *ibid.*, **65**, 375 (1961).
- (10) C. G. Hill, R. C. Reid, and M. W. P. Strandberg, *J. Chem. Phys.*, **42**, 4170 (1965).
- (11) R. L. Espino, Sc.D. Thesis, Massachusetts Institute of Technology, Cambridge, Mass., 1968.
- (12) Y. P. Lomanov, A. N. Ponomarev, and V. L. Talrose, *Kinet. Katal.*, **3**, 49 (1962).
- (13) A. N. Hughes and J. H. Purnell, *Trans. Faraday Soc.*, **61**, 2710 (1965).
- (14) R. L. Espino, J. P. Jones, R. C. Reid, and M. W. P. Strandberg, *J. Phys. Chem.*, **72**, 3689 (1968).

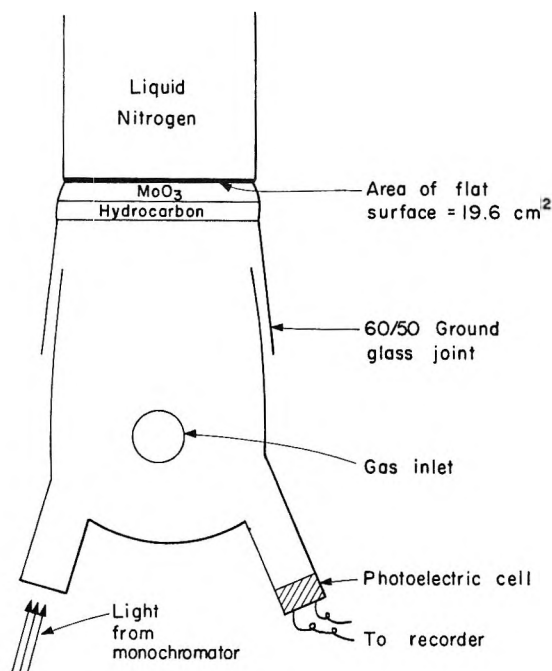


Figure 1. Schematic of Pyrex glass reactor.

position technique and film properties are described later.

The reactor, assembled, had a flat top which could be cooled by liquid nitrogen to about 77°K. An inlet tube connected the reactor to a gas-handling system where hydrocarbons and hydrogen were stored. The reactor and gas-handling system could be evacuated and purged when necessary.

After the MoO₃ film was deposited, the reactor was assembled and connected to the gas-handling system. The reactor was evacuated, and the top cup was filled with liquid nitrogen. A known volume of the desired hydrocarbon was bled slowly into the system and deposited on top of the MoO₃ film by cryopumping. The techniques used to determine the film thickness are described later.

When the system pressure had dropped to the vapor pressure of the hydrocarbon (usually less than 1 μ), a run was started. Hydrogen gas was bled in through a palladium thimble to the desired starting pressure as measured by a Barocel transducer. At time zero a 2450-MHz Raytheon Microtherm unit, connected to the inlet gas tube, was turned on to dissociate the hydrogen molecules. Hydrogen atoms then diffused into the reactor and to the film surface. Since most experiments were made with saturated hydrocarbon films, any gas phase pressure drop in the system was due entirely to reaction of the hydrogen atoms with MoO₃. In a few cases, propylene was employed as a hydrocarbon. In these experiments, the pressure decay could result from the reaction of hydrogen atoms with both propylene and MoO₃.

The reaction of hydrogen atoms with the MoO₃ film was followed by measuring the color change of the oxide.

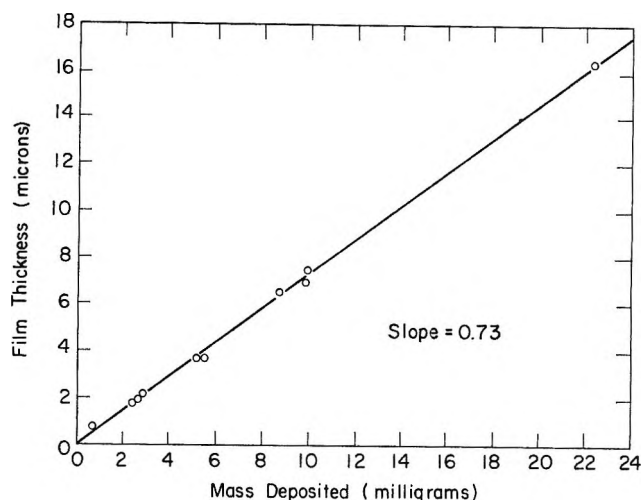


Figure 2. Propylene film thickness as a function of the mass deposited.

As seen in Figure 1, monochromatic 6150-Å light was reflected from the MoO₃ film into a photoelectric cell, and the output was recorded. The source of the light was a Bausch and Lomb Model 33-86-02 monochromator, and the focus was attained with a Model 33-86-53 achromatic condenser lens. The photoelectric cell (a Model 707L Clairex) had a peak response at 6150 Å. Outside light was minimized by covering the reactor with darkroom cloth.

Determination of Hydrocarbon Film Thickness

Previous investigators estimated the thickness of their hydrocarbon films from a material balance

$$\delta = m/\rho A \quad (1)$$

where δ is the thickness of hydrocarbon film, m the mass of hydrocarbon deposited, ρ the density of hydrocarbon, and A the area covered by hydrocarbon film.

This equation assumes that the hydrocarbon deposits are of uniform density and thickness. Although this assumption may be valid, the density of and area covered by the hydrocarbon are not readily measurable quantities.

The area must refer to all portions of the reactor below the melting point of the hydrocarbon employed. The geometric flat area in direct contact with the liquid nitrogen was 19.6 cm². The additional fin area varied with the hydrocarbon used, and a heat transfer analysis led to the additional incremental areas: propane, 0.6 cm²; propylene, 0.9 cm²; *n*-butane, 7.5 cm²; 3-methylpentane, 11.0 cm².

The density of the solid hydrocarbons is not known with much accuracy, but is believed to be about 0.8 g/cm³.¹⁵

Film thicknesses, calculated from eq 1, were checked by optical measurement. This optical technique in-

(15) H. Sackman and F. Sauerwald, *Z. Phys. Chem.*, (Leipzig), **195**, 295 (1950).

Table I: Summary of Film Thicknesses

Hydrocarbon	Film thickness calculated from material balance, μ/mg of hydrocarbon	Film thickness measured optically, μ/mg of hydrocarbon	Standard deviation for optically measured film thickness
Propane	0.62 ± 0.12	0.69 ± 0.07	0.01
Propylene	0.61 ± 0.12	0.73 ± 0.07	0.03
<i>n</i> -Butane	0.46 ± 0.10	0.44 ± 0.04	0.01
3-Methylpentane	0.41 ± 0.08	0.36 ± 0.04	0.01
Propane and 3-methylpentane (1:1)	0.47 ± 0.09	0.47 ± 0.05	0.01

volved directing monochromatic light onto the hydrocarbon film during the slow deposition process. Some of the incident light reflected directly from the hydrocarbon surface and some penetrated the hydrocarbon and reflected off the supporting surface. Interference results between these two sets of rays. Whether this interference is constructive or destructive depends, of course, on whether the two sets of rays are in phase or out of phase, and this in turn is dependent on the difference in the distances traveled by the two sets of rays. As the hydrocarbon film increases in thickness, this difference also increases; therefore, the two sets of rays are alternately in phase and out of phase. This results in a variation in the intensity of reflected light. By observing the number of cycles during the hydrocarbon deposition, one can determine the thickness of the film from

$$N\lambda = 2\delta(\mu^2 - \sin^2 i)^{1/2} + \lambda/2 \quad (2)$$

where N is the number of cycles, λ the wavelength of incident light, μ the refractive index of hydrocarbon, i the angle of incidence of light, and δ the hydrocarbon film thickness. The variations in the intensity of the reflected light were detected by a photoelectric cell which was connected to a recorder. Film thicknesses calculated from eq 2 are believed accurate to within 10%, the largest uncertainty being the value (1.45) chosen for the refractive index of the hydrocarbons.

Film thicknesses for propylene as calculated from eq 2 are plotted in Figure 2 as a function of the mass of hydrocarbon deposited. From the slope of the line in this plot, one obtains the film thickness per unit of mass deposited. The values thus obtained for the various hydrocarbons are presented in Table I along with the values that would be predicted from eq 1.

As indicated by the standard deviations given in Table I, the optical data are quite precise. It can also be seen from Table I that the film thicknesses determined by the two separate methods agree within the assumed accuracy of the calculations. The densities assumed for the hydrocarbons appear reasonable, and the films are, therefore, not frostlike structures.

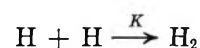
Determination of Gas Phase Hydrogen Atom Concentrations

In the experimental investigation reported here, it was not possible to measure directly the concentration of hydrogen atoms in the gas phase above the hydrocarbon film. The concentration was, therefore, estimated in an indirect manner. Previous studies¹¹ have indicated that the initial reaction rate of atomic hydrogen with solid propylene films is directly proportional to the concentration of atomic hydrogen in the gas phase. Therefore, within each set of permeation runs, additional experiments were made with 2.4- μ films of pure propylene. The initial rates of reaction of hydrogen atoms with these standard films were assumed to be proportional to the hydrogen atom concentrations, and the proportionality constant was determined from the work of Espino.¹¹

The hydrogen atom concentrations calculated in this manner are believed accurate within a factor of two.

Mathematical Model for Atomic Hydrogen Diffusion in Hydrocarbon Films

Atomic hydrogen from the gas phase penetrates the hydrocarbon interface, diffuses through the solid, and reacts with the molybdenum trioxide at the back side of the film. In addition, as it diffuses, some of the atomic hydrogen is eliminated by recombination reactions in the film



The mathematical equation encompassing the entire process can be obtained by writing a material balance over a differential thickness of the hydrocarbon film.

$$D \frac{d^2H}{dx^2} = KH^2 \quad (3)$$

D is the diffusion coefficient of hydrogen atoms in the solid, H the concentration of atomic hydrogen at point x , and K the reaction rate constant for hydrogen recombination.

To analyze the data the hydrogen atom concentration was normalized in the following manner

$$H^* = H/H_g S = H/H_s$$

where H^* is the normalized hydrogen atom concentration, H_g the gas phase concentration, H_s the solid phase concentration at the gas-hydrocarbon interface, and S the solubility constant for atomic hydrogen in the hydrocarbon. Equation 3 then becomes

$$\frac{d^2 H^*}{dx^2} = \frac{KH_s}{D} H^{*2} \quad (4)$$

From the solution of eq 4 plots similar to that in Figure 3 were constructed. The ordinate in this figure is the normalized concentration gradient at $x = \delta$, *i.e.*, at the hydrocarbon-molybdenum oxide interface. This ordinate was chosen since it is proportional to the rate at which atomic hydrogen reaches the molybdenum oxide. This latter rate was experimentally measured. The abscissa, which was the reciprocal of the film thickness, was also easily determined.

The two boundary conditions, $H = H_s$ at $x = 0$ and $H = 0$ at $x = \delta$, were chosen from the following reasoning. It was experimentally observed that the reaction rates of atomic hydrogen with bare molybdenum oxide films were orders of magnitude larger than the rates when the films were coated with hydrocarbons. Therefore, the reaction rates in the latter experiments were diffusion controlled, and it can be assumed that the hydrogen atom concentrations at the hydrocarbon-molybdenum oxide interface were essentially equal to zero. The concentration at the gas-hydrocarbon interface was assumed constant and equal to the solubility constant times the concentration in the gas phase.

Permeation Rates through Alkanes

The rate of permeation of hydrogen atoms to the MoO_3 surface was determined for various alkane films

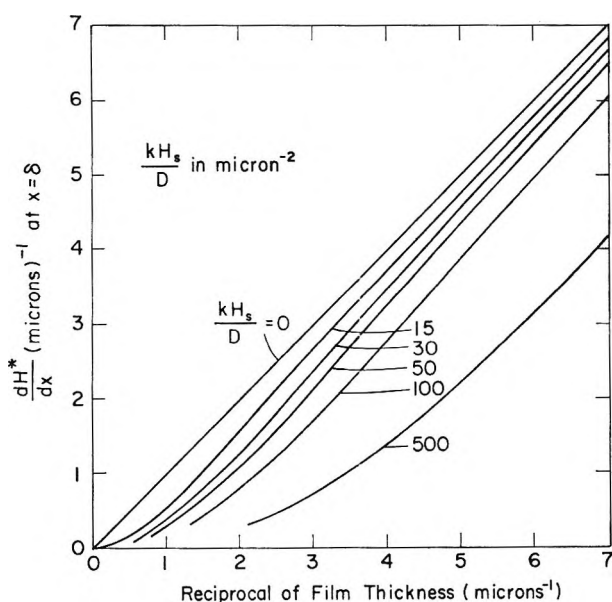


Figure 3. Theoretical curves for diffusion and recombination.

as a function of film thickness. These data are shown in Table II. Figure 4 shows these same data plotted as the ratio of the permeation rate to the gas phase hydrogen atom concentration as a function of inverse film thickness. There is some scatter, but the data for each individual run series are surprisingly linear. Several points should be noted in Figure 4. First, there are large differences in permeation rates between these low-molec-

Table II: Permeation Rates of Atomic Hydrogen through Alkanes

Alkane	Run	Film thickness, μ	Permeation rate, g-atoms/cm ² min $\times 10^{10}$	Gas phase hydrogen atom concentration, g-atoms/cm ³ $\times 10^{10}$
Propane	2a	0.20	34.4	4
	b	0.52	12.3	4
	d	1.02	7.0	4
	e	1.04	5.6	4
Propane	4a	2.0	2.7	9
	b	0.99	9.8	9
	d	0.40	26.3	9
	e	0.20	61.7	9
	f	0.15	85.6	9
	7a	1.00	4.2	3
Propane	c	0.33	21.6	3
	d	0.17	31.4	3
	10a	0.33	4.6	2
<i>n</i> -Butane	c	1.00	1.2	2
	e	0.17	9.1	2
	6a	1.00	0	4
3-Methylpentane	b	0.20	0.3	4
	8a	0.33	7.0	4
Propane, 3-methylpentane (1:1)	c	1.00	1.8	4
	e	0.17	14.4	4

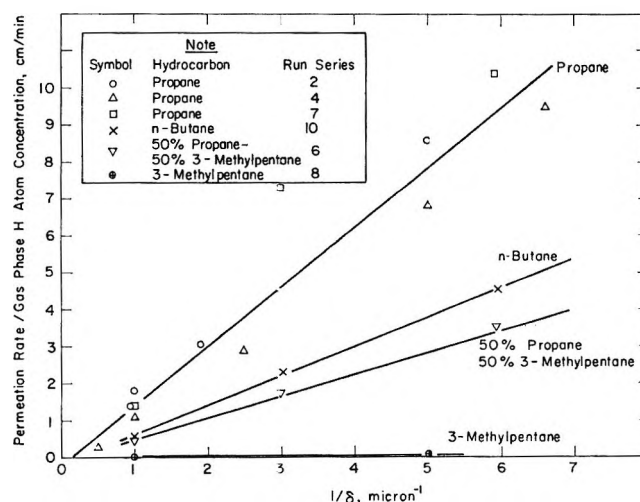


Figure 4. Alkane permeation data.

Table III: Pressure Decrease and Color Change for MoO₃ in Propylene Runs

Time, min	1- μ film		0.33- μ film		0.167- μ film	
	Pressure change, μ	Change in recorder reading	Pressure change, μ	Change in recorder reading	Pressure change, μ	Change in recorder reading
0	0	0	0	0	0	0
2	28	0	13.1	0	6.9	0.1
4	42.3	0	16.8	0	8.7	0.3
6	48.5	0	19.4	0.1	10.2	0.8
8	53.4	0	21.2	0.3	10.6	1.5
10	57.6	0	22.0	0.6	10.9	2.3
12	61.2	0	22.4	1.0	11.0	3.2
14	63.1	0	22.6	1.6	11.2	4.3
16	64.2	0	22.7	2.2	11.3	5.3
18	64.9	0	22.8	2.8	11.4	6.4
20	65.3	0	22.8	3.3	11.5	7.4
22	65.5	0.1	22.9	3.9	11.6	8.4
24	65.8	0.2	22.9	4.5		
26	65.9	0.3	23.0	5.2		
28	65.9	0.4	23.1	5.8		
30		0.6	23.1	6.3		
32		0.7				
34	66.0	0.9				
36		1.0				
38		1.2				
40	66.0	1.3				
42		1.5				

ular weight alkanes. 3-Methylpentane shows essentially no permeability unless diluted with propane. Also, though not as obvious due to the scatter and paucity of the data, the best lines (or curves) through the data do not intersect the origin at an extrapolated infinite film thickness. The latter observation might have been expected from the generalized plot of Figure 3. For finite, but small ($<500 \mu^{-2}$), values of KH_s/D , the calculated curves are close to linear at inverse film thicknesses of $1-8 \mu^{-1}$ but show a large curvature at values less than $1 \mu^{-1}$. It appears that the experimental data taken in this work confirm that KH_s/D is greater than zero but probably less than about $50 \mu^{-2}$.

A less cautious analysis might invoke the fact that, except possibly for run set 4, none of the data on Figure 4 show the inflection point that is evident on Figure 3 for cases involving a finite KH_s/D . Acceptance of this fact would lead one to postulate a very small value or negligible value of KH_s/D . If it were essentially zero, then, of course, the hydrogen atom concentration in the film would be linear with film thickness and the relation between the hydrogen flux and film thickness would be

$$J = SDH_g/\delta \quad (5)$$

J is the hydrogen atom flux, δ the film thickness, and the other terms are defined in eq 4. The product SD is often defined as the permeability constant, P . Since J , H_g , and δ are known, values of P can be determined from the slope of the lines in Figure 4. For propane it is around $2 \times 10^{-6} \text{ cm}^2/\text{sec}$ and for n -butane about

$1 \times 10^{-6} \text{ cm}^2/\text{sec}$. The reliability of these values is no better than a factor of two since H_g is not known to a greater accuracy than this. P for 3-methylpentane is at least an order of magnitude lower unless diluted with propane.

It is not known at the present time why there is such a large difference in permeation rates of hydrogen atoms through these different alkanes. From the discussion above, it does not appear that there is a significant difference in their ability to catalyze the recombination reaction.

The permeation rates appear to vary approximately in an inverse manner to the alkane freezing points; also the low permeation rate of 3-methylpentane may be due to the fact that the temperature used (77°K) is approximately half the melting point. A rough rule-of-thumb which is often invoked is that mass transport in solids become insignificant at a temperature less than one-half the melting point, *i.e.*, the so-called Tammann temperature.¹⁶ It thus appears that diffusion of hydrogen atoms becomes more difficult, or the solubility less, the farther one operates below the melting point.

Permeation of Hydrogen Atoms through Propylene Films

Three runs were made with thin propylene films covering a MoO₃ surface. In these cases, hydrogen atoms reacted with the propylene as well as diffused into the film to the MoO₃ sublayer. The pressure decrease in

(16) J. N. Sherwood, *Proc. Brit. Ceram. Soc.*, **9**, 233 (1967).

the system was indicative of the reaction of hydrogen atoms by both reactions where the color change of the MoO_3 was assumed to represent only the H-MoO_3 reaction. The data are shown in Table III. At the end of each run the propylene was essentially completely reacted. Thus almost all of the pressure drop at this time was due to reaction with the molybdenum oxide. Permeation rates calculated at the end of the runs were, as one would expect, very similar to those for the propane films.

During the first few minutes of reaction, the rate of hydrogen uptake by the propylene films was orders of magnitude larger than the permeation rates through propane films of the same thickness. Moreover, for the thin propane films, only a small fraction of the hydrogen atoms which entered the film recombined before reaching the molybdenum oxide. Therefore, it is obvious that, at the conditions of this investigation, atomic hydrogen reacts more rapidly with pure solid propylene than it recombines within the solid.

It is interesting to note that for the thicker propylene films there is no measurable color change of the molybdenum trioxide during the first few minutes. Since this is the time when hydrogen reacts most rapidly with the propylene, it is also the time when the concentration of propyl radicals is the greatest. The fact that no reaction of the radicals with the oxide was observed during this period indicates that either very few radicals reached the oxide or the reaction rate was very slow. Previous investigators¹⁷ have indicated that this reaction occurs rapidly at room temperature. However, this is not necessarily the case at liquid nitrogen temperature.

Appendix

Deposition of the MoO_3 Films. Thin, smooth MoO_3 films with surface irregularities less than about 0.05μ were desired. No previous attempt to prepare such films had been reported in the literature nor were simple techniques such as deposition from a solvent successful. The best method found was vacuum deposition in a Kinney KSE-2 system as shown schematically in Figure 5. A removable aluminum plug covered the inside walls of the glass joint to prevent deposition on the glass side walls. The diameter of the MoO_3 layer was, therefore, slightly less than that of the flat, top deposition surface. With the vacuum used, the mean-free path of the vaporized MoO_3 molecules was estimated to be over 100 cm, a length greatly in excess of the distance between the tungsten boat and deposition surface (about 5.6 cm).

The thickness of the film was estimated from kinetic theory. If ω is the total mass of MoO_3 evaporated and the solid has a density ρ in the film, then the thickness, t , of the film at a distance r from the boat is given by

$$t = (\alpha\omega n / \rho 2\pi r^2) \cos^n \theta \quad (6)$$

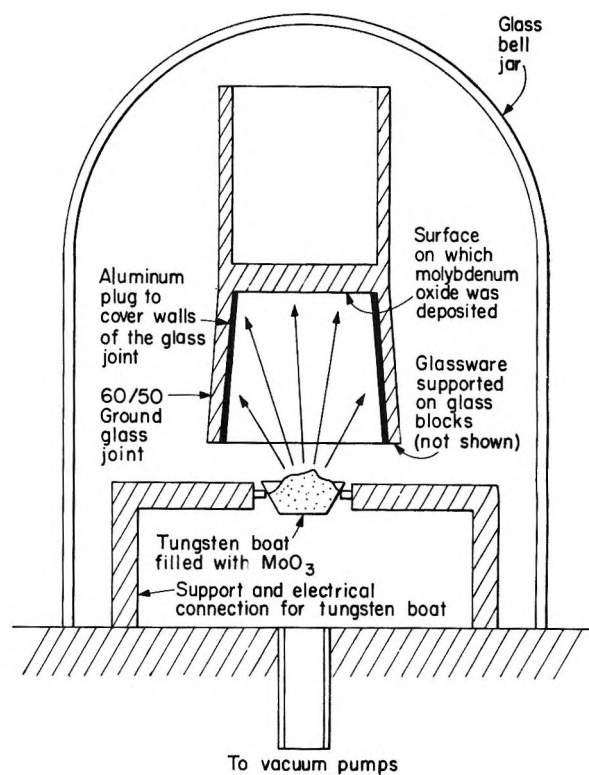


Figure 5. Vacuum deposition apparatus.

The angle θ is as shown in Figure 6. The exponent n is unity if the MoO_3 sublimation is considered to take place from a spherical particle and two if one considers sublimation to occur from a flat plane. α is the "sticking coefficient"; a value of unity would result in the thickest possible film. In this work α was chosen as 0.75.¹⁸

In the present apparatus, $d = 5.6$ cm, and the thickness at any value of a ($= d \tan \theta$) is

$$\frac{t_a}{t_0} = \frac{\cos^{n+2} \theta_a}{\cos^{n+2} \theta_0}, \theta_0 = 0^\circ \quad (7)$$

with the maximum value of a of about 2 cm

$$\theta = \tan^{-1} (2/5.6) = \tan^{-1} (0.36) = 20^\circ$$

Thus

$$\frac{t(a = 2 \text{ cm})}{t(a = 0 \text{ cm})} = (0.94)^{n+2}$$

If $n = 2$, the ratio of minimum-to-maximum thickness is 0.78; if $n = 1$, the same ratio is 0.83. Thus, though the thickness varied across the films, the variation was not great. Generally, the integrated average MoO_3 film thickness was less than 0.25μ .

The vacuum deposition procedure described above yielded sufficiently uniform films. Unfortunately, at

(17) H. W. Melville and J. C. Robb, *Proc. Roy. Soc.*, A196, 464, 479 (1949).

(18) R. C. Williams and R. C. Backus, *J. Appl. Phys.*, 20, 98 (1949).

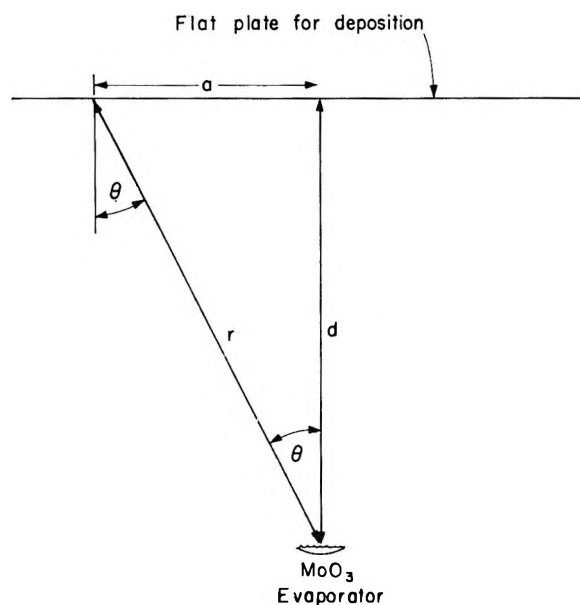


Figure 6. Deposition geometry.

the deposition conditions, the trioxide was found to be unstable with respect to dissociation into oxygen and lower oxides. Consequently, the deposited films were blue rather than the desired yellow color. This necessitated the reoxidation of the films to the trioxide. The best method found for accomplishing the oxidation was to heat the films to about 650°F in an oxygen atmosphere for about 3 days. At higher temperatures considerable mass rearrangement occurred; *i.e.*, microscopic examination showed surface irregularities on the order of 1 μ . What appeared to happen was that, due to surface tension considerations, the entire film broke up and small spheres and chains of spherelike particles formed.

To determine the dimensions of the surface irreg-

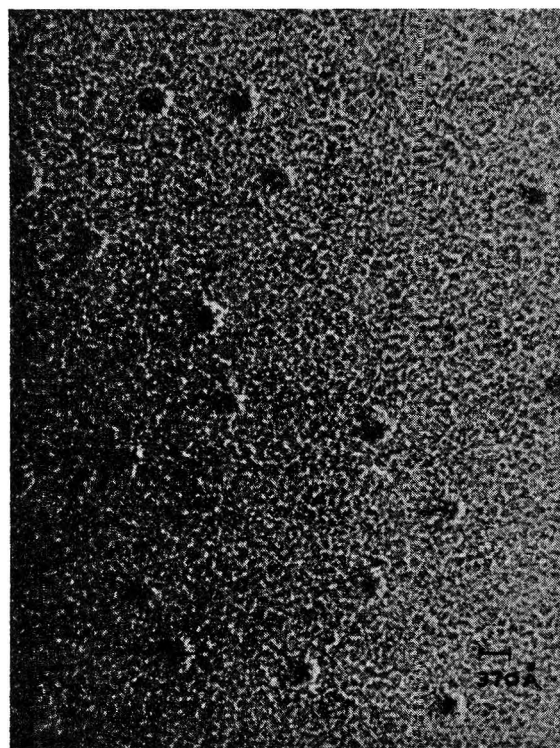


Figure 7. Electron micrograph of MoO₃ film.

ularities of the films oxidized at 650°F, the molybdenum oxide films were deposited on carbon grids, oxidized to MoO₃, and then examined in an electron microscope. A reproduction of an electron micrograph is shown in Figure 7. As can be seen, the diameter of the largest surface irregularities is about 0.03 μ . The depth is probably about half of that.

Acknowledgment. This work was supported by the National Science Foundation under Grant GK-142, and their support is most gratefully acknowledged.

An Electron Spin Resonance Study of Copper(II) O-Alkyl-1-amidinourea

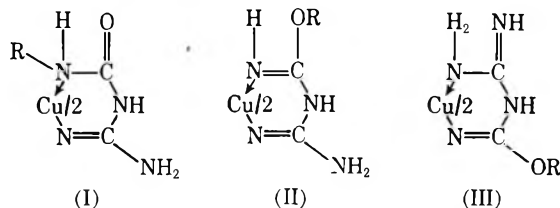
Complexes. Properties of the CuN_4^{2-} Chromophore¹by John R. Wasson^{2a} and Charles Trapp^{2b}

Department of Chemistry, Illinois Institute of Technology, Chicago, Illinois 60616 (Received March 20, 1969)

The esr and optical spectra of copper(II) O-alkyl-1-amidinourea complexes, $\text{Cu}(\text{C}_2\text{N}_4\text{H}_4\text{OR})_2$ (R = alkyl substituent), and their nitrate salts demonstrate that the metal-ligand covalency in these compounds is comparable to that found in copper(II) phthalocyanine and porphyrin complexes. The covalency of the O-alkyl-1-amidinourea complexes is attributed to the strong σ interaction of copper(II) ion with a deprotonated imino ligand bonding site and electron delocalization over the chelate ring. The unusual pink color of these planar complexes arises from high-energy "d \leftarrow d" electronic transitions and is in agreement with the strong ligand field character of the ligands ascertained from esr parameters. The bonding sites employed by the ligands, the effects of protonation of the coordinated ligands, and plausible structures for the complexes are discussed in terms of chemical and spectroscopic data as well as qualitative Hückel molecular orbital calculations. The general properties of complexes containing the equivalent CuN_4^{2-} chromophore are summarized.

Introduction

The preparation of copper(II) complexes described as guanylalkylurea chelates(I) has been reported by Dutta and Ray.³ Diana, Zalay, and Cutler⁴ studied the *n*-butyl and *n*-hexyl derivatives and showed that the compounds described by Dutta and Ray are in reality O-alkyl-1-amidinourea (R-au) complexes (II or III). In their study of nickel(II) R-au compounds,



Rasmussen and Baker⁵ found an infrared band at 1100 cm^{-1} characteristic of the ether group which would not be present in guanylalkylurea complexes. Dutta and Syamal⁶ have presented additional infrared and chemical (methoxyl group determination for O-methyl-1-amidinourea) evidence for the R-au formulation of the ligands.

Coordinated R-au ligands show a residual basicity which accounts for the large number of salts that have been characterized for these complexes.⁷ Upon treatment with ammonium salts, they are protonated, ammonia is liberated, and salts of the complexes are the result of the reaction. These observations have been cited as evidence of an amino group that remains free after complexation. Hereafter, the nitrate salts studied in the present investigation are represented by $\{\text{Cu}(\text{R-au})_2\}(\text{NO}_3)_2$.

Unlike most complexes with nitrogen-donor ligands, which are colored various shades of blue or green, the R-au complexes and their nitrate salts are pink. This

unusual coloration arises from the strong ligand field in the CuN_4^{2-} chromophore (where the 2- represents the strongly σ -bonding nitrogen atoms of the deprotonated ligands). The strong field nature of R-au ligands is also shown by their formation of diamagnetic nickel(II)⁵ and low-spin cobalt(II) complexes.⁸ As few esr studies of copper(II) ion in very strong ligand fields have been reported and the bonding sites proposed⁷ for R-au ligands are not unambiguous, we undertook an investigation of the esr and optical spectra of the copper(II) R-au compounds in order to establish the extent of covalency in the metal-ligand interaction, effects of protonation on the covalency, and to corroborate the proposed bonding sites employed by these ligands.

Experimental Section

All chemicals employed in these experiments were of the best available grade. Dicyandiamide was obtained from the Aldrich Chemical Co., Milwaukee, Wis. Analyses for C, H, and N were performed by Alfred Bernhardt, Mikroanalytisches Laboratorium, Max-

(1) From a dissertation submitted to the Graduate School of Illinois Institute of Technology by J. R. W. in partial fulfillment of the requirements for the degree of Doctor of Philosophy.

(2) (a) Department of Chemistry, University of Kentucky, Lexington, Ky. 40506; (b) Department of Chemistry, University of Louisville, Louisville, Ky. 40208.

(3) R. L. Dutta and P. Ray, *J. Indian Chem. Soc.*, **36**, 499 (1959).

(4) G. D. Diana, E. S. Zalay, and R. A. Cutler, Jr., *J. Org. Chem.*, **30**, 298 (1965).

(5) V. Rasmussen and W. A. Baker, Jr., *J. Chem. Soc.*, **A**, 580 (1967).

(6) R. L. Dutta and A. Syamal, *J. Indian Chem. Soc.*, **44**, 569 (1967).

(7) R. L. Dutta and A. Syamal, *Coord. Chem. Rev.*, **2**, 441 (1967).

(8) V. Rasmussen and W. A. Baker, Jr., *J. Chem. Soc.*, **A**, 1712 (1967).

Table I: Analyses of Complexes

Compound	Found			Calculated for			
	%C	%H	%N	%C	%H	%N	
{Cu(methyl-au) ₂ }(NO ₃) ₂	17.21	4.13	33.52	17.16	3.84	33.36	CuC ₈ H ₁₆ N ₁₀ O ₈
{Cu(ethyl-au) ₂ }(NO ₃) ₂	21.71	4.70	31.34	21.45	4.50	31.27	CuC ₈ H ₂₀ N ₁₀ O ₈
{Cu(propyl-au) ₂ }(NO ₃) ₂	25.38	5.14	29.43	25.23	5.08	29.43	CuC ₁₀ H ₂₄ N ₁₀ O ₈
{Cu(isopropyl-au) ₂ }(NO ₃) ₂	25.28	5.11	29.41	25.23	5.08	29.43	CuC ₁₀ H ₂₄ N ₁₀ O ₈
{Cu(butyl-au) ₂ }(NO ₃) ₂	28.66	5.73	27.66	28.60	5.60	27.79	CuC ₁₂ H ₂₈ N ₁₀ O ₈
{Cu(isobutyl-au) ₂ }(NO ₃) ₂	28.64	5.63	27.75	28.60	5.60	27.79	CuC ₁₂ H ₂₈ N ₁₀ O ₈
{Cu(dicyandiamide) ₂ (H ₂ O) ₂ }(NO ₃) ₂	12.44	3.23	...	12.24	3.28	35.68	Cu ₄ H ₁₂ N ₁₀ O ₈

Planck-Institut für Kohlenforschung, 433 Mülheim (Ruhr), West Germany.

Infrared spectra in the region 4000–200 cm⁻¹ were measured with a Beckman IR:12 instrument using Nujol and Fluorolube (Hooker Chemical Co) mulls on CsBr and CsI cells. Electronic spectra of mull solids were obtained by a technique described previously.⁹ A Cary Model 14 recording spectrophotometer was used to obtain the mull and solution spectra.

Esr spectra were obtained with a Varian X-band instrument and magnetic field and frequency calibration accessories described previously.¹⁰ Solution spectra were taken at room temperature using Pyrex capillary tubing as well as a quartz aqueous solution cell and a Varian E-4531/V-4531 multipurpose cavity. Cylindrical quartz sample tubes were used for the spectra of powdered and frozen solution samples.

Preparation of Complexes. {Cu(R-au)₂}(NO₃)₂. Stoichiometric amounts (1:2 metal-ligand ratio) of copper(II) nitrate trihydrate and dicyandiamide were placed in the appropriate alcohol which serves as reactant and solvent for the reaction Cu(NO₃)₂ + NH₂C(=NH)NHCN + ROH → {Cu(R-au)₂}(NO₃)₂. The reaction mixture was stirred magnetically until an appreciable amount of pink precipitate formed. The precipitate was isolated by filtration, washed with large volumes of the reactant alcohol, acetone, and ether, and then dried over anhydrous calcium chloride. This method was used to prepare the methyl, ethyl, propyl, butyl, and isobutyl derivatives. Yields were on the order of 80% of theory. The preparation described by Dutta and Ray³ involved reflux conditions.

{Cu(dicyandiamide)₂(H₂O)₂}(NO₃)₂. With isopropyl alcohol and phenyl-2-ethanol, the above preparation gave a pale green precipitate. Under reflux the green precipitate gave the pink isopropyl-au complex but no phenyl-2-ethanol derivative was obtained. Other R-au complexes could be prepared from this compound by refluxing with the appropriate alcohol.

{Cu(ethyl-au)₂}(NO₃)₂-doped samples of {Ni(ethyl-au)₂}(NO₃)₂ were prepared by adding small amounts (5% and less) of copper(II) nitrate trihydrate to the reactants used in the preparation⁵ of the orange diamagnetic nickel complex. A similar procedure was used for the methyl complex.

{Cu(methyl-au)₂}. The nitrate salt was treated with concentrated aqueous NaOH and the reaction mixture was stirred for an hour. The pink-red product was isolated by filtration, washed with small amounts of cold water and ether, and dried *in vacuo* at 65° for several days. *Anal.* Calcd for Cu(C₃H₇N₄O)₂: Cu, 21.63. Found: Cu, 21.54. Copper(II)-doped samples of Ni(methyl-au)₂ were prepared by treating the doped nitrate salts similarly. Samples of the *n*-propyl derivative were prepared in the same manner. *Anal.* Calcd for Cu(C₃H₁₁N₄O)₂: Cu, 18.16. Found: Cu, 18.21. (See Table I.)

The Hückel molecular orbital calculations were performed on an IBM Model 360-40 data processing system with a Jacobi diagonalization routine.

Results and Discussion

The Dicyandiamide Intermediate. Baker and Daniels¹¹ isolated the green dicyandiamide(dcca) complex, Cu(dcca)₂SO₄·2H₂O, and thus were able to provide evidence for the template nature of the reaction described by Dutta and Ray.³ Our isolation of the pale green complex, {Cu(dcca)₂(H₂O)₂}(NO₃)₂, from the reaction of dcca with copper(II) nitrate in the presence of isopropanol and phenyl-2-ethanol constitutes further evidence for a template mechanism in the preparation of R-au complexes. The infrared spectrum of {Cu(dcca)₂(H₂O)₂}(NO₃)₂ exhibits C≡N stretching at 2258 and a shoulder at 2220 cm⁻¹. Since dcca itself has ν(C≡N) at 2210 and 2182 cm⁻¹ and ν(C≡N) usually shifts to higher wave numbers as a result of coordination, it seems reasonable that the complex has dcca coordinated to copper through the nitrile nitrogen. No infrared evidence suggesting nitrate coordination was found. In preparing the R-au nitrate complexes at room temperature, we noted that in almost all cases a small amount of a pale green precipitate formed which was converted to the pink complexes, the rate of conversion generally decreasing with increasing molecular weight of the alcohol.

(9) J. R. Wasson, *Chemist-Analyst*, **56**, 36 (1967).

(10) J. R. Wasson, C. I. Shyr, and C. Trapp, *Inorg. Chem.*, **7**, 469 (1968).

(11) W. A. Baker, Jr., and M. Daniels, *J. Inorg. Nucl. Chem.*, **25**, 1194 (1963).

Table II: Electronic Absorption Spectra. Positions of Band Maxima^a

	Solvent ^b	λ_{max} , m μ	$1/\lambda_{\text{max}}$, cm ⁻¹	ϵ_M , M ⁻¹ cm ⁻¹
Cu(methyl-au) ₂	NM	490 (595)	20,410 (16,810)	
	Water	504 (560)	19,840 (17,860)	42 (32)
	PY	492 (550)	20,330 (18,180)	43 (33)
	DMF	492 (550)	20,330 (18,180)	42 (33)
	DMSO	489 (546)	20,450 (18,320)	42 (33)
Cu(methyl-au) ₂ (NO ₃) ₂	NM	510	19,610	...
	DMSO	555	18,020	40
Cu(ethyl-au) ₂ (NO ₃) ₂	NM	520	19,230	...
	PY	582	17,180	40
	DMF	544	18,380	40
	DMSO	558	17,920	39
Cu(<i>n</i> -propyl-au) ₂	NM	472 (550)	21,190 (16,810)	...
	DMF	490 (550)	20,410 (16,810)	42 (32)
	DMSO	490 (550)	20,410 (16,810)	42 (31)
Cu(<i>n</i> -propyl-au) ₂ (NO ₃) ₂	NM	512	19,530	...
Cu(isopropyl-au) ₂ (NO ₃) ₂	NM	510	19,610	...
Cu(<i>n</i> -butyl-au) ₂ (NO ₃) ₂	NM	522	19,160	...
Cu(isobutyl-au) ₂ (NO ₃) ₂	NM	510	19,610	...

^a Parentheses refer to shoulders. ^b NM = Nujol mull; PY = pyridine; DMF = N,N-dimethylformamide; DMSO = dimethylsulfoxide.

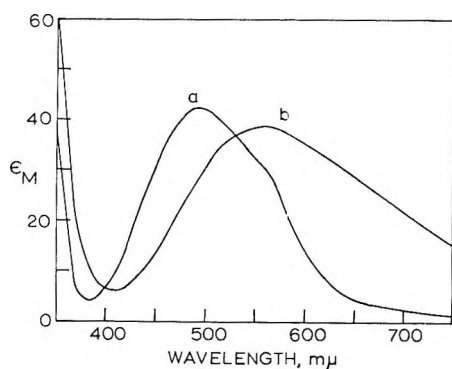


Figure 1. Absorption spectra of: a, $\{\text{Cu}(\text{methyl-au})_2\}$; and b, $\{\text{Cu}(\text{methyl-au})_2\}(\text{NO}_3)_2$ in dimethyl sulfoxide.

Electronic Absorption Spectra. The electronic spectra of R-au complexes are given in Table II and typical spectra are shown in Figure 1. In the solid state the R-au complexes exhibit a maximum at about 20,500 cm^{-1} and the nitrate salts at about 19,500 cm^{-1} . This single band is similar to that observed in planar copper(II) complexes with aldimine and pyrrole-derivative ligands,¹² the pink succinimidatocopper(II) complexes,¹³ and the closely related biguanide¹⁴ compounds. The absorption maxima in Table II agree substantially with those of R-au complex acetate salts.⁷ Unlike Cu(II)-doped $\text{ZnHg}(\text{SCN})_4$ ¹⁵ or the red-brown bis(benzimidazole)copper(II) complex¹⁶ the pink R-au complexes and their salts have no near-infrared absorption characteristic of tetrahedral geometry. The extinction coefficients ($\epsilon_M \sim 40$) of the visible absorption bands are well within the range 1–100 observed for “d ← d” transitions and the spectra are consistent with a planar geometry for the complexes. In solution, the absorp-

tion spectra of the nitrate salts become broadened and shifted, probably as a result of axial ligation by solvent molecules. Taking D_{4h} as the effective symmetry of the CuN_4^{2-} chromophore in R-au complexes (an assumption compatible with the esr spectra) a probable, but not unambiguous, “d” energy-level ordering¹⁷ is $x^2 - y^2 \gg z^2 > xy > xz, yz$. In the solid state the latter three levels are within about 2000 cm^{-1} of each other, but upon solvation the levels are shifted further apart and may be scrambled as a result of axial ligation.¹⁸ The modest 10% decrease in the absorption maxima of the R-au complexes upon protonation as well as the maintenance of the approximate equivalence of the nitrogen donor atoms and covalency changes shown by esr (discussed below) suggest that the effects of protonation are attributable to a modification of the inductive effects of the primary amino group on the chelate ring system.

While it is useful to employ Jørgensen's chromophore concept¹⁹ in general discussions of, say, NiN_6 and NiO_6 coordination clusters, the very large differences in the

(12) R. E. Clarke and J. H. Weber, *J. Inorg. Nucl. Chem.*, **30**, 1837 (1968), and references therein.

(13) S. Yamada and S. Miki, *Bull. Chem. Soc. Jap.*, **36**, 680 (1963).

(14) A. Chakravorty and S. Basu, *J. Inorg. Nucl. Chem.*, **17**, 55 (1961).

(15) D. Forster and D. M. L. Goodgame, *Inorg. Chem.*, **4**, 823 (1965).

(16) M. Goodgame and L. I. B. Haines, *J. Chem. Soc., A*, 174 (1966).

(17) C. J. Ballhausen, “Introduction to Ligand Field Theory,” McGraw-Hill Book Co., Inc., New York, N. Y., 1962.

(18) B. B. Wayland and A. F. Garito, *Inorg. Chem.*, **8**, 182 (1969).

(19) C. K. Jørgensen, “Inorganic Complexes,” Academic Press, New York, N. Y., 1963.

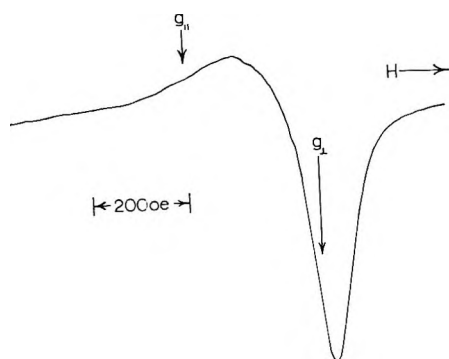


Figure 2. Room temperature esr spectrum of powdered $\{\text{Cu}(\text{methyl-}\text{au})_2\}(\text{NO}_3)_2$. Frequency 9.475 kMc. $g_{||} = 2.24$; $g_{\perp} = 2.06$

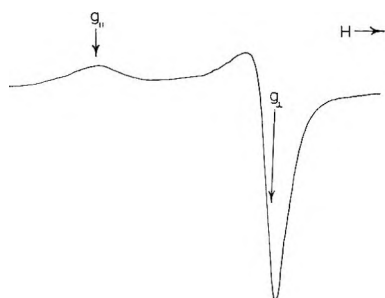


Figure 3. Room temperature esr spectrum of powdered $\{\text{Cu}(\text{dceda})_2(\text{H}_2\text{O})_2\}(\text{NO}_3)_2$. Frequency 9.475 kMc. $g_{||} = 2.354$; $g_{\perp} = 2.073$.

quadratic CuN_4 chromophores in $\text{Cu}(\text{NH}_3)_4^{2+}$ and $\text{Cu}(\text{R-}\text{au})_2$ complexes demonstrate a need for a modification of the nomenclature. For this reason we suggest that in cases where the four nitrogens are equivalent, as shown by X-ray structural analysis, single crystal electronic spectra or esr spectra, it is more appropriate to compare four-coordinate nitrogen-ligated copper(II) complexes in terms of equivalent CuN_4^{n-} chromophores when n represents the formal charge of the donor grouping. A study of the esr and optical spectra of CuN_4^{n-} chromophores is currently being carried out in these laboratories.

Analysis of the ESR Spectra. Figure 2 shows the room temperature esr spectrum of a powdered sample of $\{\text{Cu}(\text{ethyl-}\text{au})_2\}(\text{NO}_3)_2$. The spectrum yields only approximate²⁰ g values. The spectra of all the R- au complexes under the same conditions gave similar spectra with $g_{\perp} = 2.06 \pm 0.03$ and $g_{||} = 2.24 \pm 0.08$. The spectrum of the powdered dceda complex (Figure 3) shows two g values indicative of a tetragonal type symmetry about the copper(II) ion. In the absence of a suitable diamagnetic isomorphous diluent, a dispersion of a complex in a moderately high viscosity liquid in which it is not soluble can serve as an effective way of resolving hyperfine structure.²¹ From the esr spectrum of the dceda complex dispersed in benzyl alcohol-ethyl acetate (50:50 by volume) the copper

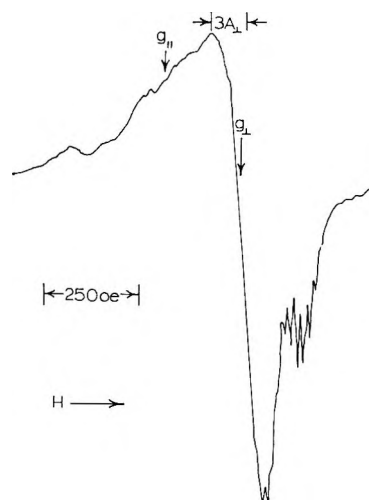


Figure 4. Room temperature esr spectrum of $\{\text{Cu}(\text{methyl-}\text{au})_2\}(\text{NO}_3)_2$ diluted into the corresponding Nickel(II) complex (about 2% copper). Frequency 9.475 kMc. $g_{||} = 2.174$; $g_{\perp} = 2.062$.

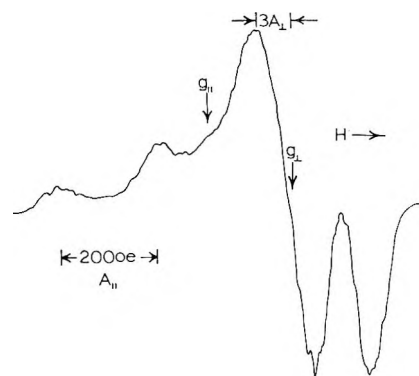


Figure 5. Frozen solution esr spectrum of $\{\text{Cu}(\text{methyl-}\text{au})_2\}$ in dimethylsulfoxide. Liquid nitrogen temperature. Frequency 9.132 kMc. $g_{||} = 2.176$; $g_{\perp} = 2.058$.

hyperfine splitting constants were determined by the method of Vännngard and Aasa.²²

The parameters $g_{||}$, g_{\perp} , $A_{||}^{\text{Cu}}$, and A_{\perp}^{Cu} can be measured²² from the anisotropic spectra of powdered magnetically dilute solids (Figure 4) and frozen solutions (Figure 5). In many instances, ligand superhyperfine structure components are also measurable but assignment of the components is not straightforward²³ since the principal axes of the superhyperfine tensor are not necessarily the same as those of the hyperfine tensor. Solution spectra (Figure 6) provide a measure

(20) J. W. Searl, R. C. Smith, and S. J. Wyard, *Proc. Phys. Soc.*, **74**, 491 (1959); *ibid.*, **78**, 1174 (1961); F. K. Kneubuhl, *J. Chem. Phys.*, **33**, 1074 (1960).

(21) D. E. O'Reilly, *J. Chem. Phys.*, **29**, 1188 (1958).

(22) T. Vännngard and R. Aasa, "Proceedings of the First International Conference on Paramagnetic Resonance, Jerusalem, 1962," Vol. 2, W. Low, Ed., Academic Press, New York, N. Y., 1963, p 509.

(23) G. F. Kokoszka and G. Gordon, "Technique of Inorganic Chemistry," H. B. Jonassen and A. Weissberger, Ed., Interscience Publishers, New York, N. Y., Vol. 8, 1968, p 151.

Table III: g Values and Hyperfine Structure Constants for Copper(II) Complexes

Complex	Medium	g_0	g_{av}^a	g_{\parallel}	g_{\perp}	$\times 10^4 \text{ cm}^{-1}$			
						$A_{\parallel}^{\text{Cu}}$	A_{\perp}^{Cu}	A_0^{Cu}	$A_0^{\text{N}^b}$
Cu(methyl-au) ₂	Ni(II) complex ^c	...	2.090	2.165	2.052	210	~20	...	15.6
	Water	2.100	91.8	15.8
	DMSO ^d	2.094	2.097	2.176	2.058	218	~25	89.0	15.8
	DMF	2.091	92.5	15.7
	PY	2.092	2.097	2.174	2.058	208	~26	93.9	15.8
{Cu(methyl-au) ₂ }(NO ₃) ₂	Ni(II) complex	...	2.104	2.174	2.062	203	~23	...	14.7
	DMSO	2.103	90.0	14.8
{Cu(ethyl-au) ₂ }(NO ₃) ₂	Ni(II) complex	...	2.096	2.174	2.057	203	~14	...	14.7
	Water	2.108	85.6	14.9
	DMSO	2.107	88.5	14.9
	DMF	2.108	86.2	14.9
	PY	2.107	82.1	...
Cu(<i>n</i> -propyl-au) ₂	DMSO	2.101	2.102	2.177	2.065	203	~25	99.0	15.9
	DMF	2.090	97.6	15.6
{Cu(dcda) ₂ (H ₂ O)}(NO ₃) ₂	Powder & dispersion	...	2.167	2.354	2.073	176	~12
Cu(II) β-phthalocyanine ^e	Free ligand	...	2.093	2.179	2.050	202	~19	...	16.7
Cu(II) tetraphenylporphine ^f	Chloroform, free ligand	2.107	2.112	2.193	2.071	202	~29	...	15.9
Cu(II) glycinate ^g	Cd(II) complex	2.267	2.055	141	10	...	8.1
Cu(II) oxinate ^h	Glass	2.172	2.042	162	~25	...	10.0
Cu(II) salicylaldoximate ^h	Glass	2.171	2.020	183	~41	...	14.0
{Cu(pyridine) ₄ }(NO ₃) ₂ ⁱ	Pt(II) complex	2.236	2.050	192	26	...	12.2

^a $g_{\text{av}} = 1/3(g_{\parallel} + 2g_{\perp})$. ^b A_{av}^{N} for powders and A_0^{N} for solutions. ^c For dilute powder samples the uncertainty in g_{\parallel} is ± 0.010 and in g_{\perp} it is ± 0.015 . ^d For frozen solutions the uncertainty in g_{\parallel} is ± 0.005 and in g_{\perp} it is ± 0.010 . ^e Reference 32. ^f Reference 33. ^g Reference 34. ^h Reference 26. ⁱ Reference 35.

of the average or isotropic g value, g_0 , as well as the isotropic hyperfine structure constant, A_0^{Cu} , and the isotropic ligand superhyperfine structure constant, A_0^{N} . Employing data obtained from the esr spectra of solids and solutions and values calculated from the relations

$$g_{\text{av}} = \frac{1}{3}(g_{\parallel} + 2g_{\perp}) \quad (1)$$

$$A_{\text{av}} = \frac{1}{3}(A_{\parallel} + 2A_{\perp}), \quad (2)$$

the parameters of the spin-Hamiltonian for the copper(II) ion in a tetragonal crystal field can be evaluated. It is noted that the use of the expressions for g_{av} and A_{av} (which are equated with the isotropic g_0 and A_0 values obtained from solution spectra) should be used with some caution since g_0 and A_0 values usually show some solvent dependence. A_{\parallel} and g_{\parallel} values, which can be accurately measured for magnetically dilute powders, can show a diluent dependence, *e.g.*, copper(II) oxinate,²⁴ and such parameters obtained from frozen solutions can show a temperature dependence, *e.g.*, copper(II) acetylacetonate.²⁵ Where possible, g_0 and g_{av} are both listed in Table III.

The spin-Hamiltonian for copper(II) ion in a tetragonal crystal field is given by

$$H = g_{\parallel}\beta H_z S_z + g_{\perp}\beta(H_x S_x + H_y S_y) + A_{\parallel}^{\text{Cu}} I_z S_z + A_{\perp}^{\text{Cu}}(I_x S_x + I_y S_y) \quad (3)$$

where β is the Bohr magneton and H is the applied

magnetic field. When ligand superhyperfine structure is present, an additional term of the general form $+S \cdot \Sigma A_n \cdot I_n$ is necessary. Here S is the total spin operator, A_n the superhyperfine structure tensor for the n ligand atoms, and I_n the ligand atom nuclear spin. The spin-Hamiltonian parameters for R-au complexes and their nitrate salts are listed in Table III. For the magnetically dilute solids the measured nitrogen superhyperfine structure parameter is listed. It was assumed that this nitrogen superhyperfine splitting observed in the high-field copper hyperfine components of the spectra corresponded closely to the average nitrogen superhyperfine splitting. This assumption is justified by the agreement between the A_0^{N} terms calculated from the spectra of powders and solutions. It is noted that the similarity of the esr spectra of {Cu(ethyl-au)₂}(NO₃)₂ in the corresponding nickel(II) complex and in solution indicate that the R-au ligand has not been replaced by solvent although the electronic spectra of solutions show that the solution species are not identical with that in the solid state. If the ligands were exchanging or the complexes decomposing, the nitrogen superhyperfine structure would probably be obliterated.²⁶

Kivelson and Neiman²⁷ have shown that g_{\parallel} is a

- (24) S. Fujiwara and K. Nagashima, *Anal. Chem.*, **38**, 1464 (1966).
 (25) H. R. Falle and G. R. Luckhurst, *Mol. Phys.*, **10**, 597 (1966).
 (26) H. R. Gersmann and J. D. Swalen, *J. Chem. Phys.*, **36**, 3221 (1963).
 (27) D. Kivelson and R. Neiman, *ibid.*, **35**, 149 (1961).

Table IV: Orbital Reduction Factors and Covalency Parameters

Complex	Medium	G	k_{\parallel}^2	k_{\perp}^2	α'^2_N	α_N^2	α_{Cu}^2	β^2	$\beta_1'^2$	$\times 10^8 \text{ cm}^{-1}$			
										ΔE_{xy}	ΔE_{zz}	β^2	$\beta_1'^2$
Cu(methyl-au)	Ni(II) complex	3.26	0.50	0.71	0.35	0.69	0.81	1.05	0.70	20.41	23.53	0.91	0.87
Cu(n-propyl-au) ₂	Frozen DMSO	2.78	0.54	0.90	0.36	0.69	0.81 ^b	0.98	0.77	20.41	23.53	0.94	0.96
{Cu(methyl-au) ₂ } (NP ₃) ₂	Ni(II) complex	2.42	0.49	0.88	0.33	0.71	0.80	1.23	0.67	19.61	21.05	1.05	0.78
{Cu(ethyl-au) ₂ } (NO ₃) ₂	Ni(II) complex	3.13	0.50	0.70	0.33	0.71	0.80	1.02	0.67	19.23	21.05	0.90	0.78
{Cu(dcda) ₂ (H ₂ O) ₂ } (NO ₃) ₂	Powder and dispersion	4.96	0.78	0.75	0.91	14.71	17.54
Cu(II) β -phthalocyanine	Free ligand	3.69	0.55	0.68	0.38	0.72	0.80	.80	.99	20.41	23.53 ^c	.87	.93
Cu(II) tetraphenylporphine	Chloroform, free ligand	2.77	0.59	0.98	0.36	0.69	0.82	1.39	0.85	20.41	23.53 ^c	1.51	1.23
Cu(II) glycinate	Cd(II) complex	5.00	0.18	0.89	0.72 ^b
Cu(II) oxinate	Glass	4.25	0.40	0.45	0.23	0.84	0.68	15.65 ^f	18.65
Cu(II) salicylaloximate	Glass	9.39	0.44	0.16	0.32	0.76	0.72	15.04 ^g	17.39
{Cu(pyridine) ₄ } (NO ₃) ₂	Pt(II) complex	4.88	0.66	0.54	0.27	0.77	0.83	0.88	0.76	18.70	18.70

^a Calculated using eq 6 and 7 with the assignments of ΔE_{xy} and ΔE_{zz} given in this table. ^b If instead of the frequently used value of 0.0360 cm^{-1} for $P = 2.0023 g_N \beta_0 \beta_N (r^{-2})$, the improved value {B. R. McGarvey, *J. Phys. Chem.*, **71**, 51 (1967)} 0.0397 cm^{-1} is used in eq 4, the estimated α^2 is reduced to 0.75 for Cu(*n*-propyl-au)₂ and 0.64 for Cu(II) glycinate. ^c Estimated values which are based on the assumption that ΔE_{xy} and ΔE_{zz} are the same as the values estimated for Cu(methyl-au)₂. ^d Reference 32. ^e Reference 33. ^f L. Morpurgo and R. J. P. Williams, *J. Chem. Soc.*, **A**, 73 (1966); ΔE_{zz} transition estimated. ^g From spectrum of the complex in DMSO. ^h Calculated using eq 6 and 7 and interchanging the ΔE_{xy} and ΔE_{zz} band assignments.

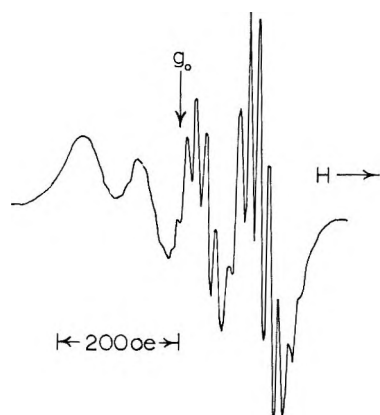


Figure 6. Solution esr spectrum of {Cu(methyl-au)₂} in dimethylformamide at room temperature. Frequency 9.422 kMc. $g_0 = 2.091$.

moderately sensitive function for indicating covalency. For ionic environments g_{\parallel} is normally 2.3 or larger and for more covalent environments it is less than 2.3. The R-au complexes, their nitrate salts, and the copper(II) phthalocyanine and tetraphenylporphine compounds listed in Table III fulfill the latter criterion for being covalent-type complexes. The qualitative validity of this conclusion is confirmed by the covalency parameters discussed below.

Esr Covalency Parameters. The esr spectra of the R-au complexes and their nitrate salts in solution exhibit nine nitrogen superhyperfine lines on the high-field $3/2 \leftarrow 3/2$ copper hyperfine splitting component which is indicative of four equivalent or nearly equivalent nitrogen atoms surrounding the copper ion. Also, in the present study the anisotropic spectra of dilute

powders and frozen solutions gave no indication of more than two g -values. In view of these results and the planar geometry suggested by the electronic spectra of the compounds an effective D_{4h} symmetry was assumed for the R-au complexes and their nitrate salts. The appropriate antibonding wave functions are

$$\psi_{B_{1g}} = \alpha d_{x^2-y^2} - 1/2 \alpha' (-\sigma_x^{(1)} + \sigma_y^{(2)} + \sigma_z^{(3)} - \sigma_y^{(4)})$$

$$\psi_{B_{2g}} = \beta_1 d_{xy} - 1/2 \beta_1' (p_y^{(1)} + p_x^{(2)} - p_y^{(3)} + p_x^{(4)})$$

$$\psi_{A_{1g}} = \alpha_1 d_z^2 - 1/2 \alpha_1' (\sigma_x^{(1)} + \sigma_y^{(2)} - \sigma_x^{(3)} - \sigma_y^{(4)})$$

$$\psi_{E_{1g}} = \begin{cases} \beta d_{zz} - \beta' / \sqrt{2} (p_z^{(1)} - p_z^{(3)}) \\ \beta d_{yz} - \beta' / \sqrt{2} (p_z^{(2)} - p_z^{(4)}) \end{cases}$$

where the notation is that of Kivelson and Neiman.²⁷ The B_{1g} and A_{1g} states account for the σ bonding. The B_{2g} and E_g states represent the in-plane and out-of-plane π bonding, respectively. The larger the square of the coefficients α' , β_1' , α_1' , and β' , the more covalent the bonding of the type associated with each parameter.²⁸ The ligand orbitals involved in the in-plane σ bonding are considered to be sp^2 -hybrid orbitals.²⁹ Overlap is included for the function describing in-plane σ -bonding, $\alpha^2 - 2\alpha\alpha'S + \alpha'^2 = 1$, where S , the overlap integral, is usually given the value 0.093.²⁷ α^2 was calculated using the expression of Kivelson and Neiman²⁷

$$\alpha^2 = -\left(\frac{A_{\parallel}}{0.036}\right) + (g_{\parallel} - 2.002) + \frac{3}{7}(g_{\perp} - 2.002) + 0.04 \quad (4)$$

(28) A. K. Wiersma and J. J. Windle, *J. Phys. Chem.*, **68**, 2316 (1964).

(29) A. H. Maki and B. R. McGarvey, *J. Chem. Phys.*, **29**, 31, 357 (1958).

and compared (Table IV) with α^2 evaluated from the overlap expression given above and α'^2 obtained from the nitrogen superhyperfine splitting. The parameter α'^2 is related to the interaction energy, W_L , by the expression.²⁷

$$W_L = \frac{4\pi}{9} \gamma_N \beta_0 \beta_N \alpha'^2 |\rho_N(0)|^2 S_z I_z^N \quad (5)$$

where γ_N is the magnetic moment of the ligand nitrogen atoms, β_0 the Bohr magneton, β_N the nuclear magneton, $|\rho_N(0)|^2$ the value of the ligand 2s function at the nitrogen nucleus, S_z the z component of the electron spin angular momentum operator, and I_z^N the z component of the spin angular momentum operator for the nucleus. $|\rho_N(0)|^2$ is taken to have a value of $33.4 \times 10^{24} \text{ cm}^{-3}$ as this value has been most frequently employed in calculating covalency parameters. The in-plane and out-of-plane π -bonding parameters, β_1 and β (Table IV), were obtained from the expressions²⁷

$$g_{\parallel} - 2.002 = - \frac{8\lambda_0 \alpha \beta_1}{\Delta E_{xy}} \left\{ \alpha \beta_1 - \alpha' \beta_1 S - \alpha' (1 - \beta_1^2)^{1/2} \frac{T(n)}{2} \right\} \quad (6)$$

$$g_{\perp} - 2.002 = - \frac{2\lambda_0 \alpha \beta}{\Delta E_{zz}} \left\{ \alpha \beta - \alpha' \beta S - \alpha' (1 - \beta^2)^{1/2} T(n) / \sqrt{2} \right\} \quad (7)$$

where α and α' were obtained using the nitrogen superhyperfine splitting, λ_0 is the spin-orbit coupling constant (-828 cm^{-1}) for the free Cu(II) ion, and $T(n)$ was set equal to 0.333.²⁷ ΔE_{xy} and ΔE_{zz} are the energies of the ${}^2B_{2g} \leftarrow {}^2B_{1g}$ and ${}^2E_g \leftarrow {}^2B_{1g}$ transitions, respectively.

In D_{4h} symmetry the g values for the Cu(II) ion with a ${}^2B_{1g}$ ground state can also be expressed^{17,30} by

$$g_{\perp} = 2.002 - 2k_{\perp}^2 \lambda_0 / \Delta E_{zz} \quad (8)$$

and

$$g_{\parallel} = 2.002 - 8k_{\parallel}^2 \lambda_0 / \Delta E_{xy} \quad (9)$$

where the k 's are the so-called orbital reduction factors and λ_0 , ΔE_{xy} , and ΔE_{zz} are as defined above. Combining the above expressions gives

$$G = \frac{g_{\parallel} - 2.002}{g_{\perp} - 2.002} = \frac{4k_{\parallel}^2 \Delta E_{zz}}{k_{\perp}^2 \Delta E_{xy}}$$

Orbital reduction factors have been used^{30,31} as a measure of covalency and are listed in Table V. In a formal manner

$$k_{\parallel}^2 = \alpha^2 \beta_1^2 - \alpha \alpha' \beta_1^2 S - \alpha' \alpha (\beta_1^2 - \beta_1^4)^{1/2} T(n) / 2$$

Since the latter terms are small, $k_{\parallel}^2 \approx \alpha^2 \beta_1^2$ and a similar expression applies for k_{\perp}^2 .

The in-plane σ -covalency parameters, α_{Cu^2} (Table IV), which are approximately the fraction of unpaired

electron density located on the copper(II) ion, calculated by the Kivelson-Neiman relation, eq 4, emphasize the similarity of the R-au complexes with copper(II) β -phthalocyanine³² and tetraphenylporphine³³ compounds but do not correspond to the analogous α^2 values (α_{N^2} in Table IV) calculated from the nitrogen superhyperfine splitting. The discrepancy is not unusual and has been explained³⁴ in terms of variation of metal 4s electron density which is assumed to be constant in the Kivelson-Neiman relation. The α_{N^2} values provide a reliable measure of the strong covalency of R-au and phthalocyanine compounds relative to copper(II) glycinate³⁴ and oxinate²⁶ which have been included in Table IV for comparison. α'_{N^2} shows the unpaired electron to be more delocalized onto the R-au and tetraphenylporphine ligands than the pyridine ligands in $\text{Cu}(\text{pyridine})_4^{2+}$, a case of the CuN_4 chromophore.³⁵ The larger σ covalency of the complexes containing the equivalent CuN_4^{2-} chromophore over that with the CuN_4 grouping is evidently due to the stronger σ interaction with the deprotonated ligand nitrogen sites. Upon protonation the R-au complexes exhibit a slight decrease in α'_{N^2} which corresponds to the qualitative argument for a covalency decrease suggested by the red shift in the electronic spectra.

While the values of α^2 and α'^2 can be accurately and unambiguously determined, the same cannot be said of β_1^2 and β^2 . β_1^2 is the in-plane π -bonding coefficient and β^2 is the out-of-plane π -bonding coefficient. Both β_1^2 and β^2 depend on the values assumed for ΔE_{xy} and ΔE_{zz} , respectively. In view of the fact that the electronic absorption spectrum consists of one very broad band we cannot unambiguously assign values to ΔE_{xy} and ΔE_{zz} . For purposes of calculation we have assumed (see Table IV) that the maximum in the band corresponds to ΔE_{xy} , and that ΔE_{zz} can be taken from the wavelength of the band, at one-half the intensity of the maximum, on the high energy side of the band. This assignment is, then, the "normal" assignment, namely, $x^2 - y^2 \gg z^2 > xy > xz, yz$.

Alternatively, if these compounds are exactly analogous to Cu(II) β -phthalocyanine^{32,36} and Cu(II) tetraphenylporphine^{33,37} then the "inverted" energy

(30) I. M. Procter, B. J. Hathaway, and P. Nicholls, *J. Chem. Soc. A*, 1678 (1968); A. A. G. Tomlinson and B. J. Hathaway, *ibid.*, 1685, 1905 (1968).

(31) M. Gerloch and J. R. Miller, *Progr. Inorg. Chem.*, **10**, 1 (1968); J. Owen and J. H. M. Thornly, *Rept. Progr. Phys.*, **29**, 675 (1966).

(32) S. E. Harrison and J. M. Assour, *J. Chem. Phys.*, **40**, 365 (1964).

(33) J. M. Assour, *ibid.*, **43**, 2477 (1965).

(34) H. A. Kuska and M. T. Rogers, *ibid.*, **43**, 1744 (1965); H. A. Kuska, M. T. Rogers, and R. E. Drullinger, *J. Phys. Chem.*, **71**, 109 (1967).

(35) W. Schneider and A. v. Zelewsky, *Helv. Chim. Acta*, **48**, 1529 (1965).

(36) J. M. Assour, J. Goldmacher, and S. E. Harrison, *J. Chem. Phys.*, **43**, 159 (1965).

(37) A. B. P. Lever, *J. Chem. Soc.*, 1821 (1965).

Table V: π -Electron Energies and HMO Parameters

	Structure							
	II	III	IV	V	VI	VII	VIII	IX
Total π -energy β units	21.304	21.288	21.302	15.248	15.246	17.652	17.955	21.364
Coulomb and Resonance Parameters								
	Atom	b		Bond		k		
	C	0.0		C-C		1.0		
	$\dot{N}\theta$	0.5		C-O		0.9		
	$\dot{N}H$	0.6		C-N		0.8		
	\dot{N}	1.5		Cu-N		0.6		
	$\ddot{O}R$	1.6						
	Cu	3.0						
Total π -Electron Energy								
	k_{Cu-N}		Structure II			Structure III		
	0.3		21.261			21.256		
	0.6		21.304			21.288		
	0.9		21.386			21.349		
	1.2		21.527			21.453		

level scheme^{32,33,36,37} $x^2 - y^2 \gg z^2 > xz, yz > xy$, is, perhaps, more appropriate. Table IV includes calculations of β_1^2 and β^2 according to both schemes.

The normal ordering of the energy levels gives rise to values of β^2 greater than unity more often than the inverted order. This is some indication that the inverted order may be preferable. However, the inverted order results in a less consistent set of values for both β^2 and β_1^2 . The fact that the normal order results in $\beta^2 > 1$ could be a result of the fact that g_{\perp} is the least accurately determined g value. We can conclude that for the compounds studied in this work the parameters calculated from the inverted scheme are not significantly better or worse than those calculated from the normal scheme. Consequently, it does not seem possible to decide which of the two schemes is the correct one. The inverted energy level scheme suggested for transition metal porphyrins is supported by the extended Hückel calculations of Zerner and Gouterman.³⁸ However, even for these compounds the experimental data^{32,33} does not seem unambiguous, since experimental values of ΔE_{xy} and ΔE_{zz} are not available.

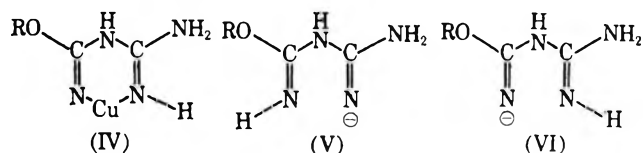
From the calculated values of the bonding parameters presented in Table IV, we conclude that strong σ bonds are present in the Cu(II) R-au complexes. The strength of the σ bonds (as manifested by α^2 values) is very similar to the σ bonds in Cu(II) β -phthalocyanine and Cu(II) tetraphenylporphines. It is also likely that moderately strong in-plane or out-of-plane (but not both) π bonding may be present, but this question cannot be answered unambiguously from the available data. In this respect the Cu(II) R-au complexes may not be exactly analogous to Cu(II) β -phthalocyanine and Cu(II) tetraphenylporphine.

Assour, Goldmacher, and Harrison³⁶ have suggested that when G (as defined above) is less than 4.0, the levels are inverted and there is strong out-of-plane π bonding; if $G > 4.0$ the normal energy level scheme is assumed. For strong ligand field complexes, G is usually less than 4.0, but this does not provide conclusive evidence for strong out-of-plane π bonding. If the energy levels are clustered together as might be expected for complexes of this type,³⁵ then $\Delta E_{zz}/\Delta E_{xy} \sim 1$, and exactly the opposite criterion for out-of-plane π -bonding applies.

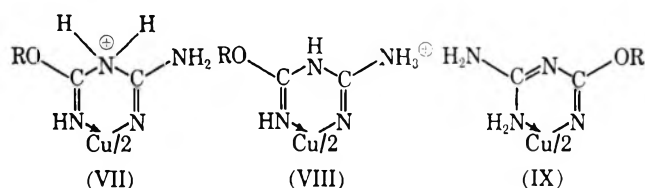
Molecular Orbital Calculations and Structural Considerations. From the above discussion it would appear that, since protonation of the R-au complexes is not accompanied by large changes in metal-ligand covalency, structure II for the R-au complexes might be the preferred one. This is in accord with the more extensive chelate ring delocalization possible relative to structure III and the ready availability of a basic primary amino group. Support for structure II is also provided by qualitative Hückel molecular orbital calculations, the results of which are listed in Table V. For these calculations a 1:1 model for the complexes was chosen and the complexes treated as planar π -electron systems. Two electrons were assigned to the copper(II) ion which was considered as a heteroatom in the fashion described by previous workers.³⁹ The Coulomb and resonance integrals employed for the copper ion assume a moderate amount of out-of-plane π interaction. The parameters employed for the Coulomb and resonance integrals $\alpha_z = \alpha_c + h\beta_{c-c}$ and $\beta_{z-y} = k\beta_{c-c}$,⁴⁰ respec-

(38) M. Zerner and M. Gouterman, *Theoret. Chim. Acta*, **4**, 44 (1966).(39) K. Fukui, A. Imamura, and C. Nagata, *Bull. Chem. Soc. Jap.*, **36**, 1450 (1963).

tively, are given in Table V. The aldimine nitrogen α'_N value was increased by 0.1 β unit per proton added. This choice was found to simulate the effect of protonation on the $\pi^* \leftarrow \pi$ electronic transition of pyridine and is in accord with HMO studies of heterocyclic compounds.⁴¹ In view of the greater electronegativity of $-\text{OH}$ and $-\text{OCH}_3$ groups⁴² over $-\text{NH}_2$ ($h_N = 1.5$) the alkoxy groups are treated as two electron heteroatoms with $h_{\text{OR}} = 1.6$. The protonation sites were considered to be removed from the π -electron system for the protonated complexes VII and VIII. As total π -elec-



tron energies and calculated resonance stabilization energies are related,⁴³ the total π -electron energies (Table V) were used as a measure of bonding site preference. Although the energy differences between comparable coordination possibilities is small, the magnitude of the energy is a moderate function of parameterization and the small differences are not unexpected in view of the slight structural differences being considered. Table V shows that (II) is favored over (III) and the isomeric form (IV). The preference of (II) over (IV) is also reflected in the π -energy differences for the anionic ligand species (V) and (VI). A consideration of the protonated R-au complexes shows that (VIII) is preferred to (VII) which agrees with the chemical properties of R-au complexes. It is noted that the calculated bonding site preferences are not a function of the Cu-N resonance integral (Table V). Although qualitative, the HMO calculations do concur with the overall covalency changes that take place upon protonation and indicate plausible structures for R-au complexes and their protonation forms.



The structure (IX) has also been proposed⁷ for R-au complexes and indeed the HMO π -electron energy (Table V) shows that it is the preferred form. However, the structural reorganization of the ligand and the infrared spectra (Figure 7) contraindicate structure IX. The infrared spectra of R-au complexes in the N-H stretching region, e.g., that of Cu(*n*-propyl-au) in Figure 7, show four sharp, strong bands attributable⁴⁴ to $\nu(\text{N-H})$ of the secondary amino group, 3345 cm^{-1} , $\nu(\text{N-H})$ of the imine group, 3265 cm^{-1} , and $\nu(\text{N-H})$ symmetric and asymmetric of the primary amino group, 3380 and 3487 cm^{-1} , respectively, whereas a similar

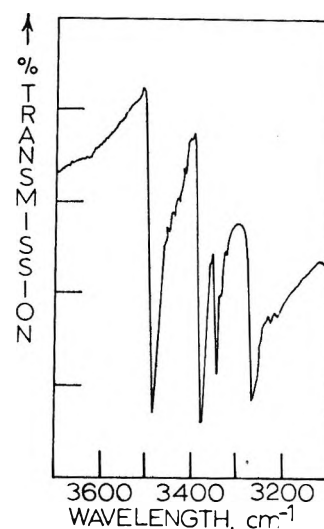


Figure 7. Infrared spectrum ($\nu(\text{N-H})$ region) of $\text{Cu}(n\text{-Pr-au})_2$.

sharp four band $\nu(\text{N-H})$ pattern would not be expected for structure IX. Mason⁴⁵ has demonstrated that there is a correlation between $\nu(\text{N-H})$ and the π -electron density on the nitrogen atom, $\nu(\text{N-H})$ decreasing as the π -electron density decreases. The π -electron densities for secondary amino group, imine nitrogen, and the primary amino group of structure II are 1.769, 1.616, and 1.861, respectively, in agreement with Mason's correlation⁴⁵ and $\nu(\text{N-H})$ assignments based on normal coordinate analyses⁴⁴ of related compounds. It is noted that forms (II) and (VIII) which are suggested for the R-au complexes and their nitrate salts are consistent with the crystal structures found for the substituted biguanide complexes 1-(2-aminoethyl)-biguanidecopper(II) sulfate monohydrate and ethylenebisbiguanidenickel(II) chloride monohydrate.⁴⁶

Conclusions

The esr spectra of the R-au complexes and their nitrate salts demonstrate that the strong covalency in these compounds is comparable to that exhibited by such strong-field ligands as phthalocyanine and tetraphenylporphine. The similarity of the complexes with

(40) A. Streitwieser, Jr., "Molecular Orbital Theory for Organic Chemists," J. Wiley and Sons, Inc., New York, N. Y., 1961.

(41) R. Zahradnik and J. Koutecky, *Advan. Heterocyclic Chem.*, **5**, 69 (1965).

(42) J. E. Huheey, *J. Phys. Chem.*, **69**, 3284 (1965); S. Chandra and S. Chandra, *Tetrahedron*, **22**, 3403 (1966).

(43) B. Pullman and A. Pullman, "Quantum Biochemistry," Interscience Publishers, New York, N. Y., 1963, p 116.

(44) P. X. Armandarez and L. Nakamoto, *Inorg. Chem.*, **5**, 796 (1966); B. B. Kedzia, P. X. Armandarez, and K. Nakamoto, *J. Inorg. Nucl. Chem.*, **30**, 849 (1968); J. A. Kieft and K. Nakamoto, *Inorg. Chim. Acta*, **2**, 225 (1968).

(45) S. F. Mason, *J. Chem. Soc.*, 3619 (1958).

(46) L. Coghi, A. Mangia, M. Nardelli, G. Pelizzi, and L. Sozzi *Chem. Commun.*, 1475 (1968); M. Nardelli, personal communication.

R–au ligands and the highly conjugated phthalocyanine and tetraphenylporphine ligands is most probably due to the deprotonated nitrogen sites in the equivalent CuN_4^{2-} chromophore. The near equivalence of the four nitrogen atoms in the CuN_4^{2-} chromophore suggests that a delocalized model employing both in-plane and out-of-plane π -bonding may be appropriate. Indeed, the agreement of the qualitative HMO

calculations with the covalency changes upon protonation, the infrared spectra, and structures suggested by analogy with those known for substituted biguanide complexes support this conclusion. The low g_{\parallel} and large A_{\parallel} values found for the R–au complexes appear to be characteristic of complexes containing the equivalent CuN_4^{2-} chromophore and are a result of the strong covalency in the complexes.

Hydrogenation of Ethylene by Zinc Oxide. I. Role of Slow Hydrogen Chemisorption

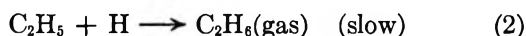
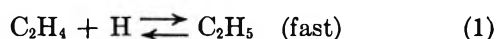
by A. L. Dent and R. J. Kokes

Department of Chemistry, The Johns Hopkins University, Baltimore, Maryland 21218 (Received March 24, 1969)

An experimental basis is provided for dividing hydrogen adsorption on zinc oxide into two types. Type I is rapid and reversible; type II is irreversible and occurs rapidly initially but slowly in the latter stages. Type I hydrogen is responsible for the observed OH and ZnH bands in the infrared and the principal source of hydrogen for the hydrogenation of ethylene. Type II does not participate in the hydrogenation of ethylene at room temperature but modifies the catalyst and enhances its activity. Neither the hydrogen adsorption nor ethylene adsorption is markedly affected by pretreating the catalyst with oxygen. The catalyst is poisoned for ethylene hydrogenation by exposure of the catalyst to oxygen provided chemisorbed hydrogen is present before the pretreatment. If care is taken to exclude chemisorbed hydrogen, the effect of oxygen pretreatment is relatively slight; hence, water (or its precursor) appears to be the poison. It is suggested that nonstoichiometry is not required for the development of active sites for hydrogenation. Instead, it is proposed that the strained sites, perhaps formed by dehydration, as suggested by Weller and Voltz, are the active sites.

Introduction

Ethylene hydrogenation over metals is a classical example of heterogeneous catalysis. Studies of this reaction and related phenomena strongly suggest that the reaction scheme includes the following *surface* processes



Such a scheme is consistent with a wide variety of data including kinetic,¹ exchange,² chemisorption and infrared studies,^{3,4} but for our purposes, we wish to focus on only two of these aspects. First, in accord with this scheme, when light ethylene reacts with deuterium over metals, a distribution of ethanes with the formula $\text{C}_2\text{H}_{6-x}\text{D}_x$ ($0 \leq x \leq 6$) is obtained. Second, the fact that active hydrogenation catalysts also are effective hydrogen–deuterium equilibration catalysts is consistent with (but not required by) the implied dissociative adsorption of hydrogen. It should be noted,

however, that while equilibration and hydrogenation are related reactions, the former is often more rapid than the latter.

Metal oxides are also catalysts for both hydrogenation of ethylene⁵ and hydrogen–deuterium exchange.⁶ Studies of hydrogenation over oxides are scarcer than such studies over metals, but the definitive work of Burwell and coworkers⁷ shows that hydrogenation over one oxide, chromia, is simpler than that over metals: for example, addition of deuterium to light ethylene

(1) For recent reviews, see: (a) G. C. Bond, "Catalysis by Metals," Academic Press, London, 1962; (b) G. C. Bond and P. B. Wells, *Advan. Catal.*, **5**, 257 (1967).

(2) T. I. Taylor, "Catalysis," Vol. V, P. H. Emmett, Ed., Reinhold Publishing Corp., New York N. Y., 1957 p. 257.

(3) R. P. Eischens and W. A. Pliskin, *Advan. Catal.*, **10**, 1 (1958).

(4) L. H. Little, "Infrared Spectra of Adsorbed Species," Academic Press, New York, N. Y., 1966, p. 100–137.

(5) D. L. Harrison, D. Nicholls, and H. Steiner, *J. Catal.*, **7**, 359 (1967).

(6) D. A. Dowden, N. MacKenzie, and B. M. W. Trapnell, *Proc. Roy. Soc.*, **A237**, 245 (1956).

yields only $C_2H_4D_2$; hence, there is no smear of the deuterium distribution in the product ethane. This result implies that the first step in the above reaction scheme is irreversible; the relatively low rate observed for isomerization of higher olefins during hydrogenation supports this conclusion. In part, this difference from metals can arise from the wide separation and lack of interaction of active sites on oxides, a suggestion first put forth by Burwell which has received some support from results recently reported from this laboratory.⁸

Attempts have been made to correlate the catalytic activity of metal oxides with the configuration of d electrons in the metal ion.^{5,6} Such correlations cannot be as general as for metals,¹ because the oxides active for ethylene hydrogenation include aluminum^{9,10} and zinc oxides¹¹⁻¹⁶ for which the metal ions have empty and filled d shells, respectively. Correlation to d shell structure alone is rendered still more suspect by recent observations that the addition of either deuterium¹⁷ or deuterium-hydrogen mixtures⁸ to ethylene over zinc oxide yields products quite similar to those obtained over chromia. On the basis of these results, together with quoted¹⁷ unpublished results of Ozaki on cobalt oxides, it has been suggested¹⁷ that the relative simplicity of the deuterogenation of ethylene over chromia may be a general characteristic of oxide hydrogenation catalysts that is independent of the d shell structure of the metal ion.

It is the purpose of this research to shed some light on the mechanism of hydrogenation over one of these oxides in the hope that it will have general validity for all of these oxides. Our candidate for this prototype is zinc oxide for a variety of reasons. First of all, it is relatively transparent in the infrared so that the kinetic runs can be supplemented by infrared studies. This aspect is particularly attractive insofar as Eischens, Pliskin and Low¹⁸ have shown that hydrogen chemisorbed on zinc oxide shows strong bands in the infrared and Bozon-Verduraz, Arghiroopoulos, and Teichner¹⁹ have studied the infrared of ethylene chemisorbed on zinc oxide. Secondly, whereas chromium oxide can show a variety of oxidation states depending on pretreatment,²⁰ zinc oxide is limited to one principal oxidation state. Mechanistic studies have been carried out on zinc oxide by Teichner and coworkers.^{14-16,19} For the most part, however, these studies have been carried out at elevated temperatures, 100 to 400°, and results with chromia⁷ suggest that the simplicity characteristic of oxides is largely lost at elevated temperatures.

The first part of this work deals with the role of fast and slow hydrogen chemisorption²¹ in hydrogenation reactions and the effect of oxygen pretreatment. These are questions that have some bearing on the behavior of chromia. Parravano and Boudart²¹ state: "It is important to note that the principal features of

hydrogen chemisorption, which are summarized above, apply equally well to other adsorbents than zinc oxide, for instance, to chromium oxide. A satisfactory explanation, therefore, must not depend on the specific properties of zinc oxide." In like vein, Weller and Voltz²² have noted that exposure to oxygen poisons chromia catalysts, a result also reported for zinc oxide.¹²⁻¹⁵ With zinc oxide it has been suggested that such oxygen poisoning occurs because it renders the catalyst more nearly stoichiometric and nonstoichiometry is required for activity.¹²⁻¹⁵ Such an explanation cannot be invoked for chromia since exposure to oxygen promotes nonstoichiometry.²² The second part of this work deals with the mechanism of the hydrogenation reaction and the possible nature of the active sites.

Experimental Section

Materials. Tank hydrogen (or deuterium) was purified by slow passage through degassed charcoal at -195° . Tank ethylene and oxygen were purified by alternate condensation, vaporization and pumping followed by distillation. Samples of hydrogen purified in this manner were shown by mass spectrographic analysis to contain less than 0.01% oxygen; gas chromatographic analysis demonstrated that the purity of the ethylene was comparable to that of the hydrogen. The oxygen purity was not checked, but prior to use it was freed from water by circulation through a liquid nitrogen trap.

The zinc oxide used for these studies was Kadox 25 supplied by the New Jersey Zinc Co.

Infrared Studies. Samples of zinc oxide weighing about 0.5 g were pressed into circular disks 20 mm in

- (7) (a) R. L. Burwell, Jr., A. B. Littlewood, M. Cardew, G. Pass, and C. T. H. Stoddart, *J. Amer. Chem. Soc.*, **82**, 6272 (1960); (b) G. Pass, A. B. Littlewood, and R. L. Burwell, Jr., *ibid.*, **82**, 6281 (1960); (c) C. T. H. Stoddart, G. Pass, and R. L. Burwell, Jr., *ibid.*, **82**, 6284 (1960); (d) A. B. Littlewood and R. L. Burwell, Jr., *ibid.*, **82**, 6287 (1960); (e) M. Cardew and R. L. Burwell, Jr., *ibid.*, **82**, 6289 (1960).
- (8) W. C. Conner and R. J. Kokes, *J. Phys. Chem.*, **73**, 2436 (1969).
- (9) J. H. Sinfelt, *ibid.*, **68**, 232 (1964).
- (10) Y. Amenomiya, J. H. B. Chenier, and R. J. Cvetanovic, *J. Catal.*, **9**, 28 (1967).
- (11) J. F. Woodman and H. S. Taylor, *J. Amer. Chem. Soc.*, **62**, 1393 (1940).
- (12) E. Molinari and G. Parravano, *ibid.*, **75**, 5233 (1953).
- (13) E. H. Taylor and J. A. Wethington, Jr., *ibid.*, **76**, 971 (1954).
- (14) J. Aigueperse and S. J. Teichner, *Ann. Chim. (Paris)*, **7**, 13 (1962).
- (15) J. Aigueperse and S. J. Teichner, *J. Catal.*, **2**, 359 (1963).
- (16) F. Bozon-Verduraz and S. J. Teichner, *ibid.*, **11**, 7 (1968).
- (17) W. C. Conner, R. A. Innes, and R. J. Kokes, *J. Amer. Chem. Soc.*, **90**, 6858 (1968).
- (18) R. P. Eischens, W. A. Pliskin, and M. J. D. Low, *J. Catal.*, **1**, 180 (1962).
- (19) F. Bozon-Verduraz, B. M. Arghiroopoulos, and S. J. Teichner, *Bull. Soc. Chim. Fr.*, 2854 (1967).
- (20) Charles P. Poole, Jr., and D. S. MacIver, *Advan. Catal.*, **17**, 223 (1967).
- (21) G. Parravano and M. Boudart, *ibid.*, **7**, 47 (1955).
- (22) S. W. Weller and S. E. Voltz, *J. Amer. Chem. Soc.*, **76**, 4695 (1954).

diameter under a pressure of 25,000 psi in a stainless steel ring. This disk was centered in a modified cylindrical gas cell with NaCl windows. The central part of the cell could be heated by nichrome windings while the windows were kept at room temperature by water-cooled copper coils wrapped around the ends of the cell. A measure of the sample temperature was provided by a thermocouple introduced into the cell *via* a glass-to-metal seal; the configuration was such that the junction formed a pressure contact with the zinc oxide disk. The cell was connected *via* tubulations on either side of the disk to a circulation loop with a magnetically driven pump so that reacting gases could be circulated over the catalyst disk. The rest of the vacuum system was a conventional BET apparatus. After assembly of the cell, the sample was degassed first at about 100°, then for 3 hr at 400° (the standard degassing procedure). If any bands due to C-H species were observed, oxygen was circulated over the catalyst for 3 hr at 400° with a liquid nitrogen trap in the line. Then, after brief degassing, the temperature was lowered to 300° and dried hydrogen was circulated over the catalyst for 3 hr. The above oxidation-reduction cycle followed by standard degassing always removed species giving rise to CH bands.

Spectra of the disk were determined with a model 112C Perkin-Elmer infrared spectrometer (modified for double pass) with NaCl optics. Normally, spectra were recorded with a spectral slit width varying from the order of 15 cm⁻¹ at 3500 cm⁻¹ to 3.5 cm⁻¹ at 1200 cm⁻¹.

Kinetic Runs. Ethylene hydrogenation was carried out in a closed system with forced circulation of gases by a magnetically driven pump. Hydrogen-ethylene or deuterium-ethylene mixtures were made up as desired in the BET system and toepled into the circulation loop. Circulation was started with the catalyst bypassed to mix the gases before the catalyst was cut into the reaction loop. The volume of the reaction system was 109 cc and the circulation rate (judged by the reaction rate with very fast catalysts) was about 300 cc/min. The fastest rate measured corresponded to about 3% per pass. The reaction was followed by periodic chromatographic analysis of small samples (~1%) of the gas in the circulation loop. All rates were computed from the initial slopes of plots of ethane formed *vs.* time. Usually, the first few points were indistinguishable from a straight line through the origin (*cf.* Figure 5).

Samples used for kinetic runs were first pressed into disks, then broken up to improve the flow characteristics. Samples 6 and 9 weighed about 1 g; sample 10 weighed about 10 g. The initial activation consisted of (a) degassing while raising the temperature to 300°, (b) circulation of hydrogen (~100 mm) over the catalyst at 300° and through a liquid nitrogen trap for 30 min, and (c) degassing for 3 hr at 450°. This treatment yielded a

sample with an area of 9.6 m²/g. In reactivation procedure (a) and (b) were repeated and the final degassing (c) was carried out at 400°. (In a few runs the above activation procedure was carried out with oxygen rather than hydrogen; such a pretreatment is referred to as O₂ activation.) Normally, the catalyst was degassed 1.5 hr at room temperature between runs and reactivated when periodic standard activity runs showed a decline in activity over 10%.

During the course of this work catalysts 9 and 10 were subjected to prolonged treatment with oxygen at 500°. After this treatment, the areas of these catalysts were 5.0 to 6.0 m²/g. Catalysts that were thus sintered bear the added label S, and in their reactivation steps a-b and c were carried out at 400 and 450°, respectively.

A comparison of the rates for different samples pretreated as described is given in Table I. Each of the

Table I: Catalytic Activity of ZnO

Sample	P _{H₂} , mm	P _{C₂H₄} , mm	Rate ^a /g of cat., molecules/sec × 10 ¹⁶	Rate ^a /cm ² of cat., molecules/sec × 10 ⁻¹¹
ZnO-6	244	24	3.04	3.2 ^b
ZnO-9	130	13	2.97	3.1
ZnO-9-S	130	13	1.82	3.0
ZnO-10-S	300	110	1.96	3.9 ^c

^a The experimentally determined orders (see later) were used to correct these rates to P_{H₂} = 130 mm and P_{C₂H₄} = 13 mm.

^b The area was not determined. Since the pretreatment was comparable to that of ZnO-9, the area was assumed to be the same.

^c This catalyst, sintered by previous experiments to an area of 5 m²/g and was hydrogen activated and degassed 16.5 hr at 450° prior to these runs.

listed numbers is the average value obtained for all runs on the freshly activated samples. There were nonsystematic variations in activity from one activation to another by as much as 20%, but the mean deviation from the average for each sample was less than 10%. The agreement of rates/cm² for different samples (after corrections for differences in area, sample size and reactant pressures) demonstrates the reproducibility of these rate measurements.

Adsorption measurements were made on a 10-g sample (ZnO-10) with a standard BET system. Adsorbed volumes were measured to within ±0.002 cc/g unless otherwise specified.

Results

Chemisorption of Hydrogen. Adsorption of hydrogen at room temperature and 128 mm on freshly activated zinc oxide is represented by the uppermost plot in Figure 1. Rapid initial adsorption is followed by a slow process which is detectable for several days. (After 24 hr the amount of hydrogen adsorbed is 0.30 to 0.34

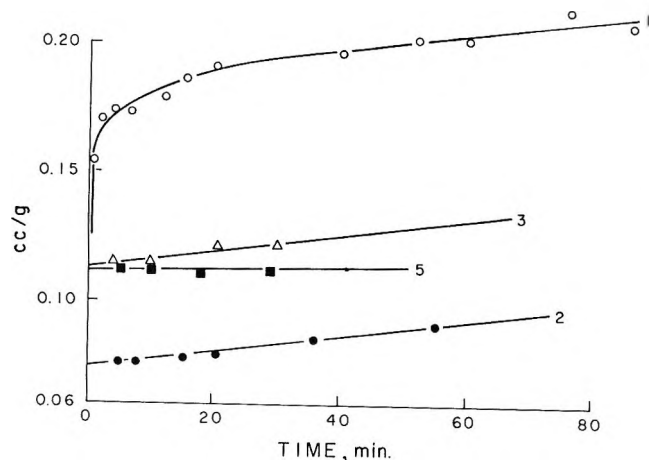


Figure 1. Adsorption of hydrogen vs. time ($P = 128$ mm): O, run 1, virgin catalyst; ●, run 2, after run 1 + 2 min degas; Δ, run 3, after run 2 + 15 min degas; ■, run 5, after run 4 (16 hr adsorption) + 30 min degas.

cc/g.) Similar behavior has been noted by others, both for zinc oxide²³⁻²⁵ and chromia.²⁶ Since the fast and slow processes appear to involve different modes of chemisorption,²⁴⁻²⁶ we looked for an experimental method of separating the fast and slow chemisorption. After the last point for run 1 was obtained, the sample was evacuated for 2 min, hydrogen was readmitted, and the amount of readsorption was measured as a function of time (curve 2). After the rapid readsorption of about 0.075 cc/g, the slow process resumes at a rate equal to that when run 1 was terminated. This process was followed for about 1 hr; at this point the catalyst was evacuated for 15 min and the readsorption was measured (curve 3). Once again, after a rapid readsorption, the slow process resumes at a rate comparable to that at the end of run 2. The catalyst was then exposed to hydrogen and the adsorption was followed for 20 hr; at this point, the slow process was undetectable over a period of 1 hr. Then, the catalyst was evacuated for 0.5 hr and the readsorption was followed (curve 5). In this run slow adsorption is not observed; hence, the amount of rapid adsorption is the total adsorption. The amount of rapid readsorption estimated from run 5 (0.112 cc/g) is quite close to the zero-time intercept for run 3 (0.113 cc/g) but substantially above the zero-time intercept for run 2 (0.074 cc/g).

The above experiments suggest: (a) fast chemisorption is removed by evacuation for more than 15 min; (b) the fast chemisorption is independent (compare runs 3 and 5) of the amount of slow chemisorption. Further support for conclusion (a) is supplied by the data in Figure 2 obtained as follows. First, the catalyst was "saturated" with slow hydrogen chemisorption by adsorption for 24 hr; total adsorption at this point was about 0.35 cc/g. Then, the catalyst was evacuated for the periods indicated and the readsorption determined

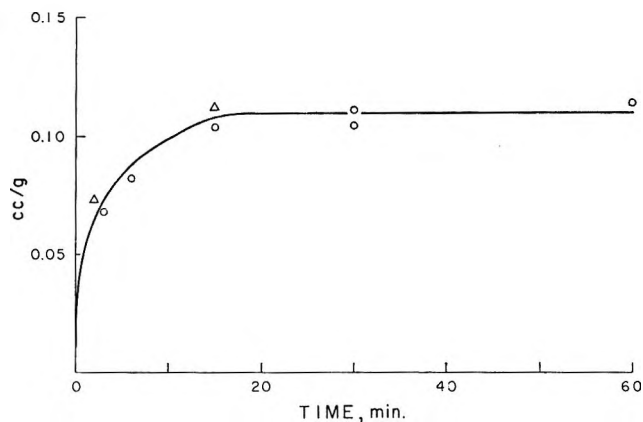


Figure 2. "Fast" hydrogen adsorption vs. degassing time ($P = 135$ mm): O, after 16-36 hr adsorption; Δ, intercepts of Figure 1, runs 2 and 3.

from data similar to that shown for run 5 (Figure 1). These data clearly support the conclusion that the "fast" hydrogen is removed by evacuation for 15 to 60 min without removal of the "slow" hydrogen.

With the above procedures we can experimentally define the amount of "fast" and "slow" chemisorption. It seems clear, however, that some of the "slow" hydrogen occurs rapidly. For example, the amount of adsorption on a freshly activated catalyst after 2 min (Figure 1) is 0.154 cc/g. Of this adsorption (in terms of our operational definitions) at most 0.112 cc/g is classified as "fast" chemisorption; hence, at least 0.042 cc/g of "slow" chemisorption occurs in 2 min. Accordingly, to avoid a misnomer, we shall designate the "fast" chemisorption as type I and the "slow" chemisorption as type II. It should be emphasized that whereas all slow chemisorption is of type II, not all type II chemisorption occurs slowly; in contrast to this, all type I chemisorption is rapid.

We can utilize the above procedure to obtain isotherms for the type I hydrogen. The catalyst is first saturated with type II hydrogen by overnight adsorption. Then, after evacuation for 0.5 hr, an isotherm is measured. This measurement is completed within 1 hr; hence, in principle, the slow process should not contribute. Figure 3 shows such a plot. Open circles are adsorption points obtained by increasing the pressure from 35 to 370 mm.; solid points are obtained by decreasing the pressure from 275 to 7 mm. The agreement of adsorption and desorption points suggests that type I adsorption, as defined, can be treated as a weak reversible chemisorption with a saturation coverage (reached above 40 mm) corresponding to about 5% of the V_m value.

The above experiments provide an operational basis

(23) H. S. Taylor and C. O. Strother, *J. Amer. Chem. Soc.*, **56**, 586 (1934).

(24) V. Kesavulu and H. S. Taylor, *J. Phys. Chem.*, **64**, 1124 (1960).

(25) M. J. D. Low, *J. Amer. Chem. Soc.*, **87**, 7 (1965).

(26) R. L. Burwell, Jr., and H. S. Taylor, *ibid.*, **58**, 697 (1936).

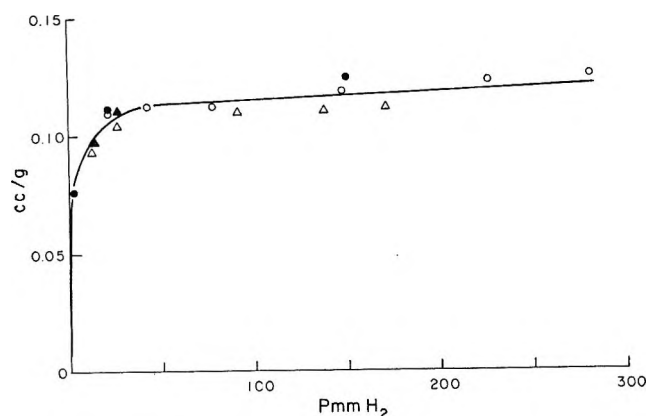


Figure 3. "Fast" hydrogen isotherms: O, hydrogen activation; Δ , oxygen activation (solid symbols denote desorption points).

for the separation of the two types of chemisorption but, for information on structure, we must turn to infrared studies. Eischens, Pliskin, and Low¹⁸ have shown that chemisorption of hydrogen on zinc oxide at room temperature produces two bands, one at 3510 cm^{-1} and the other at 1710 cm^{-1} . The former can be assigned to OH and the latter to ZnH. We have also observed these bands²⁷ and, as Eischens, *et al.*,¹⁸ have reported, we find: (a) the ratio of OH to ZnH band intensity is a constant except at the highest coverage where the OH band becomes relatively more intense; (b) the bands disappear on brief evacuation; and (c) the bands increase in intensity with increasing pressure up to 40 mm; at higher pressures, they do not show a pronounced increase in intensity. With procedures established by the chemisorption experiments, it is possible to examine the infrared spectra due to both types of chemisorption. In the absence of type I chemisorption but when type II chemisorption is about 0.24 cc/g ; *i.e.*, after adsorption for 24 hr followed by a 30 min evacuation, no bands are observed, but when about 0.10 cc/g of type I hydrogen is present, the bands exhibit their maximum intensity. This observation together with the pressure dependence of the band intensity compared to that for type I chemisorption (Figure 3) provides compelling evidence that the bands arise solely from type I chemisorption as suggested by Eischens, *et al.*¹⁸

When a degassed sample of zinc oxide is exposed to oxygen at room temperature, the background transmission increases by a factor of 2 to 4 in the wavelength region of interest. This background transmission remains unchanged after evacuation for 1 hr at room temperature; hence, this change is due to chemisorption of small amounts of oxygen ($\sim 0.005\text{ cc/g}$). Thomas²⁸ has shown that for single crystals, the absorption is directly proportional to the number of carriers. Accordingly, this change in transmission is consistent with the observations that chemisorption of small amounts of oxygen brings about a dramatic reduction in the conductivity.²⁹ Exposure to hydrogen at about

250° makes the sample opaque even after it is cooled to room temperature. This high-temperature chemisorption is that responsible for the high-temperature maximum in the isobar²³ and has been designated as type B by Kesavulu and Taylor.²⁴ In accord with infrared results, type B chemisorption increases the conductivity.³⁰ By way of contrast, neither type I nor type II chemisorption produces changes in the background transmission. Thus, it seems clear that the slow process at room temperature is different from the high temperature type B chemisorption. Some support of this view is afforded by the report²⁴ that desorption of *all* the hydrogen chemisorbed at room temperature can be effected by evacuation at 150° whereas desorption of type B chemisorption requires temperatures in excess of 250° . In conclusion, then, we disagree with the conclusions of Eischens, *et al.*,¹⁸ that "The protonic adsorption which is responsible for the high-temperature maximum of the isobar occurs to a limited extent at room temperature as a slow chemisorption." It should be noted, however, that this disagreement is based on further data and does not result from conflicting data.

The effect of oxygen on hydrogen chemisorption is of interest because of the reported poisoning effect of oxygen on the catalytic activity of zinc oxide for hydrogenation¹³⁻¹⁵ and hydrogen-deuterium exchange.¹² It was, therefore, somewhat surprising to find that although chemisorption of oxygen at room temperature had a pronounced effect on the conductivity, it had little effect on the integrated intensity of the infrared bands. This result is confirmed by the chemisorption studies. Figure 3 includes points for an isotherm obtained after the catalyst was subjected to dry oxygen treatment for 2 hr at 400° followed by 0.5

Table II: Effect of Pretreatment on Hydrogen Adsorption

Pretreatment	$V_I, \text{ cc/g}^a$	$V_{II}, \text{ cc/g}^b$
Activation	0.114	0.072
Degas 1 hr 400° , 2 hr O_2 400° , 0.5 hr degas 300°	0.110	0.082
Degas 1 hr 400° , 2 hr O_2 400° , 0.5 hr degas 150°	0.110	0.054
Degas 1 hr 475° , activation, O_2 25° , 0.5 hr degas 25°	0.095	0.062

^a Volume adsorbed at 100 mm after saturating with type II H_2 .

^b Total volume adsorbed 15 min after pretreatment minus the amount in column 2. This figure is thus a rough gauge of the amount of rapidly occurring type II chemisorption.

(27) We have also observed the ZnH band on the SP 500 zinc oxide from New Jersey Zinc Co.

(28) D. G. Thomas, *J. Phys. Chem. Solids*, **10**, 47 (1959).

(29) See, for example, R. Glemza and R. J. Kokes, *J. Phys. Chem.*, **69**, 3254 (1965).

(30) Y. Kubokawa and O. Toyama, *ibid.*, **60**, 833 (1956).

Table III: Participation of Type II Hydrogen in Hydrogenation

	Run no.				
	64	88	89	61	87
Pretreatment hr ^a	16, 0.5	16, 0.5	16, 1.5	3.5, 0.25	0.5 ^b
Initial C ₂ H ₄ , cc	1.86	1.51	1.50	1.87	1.71
Initial H ₂ , cc	3.65	16.43	16.69	4.10	19.25 ^b
Ethane formed, cc	0.73	0.89	0.87	0.77	0.61
Adsorbed D ₂ , cc ^c	0.20	0.20	0.20	0.14	~0.08
D ₂ in ethane	0.014	0.017	0.005	0.012	0.61
D ₂ in hydrogen	0.045	0.036	0.027
D ₂ on surface	0.132 ^d	0.15 ^e	0.17 ^e	...	0.028 ^d

^a The first figure pertains to the exposure time to deuterium prior to the run and the second to the evacuation time prior to the run. ^b In this run the catalyst was activated and a 0.5-hr hydrogenation run was carried out. After evacuation for 1.5 hr, the amount of deuterium on the surface was determined by exchange. ^c This figure is an estimate of the amount of type-II adsorption based on data for a different larger sample. Since the catalyst in runs 87-89 was sintered the type II adsorption is probably less. ^d These figures were determined by the measured exchange after 24-hr contact with 200-500 mm of H₂. ^e These figures were determined by mass balance.

hr degassing at 400°; within experimental error the points fall on those for the hydrogen activated sample. In an effort to see some effect, the sample was subjected to more and more intensive oxygen treatment. These results are summarized in Table II. There is a gradual decline in adsorption (ascribable to sintering) but the effect of oxygen pretreatment on hydrogen chemisorption is negligible for type I adsorption and not very large for type II adsorption; hence, the reported poisoning effect of oxygen cannot be ascribed to inhibition of hydrogen chemisorption. (It is worth noting that hydrogen activation followed by exposure to oxygen at 25° produced the biggest effect on type I adsorption. This decrease (last entry, Table II) may be due to gradual sintering or it could be evidence of the interaction of residual adsorbed hydrogen with oxygen to block out type I sites.)

Ethylene Chemisorption. Adsorption of ethylene on zinc oxide at room temperature is rapid and reversible; an isotherm is shown in Figure 4. On the time scale of these experiments (*ca.* 1 hr), we found no evidence for the dimerization reported by Ozaki and coworkers.³¹ From the amounts of adsorption at higher pressures, it appears that the number of sites for ethylene chemisorption is about five times the number available for type I hydrogen chemisorption. (The solid line indicates the extent of type I chemisorption.)

The effect of oxygen pretreatment on ethylene chemisorption was found to be small (Figure 4); hence, the reported poisoning effects of oxygen cannot be ascribed to inhibition of ethylene chemisorption.

The Role of Hydrogen in Hydrogenation. Hydrogenation of ethylene over zinc oxide at room temperature occurs at rates of the order of 0.05 cc/min. This is slower than the rate of type I adsorption and comparable to the *initial* rate of type II adsorption; hence, on this basis alone, either or both types of hydrogen chemisorption could be intermediates in the hydrogenation of ethylene.

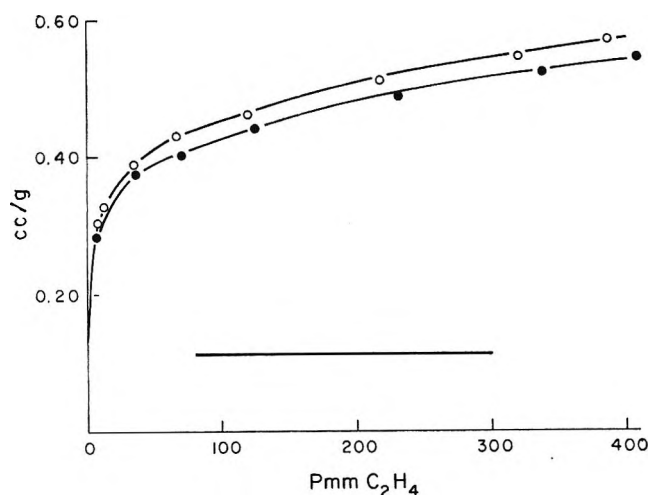


Figure 4. Ethylene Isotherms: O, hydrogen activation; ●, oxygen activation. (The horizontal line indicates the amount of type I hydrogen adsorption.)

The relative participation of type I and type II chemisorption can be assessed by tracer techniques. Consider the data for run 64 in Table III. The catalyst was first exposed to deuterium for 16 hr then evacuated for 0.5 hr. This leaves about 0.20 cc of type II D₂ on the surface. Then a regular hydrogenation run is made with H₂:C₂H₄ = 27 mm:14 mm. At the end of this run 0.73 cc of hydrogen had reacted, but even though this represents a turnover of reacting hydrogen on the surface nearly fourfold greater than the type II deuterium adsorption, analyses of the ethane shows only 1.9% of the product (0.014 cc) forms by reaction with D₂. Had all of the adsorbed deuterium reacted, 27.4% of the product (as C₂H₄D₂) would have formed *via* reaction with D₂. Analyses of the unreacted hydrogen showed the deuterium content was about 1.5%; hence, most of the ethane produced could have

(31) A. Ozaki, H. Ai, K. Kimura, presented at the Fourth International Congress on Catalysis, Moscow, 1968.

resulted from exchange of deuterium with hydrogen and its subsequent reaction. Exhaustive exchange of the catalyst with hydrogen after the reaction was complete accounted for 0.132 cc/g of deuterium, presumably still present as type II after reaction is complete. (Note that the sum of the last three entries in column 2 is 0.191 cc/g, in good agreement with the amount of type II chemisorption, 0.20 cc/g, estimated from adsorption experiments.)

Run 88 (Table III) was similar to run 64 but here the hydrogen pressure was increased to see if the type II chemisorption was labilized by the higher hydrogen pressure (120 mm). Once again, about 1.9% of the ethane formed from D₂ even though there was a turnover of reacting hydrogen on the surface more than four times the amount of type II chemisorption. Run 89 shows that if the catalyst is evacuated 1.5 hr after saturating with deuterium, the amount of incorporation of type II deuterium in the product is reduced; run 61 shows that if the amount of type II adsorption and the degassing time is decreased the incorporation of type-II deuterium in the products is still comparable to that for run 64.

Run 87b represents a basically different kind of isotopic experiment. Here a run with pure deuterium was carried out, and after evacuation the amount of type II adsorption was measured by exhaustive exchange. In the absence of ethylene, the amount of type II adsorption in 0.5 hr required for a run would be about 0.08 cc/g. In the presence of ethylene, the amount measured by exchange is 0.028 cc/g. Thus, although type II adsorption occurs in the presence of ethylene the amount is smaller. This reduction in type II adsorption may be assigned (in part) to the incorporation to form ethane.

In sum, the above data show that the predominant pathway to the hydrogenation of ethylene involves type I chemisorbed hydrogen and that the rate of type II chemisorption is reduced by a factor of 3 by the presence of ethylene.

Hydrogen Promotion. Although type II hydrogen

Table IV: Hydrogen Promotion

Run no.	Pretreatment ^a	Rate ^b mm/min	Promotion
9-62	H ₂ activation	0.533	1.33
9-63	H ₂ promotion	0.673	
9-S-75	H ₂ activation + O ₂ R.T.	0.233	1.26
9-S-76	H ₂ promotion	0.314	
9-S-80	O ₂ activation + O ₂ R.T.	0.220	1.23
9-S-81	H ₂ promotion	0.270	

^a See text. ^b Rate under standard conditions; *i.e.*, H₂:C₂H₄ = 130:13 mm.

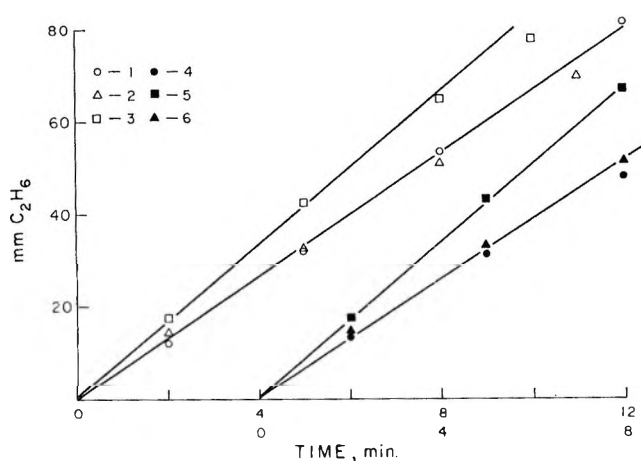


Figure 5. Ethane formation vs. time ($P_{H_2}:P_{C_2H_4} = 300:115$ mm); O, run 1, H₂ activation; Δ, run 2, repeat; □, run 3, after hydrogen promotion; ●, run 4, repeat; ■, run 5, after hydrogen promotion; ▲, run 6, repeat. (The lower abscissa is for runs 4, 5, and 6.)

chemisorption does not participate in the hydrogenation of ethylene it does promote the rate of reaction. This effect is documented in Table IV, which lists rates as a function of pretreatment. In column 2 "activation" denotes a high temperature pretreatment (see Experimental Section); the term "H₂ promotion" denotes saturating the surface with type-II chemisorption; the term "O₂ R.T." denotes exposing the catalyst to dry oxygen at room temperature followed by 0.5 hr degassing at room temperature. Data in Table IV show that hydrogen promotion increases the rate by about 30%. This promotion is evident for a catalyst subjected to standard pretreatment (9-62, 9-63), for a catalyst with chemisorbed oxygen (9-S-75, 9-S-76), and for a catalyst activated in oxygen (9-S-80, 9-S-81). Moreover, the effect seems to be about the same if the promotion is carried out with deuterium rather than hydrogen.

Although the effect of hydrogen promotion is reproducible, it only lasts for one run. Figure 5 shows a sequence of six runs on sample ZnO-10 carried out at effectively the same pressures of hydrogen and ethylene. The numbers denote the order in which the experiments were performed. Run 1 was immediately after activation and run 2 was a repeat run made after the standard run with room temperature evacuation between runs. Prior to run 3, the catalyst was saturated with type II hydrogen, *i.e.*, promoted. The rate in run 3 is about 25% greater than the average for unpromoted runs. Then, after standard evacuation, run 4 was performed and the rate, within experimental error, returned to that characteristic of unpromoted runs. Promotion with hydrogen prior to run 5 again yielded the promoted rate, but the repeat run 6 yielded the unpromoted rate. Thus, although saturation of the surface with type II hydrogen promotes the rate for the following run, the effect does not persist thereafter even though only

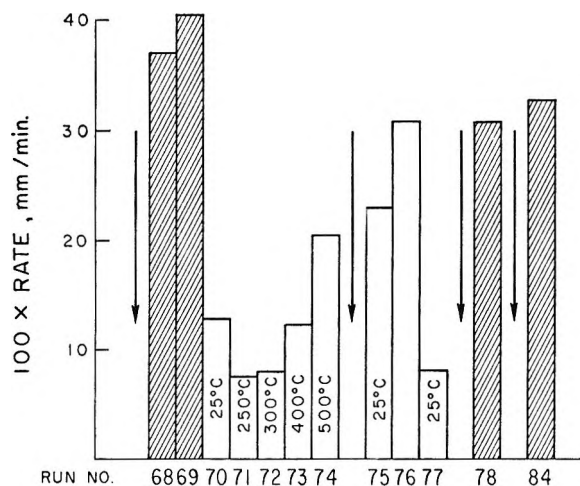


Figure 6. Effect of oxygen pretreatment on rate. Each arrow represents hydrogen activation. Cross-hatched columns indicate rates for a freshly activated catalyst or one subjected to standard degassing. Open columns that are labeled represent rates after treatment with dry oxygen for 1 hr at the indicated temperature, cooling to room temperature, and degassing 30 min. The unlabeled open column represents the rate after hydrogen promotion.

about 10% of the type II hydrogen is removed by reaction with ethylene.

Oxygen Poisoning. Oxygen poisoning effects are complex and depend on the details of pretreatment. This is illustrated by the bar graph in Figure 6 which summarizes rates for a sequence of experiments defined by run numbers. After the initial activation, two runs on a partly sintered catalyst under standard conditions (68, 69) yielded an average rate of 0.39 ± 0.02 mm/min. This is a factor of 3 greater than that for a catalyst subsequently treated with oxygen at room temperature (70). Oxygen treatment at successively higher temperatures for 1 hr by circulation over the catalyst and through a liquid nitrogen trap revealed that the rate decreased further after 250° treatment (to 0.075 mm/min) but increased at still higher temperatures. This suggests that the poisoning may arise in part from the reaction of adsorbed hydrogen with oxygen to form water.

In the next sequence, the freshly activated catalyst, presumably sintered by the 500° oxygen treatment, was exposed to oxygen at room temperature. This catalyst may have some chemisorbed hydrogen due to the pretreatment but should have less than that used in run 70 on which two hydrogenation runs had been made. Despite the presumed sintering, the reaction rate in this run (75) was nearly twice that in run 70 with similar oxygen pretreatments. To estimate the effect of interaction of oxygen with chemisorbed hydrogen, the catalyst was exposed to hydrogen overnight and run 76 was made. This yielded the already noted promotion by hydrogen insofar as the rate was increased by about 30%. This rate is a factor of more

than 3 greater than the rate after subsequent exposure to oxygen (77). Thus, the poisoning effect of oxygen is much greater in the presence of chemisorbed hydrogen than in its absence. Following this sequence, two more runs were made on a freshly activated catalyst (78, 84). These measured rates are consistent with the supposition that treatment of the catalyst with oxygen at 500° in run 74 resulted in some sintering.

The above experiments strongly suggest that oxygen poisoning stems mainly from interaction with chemisorbed hydrogen. Possibly this interaction involves the formation of water, known to be a strong poison.¹¹ Based on this sequence alone, the effect of oxygen alone is somewhat uncertain because of the possibility that some hydrogen is retained on the catalyst by the activation procedure. In one set of experiments prior to the sequence in Figure 6, however, the catalyst was first activated by circulation of dried oxygen over the catalyst at 505° for 2 hr and cooling to room temperature in dried oxygen. With this pretreatment there should be no chemisorbed hydrogen, although sintering would be expected to occur. After degassing at room temperature for 30 min the rate on this catalyst was found to be 0.378 mm/min. The catalyst was then subjected to the standard hydrogen activation. Since this activation was at lower temperatures than the oxygen activation, no sintering was expected. The rate on this catalyst was 0.370 mm/min. Thus, it appears that the poisoning due to dry oxygen is almost entirely due to interaction with chemisorbed hydrogen; if chemisorbed hydrogen is not present, poisoning by exposure to oxygen at elevated temperatures or room temperature is not observed.

Discussion

From these experiments a rather detailed picture of the hydrogenation process emerges. Adsorption of type I hydrogen, rapid and reversible, occurs on the special sites constituting about 5% of the available surface. (This assay is based on the assumption that chemisorbed hydrogen and physisorbed nitrogen have the equal effective cross sections.) The nature of these sites is open to question but adsorption on these sites gives rise to Zn-H and OH bands in the infrared. Moreover, it is this hydrogen species that is primarily responsible for the hydrogenation of ethylene.

Type II hydrogen adsorption exceeds the amount of type I adsorption by a factor of at least 2; *e.g.*, after overnight exposure to hydrogen, type I adsorption is 0.11 cc/g and type II is 0.23 cc/g. Precise assessment of the capacity of the catalyst for type II hydrogen is not possible because adsorption continued for days and saturation was never achieved.

Type II hydrogen contributes little to the hydrogenation of ethylene and does not give rise to Zn-H and OH bands. Moreover, although it may be an intermediate in the formation of the species responsible

for the high-temperature maximum in the isobar, it is experimentally distinguishable from this species. Even though type II chemisorption is unreactive, it does modify the catalyst and promotes the rate of reaction. This promotional effect does not persist after exposure to ethylene in a hydrogenation run even though only about one-fourth of the type II chemisorption is removed by such treatment. There is no experimental basis for speculation on the mechanism of this promotion but similar promotional or poisoning effects have been noted for metallic catalysts.³²

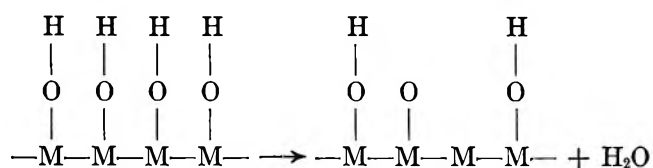
During the course of a hydrogenation run, type-II adsorption occurs concurrently. This may result in a continual promotional effect which extends the initial linear portion of plots of yield *vs.* time. Such effects will result in the apparent order of the reaction changing during the course of the reaction, a result noted by Aigueperse and Teichner.¹⁶ It seems clear that if the order for the unpromoted catalyst is desired, the order must be based on initial rates and initial pressures.

It should be emphasized that the above conclusions are restricted to room temperature. Participation of type II chemisorption may be expected to be more important at higher temperatures. Perhaps such participation, the extent varying with temperature, is the source of the complex kinetics observed by Bozon-Verduraz and Teichner.¹⁶

Oxygen chemisorption at room temperature or elevated temperatures clearly decreases the conductivity (as reflected by the background transmission). Previous workers have reported that oxygen poisons hydrogenation reactions;¹²⁻¹⁴ for example, Taylor and Wethington¹³ note that exposure to oxygen at 360° decreased the rate to less than 1% of the value before such treatment. Understandably, this has led these authors to the conclusion,¹³ "It is clear that catalytic activity, like electrical conductivity is closely related to oxygen deficiency in the oxide." Later experiments by Aigueperse and Teichner¹⁴ showed that doping with lithia or gallia had little effect on the activity, a result that led to the conclusions, "The electronic structure of the catalysts is therefore without influence on the catalytic activity." However, on the basis of poisoning experiments with oxygen, they also noted that "The formation of a nonstoichiometric oxide is a necessary condition for the catalytic activity in the hydrogenation of ethylene." Our results, however, show that exposure of the catalyst to dry oxygen at high temperatures or room temperature has a very small effect on the cata-

lytic activity *at room temperature* provided the amount of chemisorbed hydrogen on the catalyst is small during oxygen pretreatment. The fact that oxygen pretreatment of the catalyst has little effect on either type I hydrogen adsorption or ethylene adsorption is in line with these activity effects. Since oxygen pretreatment is supposed to reduce the nonstoichiometry, this clearly implies that nonstoichiometry is not a requirement for catalytic activity. It seems more likely to us that the reported poisoning with oxygen is due to interaction with adsorbed hydrogen to form water at the active sites. Thus water (or its precursor) is the poison rather than the oxygen. Similar observations have been made by Hindin and Weller on alumina³³ insofar as they find water poisons the hydrogenation activity whereas dry oxygen has little effect.

The active sites for hydrogenation on chromia and alumina have been associated with "strained sites" created by dehydration of a hydroxylated oxide surface.^{22,33} Creation of these sites for a surface terminating in close-packed hydroxyl groups can be represented as



Thus, these strained sites can be viewed as surface anion vacancies. There is reason to believe the active site on zinc oxide is similar to the one pictured above. Such a site would be isolated and noninteracting and would be poisoned by exposure to water by reversal of the foregoing equation. Some aspects of the chemistry discussed in the next paper, however, suggest the surface between active sites consists of oxide ions rather than hydroxyl ions. Such a picture has the same qualitative consequences insofar as rehydroxylation by water would still destroy the active site, *i.e.*, poison the catalyst, and the sites would be isolated. Perhaps this modification applies to chromia and alumina as well.

Acknowledgment. Acknowledgment is made to the donors of the Petroleum Research Fund, administered by the American Chemical Society, for support of this research.

(32) W. K. Hall and P. H. Emmett, *J. Phys. Chem.*, **63**, 1102 (1959).

(33) S. G. Hindin and S. W. Weller, *Advan. Catal.*, **9**, 70 (1957).

Hydrogenation of Ethylene by Zinc Oxide. II.

Mechanism and Active Sites

by A. L. Dent and R. J. Kokes

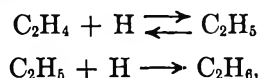
Department of Chemistry, The Johns Hopkins University, Baltimore, Maryland 21218 (Received March 24, 1969)

The rate of hydrogenation of ethylene over zinc oxide at room temperature has been determined for hydrogen pressures ranging from 23 to 583 mm and ethylene pressures ranging from 5 to 330 mm with the ratio of hydrogen to ethylene ranging from 1 to 50. Initial rates were proportional to the hydrogen pressure to the one-half power and showed a slight dependence on ethylene pressure ascribable to the extent of the surface covered with ethylene. The kinetic isotope effect was also determined for a fixed set of conditions. These measurements, supplemented by infrared studies of the sample either with chemisorbed gases (C_2H_4 , O_2 , CO) or under reaction conditions and an examination of poisoning effects of water vapor provide the basis for a model of the active site consisting of zinc ions imbedded in a close-packed oxide layer. This tentative model leads to a mechanism consistent with the kinetics and provides a plausible explanation for most of the experimental observations. It further suggests that there should be striking similarities between hydrogenation over oxides and hydrogenation over homogeneous catalysts.

Introduction

Nearly 30 years ago, Woodman and Taylor¹ discovered that zinc oxide is an effective catalyst for the hydrogenation of ethylene. Since this discovery, a number of reports¹⁻⁷ have appeared dealing with this aspect of the chemistry of zinc oxide, but the only thorough studies of kinetics have been carried out by Teichner's group^{3-6,7} at elevated temperatures, *i.e.*, roughly 100 to 400°. Under these conditions, the reaction is quite complex: orders and activation energies change from one temperature range to another,⁷ and formation of ethylene residues⁵ with consequent poisoning⁷ is evident. Since these studies span a range of temperatures in which the adsorption of hydrogen is a complex phenomenon,⁸⁻¹⁰ complexities of the related hydrogenation kinetics are to be expected. Nevertheless, the results are such that they frustrate attempts to put forth a coherent picture for the mechanism of ethylene hydrogenation.

Recently, it has been shown in this laboratory^{11,12} that room temperature catalysis of hydrogenation by zinc oxide is similar to that of chromia.^{13,14} In particular, although the mechanism of hydrogenation over these oxides may involve the same surface processes believed to occur with metal catalysts,¹⁶ *i.e.*



these oxides lead to $C_2H_4D_2$ on deuteration rather than the $C_2H_{6-x}D_x$ found with metals. Presumably, this means the first step is irreversible over oxides, *i.e.*, "alkyl reversal" does not occur, whereas on metals the first step is quite reversible. It has been suggested that this behavior of oxides is a consequence of the noninteraction of widely separated active sites.^{12,13}

The clean, 1,2-addition of deuterium to olefins over oxides is not found at elevated temperatures.¹⁴ Perhaps the specificity observed stems from the fact¹⁶ that at room temperature hydrogenation involves only the rapid reversible hydrogen chemisorption (type I). The irreversible chemisorption (type II), also present at room temperature but not effective in hydrogenation, may play a more important role at elevated temperatures and lead to a process involving two types of reactants, type I and type II chemisorption. In this event, one would expect the observed complex kinetics.

It is the purpose of this paper to examine in detail the kinetics and mechanism of hydrogenation of ethylene over zinc oxide. The major emphasis is on the reaction

- (1) J. F. Woodman and H. S. Taylor, *J. Amer. Chem. Soc.*, **62**, 1393 (1940).
- (2) E. H. Taylor and J. A. Wethington, *ibid.*, **76**, 971 (1954).
- (3) J. Aigueperse and S. J. Teichner, *Ann. Chim. (Paris)*, **7**, 13 (1962).
- (4) J. Aigueperse and S. J. Teichner, *J. Catal.*, **2**, 359 (1963).
- (5) F. Bozon-Verduraz, B. Arghiroopoulos, and S. J. Teichner, *Bull. Soc. Chim. Fr.*, 2854 (1967).
- (6) D. L. Harrison, D. Nicholls, and H. Steiner, *J. Catal.*, **7**, 359 (1967).
- (7) F. Bozon-Verduraz and S. J. Teichner, *ibid.*, **11**, 7 (1968).
- (8) H. S. Taylor and C. O. Strother, *J. Amer. Chem. Soc.*, **56**, 586 (1934).
- (9) V. Kesavulu and H. A. Taylor, *J. Phys. Chem.*, **64**, 1124 (1960).
- (10) M. J. D. Low, *J. Amer. Chem. Soc.*, **87**, 7 (1965).
- (11) W. C. Conner, R. A. Innes, and R. J. Kokes, *ibid.*, **90**, 6858 (1968).
- (12) W. C. Conner and R. J. Kokes, *J. Phys. Chem.*, **73**, 2436 (1969).
- (13) R. L. Burwell, Jr., A. B. Littlewood, M. Cardew, G. Pass, and C. T. H. Stoddard, *J. Amer. Chem. Soc.*, **82**, 6272 (1960).
- (14) A. B. Littlewood and R. L. Burwell, Jr., *ibid.*, **82**, 6287 (1960).
- (15) G. C. Bond, "Catalysis by Metals," Academic Press, London, 1962, pp 258-270.
- (16) A. L. Dent and R. J. Kokes, *J. Phys. Chem.*, **73**, 3772 (1969).

at room temperature since this is the temperature where the aforementioned simplicity is obtained. The classical techniques for kinetic studies are supplemented with infrared techniques in an attempt to gain some information on the nature of the active sites. Thus, this paper represents an extension of the results reported in part I of this series.

Experimental Section

Experimental details regarding materials, rate measurements, and infrared studies were described in a previous paper. Measurement of the effect of adsorbed water on the rate and adsorption were carried out on sample ZnO-10 in the circulating system. This sample weighed 9.5 g; it was slightly sintered in experiments preceding this so that the area was about 5 m²/g compared to 10 m²/g for a fresh catalyst.

Preliminary experiments showed that when the activated catalyst was exposed to about 2 cc of water vapor at room temperature, the pressure rapidly dropped to zero. Helium was then admitted to the circulating system and circulated through a liquid nitrogen trap in series with the sample. Contents of the trap were checked by evacuation and warmup every 30 min to see if water evolved. When this was done as a function of catalyst temperature, it was found that there was little water evolution below 300°. By heating between 300 and 450° all of the water could be recovered.

For runs reported herein, about 3 cc of water vapor was admitted to the activated catalyst. The catalyst was then conditioned by circulating helium over the catalyst of 300° for 1 hr. Since previous experiments have shown that water desorbed at 300°, this treatment should yield a uniform distribution of water throughout the catalyst bed. The catalyst was cooled to room temperature, exposed to hydrogen at about 200 mm, and the rate of adsorption was followed for 5 min. After this the catalyst was degassed for 2 hr and the rate of ethylene hydrogenation was measured for C₂H₄:H₂ = 110:310 mm. At this point, the catalyst was degassed for 2 hr at room temperature and the temperature was raised and the water evolution measured. This sequence was repeated until all of the water was removed. In another sequence, ethylene chemisorption and rate were measured as a function of adsorbed water by the same procedures.

Results

Kinetics. Rates were determined from the initial slopes of plots of conversion *vs.* time and correlated to initial pressures of reactants. Tests of order based on the changes in the reactant pressure during the course of the reaction were not attempted because the continuous promotion by type II chemisorption would be expected to frustrate such attempts.¹⁶ Typical plots of conversion *vs.* time are shown in Figure 4 (to be dis-

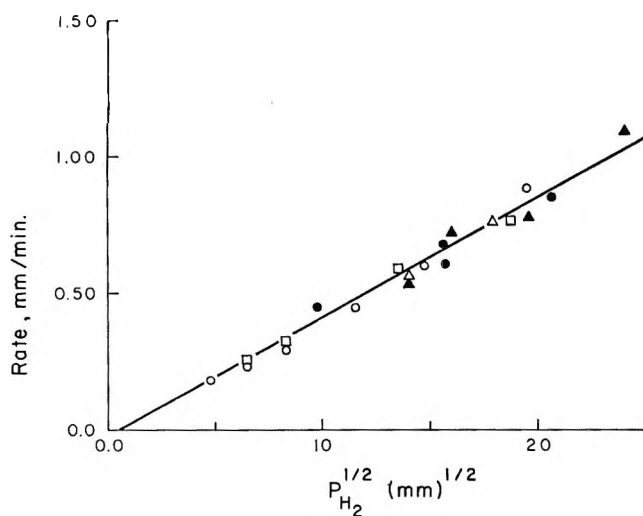


Figure 1. Order with respect to hydrogen: O, sequence 9A, $P_{C_2H_4} = 12.7$ mm, scale factor $\times 1$; \square , sequence 9B, $P_{C_2H_4} = 27.4$ mm, scale factor $\times 1.12$; Δ , sequence 9C, $P_{C_2H_4} = 71$ mm, scale factor $\times 0.90$; \blacktriangle , sequence 9D, $P_{C_2H_4} = 129$ mm, scale factor $\times 0.87$; \bullet , sequence 6A, $P_{C_2H_4} = 24$ mm, scale factor $\times 0.85$.

cussed later). It can be seen that such initial rates are well defined.

During the course of these runs the catalyst was accidentally poisoned several times and reactivation was required. Such reactivation caused a nonsystematic shift in the standard activity by as much as 20%, but the mean of standard activities after all reactivations showed a mean deviation of less than 10%.

The order with respect to hydrogen, determined for several different activation sequences at fixed ethylene pressures is illustrated by Figure 1. Since there is some dependence on ethylene pressure and the standard activity varies somewhat from one sequence to another, we have multiplied the rates for each sequence by a scale factor. These sequences, which represent a 10-fold range of ethylene pressures and a 25-fold range of hydrogen pressures, combine to give a well-defined straight line passing (nearly) through the origin when the rates are plotted *vs.* the square root of the hydrogen pressure. It is noteworthy that this plot includes data for two different samples of catalyst, ZnO-6 and ZnO-9.

The dependence of rate on ethylene pressure is shown in Figure 2. In sequence 9 (circles) hydrogen pressure was not kept constant but was varied from 70 to 314 mm. Dependence on hydrogen was factored out by dividing the rate by the square root of the hydrogen pressure. We have also included in this plot (triangles) average values of $\text{rate}/(P_{H_2})^{1/2}$ for other sequences (here no scale factor is used to bring the rates into agreement). The first four triangular points represent the sequences 9A, 9B, 9C, 9D that were used in Figure 1 to establish the order in hydrogen. As the error bars show, the average of deviations in the average values of $\text{rate}/(P_{H_2})^{1/2}$ were of the order of 6%. In

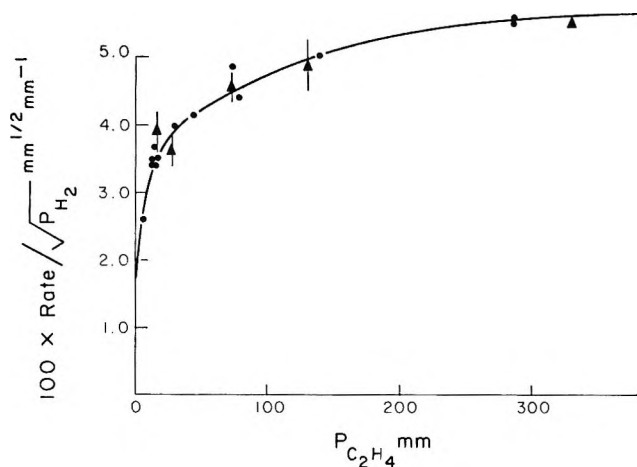


Figure 2. Order with respect to ethylene: ●, sequence 9; ▲, average values for different sequences shown in Figure 1.

toto, then, this plot not only establishes the order with respect to ethylene, but furnishes a test of the order with respect to hydrogen. These studies do not include reactant pressures with ethylene in excess, but the ratio of hydrogen to ethylene varied from 1:1 to 50:1. The pressure ranges studied vary from 5 to 330 mm for ethylene and from 23 to 583 mm for hydrogen.

The curve in Figure 2 is the same shape as an adsorption isotherm. Measurements of the adsorption isotherm for ethylene were reported in the first paper of this series (Figure 4 of ref 16). From these data and Figure 2 we can replot rate/ $(P_{H_2})^{1/2}$ vs. amount of adsorbed ethylene. Such a plot (Figure 3), although limited in range, is well represented by a straight line through the origin. Thus the empirical kinetic expression for hydrogenation of ethylene is

$$\frac{d(C_2H_6)}{dt} = k(P_{H_2})^{1/2}\theta_{C_2H_4}$$

wherein θ represents the *equilibrium* ethylene chemisorption, *i.e.*, in the absence of hydrogen, corresponding to the ethylene pressure. We recognize, of course, that ethylene adsorption under reaction conditions need not be the same as the defined θ .

Isotope Effects. Figure 4 shows a sequence of standard runs made to determine the kinetic isotope effect. Runs 57 and 59 were carried out at slightly different pressures; after correction for these differences, the average of these rates is 0.665 ± 0.017 mm/min. The corresponding rate for deuterium is 0.290 mm/min. Thus, the rate with deuterium is roughly half of the corresponding rate with hydrogen.

Parravano, Friedrik and Boudart¹⁷ have measured the rates of adsorption of deuterium and hydrogen on zinc oxide. These measurements pertain to the "slow" adsorption and show that there is no kinetic isotope effect. Thus, our observations of a normal isotope effect for the hydrogenation reaction provides additional evidence¹⁸ that the rate of "slow" adsorption

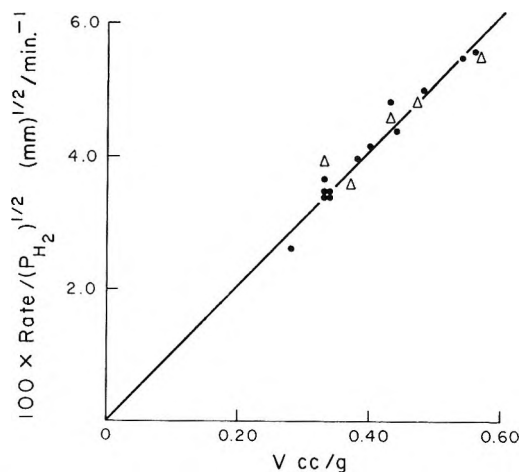


Figure 3. Order with respect to adsorbed ethylene: ●, sequence 9; ▲, average values for different sequences shown in Figure 1.

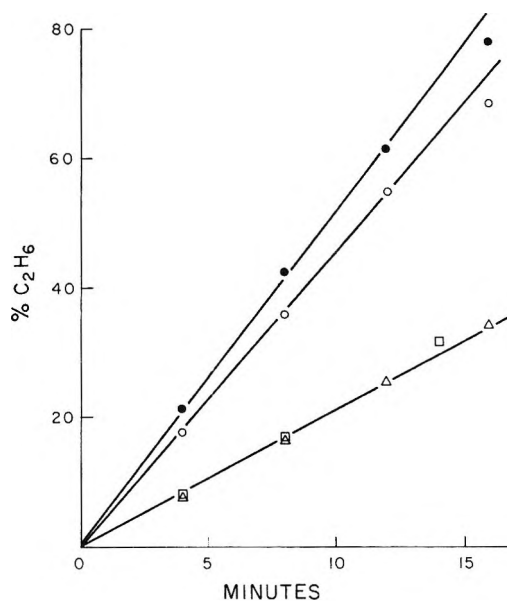


Figure 4. Hydrogen isotope effects: ○, run 57, hydrogen; □, run 58, deuterium; ●, run 59, hydrogen; ▲, run 60, deuterium.

cannot be the rate controlling step in the hydrogenation.

Infrared Studies. As shown by Eischens, Pliskin, and Low¹⁸ the reversible chemisorption of hydrogen on degassed zinc oxide gives rise to two infrared bands of comparable intensity at 3500 and 1710 cm^{-1} ; these bands are ascribed to OH and ZnH stretching bands formed by the dissociative adsorption of hydrogen. Degassed zinc oxide shows at least three bands in the 3500 cm^{-1} region, presumably due to structural OH groups in the solid, which bracket the chemisorbed OH

(17) G. Parravano, H. G. Friedrik, and M. Boudart, *J. Phys. Chem.*, **63**, 1144 (1959).

(18) R. P. Eischens, W. A. Pliskin, and M. J. D. Low, *J. Catal.*, **1**, 180 (1962).

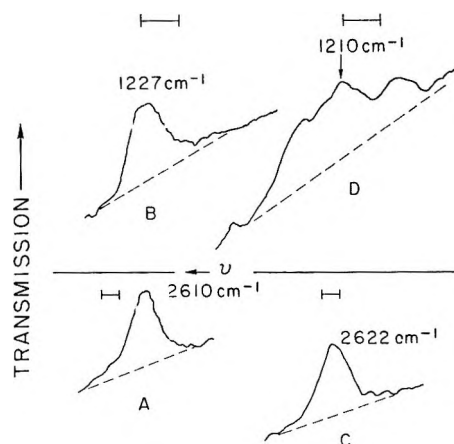


Figure 5. Effect of carbon monoxide on deuterium bonds: A, OD band, 84 mm D₂; B, ZnD band, 84 mm D₂; C, OD band, 84 mm D₂ after adding 35 mm CO; D, ZnD band, 84 mm D₂ after adding 35 mm CO. The bars indicate a $\Delta\nu$ of 10 cm⁻¹. Transmission scales are the same for OD band but for drawings B and D, they are shifted.

band. Studies of chemisorption of hydrogen are not greatly disturbed by this overlap; nevertheless, for this reason, it is more convenient to make chemisorption studies with deuterium. Chemisorption of deuterium gives rise to bands at 2610 and 1227 cm⁻¹ corresponding to OD and ZnD (Figure 5A and B). In this region, the background due to degassed zinc oxide is smooth.

At room temperature, adsorption of ethylene gave rise to no bands that were not masked by or ascribable to bands of the unsaturated hydrocarbon. When the gas phase was removed by brief evacuation, no bands due to chemisorbed hydrocarbon were observed. In particular, there was no evidence for the bands of chemisorbed ethylene observed by Bozon-Verduraz, Arghiropoulos, and Teichner⁵ at slightly higher temperatures. Our result is consistent with the adsorption experiments,¹⁶ which show rapid, reversible chemisorption of ethylene at room temperature.

Exposure of the catalyst to carbon monoxide at room temperature for about 1 hr followed by brief evacuation of the gas phase gives rise to bands due to chemisorbed carbon monoxide similar to those observed by Amberg.^{19,20} Preadsorption of such carbon monoxide followed by adsorption of deuterium yields ZnD and OD bands in the usual positions. Quantitative intensity comparisons were not made, but auxiliary experiments suggest that there was little effect on band intensities provided the catalyst was not exposed to carbon monoxide beyond 1 hr. Thus, strongly chemisorbed carbon monoxide, like chemisorbed oxygen, has little or no effect on the chemisorption of hydrogen. If, however, gaseous carbon monoxide and gaseous deuterium are both present, an effect is observed (Figure 5C and D). The band due to ZnD broadens and perhaps splits into several bands; because of the extreme broadening, it is difficult to say if the intensity de-

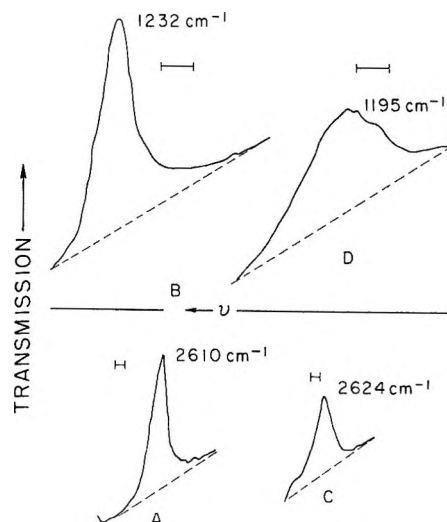


Figure 6. Deuterium bands under reaction conditions: A, OD band before and after reaction; B, ZnD band before and after reaction; C, OD band during reaction; D, ZnD band during reaction. The bars indicate a $\Delta\nu$ of 10 cm⁻¹. Transmission scales differ for OD and ZnD bands.

creases. By way of contrast, the OD band is virtually unaffected.

Exposure to water vapor followed by evacuation, results in an increase in the intensity of the structural OH bands. Bands due to chemisorption of hydrogen (or deuterium) are not observed following this treatment. Moreover, the activity for ethylene hydrogenation on this sample is reduced by about one order of magnitude. Degassing at about 400°, however, brings about a decrease in the intensity of the structural OH bands, restores the activity of the catalyst, and the sample again shows OH and ZnH bands on chemisorption of hydrogen.

As noted earlier, the cell was attached to a circulating system so that infrared observations could be made during the course of catalytic hydrogenation. In a typical kinetic run, a 10:1 mixture of deuterium and ethylene (total pressure, 220 mm) was introduced into the circulation loop with the catalyst bypassed. The ethylene was frozen out by circulation through a liquid nitrogen trap. Then the catalyst was exposed to deuterium and the spectra shown in Figure 6A and B were recorded. At this point, with circulation through the cell, the ethylene was vaporized and hydrogenation of ethylene began. The course of the reaction was monitored by observations of bands due to gaseous ethane and periodic chromatographic analysis of gas samples. Figure 6C and D shows spectra obtained during the hydrogenation. The band corresponding to ZnD broadens and shifts from 1232 to 1195 cm⁻¹ but the integrated intensity stays the same; the band cor-

(19) J. H. Taylor and C. H. Amberg, *Can. J. Chem.*, **39**, 535 (1961).

(20) C. H. Amberg and D. A. Seanor, Proceedings of the 3rd International Congress of Catalysis, Amsterdam, 1964.

responding to OD shifts from 2610 to 2624 cm^{-1} and the integrated intensity drops to 60% of the initial value. The spectra remain the same during most of the reaction. At the last stages of the reaction, however, the spectra start to change back to their initial appearance. When the reaction is complete, the spectra are identical with those shown in Figure 6A and B. It is also found that if at any point during the reaction the hydrocarbons are frozen out, the original spectra are obtained; when the hydrocarbons are revaporized, the spectra characteristic of reaction (Figure 6C and D) are obtained.

It should be recalled that the intensity of the infrared bands is relatively independent of pressure in this region.^{16,18} The fact that intensities and appearances of the spectra are the same in 200 mm of deuterium (before reaction) as in 180 mm of deuterium and 20 mm of ethane (after reaction) simply means ethane has no effect on the deuterium bands.

Poisoning Experiments. In these experiments, after an initial study of the chemisorption and activity, about 10 g of catalyst was exposed to 2.3 cc of water, which was circulated over the catalyst at 300° for 1 hr. Adsorption and activity were then measured as a function of the amount of water removed by circulation of dry helium through a liquid nitrogen trap in series with the heated catalyst. Experiments with dried catalyst showed that the water collection procedure following the sequence of activity and adsorption experiments always yielded about 0.2 cc of water. This water is presumed to come from reaction of type II hydrogen to form water in the collection procedure. (Preliminary experiments show that either the slow adsorption during adsorption measurements or the hydrogen uptake during reaction would be expected to contribute 0.2 to 0.3 cc.¹⁶ The combined effect of these experiments in sequence has not been experimentally examined.) With the assumption that all type II hydrogen was converted to water, the amount of water added agreed with that removed within 1%.

The effect of water adsorption on rate for two sequences of water adsorption and removal is shown in Figure 7. The area of this catalyst, which was sintered by previous experiments, was about 5 m^2/g . If one assigns an effective area of 10.6 \AA^2 to a water molecule,²¹ monolayer coverage corresponds to 14 cc. It is clear from Figure 7 that coverage of about 5% reduces the rate by about 50%.

Figure 8 is a plot of rates vs. adsorption for a catalyst poisoned with water to various degrees. Amounts of type I adsorption could not be estimated as in the previous runs for this would add of the order of 1 cc of type II hydrogen, convertible to water, in each run. Instead, the hydrogen adsorption after 2 min was measured. Preliminary experiments showed this included about 0.3 cc of type II adsorption. Accordingly, the total amount of hydrogen adsorbed in 2 min minus

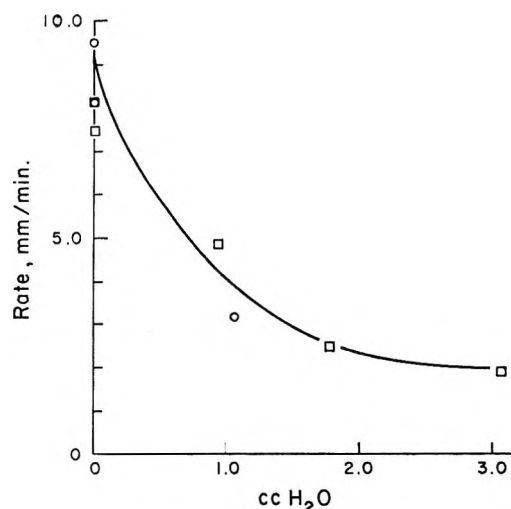


Figure 7. Activity vs. water adsorption: \square , hydrogen adsorption sequence; \circ , ethylene adsorption sequence.

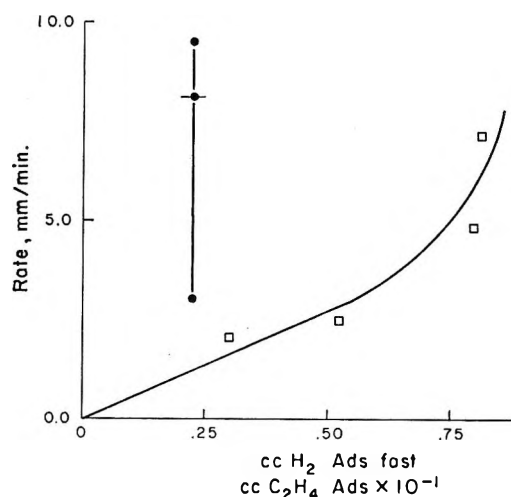


Figure 8. Correlation of rate with adsorption: \square , hydrogen adsorption sequence; \bullet , ethylene adsorption sequence.

0.3 cc was taken as a rough measure of the amount of type I chemisorption. It appears that the rate reduction brought about by water adsorption arises primarily from the associated reduction of type I chemisorption. Figure 8 is consistent with this picture insofar as it implies that the rate reduction due to water adsorption parallels a concomitant reduction of type I chemisorption, whereas ethylene chemisorption is only little affected by water chemisorption. This conclusion does not depend on the procedure used to assess the amount of type I chemisorption; at most, a more precise assessment would bring only a scale shift in the abscissa of Figure 8.

Discussion

Infrared and adsorption studies impose boundary conditions on the nature of the active sites for the

(21) S. J. Gregg and K. S. W. Sing, "Adsorption, Surface Area and Porosity," Academic Press, New York, N.Y., 1967, p 82.

hydrogenation of ethylene. The simultaneous development of ZnH and OH bands suggests the sites consist of a surface Zn-O pair. Adsorption studies¹⁶ show type I chemisorption occurs only on 5% of the total surface; hence, the number of these pair sites is limited. Moreover, since oxygen chemisorption has no effect on the type I adsorption or the associated infrared bands, the active sites are not associated with lack of stoichiometry. Accordingly, it is of interest to consider the surface structures expected for stoichiometric zinc oxide.

In zinc oxide the oxide ions are arranged in positions corresponding to hexagonal closest packing with zinc ions filling one-half the tetrahedral holes (see Figure 9a).²² The idealized structure can be viewed in terms of spheres of zinc ions and oxide ions, both in fourfold coordination, with a radius of 0.70 and 1.33 Å, respectively. (These radii are 95% of the common octahedral radii.) If the spheres corresponding to oxide ions were strictly close packed, *i.e.*, if the oxide-oxide distance were fixed at 2.66 Å, the zinc ions would have to squeeze into tetrahedral holes with a radius of 0.30 Å. The computed molar volume for such a structure is 8.0 cc compared to the experimental molar volume 14.9 cc. If, instead, we assume the close-packed layers of hard oxide spheres of radius 1.33 Å expand isotropically until the tetrahedral holes can accommodate hard zinc spheres with a radius of 0.70 Å, the oxide-oxide distance would now be 3.30 Å rather than 2.66 Å. Then, the computed molar volume would be 15.2 cc in good agreement with the experimental value. Such a structure would be very open; only 45% of the space would be filled by spheres compared to 75% for the strictly close-packed structure.

In addition to the tetrahedral holes in the oxide layers in zinc oxide, there are also octahedral and trigonal holes. The latter constitute a passageway from tetrahedral to octahedral sites. The assumed isotropic expansion increases the radius of the octahedral hole from 0.55 to 1.0 Å and increases the radius of the trigonal hole from 0.30 to 0.58 Å. Thus, in the expanded structure which approximates the real structure, the trigonal hole can almost accommodate the zinc ion. It is of some interest to note that because of the hexagonal packing, the octahedral sites lie in a straight line perpendicular to the close-packed layer. Thus, we have a straight channel of such sites, each 2.0 Å in diameter, separated by a trigonal "squeeze point" 1.2 Å in diameter.

Figure 9a provides a diagrammatic view of the layer structure in zinc oxide. The heavy solid lines represent the close-packed oxide layer; circles represent the interlayer zinc ions; the lighter lines represent the four "bonds" zinc ions make to oxide ions. Interchange of all of the zinc with all of the oxide ions yields the same structure; hence, positions of zinc ions like those of oxide ions, corresponded to an expanded, hexagonal

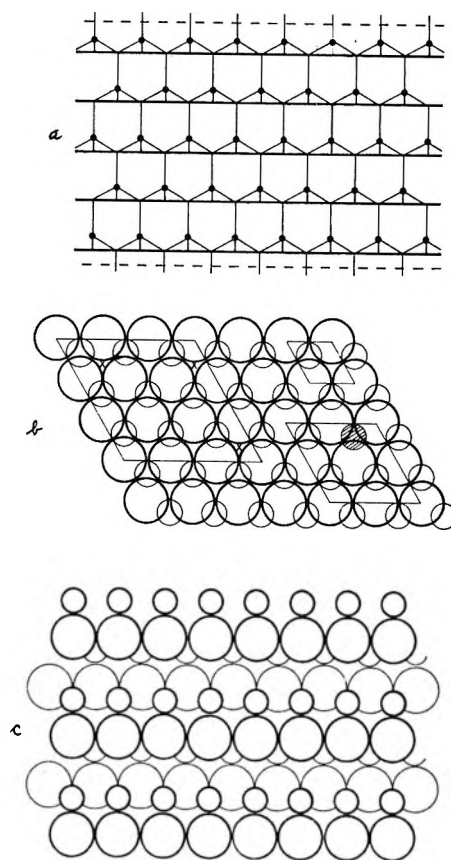


Figure 9. Structure of ZnO: A, schematic view perpendicular to the c axis. Heavy lines represent a nearly close-packed layer of oxide ions; circles represent zinc ions in tetrahedral holes; light lines represent tetrahedral "bonds;" dotted lines represent surfaces. (B) close-packed layers in 0001 surface (zinc uppermost) or 000 $\bar{1}$ surface (oxide uppermost). Larger spheres represent oxide ions. C, Layer structure for 10 $\bar{1}$ 0 surface. Larger spheres represent oxide ions.

close packing. The same drawing would also apply for the closely related zinc blende structure which differs from zinc oxide insofar as the anions show cubic rather than hexagonal close packing. The latter structure is commonly found for III-V compounds such as GaAs. For these compounds, development of close-packed planes occurs so that atoms on the surface have one rather than three dangling bonds.^{23,24} Cuts yielding such surfaces are indicated by the dashed lines in Figure 9a. Studies with etched, polished single crystals reveal that on GaAs (or GaSb) one close-packed layer (111) contains only gallium atoms; the opposite one ($\bar{1}\bar{1}\bar{1}$) contains only arsenic atoms. Because of the strong similarity in structure a similar situation holds for zinc oxide,²³ there will be one close-packed layer containing only zinc ions (0001) and one containing only oxide ions (000 $\bar{1}$). The close-packed layers for either structure are shown in Figure 9b.

(22) A. F. Wells, "Structural Inorganic Chemistry," Oxford University Press, London, 1962, p 53.

(23) H. C. Gatos, *Science*, **137**, 311 (1962).

(24) D. D. Pretzer and H. D. Hagstrum, *Surface Sci.*, **4**, 265 (1966).

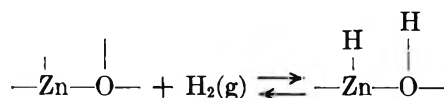
Planes other than close-packed can be formed with only one (or less) dangling bond per surface atom. For zinc oxide, these planes are parallel to the c axis and can be designated as $10\bar{1}0$ or the equivalent. Such a plane is pictured in Figure 9c. This surface consists of lines of raised zinc oxide pairs in which both the zinc and oxygen have a dangling bond. Between each line of pairs there is a groove defined by a subsurface line of pairs containing no dangling bonds. The analog of this surface in zinc blende is formed by a cut along the 110 planes. Clearly, these faces are not polar; they contain equal numbers of cations and anions.

LEED studies²⁵ on single crystals of GaAs show that the 110 plane at the surface has the same structure as in the bulk, but the 111 and $\bar{1}\bar{1}\bar{1}$ planes show rearrangement in the surface planes. The nature of these surface reconstructions are indicated by guidelines in Figure 9b. The upper right hand corner shows the ideal two-dimensional unit cell, a 1×1 net. Reconstruction on the gallium surface expands this repeat unit to a 2×2 net (lower right) whereas reconstruction on the arsenic surface expands the repeat unit to a 3×3 net (left side).²⁵ [Consider the gallium (111) surface to be represented by the drawing in Figure 9b with small spheres uppermost whereas the arsenic ($\bar{1}\bar{1}\bar{1}$) surface has large spheres uppermost.] The driving force for the rearrangement of the 111 surface appears to be the tendency of the more electropositive component, which presumably has an unfilled dangling bond,²³ to form an sp^2 rather than sp^3 bond. This can be approached if the gallium atoms in the surface move toward trigonal holes in the underlying arsenic layers. In GaAs the size of the trigonal holes is small compared to the size of the atoms; hence, such motion is accompanied by considerable strain. Macrae²⁵ proposes this strain results in loss of a superficial gallium atom or its replacement by an arsenic atom. Figure 9b shows how the systematic loss or replacement of the cross-hatched atom gives rise to a 2×2 net on the surface. Macrae²⁵ has suggested that the formation of a 3×3 net on the $\bar{1}\bar{1}\bar{1}$ surface stems from the systematic introduction of strains at the points marked by x's. It is believed²³ that the more electronegative atoms have a filled dangling bond and therefore maintain sp^3 bonding at the surface; hence, rearrangement is not the result of a driving force for rehybridization but stems from more subtle factors.

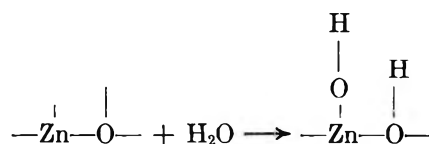
The results described above for GaAs are also obtained for the isostructural GaSb; hence, it does not seem unreasonable to extrapolate these results to the nearly isostructural zinc oxide. On this basis we would expect no surface reconstruction on the $10\bar{1}0$ planes, which are similar to the 110 surface in zinc blende, but might expect surface reconstruction on the close-packed planes. The 0001 planes, consisting of zinc ions with unfilled dangling bonds, will again tend to settle into

the underlying trigonal holes and thereby form sp^2 rather than sp^3 bonds. Because the zinc ions can almost fit into the trigonal holes, the strain will be much less than that for GaAs; hence, the surface reconstruction found for GaAs may not be needed. Accordingly, we picture the 0001 planes as a layer of zinc ions, still uppermost, but closer to the underlying oxide layer than they are in the ideal structure. The $000\bar{1}$ planes, consisting of oxide ions with filled dangling bonds, will be subject to the same kinds of forces present in GaAs. Macrae²⁵ has suggested that the 3×3 can be the result of inclusions at the x's in Figure 9b. We suggest that it is zinc ions that actually *occupy* these trigonal sites on the $000\bar{1}$ face of zinc oxide. These ions should not be viewed as deviations from stoichiometry; they result from reconstruction of the surface to stabilize the $000\bar{1}$ face. Accordingly, zinc ions located at x's in Figure 9b would not be removed by high-temperature pretreatment with oxygen if the $000\bar{1}$ faces are to persist as a reconstructed surface phase.

The picture of the active site as a zinc ion imbedded in a close-packed oxide layer has much to recommend it. The 3×3 repeat sequence would lead to sites that are not adjacent, and hence, are essentially noninteracting;^{12,13} moreover, it would assure that only a fraction of the surface contains active sites. Hydrogen adsorption on these sites occurs as



(In our model based on spheres, the outermost plane tangent to oxide spheres would be 0.53 \AA above the surface of the zinc sphere. To emphasize this point, we have shown the dangling bond of the zinc shorter than that of the oxide ion.) If, however, water is adsorbed on the zinc oxide first, we expect the following reaction to occur



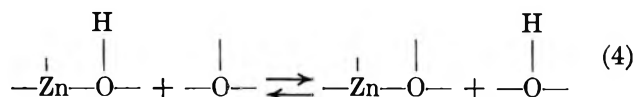
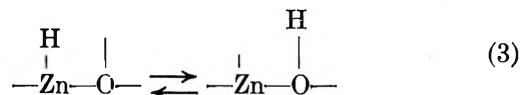
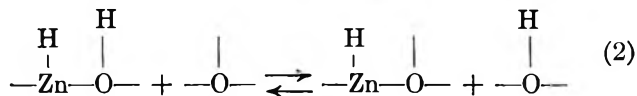
Adsorption of water vapor was shown to be strong; hence, preadsorption of water would be expected to prevent the occurrence of the first reaction, as observed. (We shall term the OH formed as a pair from water adsorption as hydroxyl in order to distinguish it from the OH formed by hydrogen chemisorption.) Hydroxylation would be expected to occur not only at active sites but also on the lines of ZnO pairs on $10\bar{1}0$ type faces (9c). The latter pairs, because of their protuberance above the surface, would be expected to retain hydroxyls more tenaciously than the active site wherein

(25) A. U. MacRae, *Surface Sci.*, **4**, 247 (1966).

the zinc ion is less accessible because it is shielded by the larger oxygen anions. In line with this three hydroxyl bands are seen even for a well degassed catalyst that shows an infrared spectra due to chemisorbed hydrogen. We would expect three hydroxyl bands from the line of hydroxylated ZnO pairs on the 10 $\bar{1}0$ faces corresponding to 0, 1, and 2 hydroxylated neighbors.²⁶ Since these hydroxyls occur on different planes from the OD groups formed by deuterium chemisorption, exchange is very slow. In addition, all hydroxyl bands including those associated with the active site occur at different frequencies from the OH bands simply because the environment is different; *e.g.*, hydroxyl groups occur in pairs.

The effect of chemisorbed carbon monoxide on the hydrogen chemisorption is also consistent with this picture. Irreversibly, slowly chemisorbed, carbon monoxide shows bands at 1575 and 1340 cm^{-1} identified as carboxylate groups which are a precursor to reduction.^{19,20} Under conditions of these experiments, strongly bound carbon monoxide covers about 5% of the oxide surface.²⁰ If this chemisorption occurs randomly on the oxide sites of all exposed planes, it would be expected to have little effect on that 5% of the surface on which type I hydrogen chemisorption occurs. This agrees with our infrared data. There is also a reversible form of chemisorbed carbon monoxide, which also covers about 5% of the surface, and shows a band at about 2174 cm^{-1} .²⁰ This species is presumed to be found by a polar interaction. As such, it might be expected to concentrate at the zinc ion of the active site. In line with this, the ZnH band for chemisorbed hydrogen is dramatically influenced by this type of chemisorption with little effect on the associated OH band.

Chemisorption of hydrogen can be represented by the set of equations



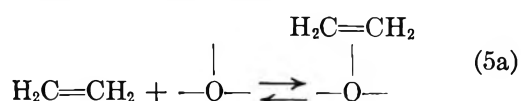
In the above, $\begin{array}{c} | \\ -\text{Zn}-\text{O}- \\ | \end{array}$ represents the active site and $\begin{array}{c} | \\ -\text{O}- \\ | \end{array}$ the oxide ions which form a wall separating active sites. (This is an oversimplification in the

sense that the zinc of the active site is likely to have several equivalent oxide nearest neighbors; nevertheless, rewriting the sequence in terms of an active site such as ZnO₃ would only greatly expand the number of equations without introducing significantly new features. For the sake of simplicity, therefore, we shall couch our discussion in terms of the simpler picture.) The first equation represents the initial adsorption act; the next equation provides for the site-to-site migration required for hydrogen-deuterium exchange which occurs readily on this catalyst.¹² Steps 3 and 4 provide a mechanism whereby hydrogen attached to zinc can exchange with hydrogens attached to oxide ions; studies by Eischens, *et al.*,¹⁸ of the exchange process seem to require such a pathway. In terms of these equilibria, we can compute the dependence of the total OH concentration (OH) on the concentration of ZnH (ZnH). As might be expected, this depends on the number of active sites (C_0) and the number of oxide sites (O^{2-}). If the latter are only sparsely covered and all equilibria lie to the right except for (2), this leads to the relation

$$(\text{OH}) = (\text{Zn-H}) + (\text{O}^{2-})(K_2K_3K_4)^{1/2} \left[\frac{(\text{ZnH})}{(C_0) - (\text{ZnH})} \right]^{1/2}$$

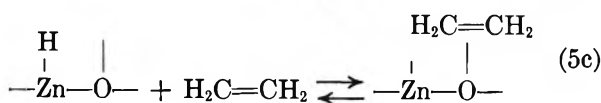
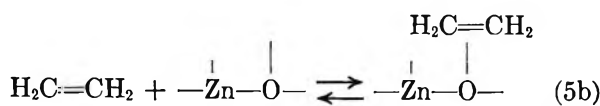
If K_2 is sufficiently small, this expression predicts that at moderate concentrations, the OH band intensity would be proportional to the ZnH band intensity, but as saturation is approached, *i.e.*, as ZnH approaches C_0 , the OH band intensity would increase dramatically relative to the ZnH band intensity. This is consistent with the infrared observations. Qualitative aspects of this result still follow even if reactions 3 and/or 4 take place only to a limited extent. This follows because as saturation is approached, the concentration of ZnO goes to zero and drives reaction 4 to the right.

Infrared studies of the adsorption of ethylene at room temperature on zinc oxide revealed no bands that could be ascribed to opening of the double bond with formation of a saturated species. Accordingly, it appears that chemisorption occurs by interaction of a π bond with the surface. For steric reasons we would not expect the ethylene to approach the imbedded zinc ion of the active site close enough for such interaction; hence, we believe ethylene adsorption is confined primarily to oxide sites. Since, however, ethylene covers about 40% of the surface (assuming an effective cross section of 23 \AA^2)²⁷ we can expect some chemisorption on oxide sites adjacent to the imbedded zinc ion. These expected modes of adsorption are



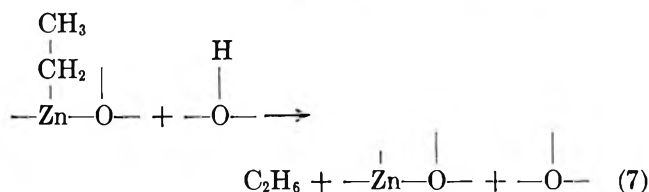
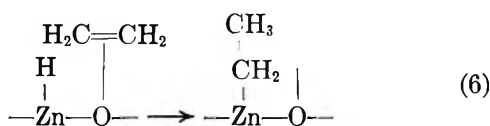
(26) For an analogous situation on aluminas, see J. B. Peri, *J. Phys. Chem.*, **69**, 220 (1965).

(27) S. J. Gregg and K. S. W. Sing, "Adsorption, Surface Area and Porosity," Academic Press, New York, N. Y., 1967, p 80.



Since adsorption of ethylene occurs on oxide sites, ethylene adsorption should inhibit adsorption of hydrogen on these sites. Moreover, since the coverage with ethylene is relatively high, at least one of the oxide sites next to a ZnH should be occupied with a resulting perturbation of the ZnH band. Thus, these equations are consistent with the observation that admission of ethylene to a sample with chemisorbed hydrogen decreases the intensity of the OH band and perturbs the ZnH band without much effect on its intensity.

Rates of adsorption of ethylene and hydrogen and the establishment of stable infrared spectra are rapid compared with the hydrogenation reaction;¹⁶ hence, it seems reasonable to assume that equilibrium is established in reactions 1 through 5. We shall further assume as a first approximation that adsorption of ethylene on oxide sites is indiscriminate and that all reactions listed as eq 5 have the same equilibrium constant. Reaction to form ethane can occur stepwise as



Since addition of deuterium to ethylene results solely in $\text{C}_2\text{H}_4\text{D}_2$,¹¹ the first step is irreversible. Bonding of an alkyl radical to a metal atom seems more likely than to an oxide ion; hence, the reactive sites have the form shown. Presumably, the steric factors that prevent π bonding with the zinc would be inoperative in the more directed σ bond of the alkyl radical.

In terms of these equations, steady-state production of ethane, R , is given by

$$R = k_6(\text{H-ZnO-C}_2\text{H}_4) \quad (8)$$

Use of eq 5 with the equilibrium assumptions yields

$$R = k_6 K_5 (\text{H ZnO}) (\text{C}_2\text{H}_{4(\text{g})}) = k_6 \frac{(\text{H ZnO})(\text{ZnO} \cdot \text{C}_2\text{H}_4)}{(\text{ZnO})} \quad (9)$$

Equations 1 through 4 can be combined to yield

$$\frac{(\text{H ZnO})}{(\text{ZnO})} = \sqrt{\frac{K_1 K_2}{K_3 K_4}} (\text{H}_2(\text{g}))^{1/2} \quad (10)$$

Substitution of eq 10 into 9 yields

$$R = k_6 \sqrt{\frac{K_1 K_2}{K_3 K_4}} (\text{ZnO} \cdot \text{C}_2\text{H}_4) (\text{H}_2(\text{g}))^{1/2} \quad (11)$$

$$\text{or } R \equiv k' \theta' (\text{H}_2(\text{g}))^{1/2}$$

where θ' represents the adsorption of ethylene on an oxide site adjacent to the exposed zinc. (Even if the three reactions listed for ethylene chemisorption have different equilibrium constants, the form of eq 11 persists with a different combination of constants for k' .) Although θ' should depend on the pressure of hydrogen as well as ethylene, the evidence from the infrared that ethylene displaces hydrogen from oxide sites suggests this dependence may be slight. Accordingly, it is reasonable as a rough approximation to assume that the adsorption of ethylene on all sites in the presence of hydrogen shows the same pressure dependence as is found in the absence. On such a basis, eq 11 is in complete accord with the experimentally determined kinetics which yield a rate proportional to the square root of the hydrogen pressure and a dependence on ethylene pressure similar to that found for ethylene adsorption. (It should be noted that eq 11 is based solely on the law of mass action and does not require assumptions regarding the form of the isotherm. Strictly speaking, k_6 should be written as k_6/γ^\ddagger , where γ^\ddagger is the activity coefficient of the activated complex, and θ' and $(\text{H}_2(\text{g}))$ should be regarded as activities; the latter will be well approximated by the pressure.)

The assumption of equilibrium prior to the rate-controlling step means that the kinetic isotope effect depends only on the partition functions of the activated complex and that for gaseous reactants. The activated complex is essentially an adsorbed alkyl radical. If we assume the reaction coordinate is the stretching of the newly formed C-H bond, the bending frequencies will be most important in determining the isotope effect. In CHCl_3 and CDCl_3 the degenerate bending frequencies are 1210 and 908 cm^{-1} , respectively. From these and the zero point energies for hydrogen and deuterium, we can estimate the isotope effect by procedures outlined by Bigeleisen and Wolfsberg.²⁸ Such a computation yields a rate with deuterium that is 69% that with hydrogen. The assumption of a slight loosening of the bending frequencies will decrease this value to that observed experimentally ($\sim 50\%$). Thus, the isotope effect is roughly consistent with the proposed mechanism. By way of contrast, one would expect significantly larger isotope effects or none were reaction 3 or 5a, respectively, the rate controlling step.

(28) J. W. Bigeleisen and M. Wolfsberg, *Advan. Chem. Phys.*, I, 15 (1958).

We feel the type II hydrogen adsorption may involve partial penetration into the bulk along the octahedral channels referred to earlier. The trigonal squeeze point with a diameter of 1.20 Å does not seem prohibitively small compared to the size of a hydrogen molecule. Thus, we tentatively suggest that type II hydrogen may occupy octahedral holes, with a nominal diameter of 2.0 Å, near the surface. Since the slow step for such sorption is likely to be expansion of the trigonal sites due to lattice vibrations, such a mechanism is consistent with the observation that the rate of type II sorption is the same with hydrogen and deuterium.¹⁷ Although the above picture is plausible, it does not provide an explanation for the promotional effects of hydrogen.

In conclusion, let us note that we have tried to fit the data to other models. None we have considered, however, yield such a clean-cut, half-order dependence on hydrogen and are also consistent with the auxiliary observations. It should be emphasized, however, that the essentials of the model we propose are that the active sites are isolated zinc oxide pairs with a pathway for limited hydrogen migration between sites. The

proposed picture of the surface structure that can give rise to these sites must be regarded as speculative even though many of the consequences seem to fit auxiliary observations. The essential features, however, bear many similarities to homogeneous catalysts which, because they are effective in dilute solution, can also be regarded as isolated, noninteracting sites. We can hope to find many analogies, therefore, in the behavior of oxides and homogeneous hydrogenation catalysts. It must, however, be emphasized that the model we propose and the relative simplicity of the kinetics would not be expected to obtain at higher temperatures where type II hydrogen plays a role. Thus, if analogies with homogeneous catalysts are to be sought, care should be taken that the temperature of the study is in a region such that the above model is applicable.

Acknowledgment. Acknowledgment is made to the donors of the Petroleum Research Fund, administered by the American Chemical Society, for support of this research. The writers also acknowledge the benefit of many helpful discussions of this work with Professor F. S. Stone.

Catalysis of the Reduction of Supported Nickel Oxide

by E. James Nowak¹

Department of Chemical Engineering, The University of New Mexico, Albuquerque, New Mexico 87106
(Received March 34, 1969)

Small amounts of metallic platinum or palladium, incorporated in alumina-supported nickel oxide catalysts, have been observed to enhance activation of the catalysts by hydrogen. By contrast, small amounts of gold and silver, which do not readily adsorb hydrogen as atoms, also do not enhance activation of the catalysts. Hydrogenolysis, isomerization, and aromatization reactions of *n*-heptane with hydrogen, used for characterizing catalytic activity, were carried out in a pulse-flow reactor coupled with a gas chromatograph. Platinum or palladium, in atom ratios to nickel (as oxide) as low as 5×10^{-3} were sufficient to cause large increases in conversion over the nickel component, while gold and silver, in atom ratios to nickel as high as 1×10^{-1} produce no such effect. There is now a preponderance of evidence favoring reduction by surface-diffusing hydrogen atoms as the mechanism for activation of supported nickel oxide by platinum and palladium.

Introduction

Commercial nickel catalysts are usually supported by refractory metal oxides such as alumina or silica-alumina, and they are activated by heating in a hydrogen-rich atmosphere which presumably reduces some or all of the nickel to its metallic form. Activation requires temperatures considerably higher than the temperature for reduction of pure bulk nickel oxide, apparently because the reducibility of nickel oxide is decreased by its strong interaction with the support

material.² Such high activation temperatures are undesirable, because they may cause sintering of the metallic nickel. It is apparent, then, that catalyzed reduction of supported nickel oxide could result in increased activity for the final catalyst by maximizing the extent of reduction at a temperature low enough to avoid appreciable loss of area due to sintering. Ac-

(1) Sandia Corporation, P. O. Box 969, Livermore, Calif. 94550.

(2) F. N. Hill and P. W. Selwood, *J. Amer. Chem. Soc.*, **71**, 2522 (1949).

tivating and stabilizing effects of platinum-group metals in nickel catalysts which could be due to catalyzed reduction have been reported in the patent and journal literature.^{3,4}

Evidence for catalyzed activation of supported nickel oxide by added platinum and palladium has been presented in a previous publication.⁵ It was shown that an atom ratio of platinum-to-nickel as low as 5×10^{-3} is sufficient to produce a striking increase in activity of the catalyst (0.6% Ni, 0.01% Pt- γ -Al₂O₃) for hydrogenolysis of *n*-heptane at 370° and 2 atm of H₂. The resulting product distribution was shown to be characteristic of metallic nickel, not of platinum, and a catalyst without nickel but with the same amount of platinum on the same support had negligible activity. Thus, platinum enhances the activity of the nickel component. Such a cooperative effect was not observed⁵ for a physical mixture of 0.6 wt % Ni-Al₂O₃ with 0.3 wt % Pt-Al₂O₃ (-60 mesh particles), showing that the metals do not interact *via* long-lived species in the gas phase; apparently direct physical contact of platinum with nickel oxide or short surface paths between particles of platinum and nickel oxide are required. Palladium produced an even more striking activation effect than platinum, and the activating effects of both metals were observed at several reduction temperatures between 370 and 480°.

Two mechanistic models for activation of nickel oxide by these metals were proposed. According to the first model, hydrogen atoms formed by adsorption of molecular hydrogen on the activating metal diffuse to nearby nickel oxide particles where they initiate reduction at a much greater rate than does molecular hydrogen. Higher reactivity of hydrogen atoms from the gas phase for reduction of nickel oxide has been established by Bergh.⁶

According to the second model, crystallites of the activating metal in contact with nickel oxide provide metallic nuclei for rapid growth of the metallic nickel phase without a high activation barrier to nucleation.

It is the purpose of this paper to report experimental evidence favoring activation *via* diffusing hydrogen atoms (the first model) and to clarify the effect of chloride ions introduced by impregnation of the catalysts with chloroplatinic acid and palladium chloride. Activating effects of Au, Ag, Pt, and Pd on NiO-Al₂O₃, with several values of chloride content, were determined and are compared at reduction temperatures of 370, 430, and 480° for *n*-heptane hydrogenolysis at 370°.

Experimental Section

Reactions were carried out in a pulse-feed tubular catalytic reactor directly coupled with an F&M Scientific Model 700 gas chromatograph with dual columns. The entire apparatus is similar in design and operation to one described previously.⁵ The catalyst bed con-

sisted of 0.20 g of catalyst particles (-8, +16 mesh) retained between two glass wool plugs. Catalyst temperatures were maintained with two cartridge-type electrical heaters in a well insulated brass block surrounding the reactor, and temperatures were measured by a thermocouple in contact with the 1/4-in. stainless steel tubing reactor wall. The 20-ft, 1/4-in. o.d. chromatograph columns were packed with Carbowax on Chromosorb and were operated at 30° for 3 min followed by a 10°/min programmed temperature increase to 100°. Hydrogen, flowing at 85 ± 2 cc/min, was the carrier gas in both columns.

Catalysts were prepared by impregnating γ -Al₂O₃ (formed by calcining Davison β -trihydrate in air for 4 hr at 590°) with aqueous solutions of suitable metal salts: H₂PtCl₆·6H₂O, Pt(NH₃)₂(NO₃)₂, PdCl₂·2H₂O, HAuCl₄·3H₂O, and AgNO₃. In some preparations, HCl was added to achieve the desired chloride ion content. Impregnation by just wetting the alumina support was followed by drying overnight at 120° and then calcining in air at 370° for 4 hr. The bimetallic catalysts were prepared in all cases by first impregnating the support with aqueous Ni(NO₃)₂ solution, drying and calcining, and then reimpregnating the catalysts with an aqueous solution of the other metal, drying, and calcining again at the same conditions. All catalysts were prerduced *in situ* with flowing hydrogen at 370 to 480°, as specified in the data tables.

The liquid feed was "Baker" *n*-heptane (bp 98-99°). Hydrogen (Airco, 99.9% pure) was passed through a De-oxo purifier to remove oxygen and then through a molecular sieve bed to remove water.

Results

Results demonstrating the lack of activation of supported nickel catalysts by Au and Ag, the activation by Pt and Pd, and the influence of catalyst chloride content are shown in Tables I and II.

The first column gives the catalyst compositions. Each catalyst batch is designated alphabetically (A,B,C, etc.). Catalysts with identical compositions but with different alphabetical designations are from different batches prepared at different times. Comparisons of these catalysts show the degree of reproducibility achieved by the preparative technique. Comparisons of different runs (second column) with the same alphabetical designation show the degree of reproducibility obtained for different catalyst charges from the same batch. The degrees of reproducibility in both cases were sufficient for reliable conclusions from

(3)(a) R. R. Sakaida, Ph.D. Thesis, California Institute of Technology, Pasadena, California, 1960; (b) R. R. Sakaida, R. G. Rinker, Y. L. Wang, and W. H. Corcoran, *A.I.Ch. E. J.*, **7**, 658 (1961).

(4) French Patent 1,372,516, Aug 10, 1964 (Imperial Chemical Industries, Ltd.).

(5) E. J. Nowak and R. M. Koros, *J. Catal.*, **7**, 50 (1967).

(6) A. A. Bergh, *Bell System Tech. J.*, **44**, 261 (1965).

Table I: Activation of Supported NiO with Added Au, Ag, Pt, Pd, and Ni

Catalyst	Run no.	Reduction pretreatment		Mole fraction n -C ₇ reacted
		Time, hr	Temp, °C	
A. 0.60 wt % Ni-Al ₂ O ₃	31	2	370	0.01
		1	430	0.04
		1	480	0.23
A. Same as above	36	2	370	0.01
		1	430	0.04
		1	480	0.16
B. Same as above	15	2	370	0.00
		1	430	0.02
		1	480	0.22
C. 0.60 wt % Ni and 0.01 wt % Pt-Al ₂ O ₃ with 6 Cl/Pt	29	2	370	0.08
		1	430	0.23
		1	480	0.48
D. Same as above	19	2	370	0.04
		1	430	0.18
		1	480	0.37
E. 0.60 wt % Ni and 0.01 wt % Pd-Al ₂ O ₃ with 6 Cl/Pd	37	2	370	0.11
		1	430	0.26
		1	480	0.48
F. Same as above	18	2	370	0.08
		1	430	0.25
		1	480	0.58
G. 0.01 wt % Pt-Al ₂ O ₃ with 6 Cl/Pt	32	2	370	0.02
		1	430	0.03
		1	480	0.01
H. Same as above	23	2	370	0.01
		1	430	0.01
		1	480	0.07
I. 0.01 wt % Pd-Al ₂ O ₃ with 6 Cl/Pd	24	2	370	0.00
		1	480	0.05
No catalyst in reactor	38	1	480	0.00
J. 0.60 wt % Ni and 0.01 wt % Au-Al ₂ O ₃ with 4 Cl/Au	21	2	370	0.00
		1	430	0.01
		1	480	0.11
K. 0.60 wt % Ni and 0.30 wt % Au-Al ₂ O ₃ with 4 Cl/Au	33	3	370	0.05
		1	430	0.13
		1	480	0.23
K. Same as above	35	2	370	0.03
		1	430	0.11
		1	480	0.23
L. 0.60 wt % Ni and 0.17 wt % Ag-Al ₂ O ₃ No chloride	34	2.2	370	0.02
		1	430	0.06
		1	480	0.18

the data. The third column gives the conditions of reduction pretreatment, and the fourth column shows the activities for conversion of *n*-heptane. The results in Table I show that neither 0.01 wt % Pt- η -Al₂O₃ nor 0.01 wt % Pd- η -Al₂O₃, each with 6 Cl⁻ per metal atom (catalysts G, H, and I), is appreciably active for the test reaction, and the same is true for the reactor containing only glass wool (run 38).

Results showing the lack of activation by Au and Ag are shown in Table I, and may be compared with the large activation by Pt and Pd also shown in Table I. Catalysts J, K, and L, containing up to 0.30 wt % Au and 0.17 wt % Ag, are no more active after pretreatment than are the reference catalysts A and B, while catalysts C, D, E, and F, containing 0.01 wt % Pt or Pd, are considerably more active. Thus, while Pt and

Table II: Influences of Chloride Content on Activation

Catalyst	Run no.	Reduction pretreatment		Mole fraction <i>n</i> -C ₇ reacted
		Time, hr	Temp, °C	
N. 0.60 wt % Ni and 0.01 wt % Pd-Al ₂ O ₃ with 30 Cl/Pd	16	2.2	370	0.12
		1	430	0.34
		1	480	0.81
F. 0.60 wt % Ni and 0.01 wt % Pd-Al ₂ O ₃ with 6 Cl/Pd	18	2	370	0.08
		1	430	0.25
		1	480	0.58
O. 0.60 wt % Ni-Al ₂ O ₃ with chloride content same as catalyst N	27	2	370	0.00
		1	430	0.02
		1	480	0.14
P. Same as above	39	2	370	0.01
		1	430	0.04
		1	480	0.18
A. 0.60 wt % Ni-Al ₂ O ₃	31	2	370	0.01
		1	430	0.04
		1	480	0.23
Q. 0.60 wt % Ni and 0.01 wt % Pt-Al ₂ O ₃ No chloride [Pt(NH ₃) ₂ (NO ₂) ₂]	20	2	370	0.01
		1	430	0.07
		1	480	0.22

Pd at atom ratios to nickel as low as 5×10^{-3} cause appreciable activation of the nickel catalyst, neither Au nor Ag at atom ratios to nickel as high as 10^{-1} have any activating effect.

The influences of catalyst chloride content are apparent from the results for catalysts F, N, O, P, and Q compared with reference catalyst A, as shown in Table II. Increasing the chloride ion content of the Pd-activated catalysts from 6 Cl-/Pd (catalyst F) to 30 Cl-/Pd (catalyst N) caused a large increase in *n*-heptane conversion which was especially noticeable after reduction at 430°. No difference in conversion was observed upon adding an equivalent amount of chloride ion to nickel catalysts without palladium, even after reduction at 480° which causes appreciable activity due to metallic nickel (catalyst O compared with catalyst A).

There is apparent synergism among Ni, Pd, and chloride ion for activation on the alumina support, but no increased activity due to increased chloride content in the absence of palladium. Platinum incorporated by impregnation with Pt(NH₃)₂(NO₂)₂ (catalyst Q) did not activate the catalyst.

Complete product distributions, including isomerization and aromatization products, were obtained for all runs. However, since the products are almost exclusively from hydrogenolysis over metallic nickel, as described previously by Nowak and Koros,⁵ only conversion data are presented here.

In summary, neither Au nor Ag enhances the activity of supported nickel oxide after reductive pretreatment with hydrogen, while Pt and Pd have a

strong activating effect. Changes in chloride content at high levels affect the activities of the Pt- and Pd-containing catalysts, but such changes do not influence the catalysts containing nickel alone; there seems to be synergism among Ni, Pd, and chloride ion in the catalysts. Changes in chloride content at low levels may affect the dispersion of the activating metal. Finally, Pt-Al₂O₃ (6 Cl-/Pt), Pd-Al₂O₃ (6 Cl-/Pd), the glass wool packing, and the reactor walls are all essentially inactive at the conditions used for the test reaction.

Discussion

The following mechanistic model for the activation of nickel oxide-on-alumina catalysts by platinum and palladium is supported by the results of this investigation. Reduction of nickel oxide particles is initiated by hydrogen atoms formed from dissociative adsorption of hydrogen on platinum or palladium particles, and the resulting rate of initiation is greater than the rate of initiation by hydrogen molecules. That gaseous atomic hydrogen is more reactive than gaseous molecular hydrogen for the reduction of nickel oxide has been established previously.⁶

Experimental evidence for this model is to be found in the results reported here. Au and Ag, which adsorb little or no hydrogen, do not activate the supported nickel catalyst, while Pt and Pd, metals which are known to adsorb copious quantities of hydrogen as mobile atoms, do activate the catalyst. This result for supported nickel catalysts parallels that of Verhoeven and Delmon,⁷ who measured rates of hydrogen reduction of unsupported nickel oxide powders containing

small amounts of finely divided foreign metals. Other papers treating the autocatalytic reductions of powdered metal oxides with and without added metal particles have appeared subsequently.^{8,9} Similar enhancement of the reduction of supported iron oxide has been reported recently.¹⁰

Results reported here also show that chloride ion added as HCl causes increased activity of Pd-activated catalysts for the test reaction. This excess chloride acts in synergism with Ni and Pd, since chloride ion added as HCl does not enhance the activity of the catalysts with nickel alone, even after they are pretreated in hydrogen to produce measurable activity, and catalysts containing chloride ion with Pd or Pt alone are inactive. The greater activating effect of Pd relative to Pt which was reported previously⁵ is now thought to be due to excess HCl inadvertently added during preparation of the PdCl₂ solution.

Whether the excess chloride enhances the rate of reduction of nickel oxide or the rate of the test reaction in concert with Pd has not been determined and should be the object of further study.

A preponderance of evidence now favors reduction by surface hydrogen atoms as the mechanism for activation

of supported nickel oxide by platinum and palladium. The alternate model invoking nucleation on added metal particles is unlikely, because it affords no satisfactory explanation for the failure of Au and Ag to activate the catalysts as do Pt and Pd. Pt, Pd, Au, and Ag all have the same crystal structure as Ni, face centered cubic, and they all have roughly comparable atomic radii. Chemical, rather than crystallographic factors seem to be controlling the activation, and, based on the differences in known chemical reactivity of the additive metals toward hydrogen, the most likely chemical intermediate is atomic hydrogen.

Acknowledgments. This work was supported by funds from a National Science Foundation Institutional Grant to The University of New Mexico and from the Research Allocations Committee for the University.

(7) W. Verhoeven and B. Delmon, *Compt. Rend., Sec. C*, **262**, 33 (1966).

(8) W. Verhoeven and B. Delmon, *Bull. Soc. Chim., Fr.*, 3065, 3073 (1966).

(9) B. Delmon and M. T. Pouchot, *ibid.*, 2677 (1966).

(10) K. M. Sancier and S. H. Inami, *J. Catal.*, **11**, 135 (1968).

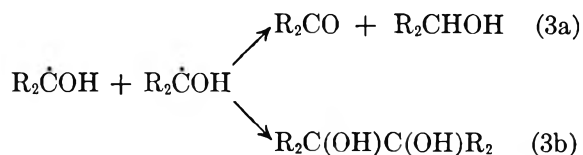
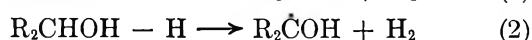
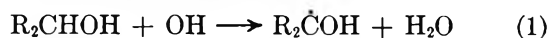
Pulse Radiolysis Study of Alcohols in Aqueous Solution

by M. Simic,¹ P. Neta,¹ and E. Hayon

Pioneering Research Laboratory, U. S. Army Natick Laboratories, Natick, Massachusetts 01760
(Received March 24, 1969)

A detailed pulse radiolysis study of aqueous solutions of methanol, ethanol, isopropyl alcohol, *n*-, iso-, and *t*-butyl alcohols, neopentanol, and cyclohexanol has been carried out. Optical absorption spectra of some of the transients have been measured down to 210 nm. Similar spectra were obtained in liquid methanol, ethanol, and isopropyl alcohol. Absorption maxima of transients have been obtained in aqueous solutions of *n*-BuOH (at 222 nm), *i*-BuOH (at 225 nm), *t*-BuOH (at 225 nm), neopentanol (at 238 nm), and cyclohexanol (at 230 nm). In alkaline solutions, dissociation of the α -hydroxyalkyl radicals ($\cdot\text{ROH}$) takes place, and the absorption spectra of the transients are considerably broadened. The dissociated form of the transients ($\cdot\text{RO}^-$) exhibit higher extinction coefficients and lower decay rate constants as compared to the undissociated form. In oxygenated-solutions absorption spectra with $\lambda_{\text{max}} \sim 240\text{--}250$ nm have been observed and are suggested to be due to the organic peroxy radicals ($\cdot\text{O}_2\text{ROH}$).

The radiolysis of aqueous solutions of simple aliphatic alcohols has been shown² to produce aldehydes (or ketones), glycols, and hydrogen. Reactions of the H atoms and OH radicals with alcohols, taking place mainly at the α -carbon position, produce radicals which subsequently disproportionate or dimerize



(1) National Academy of Sciences—National Research Council Research Associates at Natick.

(2) G. Jayson, G. Scholes, and J. J. Weiss, *J. Chem. Soc.*, 1358 (1957); J. T. Allan, E. Hayon, and J. J. Weiss, *ibid.*, 3913 (1959).

On pulse radiolysis of aqueous solutions of ethanol a transient optical absorption spectrum in the wavelength region 245–310 nm has been reported by Taub and Dorfman³ and was assigned to the α -hydroxyethyl radical $\text{CH}_3\dot{\text{C}}\text{HOH}$. This radical was found to decay by a second-order process, thus substantiating the previously postulated mechanism.² Transient absorption spectra have later been observed on pulse radiolysis of aqueous solutions of isopropyl alcohol⁴ (between 220 and 310 nm) and of methanol⁵ (between 260 and 330 nm).

Henglein and coworkers^{6,7} have observed in the pulse radiolysis of aqueous solutions of alcohols a pH dependence of the transient absorption spectra and have attributed this change to the dissociation of the transient radicals. By application of both optical and conductivity measurements pK values well below the pK values of the parent alcohols were determined.^{6,7}

Simple aliphatic alcohols are considerably employed in chemical kinetics and in mechanistic studies in radiation chemistry and photochemistry, and as H-atom donors in the quenching of triplet excited molecules. A knowledge of the absorption spectra, extinction coefficients, rates of decay, and reactivities of alcohol radicals is therefore of considerable interest. With these views in mind a rather detailed pulse radiolysis study has been made of the following alcohols: methanol, ethanol, isopropyl alcohol, *n*-, iso- and *t*-butyl alcohols, neopentanol, and cyclohexanol, using a new facility making it possible to observe transient species down to 210 nm. An attempt was also made to observe peroxy alcohol radicals hitherto postulated to be formed in oxygenated solutions.

Experimental Section

This work was carried out using a Febetron 705 System (Field Emission Corp.) which produces a pulsed electron beam of 2.3-MeV energy and constant pulse duration of about 30 nsec. Rectangular through-flow Spectrosil quartz (Thermal Syndicate, Wallsend, England) optical cells were used: 6 mm deep, 8 mm high, and 20 mm optical path. The thickness of the cell wall facing the electron beam was 0.5 mm.

The monitoring light source used was an Osram XBO 450 W xenon lamp. For work below about 260 nm, the light output from the xenon lamp was increased by a factor of 25–30 times by pulsing the lamp with pulses of about 1.2-msec duration, using the xenon lamp booster circuit developed by Hviid and Nielsen.⁸ To eliminate the effect of the magnetic field from the Febetron on the arc of the xenon lamp, the lamp was shielded by several consecutive layers of netic and conetic metal.

Two high-intensity Bausch and Lomb monochromators were used in series to reduce scattered light. At 230 and 210 nm the amount of scattered light found was 1 and 18%, respectively. Two EMI 9558 QB photomultipliers were used and a dual beam Fairchild 777 oscilloscope with selected plug-ins employed. The

photomultiplier and amplifier circuit in operation has been described elsewhere.⁹

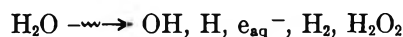
Solutions were prepared using water purified by triple distillation, radiolysis, and photolysis. Chemicals employed were analytical reagent grade or spectrograde and were supplied by Baker and Adamson and by Mallinckrodt. Solutions were buffered using perchloric acid, potassium hydroxide, sodium tetraborate, and potassium phosphate.

The total dose absorbed per pulse was determined using an N_2O -saturated aqueous solution of potassium thiocyanate as dosimeter. By measuring optical densities at 500 nm at different concentration of KCNS a plateau value for the dose employed was found at 0.1 M KCNS. Using $\epsilon^{500}_{(\text{CNS})_2^-} = 7600 \text{ M}^{-1} \text{ cm}^{-1}$,¹⁰ the total dose per pulse was determined by extrapolating the optical density of the $(\text{CNS})_2^-$ radical to "zero time." The total dose per pulse was varied by a factor of about 10 by interposing various filters between the electron beam and the optical cell. The reproducibility of the dose per pulse was better than $\pm 5\%$. The optical densities throughout this work were usually measured at 1 μsec after the pulse.

Due to the very high dose per pulse under our experimental conditions ($D_{\text{max}} \simeq 36 \text{ krad/pulse}$) it was important to ascertain that all the H, OH, and e_{aq}^- radicals produced reacted with the added solute and did not disappear by radical-radical combination. The choice of solute concentrations was therefore made on the basis of known¹¹ radical-radical and radical-solute rate constants.

Results

The optical spectra of the transient species produced on pulse radiolysis of aqueous solutions of the various alcohols studied resulted mainly from the abstraction of a hydrogen atom by the OH radicals (reaction 1), produced from the radiolysis of water



In most of our experiments the hydrated electrons were converted ($\sim 98\%$) into OH radicals by saturating the solutions with N_2O at 1 atm

(3) I. A. Taub and L. M. Dorfman, *J. Amer. Chem. Soc.*, **84**, 4053 (1962).

(4) S. Gordon, E. J. Hart, and J. K. Thomas, *J. Phys. Chem.*, **68**, 1262 (1964).

(5) M. C. Sauer, Jr., and B. Ward, *ibid.*, **71**, 3971 (1967).

(6) K. D. Asmus, A. Henglein, A. Wigger, and G. Beck, *Ber. Bunsenges. Phys. Chem.*, **70**, 756 (1966).

(7) J. Lilie, G. Beck, and A. Henglein, *ibid.*, **72**, 529 (1968); J. Lilie and A. Henglein, *ibid.*; in press.

(8) T. Hviid and S. O. Nielsen, to be published.

(9) J. P. Keene, E. D. Black, and E. Hayon, *Rev. Sci. Instr.*, **40**, 1199 (1969).

(10) J. H. Baxendale, P. L. T. Bevan, and D. A. Stott, *Trans. Faraday Soc.*, **64**, 2389 (1968).

(11) M. Anbar and P. Neta, *Int. J. Appl. Radiat. Isotopes*, **18**, 493 (1967).

Table I: Decay Rates, pK Values, and λ_{\max} for Hydroxyalkyl Radicals and Radical Anions Produced on Pulse Radiolysis of Aqueous Alcohol Solutions Saturated with N_2O

Alcohol	pH	λ_{\max} , nm	$2k/\epsilon$	λ , nm	$2k$, ($M^{-1} \text{sec}^{-1}$) ^a	pK _a
Methanol	6	<210	6.2×10^6	280	2.4×10^3	10.7 ^d
	12	<220	1.5×10^6	350	0.9×10^3	
	b	<230	5.0×10^6	230	...	
Ethanol	6	<210	4.7×10^6	280	2.3×10^3	11.6 ^d
	13	<220	5.7×10^6	300	0.5×10^3	
	b	<230	4.5×10^6	300	...	
Isopropyl alcohol	6	<210	2.1×10^6	280	1.4×10^3	12.2 ^d
	13.3	<230	2.7×10^6	300	0.4×10^3	
	b	<220	1.7×10^6	290	...	
<i>n</i> -Butyl alcohol	6	222	6.6×10^6	280	$\sim 10^3$	11.5 ^d
	13	<230	c	...		
Isobutyl alcohol	6	225	2.8×10^6	280	$\sim 10^3$	11.6 ^d
	13	<230	c	...		
<i>t</i> -Butyl alcohol	6	225	1.3×10^7	260	1.4×10^6	e
	13.5	225	1.1×10^7	260	1.2×10^9	
Neopentanol	6	238	2.0×10^6	255	$\sim 10^3$	11.3
	13	<235	c	...		
Cyclohexanol	6	230	2.1×10^6	280	$\sim 10^3$	12.1
	13.3	230	c	...		

^a These rates are better than $\pm 20\%$, and the decays were linear over at least three half-lives. ^b Liquid alcohol saturated with 1 atm of N_2O . ^c Decay trace consists of fast and slower decaying components. ^d pK value taken from ref 6. ^e No observable dissociations up to pH 13.5.



Dehydrogenation by H atoms, reaction 2, contributed a small fraction (<12%) to the over-all yield of the transients produced and was taken into consideration in calculation of the extinction coefficients of the transients.

Broad optical absorptions spectra were found on pulse radiolysis of neutral N_2O -saturated aqueous solutions of methanol and ethanol (Figures 1 and 2), with no maxima down to 210 nm. Identical spectra were observed in acid solutions down to pH 1, but in alkaline solutions broader spectra were obtained with the shape and extinction coefficient strongly dependent on the pH of the solution. While the decay rates of the transients were the same in acid and neutral solutions, they were somewhat slower at high pH values (Table I).

In neutral N_2O -saturated solutions of isopropyl alcohol, in addition to the broad transient spectrum (Figure 3), a slow first-order decaying species was found with a sharp peak at 214 nm. The optical density and decay rate constant of the slow-decaying species were found to be pH dependent with k values of 7.0×10^2 , 2.0 , 4.7×10^2 , 1.8×10^4 , and $2.4 \times 10^4 \text{ sec}^{-1}$ at pH 1, 4-6, 9.9, 10.7, and 11.8, respectively, as monitored at 225 nm. A similar but very weak absorption also appears in ethanol solutions, but none was observable in methanol solutions.

Identical spectra were obtained in irradiated solutions of isopropyl alcohol + N_2O , isopropyl alcohol + acetone, and *t*-butyl alcohol + acetone (after correction for the absorption of the *t*-butyl alcohol transient) (Figure 3). The amount of transient produced in the

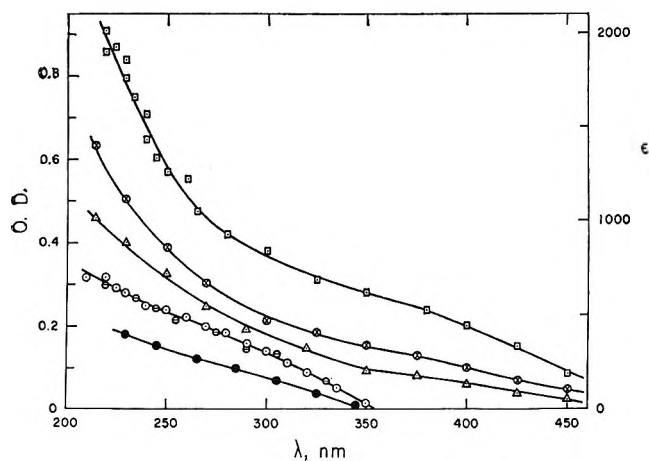


Figure 1. Absorption spectra of transients produced on pulse radiolysis of aqueous solutions of methanol: (a) 0.5 M, 1 atm N_2O , 36 krads/pulse; \ominus , pH 1; \circ , pH 6; \triangle , pH 10.4; \otimes , pH 10.8; \square , pH 12; (b) \bullet , liquid methanol, 1 atm N_2O , 28 krads/pulse, ϵ does not apply in this case.

t-butyl alcohol + acetone solution was about one-half that found in the first two solutions.

Absorption spectra of transients produced in the pulse radiolysis of liquid alcohols (Figures 1-3) are similar to the corresponding ones in aqueous solutions. No correction for the lower electron density of the alcohols was made, and no extinction coefficients were calculated, due to the uncertainty in the $G(\text{radical})$ values in pure alcohols. On a semiquantitative basis they appear, however, to be the same as those in aqueous solutions.

The absorption spectrum of CH_3CHOH both in aque-

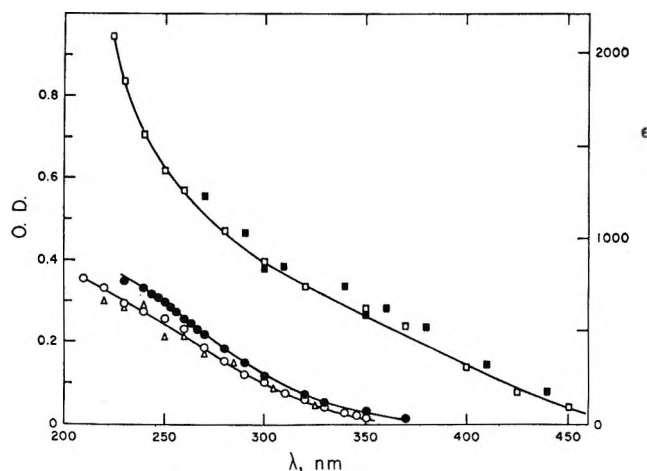


Figure 2. Absorption spectra of transients produced on pulse radiolysis of aqueous solutions of ethanol: (a) 0.1 *M*, 1 atm N_2O , 36 krad/pulse; Δ , pH 1; \circ , pH 6; \square , pH 13; (b) liquid ethanol, 1 atm N_2O , 28 krad/pulse, ϵ does not apply: \bullet , pure; \blacksquare , with NaOH added.

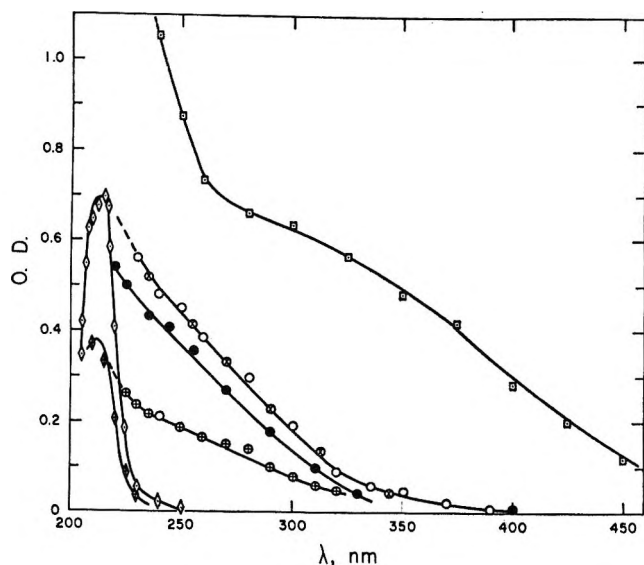


Figure 3. Absorption spectra of transients produced on pulse radiolysis of aqueous isopropyl alcohol system: (a) 0.1 *M* isopropyl alcohol, 1 atm N_2O ; \circ , pH 6, initial; \diamond , pH 6 after 80 μ sec; \square , pH 13.3, initial; (b) \otimes , 0.1 *M* isopropyl alcohol + 0.02 *M* acetone, pH 6, Ar; (c) 0.02 *M* acetone + 0.5 *M* *t*-butyl alcohol, Ar, pH 6, corrected for the *t*-butyl alcohol transient absorption: \oplus , initial; \diamond , after 80 μ sec; (d) \bullet , liquid isopropyl alcohol, 1 atm N_2O , 28 krad/pulse, ϵ does not apply here.

ous solution and in ethanol (Figure 2) is somewhat different from that previously obtained,³ where a fine structure with peaks at 247, 257, 266, and 290 nm was reported. An effort to reproduce this fine structure was not successful. Indeed, in none of the alcohols was it possible to find a fine structure in the absorption spectrum. This difference could be accounted to the technical difficulties in the spectrographic technique.³ Otherwise, the spectra obtained are in general agreement with those obtained previously.⁴⁻⁶

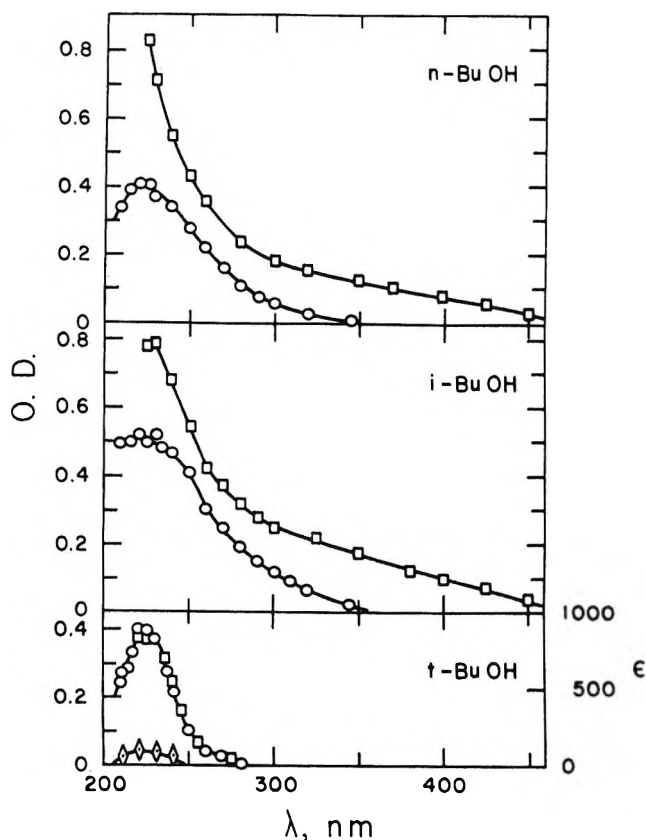


Figure 4. Absorption spectra of transients produced on pulse radiolysis of aqueous solutions of butyl alcohol: 0.1 *M* *n*-butyl alcohol, 0.1 *M* isobutyl alcohol, 0.5 *M* *t*-butyl alcohol, 1 atm N_2O , 36 krad/pulse: \circ , pH 6; \square , pH 13.3; \diamond , after 40 μ sec.

Maxima with relatively low extinction coefficients ($\sim 1000 M^{-1} \text{ cm}^{-1}$) were found on pulse radiolysis of *n*-BuOH (λ_{max} 222 nm), *i*-BuOH (λ_{max} 225 nm), *t*-BuOH (λ_{max} 225 nm), neopentanol (λ_{max} 238 nm), and cyclohexanol (λ_{max} 230 nm), and the optical spectra obtained are shown in Figures 4-6. With the exception of *t*-butyl alcohol, these radicals display a broader and stronger absorption in alkaline solutions. The decay curves of these transients, except *t*-butyl alcohol, exhibit two components. Since the fractions of the various radicals (α -, β -, etc.) produced are not known, the extinction coefficients and the decay rate constants could not be determined accurately. Only the *t*-butyl alcohol transient displays a smooth second-order decay independent of pH.

The absorption spectra of the transients produced on pulse radiolysis of neutral oxygenated aqueous solutions of methanol, isopropyl alcohol, cyclohexanol, and *t*-butyl alcohol are shown in Figure 7. The oxygenated solutions were irradiated in the presence of the corresponding ketone or in the presence of N_2O to scavenge the e_{aq}^- and eliminate the formation of HO_2 or O_2^- radicals. In all cases maxima were obtained in the region of 240 to 250 nm. The extinction coefficients of these transients are higher than those observed in oxygen-free solutions. Similar spectra were found (Figure 7)

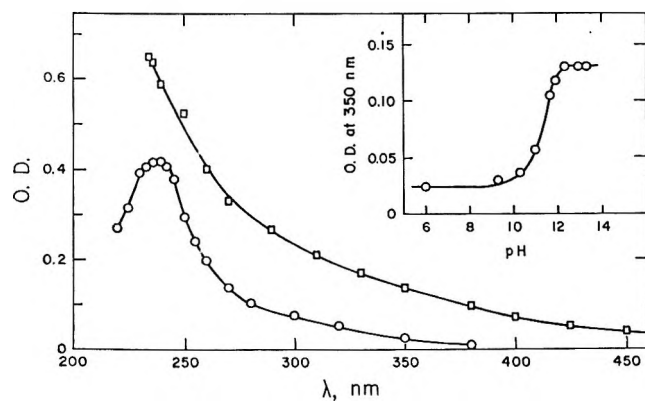


Figure 5. Absorption spectra and OD vs. pH curve of transients produced on pulse radiolysis of aqueous solutions of neopentanol, 0.1 M, 1 atm N_2O , 36 krads/pulse: \circ , pH 6; \square , pH 13.3.

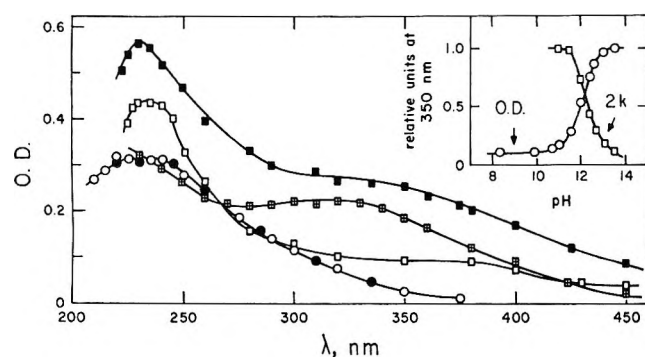
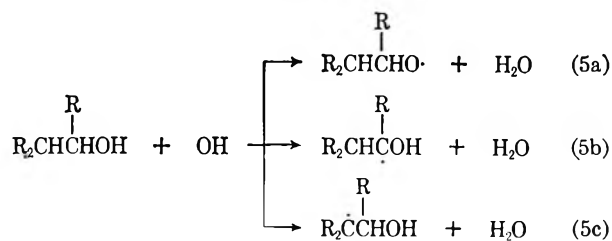


Figure 6. Absorption spectra and OD vs. pH curves of transients produced on pulse radiolysis of aqueous cyclohexanol system, 19 krads/pulse. Absorption spectra: \bullet , 0.2 M, Ar, pH 1; \circ , 0.1 M, N_2O , pH 6; \square , 0.1 M, N_2O , pH 13.3; \blacksquare , 0.1 M, 0.01 M cyclohexanone, Ar, pH 13.3; \boxplus , 0.02 M cyclohexanone, 1 M *t*-butyl alcohol, Ar, pH 13.3, corrected for the transient absorption from *t*-butyl alcohol. pK curves: 0.1 M cyclohexanol, 0.01 M cyclohexanone, Ar: \circ , normalized optical densities at 350 nm; \square , normalized second-order decay rate constants.

on pulse radiolysis of acidic (pH \sim 3) oxygenated solutions of methanol, isopropyl alcohol, and cyclohexanol; but in alkaline solutions, while λ_{max} remained the same, the extinction coefficients are higher. In the case of *t*-butyl alcohol no change was observed from pH 3 to pH 13.5.

Discussion

Hydroxyl radicals can abstract a hydrogen atom from an alcohol molecule at various positions



Reaction 5a leads to the formation of an alkoxy radical, but no evidence is presently available in support of this

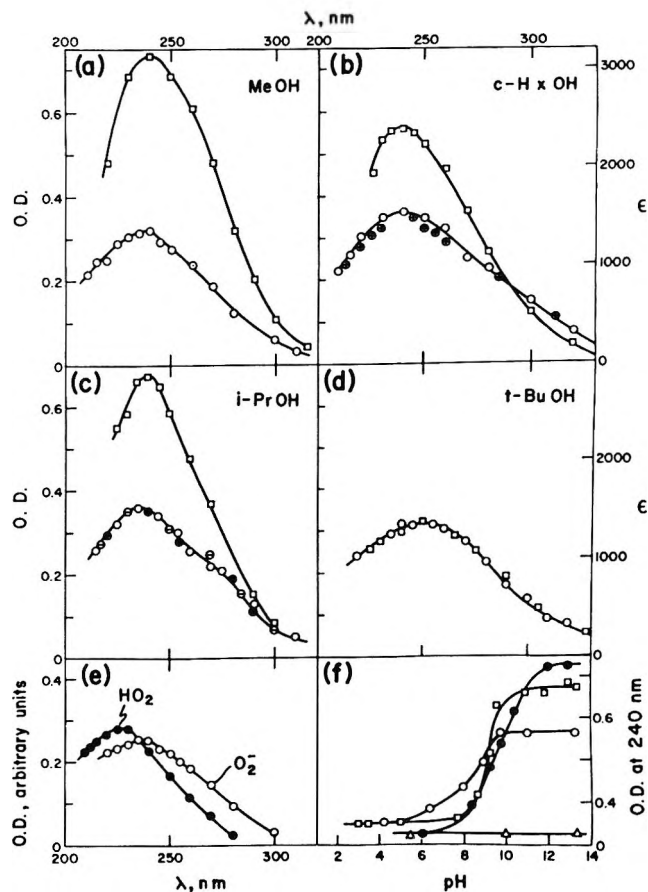


Figure 7. Absorption spectra and OD vs. pH curves of transients produced on pulse radiolysis of oxygenated aqueous solutions of alcohols, 19 krads/pulse: (a) 0.5 M methanol + 13 mM N_2O + 0.7 mM O_2 ; \circ , pH 6; \square , pH 12; (b) 0.1 M cyclohexanol + 0.01 M cyclohexanone, 1 atm O_2 ; \oplus , pH 3; \circ , pH 6; \square , pH 13.3; (c) 0.2 M isopropyl alcohol + 0.05 M acetone, 1 atm O_2 ; \oplus , pH 3; \ominus , pH 3.5; \circ , pH 6; \square , pH 13.3; (d) 1 M *t*-butyl alcohol + 13 mM N_2O + 0.7 mM O_2 ; \circ , pH 6; \square , pH 13.3; (e) 1 atm O_2 ; \bullet , pH 2-3.5; \circ , pH 8; (f) \oplus , methanol; \circ , cyclohexanol; \square , isopropyl alcohol; Δ , *t*-butyl alcohol.

reaction. (If alkoxy radicals are produced they may rapidly abstract hydrogen from α - or β -carbon position.) All the results up to date indicate that reaction 5b is the predominant process (>90%) in methanol, ethanol, and isopropyl alcohol. In *n*-propyl alcohol, *n*-butyl alcohol and isobutyl alcohol process (5c) takes place in addition to (5b).¹²

In alkaline solutions above the $pK = 11.9$ of OH radicals,¹³ the O^- radicals abstract hydrogen similarly to OH radicals,¹⁴ but this has not yet been clearly demonstrated. However, on pulse radiolysis of alkaline aqueous solutions of most alcohols significant changes have been found in the transient optical spectra at pH values

(12) M. Anbar, D. Meyerstein, and P. Neta, *J. Chem. Soc., B*, 742 (1966).

(13) J. Rabani and M. S. Matheson, *J. Phys. Chem.*, **70**, 761 (1966); J. L. Weeks and J. Rabani, *ibid.*, **70**, 2100 (1966).

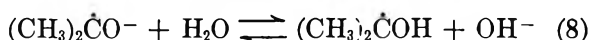
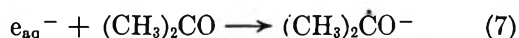
(14) G. Hughes and H. A. Makada, *Trans. Faraday Soc.*, **64**, 3276 (1968); B. L. Gall and L. M. Dorfman, *J. Amer. Chem. Soc.*, **91**, 2199 (1969).

which do not coincide with the pK of the OH radicals. In several cases these changes were observed at pH values well below the pK of OH radicals. Asmus, *et al.*,⁶ have clearly shown that these changes in spectra are due to the dissociation of the α -hydroxyalkyl radicals, and they have determined the pK values for a number of such radicals.

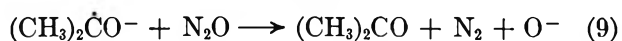


It is of interest to point out that the α -hydroxyalkyl radicals have pK_a values about 4 to 5 units below those of the parent alcohols.¹⁵

Identical transient spectra, extinction coefficients, and pK values are observed on pulse radiolysis of both N_2O -saturated solution of an alcohol and argon-saturated solution containing that alcohol and its corresponding carbonyl compound^{4,6} (Figure 3). The α -hydroxyalkyl radical anions, which are produced in the latter case by electron attachment, are in fact the ketyl radical anions of the parent carbonyl compound



The undissociated radicals of these alcohols have been shown¹⁶ to be unreactive toward N_2O , while a chain reaction occurs between the dissociated radical and N_2O (reaction 9 followed by (1))



The presence of this chain reaction should, however, have no effect on the absorption of the transient.

In neutral solutions, the α -hydroxyalkyl radicals decay with second-order rate constants of the order of $\sim 10^9 M^{-1} sec^{-1}$ (Table I). The lower decay rate constants of the transients in alkaline solutions are in agreement with the expected lower decay rate for charged species, thus substantiating the dissociation of these radicals (process 6).

In the isopropyl alcohol system the first-order slow-decaying transient, with λ_{max} 214 nm, was produced from both the reaction of OH radicals with isopropyl alcohol and the reaction of e_{aq}^- with acetone (in the presence of *t*-butyl alcohol as an OH radical scavenger) (Figure 3). The yield of this transient was about twice as high in the isopropyl alcohol + N_2O solution compared to the acetone + *t*-butyl alcohol solution, as expected. Furthermore, it is not produced in the *t*-butyl alcohol + N_2O solution. These findings exclude the possibility that this slow decaying transient is due to the alkoxy ($(CH_3)_2CHO\cdot$) or the isopropyl alcohol β radical ($\cdot CH_2CHOHCH_3$) and suggest that this species is formed from the second-order decay of $(CH_3)_2\dot{C}OH$. Since acetone has been determined¹⁷ as the main product resulting from the disproportionation of the isopropyl alcohol α -radicals, it is tentatively suggested that this disproportionation involves forma-

tion of acetone hydrate, $(CH_3)_2C(OH)_2$ (by an electron transfer mechanism). This hydrate is expected to lose a water molecule in a pH-dependent first-order reaction. Elimination of water is known to be catalyzed by both OH^- and H_3O^+ , in agreement with our findings (see Results). A more detailed examination is required before any conclusive mechanism can be offered.

Well-defined absorption maxima with λ_{max} increasing with increase in both the number of carbon atoms and the branching of the alcohol can be seen in Figures 4-6. *t*-Butyl alcohol is basically different from the other alcohols since abstraction of a hydrogen atom produces exclusively a β radical, $\cdot CH_2C(CH_3)_2OH$.¹⁸ The absence of a change in the absorption spectrum, extinction coefficient, and decay rate constant of the *t*-butyl alcohol transient up to pH 13.5 indicates that this radical is not dissociated under these conditions. Adams, *et al.*,¹⁹ did not observe an electron transfer from the *t*-butyl alcohol radical to acetophenone in alkaline solutions, while they did observe such a transfer in the case of other alcohol radicals. This can now be explained by our finding that the *t*-butyl alcohol radicals do not dissociate up to pH 13.5.

The narrowness of the absorption spectrum of the *t*-butyl alcohol radical, its low extinction coefficient (ϵ_{225} 900, ϵ_{250} 200, ϵ_{280} $30 M^{-1} cm^{-1}$), the absence of a change in its optical spectrum in the pH range 1-13.5, and its relatively high reactivity with OH radicals, $k = 2.5 \times 10^8 M^{-1} sec^{-1}$,¹¹ strongly suggest *t*-butyl alcohol as a very convenient solute for scavenging of OH radicals in pulse radiolysis studies. *t*-Butyl alcohol has been used for the study of the reaction of hydrated electrons with simple carbonyl compounds (this work), chloroaliphatic acids,²⁰ and some compounds of biological interest.²¹

The other higher alcohols investigated differ considerably from both the first three alcohols discussed and from *t*-butyl alcohol. They show a smaller change in the absorption spectrum in alkaline solutions, particularly in the region 300-400 nm. An examination of the decay of the transients indicates the presence of two components, which could not be resolved. Hydroxyl radicals abstract H atoms from these molecules at other positions in addition to the α position, and

(15) J. Murto, *Acta Chem. Scand.*, **18**, 1043 (1964).

(16) G. Scholes, M. Simic, and J. J. Weiss, *Discussions Faraday Soc.* **36**, 214 (1963); G. Scholes and M. Simic, *J. Phys. Chem.*, **68**, 1731 (1964).

(17) C. S. Munday, M.Sc. Thesis, University of Newcastle upon Tyne, 1964.

(18) R. Livingstone and H. Zeldes, *J. Amer. Chem. Soc.*, **88**, 4333 (1966).

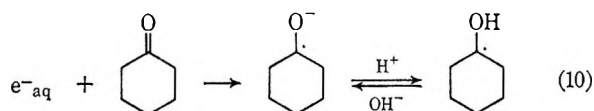
(19) G. E. Adams, B. D. Michael, and R. L. Willson, *Advances in Chemistry Series No. 81*, American Chemical Society, Washington, D. C., 1968, p 289.

(20) P. Neta, M. Simic, and E. Hayon, *J. Phys. Chem.*, in press.

(21) E. Hayon, *J. Phys. Chem.*, in press.

hence only a fraction of the radical produced are α -hydroxyalkyl radicals, which would dissociate in alkaline solutions.

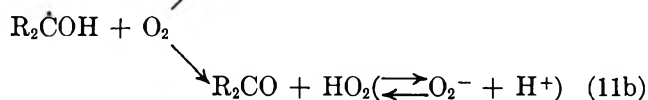
Pulse radiolysis of neutral aqueous solutions of cyclohexanol was found to produce a transient spectrum with λ_{\max} 230 nm (Figure 6). In alkaline solutions a notable difference in the absorption spectrum is found. A comparison, in the region 300–400 nm, of the transient spectra in alkaline solutions of c -HxOH + N_2O , c -HxOH + c -HxO, and t -BuOH + c -HxO (Figure 6) reveals in the first two systems a substantial formation of other radicals, in addition to the α radical. This is in contrast to the t -BuOH + c -HxO system where α radicals are formed exclusively



The fraction of CH radicals reacting with cyclohexanol to produce the α radical is estimated to be about 0.2, and the extinction coefficient of the dissociated α -radical $\epsilon_{320} \sim 2000 \text{ M}^{-1} \text{ cm}^{-1}$. The pK value of this α -hydroxycyclohexyl radical, $pK = 12.1 \pm 0.2$, was determined from both the change in optical density at 350 nm and the change in the second-order decay rate of this radical with pH , as shown in Figure 6. The other radicals formed from cyclohexanol, namely the β -, γ -, and δ -hydroxycyclohexyl radicals, are not expected to dissociate in that pH region and are not contributing to the broadening of the spectrum.

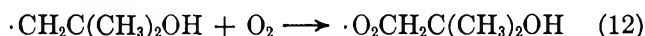
The inductive effect of various alkyl groups affecting the dissociation of simple aliphatic alcohol radicals has already been discussed,⁶ and a linear correlation between Taft's σ values and pK values presented. The similarity of the pK values for the α radicals formed from isopropyl alcohol and cyclohexanol is in good agreement with this correlation. It is of interest to point out that substituents with higher electron affinity, in the α position of the hydroxyalkyl radicals, have a considerable effect on the dissociation of these radicals. For example, the pK value for the dissociation of the hydroxy radical $X\dot{C}(\text{OH})\text{CH}_3$ where X is CH_3 , H , C_6H_5 , $\text{CH}_2=\text{CH}$, COO^- , and CH_3CO are 12.2,⁶ 11.6,⁶ 10.3,²² 10.1,⁷ 9.7,²⁰ and 4.4,⁷ respectively.

In the presence of oxygen, the alcohol radicals, produced by reaction 1, 7, 8, and 10, can react by two different processes



The rate of the reaction of oxygen with methanol and isopropyl alcohol radicals has been found to be nearly diffusion controlled,¹⁹ but no evidence in support of either reaction 11a or 11b has been presented.

In the pulse radiolysis of oxygenated solutions of t -BuOH + N_2O , the spectrum of the transient produced has λ_{\max} 250 nm and is different from the spectra of HO_2 or O_2^- (Figure 7). In addition, there is no change in the spectrum of this radical and in the extinction coefficient over a wide pH range, in contrast to significant changes observed for the perhydroxyl radical ($pK = 4.5$ and $pK \approx 9.5$).²³ While the first pK is assigned to the dissociation of HO_2 to O_2^- , the change taking place at $pH \sim 9.5$ is not yet fully understood. On the basis of these results it is concluded that the t -butyl alcohol peroxy radical is formed.



Assignment of radicals to the spectra obtained in oxygenated solutions of MeOH , i - PrOH , and c - HxOH is difficult in view of the similarity in λ_{\max} , extinction coefficients, and second-order decay rates of these transients with those of O_2^- (Figure 7). However, in the case of the perhydroxyl radical a considerable shift in the spectrum is observed due to the $\text{HO}_2 \rightleftharpoons \text{O}_2^- + \text{H}^+$ equilibrium, with $pK = 4.5$.²³ No such change has been observed in oxygenated solutions of isopropyl alcohol and cyclohexanol in the pH region 3–6. It is therefore suggested that the reaction of alcohol radicals with oxygen leads to the formation of the alcohol peroxy radicals, with $\lambda_{\max} \sim 240$ –250 nm. In alkaline oxygenated solutions of alcohols an increase in the absorption of the transient species is observed (Figure 7). This occurs at pH values in the region 8.5–9.5, which is well below the pK of the alcohol radicals. Due to the electron affinity of the peroxy group, it is suggested that the dissociation of the peroxy alcohol radical could occur at a lower pH than the pK of the parent alcohol radical. Under these conditions the $\text{R}_2(\text{O}_2)\text{CO}^-$ radical would be produced and could give rise to O_2^- radical by transfer of an electron.

Acknowledgments. We wish to thank Dr. E. D. Black for the considerable help given to E. H. in setting up this pulse radiolysis facility, and Dr. S. O. Nielsen for providing advance information on the xenon lamp booster circuit. The interest and support given by Dr. S. D. Bailey of these laboratories is gratefully acknowledged.

(22) M. Simic, P. Neta, and E. Hayon, to be published.

(23) G. Czapski and L. M. Dorfman, *J. Phys. Chem.*, **68**, 1169 (1964).

A Simple Differential Thermometric Technique for Measuring the Rates of Chemical Reactions in Solutions

by Thelma Meites, Louis Meites, and Joginder N. Jaitly¹

Department of Chemistry, Clarkson College of Technology, Potsdam, New York 13676 (Received April 1, 1969)

This paper describes the construction and operation of a constant-temperature-environment differential twin microcalorimetric apparatus for following the rate of a chemical reaction by monitoring the difference between the temperature of a reaction mixture, contained in one of two identical vessels, with that of a reference solution contained in the other. The temperatures are sensed by thermistors, whose resistances are compared in a simple Wheatstone bridge. Data on the reaction between ethyl acetate and sodium hydroxide indicate that second-order rate constants can be evaluated with accuracies and precisions of a few per cent or better even if the overall change of temperature during a reaction is as small as 0.015°. Various tests for internal consistency indicate that the measured differential temperatures are reliable to $\pm 20 \mu\text{deg}$ or better.

Introduction

There have been many studies of the rates of chemical reactions in solutions by techniques like conductometry, absorption spectroscopy, and polarography, which reveal the time dependence of the concentration of some reactant, intermediate, or product while a reaction is in progress. None of these techniques is as versatile as one might wish: electrometric ones are useless in solvents having very low dielectric constants, spectrophotometry is inapplicable to reactions in which gaseous products or precipitates are formed, and so on. Difficulties are especially likely to arise in work with biochemical substances and biological fluids, where non-reactive substances may interfere by obscuring the response of the measuring technique to variations in the concentrations of reactive ones.

Despite what would seem to be substantial advantages, thermometry has until very recently received very little attention from those engaged in kinetic work. Very many chemical reactions of interest involve enthalpy changes large enough to permit their extents to be followed, even at fairly high dilutions, with readily available temperature sensors and simple electrical circuitry. The technique should be applicable to reactions of any kind in any solvent, irrespective of the spectral, electrochemical, or other properties of the substances involved.

Several workers in classical calorimetry² have devised techniques for evaluating the overall temperature change resulting from a very slow reaction by extrapolating temperature-time data obtained while it is in progress, usually by assuming obedience to a first-order rate law. However, it was apparently Duclaux³ who first explicitly calculated kinetic parameters from such data, and Barry⁴ who first obtained reaction rates and enthalpies from the data of a single experiment. More or less traditional calorimetric apparatus and techniques have since been used for these purposes by several other

authors,^{5,6} two especially noteworthy approaches being those employed by Sturtevant. The first of these^{7,8} involved measuring the time dependence of the emf of a 20-junction copper Advance thermocouple sensing the difference between the temperatures of the reaction calorimeter and a reference calorimeter, both of which were immersed in an oil bath adjusted to follow drifts in the temperature of the reference calorimeter. Heat-exchange corrections were very small, the Newtonian heat-exchange constant for heat transfer between the bath and the reference calorimeter being only about $2 \times 10^6 \text{ sec}^{-1}$, and first-order rate constants with precisions of about $\pm 2\%$ were obtained for reactions yielding total temperature rises of the order of 25 mdeg and having half-times of 10–30 min. The other approach⁹ employed a pair of resistance thermometers, one in the reaction calorimeter and one in the reference calorimeter, connected to an ac bridge whose output, after amplification and conversion to dc by a phase-sensitive detector, was presented to an analog computer circuit serving two functions: it fed back a voltage proportional to the bridge output to a heater in the cooler calorimeter, and

(1) This paper is based in part on a thesis to be submitted by J. N. Jaitly to the Faculty of the Polytechnic Institute of Brooklyn, where this work was begun, in partial fulfillment of the requirements for the Ph.D. degree in Chemistry.

(2) Cf. J. M. Sturtevant, "Calorimetry," in "Physical Methods of Organic Chemistry," 3rd ed, Vol. I of "Technique of Organic Chemistry," by A. Weissberger, Ed., Interscience Publishers, Inc., New York, N. Y., 1959, Chapter X, pp 639–648.

(3) J. Duclaux, *Compt. Rend.*, **146**, 120 (1908).

(4) F. Barry, *J. Amer. Chem. Soc.*, **42**, 1296, 1911 (1920).

(5) K. L. Wolf and K. Merkel, *Z. Phys. Chem.*, **A187**, 61 (1940).

(6) A. K. Batalin and I. A. Shcherbatov, *J. Gen. Chem. U.S.S.R.*, **10**, 730 (1940).

(7) J. M. Sturtevant, *J. Amer. Chem. Soc.*, **59**, 1528 (1937); *J. Phys. Chem.*, **45**, 127 (1941).

(8) M. Bender and J. M. Sturtevant, *J. Amer. Chem. Soc.*, **69**, 607 (1947).

(9) A. Buzzell and J. M. Sturtevant, *ibid.*, **73**, 2454 (1951).

also provided a signal proportional to its square (and hence to the rate of consumption or liberation of heat by the reaction being studied) to an electromechanical integrator. A record of the integrator output against time was equivalent to a plot of the time dependence of the extent of reaction. A reaction yielding a total temperature change of 1.8 mdeg and having a half-time of about 6 min could be followed with a precision corresponding to uncertainties of only about 5 μ deg in the instantaneous temperature. Sturtevant and his co-workers employed this apparatus in studying the heat and rate of inactivation of pepsin,¹⁰ the hydrolyses of various amide and peptide bonds,¹¹⁻¹³ and other chemical and biochemical processes.

Most other workers have attempted to study faster reactions with simpler apparatus. Roughton¹⁴ devised a thermometric flow method for evaluating the rates of acid-base and other very fast reactions, while Bell and coworkers¹⁵⁻¹⁷ probably attained the acme of simplicity when they devised procedures based on measuring either the maximum change of temperature¹⁵ or the time at which the maximum is attained.^{16,17} Others have employed this procedure since its development¹⁸⁻²⁰ although, as was pointed out by Lueck, Beste, and Hall,²¹ it suffers from several important disadvantages: it yields only one rate datum per experiment, it propagates onto the rate constant any error in the evaluation of the Newtonian first-order heat-exchange constant ϵ , and its application to any but the simplest mechanisms would be frighteningly complex. This is because first-order kinetics are assumed in computing a rate constant from the experimental datum, so that deviations from first-order kinetics could be detected only through variations of the computed rate constant with reactant concentrations.

Lueck, Beste, and Hall²¹ employed a pair of identical glass reaction vessels immersed in a thermostat. Each vessel contained a thermistor of relatively low resistance; by connecting the thermistors to a bridge whose output was amplified and recorded, temperature-time plots were obtained. A similar arrangement was employed by Eremenko, Kolesov, and Kustova.²² Lueck, Beste, and Hall computed first-order rate constants from their recorded curves by the method of Swinbourne,²³ which not only involves a great many tedious integrations of successive portions of the recorded curve but also poses problems with reactions that are not strictly first-order.

Very recently Papoff and Zambonin²⁴ have described a quasi-adiabatic arrangement: the reaction cell is immersed in a water bath whose temperature is maintained within 0.01° of that in the cell, and the latter temperature, which is sensed by a thermistor immersed in the reaction mixture, is recorded as a function of time. After graphical correction for the heat of mixing and for secular drifts of cell temperature, this yields a plot of the extent of reaction against time, from

which the rate constant is easily deduced and on which deviations from first-order kinetics should be easily perceptible. Pseudo-first-order rate constants having average precisions of about $\pm 1\%$ were obtained for reactions having half-times between 3.5 and 30 sec and involving overall temperature changes between about 0.1 and 1 deg; in a few experiments where the overall temperature change was about 0.08 deg the precision of the rate constant was near $\pm 2\%$. A very similar arrangement, employing a single-junction thermocouple as the sensor and involving periodic measurements of its emf by means of a galvanometer driven by a photoelectric amplifier, had been used by Wyatt.²⁵ In work with reactions having half-times between 2 and 120 sec and yielding maximum temperature changes of 0.2 deg or less, Wyatt obtained first-order rate constants whose precisions were "often better than $\pm 3\%$."

This paper describes a constant-temperature-environment differential twin calorimeter and its use for the evaluation of reaction rates. Heats of dilution and stirring, the effects of power dissipation in the temperature sensor, and other phenomena that are troublesome in single-vessel techniques are compensated by the differential arrangement. Carefully aged and matched thermistors are used as temperature sensors. Second-order rate constants with precisions of a few per cent have been obtained for reactions having half-times between 18 and 300 sec and involving overall temperature changes as small as 15 mdeg.

Although many earlier workers have employed calorimeters for which heat exchange with the surroundings is relatively rapid, and although this is indeed essential to the success of the thermal maximum technique,¹⁵⁻¹⁷ it is difficult to evaluate the time dependence of the extent of reaction from the temperature-time curves ob-

(10) A. Buzzell and J. M. Sturtevant, *J. Amer. Chem. Soc.*, **74**, 1983 (1952).

(11) A. Dobry and J. M. Sturtevant, *J. Biol. Chem.*, **195**, 141 (1952).

(12) A. Dobry, J. Fruton, and J. M. Sturtevant, *ibid.*, **195**, 148 (1952).

(13) J. M. Sturtevant, *J. Amer. Chem. Soc.*, **75**, 2016 (1953).

(14) F. J. W. Roughton, *Proc. Roy. Soc.*, **A126**, 439, 470 (1930); J. B. Bateman and F. J. W. Roughton, *Biochem. J.*, **29**, 2622, 2630 (1935); F. J. W. Roughton, *J. Amer. Chem. Soc.*, **63**, 2930 (1941).

(15) R. P. Bell and J. C. Clunie, *Proc. Roy. Soc.*, **A212**, 16 (1952).

(16) R. P. Bell, V. Gold, J. Hilton, and M. H. Rand, *Discussions Faraday Soc.*, **17**, 151 (1954).

(17) R. P. Bell, M. H. Rand, and K. M. A. Wynne-Jones, *Trans. Faraday Soc.*, **52**, 1093 (1956).

(18) P. Baumgartner and P. Duhaut, *Bull. Soc. Chim. France*, 1187 (1960).

(19) N. H. Ray, *J. Chem. Soc.*, 4023 (1960).

(20) F. Becker and F. Spalink, *Z. Phys. Chem. (Frankfurt am Main)*, **26**, 1 (1960).

(21) C. H. Lueck, L. F. Beste, and H. K. Hall, Jr., *J. Phys. Chem.*, **67**, 972 (1963).

(22) L. T. Eremenko, U. R. Kolesov, and L. V. Kustova, *Zh. Fiz. Khim.*, **38**, 1259 (1964).

(23) E. S. Swinbourne, *J. Chem. Soc.*, 2371 (1960).

(24) P. Papoff and P. G. Zambonin, *Talanta*, **14**, 581 (1967).

(25) P. A. H. Wyatt, *J. Chem. Soc.*, 2299 (1960).

tained with such calorimeters. The extent of heat exchange is far too large to neglect,²¹ and corrections for it are large and uncertain. To obtain recorded curves minimally distorted by heat exchange we have designed an apparatus for which the Newtonian heat-exchange constant is as low as is consistent with reasonable simplicity of construction and use.

Description of the Apparatus

Two 5-oz PC-5 plastic cups (Sweetheart Plastics, Wilmington, Mass.) are used as the reaction and reference vessels. The normally convex bottom of such a cup is easily made concave by exerting gentle pressure on it, and it will then accommodate and stabilize the rotation of an egg-shaped Teflon-coated magnetic stirring bar. Each cup is supported in a hole, in the center of an 11-cm square platform made of $\frac{1}{2}$ -in. thick Lucite, whose diameter and taper are such that the cup is snugly supported about 1.5 cm below its top. The platforms are attached to the floor of the inner enclosure of the calorimeter by 1-in. diameter Lucite rods 6 cm long, so that the bottom of each cup is about 1 cm above the floor of the enclosure. The platforms are isolated from each other by a $\frac{1}{4}$ -in. air gap.

Each cup is closed with a tapered cover made from $\frac{1}{2}$ -in. thick Lucite. Each cover is provided with a central hole to accommodate the barrel of a B and D Multifit syringe used for reagent addition, a smaller hole to accommodate a Type 51A75 thermistor (Victory Engineering Corp., Springfield, N.J.) held in place with a small neoprene stopper, and three small glass tubes that support and provide electrical connection to a resistance heater. The entire arrangement is rigorously symmetrical around the midline of the inner enclosure.

Syringes of several different sizes were employed, and bushings of several thicknesses made from 1-in. Lucite rod were made to support them at such a height that almost all of the liquid in the syringe was submerged beneath the level of the surrounding liquid in the cup during the initial thermal equilibration. An 18-gauge Teflon needle (The Chemical Rubber Co., Cleveland, Ohio, catalog number 0312/93) cut off 5 mm below the hub was affixed to the tip of the syringe; this needle and the tip of the syringe were filled with air before the syringe was placed in position, thereby guarding against leakage of reagent out of the syringe during the thermal equilibration.

Two identical resistance heaters of about 20 ohms each were made by tightly coiling 80-cm lengths of 3-mil platinum wire on a mandrel having a diameter of 1 mm. Each end of each coil was welded to a short piece of 15-mil diameter platinum wire sealed through the end of a short length of 3-mm i.d. Pyrex tubing firmly mounted in the stopper of a cup. A few mm of mercury in each of these tubes served to make electrical connection to the source of current. A small hook of 15-mil platinum

wire at the end of a third Pyrex tube was used to support the heater at about its midpoint.

The value of the Newtonian heat-exchange constant obtained with this apparatus was typically about $2 \times 10^{-4} \text{ sec}^{-1}$. Most of the heat exchange occurs by conduction through the wires leading from the heaters to the external constant-current generator used to energize them (ϵ was about $3 \times 10^{-5} \text{ sec}^{-1}$ when these wires were removed). Since this portion of the apparatus serves only to provide a value for the thermal capacity of the reaction vessel for use in calculating the enthalpy change involved in the reaction, quite slow reactions could be followed by removing these leads if the values of ΔH were uninteresting.

The inner enclosure containing this apparatus is a rectangular box, $20 \times 10 \times 14$ in. ($w \times d \times h$) made from $\frac{1}{2}$ -in. thick Lucite. Its front face has a rectangular cutout 10×8 in. providing access to its interior; during an experiment this is covered with a $12 \times 10 \times \frac{1}{2}$ -in. Lucite plate held in place by six cylindrical Lucite knobs drilled and tapped to accommodate nylon screws cemented into the front plate of the enclosure. One small hole on the midline of this enclosure serves to lead all of the wires out of it and is sealed with silicone putty. Two $\frac{1}{2}$ -in. Lucite rods, one directly above the plunger of each syringe, projecting through both the inner and outer enclosures and passing through tightly fitting oiled felt bearings attached to the outside of both enclosures, are used to discharge the contents of both syringes simultaneously, and are withdrawn several cm immediately afterwards so as to isolate the plungers from the surroundings.

The inner enclosure is supported on four 1-in. diameter Lucite rods 4.75-in. long resting on, and cemented to, the floor of the outer enclosure. This is a double-walled box, $32 \times 22 \times 26$ in. ($w \times d \times h$) outside, made of $\frac{1}{2}$ -in. thick Lucite sheets separated by a $\frac{1}{2}$ -in. space. Provision is made for circulating thermostated water through this space for measurements at various temperatures. In the work reported here, however, all of the measurements were made at 25° and the constancy of the laboratory temperature sufficed to permit using an air-jacketed enclosure. A 1-in. diameter Lucite separator in the space directly beneath each cup was drilled to provide access for a $\frac{1}{2}$ -in. diameter hardwood shaft having a bar magnet attached to its top and fixed in place by Teflon bearings. The shafts are so adjusted that the bar magnets are a few mm below the bottom of the inner enclosure, so that stirring is accomplished without thermal contact with the surroundings, and are driven by a single variable-speed motor through a train of belts and pulleys. These expedients so nearly equalize the energies liberated by stirring the two solutions that there is no perceptible drift of the difference between their temperatures. The front of the outer enclosure is provided with a double-walled porthole having a separate inlet and outlet for thermo-

stated water; this provides access to the inner enclosure and is held in place by nylon screws and Lucite knobs similar to those used to retain the cover of the inner enclosure.

The resistances of the thermistors were compared by means of a carefully shielded dc Wheatstone bridge employing matched 100,000-ohm standard resistances whose temperature coefficients were negligibly small. The bridge voltage was usually 2.68 V, obtained from a pair of mercury batteries; it was measured with a precision potentiometer at frequent intervals to permit computing differential temperatures from recorder deflections. Corrections for the nonlinearity of the relation between these are easily applied but were usually negligible in this work. The power dissipation in each thermistor was approximately 18 μ W. In a few experiments intended to examine the effects of power dissipation a bridge voltage of 8.05 V was employed. Although the temperature of each thermistor must then have been well above that of the liquid surrounding it, no effect on the mean recorded differential temperature could be discerned. However, the noise level increased more than tenfold, evidently because of increased thermal convection. As Farm and Bruckenstein²⁶ also encountered substantial convection with power levels exceeding about 18 μ W although only a single drop of solution was in contact with each of the thermistors in their differential vapor-pressure apparatus, it appears that this convection may be confined to a very thin layer of liquid in the immediate vicinity of the thermistor rather than arising in the gas phase as they suggested.

The unbalance voltage of the bridge was recorded on a Model SRLG Y-T recording potentiometer (E. H. Sargent & Co., Chicago, Ill.), which provided sensitivities up to 0.37 mV full-scale and had an input impedance large enough to obviate significant loading of the bridge. No damping was ever employed beyond the minimum needed to suppress pen jitter at the sensitivity being employed with the input terminals of the recorder shorted. The temperature coefficients of resistance of the thermistors employed were evaluated from the resistances measured at a number of temperatures between 25 and 30° and were found to be $(-4.660 \pm 0.013) \times 10^{-2} \text{ deg}^{-1}$ at 25°. With a bridge voltage of 2.68 V this corresponds to a full-scale sensitivity of 11.57 mdeg, or 46.3 μ deg/mm, so that temperature differences as small as 5–10 μ deg should be observable. A precision of about $\pm 15 \mu$ deg in measurements of differential temperatures was obtained in this work (cf. Table I) even though the maximum sensitivity of the recorder was not employed. Indeed, the precision of measurement seemed to be simply that of measuring the pen deflection on the recorded chart. Table I illustrates the precision and sensitivity attained in a dynamic system. The experimental data in the first two columns were obtained from the final cooling portion of the curve recorded for a reaction in which the overall temperature

Table I: Precision of Differential Temperature Measurements^a

t , sec	ΔT_{obs} , mdeg	ΔT_{calcd} , mdeg	$\Delta T_{\text{obsd}} - \Delta T_{\text{calcd}}$ μ deg
1946 (= t^*)	16.008	16.039	-31
2246	15.415	15.414	+1
2396	15.125	15.112	+13
2546	14.840	14.815	+25
2696	14.524	14.524	0
2846	14.236	14.238	-2
2996	13.978	13.958	+20
3146	13.666	13.684	-18
3296	13.420	13.415	+5
3446	13.151	13.152	-1
3596	12.881	12.893	-12
3746	12.640	12.640	0

Std dev: $\pm 15.5 \mu$ deg

^a See text for experimental details. The values of ΔT_{calcd} were obtained from eq 1 with $\Delta T^* = 16.039 \text{ mdeg}$ and $\epsilon = 1.323 \times 10^{-4} \text{ sec}^{-1}$.

change was just over 16 mdeg. These were fitted to the Newtonian equation

$$\ln \Delta T = \ln \Delta T^* - \epsilon(t - t^*) \quad (1)$$

where ΔT is the measured differential temperature t sec after the addition of reagent, t^* is an arbitrarily selected time at which the reaction is considered to be complete, and ΔT^* represents the differential temperature at that instant. The values of ΔT_{calcd} in the third column of the Table were computed from the least-squares "best" values of ΔT^* and the heat-exchange constant ϵ ; the differences in the last column represent the deviations from perfect internal consistency. As these data were obtained with a recorder sensitivity of 125.5 μ deg/mm, their standard deviation corresponds to one of $\pm 0.12 \text{ mm}$ in reading the pen deflection. Another test of internal consistency leading to the same conclusion is described in connection with the computation of $\Delta R_{\text{corr}, \infty}$ below.

To achieve such a result the noise level must be extremely low. Figure 1, a portion of the record obtained in a typical experiment, illustrates the noise level attained. This arose in part from the rotation of the magnetic stirrer, but by judicious choice of stirrer speed and rigorous dehumidification of the laboratory atmosphere the total recorded noise could be kept below $\pm 1 \mu$ V at worst and could generally be made invisible. From a curve given by Farm and Bruckenstein²⁶ it appears that the noise level in their differential vapor pressure apparatus was approximately $\pm 0.5 \mu$ V, closely comparable with ours.

These results lend further support to the slowly growing belief that properly stabilized thermistors are capable of far better precision than has been thought. One

(26) R. J. Farm and S. Bruckenstein, *Anal. Chem.*, **40**, 1651 (1968).

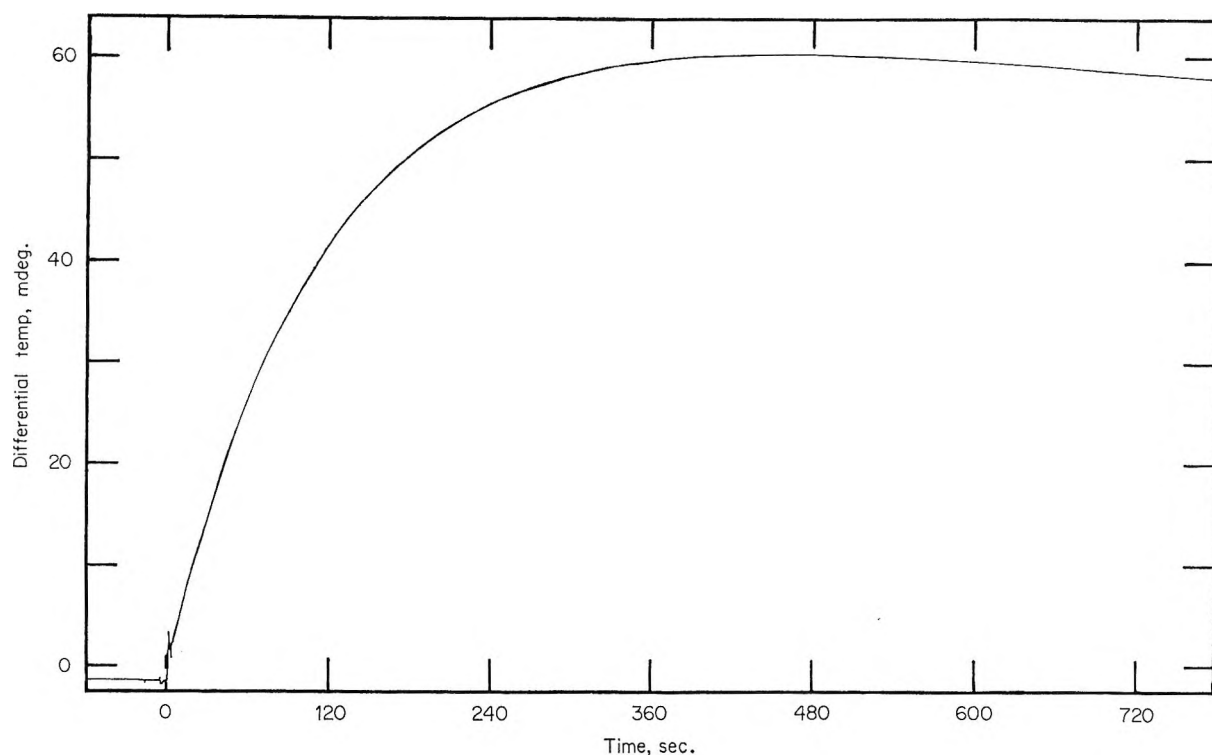


Figure 1. The unretouched initial portion of the curve obtained for the reaction between 0.0825 *F* sodium hydroxide and 4.72 *mF* ethyl acetate. The horizontal line preceding $t = 0$ represents the virtual attainment of thermal equilibrium before the addition of the reagent. The full-scale sensitivity and nominal pen speed of the recorder were 2 mV and 1 sec, respectively.

extreme view on this subject was expressed by Boucher,²⁷ who wrote "Under the best conditions of operation . . . it should be possible to achieve long-term stability in temperature measurement, using a thermistor bridge, of ± 0.01 – 0.02 deg." However, we have recorded differential curves for many hours with two thermistors side by side in the same solution without observing any transient difference even as large as 20 μ deg. Jordan,²⁸ writing about the use of 2000-ohm thermistors at power levels of about 125 μ W, stated that "No useful purpose could be served by improving the accuracy of the recorder beyond 10 μ V²⁹ . . . because random fluctuations on the order of 10 μ V are invariably apparent on thermometric titration curves." This is about the same as the noise level we obtained with a power of 160 μ W and ascribed, as noted above, to thermal convection arising from excessive heating of the thermistors; in thermometric titrations there may also be momentary variations in the efficiency with which the incoming stream of reagent is distributed throughout the solution being titrated.

At the other extreme, Tyrrell and Beezer³⁰ felt that prior amplification of the unbalance voltage of the bridge should make "temperature changes of the order of 10^{-5} deg detectable without difficulty. Boyd, *et al.*,³¹ and Nancollas and Hardy³² report having just attained such a sensitivity in work with an ac-energized thermistor bridge and phase-sensitive detector amplifier. Farm and Bruckenstein²⁶ originally claimed a precision of

about ± 20 μ deg and report³³ having further improved this to about ± 8 μ deg. Müller and Stolten³⁴ reported sixteen years ago that they were able to detect temperature differences as small as 20 μ deg by using a vacuum-tube voltmeter to observe the unbalance voltage of a dc bridge containing a single 100,000-ohm thermistor, and gave data corresponding to an average uncertainty of only about 60 μ deg in measurements made over periods of 50 min.

Thermistors having nominal resistances of 100,000 ohms at 25° were chosen for this work to minimize the power dissipation resulting from the use of a convenient bridge voltage. Twenty-one thermistors were immersed in still water in a thermostat operating at $25 \pm 0.002^\circ$ and a steady dc current of 10 μ A was passed through them. Their resistances were measured

(27) E. A. Boucher, *J. Chem. Educ.*, **44**, A935 (1967).

(28) J. Jordan, "Thermometric Enthalpy Titrations," in "Treatise on Analytical Chemistry," I. M. Kolthoff and P. J. Elving, Ed., Interscience Publishers, New York, N. Y., Part I, Vol. 8, 1968, p 5206.

(29) This corresponds to 250 μ deg under the conditions being discussed.

(30) H. J. V. Tyrrell and A. E. Beezer, "Thermometric Titrimetry," Chapman and Hall Ltd., London, 1968, p 40.

(31) S. Boyd, A. Bryson, G. H. Nancollas, and K. Torrance, *J. Chem. Soc.*, 7353 (1965).

(32) G. H. Nancollas and J. A. Hardy, *Rev. Sci. Instrum.*, **44**, 290 (1967).

(33) S. Bruckenstein, personal communication, 1969.

(34) R. H. Müller and H. J. Stolten, *Anal. Chem.*, **25**, 1105 (1953).

periodically over many months and corrected to 25.000° by employing the individual values of their temperature coefficients measured subsequently. The resistances generally fell during the first week, rose for 1–3 weeks thereafter, and then decreased to steady values (which were usually above, but occasionally below, the initial ones) reproducible within $\pm 0.003\%$.

With the aid of these data it was possible to select three matched pairs of thermistors. Each pair had resistances equal within 0.2 per cent at 25°, and one also had almost identical temperature coefficients of resistance. As thermistor mismatch would merely cause the two solutions to be unequally heated by the power dissipation in the thermistors, and as with the bridge voltage used here the power dissipation would change the temperature of 100 ml of solution only 14.6 $\mu\text{deg/hr}$ even if it were wholly uncompensated, the use of matched thermistors was merely a minor convenience in that it made trimming the standard resistors in the bridge unnecessary.

In use each thermistor is subjected to a constant current of 13 μA which is never interrupted. The currents of 100–1000 μA recommended by Jordan¹⁶ for stabilizing 2000-ohm thermistors correspond to power dissipations ranging from 0.02 to 2 milliwatts, as against the 0.017 mW used here; Müller and Stolten²¹ used a power of 1.26 mW to stabilize 100,000-ohm thermistors. It is possible that the very precise differential temperature data obtained in this work are due in part to this very low power level (which was of course chosen to eliminate deleterious effects arising from self-heating) or that thermistors having resistances of the order of 100,000 ohms are more stable than those having lower ones.

Technique of Operation

An experiment is begun by pipetting equal volumes of solvent into two clean dry cups containing magnetic stirring bars, adding a known amount of one of the desired reactants to one, and adding an equal volume of solvent to the other. We chose to investigate the potentialities and limitations of the technique by studying the well-known alkaline hydrolysis of ethyl acetate, and always placed the ester in the reaction vessel to eliminate the danger of absorption of carbon dioxide by strongly alkaline solutions exposed to the atmosphere for prolonged periods. This is an obvious precaution but one that seems to have been ignored by several of those who have investigated this reaction. Reagent-grade ethyl acetate was used without purification; it was measured into the reaction vessel by means of a small glass syringe that was weighed before and after making the addition. The weights of ethyl acetate varied from about 10 to 70 mg in different experiments.

Two identical syringes (1-, 2-, or 5-ml, depending on the volume of reagent desired) were then charged with as nearly as possible identical volumes of 5.57 *F* sodium hydroxide. This solution had been prepared by diluting

a 50% solution, from which the suspended sodium carbonate had been allowed to settle out,³⁵ with water freed from dissolved carbon dioxide. It was standardized by weight against primary-standard grade potassium hydrogen phthalate and stored in a polyethylene bottle carefully protected from atmospheric carbon dioxide. An 18-gauge Teflon needle was permanently inserted through the stopper of this bottle and was closed with a small Teflon stopper except when a syringe was being filled through it. The concentration of the stock sodium hydroxide solution was chosen with the aid of heat-of-dilution data tabulated by Parker,³⁶ which showed that this choice minimized the heats of dilution to the desired concentrations in the reaction mixture. The amounts of sodium hydroxide added to the two calorimeter vessels were always equal within $\pm 5\%$, and the difference between the heats of dilution never corresponded to a differential temperature in excess of 100 μdeg .

After weighing the filled syringes, they were inserted in their respective cups, the inner and outer enclosures were sealed, and the apparatus was allowed to come to thermal equilibrium with the stirrers on and the bridge connected to the recorder. When the differential temperature became constant, the Lucite rods above the plungers of the syringes were depressed rapidly and as nearly simultaneously as possible to begin the reaction, and the recording was allowed to proceed without further attention for something like 20 half-times. The mixing time was typically found to be 2–5 sec. This had no untoward effects in the experiments reported here, primarily because a somewhat unusual form of the second-order rate equation was employed in the computations. However, it would certainly be undesirably long if the half-time for the reaction were only a few sec,³⁷ and more efficient stirring would then be essential. This relatively long mixing time is believed to be due primarily to the fact that the density of the sodium hydroxide solution was over 20% above that of the solution to which it was added; on being ejected from the syringe, much of the reagent must have gone directly to the bottom of the cup, and it is not unreasonable that several sec should have been required to effect thorough mixing in the face of this difference of densities. The weight of sodium hydroxide solution remaining in the tip of the syringe and the Teflon needle after bottoming the plunger was determined separately and subtracted from the weight initially taken to find the weight actually added.

Because the Newtonian cooling constant is finite, the

(35) I. M. Kolthoff and E. B. Sandell, "Textbook of Quantitative Inorganic Analysis," 3rd ed, The Macmillan Company, New York, N. Y., 1952, pp 526–527.

(36) V. B. Parker, "Thermal Properties of Aqueous Uni-univalent Electrolytes," National Standard Reference Data Series, National Bureau of Standards 2, Washington, D. C., Apr 1, 1965.

(37) M. Caselli, A. Cavaggioni, and P. Papoff, *Talanta*, **15**, 1335 (1968).

recorded differential temperature always passed through a maximum.¹⁵⁻²¹ Shortly after it had done so, the recorder was set to its lowest chart speed (0.2 in./min) and the curve was recorded for 15-20 min more. Typical data obtained during this interval were shown in Table I; they were used to evaluate ϵ in eq 1. The recorder was then occasionally reset to a faster chart speed and an accurately known current between 6 and 60 mA, obtained from either a Metrohm E211 "Coulometer" or a Leeds and Northrup Type 7960 Coulometric Analyzer, was applied to the heater in the reaction vessel for a measured length of time. The recording was continued for some time after the constant-current generator had been turned off, thereby providing a second interval during which ϵ could be evaluated. These data could be used to obtain a value of the thermal capacity of the reaction vessel and its contents and thus to calculate the enthalpy change involved in the reaction. In the present work this was rarely done because the value of ΔH was of little interest; the few values that were secured were in rough agreement with, but always distinctly below, that expected. This is attributable to the loss of a little of the ester by volatilization during the protracted initial approach to thermal equilibrium.

Calculations

Second-order rate constants were computed with the aid of a Hewlett-Packard Model 9100A programmable calculator. Copies of the programs and directions for their use may be obtained from the authors.

Values of the recorder deflections ΔR (in arbitrary chart divisions and in increments of 2-5 per cent of the maximum deflection obtained) and the corresponding times t were read from the recorded chart. If the unbalance voltage of the bridge becomes appreciable the values of ΔR should be corrected for deviations from linear dependence on differential temperature. Beginning at a time t^* when the reaction is judged to be complete, the values of t and ΔR are fitted to eq 1 by a least-squares calculation to evaluate the heat-exchange constant ϵ . Corrections for heat exchange during the reaction interval are then applied by numerical integration, using the equation

$$\Delta R_{n,\text{corr}} = \Delta R_n + \frac{\epsilon}{2} \sum_{i=1}^n (\Delta R_i + \Delta R_{i-1})(t_i - t_{i-1}) \quad (2)$$

in which ΔR_i and t_i are the observed deflection (corrected if necessary for bridge non-linearity) and time, respectively, at the i th measured point, ΔR_0 and t_0 are both zero, and $\Delta R_{n,\text{corr}}$ is the deflection that would have been observed at the n th point in the absence of heat exchange. As long as ϵ is less than about a tenth of the pseudo-first-order rate constant, the integrated heat-exchange correction will be less than about 5% until the reaction is about 99% complete.

The values of ΔR_{corr} approach constancy as the reaction approaches completion. In a typical experiment,

25 successive values of ΔR_{corr} computed in the interval $508 \leq t \leq 1234$ sec had a mean (denoted below as $\overline{\Delta R_{\text{corr},\infty}}$) of 63.950 and a standard deviation of 0.056 division. The latter figure corresponds to an uncertainty of 0.14 mm in the measured deflection and to one of 17.8 μ deg in the differential temperature; the first of these uncertainties was essentially the same in all of our experiments, while the second naturally varied with the recorder sensitivity employed.

Values of the ratio $\Delta R_{\text{corr}}/\overline{\Delta R_{\text{corr},\infty}}$ are taken to be proportional to the fraction of the reaction that has taken place. Since the finite mixing time leads to an uncertainty in the instant at which the reaction is initiated, which might be appreciable if the reaction is fast, it is convenient to begin the calculations at an arbitrarily chosen time t' where the irregularities accompanying mixing have subsided. When the reaction was fast enough to require the use of the highest chart speed of the recorder, t' was usually between 3 and 6 sec; for slower reactions it was taken for convenience at the first vertical division of the chart crossed by the pen after the start of the reaction. Assuming that the value of $\Delta R'_{\text{corr}}$ at the instant $t = t'$ is proportional to the amount of the ester (= A) that has reacted at that instant, which implies that the difference between the heats of dilution in the two vessels is negligibly small but does not require that the value of t' be known, then integrated rate equation for a second-order reaction may be written in the form

$$\ln \frac{\overline{\Delta R_{\text{corr},\infty}} - (C_A^0/C_B^0)\Delta R_{\text{corr}}}{\Delta R_{\text{corr},\infty} - \Delta R_{\text{corr}}} = k(C_B^0 - C_A^0)(t - t') + \ln \frac{\overline{\Delta R_{\text{corr},\infty}} - (C_A^0/C_B^0)\Delta R'_{\text{corr}}}{\Delta R_{\text{corr},\infty} - \Delta R'_{\text{corr}}} \quad (3)$$

The equivalent form for a first-order reaction would of course be

$$\ln (\overline{\Delta R_{\text{corr},\infty}} - \Delta R_{\text{corr}}) = -kC^0(t - t') + \ln (\overline{\Delta R_{\text{corr},\infty}} - \Delta R'_{\text{corr}}) \quad (4)$$

Equation 3 is of the form $y = ax + b$ with $a = k(C_B^0 - C_A^0)$. Values of a were computed from a least-squares program, employing all of the data obtained between t' and the instant at which the reaction was 90% complete. The choice of termination times was arbitrary but clearly reflected a deviation from straightforward second-order kinetics: the computed rate constant invariably drifted upward during the last 10% of the reaction. It is by now well known^{24,28} that the alkaline hydrolysis of ethyl acetate does not exactly follow the simple second-order rate law: in fact, data obtained in the presence of excess base yield second-

(38) H. Tsujikawa and H. Inoue, *Bull. Chem. Soc. Jap.*, **39**, 1837 (1966).

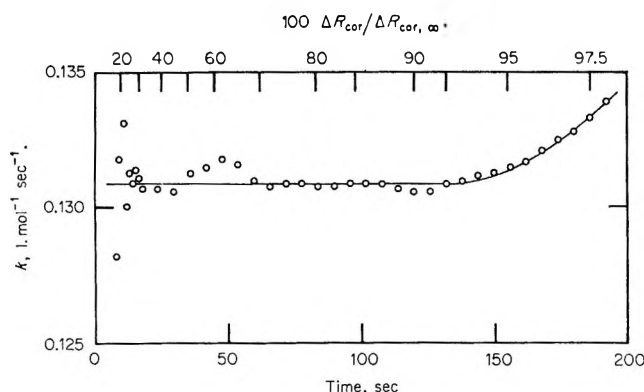


Figure 2. Plot of the second-order rate constant k , computed as described in the text, against the elapsed time (on the lower abscissa scale) and the percentage of the ethyl acetate reacted (on the upper abscissa scale) for the reaction between 0.1498 F sodium hydroxide and 6.40 mF ethyl acetate.

order rate constants about 20% larger than those obtained with excess ester or with equivalent concentrations of the two reactants.

Results

Figure 2 is a typical plot of the computed second-order rate constant against both the time (on the lower abscissa scale) and the fraction of the ester that has reacted, *i.e.*, the ratio $\Delta R_{\text{corr}}/\Delta R_{\text{corr},\infty}$ (on the upper abscissa scale). After a short initial period during which the value of k fluctuates widely because it is based on measurements of small temperature differences on a chart obtained at a recorder sensitivity chosen for convenience in measuring the larger ones obtained later in the reaction, a value stable within a few tenths of a per cent is obtained. Using the value ($k = 0.130 \text{ g l. mol}^{-1} \text{ sec}^{-1}$) finally selected to compute the values of ΔR_{corr} that would have been obtained if the data had been perfectly consistent internally, it was found that the standard deviation of the 29 experimental points measured in the range $6 \leq t \leq 130 \text{ sec}$ was $\pm 0.21 \text{ mm}$ of chart deflection or $53 \mu\text{deg}$ in the differential temperature. Much of the difference between the latter figure and the one shown in Table I is due merely to the difference of recorder sensitivity.

The upward drift of k as the reaction nears completion is consistent with results obtained by Tsujikawa and Inoue³⁸ and by Papoff and Zambonin.²⁴ The former authors observed a downward drift of k as the reaction progressed in the presence of excess ester; the latter observed an increase of k on increasing the concentration of sodium hydroxide when this was in excess.

Superimposed on this variation of k with the ratio of the concentration of base to that of ester is the expected variation of k with ionic strength. In work with solutions containing 0.50 F sodium hydroxide, Papoff and Zambonin²⁴ found that k decreased uniformly with increasing concentration of sodium chloride between 0 and 1.5 F , and asserted that their data agreed with those of

Schade.³⁹ Extrapolation to $\mu = 0$ gives $k = 0.145 \text{ l. mol}^{-1} \text{ sec}^{-1}$, and our values are in approximate agreement with this at the lowest concentrations (0.017–0.035 F) of sodium hydroxide. It is interesting to note that the values of k at the lowest concentrations of base parallel those of Arrhenius,⁴⁰ who found that k decreased slightly when the concentration of sodium hydroxide was increased from 0.003 to 0.025 F , and then rose on increasing the concentration of sodium hydroxide further to 0.05 F . However, Arrhenius' values of k are uniformly lower than ours because he obtained them with equal concentrations of base and ester. Our values are in good agreement with that deduced from the results of Amis and Siegel⁴¹ by extrapolating a plot of $\ln k$ vs. $1/D$ to D (the dielectric constant) = 78.5 and correcting to a temperature of 25°.

Table II summarizes the values we have obtained, and also includes for comparison those obtained by Papoff and Zambonin under comparable conditions. It may conservatively be concluded that the technique

Table II: Second-Order Rate Constants for the Alkaline Hydrolysis of Ethyl Acetate at 25°

Initial concentrations		Overall temperature rise	$t_{1/2}$	k , l. mol ⁻¹ sec ⁻¹
NaOH, F	EtOAc, mF	($= \Delta T_{\text{corr},\infty}$), mdeg	sec	
0.01718	2.35	19.6	285	0.152
0.0348	6.75	56.1	153	0.144
0.0357	6.73	68.3	158	0.136
0.0697	4.11	39.5	78	0.131
0.0709	10.09	94.0	81	0.130
0.0728	2.60	21.8	74	0.1305
0.0743	6.58	66.5	74	0.1315
0.0825	4.72	41.0	64	0.135
0.1079	6.31	64.8	51	0.131
0.1498	6.40	64.2	36	0.131
0.1595	1.49	15.6	32	0.138
0.2208	6.57	68.4	24	0.132
0.267	10	...	20.3	0.131 ^a
0.2744	6.26	65.0	18.3	0.140
0.502	12.1	0.137 ^a
0.505	16	...	10.2	0.137 ^a
1.01	16	...	4.9	0.141 ^a

^a Value reported by Papoff and Zambonin.¹²

is capable of yielding rate constants having accuracies and precisions of a few per cent or better over the ranges of half-times and overall temperature rises shown in Table II. Further work now in progress with other systems is aimed at revealing the smallest values of both of these parameters that can be handled.

(39) E. Schade, Thesis, Universität des Saarlandes, Saarbrücken, 1965.

(40) S. Arrhenius, *Z. Phys. Chem.*, **1**, 110 (1887).

(41) E. S. Amis and S. Siegel, *J. Amer. Chem. Soc.*, **72**, 647 (1950).

Acknowledgment. This investigation was supported by PHS Research Grant No. GM 16561 from the National Institute of General Medical Sciences. It is a

pleasure to acknowledge the help and advice given us by Professor Kenneth R. Jolls during the early stages of this work.

Differential Heat of Adsorption and Entropy of Water

Adsorbed on Zinc Oxide Surface

by Mahiko Nagao and Tetsuo Morimoto

*Department of Chemistry, Faculty of Science, Okayama University, Tsushima, Okayama, Japan
(Received April 1, 1969)*

The adsorption isotherm and the heat of immersion isotherm of water were measured on two ZnO samples pretreated at 250 and 450°, respectively. By combining these two kinds of data, we obtained the differential heat of adsorption, the free energy of adsorption, the entropy of adsorption, and the site-energy distribution for the system ZnO-H₂O. A clear hump appeared at a region of moderate relative pressure of water adsorption isotherm, but we could not find any corresponding anomaly in other properties examined here. Only in the curve of the differential entropy of adsorption could a slight abnormal change be discovered, which seemed to have some connection with the hump of adsorption isotherm. The site-energy distribution curves derived by differentiating the plot of the differential heat of adsorption vs. the amount of adsorption showed two kinds of peaks; one corresponds to a group of physisorption sites with energies less than 5 kcal/mol H₂O, and the other to that of chemisorption sites with energies of 20–25 kcal/mol H₂O.

Introduction

By combining the data of the heat of immersion and of the adsorption isotherm on a given adsorbent-adsorbate system, we can get useful information about the interaction between the solid surface and molecules. One of the most important ways to study the adsorption state is to obtain the entropy of adsorption. In 1952, Jura and Hill¹ introduced the equation which enables us to calculate the entropy of adsorption from the measurements of the heat of immersion and the adsorption isotherm. Since then, several studies on the entropy of adsorbate molecules have been published on such adsorbents as graphon,² asbestos,³ Fe₂O₃,⁴ Al₂O₃,⁵ and TiO₂.⁶ This method is distinguished by the point where the data obtained refer to the net heat of adsorption.

The present authors have investigated the interaction between the surfaces of ZnO and water molecules through the measurements of the heat of immersion⁷ and of the desorbability of chemisorbed water.⁸ As a result, the characteristic feature has been found that the adsorption isotherm of water on ZnO shows a hump at a region of moderate relative pressure of water, which has not been discovered on any polar adsorbent-polar adsorbate systems. The mechanism of this phenomenon is the problem to be worked out hereafter. The pur-

pose of the present work is to examine whether, in the case of ZnO-H₂O system in which a hump occurs in a moderate pressure region of the adsorption isotherm, a noticeable change appears in the heat of immersion isotherm and related properties. When the surfaces of metal oxides are exposed to water vapor, the chemisorption usually occurs in addition to the physisorption, each of both adsorption amounts being uncertain unless special precaution is paid. In the past investigations cited above, the energetics has been developed without analyzing in detail the role of chemisorption. In the present work, however, the contribution of chemisorp-

- (1) G. Jura and T. L. Hill, *J. Amer. Chem. Soc.*, **74**, 1598 (1952).
- (2) G. J. Young, J. J. Chessick, F. H. Healey, and A. C. Zettlemoyer, *J. Phys. Chem.*, **58**, 313 (1954).
- (3) J. J. Chessick, A. C. Zettlemoyer, F. H. Healey, and G. J. Young, *Can. J. Chem.*, **33**, 251 (1954).
- (4) F. H. Healey, J. J. Chessick, and A. V. Fraioli, *J. Phys. Chem.*, **60**, 1001 (1956).
- (5) R. L. Venable, W. H. Wade, and N. Hackerman, *ibid.*, **69**, 317 (1965).
- (6) M. Miura, H. Naono, T. Iwaki, T. Kato, and M. Hayashi, *Kogyo Kagaku Zasshi, (J. Chem. Sec. Jap., Ind. Chem. Sect.)*, **69**, 1623 (1966).
- (7) T. Morimoto, M. Nagao, and M. Hirata, *Kolloid-Z. Z. Polym.*, **225**, 29 (1968).
- (8) T. Morimoto, M. Nagao, and F. Tokuda, *Bull. Chem. Soc. Jap.*, **41**, 1533 (1968).

tion to such thermodynamical quantities as the differential heat of adsorption, and the site-energy distribution, will be discussed on the ZnO-H₂O system.

Experimental Section

Material. The original sample used in this study was zinc oxide, prepared, by burning metallic zinc in air, by the Sakai Kagaku Co. According to the maker's analysis, the purity of this sample was 99.8%, and the main impurities detected were 0.002% Pb and 0.03% water-soluble substances. Two kinds of samples were prepared from this original sample by treating under a reduced pressure of 10^{-5} Torr for 4 hr at two different temperatures, 250 and 450°, respectively.

Surface Area Measurement. The specific surface area of the samples was determined by the BET method,⁹ on the basis of the nitrogen adsorption isotherm obtained at 77°K; the area of a nitrogen molecule was assumed to be 16.2 Å². The specific surface areas of the samples treated at 250 and 450° were found to be 5.18 and 4.83 m²/g, respectively.

Water Vapor Adsorption Isotherm. On the samples treated at 250 or 450° under a reduced pressure of 10^{-5} Torr for 4 hr, the adsorption isotherm of water was measured volumetrically at 25° with an all-glass apparatus. Equilibrium pressures were read by a manometer containing Apiezon B oil.

Heat of Immersion Measurement. The sample of about 10 m² was evacuated in an ampoule under the same condition as described above, and then was exposed to water vapor of a given pressure at 25°. After the adsorption equilibrium had been attained, the ampoule was sealed. This preadsorption of water was carried out over a wide range of adsorption amounts. When a minute amount of water was supplied for adsorption, especially on the 450°-treated sample, the whole vapor was consumed at the initial stage of coverage. Under such a condition of preadsorption procedure there may be a great possibility of local adsorption. As a matter of fact, for the exact measurement of the heat of immersion isotherm, it is desirable to prepare surfaces such that all the sites with energies higher than a certain level have been perfectly covered with the adsorbate molecules after each preadsorption procedure. Although the water molecules (once adsorbed strongly on high-energy surfaces) are known to be desorbed with difficulty, we treated the sealed ampoule, which contained the sample together with a minute amount of adsorbed water, at 100° for 4 hr before the heat of immersion measurement in order to avoid strongly localized adsorption of water molecules and to make the surfaces as uniform as possible in the sense stated above. On the sample pretreated in this way, the heat of immersion in water was measured at 25° by using an adiabatic calorimeter equipped with a thermistor as a temperature-sensing element. The construction of the calorimeter and the technique of the heat of immersion

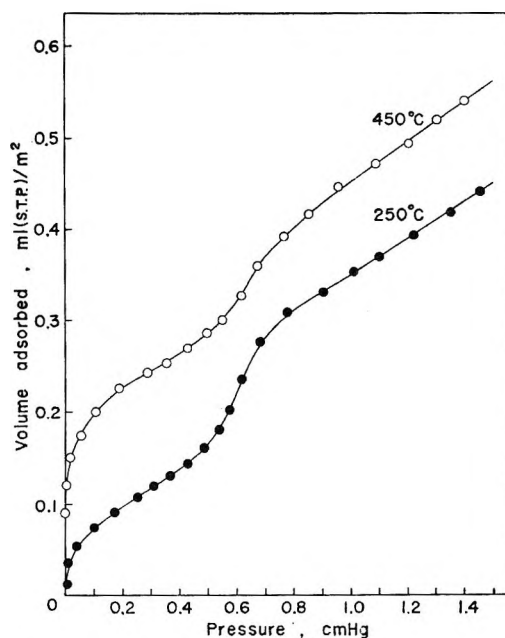


Figure 1. Adsorption isotherm of water on ZnO ($P_0 = 2.376$ cm at 25°).

measurement were the same as described previously.¹⁰ The heat of breaking of a vacant ampoule was found to be 0.28 J on the average; this was calibrated for the heat of immersion data.

Results and Discussion

The adsorption isotherms of water on ZnO are illustrated in Figure 1. Again we can see a sudden increase in the adsorption amount in the same region of relative pressure of water (0.2–0.3) as reported previously.⁸ The desorption measurements made for each sample showed no hysteresis, indicating the samples used were nonporous. Such a hump in the adsorption isotherm has been known only with the systems containing a nonpolar adsorbent and/or a nonpolar adsorbate,^{11–13} but not with those containing a polar adsorbent and a polar adsorbate. The present example is the first one in which the hump appears in the polar adsorbent–polar adsorbate system. It can be seen from Figure 1 that the shape of the two isotherms is quite the same, except that there is a nearly constant difference between the two isotherms over the whole range of the vapor pressure examined. This difference is based on the fact that the additional amount of chemisorbed water is larger with the 450°-treated sample

(9) S. Brunauer, D. H. Emmett, and E. Teller, *J. Amer. Chem. Soc.*, **60**, 309 (1938).

(10) T. Morimoto, K. Shiomi, and H. Tanaka, *Bull. Chem. Soc. Jap.*, **37**, 392 (1964).

(11) S. Ross, J. P. Olivier, and J. J. Hinchey, *Advances in Chemistry Series*, No. 33, American Chemical Society, Washington, D. C., 1961, p 317.

(12) W. R. Smith and D. G. Ford, *J. Phys. Chem.*, **69**, 3587 (1965).

(13) B. W. Davis and C. Pierce, *ibid.*, **70**, 1051 (1966).

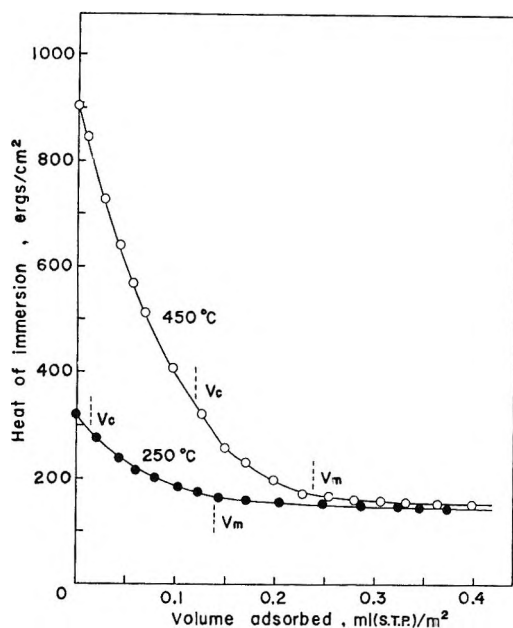


Figure 2. Heat of immersion isotherm for the system ZnO-H₂O at 25°.

than with the 250°-treated one. The V_m values calculated from the initial part of these isotherms according to the BET theory, are 0.137 and 0.246 ml(STP)/m² for the samples treated at 250 and 450°, respectively. This difference will correspond to that between the amounts chemisorbed on the two samples. Actually, in the range of pressures lower than 0.05 cm, the desorption was incomplete from these circumstances.

In Figure 2, the heat of immersion of ZnO in water is plotted against the amount of preadsorbed water. It is shown in Figure 2 that this heat of immersion isotherm decreases rapidly initially with increasing coverage and reaches a limiting value, and that there is a great difference between the heat of immersion values of the bare surfaces treated at two different temperatures. The heat value is found to be only 320 ergs/cm² on the bare surface treated at 250°, whereas it is 900 ergs/cm² on that treated at 450°. This large difference can be explained on the basis of the previous work⁷ in the following way. The plot of the heat of immersion of ZnO in water vs. the pretreatment temperature showed a maximum at about 450°. Such a phenomenon has been observed with other metal oxides as TiO₂,¹⁴ SiO₂,^{15,16} Fe₂O₃,¹⁷ etc., by many authors, and explained in terms of overlapped effect of both chemisorption and physisorption of water. Especially, there is the fact that in most cases of metal oxides the increasing part of the heat of immersion curve goes almost linearly with decreasing amount of surface water content; this indicates that the rehydroxylation of dehydrated sites on immersion in water accounts for the increasing part of the curve. There may be oxygen deficiencies on the ZnO surfaces treated at higher temperatures *in vacuo*, and if present, they do not seem to decrease when the pretreatment

temperature becomes higher than 450°. From these considerations we can deduce that oxygen deficiencies do not account for a large part of the observed heat.

The V_m value should be the sum of both amounts of water physisorbed and chemisorbed, and we can analyze them quantitatively.¹⁸ The result obtained on the present samples has shown that the amount of chemisorbed water is 0.017 and 0.118 ml(STP)/m² for 250°-treated and 450°-treated samples, respectively, as will be reported in detail in a subsequent publication.¹⁹ The symbol V_c in Figure 2 indicates the amount of chemisorbed water on each sample. The heat of immersion of ZnO in water decreases sharply in this chemisorption range, as shown in Figure 2. After the coverage has reached the V_m value, the heat of immersion decreases gradually to the surface enthalpy of water (118.5 ergs/cm²). It should be noticed that a recognizable abnormal change in the heat of immersion isotherms is not revealed in the vapor pressure region corresponding to the hump in the adsorption isotherm. This may probably be elucidated as follows: the hump in the adsorption isotherm appears after the V_m value has been attained or in the low energy region of adsorption, and, accordingly, the appearance of the hump may be unrecognizable in the energetic data of this kind.

By differentiating the heat of immersion curve, we can obtain the differential heat of adsorption as given in Figure 3. It can be seen from Figure 3 that the differential heat of adsorption curve is much higher with the 450°-treated sample than with the 250°-treated one. Moreover, the former decreases rapidly and irregularly with increasing coverage of water, whereas the latter decreases monotonically. Anyway, these features of the differential heat curve indicate that the surface of ZnO is of heterogeneous character for the water adsorption. Such descending differential heat curves have been observed in the systems: attapulgite-butylamine,²⁰ alumina-water,⁵ anatase-water,⁶ and thorium oxide-water.²¹ As the amount of chemisorbed water has not been determined on these metal oxide-water systems cited here, the differential heats obtained involve a necessarily uncertain amount of the heat due to chemisorption. In the present investigation, however, we can

(14) T. Morimoto, M. Nagao, and T. Omori, *Bull. Chem. Soc. Jap.*, **42**, 943 (1969).

(15) G. J. Young and T. P. Bursh, *J. Colloid Sci.*, **15**, 361 (1960).

(16) J. W. Whalen, *Advances in Chemistry Series*, No. 33, American Chemical Society, Washington, D. C., 1961, p 281.

(17) T. Morimoto, N. Katayama, H. Naono, and M. Nagao, *Bull. Chem. Soc. Jap.*, **42**, 1490 (1969).

(18) T. Morimoto, M. Nagao, and F. Tokuda, *J. Phys. Chem.*, **73**, 243 (1969).

(19) Unpublished data.

(20) J. J. Chessick and A. C. Zettlemoyer, *J. Phys. Chem.*, **62**, 1217 (1958).

(21) H. F. Holmes, E. L. Fuller, Jr., and C. H. Secoy, *ibid.*, **72**, 2095 (1968).

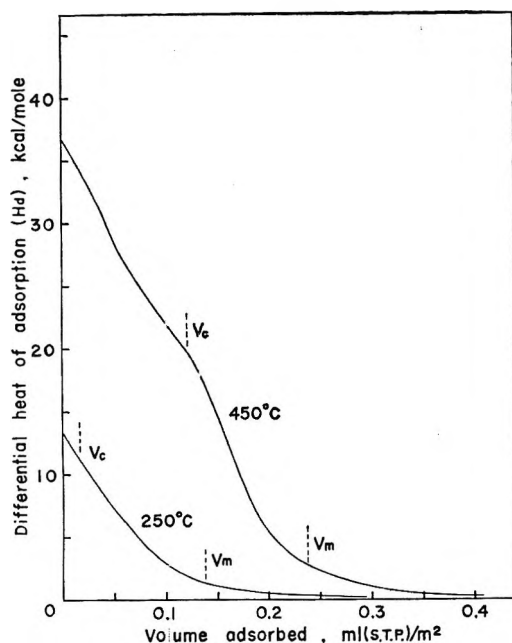


Figure 3. Differential heat of adsorption of water on ZnO.

estimate the contribution of chemisorption to the differential heats. As a result, it is found that though the differential heats on the 450°-treated surfaces are much larger than those on the 250°-treated ones, the heats due to physisorption which are obtained by eliminating the contribution of chemisorption from the data on the 450°-treated surfaces are comparable with those on the 250°-treated surfaces as indicated in Figure 3. After the coverage exceeds the V_m value, the differential heat approaches slowly to the heat of liquefaction of water. After completion of the second layer, the differential heat relative to the liquid state seems to become zero for two samples, as in the case of the $\text{Al}_2\text{O}_3\text{-H}_2\text{O}$ system.⁵

The nature of surface heterogeneity can be understood more in detail by plotting the site-energy distribution curve for ϵ given adsorption system. We can get the site-energy distribution curve by differentiating the curve of the differential heat *vs.* the amount of adsorption²⁰

$$\frac{d\Gamma}{d(H_d)} = g(\epsilon) \quad (1)$$

where Γ is the adsorption amount per unit surface, and H_d the differential heat of adsorption. The product $g(\epsilon)d(H_d)$ implies the number of molecules adsorbed on the sites which have the energies between H_d and $H_d + dH_d$. Here, the number of adsorption sites is assumed to be proportional to the adsorption amount over the whole range of coverage. The site-energy distribution curves obtained by the graphical differentiation of the curves in Figure 3 are represented in Figure 4. Apparently, the distribution curve differs for two samples, as is shown in Figure 4. It has been

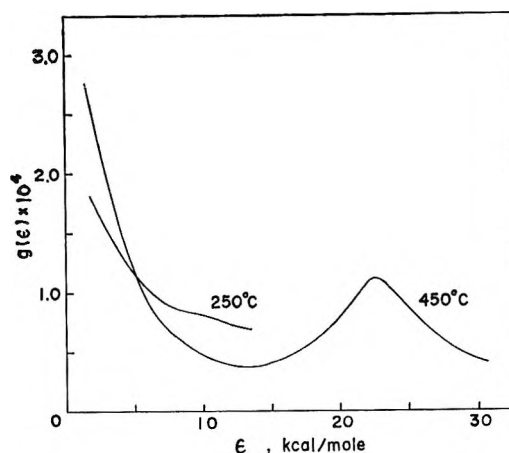
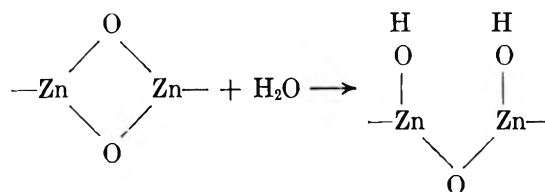


Figure 4. Site-energy distribution for the adsorption of water on ZnO.

known that surface hydroxyl groups can be removed from the surface of ZnO by the treatment at higher temperatures under a reduced pressure, and the dehydroxylated sites thus formed can be rehydroxylated rapidly when exposed to water vapor or to liquid water.^{7,8} Accordingly, with the 450°-treated sample, most of the differential heats at coverages less than the V_c value must be caused by the reaction



As is seen from Figure 4, the site-energy distribution for this rehydroxylation reaction is very wide, and shows a peak at the energy range of 20–25 kcal/mol H_2O . This value agrees well with the heat of surface hydration of ZnO, 23.5 kcal/mol of H_2O ,⁷ which has been estimated by combining the heat of immersion data and the water content of the surface. Such a peak corresponding to chemisorption energy could be found on the 450°-treated surfaces but not on the 250°-treated surfaces, because on the latter surfaces the rehydroxylation reaction occurs negligibly.

On the other hand, the physisorption of water will occur on the surface hydroxyl groups thus formed through the hydrogen bonding. The number of such physisorption sites decreases quasi-exponentially with increasing site-energy value, as is shown in Figure 4. Moreover, the energy distribution of physisorption sites is found to be approximately equal for two samples. Taking into account the errors from double graphical differentiation, the apparent difference in site-energy distribution on two samples at these coverages is not significant, which suggests that the surface hydroxyl groups removed by the treatment at 450° can be re-produced reversibly during the preadsorption process.

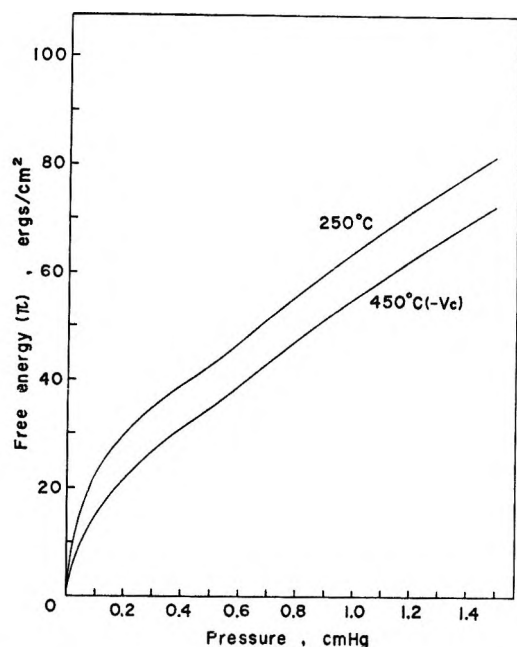


Figure 5. Free energy change of adsorption of water on ZnO.

Assuming that the perturbation of the solid surface by the adsorption of molecules can be neglected, and therefore the total change in entropy can be attributed to that of the adsorbed molecules, Jura and Hill¹ introduced the equation

$$T(S_A - S_L) = \frac{h_{I(SL)} - h_{I(S'L)}}{\Gamma} + \frac{\pi}{\Gamma} - RT \ln x \quad (2)$$

where S_A is the entropy of the adsorbed molecules, S_L the entropy of the molecules of bulk liquid, $h_{I(SL)}$ the enthalpy change on immersion (reverse sign of the heat of immersion) of the bare surface, $h_{I(S'L)}$ the enthalpy change on immersion of the surface which has preadsorbed a given amount of the adsorbate molecules, π the change in surface free energy by the adsorption, and x the relative equilibrium pressure. The change in surface free energy π can be calculated from the data of adsorption isotherm by applying the Gibbs equation

$$\pi = RT \int_0^P \Gamma d \ln P \quad (3)$$

The actual calculation of the surface free energy π was carried out by means of graphical integration, by plotting the ratio Γ/P against the vapor pressure P . The free energy change of adsorption π thus calculated is plotted against the equilibrium pressure P in Figure 5. The symbol $450^\circ (-V_c)$ in this figure means the free energy change due to only physisorption, which was obtained by integrating the adsorption data subtracted by the value V_c . Taking into account that the adsorption data obtained on the 250° -treated sample contains only a small amount of chemisorption, it may be said as a conclusion that the free energy change by physisorption of water is approximately equal for both sam-

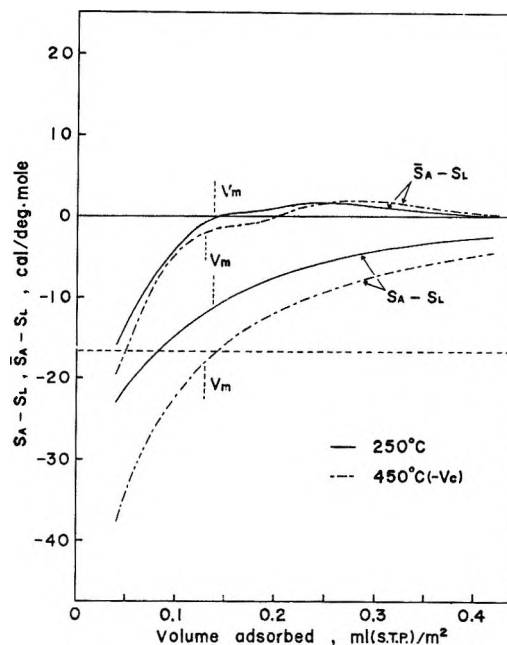


Figure 6. Integral and differential entropies of water adsorbed on ZnO.

ples, or that a large difference in free energy change between the two samples is due to the difference of the chemisorption amount, as in the case of the differential heat of adsorption. The influence of the hump in the adsorption isotherm on the free energy change should be present, but it is apparently so small that we cannot find any noticeable anomaly in the π curve.

In Figure 6, the entropy change, $S_A - S_L$, calculated by the equation (2) is plotted against the amount of preadsorbed water. Here, the values refer to the entropy of water at 25° (16.72 eu). The level of the broken line in Figure 6 indicates the entropy of water at 0°K . In the region of low relative pressures, this integral entropy of water is depressed deeply, and becomes lower than that of water at 0°K . As was pointed out by Hackerman and his coworkers in the study of water adsorption on Al_2O_3 ,⁵ this comes from the assumption that the surface is inert. In the calculation by the equation (2), the whole entropy change has been attributed only to the adsorbed molecules, despite a great possibility of the simultaneous change in the entropy of the solid surfaces themselves through strong adsorption of water molecules. As the amount of preadsorbed water increases, the entropy value approaches gradually to that of liquid water as shown in Figure 6. Here, the entropy values of the 250° -treated and the $450^\circ (-V_c)$ -treated samples go nearly in parallel. Corresponding to the hump in adsorption isotherm, any abnormal change can be expected in the integral entropy curve, but no detectable effect appears explicitly as in the case of the free energy curve.

The differential entropy of adsorption can be calculated by the equation²²

$$\bar{S}_A = \left(\frac{\partial(\Gamma S_A)}{\partial \Gamma} \right) = \Gamma \left(\frac{\partial S_A}{\partial \Gamma} \right) + S_A \quad (4)$$

where \bar{S}_A is the differential entropy of the adsorbed molecules. The differential entropy curves obtained by treating the integral entropy curves according to eq 4 are given in Figure 6. The differential entropy of water physisorbed on both samples increases steeply to the entropy value of liquid water, and after the coverage reaches the V_m value, the entropy remains almost constant in the vicinity of the entropy level of liquid water. Observing the curves of the differential entropy in more detail, we can find a very weak hump just after the

attainment of the V_m value. This may probably indicate that the sudden increase in the adsorption amount at a moderate relative pressure region is accompanied by a sudden increase in entropy. The possibility of entropy increase in this region will probably arise from the rearrangement of physisorbed water molecules or from the onset of the second layer adsorption, which gives rise to a sudden increase in freedom of the adsorbed molecules. The detailed consideration of the mechanism of this phenomenon is difficult now, but will be developed in a subsequent paper.

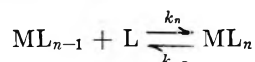
(22) T. L. Hill, P. H. Emmett, and L. G. Joyner, *J. Amer. Chem. Soc.*, **73**, 5102 (1951).

The Complexation Kinetics of Leucine with Nickel(II), Cobalt(II), and Copper(II)

by R. F. Pasternack,¹ E. Gibbs, and J. C. Cassatt²

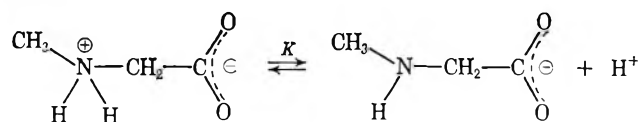
Department of Chemistry, Ithaca College, Ithaca, New York 14850 (Received April 1, 1969)

The kinetics of leucine complexation with nickel(II), cobalt(II) and copper(II) have been determined with the temperature-jump technique. The reactions are of the type

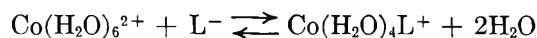


where $M = Ni^{2+}$, Co^{2+} , or Cu^{2+} , L refers to the attacking form of the ligand which is the anion in this case, and $n = 1$ or 2 . At an ionic strength of $0.1 M$ and 25° , the rate constants are: Ni^{2+} $k_1 = 1.7 \times 10^4 M^{-1} sec^{-1}$, $k_{-1} = 7.1 \times 10^{-2} sec^{-1}$, $k_2 = 4.1 \times 10^4 M^{-1} sec^{-1}$, $k_{-2} = 1.5 sec^{-1}$; Co^{2+} $k_1 = 1.3 \times 10^6 M^{-1} sec^{-1}$, $k_{-1} = 67 sec^{-1}$, $k_2 = 1.7 \times 10^6 M^{-1} sec^{-1}$, $k_{-2} = 600 sec^{-1}$; Cu^{2+} $k_1 = 1.6 \times 10^9 M^{-1} sec^{-1}$, $k_{-1} = 12 sec^{-1}$, $k_2 = 8 \times 10^8 M^{-1} sec^{-1}$, $k_{-2} = 15 sec^{-1}$. The rate constants for the reactions of Co^{2+} and Cu^{2+} with the zwitterion form of the ligand were found to be zero within experimental error. These results are consistent with the dissociative mechanism suggested by Eigen. The nonpolar side chain of leucine appears to play no significant role in determining either the forward or reverse rates. Once again, as for other ligands, $k_2^{Cu} < k_1^{Cu}$ unlike the situation found for other metal ions.

Investigations of the kinetics of complexation reactions of labile metal ions with amino acids have entered a new phase. As a result of earlier studies,³⁻⁵ it has become apparent that the zwitterion is a remarkably unreactive form and that, as a result, the reactions of the metal ions with the *anionic* form of the ligand can be studied at pH's significantly below the pK of the ligand. Hence, although the pK of sarcosine



is about ten, the reaction



could be studied at a pH of six to seven.⁶ Many advantages accrue from working at these relatively low pH's: (i) large excesses of metal ion can be employed to yield more precise values of the rate constants for the

(1) Author to whom inquiries should be addressed.

(2) Department of Chemistry, State University of New York at Buffalo, Buffalo, New York 14214.

(3) *e.g.*, K. Kustin, R. F. Pasternack, and E. M. Weinstock, *J. Amer. Chem. Soc.*, **88**, 4610 (1966).

(4) J. C. Cassatt and R. G. Wilkins, *ibid.*, **90**, 6045 (1968).

(5) A. F. Pearlmuter and J. Stuehr, *ibid.*, **90**, 858 (1968).

(6) R. F. Pasternack, K. Kustin, L. A. Hughes, and E. Gibbs, *ibid.*, in press.

formation of the monosubstituted complexes and (ii) equilibria between the fully aquated metal ion and metal-hydroxy species need not be considered. As a result there is closer agreement between the rate constant for cobalt(II) complexation⁶⁻⁸ reactions and the rate constant for water exchange of this metal ion as obtained by Swift and Connick⁹ and, secondly, the complexation kinetics of copper(II) ion can now be studied routinely.^{5,6,8}

This paper describes the reactions of several labile metal ions, Ni(II), Co(II) and Cu(II), with the α -amino acid, leucine. Leucine has a nonpolar side chain (*cf.*, Figure 1), and it is of interest to determine whether this nonpolar portion of the molecule affects the kinetics of these complexation reactions through either hydrophobic interactions or through a decrease in surface of reaction as was suggested in an earlier paper.¹⁰

Experimental Section

The leucine used in these studies was obtained from Nutritional Biochemicals Corp. Baker reagent grade nitrate salts of potassium, cobalt, nickel and copper were used. Stock solutions of the transition metal ions were prepared and the concentrations of these solutions were determined using standard analytic techniques. The indicators used in this study were Allied Chemical methyl orange, methyl red, chlorphenol red and phenol red and Eastman Organic bromothymol blue.

The temperature-jump apparatus has been described elsewhere.⁶ Solutions were freshly prepared from solid leucine and stock solutions of KNO₃ and the appropriate metal ion and indicator. The solutions were degassed and the pH was adjusted by the dropwise addition of dilute NaOH and/or HNO₃ to 0.01 pH unit. For many of the solutions, the equilibration of the pH was relatively slow taking several minutes in some cases. The pH of solutions frequently were monitored during the course of the temperature-jump experiments.

Each relaxation time represents an average of at least three photographic determinations. The relative error for these measurements is $\pm 10\%$. Test solutions of either metal ion or ligand in the absence of the other showed no discernible relaxation effects. These "blank" experiments were carried out at concentration levels of the free metal ion and ligand characteristic of solutions containing a mixture of the two. The rate

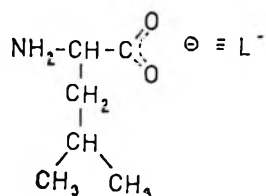
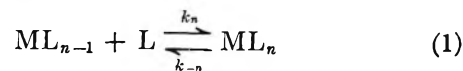


Figure 1. The leucine anion.

constants obtained in this study are being reported to $\pm 25\%$.

Results

The reactions studied were of the type



where n equals 1 or 2. The symbol "L" refers to the form of the ligand attacking the metal ion and, therefore, eq 1 could in principle represent a series of reactions differing in the degree of protonation of the ligand. The analysis of the temperature-jump data requires, for such complicated systems, a prior knowledge of the appropriate equilibrium constants. The equilibrium constants used for the analysis of these leucine systems are given in Table I.

Table I: Equilibrium Constants at 25° ($\mu = 0.1 M$)

$$K_1^a = \frac{[\text{H}^+][\text{HL}]}{[\text{H}_2\text{L}^+]} = 4.37 \times 10^{-2}{}^a$$

$$K_2^a = \frac{[\text{H}^+][\text{L}^-]}{[\text{HL}]} = 1.26 \times 10^{-10}{}^a$$

$$K_1^{\text{Ni}} = \frac{[\text{NiL}^+]}{[\text{Ni}^{2+}][\text{L}^-]} = 2.40 \times 10^6{}^a$$

$$K_2^{\text{Ni}} = \frac{[\text{NiL}_2]}{[\text{NiL}^+][\text{L}^-]} = 2.69 \times 10^4{}^a$$

$$K_1^{\text{Co}} = \frac{[\text{CoL}^+]}{[\text{Co}^{2+}][\text{L}^-]} = 1.95 \times 10^4{}^a$$

$$K_2^{\text{Co}} = \frac{[\text{CoL}_2]}{[\text{CoL}^+][\text{L}^-]} = 2.82 \times 10^3{}^a$$

$$K_1^{\text{Cu}} = \frac{[\text{CuL}^+]}{[\text{Cu}^{2+}][\text{L}^-]} = 1.29 \times 10^8{}^b$$

$$K_2^{\text{Cu}} = \frac{[\text{CuL}_2]}{[\text{CuL}^+][\text{L}^-]} = 5.36 \times 10^7{}^b$$

^a S. P. Datta, R. Leberman, and B. R. Rabin, *Trans. Faraday Soc.*, **55**, 1982 (1959). Equilibrium constants have been corrected to an ionic strength of 0.1 M using the equation suggested by D. D. Perrin and V. S. Sharma, *J. Chem. Soc.*, 724(1967). ^b P. Bretton, *J. Chim. Phys.*, **54**, 827, 837 (1957).

Whereas only two stability constants have been reported for each of the metal-leucine systems, experimental conditions for the kinetic runs were such that this limited data sufficed. The range of pH and concentrations of leucine and nickel(II) available to us was

(7) G. Davies, K. Kustin, and R. F. Pasternack, *Inorg. Chem.*, in press.

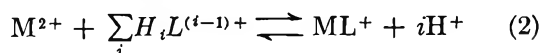
(8) R. L. Karpel, K. Kustin, and R. F. Pasternack, *Biochim. Biophys. Acta*, **177**, 434 (1969).

(9) T. J. Swift and R. E. Connick, *J. Chem. Phys.*, **37**, 307 (1962).

(10) A. Kowalak, K. Kustin, R. F. Pasternack, and S. Petrucci, *J. Amer. Chem. Soc.*, **89**, 3126 (1967).

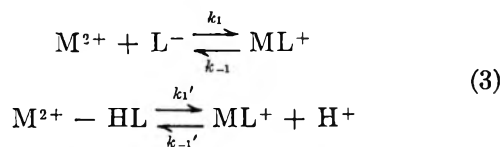
severely limited because of precipitation of what was presumed to be $\text{Ni}(\text{C}_6\text{H}_{12}\text{O}_2\text{N})_2$ at higher pH's and the relatively long relaxation times in the lower pH region. As a result of this experimental limitation it did not prove possible to analyze the nickel data in the same way that the cobalt and copper data were analyzed to determine the rate constant for the attack of the zwitterionic form of leucine. However, a stopped-flow study of this system showed that, within experimental error, the rate constant for this reaction is zero.¹¹

For both cobalt(II) and copper(II), it proved possible to obtain relaxation spectra for solutions which contained a large excess of the metal ion. For such solutions it can be assumed that the only complexation reactions of importance are



Only solutions containing $[\text{Co}^{2+}] \geq 10[\text{CoL}^+]$ or $[\text{Cu}^{2+}] \geq 4[\text{CuL}^+]$ were used in this analysis. That the condition is less stringent for the copper case is a reflection of the fact that, for glycine,⁵ sarcosine⁶ and serine⁸ $k_1^{\text{Cu}} > k_2^{\text{Cu}}$, unlike other metal ions.

In the pH range investigated, two forms of leucine needed to be considered; the anion L^- and the zwitterion HL . Then



By applying standard techniques for deriving relaxation time expressions, it can be shown that

$$1/\tau = Ak_1 + Bk_1'$$

where

$$\begin{aligned} A &= \frac{[\text{M}^{2+}]}{1 + \alpha} + [\text{L}^-] + \frac{1}{K_1 M} \\ B &= \frac{\alpha[\text{M}^{2+}]}{1 + \alpha} + [\text{HL}] + \frac{1}{K_1 M K_2^a} \left([\text{H}^+] + \alpha\beta \frac{[\text{ML}^+]}{1 + \alpha} \right) \\ \alpha &= \frac{[\text{H}^+]}{K_2^a + \beta[\text{L}^-]} \\ \beta &= \frac{K_{\text{In}} + [\text{H}^+]}{K_{\text{In}} + [\text{H}^+] + [\text{In}^-]} \end{aligned}$$

Plots were made of $(\tau B)^{-1}$ vs. AB^{-1} and are shown in Figure 2 for cobalt(II) and Figure 3 for copper(II). The slope of the lines are the respective k_1 's and the intercepts k_1' . From the plots we find that for cobalt $k_1 = 1.3 \times 10^6 M^{-1} \text{sec}^{-1}$, $k_1' \cong 0$; for copper $k_1 = 1.6 \times 10^9 M^{-1} \text{sec}^{-1}$, $k_1' \cong 0$. The zwitterion is thereby once again shown to be a remarkably unreactive species toward metal ions.

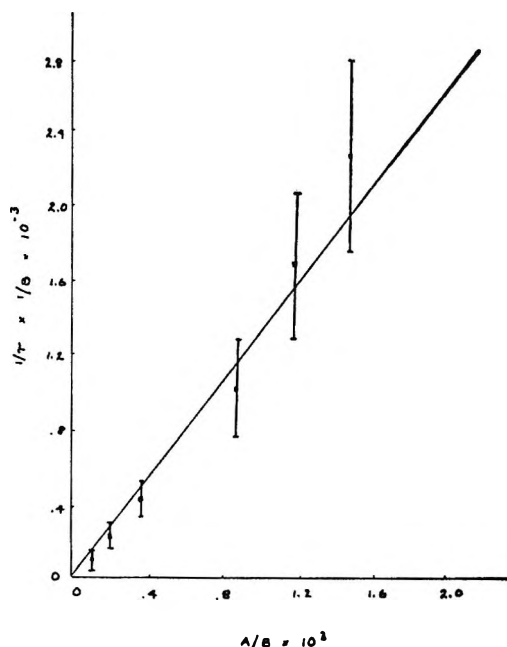


Figure 2. Plot of $(\tau B)^{-1}$ vs. AB^{-1} for cobalt(II)-leucine system. See text for definitions of A and B . The slope of this line is k_1 and the intercept is k_1' , both in units of $M^{-1} \text{sec}^{-1}$.

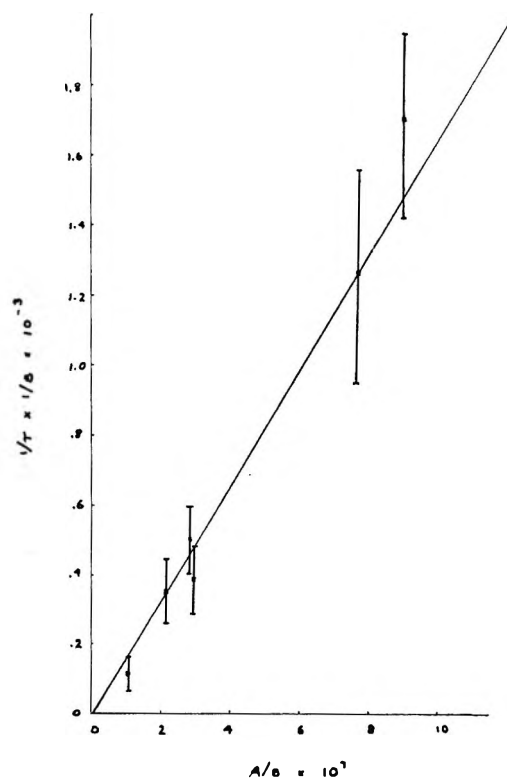
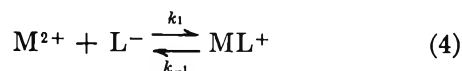


Figure 3. Plot of $(\tau B)^{-1}$ vs. AB^{-1} for copper(II)-leucine system.

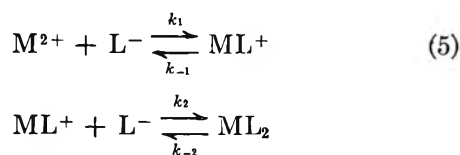
For these solutions, the only complexation reaction which need be considered is

(11) J. C. Cassatt, Ph.D. Dissertation, State University of New York at Buffalo, 1969.



It can be readily shown that a plot of $1/\tau$ vs. $[M^{2+}]/(1 + \alpha) + [L^-]$ will result in a straight line the slope of which is k_1 and the intercept k_{-1} .¹² Figure 4 shows such a plot for the cobalt(II)-leucine system while Figure 5 shows the plot for the copper(II)-leucine system. From the plots, a value of $K_1 = k_1/k_{-1}$ can be determined for each metal. For cobalt(II), the value so obtained is $2.2 \times 10^4 M^{-1}$ as compared to the literature value of $1.95 \times 10^4 M^{-1}$; for copper(II), we obtain $1.0 \times 10^8 M^{-1}$ and the literature value is $1.29 \times 10^8 M^{-1}$ (cf. Table I).

For the remaining cobalt(II) and copper(II) solutions and for all of the nickel(II) solutions, two complexation reactions need be considered



The standard treatment developed by Hammes and Steinfeld¹³ was used to determine the rate constants which resulted in the best agreement between calculated and experimental relaxation times. The experimental conditions, experimental and calculated relaxation times and the determined rate constants for leucine with nickel(II), cobalt(II) and copper(II) are given as Tables II, III, and IV, respectively. The k_1 value we obtained for nickel(II) and leucine is $1.7 \times 10^4 M^{-1} \text{sec}^{-1}$ as compared to a value of $1.5 \times 10^4 M^{-1} \text{sec}^{-1}$ obtained using a stopped-flow technique.¹¹

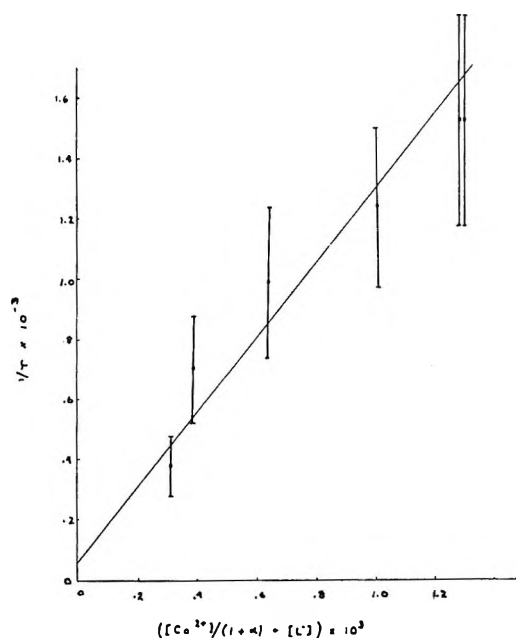


Figure 4. Plot of $1/\tau$ vs. $[Co^{2+}]/(1 + \alpha) + [L^-]$. The slope of the line is k_1 in units of $M^{-1} \text{sec}^{-1}$ and the intercept is k_{-1} in sec^{-1} .

Table II: Relaxation Spectra of Nickel(II)-Leucine Solutions^a

$[Ni^{2+}]_0 \times 10^3$	$[Lig]_0 \times 10^3$	pH	$\tau_{\text{obs}}, \text{sec}$	$\tau_{\text{calc}}, \text{sec}$
2.56	4.00	6.71	0.13	0.11
7.96	12.0	6.71	0.020	0.026
2.56	2.50	7.01	0.15	0.13
2.56	4.00	7.01	0.080	0.085
2.56	6.00	7.01	0.055	0.063
2.56	12.0	6.51	0.042	0.056
10.3	2.52	6.52	0.11	0.10
5.14	2.55	6.57	0.20	0.14
7.72	2.40	6.46	0.13	0.12
2.56	4.00	7.41	0.45	0.54
5.14	2.50	7.01	0.18	0.11

$$k_1 = 1.7 \times 10^4 M^{-1} \text{sec}^{-1} \quad k_2 = 4.1 \times 10^4 M^{-1} \text{sec}^{-1}$$

$$k_{-1} = 7.1 \times 10^{-5} \text{sec}^{-1} \quad k_{-2} = 1.5 \text{sec}^{-1}$$

^a All concentrations are molar. The subscript zero refers to the total stoichiometric concentration. $\mu = 0.1 M$, temp = 25° .

Table III: Relaxation Spectra of Cobalt(II)-Leucine Solutions^a

$[Co^{2+}]_0 \times 10^3$	$[Lig]_0 \times 10^3$	pH	$\tau_{\text{obs}}, \text{msec}$	$\tau_{\text{calc}}, \text{msec}$
2.68	4.35	7.15	1.0	0.90
2.68	2.16	7.16	1.4	1.4
5.35	6.48	6.96	0.65	0.49
2.14	2.25	7.13	2.6	2.3
2.14	5.59	7.07	1.1	0.87
5.35	7.68	6.61	0.65	0.51
8.03	9.92	6.38	0.80	0.61
8.03	52.3	6.09	0.36	0.45
8.03	69.2	6.02	0.30	0.49
8.03	85.7	6.11	0.28	0.36

$$k_1 = 1.3 \times 10^8 M^{-1} \text{sec}^{-1} \quad k_2 = 1.7 \times 10^8 M^{-1} \text{sec}^{-1}$$

$$k_{-1} = 67 \text{sec}^{-1} \quad k_{-2} = 600 \text{sec}^{-1}$$

^a All concentrations are molar. The subscript zero refers to the total stoichiometric concentration. $\mu = 0.1 M$, temp = 25° .

Discussion

The isobutyl side chain in the leucine molecule might be expected to influence the kinetics of complexation in a number of ways. As has been suggested, the non-polar group might decrease the surface of reaction of the ligand and thereby decrease the forward rate constants.¹⁰ However, hydrophobic interactions might also be of importance and these might arise from two sources. The first is an interaction in the complex itself. If the side chain of one leucine ligand interacted with the side chain of a neighboring complexed leucine, the K_2^M would be unusually high. Kinetically, it might be expected that this would be manifested in an

(12) M. Eigen and L. DeMaeyer, *Techniques in Organic Chemistry*, Vol. VIII, Part II, 2nd ed, S. L. Friess, E. S. Lewis, and A. Weissberger, Ed., Interscience Publishers, Inc., New York, N. Y., 1963.

(13) G. G. Hammes and J. I. Steinfeld, *J. Amer. Chem. Soc.*, **84**, 4639 (1962).

Table IV: Relaxation Spectra of Copper(II)-Leucine Solutions^a

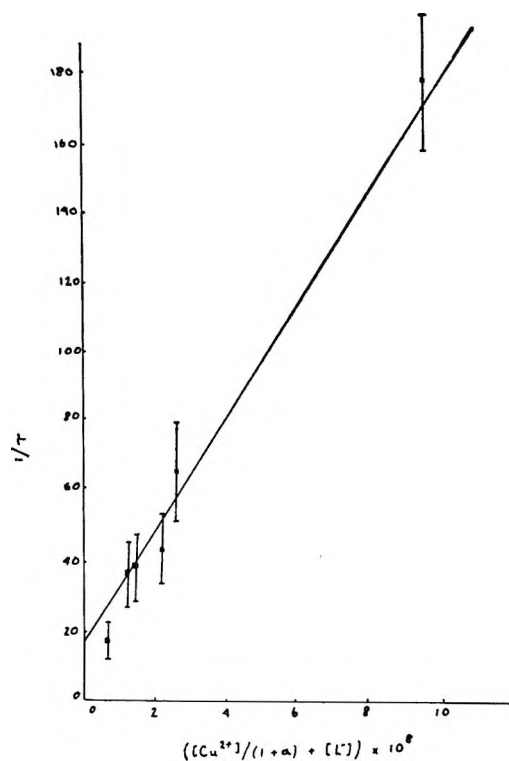
[Cu ²⁺] ₀ × 10 ³	[Lig] ₀ × 10 ³	pH	τ _{obs.} , msec	τ _{calc.} , msec
4.92	8.00	3.99	7.4	8.2
9.87	5.00	4.00	5.6	5.4
4.92	20.0	3.15	65	60
2.46	2.50	4.02	16	18
4.92	5.00	4.50	1.7	2.1
9.87	5.00	4.60	1.6	0.89
2.46	5.00	4.51	3.2	3.2
4.92	5.00	3.52	29	33
9.87	5.00	3.55	24	20
4.92	10.0	3.50	28	30

$$k_1 = 1.6 \times 10^9 M^{-1} \text{sec}^{-1} \quad k_2 = 8 \times 10^8 M^{-1} \text{sec}^{-1}$$

$$k_{-1} = 12 \text{sec}^{-1} \quad k_{-2} = 15 \text{sec}^{-1}$$

^a All concentrations are molar. The subscript zero refers to the total stoichiometric concentration. $\mu = 0.1 M$, temp = 25°.

unusually small k_{-2} . On the other hand it is possible that the side chains would sterically interfere with one another. This would result in an unusually low K_2^M with an attending large value for k_{-2} . An examination of models of metal leucine systems shows that the side

Figure 5. Plot of $1/\tau$ vs. $[Cu^{2+}]/(1 + \alpha) + [L^-]$.**Table V:** Forward Rate Constants for Metal Complexation Reactions^a

	Glycine ^{6,7}	Serine ⁸	Sarcosine ⁹	Leucine ¹⁵
$M^{2+} + L^- \xrightarrow{k_1} ML^+$				
Nickel(II)	4.1×10^4	2.9×10^4	1.3×10^4	1.7×10^4
Cobalt(II)	1.5×10^6	2.0×10^6	9.2×10^6	1.3×10^6
Copper(II)	4.0×10^9	2.5×10^9	2.8×10^9	1.6×10^9
$ML^+ + L^- \xrightarrow{k_2} ML_2$				
Nickel(II)	5.6×10^4	3.4×10^4	1.2×10^4	4.1×10^4
Cobalt(II)	2.0×10^6	2.0×10^6	1.5×10^6	1.7×10^6
Copper(II)	4×10^8	5×10^8	1×10^8	8×10^8

^a All rate constants have units of $M^{-1} \text{sec}^{-1}$. The temperature is 25° and the ionic strength is 0.1 M.

chains most likely do not interact and this type of inner interaction is unlikely. However it has been shown that the stability constants, K_2^M , for some leucine dipeptides were anomalously high.¹⁴ It was suggested at that time that side-chain (hydrophobic) interactions were responsible for this unusual stability.

A second possible effect of the nonpolar side chain might be in the ion-pair formation constant between the ligand and mono-complex. It seems possible that due to hydrophobic interactions between the side chain of the leucine attached to the metal and that in the ion-pair, the ion-pair might be unusually stable. This would result in a larger than normal k_2 . However, when the ligand is a simple α -amino acid, this interaction would result in an ion-pair in which the α -amino

acid portion would be pointed away from the metal. This configuration would probably be unreactive here but might be reactive in the oligopeptide case.

The forward rate constants obtained for the metal-leucine systems are compared with those obtained for similar systems in Table V.¹⁵ The table includes only those results which have been obtained since the advent of the low pH technique. For each metal ion, the k_1 values are in good agreement, with the nickel values showing the greatest variation. Quite clearly the large nonpolar group of leucine does not influence the forward

(14) S. P. Datta, R. Leberman, and B. R. Rabin, *Trans. Faraday Soc.*, 55, 1982 (1959).

(15) This work.

rate constant for complexation which, therefore, indicates that the smaller than normal rate constants obtained for nickel(II) and cobalt(II) with α -aminobutyric acid¹⁰ cannot be explained in terms of a decreased surface of reaction.

The k_2 values are also in good agreement for each metal ion except for nickel(II)- and copper(II)-sarcosine systems. Apparently the N-methyl group of sarcosine affects the complexation kinetics considerably more than does the isobutyl group of leucine which is attached to a nonbonding atom. There is no indication of steric hindrance nor hydrophobic interactions in the forward rates obtained for leucine.

There is considerably more variation in reverse-rate constants than forward-rate constants as is shown in Table VI. This is to be expected since these values are in practice (and especially the k_{-2} values) obtained directly from the equilibrium constants, $k_{-n} = k_n/K_n$. Since, as has been shown, the forward rate constants are relatively invariant for these ligands, any differences in stability constants will manifest themselves in the reverse-rate constants.

A comparison of the reverse-rate constants shows that the leucine values are not extreme except for copper(II). That the k_{-2} rate constant is small would be consistent with a hydrophobic interaction between the nonpolar side chains. However, the k_{-1} rate constant is comparatively even smaller. Therefore, it may well be that the variations are due more to experimental error than in any chemical interaction. We

Table VI: Reverse Rate Constants for Metal Complexation Reactions^a

	Glycine ^{6,7}	Serine ⁸	Sarcosine ⁶	Leucine ¹⁰
$ML^+ \xrightarrow{k_{-1}} M^{2+} + L^-$				
Nickel(II)	0.057	0.11	0.041	0.071
Cobalt(II)	34	93	57	67
Copper(II)	34	32	32	12
$ML_2 \xrightarrow{k_{-2}} ML^+ + L^-$				
Nickel(II)	0.93	1.6	0.50	1.5
Cobalt(II)	330	930	570	600
Copper(II)	50	150	22	15

^a All rate constants have units of sec^{-1} . The temperature is 25° and the ionic strength is 0.1 *M*.

conclude that the complexation kinetics of leucine are entirely normal and, therefore, that the large, nonpolar portion of the molecule has no influence on rates.

Having now demonstrated that the complexation kinetics involving leucine itself are quite normal, this research is being extended to studies on the complexation kinetics of leucine dipeptides.

Acknowledgments. The authors gratefully acknowledge partial support from the Petroleum Research Fund for Grant 2982B and to the National Science Foundation for Grant GP-8099.

Association of Methanol in Vapor and in *n*-Hexadecane.

A Model for the Association of Alcohols

by Edwin E. Tucker, Sutton B. Farnham, and Sherril D. Christian

Chemistry Department, University of Oklahoma, Norman, Oklahoma 73069 (Received April 1, 1969)

A new model is proposed for the self-association of methanol in nonpolar solvents and in the vapor phase. The model is based on vapor pressure measurements for methanol in *n*-hexadecane at 25, 35, and 45° and on *PVT* measurements on methanol vapor at 15, 25, and 35°. These data are best explained by assuming the presence of only two associated species: trimers and octamers. The model has been applied with success to infrared spectral data for several alcohols; it has also been tested on nmr data for alcohols in CCl₄ with mixed results.

Introduction

The nature of alcohol self-association has been discussed at length in many articles.¹ The experimental data apparently support the conclusion that many associated species are present in alcohol solutions in various nonpolar solvents. Disagreement arises primarily over whether small species such as dimer, trimer, and tetramer are cyclic or linear. A number of workers have proposed cyclic structures for one or more of these small species both in the solid state in an inert matrix and in nonpolar solvents.^{2,3} The opposing view, that small species are linear, has been supported also.^{4,5} Recently, Fletcher and Heller have claimed that it is possible to explain the spectral properties of alcohol solutions by assuming the presence of only two associated species, linear and cyclic tetramers.⁶ They agree that other species such as dimers may be present but not in sufficient concentrations to influence the mass balance of an alcohol solution.⁷

The current picture of alcohol self-association in the vapor phase is much simpler. Following Weltner and Pitzer,⁸ measurements of vapor phase heat capacities of several alcohols are thought to be best explained by assuming a monomer-dimer-tetramer equilibrium.⁹

The present report originates from a general study of the molecular complexity of hydrogen bonding systems both in the vapor phase and in nonvolatile solvents. The data reported here are vapor pressure data for methanol in the nonvolatile solvent *n*-hexadecane at 25, 35, and 45° and *PVT* data for methanol vapor at 15, 25, and 35°.

The results of these investigations indicate that it is unnecessary to assume the presence of either dimers or tetramers of methanol to obtain the best fit of both *PVT* and vapor pressure data over an activity range of 0 to 95% of the saturation vapor pressure of methanol at three temperatures.

Experimental Details

Chemicals. Reagent grade methanol, obtained from

Mallinckrodt Chemical Co., was distilled from magnesium methoxide in a 30-plate Oldershaw column. The middle cut was taken and used shortly after distillation. Separate samples were used for vapor and solution studies; precautions were taken to minimize exposure to the atmosphere. The *n*-hexadecane used was practical grade obtained from Matheson Coleman and Bell. It was treated with concentrated sulfuric acid, washed, and passed through a column of activated alumina. This product was distilled in a 12-plate Oldershaw column at 149–151° under 10 mm air pressure. The center fraction showed no impurity peaks when examined by gas chromatography.

Apparatus and Technique. Both vapor pressure and *PVT* measurements were made using Texas Instruments fused quartz precision pressure gauges. The approximate limits of resolution of the two gauges were ±0.001 mm absolute in *PVT* measurements and ±0.003 mm absolute in vapor pressure measurements. The gauges were connected to each apparatus by Pyrex capillaries of about 1-mm inside diameter wrapped with silicone rubber covered heating tapes (Glas-Col) from the pressure capsule to a short distance below the water surface in the thermostated baths. The tapes were kept at a temperature roughly equivalent to the pressure capsule temperature (45°) to prevent condensation in the capillaries at higher methanol activities above room temperature.

(1) G. C. Pimentel and A. L. McClellan, "The Hydrogen Bond," W. H. Freeman and Co., San Francisco, Calif., 1960.

(2) M. Van Thiel, E. D. Becker, and G. C. Pimentel, *J. Chem. Phys.*, **27**, 95 (1957).

(3) H. C. Van Ness, J. Van Winkle, H. H. Richtol, and H. B. Hollinger, *J. Phys. Chem.*, **71**, 1483 (1967).

(4) D. A. Ibbitson and L. F. Moore, *J. Chem. Soc., B*, **76**, (1967).

(5) W. C. Coburn, Jr., and E. Grunwald, *J. Amer. Chem. Soc.*, **80**, 1318 (1958).

(6) A. N. Fletcher and C. A. Heller, *J. Phys. Chem.*, **71**, 3742 (1967).

(7) A. N. Fletcher and C. A. Heller, *ibid.*, **72**, 1839 (1968).

(8) W. Weltner and K. S. Pitzer, *J. Amer. Chem. Soc.*, **73**, 2602 (1961).

(9) N. S. Berman, *A.I.C.H.E. J.*, **14**, 499 (1968).

Each apparatus was immersed in a constant-temperature water bath. Temperature was controlled to within $\pm 0.01^\circ$ and the absolute temperatures of the systems are estimated to be within $\pm 0.05^\circ$ from the stated temperatures.

Details of the basic vapor pressure apparatus and techniques have been described previously.¹⁰ *n*-Hexadecane was selected as an ideal solvent for studies of the present type since it is relatively inert and also has a very low vapor pressure at room temperature. The apparatus used in this study had a total volume of about 750 cc; the volume was determined by weight using water. A weighed amount of *n*-hexadecane, about 250 cc by volume, was initially added to the apparatus. The system was then evacuated at room temperature to a pressure approaching the vapor pressure of the solvent. Increments of methanol were added to the thermostated system through a mercury-covered sintered glass disk using an RGI precision micrometer buret of 0.25 ml volume. When not in use, the buret was kept in a dry chamber thermostated at 25° . The precision of the buret calibration justified reporting methanol concentrations to 10^{-4} *M*. Solution concentrations were calculated from the weight of methanol added; corrections were made for the amount of methanol in the vapor phase, dissolved air in the methanol, and the volume increase of the solution. The air and volume corrections were quite small and did not appreciably affect the statistical fit of the data later presented.

A glass Burnett-type apparatus was used for the *PVT* study on methanol vapor.¹¹ The two chambers, with volumes of approximately 1 and 3 l., respectively, were connected by a stainless steel bellows valve (HOKE 4172 G4Y). The volume ratio of the apparatus (the ratio of the large chamber volume to the total volume) was determined with dry nitrogen. Methanol additions to the apparatus were made by vapor transfer from a previously degassed liquid sample connected to the apparatus by a Fischer-Porter Teflon needle valve (795-005). A similar valve served as an evacuation port for the apparatus. The measured methanol pressures were the initial pressures in the large (*PL1*) and small (*PS1*) chambers and the final pressure in the total system (*P2*). To correct for adsorption, each pressure was monitored for a period of time to define the adsorption curve. These pressure-time data were plotted (IBM 1130, Calcomp Plotter) and the pressures were extrapolated to a specific time. The extrapolated pressures were used in the analysis of the system.

Results, Calculations, and Discussion

Vapor Pressure Measurements. Table I presents the measured vapor pressures (corrected for air) and corresponding concentrations of methanol in *n*-hexadecane at 25, 35, and 45° . If the assumption is made that in dilute solution the activity coefficient of each

species is unity, the distribution ratio for monomeric alcohol may be expressed as

$$K_D = \frac{C_A^s}{C_A^v} \quad (1)$$

where C_A^s is the molar concentration of monomeric alcohol in solution and C_A^v is the molar concentration of monomeric alcohol in the vapor phase. The formal or analytical concentration of methanol in solution, assuming an infinite series of associated species, is then given by

$$f_A = K_D C_A^v + 2K_2(K_D C_A^v)^2 + 3K_3(K_D C_A^v)^3 + \dots \quad (2)$$

where K_2 , K_3 , etc., are successive equilibrium constants. Sets of values of formal concentration in solution and monomer concentration in the vapor phase (equal to the pressure of methanol monomer divided by *RT*) may be correlated by assuming any functional dependence of formal concentration on monomer concentration consistent with eq 2. By employing a standard least-squares computer program, it is possible to assess the relative goodness of fit of a large number of assumed associated species. K_D and the successive equilibrium constants are used as parameters. The vapor pressure data were analyzed in the form of eq 2 using successively one, two, and three terms to represent associated species. The series of forms checked in this manner included a range from the simple monomer-dimer (1-2) to three parameter fits having as high as tenth-order dependence on monomer concentration (1-6-10). A variety of four-parameter fits were also tried over this range. The conditions imposed in seeking the best fit were first, a minimum in the root-mean-square deviation (RMSD)

$$\text{RMSD} = [(\sum (f_A - f_A^{\text{calc}})^2)/(n - p)]^{1/2} \quad (3)$$

(where *n* is the number of paired values of f_A and C_A^v and *p* is the number of parameters) and second, realistic temperature dependence of the equilibrium constants obtained from the fits.¹² Table II lists RMSD's for several fits at each temperature.

The results of the data analysis were surprising. No two parameter fits were satisfactory. Of the three

(10) A. A. Taha, R. D. Grigsby, J. R. Johnson, S. D. Christian, and H. E. Affsprung, *J. Chem. Educ.*, **43**, 432 (1963).

(11) E. S. Burnett, *J. Appl. Mech.*, **58**, A136 (1936).

(12) In attempting to fit data to eq 2, relative and absolute weighting of the formal concentration values were separately employed. Values of RMSD corresponding to the various choices of species fall in the same order whichever weighting scheme is used and the calculated distribution and equilibrium constants obtained by the two methods are in good agreement. Considering the techniques employed in adding samples to the solutions,¹⁰ a weighting procedure between relative and absolute (*viz.*, using weight factors proportional to N^{-1} , where *N* is the number of samples added) might have been better. However, in the *PVT* study (*vide infra*) absolute weighting is clearly preferable and, for simplicity, absolute weighting has been employed throughout.

Table I: Vapor Pressures, Measured and Calculated Concentrations of Methanol in *n*-Hexadecane

P_{MeOH} , Torr ^a	f_{MeOH} , <i>M</i>	$f_{\text{MeOH}}^{\text{cal}}$, <i>M</i> ^b	P_{MeOH} , Torr ^a	f_{MeOH} , <i>M</i>	$f_{\text{MeOH}}^{\text{cal}}$, <i>M</i> ^b
25°			25°		
3.53	0.0016	0.0016	68.84	0.0384	0.0386
8.76	0.0039	0.0039	73.48	0.0428	0.0429
13.90	0.0063	0.0062	77.63	0.0473	0.0473
18.98	0.0087	0.0086	81.32	0.0517	0.0516
23.99	0.0111	0.0110	84.64	0.0562	0.0560
28.88	0.0135	0.0133	87.66	0.0608	0.0606
33.68	0.0159	0.0158	90.37	0.0653	0.0651
38.36	0.0183	0.0183	92.82	0.0699	0.0697
42.89	0.0207	0.0208	95.08	0.0746	0.0744
47.21	0.0232	0.0233	97.12	0.0792	0.0790
51.35	0.0257	0.0258	99.02	0.0839	0.0837
5.29	0.0023	0.0023	100.79	0.0886	0.0884
10.51	0.0047	0.0047	102.44	0.0933	0.0933
15.59	0.0071	0.0070	103.95	0.0980	0.0980
20.65	0.0095	0.0094	105.38	0.1027	0.1028
25.59	0.0119	0.0117	106.72	0.1074	0.1076
30.48	0.0143	0.0141	107.98	0.1121	0.1124
35.21	0.0167	0.0166	109.17	0.1169	0.1172
39.82	0.0191	0.0190	110.28	0.1216	0.1220
44.26	0.0216	0.0215	111.35	0.1263	0.1268
48.53	0.0240	0.0241	112.36	0.1311	0.1316
52.59	0.0265	0.0266	113.32	0.1358	0.1364
56.43	0.0290	0.0291	17.34	0.0079	0.0078
60.08	0.0316	0.0317	33.82	0.0159	0.0159
63.50	0.0341	0.0342	50.10	0.0248	0.0250
66.68	0.0367	0.0368	62.58	0.0332	0.0335
69.68	0.0393	0.0394	71.75	0.0410	0.0413
74.22	0.0437	0.0437	79.95	0.0499	0.0499
78.28	0.0481	0.0480	87.76	0.0607	0.0607
81.93	0.0526	0.0524	92.92	0.0699	0.0699
85.14	0.0571	0.0568	96.84	0.0783	0.0783
88.10	0.0617	0.0613	100.57	0.0876	0.0880
90.79	0.0663	0.0659	103.17	0.0961	0.0955
7.08	0.0031	0.0031	106.06	0.1055	0.1052
12.25	0.0055	0.0055	108.60	0.1150	0.1149
20.74	0.0095	0.0094	110.86	0.1245	0.1246
28.98	0.0135	0.0134	112.89	0.1340	0.1342
36.93	0.0175	0.0175	114.54	0.1425	0.1427
44.42	0.0215	0.0216	116.38	0.1530	0.1531
51.40	0.0257	0.0258	117.94	0.1625	0.1626
57.84	0.0298	0.0301	119.32	0.1721	0.1717
63.64	0.0341	0.0344	120.61	0.1816	0.1807
35°			35°		
20.38	0.0076	0.0076	6.18	0.0023	0.0023
40.09	0.0152	0.0152	12.31	0.0045	0.0045
58.88	0.0229	0.0229	18.35	0.0068	0.0068
76.33	0.0308	0.0309	24.37	0.0091	0.0091
92.17	0.0388	0.0390	30.33	0.0114	0.0113
106.09	0.0470	0.0472	49.62	0.0190	0.0190
118.19	0.0554	0.0555	67.75	0.0268	0.0269
128.53	0.0639	0.0639	84.43	0.0347	0.0349
137.35	0.0727	0.0725	99.29	0.0429	0.0431
144.99	0.0815	0.0813	112.29	0.0512	0.0513
151.58	0.0905	0.0902	123.43	0.0596	0.0596
157.32	0.0995	0.0993	132.98	0.0683	0.0681
162.42	0.1086	0.1085	141.22	0.0771	0.0768
166.94	0.1178	0.1178	148.32	0.0860	0.0856
170.98	0.1270	0.1271	154.46	0.0950	0.0946
174.64	0.1362	0.1366	159.88	0.1040	0.1037
177.96	0.1455	0.1460	164.65	0.1132	0.1129
180.95	0.1547	0.1553	168.93	0.1224	0.1223

Table I (Continued)

P_{MeOH} , Torr ^a	f_{MeOH} , M	$f_{\text{MeOH}}^{\text{cal}}$, M^b	P_{MeOH} , Torr ^a	f_{MeOH} , M	$f_{\text{MeOH}}^{\text{cal}}$, M^b
35°			35°		
188.65	0.1827	0.1831	172.76	0.1316	0.1316
190.83	0.1921	0.1922	176.24	0.1408	0.1410
192.90	0.2014	0.2014	179.39	0.1501	0.1503
194.79	0.2108	0.2102	182.29	0.1594	0.1597
196.67	0.2202	0.2195	184.97	0.1687	0.1691
45°			45°		
23.57	0.0072	0.0072	79.74	0.0256	0.0254
46.56	0.0145	0.0144	100.73	0.0331	0.0330
68.89	0.0219	0.0217	120.67	0.0407	0.0406
90.36	0.0293	0.0292	139.25	0.0484	0.0484
110.87	0.0369	0.0368	156.49	0.0562	0.0563
130.17	0.0445	0.0445	172.18	0.0642	0.0643
148.13	0.0523	0.0524	186.39	0.0723	0.0724
164.56	0.0602	0.0603	199.16	0.0805	0.0806
179.55	0.0682	0.0684	210.60	0.0889	0.0888
193.02	0.0764	0.0765	220.89	0.0974	0.0972
205.18	0.0847	0.0848	230.15	0.1060	0.1058
216.00	0.0932	0.0931	238.52	0.1147	0.1144
225.76	0.1017	0.1016	246.19	0.1234	0.1233
234.53	0.1103	0.1102	253.08	0.1323	0.1322
242.51	0.1191	0.1189	259.30	0.1412	0.1411
249.73	0.1278	0.1278	265.18	0.1501	0.1504
256.31	0.1367	0.1367	270.11	0.1591	0.1588
262.31	0.1456	0.1457	275.05	0.1681	0.1680
267.86	0.1545	0.1549	279.57	0.1771	0.1770
272.95	0.1635	0.1640	283.74	0.1862	0.1860
11.82	0.0036	0.0036	287.88	0.1952	0.1956
37.47	0.0116	0.0116	291.27	0.2044	0.2040
57.80	0.0182	0.0181			

^a In order to analyze these data according to eq 2, values of the methanol monomer pressure were calculated from the total pressure using vapor phase constants for the 1-3-8 model obtained from Tables VII and VIII. It may be noted that the choice of associated species in the vapor phase is not at all critical in the analysis of the solution data since the maximum difference between total pressure and monomer pressure is only about 1% in each instance. Various models for association in the vapor phase lead to essentially the same conclusions concerning the nature of the associated species present in hexadecane. ^b $f_{\text{MeOH}}^{\text{cal}}$ is obtained by calculating monomer pressure, and thus C_A^V , from P_{MeOH} using constants in Tables VII and VIII and then employing eq 2 assuming that only the first, third, and eighth terms are significant.

Table II: RMSD for Several Fits of Methanol in *n*-Hexadecane

Fit	25° RMSD, M	35° RMSD, M	45° RMSD, M
1-2	0.01000 ^a	0.01260 ^a	0.00846
1-3	0.00700	0.00873	0.00552
1-4	0.00452	0.00568	0.00320
1-2-4	0.00271 ^a	0.00345 ^a	0.00200 ^a
1-3-4	0.00218 ^a	0.00274 ^a	0.00163 ^a
1-3-6	0.00102 ^a	0.00129 ^a	0.00072
1-2-8	0.00047	0.00051	0.00062
1-3-8	0.00023	0.00027	0.00018
1-4-8	0.00040	0.00053	0.00040
1-3-9	0.00039	0.00035	0.00036

^a These fits produced a negative parameter.

parameter fits having lower RMSD's the best fits were predominantly those with an eighth-order term present.

One of these, the monomer-trimer-octamer, was statistically superior at each temperature. The constants from the 1-3-8 fit had excellent temperature dependence. The least-squares values of these constants and their standard errors are given in Table III.

Table III: Distribution and Association Constants for Methanol in *n*-Hexadecane

T , °C	K_D	K_3 , M^{-2}	K_8 , M^{-7}
25	8.249 ± 0.025	83.8 ± 1.6	$(1.80 \pm 0.05) \times 10^8$
35	7.070 ± 0.029	42.6 ± 1.1	$(1.84 \pm 0.07) \times 10^7$
45	6.063 ± 0.013	25.4 ± 0.4	$(2.27 \pm 0.05) \times 10^6$

Of the four parameter fits tried, only two (1-2-4-9 and 1-3-4-9) gave lower RMSD's than the 1-3-8 fit but the temperature dependence of the dimer and trimer

Table IV: Thermodynamic Parameters for Methanol in *n*-Hexadecane^a

$$\begin{aligned} \Delta E_D^\circ &= -2.91 \pm 0.01 \text{ kcal/mol}^b & \Delta S_D^\circ &= -7.53 \pm 0.03 \text{ eu} \\ \Delta H_3^\circ &= -11.27 \pm 0.09 \text{ kcal/mol} & \Delta S_3^\circ &= -29.0 \pm 0.3 \text{ eu} \\ \Delta H_8^\circ &= -41.23 \pm 0.08 \text{ kcal/mol} & \Delta S_8^\circ &= -100.5 \pm 0.3 \text{ eu} \end{aligned}$$

^a These quantities are based on standard states of 1 mol/l. ideal solution. ^b Represents energy of solution of one mol of MeOH from the ideal gaseous state to the infinitely dilute solution in *n*-hexadecane.

Table V: Measured (*PL1*, *PS1* and *P2*) and Calculated (*P2C*) Pressures of Methanol Vapor

<i>PL1</i> , Torr	<i>PS1</i> , Torr	<i>P2</i> , Torr	<i>P2C</i> , Torr ^a
15°			
28.902	4.840	20.713	20.727
28.989	5.085	20.855	20.868
39.809	4.749	27.923	27.923
39.974	5.223	28.189	28.192
46.756	5.638	32.822	32.841
46.965	5.481	32.908	32.926
53.448	5.384	37.249	37.222
53.821	4.442	37.183	37.154
61.237	4.864	42.273	42.285
61.183	4.318	42.056	42.065
67.773	5.225	46.854	46.855
68.299	4.447	46.960	46.956
25°			
31.600	4.438	22.372	22.364
31.635	4.694	22.479	22.474
48.888	4.583	33.844	33.848
49.694	3.318	33.955	33.953
67.909	4.973	46.616	46.604
67.963	4.657	46.552	46.533
79.770	1.347	53.292	53.287
79.795	4.429	54.334	54.343
93.930	4.722	63.924	63.915
94.036	2.102	63.092	63.107
105.730	4.201	71.708	71.715
105.764	4.783	71.930	71.932
116.830	4.964	79.554	79.556
116.916	5.138	79.681	79.673
35°			
82.729	5.385	56.609	56.610
85.197	5.164	58.086	58.071
115.257	4.598	77.870	77.893
116.445	5.453	78.990	78.974
136.034	3.999	91.610	91.603
136.385	3.910	91.822	91.809
156.786	4.315	105.863	105.859
157.341	3.456	105.780	105.780
177.863	5.267	120.317	120.334
178.102	6.155	120.786	120.792
198.426	4.971	134.389	134.387
198.656	4.637	134.445	134.436
198.820	1.412	133.482	133.486

^a Apparatus volume ratio (large bulb to total) was 0.65955 ± 0.00003. *P2C* is calculated on the basis of the 1-3-8 model.

constants in these two fits was not satisfactory. The values of the thermodynamic quantities and their standard errors derived from the temperature dependence of the distribution, trimer, and octamer constants are given in Table IV.

PVT Study. Table V presents the observed pressures of methanol over an activity range to approximately 95% of the saturation vapor pressures of methanol at 15, 25, and 35°.

Assuming that all deviations from ideality in methanol vapor are due to specific complex formation, the following expressions may be used to analyze the data.

$$P = P_A + P_{A_2} + P_{A_3} + \dots \quad (4)$$

$$\pi = P_A + 2P_{A_2} + 3P_{A_3} + \dots \quad (5)$$

P is an observed pressure, *P_A*, *P_{A₂}*, and *P_{A₃}* are partial pressures of monomer, dimer, and trimer, etc., and π is a formal pressure (analogous to eq 2 for formal concentration).¹³ With the introduction of formation constants defined as

$$K_n = \frac{P_{A_n}}{(P_A)^n} \quad (6)$$

eq 4 and 5 may be expressed as

$$P = P_A + K_2 P_A^2 + K_3 P_A^3 + \dots \quad (7)$$

$$\pi = P_A + 2K_2 P_A^2 + 3K_3 P_A^3 + \dots \quad (8)$$

The solution of these equations may be accomplished by the use of a nonlinear least-squares treatment utilizing numerical optimum seeking methods.^{14,15} Using assumed values of equilibrium constants and a measured value of initial pressure, eq 7 is solved by an iteration method to obtain a value for the monomer pressure. This monomer pressure and the assumed constants are then used to calculate a formal pressure according to (8). Following this procedure for both initial pressures *PL1* and *PS1* produces two π values which are used with the volume ratio to calculate an expected π value for the system at pressure equilibrium. The calculated final value of π and the assumed association constants are used to calculate a final *P_A* value. This *P_A* value is then used to calculate the final equilibrium pressure. The measured final pressure *P2* and the calculated final pressure *P2C* are then compared. The optimizing procedure continues until the values of the constants produce a minimum in the RMSD. This procedure was carried out assuming first the presence of only one associated species and then assuming the presence of two associated species. Table VI gives RMSD's for several one- and two-parameter fits of the *PVT* data at each

(13) S. D. Christian, H. E. Affsprung, and C. Ling, *J. Chem. Soc.*, 2378 (1965).

(14) S. D. Christian, *J. Chem. Educ.*, 42, 604 (1965).

(15) D. J. Wilde, "Optimum Seeking Methods," Prentice-Hall, Inc., Englewood Cliffs, N. J., 1964.

Table VI: Comparisons of Several Fits in PVT Relationships of Methanol Vapor

Fit	15° RMSD, Torr	25° RMSD, Torr	35° RMSD, Torr
1-2	0.0550	0.0946	0.2175
1-3	0.0298	0.0360	0.0627
1-4	0.0157	0.0230	0.0693
1-2-3	0.0170 ^a	0.0224 ^a	0.0336 ^a
1-2-4	0.0163 ^a	0.0149	0.0178
1-3-8	0.0168	0.0097	0.0121

^a These fits produced a negative dimer constant.

temperature. The initial analysis of data was limited to fourth-order and lower terms since published heat capacity data for alcohol vapors had been treated satisfactorily by a monomer-dimer-tetramer model.⁹ The fact that the 1-2-4 fit gave a negative dimer constant at 15° was somewhat surprising. The unusual 1-3-8 model which best fit the vapor pressure data was then tried on the PVT data. This monomer-trimer-octamer model had no negative constants and led to a substantial decrease in RMSD over the monomer-dimer-tetramer model at 25 and 35°. Table VII

Table VII: Association Constants for Methanol Vapor

T, °C	K ₃ , Torr ⁻²	K ₈ , Torr ⁻⁷
15	(1.20 ± 0.11) × 10 ⁻⁶	(7.6 ± 1.5) × 10 ⁻¹⁷
25	(5.71 ± 0.12) × 10 ⁻⁷	(1.49 ± 0.11) × 10 ⁻¹⁸
35	(2.89 ± 0.03) × 10 ⁻⁷	(3.44 ± 0.19) × 10 ⁻²⁰

presents the least-squares values of the equilibrium constants for the methanol vapor complexes. Table VIII lists the least squares values for ΔH° and ΔS° and

Table VIII: Thermodynamic Parameters for Vapor Phase Association of Methanol^a

$\Delta H_3^\circ = -12.53 \pm 0.12$ kcal/mol	$\Delta S_3^\circ = -44.2 \pm 0.4$ eu
$\Delta H_8^\circ = -67.84 \pm 0.28$ kcal/mol	$\Delta S_8^\circ = -216.9 \pm 0.9$ eu

^a These quantities are based on standard states of 1 atm.

their standard errors for methanol trimers and octamers in the vapor phase.

While the ΔH° values in Tables IV and VIII for the formation of the associated species will not serve as unequivocal indications of the structures of these species, they will be useful for proposing structures to be later tested on other types of data.

The ΔH_8° (vapor) value is unusually large. A larger uncertainty should be attached to this value than to the

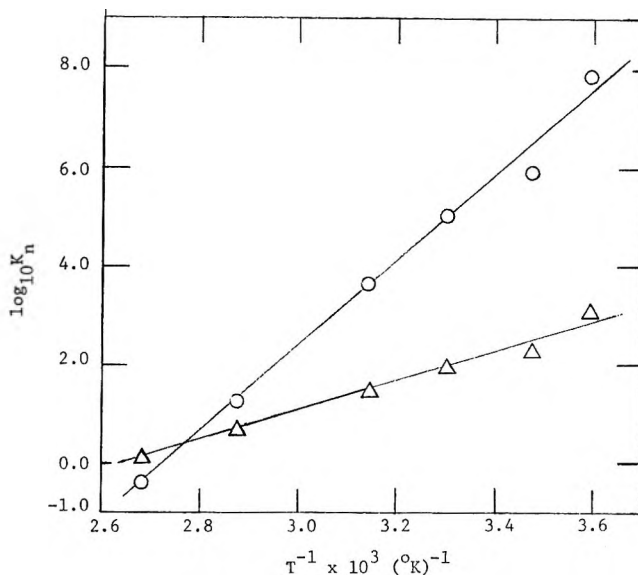


Figure 1. Van't Hoff plot of K_3 (Δ) and K_8 (O) for 1-octanol in *n*-decane.

corresponding value in solution since the amount associated in this form is very small. However, the ΔH_8° value might reasonably be accounted for by assuming a cyclic structure in which each hydroxyl group is involved in two hydrogen bonds. The ΔH_3° (vapor) value might be due to either a cyclic or a linear structure. Since nonlinear hydrogen bonds are not energetically preferred, we suggest that the trimer is probably linear.

The corresponding ΔH_3° value in solution is not greatly different from the vapor phase value, but the ΔH_8° value in solution is much smaller in magnitude than that in the vapor phase.

A smaller value of $-\Delta H_8^\circ$ in solution would be expected, owing to solvation effects,¹⁶ but the magnitude of the difference between the two ΔH_8° values is implausibly large since combination of these two values with the monomer heat of vaporization from solution leads to a negligible calculated value for the heat of vaporization of the octamer from solution.

Tests of Other Data by This Model. The marked statistical superiority of the 1-3-8 model as applied to our data suggested the possibility of using this model to fit published data for alcohol solutions, particularly infrared spectral and nuclear magnetic resonance data.

Analysis of Infrared Data. Fletcher and Heller's experimental data for 1-octanol in *n*-decane in the overtone region were fit to the 1-3-8 model using their method I computer technique⁶ which, except for the method of weighting points, is the same procedure we used in fitting eq 2. Figure 1 shows a van't Hoff plot of the octamer and trimer constants obtained from their 1-octanol data. Table IX gives the least-squares

(16) J. R. Johnson, P. J. Kilpatrick, S. D. Christian, and H. E. Affsprung, *J. Phys. Chem.*, **72**, 3223 (1968).

Table IX: Thermodynamic Parameters for the Association of 1-Octanol in *n*-Decane

$\Delta H_3^\circ = -14.0$ kcal/mol	$\Delta S_3^\circ = -37.2$ eu
$\Delta H_8^\circ = 39.5$ kcal/mol	$\Delta S_8^\circ = -108.0$ eu

Based on standard state of 1 mol/l.

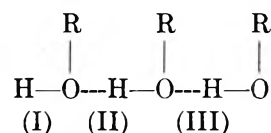
values of ΔH° and ΔS° obtained from the temperature variation of these equilibrium constants. The relative standard deviations of the 1-3-8 fit for 1-octanol are generally larger for the lower temperature data than those for a 1-4 fit. However, in the case of data at 5 and 15°, almost half the experimental points have deviations larger than $\pm 15\%$ from the calculated values for either the 1-4 or the 1-3-8 fit. The individual deviations appear to be nearly randomly distributed about zero and do not seem to vary systematically with concentration as would be expected if the data did not fit the 1-3-8 functional form.

Fletcher and Heller's data in the overtone region were fit using the assumption that the end or "dangling" OH of linear polymers does not absorb at the monomer frequency. We do not know if this assumption is justified. However, there is good evidence that a similar assumption is not applicable to absorbance data for alcohols in the fundamental region.^{17,18}

We wished to apply the 1-3-8 model to absorbance data for alcohols in CCl_4 in the fundamental OH stretching region. We were quite fortunate in obtaining from Dr. E. D. Becker the experimental data which resulted in the publication of ref 19; these consisted of absorbance data for the three alcohols, methyl, ethyl, and *t*-butyl alcohol in CCl_4 , measured over a range of temperature and concentration.

The infrared spectra of numerous alcohol solutions in CCl_4 in the region 3700-3300 cm^{-1} are quite similar. The peak near 3600 cm^{-1} is assigned to the monomer, the peak near 3500 cm^{-1} has ordinarily been assumed to exhibit approximate dimer dependence, and the peak near 3300 cm^{-1} is considered to be due to interior hydroxyl groups in large polymers. (In the following discussion we shall refer to these as the peaks at 3600, 3500, and 3300 cm^{-1} , respectively.) The degree of interference of the "dangling" OH of linear polymers at the monomer peak has often been discussed but few authors have considered this to be a serious problem. The work of Smith and Creitz¹⁷ indicated that for a hindered alcohol (2,4-dimethyl-3-ethyl-3-pentanol) the absorption by this hydroxyl group occurred only a few cm^{-1} from the monomer frequency. Coburn and Grunwald⁵ made a correction for this effect in their work with ethanol in CCl_4 . The recent article by Bellamy and Pace¹⁸ strongly supports the view that the end OH in linear polymers is virtually indistinguishable from the monomer OH. If we assume that the end OH in

linear polymers absorbs at the monomer frequency, an analysis of ir data in the fundamental region according to the 1-3-8 model is easily performed.



The linear trimer above has three different OH groups. We have already assigned OH(I) as absorbing at the monomer frequency. OH(II) should be very little different from the OH groups in the interior of a cyclic polymer and we expect it to absorb at 3300 cm^{-1} . If we assume that all polymers higher than trimer are cyclic and absorb only at 3300 cm^{-1} , we are left with one distinct bond, OH(III), and one major peak to assign. With the assignment of OH(III) as the bond responsible for the 3500- cm^{-1} peak we are now able to determine if the 1-3-8 model will provide a satisfactory fit of infrared spectral data for alcohol solutions in the fundamental hydroxyl stretching region. It may be noted here that the assumptions made above lead us to the same assignments that were made by Smith and Creitz.¹⁷

The absorbance per unit length at the monomeric frequency is expressed as

$$A_{3600} = \epsilon_M^0(C_A + K_3 C_A^3) \quad (9)$$

where we assume the ratio of absorptivities (ϵ^I/ϵ_M^0) for OH(I) and monomeric OH is unity. One might expect that this ratio would actually be somewhat larger than unity but the assumption is probably improved by the fact that OH(I) absorbs at slightly lower frequency than the monomer. The formal alcohol concentration is

$$f_A = C_A + 3K_3 C_A^3 + 8K_8 C_A^8 \quad (10)$$

The solution of these equations is accomplished by the same procedure used to obtain the least-squares values for two association constants in the *PVT* work. Using measured values of A_{3600} and ϵ_M^0 , an initial guess is made of K_3 and K_8 , eq 9 is then solved by an iteration method to give a monomer concentration which is used with K_3 and K_8 to calculate f_A . K_3 and K_8 are changed systematically until the minimum in RMSD is located.

At each of seven temperatures, 1-3-8 and also 1-2-8 fits were tried on Liddel and Becker's data. The experimental results included measurements to formal concentrations of 0.2 for methanol and ethanol and 1.0 for *t*-butyl alcohol. Two series of data for the first two alcohols were used with a combined total of about 16 points at each temperature. Only one set of data on

(17) F. A. Smith and E. C. Creitz, *J. Res. Nat. Bur. Stand.*, **46**, 145 (1951).

(18) L. D. Bellamy and R. J. Pace, *Spectrochim. Acta*, **22**, 525 (1966).

(19) U. Liddel and E. D. Becker, *ibid.*, **10**, 70 (1957).

Table X: RMSD's and Equilibrium Constants for 1-3-8 Fits of Liddel and Becker's Ir Data^a

<i>T</i> , °C	MeOH	EtOH	<i>t</i> -BuOH
-10	0.0048 $K_3 = (3.15 \pm 0.39) \times 10^3$ $K_8 = (1.63 \pm 0.28) \times 10^9$	0.0080 $K_3 = (3.16 \pm 0.65) \times 10^3$ $K_8 = (2.21 \pm 0.60) \times 10^9$	0.0048 $K_3 = (5.88 \pm 0.14) \times 10^3$ $K_8 = (1.59 \pm 0.08) \times 10^9$
	0.0047 $K_3 = (1.71 \pm 0.24) \times 10^3$ $K_8 = (9.4 \pm 1.6) \times 10^7$	0.0066 $K_3 = (1.31 \pm 0.26) \times 10^3$ $K_8 = (1.03 \pm 0.23) \times 10^8$	0.0035 $K_3 = (2.22 \pm 0.05) \times 10^3$ $K_8 = (5.08 \pm 0.22) \times 10^7$
5		0.0056 $K_3 = 84.7 \pm 15.4$ $K_8 = (2.55 \pm 0.46) \times 10^7$	0.0022 $K_3 = (1.34 \pm 0.02) \times 10^3$ $K_8 = (9.70 \pm 0.30) \times 10^6$
10	0.0042 $K_3 = 70.8 \pm 9.8$ $K_8 = (4.71 \pm 0.50) \times 10^6$		
	0.0052 $K_3 = 51.2 \pm 12.8$ $K_8 = (9.7 \pm 2.3) \times 10^6$	0.0046 $K_3 = 33.3 \pm 5.9$ $K_8 = (1.61 \pm 0.18) \times 10^8$	0.0016 $K_3 = 57.2 \pm 0.8$ $K_8 = (5.97 \pm 0.15) \times 10^6$
15	0.0011 $K_3 = 6.21 \pm 0.53$ $K_8 = (1.24 \pm 0.02) \times 10^5$	0.0041 $K_3 = 15.5 \pm 2.9$ $K_8 = (1.36 \pm 0.16) \times 10^8$	0.0024 $K_3 = 25.7 \pm 0.7$ $K_8 = (4.20 \pm 0.19) \times 10^4$
	0.0017 $K_3 = 5.38 \pm 0.54$ $K_8 = (7.6 \pm 1.6) \times 10^3$	0.0037 $K_3 = 6.7 \pm 1.5$ $K_8 = (1.51 \pm 0.50) \times 10^4$	0.0027 $K_3 = 14.0 \pm 0.6$ $K_8 = (4.50 \pm 0.28) \times 10^3$
25	0.0005 $K_3 = 1.23 \pm 0.10$ $K_8 = (2.49 \pm 0.14) \times 10^3$	0.0033 $K_3 = 2.8 \pm 1.0$ $K_8 = (3.5 \pm 1.9) \times 10^3$	0.0033 $K_3 = 8.9 \pm 0.7$ $K_8 = (6.1 \pm 0.5) \times 10^2$

^a All quantities are in molar units.

t-butyl alcohol was taken; there were nine data points at each temperature. None of the data points furnished was omitted. RMSD's and equilibrium constants calculated from Liddel and Becker's ir data for the 1-3-8 model are presented in Table X. The 1-3-8 fit was generally better than the 1-2-8 fit for all three alcohols indicating that an assumed linear trimer rather than a linear dimer is more nearly consistent with the data if the correction is made for absorbance of the nonbonded OH at the monomer peak. With the exception of the methanol trimer constant at 25°, the temperature dependence of these equilibrium constants is good. Van't Hoff plots of the trimer and octamer constants for ethanol are given in Figure 2. Several of the van't Hoff plots for these alcohols show a slight trend toward positive curvature at the two higher temperatures. This is perhaps due to error introduced by assuming the absorptivity ratio to be unity over this temperature range.

Analysis of Nmr Data. In testing the 1-3-8 model on nmr data for alcohol solutions we use assumptions similar to those used for the ir data. We assume the chemical shift for the nonbonded proton of OH(I) in the trimer is the same as that for the monomer proton (δ_1). We assume that the chemical shift for the OH(II) proton is the same as that for protons in the interior of the cyclic polymer (δ_8) and that the proton of OH(III) has a unique shift of δ_3 . These assumptions lead to the expression

$$\delta_{\text{obsd}} = (\delta_1 C_A + (\delta_1 + \delta_3 + \delta_8) K_3 C_A^3 + 8\delta_8 K_8 C_A^8) / f_A \quad (11)$$

where f_A is again formal molar alcohol concentration and δ_{obsd} is the observed chemical shift. Using values of K_3 and K_8 obtained from the temperature dependence of the constants from the ir data we were able to calculate monomer concentrations and fit eq 11 as a

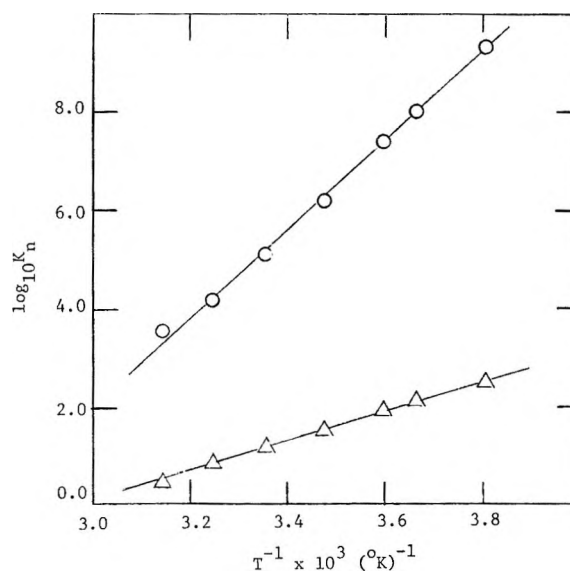


Figure 2. Van't Hoff plot of K_3 (Δ) and K_8 (\circ) for ethanol in CCl_4 .

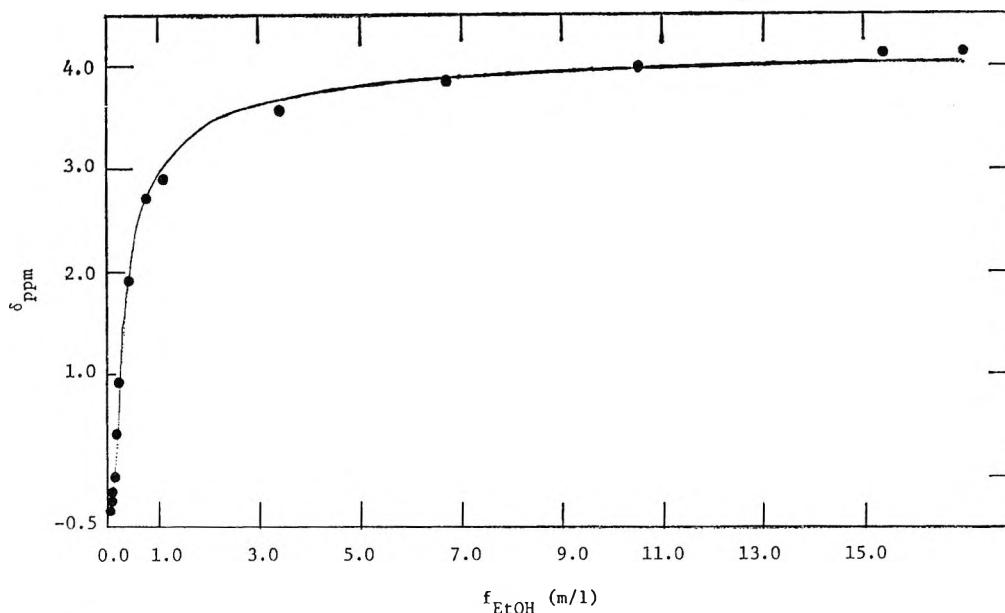


Figure 3. Chemical shift vs. molar concentration for ethanol in CCl_4 at 27° . Points are experimental. Line is calculated with $K_3 = 11.6$ (l./mol) 2 , $K_8 = 10^5$ (l./mol) 2 , and the chemical shift values in Table XI.

three-parameter problem. Several sets of nmr data from the literature were analyzed.²⁰⁻²³

Figure 3 compares the calculated (1-3-8 model) shifts with the experimental chemical shifts for ethanol in CCl_4 at 27° .²¹ The least-squares values of the parameters (δ_1 , δ_3 , and δ_8) are presented in Table XI.

Table XI: Chemical Shifts for Ethanol in CCl_4 from the 1-3-8 Model^a

$\delta_1 =$	-0.41 ± 0.07 ppm
$\delta_3 =$	1.60 ± 0.80 ppm
$\delta_8 =$	4.20 ± 0.05 ppm

^a Shifts are referred to center of methyl resonance.

These data of Becker, Liddel, and Shoolery for ethanol in CCl_4 at 27° and the data of Davis, Pitzer, and Rao for ethanol in CCl_4 at 56° , were the only sets of data which gave values of the parameter δ_3 which appeared reasonable according to the 1-3-8 model, *i.e.*, one which had a value between δ_1 and δ_8 . Perotti's ethanol data and Saunders and Hyne's *t*-butyl alcohol data gave good values for δ_1 and δ_8 but the δ_3 values were outside the expected range. This was also true for Saunders and Hyne's methanol data. This may be in part due to the minor importance of the trimer term but there are serious discrepancies between different sets of published data on the same alcohol. Two sets of nmr data on *t*-butyl alcohol in CCl_4 at 21° show very different concentration dependence.^{20,23} It would appear that new nmr studies on alcohols might be profitably undertaken.

The possibility of a proportionality between ir and

nmr shifts for hydrogen bonded species has been discussed.²⁴ It is interesting to note that the relative distances separating δ_3 and δ_8 from δ_1 in Table XI are quite similar to the separation of the associated bands from the monomer band in the ir fundamental region.

Conclusions

We believe that, in view of the limited precision of present infrared methods and the complexity of infrared spectra of alcohol solutions, assignments of structures to associated species should not be made solely on the basis of spectral data. It should be recognized that even if a particular spectral band has an absorbance which apparently depends on the n th power of the absorbance of the band assigned to the monomer, the associated OH band need not necessarily be attributed to the species A_n . Overlap between the monomer band and the band owing to the unbonded OH of an associated chain polymer should be considered and accounted for in any analysis of association based on absorbance of the free OH.

Fletcher and Heller attempted to describe the properties of alcohol solutions in terms of only two definite associated species. The 1-4 model they propose differs from that of Van Ness, *et al.*, who propose that alcohols largely associate to form linear chains of varying length.²⁵ It is known that simple alcohols

(20) J. C. Davis, Jr., K. S. Pitzer, and C. N. R. Rao, *J. Phys. Chem.* **64**, 1744 (1960).

(21) E. D. Becker, U. Liddel, and J. N. Shoolery, *J. Mol. Spectrosc.*, **2**, 1 (1958).

(22) A. Perotti, *Gazz. Chim. Ital.*, **92**, 1125 (1962).

(23) M. Saunders and J. B. Hyne, *J. Chem. Phys.*, **29**, 1319 (1958).

(24) V. S. Griffiths and G. Socrates, *J. Mol. Spectrosc.*, **21**, 302 (1966).

associate in the solid state to form long chains;¹ however, Pauling²⁶ has suggested that the liquid alcohols may consist largely of ring polymers. This supposition would account for the relatively small heat of fusion of alcohols, inasmuch as the transition from chains in the solid to cyclic aggregates in the liquid would not involve the rupture of hydrogen bonds.

If there exists a general mode of association for alcohols which are not highly hindered, then the most promising method of determining this mode is to develop a model capable of fitting several different types of data for alcohol systems. The task is not a simple one; on the basis of specific types of data, various authors have proposed very different models to account for the behavior of similar or identical alcohol-solvent systems. For example, Fletcher and Heller⁶ conclude from a study of the rate dependence of an alcohol-catalyzed reaction and the infrared spectra of 1-octanol solutions that tetramers are the predominant associated species in alcohol solutions in nonpolar solvents. However, others have claimed that if association is to be explained in terms of a single n -order polymer, an assumed monomer-trimer equilibrium provides a better fit of spectral data. Thus, Saunders and Hyne²³ have employed a 1-3 model to fit nmr data for both phenol and *t*-butyl alcohol solutions in CCl₄ and Storek and Kriegsmann²⁷ have recently confirmed the superiority of the 1-3 model in fitting nmr data for *t*-butyl alcohol in CCl₄. Fletcher and Heller's treatment of data for phenol in CCl₄ leads to a 1-3-4 fit in which the trimer is a considerably more important species than the tetramer. 1-3 and 1-4 fits of Liddel and Becker's infrared data for *t*-butyl alcohol (in which the absorbance near 3600 cm⁻¹ is assumed to be due solely to monomer) give an RMSD ratio (1-4/1-3) ranging from 2.0 at 45° to 6.0 at -10°. (We do not mean to imply here that we prefer the monomer-trimer model for *t*-butyl alcohol solutions; infrared data indicate the presence of at least two associated species and the 1-3-8 model provides a better fit than any 1- n model.)

The 1-3-8 model proposed here appears to be more generally applicable to several types of data for a number of alcohols than any proposed previously. It should be tested further with data for numerous types of compounds, including aromatic compounds such as phenols and benzyl alcohol and certain of the sterically hindered alcohols which probably do not associate beyond the trimer. If only monomer-trimer equilibrium need be considered, one would predict the presence of an absorption band near 3300 cm⁻¹ for which the absorbance increases linearly with that of a second polymer band near 3500 cm⁻¹.

Vapor pressure data provide a more severe test of an association model for alcohols than do nmr or infrared

spectral data; note that the RMSD values in Table II for the best of the 1- n fits are all more than a factor of 10 larger than the RMSD of the 1-3-8 fit at all temperatures. In spectral analysis, the incorporation of associated species into a model invariably leads to the introduction of unknown parameters in addition to the formation constants for the various aggregates (*e.g.*, chemical shifts in the case of nmr data, absorptivities in infrared studies). On the other hand, in the analysis of vapor pressure data such as those presented for the methanol-*n*-hexadecane system, the only unknown which arises in addition to the formation constants of the polymers is the distribution ratio for the monomer, K_D . We have shown that the 1-3-8 model is capable of correlating vapor pressure data for methanol in *n*-hexadecane, *PVT* data for methanol vapor, infrared spectra for methyl, ethyl, and *t*-butyl alcohol in CCl₄ and infrared spectra for 1-octanol in *n*-decane. Assumptions have been made about the nature of the three major hydroxyl-stretching peaks in the fundamental infrared region in order to analyze the data with the 1-3-8 model; the readily available spectral data are in accord with these assumptions. The proposed model promises to give a quantitative explanation of the observed chemical shift data for alcohols, although previously reported nmr measurements are not highly consistent with one another.

Finally, it should be mentioned that in proposing models involving a limited number of associated species to correlate the properties of hydrogen-bonding systems, one must admit that other species may be present at levels of concentration to which the physical methods employed are not sensitive. Thus, our interpretation of the available vapor pressure, *PVT*, and spectral data is that the population distribution of polymeric alcohol species A_n is sharply peaked at $n = 3$ and $n = 8$. To simplify the mathematical treatment and to avoid the introduction of additional parameters, the analysis includes only the trimer and the octamer. Methods more sensitive than those available at present will be required to justify the inclusion of a greater number of polymeric species in the association model.

Acknowledgments. This work was supported in part by a grant (14-01-0001-1315) from the Office of Saline Water, Department of the Interior. S. B. F. wishes to express his appreciation for a traineeship (NsG[T]-36) from the National Aeronautics and Space Administration. The authors wish to thank Dr. E. D. Becker for providing copies of infrared data.

(25) R. W. Haskell, H. B. Hollinger, and H. C. Van Ness, *J. Phys. Chem.*, **72**, 4534 (1968).

(26) L. Pauling, "The Nature of the Chemical Bond," Cornell University Press, Ithaca, N. Y., 1960.

(27) W. Storek and H. Kriegsmann, *Ber. Bunsenges. Phys. Chem.*, **72** (6), 706 (1968).

The Thermal Decomposition of Perfluorocyclobutane in a Single-Pulse Shock Tube^{1a}

by J. M. Simmie,^{1b} W. J. Quiring,^{1c} and E. Tschuikow-Roux

Department of Chemistry, University of Calgary, Calgary, Alberta, Canada (Received April 2, 1969)

The thermal decomposition of perfluorocyclobutane was studied between 1100 and 1265°K behind reflected shock waves in a modified single-pulse shock tube using dilute *c*-C₄F₈-Ar mixtures. Reflected shock temperatures were evaluated from the Rankine-Hugoniot equations using measured incident and reflected shock velocities. Analyses were carried out by mass spectrometry and gas chromatography. The observed reaction product was almost exclusively C₂F₄ except at the highest temperatures where small amounts of C₃F₆ were also observed. The principal process involves the unimolecular decomposition, *c*-C₄F₈ → 2C₂F₄. The first-order high-pressure rate constant was found to be $k^{\infty} = 10^{16.0 \pm 0.6} \exp[(-75,500 \pm 3000)/RT] \text{sec}^{-1}$ in good agreement with previous low temperature data obtained in a static system.

Introduction

The thermal decomposition of perfluorocyclobutane has been reported previously by several investigators.²⁻⁴ In a careful study carried out in a static system over the temperature range 633-833°K, Butler⁴ has shown that at pressures above 10 Torr the homogeneous unimolecular reaction *c*-C₄F₈ → 2C₂F₄ is in its high-pressure limit, with a first-order rate constant given by $k_{\text{uni}}^{\infty} = 10^{16.0 \pm 0.2} \exp[(-74,300 \pm 800)/RT] \text{sec}^{-1}$. This result is consistent with the earlier work of Atkinson³ and Trenwith^{2a} who studied this reaction over the narrow temperature range of 793-863°K. More recently, the pyrolysis of *c*-C₄F₈ has also been investigated from 1040 to 1200°K by Lifshitz, *et al.*,⁵ using a single-pulse shock tube. Although the authors claimed general agreement with the earlier report,⁴ a reexamination of their data shows such a large degree of scatter that their reported activation energy and pre-exponential factor could only be derived by extrapolation of Butler's low-temperature data (see Discussion). Inasmuch as the chemistry of the *c*-C₄F₈ ⇌ 2C₂F₄ system is of considerable practical importance, a reinvestigation of the thermal decomposition of perfluorocyclobutane at elevated temperatures seemed to be indicated.

Despite the apparent success of the single-pulse shock-tube (SPST) technique in a number of reported cases, the literature contains sufficient examples in which the kinetic SPST data either depart significantly from extrapolated lower temperature results obtained by conventional static methods or, at best, show a large degree of scatter. Over the past few years, evidence has accumulated of severe departures from ideal flow conditions in shock tubes.⁶ The importance of real flow in certain cases has prompted Strehlow⁶ to question the validity of SPST investigations in general and led to his assertion that this technique is virtually

useless for quantitative studies. Therefore, another purpose of this investigation was to reexamine the SPST technique as applied to problems in chemical reaction kinetics with the intent of answering two basic questions: is this technique applicable at all, and, if so, what are the optimum conditions? The gas dynamic aspects of this study will be reported in a more appropriate journal.⁷ Here we present data on the unimolecular dissociation of perfluorocyclobutane to tetrafluoroethylene in a modified^{8,9} SPST over the temperature range 1100-1265°K. Since satisfactory agreement with the low-temperature results of static systems was obtained, we feel this investigation may provide a working criterion for future SPST chemical kinetic studies.

Experimental

Apparatus. The shock tube was of the modified ball-valve type design⁸ and was constructed from polished brass tubing of 4.9 cm i.d. The general design was similar to that described previously,⁹ except that the single-pulse action was derived from a damping tank as described by Lifshitz, *et al.*¹⁰ The latter consisted

(1) (a) Work supported by the National Research Council of Canada; (b) National Research Council Postdoctorate Fellow, 1968-1970; (c) Graduate Fellow.

(2) (a) B. Atkinson and A. B. Trenwith, *J. Chem. Soc.*, 2082 (1953); (b) B. Atkinson and V. A. Atkinson, *ibid.*, 2086 (1957).

(3) B. F. Gray and H. O. Pritchard, *ibid.*, 1002 (1956).

(4) J. N. Butler, *J. Amer. Chem. Soc.*, **84**, 1393 (1962).

(5) A. Lifshitz, H. F. Carroll, and S. H. Bauer, *J. Chem. Phys.*, **39**, 1661 (1963).

(6) R. A. Strehlow, "A Review of Shock Tube Chemistry," Technical Report AAE 68-1, University of Illinois, 1968.

(7) E. Tschuikow-Roux, J. M. Simmie, and W. J. Quiring, *Astronaut. Acta*, submitted for publication.

(8) E. Tschuikow-Roux, *Phys. Fluids*, **8**, 821 (1965).

(9) E. Tschuikow-Roux and J. E. Marte, *J. Chem. Phys.*, **42**, 2049 (1965); *Erratum*, **43**, 1438 (1965).

(10) A. Lifshitz, S. H. Bauer, and E. L. Resler, Jr., *J. Chem. Phys.*, **38**, 2056 (1963).

of a stainless steel tank of 32.2 l. volume which was located 10 cm downstream from the diaphragm. Both channel and driver sections were of variable lengths but for most runs were set at 4.2 and 1.8 m, respectively. Prescored aluminum diaphragms of 0.15-mm thickness were used. Typical driver (helium) and driven (argon) gas pressures were of the order of 3600 and 150 Torr, respectively. Incident and reflected shock velocities were measured by recording the transit times of the incident and reflected shocks across two high-frequency pressure transducers (Kistler, Model 603A/623F) located 10 and 20 cm, respectively, from the end plate. The output from the transducers was amplified (Kistler, Model 566) and split-fed to two universal counters with 0.1- μ sec resolution (Hewlett-Packard, Model 5325A) and to a single-sweep photographic recording oscilloscope (Tektronix, Model 535A with CA plug-in). The latter provided a measure of the reaction dwell times and cooling rates. A more detailed description of the apparatus and mode of operation is given elsewhere.⁷

Materials. Perfluorocyclobutane was obtained from the Matheson Co. and purified by a freeze-pump-thaw technique and subsequently by trap-to-trap distillation. Tetrafluoroethylene was prepared by heating shavings of polytetrafluoroethylene (Teflon) *in vacuo* and purified in the same manner. The purity of the fluorocarbons was ascertained by vapor-phase chromatography using a silica gel column. Reaction mixtures of 1% perfluorocyclobutane in argon (Matheson, 99.998% stated purity) were prepared in a 35-l. stainless steel tank and allowed to mix thoroughly prior to use.

Analysis. Immediately after completion of a shock, the ball valve was closed to isolate the reaction products in the end section of the shock tube. A sample of the fully mixed gases was taken and analyzed by mass spectrometer (A. E. I. Ltd., Model MS-10). The product to reactant ratio, $[C_2F_4]/[c-C_4F_8]$, was determined by measuring the $81^+/131^+$ *m/e* peak height ratio using suitable calibration curves constructed for this purpose. The latter were checked at frequent intervals with synthetic standard mixtures.

Calculations

Temperature. Reflected shock temperatures were calculated from *measured* incident and reflected shock velocities using relations derived directly from the Rankine-Hugoniot equations

$$W_{ji} = [\beta(1 + \alpha P_{ji})]^{1/2}$$

$$T_{ji} = P_{ji}(\alpha + P_{ji})/(1 + \alpha P_{ji})$$

where W_{ji} is the shock Mach number, α and β are functions¹¹ of the heat capacity ratio $\gamma = c_p/c_v$, and T_{ji} and P_{ji} are dimensionless temperature and pressure (*i.e.*, $T_{ji} = T_j/T_i$). The subscripts denote regions across the shock front and are given by $i = 1, j = 2$

for the incident shock and $i = 2, j = 5$ for the reflected shock where the notation is that of Glass.¹¹ Since W_{22} is not determined directly, transformation from shock fixed to laboratory coordinates is achieved through

$$W_{21} = W_{22}A_{21} - U_{21}$$

where A_{21} ($= T_{21}^{1/2}$) is the relative velocity of sound, $U_{21} = (P_{21} - 1)/\gamma W_{11}$ is the fluid velocity behind the incident shock relative to the speed of sound (a_1) of the undisturbed gas ahead of the shock, and $W_{21} = v_r/a_1$ is the reflected shock Mach number, with v_r being the measured reflected shock velocity. With these equations T_{52} and T_{21} are readily evaluated and $T_5 = T_{52}T_{21}T_1$.

It is important to note that the above method of evaluating the reflected shock temperature makes no reference to any assumption concerning the particle velocity, u_5 , behind the reflected shock.

Although it is possible to compute reflected shock temperatures from either the incident or the reflected measured shock velocities, these methods of evaluation require the boundary condition of perfect shock reflection, *i.e.*, $u_5 = 0$. Our study has shown that this condition is not strictly obeyed, and leads to significant differences in computed temperatures, T_5 , and hence to severe errors in the temperature dependence of rate constants. It may be further noted, that a fourth method based on measured incident and reflected shock velocities and subject to $u_5 = 0$ compounds the error. The various methods for evaluating the reflected shock temperatures based on shock velocities have been reviewed critically and are discussed elsewhere.⁷

The decomposition $c-C_4F_8 \rightarrow 2C_2F_4$ is endothermic^{5,12} by 49.4 kcal mol⁻¹ which will cause a decrease in T_5 . For dilute (1%) mixtures of $c-C_4F_8$ in argon, this temperature drop will be small, but generally not negligible in conventional SPST studies. However, in the modified SPST equipped with a ball valve, the reactant sample is compressed to a thin slab of thickness $l = (T_{51}/P_{51})l_0$ where l_0 is the length of the bore of the ball in the ball valve. In our experiments $l \approx 15$ mm. This slab is surrounded by a large heat reservoir of inert gas (pure argon) at temperature T_5 , and therefore the effect of the endothermicity of the reaction is minimized. Calculations have shown that the resultant temperature drop was within experimental error and could therefore be neglected. It is for this reason also that the assumption of a constant γ is justified in the modified SPST.

Rate Constants. Rate constants were evaluated from the measured product/reactant ratios on the basis of the first-order rate law

(11) I. I. Glass, "Shock Tubes," University of Toronto Institute of Aerophysics, UTIA Review No. 12, Part 1 (1958).

(12) H. C. Duus, *Ind. Eng. Chem.*, **47**, 1445 (1955).

$$k^{\infty} = (1/t_d) \ln (1 + [C_2F_4]/2[c-C_4F_8])$$

The reaction dwell time, t_d , was calculated from microsecond counter and oscilloscope trace readings using the method of ref 8. Through a suitable choice of shock tube geometry and ball valve location, the measured "transducer dwell times," t_d' , were made to correspond closely to t_d , *i.e.*

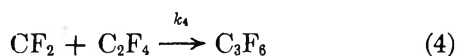
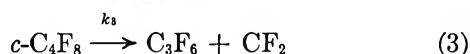
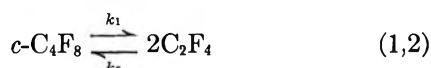
$$t_d = t_d' + (X_D - X_T)(W_{21}^{-1} + A_{51}^{-1})(L/a_1)$$

where X_D and X_T are, respectively, the positions⁸ of the reactive "sandwiched" gas and the transducer in question, both normalized with respect to the length of the driver section L . All computations were carried out with the aid of an IBM 360 electronic computer.

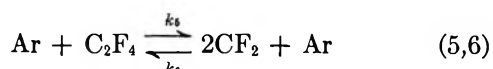
Cooling rates by the expansion fan were estimated⁸ from the slopes of oscilloscope traces to be of the order of 3×10^5 °K sec⁻¹. Thus, in view of the reasonably high activation energy of ~75 kcal and the uncertainty in reading the slopes from photographs, the effect of a finite cooling rate during the quenching process was neglected.

Results and Discussion

The pyrolysis of $c-C_4F_8$ in a single pulse shock tube at temperatures 1100–1265°K and total pressures in the range 2500–3100 Torr yields C_2F_4 as the principal reaction product. At the highest temperatures, trace amounts of perfluoropropene were also observed. This would appear to be consistent with the mechanism proposed by Butler⁴



However, using literature values for the relevant rate constants (Table I), it can be readily shown that under the experimental conditions reported here, the rate of dimerization of C_2F_4 , reaction 2, relative to its reverse, reaction 1, is totally negligible at 1254°K and for maximum conversion of $c-C_4F_8$ with $R_2/R_1 < 10^{-3}$. The rate of the parallel dissociation of C_4F_8 to yield C_3F_6 , R_3 , is less than 10% of R_1 (and probably even less as our results would indicate) at the highest temperature of 1265°K and even smaller at the lower temperatures. Reaction 4 is slow, if it occurs at all. This follows from the shock-tube work of Modica and LaGraff,¹³ who studied the thermal decomposition of C_2F_4 at 1200–1300°K using a time-resolved spectroscopic detection technique. Although the latter authors apparently did not analyze for C_3F_6 , their results indicate that the reaction



is reversible. Using their rate constant k_5 (Table I), it can be shown that at our maximum conversion of 38% and 1254°K, reaction 5 becomes important, with $R_5/R_1 \approx 2.3$. Therefore, if reaction 4 were operative one would expect the formation of C_3F_6 or its decomposition products¹⁴ at the expense of C_2F_4 . The latter is not observed; hence, we conclude that CF_2 exists in equilibrium¹³ with C_2F_4 . The dominant measured reaction in the present study is, therefore, simply the scission of perfluorocyclobutane to give tetrafluoroethylene

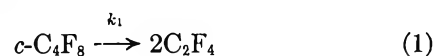


Table I: Arrhenius Rate Parameters

	Log A	E_a , kcal mol ⁻¹	Ref
k_1 , sec ⁻¹	16.0 ± 0.2	74.3 ± 0.8	a
	15.95	74.1	b
	16.32	74.3	c
	13.5 ± 0.9	58.7 ± 4.7	d
	16.1 ± 0.6	75.5 ± 3.0	e
k_3 , sec ⁻¹	17.2 ± 2.4	87.0 ± 8.0	a
	16.59	79.0	f
	11.01	25.4	b
k_2 , cm ³ mol ⁻¹ sec ⁻¹	10.4 ± 0.7	24.0 ± 2.5	a
	11.07 ± 0.03	25.64 ± 0.09	g
	11.22	26.3	h
	15.89 + 1/2 log T	55.69	i

^a Reference 4. ^b Reference 2a. ^c Reference 5. ^d Data of ref 5 recalculated. ^e This work. ^f Reference 2b. ^g G. A. Drennan and R. A. Matula, *J. Phys. Chem.*, **72**, 3462 (1968). ^h J. Lacher, G. Tompkin, and J. Park, *J. Amer. Chem. Soc.*, **74**, 1693 (1952). ⁱ Reference 13; k_5 was reported in the simple collision theory form.

Butler⁴ has shown that at pressures above 10 Torr the rate constant k_1 has attained its high-pressure limiting value. Since the mole fraction of $c-C_4F_8$ in argon in this study was 0.01 it follows that at total pressures of ~3000 Torr behind the reflected shock the partial pressure of $c-C_4F_8$ ranged from ~30 to 14 Torr corresponding to conversions from ~0.7 to 38%. Therefore, the first-order rate constants reported here are high-pressure limiting values.

The rate constants and pertinent shock-tube parameters are given in Table II. The temperature dependence of the rate constants is shown in Figure 1. The present data are denoted by open circles and the solid line is a least-squares fit. From the slope and intercept we obtain the Arrhenius expression

$$k^{\infty} = 10^{16.1 \pm 0.6} \exp[(-75,500 \pm 3000)/RT] \text{ sec}^{-1}$$

The dashed line represents an extrapolation of Butler's⁴

(13) A. P. Modica and J. E. LaGraff, *J. Chem. Phys.*, **43**, 3383 (1965).

(14) R. A. Matula, *J. Phys. Chem.*, **72**, 3054 (1968).

Table II: Experimental Results

Mach number		P_5 , Torr	T_5 , °K	t_d , μsec	$[C_2F_4]$ [<i>c</i> -C ₄ F ₈]	k_1^∞ , sec ⁻¹
W_{11}	W_{21}					
2.114	1.240	2536	1103	549	0.0141	12.8
2.128	1.246	2608	1119	500	0.0262	26.0
2.133	1.238	2639	1122	591	0.0286	35.0
2.151	1.246	2675	1133	587	0.0354	29.9
2.198	1.260	2828	1176	650	0.109	81.7
2.195	1.249	2793	1168	557	0.110	96.1
2.221	1.268	2937	1198	547	0.158	139
2.225	1.268	2968	1201	106	0.0363	170
2.228	1.265	2969	1215	492	0.474	433
2.251	1.274	3025	1231	622	0.670	465
2.265	1.274	3065	1239	599	0.910	626
2.260	1.282	3072	1238	335	0.503	670
2.272	1.274	3089	1254	490	1.246	989
2.278	1.281	3127	1265	469	1.178	989

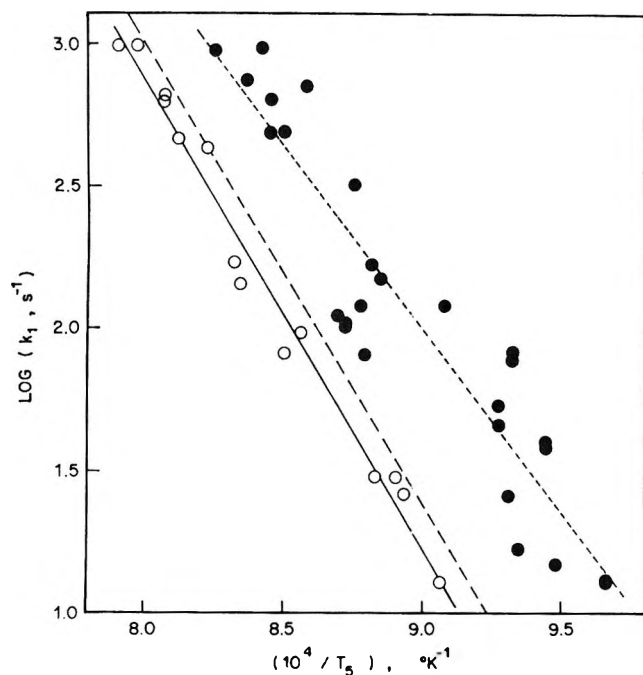


Figure 1. Temperature dependence of the rate constants: open circles, this study; filled circles, ref 5; dashed line, extrapolated data of ref 4.

expression for k^∞ determined over the temperature range 360–560°. We consider the agreement as very satisfactory considering that an extrapolation of over 5 powers of 10 in the rate constant is required.

Also shown in Figure 1 are the data of Lifshitz, *et al.*⁵ (filled circles). Although the latter authors claimed agreement with Butler's results within a factor of 2 in the preexponential factor, the large scatter of their data was obscured by the very wide temperature range (625–1250°K) of their Arrhenius plot. A least-squares analysis of their tabulated data (dotted line) yields the expression

$$k^\infty = 10^{13.5 \pm 0.9} \exp[-58,700 \pm 4700]/RT \text{ sec}^{-1}$$

which is in severe disagreement with Butler's results and those reported here. We believe this to be an example of the inadequacy, in part, of the conventional SPST technique, and one which supports the conclusions reached by Strehlow.⁶ The discrepancy appears to be particularly serious in view of the fact that Lifshitz, *et al.*,⁵ used measured incident shock velocities to compute their temperatures. As has been pointed out above, our study⁸ has shown that this method of evaluating the reflected shock temperature may lead to somewhat higher values than the true temperature, and hence result in a shift of the kinetic data to the left along the $1/T$ axis in Figure 1. Thus, the actual departure of the results of Lifshitz, *et al.*,⁵ from those of Butler may be even greater than is indicated in Figure 1.

The relatively high preexponential factor observed in the thermal decomposition of *c*-C₄F₈ may be associated with a high positive entropy of activation which, in turn, may be associated with a relatively loose cyclic transition state in which two opposite C–C bonds undergo an extension. Such a transition state has been postulated by Genaux, *et al.*,^{15,16} in their study of the thermal decomposition of cyclobutane, for which the first-order rate constant is given by $k^\infty = 4.0 \times 10^{15} \exp[-62,000/RT] \text{ sec}^{-1}$. The preexponential factor of the perfluoro compound is expected to be larger, in part, because of higher moments of inertia.⁵ A similar trend has been observed in the case of hexafluoroethane¹⁷ and its hydrocarbon analog. The activation energy in the totally fluorinated compounds also appears to be higher than in the corresponding hydrocarbon.¹⁷

(15) C. T. Genaux, F. Kern, and W. D. Walters, *J. Amer. Chem. Soc.*, **75**, 6196 (1953).

(16) A. Maccoll and P. J. Thomas, *Progr. Reaction Kinetics*, **4**, 119 (1967).

(17) E. Tschuikow-Roux, *J. Chem. Phys.*, **43**, 2251 (1965).

Electron Spin Resonance of Transient Alkyl Radicals during Alkylolithium-Alkyl Halide Reactions

by Hanns Fischer¹

Radiation Research Laboratories, Mellon Institute, Carnegie-Mellon University, Pittsburgh, Pennsylvania 15213
(Received April 2, 1969)

Transient alkyl radicals have been observed at room temperature during reactions of several alkylolithium compounds with various alkyl halides in solution. Radical structures and concentrations indicate that the reactions proceed *via* free-radical mechanisms. The room temperature hyperfine coupling constants of the radicals are discussed. Furthermore, it is suggested that an explanation of nuclear polarization during these and other reactions by the simple mechanism of chemically induced dynamic nuclear polarization derived previously is at least in part, if not generally, inadequate.

Introduction

It has been suggested that the reactions of alkylolithium compounds with alkyl halides are more likely to involve transient alkyl radicals as reaction intermediates than carbanions and carbonium ions.²⁻⁵ This suggestion has been derived from chemical evidence^{2,3} and from the observation of nuclear polarization in the nmr spectra of reaction products,^{4,5} and it is strongly supported by this report of direct electron spin resonance (esr) detection of the alkyl radical intermediates.

Experiments and Results

Because of the high reaction rates, a flow system was used. The solutions of alkylolithium compounds in hydrocarbons (Alfa Inorganics, Beverly, Mass.) were mixed with alkyl halide solutions at room temperature in a mixing chamber of simple design⁶ immediately before entering an observation tube (cylindrical 3 mm i.d. or flat 0.4×3 mm² inner cross section) which leads through the cavity of a previously described esr spectrometer.⁷ Infusion pumps (Harvard Apparatus Co., Dover, Mass.) were used to drive the solutions from syringes through the flow cell. The flow rates were varied from 1.4×10^{-3} to 1.4×10^{-1} cm³/sec. They corresponded to times between mixing and observation of 0.8 to 80 sec for the cylindrical and of 0.36 to 36 sec for the flat cell. Ether was added to the halide or to the alkylolithium solutions before reaction to uncomplex the alkylolithium hexamers.⁸ Removal of oxygen from the reactants seemed not to affect the resolution and the intensities of the observed spectra. To avoid warmup of the samples during the reactions, compressed air was blown through the cavity of the esr spectrometer. The spectra shown and the hyperfine coupling constants listed below refer to sample temperatures of $26 \pm 3^\circ$.

In general, radical concentrations increased with increasing flow rates, alkylolithium, alkyl halide, and ether concentrations. If not otherwise specified, the

esr spectra were, however, taken with a fixed concentration of alkylolithium in alkane of 1.8 or 2.3 *M*, a concentration of alkyl halide in a 6:1 benzene-diethylether mixture of 0.5 to 0.8 *M*, and flow rates of 7.7×10^{-3} cm³/sec for the alkylolithium and 1.9×10^{-2} cm³/sec for the alkyl halide solutions which correspond to a time of 4.0 sec between mixing and observation for the cylindrical cell. Under these conditions radical concentrations of 10^{-6} to 10^{-5} *M* were obtained for most systems as estimated from comparison of esr line intensities with those of galvinoxyl solutions of known concentrations. Because of experimental difficulties from lithium halide precipitation, gas evolution, and warmup during the reactions, conditions which would lead to higher radical concentrations could not be used in quantitative measurements.

Figure 1 (upper part) shows the esr spectrum of the isopropyl radical, $(\text{CH}_3)_2\dot{\text{C}}\text{H}$, during the reaction of isopropylolithium with isopropyl bromide, obtained with the standard reaction conditions. In the lower part of Figure 1 the second-order structure of some of the lines of isopropyl is resolved. When isopropyl bromide was replaced by cyclopentyl bromide, the spectrum of Figure 2 was obtained. It demonstrates the simultaneous presence of isopropyl and cyclopentyl radicals in concentrations of the same order of magnitude.

Similarly intense esr spectra as those in Figures 1

(1) On leave from Technische Hochschule and Deutsches Kunststoff-Institute, 61 Darmstadt, Germany. Correspondence should be sent to this address.

(2) D. Bryce-Smith, *J. Chem. Soc.*, 1603 (1956).

(3) K. A. Bilevitch, N. N. Bubnov, and O. Yu. Okhlobystin, *Tetradron Let.*, 3465 (1968).

(4) H. R. Ward and R. G. Lawler, *J. Amer. Chem. Soc.*, **89**, 5518 (1967).

(5) A. R. Lepley, *ibid.*, **40**, 2710 (1968).

(6) W. T. Dixon and R. O. C. Norman, *J. Chem. Soc.*, 3119 (1963).

(7) R. W. Fessenden, *J. Chem. Phys.*, **48**, 3725 (1968).

(8) G. W. Gibson and J. F. Eastham, *J. Amer. Chem. Soc.*, **85**, 2171 (1963).

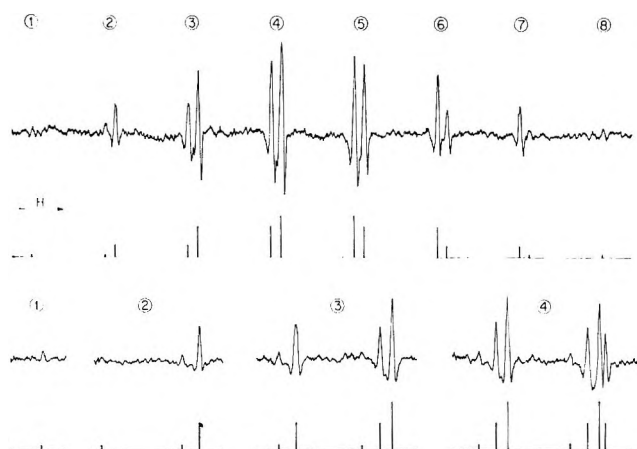


Figure 1. ESR spectrum of the isopropyl radical during the reaction of isopropyl lithium (1.86 M in n -pentane) with isopropyl bromide (0.66 M in a 6:1 benzene-diethyl ether mixture). The individual flow rates were 0.46 cm^3/min for the alkyllithium and 1.14 cm^3/min for the alkyl halide solutions. Lower part: second-order structure of some esr lines of isopropyl (second derivative presentation).

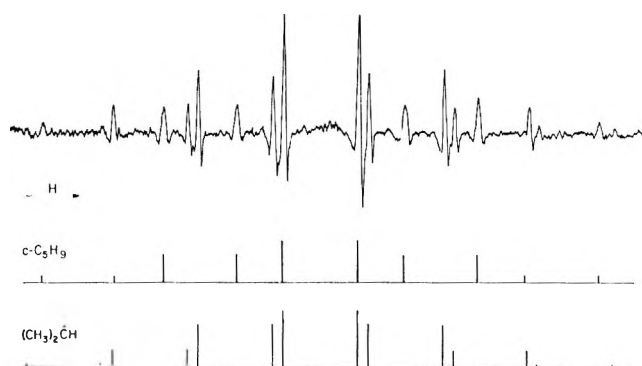
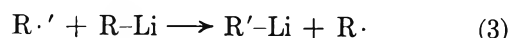


Figure 2. ESR spectrum of isopropyl $(\text{CH}_3)_2\dot{\text{C}}\text{H}$ and cyclopentyl $c\text{-C}_5\text{H}_9$ radicals during the reaction of isopropyl lithium with cyclopentyl bromide (second derivative presentation).

and 2 were also obtained from reactions of isopropyl lithium with ethyl chloride, bromide, and iodide, with n -propyl, n -butyl, n -pentyl, sec -butyl, and t -butyl bromides, from reactions of sec -butyllithium with methyl, ethyl, isobutyl, sec -butyl, t -butyl, and 3-ethyl- n -butyl bromides, and from reactions of t -butyllithium with t -butyl bromide. In all these cases, the radicals observed were those expected from a radical formation reaction



In most cases, the concentration ratio of the two radicals $\text{R}\cdot$ and $\text{R}'\cdot$ did, however, deviate from unity. So, for instance, the ratios of $\text{R}'\cdot$ and $\text{R}\cdot$ were 0.30, 0.4, 0.1, 0.8, and 1.2 for the reactions of ethyl, n -propyl, isobutyl, t -butyl, and sec -butyl bromide with isopropyl lithium. This demonstrates the occurrence of exchange reactions which lead to halogen-lithium inter-



conversions,⁹ and which have been found to proceed *via* free radical intermediates by other authors also.¹⁰⁻¹³

Under the standard reaction conditions, no free radicals were detected during reactions of methyl-, ethyl-, n -butyl-, and phenyllithium compounds presumably because of low reaction rates. A low intensity esr spectrum of the n -butyl radical which corresponded to a radical concentration of $(3 \pm 1) \times 10^{-6} M$ could however be observed during the reaction of n -butyllithium (2.25 M in n -hexane) with n -butyl bromide (0.65 M in dimethoxyethane) using the flat cell and flow rates of $1.6 \times 10^{-2} \text{ cm}^3/\text{sec}$ for the n -butyllithium and $3.9 \times 10^{-2} \text{ cm}^3/\text{sec}$ for the n -butyl bromide solutions. Under these conditions the time between mixing and observation was about 1 sec.

The dependence of radical concentrations on the reaction conditions was studied in some detail for the isopropyl lithium-isopropyl bromide reaction. For a constant molar ratio of isopropyl lithium and diethyl ether the radical concentration increased linearly with the square roots of the isopropyl lithium and isopropyl bromide concentrations, and for constant isopropyl lithium and isopropyl bromide concentrations it increased approximately linearly with the square root of the diethyl ether concentration as long as the molar ratio was lower than 0.5. For higher diethyl ether concentrations only a very slight further increase was observed. In one experiment, the dependence of radical concentrations on flow conditions was also studied. For an isopropyl lithium concentration of 1.86 M , an isopropyl bromide concentration of 0.25 M , a diethyl ether-isopropyl lithium ratio of 1.3, and a ratio of flow rates of 0.4 for the isopropyl lithium and the isopropyl bromide solutions an exponential decrease of radical concentration with time between mixing and observation was found in the time range from 1 to 80 sec. The apparent time constant was 35 sec.

These results support the validity of eq 1 since ether complexes of alkyllithium dimers are known to react.⁸ They further show that quasi-steady-state conditions for radical concentrations apply in this as in other flow systems,¹⁴ so that the radical concentrations are given by

$$[\text{R}\cdot] = (I/2k_t)^{1/2} \quad (4)$$

where I is the rate of radical formation from eq 1 and $2k_t$ is the rate constant for the radical termination reactions. Equation 4 now provides a means for compari-

(9) D. R. Applequist and D. F. O'Brien, *J. Amer. Chem. Soc.*, **85**, 743 (1963).

(10) H. R. Ward, R. G. Lawler, and R. A. Cooper, *ibid.*, **91**, 746 (1969).

(11) A. R. Lepley and R. L. Landaw, *ibid.*, **91**, 748 (1969).

(12) A. R. Lepley, *ibid.*, **91**, 749 (1969).

(13) A. R. Lepley, *Chem. Commun.*, **2**, 64 (1969).

(14) H. Fischer, *Makromol. Chem.*, **98**, 179 (1966).

Table I: Coupling Constants of the Observed Alkyl Radicals^a

Radical	T, °C	a_{α} , G	a_{β} , G	Ref
CH ₃	RT ^b	22.7 ± 0.10		This work
	20	22.68		19
	-220	23.04		16
CH ₃ -CH ₂ ·	RT	22.13 ± 0.04	26.84 ± 0.04	This work
	-180	22.39	26.81	16
CH ₃ -CH ₂ -CH ₂ ·	RT	21.89 ± 0.04	28.39 ± 0.05	This work
	-105	22.14	30.33	18
	-180	22.1	33.2	16
CH ₃ -CH ₂ -CH ₂ -CH ₂ ·	RT	21.96 ± 0.03	27.58 ± 0.03	This work
	-106	22.12	29.07	18
CH ₃ -(CH ₂) ₃ -CH ₂ ·	RT	21.89 ± 0.06	27.62 ± 0.06	This work
(CH ₃) ₂ CH-CH ₂ -CH ₂ ·	RT	21.8 ± 0.20	26.6 ± 0.20	This work
(CH ₃) ₂ -CH-CH ₂ ·	RT	21.81 ± 0.03	28.40 ± 0.05	This work
	-57	21.93	30.02	18
	-145	22.0	35.1	16
(C ₂ H ₅) ₂ -CH-CH ₂ ·	RT	21.70 ± 0.03	26.35 ± 0.03	This work
CH ₃ -CH-CH ₃	RT	21.76 ± 0.01	24.66 ± 0.01	This work
	-85	22.11	24.68	16
	-162	22.15	24.74	17
	-180	22.22	24.59	16
CH ₃ -CH ₂ -CH-CH ₃	RT	21.50 ± 0.03	24.85 ± 0.03	This work
	-90	21.90	24.63 (CH ₃) 27.20 (CH ₂)	17
	-98	21.8	24.5 (CH ₃) 27.9 (CH ₂)	17
(CH ₃) ₃ C·	RT		22.74 ± 0.05	This work
	-13		22.72	16
	-157		22.71	17
c-C ₆ H ₅ ·	RT	21.05 ± 0.06	34.86 ± 0.06	This work
	-40	21.48	35.16	16

^a The figures given are the absolute values and their mean-square errors. ^b 26 ± 3°.

son of observed radical concentrations with those predicted from kinetic results on reaction rates. Unfortunately, detailed data are available only on the *n*-butyllithium-*n*-butyl bromide system¹⁵ where we observe only low radical concentrations. However, if we insert a range of 2×10^{-2} mol/l. sec $\leq I \leq 8 \times 10^{-2}$ mol/l. sec which can be extrapolated from Shatenstein's data¹⁵ for our reaction conditions in the *n*-butyllithium-*n*-butylbromide reaction and a range of 1×10^9 l./mol sec $\leq 2kt \leq 4 \times 10^9$ l./mol sec into eq (4) we predict for the concentration of *n*-butyl radicals the range $2 \times 10^{-6} M \leq [R\cdot] \leq 9 \times 10^{-6} M$. The observed value of $[R\cdot] = (3 \pm 1) \times 10^{-6} M$ agrees with this prediction, and shows that in this reaction and very likely in others also free radical formation reactions are the only initiating reactions of alkyl lithium compounds with alkyl halides.

Discussion of Coupling Constants

Table I gives the coupling constants of the alkyl radicals observed in this work at room temperature (25 ± 3°). Also listed for comparison are literature values most of which were obtained at lower temperatures and for other solvents than those applied here.¹⁶⁻¹⁹ In our study only coupling constants of α and β protons

were detected; splittings by γ or δ protons were not resolved.

Table I shows that the absolute values of the coupling constants of α protons decrease with increasing temperature for all the radicals for which comparison is possible. For methyl radicals, this decrease has been observed before¹⁹⁻²¹ and has been attributed to an effect of the CH-bending vibration.¹⁹⁻²⁴ It is suggested that the decrease has the same origin for the other radicals. However, solvent effects on the coupling constants may also be of this same order of magnitude.¹⁶

(15) A. I. Shatenstein, E. A. Kovriezchnik, and V. M. Basmanova, *Kinet. Katal.*, **7**, 953 (1966).

(16) R. W. Fessenden and R. H. Schuler, *J. Chem. Phys.*, **39**, 2147 (1963).

(17) P. J. Krusic and J. K. Kochi, *J. Amer. Chem. Soc.*, **90**, 7155 (1968).

(18) P. J. Krusic, private communication.

(19) I. A. Zlochower, W. R. Miller, and G. K. Fraenkel, *J. Chem. Phys.*, **42**, 3339 (1965).

(20) G. B. Garbutt, H. D. Gessner, and M. Fujimoto, *ibid.*, **48**, 4605 (1968).

(21) H. Fischer and H. Hefter, *Z. Naturforsch.*, **A23**, 1763 (1968).

(22) R. W. Fessenden, *J. Phys. Chem.*, **71**, 74 (1967).

(23) R. E. Moss, *Mol. Phys.*, **10**, 399 (1966).

(24) D. H. Schrader, *J. Chem. Phys.*, **45**, 1946 (1966).

Interestingly, not noted before and in contrast to the behavior of the α proton constants, the coupling constants of β -CH₃ protons do not depend appreciably on temperature. From the CH₃-coupling constants of ethyl and isopropyl radicals (for which the α couplings do show a temperature dependence) it is therefore concluded that β -CH₃ coupling constants respond only rather weakly to the configurational changes caused by vibration at the radical carbon site. The coupling constants of β -CH₂ protons show the usual temperature dependence due to hindered rotation.²⁵ In particular our value for $a_{\beta}(\text{CH}_2)$ of the *n*-propyl radical agrees well with the temperature dependence of this coupling constant as observed by Fessenden²⁵ in the region from -180 to -50° if his curve of experimental points is extrapolated to room temperature. Somewhat noteworthy is our finding of $a_{\beta}(\text{CH}_3) = a_{\beta}(\text{CH}_2)$ for the *sec*-butyl radical at room temperature. Since at lower temperatures^{16,17} $a_{\beta}(\text{CH}_3) > a_{\beta}(\text{CH}_2)$ and since our value of $a_{\beta}(\text{CH}_2)$ cannot be the limiting value for very high temperatures²⁵ we feel that for temperatures higher than room temperature $a_{\beta}(\text{CH}_2)$ will be smaller than $a_{\beta}(\text{CH}_3)$, by possibly as much as several gauss. Thus the assumption²⁵ that $a_{\beta}(\text{CH}_3)$ represents the high temperature limiting value of $a_{\beta}(\text{CH}_2)$ has to be considered now with some reservations, though this does not affect the general conclusions of Fessenden's paper.²⁵

Comments on Nuclear Polarization Phenomena

For several of the systems studied here, emission and enhanced absorption lines have been observed in the nmr spectra of the reaction products during the reactions.^{4,5,10-13} These effects have been ascribed with some reservations to a chemically induced dynamic nuclear polarization mechanism²⁶ (CIDNP) which had been postulated to account for a nmr emission line found during reactions of phenyl radicals in the thermal decomposition of dibenzoylperoxide.^{27,28} The CIDNP-mechanism implies that in a radical formation reaction like eq 1 two radicals with antiparallel electron spins are formed simultaneously. This saturated electron spin system relaxes by magnetic electron-nuclear spin interactions in the free radicals and thereby polarizes the nuclei in the free radicals. In the product formation reaction the nuclear polarization is then transferred to the reaction products and gives rise to the nmr phenomena. As it has been noticed early,²⁶ this mechanism accounts for the polarization effects during alkyl-lithium-alkyl halide reactions very insufficiently. In its simplest form²⁸ it does not allow for the observation that in nmr multiplets of reaction products, enhanced absorption and emission lines may occur simultaneously,^{4,5,10-13} an effect which has been found during alkyl radical reactions in thermal decompositions of peroxides also.^{29,30} To overcome this difficulty, the originally developed theory was modified,³¹ and it has

been shown³¹ that CIDNP might predict the emission-absorption characteristics of the nmr spectra correctly, if the esr spectra of the radical precursors showed similar emission and enhanced absorption features. During this study, no such effect was observed for reaction conditions appropriate for nuclear polarization observations. The line intensities of the esr spectra were completely normal in most cases (see Figures 1, 2), and though some anomalies were found in *sec*-butyllithium-methyl bromide reactions, we thus believe that the CIDNP-mechanism as developed so far,^{28,31} can not be the explanation for nuclear polarizations which show the multiplet effect.

This conclusion is supported also by the following, somewhat weaker, argument which is based on the principle that the CIDNP mechanism can only explain a polarization of product nuclei if the mean lifetime of the radicals is of the same order of magnitude as the pertinent relaxation times of the nuclei in the free radicals—about 10^{-5} to 10^{-4} sec for alkyl radicals.^{28,31} Ward and Lawler⁴ have found nuclear polarization of the disproportionation products of *n*-butyl radicals during the reaction of *n*-butyllithium and *n*-butyl bromide. From the reaction conditions reported⁴ and from Shatenstein's kinetic data¹⁵ we calculate an initial reaction rate of about $I = 5 \times 10^{-4}$ M/sec for radical production. Applying quasi-steady state conditions and assuming $2k_t = 2 \times 10^9$ l./mol sec the overall mean lifetime of the radicals becomes $\tau = (2Ik_t)^{-1/2} = 10^{-3}$ sec. This lifetime is certainly a lower limit because of the approximation of assuming quasi-steady-state conditions, and it thus seems at least one order of magnitude too high to allow a dynamic nuclear polarization mechanism to be valid. In this context it should be mentioned that addition of diphenylacetylene which has been reported necessary for nuclear polarization observation⁴ did not affect radical concentrations appreciably in our esr experiments. We believe the argument on lifetimes to be valid for other reaction conditions and other reactions also. In fact, esr spectra of transient *t*-butyl radicals during thermal decompositions of *t*-butyl-trimethylperacetate³² indicate radical concentrations of 10^{-6} M. This leads to a lifetime of about 10^{-3} sec, a time again too long to allow a CIDNP explanation of the nuclear polarization of the reaction products which are observable under the same decomposition conditions.³²

Therefore, we conclude that the mechanism of polar-

(25) R. W. Fessenden, *J. Chim. Phys.*, **61**, 1570 (1964).

(26) R. G. Lawler, *J. Amer. Chem. Soc.*, **89**, 5519 (1967).

(27) J. Bargon, H. Fischer, and U. Johnsen, *Z. Naturforsch.*, **22a**, 1551 (1967).

(28) J. Bargon and H. Fischer, *ibid.*, **22a**, 1556 (1967).

(29) R. Kaptein, *Chem. Phys. Letters*, **2**, 261 (1968).

(30) J. Bargon and H. Fischer, *Z. Naturforsch.*, **A23**, 2109 (1968).

(31) H. Fischer and J. Bargon, *Accounts Chem. Res.*, **2**, 110 (1969).

(32) B. Blank and H. Fischer, unpublished observations.

ization of nuclei by relaxation processes in free radicals (CIDNP) as developed so far^{28,31} is very probably now inadequate as an explanation of all features nuclear polarization of reaction products in alkyllithium-alkyl halide and other reactions where the nmr multiplet effect occurs. The CIDNP concept is still able to explain most of the polarization phenomena in reaction products of phenyl and substituted phenyl radicals rather satisfactorily, and it seems too early to reject it completely. However, during alkyl radical reactions, another polarization mechanism must at least in part, if not generally, be operative which, as follows from the

consideration of lifetimes, induces nuclear polarization during molecule formation in the reaction transition states.^{31,33}

Acknowledgment. It is a pleasure to acknowledge stimulating discussions with Dr. R. W. Fessenden of this laboratory on many topics of this paper. This work was supported in part by the United States Atomic Energy Commission.

(33) NOTE ADDED IN PROOF. While this paper was in press similar results have been published by G. A. Russell and D. W. Lamson, *J. Amer. Chem. Soc.*, **91**, 3967 (1969).

The Kinetics of Crystal Growth of Dicalcium Phosphate Dihydrate

by Robert W. Marshall and George H. Nancollas¹

Chemistry Department, State University of New York at Buffalo, Buffalo, New York (Received April 3, 1969)

The kinetics of crystallization of dicalcium phosphate dihydrate (DCPD) has been studied by following the changes in calcium, phosphate, and hydrogen ion concentrations when stable, supersaturated solutions are inoculated with seed crystals of the salt. After a brief initial surge, the rate of growth of the crystals follows an equation that is second order with respect to concentration, $([Ca^{2+}][HPO_4^{2-}])$, over a wide range of calcium/phosphate ratios, suggesting a predominantly surface reaction controlled process. Experiments at 15, 25, and 37° have been made in supersaturated solutions over a range of calcium and phosphate concentrations and the energy of activation corresponding to the crystal growth process is 10.5 kcal mol⁻¹. Addition of sodium pyrophosphate to the supersaturated solutions has a striking inhibitory influence upon the rate of crystal growth of DCPD. The effect is analyzed in terms of adsorption, following the Langmuir isotherm, of pyrophosphate ions at the available crystal growth sites.

Dicalcium phosphate dihydrate (CaHPO₄·2H₂O; hereafter written DCPD) has long been recognized as an important product in the application of fertilizers to soils.² The main interest in this sparingly soluble salt, however, stems from its participation in the physiological formation of calcium phosphates. Thus DCPD has been proposed as an intermediate in the formation of bones and teeth,³ but there is still much discussion as to the exact nature of the precursor in the formation of hydroxyapatite (Ca₅(OH)(PO₄)₃; hereafter written HAP) under physiological conditions. DCPD may also play an important part in dental caries production. Caries is believed to result from the attack upon the dental enamel, mainly HAP, of organic acids produced by the metabolic action of the bacteria living in the vicinity of the enamel surface.³ These organic acids, with p*K* values in the range 5–7, produce acidic conditions with pH from 4 to 6.⁴ In aqueous solutions of calcium phosphate under such conditions, the stable solid phase consists of dicalcium phosphate, and the

complex species present in the solution are CaH₂PO₄⁺ and CaHPO₄.⁵

It is clear from the above brief historical outline that there is considerable interest in the mechanism of growth of DCPD crystals from supersaturated solutions of the salt. Previous studies^{6,7} have been concerned with spontaneous crystallization processes in which both nucleation and growth are occurring spontaneously. Such processes are very difficult to analyze kinetically,

(1) To whom all correspondence regarding this paper should be addressed.

(2) (a) W. E. Brown and J. R. Lehr, *Soil Sci. Soc. Amer. Proc.*, **23**, 7 (1959); (b) J. R. Lehr and W. E. Brown, *ibid.*, **22**, 29 (1958).

(3) A. E. Sobel, M. Burger, and S. Nobel, *Clin. Orthop.*, **17**, 103 (1960).

(4) J. A. Gray, *J. Dent. Res.*, **41**, 633 (1962).

(5) A. Chughtai, R. Marshall, and G. H. Nancollas, *J. Phys. Chem.*, **72**, 208 (1968).

(6) T. Hlabse and A. G. Walton, *Anal. Chim. Acta*, **33**, 373 (1965).

(7) A. G. Walton, B. A. Friedman, and A. Schwartz, *J. Biomed. Mater. Res.*, **1**, 337 (1967).

however, since the implicit assumption that only homogeneous nucleation takes place is of doubtful validity. Nucleation probably occurs heterogeneously on impurity particles which offer available sites for crystal growth. Added complications arise in deciding whether nucleation and growth occur simultaneously or consecutively. In the physiological environment, homogeneous nucleation is unlikely to occur. The process of calcification is probably initiated at suitable sites on the bone or tooth mineral or on the organic matrix. In the latter case, it is likely that the organic matrix offers a suitable conformation of binding ligand atoms to the calcium ions in the initial tissue calcification step.⁷ It has frequently been stated that normal blood serum is supersaturated with respect to the calcium hydrogen phosphate activity product $\{Ca^{2+}\}\{HPO_4^{2-}\}$, and it is clear that very special epitaxial conditions have to be met for calcification to take place. A study of the growth of added seed crystals in supersaturated solutions of calcium phosphate therefore appears to be particularly pertinent for a better understanding of the mechanism of calcification.

The present study is concerned with the kinetics of growth of DCPD crystals from solutions supersaturated with respect to this electrolyte. The existence of a well-defined metastable limit for spontaneous crystallization has made possible the preparation of supersaturated solutions stable for periods of days. The rate of growth of added seed crystals could then be measured in a highly reproducible manner in contrast to the results of experiments involving spontaneous precipitation. A temperature study has made possible the determination of the activation energy for the growth process.

Experimental Section

Materials. Reagent grade chemicals and grade A glassware were used throughout. DCPD crystals were prepared by the slow addition at 30° of 250 ml of 0.02 *M* disodium hydrogen phosphate to a mixture of 125 ml of 0.40 *M* calcium chloride and 250 ml of 0.18 *M* potassium dihydrogen phosphate. Nucleation commenced at pH 5.5 which was maintained approximately constant during precipitation by controlling the addition of the disodium hydrogen phosphate solution. The seed crystals were washed by decantation ten times with conductance water and stored as a slurry at a pH of 5.5. The regular, monoclinic crystals had an average size of 30 μ \times 12 μ . Analysis of a portion of the solid, dried at 40°, gave calcium, 23.78%, phosphate, 54.46% (theoretical for $CaHPO_4 \cdot 2H_2O$: Ca, 23.29%; P, 55.77%). The X-ray diffraction pattern and infrared spectrum were similar to those previously reported for the salt.^{8,9} Seed crystals were aged for at least 6 weeks before use. The solid phase analysis was checked periodically for more than a year, and no change in composition could be detected. Sodium pyrophosphate solutions were prepared from the Baker

Analyzed reagent (Lot No. 33159) without further purification.

Growth Experiments. The crystallization cell consisted of a 500-ml round-bottom flask with five standard-tapered necks. The glass stirrer, passing through a gland in the central neck, consisted of two glass swing-out links; the speed could be adjusted within the range 50 to 700 rpm. A nitrogen gas lead-in tube was sealed to the bottom of the flask, and additional turbulence could be effected by the bubbling of nitrogen through the cell to remove carbon dioxide. The cell was supported in a water thermostat, and growth experiments were made at 15 ± 0.02 , 25 ± 0.02 , and $37 \pm 0.03^\circ$. The pH was measured by using the electrode system contained in the cell

glass electrode|solution under study|satd KCl;

Hg₂Cl₂, Hg

together with a Corning Model 12 pH meter and Beckman Type 41263 glass electrode. The meter output was displayed on a Sargent Model SR recorder making possible continuous monitoring of pH during the crystal growth. The electrode systems were standardized before and after each experiment with NBS standard buffer solutions prepared according to Bates;¹⁰ 0.05 *m* potassium hydrogen phthalate, pH 4.008 at 25°, 3.999 at 15°, and 4.028 at 37°; 0.025 *m* potassium dihydrogen phosphate + 0.025 *m* disodium hydrogen phosphate, pH 6.865 at 25°, 6.900 at 15°, and 6.841 at 37°.

Solutions, supersaturated with respect to DCPD, were prepared by the slow addition of disodium hydrogen phosphate to a mixed solution of potassium dihydrogen phosphate and calcium chloride contained in the stirred cell. Each solution was allowed to equilibrate, with nitrogen bubbling, for at least 30 min before the addition of seed crystals in the form of a slurry containing from 18 to 180 mg of DCPD. Crystal growth commenced immediately in all cases and was followed by monitoring the pH and also by the removal of aliquots of supernatant solution for chemical analysis. Calcium analyses were made using a Perkin-Elmer Model 303 atomic absorption spectrophotometer, and phosphate was determined spectrophotometrically as the phosphomolybdate.¹¹ In addition, periodic microscopic examinations of the growing crystals were made using a Leitz Wetzlar Dialux-Pol polarizing microscope.

Results and Discussion

At the pH of the crystallization experiments both $[H_3PO_4]$ and $[PO_4^{3-}]$ concentrations are negligible,

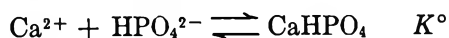
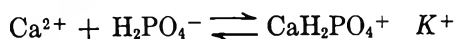
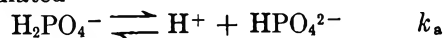
(8) P. W. Arnold, *Trans. Faraday Soc.*, **46**, 1061 (1950).

(9) E. E. Berry and C. D. Baddiel, *Spectrochim. Acta*, **23A**, 2089 (1967).

(10) R. G. Bates, "Determination of pH," John Wiley & Sons, Inc., New York, N. Y., 1963.

(11) D. N. Fogg and N. T. Wilkinson, *Analyst (London)*, **83**, 406 (1958).

and the following equilibria in the solution phase may be formulated



k_a represents the thermodynamic dissociation constant (values at 15, 25, and 37°, respectively, 5.888×10^{-8} , 6.339×10^{-8} , and 6.562×10^{-8}),¹² and K is the thermodynamic association constant for the formation of the calcium complexes.⁵ The concentrations of ionic species in the solutions were calculated as described previously;¹³ f_2 , the activity coefficient of the divalent ions was obtained from the extended form of the Debye-Hückel equation proposed by Davies.¹⁴ The thermodynamic solubility product, $K_{sp} = [\text{Ca}^{2+}][\text{HPO}_4^{2-}]f_2^2$, was obtained by allowing crystal growth experiments to proceed to equilibrium; at 25° the mean value of 21 determinations was $2.10 \pm 0.09 \times 10^{-7} \text{ mol}^2 \text{ l.}^{-2}$. This may be compared with values in the literature quoted by Bjerrum¹⁵ ($K_{sp} = 2.7 \times 10^{-7} \text{ mol}^2 \text{ l.}^{-2}$ at 18° and 2.4×10^{-7} at 37°), Farr¹⁶ ($2.18 \times 10^{-7} \text{ mol}^2 \text{ l.}^{-2}$, obtained after review of the literature), and Strates, Neuman, and Levinskas¹⁷ ($2.68 \times 10^{-7} \text{ mol}^2 \text{ l.}^{-2}$) who did not include corrections for the concentrations of calcium phosphate ion pairs. More recently, Moreno and Brown and their coworkers^{18,19} have obtained a value of $2.77 \times 10^{-7} \text{ mol}^2 \text{ l.}^{-2}$ at 25° by an extrapolation method and $2.19 \times 10^{-7} \text{ mol}^2 \text{ l.}^{-2}$ at 37° after allowing for the presence of $\text{CaH}_2\text{PO}_4^+$ and CaHPO_4 .

The results of some crystallization experiments are summarized in Table I and typical curves of concentration against time are shown in Figure 1. Reproducibility is illustrated by the agreement between the results for experiments 10 and 11 and between 26 and 27. Throughout all the crystallization experiments, the decrease in total calcium concentration in the supersaturated solutions was within 3% of the corresponding total phosphate concentration change. The resulting indication that DCPD was indeed the growing phase was confirmed by petrographic examination of the crystals. In addition, the increase in crystal size, measured microscopically, was close to that calculated from the changes in calcium and phosphate concentrations on the assumption of equal growth rates in all three dimensions. The crystal growth curves in Figure 1 are characterized by a brief initial fast period followed by a smooth decrease in concentration with time. During the latter period, which constituted the major portion of the total crystal growth, the process follows the equation (1), where the rate is expressed as a change

$$-\left(\frac{w_i}{w}\right)^{2/3} \frac{dT}{dt} = ks \left([\text{Ca}^{2+}][\text{HPO}_4^{2-}] - \frac{K_{sp}}{f_2^2} \right) \quad (1)$$

either in total calcium or total phosphate concentration

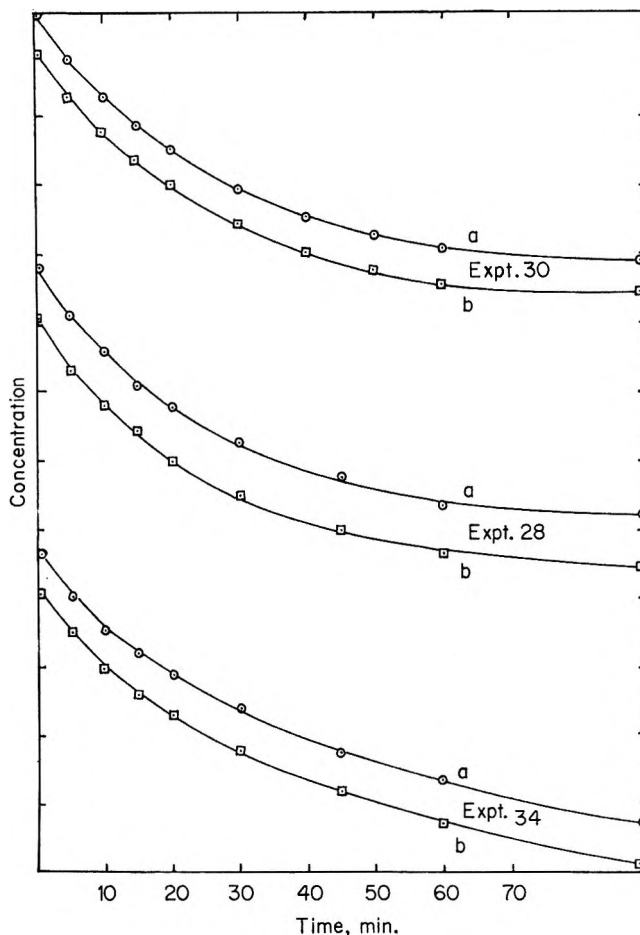


Figure 1. Plots of total calcium (a) and total phosphate (b) concentrations as a function of time. One ordinate scale division corresponds to a concentration change of $2 \times 10^{-4} M$.

with time, dT/dt . Since there is an appreciable change in crystallite size during the experiments (approximately a factor of 2 in the surface area), the correction factor $(w_i/w)^{2/3}$ is introduced to correct the rate of growth at time t to that corresponding to the initial surface area of the seed crystals. w_i is the weight of seeds crystals added initially, and w is the weight present at time t . The correction is made on the assumption of a regular three-dimensional crystal growth, and this is supported by the good agreement between the extent of

(12) R. G. Bates and S. F. Acree, *J. Res. Nat. Bur. Stand.*, **30**, 129 (1943).

(13) G. H. Nancollas, "Interactions in Electrolyte Solutions," Elsevier Publishing Co., Amsterdam, 1966.

(14) C. W. Davies, "Ion Association," Butterworth & Co., Ltd., London, 1962.

(15) N. Bjerrum, "Selected Papers," Munksgaard, Copenhagen, 1949, p 245.

(16) T. D. Farr, "Phosphorus," Chemical Engineering Report No. 8, T.V.A., Wilson Dam, Ala., 1950, p 52.

(17) B. S. Strates, W. F. Neuman, and G. J. Levinskas, *J. Phys. Chem.*, **61**, 379 (1957).

(18) E. C. Moreno, W. E. Brown, and G. Osborn, *Soil Sci. Soc. Amer. Proc.*, **24**, 94 (1960).

(19) E. C. Moreno, T. M. Gregory, and W. E. Brown, *J. Res. Nat. Bur. Stand., A*, **70**, 545 (1966).

Table I: Crystallization of DCPD from Supersaturated Solution^a

Expt no.	Total concentrations		pH	[Ca ²⁺] × 10 ²	[HPO ₄ ²⁻] × 10 ⁴	Seed crystals, mg	k, l. mol ⁻¹ min ⁻¹ (mg of seed) ⁻¹
	Calcium × 10 ²	Phosphate × 10 ³					
Temp 15°							
47	1.210	1.184	5.662	1.059	4.674	27.5	0.16
48	1.199	1.173	5.655	1.050	4.560	27.5	0.17
Temp 25°							
34	0.248	1.258	6.120	0.178	13.46	23.0	0.28
35	0.247	1.280	6.188	0.173	15.74	23.0	0.26
26	0.481	1.185	5.939	0.377	8.680	23.0	0.30
27	0.495	1.212	5.910	0.377	8.377	23.0	0.30
28	0.720	1.151	5.744	0.596	5.614	23.0	0.28
29	0.741	1.187	5.744	0.611	5.814	23.0	0.26
30	1.236	1.164	5.543	1.066	3.756	23.0	0.30
31	1.188	1.124	5.573	1.026	3.855	23.0	0.27
9	1.204	1.114	5.477	1.048	3.109	18.0	0.29
10	1.196	1.104	5.537	1.038	3.502	18.0	0.25
11	1.205	1.128	5.519	1.045	3.447	18.0	0.24
19	1.229	1.137	5.528	1.065	3.543	18.0	0.25
49	1.205	1.170	5.557	1.037	3.891	27.5	0.31
50	1.212	1.189	5.563	1.041	4.010	27.5	0.32
7	1.214	1.121	5.513	1.054	3.378	90.0	0.30
8	1.213	1.119	5.507	1.054	3.329	90.0	0.29
Temp 37°							
44	1.209	1.159	5.417	1.024	2.895	27.5	0.60
45	1.204	1.155	5.419	1.020	2.894	27.5	0.60

^a Stirring rate 120 rpm; concentrations in moles per liter.

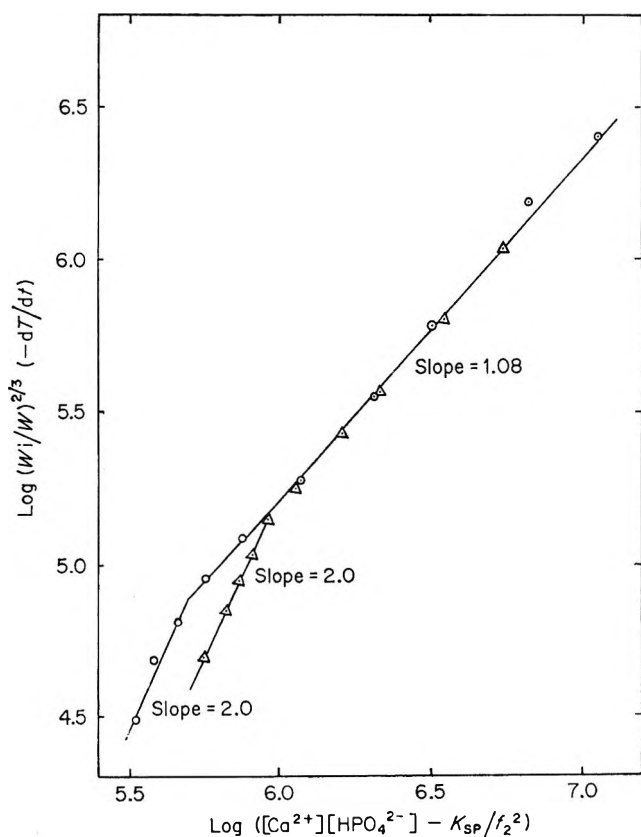


Figure 2. Plots of $\log (w_i/w)^{2/3} (-dT/dt)$ against $\log ([Ca^{2+}][HPO_4^{2-}] - K_{sp}/f_2^2)$: expt 31, \circ ; expt 34, Δ ; slopes of the lines are as indicated.

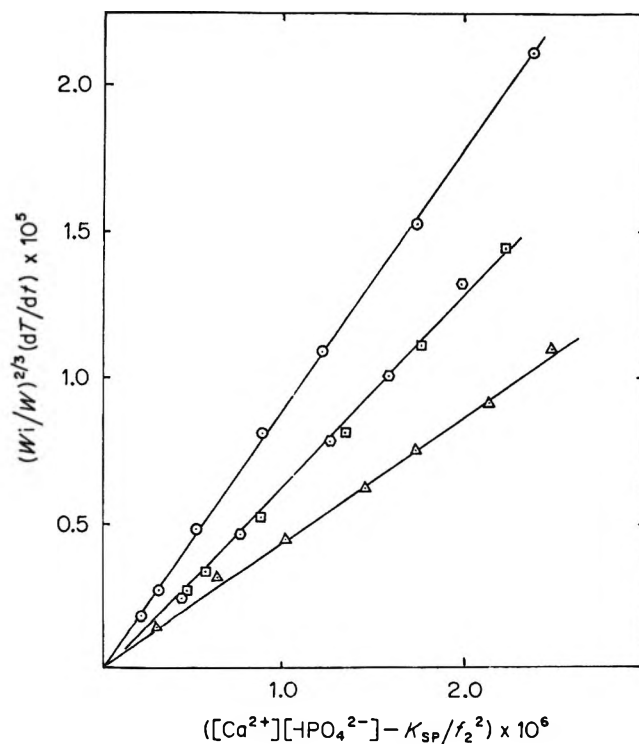


Figure 3. Plots of $(w_i/w)^{2/3} (dT/dt) \times 10^5$ against $([Ca^{2+}][HPO_4^{2-}] - K_{sp}/f_2^2) \times 10^6$: expt 49, \circ ; expt 28, \square ; expt 31, \square ; expt 19, Δ .

crystallization calculated from solution concentration changes and from microscopic measurement of crystal size during the experiments.

Typical plots of $\log [(w_i/w)^{2/3}(-dT/dt)]$ against $\log ([Ca^{2+}][HPO_4^{2-}] - K_{sp}/f_2^2)$ are shown in Figure 2. For the major portion of the crystal growth, the slope of the resulting line is unity, indicating a second-order dependence given by eq 1. During the initial surge, which was always less than 15% of the total reaction, a slope greater than unity may be interpreted in terms of the surface nucleation process used to explain a similar phenomenon observed in the growth of barium sulfate²⁰ and strontium sulfate²¹ crystals from their supersaturated solutions.

In the region following the initial surge, the linearity of the plots of $(w_i/w)^{2/3}(dT/dt)$ against $([Ca^{2+}][HPO_4^{2-}] - K_{sp}/f_2^2)$ is seen in Figure 3, and the excellent reproducibility of the experiments is exemplified by the results of experiments 28 and 31. Equation 1 is closely followed over the wide range of $[Ca^{2+}]/[HPO_4^{2-}]$ indicated in Table I. Several experiments were made with different stirring rates; changes from the normal 120 (Table I) to 600 rpm resulted in about 20% change in the value of the rate constant k in eq 1. If diffusion were rate determining, the rate would be expected to be appreciably dependent on the rate of stirring, and it is clear that within the stirring conditions used in the present work, mass transport of ions to the crystal surfaces plays only a very small part in the over-all growth process. A preliminary analysis of some of the results had indicated a diffusion-controlled crystal growth.²² However, no correction was made for the changes in crystallite size during the experiments. The conclusions here reported are based on a more extensive body of data covering a wider range of concentration and stirring conditions. By assuming a surface-controlled process, the rate of crystallization of DCPD may be expressed in terms of the bulk concentrations of the lattice ions

$$\text{rate of crystallization of DCPD} = k_s[Ca^{2+}][HPO_4^{2-}]$$

The opposing rate of solution is proportional to the available surface area

$$\text{rate of solution} = k_1s$$

In a saturated solution these rates are equal, and so $k_1 = kK_{sp}/f_2^2$. In a supersaturated solution, if diffusion plays an insignificant part in the growth process, the net rate of crystal growth will then be given by eq 1. Crystal growth experiments (Table I) were made also at 15 and 37°C, and the resulting kinetic plots are shown in Figure 4. It is seen that eq 1 is closely followed at all temperatures, and the energy of activation, obtained from the excellent linear plot of $\ln k$ against T^{-1} , is 10.5 ± 0.8 kcal mol⁻¹. This is appreciably larger than the value,²³ 4.5 kcal mol⁻¹, to be expected on the basis of pure mass transport control again pointing to the relative unimportance of the latter mechanism in the growth of DCPD crystals.

Pyrophosphate ions have long been known to have a

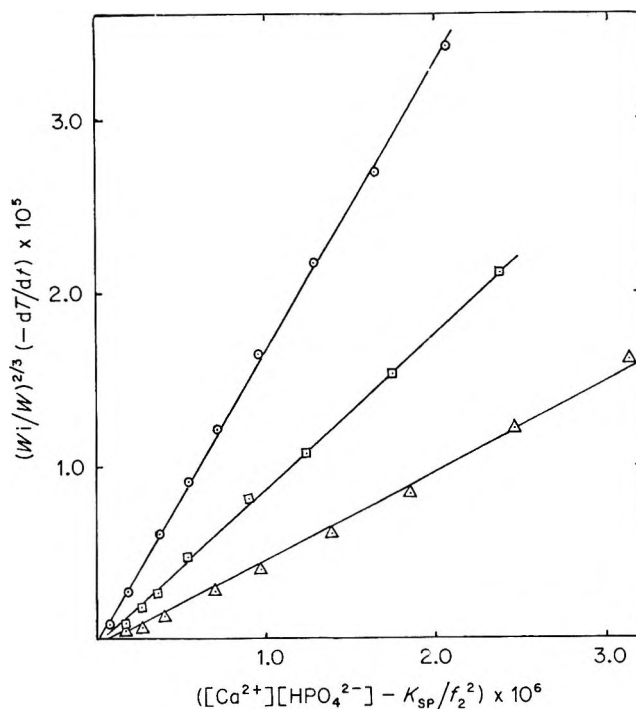


Figure 4. Plots of $-dT/dt$ against $([Ca^{2+}][HPO_4^{2-}] - K_{sp}/f_2^2)$ at different temperatures: \circ , expt 44 at 37°; \square , expt 49 at 25°; \triangle , expt 48 at 15°.

marked inhibiting influence on the precipitation of sparingly soluble salts from solution.^{21,24} Their presence, at low concentrations, in both plasma²⁵ and urine²⁶ has led a number of investigators to propose that they are also effective in preventing the precipitation of calcium phosphate from metastable solutions *in vivo*.²⁷ These observations suggest that pyrophosphate may be the effective regulator of calcification processes in the body, and it is therefore of interest to study its effect upon the rate of crystallization of DCPD.

The results of crystallization experiments made in the presence of small concentrations of sodium pyrophosphate are summarized in Table II. Some data are plotted according to eq 1 in Figure 5, and it is seen that even in the presence of pyrophosphate ion, this equation accurately represents the experimental results. If diffusion played an important part in the growth process, the addition of an additive, known to be heavily adsorbed on the surface of the crystals, might be expected to have a marked effect upon the

(20) G. E. Nancollas and N. Purdie, *Trans. Faraday Soc.*, **59**, 735 (1963).

(21) J. R. Campbell and G. H. Nancollas, *J. Phys. Chem.*, **73**, 1735 (1969).

(22) G. H. Nancollas, *J. Crystal Growth*, **34**, 335 (1968).

(23) J. R. Howard, G. H. Nancollas, and N. Purdie, *Trans. Faraday Soc.*, **56**, 278 (1960).

(24) M. Muira and H. Naono, *Bull. Chem. Soc. Jap.*, **38**, 492 (1965).

(25) H. Fleisch and S. Bisaz, *Nature*, **195**, 911 (1962).

(26) H. Fleisch, *Amer. Physiol.*, **203**, 671 (1962).

(27) H. Fleisch and W. F. Neuman, *ibid.*, **200**, 1296 (1961).

Table II: Crystal Growth in the Presence of Sodium Pyrophosphate^a

Expt no.	[Ca ²⁺] × 10 ²	[HPO ₄ ²⁻] × 10 ⁴	pH	[Py] × 10 ⁷	k', l. mol ⁻¹ min ⁻¹ (mg of seed) ⁻¹	$\frac{k}{k - k'}$
50	1.041	4.010	5.563	0	0.32	...
64	1.070	3.721	5.533	3.36	0.27	6.4
63	1.052	3.795	5.551	6.60	0.23	3.6
62	1.027	3.946	5.577	9.70	0.17	2.2
61	1.051	3.641	5.532	33.0	0.08	1.4
65	1.051	3.846	5.546	67.5	0.06	1.2
60	1.044	3.405	5.509	98.0	0.03	1.1

^a Stirring rate 120 rpm; 27.5 mg of seed crystals.

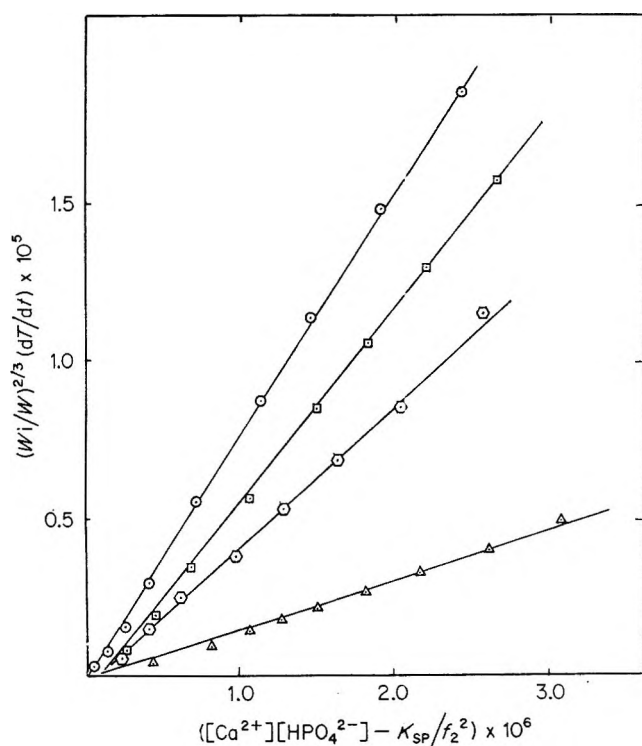


Figure 5. Kinetic plots in the presence of sodium pyrophosphate: expt 64, ○; expt 63, □; expt 62, ◇; expt 65, △.

kinetics of the reaction. That such is not the case provides additional evidence for a surface-controlled process represented by eq 1. The striking effect of the additive in reducing the rate of crystallization is illustrated in Figure 6 in which the rate constant in the presence of pyrophosphate, k' , is plotted as a function of adsorbate concentration. If we assume that the retarding action of the pyrophosphate ions is a result of their absorption at growth sites on the crystal surfaces, the Langmuir adsorption treatment should be applicable. Suppose that a fraction α of the surface is covered by adsorbed foreign ions of molar concentration $[Py]$. The rate of adsorption may be written $k_1[Py] \cdot (1 - \alpha)$, and the rate of desorption is $k_2\alpha$, where k_1 and k_2 are the corresponding rate constants. At equilibrium these rates are equal, and $\alpha = k_1[Py]/$

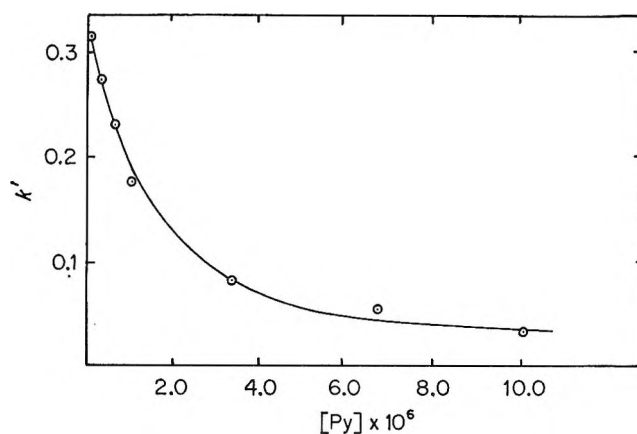


Figure 6. Plots of k' , in the presence of pyrophosphate, against [pyrophosphate].

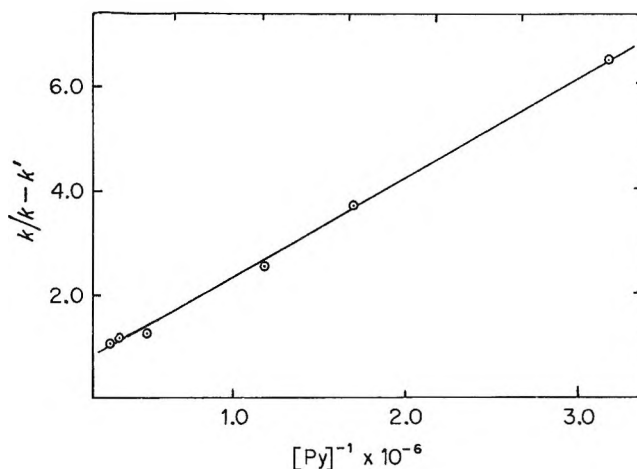


Figure 7. Langmuir isotherm plot of $k/(k - k')$ against $[pyrophosphate]^{-1}$.

$(k_2 + k_1[Py])$. Now $k' = k(1 - \alpha)$, and substituting for α we have

$$\frac{k}{k - k'} = 1 + \frac{k_2}{k_1[Py]} \quad (2)$$

In Figure 7, the left-hand side of eq 2 is plotted against $[Py]^{-1}$, and it is seen that the Langmuir isotherm satisfactorily describes the marked inhibiting effect of

the pyrophosphate ions in terms of a monomolecular "blocking" layer of foreign ions at the crystal surface.

Acknowledgments. This work is supported by Contract N00014-66-C0227 (NR 105-419), between the

Office of Naval Research, Department of the Navy, and the State University of New York at Buffalo. We also thank Union Carbide Corporation for the award of a research fellowship to R. W. M.

Plane Specificity in the Reaction of Methanol and Ethanol Vapor with Clean Germanium

by F. Meyer

Philips Research Laboratories, N.V. Philips' Gloeilampenfabrieken, Eindhoven, Netherlands (Received April 4, 1969)

The adsorption of methanol and ethanol vapor on clean germanium powder and the subsequent desorption of the decomposition products as a function of temperature have been studied. The results are interpreted in terms of a dissociative adsorption mechanism and covalent adsorption complexes are proposed. The adsorption and desorption are found to be plane specific. Twice as much is adsorbed on the (100) plane as on the (111) plane, which is in accordance with the number of dangling bonds per germanium surface atom on these planes. The desorption products from these two types of surface are different.

Introduction

The clean surfaces of germanium and silicon are highly reactive to many gases, which is due to the uncompensated (dangling) bonds of the surface atoms. This was demonstrated¹ for a number of hydrides of general formula H_xA with $x = 1, 2, 3$, *i.e.*, HCl, H₂S, NH₃, etc. These gases showed a fast adsorption up to a coverage of one molecule per $2x$ surface atoms, and a dissociative adsorption mechanism, compensating all dangling bonds at the surface, was suggested. However, hydrides with $x = 4$ such as CH₄ and SiH₄ did not adsorb chemically, and neither did organic compounds with unsaturated bonds such as ethene or benzene. Therefore, the nature of the A atom seems to be of prime importance for the adsorption.

It was the purpose of this work to study in detail the interaction between a clean germanium surface and two oxygen-containing organic compounds, namely methanol and ethanol. The results from earlier work² with ellipsometry on silicon single-crystal surfaces showed very clearly that adsorption can be dependent on the crystallographic orientation of the surface plane. In the present study gas volumetric measurements also indicate that the adsorption of alcohols on clean germanium powders is plane specific.

Experimental Section

The adsorption and desorption measurements on powders were performed in an all-glass apparatus. A

vacuum of 10^{-7} Torr was obtained with a mercury diffusion pump provided with a liquid nitrogen cold trap. Pressure readings of methanol and ethanol were taken with a McLeod manometer.

The germanium powder, obtained by crushing a high ohmic single crystal in air, was cleaned by heating to 650° at 10^{-7} Torr for 15 hr.¹ After cooling to room temperature, the methanol or ethanol vapor was admitted and the pressure decrease recorded. Because the alcohol adsorbs reversibly on the glass walls of the apparatus, blank experiments were performed at different alcohol pressures to correct for the amount removed in this way. Some typical adsorption curves for methanol are shown in Figure 1.

The excess alcohol was pumped off at room temperature until no further methanol or ethanol could be detected by the mass spectrometer connected to the adsorption apparatus. Then the temperature was raised by using an electric furnace around the reaction tube and the temperature was measured with a thermocouple imbedded in the powder. No alcohol was desorbed as such; only decomposition products were detected.

The desorption products were analyzed with an Atlas M86 mass spectrometer. Calibration curves in the appropriate pressure range for the different gases

(1) A. H. Boonstra and J. van Ruler, *Surface Sci.*, **4**, 141 (1966); A. H. Boonstra, Philips Research Reports, Suppl. No. 3, 1968.

(2) G. A. Bootsma and F. Meyer, *Surface Sci.*, **14**, 52 (1969).

were determined. The total pressure calculated from the mass spectra agreed within 3% with the total pressure in the desorption system as measured with the McLeod manometer.

The total surface area of the germanium powders was measured by applying the equation of Brunauer, *et al.*,³ to the physisorption results of krypton at liquid nitrogen temperature. For the cross-sectional area of one krypton atom, a value of 19.5 \AA^2 was taken.⁴ The specific surface area of the germanium powder was $0.13 \text{ m}^2/\text{g}$ and total surface areas of 1.8 m^2 have been used.

Some experiments were performed with 0.3 mm thick

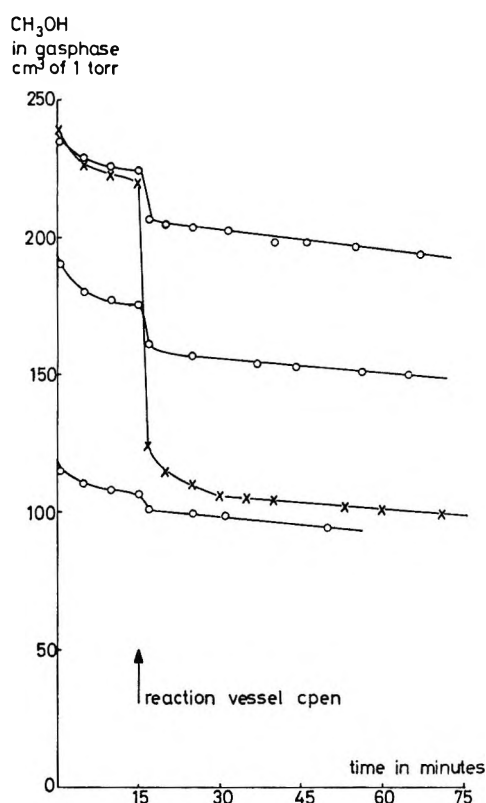


Figure 1. Adsorption of methanol: O, blank experiments in the glass apparatus without germanium; X, adsorption on clean germanium powder and glass walls.

germanium disks having a (100) oriented surface of $\sim 4 \text{ cm}^2$. Twenty-five disks were cut from a single crystal, mechanically polished, and etched in a solution of 14 cc of 40% HF, 10 cc of 60% HNO_3 , and 1 cc of ethanol. The surface was cleaned by heating to 850° under a vacuum of 5×10^{-9} Torr for 15 hr. The vacuum system was provided with metal valves and was pumped by a 50-l. Vacion pump. Low-energy electron diffraction (LEED) measurements showed that a single crystal treated in this way has a clean surface structure, the Ge(100)-2 structure.⁵ The disks were cleaned at a higher temperature than the powders since the etch layer is more difficult to remove than the oxide layers on the crushed samples.

Results and Discussion

The results of the present work show that the fast, irreversible adsorption of methanol on clean germanium powder reaches a coverage of $0.30 \pm 5\%$ molecule per surface atom. Green and Maxwell,⁶ however, claim a coverage of one methanol molecule per surface atom. This discrepancy might be partly explained by the fact that these authors did not observe a difference between the true chemical adsorption and the following reversible adsorption. Furthermore, small surface areas were used which may have introduced errors.

After the adsorption, the excess methanol was removed from the reaction vessel and the glass walls by pumping and the germanium powder was heated to various temperatures in a closed system. At 150° the first trace of desorbed hydrogen appeared in the mass spectra. The amount of desorption for the different decomposition products, hydrogen, carbon monoxide, and methane, as a function of temperature is shown in Figure 2. At each temperature, the desorption was continued until the pressures did not change. It took approximately 15 hr at 200° and 2 hr at 425° to reach these constant values.

Tamaru⁷ has shown that hydrogen adsorption on a clean germanium surface is a reversible process and the measurements of the present study are in complete agreement with this observation. The pressure dependence of the surface coverage above $\theta = 0.1$ obeys the Freundlich isotherm

$$V = Cp^{1/n}$$

Tamaru has given values of $1/n$ varying from 0.20 to 0.54 for the temperature range $218\text{--}348^\circ$. We have extended the measurements to some lower temperatures as shown in Figure 3. At 195° , a value $1/n = 0.18$ was calculated. Below 195° , the amounts of hydrogen adsorbed decrease again. This effect is probably due to the extremely low reaction rates at these temperatures which may not allow the true equilibrium value to be reached (within 24 hr). The CO and CH_4 desorptions were irreversible both with and without the presence of hydrogen. This was verified at the relevant temperatures and pressures in separate experiments with these gases. Kirovskaya,⁸ *et al.*, report CO coverages of approximately 0.01 monolayer in this pressure-temperature range.

In the present measurements, there is no significant increase in the reaction products above 425° . At this temperature, the total amount of hydrogen and carbon

(3) S. Brunauer, P. H. Emmett, and E. Teller, *J. Amer. Chem. Soc.*, **60**, 309 (1938).

(4) A. J. Rosenberg, *ibid.*, **78**, 2929 (1956).

(5) F. Jona, *I.B.M. J. Res. Develop.*, **9**, 375 (1965).

(6) M. Green and K. H. Maxwell, *Phys. Chem. Solids*, **11**, 195 (1959).

(7) K. Tamaru, *J. Phys. Chem.*, **61**, 647 (1957).

(8) I. A. Kirovskaya, L. G. Maidonovskaya, and V. N. Nagovitsin, *Russ. J. Phys. Chem.*, **41**, 1194 (1967).

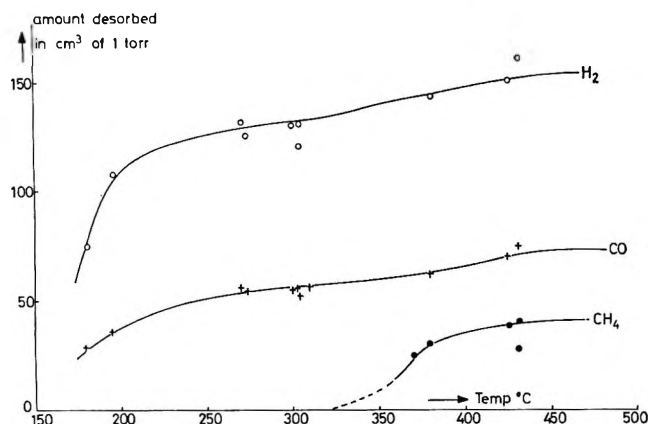


Figure 2. Amount of hydrogen (O), carbon monoxide (+), and methane (●), desorbed in a total volume of 400 cm³ as a function of temperature.

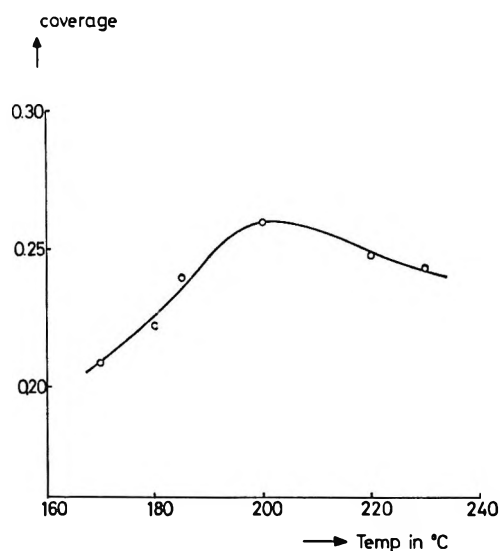
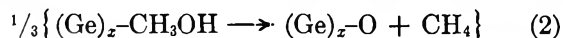
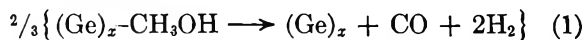


Figure 3. Number of hydrogen atoms per germanium surface atom as a function of temperature at a pressure of 0.1 Torr.

desorbed is equal to within 5% of the amounts adsorbed in the form of methanol. The oxygen is desorbed to an extent of $\frac{2}{3}$ the equivalent adsorbed. The relative amounts of H₂, CO, and CH₄ are 4:2:1, which suggests the reactions



Reaction 2 starts at a relatively high temperature. It appeared that this methane desorption is dependent on the presence of hydrogen in the system. At a pressure higher than 0.4 Torr, desorption of methane will take place. In our experiments, this was normally the case since hydrogen was evolved before the methane reaction started. It was possible, however, to desorb at 300° before any methane was formed and to remove the hydrogen-carbon monoxide mixture. If the tem-

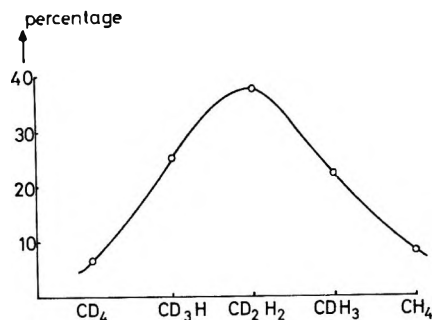
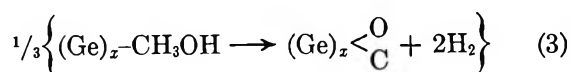


Figure 4. Percentage of deuterated methanes desorbed at 450°. A 1:1 hydrogen-deuterium mixture was present with a total pressure of 0.4 Torr.

perature is raised to 400–500°, hydrogen will desorb instead of methane according to reaction 3.



The presence of hydrogen at pressures below 0.4 Torr results in a mixture of methane and hydrogen. If deuterium gas is present during the methane desorption, the deuterium is readily incorporated in the methane as shown in Figure 4 for a 1:1 mixture of hydrogen and deuterium gas.

The fact that two completely different and independent reactions occurred on the germanium powder suggested plane specificity. Calculations⁹ have indicated that the surface of germanium powder obtained by crushing will consist of approximately 70% (111), 25% (100), and 5% (110). This leads to the assumption that reaction 1 takes place on the (111) surface and reactions 2 and 3 on the (100) surface, which is supported by the following experiment.

A clean (100) single crystal surface area of 100 cm² was prepared as described in the Experimental Section. Methanol was adsorbed, the excess was removed by pumping, and the adsorbate was subsequently desorbed with and without the presence of hydrogen. For the latter case, the only reaction product was hydrogen; neither CO nor CH₄ was observed. However, with hydrogen present (0.5 Torr), methane was the only reaction product detected. Heating the clean surface in hydrogen gave no observable products. Due to the small surface area, the amount of desorption product could not be determined accurately, but the observed data were correct within an error of 50%. Therefore these results strongly support the hypothesis that reactions 2 and 3 proceed *via* the (100) plane.

In deriving the structures of the adsorption complexes from these data, the following assumptions have been made. (1) The adsorption complex is formed in such a way that all the dangling bonds of the surface atoms are compensated. (2) The (100) surface adsorbs

(9) A. J. Rosenberg, *Phys. Chem. Solids*, **14**, 175 (1960).

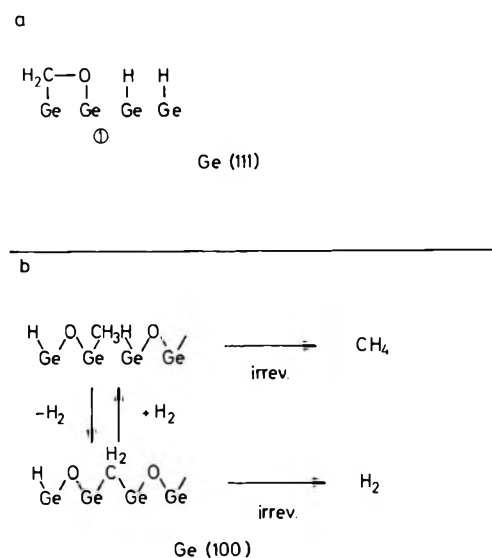


Figure 5. Structure models for the adsorption complexes of methanol on Ge(111) and Ge(100).

twice the amount of methanol per surface atom as the (111).

The desorption products showed that $\frac{2}{3}$ of the methanol was adsorbed at the (111) surface and $\frac{1}{3}$ at the (100) surface. Therefore the second assumption implies that 80% of the surface has the (111) orientation and 20% the (100) orientation, which is in reasonable agreement with the calculated values previously mentioned. Since the average coverage is 0.30 methanol molecule per surface atom, the coverage on the (111) surface is $\frac{1}{4}$ and on the (100) surface $\frac{1}{2}$ molecule per surface atom. This is supported by ellipsometry measurements of the methanol adsorption on silicon.¹⁰ (In general, silicon and germanium behave similarly in adsorption phenomena.) Here coverages were measured of $0.25 \pm 10\%$ and $0.53 \pm 10\%$ methanol molecules per surface atom for the (111) and (100) surfaces, respectively.

There are five possible structure models for a methanol molecule on the (111) surface compensating four surface bonds. Four models involve a bridge position between two adjacent surface atoms of an O atom, a CH_2 group, a CHOH group, and a CH_2O group, respectively. The fifth model has a CHO group attached to the surface *via* the carbon atom. In Figure 5a, only one model is given which has been chosen for two reasons. (1) As mentioned in the Introduction, hydrocarbons are not chemically adsorbed. Therefore, the first adsorption step will probably be the formation of the $\text{Ge}-\text{O}$ bond and not the $\text{Ge}-\text{C}$ bond, and the structure model should therefore exhibit this $\text{Ge}-\text{O}$ bond. (2) The formation of CO at relatively low temperatures (<200) suggests that the $\text{C}-\text{O}$ bond is already present in the adsorption complex.

The structure model for the adsorption complex on the (100) surface must imply the possibility of hy-

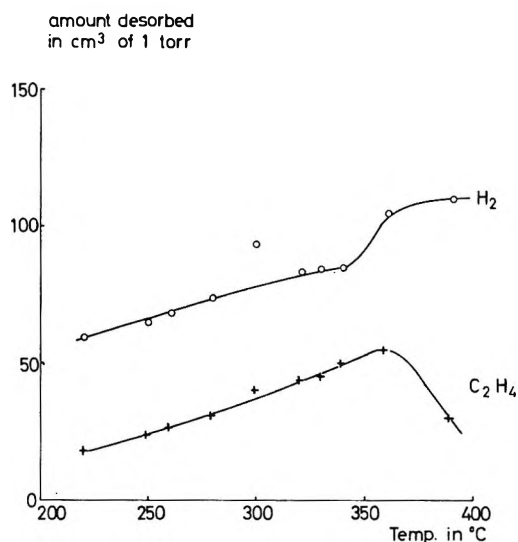
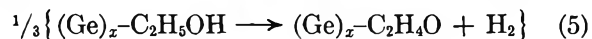
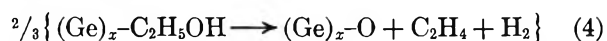


Figure 6. Amount of hydrogen (O) and ethene (+) desorbed in a total volume of 360 cm^3 as a function of temperature.

drogen exchange. The model given in Figure 5b fulfills this requirement. The fast incorporation of deuterium in the methane desorbed shows that the equilibrium reaction with hydrogen is much faster than the irreversible desorption steps.

The ethanol adsorption and desorption was studied in the same way. The average coverage after the fast irreversible adsorption was $0.20 \pm 10\%$. This was interpreted as a coverage of one ethanol on six germanium surface atoms at the (111) surface and of one ethanol on three surface atoms on the (100) surface. After removal of the excess ethanol, the germanium sample was heated and desorption took place. Figure 6 shows the amounts desorbed as a function of temperature. The desorption up to 350° can be described by the reactions



At temperatures higher than 350° , the ethene begins to react with the oxygen adsorbed on the surface forming CO , hydrogen, and a carbon deposit on the surface. Furthermore, hydrogen is adsorbed at this temperature, perhaps as $-\text{OH}$ groups. These reactions were not studied in detail.

If the desorption products at 350° are pumped off and hydrogen gas is added at a pressure of several Torr, some methane is evolved at temperatures between 400 and 500° . This amount roughly corresponds to 5% of the total amount of carbon adsorbed as ethanol. It seems, therefore, that an equilibrium with hydrogen exists just as in the case of methanol, but that the equilibrium constant is different (compare Figures 5b and 7b). In Figure 7, the same type of models is pro-

(10) F. Meyer, to be published.

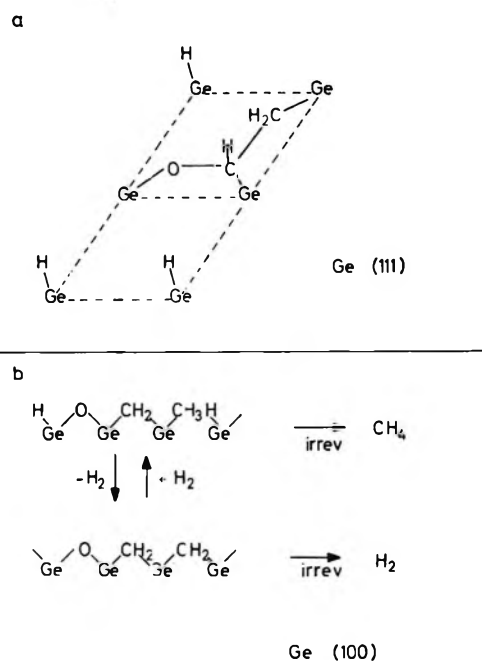


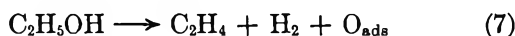
Figure 7. Structure models for the adsorption complexes of ethanol on Ge(111) and Ge(100).

posed for the adsorption complex as for the methanol case.

The reaction of ethanol vapor with clean germanium powder has been studied by Baddour and Selvidge¹¹ in a flow system. Their main decomposition product appeared to be acetaldehyde.

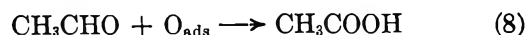


As a side-reaction, the formation of ethene was observed.



In the present work, a few experiments were performed in which the germanium sample was heated between 200 and 300° in the presence of ethanol vapor. First, ethene was formed in the same amount as expected from the previously described desorption experiments (compare Figure 6). Then the dehydrogenation reaction started, giving acetaldehyde. It seems, therefore, that this last reaction takes place at the partly covered sur-

face and is not necessarily a feature of the clean surface. A slow further reaction occurred in which the acetaldehyde was oxidized by the oxygen present on the surface to yield acetic acid.



Heating the germanium powder between 200 and 300° in the presence of methanol vapor gives carbon monoxide and hydrogen as the only reaction products. This desorption reaction is complete, constantly creating a clean surface. Sparnaay¹² reported that at higher methanol pressures (22 Torr) other reaction products are formed such as methane and ethene.

Conclusion

The interaction of gaseous adsorbates with a clean germanium surface seems to be governed by the uncompensated bonds at the surface and by the presence of an active atom in the adsorbate. It has been concluded from gas volumetric measurements on powders that the adsorption of methanol and ethanol is highly plane-specific; *i.e.*, there are large differences between the (111) and (100) planes both with respect to the amount adsorbed and the structure of the adsorption complex. This was supported by volumetric measurements on (100) oriented germanium crystals and by ellipsometric measurements on silicon surfaces.

Plane specificity will probably be a common phenomenon for chemical adsorptions on semiconductor surfaces of this type. Therefore, it is very important to obtain direct information on the structure of the adsorption complex. Techniques such as electron spectroscopy (E.S.C.A.) promise to be useful in this respect.¹³

Acknowledgment. I wish to thank Mr. P. L. M. van Boven for performing most of the adsorption and desorption experiments.

(11) R. F. Baddour and C. W. Selvidge, *J. Phys. Chem.*, **71**, 2536 (1967).

(12) M. J. Sparnaay, *Ann. N. Y. Acad. Sci.*, **101**, 973 (1963).

(13) S. Hagström, C. Nordling, and K. Siegbahn, *Phys. Lett.*, **9**, 235 (1964); F. M. Propst and T. C. Piper, *J. Vac. Sci. Technol.*, **4**, 53 (1967).

Concurrent Solution and Adsorption Phenomena in Chromatography.

III. The Measurement of Formation Constants of

H-Bonded Complexes in Solution

by D. F. Cadogan¹ and J. H. Purnell

Department of Chemistry, University College, Swansea, Wales, U.K. (Received April 7, 1969)

A gas-liquid chromatographic method for the quantitative evaluation of the stoichiometric formation constants of H-bonded complexes in nonaqueous solution is described. Theory is developed for the situation where multiple sorption occurs and methods for correcting for surface effects are described. The theory is tested by study of systems involving individual C₃-C₅ alcohols and didecyl sebacate in squalane. It is established that 1:1 complexes only are formed and formation constants and associated thermodynamic parameters are presented. The data are shown to be self-consistent and to compare well with values for other systems studied spectroscopically. The results indicate a quantitative relationship between the activity coefficients of the alcohols in squalane and the corresponding formation constants. The advantages of the glpc technique are outlined.

We have recently described² a gas-liquid partition chromatographic (glpc) method for the accurate and rapid measurement of formation constants of organic complexes in nonaqueous solution. A series of columns, each containing a complexing additive (*A*) dissolved in an inert solvent (*S*) is employed, the columns differing only in the concentration (*c_A*) of additive. Measurement of the retention volume of small samples of volatile complexing species (*X*) with each column allows calculation, sometimes directly and otherwise by extrapolation, of the corresponding apparent infinite dilution partition coefficients, *K_L*, via the well known infinite dilution retention equation connecting fully corrected (net) retention volume, *V_R*, and column liquid volume, *V_L*

$$V_R = K_L V_L \quad (1)$$

Formation constants, for 1:1 complexes (*K₁*), may then be evaluated via the equation³

$$K_L = K_L^\circ (1 + K_1 c_A) \quad (2)$$

where *K_L*[°] is the relevant infinite dilution partition coefficient (*C_{xs}*/*C_{xg}*) for distribution of *X* between *S* and the gas phase.

In principle, the above approach is applicable to the evaluation of *K₁* for complex formation via hydrogen bonding, and one such study has been described.⁴ However, almost by definition, any solvent which can be regarded as inert toward volatile H-bonding species is almost certainly a very poor solvent for such substances. In consequence, liquid bulk solubility of *X* will be low and contributions to retention from liquid surface and exposed solid surface adsorption will be substantial. This view has recently been subjected to rigorous examination^{5a} and shown^{5b} to be generally cor-

rect. It was established also that, for any volatile species, an extended form of the infinite dilution equation (1)

$$V_N = K_L V_L + K_I A_I + K_S A_S \quad (3)$$

which takes into account the surface contributions, is applicable. *K_I* and *K_S* are the infinite dilution partition coefficients relevant to liquid-gas and solid-gas interface adsorption, respectively, and *A_I* and *A_S* are the corresponding surface areas. When the surface terms are all zero, *V_N* = *V_R*. In the case where, also, complexing occurs in solution, *K_L* in eq 3 is again defined by eq 2. Evidently, if the method is to be generally applied to H-bonding studies, much more comprehensive experimentation is required than with the more amenable systems previously studied¹ if dependable values of *K_L* and, in turn, *K₁*, are to be extracted from the retention data.

The first extension of the approach demanded is immediately evident if eq 3 is rewritten in the form

$$V_N/V_L = K_L + (K_I A_I + K_S A_S)/V_L \quad (4)$$

Thus, given that values of *V_N* corresponding to infinite dilution can be obtained, a plot of *V_N*/*V_L* against *V_L*⁻¹ should then give a curve extrapolating to *K_L* at *V_L*⁻¹ = 0. It is thus necessary to employ extra sets of columns,

(1) Department of Chemistry, University of California, Riverside, Calif.

(2) D. F. Cadogan and J. H. Purnell, *J. Chem. Soc.*, A, 2133 (1968).

(3) J. H. Purnell, "Gas Chromatography 1966," A. B. Littlewood, Ed., Institute of Petroleum, London, 1967, p 3.

(4) A. B. Littlewood and F. W. Wilmott, *Anal. Chem.*, **38**, 1031 (1966).

(5) (a) J. R. Conder, D. C. Locke, and J. H. Purnell, *J. Phys. Chem.*, **73**, 700 (1969); (b) D. F. Cadogan, J. R. Conder, D. C. Locke, and J. H. Purnell, *ibid.*, **73**, 708 (1969).

of varying solvent/support ratio, *i.e.*, V_L , for each value of c_A desired, to derive the information necessary to the use of eq 4.

The second extension of the experimentation arises because, unfortunately, the occurrence of multiple sorption generally brings with it very marked peak asymmetry, which persists at even the smallest sample size which can be handled, as a consequence of the characteristics of the surface effects.^{5a,6} Hence, there is, generally, no simple route to the determination of the infinite dilution value of V_N for any multiple sorption system but, more important, because peak-maximum retention is not necessarily thermodynamically significant in these circumstances, some means to measure meaningful values of V_N with asymmetric peaks is also required. These problems have been considered at some length by us previously⁵ and have been the subject of an elegant analysis by Conder.⁷

Briefly, Conder considers the situation that a solute (X) is eluted in turn from each of a set of columns, identical in all but V_L , arbitrarily numbered $j = 0, 1, 2, 3, \dots$, to produce with each column a large asymmetric peak. He shows that a set of retention volumes corresponding to elution at a fixed gas-phase concentration of X from all columns can be obtained by finding corresponding points on the diffuse side of each peak at which the ratio [height of point above baseline:adjusted retention (from air peak)], (h_j/V_{N_i}) , is the same. This involves finding sets of h_j which fit

$$\frac{h_0}{h_j} = \frac{V_{N_0}}{V_{N_i}}$$

where the zero subscript signifies arbitrarily chosen reference data. Our experience is that this procedure, for any value of h_0 , can be carried out numerically very readily; only rarely, with the systems studied, were more than two successive approximations needed. Calculating sets for different values of h_0 yields values of V_{N_i} for each column as a function of gas-phase concentration, the data can then be corrected for pressure drop and extrapolated to yield the infinite-dilution value of V_N for each column for insertion in eq 4.

An alternative procedure to that suggested by Conder is, from the data derived by analysis of the diffuse side of each of the set of peaks, to plot a set of curves of h_j against V_{N_i} for each column. Straight lines from the origin, which correspond to fixed values of h_0/V_{N_0} , may be drawn to intersect the curves, the points of intersection along each straight line yielding the required sets of data. This procedure is undoubtedly the more effective if many data points are desired or if the numerical method requires three or more successive approximations.

We thus see that although the experimental and data-processing procedures are more tedious when H-bonding systems are under study, the glpc method again

offers a means of measurement of formation constants. Despite the added experimentation, the method is still likely to be far more rapid than alternative procedures. This paper describes a test of the theory and methods described by study of some specific systems.

Experimental Section

The low solubility of H-bonding species in inert solvents, S , previously mentioned in relation to solutes, also applies to the involatile additive A . Thus, some difficulty may be experienced in finding a suitable non-complexing diluent but it is hardly likely ever to be seriously limiting. Since in the present instance our intent was establishment of the viability of the technique, we have chosen to look for a liquid likely to H-bond with the chosen solutes (the C_3 - C_5 aliphatic alcohols) which has satisfactory solubility in squalane rather than to search for a suitable diluent for some chosen additive. We find that didecyl sebacate (DDS), a widely used glpc substrate, is suitable and this has been used throughout this work.

All columns used were 50 cm \times 0.5 cm o.d., and the solid support was 100-120 mesh (A.S.T.M.) hexamethyldisilazane-treated Sil-O-Cel. Columns of about 18% w/w solution/support were constructed with the concentration of DDS in squalane (c_A) ranging from 0 to 0.55 mol l.⁻¹ while, for the experiments at fixed c_A , columns ranging from about 7 to 32% w/w solution/support were used. In all other respects the experimental details were exactly as previously described.^{2,5}

Results

Detailed preliminary studies of the dependence of peak shape on injected sample size established that, in every case, the trailing (diffuse) edges of the elution peaks for any solute with any given column lay on a common curve. Figure 1 shows a set of peaks corresponding to elution at 50° of 0.03 to 0.11- μ l liquid samples of 2-methyl-1-propanol from a pure squalane column, which illustrates the point. This behavior, which may of course not be general, means that, for such systems, the data required in the application of Conder's method of evaluation of infinite dilution V_N can be obtained either, as he suggests, from a single massive peak or from the peak-maximum retention data of a series of peaks of different size. Conder's method is clearly more economical, but because of the exploratory nature of this study and the greater reliability of multiple measurements, we have used the peak-maximum method. Thus, in place of the single large injection we have carried out a minimum of ten elutions per system.

(6) D. E. Martire, R. L. Pecsok, and J. H. Purnell, *Trans. Faraday Soc.*, **61**, 2496 (1965).

(7) J. R. Conder, *J. Chromatogr.*, **39**, 273 (1969).

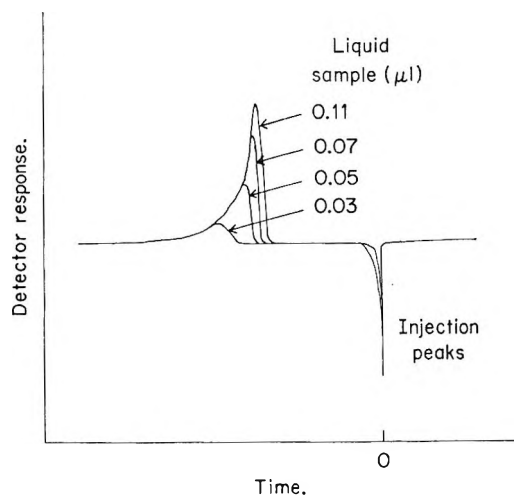


Figure 1. Illustration of dependence of peak shape on injected sample size for elution of 2-methyl-1-propanol from pure squalane at 50°.

Data processing, following Conder, was carried out as follows. For a given solute, temperature, and c_A , the data for a set of columns of differing solvent/support ratio were tabulated as sets in terms of h_j/V_{N_j} ratios corresponding to $h_j = 5, 10, 15, 20,$ and 30 chart mm peak height. The recorder attenuation setting and detector operating conditions were, of course, maintained constant at all times. The values for the most heavily loaded column were then designated h_0 and h_0/V_{N_0} in each set, and the tabulated values of h_j/V_{N_j} for all other columns were then used as a guide to carry out the numerical approximation necessary to find for each the values of h_j and V_{N_j} yielding $h_j/V_{N_j} = h_0/V_{N_0}$. As stated, this procedure was found to be quite straightforward. Having derived sets of values of V_{N_j} corresponding to constant h_j/V_{N_j} , *i.e.*, constant gas-phase concentration, two approaches are open.

First, the data may be plotted as a function of h_j and extrapolated to $h_j = 0$ to yield an infinite dilution value of V_N for each column. These data can be plotted, according to eq 4, as V_N/V_L against V_L^{-1} to give a single curve which must then be extrapolated to $V_L^{-1} = 0$ to yield K_L . The accuracy with which K_L can be determined is clearly dependent on the adequacy of extrapolation of a single curve.

The alternative method, adopted here, is to plot V_{N_j}/V_L against V_L^{-1} curves for the sets of V_{N_j} calculated for each h_0 . Since, at $V_L^{-1} = 0$, all practical sample sizes, in the range employed here at least, correspond to infinite dilution, the curves for all h_0 should extrapolate to the same value of K_L . This we find to be true in practice and the extrapolation is undoubtedly more accurate when a number of curves can be used to locate the common point. Figure 2 illustrates one set of such plots, those for 1-butanol eluted at 60° from a series of columns of $c_A = 0.14$ mol l.⁻¹.

The difference quantity $[(V_{N_j}/V_L) - K_L]$ measures

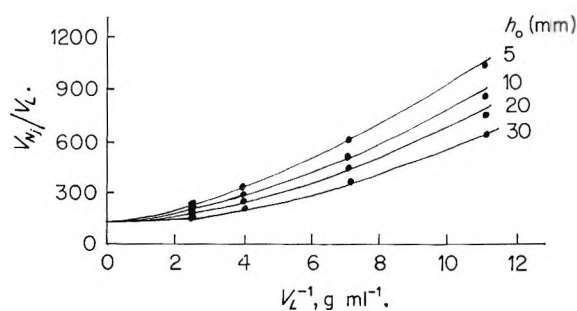


Figure 2. Plots of V_{N_j}/V_L against V_L^{-1} for various values of h_0 . Data for elution of 1-butanol at 60° from a column of 9.4% w/w DDS in squalane ($c_A = 0.14$ mol l.⁻¹). To compensate for small differences in the various columns, V_L is taken as the volume of solvent per gram of total packing.

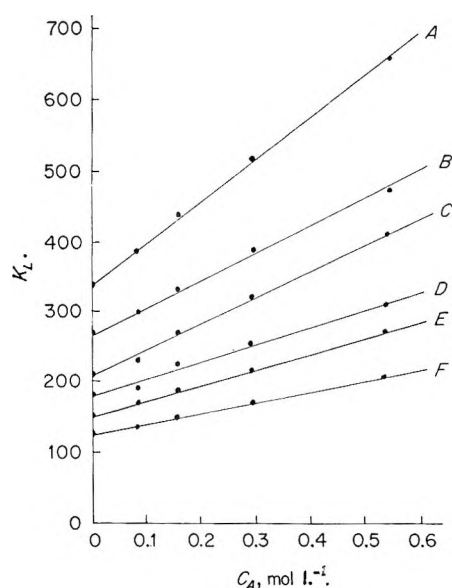


Figure 3. Plots of K_L against c_A (DDS in squalane) for (i) 2-pentanol, lines: B, 50°; D, 60°; F, 70°; and (ii) 3-methyl-1-butanol, lines: A, 50°; C, 60°; E, 70°.

the contribution of the surface terms. While K_L for any alcohol was found to depend on the value of c_A , it was found also that, for any given solvent/support ratio, the above difference was effectively independent of c_A . Thus, if this quantity is determined for a series of pure squalane columns, it can be used directly with the data for squalane-DDS columns to evaluate K_L . If this behavior is found to be general it will much reduce the volume of experimental work required.

Figure 3 illustrates typical sets of plots of derived values of K_L against c_A , for two of the alcohols, at each of three temperatures. The lines drawn are least-squares fits to the data and there is no doubt that eq 2 well describes the results. Plotted also, at $c_A = 0$, are data points obtained with squalane columns, and the agreement with the extrapolated value is excellent. These observations offer strong confirmation of the theory and procedures presented here. Formation

constants evaluated from the slopes of such plots are listed in Table I.

In order to establish that the slopes of the lines in plots such as Figure 3 do not result from mix-solvency or other effects, experiments identical with those already described were carried out with saturated hydrocarbons as solutes. Figure 4 shows a plot of K_L against

Table I: Formation Constants K_1 at 50, 60, and 70° for 1:1 Hydrogen-Bonded Complexes between Didecyl Sebacate and Aliphatic Alcohols

Alcohol	$K_1, \text{l. mol}^{-1}$		
	50°	60°	70°
2-Propanol	1.80	(1.63)	1.48
1-Butanol	1.89	1.67	1.51
2-Butanol	1.48	1.31	1.18
2-Methyl-1-propanol	1.77	1.57	1.37
2-Methyl-2-propanol	1.48	1.32	1.18
2-Pentanol	1.51	1.37	1.21
3-Methyl-1-butanol	1.83	1.65	1.51
1,1-Dimethyl-1-propanol	1.23	1.10	1.00

c_A for *n*-hexane which establishes that K_L is independent of c_A for such substances since the spread of the data is within the range $\pm 1.25\%$ which must be within any reasonable estimate of experimental and procedural error.

An indication of the errors introduced by failing to follow the procedures outlined is illustrated in Figure 5 in which we plot V_{Nj}/V_L against c_A for a range of h_0 for elution of 2-methyl-1-propanol at 50°. We see that a series of lines is obtained and that both K_L and K_1 vary by more than 10% over this small range of effective sample size. If larger samples of alcohol were used the errors could well approach 100%. Further, and most important, if data for a single h_0 were plotted, the linearity would be sufficiently good as to give no indication of error. As a final check on our procedures the data of Figure 5 can be corrected by subtracting from each the quantity $[(V_{Nj}/V_L) - K_L]$ derived from the appropriate plots of V_{Nj}/V_L against V_L^{-1} . When this is done, the four lines of Figure 5 collapse into one, with a maximum spread of $\pm 1\%$ on the points for any value of c_A .

Plots of $\log K_1$ against T^{-1} yield good straight lines; Figure 6 illustrates this with the data for four of the alcohols. The thermodynamic data derived from such plots are listed in Table II.

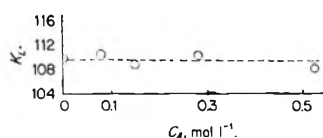


Figure 4. Plot of K_L against c_A for elution of *n*-hexane from DDS-squalane columns at 60°.

Table II: Thermodynamic Data for 1:1 Hydrogen Bonding between Aliphatic Alcohols and Didecyl Sebacate at 60°

	$-\Delta H^\circ,$ kcal mol ⁻¹	$-\Delta G^\circ,$ kcal mol ⁻¹	$-\Delta S^\circ,$ cal mol ⁻¹ deg ⁻¹
2-Propanol	2.1	0.33	5.3
1-Butanol	2.4	0.34	6.2
2-Butanol	2.5	0.18	6.9
2-Methyl-1-propanol	2.8	0.30	7.5
2-Methyl-2-propanol	2.5	0.18	6.9
2-Pentanol	2.4	0.21	6.5
3-Methyl-1-butanol	2.1	0.33	5.3
1,1-Dimethyl-1-propanol	2.3	0.06	6.6

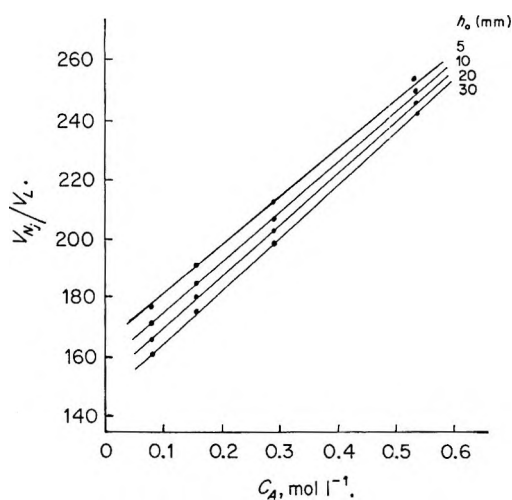


Figure 5. Plots of V_{Nj}/V_L against c_A (DDS in squalane) for data corresponding to various h_0 , uncorrected for surface effects. Elution of 2-methyl-1-propanol at 50°.

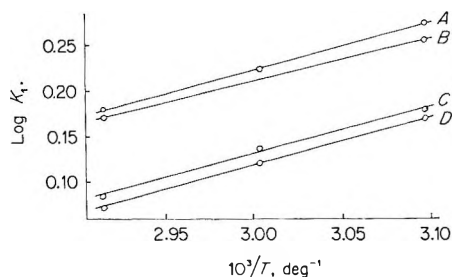


Figure 6. $\log K_1$ against T^{-1} plots for A, 1-butanol; B, 2-propanol; C, 2-pentanol; D, 2-methyl-2-propanol.

Discussion

The glpc method enjoys the considerable advantage that work at high dilution of *X* in *S* is readily possible because of the high sensitivity of available detector systems. Thus, both self-association and formation of complexes of high stoichiometry are likely to be encountered only infrequently and, further, concentration dependence of K_1 due to activity changes will be of little consequence. These assumptions underlie the basic theory adopted here and its validity is confirmed

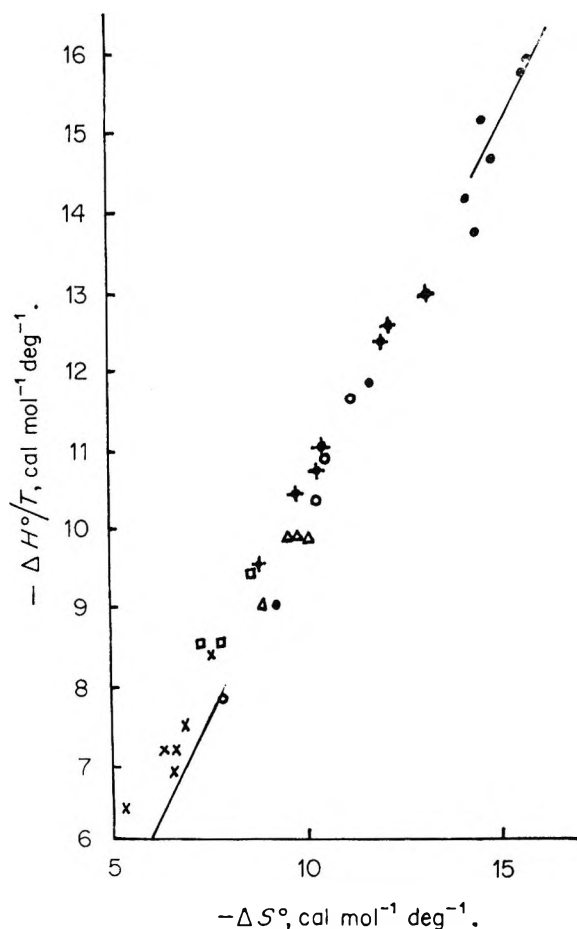


Figure 7. Plots of $-\Delta H^\circ/T$ against $-\Delta S^\circ$. Key: ●, C_1 - C_5 alcohols/di-*n*-propyl ether; ◆, C_1 - C_5 alcohols/diethyl ether;¹⁶ □, methanol, ○, ethanol, and △, *t*-butanol with acetone, benzophenone, or ethyl acetate;¹⁷ ×, this work.

by the excellent linearity of the plots in Figure 3. There is thus little question that the alcohol-DDS interaction involves formation of a single H bond in the conditions of this work.

There is, clearly, considerable self-consistency in the values of K_1 obtained since they compare in magnitude with those generally found in alcoholic systems⁸ while their sequence is the same as has been observed previously in the majority of studies.⁹ The values of $-\Delta H^\circ$ and $-\Delta S^\circ$ might be regarded as somewhat low. However, they accord well with those reported for interaction of alcohols with weak bases such as dioxane, acetone, and ethyl acetate,¹⁰⁻¹² for example. There is thus little reason to doubt these values. Figure 7 illustrates a plot of $-\Delta H^\circ/T$ against $-\Delta S^\circ$ for the data obtained here and for a wide variety of other data relating to alcohol interaction with dioxane, ketones, esters, and ethers. Our results are obviously consistent with these others. Such plots as these are not very meaningful, as we have pointed out elsewhere,^{13,14} since essentially they may merely tie together the data for systems for which K_1 lies within a fairly restricted range (the broken line corresponds to $K_1 = 1$). Even so, they

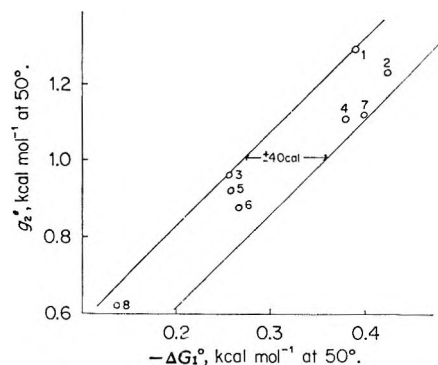


Figure 8. Plot of partial molal excess free energy of solution (g_2°) of alcohols in squalane (50°) against free energy of formation of alcohol-DDS complexes (ΔG°) at 50° . Key: 1, 2-propanol; 2, 1-butanol; 3, 2-butanol; 4, 2-methyl-1-propanol; 5, 2-methyl-2-propanol; 6, 2-pentanol; 7, 3-methyl-1-butanol; 8, 1,1-dimethyl-1-propanol.

could serve to indicate serious discrepancy, which is not apparent in the present instance.

An interesting aspect of the data is that a quantitative correlation between the partial excess free energy (g_2°) for dissolution of alcohols in squalane and the free energy of complex formation is indicated. Values of g_2° are available from our earlier work⁵ and these are plotted against $-\Delta G^\circ$ in Figure 8. Within the very reasonable error limits indicated, the data can be represented by the expression

$$g_2^\circ = (-2.5\Delta G^\circ + 0.330) \pm 0.10 \text{ kcal mol}^{-1}$$

A similar, qualitative correlation is implied in the results of an infrared study of methanol-aromatic systems by Josien and Fuson.¹⁵ The factors leading to low solubility in the nonpolar solvent are thus, in gross terms, those which lead, in the converse sense, to increasing complex stability. The data for the 1-ols in fact would fit, with negligible error, a common linear plot, thus indicating a quite direct correlation along the lines suggested. The data for the C_3 and C_4 2-ols, on the other hand, show that, whereas molecular size and point of substitution affect the value of the activity coefficient of the alcohol in squalane, they have no influence on K_1 . This illustrates that more subtle effects are at work in the solution process.

The work described appears to us to establish that the basis of the glpc approach to H-bonding studies,

- (8) A. K. Chandra and A. B. Sanigrahi, *J. Phys. Chem.*, **69**, 2494 (1965).
- (9) A. K. Chandra and S. Basu, *Trans. Faraday Soc.*, **56**, 632 (1960).
- (10) M. Tsuboi, *J. Chem. Soc. Japan, Pure Chem. Sect.*, **72**, 146 (1951).
- (11) J. J. Lindberg, *Soc. Sci. Fennica*, **20**, 5 (1957).
- (12) E. Grunwald and W. C. Coburn, *J. Amer. Chem. Soc.*, **80**, 1322 (1958).
- (13) S. H. Langer and J. H. Purnell, *J. Phys. Chem.*, **67**, 263 (1963).
- (14) S. H. Langer and J. H. Purnell, *ibid.*, **70**, 904 (1966).
- (15) M. L. Josien and N. Fuson, *J. Chem. Phys.*, **22**, 1169 (1954).

as developed here, is valid and that the technique offers much potential. The method is relatively rapid, can be employed with impure compounds, makes small demands on special experimental and theoretical skills, and requires moderately inexpensive equipment. Further, it is ideally employed in the region of infinite dilution and, most important, allows study over very wide temperature ranges. A special advantage over the infrared method is the fact that a wider range of solvents may be available since, in the latter technique, a clear solvent spectrum in the appropriate region is demanded. The one apparent drawback of the glpc

method, the required involatility of the solvent could presumably be largely or totally overcome by use of suitable pre-saturation or closed circuit gas flow techniques.^{16,17}

Acknowledgments. The authors are grateful to the Foxboro Co., Foxboro, Mass., for the award of a scholarship (D.F.C.) and of a grant for equipment and chemicals.

(16) I. Motoyama and C. H. Jarboe, *J. Phys. Chem.*, **71**, 2723 (1967).

(17) E. D. Becker, *Spectrochim. Acta*, **17**, 436 (1961).

The Kinetics of the Reaction of Trifluoromethyl Radicals with Ammonia

by Henry F. LeFevre and Richard B. Timmons

Department of Chemistry, The Catholic University of America, Washington, D. C. 20017
(Received April 7, 1969)

The gas-phase reaction of trifluoromethyl radicals with ammonia has been studied over the temperature range 81–252°. The trifluoromethyl radicals were generated by photolysis of CF₃I. The rate constant for the reaction CF₃ + NH₃ → CF₃H + NH₂ was found to be $k = (3.3 \pm 1.3) \times 10^{10} \exp\{(-8300 \pm 200)/RT\}$ in units of cm³ mol⁻¹ sec⁻¹. A comparison of CF₃ and CH₃ reactions with various polar and nonpolar molecules is presented. The difference in activation energy for these two radicals is consistently lower with polar molecules than with nonpolar substrates. However, there appears to be no simple systematic trend between the activation energy difference and the polarity of the substrate.

Introduction

The gas-phase H-atom abstraction reactions of CH₃ and CF₃ radicals have been studied with a large number of substrates. In reactions where the H atom is abstracted from a hydrocarbon the results of various workers consistently reveal that the CF₃ reactions occur with activation energies which are of the order of 3 kcal/mol lower than the corresponding CH₃ reactions. This is not surprising in view of the fact that the C–H bond-dissociation energy in CF₃H is larger than the C–H bond energy in CH₄.

In comparing CF₃ and CH₃ reactions with polar inorganic molecules the above mentioned generalization of greater CF₃ reactivity is not always observed. For example, in comparing the reactions of CF₃ and CH₃ radicals with HCl^{1,2} and HBr,^{3–5} the CF₃ reactions are reported to be slower than the corresponding CH₃ reactions. In the case of HI reactions^{5,6} the specific rate constants reported for these two radicals are very similar, resulting from the fact that although the CH₃ reaction has a higher activation energy the preexponential factor is approximately 6 times larger than

the value obtained in the CF₃ reaction. A similar situation pertains in comparing CF₃ and CH₃ reactions with SiHCl₃^{7,8} where again a higher activation energy for the CH₃ reaction is offset by a preexponential factor reported to be 20 times larger than that obtained for the CF₃ reaction. Conflicting results have been reported for CH₃ and CF₃ reactions with H₂S. The original rate constants reported for CH₃ reaction with H₂S^{9,10} are probably too high, as pointed out recently

(1) R. J. Cvetanovic and E. W. R. Steacie, *Can. J. Chem.*, **31**, 158 (1953).

(2) J. C. Amplett and E. Whittle, *Trans. Faraday Soc.*, **62**, 1662 (1966).

(3) G. C. Fettis and A. F. Trotman-Dickenson, *J. Chem. Soc.*, 3037 (1961).

(4) B. G. Tucker and E. Whittle, *Trans. Faraday Soc.*, **61**, 866 (1965).

(5) J. C. Amplett and E. Whittle, *ibid.*, **63**, 2695 (1967).

(6) M. C. Flowers and S. W. Benson, *J. Chem. Phys.*, **38**, 882 (1963).

(7) J. A. Kerr, D. H. Slater, and J. C. Young, *J. Chem. Soc.*, **A**, 104 (1966).

(8) T. N. Bell and B. B. Johnston, *Aust. J. Chem.*, **20**, 1545 (1967).

(9) N. Imai and O. Toyama, *Bull. Chem. Soc. Jap.*, **33**, 652, 1120 (1960).

by Gray, *et al.*¹¹ The two reported values for CF₃ reaction with H₂S are not in agreement, with activation energies of 3.9¹² and 1.2 kcal mol⁻¹¹³ having been observed. Because of the poor agreement among the different workers on both the CH₃ and CF₃ reactions with H₂S, it is not possible at this stage to say which reaction is the faster.

It has been suggested that larger repulsive forces between the CF₃ radical and the polar substrate may be responsible for the reversed reactivity of CF₃ and CH₃ reactions with these compounds.^{4,12} In an attempt to obtain more information on this important point, we have studied the reaction of CF₃ radicals with NH₃. The comparison of our CF₃ results with the corresponding CH₃ reaction is of particular interest in view of the highly polar character of the NH₃ molecule. In addition, the CH₃ plus NH₃ reaction has been studied on three separate occasions and the reported results are internally consistent.

Experimental Procedure

Materials. It was not possible to use the photolysis of hexafluoroacetone (HFA) as the CF₃ radical source in this study in view of the rapid reaction between HFA and NH₃. However, the photolysis of CF₃I is a convenient source for CF₃ radicals in the presence of nitrogen base compounds.¹⁴ The CF₃I was prepared by heating a 1:3 mixture of silver trifluoroacetate and iodine. The CF₃I obtained from this reaction was passed through several traps containing Ascarite in order to remove carbon dioxide. The CF₃I was further purified by fractional distillation with only the middle cut being retained.

The ammonia employed was from Matheson and had a stated minimum purity of 99.99%. This purity was confirmed by mass spectrometric analysis.

Apparatus. Reactions were carried out in a 124-cc cylindrical quartz reaction cell. The total reaction section, however, comprised a volume of 650 cc and included an all-glass gas circulation pump. The gases were circulated through the reaction cell prior to photolysis and during the course of the kinetic run. Photolysis was carried out using a G.E.-UA2 medium-pressure mercury lamp. Effective wavelengths were limited to $\lambda > 2800 \text{ \AA}$ by insertion of a filter between the lamp and the reaction cell. Circulation of pure NH₃ through the cell for 30 min produced no products noncondensable at -196°.

Photolysis was carried out over the temperature range of 81 to 252°. After a run, the products noncondensable at -196° were collected and measured in a combination Toepler pump-gas buret. Mass spectrometric analysis showed this fraction to consist of N₂ and H₂. The temperature of the traps was then raised to -154° and a second fraction collected in the gas buret. This fraction was shown to consist only of C₂F₆ and CF₃H. The ratio of C₂F₆ to CF₃H was

determined mass spectrometrically using a CEC Model 620 A mass spectrometer. The mass spectrometric cracking pattern of C₂F₆ and CF₃H was checked each day with a standard mixture of these two compounds. From a knowledge of the total moles of C₂F₆ plus CF₃H collected in the gas buret and the ratio of C₂F₆ to CF₃H obtained from the mass spectrometer, it was possible to obtain the absolute amounts of C₂F₆ and CF₃H produced.

The majority of the runs were of 2-hr duration. However, two runs were carried out for much longer periods in experiments with the absorbed intensity reduced by a factor of 10 by the insertion of a wire screen between the lamp and reaction cell. These latter experiments gave identical values for the calculated rate constant, thus showing no intensity effects are observed under our reaction conditions. In the majority of the runs the per cent conversion of the NH₃ was less than 3%. However, at the high temperature end the per cent conversion was somewhat higher, reaching 8% in one run at 251°.

Results and Discussion

The experimental results showing the rates of production of C₂F₆ and CF₃H are shown in Table I. Under our reaction conditions we can anticipate the following reaction mechanism.

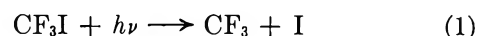


Table I: Product Yields in the Photolysis of CF₃I with Added NH₃

10 ² /T, °K ⁻¹	CF ₃ I(10%), mol/cc	NH ₃ (10%), mol/cc	CF ₃ H(10 ¹²), mol/cc sec	C ₂ F ₆ (10 ¹²), mol/cc sec	Log k ₃
1.90	0.030	1.74	8.80	2.39	7.00
1.91	0.225	1.70	18.43	17.33	7.10
2.11	0.249	1.86	7.98	17.23	6.70
2.36	0.280	2.11	2.96	15.75	6.23
2.55	0.301	4.65	2.58	13.90	5.85
2.67	0.324	4.87	1.82	12.63	5.70
2.82	0.315	8.09	1.30	11.24	5.36

The most likely fate of the NH₂ radical is reaction with iodine. As Morris and Thynne¹⁴ have pointed out, one advantage of using CF₃I as the CF₃ radical source is the fact that iodine can scavenge secondary

(10) N. Imai, *et al.*, *Bull. Chem. Soc. Jap.*, **38**, 639 (1965).

(11) P. Gray, A. A. Herod, and L. J. Leyshon, *Can. J. Chem.*, **47**, 689 (1969).

(12) N. L. Arthur and T. N. Bell, *ibid.*, **44**, 1445 (1966).

(13) J. D. Kale and R. B. Timmons, *J. Phys. Chem.*, **72**, 4239 (1968).

(14) E. R. Morris and J. C. J. Thynne, *Trans. Faraday Soc.*, **64**, 414 (1968).

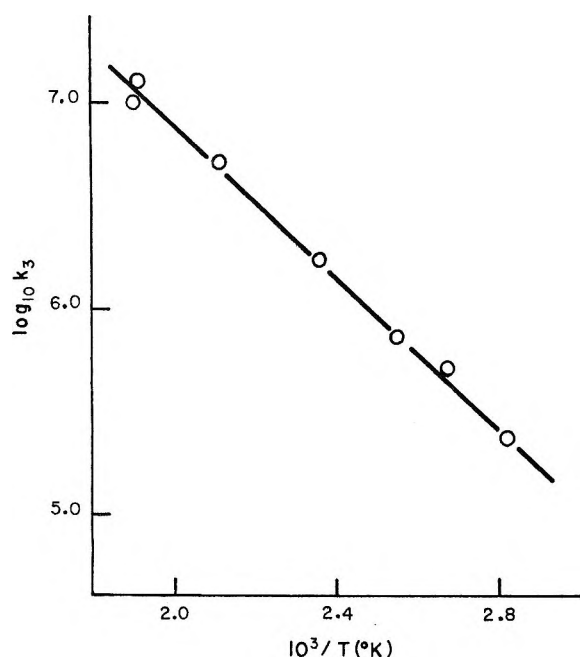


Figure 1. Arrhenius plot of the rate constant vs. reciprocal temperature for the reaction of CF_3 radicals with NH_3 .

radicals. However, we do observe small amounts of N_2 and H_2 formed in this system and presumably they arise from NH_2 reactions. The ratio of N_2 to H_2 was not reproducible from run to run, thus precluding any mechanistic interpretation of their origin.

From reactions 2 and 3, one obtains the relationship

$$\frac{R_{\text{CF}_3\text{E}}}{R_{\text{C}_2\text{F}_6}^{1/2}} = \frac{k_3[\text{NH}_3]}{k_2^{1/2}}$$

The CF_3 recombination reaction has been shown to have a nearly zero activation energy.^{15a} Using the value of $2.3 \times 10^{13} \text{ cm}^3 \text{ mol}^{-1} \text{ sec}^{-1}$ for k_2 ^{15b} and the results shown in Table I, we obtain the following result for k_3 expressed in $\text{cm}^3 \text{ mol}^{-1} \text{ sec}^{-1}$

$$k_3 = (3.3 \pm 1.3) 10^{10} \exp\{(-8300 \pm 200)/RT\}$$

The value of k_3 was calculated by the method of least squares from the plot in Figure 1. The uncertainty limits quoted are from our data and do not contain any uncertainty in the reported value for k_2 . Thus our error limits represent a lower limit.

It is of interest at this point to compare our results with the reported values for CH_3 attack on NH_3 . Three separate studies of the CH_3 reaction have produced remarkably consistent results. Activation energies of 10.0,¹⁶ 10.0,¹⁷ and 9.8¹⁸ have been reported with preexponential factors of 6.3, 7.9, and $10 \times 10^{10} \text{ cm}^3 \text{ mol}^{-1} \text{ sec}^{-1}$, respectively. Thus it is apparent that our result for the CF_3 reaction with NH_3 gives a considerably lower activation energy than the CH_3 reaction. This reaction is particularly important in view of the highly polar character of the NH_3 molecule and the suggestion that electron-electron repulsive

forces^{4,12} are more important in the CF_3 reactions. It is apparent that in the case of NH_3 such repulsive forces are not sufficiently large to reverse the reactivity of the CF_3 and CH_3 radicals.

Since a large number of reactions of CF_3 and CH_3 with the same substrate have been reported in recent years, it is of interest to compare these results. This comparison is shown in Table II where both differences in A factors and activation energies are compared. Most of the data in Table II come from references

Table II: Comparison of Arrhenius Parameters Obtained in CH_3 and CF_3 Reactions

Reactant molecule	$A_{\text{CH}_3}/A_{\text{CF}_3}$	$E_{\text{CH}_3} - E_{\text{CF}_3}$, kcal mol ⁻¹	$k_{\text{CH}_3}/k_{\text{CF}_3}$, (100°)
NH_3	2.5	1.7	0.25
SiHCl_3	2.0	1.6	0.23
HCl	3.5	-2.8	156
HBr	8.3	-1.5	63
HI	5.8	1.8	0.50
CH_3NH_2^a	0.5	1.3	0.09
$(\text{CH}_3)_2\text{NH}^a$	2.0	3.1	0.03
H_2S	1.3 ^b	-1.0	5.0
	3.2 ^c	1.7	0.32
H_2	0.04	1.5	0.005
CH_4	0.7	3.4	0.007
C_2H_6	2.1	3.8	0.013

^a Kinetic parameters refer to abstraction from the N-H group.

^b Using ref 12 for the CF_3 reaction. ^c Using ref 13 for the CF_3 reaction.

already mentioned in this paper. In some cases, for example CH_4 and C_2H_6 reactions, a simple averaging of the numerous results¹⁹ for each of these reactions was taken. The most extensive study of the CF_3 reaction with H_2 is the recent paper by Kibby and Weston²⁰ and these values have been employed. The values used for the CH_3 plus H_2 reaction are the parameters recommended by Walker.²¹ However, there is still a large uncertainty associated with the CH_3 reaction. Two sets of kinetic parameters are presented for H_2S reactions in view of the discrepancy between the two reported values for the CF_3 reactions.^{12,13} An

(15) (a) R. D. Giles and E. Whittle, *Trans. Faraday Soc.*, **61**, 1425 (1965); (b) P. B. Ayscough, *J. Chem. Phys.*, **33**, 1566 (1955).

(16) A. F. Trotman-Dickenson and E. W. R. Steacie, *ibid.*, **19**, 329 (1951).

(17) D. A. Edwards, J. A. Kerr, A. C. Lloyd, and A. F. Trotman-Dickenson, *J. Chem. Soc., A*, 621, (1966).

(18) P. Gray and J. C. J. Thynne, *Trans. Faraday Soc.*, **60**, 1047 (1964).

(19) See, for example, A. F. Trotman-Dickenson and G. S. Milne, "Tables of Bimolecular Gas Reactions," National Bureau of Standards, Reference No. NSRDS-NBS 9, U. S. Government Printing Office, Washington, D. C., 1967.

(20) C. L. Kibby and R. E. Weston, Jr., *J. Chem. Phys.*, **49**, 4825 (1968).

(21) R. W. Walker, *J. Chem. Soc., A*, 2391 (1968).

average was taken for the three reports of the CH₃ reactions with H₂S. Since the kinetic parameters reported for this reaction are also in rather poor agreement, we assume that a very large uncertainty is associated with the H₂S reactions. The CF₃ reactions with amines have been studied by Morris and Thynne.²²

It is apparent that the values for $E_{\text{CH}_3} - E_{\text{CF}_3}$ in the reactions involving hydrocarbons are considerably larger than the reactions involving inorganic molecules. This, of course, would be consistent with the concept of larger electron repulsions in the CF₃ reactions. On the other hand, there appears to be no correlation between the difference in activation energies and polarity of the substrate. For example, the dipole moment of NH₃, 1.47×10^{-18} esu, is larger than that of HCl, which is 1.08×10^{-18} esu. It would seem reasonable to expect that if electron repulsions are significantly larger in the CF₃ reactions the magnitude of such interactions would be some function of the polarity of the reactant molecule. If the reversed reactivity of CF₃ and CH₃ with HCl and HBr arises from electron repulsion then it should also be observed for molecules such as CH₃NH₂, HI, H₂S, and particularly NH₃. The fact that this is not observed is puzzling but might simply reflect the possibility that the magnitude of such electron repulsions is some complex function of the permanent dipole moment plus the polarizability of the reactant molecule.

In comparing activation energies of CF₃ and CH₃ radicals with the same substrate, it is necessary, of course, that both reactions be exothermic in order for the comparison to be meaningful. There is little doubt that this is the case for all of the substrates in Table II, with the possible exception of HCl and NH₃. If we accept the C-H bond dissociation energy in CH₄ as 104 kcal mol⁻¹²³ and the C-H bond-dissociation energy in CF₃H as 106 kcal mol⁻¹,²⁴ then the HCl reaction is also exothermic for both reactions. However, we wish to thank a reviewer for pointing out that the NH₃ reaction is not necessarily exothermic for both radical reactions. Whereas we had assumed an N-H bond dissociation energy of 103 kcal mol⁻¹ in NH₃,²⁵ this value is uncertain by at least ± 2 kcal mol⁻¹. Uncertainties in the heats of formation of NH₂, CH₃, and CF₃ radicals are sufficiently large to reverse the direction of endothermicity of one or both of these reactions depending upon the exact values chosen for the free radical heats of formation. For example, ΔH_f° for NH₂ has been tabulated to be 40 ± 2 ,²⁶ 42 ± 3 ,²⁷ 42 ± 2 ,²⁸ and 40.07 ²⁹ kcal mol⁻¹. In addition, it has been pointed out by O'Neal and Benson³⁰ that the actual value of ΔH_f° for the NH₂ radical may be as high as 46 kcal mol⁻¹. Values for the ΔH_f° of CH₃ and CF₃ radicals are also uncertain, ranging from 32 to 34 and -111 to -120 kcal mol⁻¹, respectively.²⁶⁻²⁹ In view of these uncertainties, the CH₃ and CF₃ reactions with NH₃ may both be endo-

thermic or exothermic depending upon which values are employed for the heats of formation for the various reactant and product radicals involved.

However, there has recently become available a number of other kinetic results which have a direct bearing on this question of the relative bond strengths in NH₃ and CH₄ molecules. In Table III we present a com-

Table III: Comparison of Kinetic Parameters in CH₄ and NH₃ Reactions

Reaction	Preexponential factor, cm ³ mol ⁻¹ sec ⁻¹	Activation energy, cal mol ⁻¹	Reference
O + CH ₄	2.0×10^{13}	9,200	31
O + NH ₃	4.0×10^{12}	6,600	32
CH ₃ + CH ₄	6.5×10^{11}	14,400	19
CH ₃ + NH ₃	8.1×10^{10}	10,000	19
CF ₃ + CH ₄	9.5×10^{11}	11,000	33
CF ₃ + NH ₃	3.3×10^{10}	8,300	This work

parison of the kinetic parameters obtained for the same radical (or atom) reaction with NH₃ and CH₄. The results for O + CH₄ are from Westenberg and de Haas³¹ and O + NH₃ are those of Kurylo, *et al.*³² The values for CH₃ + CH₄ and CH₃ + NH₃ were obtained by averaging the values compiled by Trotman-Dickenson and Milne.¹⁹ The results of CF₃ + CH₄ are from the paper by Carmichael and Johnston.³³ A significant fact to emerge from this comparison is the definitely lower activation energy for the abstraction reaction from NH₃. Since the CH₃ + CH₄ reaction is thermoneutral, it would seem most unlikely that the CH₃ + NH₃ reaction is endothermic as this would demand that the reaction proceeds with an extremely low activation energy. Similarly, it appears quite

(22) E. R. Morris and J. C. J. Thynne, *Trans. Faraday Soc.*, **64**, 3021 (1968). Earlier references are contained in this paper.

(23) D. M. Golden, R. Walsh, and S. W. Benson, *J. Amer. Chem. Soc.*, **87**, 4053 (1965).

(24) J. C. Amphlett, J. W. Coomber, and E. Whittle, *J. Phys. Chem.*, **70**, 593 (1966).

(25) J. A. Kerr, R. C. Sekhar, and A. F. Trotman-Dickenson, *J. Chem. Soc.*, 3217 (1963).

(26) J. A. Kerr, *Chem. Rev.*, **65**, 465 (1966).

(27) S. W. Benson, "Thermochemical Kinetics," John Wiley and Sons, Inc., New York, N. Y., 1968.

(28) V. I. Vedenev, L. V. Gurick, V. N. Kronratiev, V. A. Medvedev, and Y. L. Frankevich, "Bond Energies, Ionization Potentials and Electron Affinities," St. Martins Press, New York, N. Y., 1966.

(29) "JANAF Thermochemical Data," Dow Chemical Company, Thermal Lab, Midland, Mich., 1966.

(30) H. E. O'Neal and S. W. Benson, "Kinetic Data on Gas Phase Unimolecular Reactions," NSRDS-NBS9, U. S. Government Printing Office, Washington, D. C., in press.

(31) A. A. Westenberg and N. de Haas, *J. Chem. Phys.*, **50**, 2512 (1969).

(32) M. J. Kurylo, G. A. Hollinden, H. F. LeFevre, and R. B. Timmons, *ibid.*, in press.

(33) H. Carmichael and H. S. Johnston, *ibid.*, **41**, 1975 (1964).

certain that the $\text{CF}_3 + \text{CH}_4$ reaction is exothermic and thus the $\text{CF}_3 + \text{NH}_3$ must also be exothermic or else we would again have to invoke an unusually small activation energy for this reaction in view of the strength of the N-H bond being broken. Actually, we feel that the data in Table III are consistent with the concept that the N-H bond energy in NH_3 must be at least 2 kcal mol⁻¹ less than the C-H bond in CH_4 as it would seem most unlikely that the electron-electron repulsion encountered by a free radical in approaching an NH_3 molecule would be significantly less than encountered with CH_4 . In view of these facts, we are inclined to believe that both the CH_3 and CF_3 reactions with NH_3 are exothermic. However, more precise values for the heats of formation of the various radicals involved are certainly desirable.

Since we conclude from the results presented in Table II that no obvious correlation exists between observed activation energy differences and polarity of the substrate molecules, it is of interest to compare the experimental results with the predictions from the bond energy-bond order (BEBO) method of Johnston and Parr.³⁴ In this approach, the polarity of the reactants is not considered explicitly and electron-electron repulsions in the activated complex arise from triplet interactions between end atoms of a three-atom complex. One calculates the potential energy, V_{min} , of the reacting system along the locus of the line of constant bond order using the expression

$$V_{\text{min}} = D_{\text{N-H}} - D_{\text{N-H}}n^p - D_{\text{C-H}}(1-n)^q + D_{\text{C-N}}B(n-n^2)^\gamma[1+B(n-n^2)^\gamma] \quad (\text{I})$$

The p and q are bond-energy index parameters and n is the bond-order progress variable which is varied from 1 to 0. The last term in this equation represents the contribution from the triplet end atom interactions. The methods employed to obtain the values of p , q , and the triplet term have been discussed in detail by Johnston and Parr.³⁴ The various input data used in our calculation of the activation energies for $\text{CF}_3 + \text{NH}_3$ and $\text{CH}_3 + \text{NH}_3$ reactions are shown in Table IV. The calculated activation energies of 9.6 and 10.6 kcal mol⁻¹ are in remarkably good agreement with the experimental results. Also, the difference of 1.0

kcal mol⁻¹ for these two reactions is in reasonable agreement with the experimental result. In terms of eq 1, the lower E_{act} for the CF_3 reaction is not surprising as the same triplet interaction term must be used in both reactions and thus the difference in activation energies arises from the values D_e employed for the C-H bonds in CF_3H and CH_4 . However, it is significant that one calculates absolute values for the activation energies of these reactions in good agreement with experiment *via* a model involving a nonpolar transition state. Again, one is led to minimize the importance of increased electron-electron repulsions in CF_3 reactions as compared to the corresponding CH_3 reactions.

A second interesting experimental fact which is shown by the data in Table III is the lower preexponential factor associated with the NH_3 reactions compared to similar reactions of CH_4 . The vast majority of hydrogen-atom transfer reactions with CH_3 and CF_3 radicals have A factors in the range $10^{11.5 \pm 0.5}$ cm³ mol⁻¹ sec⁻¹. The reactions with ammonia are lower, being $10^{10.9 \pm 0.1}$ for the CH_3 reaction and $10^{10.5 \pm 0.2}$ for the CF_3 reaction.

Recently Benson²⁷ has presented an interesting method for *a priori* calculation of lower limits for A factors of bimolecular reactions based on changes in entropy between reactants and activated complex. In this approach a lower limit for ΔS^\ddagger is obtained by assuming a very tight activated complex for a particular reaction. For example, in the reaction $\text{CH}_3 + \text{NH}_3$ we would assume an activated complex of the form, $\text{CH}_3\text{-H-NH}_2$, in which the entropy of the activated complex is taken to be comparable to that of methylamine and appropriate corrections to be added for symmetry, spin, increased moments of inertia, low-frequency bending vibrations, etc. In the case of our activated complex, there is still a 3-fold symmetry axis about the C-H-N bond for the CH_3 group. Thus, no symmetry correction is required in calculating the entropy of the activated complex relative to CH_3NH_2 . Thus, adding the spin entropy correction, we can write

$$S^{\circ\ddagger}(\text{CH}_3\text{-H-NH}_2) \geq S^{\circ\ddagger}(\text{CH}_3\text{NH}_2) + R \ln 2$$

$$\Delta S^\ddagger = S^{\circ\ddagger}(\text{CH}_3\text{-H-NH}_2) - S^{\circ}(\text{CH}_3) - S^{\circ}(\text{NH}_3) \geq S^{\circ}(\text{CH}_3\text{NH}_2) + R \ln 2 - S^{\circ}(\text{CH}_3) - S^{\circ}(\text{NH}_3)$$

The entropies of CH_3NH_2 , CH_3 , and NH_3 at 298°K are taken to be 57.9, 46.0, and 46.0, respectively.²⁷ Therefore, we calculate $\Delta S^\ddagger \geq -32.7$, where this value refers to a standard state of 1 atm. We can transform to units of molarity *via* the relation $\Delta S_c^\ddagger = \Delta S_p^{\circ\ddagger} - R\Delta n - \Delta nR \ln(RT)$. In our case, $\Delta n = -1$. Therefore, we obtain $\Delta S_c^\ddagger \geq -24.4$ gibbs mol⁻¹.

Table IV: Input Values for Bond Energy-Bond Order (BEBO) Calculations^a

	Bond energies (D_e), kcal mol ⁻¹	Bond distances, Å
C-H in CF_3H	110.6	1.090
C-H in CH_4	108.2	1.090
C-N in CH_3NH_2	80.5	1.474
N-H in NH_3	107.8	1.008

^a Bond index parameters: $p(\text{N-H bond}) = 1.032$; $q(\text{C-H bond}) = 1.087$; $\beta(\text{Morse parameter}) = 1.93 \text{ \AA}^{-1}$.

(34) H. S. Johnston and C. Parr, *J. Amer. Chem. Soc.*, **85**, 2544 (1963).

The A factor for a bimolecular reaction is related to entropy changes by the equation

$$A = (ekT/h) \exp(\Delta S_c^\ddagger/R)$$

Therefore, in terms of this formulation, we predict $A \geq 7.7 \times 10^7$ l. mol⁻¹ sec⁻¹. This value is in very good agreement with the experimental result of 9×10^7 l. mol⁻¹ sec⁻¹. The comparison can be further improved by adding a correction for the increased moment of inertia of the activated complex compared to the methylamine molecule. Therefore, we conclude that the observed preexponential factors imply a very tight activated complex for this reaction.

We have carried out our calculations employing the CH₃ + NH₃ reaction instead of the CF₃ + NH₃ reaction as the entropy of the CF₃ radical is somewhat uncertain. However, rough calculations similar to that shown above lead to good agreement between theory and experiment and thus to the conclusion of a tight complex in the CF₃ + NH₃ reaction. On the other hand, if we use the Benson method to estimate the A factor for the CH₃ + CH₄ reaction, we are led to conclude that free internal CH₃ rotations are present in the activated complex in order to account for the observed A factor of 6.5×10^8 l. mol⁻¹ sec⁻¹. This latter calculation was carried out assuming an entropy for the activated complex equal to that for ethane with an added correction for the spin entropy. In this case, we calculate $A \geq 4 \times 10^8$ mol⁻¹ sec⁻¹ assuming a free CH₃ internal rotation plus an increased moment of inertia of the activated complex over that of the C₂H₆ molecule. The entropies employed for C₂H₆, CH₃, and CH₄ were 54.9, 46.0, and 44.5 gibbs mol⁻¹, respectively.²⁷ It appears that the difference in A factors of CH₃ (and CF₃) radicals with NH₃ and CH₄ can be satisfactorily accounted for in terms of entropy changes and assumptions concerning the "tightness" or "looseness" of the two activated complexes involved. Obviously this is a very important

idea with respect to reaction rate theory and it would be nice to have more kinetic data available on other radical reactions with NH₃. In general, the Benson method has led to excellent agreement of predicted A factors with experimentally observed values for a large cross section of other bimolecular reactions.

The ratio of preexponential factors for CH₃ and CF₃ reactions as shown in Table II are, in the majority of cases, close to unity. Since many of the parameters presented in Table II involve rather large experimental errors, it seems reasonable to assume that the ratio $A_{\text{CH}_3}/A_{\text{CF}_3}$ is really not significantly different from unity. Thus we conclude that the collision cross-sections for CH₃ and CF₃ reactions must be very nearly identical. Therefore, if electron-electron repulsions are significantly different in the CF₃ reactions as compared to CH₃ reactions, these interactions do not affect the respective collision frequencies.

Note Added in Revision. Subsequent to the completion of our investigation and submission for publication, a paper by Grey, *et al.*,³⁵ has appeared in which kinetic parameters for the reaction CF₃ + NH₃ are reported. Their results are in excellent agreement with our work. They report a preexponential factor of 3.5×10^{10} cm³ mol⁻¹ sec⁻¹ and an activation energy of 8.29 kcal mol⁻¹. Their work was carried out using a static system and rather different reactant concentrations than we have employed. As such, the agreement between the two sets of results is most gratifying.

Acknowledgments. Acknowledgment is made to the donors of the Petroleum Research Fund administered by the American Chemical Society for support of this research. We also wish to thank a referee for a thorough review of the manuscript and for making a number of valuable suggestions. H. F. L. was the recipient of a PRF Graduate Fellowship.

(35) P. Grey, N. L. Arthur, and A. C. Lloyd, *Trans. Faraday Soc.*, **65**, 775 (1969).

Semiempirical Calculation of Molecular Polarizabilities and Diamagnetic Susceptibilities of Fluorocarbons, Substituted Fluorocarbons, Ethers, Esters, Ketones, and Aldehydes

by J. A. Beran and L. Kevan¹

Department of Chemistry, University of Kansas, Lawrence, Kansas 66044 (Received April 9, 1969)

Empirical bond additivity and semiempirical calculational methods for molecular polarizabilities and diamagnetic susceptibilities have been applied to fluorocarbons, substituted fluorocarbons, ethers, esters, ketones, and aldehydes as well as to a few halogen-substituted alkanes and alkyl benzenes. The accuracy of the semiempirical methods is assessed for the different molecular classes investigated. It is concluded that the calculated values for the fluorocarbon systems, for which little or no experimental data exist, are of sufficient accuracy to be used for evaluation of ion-molecule and electron ionization cross sections.

I. Introduction

Molecular polarizabilities and diamagnetic susceptibilities are important for the evaluation of several kinetic aspects of positive ion chemistry. Simple ion-molecule reaction cross sections depend on the square root of the polarizability of the neutral molecule.^{2a} Electron ionization cross sections have been suggested to be proportional to molecular polarizability^{2b} as well as to diamagnetic susceptibility.³ Experimental values for polarizability and diamagnetic susceptibility exist for many simple diatomics, triatomics, and for hydrocarbons, but for most other molecular types comprehensive data are lacking.⁴ In particular, data on fluorocarbons and substituted fluorocarbons are almost entirely absent. Recent interest in the ionic reactions⁵⁻⁷ and electron ionization cross sections⁸ for fluorocarbons has created a need for polarizability and diamagnetic susceptibility data on these compounds. Previous data on electron ionization cross sections for ethers, ketones, aldehydes, and esters⁹ also require polarizabilities and diamagnetic susceptibilities for their evaluation. We have therefore investigated several semiempirical calculation methods and have calculated both polarizabilities and diamagnetic susceptibilities for fluorocarbons, substituted fluorocarbons, ethers, esters, ketones, and aldehydes.

II. Diamagnetic Susceptibility Calculations

Van Vleck¹⁰ has derived the general diamagnetic susceptibility for a molecular system as given in eq 1. The first term is the classical Langevin diamagnetic suscep-

$$\chi_M = -\frac{N_0 e^2}{6mc^2} \sum_j (\psi_0^* | r_j^2 | \psi_0) + \frac{2N_0}{3} \sum_{i \neq 0} \frac{(m_x)_i^2 + (m_y)_i^2 + (m_z)_i^2}{E_i - E_0} \quad (1)$$

tibility where N_0 is Avogadro's number, e is the electronic charge, m is the electron mass, c is the velocity of light, ψ_0 is the ground-state wave function, and r_j is the coordinate of the j th electron. The second term is the temperature-independent paramagnetic contribution to the diamagnetic susceptibility where the summation i is over all excited states, including those in the continuum, of the molecule and $(m_x)_i$ is the magnetic moment transition integral given by eq 2.

$$(m_x)_i = \left(\psi_i^* \left| \sum_j \frac{e}{2mc} M_{xj} \right| \psi_0 \right) \quad (2)$$

The summation j is over all of the electron coordinates and the orbital angular momentum operator $M_{xj} = i\hbar (y\delta/\delta z - z\delta/\delta y)$. The second term in eq 1 is zero for atoms if the coordinate origin is chosen at the nucleus, but this term is nonzero for all molecules. The first term can be calculated theoretically quite accurately for atoms and for small molecules but the second term is extremely difficult to calculate accurately because of the

(1) Department of Chemistry, Wayne State University, Detroit, Mich. 48202.

(2) (a) J. W. Otvos and D. P. Stevenson, *J. Amer. Chem. Soc.*, **78**, 546 (1956); (b) J. L. Franklin, F. H. Field, and F. W. Lampe, *ibid.*, **79**, 6129 (1957).

(3) D. P. Stevenson and D. O. Schissler in "The Chemical and Biological Action of Radiations," Vol. 5, M. Haissinsky, Ed., Academic Press, New York, N. Y., 1961, pp 182-192.

(4) H. H. Landolt and R. Bornstein, "Zahlenwerte und Functionen," 6 Auflage, "Atom and Molecular Physik," 3 Teil, Springer-Verlag, Berlin, 1950, pp 509-517.

(5) L. Kevan, *J. Chem. Phys.*, **44**, 683 (1966).

(6) L. Kevan and D. Smith, *ibid.*, **46**, 1586 (1967).

(7) J. King and D. D. Elleman, *ibid.*, **48**, 412 (1968).

(8) J. A. Beran and L. Kevan, *J. Phys. Chem.*, **73**, 3866 (1969).

(9) A. G. Harrison, E. G. Jones, S. K. Gupta, and G. P. Nagy, *Can. J. Chem.*, **44**, 1967 (1966).

(10) J. H. Van Vleck, "Electric and Magnetic Susceptibilities," Oxford University Press, London, 1932, p 275.

summation over all excited states of the molecule. Therefore, approximation methods for calculating the diamagnetic susceptibility of molecules are necessary. Several excellent, approximate calculations for diatomic molecules have been reported^{11,12} but for our purposes we shall need a more general approximate treatment which can be extended to polyatomic molecules.

Guy and Tillieu^{13,14} have utilized a variational treatment to calculate the diamagnetic susceptibility of a chemical bond. They obtained the general eq 3 where the first and second terms correspond to the first and

$$\chi_{zz} = \frac{-e^2}{4mc^2} (\psi_0^* | x^2 + y^2 | \psi_0) + \frac{e^2}{2mc^2} \frac{(\psi_0^* | x^2 - y^2 | \psi_0)}{(\psi_0^* | x^2 + y^2 | \psi_0)} \quad (3)$$

second terms in eq 1 and where $\chi_M = (N_0/3) (\chi_{zz} + \chi_{yy} + \chi_{xx})$. Note that eq 3 only includes the ground-state wave function and is therefore moderately easy to apply. For a chemical bond, ψ_0 is taken as a linear combination of hydrogen-like atomic wave functions for the two atoms in the bond and weighted according to the difference in electronegativities of the two atoms. We shall comment on this approximation later. Different atomic orbital wave functions were used corresponding to different degrees of sp hybridization of the atom. Baudet¹⁵ extended Tillieu's variation treatment to include a wide variety of bonds with each atom in various states of hybridization. Baudet then developed a systematic approach for the calculation of total molecular diamagnetic susceptibilities in which the total susceptibility is the sum of three contributions: (a) the diamagnetic susceptibility of the internal electrons or electrons not found in the valence shell, (b) the diamagnetic susceptibility of free pairs of electrons in the valence shell of atoms in various states of hybridization, and (c) the diamagnetic susceptibility of bonds with the atoms in various states of hybridization.

Table I: Calculated Diamagnetic Susceptibilities for Perfluorocarbons^{a,b}

Molecule	Haberdtz method ^c	Baudet method ^d
CF ₄	32.6	26.9
C ₂ F ₆	52.5	43.5
C ₃ F ₈	72.4	60.1
n-C ₄ F ₁₀	92.4	76.7
n-C ₆ F ₁₄	132.3	109.9
c-C ₄ F ₈	79.8	66.1
C ₂ F ₄	36.9	32.6
C ₃ F ₆	56.0	49.2
2-C ₄ F ₈	73.8	65.9
1-C ₇ H ₁₄	134.0	115.7
c-C ₈ F ₁₀	101.1	88.8

^a In units of 10⁻⁶ cgs emu/mol. ^b No experimental values are available. ^c References 18 and 19. ^d Reference 17.

Table II: Calculated Diamagnetic Susceptibilities for Substituted Fluorocarbons^a

C-F-Cl compounds	Haberdtz method ^b	Baudet method ^c	Exptl value
CF ₃ Cl	45.0	37.6	45.3 ^b
CF ₂ Cl ₂	52.0	48.4	52.2 ^d
CFCl ₃	61.8	59.2	58.7 ^d
C ₂ F ₅ Cl	65.0	54.2	
1,2-C ₂ F ₄ Cl ₂	77.5	65.0	
1,1,2-C ₂ F ₃ Cl ₃	79.1	75.8	
C-F-Br compounds			
CF ₃ Br	52.6	54.1	
CF ₂ Br ₂	67.0	81.3	
C-F-I compounds			
CF ₃ I	68.6	70.7	
C ₂ F ₅ I	88.5	87.3	
i-C ₈ F ₇ I	108.4	103.9	
C-F-H compounds			
CH ₃ F	20.8	19.0	
CH ₂ F ₂	24.8	21.6	
CHF ₃	28.6	24.2	
1,1-C ₂ H ₄ F ₂	36.9	33.0	
1,1-C ₂ H ₂ F ₂	28.7	26.9	
Other C-F-X compounds			
CHF ₂ Cl	40.8	35.0	38.6 ^d
CHFCl ₂	49.2	45.8	48.8 ^d
CF ₂ ClBr	59.4	64.8	
CF ₂ ClCFCl	102.6	108.9	
CF ₂ ClCHF ₂	96.7	95.5	
CF ₂ ClCH ₃	53.3	46.4	
CF ₂ BrCFClBr	101.0	108.7	
CF ₂ BrCHFCl	80.7	78.8	

^a In units of 10⁻⁶ cgs emu/mol. ^b References 16 and 17. ^c Reference 15. ^d "Handbook of Chemistry and Physics," 44th ed, Chemical Rubber Co., Cleveland, Ohio, 1963, p 2745.

Tables of these various contributions are provided by Baudet¹⁵ and the results reported in Tables I-III were obtained by summation of the appropriate diamagnetic susceptibility contributions.

Baudet's treatment is attractive because it is systematic, simple, and consistent. However, it gives high values for ketones and aldehydes by 10-20% and by analogy with CFCl compounds it probably gives low values for fluorocarbons. These and other discrepancies have been interpreted as due to

(11) R. M. Stevens, R. M. Pitzer, and W. N. Lipscomb, *J. Chem. Phys.*, **38**, 550 (1963); R. M. Stevens and W. N. Lipscomb, *ibid.*, **40**, 2238 (1964); **41**, 184, 3710 (1964).

(12) M. Karplus and H. J. Kolker, *ibid.*, **35**, 2235 (1961); **38**, 1263 (1963).

(13) J. Guy and J. Tillieu, *Compt. Rend.*, **239**, 1203 (1954).

(14) J. Tillieu, *Ann. Phys.*, **2**, 631 (1957).

(15) J. Baudet, *J. Chim. Phys. Physiol. Chim. Biol.*, **58**, 223 (1961).

Table III: Other Calculated Diamagnetic Susceptibilities^a

Alkyl halides	Haberditzl method ^b	Baudet method ^c	Exptl value
CH ₃ Cl	32.2	29.7	32.0 ^b
C ₂ H ₅ Cl	44.7	41.1	45.0 ^b
<i>n</i> -C ₃ H ₇ Cl	56.0	52.4	56.1 ^b
<i>n</i> -C ₄ H ₉ Cl	67.4	63.8	67.1 ^b
CH ₂ Cl ₂	46.6	43.1	46.6 ^b
CH ₂ ClBr	54.0	59.6	55.0 ^d
CHCl ₂ Br	66.6	73.0	66.3 ^d
CH ₃ Br	39.6	46.2	
Ethers			
CH ₃ OCH ₃	32.5	33.7	
C ₂ H ₅ OCH ₃	43.8	45.0	
C ₂ H ₅ OC ₂ H ₅	55.2	56.4	
<i>n</i> -C ₄ H ₉ OCH ₃	66.6	67.8	
<i>t</i> -C ₄ H ₉ OCH ₃	69.0	67.8	
(<i>n</i> -C ₃ H ₇) ₂ O	78.7	79.1	
Esters			
HCOOCH ₃	30.8	34.2	30.9 ^b
HCOOC ₂ H ₅	42.2	45.6	42.5 ^b
HCOOC ₃ H ₇	53.5	56.9	
HCOOCH(CH ₃) ₂	54.4	56.9	
HCOOC ₄ H ₉	64.8	68.3	
HCOOCH ₂ CH(CH ₃) ₂	65.6	68.3	
CH ₃ COOCH ₃	43.0	45.8	
C ₂ H ₅ COOCH ₃	54.3	57.1	
CH ₃ COOC ₂ H ₅	54.3	57.1	54.2 ^b
C ₃ H ₇ COOCH ₃	66.6	68.5	
C ₄ H ₉ COOCH ₃	77.0	79.8	
Ketones			
CH ₃ COCH ₃	34.6	39.9	34.0 ^b
C ₂ H ₅ COCH ₃	46.0	51.3	45.6 ^b
C ₃ H ₇ COCH ₃	57.4	62.6	57.4 ^b
C ₂ H ₅ COC ₂ H ₅	57.4	62.6	
<i>n</i> -C ₅ H ₁₁ COCH ₃	80.0	85.3	
<i>n</i> -C ₆ H ₁₃ COCH ₃	91.4	96.7	92.1 ^b
Aldehydes			
CH ₃ CHO	22.9	28.3	22.7 ^b
C ₂ H ₅ CHO	34.2	39.7	34.3 ^b
<i>i</i> -C ₃ H ₇ CHO	46.5	51.0	46.1 ^b

^a In units of 10⁻⁶ cgs emu/mol. ^b References 16 and 17. ^c Reference 15. ^d "Handbook of Chemistry and Physics," 44th ed., Chemical Rubber Co., Cleveland, Ohio, 1963, p 2745.

electron correlation effects between neighboring bonds. Corrections for these neighboring bond effects have been carried out in an empirical manner by Haberditzl.^{16,17} Haberditzl used Baudet's quantum mechanical values for the diamagnetic susceptibility due to inner shell core electrons and to valence shell lone electron pairs. The bonding electron susceptibilities for various bonds were determined empirically from measured diamagnetic susceptibilities for a large number of molecules. Thus, different values are obtained for primary, secondary, and tertiary carbons bonded to hydrogen or halogens. The total molecular diamagnetic

susceptibility is simply the sum of the nonbonded electron contributions for each atom in the molecule plus the empirical value for all of the bonds in the molecule. The accuracy of this method depends on the accuracy and the variety of experimental data available. It is limited as are all empirical methods, but sufficient bond types are given by Haberditzl¹⁶ that we can calculate the molecules of interest to us here. The diamagnetic susceptibility results from Haberditzl's method are also tabulated in Tables I-III as are known experimental values.

III. Polarizability Calculations

The general expression for molecular polarizability is given in eq 4. It can be seen that this expression is

$$\alpha = \frac{2}{3} \sum_{i \neq 0} \frac{(\mu_x)_i^2 + (\mu_y)_i^2 + (\mu_z)_i^2}{E_i - E_0} \quad (4)$$

where

$$(\mu_x)_i = (\psi_i^* | \sum_j e x_j | \psi_0)$$

similar to the second term in the general diamagnetic susceptibility expression (1). This term is difficult to evaluate and consequently semiempirical methods are the most fruitful for obtaining molecular polarizabilities for a wide variety of molecules. The most satisfactory procedure is to use a variational method as was done in the case of diamagnetic susceptibility.¹⁸ For diatomic molecules fairly accurate wave functions give rise to calculated polarizabilities that show reasonable agreement with experiment.^{11,19} To calculate polarizabilities for general classes of polyatomic molecules, it is only practical at present to use various semiempirical wave functions. Lippincott and Stutman²⁰ have carried out such calculations by applying the semiempirical δ -function model of chemical binding.^{21,22} The δ -function model basically consists of replacing the coulombic potentials in the Schroedinger equation of a molecular system with δ -function potentials. Molecular wave functions are obtained from linear combinations of atomic δ -function wave functions. The x component of the polarizability is then given by eq 5 where n is the number of electron equivalence classes (π , σ , etc.).

(16) W. Haberditzl, *Sitzber. Deut. Akad. Wiss. Berlin. Kl. Chem. Geol. Biol.*, No. 2 (1964).

(17) W. Haberditzl, *Angew. Chem., Int. Ed.*, 5, 288 (1961).

(18) J. O. Hirschfelder, C. F. Curtiss, and R. B. Bird, "Molecular Theory of Gases and Liquids," John Wiley and Sons, New York, N. Y., 1954, pp 941-946.

(19) H. J. Kolker and M. Karplus, *J. Chem. Phys.*, 39, 2011 (1963).

(20) E. R. Lippincott and J. M. Stutman, *J. Phys. Chem.*, 68, 2926 (1964); E. R. Lippincott, G. Nagarajan, and J. M. Stutman, *ibid.*, 70, 78 (1966).

(21) E. R. Lippincott and M. O. Dayhoff, *Spectrochim. Acta*, 16, 807 (1960).

(22) A. A. Frost, *J. Chem. Phys.*, 22, 1613 (1954); 23, 985 (1955); 25, 1150 (1956).

$$\alpha_{zz} = \frac{4nA}{a_0} (\psi_0|x^2|\psi_0)^2 \quad (5)$$

A is the δ -function strength which is empirically determined from the electronegativity of an atom, a_0 is the Bohr radius, and ψ_0 is the ground-state δ -function wave function.

Molecular polarizabilities were calculated from parallel and perpendicular components of the constituent bond polarizabilities. The parallel component of the bond polarizability was taken to be the sum of the bonding electron contribution and the contribution from the valence shell nonbonding electrons in each atom of the bond. For the bonding electrons $\bar{x}^2 = R^2/4 + [2C_R]^2$ where R is the internuclear distance and C_R is an empirical constant which is a function of the reduced electronegativities of the atoms in the bond. The second term in the expression for \bar{x}^2 is usually small compared to the first term so by eq 5 the parallel bond polarizability is proportional to the fourth power of the internuclear distance. The contribution to the parallel bond polarizability from the valence shell nonbonding electrons is determined by multiplying the fraction of nonbonding electrons to total electrons by the δ -function atomic polarizability for each atom in the bond. The atomic δ -function polarizabilities are calculated from $\bar{x}^2 = 1/A^2$. For polar bonds a correction factor, σ_i , is added which is a function of the electronegativities of the atoms in the bond. The perpendicular component of the bond polarizability was calculated by simply summing the atomic δ -function polarizabilities. Also, a polarity correction, involving Pauling's electronegativities, is applied to the perpendicular bond polarizabilities.

The average molecular polarizability, α_M , is independent of bond angles and is given by $1/3$ the sum of the parallel bond polarizabilities plus $2/3$ the sum of the perpendicular bond polarizabilities. In terms of the above

Table IV: Calculated Polarizabilities for Perfluorocarbons^a

Molecule	Lippincott-Stutman Method ^b		LeFevre method ^c	Exptl value
	Polar cor (eq 6)	No polar cor (eq 7)		
CF ₄	29.3	39.1	27.3	28.6 ^d
C ₂ F ₆	50.6	65.0	46.0	
C ₃ F ₈	73.6	94.0	64.7	
<i>n</i> -C ₄ F ₁₀	98.7	126.7	83.4	
<i>n</i> -C ₆ F ₁₄	143.9	183.3	120.9	
<i>c</i> -C ₄ F ₈	104.3	124.7	74.9	
C ₂ F ₄	43.2	54.0	41.7	
C ₃ F ₆	65.6	81.7	60.3	
2-C ₄ F ₈	90.4	111.7	79.0	
1-C ₇ F ₁₄	156.8	194.0	135.2	
<i>c</i> -C ₆ F ₁₀	122.6	145.5	107.9	

^a In units of 10^{-26} cm³. ^b Reference 20. ^c Reference 25. ^d See ref 20.

Table V: Calculated Polarizabilities for Substituted Fluorocarbons^{a, b}

C-F-Cl compounds	Lippincott-Stutman Method ^c		LeFevre method ^d
	Polar cor (eq 6)	No polar cor (eq 7)	
CF ₃ Cl	43.1	52.4	45.8
CF ₂ Cl ₂	59.2	67.7	64.3
CFCl ₃	75.4	81.8	82.8
C ₂ F ₅ Cl	66.3	81.7	64.5
1,2-C ₂ F ₄ Cl ₂	78.8	92.3	89.7
1,1,2-C ₂ F ₃ Cl ₃	96.9	108.0	101.5
C-F-Br compounds			
CF ₂ Br	50.4	60.6	56.6
CF ₂ Br ₂	73.6	83.3	85.9
C-F-I compounds			
CF ₃ I	63.2	76.2	74.4
C ₂ F ₅ I	84.2	102.2	93.1
<i>i</i> -C ₃ F ₇ I	105.8	128.9	111.8
C-F-H compounds			
CH ₃ F	25.9	29.5	26.0
CH ₂ F ₂	26.9	32.9	26.5
CHF ₃	27.8	35.5	26.9
1,1-C ₂ H ₄ F ₂	46.7	53.0	44.3
1,1,1-C ₂ H ₃ F ₃	47.1	55.6	44.7
1,1-C ₂ H ₂ F ₂	41.9	48.0	40.8
1,2-C ₂ H ₂ F ₂	42.0	48.4	40.8
Other C-F-X compounds			
CH ₂ FCI	43.0	46.8	44.9
CHF ₂ Cl	42.6	49.6	45.4
CHFCl ₂	58.5	63.5	63.9
CF ₂ ClBr	66.5	75.9	75.1
CF ₂ ClCFCII	114.6	130.0	130.1
CF ₂ ClCHFI	99.0	112.6	111.2
CF ₂ ClCH ₃	63.8	70.9	63.2
CF ₂ BrCFCIBr	109.9	123.8	133.1
CF ₂ BrCHFCI	87.0	99.0	93.4

^a In units of 10^{-26} cm³. ^b No experimental values are available. ^c Reference 20. ^d Reference 25.

discussion, the average molecular polarizabilities are given by eq 6 with bond polarity corrections or by eq 7

$$\alpha_M = 1/3 \left[\sum_i \sigma_i \alpha_{\parallel i} b_i + \sum_j f_j \alpha_j + n_{at} \frac{\sum_j X_j^2 \alpha_j}{\sum_j X_j^2} \right] \quad (6)$$

$$\alpha_M = 1/3 \left[\sum_i \alpha_{\parallel i} b_i + \sum_j f_j \alpha_j + \frac{3N - 2n_b}{N} \sum_j \alpha_j \right] \quad (7)$$

with no bond polarity corrections. The summation subscript i refers to bonds and j refers to atoms. Therefore, α_j is an atomic polarizability, f is the fraction of nonbonding electrons in the valence shell, σ is a parallel bond polarity correction, n_{at} is the number of residual degrees of polarizability freedom as defined by Lippin-

Table VI: Other Calculated Polarizabilities^a

Alkyl halides	Lippincott-Stutman method ^b		LeFevre ^c method	Denbigh ^d method	Exptl value
	Polar cor (eq 6)	No polar cor (eq 7)			
CH ₃ Cl	42.7	43.9	44.5	45.6	45.6 ^e
C ₂ H ₅ Cl	65.1	63.7	62.3	64.9	64.0 ^e
<i>n</i> -C ₃ H ₇ Cl	84.2	82.7	80.2	84.3	82.4 ^f
<i>n</i> -C ₄ H ₉ Cl	104.0	102.4	98.0	103.7	
CH ₂ Cl ₂	61.7	60.8	63.4	65.1	64.8 ^e
CH ₂ ClBr	70.1	68.5	74.2	75.0	
CHCl ₃	77.7	78.2	82.3	84.7	82.3 ^e
CHCl ₂ Br	86.2	86.2	93.1	94.6	
CCl ₄	92.5	95.0	101.2	104.3	105.0 ^e
CH ₃ Br	53.6	51.2	55.3	55.4	
Ethers					
CH ₃ OCH ₃	51.9	52.9	50.4		51.6, ^e 52.7 ^f
CH ₃ OC ₂ H ₅	72.0	75.0	68.3		
C ₂ H ₅ OC ₂ H ₅	92.1	95.0	86.1		87.3 ^e
<i>n</i> -C ₄ H ₉ OCH ₃	112.2	115.0	104.0		
(<i>n</i> -C ₃ H ₇) ₂ O	132.4	135.0	121.8		125.0 ^e
Esters					
HCOOCH ₃	56.4	51.7	51.5		
HCOOC ₂ H ₅	76.6	71.8	69.4		
HCOOC ₃ H ₇	96.7	91.8	87.2		
HCOOC ₄ H ₉	116.8	111.8	105.0		
CH ₃ COOCH ₃	76.0	71.2	69.4		
CH ₃ COOC ₂ H ₅	96.1	91.2	87.2		
C ₂ H ₅ COOCH ₃	116.3	111.8	105.0		
C ₄ H ₉ COOCH ₃	136.4	131.1	122.9		
Ketones					
CH ₃ COCH ₃	70.1	62.3	62.3	63.4	63.3, ^e 64.2 ^f
C ₂ H ₅ COCH ₃	90.3	82.3	80.2	82.8	81.3 ^e
C ₃ H ₇ COCH ₃	110.4	102.3	98.0	102.1	99.3 ^e
C ₂ H ₅ COC ₂ H ₅	110.4	102.3	98.0	102.1	99.3 ^e
<i>n</i> -C ₆ H ₁₁ COCH ₃	150.7	142.2	133.7	140.9	
<i>n</i> -C ₈ H ₁₇ COCH ₃	170.8	162.2	151.6	160.3	
Aldehydes					
CH ₃ CHO	50.5	42.9	44.5	44.0	
C ₂ H ₅ CHO	70.7	62.9	62.3	63.4	
<i>i</i> -C ₃ H ₇ CHO	90.9	82.9	80.2	82.8	
Alkyl benzenes					
C ₆ H ₆	110.5	109.6	99.1	103.1	103.2 ^f
C ₆ H ₅ CH ₃	130.6	129.6	117.0	122.5	122.6 ^e
C ₆ H ₅ C ₂ H ₅	150.6	149.6	134.8	141.9	
C ₆ H ₅ C ₃ H ₇	170.6	169.6	152.6	161.2	
C ₆ H ₅ C ₄ H ₉	190.6	189.6	170.5	180.6	

^a In units of 10⁻²⁶ cm³. ^b Reference 20. ^c Reference 25. ^d Reference 24. ^e Reference 4. ^f See ref 20.

cott and Stutman,²⁰ X is Pauling's atomic electronegativity, N is the number of atoms in the molecule, and n_b is the number of bonds in the molecule. Equations 6 and 7 can be applied in a fairly straightforward manner to many polyatomic molecules by using the atomic polarizabilities, parallel bond polarizabilities, Pauling electronegativities, and the δ -function strength A values tabulated by Lippincott and Stutman together with the experimental bond lengths in the molecule.

Equations 6 and 7 were programmed in FORTRAN IV language for a GE-625 computer²³ and the polarizabilities reported in Tables IV-VI were calculated from available experimental bond lengths.²³

Denbigh²⁴ and LeFevre²⁵ have empirically deter-

- (23) J. A. Beran, Ph.D. Thesis, University of Kansas, 1968.
 (24) K. G. Denbigh, *Trans. Faraday Soc.*, **36**, 936 (1940).
 (25) R. J. W. LeFevre, *Advan. Phys. Org. Chem.*, **3**, 1 (1966).

mined a number of perpendicular, parallel, and average bond polarizabilities from experimental values for the refractive index, dielectric constant, molar Kerr constant, and degree of polarization of scattered light. These empirical bond polarizabilities can simply be added to obtain molecular polarizabilities which are accurate to within a few per cent for those molecules from which the bond polarizabilities were determined. The empirical bond polarizabilities of Denbigh and LeFevre have been used to calculate molecular polarizabilities in Tables IV-VI. Denbigh did not determine values for the C-F and C-I bonds, so molecules containing these bonds were only calculated by LeFevre's values.

IV. Discussion

Baudet's calculated values of diamagnetic susceptibility for alkanes and alkenes agree well with experiment to within $\pm 2\%$. Some experimental values are also available in Table III to compare with Baudet's calculated values for ketones, aldehydes, ethers, and esters. The esters, ketones, and aldehydes all show high calculated values compared to experiment. The esters are high by 6-8%, the ketones by 10-16%, and the aldehydes by 18-24%. This systematic deviation indicates that the diamagnetic susceptibility of electrons in C=O bonds is sensitive to the polarity of the bond due to the substituents on carbon. The amount of deviation between experimental and calculated values increases as the C=O bond polarity increases and as the amount of double-bond character in C=O decreases. It appears that a decrease in double-bond character decreases the actual diamagnetic susceptibility of the double bond so that the experimental values are less than the calculated values. It is possible that a somewhat better approximation for ψ_0 for C=O bonds would give better results for these three classes of compounds. Introduction of a polarity parameter into ψ_0 should give quite good results. Haberditzl's results shown in Table III agree closely with experiment; this is, of course, expected since they are determined in part by the experimental values to account for neighboring bond effects.

For fluorocarbons and substituted fluorocarbons there are very few experimental values to compare with the calculated ones. Where comparison can be made the Baudet values seem to be 10-15% low compared to the experimental values. The deviation seems to be greater the more fluorines that are in the molecule. Also the deviation between Baudet's values and Haberditzl's values follows this trend of being greatest for the most highly fluorine-substituted molecules. In perfluorocarbons the deviation is always about 17% low. Presumably a more accurate calculation of the diamagnetic susceptibility of the C-F bond would give a larger value than obtained by Baudet in his simple treatment.

For comparison of diamagnetic susceptibilities with molecular ionization cross sections one is interested mainly in the difference in diamagnetic susceptibility

from molecule to molecule. For such a comparison either Haberditzl's or Baudet's calculated values should be equally valid within a given molecular class. For an overall comparison between molecular classes, we consider Haberditzl's values to be somewhat more accurate. It is suggested that Baudet's systematic method could be improved by more rigorous calculations of the diamagnetic susceptibility of C-F and C=O bonds. For more general applicability, it may be simpler to introduce a bond polarity parameter into the Baudet method as was done by Lippincott and Stutman²⁰ for molecular polarizability calculations. Other less polar molecular types such as alcohols, nitriles, sulfides, thiols, and xylenes, as calculated by Baudet, do give fairly good agreement between calculated and experimental diamagnetic susceptibilities.¹⁵

Molecular polarizabilities calculated from LeFevre's empirical bond polarizabilities average $2 \pm 2\%$ below the experimental values for the molecular classes in Table VI. Thus we consider that polarizabilities calculated by LeFevre's parameters in Table VI can be taken as a set of reference values with which to compare polarizabilities calculated by the semiempirical Lippincott-Stutman method.²⁰ It is interesting to contrast the semiempirical polarizabilities calculated with and without polarity corrections. For the alkyl halides the polarity correction makes little overall difference and the calculated polarizabilities are in good agreement with the LeFevre values. One expects the C=O polarity to increase from ethers to esters to ketones to aldehydes. It is true that the difference between the values calculated with and without polarity corrections increases in the order just cited. However, the polarity-corrected values for esters, ketones, and aldehydes show much poorer agreement with the LeFevre values and with experimental values than do the polarizabilities calculated without polarity corrections for these same classes of compounds. Thus the decision to use eq 6 with polarity corrections or eq 7 without polarity corrections to calculate molecular polarizabilities is a rather delicate one which cannot be decided on the basis of chemical reasoning alone. We conclude that for the molecular classes listed in Table VI eq 7 without polarity corrections gives the best results which are, in fact, in excellent agreement with experiment.

Only one experimental value exists for the polarizability of a perfluorocarbon (CF₄) and we found no experimental values for substituted fluorocarbons. We shall therefore consider polarizabilities calculated by LeFevre's empirical bond polarizabilities as a reference set of values with which to compare the semiempirical calculations by the Lippincott-Stutman model.²⁰ Table IV shows that it is imperative to use the polarity correction in the semiempirical calculations on perfluorocarbons to obtain values that are at all close to the LeFevre values. With polarity corrections, the polarizabilities of the perfluoroalkanes average 14% above

the corresponding LeFevre values and the values for the perfluoroalkenes average 11% above the LeFevre values. We conclude that the polarity correction is essential for all perfluorocarbons; however, we must await the measurement of more experimental values before we can conclude that the calculated semiempirical polarizabilities are significantly too high.

Table V shows that for substituted fluorocarbons polarity corrections are not unambiguously necessary to obtain satisfactory agreement with the LeFevre values. For C-F-X or C-F-H-X compounds where X is a halogen the calculated values with polarity corrections average 9% below the LeFevre values while the polarizabilities calculated with no polarity corrections average 6% above the LeFevre values. Since the LeFevre values are probably several per cent lower than the true experimental values, we conclude that for C-F-X and C-F-H-X compounds eq 7 with no polarity corrections gives the most satisfactory results. On the other hand, for C-F-H compounds calculated values

with polarity corrections average 3% above the LeFevre values while calculated values without polarity corrections average 18% above the LeFevre values. Thus for C-F-H compounds we conclude that eq 6 with polarity corrections should be used. Overall, the Lippincott-Stutman semiempirical method for calculating molecular polarizabilities gives good results with an accuracy of 10% or better. The method has the appeal of being readily extendable to complex molecules and to new molecules for which no experimental data exist; however, the decision of whether to incorporate polarity corrections or not remains largely empirical.

Both the LeFevre and the Lippincott-Stutman method appear to give sufficiently accurate polarizabilities to test for correlations between polarizability and molecular ionization cross sections.

Acknowledgment. We thank the U. S. Atomic Energy Commission for support of this research. This is AEC Document No. COO-1528-30.

Molecular Electron Ionization Cross Sections at 70 eV

by J. A. Beran and L. Kevan¹

Department of Chemistry, University of Kansas, Lawrence, Kansas 66044 (Received April 9, 1969)

Electron ionization cross sections at 70 eV have been measured for 62 hydrocarbons, fluorocarbons, and halogen-substituted hydrocarbons and fluorocarbons. These results together with previously measured results on other molecular classes have been tested against proposed correlations of ionization cross sections with polarizability, diamagnetic susceptibility, and additivity of atomic ionization cross sections. None of these correlations is generally valid but each is valid within a given molecular class. It is striking, however, that there is a single linear correlation with diamagnetic susceptibility for all nonfluorine-substituted compounds. Two empirical equations are developed, based on polarizability and based on modified additivity correlations, which reproduce the experimental cross sections for 98 molecules in a wide variety of molecular classes within average deviations of 3 and 4.5%.

I. Introduction

Electron ionization cross sections for atoms and molecules are of importance for evaluation of radiation chemical data, for mass spectrometric studies of ion-molecule reactions and thermodynamic measurements, and for plasma and space physics. They also constitute one of the fundamental problems concerning electron impact collisions. There has been considerable work on both the experimental and theoretical aspects of electron ionization cross sections. Electron ionization cross sections increase rather rapidly with energy from threshold, reach a flat maximum usually between 50 and 80 eV, and decrease slowly at higher energies. At high

electron kinetic energy (>1 keV) there is good agreement between the experimental energy dependence of the cross section and simple theory based on the Born approximation.² However, the experimental dependence of cross section on molecular structure is not satisfactorily predicted by theory. At lower electron energies which are relevant to mass spectrometric and radiation chemical studies (70 eV) the theory is even more

(1) Department of Chemistry, Wayne State University, Detroit Mich. 48202.

(2) B. L. Schram, A. J. H. Boerboom, M. J. van der Wiel, F. J. de Heer, and J. Kistemaker, "Advances in Mass Spectrometry," Vol. 3, W. L. Mead, Ed., Institute of Petroleum, London, 1966, pp 273-286.

approximate and neither theory nor experiment show particularly good agreement in themselves or with each other.^{3,4} Lacking a rigorous predictive theory one turns to semiempirical correlations. It is most desirable to find a correlation between cross sections in the approximate energy independent range near 70 eV and some ground-state molecular property. Three such correlations have been suggested which can be partially justified by approximate theory.

Otvos and Stevenson^{3a} suggested that atomic ionization cross sections in the approximate energy independent range could be calculated from the average square radius of the electrons with ionization energies less than 35 eV and that molecular cross sections could be calculated by adding the constituent atomic cross sections. Their experimental data seemed to support this postulate. Lampe, Franklin, and Field³ obtained more extensive experimental data and concluded that the additivity postulate did not hold, but that a general correlation of cross section with polarizability did exist. Stevenson and Schissler⁴ reassessed the situation in 1961 and concluded that (a) the additivity postulate does not hold in general but perhaps holds within a given molecular class of compounds, *i.e.*, alkanes; (b) simple classical theory indicates that cross sections should be proportional to the 0.5 power of the polarizability rather than the 1.0 power as suggested by Lampe, Franklin, and Field; and (c) a general correlation may exist between electron ionization cross section and diamagnetic susceptibility. The proposed cross section correlations can be summarized as: (1) additivity of atomic cross sections, (2) linear with polarizability, and (3) linear with diamagnetic susceptibility.

Part of the difficulty preventing definitive statements about semiempirical correlations has been the disagreement in the experimental cross section values. Even the most careful and recent absolute cross section measurements of two different groups of investigators^{5,6} show considerable disparity. However, relative cross sections, measured for a variety of molecules showing a wide variation of values of molecular properties, may provide a better test of such correlations. Consequently, we have measured cross sections for 62 molecules which include hydrocarbons, fluorocarbons, and halogen-substituted hydrocarbons and fluorocarbons. Our results complement those of Harrison, *et al.*,⁷ who measured cross sections for hydrocarbons, ethers, ketones, aldehydes, esters, and alkylbenzenes. Analysis of all results shows clearly that none of the three proposed correlations is generally valid but that each of the three correlations is equally valid within a given molecular class. It is striking, however, that there is a single correlation with diamagnetic susceptibility for all nonfluorine-substituted compounds. An empirical equation based on polarizability is developed here which includes most molecular classes of volatile compounds and reproduces the experimental cross sections for 98

molecules within an average deviation of 3%. A more simplified equation based on modified additivity correlations reproduces the experimental cross sections within an average deviation of 4.5%.

II. Experimental Section

All compounds were obtained commercially and were degassed before use. The quoted purities were greater than 99% for most of the compounds; a few of the fluorocarbons were only quoted as greater than 98% pure.

The ion chamber in a Nuclide 12-90G magnetic mass spectrometer was used to measure the total ionization cross section. The total number of positive ions produced by the electron beam in the ion chamber was collected on a negatively biased repeller with the ionization chamber grounded. The positive ion current collected on the repeller showed a broad maximum at -6 V and all measurements were taken at this voltage. Measurements on all compounds were taken with an electron ionizing voltage of 70 eV and on a few compounds with an electron energy of 35 and 20 eV. Other ion source parameters were trap voltage = 80 V, trap current = 50 μ A, ion chamber temperature = 50°.

The total ion current was monitored on the repeller by a Keithley 610B electrometer. To prevent leakage currents between the repeller and the ion chamber a repeller guard was installed in the original ion source. Typical ion currents were in the range of 10⁻⁹ A.

The total ion current I_t for a given gas with ionization cross section, Q_i , is given by the equation

$$I_t = Q_i I_e d N \quad (1)$$

where I_e is the ionizing electron current, d is the ionizing path length, and N is the number of molecules per cubic centimeter in the ion source. Since N is proportional to the pressure a plot of I_t vs. pressure should be linear with a slope proportional to the ionization cross section of the compound being measured. This relationship will hold only if the gas flow has similar characteristics into and out of the ion source. In our system a gold foil leak was used to admit gas to the ion source. This was shown to have effusive flow characteristics over the reservoir pressure range of 100 to 15 Torr in which we worked. The reservoir pressure was monitored by a Wallace-Tiernan gauge. The inlet system was heated with heating tape to 50°.

(3) (a) J. W. Otvos and D. P. Stevenson, *J. Amer. Chem. Soc.*, **78**, 546 (1956); (b) F. W. Lampe, J. L. Franklin, and F. H. Field, *ibid.*, **79**, 6129 (1957).

(4) D. P. Stevenson and D. O. Schissler in "The Chemical and Biological Actions of Radiations," Vol. V, M. Haissinsky, Ed., Academic Press Ltd., London, 1961, Chapter 2.

(5) R. K. Asundi and M. V. Kurepa, *J. Electron. Control*, **15**, 41 (1963).

(6) D. Rapp and P. Englancer-Golden, *J. Chem. Phys.*, **43**, 1464 (1965).

(7) A. G. Harrison, E. G. Jones, S. K. Gupta, and G. P. Nagy, *Can. J. Chem.*, **44**, 1967 (1966).

Table I: Total Electr. Ionization Cross Sections ($\text{cm}^2 \times 10^{18}$)

Code no.	Compound	70 eV			35 eV			20 eV		
		No. of runs	Cross sec.	Std dev	No. of runs	Cross sec.	Std dev	No. of runs	Cross sec.	Std dev
Rare Gases										
1.	He	7	0.417	0.11						
2.	Ne	7	0.563	0.06						
3.	Ar	16	(3.62)	0.35	7	(2.85)	0.04	13	(0.820)	0.08
4.	Kr	9	5.30	0.19	5	4.07	0.12	8	1.77	0.04
5.	Xe	4	7.50	0.14	5	6.34	0.31	7	4.33	0.28
<i>n</i> -Alkanes										
6.	CH ₄	6	4.67	0.17	6	3.65	0.16	14	1.62	0.02
7.	C ₂ H ₆	4	8.51	0.22	5	6.45	0.28	7	3.32	0.08
8.	<i>c</i> -C ₃ H ₈	4	10.6	0.14						
9.	C ₃ H ₈	4	11.5	0.36	5	8.91	0.32	7	4.79	0.12
10.	C ₄ H ₁₀	4	15.3	0.54	5	11.4	0.44	7	6.45	0.23
11.	C ₆ H ₁₂	4	18.6	0.81						
12.	C ₈ H ₁₄	5	22.5	1.3						
Alkenes										
13.	C ₂ H ₄	4	6.93	0.21						
14.	C ₃ H ₆	4	10.2	0.61						
15.	<i>i</i> -C ₄ H ₈	4	13.3	0.50						
16.	1-C ₄ H ₈	4	13.7	0.65						
17.	<i>cis</i> -2-C ₄ H ₈	4	13.9	0.56						
18.	<i>trans</i> -2-C ₄ H ₈	4	13.8	0.47						
19.	1,3-C ₄ H ₆	2	13.1	0.04						
<i>n</i> -Perfluoroalkanes										
20.	CF ₄	4	4.68	0.13	5	2.22	0.06	13	0.260	0.03
21.	C ₂ F ₆	4	7.79	0.29	5	3.89	0.04	8	0.610	0.07
22.	C ₃ F ₈	4	10.5	0.43	5	5.52	0.08	8	1.07	0.10
23.	<i>c</i> -C ₄ F ₈	5	12.5	0.84						
24.	C ₄ F ₁₀	4	13.5	0.55	5	7.25	0.07	9	1.62	0.14
25.	C ₆ F ₁₄	4	19.5	0.64						
Perfluoroalkenes										
26.	C ₂ F ₄	4	6.16	0.18						
27.	C ₃ F ₆	4	9.16	0.41						
28.	2-C ₃ F ₄	4	12.2	0.37						
29.	1-C ₇ F ₁₄	4	21.2	0.70						
30.	<i>c</i> -C ₆ F ₁₀	4	16.1	0.44						
C-F-Cl Compounds										
31.	CF ₃ Cl	3	7.79	0.11	5	5.15	0.16	8	2.02	0.05
32.	CF ₂ Cl ₂	3	11.2	0.41	5	8.52	0.37	8	4.20	0.22
33.	CFCl ₃	3	14.6	0.24	5	11.7	0.30	5	6.26	0.47
34.	C ₂ F ₅ Cl	4	10.9	0.06						
35.	1,2-C ₂ F ₄ Cl ₂	4	14.3	0.11						
36.	1,1,2-C ₂ F ₃ Cl ₃	4	17.6	0.27						
C-F-Br Compounds										
37.	CF ₃ Br	4	9.07	0.37						
38.	CF ₂ Br ₂	4	14.2	0.62						
C-F-I Compounds										
39.	CF ₃ I	4	10.9	0.48						
40.	C ₂ F ₅ I	4	13.5	0.68						
41.	<i>i</i> -C ₃ F ₇ I	4	16.6	0.42						

Table I (Continued)

Code no.	Compound	70 eV			35 eV			20 eV		
		No. of runs	Cross sec.	Std dev	No. of runs	Cross sec.	Std dev	No. of runs	Cross sec.	Std dev
C-F-H Compounds										
42.	CH ₃ F	4	4.46	0.20	5	3.03	0.09	8	1.27	0.06
43.	CH ₂ F ₂	3	4.56	0.23	5	2.75	0.03	8	0.940	0.03
44.	CHF ₃	4	4.47	0.17	5	2.41	0.03	8	0.547	0.04
45.	1,1-C ₂ H ₄ F ₂	4	7.77	0.12						
46.	1,1-C ₂ H ₂ F ₂	4	6.40	0.21						
Other C-F-X Compounds										
47.	CHF ₂ Cl	3	7.92	0.13	5	5.66	0.28	8	2.58	0.11
48.	CHFCl ₂	3	11.5	0.21	5	9.12	0.25	8	4.96	0.33
49.	CF ₂ ClBr	4	11.1	1.0						
50.	CF ₂ ClCFCII	7	27.2	6.1						
51.	CF ₂ ClCHFI	5	19.8	1.1						
52.	CF ₂ ClCH ₃	4	11.0	0.15						
53.	CF ₂ BrCFCI ₂ Br	5	23.4	1.3						
54.	CF ₂ BrCHFCl	4	15.8	0.62						
Alkyl Halides										
55.	CH ₃ Cl	4	8.68	0.30						
56.	C ₂ H ₅ Cl	4	12.0	0.21						
57.	<i>n</i> -C ₃ H ₇ Cl	4	15.6	0.21						
58.	<i>n</i> -C ₄ H ₉ Cl	5	19.9	1.2						
59.	CH ₂ Cl ₂	4	12.4	0.32						
60.	CH ₂ ClBr	5	14.7	0.95						
61.	CHCl ₂ Br	7	21.8	4.9						
62.	CH ₃ Br	4	10.1	0.42						

Table II: Comparison of Literature Values of Ionization Cross Sections (cm² × 10¹⁸)

Compound	Reference								Average ^f	% av dev
	This work ^{a,d}	3b ^{a,e}	3a ^{a,f}	7a ^{a,g}	3a ^{a,h}	6 ^b	5 ^c	5 ^b		
	70 eV	75 eV	75 eV	75 eV	75 eV	70 eV	70 eV	70 eV		
He	0.417	0.397	0.310		0.287	0.420	0.310	0.355	0.357	13
Ne	0.563	0.632	0.598	0.584		0.671	0.550	0.619	0.602	5.5
Ar	(3.62)	(3.62)	(3.62)	(3.62)	(3.62)	(3.62)	(3.62)	(3.62)	(3.62)	...
Kr	5.30	5.33	5.41	5.32	5.35	5.50	5.6	5.70	5.44	2.2
Xe	7.50	7.52		7.68		6.70	7.6	8.00	7.50	3.6
CH ₄	4.67	4.78	2.56	4.80	3.58	4.78			4.76	0.8
C ₂ H ₆	8.51	8.59	4.75	8.60	5.30				8.61	0.9
C ₃ H ₈	11.5	11.4	6.37	11.9	7.40				11.6	1.7
<i>n</i> -C ₄ H ₁₀	15.3	14.5	8.96	14.8	9.50				15.2	2.6
<i>n</i> -C ₆ H ₁₂	18.6	19.1		18.1	11.7				18.9	1.1
<i>n</i> -C ₈ H ₁₄	22.5	22.9		21.3					22.8	0.9
C ₂ H ₄	6.93	6.85	3.95	6.28	4.25	7.44			6.88	4.5
C ₃ H ₆	10.2	10.0	5.78	9.20	6.40				9.80	4.1
<i>c</i> -C ₃ H ₆	10.6	11.1		10.7					10.8	1.9
<i>i</i> -C ₄ H ₈	13.3	13.3								
1-C ₄ H ₈	13.7			11.8	8.60					
<i>cis</i> -2-C ₄ H ₈	13.9									
<i>trans</i> -2-C ₄ H ₈	13.8									
1,3-C ₄ H ₈	13.1									
CH ₂ Cl	8.68	5.41	9.70							
CH ₃ Br	10.1	6.40								
C ₂ H ₅ Cl	12.0		12.4							

^a Cross sections determined on a negatively biased repeller in a mass spectrometer. ^b Absolute cross sections. ^c Comparative cross sections determined on a Lozier type apparatus. ^d Nuclide 12-90G mass spectrometer used. ^e CEC 21-620 cycloidal mass spectrometer used. ^f Westinghouse LV mass spectrometer used. ^g AEI MS-10 mass spectrometer used. ^h CEC Diatron-20 mass spectrometer used. ⁱ Reference 3a values for hydrocarbons are not included.

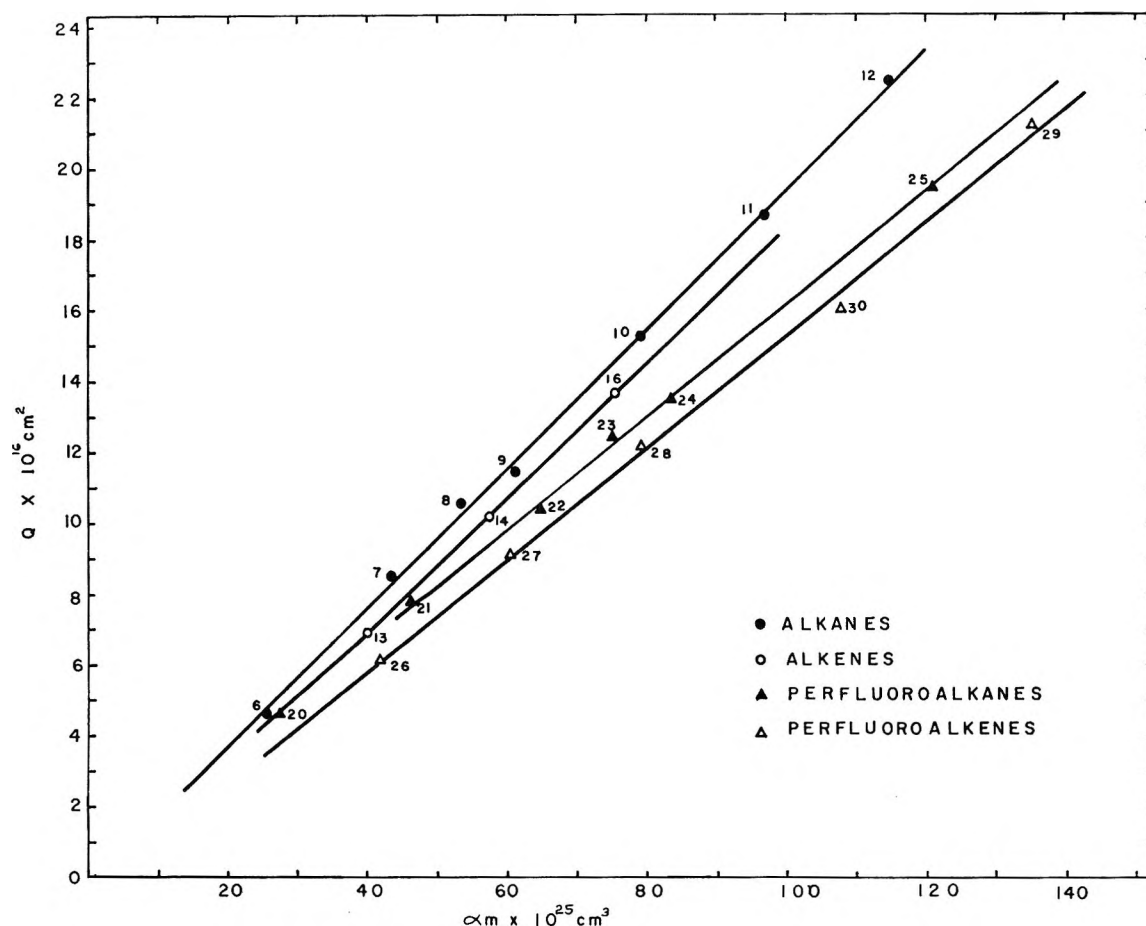


Figure 1. Total electron ionization cross sections (Q) vs. molecular polarizabilities (α_m) for alkanes, alkenes, perfluoroalkanes, and perfluoroalkenes.

As indicated by Harrison, *et al.*,⁷ liquid nitrogen trapping of the cold system may interfere with the ion current measured because of changes in pumping speed as the liquid level decreases. This problem is most serious for gases condensable at liquid nitrogen temperature. We also found this to be a serious problem and that it could be alleviated by using methanol-Dry Ice mixtures as the trap coolant instead of liquid nitrogen. Our pumping system was a 4-in. Consolidated Vacuum Corp. unit with a Model BCN baffle.

All current vs. reservoir pressure plots were linear. The slopes of the plots were determined by a computer least-squares fit to the experimental points. The standard deviation of this fit was generally within 1%. The precision was less for molecules with very low and very high cross sections. Four or more pressure plots were determined for all molecules except for three plots for six molecules and only two plots for one molecule. The standard deviations of these slopes or the total ionization cross section for most of the molecules was less than 4% and the average deviation was less than 2%. Some indication of the day-to-day reliability of the apparatus is that the standard deviation of argon slopes determined over a number of different days was only 10% while the average deviation was about 5%.

III. Results

A. Ionization Cross Sections. Relative electron ionization cross sections were measured for 62 molecules at 70 eV and for 19 molecules at 35 and 20 eV. These cross sections were always measured relative to the cross section for argon and are assigned absolute values based on Asundi and Kurepa's value⁵ for the argon ionization cross section of $3.62 \times 10^{-16} \text{ cm}^2$ at 70 eV. It should be pointed out that the absolute ionization cross section for argon is not generally agreed upon by different groups of recent workers.⁶ Our measured cross sections at 35 and 20 eV are assigned absolute values based on argon of $2.85 \times 10^{-16} \text{ cm}^2$ (35 eV) and 0.820×10^{-16} (20 eV). These values are those of Rapp and Englander-Golden⁶ multiplied by 1.15. The factor, 1.15, normalizes Rapp and Englander-Golden's data for argon at 70 eV to the data of Asundi and Kurepa⁵ for argon at 70 eV. The cross sections are summarized in Table I together with the number of current-pressure plots used for each determination and the standard deviation of these independent determinations.

Cross sections for rare gases, alkanes, and alkenes have been measured by several investigators. Table II summarizes the literature results that can be compared to our values; all values have been renormalized to a

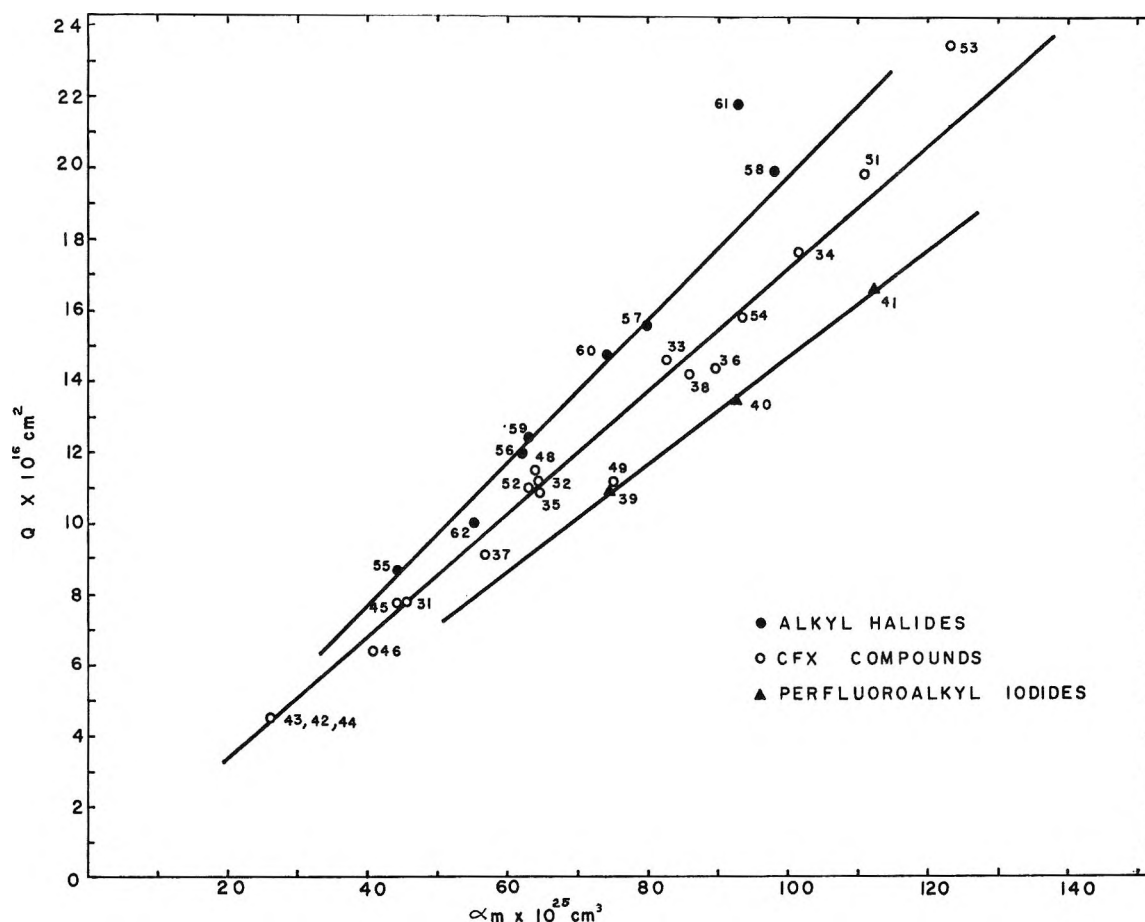


Figure 2. Total electron ionization cross sections (Q) vs. molecular polarizabilities (α_m) for alkyl halides, CFX compounds, and perfluoroalkyl iodides.

Table III: Numerical Key in Compound Identification in the Figures

Code no.	Alkynes	Code no.	Ketones
63.	HCCH	85.	CH ₃ COCH ₃
64.	CH ₃ CCH	86.	C ₂ H ₅ COCH ₃
65.	C ₂ H ₅ CCH	87.	<i>n</i> -C ₃ H ₇ COCH ₃
66.	<i>n</i> -C ₂ H ₅ CCH	88.	<i>n</i> -C ₆ H ₁₁ COCH ₃
67.	<i>n</i> -C ₄ H ₉ CCH	89.	<i>n</i> -C ₆ H ₁₃ COCH ₂
68.	<i>n</i> -C ₆ H ₁₁ CCH	90.	C ₂ H ₆ COC ₂ H ₆
	Ethers		Aldehydes
69.	CH ₃ OCH ₃	91.	CH ₃ CHO
70.	C ₂ H ₅ OCH ₃	92.	C ₂ H ₅ CHO
71.	C ₂ H ₅ OC ₂ H ₅	93.	<i>i</i> -C ₃ H ₇ CHO
72.	<i>n</i> -C ₄ H ₉ OCH ₃		
73.	<i>t</i> -C ₄ H ₉ OCH ₃		
74.	C ₃ H ₇ OC ₂ H ₅		
	Esters		Alkyl benzenes
75.	HCOOCH ₃	94.	C ₆ H ₆
76.	HCOOC ₂ H ₅	95.	CH ₃ C ₆ H ₅
77.	HCOOC ₃ H ₇	96.	C ₂ H ₅ C ₆ H ₅
78.	HCOOCH(CH ₃) ₂	97.	<i>n</i> -C ₃ H ₇ C ₆ H ₅
79.	HCOOC ₄ H ₉	98.	<i>n</i> -C ₄ H ₉ C ₆ H ₅
80.	HCOOCH ₂ CH(CH ₃) ₂		
81.	<i>n</i> -C ₄ H ₉ COOCH ₃		
82.	CH ₃ COOCH ₃		
83.	<i>n</i> -C ₃ H ₇ COOCH ₃		
84.	CH ₃ COOC ₂ H ₅		

cross section of $3.62 \times 10^{-16} \text{ cm}^2$ for argon. The agreement of our values with those of other groups is generally good except for the values of Otvos and Stevenson.

B. Correlation of Cross Sections with Molecular Parameters. The correlation of ionization cross sections with molecular polarizability is tested in Figures 1–3. The cross sections listed in Table I are plotted in 1 and 2 while the cross sections in Figure 3 are from Harrison, *et al.*,⁷ and are renormalized to our data. The numbers in the figures refer to the number of the compound in Tables I and III. The polarizabilities used are calculated from LeFevre's bond polarizabilities⁸ and are tabulated by Beran and Kevan.⁹ Polarizability values calculated by the Lippincott–Stutman method⁹ give similar correlations to those shown in Figures 1–3.¹⁰ Figure 1 shows separate linear correlations for alkanes, alkenes, perfluoroalkanes, and perfluoroalkenes. No single linear correlation holds for these different molecular types. The fluorocarbons show smaller cross sections for a given molecular polarizability than do the hydrocarbons; this will be found to be generally true.

(8) R. J. W. LeFevre, *Advan. Phys. Org. Chem.*, **3**, 1 (1966).

(9) J. A. Beran and L. Kevan, *J. Phys. Chem.*, **73**, 3860 (1969).

(10) J. A. Beran, Ph.D. Thesis, University of Kansas, 1968.

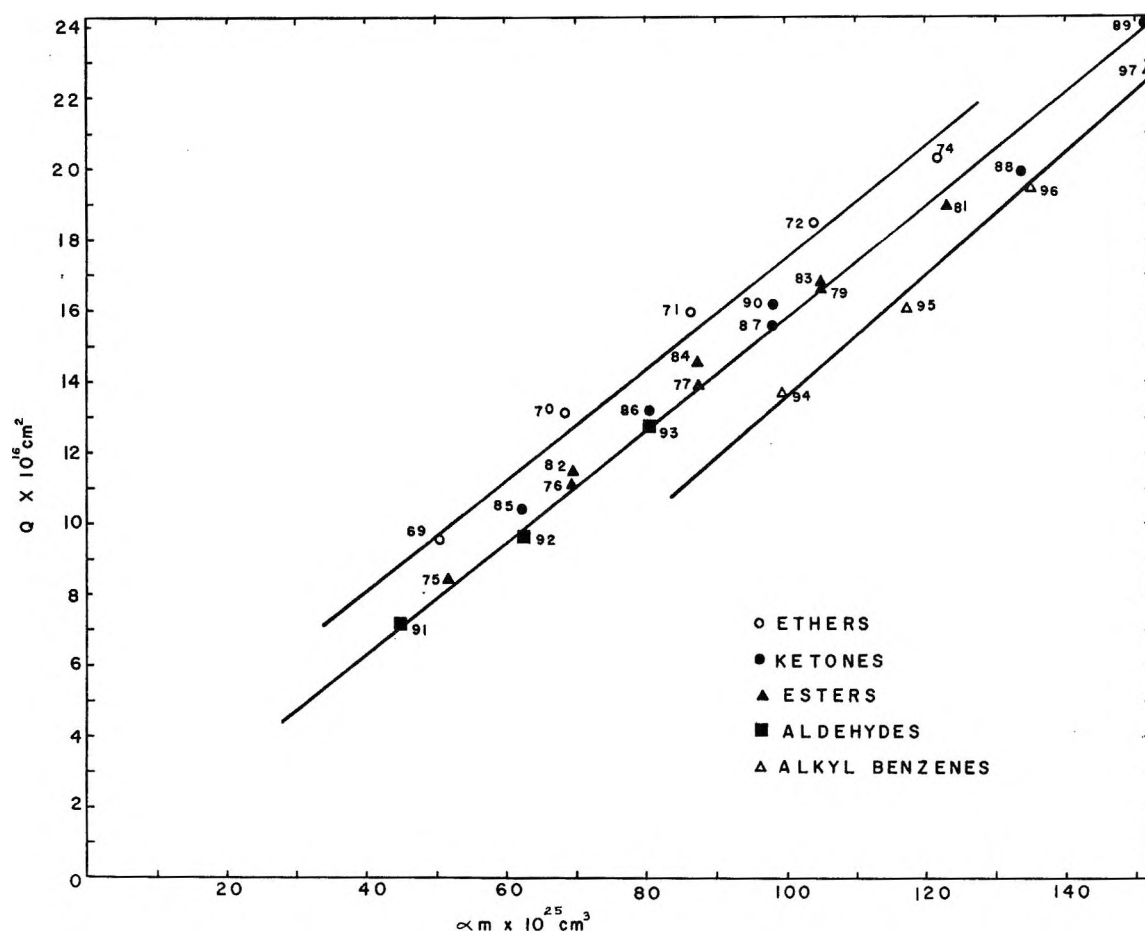


Figure 3. Total electron ionization cross sections (Q) vs. molecular polarizabilities (α_m) for ethers, ketones, esters, aldehydes, and alkyl benzenes.

Figure 2 shows separate correlations for alkyl halides, for C-F-Cl, C-F-Br, C-F-H, and other C-F-X compounds, and for perfluoroalkyl iodides. A few of the more complexly substituted compounds such as numbers 50, 53, and 61 in Table I do not fall in any of the correlations indicated in Figure 2. Figure 3 shows results on other molecular classes. The ketones, esters, and aldehydes all form a single linear correlation while the ethers and the alkyl benzenes each form other linear correlations.

In Figures 4-6 the correlation of ionization cross sections with molecular diamagnetic susceptibility is tested. The pertinent diamagnetic susceptibilities have been calculated⁹ by the semiempirical method of Haberditzl.¹¹ Figure 4 illustrates separate linear correlations for alkanes, alkenes, perfluoroalkanes, and perfluoroalkenes. In contrast to the polarizability correlation the alkene lines lie above the alkane lines for both protiated and fluorinated compounds in Figure 4. In Figure 5 the alkyl halides show a linear correlation with diamagnetic susceptibility as do the three perfluoroalkyl iodides. However, the CFCl, CFBr, CFH, and CFX compounds show poor correlation with diamagnetic susceptibility which contrasts with their rela-

tively good correlation with polarizability in Figure 2. The molecular classes in Figure 6 all seem to fit a single linear correlation in contrast to the several separate correlations observed when plotted against polarizability in Figure 3. The esters all lie below the single correlation line drawn in Figure 6 and so deviate slightly from the above generalization.

Otvos and Stevenson^{3a} originally suggested that molecular ionization cross sections are given by the sum of the constituent atomic cross sections. Mann¹² has recently calculated atomic cross sections in a more rigorous fashion than done by Otvos and Stevenson. Lin and Stafford¹³ have used Gryzinski's¹⁴ classical equation to calculate maximum atomic cross sections. Of the three theoretical evaluations of atomic cross sections, Mann's calculations appear to agree slightly better than the other calculations with the experimental data available.¹⁰ Figure 7 tests the atomic cross section additivity postulate for alkanes, perfluoroalkanes,

(11) W. Haberditzl, *Angew. Chem. Int. Ed.*, **5**, 288 (1966).

(12) J. B. Mann, *J. Chem. Phys.*, **46**, 1646 (1967).

(13) S. S. Lin and F. E. Stafford, *ibid.*, **48**, 3885 (1968).

(14) M. Gryzinski, *Phys. Rev.*, **138**, A322, A336 (1965).

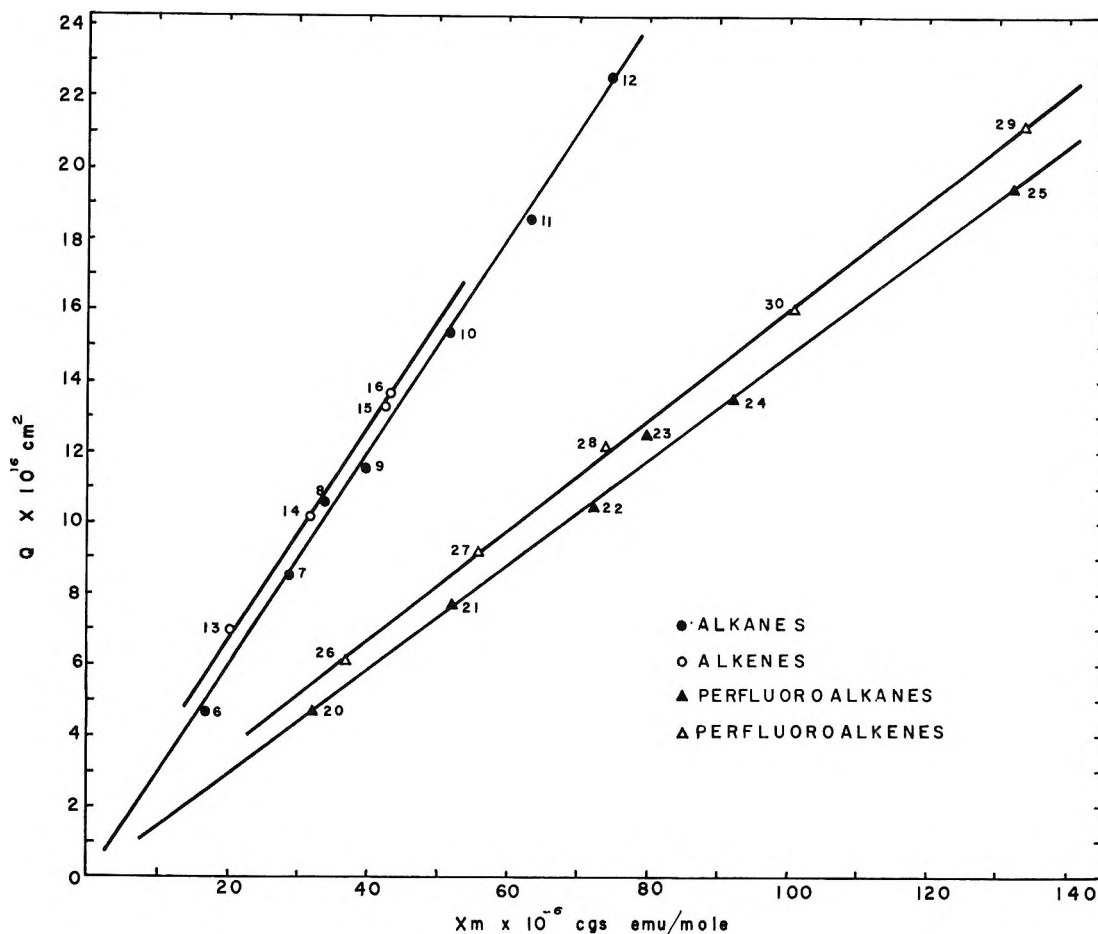


Figure 4. Total electron ionization cross sections (Q) vs. diamagnetic susceptibility (χ_m) for alkanes, alkenes, perfluoroalkanes, and perfluoroalkenes.

and several other molecular classes with Mann's calculated atomic cross sections. The correlations with other calculated values are similar. The dotted line in Figure 7 is of unit slope on which the points should fall if the additivity postulate were obeyed. Even with the improved values for the atomic cross sections it is apparent that the additivity postulate does not hold generally.

IV. Discussion

A. Semiempirical Correlations. Figures 1-7 show that the electron ionization cross sections do not form a single correlation with polarizability, diamagnetic susceptibility, or additivity of atomic cross sections. However, linear correlations within a molecular class are found for each of the three molecular properties. It is interesting that fluorine-substituted compounds show no anomalous behavior.

The polarizability correlations within each molecular class in Figures 1-3 have about the same slopes. Thus these slopes can be superimposed by multiplying the cross sections by a single coefficient for each molecular class. Small changes in slope for a molecular class can be incorporated into an equation with factors of the form n_x^R which represent the number of x atoms raised

to the power R . By utilizing these concepts a general semiempirical equation (I) has been developed which gives total ionization cross sections at 70 eV as a function of the molecular polarizability, α_m , calculated by the δ -function method with bond polarity corrections.⁹

Equation I gives calculated total ionization cross sections with an average deviation of 3% from the experimental cross sections of some 100 molecules reported in this paper and in ref 7. For the determination of the total ionization cross section of any molecule in the molecular classes studied only its polarizability need be known. The δ -function model of molecular polarizability¹⁶ provides a general method for calculating the polarizability of any molecule to the accuracy needed for eq I. For example, the total ionization cross section of CF_3COCF_3 ($\alpha_m = 74.9 \times 10^{-25} \text{ cm}^3$) should be approximately equal to

$$Q_{\text{CF}_3\text{COCF}_3} = \frac{1}{5.6 \times 10^{-9} \text{ cm}} (6^{-0.1}) \times [\alpha_m - 4.3(3)] = 9.26 \times 10^{-16} \text{ cm}^2$$

For compounds containing more than one iodine atom,

(15) E. R. Lippincott and J. M. Stutman, *J. Phys. Chem.*, **68**, 2926 (1964).

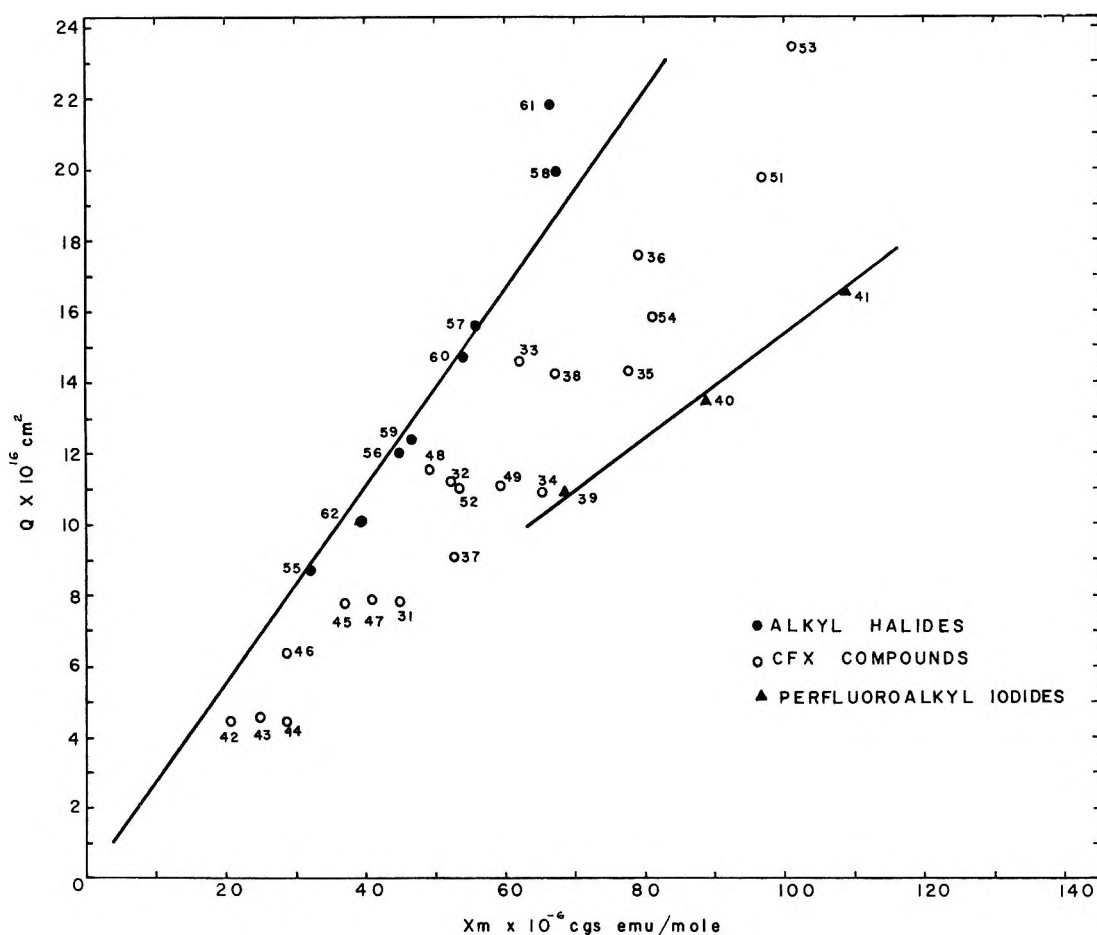


Figure 5. Total electron ionization cross sections (Q) vs. diamagnetic susceptibility (χ_m) for alkyl halides, CFX compounds, and perfluoroalkyl iodides.

a factor of approximately $n_1^{0.3}$ should be included in eq I.

$$Q_{\text{exptl}} = \frac{1}{5.6 \times 10^{-9} \text{ cm}} n_F^{-0.1} n_{\text{Cl}}^{0.16} n_{\text{Br}}^{0.255} \times$$

$$\left[\begin{array}{l} \alpha_m \text{ (alkanes)} \\ 0.91 \alpha_m \text{ (alkenes)} \\ \alpha_m + 4.2 - 4.0(n_C - 2) \text{ (ethers)} \\ \alpha_m - 4.3n_C \text{ (ketones)} \\ \alpha_m - 4.0(n_C + 1) \text{ (aldehydes)} \\ \alpha_m - 4.5n_C \text{ (esters)} \\ \alpha_m - 4.2(n_C + 2) \text{ (alkylbenzenes)} \end{array} \right] \times$$

$$\left[\begin{array}{l} 0.925 \text{ (monofluoro compounds)} \\ 1.1 \text{ (monochloro compounds)} \\ 1.1 \text{ (monobromo compounds)} \\ 1.1 \text{ (monoiodo compounds)} \end{array} \right] \quad (\text{I})$$

where $n > 1$; if $n = 0$, let $n_z^R = 1$. α_m is the δ -function molecular polarizability with bond polarity corrections and is in units of $\times 10^{-25} \text{ cm}^3$.

In contrast to the polarizability correlations which have about the same slope, the diamagnetic susceptibility correlations in Figures 4–6 show distinctly different slopes for hydrocarbons and fluorocarbons. Further-

more, partially fluorine-substituted compounds do not form very good linear correlations within a given molecular class like CFCl or CFH compounds. Instead, these compounds scatter widely between the two slopes defined by alkanes and perfluoroalkanes. It is possible that some of this scatter is due to inaccurate values of χ_m . As the data stand, however, it is difficult to devise a semiempirical equation like eq I which is based on χ_m .

If the fluorine-substituted compounds in Figures 4–6 are ignored, it is most striking that all of the remaining molecular classes (alkanes, alkenes, alkyl halides, ethers, esters, ketones, and aldehydes) do fall on a single linear correlation passing through the origin with no adjustments being necessary. The equation is

$$Q (\times 10^{16} \text{ cm}^2) = 0.278 \chi_m \times$$

$$(\times 10^{-6} \text{ cgs emu/mol}) \quad (\text{II})$$

Equation II is consistent with Stevenson's suggestion⁴ of a general correlation between ionization cross section and diamagnetic susceptibility. However, the fluorine-substituted compounds disprove the apparent generality of this correlation. More extensive and accurate experimental values of χ_m for fluorine-substituted compounds could possibly change this conclusion but

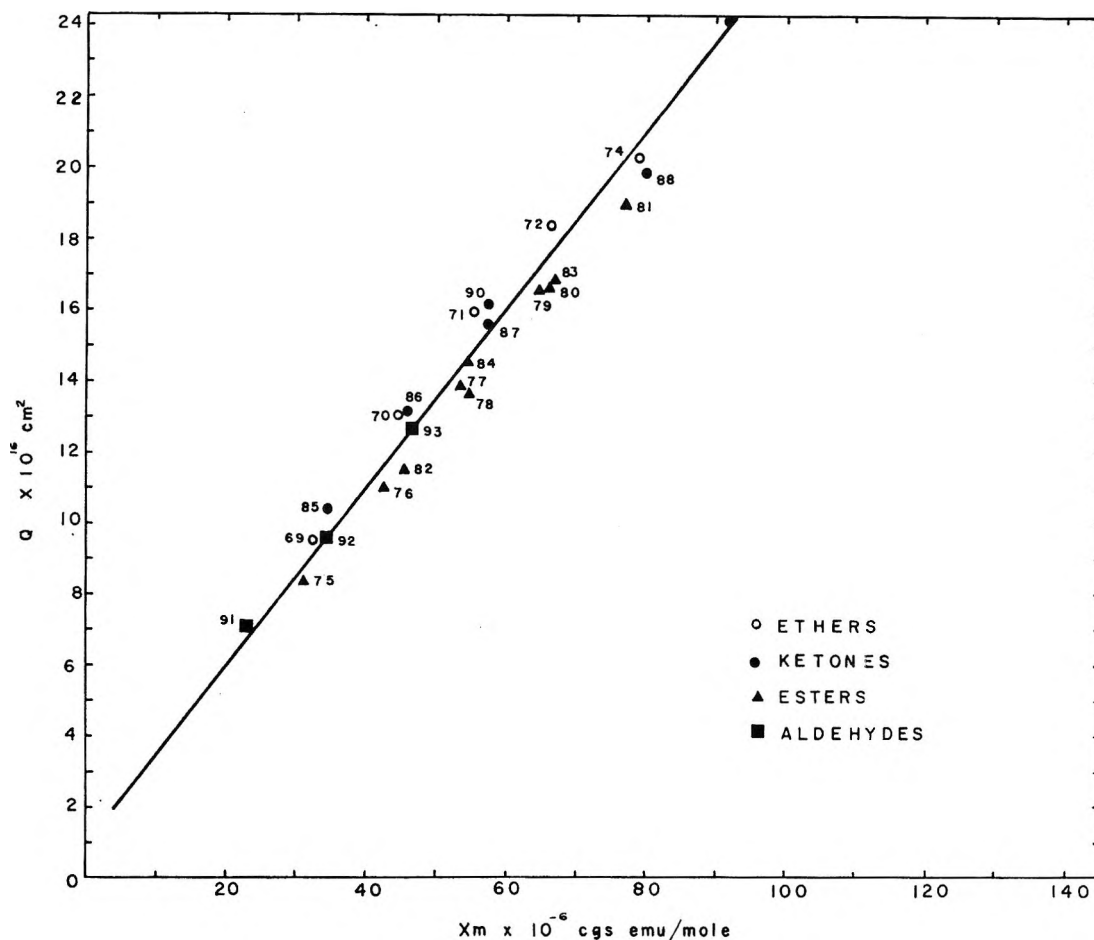


Figure 6. Total electron ionization cross sections (Q) vs. diamagnetic susceptibility (χ_m) for ethers, ketones, esters, and aldehydes.

the experimental values available do not make it seem likely.⁹ It is, however, true that for nonfluorine-substituted compounds ionization cross sections do show a single general correlation with diamagnetic susceptibility and not with polarizability.

Linear correlation for different molecular classes with additivity of atomic cross sections is demonstrated in Figure 7. This type of correlation is equivalent to one between ionization cross section and the number of different kinds of atoms in the molecule. Such modified additivity correlations have been derived previously for several molecular classes.⁷ We have generalized this approach and derived eq III in which n_X is the number of X atoms and n_{CC} refers to the number of carbon-carbon bonds irrespective of bond type. The factors 2.21, 0.3, and 1.68 in front of the number of carbon, hydrogen, and oxygen atoms, respectively, are Mann's¹² calculated atomic cross sections normalized to 3.62 for argon. Equation III gives calculated total ionization cross sections with an average deviation of 4.5% from the experimental cross sections of some 100 molecules reported in this paper and in ref 7.

The two semiempirical equations (I and III) that have been derived in this work can be applied to most

$$Q_{\text{exptl}} = 1.34 \times \left[\begin{array}{l} 2.21n_C \\ +0.3n_H \\ +0.16n_F \\ +3.3n_{Cl}(\text{chlorohydrocarbons}) \\ +2.9n_{Cl}(\text{chlorohalohydrocarbons}) \\ +4.33n_{Br} \\ +5.3n_I \\ +1.68n_O \\ -0.4n_{CC}(\text{alkenes}) \text{ no. of CC bonds} \end{array} \right] \times$$

$$\left[\begin{array}{l} 0.9 \text{ (ethers)} \\ 0.7 \text{ (esters)} \\ 0.76 \text{ (ketones)} \\ 0.73 \text{ (aldehydes)} \\ 0.7 \text{ (alkylbenzenes)} \\ 0.7 \text{ (alkynes)} \end{array} \right] \times 10^{-16} \text{ cm}^2 \quad \text{(III)}$$

molecules that can be vaporized into a mass spectrometer. Equation I appears to be more accurate. It has the disadvantage, however, of being somewhat cumbersome to use and requires the polarizability of the molecule to be known or calculable. Equation III is much easier to use than eq I. It has the added feature that no other property of the molecule has to be known

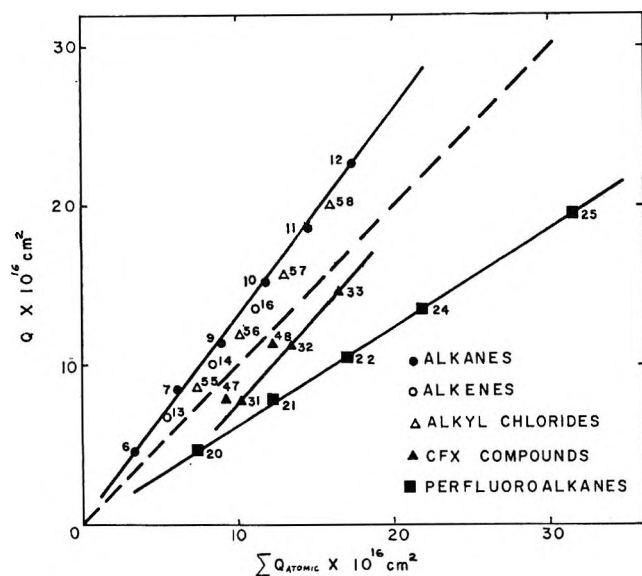


Figure 7. Total electron ionization cross sections (Q) vs. the sum of atomic electron ionization cross sections for alkanes, alkenes, alkyl chlorides, CFX compounds, and perfluoroalkanes.

except its molecular formula. It appears that eq II can be validly used for nonfluorine-substituted compounds if the diamagnetic susceptibility is known.

B. Hydrogen vs. Fluorocarbon Cross Sections. One of the interesting findings in this work is that ionization cross sections for fluorocarbons are less than those for the corresponding hydrocarbons. Pairs of molecules which show this trend are C_2F_6 (7.79) vs. C_2H_6 (8.51), C_3F_8 (10.5) vs. C_3H_8 (11.5), C_4F_{10} (13.5) vs. C_4H_{10} (15.3), C_2F_4 (6.16) vs. C_2H_4 (6.93), and C_3F_6 (9.16) vs. C_3H_6 (10.2). Also whenever a fluorine atom is substituted for a hydrogen atom in a molecule the cross section decreases and when substituted for another halogen atom the cross section decreases substantially. Typical examples of this trend in cross sections appear in the compounds CF_3Cl (7.79) vs. CHF_2Cl (7.92) and CF_3Br (9.07) vs. CH_3Br (10.1).

These observations are real since total ionization efficiency curves for fluorocarbons as well as for hydrocarbons show that 70 eV electron energy is about 5–15 eV above the energy at which the maximum total ionization cross section occurs. Thus the measurements are compared in the nearly energy-independent region for the ionization cross section.

However, it would seem that the decrease in 70-eV ionization cross section with increasing fluorine substitution reflects the somewhat unique properties of the ground-state fluorine atom. The high electronegativity and high ionization potentials of fluorine compared to hydrogen and other halogen atoms are emphasized in Table IV. For fluorosubstituted hydro- or halohydro-

Table IV: Ionization Potentials^a and Electronegativities^b of Some Elements

Element	Ionization potentials ^c				Electronegativity
	I	II	III	IV	
Ar	15.68	27.76	40.75	...	0
H	13.527	2.1
F	17.34	34.81	62.35	86.72	4.0
Cl	12.952	23.76	39.69	53.16	3.0
Br	11.80	19.1	25.7	...	2.8
I	10.6	19.4	2.5

^a "Handbook of Chemistry and Physics," 44th ed, The Chemical Rubber Publishing Co., Cleveland, 1963. ^b Pauling's electronegativity scale. ^c Units of volts.

carbons, fluorine, because of its high electronegativity, not only has its own lone-pair orbital electrons bound tightly but also increases the energy of the electron pair in the C–F bond. This qualitatively decreases the probability of ionization of the entire molecule. One expects the chemical properties of fluorine to be an even more decisive factor at electron impact energies below the energy of the maximum total ionization cross section.

The total ionization cross sections for the series CH_nF_{4-n} at 70 eV are nearly the same but as the energy is decreased from 70 to 35 to 20 eV, a trend in cross sections develops in which $CH_4 > CH_3F > CH_2F_2 > CHF_3 > CF_4$. This fact is also shown in the perfluoroalkane and the CF_nCl_{4-n} series. As the electron energy decreases, the slope of the cross section vs. polarizability decreases for the perfluoroalkanes and increases for the CF_nCl_{4-n} series.

Acknowledgment. We thank the U. S. Atomic Energy Commission for support of this research. This is AEC Document No. COO-1528-31.

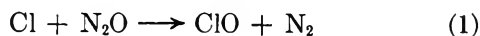
Matrix Infrared Studies of OF Radical Systems¹

by Alfred Arkell

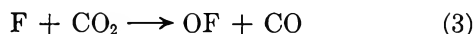
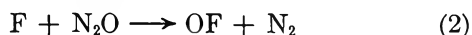
Contribution No. 1463, Texaco Research Center, Beacon, New York 12508 (Received April 11, 1969)

The photolysis of OF₂-N₂O or OF₂-CO₂ combinations in a nitrogen matrix at 4°K has produced increased yields of OF radical compared to OF₂ without added N₂O or CO₂. The OF radical was also observed when F₂-N₂O was photolyzed in a nitrogen or argon matrix at 4°K. This latter observation confirms a previously proposed mechanism and supports a lower-limit estimate of about 40 kcal/mol for the bond energy of OF. No radical was observed during the photolysis of F₂-CO₂ in nitrogen and alternate mechanisms involving CO₃ are proposed.

During the course of previous work² in which the OF radical was produced by photolysis of OF₂ in N₂ or Ar at 4°K, it was also observed that the addition of N₂O to the matrix gave a pronounced increase in OF radical production. A similar but less pronounced increase in OF radical production was also observed when CO₂ was added to the matrix. According to previous observations by Kaufman, *et al.*,³ it was proposed that ClO radical was produced by reaction of atomic chlorine with N₂O



Therefore, it was assumed that similar reactions of atomic fluorine with N₂O and CO₂



could account for increased OF radical production. Subsequent work has now shown that reaction 2 does occur but that reaction 3 does not. It is of interest to note that Ogden and Turner⁴ have completed a similar study of the F + N₂O reaction and, although they did not observe the OF radical directly, their results supported the conclusion that OF radical was an intermediate in the reaction. The present low-temperature matrix studies describe the effects of photolyzing OF₂ or F₂ in matrices containing N₂O or CO₂.

Experimental Section

The low-temperature infrared cell, Beckman IR-9 spectrophotometer, and high-pressure mercury arc (General Electric BH6) used in this work have been described previously.² Two component gas blends were prepared by standard manometric procedure using a matrix to reactant ratio (M:R) of 40. Three-component gas mixtures were produced by simultaneous deposition from two manifolds, and flow rates were adjusted to give the desired M:R. The N₂ (Airco, prepurified), argon (Airco), OF₂ and F₂ (Allied Chemical Co.), CO₂ and N₂O (Matheson) were used without further purification. A summary of the runs to be discussed is given in Table I. Deposition rates were 0.12 and 0.06 mmol/min for runs 1-3 and 4-6, respectively.

In all runs a deposition time of about 30 min was required. Photolyses were carried out using a BH6 water filter (5-cm quartz cell, 2200-9000 Å) combination.

Results

Photolysis of OF₂ in an N₂ Matrix. As shown in Table II and Figure 1 the photolysis of OF₂ in an N₂ matrix appeared to be reaching a steady-state production of OF radical; that is, a balance between formation, recombination, and secondary photolysis, in the 120-130 absorbance (× 10³) region. Diffusion (4-42-4°K) in this run showed complete loss of the OF radical absorptions, a large increase in OF₂, and trace formation of O₂F₂ and O₃.

In contrast to this, when N₂O was added to the matrix (run 2), several changes occurred. The level of OF radical production was increased significantly and the relative intensities of the two OF radical absorptions at 1030 and 1026 cm⁻¹ were reversed. After 51 min photolysis, and during a liquid helium refill, an exotherm⁵ occurred which temporarily increased the temperature to about 18°K. An infrared spectrum after the refill showed that the OF radical absorbances had decreased. Continued photolysis up to the 101 min total indicated (Figure 1) that the OF radical was being produced at about the same rate as it was prior to the exotherm. A trace of O₂F also formed during photolysis. Diffusion (4-40-4°K) in this run gave as the major product O₂F₂ and a trace of O₃; however, no increase in OF₂ was found.

(1) This work was supported by the Research and Technology Division, AFSC, Edwards, Calif., under Contract AF 04(611)-9577.

(2) A. Arkell, R. R. Reinhard, and L. P. Larson, *J. Amer. Chem. Soc.*, **87**, 1016 (1965).

(3) F. Kaufman, N. J. Gerri, and D. A. Pascale, *J. Chem. Phys.*, **24**, 32 (1956).

(4) J. S. Ogden and J. J. Turner, *J. Chem. Soc., A*, 1483 (1967). The OF radical may not have been observed in the work by Ogden and Turner because of the presence of SiF₄ in their fluorine sample. Silicon tetrafluoride has a strong absorption in the OF radical region.

(5) Exotherms, or temperature spikes, ranging from 5 to 20°K increase in temperature were observed many times in this and other radical work. If the liquid He container was near empty or in the process of being filled then the exotherm showed on the temperature recorder as a spike. However, if the liquid He container had a sufficient reserve at the time of the exotherm then no temperature spike was observed but an increase in the liquid He loss rate occurred.

Table I: Summary of Runs. Photolysis of OF₂ or F₂ in Matrices Containing N₂O or CO₂ at 4°K

Run no.	Components (mole ratio)					μMol used		Photolysis ^a time, min	Table and/or figure	
	N ₂	Ar	OF ₂	F ₂	N ₂ O	CO ₂	OF ₂ or F ₂			N ₂ O or CO ₂
1	40		1				90		18-69	I, II
2	40		1		1		90	90	24-101	I, II
3	40		1			1	90	90	24-91	I, II
4		40		1	1		48	48	8-70	
5	40			1	3		48	160	11-110	2
6	40			1		1	48	48	7-38	

^a Photolysis using BH6 + H₂O Filter (2200-9000 Å).

Table II: The Effect of N₂O and CO₂ on the Photolysis of OF₂ in N₂ at 4°K

Run no.	Composition	Photolysis time, min	Absorbance × 10 ⁴			Ratio 1030:1026
			1030 cm ⁻¹	1026 cm ⁻¹	Total	
1	OF ₂ + N ₂	18	44	26	70	1.7:1
		36	67	36	103	1.9:1
		53	77	37	114	2.1:1
		69	83	45	128	1.8:1
2	OF ₂ + N ₂ + N ₂ O	24	44	83	127	1:1.9
		51	61	150	211	1:2.5
		51 ^a	57	104	161	1:1.8
		76	74	169	243	1:2.3
		101	84	214	298	1:2.5
3	OF ₂ + N ₂ + CO ₂	24	32	56	88	1:1.8
		49	44	106	150	1:2.4
		74	56	93	149	1:1.7
		91	62	126	188	1:2.0

^a Second infrared spectrum taken after liquid helium refill because of exotherm during refill (4-18-4°K).

In run 3, in which CO₂ was added, the results were very similar to the system containing N₂O. The 1026 cm⁻¹ absorption was, on the average, twice as large as the 1030 cm⁻¹ absorption and the total OF radical absorbance was again considerably higher than that found in the nonadditive system. No diffusion could be made in this run because of a shortage of liquid helium.

Photolysis of F₂ + N₂O in N₂ or Ar at 4°K. The photolysis of F₂ + N₂O + N₂ (1:3:40) gave steady production of both OF radical and OF₂. After 11 min of ultraviolet irradiation (Figure 2, curve B) the OF radical absorption at 1026 cm⁻¹ was about twice as large as the OF₂ absorption at 822 cm⁻¹. A high-resolution scan of the OF radical absorption showed that only one band was present at 1026 cm⁻¹. This was of interest because all previous work with OF₂ had shown that two OF radical absorptions at 1026 and 1030 cm⁻¹ were produced on photolysis. As shown in Figure 2 (curves C and D) total photolysis times of 44 min and 77 min showed formation of the split ν₁ bands of OF₂ in the 920 cm⁻¹ region. There was also a continued increase in both OF and OF₂ absorptions. A second high-resolution scan of the OF radical absorption after 77 min photolysis still showed only a single absorption at 1026 cm⁻¹. Diffusion (4-29-4°K) of this sample gave com-

plete loss of OF radical (1026 cm⁻¹, Figure 2, curve E), a small increase in OF₂, and formation of O₂F₂, as evidenced by the doublet near 620 cm⁻¹ and the bending vibration near 460 cm⁻¹. The small absorption at 900 cm⁻¹ remains unidentified.

The photolysis of F₂ + N₂O + Ar (1:1:40) gave essentially the same results as in the nitrogen matrix except that the OF radical absorption was at 1028 cm⁻¹ which is in agreement with previous work.² As a consequence of the higher F₂:N₂O ratio (1:1) in this run compared to the previous run (1:3), the diffusion operation gave both OF₂ and O₂F₂ as major products.

Photolysis of F₂ + CO₂ in N₂ at 4°K. The photolysis of F₂ + CO₂ + N₂ (1:1:40) gave no evidence of new band formation after photolysis times of 7 and 38 min. No additional photolysis was attempted because of the complete absence of new bands after 38 min of irradiation.

Discussion

As shown in Figure 1 the photolysis of OF₂ in a matrix leads to the formation of OF radical with a gradual increase in its absorbance (× 10³) up to about 120 at which point it appears to have reached a steady-state concentration. It was therefore considered of interest to determine how the addition of N₂O or CO₂ to the

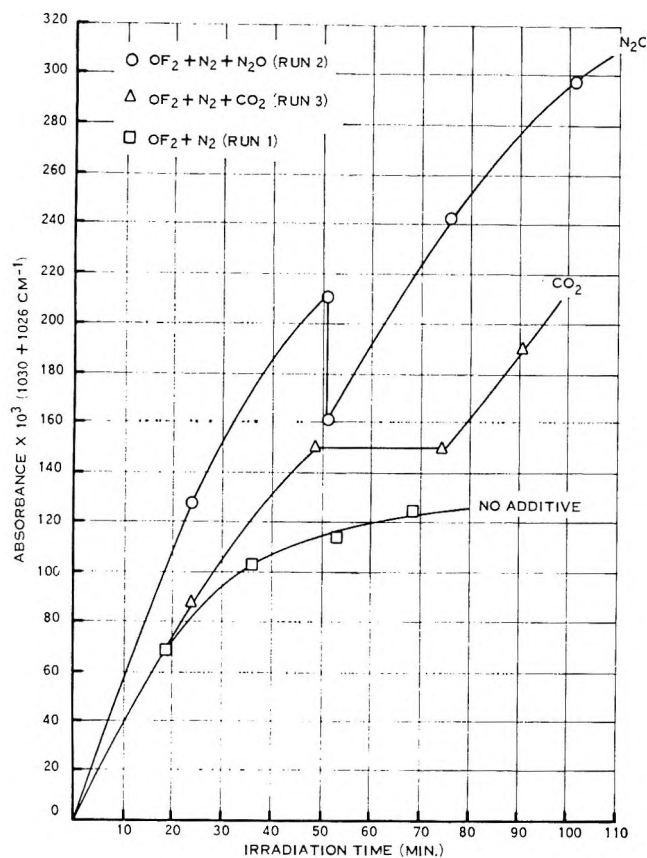
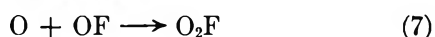
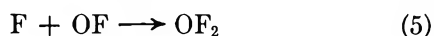
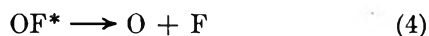


Figure 1. Effect of N_2O and CO_2 on OF radical formation.

matrix would allow significantly greater concentrations of OF radical to accumulate. It can be assumed that OF radical may be lost by any combination of the equations shown below



It should be noted that the loss of OF by decomposition as in (4) or (6) is particularly bad because it increases the concentration of O and F atoms in the matrix, both of which are capable of removing additional OF as in eq 5 and 7. Considering eq 4, the decomposition of OF^* could occur if the radical is in a vibrationally excited state. In this case the N_2O or CO_2 may be acting as a stabilizer by allowing the transfer of this excess vibrational energy from diatomic OF^* to the multiply bonded triatomic additives N_2O or CO_2 . Although stabilization by N_2O and CO_2 cannot be rigorously excluded it seems quite probable that the two different environments provided by N_2O and CO_2 in the same cage with OF radical would have caused a perturbation of the OF radical absorption. However, this was not observed as evidenced by the fact that OF radical absorptions were at the same frequencies in both N_2O and CO_2 runs.

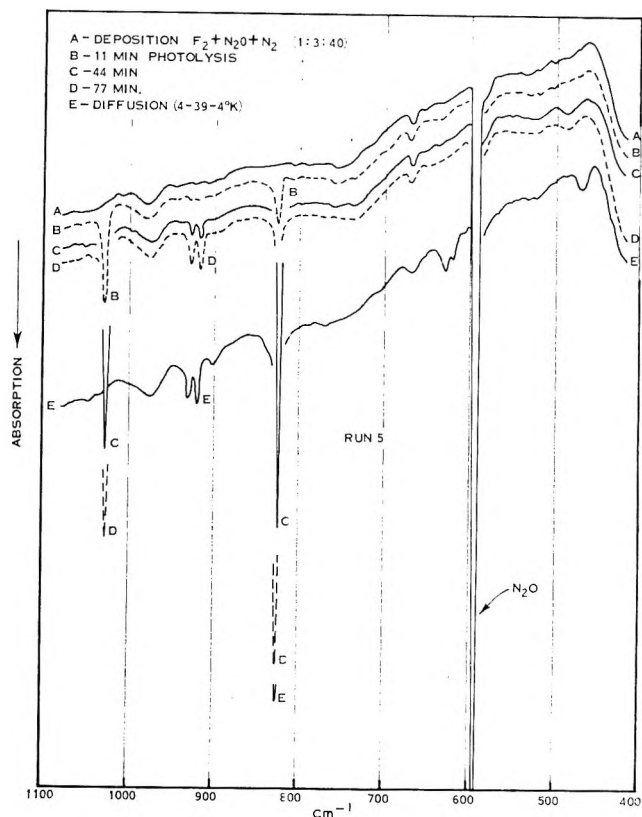


Figure 2. Photolysis of $F_2 + N_2O + N_2$ at $4^\circ K$.

If it is assumed that (5) is the most likely path by which OF radical is lost, that is by recombination, then anything which tends to remove atomic fluorine should allow a greater accumulation of OF radical. As shown by the $F + N_2O$ reaction (run 5, Figure 2), N_2O not only effectively removes F by reaction but it produces another OF radical in the process. A comparison of the

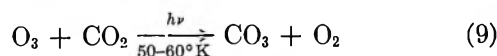


absorbances in runs 1 and 2 (Figure 1) shows that about twice as much OF is being produced in run 2 (eq 8) compared to run 1. Additional evidence regarding the availability of fluorine atoms was found by comparing the products of diffusion from the two runs. In run 1 the formation of OF_2 as the major product after diffusion showed that atomic F was readily available in the matrix. However, in run 2, in which atomic F was reacted (2) as it formed, the major product after the diffusion operation was O_2F_2 produced by combination of OF radicals.

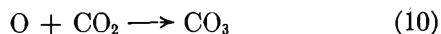
In view of the improved OF radical production from OF_2 when CO_2 was present (run 3, Figure 1) and the absence of reaction between atomic F and CO_2 (run 6) it is necessary to consider alternate mechanisms for improved OF radical production in run 3. In recent work by Moll, *et al.*,⁶ it was shown that the new species

(6) N. G. Moll, D. R. Clutter, and W. E. Thompson, *J. Chem. Phys.*, **45**, 4469 (1966).

CO₃ could be produced by the photolysis (9) of O₃ in a CO₂ matrix. They proposed that



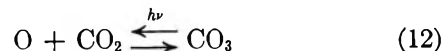
CO₃ was produced by the reaction of atomic oxygen from O₃ with CO₂. In the present study it was suggested that a limiting factor to OF radical production may be photolysis of the radicals as shown in eq 6 to give oxygen and fluorine atoms. If the generated oxygen atoms⁷ react (eq 10) with CO₂ to give CO₃ then OF radicals could be regenerated by the reaction (eq 11)



of atomic F with CO₃. In this manner, CO₂ would be acting as an oxygen transfer agent and would offset the photolytic loss of OF radical by allowing for the reformation of OF as shown in eq 10 and 11. If this proposed mechanism is valid, then the magnitude of the observed improvement (run 3, Figure 1) in the presence of CO₂ suggests that photolytic loss of OF (eq 6) contributes significantly to total OF losses. The absence of observed infrared absorptions⁶ for CO₃ in the CO₂ run was not considered as negative evidence for their presence in view of their transient existence in this system.

An alternate function for CO₃ must also be considered because of the previous observation⁶ that CO₃ itself is subject to photolytic decomposition to give O atoms and

CO₂. The overall effect of improved OF radical production would be the same as in the previous mechanism; however, in this case it would be unnecessary to invoke the F + CO₃ reaction. The improved OF radical production would occur because the reversible reaction



would increase the range of migration of O atoms within the matrix. Thus, in the absence of CO₂ the generated O and F atoms from OF decomposition would migrate to isolated matrix sites. However, in the presence of CO₂ throughout the matrix, reaction 12 could increase the range of O atom migration and thereby increase the probability of an O + F reaction to regenerate OF.

OF Radical Bond Energy. The observation of OF radical formation during photolysis of F₂-N₂O mixtures confirms the presence of this intermediate in the formation of OF₂, as previously proposed by Ogden and Turner.⁴ It also supports their lowerlimit estimate of about 40 kcal/mol for the OF radical bond energy based on the energy requirements for reaction 2.

Acknowledgments. The author wishes to thank Drs. P. H. Lewis and S. A. Francis for helpful discussions and Mr. G. H. Post for his help with the experimental portion of the work.

(7) As suggested by a reviewer it should be noted that eq 10 assumes the dissipation of hot O atom energy in the formation of CO₃.

Ion-Solvent Interactions. Infrared Studies of Solvation of the Sodium Ion^{1,2}

by E. G. Höhn,³ J. A. Olander, and M. C. Day

Department of Chemistry, Louisiana State University, Baton Rouge, Louisiana 70803 (Received April 14, 1969)

The specific solvation of the sodium ion by tetrahydrofuran has been observed by infrared techniques. Unperturbed ν_{COO} bands occur at 1071 and 913 cm⁻¹. In the presence of the sodium ion, new bands occur at ~1053 and ~895 cm⁻¹, respectively, indicating complexation of the sodium ion. The band intensities are observed to be dependent on the ratio of ether:salt. This is used to approximate stability constants for the stepwise complexation of the sodium ion by tetrahydrofuran.

Introduction

The importance of ion-solvent interactions on ionic conductance and extent of ion pairing was clearly pointed out by Gilkerson⁴ and has been extensively studied by several research groups.⁵⁻⁹ More recently there has been considerable interest in the effects of solvent interactions on the rates of anionic polymerization reactions,¹⁰⁻¹³ but in spite of the large amount of re-

search in this area, there are yet numerous unanswered questions concerning the nature of the solvated species

(1) Reprint requests should be sent to M. C. Day.

(2) Presented in part at Southwestern Meeting of the American Chemical Society, Dec 1967.

(3) Department of Chemistry and Chemical Engineering, University of Saskatchewan, Saskatoon, Sask.

(4) W. R. Gilkerson, *J. Chem. Phys.*, **25**, 1199 (1956).

and the effect solvation may have on the type of ion pair present in solution.

The stability of a complex between a cation and a Lewis base should be dependent on the size of the cation and the basicity of the coordinating species. In order to obtain a strong ion-solvent interaction, it is necessary to have a salt with a small cation. It is also desirable to be able to control the concentration of the coordinating species. This requires the use of a solvent that is inert, or at least, a relatively poor coordinating agent to which the coordinating species can be added in controlled amounts. Unfortunately, salts containing small cations are not generally soluble in noncoordinating solvents. As a consequence, in the use of mixed solvent systems, the study of the complexation of a small cation by a coordinating species is normally complicated by competition with the solvent.

Recently, we have shown that the specific solvation of the cation can be studied in mixed systems by nmr¹⁴ and conductance¹⁵ methods. Sodium tetrabutylaluminate (NaAlBu_4) has the unique property of being soluble in saturated hydrocarbon solvents, and it was shown that there is no significant interaction between the NaAlBu_4 and the hydrocarbon solvent.¹⁴ The solvent can thus be considered to act essentially as a dispersing medium for the salt. This overcomes the problem of competitive solvation normally found in mixed solvent systems, and the effect of the controlled addition of a complexing species can then be followed. We wish to report here the use of infrared spectroscopy in the study of the specific complexation of the sodium ion by tetrahydrofuran (THF).

Experimental Section

Infrared spectra were recorded using a Beckman IR-7 spectrophotometer and Beckman Model FH-01 vacuum-tight liquid cells equipped with potassium bromide windows. Amalgamated lead spacers were used to give a path length of 0.03 mm. The spectra were recorded at ambient temperature of ca. 25°.

Preparation of Sodium Tetrabutylaluminate. NaAlBu_4 was prepared by direct addition of 1 mol of aluminum tributyl (198 g) to a sodium dispersion containing an excess of sodium (23 g) in 200 ml of *n*-heptane. The mixture is stirred and refluxed under a nitrogen atmosphere for 2 hr and then filtered through a fine-fritted glass funnel in a nitrogen atmosphere drybox.¹⁵ The *n*-heptane is removed from the NaAlBu_4 by vacuum evaporation, after which the product is recrystallized from *n*-pentane at Dry Ice temperatures. The white, crystalline NaAlBu_4 is then dried under vacuum.

Sodium tetraethylaluminate (NaAlEt_4) and sodium tetraoctylaluminate (NaAlOct_4) were prepared by the general method described for NaAlBu_4 with toluene used as a reaction solvent rather than heptane and the

appropriate aluminum alkyl, AlOct_3 or AlEt_3 , used in place of AlBu_3 .

Solvents. Cyclohexane was treated with an H_2SO_4 - HNO_3 mixture, dried over KOH, and distilled from CaH_2 . THF and Bu_2O were dried over KOH and distilled from LiAlH_4 . Distillation and collection of solvents were carried out under a nitrogen atmosphere.

Preparation of Solutions. Solutions of varying THF concentration and a constant NaAlBu_4 concentration were prepared by adding an aliquot of a standard NaAlBu_4 solution in cyclohexane to a weighed portion of THF and diluting to volume with cyclohexane. All manipulations involving exposure of NaAlBu_4 , solvents, or solutions were carried out in a nitrogen drybox.

Experimental Procedure. In order to determine the concentration of unperturbed THF in NaAlBu_4 -THF-cyclohexane solutions, spectra of solutions of THF in cyclohexane of a known THF concentration were recorded from 900 to 1150 cm^{-1} . The intensity of the 1071- cm^{-1} band of THF in these solutions was obtained by constructing an artificial base line¹⁶ and using it to obtain a value for the incident radiation ($\%T_0$). The per cent transmittance ($\%T$) was read from the point of maximum absorption for the band. These per cent transmittances were then converted to the respective absorbances (A_0 and A), and their difference ($A - A_0$) was plotted vs. concentration of THF. Linear plots were obtained in all cases.

The concentration of unperturbed THF in NaAlBu_4 -THF-cyclohexane solutions was then found by determining an ($A - A_0$) value for the 1071- cm^{-1} band as was done for the standard solutions. This value was then used to determine the concentration of unperturbed THF from the standard plot. Some error is inherent in this method since the ~1053- and 1071- cm^{-1} bands are not completely separated; thus, the intensity of either band will be enhanced due to overlap with the other. This error is considered to be a minor one and

(5) R. M. Fuoss, *et al.*, *J. Phys. Chem.*, **69**, 2576 (1965), and many others in the series.

(6) C. A. Kraus, *J. Chem. Educ.*, **35**, 324 (1958).

(7) W. R. Gilkerson and J. B. Ezell, *J. Amer. Chem. Soc.*, **89**, 808 (1967).

(8) T. E. Hogen-Esch and J. Smid, *ibid.*, **88**, 318 (1966).

(9) A. D'Aprano and R. Triolo, *J. Phys. Chem.*, **71**, 3474 (1967).

(10) T. Shimomura, J. Smid, and M. Szwarc, *J. Amer. Chem. Soc.*, **89**, 5743 (1967).

(11) J. E. L. Roovers and S. Bywater, *Can. J. Chem.*, **46**, 2711 (1968).

(12) F. A. Dainton, *et al.*, *Makromol. Chem.*, **89**, 257 (1965).

(13) J. E. L. Roovers and S. Bywater, *Trans. Faraday Soc.*, **62**, 701 (1966).

(14) E. Schaschel and M. C. Day, *J. Amer. Chem. Soc.*, **90**, 503 (1968).

(15) C. N. Hammonds and M. C. Day, *J. Phys. Chem.*, **73**, 1151 (1969).

(16) H. H. Willard, L. L. Merritt, Jr., and J. A. Dean, "Instrumental Methods of Analysis," 4th ed. D. Van Nostrand Co., Inc., Princeton, N. J., 1965.

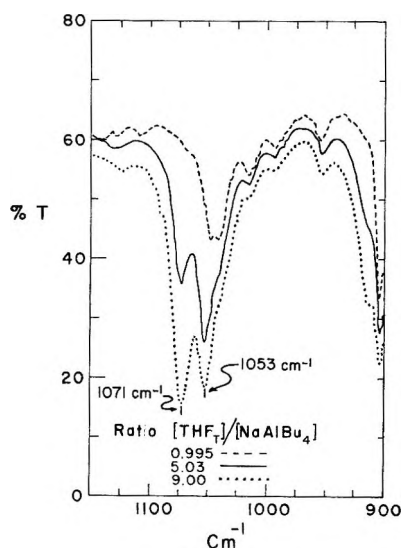


Figure 1. Infrared spectra of NaAlBu_4 -THF-cyclohexane solutions of constant salt concentration and varying THF concentration.

relatively unimportant within the experimental procedures used.

To ensure that cell constants did not change in the course of a study, alternating series of spectra of standard THF-cyclohexane and NaAlBu_4 -THF-cyclohexane solutions were obtained.

Results and Discussion

The infrared spectra of NaAlBu_4 -THF-cyclohexane solutions of constant NaAlBu_4 concentration and varying THF concentration in the 900–1150- cm^{-1} region are shown in Figure 1. The asymmetric C–O–C stretching vibration of THF appears at 1071 cm^{-1} ¹⁷ while the symmetric C–O–C mode appears at 913 cm^{-1} .¹⁸ Bands at 902, 1015, and 1040 cm^{-1} are due to cyclohexane. The AlBu_4^- anion shows broad absorptions centered at 1060 and 1145 cm^{-1} , and moderately intense absorptions at 992 and 955 cm^{-1} . As can be seen from Figure 1, the 1071- and 913- cm^{-1} bands of THF are not evident at THF:salt ratios below 1:1, but a new band appears at ~ 1048 cm^{-1} . A second new band appears in the 900- cm^{-1} region but is masked by the 902- cm^{-1} band of cyclohexane. As the THF:salt ratio is increased past the 1:1 ratio, the band at ~ 1048 cm^{-1} shifts toward a final value of 1053 cm^{-1} and increases in intensity. Correspondingly, the 1071- cm^{-1} band becomes evident, and the band at 913 cm^{-1} appears as a shoulder on the 902- cm^{-1} band of cyclohexane, thus indicating the presence of free THF. The growth of the band at ~ 902 cm^{-1} with an increase in THF concentration can be attributed to the overlap of the perturbed C–O–C symmetric THF band and the 902- cm^{-1} cyclohexane band.

The complexation of THF to group III halides has been shown to shift the frequencies of both the symmetric and asymmetric C–O–C stretching modes of

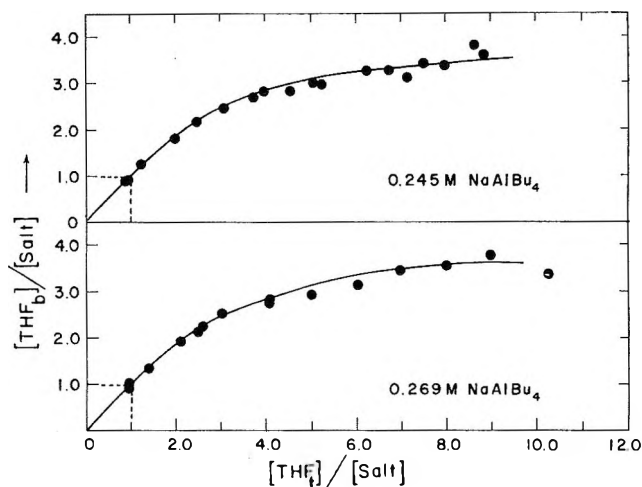
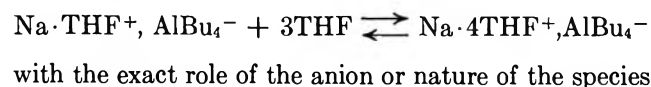


Figure 2. Average value plots, \bar{n} , of the ratio of bound THF:salt vs. ratio of total THF:salt for NaAlBu_4 concentrations of 0.245 and 0.269 M .

THF to lower values.¹⁹ The new band at ~ 1053 cm^{-1} is thus considered to result from the C–O–C stretch of THF molecules complexed with the sodium ion. Spectra of NaAlEt_4 and NaAlOctyl_4 in THF show essentially the same perturbed bands observed with the NaAlBu_4 -THF-cyclohexane system, thereby substantiating the interpretation that the complexation occurs with the sodium ion. Other similar complexing agents should exhibit analogous behavior. This was shown to be true for di-*n*-butyl ether which shows a shift from the unperturbed ν_{COC} of 1125 cm^{-1} to a perturbed value of 1083 cm^{-1} upon complexation.

As can be seen from Figure 1, the absence of the 1071 cm^{-1} band at ratios of THF:salt less than 1:1, and the relative intensity changes as the THF:salt ratio is varied indicate an equilibrium between the 1:1 complex and additional THF molecules. In Figure 2, average value plots (\bar{n}) of the ratio of (bound THF):salt vs. (total THF):salt ($[\text{THF}_b]:[\text{salt}]$ vs. $[\text{THF}_t]:[\text{salt}]$) are shown for salt concentrations of 0.245 and 0.269 M . Below a ratio of 1:1, within experimental limitations, all of the THF is observed to be in the complexed form. The 1:1 complex is then in equilibrium with additional THF molecules, giving a limiting average value of 4, indicating a maximum coordination of 4 for THF and sodium ion under these conditions. This can be considered as



(17) G. M. Barrow and S. Searles, *J. Amer. Chem. Soc.*, **75**, 1175 (1953).

(18) N. B. Colthup, L. H. Daly, and S. E. Wiberley, "Introduction to Infrared and Raman Spectroscopy," Academic Press, New York, N. Y., 1964, p 272.

(19) J. Lewis, J. R. Miller, R. L. Richards, and A. Thompson, *J. Chem. Soc.*, 5850 (1965).

Table I: Approximate Stepwise Stability Constants for $(\text{Na} \cdot x\text{THF})^+$

Salt concn, M	k_1	k_2	k_3	k_4
0.269	Large	28	4.6	0.9
0.245	Large	33	5.5	0.9

(*e.g.*, solvent-separated or contact ion-pair, etc.) not known.

Using Bjerrum's method²⁰ of plotting \bar{n} vs. the negative logarithm of free ligand concentration ($p[\text{THF}_f]$), approximations to the stepwise stability constants for the THF complex with the sodium ion have been made. These are listed in Table I for both the 0.245 and 0.269 M solutions of NaAlBu_4 .

These values are only first order approximations to the stability constants but do give representative orders of magnitude. The discrepancies between the values for the two concentrations are on the order of the accuracy of the system.

From the above, it can be concluded that the sodium ion forms a very stable 1:1 complex with THF, and this is in equilibrium with three additional THF molecules forming a four-coordinated species. Previous studies of this system using nmr¹⁴ and conductance¹⁶ techniques have led to an analogous, but less definitive, interpretation. Although there may be a concentration dependence as well as solvent dependence of the solvation number of the sodium ion, it would seem that the maximum coordination number of 4 is now established for this particular system at a salt concentration in the region of 0.25 M .

Acknowledgment. Support of this work by National Science Foundation Grants GP 1967 and GP 6421 and a National Aeronautics and Space Administration Traineeship for J. A. Olander is gratefully acknowledged.

(20) J. Bjerrum, "Metal Ammine Formation in Aqueous Solution," P. Haase and Son, Copenhagen, 1941.

The Radiation-Induced Isotopic Exchange in Gaseous Hydrogen-Deuterium Mixtures

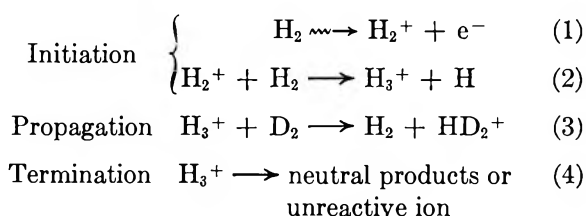
by T. Terao¹ and R. A. Back

Publication No. 11002 from the Division of Pure Chemistry, National Research Council of Canada, Ottawa, Canada
(Received April 14, 1969)

Isotopic exchange in H₂-D₂ mixtures induced by γ -rays and X-rays has been studied in static and flow systems at dose rates from about 2×10^{10} to 1×10^{12} eV cc⁻¹ sec⁻¹, using very pure reagent gases. Highest yields of exchange were obtained using X-rays in a well-baked flow system continuously flushed with equimolar H₂ and D₂ at atmospheric pressure, introduced through Pd thimbles. Values of the ion-pair yield, $M/N[\text{HD}]$, as high as 2.37×10^7 were obtained, corresponding to $G(\text{exchange}) = 1.3 \times 10^8$. The exchange is highly sensitive to impurities, which undoubtedly account for the much lower values ($M/N[\text{HD}] = 2 \times 10^4$) previously reported. Electric fields applied during the irradiation strongly suppressed the exchange, confirming the ionic chain mechanism suggested earlier by Thompson and Schaeffer. An average rate constant of $(3.3 \pm 0.5)10^{-10}$ cc molecule⁻¹ sec⁻¹ was estimated for the chain propagation step, $\text{H}_3^+ + \text{D}_2 \rightarrow \text{H}_2 + \text{HD}_2^+$ (and its isotopic variants), which is thus shown to be a typically fast proton-transfer reaction. This value was obtained by a method in which the propagation reaction competed with removal of ions by an electric field. The data from three sets of experiments, with $[\text{H}_2] = [\text{D}_2]$, $[\text{H}_2] \gg [\text{D}_2]$, and $[\text{D}_2] \gg [\text{H}_2]$, were indistinguishable after corrections for differences in composition and ion mobility.

Introduction

Early studies of the radiation-induced atomic exchange in hydrogen gas were interpreted in terms of the simple hydrogen-atom chain reaction which is well established in the photochemical and thermal systems.²⁻¹⁰ The work of Thompson and Schaeffer¹¹ in 1958, however, on the effect of added noble gases on the exchange in H₂-D₂ mixtures induced by α -rays, provided very strong evidence that the exchange occurs almost entirely by an ionic chain mechanism. Small amounts of xenon (and, less effectively, krypton) suppressed the exchange almost completely, while large additions of argon, neon, or helium had only minor effects. Thompson and Schaeffer suggested the following chain mechanism



All the possible isotopic variations of these reactions occur. Since reaction 2 is known to be very fast, H₃⁺ (or its isotopic equivalent) is the predominant ion in the system. The proton-transfer reaction, 3, is the propagation step in the chain which leads ultimately to HD formation, and in the experiments of Thompson and Schaeffer, occurred about 2×10^4 times for each initiation or termination step. They originally suggested that xenon and krypton intercepted the ionic chain by simple charge transfer from H₂⁺ or H₃⁺ (which is in

fact endothermic), but later proposed that this occurred by proton transfer.¹²

Subsequent studies of these systems in a mass spectrometer,¹³ in a glow discharge,¹⁴ and with tritium β -rays¹⁵ have confirmed the ionic chain mechanism suggested by Thompson and Schaeffer. There has been some debate about the rate constant for reaction 3. Volpi, *et al.*,¹³ estimated a relatively low value of 8×10^{-13} cc molecule⁻¹ sec⁻¹, while Dawson and Tickner¹⁴ suggested a value of 3×10^{-10} to account for the ex-

(1) National Research Council of Canada Postdoctoral Fellow, 1966-68; Department of Engineering Sciences, Nagoya Institute of Technology, Gokiso-cho, Showa-ku, Nagoya, Japan.

(2) P. C. Capron, *Ann. Soc. Sci. Bruxelles*, **55**, 222 (1935).

(3) W. Mund, L. Kaertkemeyer, M. VanPee, and A. Van Tiggelen, *Bull. Soc. Chim. Belges*, **49**, 187 (1940).

(4) W. Mund, T. de Menten de Hornes, and M. Van Meersche, *ibid.*, **56**, 386 (1947).

(5) W. Mund and M. Van Meersche, *ibid.*, **57**, 88 (1948).

(6) H. Eyring, J. O. Hirschfelder, and H. S. Taylor, *J. Chem. Phys.*, **4**, 479 (1936).

(7) L. M. Dorfman and H. C. Matraw, *J. Phys. Chem.*, **57**, 723 (1953).

(8) H. C. Matraw, C. F. Pachucki, and L. M. Dorfman, *J. Chem. Phys.*, **20**, 926 (1952).

(9) S. O. Thompson and O. A. Schaeffer, *ibid.*, **23**, 759 (1955).

(10) L. M. Dorfman and F. J. Shipko, *J. Phys. Chem.*, **59**, 1110 (1955).

(11) S. O. Thompson and O. A. Schaeffer, *J. Amer. Chem. Soc.*, **80**, 553 (1958).

(12) O. A. Schaeffer and S. O. Thompson, *Radiat. Res.*, **10**, 671 (1959).

(13) V. Aquilanti, A. Galli, A. Giardini-Guidoni, and G. G. Vopli, *J. Chem. Phys.*, **43**, 1969 (1965).

(14) P. H. Dawson and A. W. Tickner, *ibid.*, **37**, 672 (1962).

(15) W. M. Jones, *ibid.*, **47**, 4675 (1967).

change observed in the glow discharge. Thompson and Schaeffer calculated that if k_3 were equal to k_2 (i.e., $\sim 1.4 \times 10^{-9}$ cc molecule⁻¹ sec⁻¹), then their ion-pair yield, $M/N[\text{HD}]$, should have been about 2×10^7 rather than 2×10^4 as they observed. They concluded that the chain length was probably limited by impurities, despite rigorous purification. Earlier work by Dorfman and Shipko¹⁰ had demonstrated the great sensitivity of the reaction to impurities. If on the other hand k_3 were much lower, the exchange rate obtained by Thompson and Schaeffer could have been close to its impurity-free limit, with chains terminated by ion neutralization.

The present investigation of the radiation-induced exchange was undertaken to determine whether $M/N[\text{HD}]$ from H₂ + D₂ could be raised above 2×10^4 by further purification, to examine the effects of electric fields on the exchange, to attempt to measure ion lifetimes and ion concentrations by an intermittent-field method, and finally, if possible, to obtain a value of k_3 .

Experimental Section

All irradiations were done in cylindrical Pyrex vessels, 3.2 cm i.d., 11.8 cm long, equipped with central axial electrodes 4 mm in diameter and outer cylindrical electrodes which were a close fit inside the Pyrex cylinders. A number of small holes in the electrodes facilitated evacuation of the space between the electrodes and Pyrex walls. In some preliminary experiments the vessel was thoroughly baked under vacuum on a mercury-free line, filled with an H₂-D₂ mixture, sealed, and irradiated. H₂ and D₂ were introduced separately into the vacuum line through heated palladium thimbles.

Most of the experiments were done in a flow system to which H₂ and D₂ from cylinders were admitted continuously through Pd thimbles at 200-350°. Flow rates of H₂ and D₂ were controlled by the pressure differential across the thimbles and their temperature. Each gas flowed through 50 cm of 1-mm bore capillary (to prevent back diffusion of the mixed gases to the hot palladium and consequent isotopic mixing) to a small mixing bulb (10 cc), and thence the H₂-D₂ mixture (containing from 0.02 to 0.8% HD) entered the reaction vessel. The exit gases from the vessel flowed through a long capillary to prevent back diffusion of impurities, and then via glass and polythene tubing to the pick-up of a gas chromatograph. Total flowrates of gases through the system were varied between 5 and 10 cc/min which gave average residence times from about 8 to 16 min in the 83 cc reaction vessel. Typical procedure in the flow experiments was first to measure the total flowrate and the initial composition of the gas in the absence of radiation. The irradiation was then begun, and repeated analyses made until a steady HD content in the effluent gas was established. The reac-

tion vessel and inlet system could be baked to temperatures of 400°, and could be evacuated *via* a mercury-free high-vacuum line. All experiments in the flow system were done at atmospheric pressure and 25°.

Radiation sources and dosimetry. Most of the work was done with X-rays from a Machlett OEG-60 tube equipped with a beryllium window and operated from 20 to 60 kV and 10 to 50 mA. Some experiments in sealed vessels were done with ⁶⁰Co γ -radiation. All dosimetry was based on direct measurement of saturation ion-currents in the reaction vessel itself. The outer cylindrical collecting electrode was made with a portion about 2-cm long at one end telescoped. After final glass-blowing operations on that end of the vessel, the electrode was extended to the closed end, thus encompassing the entire volume of the vessel, so that there was virtually no dead space. Good saturation plateaus were always obtained. Electrode materials presented some problems, as tests showed that graphite, Kovar, tungsten, copper, and silver caused relatively rapid exchange in the absence of radiation. Oxide-free copper and silver were fairly inert, but traces of oxide, difficult to avoid in the glass-blowing operations, were very efficient catalysts for exchange. Stainless steel was found to cause virtually no exchange, and was used for electrodes in most of the experiments. Reaction of hydrogen with the carbon (<0.15%) in the type 303 stainless steel employed apparently produced hydrocarbon impurities, and low-carbon (<0.03%) stainless steel (Type 304-L) was finally used to minimize this complication.

Analysis. Mixtures of H₂, HD, and D₂ were analyzed by gas chromatography, using a 2-m alumina column treated with MnCl₃ and operated at -196°. ¹⁶ With helium carrier gas the three components were quite well resolved, and this was used to measure H₂/D₂ ratios and in some measurements of HD. Accurate area measurements of small HD peaks was difficult, as they came out on the tail of the large H₂ peak. For greater accuracy, therefore, H₂ was used as a carrier gas, eliminating the H₂ peak, and thus permitting better measurement of HD/D₂ ratios. Because relatively large samples of gas were available for analysis, a simple thermal conductivity detector was sensitive enough with both carrier gases, despite the small differences in thermal conductivity. Peak areas were shown by calibration experiments to be very nearly proportional to the quantity of each component, and were used throughout.

Results and Discussion

Experiments in sealed vessels. A series of experiments in sealed vessels showed that values of the ion-pair yield, $M/N[\text{HD}]$, could indeed be obtained that were higher than the highest value previously observed

(16) I. Yasumori and S. Ohno, *Bull. Chem. Soc. Jap.*, 39, 1302 (1966).

($\sim 2 \times 10^4$). Values in the range $1-3 \times 10^5$ could be obtained fairly regularly, but higher and lower values were also observed. These varied from $\sim 10^3$ to 2.9×10^6 , the highest value measured in a sealed vessel. The data showed no particular correlation with any experimental parameters, although in general higher values of $M/N[\text{HD}]$ were obtained with more prolonged baking of the vessel and when lower residual pressures were achieved before filling. There seems little doubt that the scatter was due to trace impurities intercepting the ionic chain, which because of the enormous chain length is highly susceptible to such effects.

Flow experiments. These were undertaken to avoid the exposure to air, glassblowing, evacuation, baking, filling and sealing involved in each experiment with the sealed vessels. Once the flow system was assembled, the reaction vessel was exposed only to flowing hydrogen for long periods of time, and experiments could be done in quick succession without risk of altering the conditions. There were several ways of preparing the reaction system for an experiment. The vessel could be baked under vacuum with the Pd thimbles at 100° and thus not passing hydrogen. It could be baked open to the vacuum line with thimbles hot, thus flushing with a few milli Torr pressure of hydrogen, or with hydrogen flowing at atmospheric pressure. Preirradiation with X-rays during or after baking was also tried, and irradiation was normally continued, with repeated analyses, until approximately steady values of $M/N[\text{HD}]$ were obtained.

The flow experiments gave yields of HD considerably higher than those found with the static sealed vessels, but again there was a good deal of scatter from day to day and with various treatment of the vessel. There was some evidence that hydrogen reacted with the $<0.15\%$ carbon present in the type-303 stainless steel electrodes, during irradiation or baking, to form hydrocarbon impurities which may have lowered the yield of exchange and contributed to the irreproducibility of the results. A reaction vessel made with low-carbon ($<0.03\%$) type 304L stainless steel electrodes gave considerably better results, and was used in all subsequent experiments. Values of $M/N[\text{HD}]$ measured in this vessel over a period of several months with equimolar $\text{H}_2\text{-D}_2$ mixtures ranged from 1.5×10^6 to 2.37×10^7 . The values obtained depended to some extent on the conditioning of the system, with the highest values usually following prolonged baking of the vessel with hydrogen flowing through the thimbles and continuous pumping. Values between about 1 and 2.37×10^7 were obtained consistently in a series of experiments lasting about 6 weeks. Typical data from these experiments, which presumably correspond to the highest purity of reagent gases that we were able to attain, are shown in Table I. These are crude experimental yields of HD, uncorrected for back reaction or for slight deviations of the H_2/D_2 ratio from unity. The highest value ob-

Table I: Isotopic Exchange in $\text{H}_2\text{-D}_2$ Mixtures ($\text{H}_2 = \text{D}_2$, Initial HD = 0.2-0.6%; X-Ray Tube Current = 10 mA at 16-18 kV; Dose Rates from 6 to 14×10^9 eV $\text{cc}^{-1} \text{sec}^{-1}$)

Saturation current, amp $\times 10^9$	Final HD, %	Flow rate, cc/min	$M/N[\text{HD}] \times 10^{-7}$
4.80	17.37	5.0	1.17
4.40	13.49	5.9	1.15
4.40	25.70	4.4	1.67
2.16	18.01	4.4	2.37
2.20	7.30	5.3	1.09
2.20	10.23	5.2	1.53
2.60	9.51	5.3	1.20
2.20	8.26	4.8	1.14
2.24	15.09	4.7	2.04
2.24	14.21	4.7	1.92
2.24	15.12	4.7	2.00
2.24	12.10	4.5	1.54
2.24	9.43	3.9	1.03
2.24	13.9	3.9	1.57

tained, 2.37×10^7 , corresponds to a value of $G(\text{exchange})$ (defined in the usual way to take account of the exchange of like atoms) of $2 \times 100 \times 2.37 \times 10^7/W = 1.3 \times 10^8$, which must be one of the highest G values ever observed in radiation chemistry. Values of $M/N[\text{HD}]$ consistently lower than those in Table I were obtained at other times, often associated with replacement of a deuterium cylinder or of the palladium thimbles, which became badly deformed in use and eventually cracked.

The effect of electric fields on the exchange. Electric fields were applied during irradiation in the flow system under conditions yielding a considerable range of values of $M/N[\text{HD}]$ in the absence of a field (presumably corresponding to various degrees of purity of the reagent gases). The field reduced the amount of exchange to an extent which depended markedly on these initial field-free values. Thus if $M/N[\text{HD}]$ was low, the field had little effect, while if $M/N[\text{HD}]$ was high, the field reduced it much more sharply; this is illustrated in Figure 1. This behavior is in accord with termination of the ion chain by impurities rather than by neutralization, except perhaps at the highest values of $M/N[\text{HD}]$. Thus if an ion reacted with an impurity molecule long before neutralization, more rapid neutralization by removal to an electrode by an applied field would have little effect. As impurities were reduced, the H_3^+ ion chain would persist longer before termination by an impurity molecule, and application of the same field would reduce the chain length and the yield of HD to a much greater extent.

Ion-lifetime measurements were attempted by an intermittent-field method, previously described.¹⁷ Be-

(17) C. J. Wood, R. A. Back, and D. H. Dawes, *Can. J. Chem.*, **45**, 3071 (1967).

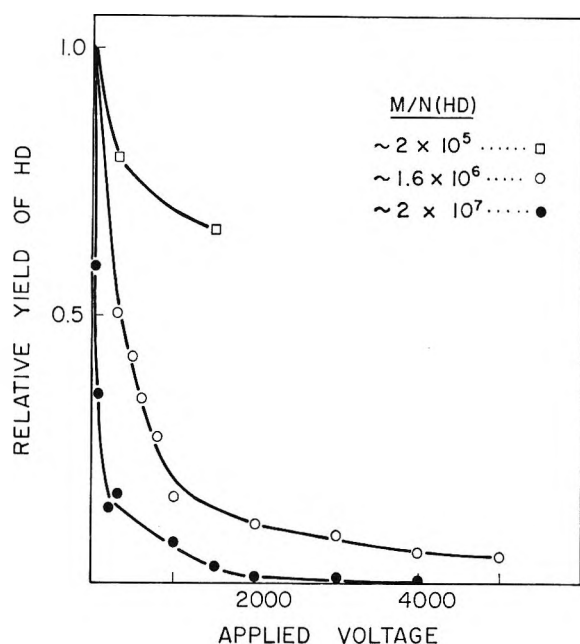


Figure 1. Effect of applied field on the yield of HD.

havior was (as expected) characteristic of systems having free electrons rather than negative ions, and with mixed ion loss, by both homogeneous combination and diffusion to the walls. Because such systems are not amenable to accurate lifetime measurements by this method,¹⁸ and because lifetime with respect to neutralization was not apparently the meaningful lifetime for the ion-chain reaction, these measurements were not pursued further.

The considerable scatter in values of $M/N[\text{HD}]$, even in the best experiments in the flow system (Table I), indicated that chains were still being terminated to some extent by impurities, making quantitative kinetic studies of the exchange difficult. The effect of applied fields, however, suggested a means of estimating k_3 , even in the presence of trace impurities. When a field is applied, ions are drawn to the electrodes, and as the field strength is increased, ions are removed more and more rapidly from the gas phase, with the average time of transit to the collecting electrode varying inversely with the field strength. At low field strengths, gas-phase combination and diffusion to the walls would contribute to the removal of ions, but at higher field strengths these would become negligible, and ion lifetime should become strictly proportional to the inverse of the field strength. Similarly, at low field strengths, the lifetime of the ionic chain propagated by H_3^+ and its isotopic variants is probably limited by reaction with impurities and perhaps partly by neutralization. At sufficiently high field strengths, however, removal to the electrode should become the dominant controlling factor; in other words, H_3^+ ions will be removed from the gas phase so quickly that no encounters with impurities can occur in transit. Under these conditions,

ions would drift toward the collecting electrode with a velocity EK , where E = field strength and K = ion mobility. For parallel-plate electrodes and uniform irradiation, it is easily seen that the average time required for an ion to reach the collecting electrode from its point of formation would be equal to $d^2/2VK$, where d is the distance between the plates and V the applied voltage. The ion reaching the electrode would not, of course, be the original ion, as the chain-propagating proton-transfer reaction, 3, (and its isotopic variants) would have occurred many times during transit. The average number of occurrences, which is simply the yield per ion pair for reaction 3, will be given by

$$M/N(3) = k_3[\text{H}_2 + \text{HD} + \text{D}_2]d^2/2VK \quad (5)$$

where k_3 is an appropriate average second-order rate constant. Equation 5 is based on the assumption that normal random thermal motion of the ions is virtually unaffected by the electric field, the drift velocity being much smaller than the average velocity of thermal motion. Our experiments were in fact done in a cylindrical rather than a parallel-plate vessel, and it can be shown that the corresponding expression for cylindrical geometry is

$$M/N(3) = \frac{k_3[\text{H}_2 + \text{HD} + \text{D}_2](r_2^3 + r_1r_2^2 - r_1^2r_2 - r_1^3) \ln(r_2/r_1)}{4(r_2 + r_1)VK} \quad (6)$$

where r_1 and r_2 are the radii of the inner and outer electrodes, respectively. Substituting our experimental values of $r_1 = 0.2$ and $r_2 = 1.5$ cm, this becomes

$$M/N(3) = 1.1133k_3[\text{H}_2 + \text{HD} + \text{D}_2]/VK \quad (7)$$

To relate $M/N(3)$ to $M/N[\text{HD}]$, it should be noted that four ions (H_3^+ , H_2D^+ , HD_2^+ and D_3^+) are present in the system, and each can react with either H_2 , HD or D_2 in a total of 18 possible isotopic variants of reaction 3 (this includes reactions in which like atoms are exchanged). If the rate constants are all equal, and the relative concentrations of the four ions are statistically equilibrated, it can easily be shown that in an equimolar mixture of H_2 and D_2 , only one half of the reactions occurring give rise to HD . More generally, it can be shown that for any mixture of H_2 , HD and D_2 , there is an efficiency factor of $2f_{\text{H}}f_{\text{D}}$ for the production of HD , where f_{H} and f_{D} are atom fractions of H and D present. The net yield of HD is further reduced because it can be destroyed in reaction 3, and taking this into account, a net efficiency factor of $2f_{\text{H}}f_{\text{D}} - f_{\text{HD}}$ results, where f_{HD} is the mole fraction of HD present. Thus

$$M/N(\text{HD}) = (2f_{\text{H}}f_{\text{D}} - f_{\text{HD}})M/N(3) \quad (8)$$

(18) T. Terao and R. A. Back, to be published.

Three sets of experiments were carried out with $[H_2] = [D_2]$, $[H_2] \gg [D_2]$, and $[D_2] \ll [H_2]$, all in the flow system at atmospheric pressure, with voltages applied ranging from 0 to 5000 V. The per cent reaction in each of these sets was held roughly constant by increasing the X-ray intensity to compensate for the decrease in $M/N[HD]$ with increasing field strength. The absorbed dose rate varied from 2 to 120×10^{10} eV cc⁻¹ sec⁻¹. Data from these experiments are shown

Table II: Effect of Electric Fields on the Isotopic Exchange

Applied voltage	Dose rate, eV cc ⁻¹ sec ⁻¹ $\times 10^{-10}$	$M/N[HD]$ $\times 10^{-4}$	$M/N(3)$ $\times 10^{-4}$
$[H_2] = [D_2], 2f_{HD} = 0.5$			
0	7.8	16.0	37.3
500	7.8	6.80	14.6
1000	97	0.840	1.87
3000	23	2.61	5.63
2000	68	1.43	3.19
0	53	1.78	4.00
0	7.5	16.7	39.0
800	7.5	16.5	38.5
4000	18	4.5	9.95
300	96	0.947	2.12
600	7.1	8.38	18.1
0	13.5	5.74	12.7
700	5.4	16.9	38.0
700	7.7	5.94	12.7
700	15.4	4.80	10.6
700	10.9	5.40	11.7
700	18.6	4.70	10.5
1500	38	2.50	5.65
3000	65	1.37	3.05
$[H_2] \gg [D_2], 2f_{HD} = 0.0524$			
0	5.4	1.09	21.8
1000	15.8	0.351	7.01
2000	20	0.226	4.48
700	6.8	0.472	9.25
1500	13.5	0.296	5.84
4000	34	0.132	2.61
800	4.4	0.487	9.47
1200	7.0	0.339	6.61
2500	14.3	0.200	3.91
0	3.9	1.177	23.4
500	3.9	0.621	12.1
900	5.9	0.424	8.28
600	4.0	0.547	10.7
$[D_2] \gg [H_2], 2f_{HD} = 0.1806$			
500	37	2.72	16.1
1500	95	1.10	6.55
1000	54	1.57	9.29
1200	54	1.38	8.13
600	2.5	2.42	14.2
2000	8.1	0.967	5.71
800	3.3	1.933	11.3
900	3.3	1.760	10.3
3000	93	0.661	3.88
700	2.1	1.980	11.5
4000	123	0.506	2.97

in Table II. Fields applied during these experiments were always sufficient to obtain saturation ion-currents. At the higher voltages ion currents were appreciably (up to 10%) higher than the saturation values because electrons accelerated in the field caused some additional ionization. In calculating values of $M/N[HD]$ in Table II, N is based on the actual observed ion current rather than the saturation value, thus taking account of the extra ions formed by electron impact. Values of $M/N(3)$ shown in Table II were obtained from $M/N[HD]$ via eq 8, taking for f_{HD} a simple average of that for the inlet and outlet gases (this implies "plug" flow through the reaction vessel). In order to compare the three systems studied, it may be noted that the isotopic composition of the gas can affect the data in two ways, first through an isotope effect in the value of k_3 , and secondly, through a variation in the mobility, K . The latter effect seems fairly well understood, as most theories of ion mobility predict that the average mobility (for Langevin conditions at zero field) in mixtures of H_2 , HD and D_2 should vary approximately inversely with $M^{1/2}$ where M is the average molecular weight of the gas.¹⁹ There is fair confirmation of this in the mobility studies of Rose on H_2 and D_2 .²⁰ To take account of the dependence of K on the isotopic composition, we have normalized the values of $M/N(3)$ obtained from the $[H_2] \gg [D_2]$ and $[D_2] \gg [H_2]$ mixtures, assuming $M/N(3)$ to vary inversely with K and hence directly with $M^{1/2}$, taking the equimolar H_2 - D_2 mixture as the norm. In Figure 2, values of $M/N(3)$ normalized in this way are plotted against $1/V$, which from eq 7 should yield a straight line through the origin at sufficiently high field strengths.

The data in Figure 2 follow the expected behavior, with values of $M/N(3)$ falling off from the initial linear relation at voltages less than about 1200 V. This fall-off is compatible with a levelling out at the field-free value which in these experiments ranged from 2 to 4×10^6 . In several other series of experiments, not shown in Figure 2, field-free values of $M/N(3)$ were markedly lower, presumably due to impurities, and the falloff from the linear relation occurred at lower values of $1/V$, and was more severe. At the highest voltages, however, values of $M/N(3)$ came into line with the data in Figure 2, lending support to the postulate that these data in the high-voltage limit were unaffected by impurities.

It is also evident from Figure 2 that within the experimental accuracy, the data from the three systems, normalized to take account of the dependence of K on isotopic composition, are indistinguishable. This suggests that effective values of k_3 in the three systems are

(19) P. G. Davies, J. Dutton, F. Llewellyn-Jones, and E. M. Williams, *Phil. Trans. Roy. Soc. London*, **A259**, 299 (1966); J. Dutton, F. Llewellyn-Jones, W. D. Rees, and E. M. Williams, *ibid.*, **A259**, p 339 (1966).

(20) D. J. Rose, *J. Appl. Phys.*, **31**, 643 (1960).

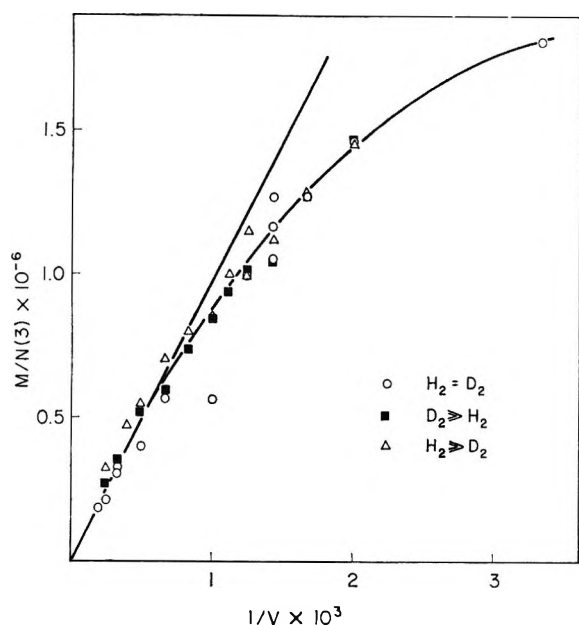


Figure 2. Plot of eq 7, with $M/N(3)$ normalized for differences in ionic mobility, K .

similar; it does not follow, however, that k_3 has no isotopic dependence, since the value obtained in each system is a very complex weighted mean for the 18 possible isotopic variants of reaction 3. The weighting depends on the relative proportions of the 4 ions and 3 molecules present, and upon which variants give rise to HD. Furthermore, isotope effects in reaction 3 itself are threefold in nature, depending on the isotopic composition of the reacting ion, on whether H⁺ or D⁺ is transferred, and on whether H₂, HD, or D₂ is the acceptor. It seems probable that these effects will tend to cancel one another in the weighted mean values of k_3 that are obtained. It is clear that there must be some overall isotope effect in k_3 ; this was shown by several experiments in which sealed vessels containing H₂ and D₂ were irradiated with γ -rays until a steady concentration of HD was reached. Values of $[HD]^2/[H_2][D_2]$ close to the thermodynamic equilibrium value of 3.27 were obtained confirming earlier observations.^{15,21} The observed deviation from the statistical value of 4 must be reflected in an isotope effect in k_3 , but it is evident that the accuracy of the present data does not permit its detection.

From the slope of the straight line drawn through the initial points in Figure 2, a value of $k_3 = 3.14 \times 10^{-10}$ cc molecule⁻¹ sec⁻¹ may be obtained, taking a value of $K = 8.82$ cm² V⁻¹ sec⁻¹ for a $[H_2] = [D_2]$ mixture, which is based on a value of 10.8 for H₂¹⁹ and the assumption that K depends inversely upon $M^{1/2}$. The accuracy of this estimate of k_3 is difficult to assess precisely, but several possible sources of error may be pointed out. Any error in K , either in the value of 10.8 taken for pure H₂, or in the assumed dependence upon isotopic composition, will be reflected directly in k_3 .

There seems fair agreement on the former figure for H₂ of high purity^{19,22} and general theoretical (and some experimental) support for the latter assumption. It should be noted that in almost all of the present experiments the values of E/p were less than 10 Vcm⁻¹ Torr⁻¹ (the highest value was 16.8 at the central electrode with 5000 V applied). This is within the "zero field" region where K is independent of field,¹⁹ and where ion mobility should closely approximate simple Langevin behavior. It should also be noted that while the maximum voltage gradient in our experiments was perhaps 500 times higher than that typically used in the reaction chamber of a mass spectrometer used to study ion-molecule reactions, this was more than balanced by the reduction in mean free path. Thus the average energy of reacting ions may be estimated at about 0.05 eV at our highest voltage (5000 V), so that our value of k_3 is comparable to the field-free values for ion-molecule reactions such as those measured by pulse techniques rather than to those measured using a withdrawing field during the reaction.²³

A second possible source of error in k_3 is the assumption implicit in Figure 2, in which the straight line is drawn through the origin, that nonionic reactions (notably the atomic chain reaction) made a negligible contribution to isotopic exchange. Our justification for this assumption is the conclusion of Schaeffer and Thompson^{11,12} that M/N due to the atomic reaction was less than 100, which is supported by estimates based on the known rate constants of the atomic exchange reaction. The present data would permit a positive intercept as high as 1×10^5 , but are equally compatible with a line through the origin. It is also probably true that excitation and dissociation by electron impact in the electric field could sharply enhance the yield of hydrogen atoms relative to that of ions, but since the latter was only increased by $\sim 10\%$ at the highest voltages used, it seems doubtful that the yield of atoms would be more than doubled. If the estimate of Schaeffer and Thompson is correct, the atomic exchange reaction would still be negligible in Figure 2.

Finally, there is some error in the assumption of "plug" flow in the reaction vessel in the correction for the back reaction of HD. It can be shown that the assumption of complete mixing in the reaction vessel would lead to values of k_3 from 4 to 8% higher. True flow condition in the vessel were somewhere between these two extremes, and k_3 should probably be adjusted upwards by about 3%.

Taking all these factors into account, an estimate of

(21) S. O. Thompson and O. A. Schaeffer, *J. Chem. Phys.*, **23**, 759 (1955).

(22) T. M. Miller, J. T. Moseley, D. W. Martin, and E. W. McDaniel, *Phys. Rev.*, **173**, 115 (1968).

(23) A. G. Harrison, J. J. Myher, and J. C. J. Thynne, "Ion-Molecule Reactions in the Gas Phase" *Advances in Chemistry Series No. 58*, American Chemical Society, Washington, D. C., 1965, p 150.

$(3.3 \pm 0.5)10^{-10}$ cc molecule⁻¹sec⁻¹ is probably not unrealistic for the best value and limits of uncertainty of k_3 . This is in excellent agreement with the value of 3×10^{-10} estimated by Dawson and Tickner,¹⁴ but much higher than the low value of 8×10^{-13} suggested by Volpi, *et al.*¹³ Our very high value of $M/N[\text{HD}]$ in highly purified H₂-D₂ mixtures is also strong support for the high value of k_3 , and it seems clear that reaction 3 is a typically fast proton-transfer reaction, about half the speed of the very fast reaction 2,²³ and that any suggestion of an activation energy¹⁵ is most unlikely.

Finally, the possibility that H₅⁺ rather than H₃⁺ is the ion involved in reaction 3 should be noted. This has been discussed by Jones, *et al.*,¹⁹ whose drift experiments offer some support to the suggestion that H₅⁺ is the dominant ion in hydrogen at atmospheric pressure and low field strengths. Presumably H₅⁺ would then be the carrier of the ionic chain; the present observations and conclusions would be little affected, although the meaning of k_3 would be altered.

Summary

(1) Values of the ion-pair yield, $M/N[\text{HD}]$, as high as 2.37×10^7 have been observed in the X-ray induced isotropic exchange in H₂-D₂ mixtures, corre-

sponding to $G(\text{exchange}) = 1.3 \times 10^8$. The exchange is highly sensitive to impurities, and it seems clear that in previous studies in which maximum value of $M/N(\text{HD})$ of about 2×10^4 were obtained, the reaction chain length was severely limited by interaction with impurities. (2) Application of electric fields during the irradiation strongly inhibited the exchange, confirming previous conclusions that the reaction proceeds by an ionic mechanism. (3) A rate constant of $(3.3 \pm 0.5) 10^{-10}$ cc/molecule sec has been estimated for the chain propagating step, thought to be $\text{H}_3^+ + \text{D}_2 \rightarrow \text{H}_2 + \text{HD}_2^+$ (and its isotopic variants), which is thus a typically fast proton-transfer reaction. This value was determined from experiments in which the propagation reaction competed with removal of ions from the gas phase by an electric field, a method common in mass spectrometry at much lower pressures, but not employed previously under conventional high-pressure radiolysis conditions. (4) The rate constant for the propagation reaction was obtained from three mixtures, with $[\text{H}_2] = [\text{D}_2]$, $[\text{H}_2] \gg [\text{D}_2]$, and $[\text{D}_2] \ll [\text{H}_2]$. After correcting for differences in ion mobility, the data were superimposable; there was thus no overall isotope effect between the three systems. It seems probable that isotope effects in the 18 possible variants of the propagation reaction tended to cancel.

Some Energetics and the Kassel Fit Parameter s_K in Unimolecular Reactions

by E. Tschuikow-Roux

Department of Chemistry, University of Calgary, Calgary, Alberta, Canada (Received April 14, 1969)

Experimental Kassel fit parameters s_K for thirteen unimolecular reactions involving molecules of varying complexity and diverse frequency patterns are compared with calculated s values based on $\langle E^{\infty}_{th} \rangle_t$, the average energy of reacting species produced by thermal collisional activation in the high-pressure limit. The discussion is carried out within the framework of the quantum-statistical RRKM theory of unimolecular reactions. Explicit expressions for $\langle E^{\infty}_{th} \rangle_t$ are derived in terms of an energy distribution function for reacting species using a rotation-vibration energy level sums approximation, or in terms of the temperature dependence of the high pressure limiting rate constant k^{∞} .

Comparison of s and s_K shows that the correlation previously reported for small molecules at elevated temperatures diminishes with (a) increasing complexity of the species, (b) increasing frequency pattern, and (c) decreasing working temperature. It is concluded that s_K of classical Kassel theory is strictly an empirical fit parameter and that its common interpretation as the number of "effective oscillators" is a misnomer.

Introduction

In the discussion of intermolecular energy transfer in connection with collisional activation-deactivation probabilities in chemical reaction kinetics, a knowledge of the average energy of reacting species is frequently necessary. Several such levels of excitation have been distinguished^{1,2} corresponding to low and high-pressure limits, and type of activation (collisional or chemical). An estimate of the average energy of reacting species also finds use in comparisons² of the classical RRK and the quantum-statistical RRKM (Rice-Ramsperger-Kassel-Marcus) theories of unimolecular reactions.

Despite the general acceptance of the RRKM theory³ in the interpretation of unimolecular reactions, the classical RRK theory, and particularly the Kassel parameter s_K continue to be used in the representation and interpretation of experimental data, with s_K commonly referred to as the number of "effective oscillators," *i.e.*, the effective number of classical oscillators when the systems behave in a true classical unimolecular fashion. It has been pointed out² that the frequently used estimate of s_K as being equal to $1/2 t$ to $2/3 t$, where t is the total number of vibrational degrees of freedom is not generally correct, since s depends on several factors, including the frequency patterns of the activated complex and molecule, the critical energy E_0 , as well as the working temperature.

It has been shown by Placzek, *et al.*,² that the average energy of reacting systems in the high pressure region, $\langle E^{\infty}_{th} \rangle_t$, or the average internal energy of all molecules, $\langle E_{all} \rangle_K$, can provide a measure of the "effective" number of oscillators, *i.e.*, $s = (\langle E^{\infty}_{th} \rangle_t - E_0) / RT$ or $s' = \langle E_{all} \rangle / RT$, which within certain limitations, may be associated with the Kassel empirical-fit parameter, s_K . A reasonable correlation was obtained in the case of CH_4 and CF_3H (which have comparatively high E_0 values) at elevated temperatures. It was stressed that even so the calculated values of s and s'

were roughly of similar magnitude as the Kassel fall-off parameter s_K , the three values could not be identical since each corresponds to different aspects of empirical fit. It was also indicated that the relative correspondence of the various s values in relation to t , T , and the critical energy E_0 , would be perturbed somewhat for systems with lower E_0 and/or higher t values. Nevertheless, the treatment of Placzek, *et al.*,² could be taken to infer that a general "order of magnitude" correspondence between the various s values could be anticipated.

The present communication extends this comparison of s parameters based on RRKM average-energy calculations with s_K values reported in the literature for various unimolecular systems, and it is shown, that the correlation diminishes with increasing complexity of the molecule and decreasing working temperature. For 12-atom molecules such as butene-2 there appears to be no correlation at all (see Discussion).

Furthermore, it appears that although the evaluation of average energies has been carried out numerically in numerous applications of the RRKM theory, an explicit integrated form has not been given in the literature. Therefore, we consider first several alternate methods of evaluating $\langle E^{\infty}_{th} \rangle_t$ or $\langle E^{\dagger}_{th} \rangle_t$ in terms of either an energy distribution function $f(E)$ and making use of the rotation-vibration energy level sums approximation of Whitten and Rabinovitch,⁴ or in terms of the

(1) B. S. Rabinovitch and D. W. Setser, *Advan. Photochem.*, **3**, 1 (1964). This article should be consulted for numerous references to RRKM theory applications.

(2) D. W. Placzek, B. S. Rabinovitch, G. Z. Whitten, and E. Tschuikow-Roux, *J. Chem. Phys.*, **43**, 4071 (1965).

(3) (a) R. A. Marcus and O. K. Rice, *J. Phys. Colloid Chem.*, **55**, 894 (1951); (b) R. A. Marcus, *J. Chem. Phys.*, **20**, 359 (1952); (c) G. M. Wieder and R. A. Marcus, *ibid.*, **37**, 1835 (1962); (d) R. A. Marcus, *ibid.*, **43**, 2658 (1965).

(4) (a) G. Z. Whitten and B. S. Rabinovitch, *ibid.*, **38**, 2466 (1963); (b) *ibid.*, **41**, 1883 (1964).

temperature dependence of the high-pressure limiting first-order rate constant, k^∞ .

Theoretical Considerations

$\langle E^{\infty}_{\text{th}} \rangle_t$ in terms of $f(E)$. The average energy of reacting species produced by thermal collisional activation in the high-pressure region is given by^{1,2}

$$\langle E^{\infty}_{\text{th}} \rangle_t = \int_{E_0}^{\infty} E f(E) dE \quad (1)$$

where E_0 is the critical energy and $f(E)$ is a normalized energy distribution function derived from the thermal quantum-statistical Boltzmann distribution, $K(E)$, weighted by the specific reaction probability, $k(E)$,

$$f(E) dE = \frac{k(E) K(E) dE}{\int_{E_0}^{\infty} k(E) K(E) dE} \quad (2a)$$

$$= \frac{\sum_{E^\ddagger} P(E^\ddagger) \exp(-E^\ddagger/RT) dE^\ddagger}{\int_0^{\infty} \sum_{E^\ddagger} P(E^\ddagger) \exp(-E^\ddagger/RT) dE^\ddagger} \quad (2b)$$

where eq 2b follows from the RRKM theory formulation^{1,3} of $k(E)$ and $K(E)$, and the fact that the total energy $E = E_0 + E^\ddagger$, E^\ddagger being the nonfixed energy of the activated complex. The symbol $\sum P(E^\ddagger)$ denotes the total sum of the degeneracies of all possible energy eigenstates of the active⁵ degrees of freedom of the activated complex at energy E^\ddagger and can be readily evaluated by the approximate but accurate methods of Whitten and Rabinovitch.⁴ For the general case of an activated complex possessing s^\ddagger vibrational degrees of freedom and r^\ddagger active internal rotations the rotation-vibration energy level sum approximation⁴ has the form

$$\sum_{E^\ddagger} P(E^\ddagger_{\text{vr}}) = C_1 (E^\ddagger + a^\ddagger E^\ddagger_z)^n \quad (3)$$

where C_1 is a constant,⁶ $E^\ddagger_z = 1/2 \sum \omega_i^\ddagger$ is the zero point energy of the activated complex, ω_i^\ddagger being the i th vibrational frequency, and n is defined as

$$n = s^\ddagger + 1/2 r^\ddagger$$

The quantity a^\ddagger depends weakly on the ratio E^\ddagger/E^\ddagger_z and approaches unity as E^\ddagger becomes very large.^{4a} As a first approximation, then, we shall treat a^\ddagger as a constant.

The denominator in eq 2b is the normalization constant D . With $\sum P(E^\ddagger_{\text{vr}})$ written as in 3 and setting $x = E^\ddagger/E^\ddagger_z$, and $b = E^\ddagger_z/RT$, a further change of variable $y = (x + a^\ddagger)b$ leads to

$$D = C_1 (RT)^{n+1} e^\phi \int_\phi^\infty y^n e^{-y} dy \quad (4)$$

where $\phi = ba^\ddagger$.

The total energy of the reacting species is $E = E_0 + E^\ddagger$, thus with eq 2 to 4 in 1, and upon the change of variable indicated above, we obtain

$$\begin{aligned} \langle E^{\infty}_{\text{th}} \rangle_t &= \frac{C_1}{D} \int_{E^\ddagger=0}^{\infty} (E_0 + E^\ddagger) (E^\ddagger + a^\ddagger E^\ddagger_z)^n e^{-E^\ddagger/RT} dE^\ddagger \\ &= RT \frac{\int_\phi^\infty y^{n+1} e^{-y} dy}{\int_\phi^\infty y^n e^{-y} dy} + E_0 - a^\ddagger E^\ddagger_z \end{aligned} \quad (5)$$

The evaluation of the integrals in eq 5 is straightforward by successive integration by parts and we obtain

$$\langle E^{\infty}_{\text{th}} \rangle_t = E_0 + (n+1)(1+\theta)RT - a^\ddagger E^\ddagger_z \quad (6)$$

where for integer values of n ($r^\ddagger = \text{even}$)

$$\theta = \phi^{n+1}/(n+1)! \sum_{j=0}^n [\phi^{n-j}/(n-j)!] \quad (7)$$

In the case when n is half-integer ($r^\ddagger = \text{odd}$) we have

$$\theta' = \phi^{n+1}/\Gamma(n+2) \times \left\{ \sum_{j=0}^{n-1/2} [\phi^{n-j}/\Gamma(n-j+1)] + e^\phi [1 - \text{erf}(\phi^{1/2})] \right\} \quad (8)$$

where to a good approximation we may neglect the last term

$$e^\phi [1 - \text{erf}(\phi^{1/2})] \simeq (\pi\phi)^{-1/2}$$

relative to the sum in the denominator of eq 8 even for small molecules at elevated temperatures.

The average energy above the critical threshold which is also the nonfixed energy of the activated complex in the high pressure limit is

$$\langle E^\ddagger \rangle = (n+1)(1+\theta)RT - a^\ddagger E^\ddagger_z \quad (9)$$

and the number of "effective oscillators" may be identified with

$$s = (\langle E^{\infty}_{\text{th}} \rangle_t - E_0)/RT \quad (10a)$$

$$= (n+1)(1+\theta) - \phi \quad (10b)$$

As a first approximation we can take $a^\ddagger = 1$ and thus $\phi = E^\ddagger_z/RT$ to evaluate $\langle E^\ddagger \rangle_{a^\ddagger=1}$ and x_1 . This corresponds to the semiclassical approximation. With this value of x_1 we evaluate a^\ddagger from its definition,^{4a} eq 11, to find a new value of ϕ and hence of $\langle E^\ddagger \rangle$,

$$a^\ddagger = 1 - \beta^\ddagger w(x) \quad (11)$$

where $w(x)$ has been tabulated^{4a} and

$$\beta^\ddagger = [(s^\ddagger - 1)(s^\ddagger + 1/2 r^\ddagger)/s^\ddagger] \sum \omega_i^\ddagger / (\sum \omega_i^\ddagger)^2 \quad (12)$$

In practice it is found that 2 or 3 iterations suffice to achieve convergence.

Equation 6 shows that the RRKM average energy of

(5) For a definition of active and adiabatic degrees of freedom and other nomenclature ref 1 and 3c should be consulted.

(6) $C_1 = Z^\ddagger_{\text{R}}/(RT)^{1/\sigma^\ddagger} \Gamma(s^\ddagger + 1 + 1/2 r^\ddagger) \Pi \omega_i^\ddagger$, where Z^\ddagger_{R} is the partition function for the active rotational degrees of freedom of the activated complex. Although it appears that $C_1 \propto T^{-1/\sigma^\ddagger}$, a factor of T^{1/σ^\ddagger} is normally contained in Z^\ddagger_{R} and hence C_1 is temperature independent. In eq 2b the constants C_1 will cancel out.

reacting molecules, and hence the number of "effective oscillators," s , (eq 10b), is a function of (1) the total number of active degrees of freedom of the activated complex, which includes all vibrations and internal rotations, (2) the magnitude of the fundamental vibrational frequencies, and (3) the temperature. In this connection some limiting cases are of interest here. At sufficiently high temperature ϕ will become very small and θ will become negligible ($\lim_{T \rightarrow \infty} \theta = 0$), thus eq 6 reduces to

$$\langle E^{\circ}_{\text{th}} \rangle_t = E_0 + (n + 1)RT - a^\dagger E^\ddagger \quad (13)$$

and at temperatures so high that $(n + 1)RT \gg a^\dagger E^\ddagger$,

$$\langle E^{\circ}_{\text{th}} \rangle_t \cong E_0 + (n + 1)RT \quad (14)$$

which is the classical limit.⁷ At very low temperature ϕ becomes very large and the first term in the summation in eq 7 or 8 will predominate over all others. Thus in the limit of very low T

$$\lim_{T \rightarrow 0} \theta = \phi / (n + 1) \gg 1 \quad (15)$$

and substitution in eq 9 leads to $E^\ddagger = 0$, as it should.

$\langle E^{\circ}_{\text{th}} \rangle_t$ in terms of k^∞ . An alternate procedure in deriving the average energy of reacting molecules is provided in the case when the experimental high-pressure limiting-rate constant is known as a function of temperature.

From the definition^{1,3} of $k(E)$ and $K(E)$ we have

$$k(E)K(E)dE = \frac{C_2}{Z^*_{\text{vr}}} \sum P(E^\ddagger) e^{-E/RT} dE \quad (16)$$

where C_2 is a constant,⁸ and $Z^*_{\text{vr}} = Z^*_{\text{v}} Z^*_{\text{r}}$ is the product of the vibrational and rotational partition functions for the active degrees of freedom of the active molecule. Noting that the denominator in eq 2a defines the high-pressure limiting-rate constant k^∞ , then by eq 16

$$k^\infty = \int_{E_0}^{\infty} k(E)K(E)dE \quad (17a)$$

$$= \frac{C_2}{Z^*_{\text{vr}}} \int_{E_0}^{\infty} \sum P(E^\ddagger) e^{-E/RT} dE \quad (17b)$$

Since k^∞ and Z^*_{vr} are functions of $\beta = 1/(RT)$ while $\sum P(E^\ddagger)$ is not, eq 17b may be rewritten

$$k^\infty(\beta) = \frac{C_2}{Z^*_{\text{vr}}(\beta)} \int_{E_0}^{\infty} \sum P(E^\ddagger) e^{-\beta E} dE \quad (18)$$

Differentiation of eq 18 with respect to β and making use of eq 17b leads to

$$\frac{dk^\infty(\beta)}{d\beta} = -k^\infty(\beta) \frac{d}{d\beta} \ln [Z^*_{\text{vr}}(\beta)] - \frac{C_2}{Z^*_{\text{vr}}(\beta)} \int_{E_0}^{\infty} E \sum P(E^\ddagger) e^{-\beta E} dE \quad (19)$$

The last term in eq 19 may be written, in view of eq 16, and eq 1 and 2a, as

$$\begin{aligned} \int_{E_0}^{\infty} E \frac{C_2}{Z^*_{\text{vr}}(\beta)} \sum P(E^\ddagger) e^{-\beta E} dE &= \int_{E_0}^{\infty} E k(E) K(E) dE \\ &= \langle E^{\circ}_{\text{th}} \rangle_t \int_{E_0}^{\infty} k(E) K(E) dE \\ &= \langle E^{\circ}_{\text{th}} \rangle_t k^\infty(\beta) \end{aligned} \quad (20)$$

Substitution of eq 20 in 19 and solving for $\langle E^{\circ}_{\text{th}} \rangle_t$ gives

$$\begin{aligned} \langle E^{\circ}_{\text{th}} \rangle_t &= - \frac{d}{d\beta} \ln [Z^*_{\text{vr}}(\beta)] - \frac{d}{d\beta} \ln k^\infty(\beta) \\ &= \frac{r}{2} RT + RT \sum_{i=1}^t (H^\circ - H^\circ_0)_i / RT - \frac{d}{d\beta} \ln k^\infty(\beta) \end{aligned} \quad (21)$$

where r is the number of active (internal) rotations and $\sum (H^\circ - H^\circ_0)_i / RT$ are the Planck-Einstein harmonic oscillator functions for the molecule. It should be emphasized that eq 21 is independent of the properties of the activated complex. In order to obtain the "effective" number of oscillators the critical energy is required. Writing k^∞ in terms of its integrated form^{3c}

$$k^\infty = \alpha \left(\frac{kT}{h} \right) \frac{Z^\ddagger_1 Z^\ddagger_{\text{R}} Z^\ddagger_{\text{V}}}{Z^*_{\text{R}} Z^*_{\text{V}}} e^{-E_0/RT} \quad (22)$$

and performing the differentiation indicated in eq 21, we obtain $\langle E^{\circ}_{\text{th}} \rangle_t$ in terms of activated complex properties

$$\begin{aligned} \langle E^{\circ}_{\text{th}} \rangle_t &= E_0 + 1/2(r^\ddagger + 2)RT + \\ &RT \sum_{i=1}^{s^\ddagger} (H^\circ - H^\circ_0)_i / RT \end{aligned} \quad (23)$$

and the value of s follows from eq 10a

$$s = 1/2(r^\ddagger + 2) + \sum_{i=1}^{s^\ddagger} (H^\circ - H^\circ_0)_i / RT \quad (24)$$

$\langle E_{\text{a11}} \rangle_K$ in Terms of $K(E)$. The third method of finding the s parameter is by fitting the average internal energy of all the molecules at the temperature in question.² We start with

$$\langle E_{\text{a11}} \rangle_K = \int_0^{\infty} EK(E)dE \quad (25)$$

where $K(E)$ is the Boltzmann distribution function for those internal degrees of freedom which are classified as active modes (vibrations and internal rotations) in the energized molecule,

(7) Although n refers to the activated complex, the factor $(n + 1)$ which is obtained in this formulation corresponds to the inclusion of the reaction coordinate. In the absence of internal rotations $(n + 1)$ is the number of vibrational degrees of freedom in the molecule, and hence eq 14 represents the classical limit.

(8) $C_2 = Z^\ddagger_1 / h Z^*_1$, where Z^\ddagger_1 and Z^*_1 are the partition functions for the adiabatic (overall) rotational degrees of freedom of the activated complex and molecule, respectively, and h is Planck's constant.

$$K(E)dE = \frac{N(E)e^{-E/RT}dE}{\int_0^\infty N(E)e^{-E/RT}dE} \quad (26)$$

and $N(E)$ is the rotation-vibration energy-level density. Since $N(E)$ is not a function of RT , then again setting $\beta = 1/(RT)$ we have

$$\begin{aligned} \int_0^\infty EN(E)e^{-E\beta}dE &= -\frac{d}{d\beta} \int_0^\infty N(E)e^{-E\beta}dE \\ &= -\frac{dZ_{vr}}{d\beta} \end{aligned} \quad (27)$$

where we have identified the denominator in eq 26 with $Z_{vr} = Z_v Z_r$, the product of the vibrational and internal rotational partition functions. Substitution of eq 26 and 27 in 25 gives

$$\begin{aligned} \langle E_{all} \rangle_K &= -\frac{d}{d\beta} [\ln Z_{vr}] \\ &= \frac{1}{2}rRT + RT \sum_{i=1}^t (H^0 - H^0_0)_i/RT \end{aligned} \quad (28)$$

where r is the number of such internal (free) rotations. The parameter s' is then simply

$$s' = \langle E_{all} \rangle_K/RT \quad (29)$$

Results and Discussion

The preceding section outlines two simple methods of computing the average internal energy of reacting molecules, $\langle E^{\text{th}} \rangle_t$; or the average nonfixed energy $\langle E^\ddagger \rangle$ of the activated complex in a system undergoing thermal unimolecular decomposition in the high-pressure limit (*i.e.*, $\langle E^\ddagger \rangle = \langle E^{\text{th}} \rangle_t$). The quantity $\langle E^\ddagger \rangle$ is of interest because it is one of the system parameters probed by investigations of reaction kinetics. Following an earlier suggestion² these average energies and the average internal energy for all molecules, $\langle E_{all} \rangle_K$, are used to evaluate a parameter s which, in certain cases, may be associated with the number of "effective oscillators" in classical reaction rate theory.

The calculations were carried out with an electronic desk calculator (Hewlett-Packard, Model 9100 A). Activated-complex models were mostly selected from the literature and are summarized in the Appendix. A comparison of the $\langle E^\ddagger \rangle$ and s values obtained from eqs 9 and 10b with the exact quantum-statistical calculations² and the classical values for methane and fluoroform is given in Table I for different temperatures. Some details of the calculations and the semiclassical approximation ($\alpha^\ddagger = 1$) are also listed. Even at the highest temperatures (2000°K for CH₄ and 1800°K for CHF₃) the classical limit greatly overestimates $\langle E^\ddagger \rangle$. The semiclassical approximation, on the other hand, yields a somewhat lower value than the exact result. A significant improvement is achieved by a single iteration. The iterative process is seen to yield a

damped oscillating, but rapidly converging value of $\langle E^\ddagger \rangle$ which lies somewhat below $\langle E^\ddagger \rangle_{\text{exact}}$. The agreement improves with increasing temperature and/or with a lowering of the frequency pattern.

In Table II the s parameters evaluated by methods 1, 2, and 3 (corresponding to eqs 10b, 24, and 29, respectively) for 13 molecules and activated complexes of varying complexity and diverse frequency patterns are compared with the corresponding Kassel fit parameters, s_K , reported in the literature at the temperatures indicated. These s_K values are denoted as F.O. if determined by fitting the fall-off curvature or L.P. if determined by fitting low-pressure data in the second-order region.⁹

Inspection of Table II shows that reasonable agreement between the three methods and the reported s_K values is obtained only in the case of small molecules. For larger molecules such as *c*-C₃H₆, *cis*-butene-2, and methylcyclopropane (MCP) all calculated s values are *much lower* than those obtained from curve fitting. At the same time the three methods of evaluation show increasing internal disparity with increasing complexity of the molecule and complex. Finally the relative difference between the various s values increases with decreasing working temperature in a particular study.

The evaluation of s by methods 1 and 2 is formally the same but differs in the computational stages. Both these methods depend on a chosen activated complex model; however, method 1 requires the explicit use of the distribution function $f(E)$ in terms of the rotation-vibration energy level sums approximation. Since both methods predict that the average energy of reacting species will steadily increase with temperature toward the limit $E_0 + (n+1)RT$, the degree of disparity between the two methods in the case of larger molecules possessing a large number of *high* frequencies appears somewhat surprising. The reason for this is not quite clear but may reside in the inaccuracy of the energy level sums approximation at lower energies.

It may, of course, be argued that the difference between the calculated s parameters and those obtained from fitting the fall-off curvature may be due, in part, to a poor choice of activated-complex models. If so, the evaluation of s and matching it roughly with s_K would provide a stringent test of the activated-complex model. At a fixed temperature the lowering of vibrational frequencies in the activated complex results in an increase in the average internal energy and hence in s . However, activated-complex models used in the present study were mostly those found to be adequate in RRKM theory interpretation of unimolecular reaction rate data.^{1,3c} For example, lowering E^\ddagger_z for MCP by 20% (Method 1) increases s by only 50%, still far short from the reported $s_K = 19$. A further lowering of

(9) E. K. Gill and K. J. Laidler, *Proc. Roy. Soc. (London)*, **A250**, 121 (1959).

Table I: Summary of Computations of $\langle E^\ddagger \rangle$ and s for CH_4 and CHF_3

T , °K	a^\dagger	θ	$\langle E^\ddagger \rangle^a$ kcal	s^b	$\langle E^\ddagger \rangle^c$ kcal	s^c	$\langle E^\ddagger \rangle_{\text{class}}^d$ kcal	t
CH₄								
600	1	1.0726	1.989	1.67				
	0.7593	0.6519	2.349	1.97				
	0.7671	0.6651	2.333	1.96				
	0.7668	0.6645	2.333	1.96	2.899	2.43	10.73	9
1000	1	0.3931	4.664	2.35				
	0.8042	0.2244	5.612	2.82				
	0.8154	0.2332	5.543	2.79				
	0.8146	0.2326	5.548	2.79	7.074	3.56	17.88	9
2000	1	0.0422	17.03	4.28				
	0.8856	0.0245	18.71	4.71				
	0.8913	0.0252	18.62	4.69				
	0.8910	0.0252	18.63	4.69	20.81	5.24	35.77	9
CHF₃								
600	1	0.2708	3.170	2.66				
	0.8446	0.1669	3.682	3.09				
	0.8527	0.1718	3.650	3.06				
	0.8524	0.1716	3.650	3.06	4.092	3.43	10.73	9
1000	1	0.0486	8.287	4.17				
	0.8976	0.0303	9.033	4.55				
	0.9021	0.0310	8.998	4.53				
	0.9019	0.0310	8.999	4.53	9.842	4.95	17.88	9
1800	1	0.00233	21.79	6.09				
	0.9445	0.00164	22.35	6.25				
	0.9455	0.00165	22.34	6.25				
	0.9452	0.00164	22.34	6.25	23.02	6.44	32.19	9

^a From eq 9. ^b From eq 10b. ^c Exact values from ref 2, activated complex models 2. ^d $\langle E^\ddagger \rangle_{\text{class}} = tRT$.

Table II: Comparison of Kassel Fit Parameter s_K with Calculated s Values^a

Reaction	E_a^∞ , kcal	T , °K	s_K	Fit	Kinetics ref	s^\dagger	r^\dagger	s eq 10b	s eq 24	s eq 29
$\text{N}_2\text{O} \rightarrow \text{N}_2 + \text{O}$	61.1	888	2 ^b	F.O.	<i>c</i>	3	0	2.53	2.53	1.60
$\text{NO}_2\text{Cl} \rightarrow \text{NO}_2 + \text{Cl}$	29.5 ^d	500	3.5	L.P.	<i>e</i>	5	0	2.44	2.89	1.82
$\text{CH}_4 \rightarrow \text{CH}_3 + \text{H}$	102 ^d	2000	6.2	F.O.	<i>f</i>	8	0	4.69	5.21	4.05
$\text{CHF}_3 \rightarrow \text{CF}_2 + \text{HF}$	69 ^d	1800	8.3	F.O.	<i>f</i>	8	0	6.25	6.48	5.53
$\text{CH}_3\text{NC} \rightarrow \text{CH}_3\text{CN}$	37.9 ^d	504	3.6 ^g	F.O.	<i>h</i>	11	0	1.94	2.59	2.07
$\text{N}_2\text{F}_4 \rightarrow 2\text{NF}_2$	19.8	400	6 ⁱ , 4 ^j	L.P.	<i>i,j</i>	10	1	4.42	6.05	3.34
$\text{N}_2\text{O}_5 \rightarrow \text{NO}_2 + \text{NO}_3$	20.9 ^d	300	10 ^k , 7 ^b	L.P.	<i>k</i>	9	6 ^l	2.31	4.45	...
$\text{C}_2\text{H}_5 \rightarrow \text{C}_2\text{H}_4 + \text{H}$	40.0	791	7	F.O.	<i>m</i>	14	1 ⁿ	3.43	5.53	...
$c\text{-C}_3\text{H}_8 \rightarrow \text{CH}_3\text{CHCH}_2$	65.0	765	12-13	F.O.	<i>o</i>	20	0	3.48	6.43	4.91
<i>cis</i> -Butene-2 \rightarrow <i>trans</i> -Butene-2	62.8	742	>24 ^{p,q}	F.O.	<i>q</i>	29	0	4.14	8.72	...
MCP \rightarrow Butenes	65.0	764	19	F.O.	<i>r</i>	29	0	5.28	10.11	8.28
$c\text{-C}_4\text{H}_8 \rightarrow 2\text{C}_2\text{H}_4$	62.5	722	~23	F.O.	<i>s</i>	29	0	4.18	8.96	...
$c\text{-C}_4\text{F}_8 \rightarrow 2\text{C}_2\text{F}_4$	74.3	838	21-26	F.O.	<i>t</i>	29	0	17.1	19.2	...

^a Decimals in last three columns have only qualitative significance. ^b Reference 9. ^c H. S. Johnston, *J. Chem. Phys.*, **19**, 663 (1951). ^d Critical energy, E_0 . ^e H. F. Cordes and H. S. Johnston, *J. Amer. Chem. Soc.*, **76**, 4264 (1954). ^f Reference 2. ^g Reference 10b. ^h Reference 10a. ⁱ Reference 17. ^j A. P. Modica and D. F. Hornig, *J. Chem. Phys.*, **49**, 629 (1968). ^k H. S. Johnston and R. L. Perrine, *J. Amer. Chem. Soc.*, **73**, 4782 (1951). ^l See Appendix, item (b). ^m J. H. Purnell and C. P. Quinn, *Proc. Roy. Soc. (London)*, **A270**, 267 (1962); C. P. Quinn, *Proc. Roy. Soc. (London)*, **A275**, 190 (1963). ⁿ See Appendix, item (i). ^o H. O. Pritchard, R. G. Sowden, and A. F. Trotman-Dickenson, *Proc. Roy. Soc. (London)*, **A217**, 563 (1953). ^p Reference 11. ^q B. S. Rabinovitch and K. W. Michel, *J. Amer. Chem. Soc.*, **81**, 5065 (1959). Fall-off behavior was interpreted in terms of Slater's parameter n ; although $n = 28$ was found formally the confidence limit was placed¹¹ at $n > 20$. The value $s_K > 24$ was estimated from the graphical relationship between n and s_K in ref 11 for $E_0/RT = 42$. ^r J. P. Chesick, *ibid.*, **82**, 3277 (1960). ^s H. O. Pritchard, R. G. Sowden, and A. F. Trotman-Dickenson, *Proc. Roy. Soc. (London)*, **A218**, 416 (1953). s_K was estimated from quoted Slater parameter $n = 20$ (ref q) using graphical interpolation.¹¹ ^t J. N. Butler, *J. Amer. Chem. Soc.*, **84**, 1393 (1962).

the frequencies would result in an unrealistic activated-complex model.

In conclusion it may be stated that while the above theoretical treatment provides a simple and useful estimate of average energies, it can hardly serve, *in general*, as a predictive method for estimating the Kassel fit parameter s_K . An exception is found in the case of very small molecules at high temperatures or molecules with a very low frequency pattern such as *c*-C₄F₈. For such molecules the classical error is usually small and s_K can be successfully estimated by the classical operation of dividing an average energy of the actual systems by RT , a quantity dictated by the classical equipartition of energy for one vibrational degree of freedom. However, the classical error is large for molecules with many high-frequency vibrational modes when the temperature is relatively low. In these cases the Kassel fit parameter s_K may still be interpreted, if one wishes, as the effective number of classical oscillators corresponding to the *hypothetical* condition when the systems are acting in a classical manner. However, the s_K parameter cannot be estimated by computing the number of classical oscillators corresponding to the average energy of *non-classical* reacting systems.

It is concluded, therefore, that for these *real* systems s_K is simply an empirical fit-parameter of doubtful theoretical value. Further, it is suggested that the unqualified use of the term "effective oscillators" may be misleading. This is corroborated further by the observation that while the calculated s values tend toward a limiting value of $(n + 1) = t$ as the temperature increases without limit, the s_K values exhibit a maximum^{2,10} and could force $s_K > t$ for large molecules.¹¹

Finally, the lack of a physical meaning of the term "effective oscillators" is further exemplified by the observation that while the original RRKM theory formulation^{3b} classified the degrees of freedom of the active molecules with respect to their role in intramolecular energy transfer as "active" or "inactive" (in addition to those terms "adiabatic"), numerous successful applications of this theory have shown that all vibrational degrees of freedom are active.^{1,3c}

Appendix

Vibrational Frequency Assignment. Activated complex frequencies for N₂O, N₂O₅, *c*-C₃H₆, *c*-C₄H₈, *cis*-butene-2, and methylcyclopropane were those used by Wieder and Marcus^{3c} in RRKM theory applications. These were grouped in multiples of the lowest frequency in each case; the number in each group is listed in parentheses.

Molecular frequencies were taken from the literature. In units of kcal the activated complex frequencies are:

(a) *Nitrous oxide*: 1.68 (2), 3.36. Molecular frequencies have been listed by Herzberg.¹²

(b) *Nitrogen pentoxide*: 2.06 (2), 2.15, 2.36, 3.00, 3.78, 4.04 (2), 4.62. The overall rotations of the ac-

tivated complex were taken to be those of a quasi-diatom molecule with masses of NO₂ and NO₃. The NO₂ and NO₃ groups in the loose complex are considered essentially free and hence possess three rotational degrees of freedom each, for a total of six internal rotations of the complex.

(c) *Cyclopropane*: 0.64 (2), 1.92 (2), 2.56 (2), 3.20 (5), 4.48 (3), 8.96 (6). A complete molecular frequency assignment is available from the work of Mathai, *et al.*,¹³ and Günthard, *et al.*¹⁴

(d) *Cyclobutane*: 0.26, 0.52 (3), 2.60 (5), 3.38 (8), 4.16 (4), 8.32 (8).

(e) *cis-Butene-2*: 0.66 (3), 1.98 (3), 2.64 (3), 3.30 (5), 3.96 (7), 8.58 (8).

(f) *Methylcyclopropane*: 1.03 (5), 2.06 (5), 3.09 (7), 4.12 (5), 8.24 (7). An approximate assignment of molecular frequencies has also been given by Wieder and Marcus.^{3c}

For methane and fluoroform the activated complex frequency patterns of ref 2, model 2, respectively, were adopted and are listed below in kcal. Molecular frequencies for methane have been summarized by Herzberg,¹² and for fluoroform by Rank, Shull, and Pace.¹⁵

(g) *Methane*: 1.46 (2), 3.29, 4.22 (2), 8.64 (3).

(h) *Fluoroform*: 1.45 (2), 1.96, 1.99, 2.57, 3.19, 3.93, 4.38.

(i) *Ethyl*: 0.86 (2), 2.20, 2.74 (3), 3.68 (2), 4.37 (2), 8.71 (4). The frequency pattern of ref 1 was adopted here. One of the rotational degrees of freedom is treated as active.

(j) *Methyl Isocyanide*. Activated complex frequencies used were those from the detailed study of this system by Schneider and Rabinovitch^{10a} for their 300 model. These are, in units of kcal: 0.77, 1.72, 2.98 (2), 4.13 (3), 5.69, 8.57 (3). Molecular frequencies have been reported by Pillai and Cleveland.¹⁶

(k) *Tetrafluorohydrazine*. The activated complex was assumed to be planar and the torsional vibration about the N-N bond was allowed to become a free rotation.^{17a} Vibrational frequencies of the complex were those suggested by Brown:^{17b} 0.21 (4), 1.43, 1.72, 2.66 (2), 313 (2) kcal. The assignment for the molecule has been given by Durig and Lord.¹⁸

(10) (a) F. W. Schneider and B. S. Rabinovitch, *J. Amer. Chem. Soc.*, **84**, 4215 (1962); (b) *ibid.*, **85**, 2365 (1963).

(11) E. W. Schlag, B. S. Rabinovitch, and F. W. Schneider, *J. Chem. Phys.*, **32**, 1599 (1960).

(12) G. Herzberg, "Infrared and Raman Spectra," D. Van Nostrand Co., New York, N. Y., 1960.

(13) P. M. Mathai, G. G. Shepherd, and H. L. Welsh, *Can. J. Phys.*, **34**, 1448 (1956).

(14) Hs. H. Günthard, R. C. Lord, and T. K. McCubbin, Jr., *J. Chem. Phys.*, **25**, 768 (1956).

(15) D. H. Rank, E. R. Shull, and E. L. Pace, *ibid.*, **18**, 885 (1950).

(16) M. E. K. Pillai and F. F. Cleveland, *J. Mol. Spectrosc.*, **5**, 212 (1960).

(17) (a) L. M. Brown and B. de B. Darwent, *J. Chem. Phys.*, **42**, 2158 (1965); (b) L. M. Brown, Ph.D. Thesis, The Catholic University of America, 1964, University Microfilms, Ann Arbor, Mich.

(l) *Nitryl chloride*. The N-Cl stretching frequency in NO_2Cl was assigned to the reaction coordinate in the activated complex. Three of the frequencies were assigned values intermediate between those in the NO_2Cl molecule¹⁹ and NO_2 .¹² The in- and out-of-plane Cl bending frequencies were arbitrarily lowered to one-half their value in the molecule. The assignment of the complex was thus: 0.53, 0.59, 2.21, 3.74, 4.72 kcal.

(m) *Perfluorocyclobutane*. The ring-stretching vibration was taken as the reaction coordinate. Eleven of

the bending and deformation modes were arbitrarily lowered by 50% from those in the $c\text{-C}_4\text{F}_8$ molecule.²⁰ The resulting activated complex assignment used was: 0.12, 0.27, 0.37 (2), 0.41 (2), 0.49 (2), 0.51, 0.63 (2), 0.71, 0.78 (2), 0.81 (2), 0.87, 0.94, 1.07, 2.75 (2), 2.88, 3.50 (2), 3.67, 3.83 (2), 4.02 (2) kcal.

(18) J. R. Durig and R. C. Lord, *Spectrochim. Acta*, **19**, 1877 (1963).

(19) R. Ryason and M. K. Wilson, *J. Chem. Phys.*, **22**, 2000 (1954).

(20) H. H. Claassen, *ibid.*, **18**, 543 (1950).

A Nuclear Magnetic Resonance Study of the Effect of Charge on Solvent Orientation of a Series of Chromium(III) Complexes¹

by Lawrence S. Frankel²

Department of Chemistry, University of Massachusetts, Amherst, Massachusetts 01002 (Received April 23, 1969)

Relative proton spin-spin relaxation times of N,N-dimethylformamide, N,N-dimethylacetamide and methanol in the solvation shell (second coordination sphere) of a variety of paramagnetic Cr(III) compounds have been obtained. The orientation of the ligands in the second coordination sphere may be flipped end to end depending on the charge of the solute. An ion dipole model is examined to explain the results. For ± 3 charged solutes the ligands in the second coordination sphere are essentially completely oriented along the ligand dipole-moment vector. For solutes of lower charge the orientation is not complete. The effect of temperature is reported.

Introduction

Relatively little is known about the chemistry of the first solvation shell (second coordination sphere) of transition metal complexes. Neutral molecules in the second coordination sphere generally interact weakly with the solute. Consequently, these interactions usually do not bring about an observable change in the electronic spectrum of the solute. The effect of the solute on a property of the solvent is often small and generally open to various interpretations.

The direct study of second sphere preferential solvation^{3,4} and its kinetic significance^{5,6} has recently been reported. The primary objective of this report is to examine the effect of charge on the average orientation of solvent in the second coordination sphere of a series of nonlabile Cr(III) compounds. Basically the experiment undertaken requires a solvent which contains two or more nonequivalent protons and a subsequent comparison of the spin-spin relaxation times which result upon the addition of a nonlabile paramagnetic Cr(III) complex. Matwiyoff⁷ has used this approach to study the orientation of N,N-dimethylformamide (DMF) in

the primary coordination sphere of $\text{Co}(\text{DMF})_6^{2+}$. Luz and Meiboom in a study of $\text{M}(\text{CH}_3\text{OH})_6^{2+}$ ($\text{M} = \text{Co}, \text{Ni}$) in methanol note that when the primary-sphere ligands do not exchange, the methanol molecules in the second coordination sphere have a preferred orientation.⁸ In this study DMF, N,N-dimethylacetamide (DMA) and methanol were employed as second-sphere ligands.

(1) We gratefully acknowledge the support of the Directorate of Chemical Science, Air Force Office of Scientific Research under grant AFOSR 212-65.

(2) Rohm and Haas Company Research Laboratory 13, 5000 Richmond Street, Philadelphia, Pa. 19137.

(3) L. S. Frankel, T. R. Stengle, and C. H. Langford, *Chem. Commun.*, 393 (1965).

(4) L. S. Frankel, T. R. Stengle, and C. H. Langford, Paper No. 222, Division of Physical Chemistry, 156th National Meeting, American Chemical Society, Atlantic City, N. J., Sept 1968.

(5) C. H. Langford and J. F. White, *Can. J. Chem.*, **47**, 3049 (1967).

(6) S. Behrendt, C. H. Langford, and L. S. Frankel, *J. Amer. Chem. Soc.*, **91**, 2236 (1969).

(7) N. A. Matwiyoff, *Inorg. Chem.*, **5**, 788 (1966).

(8) Z. Luz and S. Meiboom, *J. Chem. Phys.*, **40**, 2686 (1964).

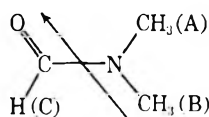


Figure 1. System of labeling employed for amides. The approximate dipole moment vector is indicated by the arrow.

Experimental Section

Spectra were obtained on a Varian A-60 spectrometer equipped with commercially available temperature accessories. The concentration of the solute was adjusted ($\approx 1 \times 10^{-2} M$) to obtain the best balance between overlapped peaks, $\text{CH}_3(\text{A})$ and $\text{CH}_3(\text{B})$ (Figure 1), and significant relaxation-time changes. No time effects were observed in the time required to obtain three repetitive slow-scan spectra with the lone exception of $\text{Cr}(\text{H}_2\text{O})_6^{3+}$ in DMA and DMF where small changes are observed. For these systems spectra were obtained as rapidly as possible. The ratio of the relaxation times is generally good to $\pm 10\%$.

Reagent grade DMF was obtained from Eastman and purified as previously described.⁹ The pmr spectrum of DMA obtained from E. I. duPont, taken at an amplitude setting at which the ^{13}C splittings are observed, did not reveal any impurities; the DMA was used without purification. Reagent grade methanol obtained from Baker and Adamson was used without further purification.

$\text{K}_3[\text{Cr}(\text{ox})_3] \cdot 3\text{H}_2\text{O}$ (ox = oxalate),¹⁰ *cis*- $[\text{Cr}(\text{en})_2\text{Cl}_2]\text{Cl}$ (en = ethylenediamine),¹¹ $\text{Cr}(\text{acac})_3$ (acac = acetylacetonate)¹² and $\text{Cr}(\text{acacNO}_2)_3$ ¹³ were prepared and purified as previously described. $\text{K}_3[\text{Cr}(\text{NCS})_6]$ was obtained from Alfa Inorganics and recrystallized from ethanol. Reagent grade $\text{NH}_4[\text{Cr}(\text{NH}_3)_2(\text{NCS})_4]$ and $\text{NH}_4[\text{Cr}(\text{an})_2(\text{NCS})_4]$ (an = aniline) were obtained from Fisher Scientific Co. $\text{Cr}(\text{en})_3(\text{ClO}_4)_3 \cdot 2\text{H}_2\text{O}$ was a gift of Mr. J. Votano.

Nuclear Magnetic Resonance Theory

Under rapid exchange conditions, the observed spin-spin relaxation time T_2 , is given by

$$1/T_2 = P_s/T_{2s} + P_b/T_{2b} \quad (1)$$

where P_s is the probability that a solvent molecule is in environment s , T_{2s} is the relaxation time in environment s and P_b and T_{2b} refer to the same quantities in environment b .¹⁴ In the proposed experiment environment s refers to the second coordination sphere and b to the bulk solution. The relaxation time T_{2b} is simply the relaxation time in a solution free of paramagnetic solute. For reasonably dilute solutions P_b is near unity, therefore $\pi(\Delta\nu - \Delta\nu_b) = P_s/T_{2s}$, where $\Delta\nu$ is the line width at half height and is related to the relaxation time by the equation $\pi\Delta\nu = 1/T_2$.

Equation 1 is valid if the rate of exchange of the ligands between the second coordination sphere and

the bulk solution is large compared with (1) the reciprocal of the difference of the Larmor frequencies, $\Delta\omega$, for the two environments and (2) the relaxation rate of the solvent molecules in environment s . In this experiment $1/T_{2s} \approx 10^4$ while $\Delta\omega \approx 0$. The exchange rate is probably exceedingly rapid, so that the limiting conditions which leads to eq 1 are easily satisfied.

Both nuclear magnetic dipole electron magnetic dipole^{15,16} and contact¹⁷ mechanisms lead to relaxation. In this experiment the contact term may be neglected. This simplification is justified by the experimental observation that the contact shift equals zero. The dipolar contribution is given by

$$\frac{1}{T_{2s}} = \frac{C}{r^{-6}} \left[7\tau_c + \frac{13\tau_c}{1 + \omega_s^2\tau_c^2} \right] \quad (2)$$

where C is a constant; τ_c , is the dipolar correlation time and ω_s , is the electron precessional frequency. If the relaxation times of two nuclei of the same molecule are compared, and it can be shown that τ_c is the same for both protons then

$$\Delta\nu_1/\Delta\nu_2 = r_2^{-6}/r_1^{-6}$$

where the subscripts refer to the two protons of the same molecule. Thus the orientation of the second-sphere ligands relative to the paramagnetic complex is obtained.

In the preceding discussion it has been assumed that $1/T_{2s}$ is entirely due to one labile sphere of molecules. Actually $1/T_{2s}$ contains a contribution from the next sphere of solvent molecules. Since the number of solvent molecules increases by a geometric factor ($4\pi r^2$) the observed distance dependence may be less than r^{-6} .⁸

Results and Discussion

The solutes in the solvents in question are assumed to be in the form indicated in Table I in solution. From the limited data available ion association with resulting charge neutralization seems to be in general small for these solvents.^{18,19} However, ion association constants

(9) D. W. Meek, R. S. Drago, and T. S. Piper, *Inorg. Chem.*, **1**, 285 (1962).

(10) D. M. Yost, *Inorg. Syn.*, **1**, 37 (1939).

(11) C. L. Rollinson and J. C. Bailar, Jr., *ibid.*, **2**, 200 (1946).

(12) B. E. Bryant and W. C. Fernelius, *ibid.*, **5**, 188 (1953).

(13) J. P. Collman, R. L. Marshall, W. L. Young, and S. D. Golby, *Inorg. Chem.*, **1**, 704 (1962).

(14) T. J. Swift and R. E. Connick, *J. Chem. Phys.*, **37**, 307 (1962).

(15) I. Solomon, *Phys. Rev.*, **99**, 559 (1955).

(16) N. Bloembergen and L. O. Morgan, *J. Chem. Phys.*, **34**, 842 (1961).

(17) N. Bloembergen, *ibid.*, **27**, 572 (1957).

(18) P. G. Sears, E. D. Wilhoit, and L. R. Dawson, *J. Phys. Chem.*, **59**, 373 (1955).

(19) G. R. Lester, T. A. Gover, and P. G. Sears, *ibid.*, **60**, 1076 (1956).

Table I: The Relative Second Coordination Sphere Line Widths of DMA, DMF, and Methanol as a Function of Paramagnetic Solute

Solute	DMA		DMF		Methanol OH/CH ₃
	(C)/(B)	(A)/(B)	(C)/(B)	(A)/(B)	
Cr(H ₂ O) ₆ ³⁺	2.80	1.50	3.75	1.30	
Cr(en) ₃ ³⁺	1.90	1.60	2.75	1.60	
Ni(CH ₃ OH) ₆ ²⁺					1.65 ^c
Co(CH ₃ OH) ₆ ²⁺					1.55 ^c
<i>cis</i> -Cr(en) ₂ Cl ₂ ¹⁺	1.20	1.10	1.50	1.00	
Cr(acac) ₃	1.05	1.35	0.90	0.80	2.40
Cr(acacNO ₂) ₃	1.00	0.90	1.00	1.00	
Cr(NCS) ₄ (an) ₂ ¹⁻	0.85	0.80	1.20	0.70	
Cr(NCS) ₄ (NH ₃) ₂ ¹⁻	0.85	0.80	1.35	0.90	1.40
Cr(ox) ₃ ³⁻	0.50 ^a	0.50 ^a	0.55 ^b	0.55 ^b	
Cr(NCS) ₆ ³⁻	0.28	0.30	0.35	0.50	1.25

^a Aqueous DMA mixed solvent, mol fraction DMA varied from 0.04 to 0.39. ^b Aqueous DMF mixed solvent, mol fraction DMF 0.32. ^c Data of Luz and Meiboom, ref 8.

are generally determined in the concentration range 1×10^{-4} – 5×10^{-3} M. Our experiments require a concentration of 1×10^{-2} M and it is therefore difficult to assess the degree of ion association. The results of Fuoss commonly used to estimate ion association constants (K_A)²⁰ give $K_A \approx 10$ l. mol⁻¹ in 1:1 electrolytes. The data of Miller and Watts²⁰ suggest that an exception to the above is *cis*-[Cr(en)₂Cl₂]Cl in which a specific chemical interaction gives rise to unusually large values for K_A in the solvents under consideration. For higher charged electrolytes the degree of ion association is obviously larger and further complicated by more than one equilibria. The relatively high concentrations required in our experiment is an admitted shortcoming.

The nmr spectra of DMF and DMA at room temperature where rotation around the C–N bond is slow²¹ consist of three peaks. Based on long-range coupling constants,²² contact shifts²³ and relaxation times⁷ the high field methyl peak has been assigned to CH₃(A). The CH₃(B) resonance is 0.17 ppm downfield and the formyl peak approximately 5.08 ppm still further downfield (Figure 1). For DMA CH₃(C) is the high field peak and CH₃(A) and CH₃(B) are in the same relative order as in DMF. Under high resolution DMF shows long range coupling, $J_{\text{CH}_3(\text{A}),\text{H}(\text{C})} = 0.7$ cps and $J_{\text{CH}_3(\text{B}),\text{H}(\text{C})} = 0.3$ cps. The full line width of the doublets for each methyl group were measured and subsequently remeasured upon the addition of paramagnetic solute. The resulting difference was taken as the quantity of interest. DMA is somewhat better suited for this study since no long range coupling is resolved although line width results suggest some very small long range coupling between CH₃(A) and CH₃(C).

A value of 3.82 D has been reported for the dipole moment of DMF.²⁴ From bond moment vector addition²⁵ we estimate that the direction of the dipole-moment vector deviates from that of the C=O group by

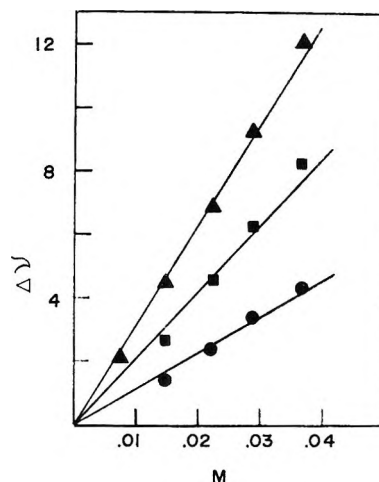


Figure 2. The concentration dependence of the proton line widths of DMF in Cr(en)₃³⁺: ▲, H(C); ■, CH₃(A); ●, CH₃(B).

only a few degrees and is so indicated in Figure 1 (not drawn to scale). If second-sphere orientation effects are primarily governed by an ion-dipole interaction a paramagnetic cation will orient the ligand so that the oxygen atom of the solvent is closest to the paramagnetic center. The three proton peaks of the ligand would then show the following line-width relation $\Delta\nu(\text{C}) > \Delta\nu(\text{A}) > \Delta\nu(\text{B})$. A paramagnetic anion would completely reverse the above order. The results are summarized

(20) W. A. Miller and D. W. Watts, *J. Amer. Chem. Soc.*, **89**, 6858 (1967).

(21) L. H. Piette, J. D. Ray, and R. A. Ogg, *J. Mol. Spectrosc.*, **2**, 66 (1958).

(22) J. V. Hatton and R. E. Richards, *Mol. Phys.*, **3**, 253 (1960).

(23) B. B. Wayland, R. S. Drago, and H. F. Henneke, *J. Amer. Chem. Soc.*, **88**, 2455 (1966).

(24) M. H. Hutchinson and L. E. Sutton, *J. Chem. Soc.*, 4382 (1958).

(25) C. P. Smyth, "Dielectric Behavior and Structure," McGraw-Hill Book Co., Inc., New York, N. Y., 1955, pp 31, 244–6.

in Table I. Satisfactory linear results of a concentration study for $\text{Cr}(\text{en})_3^{3+}$ in DMF are shown in Figure 2.

Two extreme ligand orientations are considered (X,Y). These orientations correspond to the negative and positive end of the dipole-moment vector of the solvent. Based on an ion-dipole model the ratio of the populations of the two extreme orientations is given by

$$K = N(\text{X})/N(\text{Y}) = e^{-unq/a^2RT} \quad (3)$$

where u is the dipole moment of the ligand, nq the charge of the paramagnetic solute and a the distance from the paramagnetic solute to the center of the ligand dipole moment. Assuming any reasonable value for a , substitution into eq 3 leads to the conclusion that if $n \neq 0$ every molecule should be completely oriented along X or Y. In the above calculation we have substituted the formal charge of the paramagnetic ion. Actually the presence of the primary coordination sphere will cause a reduced effective charge for the ligands in the second coordination sphere.

A fundamental question which is considered is whether all the ligands in the second coordination sphere are completely oriented by the paramagnetic solute for any of the systems in Table I. To answer this question the distance from the center of the paramagnetic solute to two protons in the second coordination sphere must be estimated. We restrict attention to H(C) and CH₃(B) since they are at opposite extremes of the dipole moment and consider the most favorable cases $\text{Cr}(\text{H}_2\text{O})_6^{3+}$ and $\text{Cr}(\text{NCS})_6^{3-}$. The complex-ion radius was estimated as described by Morgan, *et al.*,²⁶ $\text{Cr}(\text{H}_2\text{O})_6^{3+} = 3.3 \text{ \AA}$, $\text{Cr}(\text{NCS})_6^{3-} = 4.9 \text{ \AA}$. The molecular bond distances and angles for DMF were taken from the data summarized by Matwiyoff.⁷ For this calculation the dipole-moment vector of DMF was assumed to be colinear with the carbonyl group. The distance r was calculated as the sum of the complex-ion radius plus a weak hydrogen bond 2.0 Å plus the intramolecular bond distance effects which were subject to the constraint of dipole orientation. Evaluating the sixth-power dependence gives for $\text{Cr}(\text{H}_2\text{O})_6^{3+}$ $\Delta\nu(\text{C})/\Delta\nu(\text{B}) = 4.0$ and $\text{Cr}(\text{NCS})_6^{3-}$ $\Delta\nu(\text{C})/\Delta\nu(\text{B}) = 0.28$ in reasonable agreement with the results in Table I. Similar quantities for DMA give 2.5 and 0.35. An error of $\pm 0.2 \text{ \AA}$ in r leads to an uncertainty of approximately 5% in the line-width ratios. Considering the crudeness of the distance approximations, the exact numerical results should not be taken too literally. These calculations support the contention that for ± 3 charged solutes the average orientation occurs along the dipole-moment vector. The decrease in ratios for $\text{Cr}(\text{en})_3^{3+}$ is probably due to the increasing complex-ion radius. The data in Table I suggest that only for ± 3 charged solutes is the orientation essentially complete. This conclusion is not in agreement with the predictions of an ion-dipole model.

The average relative orientation of the C and B protons in DMF and DMA in the second coordination sphere of -1 solutes is reversed. The cause of this reversal is not immediately apparent and is in obvious disagreement with an ion-dipole model.

Some combination of at least four different types of chemical interactions may tend to offset the electrostatic effect. These are (1) solvent structure, second-sphere bulk solution interactions; (2) steric effects and solvent close-packing around the complex; (3) first-sphere ligand second-sphere ligand interaction; (4) intramolecular electronic effects, acidic protons. Solvent structure (1) is not thought to be a dominant effect since the solvent can be flipped end to end and for $n = 0$ only small orientation effects are observed.

For $\text{Cr}(\text{H}_2\text{O})_6^{3+}$ in DMF and DMA a specific interaction between the first-sphere ligand and the second-sphere ligand (hydrogen bonding between water and the C=O solvent group) would produce a similar orientation to an ion-dipole interaction. Therefore, we can not unambiguously attribute the origin of the orientation. The results for $\text{Cr}(\text{NCS})_6^{3+}$ do not present this difficulty.

The results for methanol are summarized in Table I. Relative to the methyl protons the hydroxy proton is preferentially aligned with the solute independent of the charge of the solute. This is diagnostic of an important solvent structure effect. Since methanol is a well-ordered strongly interacting liquid, this type of effect would not be surprising. However, one would expect the exact opposite results with the methyl group closer to the paramagnetic solute since the solvent interaction is primarily between the hydroxy groups. We believe the methanol results are explained by the fact that in both orientations of the dipole the hydroxy proton is closer to the solute than the methyl group protons. The data for $\text{Cr}(\text{acac})_3$ has been shown to correspond to a specific hydrogen bond interaction with the acac ring.^{27,28}

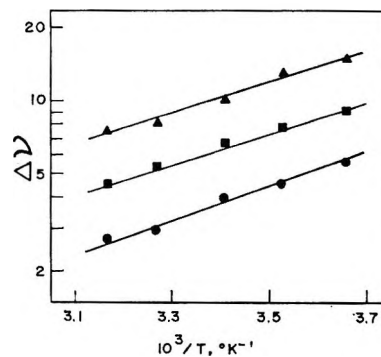


Figure 3. The temperature dependence of the proton line widths of DMF in $\text{Cr}(\text{en})_3^{3+}$: \blacktriangle , H(C); \blacksquare , CH(A); \bullet , CH(B). The salt concentration is $2.8 \times 10^{-2} M$.

(26) L. O. Morgan, A. W. Nolle, R. L. Hull, and J. Murphy, *J. Chem. Phys.*, 25, 206 (1956).

The effect of temperature on the proton relaxation times of DMF containing $\text{Cr}(\text{en})_3^{3+}$ is given in Figure 3. Within experimental error all three proton resonances give the same activation energy, 2.8 kcal. The value of the activation energy is typical of rapid exchange conditions for $\text{Cr}(\text{III})$.^{8,16,29} The fact that the same activation energy is obtained for all protons indicates that the correlation time can be neglected when considering relative relaxation times. DMA was studied at temperature extremes to see if a thermal effect could be detected. The solute was $\text{Cr}(\text{en})_3^{3+}$. The relative line widths at -20° were identical to those reported in Table I. At 118° the barrier to internal rotation about the C-N bond is no longer observed and the methyl groups are equivalent. Under these conditions $\Delta\nu(\text{C})/\Delta\nu(\text{A} = \text{B}) = 1.40$. This value is comparable to the appropriately weighted room temperature results. The ion-dipole model predicts no thermal effects since $unq/a^2 \gg RT$ over the temperature range reported.

The effect of varying amounts of water to DMA was studied in the presence of $\text{Cr}(\text{NCS})_4(\text{NH}_3)_2^{1-}$. The mol fraction of DMA was varied from 1.00 to 0.11. Considering the mole fraction range the second coordination sphere probably consists of a mixed solvation shell and depends on the composition of the bulk solution.⁴ Only small effects which are close to experimental error ($\pm 10\%$) are observed. This suggests that steric effects and solvent close packing are not dominant in this case. In general it would not be surprising to find cases where this effect could be large.

Acknowledgment. We gratefully acknowledge the help of Warren Muir.

(27) L. S. Frankel, Ph.D. Thesis, University of Massachusetts, Amherst, Mass., 1966.

(28) T. S. Davis and J. P. Fackler, Jr., *Inorg. Chem.*, **5**, 242 (1966).

(29) T. R. Stengle and C. H. Langford, *J. Phys. Chem.*, **69**, 3299 (1965).

Electron Paramagnetic Resonance Study of the Anion Radical of Phenyl Methyl Sulfone and of 4-Nitrophenyl Methyl Sulfone

by Sr. Elizabeth Keller, C. S. J., and Robert G. Hayes

Department of Chemistry, University of Notre Dame, Notre Dame, Indiana 46556 (Received April 24, 1969)

The anion radicals of phenyl methyl sulfone and 4-nitrophenyl methyl sulfone have been prepared by electrolytic reduction in liquid ammonia and acetonitrile, respectively. The proton and nitrogen coupling constants have been measured and compared with the predictions of semiempirical theories. We find that our data may be rationalized using a single d orbital, symmetrical across the O-S-O plane, to describe the conjugation of the sulfone group. Other orbitals of the sulfone are permitted to interact owing to the low symmetry of the compounds we have studied, but their effect is not measurable.

The radical anions of a number of sulfones have been studied by epr spectroscopy. These have included the anions of thioxanthane dioxide,¹ thianthrene tetroxide,² dibenzothiophene dioxide,³ and diphenyl sulfone.⁴ The spectra have been used to decide how much the sulfone group engages in conjugation.

In an early study of conjugation involving sulfur, Koch and Moffitt⁵ pointed out that the sulfone group could conjugate with p orbitals on its substituents both when the p orbital is oriented with its axis parallel to the O-O direction, as in planar sulfones, and when the axis of the p orbital lies in the plane containing S and normal to the O-O direction. These were called case I conjugation and case II conjugation, respectively.

Koch and Moffitt pointed out that the sulfone grouping presented two types of orbitals for either case I or case II conjugation. One type is symmetrical across the OSO plane and consists of an empty d orbital. The other type is antisymmetric across the OSO plane and consists of a filled orbital which forms part of the sul-

(1) G. Vincow, *J. Chem. Phys.*, **37**, 2484 (1962).

(2) E. T. Kaiser and D. H. Eargle, *ibid.*, **39**, 1353 (1963).

(3) D. H. Eargle, Jr., and E. T. Kaiser, *Proc. Chem. Soc.*, **22** (1964).

(4) R. Gerdil and E. A. C. Lucken, *Mol. Phys.*, **9**, 629 (1965). A recent review of work on this and other sulfones appears in "Radical Ions," L. Kevan and E. T. Kaiser, Ed., Interscience, New York, N. Y., 1968, p 301.

(5) H. P. Koch and W. E. Moffitt, *Trans. Faraday Soc.*, **47**, 7 (1951).

fur-oxygen π system. The studies of sulfones which have been reported so far have provided information about the symmetrical type of interaction, involving d orbitals, because in all cases the orbital bearing the unpaired electron has been symmetrical. The anions we have studied, those of phenyl methyl sulfone and 4-nitrophenyl methyl sulfone, have no symmetry across the OSO plane, so the orbital containing the unpaired electron may contain contributions from both types of conjugation.

Results

The spectra of the anion radicals of phenyl methyl sulfone and 4-nitrophenyl methyl sulfone are simple, and it is not very difficult to assign coupling constants to them. The coupling constants of the phenyl methyl sulfone radical anion appear in Table I. This ion was observed in liquid NH_3 using electrolysis to generate the ion. The lines were broad. Peak-to-peak derivative line widths were about 1 G.

Table I: Coupling Constants of Phenyl Methyl Sulfone Anion

Position	A_H , G
Methyl	1.96
2	3.84
3	<0.9
4	8.96

The only ambiguity in the assignment of the coupling constants to positions in Table I is in the assignment of the 3.84-G coupling constant. We have assigned it to the *ortho* position because the *para* coupling constant is large.

Table II displays the coupling constants of 4-nitrophenyl methyl sulfone anion. This ion was prepared by electrolysis in acetonitrile. The lines were about 0.2 G wide.

Table II: Coupling Constants of 4-Nitrophenyl Methyl Sulfone Anion

Position	$A_{(HN)}$, G
Methyl	0.78
2	<0.24
3	3.81
Nitrogen	7.84

Once again, one coupling constant has to be assigned by assumption. We have assigned the 3.81-G coupling to position 3 by analogy with nitrobenzene radical anion. Both this assumption and the assumption made in the assignment of the coupling constants of phenyl methyl sulfone are consistent with the spin densities calculated using any reasonable set of parameters.

Experimental Section

Phenyl methyl sulfide was purchased from Aldrich Chemical Co. *p*-Nitrophenyl methyl sulfide was prepared using the technique of Truce and coworkers.⁶

The sulfides were oxidized to sulfones in glacial acetic acid, using 30% hydrogen peroxide. The sulfones were recrystallized from ethanol-water mixtures until sharp melting points were obtained.

Reductions in liquid NH_3 were carried out in a cell like the cell described by Levy and Myers.⁷ Tetramethylammonium iodide was used as a supporting electrolyte. Reductions in acetonitrile were carried out in a Varian aqueous solution cell using a mercury pool cathode and a modified calomel electrode as second washing electrode. Tetramethylammonium perchlorate was the electrolyte.

Spectra were recorded using a Varian V-4500-13 spectrometer equipped with Fieldial.

Discussion

There is no compound which one can use for comparison to provide direct evidence of the presence or absence of effects due to the lack of symmetry in phenyl methyl sulfone. That is, there is no anion which should have exactly the same π -electronic structure if there were no involvement of orbitals antisymmetric across the OSO plane in conjugation. The best one can do is compare the distribution of unpaired electron in the anion of phenyl methyl sulfone with the distribution which is calculated, using some approximate theory, with parameters which give a good fit for the anions of other sulfones. Gerdil and Lucken⁴ were able to obtain good agreement between calculated coupling constants, and their observations on the anion of diphenyl sulfone by using the parameters $\alpha_s = \alpha_0 - 2\beta_0$, $\beta_{sc} = 0.8\beta_0$ to describe the sulfone group. They had to use McLachlan's⁸ treatment, which includes interelectronic repulsion in an approximate way, though, to get good results.

Table III compares the experimental results on the anions of phenyl methyl sulfone and *p*-nitrophenyl methyl sulfone with calculated spin densities, using Gerdil and Luckens parameters. It also shows the agreement between calculations and experiment for the anion of diphenyl sulfone. The coupling constants were assumed to be proportional to spin densities. No dependence on charge was assumed. The constants of proportionality used were 25 G for the proton couplings and 35 G for the nitrogen coupling. Bonding parameters for the nitro group were taken from the work of Rieger and Fraenkel.⁹ The ring positions are in all cases numbered from the sulfone grouping, so the positions *ortho* to sulfone is 2.

(6) W. E. Truce, D. P. Tate, and D. N. Burdge, *J. Amer. Chem. Soc.*, **82**, 2872 (1960).

(7) R. J. Myers and D. H. Levy, *J. Chem. Phys.*, **41**, 1062 (1964).

(8) A. D. McLachlan, *Mol. Phys.*, **3**, 233 (1960).

(9) P. N. Rieger and G. K. Fraenkel, *J. Chem. Phys.*, **39**, 609 (1963).

Table III: Calculated and Experimental Ring Spin Densities in Diphenyl Sulfone, Phenyl Methyl Sulfone, and *p*-Nitrophenyl Methyl Sulfone

Compound and position	$p(\text{Hückel})$	$p(\text{McLachlan})$	$p(\text{exptl})$
Diphenyl sulfone			
2	0.075	0.087	0.096
3	0.017	-0.022	0.026
4	0.133	0.179	0.186
Phenyl methyl sulfone			
2	0.122	0.122	0.153
3	0.048	-0.016	<0.05
4	0.282	0.399	0.359
4-Nitrophenyl methyl sulfone			
2	0.017	-0.026	<0.01
3	0.096	0.120	0.127
N	0.199	0.208	0.244

As Table III shows, Gerdil and Lucken's parameters describe the asymmetric sulfones about as well as they describe diphenyl sulfone, so there is no evidence for any difference in conjugation in the two cases. There is, thus, no evidence for the involvement of a sulfone orbital antisymmetric across the OSO plane.

One may try to understand the methyl splitting in various ways. It is accepted that methyl couplings in epr spectroscopy are due primarily to hyperconjugative effects,¹⁰ so one should include the methyl group in the π system to calculate the expected couplings. On the other hand, if one considers only anions, the methyl couplings are, to a good approximation, proportional to the spin density at the adjacent atom. In the two compounds we have studied the sulfur 3d spin densities are 0.118 and 0.029 in phenyl methyl sulfone anion and 4-nitrophenyl methyl sulfone anion, respectively. These were calculated using the same parameters which gave the spin densities in Table III, using McLachlan's method. The corresponding methyl coupling constants are 1.96 and 0.78 G. These are not in constant ratio, of course, but not very much can be concluded from this because calculated spin densities are often in error by substantial amounts, especially when they are small.

We have also calculated the methyl couplings by including the methyl group in the π system and doing a Hückel calculation including overlap, similar to the calculations performed by Colpa and de Boer.¹⁰ We performed this calculation to see if the parameters deduced for the sulfone group would also give decent results for the methyl couplings. To perform the calculation one needs overlap integrals as well as the various matrix elements of the Hückel Hamiltonian, which are available. We followed Colpa and de Boer in setting the several $C_{ar}-C_{ar}$ overlaps equal to 0.25

and the $C_{me}-(H_3)$ overlap equal to 0.50. The remaining overlaps were calculated on Slater-type orbitals using the usual methods.¹¹ The results appear in Table IV. In this table $n\mu$ is the effective nuclear charge. Slater's rules were used to obtain μ for all orbitals except the sulfur 3d, for which we followed the suggestion of Craig and Zauli.¹² The r_{ab} values were taken from similar compounds.¹³

Table IV: Overlap Integrals

Bond ab	μ_a	μ_b	$r_{ab}, \text{Å}$	S_{ab}
C(2p π)-S(3d π)	1.63	1.2	1.80	0.53
N(2p π)-C(2p π)	1.95	1.63	1.50	0.16
N(2p π)-O(2p π)	2.28	1.96	1.20	0.17

The results of our calculations appear in Table V. In calculating a spin density from the methyl hyperfine coupling constant we have assumed that the entire methyl hyperfine interaction arises from unpaired spin in hydrogen 1s orbitals. This is not quite correct because the π orbital on the adjacent carbon has non-vanishing spin density at the proton, but the term we keep is dominant.

Table V: Spin Densities Calculated Including Overlap and Hyperconjugation

Compound and position	$p(\text{calcd})$	$p(\text{exptl})$
Phenyl methyl sulfone		
2	0.134	0.153
3	0.025	<0.05
4	0.233	0.359
Me	0.057	0.012
4-Nitrophenyl methyl sulfone		
2	0.029	<0.01
3	0.095	0.127
N	0.202	0.224
Me	0.011	0.005

The spin densities in the ring do not change much with the method of calculation. The methyl couplings come out in the right order, but the absolute values are poor, especially in phenyl methyl sulfone. The agreement can be improved some by varying some of the

(10) J. P. Colpa and E. de Boer, *Mol. Phys.*, **1**, 333 (1964).(11) R. S. Mulliken, C. A. Rieke, D. Orloff, and H. Orloff, *J. Chem. Phys.*, **17**, 1248 (1949).(12) D. P. Craig and C. Zauli, *ibid.*, **37**, 601 (1962).

(13) A. D. Mitchell and L. C. Cross, Ed., "Interatomic Distances," The Chemical Society, Burlington House, London, W1, 1958.

several parameters, but this is not a fruitful course of action.

In summary, one may describe the conjugation of the sulfone group in phenyl methyl sulfone and 4-nitrophenyl methyl sulfone using a single unfilled d orbital with the parameters appropriate to diphenyl sulfone. This description is very satisfactory for everything but

the methyl coupling constant, which is predicted only roughly by the model.

Acknowledgment. This work was supported by the National Center for Radiological Health under Grant RH-00405. This support is acknowledged gratefully. We also thank Professor O. G. Ludwig and Richard Noren for the use of some of their computer routines.

The Photochemistry of Methylamine at 1470 Å

by John J. Magenheimer, Robert E. Varnerin, and Richard B. Timmons

Department of Chemistry, The Catholic University of America, Washington, D.C. 20017 (Received April 24, 1969)

The products produced in the vacuum uv photolysis of methylamine at room temperature using a Xe resonance lamp have been determined. From the photolysis of CH_3NH_2 and CD_3NH_2 both in the presence and absence of added free radical scavengers, the relative quantum yields for various primary steps have been calculated. The main primary process is the formation of hydrogen atoms. In contrast with the longer wavelength studies of methylamine, we find that the major portion of these H atoms arise from hydrogens attached to the carbon atom as shown by the experiments with CD_3NH_2 . The direct molecular elimination of hydrogen definitely occurs at 1470 Å. However, the total hydrogen formed by this route represents a relatively minor percentage of the overall decomposition. Only a small fraction of the decomposition occurs *via* methyl radical formation.

Introduction

The vacuum uv photolysis of simple molecules has become an increasingly active research area in recent years. Of the work so far reported, the larger effort has dealt with the photochemistry of hydrocarbons. A number of interesting results have been obtained including the consistent observations of molecular elimination as one of the primary photolytic steps at these shorter wavelengths. In addition, it appears that in the case of alkane photolysis the molecular hydrogen formation arises mainly from hydrogens located on the same carbon atom.¹

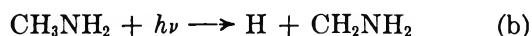
We now wish to report on the photochemistry of methylamine at 1470 Å. In view of the previous work with hydrocarbons, we were interested in determining the importance of molecular elimination in this photolysis and, in particular, if such elimination comes predominantly from the carbon or nitrogen atom. In addition, it is of interest to compare the photochemistry of methylamine at 1470 Å with the results obtained at longer wavelengths.

The photolysis of methylamine has been the subject of two recent investigations. Using 1849 Å radiation and esr radical detection, Hadley and Volman² have shown that the primary step

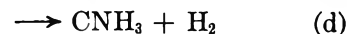


is the only major free radical-producing process at 77°K.

The most detailed gas-phase study of this molecule is that work of Michael and Noyes³ where photolysis was carried out at room temperature and wavelengths between 1940 and 2440 Å. From their results, they conclude that reaction a accounts for at least 75% of the overall photolysis and the reaction



represents about 10% of (a). In addition, primary steps



were shown to be of minor importance.

In the work we have carried out, major emphasis was placed on the analysis of products noncondensable at 77°K obtained in the photolysis of CH_3NH_2 or CD_3NH_2 in the presence and absence of added scavengers. As observed by other workers in studying the photolysis of methylamine, polymer formation and

(1) H. Okabe and J. R. McNesby, *J. Chem. Phys.*, **34**, 668 (1961).

(2) S. G. Hadley and D. H. Volman, *J. Amer. Chem. Soc.*, **89**, 1053 (1967).

(3) J. V. Michael and W. A. Noyes, Jr., *ibid.*, **85**, 1228 (1963).

other nitrogen containing products are also produced in this system. The reproducibility obtained from run to run with these condensable products was rather poor, most likely caused by the polymer formation. Fortunately the fraction noncondensable at 77°K, hydrogens and methanes, was very reproducible and we were able to accomplish our primary objective of establishing the important primary steps in this photolysis at 1470 Å.

Apparatus and Procedure

The high-vacuum reaction system was of comparable design to that normally employed in gas phase photochemical work. It contained an all-glass gas circulation pump, and greaseless stopcocks were employed. The lamp was similar to the one described by Ausloos and Lias.⁴ It contained a number of titanium wires used as getters and vaporized as required. A thin LiF window was joined to the lamp body by a Ag-AgCl graded seal. The lamp was operated at a xenon pressure of 0.1 Torr and light emission was obtained *via* microwave discharge. Under these conditions, the effective wavelength output is mainly the 1470 Å Xe resonance line accompanied by a much less intense emission at 1296 Å.

Most of the photolytic runs were of 30-min duration and conversion of the methylamine was always less than 1%. The fraction noncondensable at 77°K was collected and measured in a combination Toepler pump-gas buret. This fraction was analyzed mass spectrometrically and shown to consist only of hydrogen, methane and nitrogen.

Methylamine was prepared from Eastman Kodak Co. methylamine hydrochloride. It was recrystallized from water and the amine was liberated by reaction with anhydrous calcium oxide. The only measurable impurity was a small trace of NH₃. The CD₃NH₂ was prepared by reacting a sample of CD₃NH₂·HCl (Brinkman Chemical Co.) with concentrated KOH. Water vapor was removed by distilling the CD₃NH₂ through a drying tube filled with P₂O₅. The CD₃NH₂ had a stated minimum D atom purity of 97% on the carbon atom. We confirmed this *via* nmr analysis obtaining a maximum H atom impurity of 2 atom % on the carbon atom.

The C₂H₄ (Phillips Petroleum, research grade) and C₂D₄ (Stohler Isotopic Chemicals, 97 atom % D) were used without further purification.

Because of the deposition of polymer on the LiF window during the course of a run, it was necessary to clean the window between successive runs. This was accomplished by washing the window with ethanol followed by overnight evacuation of the reaction cell. In some runs a prephotolysis of the system was carried out prior to the actual photolysis of the methylamine but after the window had been cleaned. Such prephotolysis produced minor amounts of noncondensa-

bles which are not significant when compared to the amounts of noncondensable produced during the methylamine photolysis. It was observed that photolysis of the polymer on the LiF window produced noncondensable products which were surprisingly rich in N₂. If repeated photolysis of the methylamine was carried out without first removing the polymer from the window, the total yield of noncondensable decreased from run to run.

From a series of runs with varying pressures of methylamine it was found that at pressures about 2 Torr the rate of production of hydrogen was independent of CH₃NH₂ pressure. In other words, all photons were absorbed at pressures above 2 Torr. We also observed that the rate of polymer deposition on our LiF window increased rapidly with increasing CH₃NH₂ pressure. In our experimental runs, we wanted to minimize this polymer formation but, at the same time, operate under conditions where we could obtain reasonable amounts of noncondensables for analytical purposes while keeping the percent conversion of the methylamine to a low value (<1%). We found that these goals could be accomplished using pressures of CH₃NH₂ of the order of 10 Torr.

Results and Discussion

The initial experiments were carried out using CH₃NH₂ with C₂D₄ as the added radical scavenger. These results are shown in Table I. In order to scav-

Table I: Rates of Production of Products in the Photolysis of CH₃NH₂-C₂D₄ Mixtures at Room Temperature (Photolysis Time Was 30 Min)

$P_{\text{CH}_3\text{NH}_2}$, Torr	$P_{\text{C}_2\text{D}_4}$, Torr	$R_{\text{H}_2}^a$	R_{HD}	R_{D_2}
10.8	0	21.8	0	0
10.8	0	22.4	0	0
10.9	0.21	10.2	0.71	0.36
10.3	0.68	5.9	0.99	0.40
10.7	0.86	5.20	1.06	1.24
10.4	0.87	5.02	1.10	1.26

^a All rates are in units of mol sec⁻¹ × 10¹⁰.

enge all the H atoms it was necessary to work at pressures of C₂D₄ up to about 5% of the CH₃NH₂. At these concentrations of added scavengers some C₂D₄ photolysis also takes place as revealed in Table I where the D₂ yield is shown to increase with increasing C₂D₄ pressure. The per cent ethylene required in our experiments to remove all H atoms is somewhat larger than that usually required in typical hydrocarbon photolysis as the bimolecular reaction of H atoms with CH₃NH₂ is probably much faster than the correspond-

(4) P. Ausloos and S. G. Lias, "The Chemistry of Ionization and Excitation," Taylor and Francis Ltd., London, 1967, p 79.

Table II: Rates of Production of Products in the Photolysis of $\text{CD}_3\text{NH}_2\text{-C}_2\text{D}_4$ and $\text{CD}_3\text{NH}_2\text{-C}_2\text{H}_4$ Mixtures at Room Temperature (Photolysis Time Was 30 Min)

Run No.	$P_{\text{CD}_3\text{NH}_2}$ Torr	$P_{\text{C}_2\text{D}_4}$ Torr	$R_{\text{H}_2}^a$	R_{HD}	R_{D_2}	$R_{\text{CD}_3\text{H}}$	R_{CD}
1	10.4	0	2.64	7.18	5.02	0.41	0.15
2	10.0	0	2.75	6.64	4.58	0.32	0.12
3	10.4	0	2.76	6.66	4.47	0.35	0.14
4	10.7	0	2.55	7.66	5.32	0.40	0.14
5	10.9	0.07	1.63	3.13	2.64	0.12	0.06
6	11.2	0.12	1.54	2.71	2.37	0.11	0.06
7	10.7	0.19	1.65	2.48	2.22
8	10.5	0.21	1.87	2.32	2.23
9	10.7	0.36	1.65	2.00	2.18
10	10.2	0.48	1.33	1.67	1.99
11	10.4	0.67	1.02	1.29	1.91
12	10.6	0.80	0.95	1.36	2.27
13	9.9	1.05	0.96	1.21	2.31
		$P_{\text{C}_2\text{H}_4}$ Torr					
14	10.6	0.19	2.50	3.03	1.74	0.11	0.05
15	10.8	0.31	2.12	2.15	1.21	0.08	0.02
16	11.0	0.79	2.64	1.62	0.81
17	10.4	0.96	2.80	1.49	0.66
18	10.2	0.49	2.12	1.81	0.95

^a All rates are in $\text{mol sec}^{-1} \times 10^{10}$. ^b The blanks in the methane yields represent runs in which the total methane yield was too small to be analyzed.

ing H atom-hydrocarbon reaction. It is also apparent from the data in Table I that small, but significant, amounts of HD are produced even in the completely inhibited reaction. The HD produced is certainly too large to be explained as arising from a H atom impurity in C_2D_4 . Although we cannot prove conclusively how this HD is produced, we feel that it arises from D atom reactions with the polymer on the walls. The D atoms will be produced by addition of H atoms to C_2D_4 followed by unimolecular decomposition of the chemically activated $\text{C}_2\text{D}_4\text{H}$. Or, alternately, the $\text{C}_2\text{D}_4\text{H}$ could undergo a bimolecular reaction with polymer on the walls producing HD. It seems reasonable to expect that such a heterogeneous reaction would have a low activation energy and thus still be of importance even in the presence of large amounts of added C_2D_4 . It should be pointed out that at pressures above 5 Torr the deactivation of the chemically activated $\text{C}_2\text{D}_4\text{H}$ would normally be faster than decomposition. However in these experiments the photochemically produced H atom is presumably "hot" and the lifetime of the activated $\text{C}_2\text{D}_4\text{H}$ species with respect to decomposition could be very short and thus, of importance, even at pressures above 5 Torr. In addition, HD production via a homogeneous disproportionation reaction of H plus $\text{C}_2\text{D}_4\text{H}$ is also possible.

From Table I, we calculate that the percent hydrogen arising from molecular elimination in the photolysis of methylamine is 20%, the remaining H_2 arising from H atom attack on CH_3NH_2 . This figure of 20%

represents an upper limit and the actual molecular H_2 is somewhat lower. We observed that photolysis of the polymer on the LiF window in the presence of added C_2D_4 produced small, but not insignificant, amounts of H_2 . In order to determine the amount of H_2 produced from the polymer photolysis we carried out some runs by varying the duration of the photolysis of the CH_3NH_2 plus C_2D_4 mixtures. At very short photolysis times (10 min), the rate of H_2 production in the fully inhibited reaction was about 15% lower than in the runs of 30 min duration. It was not possible to reduce the photolysis time to less than 10 min because a large uncertainty is involved in determining the small amounts of H_2 produced. Using the 15% lower rate of H_2 production in the 10-min run, we obtain a figure of 17% for molecular H_2 formation in CH_3NH_2 photolysis. This again represents an upper limit and the exact figure might be slightly lower.

In order to determine the fraction of H atoms and molecular H_2 arising from the C atom and N atom of methylamine, we carried out experiments using CD_3NH_2 . In some experiments C_2H_4 was used as scavenger and, in others, C_2D_4 was employed. The results we obtained are summarized in Table II. In general, the combination $\text{CD}_3\text{NH}_2\text{-C}_2\text{H}_4$ was used to determine the importance of D atom and D_2 production in the primary photolysis, and the combination $\text{CD}_3\text{NH}_2\text{-C}_2\text{D}_4$ was used to measure the importance of H atom and H_2 formation arising from hydrogen located on the nitrogen atom. This approach was necessary

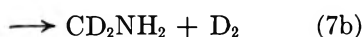
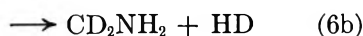
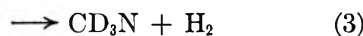
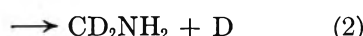
Table III: Average Rates^a of Production of H₂, HD and D₂ in Terms of Molecular and Atomic Yields

Run No.	$R_{H_2}(M)$	$R_{H_2}(T)$	$R_{H_2}(A)$	$R_{HD}(M)$	$R_{HD}(T)$	$R_{HD}(A)$	$R_{D_2}(M)$	$R_{D_2}(T)$	$R_{D_2}(A)$
11 to 13	0.98
11 to 13, 16 to 18	1.45
1 to 4	...	2.67	1.69	...	7.05	5.60	...	4.85	4.04
16 to 18	0.81

^a All rates are in units of mol sec⁻¹ × 10¹⁰.

because of the two-fold problem of polymer photolysis and photolysis of the added ethylene. Thus the combination CD₃NH₂-C₂D₄ leads to anomalously high D₂ formation whereas the CD₃NH₂-C₂H₄ runs yield too much H₂. We are confident that this procedure leads to quantitative determinations of the amounts of H₂ and D₂, respectively. This is shown in Figure 1(b) where the H₂ yield is seen to be independent of C₂D₄ concentration over a wide change in C₂D₄ pressure and, in Figure 1(a), the yield of D₂ is shown to be independent of C₂H₄ pressure over a similarly wide range.

In order to determine the relative importance of H and D atoms in the primary photolytic steps, we treat the data in terms of the following mechanism



We let $R_{H_2}(T)$ represent the overall rate of H₂ production in the photolysis of CD₃NH₂ in the absence of added scavenger and $R_{H_2}(M)$ represent the limiting rate of H₂ obtained under conditions of complete H atom scavenging by C₂D₄. The rate $R_{H_2}(A)$ representing hydrogen arising from an atomic process is then given as the difference between $R_{H_2}(T)$ and $R_{H_2}(M)$. Similar designations can be given to HD and D₂ production. Using this procedure, the results obtained are given in Table III.

In order to accomplish our goal of determining the yields of H atoms and D atoms in the primary photolysis we have to calculate the relative amounts of HD arising *via* reactions 6b and 7a. From the proposed mechanism, we can write

$$\frac{R_{H_2}(A)}{R_{HD}(A,H)} = \frac{k_{6a}}{k_{6b}} \quad \frac{R_{HD}(A,D)}{R_{D_2}(A)} = \frac{k_{7a}}{k_{7b}}$$

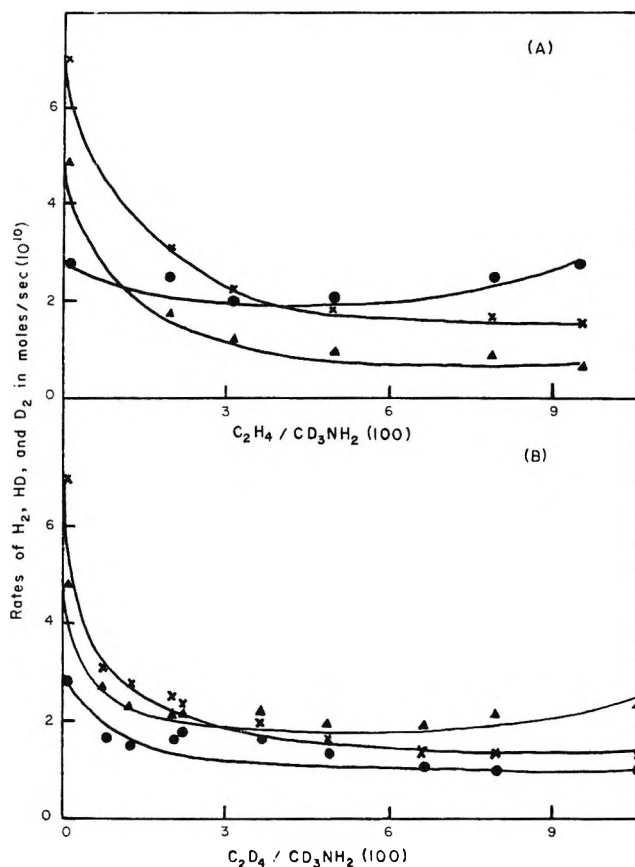


Figure 1. Rates of Production of H₂, HD and D₂ in the Photolysis of CD₃NH₂-Ethylene Mixtures H₂, ●; HD, ×; and D₂, ▲. (A) CD₃NH₂-C₂H₄ system; (B) CD₃NH₂-C₂D₄ system.

where $R_{HD}(A,H)$ and $R_{HD}(A,D)$ represent rates of HD production from H atom and D precursors, respectively. To a very good approximation, we can assume that the selectivity ratio for H or D atom abstraction from CD₃NH₂ is essentially the same for attack by either a H or D atom, *i.e.*

$$\frac{k_{6a}}{k_{6b}} = \frac{k_{7a}}{k_{7b}}$$

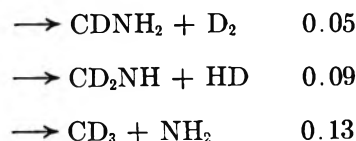
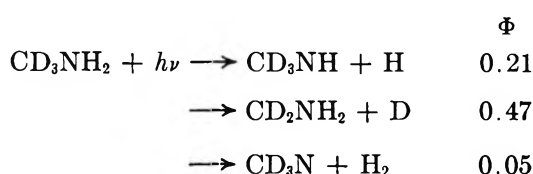
The total rate of HD production from atom precursors is 5.60×10^{-10} mol sec⁻¹. If we let α be the fraction of HD arising from reaction 6b, then $(1 - \alpha)$ is the fraction from reaction 7a. Therefore, we have (Table III)

$$\frac{1.69}{\alpha(5.60)} = \frac{(1 - \alpha)5.60}{4.04}$$

Solving, we obtain values for α of 0.68 and 0.32. With α 0.68, the ratio $R_{\text{H}_2}(\text{A})/R_{\text{HD}}(\text{A,H})$ is 0.42. With α 0.32, this ratio is equal to 0.94. In order to choose between the two values of α , we turn to the data of Michael and Noyes³ on the uv photolysis of CD_3NH_2 . In their work, molecular hydrogen elimination is of negligible importance and essentially all of the H_2 , HD and D_2 arises from atomic precursors. Treating their data in essentially the same way as we have done above, we obtain values of $R_{\text{H}_2}(\text{A})/R_{\text{HD}}(\text{A,H})$ of 4.75 and 1.13. Furthermore, the value of 1.13 for this ratio is internally consistent with a primary photolytic step of H atom production as the overwhelmingly most important primary step. This is in accord with the esr experiments.² On the other hand, the value of 4.75 for the ratio of rate constants 6a and 6b leads to the conclusion that the uv photolysis of CD_3NH_2 produces essentially equal amounts of H and D atoms. This, of course, is contrary to the experimental evidence. The agreement between the value of 1.13 from the work of Michael and Noyes, and 0.94 obtained in our experiments is very satisfactory. Thus we conclude that within experimental error the ratio k_{6a}/k_{6b} is close to unity.

Unfortunately, this rate-constant ratio does not appear to have been measured by other workers. Recent work has been done, however, using CH_3 and CF_3 reactions with CD_3NH_2 . In the CH_3 reactions, one calculates a selectivity ratio for abstraction of H atom to D atom equal to 74 by extrapolating to 300°K the results of Gray and Thynne^{5a} obtained at higher temperatures. However, their activation energies of 10.1 and 6.0 kcal mol⁻¹ for abstraction from the C-D and N-H bonds, respectively, represents a much larger difference than the value of 1.3 kcal mol⁻¹ reported by Michael^{5b} for the same two reactions. Michael's results for CD_3NH_2 coupled with his data for CH_3ND_2 indicates that the methyl radical can abstract from either end of the methylamine molecule with about equal ease. In the CF_3 reactions, this same ratio is 1.5 at 300°K where we have extrapolated the results of Morris and Thynne⁶ from higher temperatures. In view of the results obtained with CH_3 and CF_3 radicals, a selectivity ratio of unity obtained in our H atom reactions with CD_3NH_2 seems quite reasonable.

From our observed ratio of k_{6a} to k_{6b} of 0.94, we calculate the following relative quantum yields in the photolysis of CD_3NH_2 .



The importance of the last step is calculated from the methane yields in Table II. The elimination of methane upon the addition of ethylene reveals the absence of molecular methane formation as one of the primary steps. The products from the photolysis of methylamine were analyzed for ethane production. It was found that the ethane yield was 2.5 times larger than the methane production in the unscavenged runs.

Of the primary steps listed above the only process with which a large uncertainty is associated is the one leading to molecular HD formation. The reason for the large uncertainty in this value is that it is determined under conditions identical to those shown in Table I where significant amounts of HD were produced in the $\text{CH}_3\text{NH}_2\text{-C}_2\text{D}_4$ photolysis. This will lead to values of molecular HD which are undoubtedly too high and thus our reported relative quantum yield of 0.09 is to be considered only as an upper limit.

In both our work and that of Michael and Noyes it has been assumed that the fate of the H and D atoms is reaction with methylamine. This is to be contrasted with the recent study of methane photolysis⁷ where it is assumed all atoms produced disappeared by atom recombination rather than by abstraction from methane. However, the H atom reaction with CH_4 has a rather high activation energy, 11.8 kcal mol⁻¹.⁸ On the other hand, abstraction of H atoms from methylamine by CH_3 and CF_3 have much lower activation energies.^{5,6} Therefore, the assumption that the fate of the H atoms and D atoms in abstraction from methylamine does not seem unreasonable under our reaction conditions.

Although we do not have quantitative data available on other products we did make a number of interesting observations. In all runs small amounts of N_2 were produced including runs carried out in the presence of ethylene. The addition of ethylene did not decrease the small N_2 yields. This is in accord with the experimental findings of Michael and Noyes. However, in addition, we observed that photolysis of the cell containing no methylamine but with polymer deposition on the walls and the LiF window produced noncondensable products which were surprisingly rich in N_2 . Actually the N_2 produced in these experiments

(5) (a) P. Gray and J. C. J. Thynne, Tenth Symposium (International) on Combustion, The Combustion Institute, 1965. (b) J. V. Michael, Ph.D. Thesis, University of Rochester, 1962.

(6) E. R. Morris and J. C. J. Thynne, *Trans. Faraday Soc.*, **64**, 2124 (1968).

(7) A. H. Laufer and J. R. McNesby, *J. Chem. Phys.*, **49**, 2272 (1968).

(8) M. J. Kurylo and R. B. Timmons, *ibid.*, **50**, 5706 (1969).

was sufficiently large to account for all the N_2 produced during the methylamine photolysis. Therefore, we feel that the N_2 we observe comes from the polymer photolysis and not from decomposition of ammonia or other nitrogen-containing compounds as suggested in the work at longer wavelengths.³

We made a determined effort to detect any HCN which might have been produced in this system. At the wavelength employed it is energetically possible that excited species such as $CD_2NH_2^*$ or CD_3NH^* produced in the initial step could further decompose to hydrogen and HCN. We employed both gas chromatography and mass spectrometry in searching for HCN but we observed only insignificantly small amounts of this product.

Conclusion

The photolysis of methylamine proceeds primarily by an atomic mechanism with molecular elimination processes representing relatively minor contributions to the overall photodecomposition. Surprisingly, we find that D atom formation in CD_3NH_2 photolysis is more important than H atom formation. This is contrary to the methylamine photochemistry at longer wavelengths. The deposition of copious quantities of polymer on the walls and window of the reaction cell severely complicates this system and limits the quantitative data to products noncondensable at 77°K. The molecular yields we report are to be considered as maximum amounts and this is particularly true in the case of HD formation.

Acid Dissociation in Acetone-Water Mixtures. An Anomalous Medium

Effect When London Dispersion Forces Are Large

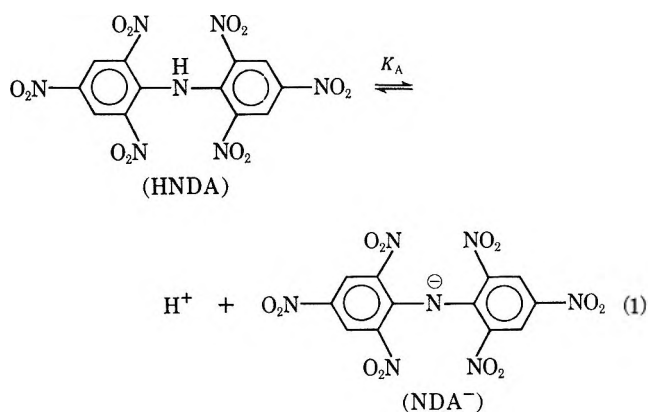
by Dodd-Wing Fong and Ernest Grunwald

Department of Chemistry, Brandeis University, Waltham, Massachusetts 02154 (Received April 29, 1969)

2,4,6,2',4',6'-Hexanitrodiphenylamine (HNDA) undergoes acid dissociation according to $HNDA \rightleftharpoons H^+ + NDA^-$. At 25°, $pK_A = 2.75$ in water, 2.13 in 12 wt % acetone-water, and 1.26 in 24 wt % acetone-water; 0.1 M *p*-cyanophenol and 0.1 M *p*-methoxyphenol likewise raise the dissociation constant. The direction of these changes is contrary to prediction based on the charge-in-dielectric-continuum model, but is consistent with the expected large increase in solvation energy of NDA^- , when acetone is added to water, as a result of London dispersion forces.

For acid dissociation of the charge type $HA = H^+ + A^-$, the usual medium effect when acetone is added to an aqueous solution is for K_A to decrease.¹ This effect is attributed primarily to the lowering of the dielectric constant, which opposes the formation of the ions.² The change in solvent basicity is thought to be small, as long as water remains in large molar excess.³ The change in solvation energy by van der Waals-London dispersion forces is likewise thought to be small, or at least not to be dominant.

We find, on the contrary, that for acid dissociation of 2,4,6,2',4',6'-hexanitrodiphenylamine (HNDA),^{4,5} K_A not only fails to decrease but actually increases by more than 30-fold as acetone, up to 24 wt %, is added to an aqueous solution. Our data are listed in Table I, and pK_A values covering the entire acetone-water system are cited in Table II. We find, moreover, that *p*-methoxyphenol and *p*-cyanophenol also raise the K_A of



(1) J. F. J. Dippy, S. R. C. Hughes, and A. Rozanski, *J. Chem. Soc.*, 1441 (1959), and references cited therein.

(2) W. F. K. Wynne-Jones, *Proc. Roy. Soc.*, **A140**, 440 (1933).

(3) Acetone is a much weaker base than water. See, for example, N. C. Deno and M. J. Wisotsky, *J. Amer. Chem. Soc.*, **85**, 1735 (1963).

Table I: pK_A of 2,4,6,2',4',6'-Hexanitrodiphenylamine at 25° in Acetone-Water Mixtures

[Acetone], <i>M</i>	p_0H^a	[A ⁻], ^b μM	[A ⁻]/[HA]	pK_A^c
0.0	2.701	11.75 ± 0.43	0.96 ± 0.07	2.72 ± 0.03
	3.000	15.34 ± 0.17	1.78 ± 0.06	2.75 ± 0.01
	3.230	18.09 ± 0.21	3.07 ± 0.15	2.74 ± 0.02
	3.421	19.49 ± 0.32	4.35 ± 0.41	2.78 ± 0.04
			(Av)	2.75 ± 0.02
2.03	2.002	11.35 ^d	0.80	2.11
	2.223	13.73 ^d	1.13	2.17
	2.399	16.21 ± 0.04	1.68 ± 0.01	2.17 ± 0.01
	2.700	20.76 ± 0.12	4.06 ± 0.12	2.09 ± 0.01
	3.002	23.08 ± 0.06	8.24 ± 0.20	2.11 ± 0.01
			(Av)	2.13 ± 0.04
4.06	1.524	34.64 ± 0.21	2.02 ± 0.04	1.22 ± 0.01
	1.700	38.47 ± 0.09	2.90 ± 0.03	1.24 ± 0.01
	1.855	39.55 ± 0.72	3.24 ± 0.27	1.34 ± 0.03
	1.922	42.16 ± 0.21	4.40 ± 0.12	1.28 ± 0.01
	2.002	43.98 ± 0.26	5.66 ± 0.23	1.25 ± 0.01
			(Av)	1.26 ± 0.04

^a $p_0H = -\log [H^+]$, where $[H^+]$ = molar concentration of hydrogen ion at a given solvent composition. ^b Mean and standard deviation, based on several absorbancy measurements between 4400 and 5000 Å. ^c $K_A = [H^+][A^-]/[HA]$, in molar concentrations. No attempt is made to estimate molar activity coefficients. ^d Initial measurement.

Table II: Effect of *p*-Methoxy- and *p*-Cyanophenol and of Acetone on pK_A of 2,4,6,2',4',6'-Hexanitrodiphenylamine at 25°

Acetone, wt %	Phenol 0.1 <i>M</i>	pK_A^a
0	...	2.75 ± 0.02
12 ^b	...	2.13 ± 0.04
	<i>p</i> -OCH ₃	1.83 ± 0.03
	<i>p</i> -CN	1.73 ± 0.01
24 ^c	...	1.26 ± 0.04
	<i>p</i> -OCH ₃	1.12 ± 0.01
	<i>p</i> -CN	1.15 ± 0.05
42	...	2.5 ± 0.1 ^d
76.5	...	2.9 ± 0.1 ^d
100	...	3.3 ± 0.3 ^d

^a Unless otherwise specified, K_A is the equilibrium constant in terms of molar concentrations at the given solvent composition. ^b 2.03 *M*; Table I. ^c 4.03 *M*; Table I. ^d Results extrapolated to infinite dilution. D. J. Glover, ref 5.

HNDA in water-rich media (Table II), so that this unusual effect is not characteristic of acetone alone. In fact, on a molar basis the effects produced by the phenols are even greater than those produced by acetone. In 12 wt % acetone, $\delta \log K_A / \delta c$ is 3 for *p*-methoxyphenol, 4 for *p*-cyanophenol, and 0.37 for acetone, where c denotes the molar concentration of added phenol or acetone. The fact that the two phenols produce similar effects, in spite of the different electron donor-acceptor properties of their substituents, seems to rule out possible explanations that involve the formation of specific charge-transfer complexes.

We believe that the medium effect on K_A is in this case dominated by London dispersion forces. Some years ago, Grunwald and Price applied London's

theory for complex molecules⁶ to the prediction of medium effects on relative acid strength and described certain conditions under which the dispersion forces should be especially large.⁷ The following conditions apply here. The acid, HNDA, absorbs in the ultraviolet while the conjugate base also absorbs strongly in the visible. Thus the chromophoric groups (the amino-nitrogen atom and the six nitro groups) become very strong centers of van der Waals attraction in the NDA⁻ ions,⁷ and we must expect a relatively large change in solvation energy by London dispersion forces on acid dissociation. Any change in solvent that improves the van der Waals attraction of solvent molecules for solute molecules will tend to promote acid dissociation.

Our data suggest the following interpretation. Water is a poor solvating agent by the London dispersion mechanism.⁷ When acetone or phenol is added to water, solvation by the London dispersion mechanism improves and the gain in interaction energy is greater for the NDA⁻ ion than for HNDA. Up to 24 wt % acetone, this effect is large enough to outweigh the opposing effect of the lowered dielectric constant, and our data show that K_A increases. At still higher concentrations of acetone, the balance of opposing effects changes, and Glover's data⁹ show that K_A decreases above 40% acetone (Table II).

Because of the dramatic increase in K_A up to 24 wt % acetone disclosed by our data, we believe that there is

(4) R. Stewart and J. P. O'Donnell, *J. Amer. Chem. Soc.*, **84**, 493 (1962); *Can. J. Chem.*, **42**, 1694 (1964).

(5) D. J. Glover, *J. Amer. Chem. Soc.*, **87**, 5275 (1965).

(6) F. London, *J. Phys. Chem.*, **46**, 305 (1942).

(7) E. Grunwald and E. Price, *J. Amer. Chem. Soc.*, **86**, 4517 (1964).

an enrichment of acetone in the solvent shells around the NDA^- ions. However, the NDA^- ions are fairly large and can accommodate quite a few acetone molecules on adjacent sites. The displacement of water molecules by acetone molecules seems to take place gradually, and its effect on K_A does not become saturated until the acetone concentration is in excess of 24 wt %. That saturation occurs eventually is shown by the much smaller effect of added phenol in 24 wt % acetone than in 12 wt % acetone (Table II).

Experimental Part

Materials. Fisher certified acetone was distilled once before use. Eastman White Label 2,4,6,2',4',6'-hexanitrodiphenylamine (HNDA) and *p*-methoxyphenol were recrystallized from acetone and dried *in vacuo*. *p*-Cyanophenol from Aldrich Chemical Co. was recrystallized from methanol-water and dried *in vacuo*. Chemically pure, deionized water was used without further purification.

K_A Measurements. To obtain K_A , we measured $[\text{NDA}^-]$ spectrophotometrically in solutions of known p_cH and known total $[\text{HNDA}]$ concentration. (Quantities in brackets denote molar concentrations. $\text{p}_c\text{H} = -\log [\text{H}^+]$.) Optical densities were recorded between 4400 and 5000 Å at 25°, using a Beckman model DU-2 spectrophotometer and matched 1-cm cells. Absorption of light in this range is due entirely to the NDA^- ions. Stock solutions of the separate reactants were brought to 25° before mixing, so that after mixing, it required only a few minutes to reach thermal equilibrium in the thermostated cell compartment of the spectrophotometer. Optical densities were measured 10–15 min after mixing.

The p_cH of the solutions was measured with a calibrated Beckman research pH meter. At the higher HCl concentrations ($>0.02 F$), it could be assumed that $[\text{H}^+]$ is equal to the molar concentration of added HCl because $[\text{HNDA}]$ is relatively small. Solutions with $[\text{H}^+] \approx 0.03 M$ served as pH standards to make the pH meter direct reading in p_cH for measurements in the more dilute HCl solutions at the given solvent composition. Experience accumulated in this laboratory has shown that p_cH measured in this manner is equal

to $-\log [\text{H}^+]$ at the given solvent composition within close limits.

The concentrations of un-ionized HNDA and of NDA^- were less than 60 μM in all measurements. The pH ranged from 1.5 to 3.5. The data in Table I are typical.

Molar extinction coefficients in water were measured for 38 μM $[\text{NDA}^-]$ in the presence of 0.05 *F* NaOH. Our results were in good agreement with Glover's.⁵ Although alkaline solutions of NDA^- in water have optical densities that are stable for days, solutions of $[\text{NDA}^-]$ in 0.05 *F* NaOH in 12 and 24 wt % acetone change color soon after mixing of the components, and the optical density is highly unstable. However, stable optical densities could be obtained in both mixed solvents when NaOH was added so as to be only slightly in excess of the HNDA, which was on the order of 50 μM . In 24 wt % acetone, molar extinction coefficients obtained under such near-neutral conditions were identical with extinction coefficients obtained for solutions containing only 50 μM HNDA. It should be noted that acid dissociation is expected to be virtually complete for an acid of $\text{p}K_A$ 1.26 at a formal concentration of 50 μM .

The molar extinction coefficients in 12 and 24 wt % acetone were only slightly different from those in water, in agreement with Glover,⁵ showing that except for solvation effects, the light-absorbing species is the same.

Because solution of solid HNDA in the acetone-water mixtures was inconveniently slow, the solid was dissolved in pure acetone and the resulting solution was diluted with water. Some of the aqueous acetone solutions were found to be metastable in the presence of HCl, because HNDA crystallized out overnight. However, crystallization was so slow as to be imperceptible during the time required to measure the optical densities, except in 12 wt % acetone below pH 2.3, where the change was less than 10% in 15 min. Here K_A was calculated from the initial readings.

Acknowledgment. It is a pleasure to thank Professor Allan K. Colter for helpful discussions. We gratefully acknowledge the support of this work by the Petroleum Research Fund of the American Chemical Society and by the National Science Foundation.

An Electron Impact Study of Ionization and Dissociation of Monosilane and Disilane¹

by P. Potzinger and F. W. Lampe

Department of Chemistry, The Pennsylvania State University, University Park, Pennsylvania 16802
(Received May 7, 1969)

Appearance potentials of the principal positive ions from monosilane and disilane have been determined and upper limits to the heats of formation of the various ions have been derived, as well as a value of $\Delta H_f^\circ(\text{SiH}_3) = 51$ kcal/mol. From the energetic onsets of some of the resonance-capture processes and pair-production processes, thermochemical data for some of the negative ions from monosilane are derived. This is not possible in the case of disilane because it appears that all the negative ions are formed in different dissociation channels of common parent $\text{Si}_2\text{H}_6^{-*}$ ions and Si_2H_8^* molecules.

Introduction

Ionization and dissociation of the simple paraffinic hydrocarbons by electron impact have been the subject of numerous studies and there exists general agreement concerning the appearance potentials and the standard heats of formation of the principal ions and free radicals formed.² The structurally similar silanes, on the other hand, have received only scant attention and some of the available electron impact data are not in good agreement.³⁻⁷

As part of a general program of study concerned with the effects of ionizing radiation on silanes and simple organosilanes, we have had occasion to study the major ionization and dissociation processes that occur from the impact of electrons on monosilane and disilane. In the hope that our results may contribute to a clearer understanding of the energetics and thermochemistry involved, we report them herewith.

Experimental Section

All the measurements reported herein were carried out in a Nuclide Associates 12-90G mass spectrometer (12-in. radius of curvature, 90° sector field). All studies of positive ions were made using the retarding-potential difference (rpd) method⁸ of obtaining ionization efficiency curves that originate from the impact of electrons which are monoenergetic within about ± 0.1 eV.

At least three replicate determinations were carried out for each ion with the experimental errors reported being the average deviation from the average value. In these rpd experiments, the electron beam was pulsed at 100 kHz, obtaining an average electron current of about 5 μA . A 22-Hz square wave, having a peak-to-peak amplitude of 0.1 V and clamped about 1-V negative with respect to the filament, was applied to the retarding grid in a three-grid electron gun. The output of the electron-multiplier detector, consisting of a 22-Hz square-wave signal superimposed on an

essentially dc level, (rms multiplier current caused by ions arriving at 100 kHz) was fed to a Princeton Applied Research lock-in amplifier (par), tuned to 22 Hz and proper phase. The par amplifies the entire signal, extracts the 22-Hz rpd component as a dc signal which is displayed on the y axis of a Moseley 135-AM X-Y recorder. Since the electron energy, scanned by means of an appropriate motor drive, is displayed on the x axis of the recorder, direct continuous rpd ionization-efficiency curves are obtained. Typical curves for SiH_3^+ and SiH_2^+ from SiH_4 are shown in Figure 1. Argon ($I_z = 15.77$ eV) was used to calibrate the electron energy scale and all measurements were done in at least triplicate.

The rpd technique was not used in the study of negative ions, since the ion intensities were considerably lower than obtained during the study of positive ions. The electron energy scale for negative ion measurements was calibrated using the onset (9.2 eV) for the resonant capture formation of O^- from CO .⁹

Monosilane was obtained from Air Products, Inc. It was purified by fractionation on a high-vacuum line immediately before use until satisfactory purity by mass spectral standards was obtained. Disilane was prepared by the reduction of hexachlorodisilane (Peninsular Chemical Co.) with lithium aluminum hy-

- (1) AEC Document No. NYO-3570-9.
- (2) F. H. Field and J. L. Franklin, "Electron Impact Phenomena," Academic Press, New York, N. Y., 1957.
- (3) H. Neuert and H. Clasen, *Z. Naturforsch.*, **7a**, 410 (1952).
- (4) W. C. Steele, L. D. Nichols, and F. G. A. Stone, *J. Amer. Chem. Soc.*, **84**, 4441 (1962).
- (5) W. C. Steele and F. G. A. Stone, *ibid.*, **84**, 3599 (1962).
- (6) F. E. Saalfeld and H. J. Svec, *Inorg. Chem.*, **2**, 46 (1963); (b) F. E. Saalfeld and H. J. Svec, *ibid.*, **2**, 50 (1963).
- (7) G. G. Hess, F. W. Lampe, and A. L. Yergey, *Ann. N. Y. Acad. Sci.*, **136**, 106 (1966).
- (8) R. E. Fox, W. M. Hickam, D. J. Grove, and T. Kjeldaas, *Rev. Sci. Instrum.*, **26**, 1101 (1955).
- (9) G. J. Schulz, *Phys. Rev.*, **128**, 178 (1962).

Table I: Energetics of Positive Ion Formation in Monosilane^a

Ion	AP, eV	Process assigned	ΔH_f° (ion), kcal/mol
SiH_3^+	12.30 ± 0.03	$\text{SiH}_4 + e \rightarrow \text{SiH}_3^+ + \text{H} + 2e$	239
SiH_2^+	11.90 ± 0.02	$\text{SiH}_4 + e \rightarrow \text{SiH}_2^+ + \text{H}_2 + 2e$	282
SiH^+	15.3 ± 0.3	$\text{SiH}_4 + e \rightarrow \text{SiH}^+ + \text{H}_2 + \text{H} + 2e$	308
Si^+	13.56 ± 0.08	$\text{SiH}_4 + e \rightarrow \text{Si}^+ + 2\text{H}_2 + 2e$	318

^a $\Delta H_f^\circ(\text{SiH}_4)$ was taken to be 7.3 kcal/mol after S. R. Gunn and L. G. Green, *J. Phys. Chem.*, **65**, 779 (1961).

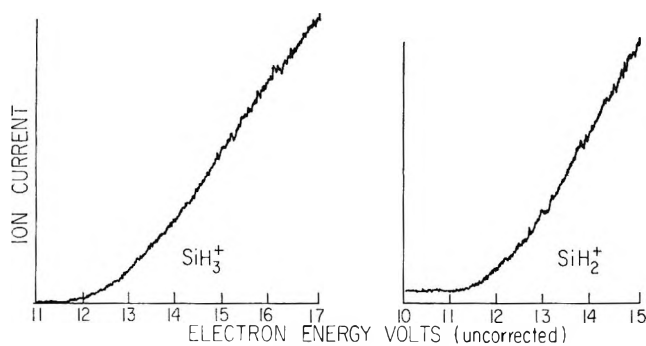


Figure 1. Ionization-efficiency curves of SiH_3^+ and SiH_2^+ from SiH_4 .

dride using bis[2-(2-methoxyethoxy)ethyl] ether as solvent. When the gases formed in this reaction were separated by fractionation on the vacuum line, it was found that the Si_2H_6 fraction contained SiH_3Cl as an impurity. In order to remove this impurity, the gases evolved from the reaction mixture were collected and treated again with lithium aluminum hydride. Fractionation of the gases subsequent to the second treatment with lithium aluminum hydride yielded a sample of disilane free of SiH_3Cl and sufficiently pure for our purposes.

Results and Discussion

1. *Positive Ions from SiH_4 .* The 70-eV mass spectrum of SiH_4 is in excellent agreement with that reported by previous investigators^{3,6a} and therefore is not reproduced here. The lowest threshold potentials of the principal positive ions are tabulated in Table I. In addition, Table I presents the formation processes assigned and the standard heats of formation of the ions, as calculated from the assigned processes and the assumption that the minimum appearance potentials are equal to the enthalpy changes of the assigned reactions.

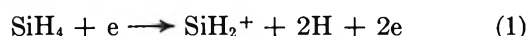
SiH_3^+ (m/e 31). Our value for the threshold potential of this ion is in excellent agreement with the value reported by Steele, Nichols, and Stone⁴ and within the combined experimental errors agrees with the value reported by Neuert and Clasen.³ It is in serious disagreement with the value reported by Saalfeld and Svec.^{6a} Since there is no doubt, in the case of this ion, about the formative process, and since Saalfeld

and Svec^{6a} found no evidence of kinetic energy effects in the silane fragment ions, we conclude that $\Delta H_f^\circ(\text{SiH}_3^+) = 239 \pm 2$ kcal/mol. Two discontinuities in the ionization-efficiency curve were found at 13.1 ± 0.2 and 14.2 ± 0.3 eV in all experiments. These breaks are indicative of the onset of other formation processes of SiH_3^+ and, although the nature of the processes cannot be ascertained, they must represent the onsets of different states of excitation of the SiH_3^+ ion.

Isotopic interference may be an influence in the determination of the appearance potential of SiH_3^+ , since the appearance potential of SiH_2^+ is lower by about 0.5 eV. The presence of $\text{Si}^{29}\text{H}_2^+$ in the ionization-efficiency curve of m/e 31 would be indicated by a slight tailing near onset with a slope that is 5% of the initial slope of m/e 30 (SiH_2^+). Inspection of Figure 1 shows that at our level of detection sensitivity such tailing is not significant.

SiH_2^+ (m/e 30). The threshold potential for the appearance of this ion is likewise in excellent agreement with the value reported by Steele, Nichols, and Stone.⁴ Within the combined experimental errors it can be considered to agree with the work of Neuert and Clasen³ (after correction of an obvious erroneous mass assignment by these authors) and with that of Saalfeld and Svec.^{6a} Thus, one may conclude with confidence that $\Delta H_f^\circ(\text{SiH}_2^+) = 282 \pm 1$ kcal/mol.

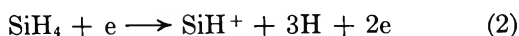
A reproducible break was found at 13.0 ± 0.2 eV. Since a similar break was found in SiD_2^+ by Hess and Lampe¹⁰ and since there is no such low-lying electronic state of H_2 , we believe that this break corresponds to formation of SiH_2^+ in a different state of excitation. Saalfeld and Svec^{6a} have reported an even higher appearance potential of SiH_2^+ at 16.5 ± 0.3 eV which corresponds to the process



In only one of our continuous rpd curves have we been able to detect a break beyond that at 13.0 eV. This particular break exhibited only a very slight change of slope and although its occurrence was at 16.4 ± 0.2 eV, its absence in the other curves prevents us from reporting a definite confirmation of (1).

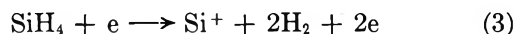
(10) G. G. Hess and F. W. Lampe, *J. Chem. Phys.*, **44**, 2257 (1966).

SiH^+ (m/e 29). The ionization-efficiency curve for this ion showed a long tail and is indicative of a formation process involving considerable excess energy, although in this case the tail may be partly due to contribution from Si^{29+} . We did not attempt to correct this tail for the contribution for Si^{29+} , since the very small slope of the Si^{28+} curve over a large energy range suggested that the contribution was small. Extrapolation of the tail to onset yielded a value of 15.3 ± 0.3 eV for the minimum appearance potential. This value lies between those reported by Neuert and Clasen³ and Saalfeld and Svec,^{6a} although with the rather large combined experimental error, could be considered in agreement with the former authors. In agreement, with Saalfeld and Svec^{6a} we found a second appearance potential at 20.0 ± 0.2 for this ion which most likely corresponds to



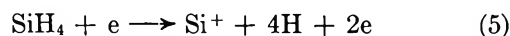
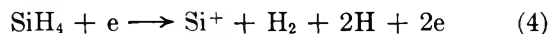
Saalfeld and Svec^{6a} employed a linear extrapolation method to obtain their appearance potentials, and since it is known that this method gives results too high for curves exhibiting long tails, we take our value to be more nearly correct and conclude $\Delta H_f^\circ(\text{SiH}^+) = 308 \pm 7$ kcal/mol.

Si^+ (m/e 28). The threshold for the appearance of Si^+ was found to be quite reproducible at 13.56 ± 0.08 eV. This value is not in good agreement with the value of 11.7 eV reported by Saalfeld and Svec^{6a} nor with the value of 14.5 reported by Neuert and Clasen.³ The standard heat of formation of gaseous Si is calculated from vapor pressure measurements to be 105 kcal/mol¹¹ and this value combined with the ionization potential of Si (8.15 eV¹²) yields a heat of formation of Si^+ of 293 kcal/mol. The value of 11.7 eV³ is simply too low to be compatible with this figure. If we take our minimum-energy process to be



we calculate $\Delta H_f^\circ(\text{Si}^+)$ to be 318 kcal. For a process where so many bonds are broken such a large excess energy is not unexpected and hence, as is often true in electron impact fragmentation, the appearance potential is an upper limit to the heat of reaction.

Reproducible breaks were observed at 14.8 ± 0.2 , 18.4 ± 0.2 , 20.2 ± 0.2 , and 22.9 ± 0.2 eV, with the breaks at 18.4 and 22.9 eV probably signifying the onsets of the two processes



The other discontinuities at 14.9 and 20.2 eV do not correspond to known excited states of Si^+ .

2. *Negative Ions from SiH_4 .* Negative ion mass spectra of SiH_4 at three different electron energies are shown in Table II. The spectra shown have been

Table II: Negative Ion Mass Spectra of SiH_4

Ion	Relative intensity at		
	20 eV	50 eV	70 eV
SiH_3^-	100	100	100
SiH_2^-	33	38	33
SiH^-	39	76	64
Si^-	4.8	52	54

corrected for isotopic contributions from Si^{29} and Si^{30} and so represent the monoisotopic spectra of Si^{28} .

The negative ion ionization-efficiency curves were recorded from 0 to 30 eV nominal electron energy. However, below 4 eV the trap current decreased so rapidly that quantitative ion intensities could not be obtained in this region. In addition to measuring onset potentials of the negative ions, the cross sections of the highest resonance peak of all negative ions were measured relative to those for the resonance peak of O^- from CO ($\sigma = 1.610 \cdot 10^{-19}$ cm²).⁹ These data are shown in Table III.

SiH_3^- (m/e 31). The ionization-efficiency curve of SiH_3^- shows a resonance peak having an onset at 2.5 ± 0.3 eV and a second resonance peak at 6.7 eV. A third onset at approximately 11 eV is probably also due to a resonance process while at 15.5 ± 0.5 eV a pair-production process sets in with yet another resonance peak superimposed on it.

From the appearance potential of the lowest-energy resonance peak we calculate a maximum heat of formation of SiH_3^- , namely $\Delta H_f^\circ(\text{SiH}_3^-) \leq 0.5$ eV. Combination of this result with the heat of formation of the SiH_3 radical leads to a minimum electron affinity of 41.5 kcal/mol for SiH_3 .

The resonance processes at 6.7 eV and 11 eV may result in an electronically excited SiH_3^- ion or the energy may go in kinetic and/or vibrational energy of the fragments formed, but we are unable to say more about these processes.

The onset of the pair-production process gives the value $\Delta H_f^\circ(\text{SiH}_3^-) \cong 0.0 \pm 0.5$ eV, which is somewhat lower than the upper limit obtained above from the lowest-energy resonance peak.

SiH_2^- (m/e 30). This ion also shows a resonance peak at 2.5 eV. In addition, there are two further resonance peaks, one at 7.7 eV and a very broad one with an onset at around 13 eV. A sharp pair-production onset appears at 20 ± 0.5 eV.

The first resonance peak exhibits the same threshold potential as the corresponding resonance peak for SiH_3^- , suggesting that this peak is characteristic of the vertical transition of the SiH_4 molecule to SiH_4^- and is not

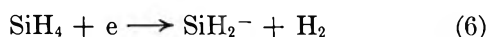
(11) "JANAF Thermochemical Tables," Dow Chemical Co., Midland, Mich., 1965.

(12) C. E. Moore, National Bureau of Standards Circular 467, Vol. 2, U. S. Government Printing Office, Washington, D. C., 1952.

Table III: Cross Section of the Highest Resonance Peak of the Negative Fragment Ions of SiH₄

Ion	Assigned process	Cross section	AP, eV
SiH ₃ ⁻	SiH ₄ + e → SiH ₃ ⁻ + H	1.76 × 10 ⁻¹⁹ cm ²	6.7
SiH ₂ ⁻	SiH ₄ + e → SiH ₂ ⁻ + 2H(H ₂)	6.7 × 10 ⁻²⁰ cm ²	7.7
SiH ⁻	SiH ₄ + e → SiH ⁻ + H + H ₂	4.8 × 10 ⁻²⁰ cm ²	7.7
Si ⁻	SiH ₄ + e → Si ⁻ + H ₂ + 2H(?)	1.0 × 10 ⁻²⁰ cm ²	2.5

characteristic of either of the specific fragment ions. (Isotopic interference of Si²⁹H₂⁻ with Si²⁸H₃⁻ can be ruled out because the intensity of the resonance peaks in both cases are approximately the same and it is, therefore, very unlikely in the SiH₃⁻ case that the peak is due to Si²⁹H₂⁻). This means, of course, that the onset energy of these peaks gives only upper limits to thermochemical values for the ions. Thus we conclude that $\Delta H_f^\circ(\text{SiH}_2^-) \leq 2.8$ eV, if the formation process is

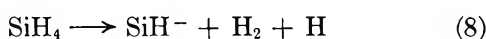


If the equation



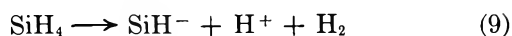
describes the pair-production process whose onset is at 20 eV, we get $\Delta H_f^\circ(\text{SiH}_2^-) = 2.3$ eV, a value compatible with that obtained from (6).

SiH⁻ (*m/e* 29). This ion does not show the resonance peak at 2.5 eV, but we do observe a resonance peak with an onset at 7.7 eV. If it is only for an energetic reason that we do not observe a resonance peak at 2.5 eV for SiH⁻, then from the threshold potential of the lowest-energy process, *viz.*



we must have $2.5 \text{ eV} < A(\text{SiH}^-) < 7.7 \text{ eV}$ for the minimum appearance potential. From this inequality we may derive for the standard heat of formation of SiH⁻, the limits, $0.5 \text{ eV} < \Delta H_f^\circ(\text{SiH}^-) < 5.7 \text{ eV}$.

In addition to a second resonance peak at 11.5 ± 0.5 eV, there are two pair-production processes with onsets at $18 \text{ eV} \pm 0.5$ and at 22.5 ± 0.5 eV. The lower value would give us $\Delta H_f^\circ(\text{SiH}^-) = 2.5 \pm 0.5$, a value compatible with our limits, if the process is described by the equation

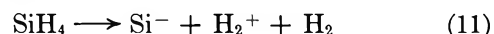


Moreover, the difference in the appearance potentials of these two pair-production processes suggests strongly that, for the higher value, the following process obtains



Si⁻ (*m/e* 28). This ion exhibits a resonance peak at 8.5 eV, a second at about 12.5 eV, and at least three pair-production onsets, of which only the first at 22 eV can be established with a reasonable degree

of accuracy. If this latter value corresponds to the minimum-energy process, *viz.*



one obtains $\Delta H_f^\circ(\text{Si}^-) = 4.7$ eV. This value is 0.8 eV lower than the $\Delta H_f^\circ(\text{Si})$ we get from combining process 3 with the ionization potential of Si.¹² If the excess energies of processes 3 and 11 were the same, the electron affinity of Si would then be 0.8 eV, but this argument is of course highly conjectural.

3. *Positive Ions from Si₂H₆*. In Table IV the 70-eV mass spectrum of the monoisotopic Si₂²⁸H₆ is shown. The agreement with the published mass spectrum of Saalfeld and Svec^{6b} is fair in the upper mass region but not so in the lower. We find the intensities of *m/e*

Table IV: Positive Ion Mass Spectrum of Si₂H₆ at 70 eV

<i>m/e</i>	Ion	Intensity	% of natural peak that contains only Si ²⁸
29	SiH ⁺	23.4	98
30	SiH ₂ ⁺	9.8	86
31	SiH ₃ ⁺	18.9	94
56	Si ₂ ⁺	29.6	100
57	Si ₂ H ⁺	41.4	93
58	Si ₂ H ₂ ⁺	64.2	91
59	Si ₂ H ₃ ⁺	20.7	69
60	Si ₂ H ₄ ⁺	100.0	94
61	Si ₂ H ₅ ⁺	30.5	73
62	Si ₂ H ₆ ⁺	51.5	84

31, 30, 29 to be considerably higher than reported by these authors.^{6b} Since the relative intensities reported by Saalfeld and Svec^{6b} for *m/e* 31, 30, and 29 stand in similar discrepancy to those reported by Pupezin and Zmbov,¹³ we think that mass discrimination of low-mass ions may have been severe in the experiments of the former authors,^{6b} as indeed first suggested by them. The agreement of our appearance potential of SiH₃⁺ formation from Si₂H₆ with that reported by Steele and Stone⁵ supports our conclusion that impurities of SiH₄ in the Si₂H₆ are not playing a role in our experiments or theirs.⁵

The appearance potentials of all the mass peaks

(13) J. D. Pupezin and K. F. Zmbov, *Bull. Inst. Nucl. Sci. Boris Kindrich* (Belgrade), **8**, 89 (1958).

Table V: Energetics of Positive Ion Formation in Disilane^a

Ion	AP, eV	Process assigned	ΔH_f° (ion), kcal/mol
SiH ₂ ⁺	11.95 ± 0.10	Si ₂ H ₆ + e → SiH ₂ ⁺ + SiH ₄	285
SiH ₃ ⁺	11.95 ± 0.15	Si ₂ H ₆ + e → SiH ₃ ⁺ + SiH ₃	51 ^b
Si ₂ ⁺	13.0		...
Si ₂ H ⁺	12.90 ± 0.2	Si ₂ H ₆ + e → Si ₂ H ⁺ + 2H ₂ + H	263
Si ₂ H ₂ ⁺	11.80 ± 0.10	Si ₂ H ₆ + e → Si ₂ H ₂ ⁺ + 2H ₂	290
Si ₂ H ₃ ⁺	12.50 ± 0.10	Si ₂ H ₆ + e → Si ₂ H ₃ ⁺ + H ₂ + H	254
Si ₂ H ₄ ⁺	10.85 ± 0.10	Si ₂ H ₆ + e → Si ₂ H ₄ ⁺ + H ₂	268
Si ₂ H ₅ ⁺	11.40 ± 0.10	Si ₂ H ₆ + e → Si ₂ H ₅ ⁺ + H	229
Si ₂ H ₆ ⁺	10.15 ± 0.10	Si ₂ H ₆ + e → Si ₂ H ₆ ⁺	252

^a ΔH_f° (Si₂H₅) was taken to be 17.1 kcal/mol. (See ref *a* in Table I.) ^b ΔH_f° of SiH₂ free radical.

except *m/e* 28 and *m/e* 29 have been measured. The ionization-efficiency curves of all of the fragment ions from Si₂H₆ show a more-or-less strong tailing (most likely due in part to isotopic interferences) near onset and if point-by-point rpd measurements had been made, one would perhaps be tempted to approximate the continuous curve by linear segments, thereby creating breaks which in actuality do not exist. The continuous ionization-efficiency curves we obtain do not lead to this temptation and the considerable tailing completely obscures any structure near onset. Therefore, we report only the minimum onset potential of the positive ions from Si₂H₆. In Table V are presented the minimum appearance potentials of the ions, the process of formation assigned to the ion, and the heats of formation of the ions computed with the assumption of no excess energy. As usual, because of possibility of excess energy, these heats of formation are, in actuality, upper limits to the true values.

Our appearance potentials of SiH₃⁺ and SiH₂⁺ from Si₂H₆ are in excellent agreement with the values reported by Steele and Stone.⁵ Moreover, the values of ΔH_f° (SiH₂⁺) computed from the appearance potentials of this ion from SiH₄, and Si₂H₆ and the assigned processes (Tables I and V) are also in good agreement, suggesting that little excess energy is involved in the electron impact formation of SiH₂⁺ from both molecules. Assuming no excess energy in SiH₃⁺ formation from Si₂H₆ and SiH₄ we calculate a value of 51 kcal/mol for ΔH_f° (SiH₃⁺); this is in excellent agreement with the value of 49.5 reported by Steele, Nichols, and Stone.⁴ On the other hand, our value for A (SiH₃⁺) from Si₂H₆ is in serious disagreement with the value reported by Saalfeld and Svec.¹⁴ We do not understand the reason for this disagreement.

In measurements of the appearance potentials of the ions containing two silicon atoms, there is a problem of nonnegligible isotopic mass interference by ions of different chemical composition than that containing only the Si²⁸ isotope. The effect of this mass overlap is probably a major reason for the tailing observed in the ionization-efficiency curves and the magnitude of

the overlap at 70 eV for the various ions can be judged by inspection of the fourth column of Table V. The effect of this overlap on the accuracy of the onset potentials is difficult to assess, although it is quite clear that for those ions with the smallest overlap (larger the percentage in column 4 of Table V) the more accurate is the appearance potential. We do not think the effect of overlap on the appearance potentials is very serious, however, because from *m/e* 62 (84% being Si₂H₆⁺) we obtain the ionization potential of Si₂H₆ as 10.15 ± 0.10 eV which is in good agreement with the value of 10.6 ± 0.3 reported by Saalfeld and Svec.^{6b} In computing the ionic heats of formation shown in Table V we have assumed that this mass overlap has a negligible effect.

In a study of ion-molecule reactions in pure monosilane, Hess and Lampe¹⁰ reported that only the SiH₂⁺ ion reacts on collision with SiH₄ and the products of these collision reactions are SiH₃⁺, Si₂H⁺, Si₂H₂⁺, Si₂H₃⁺, Si₂H₄⁺, and Si₂H₅⁺; the SiH₃⁺ ion was found to be quite unreactive toward SiH₄, being formed by hydride ion transfer to SiH₂⁺ more rapidly than it could have been reacting with SiH₄. As is easily verified from the heats of formation of Tables I and V, all reactions of SiH₃⁺ with SiH₄ to form the product ions containing two silicon atoms are quite endothermic except the reaction forming Si₂H₅⁺ and H₂. It is possible that this latter reaction may, in fact, occur in monosilane (although it would not have been detectable in the experiments of Hess and Lampe¹⁰), but this is the only reaction of SiH₃⁺ that is energetically feasible and the extent of all reactions forming Si₂H₅⁺ is small.

All the reactions¹⁰ of ground-state SiH₂⁺ with SiH₄ are thermoneutral or exothermic except those producing Si₂H⁺ and Si₂H₃⁺. This means that these ions must be formed by collision of SiH₂⁺ ions that contain excess energy as electronic or vibrational energy. As already discussed, the ionization-efficiency curve of SiH₂⁺ shows a reproducible break at 13.0 ± 0.2 eV,

(14) F. E. Saalfeld and H. J. Svec, *Inorg. Chem.*, **3**, 1442 (1964).

Table VI: Cross Section of the First Resonance Peak of Si_2H_6

Ion	$\sigma_{\Sigma}, \text{cm}^2$	σ_1, cm^2	σ_2, cm^2
SiH^-	7.2×10^{-20}	2.5×10^{-20}	4.7×10^{-20}
SiH_2^-	8.7×10^{-20}	5.6×10^{-20}	3.1×10^{-20}
SiH_3^-	10.5×10^{-20}	6.3×10^{-20}	4.2×10^{-20}
Si_2^-	12.2×10^{-20}	6.0×10^{-20}	6.2×10^{-20}
Si_2H^-	5.4×10^{-20}	2.1×10^{-20}	3.3×10^{-20}
Si_2H_2^-	10.6×10^{-20}	6.4×10^{-20}	4.2×10^{-20}
Si_2H_3^-	5.4×10^{-20}	1.7×10^{-20}	3.7×10^{-20}
Si_2H_4^-	2.4×10^{-20}	1.0×10^{-20}	1.4×10^{-20}
Si_2H_5^-	1.0×10^{-20}	4.0×10^{-21}	6.0×10^{-21}

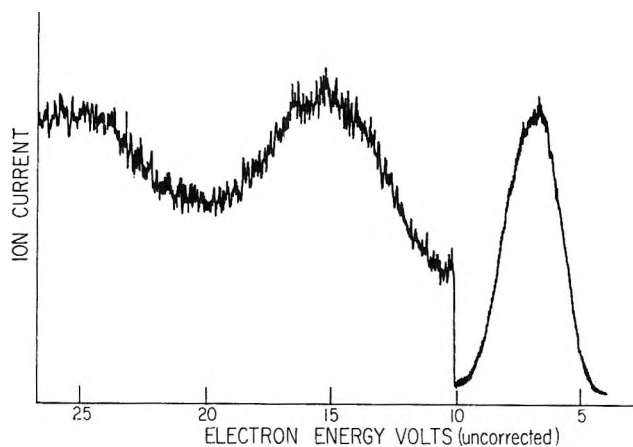
and if this break corresponds to formation of an excited state of SiH_2^+ , then reaction of SiH_2^+ , in this excited state, with SiH_4 would be energetically feasible. Alternatively, SiH_2^+ may retain sufficient vibrational energy from the electron impact process to make reactions with SiH_4 to form Si_2H^+ and Si_2H_3^+ feasible. For example, our data in Table I indicate that the decomposition reaction



is endothermic by 36 kcal. The occurrence of a metastable ion in monosilane at an apparent mass of 26.1 ($30^+ \rightarrow 28^+ + 2$), proves that some SiH_2^+ ions carry sufficient vibrational energy to undergo (12) and hence also may undergo reaction with SiH_4 to form Si_2H^+ and Si_2H_3^+ .

4. *Negative Ions form Si_2H_6^- .* The ionization-efficiency curves of the negative ions of Si_2H_6 are peculiar insofar as the energetic onsets of the resonance peaks and of the ion-pair production processes are independent of the particular ion being studied. A typical ionization-efficiency curve is shown in Figure 2.

This complete lack of specificity must mean that capture of the electron in a Franck-Condon transition yields such a highly excited Si_2H_6^- ion that all dissociation channels are energetically possible and the intensities of the various peaks are determined solely by the shape of the potential energy surface. In the case of pair production processes, the observation must mean that Franck-Condon excitation to the lowest state of Si_2H_6^* that correlates with ionic fragments results in sufficient excitation for all the ionic dissociation channels to be possible. It is clear that no

Figure 2. Ionization-efficiency curves of SiH_3^- from Si_2H_6 .

useful thermochemical data can be derived from the onsets found in these ionization-efficiency curves.

Upon closer inspection of the first resonance peak it is found that in actuality it consists of two overlapping resonance peaks. Defining the cross section of the low-energy component of the doublet by σ_1 and that of the high-energy component by σ_2 we have resolved this resonance peak into its two components, with the aid of a DuPont curve resolver, and give the cross sections at the two peaks for the various ions in Table VI. The relative intensities of the two components differ from ion to ion but the significance of this is not clear.

Acknowledgment. This work was supported by Contract No. AT(30-1)-3570 with the U. S. Atomic Energy Commission. We also wish to thank the National Science Foundation for providing funds to assist in the original purchase of the mass spectrometer.

A Kinetic Investigation of an Isomerization of

Aqueous Lysozyme near Neutral pH¹

by Jeffrey D. Owen, Edward M. Eyring,² and David L. Cole

Department of Chemistry, University of Utah, Salt Lake City, Utah 84112 (Received May 8, 1969)

The temperature-jump relaxation method was used to study the kinetics of an isomerization of aqueous lysozyme at 10 and 25° near neutral pH. A single relaxation time τ of the order of 2 msec was observed and identified on the basis of its pH dependence with an ionizable group in the protein having a $pK = 7.3$. A deuterium oxide solvent kinetic isotope effect (k_{H_2O}/k_{D_2O}) = 2.5 at 25° indicates that protons are involved in the isomerization mechanism. The possibility that a reported dimerization of lysozyme under similar conditions of protein concentration and pH is responsible for the observed relaxation has been ruled out.

Introduction

In the egg white lysozyme molecule there are 129 amino acid residues cross-linked by four disulfide bridges on a single polypeptide chain.^{3,4} Although lysozyme was the first enzyme for which the three dimensional structure was resolved to 2 Å by X-ray diffraction,⁵ there is still much to be learned regarding the specific interactions between amino acid residues in aqueous solution. The present kinetic study indicates that aqueous lysozyme in the absence of substrate and near neutral pH "isomerizes" to the extent of rapidly exposing a new acid group to solution when subjected to a $\sim 10^\circ$ temperature jump.

Experimental Section

Worthington salt-free, twice recrystallized chicken egg white lysozyme was used without further purification after an analytical amberlite column chromatography run showed that over 95% of the material emerged as a single sharp peak on an absorbance (280 nm) vs. time graph. We effected this separation with sodium form Bio-Rex 70 (200–400 mesh) analytical grade cation exchange resin in a 0.9×20 cm Sephadex column using a 0.2 M potassium phosphate buffer (pH 7.09) as eluent. We checked enzyme concentrations on a Cary Model 14 spectrophotometer at 280 nm where the extinction coefficient is 26.0 for a 1% by weight aqueous lysozyme solution.^{6–8} Eastman phenolsulfonephthalein (phenol red) and 3',3''-dichlorophenolsulfonephthalein (chlorophenol red) were purified by reprecipitation⁹ and used as colorimetric indicators at 560 and 580 nm, respectively. Matheson Coleman and Bell *p*-nitrophenol was also used in a few of our kinetic experiments at a wavelength of 420 nm.

A single-beam temperature-jump apparatus closely resembling that of Hammes and Steinfeld¹⁰ was used to perturb the aqueous lysozyme equilibrium. Sample solutions were prepared with boiled, demineralized, distilled water made 0.1 M in KCl to facilitate rapid

heating. A Beckman 1019 Research pH meter was used to determine the pH of sample solutions. Freshly prepared lysozyme solutions were used in all cases, and relaxation times obtained from only the first half-dozen 25-kV 0.1- μ F pulses of a given sample solution were retained in our compilation of data (Table I and Figures 1 and 2). Blank solutions containing indicator and KCl but no protein were tested for the absence of detectable relaxation times before each sample run. Relaxation times were obtained from the exponential oscilloscope traces using semilogarithmic plots of absorbance vs. time to verify the presence of only one relaxation.

HCl and KOH were used to adjust pH of the aqueous sample solutions, while the pD of solutions in D₂O was varied with KOD. The purity of the Columbia D₂O was checked by adding known amounts of water to D₂O and noting the increased nmr signal amplitude on a Varian A-60 spectrometer. Signals extrapolated back to zero amplitude indicated less than 1% H₂O initially present in the D₂O.

Results

In Figures 1 and 2 we have displayed the relaxation times measured in water at 10 and 25° and in D₂O at 25° with solutions that were 8×10^{-4} M in lysozyme

(1) Supported in part by Grant AM 06231 from the National Institute of Arthritis and Metabolic Diseases.

(2) To whom reprint requests should be sent.

(3) J. Jolles, J. Jauregui-Adell, I. Bernier, and P. Jolles, *Biochim. Biophys. Acta*, **78**, 668 (1963).

(4) R. E. Canfield, *J. Biol. Chem.*, **238**, 2698 (1963).

(5) D. C. Phillips, *Proc. Nat. Acad. Sci. U. S.*, **57**, 484 (1967).

(6) R. A. Bradshaw, L. Kanarek, and R. L. Hill, *J. Biol. Chem.*, **242**, 3789 (1967).

(7) N. Arnheim, Jr., and A. C. Wilson, *ibid.*, **242**, 3951 (1967).

(8) C. O. Stevens, H. E. Sauberlich, and G. R. Bergstrom, *ibid.*, **242**, 1821 (1967).

(9) W. R. Ordorff and R. W. Sherwood, *J. Amer. Chem. Soc.*, **45**, 486 (1923).

(10) G. G. Hammes and J. I. Steinfeld, *ibid.*, **84**, 4639 (1962).

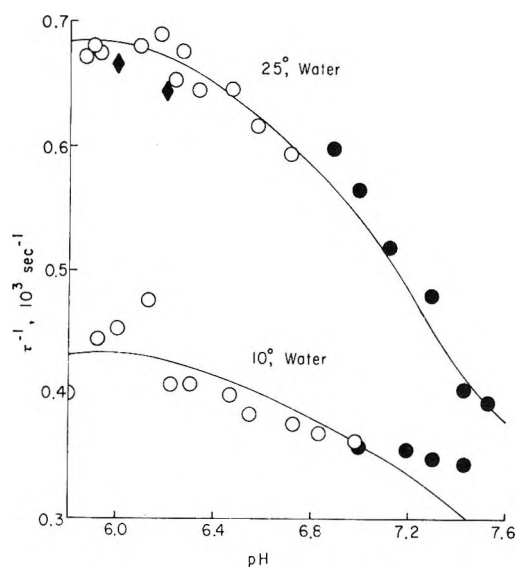


Figure 1. Lysozyme isomerization in water at 25° and 10°. Enzyme concentration is 0.8 mM. Open circles and filled circles denote τ^{-1} values obtained with 0.02 mM chlorophenol red and 0.02 mM phenol red, respectively. Diamond shaped points on the 25° curve denote τ^{-1} values obtained with 0.54 mM *p*-nitrophenol. The solid line is a theoretical curve obtained by an iterative least-squares analysis of eq 20 of the text.

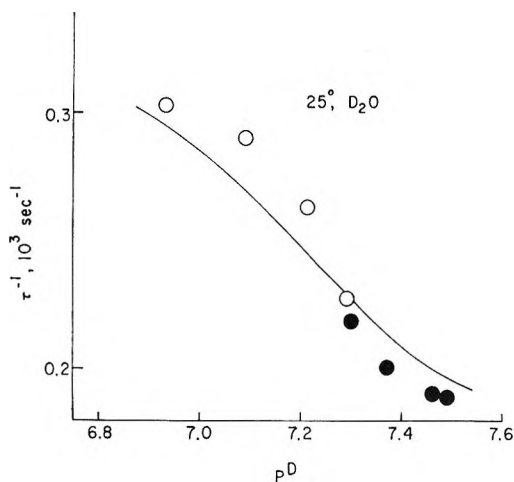


Figure 2. Lysozyme isomerization in heavy water at 25°. Enzyme concentration is 0.8 mM. Open circles and filled circles denote τ^{-1} values obtained with 0.2 mM chlorophenol red and 0.02 mM phenol red, respectively. The solid line is a theoretical curve obtained by an iterative least-squares analysis of eq 20.

(assuming 14,400 for the molecular weight¹¹), 2×10^{-5} M in chlorophenol red or phenol red, or 5.4×10^{-4} M in *p*-nitrophenol, and 0.1 M in KCl. Values of pD are taken to be the glass electrode pH vs. sce plus 0.4 pH unit. In Table I we give additional relaxation times measured in water at 25° for other concentrations of enzyme and indicator.

In a typical relaxation experiment at 8×10^{-4} M lysozyme, pH 7.15, 2×10^{-5} M phenol red, and 0.1

Table I: Joule Heating Temperature-Jump Relaxation Times Measured in Aqueous Lysozyme Solutions at 25° and Ionic Strength $\mu = 0.1$ M Adjusted with KCl

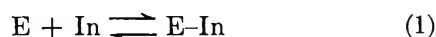
$c_0,^a 10^{-4} M$	pH ^b	$c_0',^c 10^{-5} M$	$\tau,^d msec$
4.0	7.18	2	1.65
4.0	7.18	2	1.85
8.0	7.11	2	1.85
16.0	7.11	2	1.95
16.0	7.11	2	1.63
16.0	7.13	2	1.50
35.0	7.04	2	2.00
33.0	7.04	2	1.85
8.0	7.00	2	1.90
8.0	7.02	2	1.51
7.0	7.00	2	2.00
6.7	7.04	2	2.00
7.7	7.19	6	1.90
7.9	7.16	4	1.93
8.0	7.19	2	1.83

^a Total molar concentration of lysozyme calculated on the basis of a molecular weight of 14,400. ^b Glass electrode pH of the sample solution. ^c Molar concentration of phenol red indicator. ^d Experimental relaxation time in milliseconds.

M KCl, the amplitude of the effect was observed to be 25 mV in the direction of increasing absorbancy. Light-to-dark signal and peak-to-peak high-frequency noise under these typical conditions were 24.0 V and 45 mV, respectively.

Chipman and Schimmel¹² recently made a temperature-jump relaxation rate study of oligosaccharide binding at the active site of hen egg white lysozyme. They observed no relaxation in the 10 μ sec to 100 msec time range when 2 to 8×10^{-5} M lysozyme and 5.4×10^{-4} M *p*-nitrophenol but no oligosaccharide was present in their pH 6.0, 0.1 M aqueous NaCl sample solutions. However, their null result does not preclude the observability of relaxations in this time range at substantially higher concentrations of lysozyme. When the lysozyme concentration is increased to 8×10^{-4} M, a relaxation does appear with 5.4×10^{-4} M *p*-nitrophenol (pH 6.0, λ 420 nm, ionic strength $\mu = 0.1$ M). As is evident from the diamond shaped points of Figure 1, this relaxation in the presence of *p*-nitrophenol is consistent with those observed using chlorophenol red indicator.

One possible explanation for the observed relaxations would be the binding of indicator to enzyme



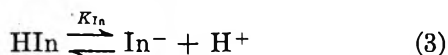
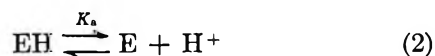
However, the following experiments tend to rule out this possibility: At 580 nm the light absorbance of 5×10^{-4} M lysozyme plus 2×10^{-5} M chlorophenol red (pH 6.14 in 0.1 M aqueous KCl) equals the sum

(11) A. J. Sophianopoulos, C. K. Rhodes, D. N. Holcomb, and K. E. Van Holde, *J. Biol. Chem.*, **237**, 1107 (1962).

(12) D. M. Chipman and P. R. Schimmel, *ibid.*, **243**, 3771 (1968).

of the absorbances of separate aqueous lysozyme and chlorophenol red solutions at the same conditions of pH and ionic strength to within 0.002 absorbance unit measured on a Cary Model 14 spectrophotometer. A similar result is obtained with $5 \times 10^{-4} M$ lysozyme and $2 \times 10^{-5} M$ phenol red at pH 7.12 and 560 nm. Thus, there is no spectral evidence of indicator-enzyme binding at concentrations like those of our kinetic study. Also, the measured relaxation times were independent of indicator concentration within the approximately $\pm 10\%$ precision of measurement of relaxation times. It can be shown that for a reaction involving indicator to lysozyme binding the relaxation time would decrease with increasing enzyme concentration.

Sedimentation equilibrium data indicate¹³ that aqueous lysozyme (0.15 M KCl and 23°) undergoes rapid, reversible dimerization in the pH range 5 to 9 at protein concentrations of ~ 1.5 g/100 ml. Increasing the pH leads to further polymerization above pH 11. These authors¹³ conclude that dimerization occurs principally between two monomers each of which has lost a proton from a group of $pK_a = 6.2$. Upon dimerization, the pK_a of this group is shifted below 5.4. They explicitly reject an alternative mechanism in which an isomerization rather than dimerization is the pH dependent step. Light-scattering data¹⁴ confirm the existence of a rapid, reversible dimerization near pH 7 that proceeds to higher polymers for lysozyme concentrations in excess of 2% by weight. The reported¹⁴ monomer-dimer equilibrium constant is $K = 5 \times 10^2 M^{-1}$. Thus, we need to test the fit of our relaxation data by the mechanism



where we assume that each of the first two protolytic reactions are so rapid as to lie outside the time range accessible to our Joule heating temperature jump apparatus.

Deleting superscript electronic charges for simplicity and denoting small instantaneous changes in dimer concentration by δE_2 , the equilibrium concentration by \bar{E}_2 , etc., it follows from the rate expression

$$\frac{d\delta E_2}{dt} = 2k_1\bar{E}\delta E - k_{-1}\delta E_2 \quad (5)$$

and the conservation relations

$$-\delta E = \delta EH + 2\delta E_2 \quad (6)$$

$$-\delta H = \delta EH + \delta HIn \quad (7)$$

$$-\delta In = \delta HIn \quad (8)$$

$$K_{In}\delta HIn = \bar{In}\delta H + \bar{H}\delta In \quad (9)$$

$$K_a\delta EH = \bar{E}\delta H + \bar{H}\delta E \quad (10)$$

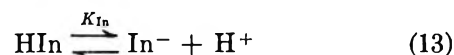
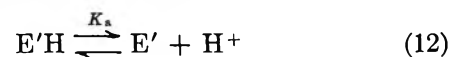
that the relaxation time τ is given by

$$1/\tau = \frac{4k_1\bar{E}}{\bar{H}(K_{In} + \bar{H} + \bar{In})} + k_{-1} \quad (11)$$

$$1 + \frac{K_a(K_{In} + \bar{H} + \bar{In}) + \bar{E}(K_{In} + \bar{H})}{K_a(K_{In} + \bar{H} + \bar{In}) + \bar{E}(K_{In} + \bar{H})}$$

A slope-intercept plot of all the 25° data of Table I and of Figure 1 yields an unacceptable negative value of k_1 indicating that our postulated dimerization mechanism, eq 2-4, does not apply. The values of pK_{In} used in these calculations were¹⁵ 5.98 and 7.78 for chlorophenol red and phenol red, respectively. The fact that the dimerization mechanism does not fit our experimental data should not be misconstrued as evidence that the well documented dimerization does not occur. It may lie outside the 0.02-100-msec range accessible to us.

Now let us consider an isomerization mechanism that exposes an ionizing group like the one French and Hammes¹⁶ proposed for aqueous ribonuclease.



Here we assume that the slow, observed relaxation time is associated with the conformational change of EH to its isomer E'H. Combining the conservation relations

$$\delta EH + \delta E'H + \delta E' = 0 \quad (15)$$

$$K_a\delta E'H = \bar{H}\delta E' + \bar{E}'\delta H \quad (16)$$

$$-\delta H = -\delta E' - \delta In \quad (17)$$

with eq 8 and 9, we obtain from

$$\frac{-d\delta EH}{dt} = k_1\delta EH - k_{-1}\delta E'H \quad (18)$$

the relaxation time

$$1/\tau = k_1 + \frac{k_{-1}}{1 + \frac{K_a}{\bar{H} + \frac{\bar{E}'(K_{In} + \bar{H})}{K_{In} + \bar{H} + \bar{In}}}} \quad (19)$$

(13) A. J. Sophianopoulos and K. E. Van Holde, *J. Biol. Chem.*, **239**, 2516 (1964).

(14) M. R. Bruzzesi, E. Chiancone, and E. Antonini, *Biochemistry*, **4**, 1796 (1965).

(15) I. M. Kolthoff, *J. Phys. Chem.*, **34**, 1466 (1930).

(16) T. C. French and G. G. Hammes, *J. Amer. Chem. Soc.*, **87**, 4669 (1965).

Since we do not know the equilibrium constant k_1/k_{-1} *a priori*, we cannot calculate \bar{E} , and thus are unable to use eq 19. Instead we adopt the assumption of French and Hammes¹⁶ that the enzyme concentration is high enough to act as a pH buffer and hence $\delta H = 0$. We then obtain in place of eq 19 the similar, yet simpler expression (eq 8 of French and Hammes¹⁶)

$$1/\tau = k_1 + \frac{k_{-1}}{1 + \frac{K_a}{\bar{H}}} \quad (20)$$

The solid lines in Figures 1 and 2 are theoretical curves obtained from an iterative least-squares analysis of eq 20. Initially, values for k_1 , k_{-1} , and K_a were assumed and the root-mean-square error in τ^{-1} at $\text{pH} = \text{p}K_a$ was plotted against the assumed value for $\text{p}K_a$. A minimum in this curve for lysozyme in water at 25° was seen at $\text{p}K_a = 7.3$. The values for k_1 and k_{-1} obtained using this iterative least-squares method are listed in Table II. The accuracy of the

Table II: Temperature-Jump Lysozyme Isomerization Rate Constants Deduced from Eq 20

Condition	k_1, sec^{-1}	k_{-1}, sec^{-1}	$\text{p}K_a$
H ₂ O, 25°	210	495	7.3
H ₂ O, 10	155	285	7.4
D ₂ O, 25	83	290	7.3

rate constants and $\text{p}K$ values is estimated to be not better than $\pm 15\%$. The values of $k_{\text{H}_2\text{O}}/k_{\text{D}_2\text{O}}$ for k_1 and k_{-1} were 2.5 and 1.7, respectively. The activation parameters for k_1 and k_{-1} at 25° are, respectively, ΔG° , 14.2 and 13.8 kcal/mol; ΔH° , 3.4 and 6.1 kcal/mol; and ΔS° , -37 and -26 eu. The thermodynamic parameters for the isomerization at 25° are $\Delta G^\circ = 0.4$ kcal/mol, $\Delta H^\circ = -2.7$ kcal/mol, and $\Delta S^\circ = -11$ eu.

Discussion

From the preceding treatment of our experimental relaxation times we have concluded that τ is attributable to an isomerization rather than a dimerization or indicator-enzyme interaction. Although recent

conformational studies by solvent perturbation have been concerned with specific residue interactions in lysozyme, the detailed description of the isomerization or isomerizations is still unknown.¹⁷⁻¹⁹ In Table III

Table III: $\text{p}K$ Values for Buried Groups in Ribonuclease and Lysozyme

Ribonuclease	Solvent perturbation	6.5	Timasheff and Gorbunoff ²⁰
Ribonuclease	Temperature jump	6.1	French and Hammes ¹⁶
Lysozyme	Solvent perturbation	6.8	Timasheff and Gorbunoff ²⁰
Lysozyme	Temperature jump	7.3	This work

we compare results of recent solvent perturbation-titration studies of ribonuclease and lysozyme histidine residues,²⁰ a temperature-jump relaxation method study of ribonuclease,¹⁶ and our present temperature-jump study of lysozyme.

The deuterium isotope effect for k_1 and k_{-1} indicates that one or more protons are involved in the isomerization. It is possible that the structure of lysozyme is different in D₂O than in water, but it has been shown that the activity and stability of this enzyme were unaltered in heavy water.²¹

There are no striking dissimilarities between the thermodynamic quantities reported here and those for ribonuclease.¹⁶ On the other hand, the solvent kinetic isotope effects are somewhat smaller than for ribonuclease isomerization and are more consistent with those obtained in temperature jump studies of intramolecular hydrogen bond breaking in simple organic acids.²²

(17) E. J. Williams and M. Laskowski, Jr., *J. Biol. Chem.*, **240**, 3580 (1965).

(18) E. J. Williams, T. T. Herskovits, and M. Laskowski, Jr., *ibid.*, **240**, 3574 (1965).

(19) K. Hamaguchi, K. Hayashi, and T. Imoto, *J. Biochem. (Tokyo)*, **55**, 24 (1964).

(20) S. N. Timasheff and M. J. Gorbunoff, *Ann. Rev. Biochem.*, **36**, 13 (1967).

(21) D. Shugar and E. Gajewsha, *J. Polymer Sci.*, **31**, 281 (1958).

(22) J. L. Haslam and E. M. Eyring, *J. Phys. Chem.*, **71**, 4470 (1967).

Infrared Spectra and Bonding in the Sodium Superoxide and Sodium Peroxide Molecules

by Lester Andrews

Chemistry Department, University of Virginia, Charlottesville, Virginia 22901 (Received May 12, 1969)

Sodium superoxide has been produced for infrared spectral study by condensing sodium atoms and oxygen molecules at high dilution in argon on a CsI window at 15°K. Use of oxygen isotopic mixtures and comparison with lithium superoxide verify the molecular identity and indicate a symmetrical triangular structure. Nine frequencies from three isotopic molecules determine the potential constants $F_{O-O} = 5.46 \pm 0.05$, $F_{Na-O} = 0.80 \pm 0.02$, $F_{Na-O,Na-O} = -0.12 \pm 0.02$ mdyn/Å. The oxygen-oxygen stretching force constant for NaO₂ is near those for LiO₂ and O₂⁻ which suggests that the NaO₂ molecule is highly ionic and may consist of a sodium cation bonded to a superoxide anion by coulombic forces. Further reaction of NaO₂ with sodium atoms produces NaO₂Na which has been identified and compared to lithium peroxide.

Introduction

Recently, we have produced the lithium superoxide^{1,2} and lithium peroxide² molecules for infrared spectral study by the reaction of lithium atoms and oxygen molecules using the matrix isolation technique. Mixed oxygen isotopic experiments indicate that LiO₂ has C_{2v} symmetry, and the oxygen-oxygen stretching force constant agrees with that calculated for the isolated superoxide ion from Raman spectra.³ This comparison suggests ionic bonding between a lithium cation and superoxide anion in the lithium superoxide molecule. Indeed, LiO₂ is a unique molecule, and the infrared spectra of further alkali metal analogs are of interest to determine the generality of the bonding and structure found for LiO₂.

The symmetrical bonding of molecular oxygen to a metal atom has been observed in several of the more reactive complexes. The oxygen-oxygen distance and the tendency to bond oxygen increase as the ancillary ligands become more electron releasing. Oxygen-oxygen distances of 1.30 and 1.51 Å have been reported^{4,5} which correspond, respectively, to the superoxide and peroxide internuclear distances. The catalytic⁶ and possible biochemical⁴ usefulness of these compounds have been recently discussed.

Reaction of sodium with excess oxygen gives mainly the peroxide. Further oxidation at 500° and 300 atm produces the superoxide, but the resulting product is a mixture of crystalline sodium superoxide and sodium peroxide.⁷ X-Ray diffraction measurements on crystalline NaO₂ yield an oxygen-oxygen internuclear distance of 1.33 ± 0.05 Å in the superoxide anion,⁸ and in NaO₂Na crystal an O-O distance of 1.50 ± 0.03 Å is found for the peroxide anion.⁹ Infrared spectra of crystalline NaO₂ and NaO₂Na showed no absorption¹⁰ due to the homopolar nature of the superoxide and peroxide anions. The infrared spectra of molecular

NaO₂ and NaO₂Na are of interest for comparison to those of their analogous lithium compounds and for observation of sodium-oxygen vibrational frequencies which have heretofore not been reported. Accordingly, we have prepared the NaO₂ and NaO₂Na molecules for infrared spectral study using the matrix reaction of sodium atoms and oxygen molecules.

Experimental Section

The 15°K refrigeration system, vacuum vessel, alkali metal atom source, and experimental technique have been described earlier.¹¹ Sodium metal (J. T. Baker, lump), oxygen gas (Linde, welding) and isotopically enriched oxygen 99.3% ¹⁸O₂ (O.R.N.L.) were used without purification. The oxygen isotopic mixture ¹⁸O₂-¹⁶O¹⁸O-¹⁸O₂ was prepared by discharging equimolar amounts of ¹⁶O₂ and ¹⁸O₂ for 6 hr in a 3-l. bulb using a tesla coil.

A fresh 6-mm cube of sodium metal was cut under an argon atmosphere, washed with dry hexane, dried by evaporation, and placed in the Knudsen cell which was sealed with a tantalum gasket. The Knudsen cell was positioned in a resistance wire wound ceramic heater, and the vacuum vessel was immediately evacuated.

- (1) L. Andrews, *J. Amer. Chem. Soc.*, **90**, 7368 (1968).
- (2) L. Andrews, *J. Chem. Phys.*, **50**, 4228 (1969).
- (3) J. Rolfe, W. Holzer, W. F. Murphy, and J. H. Bernstein, *ibid.*, **49**, 963 (1968).
- (4) S. J. La Placa and J. A. Ibers, *J. Amer. Chem. Soc.*, **87**, 2581 (1965).
- (5) I. A. McGinnety and J. A. Ibers, *Chem. Commun.*, 235 (1968).
- (6) J. P. Collman, *Accounts Chem. Res.*, **1**, 136 (1968).
- (7) S. E. Stephanou, W. H. Schechter, W. J. Arsinger, Jr., and J. Kleinberg, *J. Amer. Chem. Soc.*, **71**, 1819 (1949).
- (8) H. H. Templeton and C. H. Dauben, *ibid.*, **72**, 2251 (1950).
- (9) H. Floppl, *Z. Anorg. Allg. Chem.*, **291**, 12 (1957).
- (10) E. G. Brame, Jr., S. Cohen, J. L. Margrave, and W. V. Meloche, *J. Inorg. Nucl. Chem.*, **4**, 90 (1957).
- (11) L. Andrews, *J. Chem. Phys.*, **48**, 972 (1968).

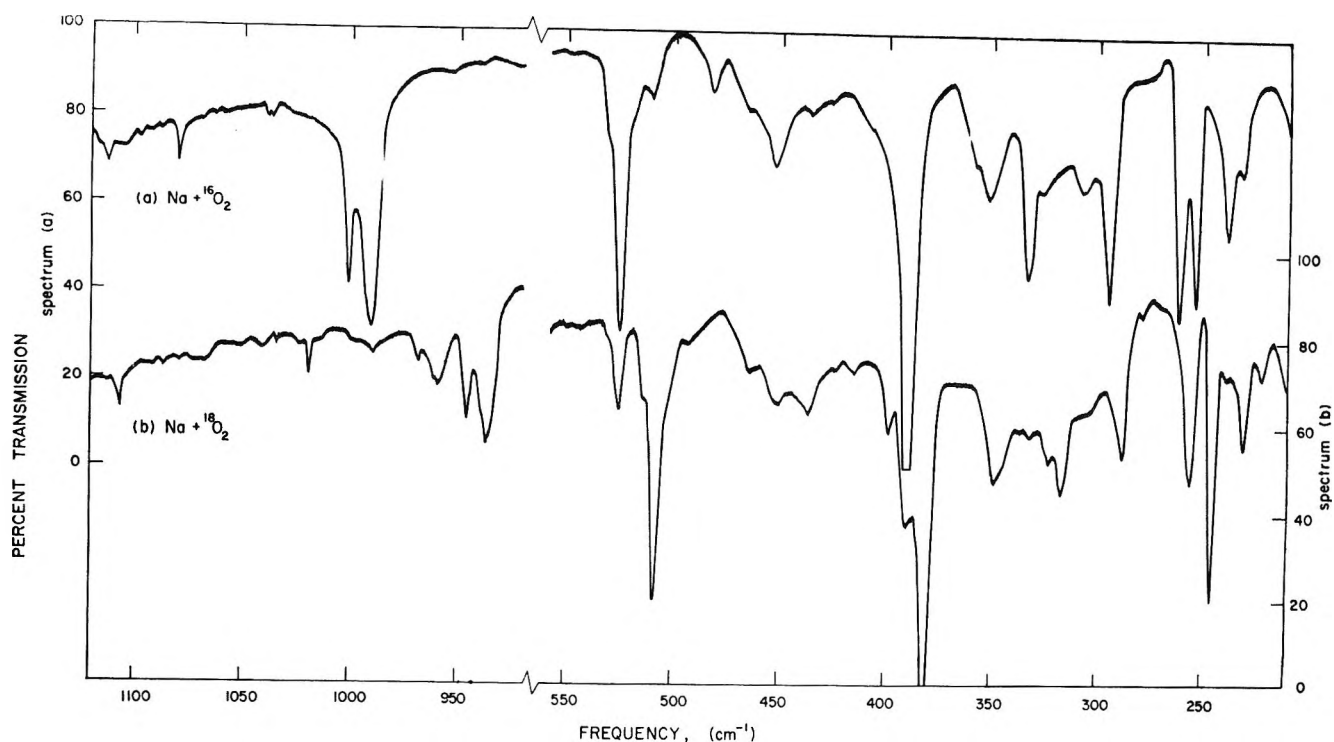


Figure 1. Infrared spectra in the 210–560- and 920–1120- cm^{-1} spectral regions for sodium atoms deposited with oxygen molecules in an argon matrix at 15°K: spectrum a, $\text{Ar}/^{16}\text{O}_2 = 100$, $\text{Ar}/\text{Na} \approx 200$; spectrum b, $\text{Ar}/^{18}\text{O}_2 = 150$, $\text{Ar}/\text{Na} \approx 200$.

After cooling the sample window to 15°K, the deposition of oxygen in argon ($M/R = 100:1$ to $300:1$) or pure oxygen at 2.0 mmol/hr was started, and the Knudsen cell was warmed to 240° where the vapor pressure of sodium is near 1μ .¹² Deposition times for the argon matrix experiments typically ranged from 20 to 30 hr. Infrared spectra were recorded during and after sample deposition on a Beckman IR-12 filter-grating spectrophotometer in the 200–2000- cm^{-1} spectral region. In certain experiments the deposited sample was warmed to near 40°K by bucking the refrigerator with electrical heaters after which it was allowed to recool to 15°K. During this operation the sample window temperature was monitored with a gold–2.1% cobalt *vs.* copper thermocouple. Frequency accuracy is $\pm 0.5 \text{ cm}^{-1}$ with spectral slit widths near 0.8 cm^{-1} at 1100, 900, and 700 cm^{-1} , 2.4 cm^{-1} at 500 cm^{-1} , and 4.0 cm^{-1} at 300 cm^{-1} .

Results

Argon Matrix. A sample of oxygen was deposited in argon ($\text{Ar}/\text{O}_2 = 100$) without alkali metal, and no infrared absorptions were observed in addition to the usual traces of CO_2 and H_2O . Figure 1 contrast spectra in the 210–560 and 920–1120- cm^{-1} spectral regions for samples of oxygen (a) $\text{Ar}/^{16}\text{O}_2 = 100$ and (b) $\text{Ar}/^{18}\text{O}_2 = 150$ deposited with sodium ($\text{Ar}/\text{Na} \approx 200$), which illustrates the oxygen isotopic shifts. The observed frequencies and optical densities are listed in Table I.

Figure 2 shows the spectrum recorded for the major absorptions using a 1:2:1 mixture of $^{16}\text{O}_2$ – $^{16}\text{O}^{18}\text{O}$ – $^{18}\text{O}_2$

Table I: Infrared Absorptions (cm^{-1}) Produced by the Reaction of Sodium Atoms and Oxygen Molecules in an Argon Matrix^a

$\text{Na} + ^{16}\text{O}_2$ $\text{Ar}/\text{O}_2 = 200$	$\text{Na} + ^{18}\text{O}_2$ $\text{Ar}/\text{O}_2 = 150$	Concentration ^b effects Na/O_2	Diffusion ^c behavior
1112.5 (0.04)	1106.5 (0.04)	Dec ^d	Con
1080.0 (0.05)	1019.1 (0.04)	Con/con	Dec
1001.0 (0.43)	946.0 (0.16)	Con/dec	Inc
991.0 (0.61)	936.8 (0.19)	Con/dec	Inc
524.5 (0.53)	507.4 (0.58)	Dec/inc	Dis
453 (0.08)	451 (0.05)	^e	Con
390.7 (0% T) ^f	381.5 (0% T)	Reference	Dec
350 (0.11)	348 (0.18)	^f	Inc
332.8 (0.24)	317.8 (0.16)	Con/con	Dec
295.5 (0.32)	289.0 (0.16)	Con/con	Inc
262.0 (0.58)	256.4 (0.29)	Dec/inc	Inc
254.0 (0.47)	246.0 (0.68)	Dec/inc	Dis
239.0 (0.28)	231.0 (0.18)	Dec/inc	Dis
232 (0.16)	223 (0.06)	Dec/inc	Con

^a Optical densities are shown parenthetically. ^b Changes (decrease, increase, or constant) in relative intensities between experiments relative to data in first column of this table using 390.7- cm^{-1} band as an internal reference. ^c Bands increased, decreased, disappeared, or remained constant on diffusion. ^d Not observed in appropriate experiment. ^e Quantitative measurement of broad bands not possible. ^f The relative optical densities of the 390.7-, 332.8-, and 1080.0- cm^{-1} bands measured before the 390.7- cm^{-1} band became completely absorbing were 40:4:1.

(12) W. T. Hicks, *J. Chem. Phys.*, **38**, 1873 (1963). The equilibrium vapor contained less than 0.4% Na_2 at 500°K as calculated from thermodynamic data tabulated by W. H. Evans, R. Jacobson, T. R. Munson, and D. D. Wagman, *J. Res. Natl. Bur. Stand.*, **55**, 83 (1955).

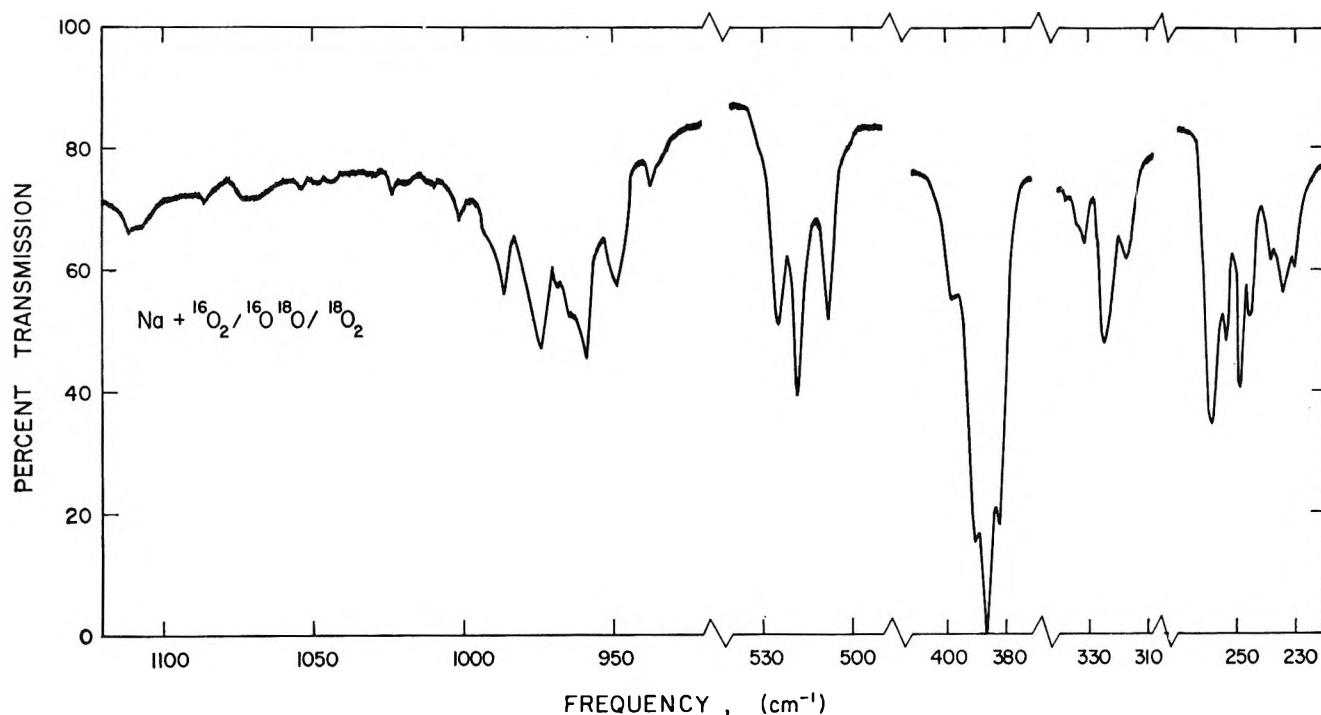


Figure 2. Infrared spectra showing oxygen isotopic splittings for sodium atoms deposited with a 1:2:1 mixture of $^{16}\text{O}_2$ - $^{16}\text{O}^{18}\text{O}$ - $^{18}\text{O}_2$ in argon ($\text{Ar}/\text{O}_2 = 100$, $\text{Ar}/\text{Na} \approx 200$) at 15°K .

Table II: Major Infrared Absorptions Produced by the Reaction of Sodium Atoms with a 1:2:1 Mixture of $^{16}\text{O}_2$ - $^{16}\text{O}^{18}\text{O}$ - $^{18}\text{O}_2$ in an Argon Matrix with $\text{Ar}/\text{O}_2 = 100$

Absorptions, cm^{-1}	Absorptions, cm^{-1}
1001.0	332.6
991 (sh)	325.2
986.5	317.5
975.0	
963.5 (sh)	
959.5	259.5
948.5	
936.5	
524.0	254.3
518.0	249.7
507.4	246.0
390.3	239.0
386.7	235.0
381.5	231.0

($\text{Ar}/\text{O}_2 = 100$) deposited with sodium ($\text{Ar}/\text{Na} \approx 200$), and the frequencies are listed in Table II. Additional experiments were run with $\text{Ar}/\text{O}_2 = 100$, $\text{Ar}/\text{Na} \approx 800$, $\text{Ar}/\text{O}_2 = 150$, $\text{Ar}/\text{Na} \approx 200$, and $\text{Ar}/\text{O}_2 = 300$, $\text{Ar}/\text{Na} \approx 300$ in order to study the effect of concentration of both sodium atoms and oxygen molecules on the relative intensities of the absorptions produced in these experiments. The behavior of the absorptions in these experiments is summarized under concentration effects in Table I by listing the change in band intensity *relative* to the 390.7-cm^{-1} band when the sodium concentra-

tion is decreased at constant oxygen concentration and when oxygen concentration is decreased at constant sodium concentration. During all of the above experiments the bands at 1080.0 , 390.7 , and 332.8 cm^{-1} maintain approximately constant relative intensities as do the three absorptions at 524.5 , 254.0 , and 239.0 cm^{-1} .

Oxygen Matrix. Two experiments were run trapping sodium vapor in an oxygen matrix using evaporation temperatures of 221 and 249° . The observed frequencies and optical densities are listed in Table III. Obviously, an oxygen matrix provides the upper limit on oxygen concentration. Several of the absorptions

Table III: Infrared Absorptions (cm^{-1}) Produced by the Reaction of Sodium Atoms in an Oxygen Matrix^a

Knudsen cell t , $^\circ\text{C}$	249 ± 3		221 ± 2		
	Approximate O_2/Na		500		
Deposition, T , $^\circ\text{K}$	15		15		Warm to 37
	b				
	1080.8 (0.09) ^d		1109 (0.13)	(0.08) ^c	
	998 (0.44)		1081.0 (0.085)	(0.02)	
	351 (0.23)		998 (0.18)	(0.03)	
	306.0 (1.0) ^d		350 (0.15)	(0.20)	
	259.5 (0.42) ^d		306.0 (0.90)	(0.15)	
	242.6 (0.13)		259.0 (0.32)	(0.06)	
			242.8 (0.11)	(0.00)	

^a Optical densities are shown parenthetically. ^b Not observed here. ^c Optical densities recorded after warming sample to 37°K and recooling to 15°K . ^d Assigned, respectively, to ν_1 , ν_2 , and ν_3 of NaO_2 in an oxygen matrix.

produced in the argon matrix reaction are not observed in the oxygen matrix as comparison of Tables I and III shows.

Diffusion Experiments. When the argon matrix samples are warmed to 38–40°K and recooled to 15°K, the absorptions listed in Table I remain approximately constant, increase, or decrease in intensity or disappear completely. The diffusion operation is accompanied by increased light scattering and poorer spectral operating conditions; however, certain trends are clear, and the diffusion behavior of the observed absorptions is summarized in Table I. After warming the oxygen matrix samples to 36–37°K and recooling to 15°K, most of the absorptions decrease in intensity as is shown in Table II.

Discussion

We are interested in identifying the molecular species responsible for the infrared absorptions reported here and determining their structures and vibrational potential constants.

Identification of New Molecular Species. In the previous study^{1,2} of the reaction of lithium atoms with oxygen molecules, mixed lithium isotopic experiments showed that the major product species contained a single lithium atom, and that the second most intense absorptions were due to a species containing two equivalent lithium atoms. Unfortunately sodium has only one stable isotope so we are left with concentration variation studies to determine the number of sodium atoms present in the species observed here. In the lithium work, conclusions from mixed lithium isotopic experiments parallel those from concentration variation experiments.

NaO₂. The 390.7-cm⁻¹ band is by far the most intense feature observed in the reaction of sodium atoms with oxygen molecules in an argon matrix, and we attribute it to the species NaO₂ since the most intense band in lithium–oxygen experiments was due to LiO₂. The features at 1080.0 and 332.8 cm⁻¹ listed in Table I are the only absorptions which show constant concentration dependence and the same diffusion behavior as the 390.7-cm⁻¹ band. The mixed oxygen isotopic experiment illustrated in Figure 2 shows that the 390.7- and 332.8-cm⁻¹ bands become 1:2:1 relative intensity triplets indicating that two equivalent oxygen atoms are present in the species NaO₂. Unfortunately, insufficient NaO₂ was produced in this experiment to observe the three isotopic components of the much weaker bands in the 1019- to 1080-cm⁻¹ region. Increased light scattering in this spectral region makes it more difficult to detect very weak bands after 24 hr of sample deposition. We conclude that the 1080.0-, 390.7-, and 332.8-cm⁻¹ absorptions are due to the NaO₂ molecule.

NaO₂Na. The absorptions at 524.5, 254.0, and 239.0 cm⁻¹ decrease relative to the 390.7-cm⁻¹ band with a

decrease in sodium concentration and increase relative to the 390.7-cm⁻¹ absorption with a decrease in oxygen concentration. Counterparts of the above bands are not observed in the pure oxygen matrix experiments. These three bands disappear completely upon sample warming, as is shown in Table I. The triplet structures illustrated in Figure 2 for these absorptions indicates that two equivalent oxygen atoms are present in this molecular species. The intensity changes observed on concentration variation suggest that the molecule contains at least one more sodium atom than NaO₂. Failure to observe counterparts of these bands in the pure oxygen matrix experiments is consistent with the formation of this species by adding Na to NaO₂, a reaction made improbable in the oxygen matrix experiments. The concentration and diffusion behavior of the intense 524.5- and 254.0-cm⁻¹ bands parallel earlier observations for LiO₂Li. We assign the 524.5- and 254.0-cm⁻¹ bands to NaO₂Na and tentatively associate the 239.0-cm⁻¹ absorption with NaO₂Na.

Dimer. The intense doublet at 1001 and 991 cm⁻¹ in the argon matrix experiments shows a decrease relative to the 390.7-cm⁻¹ band with decreasing oxygen concentration but remains constant relative to the 390.7-cm⁻¹ feature with decreasing sodium concentration in the range presently studied. In the oxygen matrix experiments, a decrease in sodium atom concentration produces an apparent decrease in the 998-cm⁻¹ band relative to the 306-cm⁻¹ absorption. However, both bands are broad and accurate quantitative comparison is difficult. Upon sample warming, the intense doublet shifts to 1008 and 1002 cm⁻¹ with a marked increase in intensity. The 1002-cm⁻¹ component is more intense than the 1008-cm⁻¹ peak after warmup.^{12a}

In the experiment whose spectrum is illustrated in Figure 1b, the presence of about one-sixth ¹⁶O₂ is indicated by the observation of the 524.5- and 390.7-cm⁻¹ bands. For a species containing two equivalent oxygen molecules, we expect to see features due to (¹⁶O₂)₂, (¹⁶O₂)(¹⁸O₂), and (¹⁸O₂)₂ with 1:10:25 statistical weights. The bands at 968.8 and 959.0 cm⁻¹ could be due to a ¹⁶O₂¹⁸O₂ containing sodium compound since the observed intensities are in excellent agreement with the statistical prediction for such a species.

Figure 2 shows the spectrum for a 1:2:1 mixture of ¹⁶O₂–¹⁶O¹⁸O–¹⁸O₂. For this mixture six possible associations of two oxygen molecules exist with heavier statistical weights for the intermediate mixed isotopes. Owing to overlap of the doublet absorptions, we cannot make definite assignments to each of the six isotopic molecules from the spectrum in Figure 2, but we can conclude that the observed absorptions are likely due to

(12a) NOTE ADDED IN PROOF. Experiments in progress reacting potassium atoms with oxygen molecules yield a single sharp, intense feature at 993 cm⁻¹ in an argon matrix. This observation suggests that the doubling of the absorption near 1000 cm⁻¹ in the sodium experiments may be due to an argon matrix site effect.

a species containing two equivalent oxygen molecules, the same conclusion reached from the spectrum in Figure 1b.

Since we did not observe² a molecule containing one lithium atom and two oxygen molecules, even in pure oxygen matrix experiments, we believe that the 1001- and 991-cm⁻¹ bands observed here could be due to the dimer of NaO₂. This tentative assignment is supported by the decrease of NaO₂ and growth of (NaO₂)₂ on diffusion in the argon matrix experiments.

The 295.5- and 262.0-cm⁻¹ absorptions may be associated with (NaO₂)₂ since they also grew markedly upon sample warming. Our data are insufficient to make a definite assignment of the 295.5- and 262.0-cm⁻¹ bands; however, their marked growth on diffusion definitely associates them with an aggregate species.

Vibrational Assignments. NaO₂. The spectrum observed in the mixed oxygen isotopic experiment indicates that the two oxygen atoms are equivalent in NaO₂ and that the molecule has the isosceles triangular structure. This species belongs to the C_{2v} point group and has three normal modes, ν_1 (a₁, symmetric O–O stretch), ν_2 (a₁, symmetric Na–O stretch), and ν_3 (b₁, antisymmetric Na–O stretch) all of which are infrared active. The 1080.0-cm⁻¹ band shifts to 1019.1 cm⁻¹ when ¹⁸O₂ is substituted for ¹⁶O₂ in the argon matrix experiments and to 1081.0 cm⁻¹ in the pure ¹⁶O₂ matrix. ν_1 of ⁷Li¹⁶O₂ at 1096.9 cm⁻¹ was observed² at 1035.2 cm⁻¹ with ¹⁸O₂ and at 1098.7 cm⁻¹ in an oxygen matrix. Therefore, the 1080.0-cm⁻¹ band observed here is assigned to ν_1 of NaO₂. The larger oxygen isotopic shift found for the 332.8-cm⁻¹ band indicates² its assignment as ν_3 while the smaller oxygen isotopic shift observed for the 390.7-cm⁻¹ absorption dictates its assignment as ν_2 of NaO₂. The difference between oxygen and argon matrix shifts is a factor 4.0 ± 0.3 greater for NaO₂ than for LiO₂. Vibrational assignments for NaO₂ are listed in Table IV.

Table IV: Frequencies (cm⁻¹) Assigned to NaO₂ and NaO₂Na in an Argon Matrix^a

NaO ₂			
Isotope	ν_1	ν_2	ν_3
23-16-16	1080.0	390.7	332.8
23-16-18	(1049.6) ^b	386.7	325.2
23-18-18	1019.1	381.5	317.8
NaO ₂ Na			
Isotope	ν_4	ν_5	ν_6
23-16-16-23	239.0	524.5	254.0
23-16-18-23	235.0	518.0	249.7
23-18-18-23	231.0	507.4	246.0

^a Frequency accuracy is ±0.3 cm⁻¹ for ν_1 of NaO₂ and ±0.5 cm⁻¹ for all other frequencies. ^b Estimated by averaging 23-16-16 and 23-18-18 values. An analogous average is within the average frequency accuracy for both lithium isotopes of Li¹⁶O¹⁸O.

NaO₂Na. We have discussed² the possible structures containing two equivalent alkali metal and two equivalent oxygen atoms and concluded that the molecule likely is a planar rhombus with D_{2h} symmetry. Our data suggest that NaO₂Na is formed by the addition of a second sodium atom to NaO₂.

A rhombus structure has three Raman active and three infrared active vibrational modes. The two most intense absorptions assigned to NaO₂Na are considered for assignment to ν_6 (B_{2u}) and ν_5 (B_{3u}) using the normal mode description and notation of Berkowitz.¹³ By analogy with NaO₂, the higher frequency vibration is ν_5 (B_{2u}) which corresponds to the motion of sodium cations perpendicular to the peroxide anion, whereas the lower frequency vibration ν_6 (B_{3u}) corresponds to the motion of sodium cations parallel to the peroxide anion. Since these two vibrations are alone in their respective symmetry classes, we can estimate the O–Na–O angle γ using the calculation detailed by White and coworkers.¹⁴ The primary assumption in this calculation is that the stretch–stretch interaction force constants F_{12} and F_{14} are equal, which should be a reasonably good approximation. For two sets of isotopic data, the frequency ratio ν_5/ν_6 is 2.065 which yields $\gamma = 51.7^\circ$.

The weaker absorption at 239.0 cm⁻¹ which may be associated with NaO₂Na is considered for the remaining infrared-active fundamental ν_4 (B_{1u}), the out-of-plane bending motion. Since this mode usually has a lower frequency than ν_5 and ν_6 , the 239.0-cm⁻¹ band is a reasonable assignment to ν_4 of NaO₂Na. Vibrational assignments for NaO₂Na are given in Table IV.

Force Constant Calculations. NaO₂. To do normal coordinate calculations, we need estimates of structural parameters for NaO₂. Since preliminary force constant calculations show the oxygen–oxygen stretching force constant to be near 5.5 mdyn/Å which is close to the 5.6 mdyn/Å calculated for O₂⁻ from Raman data, we assume the O–O internuclear distance in NaO₂ to be 1.33 ± 0.06 Å which was determined for crystalline NaO₂. Product rule and normal coordinate calculations based on an abundance of isotopic data for LiO₂ showed that the Li–O distance is likely near 1.77 ± 0.07 Å, a value bracketed by internuclear distances for the gas phase LiF (1.564 Å)¹⁵ and LiCl (2.021 Å)¹⁶ molecules. Accordingly, we take the internuclear distances of the NaF (1.925 Å)¹⁷ and NaCl (2.360 Å)¹⁸ diatomic molecules as defining a likely range for the Na–O bond length in our calculations for NaO₂. That this is a

(13) J. Berkowitz, *J. Chem. Phys.*, **29**, 1386 (1958).

(14) D. White, K. S. Seshadri, D. F. Dever, D. E. Mann, and M. J. Linevsky, *ibid.*, **39**, 2463 (1963).

(15) L. Wharton, W. Klemperer, L. P. Gold, R. Strauch, J. J. Gallagher, and V. E. Derr, *ibid.*, **38**, 1203 (1963).

(16) D. R. Lide, Jr., P. Cahill, and L. P. Gold, *ibid.*, **40**, 156 (1964).

(17) S. E. Veazy and W. Gordy, *Phys. Rev.*, **138**, A1306 (1965).

(18) A. Honig, M. Mandel, M. L. Stitch, and C. H. Townes, *ibid.*, **96**, 629 (1954).

reasonable range of Na–O bond lengths if verified by an estimate of 2.07 Å from the empirical correlations of Herschbach and Laurie,¹⁹ using a preliminary Na–O force constant of 0.8 mdyne/Å.

Force constant calculations were done for Na–O bond lengths of 1.90, 2.04, 2.20, and 2.35 Å using the nine isotopic frequencies listed in Table IV. The calculations were performed on a least-squares adjustment program FADJ written by J. H. Schachtschneider using the Wilson FG matrix method. Since the off-diagonal constants F_{12} and F_{13} were very small (<0.05 mdyne/Å) for LiO₂ and insufficient data are available to uniquely determine all six potential constants here, we fixed these two constants at zero. The internal coordinate force constants for the 2.04 Å Na–O bond length were as follows: $F_{O-O} = 5.47$, $F_{Na-O} = 0.80$, $F_{Na-O, Na-O} = -0.12$, all in millidynes per ångström units. The average difference between calculated and observed frequencies was 0.3 cm⁻¹ for this potential function, which is near the average experimental frequency accuracy of ± 0.4 cm⁻¹. Use of the other Na–O bond lengths in the calculation produced negligible changes in the potential constants and frequency fit. The Na–O bond length of 2.07 Å determined by the Herschbach–Laurie¹⁹ correlation provides the best estimate of the Na–O distance in the NaO₂ molecule. The excellent fit of nine isotopic frequencies to an average difference between calculated and observed of 0.3 cm⁻¹ is strong support for our vibrational assignments to a triangular NaO₂ molecule.

NaO₂Na. As we previously discussed, normal coordinate calculations for ν_5 and ν_6 of NaO₂Na estimate the O–Na–O bond angle to be near 51.7°. For this bond angle the symmetry coordinate force constants F_{2u} and F_{3u} are calculated to be 0.944 mdyne/Å. Using the O–O internuclear distance from sodium peroxide crystal of 1.50 Å as the rhombus diagonal opposite the 51.7° angle, a Na–O bond length of 1.72 Å is calculated. Since this Na–O bond length is somewhat shorter than gas phase NaF (1.925 Å),¹⁷ we feel that a bond length near 1.90 Å would be more appropriate for NaO₂Na. This estimate of the Na–O internuclear distance defines the O–Na–O angle to be 46.6° and symmetry coordinate force constants $F_{2u} = 0.907$ and $F_{3u} = 1.148$ mdyne/Å which combine to give $F_{Na-O} = 1.03$ mdyne/Å.

We calculate the out-of-plane bending force constant $k\Delta/l^2$ using the change in the angle between the Na–O bonds and the plane of the molecule as the internal coordinate. This calculation gives $k\Delta/l^2 = 0.32$ mdyne/Å for bending four Na–O bonds out of the molecular plane.

Conclusions

These results are of interest since sodium–oxygen stretching frequencies have not been reported previously. The symmetrical structure of the sodium super-

oxide molecule merits further analysis of the bonding in this molecule.

Na–O Force Constants. The sodium–oxygen stretching force constant in NaO₂ is 0.80 mdyne/Å, approximately two-thirds of its LiO₂ counterpart. For the NaO₂Na molecule, F_{Na-O} is near 1.0 mdyne/Å, which is also less than F_{Li-O} for LiO₂Li. The negative stretch–stretch interaction force constant is usually interpreted to mean that stretching one bond weakens the other. This is consistent with ionic bonding in NaO₂ which decreases for both Na–O bonds as the Na–O₂ distance is increased. F_{23} for NaO₂ is also two-thirds of its LiO₂ counterpart.

The out-of-plane bending force constant (0.32 mdyne/Å) calculated here for NaO₂Na is slightly larger than its LiO₂Li counterpart (0.25 mdyne/Å).² This is a surprising trend; however, comparatively little is known about this type of vibrational mode, and these assignments cannot be regarded as definitive.

O–O Force Constant. Recent laser Raman observations of potassium superoxide doped into alkali halide lattices³ have estimated the vibrational frequency of isolated superoxide ion to be near 1090 cm⁻¹. Based on this frequency, F_{O-O} for O₂⁻ is readily calculated to be 5.59 mdyne/Å.

The oxygen–oxygen stretching force constant for NaO₂ is 5.46 ± 0.01 mdyne/Å for a wide range of Na–O bond lengths. Comparing the analogous potential function, the oxygen–oxygen force constant for LiO₂ is 5.55 mdyne/Å, only slightly larger than its NaO₂ counterpart. These O–O force constants are lower than those for XO₂ radicals and O₂ itself.²

Bonding in NaO₂ and NaO₂Na. We suggested earlier^{1,2} that the close agreement between oxygen–oxygen force constants for LiO₂ and O₂⁻ indicates complete electron transfer from lithium to the oxygen molecule with coulombic forces binding a lithium cation and a superoxide anion. Even though the ionization potential and electronegativity of sodium are slightly less than those of lithium, if the valence electron of Li is completely transferred to O₂ in LiO₂, then the Na atom can do no more than completely transfer its valence electron to O₂ in the sodium superoxide molecule. The close agreement of the O–O force constants for LiO₂ and NaO₂ support this argument.

The valence electron of sodium is added to one of the antibonding π molecular orbitals on O₂ which results in a decrease in the oxygen–oxygen force constant and bond order. This effect is discussed in the bonding of XO₂ radicals by Spratley and Pimentel.²⁰

One may reasonably expect the smaller lithium cation to polarize the superoxide anion more effectively than

(19) D. R. Herschbach and V. W. Laurie, *J. Chem. Phys.*, **35**, 458 (1961).

(20) R. D. Spratley and G. C. Pimentel, *J. Amer. Chem. Soc.*, **88**, 2394 (1966).

the slightly larger sodium cation, thus decreasing the antibonding electron density in the O₂ part of LiO₂ relative to that for NaO₂. However, the difference between polarizing power for Li⁺ and Na⁺ is very small which can be seen by comparing observed dipole moments for LiF (6.284 D),¹⁵ LiCl (7.12 D),¹⁶ NaF (8.123 D),¹⁷ and NaCl (8.5 D)¹⁸ with the product of a single electronic charge and the internuclear distance ($e \times r$) for these gaseous alkali halides. The observed dipole moments for LiF and NaF are 0.84 and 0.88 times their respective ($e \times r$) values and the dipole moments for LiCl and NaCl are 0.73 and 0.75 times their respective ($e \times r$) values. Thus, the differences in charge distribution or relative covalent and ionic character between these lithium and sodium halides is only a few per cent. Therefore, we expect the anionic character of the O₂ parts of LiO₂ and NaO₂ to be nearly the same, an expectation supported by the oxygen-oxygen stretching force constants. The fact that the O-O force

constant for NaO₂ is approximately 2% lower than that for LiO₂ is attributed to a very small amount of alkali metal motion in this normal coordinate, which is necessary for this mode to be infrared allowed.

We suggest that the sodium peroxide molecule is formed by the addition of a second sodium atom to the sodium superoxide molecule. Unfortunately, the O-O stretching frequency for NaO₂Na is not infrared active, so conclusions about the bonding in NaO₂Na can only be suggested by comparison to NaO₂. The most reasonable structure for NaO₂Na is two equivalent sodium cations bonded to a peroxide anion in a planar configuration. We expect a higher Na-O force constant for NaO₂Na than for NaO₂ since the sodium cations in NaO₂Na feel a higher effective anionic charge.

Acknowledgment. The author gratefully acknowledges financial support for this research by the National Science Foundation under Grant GP-8587.

Chemical Effects Following N¹⁴(n,p)C¹⁴ in Magnesium Nitride

by Ronald D. Finn, Hans J. Ache,

Chemistry Department, Virginia Polytechnic Institute, Blacksburg, Virginia 24061

and Alfred P. Wolf

Chemistry Department, Brookhaven National Laboratory, Upton, New York 11973 (Received May 14, 1969)

The reactions of carbon-14 recoil species produced by the N¹⁴(n,p)C¹⁴ nuclear reaction have been investigated in magnesium nitride. The major reaction products observed upon dissolution in water are C¹⁴H₄, C¹⁴N⁻, and C¹⁴N₂²⁻. Thermal annealing of the neutron-irradiated magnesium nitride resulted in a sharp drop of the C¹⁴N⁻ and C¹⁴N₂²⁻ yields and a new product of C¹⁴H₂=NH was observed. In a sample annealed at 500° for 2.5 days, up to 65% of the total C¹⁴ activity was found in the latter compound. The product distribution was also found to be a function of the pH of the aqueous solvent used for dissolution.

Introduction

Recent studies by several investigators^{2,3} have shown that carbon atoms produced by nuclear processes such as C¹²(p,pn)C¹¹, N¹⁴(p,α)C¹¹, etc., display an extremely high reactivity toward oxygen when they reach thermal energies. Welch and Wolf⁴ studied the reactions of carbon species generated by the decomposition of carbon suboxide *via* microwave discharges. They found an upper limit for the reaction rates of these carbon species with saturated hydrocarbons, which is approximately 10⁻⁵ times that for the reaction with molecular oxygen and only 10⁻¹⁰ times that for carbon-carbon recombination. Other approaches of

studying the reactions of carbon atoms include techniques developed by Skell⁵ and Libby.⁶

All of these investigations were done either in the gas phase or by using experimental techniques involving

(1) Research performed under the auspices of the U. S. Atomic Energy Commission.

(2) H. J. Ache and A. P. Wolf, unpublished results.

(3) G. Stöcklin and A. P. Wolf in "Methods of Preparing Marked Molecules," Euratom, Brussels, 1964, p 181.

(4) M. Welch and A. P. Wolf, *Chem. Commun.*, 117 (1968).

(5) P. S. Skell and R. R. Engel, *J. Amer. Chem. Soc.*, **89**, 2917 (1967) and preceding papers.

(6) J. L. Sprung, S. Winstein, and W. F. Libby, *ibid.*, **87**, 1812 (1965).

the surfaces of organic films. Very little information is available about hot and thermal reactions of carbon species in solid inorganic matrices.⁷⁻¹⁵ In the light of the current investigation on the reactions of thermal carbon atoms it seemed most interesting to extend the present research to the study of the fate of recoil carbon in solid inorganics.

The general approach of determining the fate of a trapped recoil particle in a solid matrix usually involves the dissolution of samples of different solvents followed by radiochemical analysis of the resultant solution. As a result of the interaction of the different product species with the solvent, new species are produced in the solution. Especially interesting are those cases in which an atomic species, not identical with those elements already in the lattices, is introduced into a particular crystal by a recoil technique. Thus one can in principle investigate the chemical reactivity of this species within the crystal lattice. From the products obtained by dissolution, one can speculate on the original chemical state of the recoil particle. Results obtained in the magnesium nitride system are described and a discussion of the data is given.

Experimental Section

Sample Preparation and Irradiation. Sixteen grams of reagent grade magnesium nitride was placed in a quartz vessel under an argon or helium atmosphere. The vessel was then evacuated and sealed under vacuum. Irradiations were performed at the Brookhaven National Laboratory, HFBR, or BMR reactors. Fluxes and total irradiation time are noted in the tables for each sample listed. The temperature during irradiation was kept between 50 and 80°. The samples were analyzed shortly after their irradiation unless otherwise specified. All samples were carefully protected against contact with air.

Materials. Magnesium nitride samples were obtained from K and K Laboratories. Analysis showed the following composition: 70.03% Mg and 24.06% N. The carrier gases methane, carbon monoxide, carbon dioxide, and methylamine were purchased from Matheson Company, Inc., the methane being of UHP grade, carbon monoxide of CP grade, carbon dioxide of bone-dry grade, and methylamine of anhydrous grade.

Determination of Total C^{14} Produced. The total C^{14} activity of the sample, produced by the $N^{14}(n,p)C^{14}$ nuclear reaction was determined from an acetanilide flux-monitor. The acetanilide was combusted to $C^{14}O_2$ and the $C^{14}O_2$ assayed by internal gas counting. In a typical 10-hr neutron irradiation (flux 4.8×10^{13} n cm^{-2} sec^{-1}) the C^{14} activity was approximately 10 nCi/mg of N.

Reaction Products. The magnesium nitride sample (about 0.5-1.0 g) was contained in an evacuated glass vessel to which CH_4 and CO gas were added as carrier. After dissolution of the sample in 10 cc of 2 N NaOH,

carried out under the carrier gases and at 0°, the gases were flushed into a storage bulb using a helium gas stream. Aliquots were taken from the storage bulb.

Methane, carbon monoxide, and methylamine were analyzed by the usual radiogas chromatographic methods coupling a Perkin-Elmer 811 with a flow proportional counter.¹⁶ Three different gas chromatographic columns were used in this analysis: (1) 1.5 m \times 0.5 cm i.d. activated charcoal column (used at 70°); (2) 10 m \times 0.5 cm i.d. 20% dimethylsulfolane on Chromosorb W (used at 25°); and (3) 2 m \times 0.5 cm i.d. Porapak Q coated with polyethylenimine (used at 100°).

In the analysis of thermally annealed samples, measurements indicated the presence of a gas of unknown composition which accounted for the majority of the gas-phase activity. The gas had a retention time close to that of methane on a Porapak column used at 100°.

The unknown gas was identified as methylenimine by converting it into formaldehyde using a technique described previously by Cacace and Wolf.¹⁷ An aliquot of the sample was condensed into 5 ml of 7 N H_2SO_4 containing 39 mg of carrier formaldehyde. The ampoule was sealed and heated for 20 min at 100°. The contents of the ampoule were added to a saturated solution of dimedone and the derivative was collected. It was recrystallized from ethanol-water mixtures.¹⁸ The reduction of the unknown gas in a hydrogen stream with Raney Ni as catalyst deposited on firebrick (40-60 mesh) resulted in the formation of methylamine.

After the removal of methane, carbon monoxide, methylamine and methylenimine, a known amount of sodium cyanide was added to the target solution. This was followed by the addition of an excess of silver nitrate. The system was again evacuated and the solution acidified to liberate the carbon dioxide from the "target solution." Carbon dioxide was flushed into a storage bulb from which aliquots were taken and analyzed by radiogas chromatography¹⁴ (*vide supra*). The silver cyanide was removed from the "target solution" by filtration, and recrystallized from concen-

(7) P. E. Yankwich and J. D. Vaughan, *J. Amer. Chem. Soc.*, **78**, 1560 (1956).

(8) P. E. Yankwich and J. D. Vaughan, *ibid.*, **76**, 5851 (1954).

(9) P. E. Yankwich and W. R. Cornman, *ibid.*, **77**, 2096 (1965).

(10) P. E. Yankwich, *J. Chem. Phys.*, **15**, 374 (1947).

(11) P. E. Yankwich and P. J. Marteney, "Chemical Effects of Nuclear Transformations," Vol. II, International Atomic Energy Association, Vienna, 1965, p 81.

(12) L. T. Sharman and K. T. McCallum, *J. Amer. Chem. Soc.*, **7**, 2989 (1955).

(13) F. S. Rowland and W. F. Libby, *J. Chem. Phys.*, **21**, 1493 (1953).

(14) J. G. Kuhry and J. P. Adloff, *Bull. Soc. Chim.*, 2402 (1967).

(15) J. G. Kuhry and J. P. Adloff, *ibid.*, 1967, 3414.

(16) G. Stöcklin, F. Cacace, and A. P. Wolf, *Z. Anal. Chem.*, **194**, 406 (1963).

(17) F. Cacace and A. P. Wolf, *J. Amer. Chem. Soc.*, **87**, 5301 (1965).

(18) J. Yang and A. P. Wolf, *ibid.*, **82**, 4488 (1959).

Table I: Labeled Products from Neutron-Irradiated Magnesium Nitride (Exposure Time 10.5 hr)

Reactor type	BMR ^a	BMR ^b	BMR ^c	BMR ^c	BMR ^c	BMR ^c	BMR ^b	BMR ^b	HFBR ^b
Neutron flux, cm ⁻² sec ⁻¹	4.8 × 10 ¹³	4.8 × 10 ¹³	4.8 × 10 ¹³	4.8 × 10 ¹³	4.8 × 10 ¹³	4.8 × 10 ¹³	4.8 × 10 ¹³	4.8 × 10 ¹³	2 × 10 ¹⁴
Preirradiation treatment					500° 5 days	500- Mrad γ irradiation			
Postirradiation treatment									
Solvent	2 N NaOH	2 N NaOH	2 N NaOH	2 N NaOH	2 N NaOH	2 N NaOH	2 N H ₂ SO ₄	2 N H ₂ SO ₄	2 N NaOH
Thermal anneal time, days		5	5					5	
temp, °C		500	500					500	
γ irradiation			500-Mrad 1. γ irradiation 2. therm	500-Mrad					
	% C ¹⁴ of total produced in								
C ¹⁴ O	0.01	0.02	0.01	0.01	<0.01	0.05	<0.01	<0.01	<0.01
C ¹⁴ H ₄	11.6	23.2	31.5	11.5	17.9	15.1	23.17	52.3	11.0
C ¹⁴ O ₂	0.06	0.17	0.4	0.4	<0.01	1.27	2.22	2.23	3.7
[C ¹⁴ N] ⁻	41.3	3.8	3.8	43.3	41.0	41.3	20.1	0.57	41.6
[C ¹⁴ N ₂] ²⁻	18.1	2.7							
C ¹⁴ H ₂ =NH	3.6	66.2						4.7	
C ¹⁴ H ₃ NH ₂	<0.01	5.0							

^a Average of 7 runs. ^b Average of 3 runs. ^c One run.

trated ammonium hydroxide solution. The absolute activity of the silver cyanide was determined by counting the C¹⁴O₂ obtained by quantitative oxidation of the cyanide to C¹⁴O₂. Gas-phase proportional counters were used to determine the radioactivity.

After removal of C¹⁴N⁻ an excess of cyanamide (0.3 g) was added to an aliquot of the acidic solution. The solution was heated and concentrated. Upon cooling the bulk of cyanamide precipitated. It was recrystallized (from water) to constant specific activity. The dimedone derivative of formaldehyde was made by adding a neutralized aliquot of target solution containing formaldehyde carrier to a saturated ethanol solution of dimedone. The oxalate derivative of urea was made from a neutralized aliquot of target solution with urea carrier by adding to it a saturated solution of oxalic acid. The derivative was recrystallized from hot water.

The C¹⁴-activity incorporated in cyanamide, in the derivatives of formaldehyde, and in urea was measured by liquid scintillation counting.

The picrate of guanidine was made by adding an aliquot of degassed target solution containing guanidine carrier to a boiling solution of 0.35 g picric acid in 30 ml of water. Upon cooling, guanidine picrate was removed by filtration, washed with cold water, recrystallized from hot water and then dried for 1 hr at 75°. The sample was combusted and the activity determined as previously described.

The total activity in the target solution, after complete degassing and precipitation of silver cyanide was

found to be less than 5% of the total activity produced. If 2 N H₂SO₄ was used as solvent, the procedures described above were slightly altered, C¹⁴O, C¹⁴H₄, C¹⁴O₂ and a fraction of HC¹⁴N were liberated upon dissolution and measured directly by radiogas chromatography.

Pre- and Postirradiation Treatment. Samples of magnesium nitride were sealed under vacuum into quartz ampoules and thermally annealed in a thermostatically controlled air oven. Pre- and post-γ irradiation was done using the BNL High Flux Irradiation Facilities.

Results

The results obtained when neutron-irradiated magnesium nitride is dissolved in aqueous solutions show evidence for a diversity of products arising from the reactions of trapped carbon-14 species with the solvent. Major products found in a freshly analyzed sample include C¹⁴H₄, H C¹⁴N, and H₂NC¹⁴N (Table I). C¹⁴O, C¹⁴O₂, and others such as C¹⁴H₃NH₂, C¹⁴H₂O, C¹⁴O-(NH₂)₂ and C¹⁴NH(NH₂)₂, are usually observed in yields of less than 5%.

Several series of experiments were carried out to study the effects of the various parameters, such as pH of the solvent, pre- and postirradiation (thermal and radiation) annealing, and radiation dose rate on the spectrum of the carbon-14-labeled reaction products.

Solvent Effects. The results (Table I) obtained by dissolution of freshly irradiated magnesium nitride

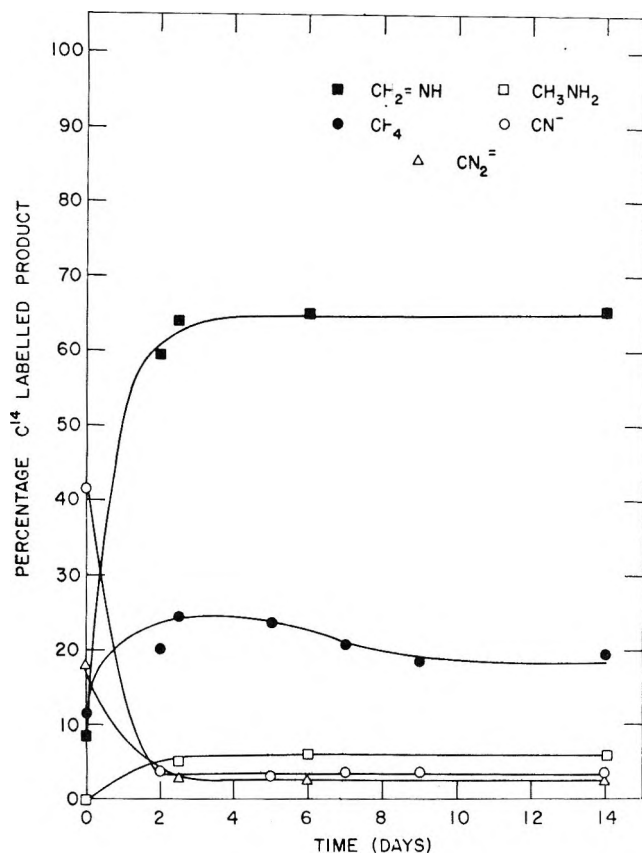


Figure 1. Effect of postirradiation annealing on C^{14} product distribution following $N^{14}(n,p)C^{14}$ in magnesium nitride. Annealing temperature, 500° ; Solvent, $2 N NaOH(aq)$.

samples in $2 N H_2SO_4(aq)$ and $2 N NaOH(aq)$, indicate that the choice of the solvent has a pronounced effect on the product spectrum. It can be seen that there is a drop in the yield of $HC^{14}N$ from 41.3% to 20.1% and an increase in the yield of $C^{14}H_4$ from 11.6% to 23.2% in going from a basic solution [$2 N NaOH(aq)$] to an acidic solution [$2 N H_2SO_4(aq)$]. This effect is even more pronounced in the case of samples, which have been annealed at 500° for a period of 5 days after the neutron irradiation, where the corresponding numbers are 3.8% and 0.6% for $[C^{14}N]^-$ and 23.2% and 52.3% for $C^{14}H_4$.

Pre- and Postirradiation Treatment. Treatment of the magnesium nitride prior to neutron irradiation, e.g., thermal annealing for 5 days at 500° or γ irradiation (total dose 500 Mrads), results in a change in the $C^{14}H_4$ yields. The $C^{14}H_4$ increases from 11.6% to 17.9% and 15.1%, respectively. There is essentially no effect on the $[C^{14}N]^-$ yields when the samples are dissolved in $2 N NaOH(aq)$ (Table I). A γ irradiation up to 500 Mrads when applied after the neutron irradiation of the magnesium nitride sample resulted in no observable effect.

Figures 1 and 2 show the results obtained from the neutron-irradiated magnesium nitride samples when dissolution of the samples was achieved in $2 N NaOH$

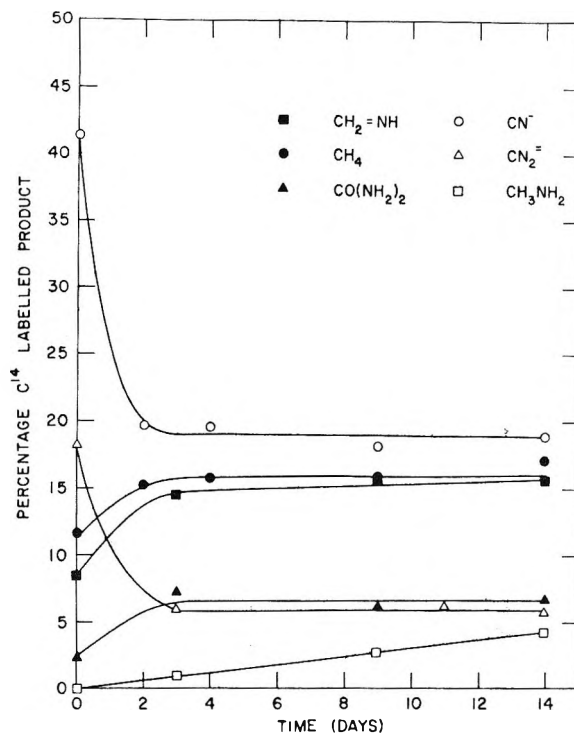


Figure 2. Effect of postirradiation annealing on C^{14} product distribution following $N^{14}(n,p)C^{14}$ in magnesium nitride. Annealing temperature, 300° ; Solvent, $2 N NaOH(aq)$.

solution after the annealing had been completed. Annealed samples of solid magnesium nitride which were decomposed with $2 N NaOH$, liberated the majority of the carbon-14 activity in the form of the two gases, $C^{14}H_4$ and $C^{14}H_4=NH$. Lesser amounts of $C^{14}H_3NH_2$, $C^{14}O_2$, and $C^{14}O$ were also seen. The thermal annealing curves were obtained at temperatures of 500 and 300° . Although the shapes of the two curves are quite different, it should be noted that it was possible to make the transition at any time from the lower curve to the upper curve, by changing the temperature. This means to say that the product distribution at the lower annealing temperature can be transformed into that which appears at the higher temperature simply by raising the temperature from 300 to 500° for any time interval required. The most noticeable change is the sharp drop in the $[C^{14}N]^-$ yields even after short annealing times and the marked increase of the product which we believe to be $C^{14}H_2=NH$. Less pronounced is the increase in the yield of $C^{14}H_4$.

Radiation Dose Rate Effects. The effect of the dose rate on the final carbon-14 distribution was studied by irradiating the magnesium nitride in the Brookhaven Medical Reactor and the High Flux Beam Reactor with fluxes of 4.8×10^{13} and $2 \times 10^{14} n cm^{-2} sec^{-1}$, respectively. The dose rate in the HFBR was higher by a factor of ~ 5 as compared to the dose rate in the BMR. No significant variation in the C^{14} product spectrum could be observed.

Discussion

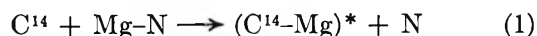
The carbon-14 species is created, stripped of some of its electrons, by the $N^{14}(n,p)C^{14}$ nuclear reaction. It has an initial kinetic energy of about 40 keV.⁷ The energy of the recoil species is dissipated by producing displaced atoms and also by heating a small region of the crystal. It is reasonable to assume that this region encompasses approximately 1000 atoms which may reach temperatures of nearly 2500°K for a time period of 10^{-11} sec.¹⁹ During this time chemical reactions of the recoil species are initiated, but due to the rapid quenching of the hot zone and the rates of some of the reactions, all reactions cannot proceed to completion. Trapped in this hot zone are various types of disorder such as vacancies, interstitial atoms, free radicals, and other relatively reactive chemical species and sites. This means that at least hypothetically, the carbon species may be present in atomic, cationic, anionic, molecular or combined forms.

Yankwich and Cornman⁹ argued that in simple ionic crystals, the energetic carbon recoil species come to rest in terminal hot spots, where they exhibit a more or less "symmetrical" distribution among various final oxidation states. These arguments were based on results obtained from the Be_3N_2 system.⁹ Although this system is not completely comparable with the one described in this paper, it is obvious from the results shown in Table I, that there are basic differences, certainly insofar as the $C^{14}H_4$ and $[C^{14}N]^-$ yields are concerned. More $HC^{14}N$ and less $C^{14}O_2$ are formed in the Mg_3N_2 system, than reported by Yankwich for Be_3N_2 and no equal distribution of radiocarbon between the various formal oxidation states of carbon were observed. Kuhry and Adloff¹⁵ investigated a series of nitrides and obtained an interesting relationship between the percent $C^{14}H_4$ produced and the ratio $p = r^2Me/R^2N$, where r and R are the radii of the metal and the nitrogen in the nitride lattice and Me and N are the numbers of metal and nitrogen atoms in the lattice, *i.e.*, the ratio of the geometrical cross sections each type of atom exhibits to the recoil carbon species.

It is necessary to study the fate of the C^{14} recoil species in the lattice in greater detail in order to correlate the isolable products with their possible precursors in the lattice. The structure of magnesium nitride may be regarded as a derivation of the fluorite structure with regular removal of one quarter of the cations and a slight adjustment in the positions of the remaining atoms.^{20,21} In order to simplify matters one can postulate that when magnesium nitride is subjected to neutron irradiation, the generated carbon-14 ends up in two different environments. It is clear that the crystal structure of magnesium nitride is altered due to the nuclear and radiation processes, but it is hard to envision complete degradation of the structure. Chemically the result may be the formation of bonds between the carbon recoil species and nitrogen or metal

atoms. Some of these compounds and intermediates may be rather stable and can be observed after dissolution. Some will react with the solvent.

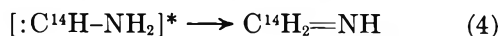
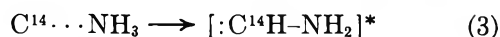
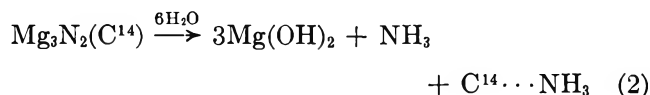
One reaction to be considered would be that of the carbon with a metal atom to form a metal carbide (Mg_2C). Methane is known to be the hydrolysis product of magnesium carbide and it is reasonable to postulate that Mg_2C^{14} can be a precursor of $C^{14}H_4$. Two possible modes of carbide formation could involve either a carbon-14 atom occupying an interstitial position with the metal atom being in its normal lattice position or the carbon could reside in a cation vacancy



The same result could also be obtained by the displacement of a nitrogen anion by the recoil carbon-14.

In a second reaction the carbon recoil species may undergo formation of stable or metastable chemical bonds with the nitrogen, resulting in formation of $[C^{14}N]^-$ and $[C^{14}N_2]^{2-}$ upon dissolution in aqueous solvents. It seems noteworthy that HCN has also been observed as the main product in the gas-phase reaction of recoil carbon-11 with nitrogen.²² Perhaps the most striking observation is the drastic change in the yields of $[C^{14}N]^-$ and $[C^{14}N_2]^{2-}$ upon thermal annealing at 500°. Since this is accompanied by a simultaneous increase of the C^{14} found incorporated in "methylenimine" it can be suggested that thermal annealing transforms the precursors of $[C^{14}N]^-$ and $[C^{14}N_2]^{2-}$ to the precursor of "C-14-methylenimine."

As a consequence of an increase in temperature of the magnesium nitride, the defects in the crystal disappear, which means to say that displaced nitrogen can start reoccupying its original position in the lattice. Thus the precursors of $[C^{14}N]^-$ and $[C^{14}N_2]^{2-}$ if not in their fully bonded form, but rather in some state which leaves the C^{14} to N bonds weaker than in the fully formed $[C^{14}N]^-$ or $[C^{14}N_2]^{2-}$, can be altered by C^{14} to N bond separation in the annealing process to give other intermediates and products. The attack of the solvent can then lead in the first step to NH_3 (rather than $C^{14}N$, a necessary consequence if the C to N bonds were fully formed) but to which a carbon atom is still loosely attached



(19) G. Harbottle and N. Sutin, in "Advances in Inorganic and Radiochemistry," Vol. I, H. J. Emeleus and A. G. Sharpe, Ed., Academic Press, New York, N. Y., 1959, pp 268-312.

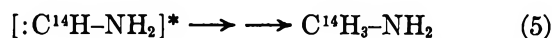
(20) R. Paulus, *Z. Phys. Chem.*, **22**, 353 (1933).

(21) R. Wyckoff, "Crystal Structure," Vol. 2, Interscience Publishers, New York, New York, 1964, pp 2-6.

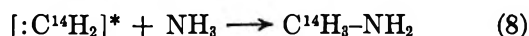
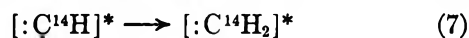
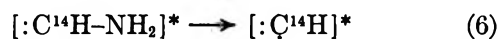
(22) H. J. Ache and A. P. Wolf, *Radiochim. Acta*, **6**, 32 (1966).

The resulting complex [*] formed by hydrogen migration is similar or equivalent to the reaction complex postulated by Cacace and Wolf⁷ for the reactions of "hot" carbon-11 with ammonia, eq 3 and 4. (Clearly at some stage (2) or (3) carbon atom C-H insertion might occur.)

Applying these postulates the observed increase in $C^{14}H_3NH_2$ after annealing (Figures 1 and 2) could then likewise be understood in terms of the direct reduction of $C^{14}H_2=NH$ or its precursor by the surrounding molecules

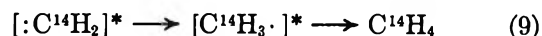


The reaction complex $[:C^{14}H-NH_2]^*$ could also decompose to $:C^{14}H$ (methyne) which can pick up one hydrogen to give $:C^{14}H_2$ (methylene). The methylene- C^{14} can insert into NH_3 (produced in excess by the decomposition of Mg_3N_2) to give $C^{14}H_3NH_2$



In a similar way the increase in the yield of $C^{14}H_4$ with

annealing might be postulated to occur *via* a successive hydrogen abstraction mechanism



An alternate explanation for the latter observation (*vide supra*) suggests that during the annealing process, carbon is occupying anion sites in the lattice so that a carbide structure is obtained which gives $C^{14}H_4$ upon dissolution in aqueous media.

Very little can be said at the present time about the solvent effect but it seems reasonable to suggest that the stability and the reactions of the various intermediates involved display pH dependence.

In the present investigation, *e.g.*, $HC^{14}N$, $H_2NC^{14}N$, and $C^{14}H_2-NH$ are observed, which are the same reaction products as obtained in hot carbon reactions with N_2 ²² or NH_3 .¹⁷ Yankwich¹¹ found $C^{14}H_3NH_2$ to be the major product following $N^{14}(n,p)C^{14}$ in NH_4Cl in analogy with "hot" carbon reactions on NH_3 .¹⁷ In conclusion it seems noteworthy to point out that carbon recoil reactions in the solid systems reflect the reactions and reaction products obtained or postulated in gas-phase reactions with the same elements.

Solvation Enthalpies of Various Ions in Water, Propylene Carbonate, and Dimethyl Sulfoxide¹

by C. V. Krishnan and Harold L. Friedman

Department of Chemistry, State University of New York at Stony Brook, Stony Brook, Long Island, New York 11790
(Received May 15, 1969)

The data previously surveyed² have been considerably extended by new determinations of heats of solution in propylene carbonate (PC), dimethyl sulfoxide (DMSO), water, and D₂O. It is found that the enthalpy of transfer of the R₄N⁺ ions to PC from DMSO comprises additive contributions from the CH₂ groups, and these CH₂ terms are the same as those for the PC ← DMSO transfers of the primary alcohols.³ This is the basis of a simple method to get single-ion contributions to enthalpies of transfer of the electrolytes. In this way it is found that the enthalpy of transfer of Ph₄As⁺ is the same as that of Ph₄B⁻, just as has often been assumed for other solvent pairs. The enthalpies of the PC ← DMSO transfer of the alkali metal ions are an order of magnitude larger than one would expect from the Born charging equation. These large effects seem to reflect the difference in basicity of the two solvents. The enthalpy of transfer of the R₄N⁺ ions to PC from water is dominated by an effect which does not comprise additive contributions from the methylene groups. Indeed, it reaches a maximum value (as a function of chain length) at tetraamylammonium ion. This effect is attributed to structural changes ("icebergs") in the water in the neighborhood of the ions in aqueous solution. Part of the evidence for this interpretation is the finding that the nonadditive effect is 5% larger in D₂O than in H₂O, just as for the corresponding term in the hydration of the primary alcohols.³

I. Introduction

Ionic solvation enthalpies are fundamental quantities for understanding ionic solutions but are accessible to experimental interpretation only for the monatomic ions and the very few polyatomic ions whose energies of formation may be accurately determined in the gas phase. If one deals with differences of solvation enthalpies in two solvents, that is with enthalpies of transfer to one solvent from another rather than to the gas phase from a solvent, then the accessibility problem is relieved, but there is of course a price to pay in the increased difficulty of interpretation of the results. The work reported here is aimed at working around this difficulty by combining data for electrolytes and nonelectrolytes in several different solvents.

This is a continuation of interpretive² and experimental³⁻⁵ work reported earlier. In the meantime there has appeared a valuable review of a special part of this field of study, namely, thermodynamics of transfer to H₂O from D₂O.⁶ Much of the interest in these studies derives from their relevance to the problem of structural ("iceberg") effects induced in water by nonpolar solutes or nonpolar groups on solute molecules; these effects in turn may contribute in a decisive way in determining the conformations of large molecules in aqueous solution.

This report deals mostly with cations. While of necessity the experiments include anions and the new anion results obtained are all reported here, not enough species have been investigated to provide a firm basis for interpretation of the data. This caution may be

more easily understood after one sees the variety of behavior of the cations.

A simple notation introduced and explained in the preceding report³ is employed here: (X)_{B←A} is the enthalpy change when solute species X is transferred to a state of infinite dilution in solvent B from a state of infinite dilution in solvent A.

II. Experimental and Results Section

The instrumental aspects have been described.³⁻⁵ New materials problems were handled as follows: Pr₄NBr, Pr₄NI, Me₃PhNI, PrPh₃PBr, and Ph₄SbBr were recrystallized from methanol-ether mixtures, while Pr₄NCl, Bu₄NCl, Bu₄NBr, Bu₄NI, Am₄NCl (Am = *n*-C₅H₁₁), Am₄NBr, and Am₄NI were recrystallized from acetone-ether mixtures. Ph₄PCl and Ph₄AsCl were dissolved in hot ethanol and filtered, and the filtrate was concentrated by evaporation before the addition of ether to precipitate the product^{7,8} which was then recrystallized from methylene chloride. For all of the preceding the starting materials were com-

(1) Grateful acknowledgment is made of the support of this work by the National Institutes of Health.

(2) H. L. Friedman, *J. Phys. Chem.*, **71**, 1723 (1967).

(3) C. V. Krishnan and H. L. Friedman, *ibid.*, **73**, 1572 (1969).

(4) Y. C. Wu and H. L. Friedman, *ibid.*, **70**, 2020 (1966).

(5) Y. C. Wu and H. L. Friedman, *ibid.*, **70**, 501 (1966).

(6) E. M. Arnett and D. R. McKelvey in "Solute-Solvent Interactions," J. F. Coetzee and C. D. Ritchie, Ed., Interscience Publishers, New York, N. Y., 1969.

(7) H. H. Willard, L. R. Perkins, and F. F. Blicke, *J. Amer. Chem. Soc.*, **70**, 737 (1947).

(8) F. F. Blicke and E. Monroe, *ibid.*, **57**, 720 (1935).

mercially available. Bu_4PBr was prepared by mixing equimolar amounts of tributylphosphine and butyl bromide and storing at 0° for 2 weeks. The crystals which formed were filtered off, washed with ether, and recrystallized from acetone. The perchlorates were prepared from halides by metathesis with aqueous NaClO_4 and recrystallized from acetone. Hex_4NBr ($\text{Hex} = n\text{-C}_6\text{H}_{13}$) received from Eastman Organic Chemicals could not be recrystallized by any of several procedures which were attempted. The material was just washed with ether and dried. Each salt used was dried under vacuum, ground, and dried under vacuum again. Other salts used were from earlier preparations.^{4,5}

The purity of some of the salts used was checked by measurement of the electrical conductivity of an aqueous solution as described before.⁵ Results for the ratio $\Lambda_{\text{est}}^\circ$ obtained from our measurements to $\Lambda_{\text{lit}}^\circ$ obtained from the tabulations of ionic conductivities of Evans and Kay⁹ or Robinson and Stokes¹⁰ follow: Pr_4NBr , 0.9978; Pr_4NI , 0.9986; Bu_4NCl , 0.9987; Bu_4NBr , 0.9990; Bu_4NI , 0.9960; Am_4NBr , 0.9967; Ph_4AsCl , 0.9996.¹¹ In other cases the purity was checked by estimation of the halide and found to be better than 99.7%, except in the case of Am_4NI in which case the purity criterion was that further recrystallization of the salt did not change its heat of solution.

The 99.77% D_2O obtained from Columbia Organic Chemicals was used as received.

The heats of solution of Ph_4PClO_4 and $\text{Ph}_4\text{AsClO}_4$ in water were obtained from heats of precipitation when the dry halide salts were mixed with 10 mM aqueous NaClO_4 in the calorimeter.⁴ However, a small part of the salt was found to react slowly, perhaps due to the formation of the precipitate on its surface, and a better procedure was found to be to mix solid NaClO_4 with a dilute (<5 mM) aqueous solution of Ph_4AsCl or Ph_4PCl in the calorimeter. A saturated aqueous solution (~ 2 mM) of Hex_4NBr was used in a similar procedure to get the heat of precipitation of $\text{Hex}_4\text{NClO}_4$. Heats of solution of Bu_4NI and Am_4NI in water could not be obtained, apparently because the materials floated on the water and did not dissolve properly. The heat of solution of Hex_4NBr in water could not be obtained, apparently because the micelles which formed as the material reacted with water were slow to dissociate.

The dissolution and mixing processes were found to be practically complete within 2–10 min except as just noted and as follows: Me_4NClO_4 , Am_4NClO_4 , Ph_4SbBr in PC, and Me_4NBr , Me_4NI , Me_4NClO_4 , Am_4NClO_4 , $\text{Ph}_4\text{AsClO}_4$, BuPh_3PBr in DMSO, 15–30 min.

All the measurements were made at 25.0° . The results are given in Table I, where each value given is the average of two or more independent observations agreeing within 0.05 kcal/mol.

Based on the convention that $(\text{Ph}_4\text{As}^+)_{\text{PC} \leftarrow \text{DMSO}} =$

Table I: Enthalpies of Solution of Pure Substances at 25° (Values in kcal/mol)

Solute	Solvent			
	H_2O	D_2O	PC	DMSO
Me_4NBr		6.29		3.05
Me_4NI				3.30
Me_4NClO_4			3.90	3.45
Et_4NBr		1.79		
Et_4NClO_4			3.58	3.75
Pr_4NCl	-5.30		3.78	3.13
Pr_4NBr	-1.03, -1.10 ^a	-0.99	5.02	3.83
Pr_4NI	2.76, 2.765 ^b		4.74	3.76
Pr_4NClO_4			5.37	5.90
Bu_4NCl	-7.14		3.38	3.22
Bu_4NBr	-2.02	-2.17	5.70	4.95
Bu_4NI			7.85	7.27
Bu_4NClO_4			3.03	3.95
Am_4NCl	-9.13		1.92	2.13
Am_4NBr	0.77	0.49	8.95	8.60
Am_4NI			12.25	12.07
Am_4NClO_4			11.13	12.44
Hex_4NBr			4.10	3.99
$\text{Hex}_4\text{NClO}_4$	12.10		12.41	14.20
Bu_4PBr	-2.85		4.80	3.92
Ph_4AsCl	-2.57, -2.60 ^c	-2.47	0.25	-0.92
Ph_4AsBr	1.80		1.75	-0.03
$\text{Ph}_4\text{AsClO}_4$	12.82		6.18	6.22
Ph_4PCl	-2.19	-2.07	0.90	0.07
Ph_4PClO_4	12.85		5.98	
Ph_4SbBr	2.84		3.79	0.25
Me_3PhNI	9.45		4.68	1.93
PrPh_3PBr	4.65			3.14
BuPh_3PBr	5.40			4.95
KBPh_4				-1.71
RbBPh_4				0.92
CsBPh_4				1.72

^a R. H. Boyd and P. S. Wang, Abstracts of papers, 155th National Meeting of the American Chemical Society, San Francisco, Calif., April 1968. ^b O. N. Bhatnagar and C. M. Criss, **73**, 174 (1969). ^c E. M. Arnett, W. G. Bentrude, J. J. Burke, and P. M. Duggleby, *J. Amer. Chem. Soc.*, **87**, 1541 (1965).

$(\text{BPh}_4^-)_{\text{PC} \leftarrow \text{DMSO}}$, we obtain the single-ion enthalpies of transfer given in Table II. The figures in the body of the table are the enthalpies of transfer of the salts; the plain figures are obtained from differences of enthalpies of solution while the figures in parentheses are obtained from the ionic values on the border of the table. The ionic values have been chosen to minimize the differences between the plain figures and those in parentheses. It is clear that these differences are mostly less than 0.1 kcal/mol as expected from the claimed accuracy of the calorimetry. The exceptions are pre-

(9) D. F. Evans and R. L. Kay, *J. Phys. Chem.*, **70**, 366 (1966).

(10) R. A. Robinson and R. H. Stokes, "Electrolyte Solutions," Butterworth and Co., Ltd., London, 1955.

(11) R. L. Kay and G. P. Cunningham, private communication.

Table II: Enthalpies of Transfer to Propylene Carbonate from Dimethyl Sulfoxide at 25° (Values in kcal/mol)^a

	Single-ion values ^b	Cl ⁻	Br ⁻	I ⁻	ClO ₄ ⁻	BPh ₄ ⁻
		1.82	2.41	2.27	0.67	-0.65
Li ⁺	7.04	9.03 ^c (8.86)	9.45 ^c (9.45)	8.97 ^c (9.31)		
Na ⁺	4.18			6.45 ^{d,e} (6.45)		3.53 ^{d,e} (3.53)
K ⁺	3.10		5.49 ^{c,d} (5.51)	5.40 ^{c,d} (5.37)		2.45 ^d (2.45)
Rb ⁺	2.14					1.49 ^d
Cs ⁺	1.31					0.66 ^d
Me ₄ N ⁺	-0.23		2.22 (2.18)	2.04 (2.04)	0.45 (0.44)	
Et ₄ N ⁺	-0.84	0.93 (0.98)	1.63 (1.57)	1.38 (1.43)	0.17 (0.17)	
Pr ₄ N ⁺	-1.23	0.65 (0.59)	1.19 (1.18)	0.98 (1.04)	-0.53 (-0.56)	
Bu ₄ N ⁺	-1.66	0.16 (0.16)	0.75 (0.75)	0.58 (0.61)	-0.92 (-0.99)	
Am ₄ N ⁺	-2.03	-0.21 (-0.21)	0.35 (0.38)	0.18 (0.24)	-1.31 (-1.36)	
Hex ₄ N ⁺	-2.38		0.11 (0.03)		-1.79 (-1.71)	
Bu ₄ P ⁺	-1.53		0.88			
Me ₃ PhN ⁺	0.48			2.75		
Ph ₄ P ⁺	-0.99	0.83				
Ph ₄ As ⁺	-0.65	1.17 (1.17)	1.78 (1.76)		-0.04 (0.02)	
Ph ₄ Sb ⁺	1.13		3.54			

^a The values in parentheses are obtained by adding the ionic heats along the margins. The other values in the body of the table are experimental. The ionic heats are chosen to make the two sets as similar as possible. ^b Single-ion values based on the convention that values for Ph₄As⁺ and Ph₄B⁻ are the same. ^c These experimental values are obtained by combination of ionic differences from Table III with data on (MX)_{DMSO←w} from R. F. Rodewald, K. Mahendran, J. L. Bear, and R. Fuchs, *J. Amer. Chem. Soc.*, **90**, 6698 (1968). ^d These data depend on heats of solution in propylene carbonate from Y. C. Wu and H. L. Friedman, *J. Phys. Chem.*, **70**, 501, 2020 (1966). ^e These data depend on heats of solution in dimethyl sulfoxide from E. M. Arnett and D. R. McKelvey, *J. Amer. Chem. Soc.*, **88**, 2598 (1966).

sumed to indicate impurity problems, but in spite of these the data seem satisfactory for the purpose at hand.

In the same way, with the convention that (Ph₄As⁺)_{PC←w} = (BPh₄)_{PC←w}, we obtain the single-ion enthalpies of transfer for the transfer to propylene carbonate from water in Table III. Finally, the enthalpies of transfer of several bromides to H₂O from D₂O are given in Table IV.

III. Enthalpies of Transfer to Propylene Carbonate from Dimethyl Sulfoxide

The ionic enthalpy change for this process is given as a function of ionic radius in Figure 1, together with the Born-charging approximation for the same quantity. This is computed on the basis of the dielectric properties of propylene carbonate² ($\epsilon = 65$, $d \ln \epsilon/dT = -3.7 \times 10^{-3}/\text{deg}$) and dimethyl sulfoxide¹² ($\epsilon = 45$, $d \ln \epsilon/dT = -4.1 \times 10^{-3}/\text{deg}$). It is at once clear that the Born-charging process, which must contribute as a result of the polarization of the solvent at a distance from the ion, contributes negligibly to the effects that are found here.

It is striking that the enthalpy of transfer of the tetraalkylammonium ions is negative and linear in the ionic radius. It is also linear in the carbon number; for the bromides in Table II from tetraethyl to tetrahexyl, we find

$$(R_4NBr)_{PC \leftarrow DMSO} = 2.40 - 0.100N \pm 0.10 \text{ kcal/mol} \quad (1)$$

where N is the number of carbon atoms in the cation and where the maximum deviation is shown. It is recalled that the data³ for the primary alcohols fit the equation

$$(C_NH_{2N+1}OH)_{PC \leftarrow DMSO} = 1.93 - 0.09N \text{ kcal/mol} \quad (2)$$

so there is a clear implication that the solvation of tetraalkylammonium ions in these solvents is accounted for by additive contributions from the methylene groups and that the solvation of the methylene groups is the same whether they are in R₄N⁺ or in ROH. This being

(12) H. L. Schlafer and W. Schaffernicht, *Angew. Chem.*, **72**, 618 (1960).

Table III: Enthalpies of Transfer to Propylene Carbonate from Water at 25° (Values in kcal/mol)^a

	Single-ion values ^b	Cl ⁻	Br ⁻	I ⁻	ClO ₄ ⁻	BPh ₄ ⁻	CF ₃ CO ₂ ⁻
		6.31	3.24	-0.78	-3.93	-3.49	7.79
Li ⁺	0.73						
Na ⁺	-2.44						
K ⁺	-5.24						
Rb ⁺	-5.87						
Cs ⁺	-6.40						
Me ₄ N ⁺	-3.89						
Et ₄ N ⁺	0.17						
Pr ₄ N ⁺	2.79	9.08	6.05	1.98	-3.77		
		(9.10)	(6.03)	(2.01)	(-3.76)		
Bu ₄ N ⁺	4.39	10.52	7.72				
		(10.70)	(7.53)				
Am ₄ N ⁺	4.79	11.05	8.18				
		(11.10)	(8.13)				
Hex ₄ N ⁺	4.24				0.31		
Ph ₄ P ⁺	-3.22	3.09			-6.87		
		(3.09)			(-7.15)		
Ph ₄ As ⁺	-3.49	2.82	-0.05		-6.64		
		(2.82)	(-0.25)		(-7.42)		
Ph ₄ Sb ⁺	-2.29		0.95				
Bu ₄ P ⁺	4.41		7.65				
Me ₃ PhN ⁺	5.55			4.77			

^a New data are the plain numbers in the body of the table. Numbers in parentheses are derived by adding the ionic enthalpies. The latter have been chosen as in Table II, except as noted.^b ^b The anion values and the cation values for Li⁺ through Et₄N⁺ have been taken from Wu and Friedman (ref 4) but shifted to accord with the convention: (Ph₄As⁺)_{PC←w} = (BPh₄⁻)_{PC←w}.

Table IV: Enthalpies of Transfer to H₂O from D₂O at 25° (Values in kcal/mol)

Me ₄ NBr	Et ₄ NBr	Pr ₄ NBr	Bu ₄ NBr	Am ₄ NBr	Ph ₄ AsBr	Ph ₄ PBr
-0.37	-0.30	-0.04	0.15	0.28	-0.24 ^b	-0.26 ^b
-0.52 ^a						

^a From Arnett and McKelvey (ref 6). All other values from Table I. ^b From chloride data in Table I combined with Cl-Br difference of 0.135 kcal/mol from Arnett and McKelvey (ref 6).

Table V: Phenyl Group Contributions to Enthalpy of Transfer to PC from DMSO Deduced from Transfer Data for Various Solutes

Solute	Hydrocarbons ^a	Me ₃ PhN ⁺	Ph ₄ As ⁺	Ph ₄ B ⁻	Ph ₄ P ⁺	Ph ₄ Sb ⁺
Ph contribution, kcal/mol	-0.17 to -0.26	0.75	-0.16	-0.16	-0.25	0.28

^a Data from ref 3.

the case, the $N = 0$ intercept of eq 1 fixes the enthalpy of transfer of the bromide ion itself (Br⁻)_{PC←DMSO} = 2.40 kcal/mol. It is very satisfactory that the single-ion value determined by this assumption is practically the same as the one determined by the convention used in Table II. Similar results are obtained if the same series of steps is repeated beginning with the data for the R₄NCIO₄, R₄NCl, or R₄NI salts.^{13,14}

The corresponding additivity principle does not work

(13) B. E. Conway, R. E. Verrall, and J. E. Desnoyers [*Trans. Faraday Soc.*, 62, 2738 (1966)] devised a similar method for obtaining single ion values of limiting partial molar volumes from the data for aqueous solutions of tetraalkylammonium salts. They plotted V_2^0 for the salts against the molecular weight of the cation and obtained nearly linear plots for each halide; the intercepts at zero molecular weight could consistently be interpreted as the ionic volumes of the halides. Their data, which are relatively considerably more accurate than ours, show small deviations from linearity which are quite consistent with the nonlinearity of the "iceberg" effect discussed in section IV of the present report. Therefore, it should perhaps be expected that this method of getting single-ion values of thermodynamic properties will work even better for nonaqueous electrolyte solutions, as in the present example.

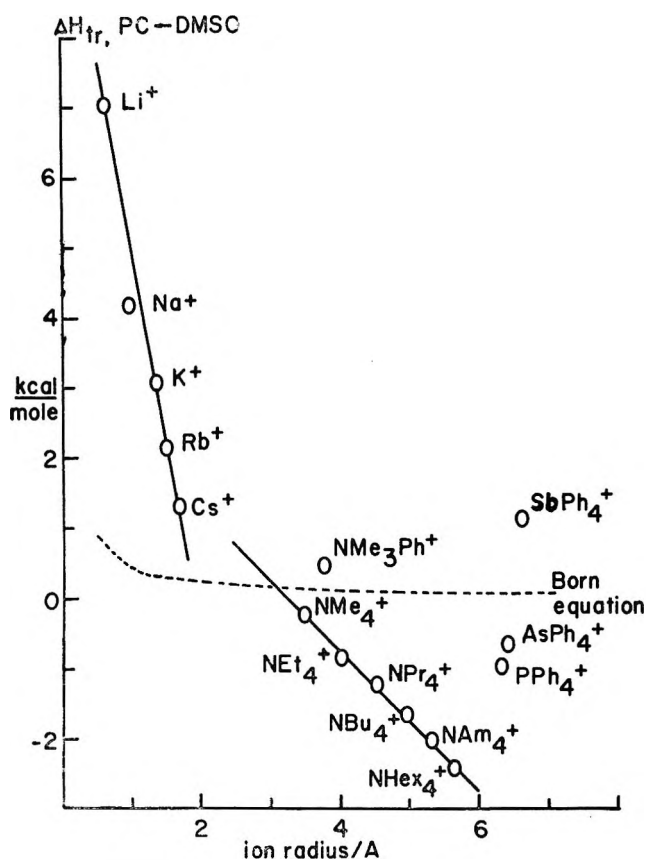


Figure 1. Ionic enthalpies of transfer to propylene carbonate from dimethyl sulfoxide based on the data in Table II. These depend on the convention that the enthalpy of transfer is the same for Ph_4As^+ and Ph_4B^- .

for the arylsubstituted ions. This is most easily demonstrated by assuming that for these ions the enthalpy of transfer is a sum of contributions from the peripheral groups with the methyl group contribution being 0.09 kcal/mol. The results given in Table V demonstrate that the solvation of the phenyl group is quite sensitive to what it is bound to. Some evidence for this was also found in the study of nonelectrolytes.³

The alkali metal ion data in Figure 1 seem to reflect an interaction of the ions as Lewis acids with the solvents as Lewis bases, since DMSO is more basic than PC and Li^+ is more acidic than Na^+ , etc. While there is no quantitative treatment to apply to this situation, it is easily shown to be consistent with the difference in ability of these solvents to act as hydrogen bond acceptors. A measure of this is the enthalpy of transfer³ of the normal alcohols, after correction for an additive effect of the methylene groups $(\text{HO}\cdots\text{H})_{\text{PC}\leftarrow\text{DMSO}} = 1.93$ kcal/mol which is close to the enthalpy of transfer of Rb^+ . The electric field at the surface of an isolated Rb^+ is 2.2×10^6 cgs units and is assumed to be a measure of the ability of the ion to discriminate between the weak base PC and the stronger base DMSO. The field in the neighborhood of the hydroxyl group of an alcohol (dipole moment = 1.7 D) has this

same value at a point 1.1 Å from the electrical center of the dipole and in line with the dipole. This does seem to be a reasonable point for the closest approach of the "surface" of the base.

IV. Enthalpies of Transfer to Propylene Carbonate from Water

The enthalpy of transfer as a function of ion radius is given in Figure 2. Some of these data have been presented and discussed before;² in particular the trend from Li^+ to Cs^+ was associated with the change of the aqueous ions from strongly hydrated to structure breaking. Also the trend from Cs^+ to Et_4N^+ was associated with "iceberg" formation induced in water by tetraalkylammonium ions.

Now it may be remarked that the trend from Li^+ to Cs^+ in Figure 1 is very similar to that in Figure 2, but rather different interpretations have been offered in the two cases: difference in basicity for the $\text{PC} \leftarrow \text{DMSO}$ transfer, but specific hydration effects for the $\text{PC} \leftarrow \text{w}$ transfer. Perhaps this is most simply justified on the basis of the difference in the single-ion values in the two systems. While there is some uncertainty that the values in Figure 2 are single-ion values, it also seems quite impossible that the error is enough to shift $(\text{Cs}^+)_{\text{PC}\leftarrow\text{w}}$ to a positive value.

A remarkable feature of the new data is the trend of the enthalpy of transfer as a function of size for the larger R_4N^+ ions. In view of the regularity of the $\text{PC} \leftarrow \text{DMSO}$ transfers of these ions (Figure 1) the curvature and maximum in the $\text{PC} \leftarrow \text{H}_2\text{O}$ transfer (Figure 2) certainly reflects some phenomenon in the aqueous rather than the PC phase. In fact this curvature is very similar to an effect in the hydration of the primary alcohols,³ where it is found that the hydration enthalpies depend nonlinearly on the number of methylene groups in the chains.

To probe the extent of this similarity, the R_4N^+ data in Figure 2 are compared with the enthalpies of the $\text{H}_2\text{O} \leftarrow \text{D}_2\text{O}$ transfers (Table IV) by an extension of the technique introduced in the investigation of the alcohols.³ Thus it is assumed that the term in the enthalpy

(14) An estimate of the enthalpy of transfer of a methylene group to PC from DMSO can also be made on the basis of the theory of regular solutions: J. H. Hildebrand and R. L. Scott, "The Solubility of Nonelectrolytes," 3rd ed, Reinhold Publishing Corp., New York, N. Y., 1950. From this theory it may be deduced that the enthalpy of transfer of species C to solvent A from solvent B is

$$(C)_{\text{A}\leftarrow\text{B}} = v_C(\delta_A - \delta_B)(\delta_A + \delta_B - 2\delta_C)$$

where v_C is the partial molar volume of species C in either solvent, assumed to be the same as the molar volume, and δ_i is the solubility parameter for species i , estimated to be 12.3 for PC and 12.8 for DMSO. On the basis of this equation one finds that both the normal hydrocarbons and the normal alcohols should fit an equation of the form of eq 1, but in each case the term in N is $-0.07N$ rather than the experimentally observed $-0.10N$. The difference is not significant in view of the uncertainties in the δ_i values of the solvents, which were estimated from the boiling points using Trouton's rule. The constant term estimated was in fair agreement for the hydrocarbons, although of course not for the alcohols. The degree of agreement found is impressive in view of the assumptions on which this theory is based. However, it is not in agreement with the data for $\text{PC}\text{-H}_2\text{O}$ transfers.

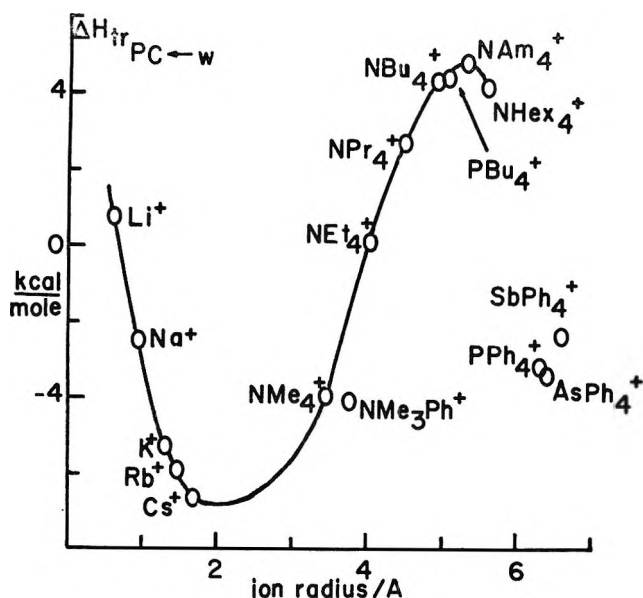


Figure 2. Ionic enthalpies of transfer to propylene carbonate from water based on the data in Table III. These depend on the convention that the enthalpy of transfer is the same for Ph_4As^+ and Ph_4B^- . The curves are merely drawn in to connect the experimental points.

of hydration of R_4N^+ which depends nonlinearly on the chain length N of $\text{R} = n\text{-C}_N\text{H}_{2N+1}$ is due to a structural ("iceberg") effect in water near the ion and that it will have the same N dependence, except for a scale factor, in D_2O as in H_2O . Then we plot

$$\text{H}^{\text{red}} = (\text{R}_4\text{NBr})_{\text{PC} \leftarrow \text{w}} - \gamma^{-1}(\text{R}_4\text{NBr})_{\text{w} \leftarrow \text{d}} \quad (3)$$

where d is D_2O , and where γ is a parameter, independent of N determined by the requirement that H^{red} should be linear in N . The experimental uncertainties are large owing to the fact that our calorimeter is not well designed to measure the small differences needed to get the $\text{d} \leftarrow \text{w}$ transfers, but the result in Figure 3 seems adequate to show that the structural effect of alkyl groups in D_2O is about 5% larger than in water at 25° . The interpretation in terms of structural effects is supported by the fact that γ is the same for R_4N^+ as for ROH within experimental error.

The strongly nonlinear radius dependence of the structural effect on the enthalpy of aqueous solutes is no doubt one of the difficulties which have impeded earlier efforts to understand this effect.⁶

A possible manifestation of this nonlinear effect in the partial molal volumes of tetraalkylammonium ions was mentioned above.¹³ A more definite independent indication of the same thing is found in the effect of these ions on the self-diffusion coefficient of water in 1 M solutions of tetraalkylammonium salts.¹⁵ The cations all reduce the self-diffusion coefficient of water, but the effect is about the same for Bu_4N^+ as for Pr_4N^+ but much smaller for Et_4N^+ and still smaller for Me_4N^+ .

In the same connection it is interesting to note that the shape of the greater part of the cation curve drawn

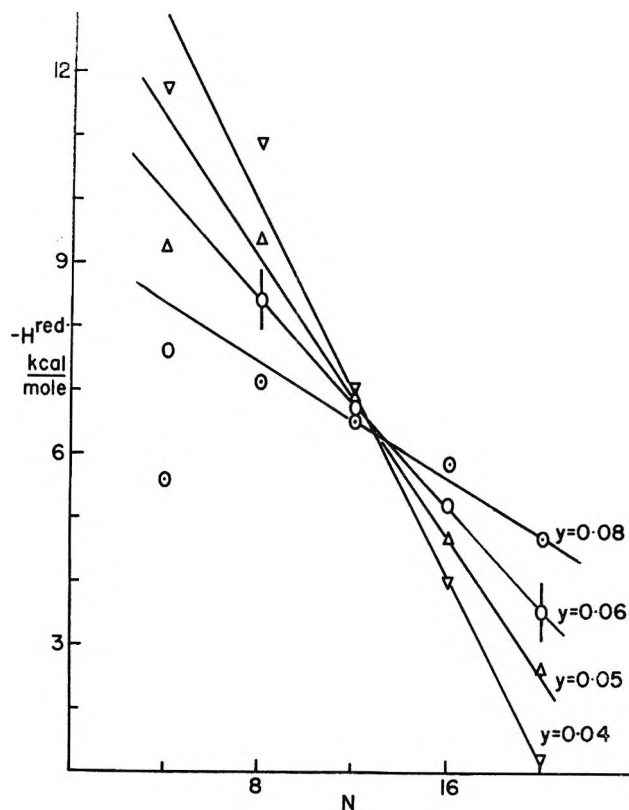


Figure 3. Test of the assumption that the structural effect in aqueous solutions of R_4N^+ salts dominates both the transfer to water from D_2O and the transfer to propylene carbonate from water.

in Figure 2 is reflected by the curve representing the radius dependence of the coefficient

$$dT_1^{-1}/dm$$

where T_1 is the nmr spin-lattice relaxation time of the solvent protons in moderately dilute aqueous solutions of various electrolytes and m is the molality of the electrolyte. This result has been recently reported by Hertz and Engel and interpreted in terms of the same structural effects which have been invoked to interpret the curve in Figure 2.¹⁶ This kinetic manifestation of the effect tends to support the structural interpretation of the thermodynamic data.

If one believes that the conventional ionic enthalpies in Figure 2 are close to the real ones, then he may conclude that, by the solvation-enthalpy criterion, Me_4N^+ is a net structure breaker, structure making and breaking mutually cancel for Et_4N^+ , and structure-making effects dominate for Pr_4N^+ , Bu_4N^+ , and Am_4N^+ . It is intriguing that these conclusions have been reached by other investigators on the basis of other experimental probes: Kay and his associates^{17,18}

(15) H. G. Hertz, B. Lindman, and V. Siepe, *Ber. Bunsenges. Phys. Chem.*, in press.

(16) G. Engel and H. G. Hertz, *Ber. Bunsenges. Phys. Chem.*, **72**, 808 (1965).

(17) R. L. Kay and D. F. Evans, *J. Phys. Chem.*, **70**, 2325 (1966).

from the ratio of Walden products of the ions in H₂O and D₂O, Wood and Anderson¹⁹ from heats of mixing of ionic solutions, and Bunzl²⁰ from the temperature dependence of the shift of the 0.97- μ infrared band in aqueous solutions of tetraalkylammonium bromides.

V. Special Properties of Phenyl Groups

The peculiar behavior of phenyl groups in the PC \leftarrow DMSO transfers has already been summarized in Table V. These data are to be compared with a ΔH of -0.2 to -0.3 kcal/mol expected if the transfer of a phenyl group is like that of an ethyl or propyl group, as might be expected if size is the dominant factor, or a ΔH of -0.3 kcal/mol if the dominant interaction is that of the solvent dipole with the solute polarizability $\alpha\mu^2/r^6$.³ It seems rather more clear in the present case than in the case of the nonelectrolytes³ that there is a strong contribution to the solvation from some interaction that is very sensitive to the detailed state of the phenyl group, perhaps the charge-transfer interaction.

In the case of the PC \leftarrow w transfers (Figure 2) there is a roughly constant contribution of -2 kcal/mol per phenyl group. This figure is obtained simply from the displacement of the phenyl-substituted ions from the R₄N⁺ curve in Figure 2 so it represents the difference in enthalpy of transfer of the phenyl group compared to an alkyl group of about the same size. Now the question is, does it represent a difference in solvation of phenyl and alkyl groups in the water or in the propylene carbonate or, perhaps, both? The fact that the PC \leftarrow DMSO transfer distinguishes phenyl from alkyl groups implies that PC solvation itself does; indeed this is established by the nonelectrolyte study³ which showed that the enthalpy of solvation of a phenyl group in PC is about -7.5 kcal/mol while that of an ethyl group is about -1.5 and that of a propyl group about -2.5 kcal/mol. These data are not consistent with the -2 kcal/mol difference noted above, so apparently there is also a sizable difference in solvation of the

alkyl and phenyl groups in the water. This also is suggested by the data for transfer of nonelectrolytes,³ but one cannot say more on the basis of the PC \leftarrow w transfers because of the failure to find a group contribution of phenyl in the hydration enthalpies of the nonelectrolytes.

It is of interest to compare the H₂O \leftarrow D₂O transfers of aryl- and alkyl-substituted cations (Table IV). We see that by this rather important measure of the structural effect both Ph₄As⁺ and Ph₄P⁺ are quite close to Et₄N⁺ as one would expect from the similarity of sizes of phenyl and ethyl groups if this were the controlling factor.

On the other hand, Masterton²¹ has found that the partial molar thermal expansion of benzene in water is positive, while that of the aliphatic hydrocarbons is negative.

Very recently NaBPh₄(aq) has been found to have a very large partial molar heat capacity;²² this effect has often been taken as diagnostic of iceberg effects. However $C_{p,2}^\circ$ for this electrolyte is very much larger than for *n*-Bu₄NBr, although the reverse would be expected on the basis of the relative sizes of the icebergs as indicated by the PC \leftarrow w transfers. These differences may be associated with the fact that clathrate hydrate compounds are reported with many aliphatic hydrocarbons and tetraalkylammonium salts as guests but none with benzene or tetraphenyl salts.²³

In summary it is still hard to decide whether the hydration of phenyl groups is qualitatively very different from that of alkyl groups.

(18) R. L. Kay, T. Vituccio, C. Zawoyski, and D. F. Evans, *J. Phys. Chem.*, **70**, 2336 (1966).

(19) R. H. Wood and H. L. Anderson, *ibid.*, **71**, 1871 (1967).

(20) K. W. Bunzl, *ibid.*, **71**, 1358 (1967).

(21) W. L. Masterton, *J. Chem. Phys.*, **22**, 1830 (1954).

(22) J. C. Ahluwalia and S. Subramanian, *J. Phys. Chem.*, **72**, 2525 (1968).

(23) G. A. Jeffrey and R. K. McMullan, "Progress in Inorganic Chemistry," Vol. 8, F. A. Cotton, Ed., Interscience Publishers, New York, N. Y., 1967.

Estimation of Activation Energies for Nitrous Oxide, Carbon Dioxide, Nitrogen Dioxide, Nitric Oxide, Oxygen, and Nitrogen Reactions by a Bond-Energy Method

by S. W. Mayer

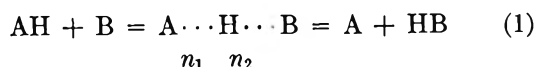
Laboratory Operations, Aerospace Corporation, El Segundo, California (Received May 16, 1969)

A trial method is described for estimating the activation energies of bimolecular transfer reactions of such multivalent gaseous compounds as O_2 , N_2 , NO , N_2O , NO_2 , CO , and CO_2 . It is also applicable when the monatomic reactants O , N , and H , and the OH radical are involved. The method uses trial relationships between bond dissociation energy, bond length, and bond order. This semiempirical calculation avoids the use of adjustable parameters. The agreement between calculated and experimental activation energies is very good when spin conservation in the transition state is considered in the computation procedure. Spin conservation is applied specifically to N_2O and CO_2 transfer reactions. A convenient rule has also been formulated that predicts the activation energy will be negligible in exothermic bimolecular reactions between radicals when the transition-state formula corresponds to that of a compound having stable bonds. No exceptions to this rule have been found.

Introduction

Transition-state computations^{1,2} of activation energies and rate constants for hydrogen atom transfers in the gas phase exhibit good agreement with measured activation energies and rate constants when several trial assumptions involving bond energy, bond order, and bond length interrelationships are used. Included are the assumptions that (1) the Pauling³ "rule" for the relationship between bond length and bond order applies in the transition state; (2) the Lennard-Jones 6-12 energy and distance parameters⁴ for the noble gases represent the zero bond order energies and internuclear distances for elements in the corresponding rows of the periodic table; (3) an approximately linear relationship exists between the logarithm of bond energy and the logarithm of bond order¹; (4) the triplet repulsion energy arising from uncoupled spins in the transition state is represented by a Sato⁵ anti-Morse function similar to that for the triplet³ Σ_u^+ state of H_2 . It is possible (although open to serious question) that the changes in potential energy of dissociating bonds or forming bonds may be described, as a function of bond length or nominal bond order, within some arbitrary error such as 2 kcal/bond by such postulates derived empirically from energy data for a series of bonds covering a range of bond orders.³

The aforementioned activation energy computing method does not utilize adjustable parameters. It does, however, use a tentative model of the transfer reaction



whereby the sum of the bond orders n_1 and n_2 in the transition state is constant at unity, corresponding to the initial univalent bond order of the reactant, AH , and of the final bond order of the product, HB . For this model, the activation energy of the transition state is calculated for one line,^{1,2} rather than a surface as in the basic London-Eyring-Polanyi absolute rate treatment.⁶

Because of the relative success^{1,2} of this rather empirical bond-energy bond-order (BEBO) model in predicting rate constants for H-atom transfers, it was decided⁷ to investigate its applicability to reactions in which the transferred univalent atom was larger than the hydrogen atom and, eventually, to reactions in which multivalent atoms were transferred. A reduced-variable treatment was introduced so that larger, univalent atoms such as the halogens were scaled relative to hydrogen. The computed activation energies and rate constants were found to agree very well with the measured values of those relatively few halogen transfer

(1) (a) H. S. Johnston and C. Parr, *J. Amer. Chem. Soc.*, **85**, 2544 (1963); (b) H. S. Johnston, "Gas Phase Reaction Rate Theory," The Ronald Press Co., New York, N. Y., 1966.

(2) (a) S. W. Mayer, L. Schieler, and H. S. Johnston, *J. Chem. Phys.*, **45**, 385 (1966); (b) S. W. Mayer and L. Schieler, *J. Phys. Chem.*, **72**, 236 (1968).

(3) L. Pauling, "The Nature of the Chemical Bond," Cornell University Press, Ithaca, N. Y., 1960.

(4) J. O. Hirschfelder, C. F. Curtiss, and R. B. Bird, "Molecular Theory of Gases and Liquids," John Wiley & Sons, Inc., New York, N. Y., 1964.

(5) S. Sato, *J. Chem. Phys.*, **23**, 592, 2465 (1955).

(6) S. Glasstone, K. J. Laidler, and H. Eyring, "Theory of Rate Processes," McGraw-Hill Book Co., Inc., New York, N. Y., 1941.

(7) S. W. Mayer, L. Schieler, and H. S. Johnston, "Proceedings of the Eleventh International Symposium on Combustion," The Combustion Institute, Pittsburgh, Pa., 1967, p 837.

Table I: Molecular and Bond Data^a

	N ₂	NO	O ₂	CO	NO ₂	N ₂ O	N(NO)	CO ₂
Dissociation energy, D_e , kcal/mol	228.6	152.8	120.3	258.9	73.7	41.0	116.2	128.4
Bond length, $r_e \times 10^{-8}$ cm	1.098	1.151	1.207	1.128	1.197	1.186	1.126	1.159
Vibrational wave number, ω_e , cm ⁻¹	2358	1904	1580	2170	1330	1410	1685	1720
Bond energy, B_e , kcal/mol	228.6	152.8	120.3	258.9	113.2	110	158	193.5
Bond order	3.0	2.5	2.0	3.0	1.75	1.75	2.5	2.0
Ground state	¹ Σ	² π	³ Σ	¹ Σ	² Σ	¹ Σ	¹ Σ	¹ Σ
Single-bond values used								
Dissociation energy, D_1 , kcal/mol	39.7	49.5	35.0	85.7	32.2	18.1	29.1	55.6
Bond length, $r_1 \times 10^{-8}$ cm	1.48	1.44	1.47	1.43	1.44	1.44	1.48	1.43
Vibrational wave number, ω_1 , cm ⁻¹	1370	1220	1120	1180	1080	1090	1105	1180
Bond energy, B_1 , kcal/mol	39.7	49.5	35.0	85.7	49.5	49.5	39.7	84.0

^a The JANAF Thermochemical Tables⁸ (with supplements to December, 1968) were the primary source of data. Energies were computed on the basis of the potential energy curve and, consequently, included the zero-point energy. In polyatomic molecules, D_e for the bond broken or formed is not equal to the bond energy since the other bonds in the molecule change in energy when one bond is broken or formed. For N₂O, which can dissociate to form either N₂ or NO, the total gas phase dissociation energy of 268 was partitioned between the ON and NN bonds on the basis of their estimated bond orders.

reactions for which the experimental kinetic data were available.⁷ Further modifications of the method¹ are needed to extend it to transfer reactions in which a multivalent bond is broken or formed. The multivalency clearly voids the use of the simple BEBO reaction model in which it was assumed that n_2 equals $1 - n_1$ for univalent bonds in the transition state. This assumption is equivalent to stating that, in univalent reactions, the bond order n_2 of H···B is equal to the decrease in bond order n_1 of A···H from its initial single bond. An extension of this trial assumption to multivalent transfers can be made by choosing a transition-state model in which the bond order n_2 continues to be linearly related to the decrease in the bond order of the dissociating bond A···X, where X is the transferred atom. The computation procedure associated with this model is described in the next section.

Computation Procedures

A. Multivalent, Dissociation Energy. The aforementioned transition-state model for multivalent transfers in which the bond order n_2 of the formed bond X···B was linearly dependent on the decrease in bond order of the dissociating bond was satisfied by the relationship

$$n_2 = (n_{XB}/n_{AX})(n_{AX} - n_1) \quad (2)$$

where n_{AX} and n_{XB} are, respectively, the initial bond order of the reactant AX and the final bond order of the product XB, X is the transferred atom (*e.g.*, nitrogen or oxygen), and n_1 is the bond order of A···X in the transition state. Equation 2 meets the requirement that when n_2 is zero (at the initiation of the reaction) n_1 equals n_{AX} , and that n_2 equals n_{XB} when n_1 is zero at the conclusion of the bimolecular transfer reaction. When X

is a univalent atom such as hydrogen, eq 2 reduces to the BEBO trial assumption that $n_1 + n_2$ equals 1.

In order to compute activation energies for transfers involving a multivalent bond by modified BEBO method, it was necessary to extend the bond-energy bond-order relationship to orders above 1. Since a linear relationship between $\log D_e$ (where D_e is the gas phase dissociation potential energy of the bond) and $\log n$ was used for bond orders not exceeding 1, a linear $\log D_e/\log n$ relationship was used for n greater than 1. Then, the slopes π' and π'' of these lines for the multivalent region are given by

$$\pi' = [\log(D_{e,AX}/D_1)]/\log n_{AX} \quad (3A)$$

$$\pi'' = [\log(D_{e,XB}/D_2)]/\log n_{XB} \quad (3B)$$

where D_1 and D_2 are the single-bond dissociation potential energies (Table I) of AX and XB, respectively. D_e includes the zero-point energy, as shown in Table I, since it is based on the minimum of the potential energy curve. For diatomic species, the dissociation energy is equal to the bond energy B_e , but this equality does not hold for polyatomic species since the bond energies of the other bonds in the molecule generally change when a bond is broken or formed.³ The values of D_e in Table I were obtained in a straightforward manner from thermochemical data,⁸ but the values of D_1 for the triatomic molecules were estimated because they have not been measured. The estimations were based on the simple assumption that the ratio of D_1 to B_1 was the same as that for D_e to B_e .

(8) D. R. Stull, Ed., "JANAF Thermochemical Tables, with Supplements," Dow Chemical Co., Midland, Mich., 1968.

$$D_1/B_1 = D_e/B_e \quad (4)$$

This expression also implies that the slope π' is unchanged if B_1/B_1 is used in eq 3 instead of D_e/D_1 .

With these modifications, the potential energy V of transition-state formation in multivalent bimolecular transfer reactions was calculated in a manner similar to that used for univalent transfers.^{1,2}

$$V = (D_{e,AX} - D_{1,AX}n_1^{\pi'}) - D_{2,XB}n_2^{\pi''} + V_r \quad (5)$$

where V_r is the triplet repulsion as calculated by the reduced variable treatment of eq 10 in ref 7. When a bond order, n_1 or n_2 , is less than 1, the slope π in eq 5 is replaced by the slope p calculated for the bond-order region below 1. In a manner similar to that of previous investigations,^{1,2} the computer program modified for multivalent bonds determines the value of n_2 that corresponds to the peak in the potential energy V of the linear transition-state model $A \cdots X \cdots B$. The computed activation energy for this model is equal to the potential energy peak height plus a small zero-point energy correction.⁶

B. Spin Conservation in the Transition State. The dissociation energies D_e shown in Table I correspond, as is customary, to dissociation to ground-state products. In thermal dissociation, the ground-state atomic oxygen dissociated from $\text{CO}_2(^1\Sigma)$ and $\text{N}_2\text{O}(^1\Sigma)$ probably⁹ is triplet $\text{O}(^3\text{P})$, but spin would be conserved if a singlet $\text{O}(^1\text{D})$ atom were dissociated from the parent molecule. For these bimolecular transfers, it is not known whether dissociation of CO_2 or N_2O starts by splitting off a singlet $\text{O}(^1\text{D})$ atom and is followed by spin conversion deexcitation of the singlet to the triplet $\text{O}(^3\text{P})$. It is conceivable that prior to the dissociation the molecule transforms to an excited state *via* an internal spin change and that $\text{O}(^3\text{P})$ is then formed directly by dissociating from an excited molecule, or the oxygen atom dissociated from ground state N_2O or CO_2 could cross over in the transition state to $\text{O}(^3\text{P})$. From a kinetics point of view, it appears that the most direct mode of beginning to break the oxygen bond in bimolecular transfers involving N_2O or CO_2 could well be by the formation of single $\text{O}(^1\text{D})$. From that point of view, it is clearly desirable to consider a transition-state model, when N_2O or CO_2 are involved in the bimolecular transfer of an oxygen atom, in which the dissociating oxygen (*i.e.*, X in $A \cdots X \cdots B$) is in the $\text{O}(^1\text{D})$ state. This can be done quite readily in computations of the activation energy by adding the difference in energy between $\text{O}(^3\text{P})$ and $\text{O}(^1\text{D})$ (45.4 kcal/mol) to D_e when the described computation procedure is used for multivalent transfers. In contrast with the dissociation spin-conservation requirements for N_2O and CO_2 , it is possible for ground state $\text{O}(^3\text{P})$ to dissociate directly with spin conservation from the other molecules of Table I: NO , CO , NO_2 , and O_2 . Consequently, a transition-state model for oxygen transfers involving only the latter molecules need not

consider the possibility that $\text{O}(^1\text{D})$ is the state of the transferred atom.

C. Bond Formation in the Transition State Without Corresponding Dissociation. When the modified BEBO method was applied^{1,2,7} to univalent bonds such as those in F_2 or H_2 , the model of the transition state logically involved the assumption that dissociation of the bond of reactant AX must occur in proportion to the formation of the product bond XB . This proportionality is expected since the XB bond is formed with the participation of an electron that had been used in the AX bond. In multivalent reactions, the situation can be more complex. For example, in the case of NO_2 reactant, the valence electrons are not in a completely bonded form, as indicated by the electron spin. It is possible, therefore, that a model for the oxygen-transfer reaction of NO_2 with H could consist of the formation of a species such as $\text{H} \cdots \text{ONO}$, where the bond order of $\text{H} \cdots \text{O}$ increases without a similar decrease in the ON bond. The criterion for selecting those transition states for which this model is considered possibly applicable is the existence of a stable compound that corresponds to the transition-state formula. A stable compound, in this context, can tentatively be defined as one with a bond dissociation energy of at least 25 kcal/mol for each bond. In the cited case, nitrous acid would be the stable compound, with a dissociation potential energy of 78 kcal/mol for the $\text{H}-\text{O}$ bond.⁸ Other compounds with formulas similar to those of relevant transition-state models are N_2O , NO_2 , and O_3 . Since the formation of the new bond in the transition state will release energy to the transition state, estimates of activation energy based on this model can be made by subtracting a term from the right-hand member of eq 5 that corresponds to the potential energy of the bond formed by one reactant with the other reactant (*e.g.*, H and ONO).

D. Bond-Energy Dissociation. The dissociation models previously used¹ for polyatomic molecules allow the dissociation of an atom from a reactant to proceed slowly enough so that the other bonds in the reactant reach their ground state before the $A \cdots X$ bond (where A is not monatomic) is completely broken. Consequently, the dissociation energy rather than the bond energy was used for computations based on this model. It is conceivable, however, that for some polyatomic molecules the bond $A \cdots X$ may break so rapidly in the transition state that the other bonds in A remain unchanged in the transition state. When computations were made for oxygen or nitrogen transfers based on this model, the calculated activation energies did not usually agree well with the measured values. For this model, computations were made by using the bond energy data of Table I rather than the dissociation energies.

E. Simultaneous Polyvalent Bond Formation and Dis-

(9) E. K. Gill and K. J. Laidler, *Can. J. Chem.*, **36**, 1570 (1958).

Table II: Comparison of Computed Activation Energies with Observed Activation Energies

Reaction AX + B = A + BX	Observed E_0	Computed activation energies ^a					
		Spin conser- vation	Multi. dissoc. energy	No triplet	Single- bond energy	Multi. bond energy	Poly. simul- taneous
N ₂ O + NO = N ₂ + NO ₂	50 ^{b,c}	48	2	46	31	13	1
N ₂ O + O = N ₂ + O ₂	27 ^d	28	0	26	0	35	..
N ₂ O + H = N ₂ + OH	15 ^e	15	0	14	0	1	0
O ₂ + CO = O + CO ₂	50 ^f	49	37	48	..	73	5
HO + CO = H + CO ₂	0 ^g	1	0	0	0
NO ₂ + CO = NO + CO ₂	32 ^h	28	1	26	0	34	0
ONN + O = ON + NO	27 ^{i,j}	29	24	25	48	40	0

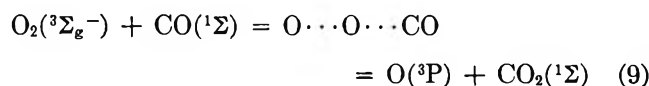
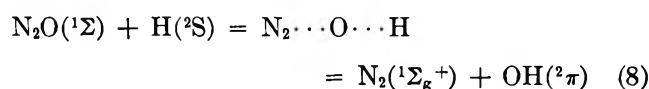
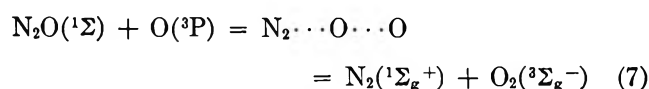
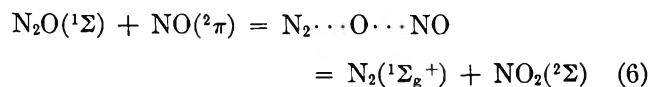
^a Energies expressed in kcal/mol. ^b F. Kaufman and J. R. Kelso, *J. Chem. Phys.*, **23**, 602 (1955). ^c E. S. Fishburne and R. Edse, *ibid.*, **41**, 1297 (1964). ^d D. Gutman, R. L. Belford, A. J. Hay, and R. Panirow, *J. Phys. Chem.*, **70**, 1793 (1966). ^e G. Dixon-Lewis, M. M. Sutton, and A. Williams, "Tenth International Symposium on Combustion," Combustion Institute, Pittsburgh, Pa., 1965, p 495. ^f K. G. P. Sulzmann, B. F. Myers, and E. R. Bartle, *J. Chem. Phys.*, **42**, 3969 (1965). ^g G. Dixon-Lewis, W. E. Wilson, and A. A. Westenberg, *ibid.*, **44**, 2877 (1966). ^h H. S. Johnston, W. A. Bonner, and B. J. Wilson, *ibid.*, **26**, 1002 (1957). ⁱ K. Schofield, *Planetary Space Sci.*, **15**, 643 (1967). ^j R. M. Fristrom and A. A. Westenberg, "Flame Structure," McGraw-Hill Book Co., Inc., New York, N. Y., 1965, pp 355, 371, 372.

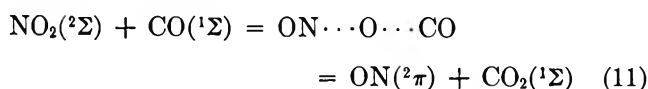
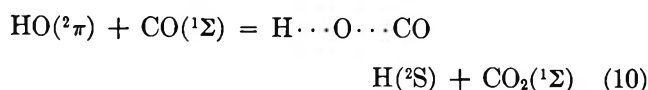
sociation. It is characteristic of the transition-state models previously described that bond formation proceeds first *via* formation of the single bond, which then becomes a polyvalent bond as the reaction progresses. It is clearly possible that the formation of a polyvalent bond in the transition state does not proceed through any recognizable single-bond state such as those for which data are presented in Table I, but that the molecular orbital changes involved in the formation of a polyvalent bond proceed directly from the zero bond to the final bond without the intermediate step of passing through a bond characteristic of single bonds in stable molecules. Similarly, the dissociation of the polyvalent bond A...X in the transition state could proceed directly to the zero-bond state without following the potential energy bond-order path suggested by the dissociation energy D_1 of a single bond. By using the D_e and r_e of Table I and the Johnston-Parr trial assumption¹ that the Lennard-Jones 6-12 energy and distance parameters for neon⁴ represent the zero bond-order energies and internuclear distances of N and O bonds, values of π' and π'' were calculated for use in eq 5 over the entire bond-order range rather than limiting the use of π' and π'' to bond orders above 1. The activation energies computed for this model gave poor agreement with experiment for most of the reactions studied, but not for reactions of an atom with a diatomic species. In the latter cases, the transition state is triatomic, and the only bonds in the transition state are the breaking and forming bonds so that, in exothermic reactions, the energy involved initially is absorbed in these two bonds. This special situation will be considered later, in connection with Table III.

Results and Discussion

Computed activation energies are compared with experimental activation energies in Table II. All of the

reactions are written in the exothermic direction. None of the reactions in Table II is of the atomic plus diatomic type. The "multivalent dissociation energy" column summarizes the E_0 's computed with the spin conservation ignored. The computed E_0 's of particular interest, however, are in the spin conservation column. This column summarizes the computed E_0 's obtained by combining the postulate of spin conservation for dissociation of the multivalent bond, described in the section on Computation Procedures, with the linear bond-order relationships for multivalent bonds as embodied in eq 2-5. The agreement is very good between the E_0 's computed by this method and the experimental E_0 's. Among the first six reactions, spin conservation involves the formation or reaction of an O(¹D) atom in the transition state since CO₂ or N₂O is a reactant or product. The agreement between computed and measured E_0 's is superior when such spin conservation is assumed. The electron spin states consistent with spin conservation, if the transferred oxygen atom in the activated complex remains in the O(¹D) state, are shown in the following equations for reactions involving ground state, singlet N₂O or CO₂





The Wigner-Wittmer rules¹⁰ for spin conservation are extended to the transition state in eq 6-11.

For reaction 6 the observed activation energy is about 50 kcal/mol (as shown in Table II) despite the fact that the reaction is written in the exothermic direction. If spin conservation of the atomic oxygen in the transition state is not postulated and the alternate assumption is made that the oxygen of N₂O changes spin to form O(³P) as it apparently⁹ does in the thermal decomposition of N₂O, the computed E_0 was only 2 kcal/mol. However, if the postulate is used, as proposed in this study, that spin is conserved in the transition state, the computed E_0 was 48 kcal/mol, which was in much better agreement with the observed activation energy. For spin conservation, the maximum in the value of V , the potential energy of activation in eq 5, was calculated to occur when the bond order n_2 was equal to 0.75. At this bond order, the bond energy of the new bond (X \cdots B or O \cdots NO) was calculated to be 23 kcal/mol. The energy required to break the old bond (A \cdots X or N₂ \cdots O) to the bond order n_1 given by eq 2 at n_2 equal to 0.75 was calculated to be 71 kcal/mol in accordance with the terms in the parentheses of eq 5. Thus, the energy required to break the old bond exceeded by 48 kcal/mol the energy supplied by the formation of the new bond at maximum V . In the case of reaction 6, V_r was 1.6 kcal/mol which was counterbalanced by the zero-point energy correction.⁶

For reactions 6-11, the trial postulate of spin conservation provided good agreement with experimental E_0 (Table II), whereas the assumption of ground-state O(³P) as the transferred oxygen species in the transition gave poor agreement except in reaction 10. The last reaction in Table II did not, however, show significantly better agreement for spin conservation, which required that the transferred N atom remain in a doublet, excited state such as N(²D).

The "no triplet" column presents E_0 's computed by the procedure used for the spin conservation column, except that triplet repulsion V_r was arbitrarily set at 0. From the results listed in this column it can be seen that, for almost all of these reactions, the triplet repulsion made only a small contribution to the activation energy, compared to the contributions of the bonding terms in eq 5. The "single-bond energy" column lists E_0 's computed by the procedures used for the spin conservation column, except that the single-bond energy B_1 was used for eq 3 and 5, rather than the corresponding dissociation energy D_1 . It is evidently incorrect, as anticipated, to use B_1 rather than D_1 since the computed

E_0 's do not generally exhibit satisfactory agreement with experiment when B_1 is thus employed.

For the multivalent bond energy column, the method described in the Computation Procedures section under "Bond-Energy Dissociation" was used. Examination of the computed E_0 's in this column of Table II shows that they do not generally agree with the experimental E_0 's although there are some cases of agreement. For the polyvalent simultaneous column, the method used was described in the Computation Procedures section under "Simultaneous Polyvalent Bond Formation and Dissociation." This model for the bonding changes during a reaction does not give agreement with experiment for those reactions having a transition state with more than two bonds.

The structural formulas of the transition state in the first six reactions of Table III are similar to those of

Table III: Reactions That Have a Transition-State Formula Similar to a Stable-Molecule Formula

Reaction AX + B = A + BX	Transition state formula	Observed E_0	Computed E_0^a Multi sim- dissoc. ta- energy neous	En- ergy ^b of new bond (kcal/ mol)
ONO + H = ON + OH	HNO ₂	0 ^c	1	78
ONO + O = ON + O ₂	NO ₃	0 ^d	3	49
ON + N = O + N ₂	N ₂ O	0 ^d	25	61
ON + O = O + NO	NO ₂	~0 ^e	25	72
O ₂ + O = O + O ₂	O ₃	~0 ^e	51	26
HO + O = H + O ₂	HO ₂	0 ^f	25	63
O ₂ + N = O + NO	...	7 ^f	27	8

^a For all the reactions in Table III, spin conservation in the transition state can occur without involving excited atoms such as O(¹D) or N(²D). Therefore, the E_0 computed by the multivalent dissociation-energy model is equal in these cases to the E_0 computed for the spin-conservation model. All energies here are in kcal/mol. ^b Bond-energy data based on "JANAF Tables." In each of these six reactions, this bond energy is easily sufficient to supply all the activation energy that would have been needed, based on E_0 computed by the appropriate model. Consequently, observed E_0 should be negligible (*i.e.*, 0 or 1 kcal/mol). ^c L. F. Phillips and H. I. Schiff, *J. Chem. Phys.*, **37**, 1233(1962). ^d L. F. Phillips and H. I. Schiff, *ibid.*, **36**, 1509 (1962). ^e J. T. Herron and F. S. Klein, *ibid.*, **40**, 2751 (1964); **41**, 1285 (1964). ^f R. M. Fristrom and A. A. Westenberg, "Flame Structure," McGraw-Hill Book Co., Inc., New York, N. Y., 1965, pp 355, 371, 372.

stable species⁸ (*e.g.*, HONO, N₂O, NO₂, NO₃, O₃, and HO₂). For this specific class of reactions, E_0 can be computed as outlined under "Bond Formation in the Transition State without Corresponding Dissociation" of the Computation Procedures section. In this group of reactions between two radicals, E_0 in the exothermic direction is almost zero, possibly because sufficient en-

(10) G. Herzberg, "Spectra of Diatomic Molecules," 2nd ed, D. Van Nostrand Co., Inc., Princeton, N. J., 1959, p 315 ff.

ergy is initially provided by the preliminary partial formation of the new bond in the transition state to supply the subsequent dissociation energy requirement of the old bond, with virtually no net potential energy of activation. It is, therefore, postulated on a trial basis that the absence of activation energy barriers will be characteristic of exothermic bimolecular transfer reactions for which the transition-state structural formula corresponds to that of a stable compound, if the bond formed between the two radical reactants has a binding energy larger than the activation energy predicted by the appropriate model of Table III. Of the six reactions in this group in Table III, four are the monatomic-plus-diatomic polyvalent reaction type for which the simultaneous bond-formation model (see Computation Procedures section) may be justified. The potential value of the simultaneous model is further indicated by the results in Table III for the last reaction, $\text{NO} + \text{O} = \text{N} + \text{O}_2$, which does not have a transition-state formula that corresponds to a stable compound.⁸ The E_0 computed by the simultaneous model for this reaction agrees very well with experiment, whereas the E_0 's computed by models involving typical single-bond energies for N-O and O-O are much too high. Another indication of the possible merit of the simultaneous model is given by the data in Table III for the $\text{O}_2 + \text{O}$ oxygen exchange reaction, which has almost no potential energy barrier. The standard enthalpy for the association⁸ of $\text{O}_2 + \text{O}$ to form O_3 is only about -26 kcal/mol at 300°K . Therefore, the energy of the bond formed between the two reactant radicals cannot supply the 51 kcal/mol required to eliminate the activation energy barrier computed by the "multivalent dissociation energy" model, which postulates that bond formation and dissociation proceed *via* the characteristic single-bond energy state. The simultaneous model on the other hand, is satisfactory for this exchange reaction since it leads to a computed E_0 requirement of only 4 kcal/mol which can readily be supplied from part of the 26 kcal/mol available in the association of the radical O_2 with O.

A hypothetical justification of the suggested uniqueness of triatomic transition states in following the simultaneous model can be formulated in the following manner. Consider the $\text{O}\cdots\text{O}\cdots\text{O}$ transition state in the $\text{O}_2 + \text{O}$ exchange reaction. The 120 kcal/mol bond energy (Table I) of the double-bonded O_2 product and reactant is to be contained in the two bonds of this

transition state. In view of the symmetry of the reaction, the bond order of the forming bond should be one when the bond order of the breaking bond is one. Since the characteristic bond energy of the oxygen single-bond is only 35 kcal/mol (Table I), the energy that could be stored in two such normal single bonds is only 70 kcal, in contrast with the 120 kcal. Consequently, bond breaking and formation would have a tendency not to proceed through the usual state characterized by a bond energy of 35 kcal/mol at a bond order of one, but would prefer a path that allowed almost all the 120 kcal to be distributed between the breaking and forming bond when they each have a bond order of one. (It should not be assumed that this hypothesis is justified for univalent reactions; the latter attain a bond order of one only at the beginning and end of the reaction.) If the transition state is larger than triatomic, it is noteworthy that breaking and forming of bonds can, however, more readily proceed through a normal single bond since the excess energy (such as the ~ 50 kcal/mol in the case of the $\text{O}_2 + \text{O}$ exchange) can be stored in exciting the vibrations of the other bonds and in the higher rotational energies due to greater moments of inertia of the nonlinear, larger transition states. The data of Tables II and III indicate that the use of the simultaneous model should be reserved for transfer reactions between monatomic and diatomic species.

To summarize, the trial postulates found to be of value in these semiempirical calculations are (1) spin conservation for the transferred atom is maintained in the transition state; (2) the activation energy (exothermic direction) is almost zero when the structural formula of the transition state corresponds to that of a reasonably stable molecule; (3) the dependence of potential energy on bond order in the transition state is represented within about 2 kcal/mol by eq 5, as supplemented by eq 2-4; and (4) in reactions of atoms with diatomics involving polyvalent bonds, the direct, simultaneous formation and dissociation of polyvalent bonds can occur. As new experimental data on the kinetics of multivalent, bimolecular transfer reactions become available, it should be possible to determine the value of these empirical trial postulates.

Acknowledgment. It is a pleasure to acknowledge the valuable correspondence with Professor H. S. Johnston of the University of California, Berkeley, Calif.

The Surface Hydroxylation of Silica

by C. G. Armistead, A. J. Tyler, F. H. Hambleton, S. A. Mitchell, and J. A. Hockey

Unilever Chemicals Development Centre, Warrington, England, and Chemistry Department, University of Manchester Institute of Science and Technology, Manchester, England (Received May 19, 1969)

The surface hydroxylation of silica gels and powders has been studied by determining the stoichiometry of the reactions of SiMe_2Cl_2 , TiCl_4 , and BCl_3 with the surface hydroxyl groups. The results demonstrate that the fully hydroxylated silica surfaces studied carry two distinct types of surface hydroxyl sites, which are distributed as follows: 1.4 ± 0.1 single surface hydroxyls (type A sites), and about 3.2 ± 0.1 interacting hydroxyl groups arranged in pairs (1.6 ± 0.1 type B sites). On heating the silicas above ambient temperatures, *in vacuo*, the type B sites are progressively removed. By correlating this result with earlier studies, it is concluded that at temperatures of $500 \pm 50^\circ$, *in vacuo*, virtually all the type B sites are eliminated. However, the type A site concentration remains constant at evacuation temperatures up to $600 \pm 50^\circ$ at around 1.4 ± 0.1 A sites/100 \AA^2 .

These conclusions suggest that the silica surface corresponds to an array of different crystal planes, some of which contain OH groups at relatively large interhydroxyl spacings and others containing OH groups held in such a way as to promote interhydroxyl hydrogen bonding.

The surfaces of all metal and metalloid oxides are covered to varying degrees by hydroxyl groups or ions which play an important role in the adsorption processes occurring at oxide surfaces. The surface properties of silica are of great theoretical and practical importance and consequently this oxide has been the subject of a great deal of research. The parameters which require definition for a satisfactory description of the surface properties are the concentration, coordination and stereochemistry of the surface hydroxyls. A number of experimental techniques have proved to be of particular value in this respect.

Using thermogravimetric methods, de Boer and Vleeskens¹ found that silicas approached a limiting surface coverage or concentration of 4.6 hydroxyl groups per 100 \AA^2 of surface ($n_{\text{OH}} = 4.6$) after they had been repeatedly rehydroxylated and annealed at 450° . They concluded that the fully annealed and rehydrated surface of silica closely resembled the rhombohedral face of β -tridymite, in which each of 4.6 surface silicon atoms per 100 \AA^2 of surface carried one hydroxyl group. The hydroxyls in excess of this limiting value were attributed to surface defects and arrangements whereby some of the surface silicon atoms carried more than one hydroxyl. Other workers²⁻⁴ utilizing infrared spectroscopic techniques have since attributed the excess hydroxyl concentration to hydroxyl groups located within the bulk of the solid. Such bulk hydroxyls are removed during thermal treatment and only a very few are regenerated during the rehydroxylation process.⁵

As a result of such studies, it has become apparent that the model of de Boer,¹ *et al.*, for the surface hydroxylation of silica is insufficient to explain the observed results. Its major defect is that it predicts that the limiting surface contains hydroxyl groups in such a way that their oxygen atoms are 5 \AA apart,

hence implying that interhydroxyl hydrogen-bonding interactions cannot occur due to this relatively large distance. It has been clearly demonstrated that a substantial fraction of the hydroxyl groups of both freshly prepared and hydroxylated annealed silicas undergo hydrogen-bonding interactions.²⁻⁴

In a recent publication, Peri and Hensley⁶ have produced a different model for the silica surface. These workers have used computer techniques to simulate *via* "Monte Carlo" statistical methods, crystallographically viable surface hydroxylation patterns. In their paper, Peri and Hensley⁶ produce two possible models for the surface hydroxylation. One (see Figure 3, ref 6) corresponds to a randomly hydroxylated 0001 face of β -tridymite, which contains approximately 1.5 single or non-hydrogen-bonded hydroxyls per 100 \AA^2 of surface and about 3-3.5 hydrogen-bonded hydroxyls per 100 \AA^2 of surface. However, Figure 3 in Peri and Hensley's paper⁶ shows no differentiation between first (*i.e.*, surface) and second-layer silicon atoms. This cannot therefore be a correct model for the silica surface and any discussion based on it is likewise invalid. The other model (see Figure 4 of ref 6) corresponds to a surface resembling an idealized 100 face of β -cristobalite. When this model is fully hydroxylated each silicon atom carries two hydroxyl groups giving a total concentration of 7.9 hydroxyls per 100 \AA^2 of surface.

(1) J. H. de Boer, M. E. A. Hermans, and J. M. Vleeskens, *Proc. Koninkl. Ned. Akad. Wetenschap.*, B, **60**, 44 (1957).

(2) F. H. Hambleton, J. A. Hockey, and J. A. G. Taylor, *Trans. Faraday Soc.*, **62**, 801 (1966).

(3) J. J. Fripiat and U. Uytterhoeven, *J. Phys. Chem.*, **66**, 800 (1962).

(4) V. Ya. Davydov, U. V. Kiselev, and L. T. Zhuravlev, *Trans. Faraday Soc.*, **60**, 2254 (1964).

(5) F. H. Hambleton, J. A. Hockey, and A. J. Tyler, *J. Catal.*, **13**, 35 (1969).

(6) J. B. Peri and A. L. Hensley, Jr., *J. Phys. Chem.*, **72**, 2926 (1968).

Experimentally the surface concentrations of single (A site) and paired (B site) hydroxyls may be assessed by considering the stoichiometry of the chemical reaction of the surface hydroxyls with hydrogen-sequestering reagents. As a result of their own studies using AlCl_3 and SiCl_4 , Peri and Hensley⁶ have chosen the 100 β -cristobalite model, since they state that their experimental results show that all the hydroxyls react in pairs even after evacuation of some of the solids at temperatures in excess of 600° .

The object of the present paper is to show that there exists a significant body of experimental evidence in favor of a silica surface containing both A and B sites and also to postulate a theoretical model in accord with these observations.

Experimental Section and Results

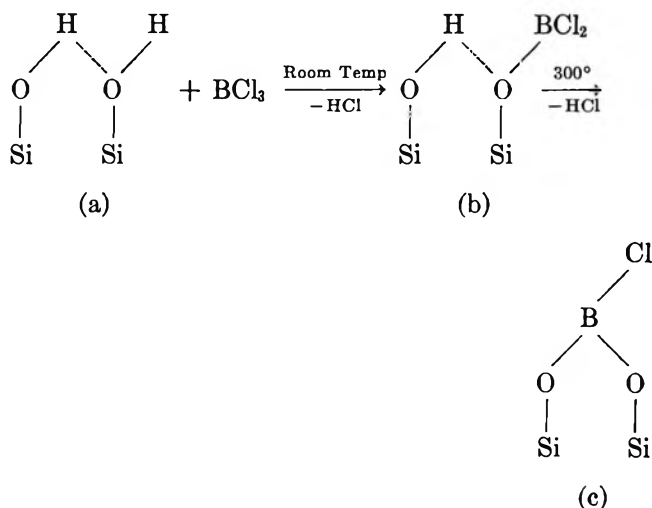
The results of the infrared, thermogravimetric and adsorption studies referred to in this paper have been published elsewhere⁷⁻¹⁰ and the reader is thus referred to this literature as required. The only experimental data reported here is that which concerns the chemical reactions of TiCl_4 , BCl_3 and SiMe_2Cl_2 with the surface hydroxyls of a range of silica gels and powders. All the experimental techniques have one common important feature. All the reactions were investigated by chemical analysis of the solid phase for residual chlorine, thereby circumventing any possible artifactual results produced by the reactions of the halogen compounds with any vacuum stopcocks, greased or otherwise. In our experience, BCl_3 , TiCl_4 and halogenosilanes react with the organic polymer diaphragms of greaseless stopcocks and vacuum greases to produce gaseous HCl in significant quantities.

It is also important to recognize that if the surface hydroxyls of a silica, which also contains bulk hydroxyls, are reacted with halogen compounds at low temperatures ($\leq 200^\circ$) then the bulk hydroxyls remain unaffected. If the unreacted solid is then heated to 600° , the bulk hydroxyls condense, releasing water from the interior of the particles. This water hydrolyzes the halogen containing surface products thereby producing HCl in the gas phase. All freshly prepared silicas in our experience contain an appreciable quantity of such bulk hydroxyls often equivalent to an n_{OH} value of 1-2 per 100 \AA^2 .

The following experiment is reported as an illustration of this point. A silica containing "bulk hydroxyls"^{5,8,10} (*i.e.*, hydroxyls unavailable for reaction with molecules such as D_2O , BCl_3 , AlCl_3 , $\text{SiMe}_2\text{Cl}_{(4-x)}$) was mounted in a cell¹¹ and its spectrum recorded after evacuation at 2×10^{-4} Torr at room temperature. The spectrum obtained is shown in Figure 1a and is similar to that obtained by Davydov and his coworkers⁴ for similar internally hydroxylated silicas. Reaction with BCl_3 at room temperature leaves a broad residual OH absorption band corresponding to the internal

hydroxyls as defined by this reagent. The excess BCl_3 vapor and the HCl produced in the reaction were then evacuated at room temperature as before and the corresponding spectrum recorded (Figure 1b). The cell was then closed from the pumps and the sample heated *in situ* for 90 min at 300° . The spectrum (Figure 1c) was then recorded once more without evacuating the cell. This spectrum illustrates that this procedure leads to the production of a surface containing SiOH and BOH species of the type described previously⁷ and also to the production of gaseous HCl as evidenced by the finely resolved absorption pattern observed around 2890 cm^{-1} .

Another suggested explanation¹² of the spectra shown in Figure 1 is that the residual absorption band at 3650 cm^{-1} (1b) corresponds to interacting surface hydroxyls that cannot react completely as pairs with BCl_3 at ambient temperatures owing to steric hindrance—a possibility suggested by Peri and Hensley⁶—but can react to completion on subsequent heating to 300° .



However, the second reaction at 300° on this scheme, although producing HCl in the gas phase as observed (Figure 1c), would not produce the observed hydroxylated species SiOH and BOH (Figure 1c). Noting the results of our other studies on the BCl_3 , SiO_2 , H_2O - D_2O system^{2,5,7} and spectrum c, we conclude that the hydrolyzing reagent produced on heating the room temperature reacted species (Figure 1b) must be HOH and

(7) F. H. Hambleton and J. A. Hockey, *Trans. Faraday Soc.*, **62**, 1694 (1966).

(8) C. G. Armistead and J. A. Hockey, *ibid.*, **63**, 2549 (1967).

(9) J. A. G. Taylor and J. A. Hockey, *J. Phys. Chem.*, **70**, 2169 (1966).

(10) A. J. Tyler, Ph. D. Thesis, Manchester University, Manchester, England, 1968.

(11) C. G. Armistead, F. H. Hambleton, J. A. Hockey, and J. W. Stockton, *J. Sci. Instrum.*, **44**, 872 (1967).

(12) We thank one of the referees for bringing this possibility to our notice. However, as is now indicated in the text, we do not believe it to be a viable explanation of the experimental results summarized by the spectra in Figure 1.

Table I

Sample	Reagent	Site concn/100Å ²	
		Type A	Type B
R. A. 3	TiCl ₄	1.4 ± 0.1	3.2 ± 0.1
R. R. A. 3/700	TiCl ₄	1.4 ± 0.1	3.2 ± 0.1
R. A. 3/700	TiCl ₄	1.3 ± 0.1	...
R. A. 3	SiMe ₂ Cl ₂	1.3 ± 0.1	... ^a
R. R. A. 3/700	SiMe ₂ Cl ₂	1.3 ± 0.1	... ^a
R. A. 3/700	SiMe ₂ Cl ₂	1.2 ± 0.1	... ^a

^a Indeterminable with SiMe₂Cl.

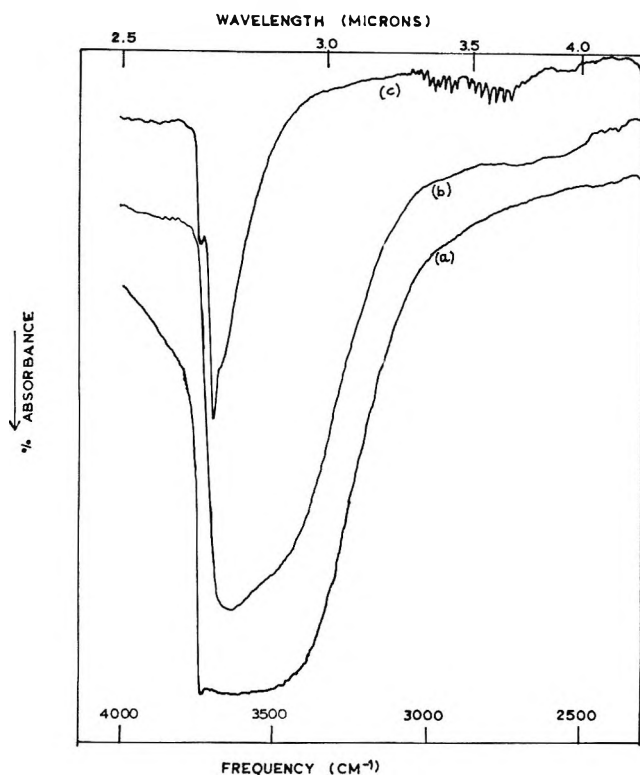


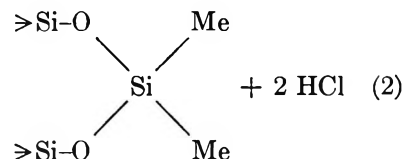
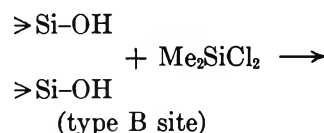
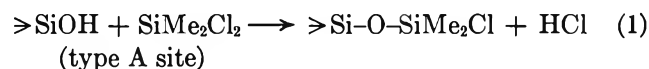
Figure 1. Spectrum of silica holding both surface and "bulk" hydroxyls (a) before reaction with BCl₃, (b) after reaction with BCl₃ followed by evacuation at room temperature, and (c) after subsequent heating for 90 min at 300° without evacuation.

not OH. Hence we do not feel that this "steric hindrance" viewpoint is tenable.

Thus an experimental procedure of this type, which corresponds closely to that of Peri and his coworkers,⁶ leads to the production of HCl in excess of that obtained from the reaction of BCl₃ and the surface hydroxyls. Similar results are obtained with other multichlorinated hydrogen-sequestering agents. Thus, if the stoichiometry of the reactions of such reagents with the silica surface hydroxyls are determined by measuring the HCl produced in an experiment of the type described above, a false picture of the reaction is obtained. One would conclude from such results that more of the surface hydroxyls were "paired" than was actually the case.

In Table I, the silicas that we have studied are listed, together with the results obtained for their surface hydroxylation in terms of the analyses carried out as described below.

SiMe₂Cl₂. (For full experimental details see ref 8.) The silica R. A. 3 was evacuated to constant weight at 300° followed by reaction with SiMe₂Cl₂ vapor to constant weight and final evacuation at 300° and 1 × 10⁻⁴ Torr. The solid reaction product contained chlorine equivalent to 1.3 ± 0.1 chlorine atoms per 100 Å² of surface. Considering the reactions of SiMe₂Cl₂ with type A and type B sites, we have



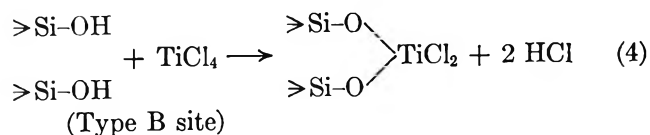
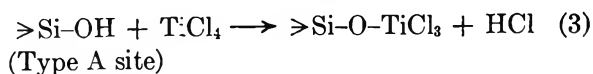
It can be seen from this reaction scheme that only Type A sites can lead to residual chlorine in the reaction products. Furthermore, the number of type A sites is equal to the number of residual chlorine atoms, that is 1.3 ± 0.1 type A sites/100 Å². Reaction of an R. A. 3 silica, that had been evacuated to constant weight at 500°, with SiMe₂Cl₂ at 300° again gives a type A site concentration of 1.3 ± 0.1 per 100 Å² of surface.

On the basis of the model chosen and discussed by Peri and Hensley⁶ only reaction 2 should occur, which would result in there being no residual chlorine on the silica surface after treatment with SiMe₂Cl₂.

TiCl₄. Infrared spectroscopic studies¹³ have shown that TiCl₄ reacts with all the 4.6 hydroxyl groups present on the surface of a fully hydroxylated annealed

(13) J. Murray and J. A. Hockey, unpublished results.

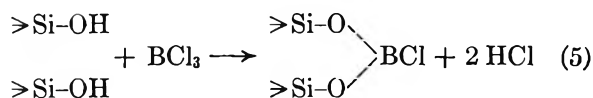
Aerosil (R. R. A. 3/700).⁵ The silicas were evacuated at 2×10^{-5} Torr at room temperature to constant weight on a MacBain balance. The weight change, produced by the reaction of the sample with TiCl_4 vapor *in situ* was measured directly, after complete removal by evacuation of the excess reagent. The observed weight changes are in accord with the reactions 3 and 4 shown below occurring in almost equal preponderance.



For a silica with a B. E. T. surface area of $150 \text{ m}^2/\text{g}$ carrying $4.6 \text{ OH}/100 \text{ \AA}^2$ of surface, the weight increase per gram of silica on reaction with TiCl_4 , assuming that there are $1.4 \text{ OH}/100 \text{ \AA}^2$ reacting as in eq 3 and 3.2 hydroxyl groups reacting as 1.6 type B sites, as in eq 4, is equal to 101 mg per gram of solid.

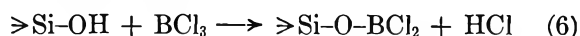
For the same silica reacting as in eq 4 only, as it would were Peri and Hensley's model correct, 2.3 hydroxyl pairs or type B sites/ 100 \AA^2 would react. This would produce a weight change of 67 mg per gram of solid. The observed weight changes were always within $1\text{--}2\%$ of the first figure of 101 mg per gram of solid.

BCl_3 . Two grams of silica was dried to constant weight at 180° *in vacuo* and exposed to BCl_3 vapor at room temperature. Under such conditions, all the surface hydroxyls react, as was confirmed by infrared spectroscopic techniques.⁵ After prolonged evacuation of the HCl and excess BCl_3 at 100° , the chlorine content of the reacted solid was determined by dissolving it in 1 M sodium hydroxide solution and titrating this solution for chloride potentiometrically. This process was repeated for another sample of the same silica after it had been evacuated to constant weight at 450° . The analyses were duplicated and agreement of 3% or better was obtained in all cases. Taking the chloride analyses in Table II for the 450° evacuated samples and assuming that the surface contains only type B sites as postulated by Peri and Hensley,⁶ we have the following reaction



We note that each chlorine atom in the solid reaction product is equal to two surface hydroxyls. On this basis, after evacuation at 450° , all the silicas studied carry between $4.4\text{--}6.6$ surface hydroxyls per 100 \AA^2 . However, independent thermogravimetric analyses of the same samples show that the total hydroxylation including any bulk hydroxyls still present is less than

3 hydroxyl groups/ 100 \AA^2 of surface. Similarly, using reaction 5 to analyze the data obtained at 180° yields n_{OH} values between 7.4 and 9.2 . Thermogravimetric analysis again shows the total n_{OH} value, including any bulk hydroxyls present, to be always less than 6 for each of the samples. Consequently we conclude that analysis of the data on the basis of eq 5 alone cannot be correct. Calculations consistent with the observed chlorine contents can only be obtained if we include another reaction (6)



which would produce two chlorine atoms for each hydroxyl group. By assuming that all the interacting hydroxyls on type B sites have been removed by prolonged evacuation at 450° , the only reaction which could occur on these silicas is that presented in eq 6 above. Analyzing the data in Table II for the 450° sample in this way produces a surface hydroxyl concentration of 1.4 ± 0.1 hydroxyl groups per 100 \AA^2 . (This value may be a little high due to the incomplete removal of all the type B sites at 450° .) By subtracting from the total chlorine content of the 180° sample the contribution due to these 1.4 single surface hydroxyls we obtain the chlorine content due to reactions occurring at the paired type B hydroxyl sites. The total hydroxyl contents are below the limiting room temperature value of $4.6/100 \text{ \AA}^2$ due to the fact that at 180° a number of the type B sites have already been removed.

There are other data in the literature supporting this picture of approximately equal numbers of type A and type B sites per 100 \AA^2 on a fully hydroxylated surface. Boehm, *et al.*,¹⁴ show that the Cl:B ratio of the solid product varies with the prior outgassing temperature of the silica, gradually increasing with temperature to a value of $2:1$ after prior evacuation at 450° . Clearly this increasing ratio is only consistent with an increasing predomination of reaction 6 as the silica surface is dehydroxylated progressively by removal of the type B sites.

Fripiat¹⁶ and his coworkers have studied the reaction of diborane with the surface hydroxyls of silica. They analyzed the surface reactions by studying the ratio of the hydrogen evolved to the diborane consumed on reacting hydroxylated silicas with the diborane—they called this ratio the "primary hydrolysis ratio." They also measured the hydrogen evolved when the evacuated solid reaction product was hydrolyzed by water vapor; this ratio they called the "secondary hydrolysis ratio." This secondary ratio corresponds to the volume of hydrogen produced on treatment with water vapor to the volume of diborane initially consumed.

Fripiat, *et al.*,¹⁵ also showed that the diborane dis-

(14) H. P. Boehm, M. Schneider, and F. Arendt, *Z. Anorg. Allg. Chem.*, **320**, 43 (1966).

(15) J. J. Fripiat and M. Van Tongelen, *J. Catal.*, **5**, 158 (1966).

rows (see Figure 4 of ref 6) with each silicon atom carrying two hydroxyl groups. Equally important is the fact that the terminal Si-O(OH) bond axis is at a low angle to the surface plane $[(180 - 109^\circ 28')/2 \simeq 35^\circ]$ and point in such a way that the oxygen atoms of the hydroxyl groups on adjacent surface silicon atoms are held close together. Such an arrangement would produce paired hydrogen-bonded hydroxyls.

Dehydroxylation of such a surface, by the elimination of one molecule of water per pair of interacting hydroxyls would be relatively easy and proceed in such a manner as to leave only paired hydroxyls remaining on the surface and a corresponding number of strained siloxane links.

Proceeding now to consider the extent of the hydroxylation of each of these crystal planes, we note that the single hydroxyl concentration as measured by both chemical and infrared spectroscopic techniques remains constant at ignition temperatures up to $600 \pm 50^\circ$. We therefore conclude that those parts of the equilibrium room-temperature silica surface which corresponds to the 0001 β -tridymite (or equivalent) crystal plane are fully hydroxylated between 0 and 600° . Thus, out of the total surface area of the solid approximately 1.4/4.6, *i.e.*, $\sim 30\%$ of the surface corresponds to the 0001 face of β -tridymite or its equivalent face in β -cristobalite.

Were it fully hydroxylated, a surface corresponding to the 100 plane of β -cristobalite would contain 7.9 hydroxyl groups per 100 \AA^2 . Therefore, by analogous arguments to those presented above we may conclude that those parts of the equilibrium room-temperature surface which correspond to the 100 β -cristobalite or equivalent crystal plane are hydroxylated to only about 60% of their maximum possible hydroxylation. That is to say that 70% of the equilibrium room-temperature silica surface corresponds to a partially dehydroxylated 100 plane of β -cristobalite (or its equivalent face in β -tridymite) giving a concentration of 3.2 interacting hydroxyls (or 1.6 type B sites) per 100 \AA^2 of total surface area.

With the exception of Peri and Hensley,⁶ previous workers in this field^{1,16} have assumed that fully hydroxylated surfaces (*i.e.*, after evacuation at 25°) are indeed fully hydroxylated. Perhaps a more realistic view can be achieved if one considers that the concentration of interacting surface hydroxyls decreases steadily as the sample is heated from room temperature upwards. In view of this there seems little *a priori* evidence that significant dehydroxylation has not occurred on ignition *in vacuo* at 25° . That is to say that if dehydroxylation has proceeded to a certain extent at say 450°K , then one should not assume that a similar, though less extensive, depopulation has not occurred at 300°K .

The presence after room temperature evacuation of strained siloxane links would imply that adsorbing

water onto a nonmicroporous room-temperature evacuated silica would result in the creation of interacting paired hydroxyls and also to a spatial relaxation of the silica lattice. In the case of the production of interacting hydroxyls at strained siloxane links it should be noted that Anderson and Wickersheim¹⁷ have shown that the adsorption of water onto silicas at room temperature led to an increase in the intensity of the infrared absorption band at 3550 cm^{-1} . In the case of the spatial relaxation of the silica lattice during this rehydration process, Folman and Yates¹⁸ have noted that adsorbing water onto silicas evacuated at room temperature results in an expansion of the sample.

Conclusions

The results presented in this paper suggest that at ambient temperatures the surface hydroxylation of "fully" hydroxylated silicas corresponds to a surface containing about 4.6 hydroxyl groups per 100 \AA^2 of total surface area. Of these about 1.4 ± 0.1 groups exist as single non-hydrogen-bonded species (1.4 A type sites/ 100 \AA^2). The remaining 3.2 hydroxyls exist as pairs (1.6 ± 0.1 B type sites/ 100 \AA^2).

Dehydroxylation of such a surface results in the complete removal of type B sites at temperatures of $500 \pm 50^\circ$. At this stage of dehydroxylation the surface contains only 1.4 isolated or single hydroxyls/ 100 \AA^2 of surface.

Referring to infrared spectroscopic data published elsewhere⁵ this model is in accordance with the assignment of the "high" frequency (3750 cm^{-1}) absorption band to the single hydroxyl species and the assignment of the 3550 cm^{-1} absorption band to the hydrogen-bonded surface species. As shown in ref 5, the non-exchangeable band centered at 3650 cm^{-1} observed in freshly prepared silicas corresponds to hydrogen-bonded internal or bulk hydroxyls.

It is noticeable that the mysterious¹⁵ value of $n_{\text{OH}} = 1.4 \pm 0.1$ discussed by a number of workers in recent years,^{6,8,15,19-21} is equal to the single surface hydroxyl concentration/ 100 \AA^2 . The persistent value of 1.4 ± 0.1 single groups obtained up to temperatures of at least 600° indicates their temperature stability, whereas the progressive removal of the B sites by steadily increasing outgassing temperatures implies a sterically controlled dehydroxylation process of the type described previously.²

Finally, lest the purpose of this paper be in part

(17) J. H. Anderson, Jr., and K. A. Wickersheim, *Surface Science*, **2**, 252 (1964).

(18) M. Folman and D. J. C. Yates, *Trans. Faraday Soc.*, **54**, 429 (1958).

(19) J. B. Peri, *J. Phys. Chem.*, **70**, 2937 (1966).

(20) J. Yu. Babkin, V. S. Vasil'eva, I. V. Drogaleva, A. V. Kiselev, A. Ya. Korolev, and K. D. Shcherbakova, *Dokl. Akad. Nauk SSSR*, **129**, 1 (1959).

(21) H. P. Boehm, *Angew. Chem., Int. Ed.*, **5**, 553 (1966).

misconstrued, it is not intended that it should detract in any way from the undoubted usefulness of the "Monte Carlo" method as originally applied by Peri. This technique would seem to us to be one of the ways in which future experimental determination of the surface hydroxylation of oxide surfaces may be correlated with realistic theoretical models.

Acknowledgments. We thank Miss J. Murray for the TiCl_4 experimental data. We thank S. R. C. for a personal grant to A. J. T. and Unilever Chemicals Development Centre for a personal grant to C. G. A. We also thank Unilever Chemicals Development Centre and S. R. C. for other generous financial support of part of this work.

The Density Function for End-to-End Lengths of Self-Avoiding Random Walks on a Lattice

by Frederick T. Wall^{1a} and Stuart G. Whittington^{1b}

Department of Chemistry, University of California, San Diego, La Jolla, California 92037

Accurate coordinate density functions are calculated for the end-to-end separations of short self-avoiding random walks on the tetrahedral and face-centered cubic lattices. The results are extrapolated to describe long walks by assuming an approach to spherical symmetry with increase in number of steps. The form of the density functions so obtained can be represented by an equation used by Domb to describe his exact enumeration data on the cubic lattice. It is suggested that the essential form of the density function is independent of the lattice for long walks.

Introduction

The number and configurational properties of self-avoiding random walks is of importance in the theory of polymer molecules,² percolation problems³ and the susceptibility expansion of the Ising model.⁴ There is overwhelming evidence from exact enumeration results⁵ and Monte Carlo calculations⁶ that the mean square end-to-end length, $\langle r_n^2 \rangle$, of an n -step self-avoiding walk on a lattice has the functional form

$$\langle r_n^2 \rangle = An^\gamma \quad (1)$$

where $1.18 < \gamma < 1.22$ for walks in three dimensions. There is strong evidence from exact enumeration studies that γ is exactly $6/5$, a conclusion also derived theoretically by Edwards,⁷ using a self-consistent field approach for a continuum model. Reiss⁸ has recently criticized Edwards' approach to the problem and, using a variation principle, has obtained a value of $\gamma = 4/3$ in a continuum. It has since been shown, however, that Reiss' solution of the resulting self-consistent field equation was not sufficiently accurate.⁹

Until recently, relatively little work had been carried out on the probability density function of end-to-end separations of self-avoiding walks. Domb¹⁰ and co-workers have fitted exact enumeration data on the cubic lattice to a distribution of the form

$$F(x) = A \exp \{ -(x/\sigma)^\nu \} \quad (2)$$

In this expression, $F(x)$ is the density function of the x coordinate of the end point of the walk, with $\nu = 2.5$ for three-dimensional systems. The arguments of Fisher¹¹ are in agreement with this result, and Reiss⁸ also predicts a non-Gaussian distribution, although Edwards'⁷ approach suggests that the distribution over r is a *displaced* Gaussian.

It is the purpose of this paper to calculate $F(x)$ exactly for short walks on the tetrahedral and face-centered cubic lattices and to use a procedure for longer walks that assumes an approach of the radial distribu-

(1) (a) American Chemical Society, 1155 Sixteenth St., N. W., Washington, D. C. 20036. (b) Unilever Research Laboratory, The Frythe, Welwyn, Hertfordshire, England.

(2) F. T. Wall and L. A. Hillel, *Ann. Rev. Phys. Chem.*, **5**, 267 (1954).

(3) S. R. Broadbent and J. M. Hammersley, *Proc. Camb. Phil. Soc.*, **53**, 629 (1957).

(4) M. E. Fisher and M. F. Sykes, *Phys. Rev.*, **114**, 45 (1959).

(5) C. Domb, *J. Chem. Phys.*, **38**, 2957 (1963).

(6) F. T. Wall and J. J. Erpenbeck, *ibid.*, **30**, 634 (1959).

(7) S. F. Edwards, *Proc. Phys. Soc.*, **85**, 613 (1965).

(8) H. Reiss, *J. Chem. Phys.*, **47**, 186 (1967).

(9) I. McC. Torrens, *ibid.*, **48**, 1488 (1968).

(10) C. Domb, J. Gillis, and G. Wilmers, *Proc. Phys. Soc.*, **85**, 625 (1965).

(11) M. E. Fisher, *J. Chem. Phys.*, **44**, 616 (1966).

tion to spherical symmetry. This procedure has been carried out to about 90 steps, with results consistent with the form of $F(x)$ suggested by the exact enumeration studies of Domb, *et al.*¹⁰

The Generating Function of Short Walks. Suppose that $N_n(x,y,z)$ and $N_n^\circ(x,y,z)$ are, respectively, the numbers of self-avoiding and unrestricted walks which, starting at the origin, have reached the point (x,y,z) after n steps. Let us define two generating functions $G_n(\alpha,\beta,\gamma)$ and $G_n^\circ(\alpha,\beta,\gamma)$ as

$$G_n(\alpha,\beta,\gamma) = \sum_{x,y,z} N_n(x,y,z) \alpha^x \beta^y \gamma^z \quad (3)$$

and

$$G_n^\circ(\alpha,\beta,\gamma) = \sum_{x,y,z} N_n^\circ(x,y,z) \alpha^x \beta^y \gamma^z \quad (4)$$

It is clear that c_n , the total number of walks of n steps, is equal to $G_n(1,1,1)$ and, as shown in Appendix 2, that

$$c_n \langle x_n^2 \rangle = \left[\frac{\partial}{\partial \alpha} \left\{ \frac{\alpha \partial G_n(\alpha,\beta,\gamma)}{\partial \alpha} \right\} \right]_{\alpha=\beta=\gamma=1} \quad (5)$$

where $\langle x_n^2 \rangle$ is the mean square x coordinate of the end point of the walk. Hence, for a lattice with cubic symmetry

$$c_n \langle r_n^2 \rangle = 3 \left[\frac{\partial}{\partial \alpha} \left\{ \frac{\alpha \partial G_n(\alpha,\beta,\gamma)}{\partial \alpha} \right\} \right]_{\alpha=\beta=\gamma=1} \quad (6)$$

Similar equations are applicable to the unrestricted walk.

For an unrestricted walk on the tetrahedral lattice, the successive vectors representing steps must be chosen alternately from two groups, A and B, each with x , y , and z coordinates as follows¹²

A			B		
x	y	z	x	y	z
1	1	1	$\bar{1}$	$\bar{1}$	$\bar{1}$
1	$\bar{1}$	$\bar{1}$	$\bar{1}$	1	1
$\bar{1}$	1	$\bar{1}$	1	$\bar{1}$	1
$\bar{1}$	$\bar{1}$	1	1	1	$\bar{1}$

Each vector in group B is the negative of a vector in group A and each group constitutes a tetrahedral set. For the purpose of establishing a generating function like eq 3 or 4, we first define a factor g_1 to symbolize the vectors in group A

$$g_1 = (\alpha\beta\gamma + \alpha/\beta\gamma + \beta/\alpha\gamma + \gamma/\alpha\beta) \quad (7)$$

In this factor, the exponents of α , β , and γ , occurring in each term, correspond to the x , y , and z components of the corresponding tetrahedral vectors. For group B, a similar factor, g_2 , is defined

$$g_2 = (1/\alpha\beta\gamma + \beta\gamma/\alpha + \alpha\gamma/\beta + \alpha\beta/\gamma) \quad (8)$$

It is now clear that the generating function for the unrestricted tetrahedral walk assumes the form

$$\begin{aligned} G_0^\circ &= 1 \\ G_1^\circ &= g_1 \\ G_2^\circ &= g_1 g_2 \\ G_{2p-1}^\circ &= g_1^p g_2^{p-1} \\ G_{2p}^\circ &= g_1^p g_2^p \end{aligned} \quad (9)$$

We shall now assume that the generating functions for self-avoiding walks can be derived from the generating functions for unrestricted walks by introducing appropriate correction terms for loops of 2, 4, 6, ..., $2p$, ... steps. (On a more general lattice, loops of an odd number of steps might also be involved.) Thus, on the tetrahedral lattice, the first three generating functions become

$$\begin{aligned} G_0 &= 1 \\ G_1 &= g_1 G_0 = g_1 \\ G_2 &= g_2 G_1 - 4G_0 = g_1 g_2 - 4 \\ G_3 &= g_1 G_2 - \beta G_1 = g_1^2 g_2 - 7g_1 \end{aligned} \quad (10)$$

The term $-4G_0$ in G_2 removes the four walks that return to the origin at the second step, there being four configurations involving second steps that are the exact reverse of the first steps. The term $-3G_1$ appearing in G_3 is the generating function of a "tadpole" consisting of a stem of one step and a loop of two. The coefficient 3 reflects the fact that there can be precisely three such "tadpole" configurations associated with each stem; they are, of course, disallowed in self-avoiding walks. If the walks were only restricted by forbidding loops of two, the general recurrence relations for the generating function with $p > 1$ would be

$$\begin{aligned} G_{2p} &= g_2 G_{2p-1} - 3G_{2p-2} \\ G_{2p+1} &= g_1 G_{2p} - 3G_{2p-1} \end{aligned} \quad (11)$$

It follows immediately that

$$c_n = 4c_{n-1} - 3c_{n-2} \text{ for } n \geq 3 \quad (12)$$

from which a solution is readily obtained, namely

$$c_n = 4 \times 3^{n-1} \quad (13)$$

as required.

It is important to notice that the factor 4 appearing in G_2 and the factor 3 appearing in G_3 and in succeeding G_i reflects the difference in the numbers of ring closures attributable to loops of two at the origin and at points other than the origin.¹³

Presumably higher loops can be corrected for in a similar way, and with this end in mind, we shall employ a method which in our judgment is highly plausible

(12) See, *e.g.*, F. T. Wall, S. Windwer, and P. J. Gans, *Methods Computational Phys.*, **1**, 220 (1963).

(13) F. T. Wall, L. A. Hiller, and D. J. Wheeler, *J. Chem. Phys.*, **22**, 1036 (1956).

although not rigorous. Pursuing this line of reasoning, we write that

$$G_{2p} = g_2 G_{2p-1} - \sum_{k=1}^{p-1} q_{2k} G_{2p-2k} - u_{2p} G_0 \quad (14)$$

and

$$G_{2p+1} = g_1 G_{2p} - \sum_{k=1}^p q_{2k} G_{2p-2k+1} \quad (15)$$

where u_{2p} is the number of polygons of $2p$ steps (or the number of returns to the origin), and q_{2k} corrects for ring closures to points other than the origin. (Actually, q_{2k} equals the number of tadpole configurations of total length n and loop size $2k$ divided by c_{n-2k} .) A further element of complexity enters when star graphs¹⁴ can occur on the lattice. These graphs represent walks containing more than one loop but no cut points. The treatment described above would correct for such configurations more than once, so it becomes necessary to make appropriate compensation. The net result is that q_{2k} is not just a count of tadpoles, but is also weakly dependent upon n .

Leaving aside the problem of the treatment of the star graphs, we turn first to the more immediate calculation of the u_{2p} . By successive application of the recurrence relations, G_{2p} can be expressed as a linear combination of the generating functions of unrestricted walks in the form

$$G_{2p} = \sum_{i=0}^p b_{2i} G_{2i}^\circ - u_{2p} G_0^\circ \quad (16)$$

in which the term $u_{2p} G_0^\circ$ simply represents the number of additional returns to the origin not accounted for in the expression beneath the summation sign. Hence u_{2p} must be so chosen as to make the value of the coefficient of $(\alpha\beta\gamma)^\circ$ in the total expression for G_{2p} equal to zero. In Appendix II it is shown that the value of the coefficient of $(\alpha\beta\gamma)^\circ$ in the expression for G_{2p}° is given by

$$\eta(2p) = \sum_{i,j,k,l} \binom{p!}{i!j!k!l!} \quad (17)$$

where the summation is taken over all nonnegative values of $i, j, k,$ and l satisfying the condition $i + j + k + l = p$. The first few values of $\eta(2p)$ are given in Table I.

Table I

p	$\eta(2p)$
0	1
1	4
2	28
3	256
4	2716
5	31504

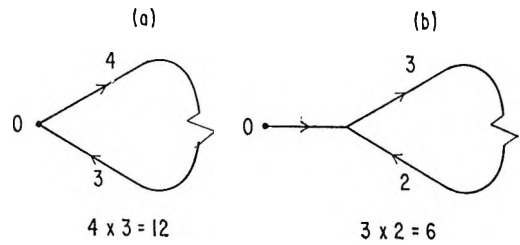


Figure 1. Schematic representations of loop closures (a) and tadpole configurations (b) with approximate relative weighting factors.

Knowing the values of b_{2i} and $\eta(2i)$, we can calculate u_{2p} using

$$u_{2p} = \sum_{i=0}^p b_{2i} \eta(2i) \quad (18)$$

Applying this approach to G_4, G_6 and G_8 we obtain

$$\begin{aligned} G_4 &= g_2 G_3 - 3G_2 & u_4 &= 0 \\ G_5 &= g_1 G_4 - 3G_3 \\ G_6 &= g_2 G_5 - 3G_4 - 24G_0 & u_6 &= 24 \end{aligned} \quad (19)$$

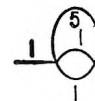
That $u_4 = 0$ simply means that there are no ways of closing a loop of four steps in the tetrahedral lattice, whereas $u_6 = 24$ means that there are precisely 24 ways of returning to the origin in six steps. For seven steps it is necessary to determine a value of g_6 . In forming a loop back to the origin, it is obvious that there are four ways to leave the origin and three ways to return; on the other hand, to form a loop with a stem, it is clear that there are three ways to leave a stem and, at most, two ways to return, without first forming another loop. (See Figure 1.) The ratio of these net counts is $(4 \times 3)/(3 \times 2)$ or 2; hence, in the absence of star graphs, $q_{2p}/u_{2p} = 1/2$. However, it is necessary to take into account the first θ graphs,¹⁴ $\theta(5,1,1)$ of which there are $u_6/4$ in each of the positions associated with G_1 . Hence

$$G_7 = g_1 G_6 - 3G_5 - (u_6/2 - u_6/4)G_1$$

or

$$G_7 = g_1 G_6 - 3G_5 - 6G_1 \quad (20)$$

At eight steps we must take account of polygons of eight steps and the "generalized tadpole"



which is a $\theta(5,1,1)$ with a unit-length stem. At ten steps a further complexity arises because of the star graph $\theta(6,2,2)$. Nevertheless, by proceeding as described above in deriving G_7 , we find that

(14) M. F. Sykes, *J. Math. Phys.*, 2, 52 (1961).

$$\begin{aligned} G_8 &= g_2 G_7 - 3G_6 - 8G_2 - 48G_0 \\ G_9 &= g_1 G_8 - 3G_7 - 8G_3 - 12G_1 \\ G_{10} &= g_2 G_9 - 3G_8 - 8G_4 - 10G_2 - 480G_0 \end{aligned} \quad (21)$$

The values of u_{2p} and c_n obtained from these generating functions agree with the counts of Sykes and Essam.¹⁵ This approach might be continued somewhat further, but it rapidly becomes exceedingly laborious without any assurance of a significant improvement in the ultimate extrapolation. Accordingly, we shall now turn our attention to a procedure leading to an extrapolation for large n .

The Generating Function Projected on One Dimension. To facilitate carrying our method further, we now find it expedient to project our walks onto one axis. It follows immediately from eq 3 that

$$G_n(\alpha, 1, 1) = \sum_{x,y,z} N_n(x,y,z) \alpha^x = \sum_x F_n(x) \alpha^x \quad (22)$$

where $F(x)$ is the total number of walks allowed in three dimensions with a component of the end-to-end distance equal to x . From eq 7 and 8 we see that

$$G_n^\circ(\alpha, 1, 1) = (2\alpha + 2/\alpha)^n \quad (23)$$

so that

$$F_n^\circ(x) = \sum_{y,z} N_n^\circ(x,y,z) \quad (24)$$

Evidently $F_n^\circ(x)$ satisfies the difference equation

$$F_n^\circ(x) = 2\{F_{n-1}^\circ(x-1) + F_{n-1}^\circ(x+1)\} \quad (25)$$

For a self-avoiding walk, we can write

$$F_{2p}(x) = 2\{F_{2p-1}(x-1) + F_{2p-1}(x+1)\} - \sum_{k=1}^{p-1} q_{2k} F_{2p-2k}(x) - u_{2p} F_0(x) \quad (26)$$

and

$$F_{2p+1}(x) = 2\{F_{2p}(x-1) + F_{2p}(x+1)\} - \sum_{k=1}^p q_{2k} F_{2p-2k+1}(x) \quad (27)$$

where u_{2p} and q_{2k} are precisely the same as those appearing in eq 14 and 15, with q_{2k} weakly dependent on the length of the walk.

The Approach to Spherical Symmetry. It is well known that the distribution function of an unrestricted random walk approaches spherical symmetry for large n , and Domb, *et al.*,¹⁰ have presented numerical evidence that this is also true for a self-avoiding walk. In Appendix III it is shown that, for walks that are statistically spherically symmetric

$$\left[\frac{d^2 F_n(x)}{dx^2} \right]_{x=0} = 0 \quad (28)$$

Expressed in finite difference form for walks of $2p$ steps on the tetrahedral lattice, we see that

$$F_{2p}(-2) - 2F_{2p}(0) + F_{2p}(2) = 0 \quad (29)$$

a statement which should be asymptotically correct for large values of p . Since $F_n(x) = F_n(-x)$, it is also clear that for large p

$$F_{2p}(0) = F_{2p}(2) \quad (30)$$

In principle, this should enable us to estimate values of u_{2p} , as follows. From eq 26 we see that

$$u_{2p} = -F_{2p}(0) + 2\{F_{2p-1}(-1) + F_{2p-1}(1)\} - \sum_{k=1}^{p-1} q_{2k} F_{2p-2k}(0) \quad (31a)$$

and

$$0 = -F_{2p}(2) + 2\{F_{2p-1}(1) + F_{2p-1}(3)\} - \sum_{k=1}^{p-1} q_{2k} F_{2p-2k}(2) \quad (31b)$$

By subtracting eq 31b from 31a, and recognizing that $F_n(1) = F_n(-1)$, we find

$$u_{2p} = \{F_{2p}(2) - F_{2p}(0)\} + 2\{F_{2p-1}(1) - F_{2p-1}(3)\} + \sum_{k=1}^{p-1} q_{2k} \{F_{2p-2k}(2) - F_{2p-2k}(0)\} \quad (32)$$

If eq 30 were valid for all values of $2p$, then eq 32 would simplify considerably. Actually the term in the summation of eq 32 cannot be neglected for values of k approaching p . Accordingly, we proceeded with numerical calculations as follows. For long walks, we assumed that¹³

$$q_{2k} = \zeta u_{2k} \quad (33)$$

where ζ is assumed to be independent of k . In the absence of star graphs, other than $(n, 1, 1)_\theta$, $q_{2k} = u_{2k}/3$, so that we expect $\zeta < 1/3$. Since spherical symmetry is not realized for short walks, we shall provide for a gradual approach to spherical symmetry by assuming that

$$F_{2p}(0) = F_{2p}(2)(1 + \lambda/2p) \quad (34)$$

for values of $p \gtrsim 5$, with λ chosen to make the equation numerically correct for $p = 5$. For smaller values of p , exact enumeration data have been used throughout.

In Table II, values of $\langle r_n^2 \rangle$ calculated by the method described above are compared with Monte Carlo data. Three different values of ζ were used for the calculation. The agreement with Monte Carlo data is quite good when ζ is equal to $1/6$. The dependence of $\langle r_n^2 \rangle$ on n is shown in Figure 2 and the limiting gradient indicates that $\gamma = 1.20 \pm 0.02$. The dependence of c_n on n suggests the connective constant, k , is given by $e^k = 2.876$, close to the values derived from exact enumeration¹⁵ (2.878) and Monte Carlo studies⁶ (2.884).

(15) M. F. Sykes and J. W. Essam, *Physica*, 29, 378 (1963).

Table II: Table of $\langle r_n^2 \rangle$ on Tetrahedral Lattice^a

n	Monte Carlo	$\zeta = 0.15$	$\zeta = 1/6$	$\zeta = 0.18$
20	46.51	46.24	46.38	46.49
30	75.84	74.75	75.29	75.39
40	106.9	105.2	106.4	106.6
50	139.4	137.5	139.5	139.9
80	247.2	243.5	249.0	250.1

^a Calculations made for $\lambda = 0.1286$.

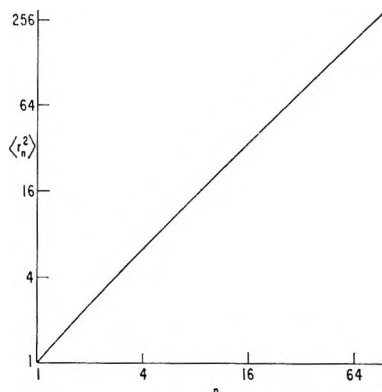


Figure 2. Log-log graphs of $\langle r^2 \rangle$ vs. n for self-avoiding walks on tetrahedral lattice; $\zeta = 1/6$.

The density function $F_n(x)$ is plotted in Figure 3 for $n = 64$ and the density function for the unrestricted walk is shown in the same figure for comparison, both functions being normalized so that the total number of walks is equal in the two cases. Values of $F_n(x)$ calculated from eq 2 are shown in the same figure. The number of walks reaching a distance r from the origin after n steps $P_n(r)$ is given by (see Appendix III)

$$P_n(r) = 4\pi r^2 f_n(r) \propto r F_n'(r) \tag{35}$$

and the dependence of $P_{64}(r)$ on r is shown in Figure 4.

Walks on the Face-Centered Cubic Lattice. The generating function of an unrestricted walk on the face-centered cubic lattice is given by

$$G_n^\circ(\alpha, \beta, \gamma) = [(\alpha + 1/\alpha)(\beta + 1/\beta) + (\alpha + 1/\alpha)(\gamma + 1/\gamma) + (\beta + 1/\beta)(\gamma + 1/\gamma)]^n \tag{36}$$

and the one-dimensional generating function of a self-avoiding walk can be written as

$$G_n(\alpha, 1, 1) = gG_{n-1}(\alpha, 1, 1) - \sum_{k=2}^{n-1} a_k G_{n-k}(\alpha, 1, 1) - u_k G_0(\alpha, 1, 1) \tag{37}$$

where $g = 4(\alpha + 1 + 1/\alpha)$ and the a_k are again weak functions of n .

Exact values of c_n and u_n are available¹⁶ up to $n = 12$ and $\langle r_n^2 \rangle$ is known exactly⁴ to $n = 7$.

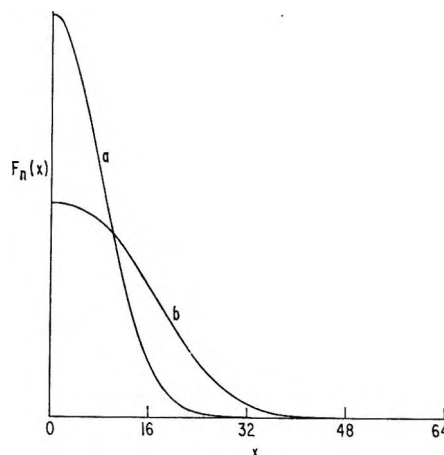


Figure 3. $F_n(x)$ vs. x for $n = 64$ on tetrahedral lattice, (a) unrestricted walks; (b) self-avoiding walks calculated for $\zeta = 1/6$.

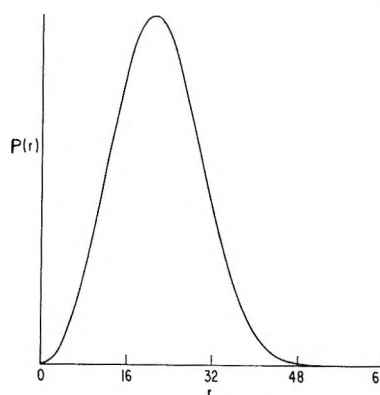


Figure 4. $P_{64}(r)$ vs. r for self-avoiding walks on tetrahedral lattice; $\zeta = 1/6$.

On this lattice we have made explicit use of the exact data to estimate a_k and its dependence on n for $n \leq 12$. We first allowed a_k to assume two values a_k^* and a_k depending on whether the k loop appears for the second or subsequent time. By choosing the a_k to force agreement with exact numeration values of c_n , u_n , and $\langle r_n^2 \rangle$ we obtain the values of a_k shown in Table III.

Since $a_k^* \simeq a_k$ it seems reasonable to use only the initial values of u_k and the limiting values of a_k . We have adopted this procedure up to $n = 12$ using exact

Table III

k	u_k	a_k^*	a_k
2	12	11	11
3	48	36	36
4	264	165.995	166.147
5	1680	904.329	906.496

(16) J. L. Martin, M. F. Sykes, and F. T. Hioe, *J. Chem. Phys.*, **46**, 3478 (1967).

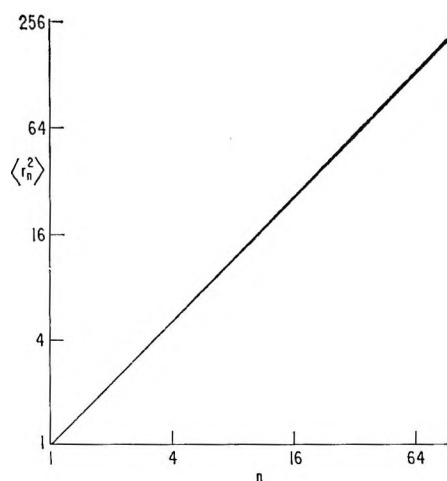


Figure 5. Log-log graph of $\langle r^2 \rangle_n$ vs. n for self-avoiding walks on face-centered cubic lattice.

values of c_n and u_n and have fitted the values of a_k and u_k to an equation of the form

$$a_k = u_k(\alpha_0 + \alpha_1/k + \alpha_2/k^2) \quad (38)$$

After 12 steps we proceed by forcing the approach to spherical symmetry by imposing the condition

$$F_n(0) = F_n(1)(1 + \lambda_1/n + \lambda_2/n^2) \quad (39)$$

where λ_1 and λ_2 are chosen to make the equation fit best at $n = 10, 11$, and 12 .

When $\alpha_0 = 0.2141$, $\alpha_1 = 0.6667$, $\alpha_2 = 7.0$, $\lambda_1 = 0.076$, and $\lambda_2 = 0.396$, the dependence of $\langle r_n^2 \rangle$ on n is shown in Figure 5 and the coordinate and radial distribution functions are shown in Figures 6 and 7. With a proper choice of the parameter σ , $F(x)$ calculated from Domb's eq 2 can be essentially superimposed on the curve of Figure 6.

Discussion

The agreement between values of $\langle r_n^2 \rangle$ calculated by the present method with those obtained by Monte Carlo methods and by exact enumeration coupled with extrapolation techniques, as well as the agreement between the estimated values of the attrition coefficient, lends considerable support to the validity of the density function obtained. The shape of the density function is only weakly dependent on parameters such as ζ . The form of the density function is qualitatively in agreement with the forms proposed by Domb, *et al.*,¹⁰ and by Reiss⁸ and, with a proper choice of parameters, the agreement with Domb's results can be made quantitative except for the region in the immediate vicinity of the origin. This discrepancy was also noted by Domb.¹⁰ Since the form (eq 2) can be fitted to numerical results for the cubic lattice¹⁰ as well as for the tetrahedral and face-centered cubic lattices studied here, it appears that the limiting form of the density function is probably independent of the particular lattice being studied.

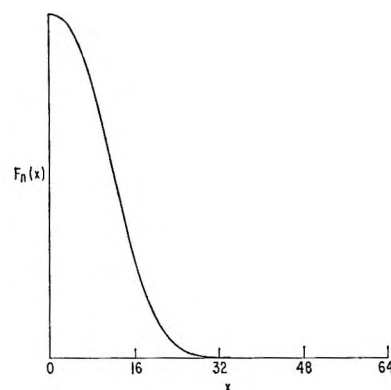


Figure 6. $F_n(x)$ vs. x for self-avoiding walks on face-centered cubic lattice; $n = 64$.

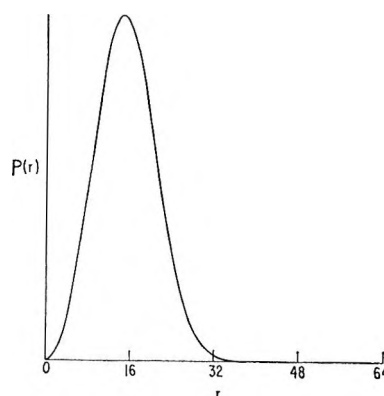


Figure 7. $P_{64}(r)$ vs. r for self-avoiding random walks on face-centered cubic lattice.

Appendix I

The Relation between the Generating Function and the Mean Square x Coordinate of the End Point of an n -Step Walk. The generating function $G_n(\alpha, \beta, \gamma)$ is defined as

$$G_n(\alpha, \beta, \gamma) = \sum_{x,y,z} N_n(x,y,z) \alpha^x \beta^y \gamma^z$$

Now

$$\frac{\partial}{\partial \alpha} \left(\alpha \frac{\partial G}{\partial \alpha} \right) = \sum_{x,y,z} N_n(x,y,z) x^2 \alpha^{x-1} \beta^y \gamma^z$$

so that, when $\alpha = \beta = \gamma = 1$

$$\begin{aligned} \frac{\partial}{\partial \alpha} \left(\alpha \frac{\partial G}{\partial \alpha} \right) \Big|_{\alpha=\beta=\gamma=1} &= \sum_{x,y,z} N_n(x,y,z) x^2 \\ &= c_n \langle x^2 \rangle_n \end{aligned}$$

Appendix II

The Number of Returns to the Origin at the $2p$ th Step of an Unrestricted Random Walk on the Tetrahedral Lattice. The generating function of the unrestricted walk is given by

$$G_{2p}^o(\alpha, \beta, \gamma) = (g_1 g_2)^p$$

Expanding by the multinomial theorem

$$G_{2p}^{\circ} = \sum_{i,j,k,l} \frac{p!}{i!j!k!l!} (\alpha\beta\gamma)^i (\alpha/\beta\gamma)^j (\beta/\alpha\gamma)^k (\gamma/\alpha\beta)^l \times \\ \sum_{m,n,q,r} \frac{p!}{m!n!q!r!} (\alpha\beta\gamma)^{-m} (\alpha/\beta\gamma)^{-n} (\beta/\alpha\gamma)^{-q} (\gamma/\alpha\beta)^{-r}$$

where $i + j + k + l = m + n + q + r = p$. In order that the exponents of α , β , and γ all be zero, the following additional conditions must be satisfied

$$i + j - k - l - m - n + q + r = 0$$

$$i - j + k - l - m + n - q + r = 0$$

$$i - j - k + l - m + n + q - r = 0$$

To satisfy these conditions it is necessary that $i = m$, $j = n$, $k = q$ and $l = r$ so that the coefficient of $\alpha^{\circ}\beta^{\circ}\gamma^{\circ}$ in G_{2p}° is

$$\eta(2p) = \sum_{i,j,k,l} \left(\frac{p!}{i!j!k!l!} \right)^2$$

where the summation is taken over all nonnegative values of i , j , k , and l such that $i + j + k + l = p$.

Appendix III

The Effect of Spherical Symmetry on the Behavior of the Coordinate Density Function $F_n(x)$ around $x = 0$. Suppose that $f_n(\mathbf{r})$ is the number of walks which are at point \mathbf{r} after n steps. Define the coordinate density function $F_n(x)$ by

$$F_n(x) = \int_{-\infty}^{\infty} \int_{-\infty}^{\infty} f_n(\mathbf{r}) dy dz$$

Let $p^2 = r^2 - x^2 = y^2 + z^2$. Assuming spherical symmetry, then

$$F_n(x) = 2\pi \int_0^{\infty} f_n \{ (x^2 + p^2)^{1/2} \} p dp = 2\pi \int_x^{\infty} f_n(\xi) \xi d\xi$$

Differentiating with respect to x gives¹⁷

$$F_n'(x) = -2\pi f_n(x)x$$

$$F_n''(x) = -2\pi \{ f_n(x) + x f_n'(x) \}$$

For a self-avoiding walk $f_n(0) = 0$ so that

$$F_n''(0) = 0$$

(17) This result has been derived by Domb, *et al.*¹⁰

Heats of Mixing Aqueous Electrolytes. VII. Calcium Chloride and Barium Chloride with Some Alkali Metal Chlorides

by R. H. Wood and M. Ghamkhar

Department of Chemistry, University of Delaware, Newark, Delaware (Received January 20, 1969)

The heats of mixing aqueous solutions of calcium chloride and barium chloride with some alkali metal chlorides have been measured at constant molal ionic strength and 25°. The results are similar to those for magnesium chloride with alkali metal chlorides. At lower concentrations, $RT h_0$ becomes more positive and the mixing with lithium chloride gives the lowest slope. The mixture with sodium chloride gives the largest value of $RT h_0$. If the contributions of oppositely charged ions are estimated and subtracted from the heat of mixing, the sign of the remainder correlates in most cases with the properties of the water structure around the two cations. The heats of mixing at constant molal ionic strength, molar ionic strength and equivalents per kilogram of water are calculated and compared. The heats of mixing at constant molal and molar ionic strengths are not very different. The heats of mixing at constant equivalents per kilogram are as small as the other heats of mixing and this may be the preferred concentration scale at high salt concentrations.

Introduction

Previous work on the heat of mixing magnesium chloride with alkali metal chlorides at constant molal ionic strength¹ has shown that the magnitude of the heat of mixing is similar to the magnitude of the heat of mixing two alkali metal chlorides. In addition, the

signs of the cation-cation interactions correlated fairly well with the structure of the water around the two ions. Because the previous work was the first systematic investigation of charge-asymmetric mixtures,²

(1) R. H. Wood, J. D. Patton, and M. Ghamkhar, *J. Phys. Chem.*, **73**, 346 (1969).

this investigation was undertaken in order to provide data to see if the conclusions derived from magnesium chloride mixtures would be confirmed by measurements on calcium chloride and barium chloride mixtures.

Experimental Section

Except for the cesium chloride solution, all stock solutions were prepared from reagent grade salts and all impurities reported for these salts were less than 0.01%. Stock solutions were analyzed for chloride ion by a gravimetric silver chloride precipitation. The calcium chloride and barium chloride stock solutions had pH 3.6 and 5.7, respectively, and each of the alkali chloride solutions had a pH between 5 and 6.5. The low pH was used so that hydrolysis of the calcium and barium ions would be negligible.

Technical grade cesium chloride³ was purified by precipitating the 1.2% sulfate impurity with a 0.005% excess of barium chloride. The other reported impurities in this salt were negligible except for 0.1% rubidium. The stock solution was analyzed by a tetraphenylborate precipitation of the cesium ion. Duplicate determinations agreed to within 0.1%. The procedure and calorimeter are the same as described earlier.^{4,5}

Results and Discussion

The experimental data were fitted by the method of least-squares to the equation

$$\Delta H_m(\text{cal/kg of solvent}) = RTI^2y(1 - y)[h_0 + (1 - 2y)h_1] \quad (1)$$

where I is the molal ionic strength and y is the ionic strength fraction of either calcium chloride or barium chloride, h_0 is a measure of the magnitude of the interaction, and h_1 is a measure of the skew of the interaction. The heats of mixing were measured in the range $y = 0$ to $y = 0.2$ and $y = 0.8-1.0$. The results together with the number of data points are given in Table I. Any points which differed from the least-squares fit by more than about twice the standard deviation were rejected.

Zdanovskii and Deryabina⁶ have measured heat of mixing MgCl_2 with LiCl , NaCl , and KCl and CaCl_2 with NaCl and KCl . The mixtures were not made at constant ionic strength, so comparison with the present results is difficult. However, interpolating Zdanovskii and Deryabina's results to constant ionic strength gives values roughly comparable to the present results and to previous results from this laboratory.^{1,2} A quantitative comparison is not justified.

An examination of Table I shows that the heats of mixing of calcium chloride and barium chloride with alkali metal chlorides are of the same order of magnitude as the magnesium chloride mixings.¹ Also, the three series of charge-asymmetric mixings have heats of mixing which are the same order of magnitude as those of the alkali metal chlorides with themselves.^{5,7}

It was observed that RTh_0 for the magnesium chloride with alkali metal chloride mixtures became more positive as the concentration decreased and this was ascribed to the higher order limiting law which requires that $RTh_0 = -633 \log I$, for these mixtures at sufficiently low concentrations.^{1,8} An examination of Table I and Figure 1 shows that the same increase in RTh_0 as the concentration decreases is apparent in the calcium chloride and barium chloride results. However, no approach to the limiting law is seen at these concentrations. The size of the ion seems to govern the concentration dependence of RTh_0 since for all three alkaline earths, the mixture with lithium chloride has the lowest slope. Also, the magnesium chloride-cesium chloride mixture has the largest slope. Another interesting feature of the results is that the mixture with sodium chloride gives the largest value of RTh_0 for MgCl_2 , CaCl_2 , and BaCl_2 .

The value of RTh_0 for $\text{BaCl}_2\text{-LiCl}$ at $I = 3$ looks a little out of place on Figure 1. The experiments were repeated with identical results and no sign of a precipitate was found in the mixed solutions. In addition, Mr. Alan Levine repeated the measurements on a completely different calorimeter and found $RTh_0 = -32.6 \pm 1$ after three measurements.

It has been shown earlier that the sign of the heat of interaction of like-charged ions can be predicted on the basis of the effect of the ions on the water structure.⁹⁻¹¹ The rule is that two structure-making ions or two structure-breaking ions give a positive value of RTh_0 whereas mixing a structure maker with a structure breaker gives a negative RTh_0 . The heats of interaction of the like-charged ions in a charge-asymmetric mixing can be estimated in the following manner to see if the structure rule holds.¹ The limiting law is neglected and the oppositely charged ion interaction is estimated from Guggenheim's equation^{1,12,13}

(2) For the purposes of this paper, a charge-asymmetric mixture is a mixture of two or more electrolytes having two or more different charge types. Thus, in a $\text{MgCl}_2\text{-CaCl}_2$ mixture, the electrolytes are of the same charge type and the mixture is charge symmetric.

(3) Obtained from Penn Rare Metals Division of the Kawecki Chemical Co., New York, N. Y.

(4) H. S. Jongenburger and R. H. Wood, *J. Phys. Chem.*, **69**, 4231 (1965).

(5) R. H. Wood and R. W. Smith, *ibid.*, **69**, 2974 (1965).

(6) A. B. Zdanovskii and L. D. Deryabina, *Russ. J. Phys. Chem.*, **39**, 357, 485, 774 (1965); **41**, 1965 (1967).

(7) Y. C. Wu, M. B. Smith, and T. F. Young, *J. Phys. Chem.*, **69**, 1868 (1965).

(8) H. F. Friedman, "Ionic Solution Theory," Interscience Publishers, New York, N. Y., 1962, p 244.

(9) T. F. Young, Y. C. Wu, and A. A. Krawetz, *Discussions Faraday Soc.*, **24**, 37, 77, 80 (1957).

(10) Y. C. Wu, M. B. Smith, and T. F. Young, *J. Phys. Chem.*, **69**, 1868 (1965).

(11) R. H. Wood and H. L. Anderson, *ibid.*, **71**, 1869 (1967).

(12) E. A. Guggenheim, *Phil. Mag.*, **19**, 588 (1935).

(13) G. N. Lewis and M. Randall, "Thermodynamics," 2nd ed, revised by K. S. Pitzer and L. Brewer, McGraw-Hill Book Co., New York, N. Y., 1961, Chapter 25 and Appendix 4.

Table I: Heat of Mixing Calcium Chloride and Barium Chloride with Some Alkali Metal Chlorides at 25°

Salt pair	I^a	RTh_0^b	RTh_1	N^c
LiCl-CaCl ₂	0.5	-18 ± 2	-3 ± 3	6
	1	-21.8 ± 1	-2.6 ± 1	8
	2	-26.2 ± 0.3	-1.4 ± 0.5	8
	3	-29.3 ± 0.5	-1.1 ± 0.7	14
NaCl-CaCl ₂	0.5	168 ± 5	-5 ± 8	8
	1	137 ± 2	-9 ± 2	8
	2	113 ± 3	-12 ± 5	7
	3	87 ± 3	-15 ± 5	15
KCl-CaCl ₂	0.5	70 ± 5	-5 ± 5	8
	1	48.3 ± 1.0	-2.8 ± 2	7
	2	20.5 ± 0.3	-1.0 ± 0.5	8
	3	-0.5 ± 0.2	1.9 ± 0.3	15
LiCl-BaCl ₂	0.5	-30 ± 3	-5 ± 4	8
	1	-33.7 ± 0.7	-1 ± 1	8
	2	-41.6 ± 0.7	0 ± 1	8
	3	-30.4 ± 0.2	0.8 ± 0.4	16
NaCl-BaCl ₂	0.5	103.7 ± 1.0	-4.0 ± 2	15
	1	85.3 ± 0.4	-4.8 ± 0.6	16
	2	58.7 ± 0.2	-4.5 ± 0.2	13
	3	40.4 ± 0.6	-3 ± 1.0	13
KCl-BaCl ₂	0.5	23 ± 3.0	-7 ± 4	6
	1	-8.0 ± 0.3	-1.0 ± 0.6	12
	2	-29.6 ± 0.1	4.2 ± 0.2	10
	3	-41.7 ± 0.2	7.7 ± 0.3	14
CsCl-BaCl ₂	1	-39.6 ± 1.0	-5.4 ± 2	8

^a Molal ionic strength of the solutions. ^b Units are calories per kilogram of solvent per ional squared. This gives ΔH_m in calories per kilogram of solvent. ^c Number of experimental points.

$$RTh_0(+, -) = \frac{-2.303RT^2}{3} \left[\frac{1}{3} \frac{\partial B_{MgCl_2}}{\partial T} - \frac{\partial B_{MCl}}{\partial T} \right]$$

where B is the oppositely charged pairwise interaction coefficient. Values of $\partial B/\partial T$ were taken from Lewis and Randall¹¹ and the calculated values of $RTh_0(+, -)$ are given in Table II. The difference between the experimental RTh_0 and that calculated by eq 2 should then be equal to the like-charged pair interaction plus any triplet interactions. If the triplet interactions are small, as they are for the alkali halides,⁴ and if the Cl⁻-Cl⁻ interaction is small, then the structural correlation should hold. In Table II the last column shows the value of $RTh_0(+, +)$ obtained when the oppositely charged pairwise interactions are subtracted from RTh_0 . The rule predicts that mixtures of LiCl or NaCl with CaCl₂ or BaCl₂ (structure maker, structure maker) should have a positive $RTh_0(+, +)$ and mixtures of KCl or CsCl with CaCl₂ or BaCl₂ should have a negative $RTh_0(+, +)$. The prediction is correct except for KCl-CaCl₂ at $I = 0.5$. For the magnesium chloride with alkali metal chloride mixings, the prediction failed only for the KCl-MgCl₂ mixings at $I = 0.5$ and 1.0. This failure at the lower concentrations may be due to the neglect of the limiting law contribution to RTh_0 which is large at low concentrations.¹

One of the goals of the investigation of the properties of mixed electrolytes is the prediction of their properties from as few measurements as possible. For charge-

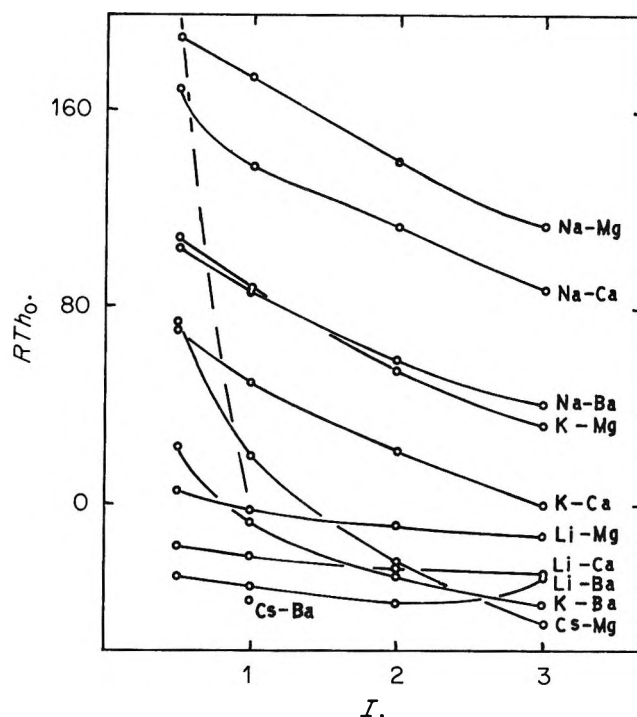


Figure 1. Values of RTh_0 plotted vs. I for mixtures of alkali metal chlorides with alkaline earth chlorides. The limiting law is indicated by a dashed line.

symmetrical mixtures, when only measurements on pure electrolytes are available, the best prediction

seems to be the assumption that the heat or free energy of mixing is zero for a common-ion mixture at constant ionic strength. This is Young's rule¹⁴ applied only to common-ion mixtures where it should be most accurate. This is equivalent to assuming that all $RT\bar{h}_0$ (or $RT\bar{g}_0$ if free energies are being calculated) are zero in the equation proposed by Wood and Anderson¹⁵ since the $RT\bar{h}_0$ terms in this equation are for common-ion mixtures only. In the derivation of this equation, it is shown

activity is negligible.⁶ Their data indicate that this is another reasonable first approximation.

With charge-asymmetric mixtures, it is impossible to mix at constant ionic strength and to cancel out all oppositely charged pair interactions. There is some evidence that at least for reasonably concentrated strong electrolytes (say about 0.2 to about 2 ional) the interaction of an ion with its ion atmosphere does not change very rapidly with concentration. In the first place, activity coefficients do not generally change rapidly in this region (± 20 to 30%). Also, $RT\bar{g}_0$ and $RT\bar{h}_0$ which include ion-atmosphere effects are often not strongly concentration dependent in this concentration range.^{5,17} This raises the question of whether it might be better to neglect ion-atmosphere effects by not mixing at constant ionic strength than to neglect oppositely charged pairs.

The contributions of oppositely charged pairs can be canceled out by mixing at a constant concentration of the common ion. For charge-asymmetric mixtures, this means mixing at a constant concentration expressed as equivalents per liter (normality) or equivalents per kilogram of water. For convenience, the concentration scale equivalents per kilogram of solvent will be used and this will be symbolized by

$$E = (1/2) \sum_i m_i |z_i| = \sum_+ m_+ z_+$$

where m_i and z_i are the molalities and charges of the ions and $+$ indicates positive ions only. For instance, a mixing at $E = 1.0$ would be a mixing of 1 *m* NaCl with $1/2$ *m* MgCl₂ with the concentration of chloride ion equal to 1.0 molal in both solutions.

The constant E mixing process was suggested by Young as an alternative to the constant I process in a footnote to his 1949 review article.¹⁸ This kind of concentration scale is useful in the study charge-asymmetric fused salt mixtures,^{19,20} and this gives plausibility to the idea that mixing at constant E will give the best predictions in very concentrated solutions. Of course as the Debye-Hückel region is approached, this approximation will be very poor.

The heat of mixing at constant number of equivalents per kilogram of solvent can be calculated from the heat of mixing at constant molal ionic strength using the thermodynamic cycle

Table II: Estimation of Cation-Cation Pair Interactions

Salt pair	Ionic strength	$RT\bar{h}_0$ (+, -)	$RT\bar{h}_0$ (+, +) ^a
LiCl-CaCl ₂	0.5	-90	72
	1	-90	68
	2	-90	64
	3	-90	61
NaCl-CaCl ₂	0.5	39	129
	1	39	98
	2	39	74
	3	39	48
KCl-CaCl ₂	0.5	54	16
	1	54	-6
	2	54	-33
	3	54	-55
LiCl-BaCl ₂	0.5	-107	77
	1	-107	73
	2	-107	65
	3	-107	77
NaCl-BaCl ₂	0.5	22	82
	1	22	63
	2	22	37
	3	22	18
KCl-BaCl ₂	0.5	37	-14
	1	37	-45
	2	37	-67
	3	37	-79
CsCl-BaCl ₂	1	147	-187

^a This is the cation-cation pair interaction estimated by subtracting the cation-anion pair interactions, $RT\bar{h}_0(+, -)$, from the value of $RT\bar{h}_0$.

that, by taking as components the correct amounts of pure electrolytes, the oppositely charged pairwise interactions in the final solution are equal to those in the initial pure electrolytes. Thus, Wood and Anderson's component rule with $RT\bar{h}_0$ assumed to be equal to zero is an approximation based on both Brønsted's principle of specific ion interaction¹⁶ and Young's rule.¹⁴

For charge-asymmetric mixtures of alkali metal chlorides with alkaline earth chlorides, the assumption that the heat of common ion mixing is zero is about as good (or as poor) as it is for charge-symmetric mixtures of alkali metal chlorides since the values of $RT\bar{h}_0$ are of the same order of magnitude.

Zdanovskii and Deryabina recommend the approximation that the heat of mixing at constant water

(14) T. F. Young and M. B. Smith, *J. Phys. Chem.*, **58**, 716 (1954).

(15) R. H. Wood and H. L. Anderson, *ibid.*, **70**, 992 (1966).

(16) J. N. Brønsted, *J. Amer. Chem. Soc.*, **44**, 877, 938 (1922); **45**, 2898 (1923).

(17) A. K. Covington, T. H. Lilley, and R. A. Robinson, *J. Phys. Chem.*, **72**, 2759 (1968).

(18) T. F. Young, *Chem. Rev.*, **44**, 93 (1949).

(19) S. V. Mischel and O. J. Kleppa, *J. Phys. Chem.*, **46**, 1853 (1967).

(20) H. Flood, T. Fjorland, and K. Grjotheim, *Z. Anorg. Allg. Chem.*, **276**, 289 (1954).

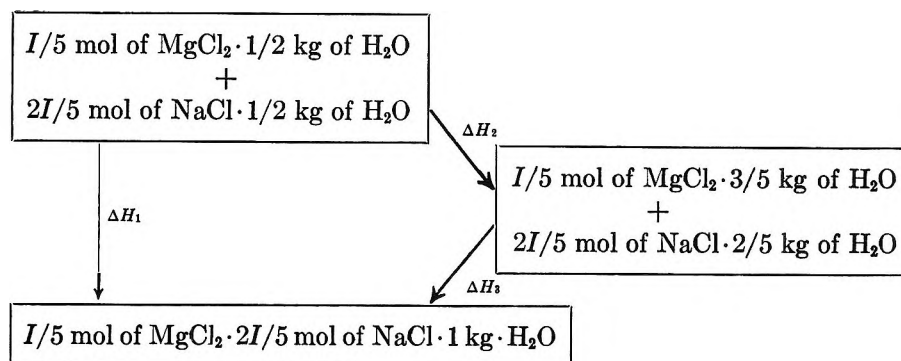


Table III: RTh_0 for Mixing Solutions of the Same Molal Ionic Strength, I , Molar Ionic Strength μ , and Equivalents per Kilogram of Solvent, E

Salt pair	$I = 0.5$			$I = 1$			$I = 2$			$I = 3$		
	I	μ	E^a	I	μ	E	I	μ	E^a	I	μ	E
Mg ₂ Cl-LiCl	5.	5	33	-1.8	-3	3	-8.7	-11	1	-12.8	-17	0
-NaCl	189	192	123	172.5	176	106	138.8	146	95	113.6	123	63
-KCl	108	112	22	86.7	94	-18	54.0	64	-45	31.7	44	-66
-CsCl	73	78	-101	19.0	30	-163	-23.7	-10	-184	-49.6	-31	-202
CaCl ₂ -LiCl	-18	-18	16	-21.8	-23	-1	-26.2	-29	-5	-29.3	-34	-3
-NaCl	168	171	120	137	140	84	113	119	76	87	93	46
-KCl	70	72	-18	48.3	54	-44	20.5	28	-75	-0.5	7	-92
BaCl ₂ -LiCl	-30	-30	+21	-33.7	-36	7	-41.6	-46	-2	-30.4	-33	+23
-NaCl	104	105	46	85.3	88	33	58.7	62	21	40.4	43	3
-KCl	23	24	-66	-8.0	-6	-102	-29.6	-26	-124	-41.7	-39	-127
-CsCl				-39.6	-32	-194						

^a Values in this column are RTh_0 at a constant E equal to $0.8 I$.

where the ΔH_1 mixing is at constant number of equivalents per kilogram of water, $E = 4I/5$. The enthalpy change in calories for this step is

$$\Delta H_1 = RTh_0^E(E)^2y(1-y)W \\ = RTh_0^E(4I/5)^2(1/4)(1) \quad (2)$$

where RTh_0^E is the heat of mixing coefficient at $E = 4I/5$, y is equivalent fraction of one salt, W is the total weight of solvent, and ΔH is in calories. Similarly, the ΔH_3 mixing is at constant ionic strength and

$$\Delta H_3 = RTh_0^I(I)^2y(1-y)W = \\ RTh_0^I(I)^2(2/5)(3/5)(1) \quad (3)$$

Also

$$\Delta H_2 = (I/5)[\phi_L(\text{MgCl}_2, I/3) - \phi_L(\text{MgCl}_2, 2I/5)] \\ + (2I/5)[\phi_L(\text{NaCl}, I) - \phi_L(\text{NaCl}, 4I/5)] \quad (4)$$

Substituting eq 2, 3, and 4 into $\Delta H_1 = \Delta H_2 + \Delta H_3$ gives

$$RTh_0^E = (3/2)RTh_0^I + (5/4I)[\phi_L(\text{MgCl}_2, I/3) \\ - \phi_L(\text{MgCl}_2, 2I/5)] + (5/2I)[\phi_L(\text{NaCl}, I) \\ - \phi_L(\text{NaCl}, 4I/5)] \quad (5)$$

where RTh^E is at the concentration $E = 4I/5$ and RTh^I is at the concentration I .

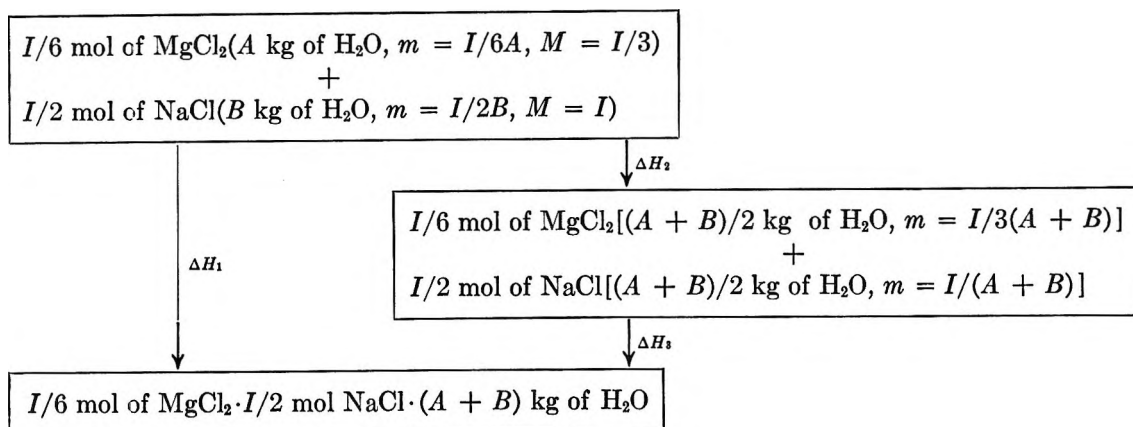
The values of RTh_0^E in Table III were calculated using the heat of dilution data of Parker²¹ for the alkali metal chlorides and NBS Circular 500²² data for the alkaline earth chlorides. Above 1 *m* the CsCl heat of dilution was taken from Levine and Wood.²³

As a further test, the heat of mixing with initial solutions at a constant molar since strength (μ) was also calculated from the heat of mixing at constant molal ionic strength using the thermodynamic cycle

(21) V. B. Parker, "Thermal Properties of Aqueous Uni-Univalent Electrolytes," U. S. National Bureau of Standards, NSRDS-NBS-2, Washington, D. C., 1965.

(22) F. D. Rossini, *et al.*, National Bureau of Standards Circular 500, U. S. Government Printing Office, Washington, D. C., 1952.

(23) A. S. Levine and R. H. Wood, *J. Chem. Eng. Data*, in press.



Calculating the values for each step in calories gives

$$\Delta H_1 = RT h_0^\mu (\mu)^2 y (1 - y) V = RT h_0^\mu (I)^2 (1/4)(1) \quad (6)$$

where $RT h_0^\mu$ is the heat of mixing coefficient based on molar ionic strength (μ), y is the molal ionic strength fraction, and V is the total volume of the solutions before mixing. Similarly

$$\Delta H_3 = RT h_0^I (I)^2 y (1 - y) W = RT h_0^I (I/(A + B))^2 (1/4)(A + B) \quad (7)$$

where $RT h_0^I$ is the usual heat of mixing coefficient at constant molal ionic strength (I), y is the molal ionic strength fraction, and W is the total weight of solvent in the solutions. Also

$$\Delta H_2 = (I/6) [\phi_L(\text{MgCl}_2, I/3(A + B)) - \phi_L(\text{MgCl}_2, I/6A)] + (I/2) [\phi_L(\text{NaCl}, I/(A + B)) - \phi_L(\text{NaCl}, I/2B)] \quad (8)$$

where $\phi_L(\text{MgCl}_2, I/6(A + B))$ denotes the ϕ_L for magnesium chloride at a molality of $I/6(A + B)$. Combining these equations with the equation $\Delta H_1 = \Delta H_2 + \Delta H_3$ gives the result

$$RT h_0^\mu = RT h^I/(A + B) + (2/3I) [\phi_L(\text{MgCl}_2, I/3(A + B)) - \phi_L(\text{MgCl}_2, I/6A)] + (2/I) [\phi_L(\text{NaCl}, I(A + B)) - \phi_L(\text{NaCl}, I/2B)] \quad (9)$$

where $RT h^I$ is to be evaluated at the molal ionic strength of the mixing which is $I/(A + B)$.

Values of A and B were calculated using the partial molal volume data of Vaslow²⁴ and Owen and Brinkley.²⁵

The results of the calculations are compared in Table III. The corrections to constant E and μ are subject to rather large uncertainty because of the inaccuracy of most of the heat of dilution data. Errors in $RT h^E$ as high as 30 cal kg/eq² at $E = 0.4$ and 5 at $E = 2.4$ and errors in $RT h^\mu$ as high as 2 cal l./mol² at $\mu = 0.5$ and 5 at $\mu = 3.0$ are quite possible.

Table III shows that the constant μ approximation is

very close to the constant I approximation at these concentrations. The constant I approximation is preferred because it is a more convenient concentration unit. It may be that in much more concentrated solutions, the constant μ mixing will be preferable.

Table III also shows that the approximation $RT h^E = 0$ is about as good as assuming the heats of the other mixings are zero. If the effect of the change in ionic strength is negligible, then the values of $RT h^E$ in Table III should be due to like-charged pairs and triplet interactions because the like-charged pair interactions are the same in the initial and final solutions. If this is correct, one would expect the values of $RT h_0$ to follow the structure rule for like-charged pair interactions since the triplet interactions are relatively small. The rule is that mixtures of a structure-maker with a structure-maker (all LiCl and NaCl mixings in Table III) should have positive values of $RT h_0$ and mixtures of a structure-breaker with a structure-maker (all KCl and CsCl mixings in Table III) should have negative values of $RT h_0$.⁹⁻¹¹ It is encouraging that for most of the mixtures in Table III the structure rule holds or is wrong by a small amount. However, the earlier method of estimating the like-charged pairs²⁶ gives quite different results. For instance, at $I = 3.0$ the estimates of the like-charged pair interactions from Table II are: Li⁺-Ca²⁺, 61; Na⁺-Ca²⁺, 48; K⁺-Ca²⁺, -55; while the estimates from Table III at $E = 2.4$ are: Li⁺-Ca²⁺, -3; Na⁺-Ca²⁺, 46; K⁺-Ca²⁺, -92.

It seems worthwhile investigating the use of this concentrations scale further. The present evidence indicates that assuming $RT h^E = 0$ is about as good as assuming $RT h^I = 0$ in the concentration range $I = 0.5$ to 3.0. If more accurate predictions are desired, the equations of Wood and Anderson¹⁵ for predicting many component mixings are easily extended to charge-asymmetric mixtures if E is used instead of I as the concentration scale. The equations of Wood and

(24) F. Vaslow, *J. Phys. Chem.*, **70**, 2286 (1966).

(25) B. B. Owen and S. R. Brinkley, *Chem. Rev.*, **29**, 461 (1941).

(26) See Table II of this paper and ref 1.

Anderson extended to constant E mixings correct for all triplet interactions except like-charged triplets while neglecting ion-atmosphere effects. This will probably be the most accurate method of predicting the properties of charge-asymmetric mixtures at high concentration since the concentration dependence of triplet interactions is probably much higher than the concentration dependence of ion-atmosphere effects.

Acknowledgment. The authors gratefully acknowledge the support of this work by the Office of Saline Water, U. S. Department of the Interior. The authors also wish to thank Miss Nalini Bhatt for help with the calorimetric measurements, Mr. Alan Levine for checking the BaCl_2 with LiCl measurement at $I = 3$, and Dr. Peter Reilly and Professor R. A. Robinson for helpful discussions.

Equilibria in Propylene Carbonate. I. Viscosity and Conductance Studies^{1a} of Some Lithium and Quaternary Ammonium Salts

by L. M. Mukherjee^{1b} and David P. Boden

Chemistry Department, Polytechnic Institute of Brooklyn, Brooklyn, New York 11201
(Received February 17, 1969)

Results of conductance and viscosity measurements of solutions of LiCl , LiBr , LiClO_4 , Et_4NCl , Et_4NClO_4 , $n\text{-Bu}_4\text{NBr}$, and $n\text{-Bu}_4\text{NClO}_4$ in propylene carbonate are reported. All conductance data have been treated by the method of Fuoss and Accascina. Lithium chloride and lithium bromide are found to be associated, having association constants of 557 and 19, respectively, whereas no association could be detected for the other systems. The significance of the values of viscosity F coefficient and a^0 parameter in different cases is discussed.

Introduction

Propylene carbonate (PC) is a stable substance of convenient liquid range (mp -49.2° ; bp 241.7°) and moderately high dielectric constant (64.4^2 at 25°). It is a good solvent²⁻⁶ for a variety of inorganic and quaternary ammonium salts. In recent years, it has been considered a specially suitable solvent for "high energy" electrochemical reactions.³

Reports on fundamental studies⁴⁻⁸ of the behavior of solutions of electrolytes in PC, however, are few and indicate lack of correlation in some instances. Fuoss,⁴ *et al.*, studied the conductance of tetra-*n*-butylammonium tetraphenylboride in this solvent and concluded that ion association was negligible. Wu and Friedman⁵ investigated the conductances and heats of solution of several alkali metal iodides, perchlorates, trifluoroacetates, and tetraphenylborates. Their preliminary studies indicate that the perchlorates in general are "strong" electrolytes whereas the corresponding trifluoroacetates give evidence of considerable ion association, and suggest that the predominant associated form of lithium trifluoroacetate is an ion-pair dimer. In the case of lithium perchlorate solutions, the conductance data⁵ indicate negligible ion association whereas those on heat of solution show a strong concen-

tration dependence indicating the existence of very large ionic interactions. Butler⁶ studied potentiometrically the equilibria of the chloro complexes of silver(I) in PC, and Boden⁷ and Reddy and McClure⁸ have investigated the behavior of glass electrodes in solutions of alkali metal and alkaline earth metal salts in this solvent.

In this work, solutions of a selected group of 1:1 electrolytes in PC have been carefully investigated through conductance and viscosity measurements. The sys-

(1) (a) Presented at the 157th National Meeting of the American Chemical Society, Minneapolis, Minn., April 1969. The material forms a part of a thesis to be submitted by D. P. Boden to the Graduate School of the Polytechnic Institute of Brooklyn, Brooklyn, N. Y., in partial fulfillment of the requirements for the degree of Doctor of Philosophy; (b) Chemistry Department, Illinois State University, Normal, Ill. 61761, to which all correspondence should be sent.

(2) W. H. Harris, Ph.D. Thesis, University of California, Berkeley, Calif., 1958, UCRL Report 8381.

(3) R. J. Jasinski, "High Energy Batteries," Plenum Press, New York, N. Y., 1967.

(4) R. M. Fuoss, J. B. Berkowitz, E. Hirsch, and S. Petrucci, *Proc. Nat. Acad. Sci. U. S.*, **44**, 27 (1958).

(5) Y.-C. Wu and H. L. Friedman, *J. Phys. Chem.*, **70**, 501 (1966).

(6) J. N. Butler, *Anal. Chem.*, **39**, 1799 (1967).

(7) D. P. Boden, paper presented at the Electrochemical Society Meeting, Dallas, Texas, May 1967.

(8) J. E. McClure and T. B. Reddy, *Anal. Chem.*, **40**, 2064 (1968).

tems studied include lithium chloride, lithium bromide, lithium perchlorate, tetraethylammonium chloride, tetraethylammonium perchlorate, tetra-*n*-butylammonium bromide, and tetra-*n*-butylammonium perchlorate. The behavior of these different salts in PC is explained on the basis of the limiting equivalent conductance, the viscosity effects, the a° parameter and, where appropriate, the association constant.

Theory

In cases where ion association cannot be neglected, the conductance equation for a 1:1 electrolyte takes the form⁹

$$\Lambda(1 + Fc) = \Lambda_0 - Sc^{1/2}\gamma^{1/2} + Ec\gamma \log(c\gamma) + Jc\gamma - K_A c\gamma f^2 \Lambda(1 + Fc) \quad (1)$$

where c is the molar concentration, γ is the degree of dissociation of the solute, and K_A is the association constant defined as

$$K_A = \frac{1 - \gamma}{c\gamma^2 f^2} \quad (2)$$

f being the mean ionic activity coefficient.

For PC at 25° S , E , and J can be expressed as

$$S = 0.30833\Lambda_0 + 24.27178$$

$$E = 0.95694\Lambda_0 - 11.03162$$

$$J = 0.8311\Lambda_0[h_b + \ln a^\circ - 0.10595] + 7.4838 + 8.0754a^\circ - 9.58178[\ln a^\circ + 0.00365]$$

The coefficient F can be obtained from the viscosity data by the use of the Jones and Dole equation which is usually expressed in the form

$$\eta/\eta_0 = 1 + Ac^{1/2} + Fc \quad (3)$$

Thus, by plotting $(\eta/\eta_0 - 1)/c^{1/2}$ vs. $c^{1/2}$ a straight line should be obtained whose slope would give F and intercept, A .

If, on the other hand, ion association is negligible the conductance equation for a 1:1 electrolyte simplifies to

$$\Lambda = \Lambda_0 - Sc^{1/2} + Ec \log c + Jc - F\Lambda_0 c \quad (4)$$

Since the J term is always larger than the term in E and since in general the F term is small, the experimental Λ vs. $c^{1/2}$ plot will lie above the limiting tangent given by the Onsager equation.

The latter behavior can be used as a criterion to judge whether ion association exists since if association is appreciable, the γ term in the conductance equation (cf. eq 1) will depress the curve below the limiting tangent.

Electrolytes in general can then be divided into two classes: (1) where the measured conductance curve lies below the limiting tangent and therefore eq 1 is to be used to evaluate the data, and (2) where the measured conductance curve lies above the limiting tangent and eq 4 is applicable. The method of treating conductance

data using eq 1 or 4 has been thoroughly discussed in the monograph by Fuoss and Accascina¹⁰ and a detailed description has been omitted in this paper.

Experimental Section

Chemicals. Solvent. Technical grade PC (Jefferson) was distilled twice under vacuum (1 mm) from anhydrous CaO, a middle fraction being taken each time. The specific conductance of the twice-distilled solvent ranged between $\sim 1.0 \times 10^{-8}$ and $\sim 2.0 \times 10^{-8}$ ohm⁻¹ cm⁻¹. Analysis by vapor phase chromatography indicated the absence of any appreciable impurities. The CO₂ content is estimated to be <0.02 mol % and no other extraneous peak was observed. Karl Fisher titration failed to detect any water.

Salts. Lithium Perchlorate. Anhydrous salt (G. F. Smith) was recrystallized twice from distilled water, dehydrated at 120° under vacuum, and then the anhydrous product obtained in this manner was recrystallized from anhydrous ether following the procedure used by Berglund and Sillen.¹¹ The recrystallized salt was then heated under vacuum at 120° for 16 hr before use.

Lithium Chloride and Bromide. Fisher Certified Reagent grade LiCl and anhydrous reagent grade LiBr (Matheson Coleman and Bell) were used without further purification. Both salts were heated at 60° under vacuum for 16 hr before use.

Tetraethylammonium Chloride. Highest purity salt (Fisher) was recrystallized from a mixture of 1:2 dichloroethane and ethanol. It was then dried at 60° for 16 hr before use.

Tetraethylammonium Perchlorate. Highest purity salt (Eastman) was dried at 60° under vacuum for 16 hr. No trace of any bromide impurity was detected in the sample.

Tetra-*n*-butylammonium Bromide. Polarographic grade (Southwestern Chemicals) salt (mp 102.5-103.5°) was used without any further treatment.

Tetra-*n*-butylammonium Perchlorate. This salt was prepared by reaction between tetra-*n*-butylammonium hydroxide and perchloric acid. The product was recrystallized from ethanol: mp 213-14°.

Conductance Measurements. The conductance measurements were made in a 500 ml Kraus and Bray-type cell which had a cell constant of 0.33350 cm⁻¹. A Wayne Kerr Autobalance Universal Bridge (Type B 641) was used to measure the conductance values at a frequency of 1550 cps. All measured values of the solution conductance were corrected for the conductance of the solvent and are considered reliable to $\pm 0.01\%$.

(9) R. M. Fuoss and L. Onsager, *J. Phys. Chem.*, **61**, 668 (1957).

(10) R. M. Fuoss and F. Accascina, "Electrolytic Conductance," Interscience Publishers, Inc., New York, N. Y., 1959, pp 191-205, 207-247.

(11) U. Berglund and L. G. Sillen, *Acta. Chem. Scand.*, **2**, 116, (1948).

Table I: Summary of Results of Conductance Measurements in Propylene Carbonate at 25°

LiCl		LiBr		LiClO ₄		Et ₄ N·Cl		Et ₄ N·ClO ₄		n-Bu ₄ N·Br		n-Bu ₄ N·ClO ₄	
C(M) × 10 ³	Δ	C(M) × 10 ³	Δ	C(M) × 10 ³	Δ	C(M) × 10 ³	Δ	C(M) × 10 ³	Δ	C(M) × 10 ³	Δ	C(M) × 10 ³	Δ
0.888	19.899	0.558	26.276	2.011	24.649	1.441	30.416	0.934	31.613	0.642	27.782	1.503	26.967
2.961	14.4195	0.837	25.995	4.030	24.076	1.878	30.197	1.173	31.496	0.803	27.690	1.878	26.819
4.440	12.914	1.674	25.285	6.006	23.610	2.694	29.974	1.578	31.301	1.070	27.580	2.505	26.623
5.920	11.559	2.182	24.945	8.010	23.210	3.443	29.794	2.408	30.982	1.606	27.306	3.757	26.3085
7.401	10.654	3.131	24.346	10.00	22.901	4.767	29.511	3.268	30.711	2.141	27.144	5.010	26.056
8.881	9.944	5.5405	23.097	20.03	20.601	5.902	29.310	5.084	30.272	3.212	26.791	7.515	25.606
11.84	8.840	9.004	21.8665	28.01	20.910	7.747	29.046	6.779	29.927	4.283	26.529		
17.76	7.574	12.005	20.980			10.33	28.733	10.17	29.386	6.425	26.050		
		14.41	20.3405					13.55	28.997	8.566	25.623		
		17.96	19.4625							12.25	24.985		

Table II: Results of Viscosity Measurements at 25°

LiCl		LiBr		LiClO ₄		Et ₄ N·Cl		Et ₄ N·ClO ₄		n-Bu ₄ N·Br		n-Bu ₄ N·ClO ₄	
C(M) × 10 ³	η ^a (cP)	C(M) × 10 ³	η ^a (cP)	C(M) × 10 ³	η ^a (cP)	C(M) × 10 ³	η ^a (cP)	C(M) × 10 ³	η ^a (cP)	C(M) × 10 ³	η ^a (cP)	C(M) × 10 ³	η ^a (cP)
3.111	2.496	7.554	2.5085	3.650	2.491	2.479	2.486	4.067	2.488	1.928	2.484	1.879	2.483
6.222	2.503	15.02	2.534	7.300	2.502	4.959	2.4905	8.136	2.491	3.855	2.489	3.757	2.488
12.44	2.514	22.66	2.560	10.95	2.510	9.918	2.499	12.20	2.496	6.4255	2.496	7.515	2.496
18.67	2.526	30.22	2.583	14.60	2.524	16.53	2.506	16.27	2.501	8.996	2.501	12.81	2.507
24.89	2.537	37.77	2.607	18.25	2.538	20.66	2.513	20.34	2.510	12.85	2.511	25.62	2.536
31.11	2.552							29.985	2.521			51.25	2.588
								49.97	2.548				
								99.95	2.614				

^a η_{solvent} = 2.480 cP.

Viscosity Measurements. A Cannon-Fenske type viscometer having an efflux time of 870.3 seconds with PC was used for all measurements. The densities of the solutions were determined in a conventional way by using a pycnometer. All measurements were carried out in an oil bath maintained at 25.00 ± 0.01°. Preparation of all working solutions and other manipulations were carried out in a glove box in a current of Matheson high-purity argon containing water (7.8 ppm), oxygen (8.0 ppm), nitrogen (20 ppm), hydrogen (1.0 ppm) carbon dioxide (< 2.0 ppm) and hydrocarbons as methane (< 1.0 ppm).

Results and Discussions

The results of conductance measurements on the different systems are given in Table I. The equivalent conductances of lithium chloride and lithium bromide when plotted as functions of the square roots of their concentrations fall on curves which lie below the limiting tangent, indicating thereby that ion-association presumably occurs in these two cases. On the contrary, similar plots for the remaining electrolytes, *viz.*, lithium perchlorate, tetraethylammonium chloride, tetraethylammonium perchlorate, tetra-*n*-butylammonium bromide and tetra-*n*-butylammonium perchlorate, are found to lie above the limiting tangent, and these systems are, therefore, considered to be unassociated.

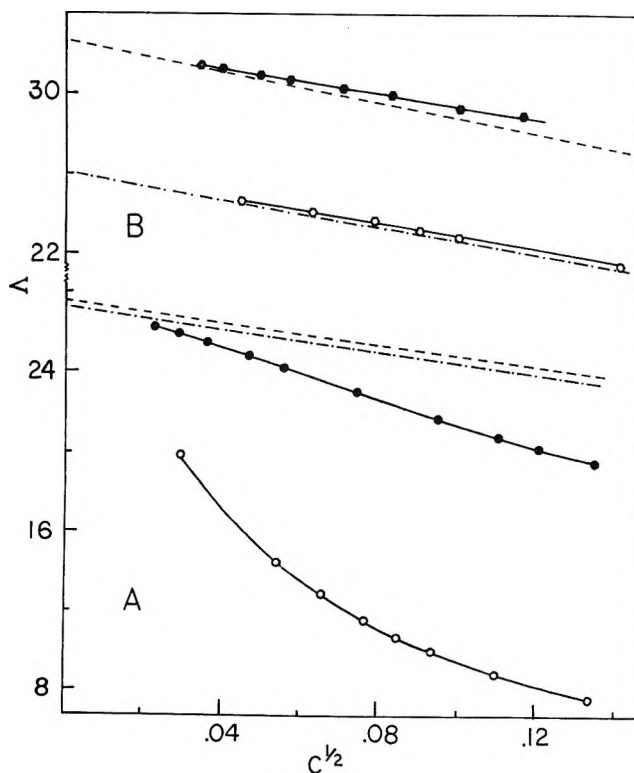


Figure 1. Plot of Δ vs. $c^{1/2}$. \circ (LiCl), \bullet (LiBr), \circ (LiClO₄), \bullet (Et₄N·ClO₄). Limiting tangents: A - - - - (LiCl), - - - (LiBr); B - - - - (LiClO₄), - - - (Et₄N·ClO₄).

Table III: Physical Constants Determined from Analysis of Conductance Data^a

Salt	Λ_0	K_A^b	a° exptl, Å	$r_+ + r_-^d$ Å	F
LiCl	27.50	557	2.525	2.41	...
LiBr	27.35	19	2.66	2.55	1.25 (± 0.02)
LiClO ₄	26.08		2.75	3.66 ^e	1.30 (± 0.14)
Et ₄ N·Cl	31.64		4.73	5.81	0.51 (± 0.03)
Et ₄ N·ClO ₄	32.65		3.60	7.06 ^e	0.54 (± 0.025)
<i>n</i> -Bu ₄ N·Br	28.65		3.525	6.90	0.96 (± 0.03)
<i>n</i> -Bu ₄ N·ClO ₄	28.17		5.00	8.01 ^e	0.83 (± 0.015)

^a J values: LiCl (55.1); LiBr (57.0); LiClO₄ (57.5); Et₄N·Cl (108.6); Et₄N·ClO₄ (83.0); *n*-Bu₄N·Br (76.0); *n*-Bu₄N·ClO₄ (106.3).
^b Eq 2; f calculated using the Debye-Hückel equation in the form $-\log f = 0.6851c^{1/2}\gamma^{1/2}/(1 + 0.3629 \times 10^8 \cdot a^\circ \cdot c^{1/2}\gamma^{1/2})$. ^c Estimated uncertainty: $\sim 2\%$. ^d Crystallographic radius (ref 14). ^e Estimated.

Typical plots obtained for LiCl and LiBr, and LiClO₄ and (Et₄)₄NClO₄ are shown in Figure 1.

In Table II the results of viscosity measurements are presented. All data except those of LiCl are found to conform well to the Jones and Dole equation. Plots of $(\eta/\eta_0 - 1)/c^{1/2}$ vs. $c^{1/2}$ for LiCl indicate considerable curvature and tend towards a physically unreasonable value of A . Because of this, in the treatment of conductance data of LiCl viscosity correction was omitted.

The values of Λ_0 , a° , K_A and F for the various electrolytes are summarized in Table III. The J values corresponding to the interpolated a° values are given in the footnote.

In the case of LiCl and LiBr the association constants are found to be 557 and 19 respectively, the larger bromide ion with its lower surface charge density appearing to have a much lower affinity for the lithium ion than the smaller chloride ion. Lithium perchlorate, on the other hand, appears to be completely dissociated in agreement with the earlier studies.⁵ This increase in the association constant as the anion size decreases agrees with the general contention of the theories of Denison and Ramsey,¹² and Gilkerson.¹³ The viscosity F coefficients for lithium bromide and lithium perchlorate are greater than those for the tetraalkylammonium salts (Table III); considering the contribution of the anions to be small in each case this would indicate that Li⁺ is likely to be highly solvated. On this basis, it appears that of the three cations the extent of interaction with the solvent varies in the order: Li⁺ > *n*-Bu₄N⁺ > Et₄N⁺. For the lithium salts the agreement between the a° values obtained from the conductance data and the sums of the crystallographic radii¹⁴ is generally good indicating that in the event of ion-ion contacts, the bare ions rather than their solvated co-spheres are presumably involved.

No evidence of ion association could be found for the tetraethylammonium and tetra-*n*-butylammonium salts (Table III). The limiting conductances of the series of perchlorate salts follow the sequence Et₄N·ClO₄ (32.65) > *n*-Bu₄N·ClO₄ (28.17) > LiClO₄ (26.08). This

leads to the interesting observation that the mobility of Li⁺ is lower than that of either Et₄N⁺ or *n*-Bu₄N⁺ and suggests that the effective (solvated) sizes of the cations are in the order of Li⁺ > *n*-Bu₄N⁺ > Et₄N⁺. Considering the viscosity F coefficient to be a measure of the combined effect of the ionic sizes and interaction of the ions with the solvent¹⁵ one would expect in this particular series of salts that the values of F would follow the order LiClO₄ > *n*-Bu₄N·ClO₄ > Et₄N·ClO₄. As shown by the data in the last column of Table III, this expectation is very well borne out.

Based on the Λ_0 values of the pairs LiBr-LiClO₄ and Bu₄NBr-Bu₄NClO₄ and assuming that additivity of ion conductances is valid in PC, λ_{0Br^-} is found to be greater than $\lambda_{0ClO_4^-}$. In this connection, the small difference in Λ_0 of LiCl and LiBr would indicate that both Cl⁻ and Br⁻ ions have about the same mobilities. Comparison of LiCl-LiClO₄ data suggests that λ_{0Cl^-} is greater than $\lambda_{0ClO_4^-}$. The Et₄NCl-Et₄NClO₄ pair, however, indicates for some unknown reason a reverse order in the relative magnitudes of λ_{0Cl^-} and $\lambda_{0ClO_4^-}$.

The actual values of a° for the different tetraalkylammonium salts are not too unreasonable. Apparently, however, there is a tendency for a° to be substantially less than the sum of the crystallographic radii of the ions.

The trend in the actual magnitude of the a° values is not clearly understood; for example, the a° values for Et₄N·ClO₄ and *n*-Bu₄N·Br appear to be smaller than that for Et₄N·Cl which seems rather unreasonable. No explanation for this discrepancy can be presented at this stage.

Acknowledgment. D. P. Boden acknowledges the cooperation received from ESB, Inc., Yardley, Pa.

(12) J. T. Denison and J. B. Ramsey, *J. Amer. Chem. Soc.*, **77**, 2615 (1955).

(13) W. R. Gilkerson, *J. Chem. Phys.*, **25**, 1199 (1956).

(14) L. Pauling, "The Nature of the Chemical Bond," Cornell University Press, Ithaca, N. Y., 1948; F. Evans and R. L. Kay, *J. Phys. Chem.*, **70**, 366 (1966).

(15) R. H. Stokes and R. Mills, "Viscosity of Electrolytes and Related Properties," Pergamon Press, New York, N. Y., 1965, pp 33-45.

The Electric Moments of the Halotrifluoroethylenes¹

by E. J. Gauss and Theodore S. Gilman²

Department of Chemistry, University of Colorado, Boulder, Colorado 80302 (Received February 21, 1969)

The dipole moments of CF_2Cl_2 , $\text{CF}_2=\text{CFCl}$, $\text{CF}_2=\text{CFBr}$, and $\text{CF}_2=\text{CFI}$ have been measured, with values of 0.50, 0.58, 0.76, and 1.04 D, respectively, being obtained. The moments of the trifluorovinyl compounds are discussed in terms of possible mesomeric and inductive effects. It is concluded that the magnitude of and trend in these moments are best explained on the basis of inductive effects.

Introduction

The change in dipole moment when an alkyl group is replaced by an alkenyl or aryl group or when the hydrogens of an alkyl group are replaced by fluorines is often attributed to mesomeric or inductive effects.³⁻⁵ For example, mesomerism can be used to explain the lowering of the dipole moment when the ethyl group in $\text{C}_2\text{H}_5\text{Cl}$ is replaced by a vinyl or phenyl group. On the other hand, replacement of the hydrogens in the methyl halides by fluorines causes the trend in polarity to reverse. In the CH_3X series ($\text{X} = \text{Cl}, \text{Br}, \text{or I}$), the electric moment of the chloride is greatest and that of the iodide the least; whereas in the CF_3X series the trend in moments is in the opposite direction. This reversal has been attributed to inductive effects.⁶

The dipole moments of the halotrifluoroethylenes are therefore of interest since both mesomeric and large inductive effects are possible. These moments are reported in this paper, and the values are interpreted in terms of the above-mentioned effects.

Experimental Section

Materials. (i) Bromotrifluoroethylene was prepared by a method, developed in these laboratories,⁷ which involved the bromination of trifluoroethylene and subsequent dehydrobromination of the adduct, 1,2-dibromo-1,1,2-trifluoroethane, in a suspension of KOH in mineral oil. The gaseous product, after fractional distillation, boiled at -12.0° at 630 mm pressure. (ii) The preparation of iodotrifluoroethylene has been reported elsewhere.⁸ The sample used was shaken with mercury after fractional distillation (bp 27° (632 mm)). (iii) Gaseous dichlorodifluoromethane and chlorotrifluoroethylene (E.I. du Pont de Nemours and Co.) were used directly from cylinders. (iv) The ammonia used to calibrate the dielectric constant cell was purified on a vacuum line by three successive trap-to-trap distillations, with the middle fraction being saved in each instance.

Apparatus and Procedure. The heterodyne beat apparatus, dielectric constant cell, and procedure used have been described previously.⁹ The cell constant was 79.14 pF, as found by calibration with ammonia whose dielectric constant is accurately known.¹⁰ Each

of the gases studied was admitted to the cell at various pressures ranging from 200 to 650 mm at each of four or five temperatures between 25 and 150° . Capacitance readings were taken; then the cell was immediately evacuated and the empty cell capacitance was read. This procedure tended to minimize the effects of drift in the electrical circuits and of gas absorption on the plates in the cell; it was found that there was a slow decrease in capacitance of the empty cell upon evacuation which was presumably the result of slow gas desorption.

Results

For each of the gases and at each temperature, values of ΔC , the difference in capacitance between the full and empty cell, were plotted *vs.* the pressure of the gas in the cell. A value of ΔC for 1 atm was obtained by extrapolation of the best straight line drawn through the points, thus minimizing the effect of possible gas imperfections. Values of $\epsilon - 1$ at 1 atm were obtained by dividing the corresponding ΔC 's (1 atm) by the cell constant ($\epsilon =$ dielectric constant). The total molar polarization P was then calculated by

$$P \text{ (cc/mol)} = \frac{82.05T}{3} (\epsilon - 1)$$

in which ideal gas behavior is assumed and in which $\epsilon + 2$ has been replaced by 3 since ϵ is so close to unity. The values of P thus obtained at different temperatures for the four gases studied are given in Table I.

(1) Based in part on the M.A. Thesis of E. J. Gauss, University of Colorado.

(2) Deceased on February 11, 1969. Reprint requests may be addressed to Chairman, Department of Chemistry, University of Colorado, Boulder, Colorado 80302.

(3) C. P. Smyth, "Dielectric Behavior and Structure," McGraw-Hill Book Co., Inc., New York, N. Y., 1955, Chapters VIII-X.

(4) R. J. W. Le Fevre, "Dipole Moments," 3rd ed, John Wiley & Sons, Inc., New York, N. Y., 1953, Chapter IV.

(5) J. W. Smith, "Electric Dipole Moments," Butterworth and Co. Ltd., London, 1955, Chapter 7.

(6) A. Di Giacomo and C. P. Smyth, *J. Amer. Chem. Soc.*, **77**, 774 (1955).

(7) R. J. Seffl, Ph.D. Thesis, University of Colorado, 1954.

(8) J. D. Park, R. J. Seffl, and J. R. Lacher, *J. Amer. Chem. Soc.*, **78**, 59 (1956).

(9) E. J. Gauss and T. S. Gilman, *Rev. Sci. Instr.*, **31**, 164 (1960).

(10) A. van Otterbeek and K. de Clippelier, *Physica*, **14**, 349 (1948).

Table I: Total Polarization at Various Temperatures

<i>T</i> , °K	<i>P</i> , cc/mol	<i>T</i> , °K	<i>P</i> , cc/mol
CF ₂ Cl ₂		CF ₂ =CFCl	
298.2	22.88	297.6	21.19
323.2	22.12	324.2	20.62
359.0	21.46	373.2	19.73
373.2	21.54	423.3	19.16
423.2	21.35		
CF ₂ =CFBr		CF ₂ =CFI	
298.1	27.82	298.2	51.37
323.0	27.01	326.2	45.54
373.3	25.03	363.2	42.18
424.2	24.48	393.6	39.45

With the exception of CF₂=CFI, plots of *P* vs. 1/*T* extended over a sufficiently wide temperature range to justify determination of the slopes *B* and intercepts *P*_D, the distortion polarization, by the least-squares method. The values thus obtained for *P*_D and for the dipole moment *μ*, calculated from *B* by means of μ (D) = 0.01281√*B*, are given in Table II.

Table II: Distortion Polarizations and Dipole Moments

<i>P</i> _D (cc/mol) →	<i>μ</i> (D)
CF ₂ Cl ₂ 17.44	→ 0.50 ± 0.06 0.58 ± 0.04 0.76 ± 0.05 1.04 ± 0.10 ^b
CF ₂ =CFCl 14.27	
CF ₂ =CFBr 15.90	
CF ₂ =CFI 24 ^a	

^a Estimated (see below). ^b The average of three *μ* values (1.07, 1.04, and 1.00 D) calculated from the total polarizations at 326.2, 363.2, and 393.6°K, respectively, by the refractivity method.

The uncertainties in the values of *μ* were computed by determining by how much the slopes *B* would be increased if the least-squares values of *P* at *T*_{min} and *T*_{max} were increased and decreased, respectively, by the calculated standard deviation in *P*.

Least-squares treatment of the data for CF₂=CFI yielded a dipole moment of about 1.5 D and a value of 2.85 cc/mol for *P*_D. Since the distortion polarization of CF₂=CFI can hardly be less than that of CF₂=CFBr, it was clear that the slope of the polarization vs. 1/*T* data could not be used to evaluate the dipole moment in this instance. Reproducible polarization data were obtained only between 326 and 394°K, which is too small a temperature interval for the evaluation of a reliable slope and intercept. Dielectric constant measurements for CF₂=CFI were in fact made at 298 and 423°K as well, but a large scatter of the data points was observed at each of these temperatures. This was attributed to partial condensation of the gas at the lower temperature (even though the pressure in the cell never exceeded 430 mm) and to decomposition or re-

arrangement at the higher temperature. It was therefore necessary to resort to the refractivity method¹¹ for the determination of the dipole moment of CF₂=CFI.

In this method *P*_D is estimated from refraction or other data and subtracted from the total observed polarization at a certain temperature to obtain the orientation polarization. The dipole moment is then calculated with the relation

$$\mu$$
 (D) = 0.01281[(*P* - *P*_D)*T*]^{1/2}

The following evidence was used to arrive at a value of 24 cc/mol for *P*_D of CF₂=CFI. (a) The values of *P*_D for CF₂=CFCl and CF₂=CFBr given in Table II differ by 1.6 cc/mol; the same difference in *P*_D has been found for CF₃Cl and CF₃Br.⁶ Furthermore, *P*_D for CF₃I exceeds that of CF₃Br by 7.7 cc/mol.⁶ Thus, if this same excess holds for the corresponding trifluorovinyl compounds, *P*_D for CF₂=CFI should be 23.6 cc/mol. (b) The molar refraction (*n* line) of CF₂=CFCl has been found¹² to be 15.75 cc/mol. The *n* line atomic refraction of iodine exceeds that of chlorine by 7.93 cc/mol.¹³ Thus the molar refraction of CF₂ + CFI should be about 23.7 cc/mol, which indeed is the value one obtains by adding atomic refractions,¹³ using 1.1 cc/mol for the atomic refraction of fluorine.¹² (c) On the basis of refraction data for a number of perhalogenated olefinic compounds, Fainberg and Miller¹⁴ give 10.15 cc/mol for the refraction of the CF₂=CF— group. Adding 13.9 cc/mol for atomic refraction of iodine¹³ gives 24.2 cc/mol for CF₂=CFI.

Hence to the extent that the distortion polarization is approximately equal to the *n* line molar refraction, a value of 24 cc/mol should be a reasonable estimate of the former quantity for CF₂=CFI. Actually, since the total polarization is about twice as great as the distortion polarization for this compound, considerable uncertainty in the latter can be tolerated. For example an uncertainty of 2 cc/mol in *P*_D leads to one of only about 0.06 D in the dipole moment.¹⁵

Discussion

The dipole moments of both CF₂Cl₂ and CF₂=CFCl have been determined previously. That of the first compound was measured to check the reliability of our method and apparatus, while the other was determined in order to have data for the three members of

(11) See, for example, ref 4, pp 13–15, 25, and 26.

(12) M. T. Rogers, J. G. Malik, and J. L. Spiers, *J. Amer. Chem. Soc.*, **78**, 46 (1956). These authors measured the refractive index for the mercury green line. Adjustment to the *n* line amounted to only 0.02 cc/mol.

(13) K. Fajans, "Technique of Organic Chemistry," A. Weissberger, Ed., 2nd ed., Vol. I ("Physical Methods") part II, Interscience Publishers, Inc., New York, N. Y., 1949, p 1163.

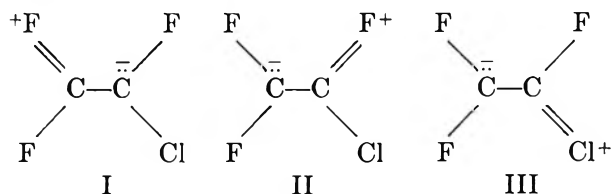
(14) A. H. Fainberg and W. T. Miller, Jr., *J. Org. Chem.*, **30**, 864 (1965).

(15) A value of 22.8 cc/mol for the molar refraction can be calculated from the refractive index (*n* line) and density of CF₂=CFI at 0° measured by Park, Seffl, and Lacher.⁸

the $\text{CF}_2=\text{CFX}$ series measured under the same conditions.

For CF_2Cl_2 there is good agreement with the value 0.51 D reported by Smyth and McAlpine;¹⁶ a somewhat higher value (0.55 D) was found by Epprecht¹⁷ and Fuoss.¹⁸ A greater spread of moment values has been reported in the literature for $\text{CF}_2=\text{CFCl}$: 0.38,¹⁹ 0.40,⁶ and 0.16 D.²⁰

From one point of view, a dipole moment of about 0.6 D for $\text{CF}_2=\text{CFCl}$ might seem unexpectedly large were it not for mesomeric effects involving structures such as



One can cite several sets of data which suggest that the moment should be smaller than the observed value in the absence of mesomerism. In this regard Rogers and Pruett have pointed out¹⁹ that the moment might be expected to be close to the difference between the moments of fluorobenzene and chlorobenzene, about 1.6 and 1.7 D,²¹ respectively, in the gaseous state. Other evidence supporting this argument is the small difference between the moments of (a) vinyl fluoride and vinyl chloride, both about 1.43 D,²¹ and (b) 1,1-difluoroethylene, 1.37 D,²¹ and 1,1-dichloroethylene, 1.2–1.3 D (from solution measurements).²¹ On the basis of this type of argument, then, contributions from mesomeric structures I, II, or III are needed to explain the observed moment of $\text{CF}_2=\text{CFCl}$.

Bond length considerations have been used to decide whether structures with the double bond to fluorine (I or II) are more significant than those with the double bond to chlorine (III). Since the decrease in C–F bond distance which occurs in methane derivatives as the degree of fluorine substitution increases has been interpreted as indicating increasing double bond character,²² Rogers and Pruett concluded¹⁹ that the contribution of structures with the double bond to fluorine is more important. (They also inferred that a structure similar to I, with the chlorine end negative, would be preferable to II or III because the dipole moment of chlorobenzene is somewhat greater than that of fluorobenzene.) Other bond distance evidence which supports this viewpoint is the unusually short C–F bond length in $\text{CF}_2=\text{CF}_2$ (1.30–1.31 Å²³), as compared to 1.34 or 1.35 Å in vinyl fluoride,²⁴ whereas no such similar effect has been observed in the corresponding chloro compounds.²⁵ Furthermore, with increasing atomic size, there seems to be a decreasing tendency toward the formation of double bonds involving the overlap of p orbitals; thus, on this basis as well, structures I and II are preferable to III, particularly since

an interpretation is sought which will take into account the moments of the bromo and iodo compounds as well. Bond length evidence supporting any of the structures I, II, or III is, however, somewhat inconclusive in that a slightly longer than usual C=C bond distance should result from the contribution of such structures. Yet in the similar compounds, $\text{CF}_2=\text{CF}_2$ and $\text{CF}_2=\text{CH}_2$, this distance is, if anything, shorter than the normal C=C double bond distance of 1.34 Å.^{23,26}

On the other hand, as the data in Table II indicate, the dipole moments in the $\text{CF}_2=\text{CFX}$ series increase as X changes from Cl to Br to I; this strongly suggests that the nonfluorine halogen atom X is at the positive end of the dipole. If such is the case, then contributions from structures like I, which have X at the negative end, must be relatively unimportant; otherwise, the $\text{CF}_2=\text{CFX}$ molecules would have moments which, in the absence of mesomeric effects, would be even greater than those observed. This seems highly unlikely in view of the fact that the polarities of the various carbon–halogen bonds are generally regarded as differing at most by only 0.2 or 0.3 D. Moreover, structures like II fail to account for the substantial increase in moments noted above.

In contrast to the problems encountered with finding a satisfactory mesomeric explanation of the magnitude of and trend in the electric moments in the $\text{CF}_2=\text{CFX}$ series, a qualitative interpretation in terms of inductive effects is fairly straightforward. For example, were it not for induction, the dipole moments of *trans*-1,2-chlorofluoroethylene and chlorotrifluoroethylene should be about the same, since the over-all moments in both molecules might be regarded as the resultant of a C–Cl and a C–F bond moment pointing in opposite directions. Indeed the moment of the first compound should be close to zero, because as indicated earlier, the moments of the C–Cl and C–F bonds differ by only 0.1 D or less.²⁷ But, with $\text{CF}_2=\text{CFCl}$ this should no longer be

(16) C. P. Smyth and K. B. McAlpine, *J. Chem. Phys.*, **1**, 190 (1933).

(17) G. W. Epprecht, *Z. Angew. Math. Phys.*, **1**, 138 (1950).

(18) R. M. Fuoss, *J. Amer. Chem. Soc.*, **60**, 1633 (1938).

(19) M. T. Rogers and R. D. Pruett, *ibid.*, **77**, 3686 (1955); *ibid.*, **79**, 6575 (1957).

(20) J. E. Boggs, C. M. Crain, and J. E. Whiteford, *J. Phys. Chem.*, **61**, 482 (1957).

(21) A. L. McClellan, "Tables of Experimental Dipole Moments," W. H. Freeman & Co., San Francisco, Calif., 1963.

(22) L. Pauling, "The Nature of the Chemical Bond," 2nd ed, Cornell University Press, Ithaca, N. Y., 1940, p 235.

(23) I. L. Karle and J. Karle, *J. Chem. Phys.*, **18**, 963 (1950); T. T. Brown and R. L. Livingston, *J. Amer. Chem. Soc.*, **74**, 6084 (1952).

(24) H. W. Morgan and J. H. Goldstein, *J. Chem. Phys.*, **30**, 1025 (1959); B. Bak, D. Christensen, L. Hansen-Nygaard, and J. Rastrup-Andersen, *Spectrochim. Acta*, **13**, 120 (1958).

(25) L. E. Sutton, Ed., "Tables of Interatomic Distances and Configuration in Molecules and Ions," Special Publication No. 11, The Chemical Society, London, 1958.

(26) A. Roberts and W. F. Edgell, *J. Chem. Phys.*, **17**, 742 (1949).

(27) The dipole moment of *trans*-1,2-chlorofluoroethylene apparently has not been determined.

the case; the opposing C-Cl and C-F bond moments (and also the opposing C-F moments for that matter) should not effectively cancel each other out. This is because through mutual induction, carbon-halogen bonds lower the moments of other carbon-halogen bonds to the same carbon.²⁸ The C-F bond has the greatest ability to lower the moments of other bonds, and the extent to which the moment of a C-X bond is lowered increases with the polarizability of X. Thus a C-F bond has a greater effect than a C-Cl bond in lowering the moment of a C-X bond to the same carbon, and the moment of a C-Cl bond is lowered more than that of C-F bond by a C-X bond.

As a result of this type of interaction, then, the polarity of the C-Cl bond in $\text{CF}_2=\text{CFCl}$ will be lowered more than that of the opposing C-F, and a moment for the whole molecule greater than that expected on the basis of simple bond moment considerations will result. Moreover, as a consequence of the increase in polarizability, replacing the chlorine with bromine or iodine should cause increasingly greater lowering of the C-Br or C-I bond moment and hence an increase in the moment of the molecule as a whole, as has been found by experiment. A similar type of argument was used to explain the increase in moment in the CF_3X series.⁶

A rough estimate of the magnitude of the moment of $\text{CF}_2=\text{CFCl}$ resulting from inductive¹ effects can be made with the aid of the following bond moment lowering data computed by Smyth and McAlpine.¹⁶ For chlorine and/or fluorine bonded to the same carbon with tetrahedral angles, the lowerings were calculated to be: C-F by C-F, 0.21 D; C-Cl by C-F, 0.56 D; C-F by C-Cl, 0.11 D. With these figures, one can estimate that, at the CF_2 end of the molecule, the lowering should be about 0.4 D and at the CFCl end, about 0.7 D, leaving a net induced moment of about 0.3 D, with the CF_2 end being the negative end of the dipole.^{29,30} It thus appears that roughly one-half of the total moment of $\text{CF}_2=\text{CFCl}$ is attributable to isolated inductive effects at each end of the molecule, since as mentioned earlier, on the basis of bond moments alone the total moment should be only 0.1 D or less. The rest of the total moment of about 0.6 D can be accounted for in terms of effects which are best revealed by a comparison of the moments in the trifluoromethyl and trifluorovinyl series, which is given in Table III.

On the basis of inductive action, one would expect the moments in the trifluoromethyl series to be larger because there are three fluorines to lower the moment of

Table III: Comparison of Dipole Moments

X	μ of CF_3X , ^a D	μ of $\text{CF}_2=\text{CFX}$, D
Cl	0.46	0.58
Br	0.65	0.76
I	0.92	1.04
H	1.62	1.32 ^b

^a See ref 6. ^b O. L. Stiefvater and J. Sheridan, to be published.

the C-X bond. Hence the fact that the moments of the trifluorovinyl halides are greater suggests that the inductive influence of the CF_2 group at one end of the molecule is transmitted through the double bond and that the double bond itself is polarized, thus giving rise to a charge separation over a greater distance than is possible with the trifluoromethyl compounds. The constant difference between the moments in the two series can thus be regarded as the contribution of this charge separation, plus possibly a small contribution from mesomerism.

For the first three members in each series (X = halogen only), the data in Table III exhibit a parallelism which becomes more evident and meaningful when the dipole moments in each series are plotted against the atomic refraction of the corresponding halogen. The fact that two parallel lines result supports the plausibility of an inductive effect interpretation of the dipole moments since atomic refraction can be considered to be proportional to polarizability. Such a simple correlation between dipole moment and polarizability can only be expected in a series of compounds in which one element is replaced by another with the same outer electron configuration and with about the same bond moment. The last line of Table III, referring to the hydrogen compound, seems to indicate that a mutual polarization of bond moments is transmitted and intensified by the C=C bond only to halogens, but not to hydrogen.

Acknowledgments. The financial support of a grant from the Research Corporation is gratefully acknowledged. We are also indebted to Professor Joseph D. Park for making available samples of the compounds studied.

(28) See ref 3, pp 235-239.

(29) The fact that the pertinent bond angles in $\text{CF}_2=\text{CFCl}$ are about 114° ³⁰ instead of 109.5° causes small decreases in the calculated lowerings which can be neglected in this approximate treatment.

(30) P. A. Akisin, L. V. Vilikov, and Ju. I. Vesnin, *Dokl. Akad. Nauk SSSR*, **126**, 310 (1959).

Infrared Spectroscopic Study of Oxygen Species in Vanadium Pentoxide

with Reference to Its Activity in Catalytic Oxidation

by Yoshiya Kera and Kozo Hirota

Department of Chemistry, Faculty of Science, Osaka University, Toyonaka, Osaka, Japan
(Received February 27, 1969)

To clarify the nature of the exchangeable oxygen in vanadium pentoxide catalyst during the oxidation reaction, an infrared technique combined with the ^{18}O tracer technique was applied to the samples isotopically substituted by treatment with carbon dioxide- ^{18}O . The bands appearing at 1019 and 818 cm^{-1} can be identified to be the $\text{V}=\text{O}$ and $\text{V}-\text{O}-\text{V}$ groups, respectively, because the corresponding shift of both bands appeared by isotopic substitution. Exchange experiments between gaseous carbon dioxide and vanadium pentoxide were carried out at 290, 370, 410, and 450° , and the ^{18}O balance was investigated, taking the intensity of the above infrared bands into account. Thus, the behavior of the oxygen species at the surface and in the bulk could be determined; (a) Direct exchange of the oxygen on the surface $\text{V}=\text{O}$ groups with gaseous oxygen is very rapid at the initial stage of reaction. (b) Oxygen exchange between $\text{V}=\text{O}$ and $\text{V}-\text{O}-\text{V}$ groups may occur rapidly near the lattice dislocations on the (010) surface as well as on other surfaces. (c) The exchange within the $\text{V}-\text{O}-\text{V}$ net plane is the easiest of all the processes, so that it becomes predominant in the reaction even at the intermediate stage. (d) The exchange between the $\text{V}=\text{O}$ and $\text{V}-\text{O}-\text{V}$ groups on the surfaces is important from the standpoint of catalytic oxidation.

According to our "triangular" reaction scheme¹ for carbon monoxide oxidation over vanadium pentoxide powders, oxygen atoms in the $\text{V}=\text{O}$ groups projecting from the $\text{V}-\text{O}-\text{V}$ net planes of the oxide are repeatedly regenerated by new ones. However, it was shown also that such exchangeable oxygen species are not restricted to the $\text{V}=\text{O}$ groups on the surface, but the oxygen species in the oxide bulk relate to the reaction. Therefore, the behavior of oxygen has to be clarified in the oxidation scheme, even though such a scheme has been implicitly accepted without any direct evidence by most of the researchers.

As reported preliminarily,² a new band appeared at 962 cm^{-1} in the infrared spectra of the oxide substituted by isotopic oxygen ^{18}O , so that the 1019-cm^{-1} band was confirmed to be the stretching vibration of the $\text{V}=\text{O}$ group, projecting perpendicularly to the $\text{V}-\text{O}-\text{V}$ net plane, *i.e.*, the (010) plane. There is also the possibility of finding additional isotopic bands produced by oxygen species in the oxide.

It is the object of the present report to investigate the behavior of various oxygen species in vanadium pentoxide and to establish their role in the catalytic oxidation in more detail by using an ir technique in combination with the ^{18}O tracer technique and also to discuss the relation between the exchangeability of oxygen and the catalytic activity of the oxide.

Experimental Section

Catalyst. The same lot of vanadium pentoxide powders as in the previous paper¹ (Mitsuwa Chemical Co., special grade) was used without any treatment. Surface area of the powders was determined to be 2.5

m^2/g from the BET method, using carbon dioxide as adsorbate at -78° .

Procedure of Experiment E. To determine the ir band due to the exchangeable oxygen, the ^{18}O -substituted powders were prepared by the isotopic exchange reaction of carbon dioxide- ^{18}O (including oxygen- ^{18}O (10:13)) with the powders. The scheme of this exchange process has been previously studied¹ and is examined in more detail in this paper.

The apparatus is shown in Figure 1. The procedure was similar to that of experiment B in the previous paper.¹ After the substitution, the oxide powders were taken out of the reaction tube, and their ir spectra were measured, using a Japan Spectroscopic Co., Type DS-402G, apparatus.

Procedure of Experiment F. For the sake of determining the relation between the ir bands and the isotopic exchange reaction on the catalyst, the ir spectra of the oxide were investigated as a function of the progress of the exchange reaction between carbon dioxide- ^{18}O and the oxide. The apparatus shown in Figure 2 was used with the following procedure.

Four side tubes, each accompanying a tap, were attached to a main reaction tube R. (Only two side tubes are shown in Figure 2.) Each side tube was charged with oxide powders for measurement of the infrared spectra. The total amount of the oxide was 34 mg for each experiment, 1.5 mg in each side tube, and 28 mg in the main tube, which was attached in order to

(1) K. Hirota, Y. Kera, and S. Teratani, *J. Phys. Chem.*, **72**, 3133 (1968).

(2) Y. Kera, S. Teratani, and K. Hirota, *Bull. Chem. Soc. Jap.*, **40**, 2458 (1967).

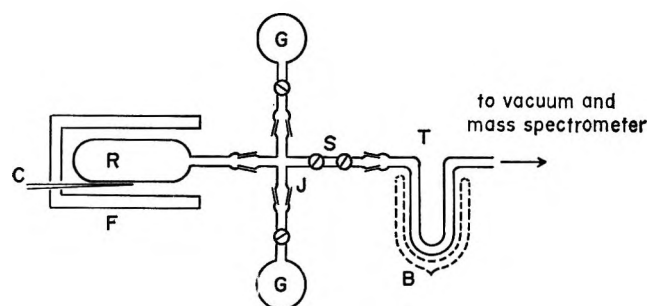


Figure 1. Reaction apparatus: R, reaction tube; G, gas reservoir; S, sampling part; B, Dry Ice-acetone bath; F, electric furnace; C, chromel-alumel thermocouple; J, joint; T, trap.

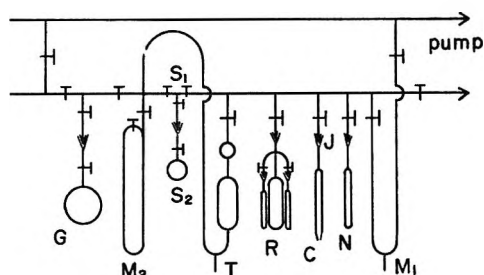


Figure 2. Reaction apparatus: R, reaction tube; G, gas reservoir; S₁, sampling part; S₂, sampling tube; M₁, M₂, mercury manometer; T, Toepler pump; C, calcium chloride tube; J, joint; N, the collecting part of the reacting gas.

reduce any change in composition incurred upon the removal of a part of the catalyst for analysis.

Prior to each experiment, a calcium chloride tube, which had an open end to the air, was attached to the joint J. Then, R was heated with an electric furnace at 490° for 1 hr and then was degassed with a mercury diffusion pump at 490° for 2 hr, until the degree of vacuum reached about 10⁻⁵ mm, according to an ionization gauge. The reaction temperature was regulated to be constant within ±1°.

After the above-mentioned treatment, a constant amount of carbon dioxide labeled with ¹⁸O was introduced with a Toepler pump, and the reaction was begun. At a given time, about 1% of the gas reacting in R was removed in the part S₁ (ca. 1 cm³) for the analysis, and a side tube was simultaneously taken away from the system successively for the infrared measurement. Before the side tube was removed, the reaction gas was collected in the part N by immersing the part in liquid nitrogen to prevent a part of the reaction gas from being lost to the system.

Gaseous Reactant. A mixture of oxygen and carbon dioxide, both containing ca. 60 atom % ¹⁸O, was used in experiment E. Carbon dioxide-¹⁸O used in experiment F was prepared from the carbon monoxide-¹⁸O, which was obtained by contacting the gaseous oxygen-¹⁸O with active charcoal at about 900°. By allowing gaseous oxygen-¹⁸O to react with carbon monoxide-¹⁸O at

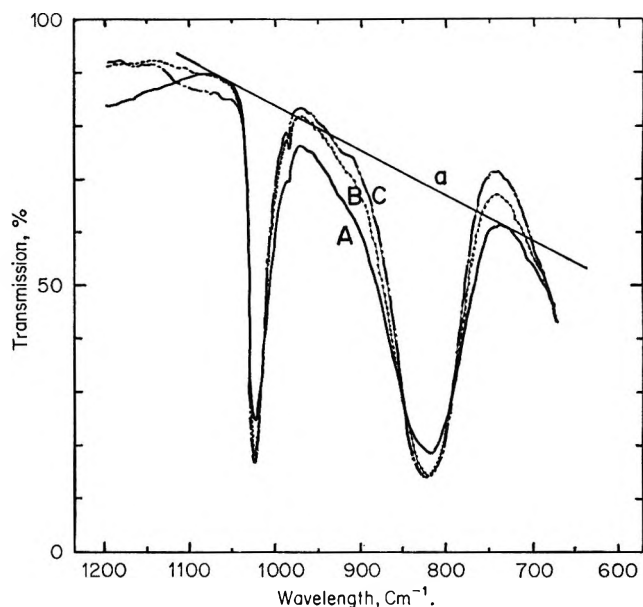


Figure 3. The change in the ir spectrum of the oxide with degree of pulverization. Curve A shows the ir spectrum observed after the first pulverization, B after repeating the pulverization, and C after again repeating the pulverization.

350° on a platinum black catalyst, carbon dioxide-¹⁸O was prepared. The concentration of ¹⁸O in carbon dioxide thus obtained was about 38 atom %, and the gas was mass spectroscopically free from other substances.

The oxygen-¹⁸O used in both experiments was prepared by our laboratory as in the previous paper.³ For the isotopic analysis, a Hitachi Co. Type RMU-5B apparatus was used.

Ir Measurement. Ir absorption spectra of vanadium pentoxide powders were measured by the KBr disk method over the range from 400 or 650 to 1200 cm⁻¹. To determine quantitatively the ¹⁸O concentration in the V=O group, a "compensation method" was adopted by inserting the untreated oxide powders in the optical path of the reference light.

The samples for the KBr disk method were prepared by pulverizing a mixture of the oxide and KBr powders in an agate mortar and pressing them in the usual way. The shape of the Ir spectrum changed gradually as shown by curves A, B, and C in Figure 3, depending on the degree of the pulverization. The integrated absorption intensities of the band at 1019 cm⁻¹ of these three spectra are approximately equal, in spite of the absorbances at the band maxima being different for the different cases. Most measurements were done on the samples, corresponding to the A curve, and the baseline **a** was assumed to be approximately linear. The absorbance of the band at 1019 cm⁻¹ was determined for various concentrations of the oxide powders, in order to

(3) K. Hirota, Y. Kobayashi, M. Takahashi, and Y. Yoshikawa, *Isotopes Radiation* (Tokyo), 2, 235 (1959).

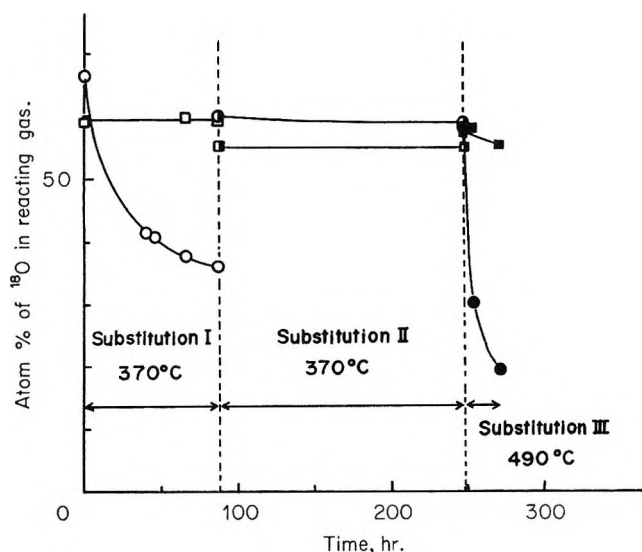


Figure 4. Changes of ^{18}O concentration in oxygen and carbon dioxide during the ^{18}O -substituted reaction of vanadium pentoxide. Circles indicate carbon dioxide and squares oxygen.

draw a calibration curve for the concentration of oxide in the disk. A linear relationship was confirmed well over the concentration range from 0.007 to 0.7 (mg of $\text{V}_2\text{O}_5/200$ mg of KBr). However, the compensation was carried out in the present experiment by adjusting the concentration of the oxide in the range between 0.4 and 0.6 (mg of $\text{V}_2\text{O}_5/200$ mg of KBr).

The ^{18}O concentration in the V-O-V groups was investigated as in the V=O group, as will be explained in experiment E-2, but the attempt was unsuccessful.

Results

Experiment E-1. Identification of the Stretching Band Ascribable to the V=O Group. Vanadium pentoxide powders were treated with a mixture of oxygen and carbon dioxide, both gases containing ca. 60 atom % of ^{18}O , for 88 hr at 370° (substitution I). Such treatment was repeated for 160 hr at the same temperature (substitution II) with a fresh mixture and again for 24 hr at 490° (substitution III). Changes of ^{18}O concentration in both gases during the treatment are shown in Figure 4, with time as the abscissa. ^{18}O concentration in carbon dioxide (circles) decreases rapidly, while that in oxygen (squares) did not change at 370° , as can be expected by the result of Figure 4 in the previous research.¹ However, a decrease of ^{18}O concentration was observed at 490° on oxygen also, while the isotopic composition of the gaseous oxygen ($^{16}\text{O}_2:^{16}\text{O}^{18}\text{O}:^{18}\text{O}_2$) did not change as below 490° .

The infrared spectra of the samples after the three substitution treatments are shown by curves B, C, and D, respectively, in Figure 5, where curve A is the spectrum without such treatment. The spectra B, C, and D did not change even after keeping the sample in air for several months.

Comparing these spectra, a new band appeared in the

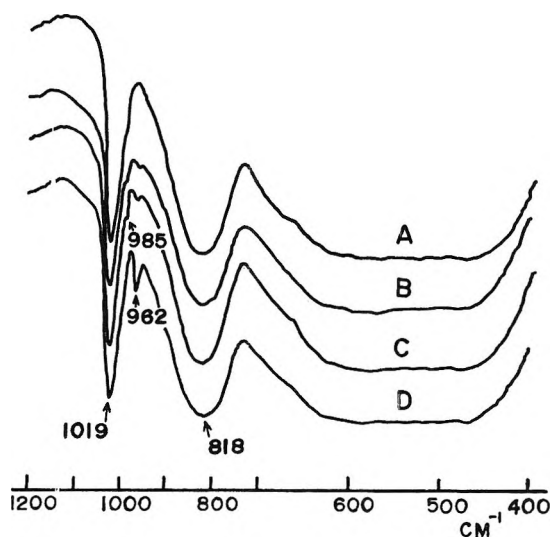


Figure 5. Change in the ir spectra by repetition of the ^{18}O substitution. A shows the spectrum without substitution, B the spectrum obtained after substitution I, C after substitution II, and D after substitution III.

treated samples at 962 cm^{-1} near the strong band at 1019 cm^{-1} . Its intensity becomes stronger with repetition of the treatment. Also, a weak shoulder band often appeared at ca. 985 cm^{-1} , as already reported.⁴

Eichhoff and Weigel⁵ and Miller and Cousins⁶ investigated both ir and Raman spectrum of VOCl_3 and assigned the strong sharp band observable at 1035 cm^{-1} to the V=O stretching vibration. Several authors^{7,8} report that a strong sharp band of this kind also appears near 1000 cm^{-1} on some vanadyl compounds. Since vanadium pentoxide crystal contains the vanadyl group in its structure, they ascribed the 1020-cm^{-1} band in vanadium pentoxide to the V=O stretching vibration. The same assignment is adopted for the 1019-cm^{-1} band in the present paper.

Then, under the assumption that the oxygen atom forms a bond with an atom of infinite mass, the isotopic band produced by ^{18}O substitution was calculated. The value thus calculated, 961 cm^{-1} , coincides well with the observed, 962 cm^{-1} . The above assumption is plausible due to the reason that the V=O groups project perpendicularly to the V-O-V net plane, considering the crystal structure of this oxide (Figure 6).⁹ Hence the stretching vibrational mode of the V=O

(4) M. Adachi, T. Imanaka, and S. Teranishi, *Nippon Kagaku Zasshi*, **89**, 446 (1968).

(5) H. I. Eichhoff and F. Weigel, *Z. Anorg. Allg. Chem.*, **275**, 267 (1954).

(6) R. A. Miller and L. R. Cousins, *J. Chem. Phys.*, **26**, 329 (1957).

(7) C. G. Barraclough, J. Lewis, and R. S. Nyholm, *J. Chem. Soc.*, 3552 (1959).

(8) L. D. Frederickson, Jr., and D. M. Hansen, *Anal. Chem.*, **35**, 818 (1963).

(9) A. Byström, K. A. Wilhelm, and O. Brotzen, *Acta Chem. Scand.*, **4**, 1119 (1950).

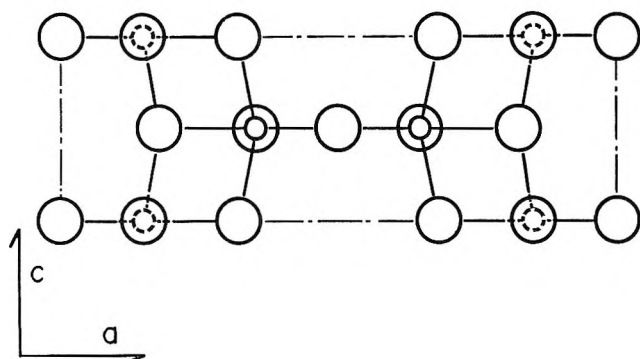
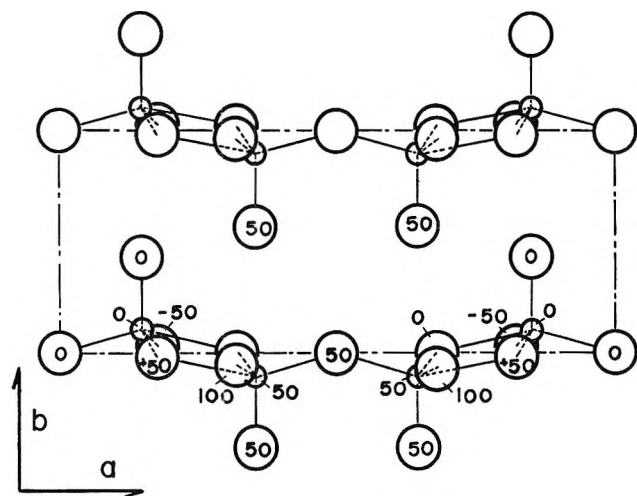


Figure 6 (a) Projection of the structure on the (001) plane of V_2O_5 : small circles denote V atoms; large circles O atoms. The figure denotes the height of the atoms in fractions of c . Superimposed oxygen atoms are symmetrically displaced. The cell dimensions: $a = 11.519$, $b = 4.373$, $c = 3.564$ Å. (b) Projection of the structure for the (010) plane of V_2O_5 .

groups can approximately be regarded as independent of the other vibrational modes, and the 1019- and 962- cm^{-1} bands can be conclusively assigned to the $V=^{16}\text{O}$ and $V=^{18}\text{O}$ stretching vibrations, respectively.

However, the assignment of the weak band at 985 cm^{-1} is difficult at the present stage of investigation.

Figure 4 shows that the ^{18}O -exchange reaction probably reaches equilibrium by both substitution treatments I and II at 370° but that further exchange occurred by elevating the reaction temperature to 490° in substitution III. The above findings seem to indicate that ^{18}O concentration is not homogenized so easily in vanadium pentoxide powders at the lower temperature; *i.e.*, the isotopic exchange of oxygen species in the inner bulk is a slow process.

As shown in Figures 4 and 5, in spite of the fact that the ^{18}O concentration in the gaseous reactant after the substitution III becomes lower than that after the substitutions I and II, the 962- cm^{-1} band of the former samples is much more intense than that of the latter sample. This result suggests that the oxygen in the $V=O$ groups becomes much more mobile with rising

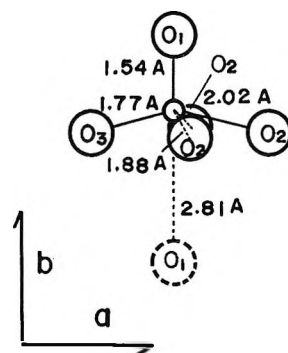


Figure 7. The coordination around one vanadium atom. Solid lines correspond to the five strong V-O bonds, and the dotted line shows the sixth, much weaker bond; bond lengths are in angstroms.

temperature. Such peculiar behavior of oxygen in the catalyst will be reported in more detail (experiment F).

Experiment E-2. Identification of the Stretching Band Assignable to the V-O-V Groups. In Figure 5, there appear two broad bands at shorter wavelengths (*ca.* 800 and 500-600 cm^{-1}). However, an isotopic shift of the band could not be confirmed in all the curves, presumably because the band is a composite one and becomes too broad. This may be plausible, considering that there are three kinds of V-O distances in the net plane—1.77, 1.88, and 2.02 Å—as Figure 7 shows,⁹ where the O_1 atom belongs to the $V=O$ group and O_2 and O_3 belong to the V-O-V groups. The small circle denotes the vanadium atom.

Siebert¹⁰ measured Raman spectrum of the tetrahedral VO_4^{3-} ion in aqueous solution and assigned the bands at 870 and 825 cm^{-1} to be of the symmetric and asymmetric stretching modes, respectively. Barraclough, Lewis, and Nyholm⁷ compared ir spectra of various tetrahedral anions (CrO_4^{2-} , MoO_4^{2-} , MnO_4^- , and VO_4^{3-}) with one another and indicated that the mode of their metal-oxygen stretching vibration is not simple, but is triply degenerate, so that a slight distortion from tetrahedral symmetry can lead to a broad band actually observable in the 800-900- cm^{-1} region. Now, vanadium pentoxide can be regarded as polymeric, and its structure may be viewed as a distorted VO_5 trigonal-bipyramide sharing four corners, according to the X-ray data^{9,11} (*cf.* Figure 6). They considered, therefore, that the broad band at 825 cm^{-1} represents the stretching vibration of the V-O-V group in the lattice layer, corresponding to the (010) plane.

To estimate the nature of the 818- cm^{-1} band in Figure 5, the band produced by its isotopic shift was investigated by the compensation method. Compensated spectra (III) of ^{18}O -enriched samples by substitution are shown with dotted curves in Figure 8.

(10) H. Siebert, *Z. Anorg. Allg. Chem.*, **275**, 225 (1954).

(11) H. G. Bachmann, F. R. Ahmed, and W. H. Barnes, *Z. Kristallogr.*, **115**, 110 (1961).

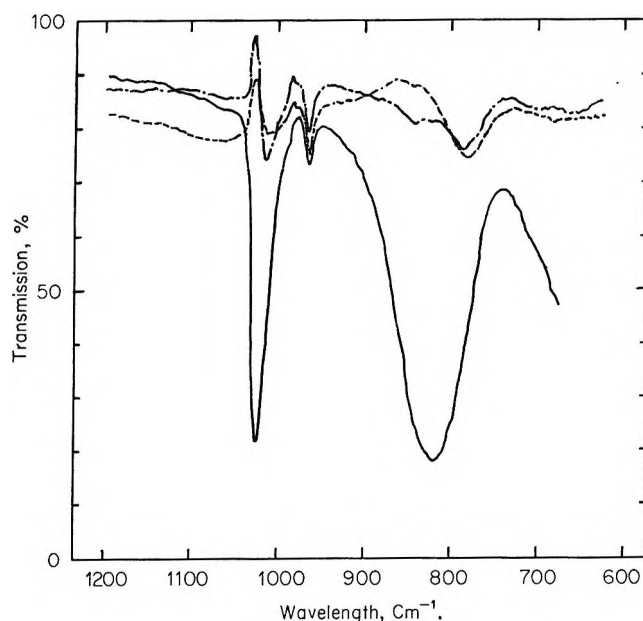


Figure 8. Ir spectrum of the ^{18}O -substituted vanadium pentoxide powders and their compensated spectra. The solid curve shows the ir spectrum of the ^{18}O -substituted powders, and the dotted curves then compensated spectra.

The attempt was successful to some extent, because a new band always appeared at *ca.* 780 cm^{-1} . However, since the position of the appearing band was different and the base line and the form of the compensated spectra changed from experiment to experiment, it became difficult to carry out the quantitative analysis on the band.

Under the assumption that the reduced mass of this unknown group giving the band is approximately equal to that of a V–O–V bond, the isotopic shift due to ^{18}O substitution for ^{16}O was again calculated, and 47 cm^{-1} was obtained. If this is correct, the corresponding band should be observed at 771 cm^{-1} in the ^{18}O -substituted substance. Experimentally, the mean maximal position of the compensated band in both spectra shown by dotted curves in Figure 8 is *ca.* 780 cm^{-1} . Thus, the calculated value is larger by 12% (9 cm^{-1}) than the observed value. This somewhat large discrepancy indicates that the oxygen giving the 818-cm^{-1} band cannot be regarded as a simple V–O–V bonding state, and this bonding state is different in nature from that of the band at 1019 cm^{-1} . Therefore, the band near the 818-cm^{-1} band may be ascribed to the V–O–V stretching vibrational mode. Such failure in quantitative explanation of this band seems to be due to the situation that contrary to the stretching vibration of the V=O group, the stretching vibration of each V–O group depends in a complicated way on many other vibrations in the V–O–V plane.

Experiment F. Distribution of ^{18}O among the Various Lattice Oxygens in Vanadium Pentoxide during the Exchange Reaction. 1. Degree of ^{18}O Distribution in the V=O Group. The isotopic exchange reaction between

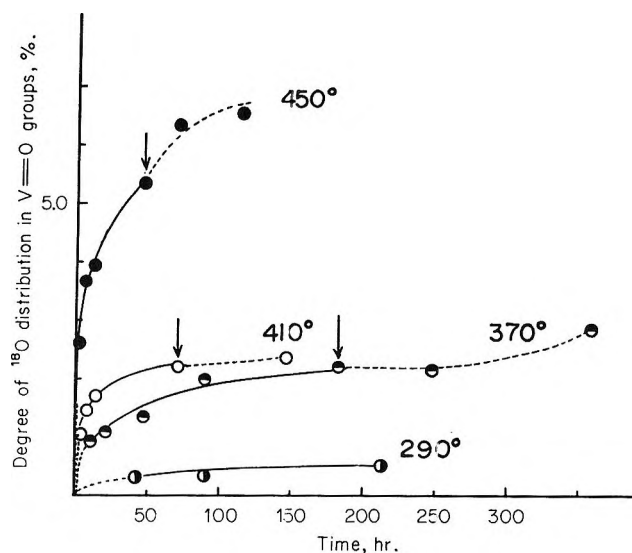


Figure 9. Temperature effect of the degree of ^{18}O distribution in the V=O group.

carbon dioxide and vanadium pentoxide was carried out at 290 , 370 , 410 , and 450° the pressures of carbon dioxide being 18.8 , 18.4 , 17.1 , and 21.0 mm , respectively. The course of the reaction at the four temperatures can be shown by the ^{18}O concentration in carbon dioxide *vs.* reaction time, necessary data being given in Table I.

Due to experiment E-1, the linearity of the calibration curve of the 1019-cm^{-1} band was confirmed, so that the absorbance of the 1019-cm^{-1} band in the uncompensated sample ($\log(I_0/I)_{1019}$) and that of the 962-cm^{-1} band in the compensated ($\log(I_0/I)_{962}$) can be regarded as proportional, respectively, to the amount of the V= ^{18}O and V= ^{16}O groups existing in the sample. Therefore, under the plausible assumption that an isotope effect does not exist in the extinction coefficient of both bands, the percentage of V= ^{18}O groups V= $^{18}\text{O}\%$, in Table I can be calculated by eq 1

$$\begin{aligned} \text{V}=\text{}^{18}\text{O}\% &= \frac{(\text{V}=\text{}^{18}\text{O})}{(\text{V}=\text{}^{16}\text{O}) + (\text{V}=\text{}^{18}\text{O})} \times 100 \\ &= \frac{\log(I_0/I)_{962}}{\log(I_0/I)_{1019} + \log(I_0/I)_{962}} \times 100 \end{aligned} \quad (1)$$

Hereafter, the degree of ^{18}O distribution in the V=O group will be estimated by V= $^{18}\text{O}\%$. In Figure 9, these values are plotted *vs.* reaction time at the four temperatures. The data indicated by arrows, lying on the dotted lines, were obtained by heat treatment of the samples in a vacuum at the same temperature. The result shows that the higher the temperature, the larger the V= $^{18}\text{O}\%$, and that the value increases by heating the samples in a vacuum after the exchange reaction, due to migration of ^{18}O from other combined states.

2. Degree of ^{18}O Distribution in the V–O–V Groups. As mentioned in experiment E-II, direct estimation of

Table I: Distribution of ^{18}O in Vanadium Pentoxide during the Exchange Reaction

Expt	Time, hr	$^{18}\text{O}_g$, %	$^{18}\text{O}_L$, 10^{18} atoms	$\text{V}=\text{}^{18}\text{O}$		$\text{V}-^{18}\text{O}-\text{V}$	
				%	10^{18} atoms	%	10^{18} atoms
F-a (450°)	0	39.9					
	2	32.5	11.7	2.6	5.8	1.8	5.9
	6	27.1	19.6	3.7	7.7	3.7	11.9
	12	21.2	28.0	3.9	7.9	6.6	20.1
	46	13.5	35.5	5.4	9.6	9.5	25.9
	24	...	35.5	6.3	11.4	8.8	24.2
	68	...	35.5	6.5	11.8	8.7	23.8
F-b (410°)	0	34.2					
	4	30.4	4.9	1.0	2.2	0.8	2.7
	8	27.1	8.9	1.5	3.0	1.9	5.9
	14	23.5	13.1	1.7	3.4	3.2	9.7
	71	12.8	23.5	2.2	3.9	7.3	19.6
	75	...	23.5	2.4	4.2	7.2	19.3
F-c (370°)	0	40.9					
	10.5	35.0	8.1	0.9	2.0	1.9	6.1
	21	30.6	13.8	1.1	2.2	3.7	11.6
	47	27.0	18.2	1.3	2.7	5.2	15.5
	89	24.0	21.3	2.0	3.7	6.2	17.6
	183	17.7	27.3	2.2	3.9	8.7	23.4
	65	...	27.3	2.1	3.8	8.7	23.5
	175	...	27.3	2.8	5.1	8.3	22.3
F-d (290°)	0	36.6					
	42	30.0	9.3	0.3	0.7	2.6	8.6
	90	24.0	17.4	0.3	0.7	5.3	16.7
	213	22.9	18.1	0.5	1.0	5.7	17.1

^a Data below the dotted lines at each temperature were obtained by keeping the catalyst in a vacuum after the measurement just above the dotted lines.

^{18}O concentration in the V-O-V groups was difficult. However, the ^{18}O concentration in the groups can be determined indirectly from the material balance of ^{18}O atoms disappearing from the gaseous phase and of ^{18}O atoms going into the V=O groups in the oxide lattice. They are given in the fourth and sixth columns in Table I, where O_L denotes the total oxygen species in the oxide.

Oxygen in crystalline vanadium pentoxide may be classified roughly into two kinds: oxygen in the V=O group and that in the net plane of the V-O-V groups, even though at least two types of V-O bond exist in the V-O-V net plane^{9,11} (cf. Figures 6 and 7). Therefore, it can be considered that ^{18}O atoms which disappear from the gaseous phase during the exchange reaction migrate into the oxide lattice and distribute themselves between oxygen species in the V=O groups and those in the V-O-V net planes (V-O-V groups).

From this, the amounts of V- ^{18}O -V are calculated by eq 2, using the data in Table I

$$(\text{V}-^{18}\text{O}-\text{V}) = (^{18}\text{O}_L) - (\text{V}=\text{}^{18}\text{O}) \quad (2)$$

The percentage of V- ^{18}O -V groups, V- ^{18}O -V %, which

will be called the degree of ^{18}O distribution in this group hereafter, is given by eq 3

$$\text{V}-^{18}\text{O}-\text{V} \% = (\text{V}-^{18}\text{O}-\text{V})/(\text{V}-\text{O}-\text{V})_{\text{total}} \times 100 \quad (3)$$

Thus calculated values are given in the last two columns in Table I.

To show clearly the change of the V- ^{18}O -V % during the course of the exchange at each temperature, Figure 10 was prepared, where V- ^{18}O -V % is plotted against the total $^{18}\text{O}_L$ atoms. Equilibrium ^{18}O concentration of the isotopic exchange reaction and mean ^{18}O concentration in the oxide are described by horizontal lines at the top of the figure and a straight line drawn from the origin, respectively. Conversions in the exchange reactions can be calculated by the ratios of the two concentrations in Figure 10, and the conversions thus obtained in the first and the last measurements at each temperature are as follows: 24 and 81% at 450°; 14 and 72% at 410°; 19 and 66% at 370°; 24 and 48% at 290°. The values indicate that the data obtained in the present experiment give information about the inner bulk, rather than the surface layer of the oxide.

Now, by comparing each curve in Figure 10 with the

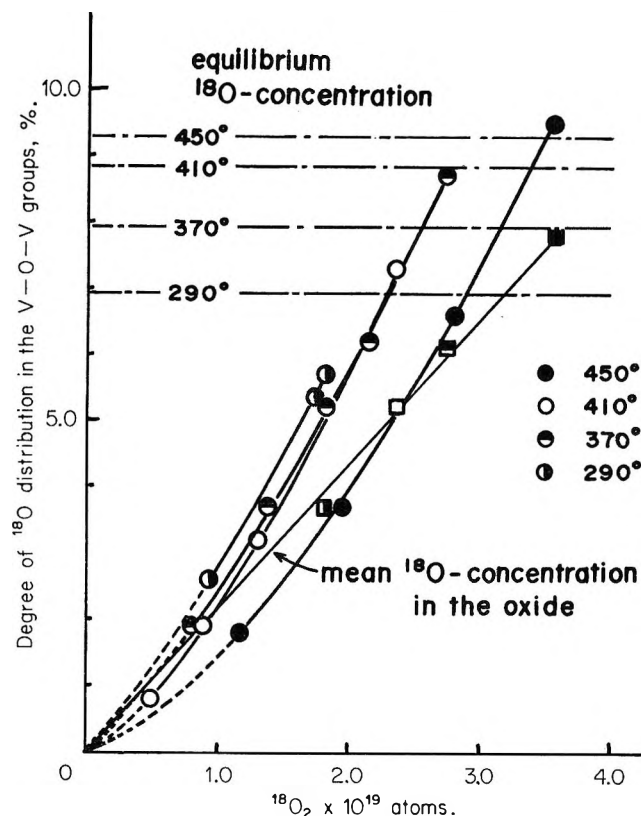


Figure 10. Temperature effect of the degree of ^{18}O distribution in the V-O-V groups.

curve of the mean ^{18}O concentration in the oxide, it is understood that the V-O-V % is larger than the $\text{V}=\text{}^{18}\text{O}$ %, except for the initial stage at higher temperature, because nearly all the curves fall above the straight line of mean ^{18}O concentration. Moreover, the lower the temperature, the larger the degree of ^{18}O distribution in the V-O-V groups, if the total amount of the ^{18}O atoms going into the catalyst is made equal. The result indicates a difference in behavior of oxygen between the $\text{V}=\text{O}$ and V-O-V groups.

Discussion

Considering the nature of exchange reactions, it will be assumed in the present discussion that the crystal structure of vanadium pentoxide is invariant during the reaction. Of course, various lattice imperfections always exist, and they can change to some extent by chemical or thermal treatment, as esr signals of the oxide indicate.¹²

To demonstrate how the ^{18}O distribution between the $\text{V}=\text{O}$ and V-O-V groups changes during the exchange reaction, Figures 11 and 12 were drawn up, in which ratios of the $\text{V}=\text{}^{18}\text{O}$ % to the $\text{V}-\text{}^{18}\text{O}-\text{V}$ % are plotted against time and the total amount of $^{18}\text{O}_L$, respectively. The ratios were calculated by using the values in Table I. Based on both figures, the behavior of the oxygen species in the oxide during the exchange reaction can be discussed.

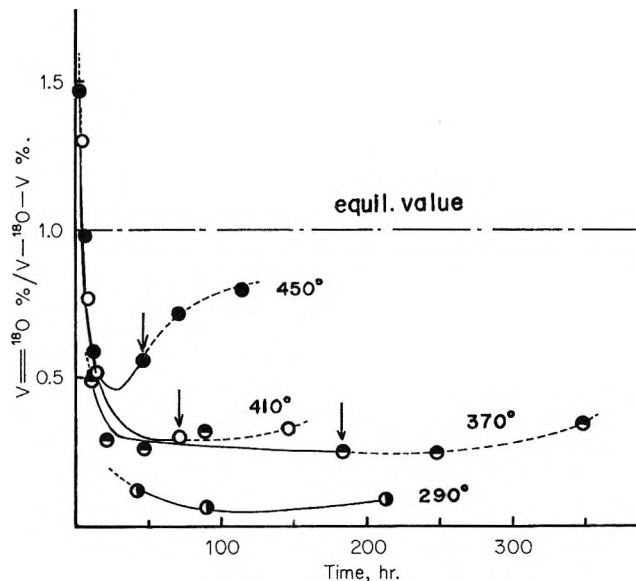
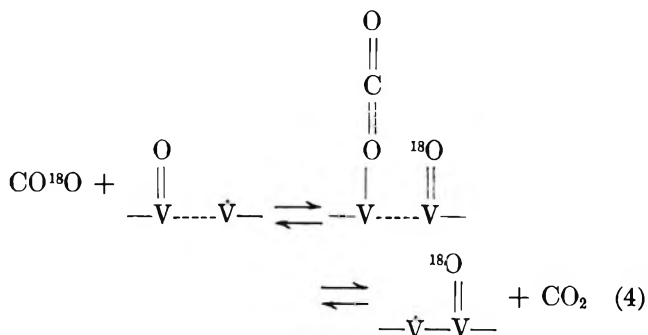


Figure 11. Changes in the ^{18}O distribution between the $\text{V}=\text{O}$ and V-O-V groups with reaction time.

1. *Behavior of Oxygen Species on the Surface.* In the previous paper,¹ the isotopic exchange of carbon dioxide with gaseous oxygen proceeds rapidly by eq 4



At the same time, migration of ^{18}O into the oxide bulk was pointed out as a slower process. The former rapid process can be estimated by Figure 11 in which the ratios decrease markedly with time in the initial stage at each temperature, except the run at 290° , because if the initial ratio is estimated by extrapolating it to $t = 0$, very large values are obtained, especially at 410° and 450° .

However, it is noteworthy that the curves show a tendency to decrease from initial values above unity immediately to the values below 0.5, especially in the runs at 410° and 450° . In the first experimental points of each temperature, conversions of the exchange were about 15–25%, as indicated by the result of expt F-2. They are too large by about a factor of 10^2 if only the $\text{V}=\text{O}$ group in the surface (010) plane relates to the reaction under the assumption that the oxide is com-

(12) K. Tarama, S. Teranishi, S. Yoshida, and H. Yoshida, *Bull. Chem. Soc. Jap.*, **34**, 1195 (1961); K. Hirota and K. Kuwata, *ibid.*, **36**, 229 (1963); E. Gillis and E. Boesman, *Phys. Status Solids*, **14**, 337 (1966).

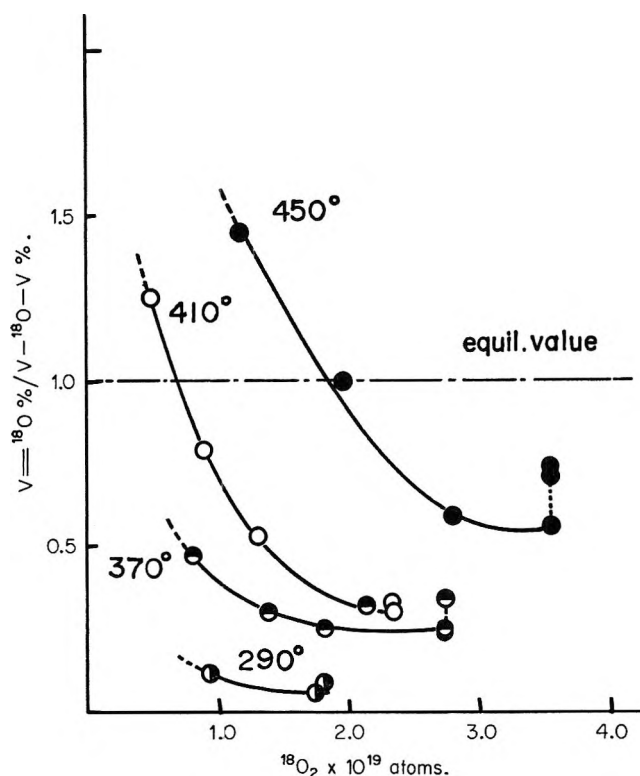


Figure 12. Changes in the ^{18}O distribution between the $\text{V}=\text{O}$ and $\text{V}-\text{O}-\text{V}$ groups plotted against the total amount of $^{18}\text{O}_L$ going into the oxide.

posed of cubic particles (see Appendix). This indicates that they contain already information from the inner bulk to some extent.

2. *Behavior of Oxygen Species in the Oxide.* According to Figure 12, the ratios of $\text{V}=\text{O}$ to $\text{V}-\text{O}-\text{V}$ % change with the total amount of $^{18}\text{O}_L$, and the curves have a minimum, whose value remarkably depends on the reaction temperature. Moreover, the higher the temperature, the more the minimal region of the curves shifts toward the larger value of $^{18}\text{O}_L$.

Since the isotope effect might be so small that the equilibrium ratio is approximately unity, the findings obtained from Figure 12 can be explained by the difference in the temperature effects on the exchangeability of oxygen in the $\text{V}=\text{O}$ and $\text{V}-\text{O}-\text{V}$ groups. Specifically the activation energy for the exchange of the $\text{V}-\text{O}-\text{V}$ groups is somewhat smaller than for the $\text{V}=\text{O}$ groups in the bulk. Additional support to the above conclusion seems to be given by the increase of the dotted lines after the heat treatment in Figure 9, because this tendency indicates that the equilibration of ^{18}O occurred from the $\text{V}-\text{O}-\text{V}$ groups to the $\text{V}=\text{O}$ group.

In the exchange of oxygen species in the oxide bulk with those on the surface layer, three kinds of processes need to be considered: (I) exchange in the $\text{V}-\text{O}-\text{V}$ net plane itself; (II) exchange parallel to the $\text{V}-\text{O}-\text{V}$ net planes *via* $\text{V}=\text{O}$ groups; (III) exchange perpendicular to the net plane. Process I involves only the $\text{V}-\text{O}-\text{V}$ groups, while process II involves only $\text{V}=\text{O}$ groups.

On the other hand, in process III oxygens of both the $\text{V}=\text{O}$ and $\text{V}-\text{O}-\text{V}$ groups, participate so that process III has to include two steps: the exchange of oxygens in the $\text{V}=\text{O}$ groups with each other and the repeated exchange of the oxygens in the $\text{V}=\text{O}$ groups with those in the $\text{V}-\text{O}-\text{V}$ groups. Therefore, the conclusion reached in the last paragraph on the inner exchange points to a smaller activation energy for process I.

From the structural standpoint, Gillis indicated that the diffusion of oxygen in the directions [001] and [010] may be more favorable, because there are channels which are large enough for an oxygen atom to go through in the V_2O_5 crystal, in both directions.¹³ Based on this fact, he proposed a mechanism of phase transition between V_2O_5 and V_6O_{13} in which only oxygens in the $\text{V}=\text{O}$ groups take part. However, Gillis' proposition on the behavior of oxygen in the oxide is not supported by the present conclusion, because it can be regarded as the faster diffusion of oxygens in the $\text{V}=\text{O}$ groups in the directions [001] and [010], corresponding to processes II and III, respectively.

3. *Oxygen Exchange between the $\text{V}=\text{O}$ and the $\text{V}-\text{O}-\text{V}$ Groups.* Process III can be realized by repeated oxygen exchange between the $\text{V}=\text{O}$ and the $\text{V}-\text{O}-\text{V}$ groups, though not so quickly as process I. This possibility was already pointed out by the increase of the dotted line curves in Figure 9. The possibility of some sort of process III in the reaction scheme must therefore be admitted. Of course, if this process is considered to be faster than process I, the experimental line shown in Figure 11 cannot be explained, because otherwise the ratios ($\text{V}=\text{O} \text{ } ^{18}\text{O} \text{ } \%/ \text{V}-\text{O}-\text{V} \text{ } \%$) must decrease asymptotically to unity from the initial value. Nevertheless, this exchange reaction has to be regarded as important in catalysis, as will be explained.

From the structural standpoint (*cf.* Figure 6), it seems plausible that not only are the oxygen species in the $\text{V}=\text{O}$ group on the (010) surface easily exchangeable, but also all the oxygen species in the $\text{V}-\text{O}-\text{V}$ groups on the (100) and (001) surface. Ketelaar found that the cleavage along the (010) plane was perfect, and that cleavage along (100) could also occur, but only with difficulty along the (001) plane.¹⁴ On the basis of the Ketelaar's finding, the oxygen in the $\text{V}=\text{O}$ group may be different in nature from that in the $\text{V}-\text{O}-\text{V}$ groups on the (010) surface, but both groups may be the same in nature on the (001) and (100) surfaces, because the cleavage plane of the crystal may not be smooth in both (100) and (001) planes. However, with an electron microscope, Gillis and Renault clearly observed the gradual growth of some dislocations even on the (010) surface of a single vanadium pentoxide crystal under evacuation.¹⁵

(13) E. Gillis, *Compt. Rend.*, **258**, 4765 (1964).

(14) J. A. A. Ketelaar, *Nature*, **137**, 316 (1936).

(15) E. Gillis and G. Renault, *Compt. Rend.*, **262B**, 1215 (1966).

On the basis of both structural investigations, it seems plausible that the oxygen in the V=O and V-O-V groups on the (010) surface are equivalent in their activity near the dislocations. That is, the oxygen near the dislocations can exchange between V=O and V-O-V groups easily on the (010) plane, as for the (100) and (001) surfaces. The (100) and (001) surfaces can be simply regarded as consisting of numerous dislocations.

4. *General Scheme of the Oxygen Exchange and Catalyst Activity.* From the above discussion, the isotopic exchange of gaseous oxygen with the oxide begins mainly at the V=O groups belonging to all the surface planes. The exchange in the V-O-V net plane, however, proceeds the fastest of all the exchange processes in the bulk, as the second stage of total reaction. It means that the exchange between the V=O groups and the V-O-V groups is comparatively slow, but such an exchange process may not be neglected in the catalytic oxidation.

Teranishi, *et al.*,⁴ studied the adsorption of formic acid on vanadium pentoxide by using the ir technique and proposed a dynamic model in which the V=O and V-O-V groups on the (010) plane were converted into each other by adsorption and desorption of the reactant. This scheme may be understood from the above explanation, based on the role of the dislocations.

The above conclusion is noteworthy in connection with the catalytic activity of vanadium pentoxide, because even though the V=O group projecting from the (010) surface has often been regarded as the active site, the active group probably exists near the dislocations. Besides, the oxygen species on the (100) and (001) surfaces may also have similar catalytic activity,

according to the discussion in the last paragraph of section 3. This proposition will be a subject of future investigation.

Acknowledgment. The authors wish to express their sincere thanks to Professor S. Teranishi and Dr. Shousuke Teratani for their valuable discussions.

Appendix

The Amounts of Oxygen Existing on the Surface of the Vanadium Oxide at the Initial Stage. Under the assumption that each particle of the vanadium oxide has a cubic form, the following two relations will exist among the length of an edge of the cube (x), the specific density (ρ), the surface area per gram (S), and the number of particles per gram (n)

$$n \cdot x^3 = \frac{1}{\rho}, 6 \cdot n \cdot x^2 = S \quad (\text{A1})$$

From eq A1

$$x = \frac{6}{\rho S} \quad (\text{A2})$$

Adopting 3.36 g/cm³ as ρ and 2.5×10^4 cm²/g as S , x of the oxide used is calculated to be about 7100 Å by eq A2. Therefore, using the value of 4.37 Å as the layer interval between two (010) planes (*cf.* Figure 6), each particle can be estimated to consist of about 1600 layers. This means that the order of magnitude of easily exchangeable oxygen species existing only in the surface layer is *ca.* 10^{-3} or 0.1% of the total oxygen in the particle. This value is much smaller than the 15-25% conversion noted earlier in this paper.

Rate Constants for Quenching of Biacetyl Triplets in Benzene

by R. B. Cundall, G. B. Evans,

Department of Chemistry, The University, Nottingham, England

and E. J. Land

Petersen Laboratories, Christie Hospital and Holt Radium Institute, Manchester, England (Received April 17, 1969)

The quenching of the biacetyl triplet by a number of molecules including a stable triplet, free radicals, a paramagnetic complex, and some diamagnetic species has been studied. There is only a small variation in the rate constants for the efficient quenchers ($5.5\text{--}2.4 \times 10^9 M^{-1} \text{sec}^{-1}$). The role of spin statistical factors and complex formation in reducing the rate below diffusion control is discussed.

Excited triplet states may be deactivated by bimolecular processes which involve energy transfer or other mechanisms which are not yet clearly defined. It is usually stated that if the energy-transfer process is exothermic, the rate of transfer is diffusion controlled. Although this seems true for solvents of high viscosity, it may not apply to solutions of low viscosity ($\eta < 3$ cP).¹ The fact that most published rate constants for triplet quenching are about $5 \times 10^9 M^{-1} \text{sec}^{-1}$ whereas calculated diffusion rates are 3 to 5 times higher than this does not support this generalization in the less viscous solvents.² On the other hand, the experimental finding that all measured triplet quenching rate constants have almost the same value within the limits of experimental accuracy has been used to support unit efficiency for the deactivation process. Contrary evidence has been obtained by Hammond and coworkers,³ who show that some triplet deactivation processes are subject to steric hindrance and so cannot be truly diffusion limited. Reversal of energy transfer is possible if the excitation energies of the donor and acceptor triplets are similar as shown by Sandros.⁴ Recently Nordin and Strong⁵ have also indicated that if the energy difference ΔE is not too large, energy transfer efficiencies should differ from diffusion control to an extent which depends upon the actual lifetimes of the acceptor and donor triplet states.

We wish here to report some results obtained on the quenching of biacetyl phosphorescence by a number of species including free radicals and bis-galvinoxyl which exists in its ground state as a triplet.⁶ Pulse radiolysis has been used to populate the excited states of biacetyl, largely by energy transfer from the solvent benzene, and to follow the subsequent decay of the phosphorescing triplet. Quenching solutes were present in low concentration and direct excitation of quencher was avoided.

Experimental Section and Results

Pure crystallizable benzene (B.D.H.) was shaken several times with concentrated sulfuric acid, washed,

dried (with Na_2CO_3) and then fractionally crystallized three times. It was dried once more using P_2O_5 or silica gel and was fractionally distilled. All other materials were distilled or recrystallized samples.

The pulse radiolysis apparatus has been described by Keene.⁷ In these experiments the biacetyl phosphorescence was viewed under strictly comparable conditions for the different solutions. The solutions were reproducibly deoxygenated by bubbling with argon and all experiments were carried out at room temperature (25°).

The decay of the biacetyl triplet is a function of radiation dosage.⁸ Using $2 \mu\text{sec}$ pulses of 4-MeV electrons at doses below 1000 rads the lifetime of the biacetyl triplet was sufficiently long for its decay to be studied. It proved convenient to use pulses of 60 rads in the quenching experiments since under these conditions, interference from secondary processes, such as radiolytic product quenching, seemed negligible, or at least independent of dose. The excellence of the observed first-order decay behavior and low noise level inherent in emission measurements allowed the determination of precise first-order rate constants. There was no detectable formation of biacetyl triplets after the pulse. The observed spectrum for biacetyl phosphorescence⁹ agreed very closely with the long-lived biacetyl emission spectra published by Bäckström and Sandros⁹ and Dubois and Wilkinson.¹⁰ The form of the spectrum

(1) P. J. Wagner and I. Kochevar, *J. Amer. Chem. Soc.*, **90**, 2232 (1968).

(2) *e.g.*, J. T. Dubois and R. L. van Hamert, *J. Chem. Phys.*, **40**, 923 (1964).

(3) G. S. Hammond and R. P. Foss, *J. Phys. Chem.*, **68**, 3739 (1964); W. G. Herkstroeter, L. B. Jones, and G. S. Hammond, *J. Amer. Chem. Soc.*, **88**, 4777 (1966).

(4) K. Sandros, *Acta Chem. Scand.*, **18**, 2355 (1964).

(5) S. Nordin and R. L. Strong, *Chem. Phys. Lett.*, **2**, 429 (1968).

(6) E. A. Chandross, *J. Amer. Chem. Soc.*, **86**, 1263 (1964).

(7) J. P. Keene, *J. Sci. Instr.*, **41**, 493 (1964).

(8) R. B. Cundall, G. B. Evans, P. A. Griffiths, and J. P. Keene, *J. Phys. Chem.*, **72**, 3871 (1968).

(9) H. L. J. Bäckström and K. Sandros, *Acta Chem. Scand.*, **14**, 48 (1960).

was independent of biacetyl concentration although the intensity increased to a limiting value at about $3 \times 10^{-2} M$ biacetyl. In the experiments reported here the biacetyl concentration was fixed at $10^{-2} M$ and added quencher concentration varied between 5×10^{-7} and $10^{-4} M$.

The rate of decay of biacetyl phosphorescence was dependent on the purity of the solvent and in particular the amount of residual oxygen as well as the radiation dose. Most batches of benzene gave observed lifetimes ($1/e$ values) of about 230 μsec . This is a value less than that achieved under photochemical conditions,⁸ and may be due to excited state quenching by radicals. Repeated pulsing of a solution sometimes resulted in small increases of biacetyl triplet lifetime, presumably due to the consumption of small amounts of O_2 by radiolytic intermediates. This test was applied to all the observations.

The method for measuring the rate constant for quenching of the biacetyl phosphorescence was as follows. τ_0 , the lifetime of the biacetyl triplet state in the absence of quencher, and τ , the lifetime in the presence of the quencher at concentration $[Q]$, were measured from the oscilloscope traces. From plots

of τ^{-1} vs. $[Q]$, k_q the quenching rate constant could be determined from

$$1/\tau = 1/\tau_0 + k_q[Q]$$

The results are shown in Table I.

Discussion

The results for the various rate constants are consistent with many data in the literature. The highest quenching rate constants for DPPH and bis-galvinoxyl do not exceed other values which have been reported for this type of process. They are less than values expected if the most efficient quenching process in benzene was completely diffusion controlled. The modified Debye equation used by Osborne and Porter,¹¹ viz.

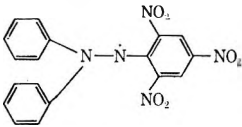
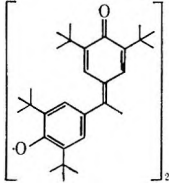
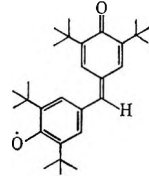
$$k_{diff} = \frac{8RT}{2000\eta}$$

gives a value of $1.55 \times 10^{10} M^{-1} \text{sec}^{-1}$ for benzene at 25° . It has been indicated that more complex expressions, which should presumably be more accurate, increase the predicted value.¹ Spectrofluorimetric studies which we have made give a value of $4.0 \times 10^{10} M^{-1} \text{sec}^{-1}$ for the quenching of the first excited singlet state of benzene by biacetyl. This supports the evidence of Dubois and van Hemert² that the Debye equation yields values close to those of experiment in singlet-quenching experiments, even when dipole-dipole transfer effects are expected to be negligible and allowance made for the possibility of energy migration through the liquid.

The value for *trans*-stilbene corresponds closely with $4.4 \times 10^9 M^{-1} \text{sec}^{-1}$ obtained by Bäckström and Sandros.⁹ Ferric acetylacetonate, which has five unpaired electrons, gives a value in satisfactory agreement with the results of Hammond¹² using a number of different sensitizers, and also Linschitz,¹³ using benzophenone. The k_q value for ferrocene is about three times smaller than the high value of $7.0 \times 10^9 M^{-1} \text{sec}^{-1}$ measured by Hammond for the quenching of the benzil triplet. However, the values obtained by Hammond and his coworkers¹² vary with the triplet being quenched and so there may be no other significance in the discrepancy.

There is no obvious correlation with the magnetic moment or number of unpaired electrons of the quenching molecule as first shown for the triplets of naphthalene and anthracene by Porter and Wright.¹⁴ The

Table I: Quenching Rate Constants (k_q) for Biacetyl Phosphorescence in Benzene-Biacetyl Solutions

Added quencher	$k_q, M^{-1} \text{sec}^{-1} \times 10^{-9}$
Diphenylpicrylhydrazyl (DPPH)	5.5 ± 0.5
	
bis-Galvinoxyl (g.s. triplet)	5.5 ± 1.0
	
<i>trans</i> -Stilbene	4.0 ± 0.2
Ferric Acetylacetonate	3.1 ± 0.5
Galvinoxyl (free radical)	2.9 ± 1.0
	
Azulene	2.4 ± 0.2
Ferrocene	2.4 ± 0.2
Cyclohexene	$(1.18 \pm 0.10)10^{-4}$
Biacetyl	$(5 \pm 1)10^{-5}$

(10) J. T. Dubois and F. Wilkinson, *J. Chem. Phys.*, **39**, 377 (1963).

(11) A. D. Osborne and G. Porter, *Proc. Roy. Soc. A*, **284**, 9 (1965).

(12) A. J. Fry, R. S. H. Liu, and G. S. Hammond, *J. Amer. Chem. Soc.*, **88**, 4781 (1966).

(13) J. A. Bell and H. Linschitz, *ibid.*, **85**, 528 (1963).

(14) G. Porter and M. R. Wright, *J. Chim. Phys.*, **55**, 705 (1958); *Discussions Faraday Soc.*, **27**, 18 (1959).

influence of electronic spin statistical factors is not clear and would depend on the nature of the collision complex. It is possible that the failure of the triplet quenching processes to have rate constants which are effectively diffusion controlled when other factors seem favorable may partly be due to this effect. Porter and Wright interpreted some of the variation in quenching efficiency in just this way. If the spin number of the quencher is $>1/2$ and unchanged in the deactivation process, then the efficiency should be reduced $1/3$. In addition, the probability of quenching should be further affected by variation in stability of the triplet-quencher complex. For the situation under discussion this second factor should have a value between 1 and $1/4$ which decreases with the extent of interaction in the quenching process. If formation of a well-defined complex as distinct from a very short lived encounter is essential to transfer then the effectiveness of an encounter may be reduced even further by steric and solvation effects, as seems to be the case for the first transition and lanthanide series of ions in aqueous solution.^{13 14}

Quenching of biacetyl triplet by bis-galvinoxyl is analogous to the mixed triplet-triplet interactions which lead to delayed (P-type) fluorescence studied by Parker.¹⁵ The overall efficiency of triplet quenching is not high, especially if long range dipole-dipole transfer is possible as has been suggested for this type of process in the polyacenes. Parker¹⁵ has shown that the efficiency of the triplet-triplet interaction varies between 0.56 and values which, in the case of two dyes, may be as low as 10^{-4} when compared with the diffusion rate calculated from the Debye equation. Spin statistical factors may operate here as indicated by Birks¹⁶ in a somewhat different context.

The results quoted are consistent with the view that some chemical complex formation involving steric

and probably other restrictions is involved in the bimolecular deactivation of the triplet state.³ In all the cases where the quenching is efficient electronic excitation-energy transfer could be a more significant mechanism than the catalyzed $T \rightarrow S$ intersystem crossing without electronic change in the quencher when both are possible. This has been demonstrated by Binet, Goldberg, and Forster¹⁷ for quenching of benzil phosphorescence by chromium complexes. It should be possible to study this type of process in detail by pulse radiolysis. In none of the investigated cases is reverse energy transfer expected to lead to an apparent decrease in efficiency of quenching since acceptor-donor energy differences are all likely to be greater than at least 5 kcal (ΔE for biacetyl-*trans*-stilbene).¹⁸ Also in the case of stilbene the lifetime of the triplet is probably too short in the *fluid* state for significant reverse transfer, as required by the scheme of Nordin and Strong.⁵

The quenching by cyclohexene is almost certainly a chemical effect as suggested by Bäckström and Sandros.⁹ The quenching by ground-state biacetyl is more marked than found by these authors ($460 M^{-1}$) and is probably due to a product formed by the reaction of a radiolytic intermediate with biacetyl.

These experiments, which we hope to extend, show how pulse radiolysis can be used with advantage to study the behavior of excited states when practical difficulties would make similar photochemical experiments difficult.

(15) *e.g.*, C. A. Parker, "Fast Reactions and Primary Processes in Chemical Kinetics," S. Claesson, Ed., Interscience Publishers, New York, N. Y., 1967, p 317.

(16) J. B. Birks, *Phys. Lett.*, **24A**, 479 (1967).

(17) D. J. Binet, E. L. Goldberg, and L. S. Forster, *J. Phys. Chem.*, **72**, 3017 (1968).

(18) W. G. Herkstroeter and G. S. Hammond, *J. Amer. Chem. Soc.* **90**, 4769 (1966).

Transport Processes in Hydrogen Bonding Solvents. III. The Conductance of Large Bolaform Ions in Water at 10 and 25°

by T. L. Broadwater¹ and D. Fennell Evans²

Department of Chemistry, Case Western Reserve University, Cleveland, Ohio 44106 (Received May 1, 1969)

Precise conductance measurements were carried out on $\text{Bu}_3\text{N}(\text{CH}_2)_8\text{NBu}_3\text{Br}_2$, $\text{Pr}_3\text{N}(\text{CH}_2)_6\text{NPr}_3\text{Br}_2$, $\text{Et}_3\text{N}(\text{CH}_2)_4\text{-NEt}_3\text{Br}_2$, $\text{MeN}(\text{CH}_2\text{CH}_2)_3\text{NMeBr}_2$, and $\text{MeN}(\text{CH}_2\text{CH}_2)_3\text{NMeI}_2$ in water at 10 and 25° and on $\text{Bu}_3\text{N}(\text{CH}_2)_8\text{-NBu}_3\text{Br}_2$ in methanol in 10 and 25°. From a comparison of the limiting ionic mobilities and concentration dependence of the tetraalkylammonium ions and these large bolaform ions, it is concluded that cation-cation pairing does not make a significant contribution to the concentration dependence of R_4N^+ ions in dilute aqueous solutions. In addition, when the concentration dependence for these salts in aqueous solution is compared to that observed in other hydrogen bonding solvents, many similarities are observed. It is likely that part of their peculiar behavior which has been attributed to the structural features of aqueous solution is a general property of hydrogen bonding solvents.

Introduction

Water structure effects have been shown to be an important factor in determining the magnitude of limiting ionic properties.³ However, the extent to which they are responsible for the anomalous concentration dependence in aqueous electrolyte solutions is not understood. In the case of the tetraalkylammonium salts, several explanations have been advanced based on ionic aggregation induced or enforced by water structure.³⁻⁹ It has been suggested that cation-cation pairing could be responsible for these effects and several recent papers have lent support to this argument.

Wen and Nara studied the volume change associated with mixing of solutions of R_4N halides and alkali metal halides.¹⁰ Analysis of the data using Friedman's ionic solution theory showed that when the R_4N ions were large, cation-cation interaction was found to predominate. Wen, Nara, and Wood calculated the volume change upon dimerization of Bu_4N^+ and found it to be -11 cc/mol .¹¹

Due to its labile nature, the isolation and direct study of a cation-cation pair is impossible. This difficulty can be circumvented, at least in part, by the study of appropriate model compounds. In a previous paper the preparation and partial molar volume measurements on $\text{Bu}_3\text{N}-(\text{CH}_2)_8\text{NBu}_3(\text{Br})_2$, a large bolaform electrolyte, were reported.¹² This compound can be likened to two tetraalkylammonium ions held in close proximity. The change of ϕ_2 with concentration for DiBuBr_2 was similar to that observed for Bu_4NBr , with ϕ_2 decreasing to a minimum $\phi_2(\text{min}) = \text{DiBu} \cdot 55\text{H}_2\text{O}$ and increasing with concentration. The ratio $\bar{V}_2^\circ(\text{DiBu}^{2+})/\bar{V}_2^\circ(\text{Bu}_2\text{N}^+)$ was found to be 1.91 and the volume change upon dimerization was estimated to be $-11.5 \text{ cm}^3/\text{mol}$. If the value of the partial molar volume for DiBuBr_2 is corrected by a factor of 2, then

the curve of ϕ_2 for the bolaform salt may be almost superimposed on that for Bu_4NBr .

In an effort to explore further the implications of cation-cation pairing in aqueous solutions of the tetraalkylammonium ions, we have studied the conductance of a number of bolaform ions of the general form $(\text{C}_n\text{H}_{2n+1})_3\text{N}^+(\text{C}_{2n}\text{H}_{4n})\text{N}^+(\text{C}_n\text{H}_{2n+1})_3$. These bolaform cations will be abbreviated as DiBu^{2+} , DiPr^{2+} , and DiEt^{2+} for the butyl, propyl, and ethyl derivatives, respectively. As suggested by Fuoss,¹³ DMD^{2+} will be used for the dimethyl derivative; it differs from the others in that two charged nitrogens are paired through three side chains.

Experimental Section

The dibromide salts of DiBu^{2+} (mp 123-125°),¹² DiPr^{2+} (mp 227-229°), and DiEt^{2+} (mp 268-269.5°) were made by refluxing an excess of trialkylamine with the appropriate alkyldibromide in methanol or ethanol. Recrystallizations were from methanol-ether mixtures. DMDBr_2 and DMDI_2 were made by reaction of 1,4-diazocyclo(2,2,2)octane in methanol with the

(1) For further details, cf. T. L. Broadwater, Ph.D. Thesis, Case Western Reserve University, Sept 1968.

(2) To whom all correspondence should be addressed.

(3) R. L. Kay and D. F. Evans, *J. Phys. Chem.*, **70**, 2325 (1966).

(4) S. Lindenbaum and G. E. Boyd, *ibid.*, **68**, 511 (1964).

(5) W. Y. Wen and S. Saito, *ibid.*, **68**, 2639 (1964).

(6) F. Franks and H. T. Smith, *ibid.*, **68**, 3581 (1964).

(7) F. Franks and H. T. Smith, *Trans. Faraday Soc.*, **63**, 2586 (1967).

(8) B. E. Conway, R. E. Verrall, and J. E. Desnoyers, *ibid.*, **62**, 2738 (1966).

(9) D. F. Evans and R. L. Kay, *J. Phys. Chem.*, **70**, 366 (1966).

(10) W. Y. Wen and K. Nara, **71**, 3907 (1967); **72**, 1137 (1968).

(11) W. Y. Wen, K. Nara, and R. H. Wood, *ibid.*, **72**, 3048 (1968).

(12) T. L. Broadwater and D. F. Evans, *ibid.*, **73**, 164 (1969).

(13) J. E. Lind, Jr., and R. M. Fuoss, *ibid.*, **66**, 1749 (1962).

Table I: Equivalent Conductances of the Diammonium Salts

10^4C	A	10^4C	A	10^4C	A	10^4C	A
$H_2O, 25^\circ$				$H_2O, 10^\circ$			
DMDBr ₂		DMDI ₂		DMDBr ₂		DiEthBr ₂	
$10^7\kappa = 1.49$	$A = 0.197$	$10^7\kappa = 1.95$	$A = 0.221$	$10^7\kappa = 0.67$	$A = 0.197$	$10^7\kappa = 1.16$	$A = 0.094$
		(Run I)					
2.436	149.59	5.457	145.43	0.853	108.67	0.675	83.95
4.418	147.82	10.339	142.51	2.074	106.98	1.357	83.25
7.585	145.67	15.755	140.04	3.528	105.92	2.277	82.53
10.831	143.95	20.797	138.13	5.337	104.87	4.368	81.41
15.650	141.31	25.264	136.65	7.643	103.77	6.485	80.51
22.708	139.29	28.998	135.52	10.918	102.52	9.240	79.56
31.469	136.76	33.171	134.35	15.564	101.09	14.565	78.07
		37.505	133.24	25.880	98.56	20.802	76.68
DiEthBr ₂		DiPrBr ₂		DiPrBr ₂			
$10^7\kappa = 1.84$	$A = 0.094$	$10^7\kappa = 1.82$	$A = 0.221$	$10^7\kappa = 1.06$	$A = 0.063$		
		(Run II)					
0.507	119.71	1.499	149.08	0.574	75.69		
1.426	118.26	2.740	147.66	1.407	74.85		
2.485	117.22	4.378	146.20	2.340	74.25		
4.320	115.84	6.047	144.97	3.997	73.45		
6.707	114.45	8.168	143.63	6.197	72.59		
9.751	113.01	11.943	141.64	8.919	71.70		
13.985	111.36	22.623	137.42	12.599	70.71		
20.029	109.45			17.565	69.60		
				23.385	68.50		
DiPrBr ₂		DiBuBr ₂		DiBuBr ₂		DiBuBr ₂	
$10^7\kappa = 1.16$	$A = 0.063$	$10^7\kappa = 2.00$	$A = 0.065$	$10^7\kappa = 1.36$	$A = 0.065$	$10^7\kappa = 0.73$	$A = 0.065$
		(Run I)		(Run I)		(Run I)	
0.668	107.78			0.506	72.37	1.108	71.81
1.298	106.90	1.177	102.28	1.296	71.57	1.810	71.32
2.218	105.95	3.687	100.22	2.507	70.83	3.231	70.54
3.667	104.83	6.729	98.60	4.874	69.79	5.337	69.68
5.745	103.65	11.067	96.89	7.650	68.86	8.175	68.75
9.050	102.13	16.036	95.35	10.866	67.98	11.858	67.77
13.115	100.63	21.186	94.02	14.213	67.20	16.753	66.70
18.247	99.06	27.014	92.70	18.941	66.25	22.085	65.72
24.421	97.47	31.964	91.72	24.141	65.35		
				29.563	64.52		
				35.226	63.75		
				41.066	63.01		
DiBuBr ₂				MeOH, 25°		MeOH, 10°	
$10^7\kappa = 2.29$	$A = 0.065$			DiBuBr ₂		DiBuBr ₂	
	(Run II)			$10^7\kappa = 0.79$	$A = 0.224$	$10^8\kappa = 0.98$	$A = 0.224$
0.721	102.79			0.181	102.98	0.366	81.50
1.784	101.45			0.372	100.87	0.751	79.35
3.348	100.22			0.570	99.29	1.161	77.68
5.042	99.27			0.788	97.87	1.586	76.23
7.407	98.13			0.999	96.69	2.084	74.77
9.790	97.17			1.279	95.33	2.684	73.28
13.280	95.97			1.675	93.64	3.408	71.76
17.392	94.77			2.076	92.17	3.992	70.67
23.161	93.33			2.938	89.53	4.833	69.28
28.739	92.12			3.815	87.31		
				4.994	84.85		
				6.327	82.54		
				7.895	80.26		
				10.018	77.70		
				13.347	74.53		

appropriate methyl halide. Both salts were purified by several recrystallizations from hot methanol. All of the salts were dried overnight in a vacuum oven at 60° and,

except for DMDI₂, were analyzed by Galbraith Laboratories, Knoxville, Tenn.

The preparation of the solvents, the electrical

Table II: Conductance Parameters for the Diammonium Salts

Salt	Solvent	T, °C	Λ_0	\bar{a}	σ	J
DMDBr ₂	H ₂ O	10	109.93 ± 0.16	1.23 ± 0.24	0.29	53.78
		25	154.05 ± 0.06	2.00 ± 0.06	0.09	75.83
DMDI ₂	H ₂ O	25	152.35 ± 0.05	1.87 ± 0.03	0.06	75.37
		25	152.54 ± 0.05	1.59 ± 0.08	0.09	75.56
DiEthBr ₂	H ₂ O	10	85.26 ± 0.04	1.52 ± 0.11	0.07	29.11
		25	121.31 ± 0.05	1.93 ± 0.11	0.09	43.09
DiPrBr ₂	H ₂ O	10	76.83 ± 0.02	1.84 ± 0.07	0.04	20.68
		25	109.58 ± 0.04	2.22 ± 0.08	0.08	31.36
DiBuBr ₂	H ₂ O	10	73.38 ± 0.02	2.09 ± 0.03	0.04	17.23
		10	73.46 ± 0.01	1.97 ± 0.04	0.02	17.31
		25	104.70 ± 0.02	2.50 ± 0.04	0.04	26.48
	MeOH	25	104.55 ± 0.04	2.38 ± 0.07	0.07	26.33
		10	85.20 ± 0.10	1.15 ± 0.17	0.11	39.70
		25	106.40 ± 0.20	0.43 ± 0.14	0.15	49.95

equipment, conductance cells, cup dropping device, and general techniques were as previously described.^{9,14}

Results

The measured equivalent conductances and corresponding molar concentrations are given in Table I. The specific conductance of the solvent and density constants, A , are also included in the table for each run. Density measurements were carried out on the most concentrated solution from each conductance run and the density was assumed to follow the relationship $d = d_0 + A\bar{m}$, where d_0 is the density of the solvent and \bar{m} the concentration in moles of salt per kilogram of solution. The A value obtained at 25° was also used to calculate density changes at 10°, a valid assumption for TAA salt solutions.⁹

The data were analyzed with the Fuoss–Onsager conductance theory¹⁵ for nonassociated electrolytes in the form

$$\Lambda = \Lambda_0 - SC^{1/2} + EC \ln C + JC \quad (\text{I})$$

The parameters Λ_0 and \bar{a} are recorded in Table II and were calculated with a computer program written by Kay.¹⁶ The program was modified to correct the terms α , β , κ , and b for the case of unsymmetrical electrolytes; these functions are defined elsewhere.^{1,16} The required values of the dielectric constant and viscosity of the solvents and the limiting conductance of the anions were taken from the literature,³ except $\lambda_0(\text{Br}^-) = 45.5$ in MeOH at 10°.¹⁷ Table II also contains σ , the standard deviation, and J . Because DiBuBr₂ appeared to be associated in methanol, only those points below $2 \times 10^{-4} M$ were analyzed.

Discussion

Comparison of Limiting Ionic Conductance. Values of $\lambda_0 + \eta$ at 10 and 25° are recorded in Table III for each salt, along with the value of

$$C_{10}^{25} = (\lambda_0\eta)_{25}/(\lambda_0\eta)_{10} \quad (\text{II})$$

The bolaform ions show the same temperature dependence as R_4N^+ ions, the larger ones being structure makers ($C_{10}^{25} > 1$) and the smallest, DMD,¹² being a structure breaker. DiEth²⁺ shows little if any temperature dependence, a behavior similar to that observed for Et₄N⁺ ion. The corresponding values for the R_4N^+ ions are 1.049, 1.033, 1.002, and 0.979 for the butyl through methyl derivatives.⁹

Table III: Mobility Ratios of 10 and 25°

Ion	T, °C	λ_0^+	C_{10}^{25}	M
DiBu	25	26.40		
	10	17.27	1.040	1.36
DiPr	25	31.36		
	10	20.68	1.034	1.36
DiEth	25	43.09		
	10	29.11	1.011	1.34
DMD	25	75.56		
	10	53.78	0.962	1.70

In order to compare the mobilities of the tetraalkylammonium ions and the corresponding dimers on a similar basis, the ratio, M , defined as

$$M = \frac{\lambda_0(\text{DiR}^{2+})}{\lambda_0(\text{R}_4\text{N}^+)} \quad (\text{III})$$

was calculated at 25°, and the values are given in Table III. Except for DMD²⁺, the mobilities of the bolaform ions are larger than those for the R_4N^+ ions by about 35%. This discrepancy can be largely accounted for by the difference in geometry of the bolaform ions as

(14) (a) D. F. Evans, C. Zawoyski, and R. L. Kay, *J. Phys. Chem.*, **69**, 3878 (1965); (b) J. L. Hawes and R. L. Kay, *ibid.*, **69**, 2420 (1965); (c) C. G. Swain and D. F. Evans, *J. Amer. Chem. Soc.*, **88**, 383 (1966).

(15) R. M. Fuoss and F. Accascina, "Electrolytic Conductance," Interscience Publishers, Inc., New York, N. Y., 1959.

(16) R. L. Kay, *J. Amer. Chem. Soc.*, **82**, 2099 (1960).

(17) R. L. Kay, private communication.

compared to the corresponding symmetrical R_4N^+ ions.

Using the formula of Perrin¹⁸

$$\mu = \frac{1}{6\pi N A}$$

where μ is the mobility and A is a geometrical coefficient, the mobility of the bolaform ions can be predicted. If the bolaform ions are considered to be rigid ellipsoids, then

$$A = (b^2 - a^2)^{1/2} / \ln \left(\frac{b}{a} + \left[\left(\frac{b}{a} \right)^2 - 1 \right]^{1/2} \right)$$

where a and b are the semiminor and semimajor axes, respectively. In the calculation, b was set equal to $2a$, where a is the radius of the tetraalkylammonium ion monomer unit.³ Using these relationships, the values of λ_0 can be calculated from $\lambda_0 = (0.65 \times 10^4) Z_i e \mu / 300$ and are found to be $\lambda_0^{e11}(\text{DiBu}^{2+}) = 28.4$, $\lambda_0^{e11}(\text{DiPi}^{2+}) = 31.0$, $\lambda_0^{e11}(\text{DiEth}^{2+}) = 35.0$ and $\lambda_0^{e11}(\text{DMD}^{2+}) = 40.4$ in H_2O at 25° . Comparison of the calculated values with those in Table II shows that for the larger ions the agreement is within 8%. There is serious disparity in the case of the smallest ion, DMD^{2+} which does not have the same geometrical relationship to its tetraalkylammonium analog. It should be noted that dimerization of the Bu_4N^+ ions in a Bu_4NBr solution at infinite dilution would result in an increase in the conductance since the *equivalent* conductance would change from 97.53 to 104.70.

Concentration Dependence. If cation-cation pairing is to explain the concentration dependence of these aqueous solutions then it must lead to a substantial decrease in the conductance with concentration. The extent to which this explanation is compatible with experimental observation can be seen from the following calculation.¹⁹ In this discussion, R_4N^+ will be denoted by the subscript 1, $(R_4N)_2^{2+}$ by 2 and x^- , the anion, by 3. At some finite concentration, the conductance of the solution can be expressed as $\kappa_{\text{soln}} = \kappa_1 + \kappa_2 + \kappa_3$, where κ_i is the specific conductance $\times 1000$. The equivalent conductance is obtained by dividing κ_{soln} by the concentration of electrolyte in equivalents per liter. The equivalent conductance for a solution of several species is defined by

$$\Lambda = \sum \lambda_i = \sum_i (\kappa_i / Z_i C_i) \quad (\text{IV})$$

where Z_i is the absolute magnitude of the valence and C_i the concentration of the species in moles per liter. If C is the concentration of salt in moles per liter and α the fraction of R_4N^+ ions dimerized to $(R_4N)_2^{2+}$ then $C_1 = (1 - \alpha)C$, $C_2 = (\alpha/2)C$ and $C_3 = C$, and

$$\Lambda_{\text{soln}} = (1 - \alpha)\lambda_1 + \alpha\lambda_2 + \lambda_3 \quad (\text{V})$$

In eq V, Λ_{soln} is the conductance which would be measured at some concentration C , if $(1 - \alpha)C$ parts of

R_4NX were mixed with $(\alpha/2)C$ parts of $(R_4N)_2X_2$, assuming that they are both strong electrolytes. Denoting the conductance of R_4NX , the monomer, by Λ_m and $(R_4N)_2X_2$, the dimer, by Λ_D , then

$$\Lambda_{\text{soln}} = (1 - \alpha)\Lambda_m + \alpha\Lambda_D \quad (\text{VI})$$

Now, $\Lambda_i = \Lambda_i^0 - S_i \Gamma^{1/2}$ where, if C is in moles per liter, $\Gamma = \sum C_i Z_i^2 = (1 - \alpha)C + 4(\alpha/2)C + C = (2 + \alpha)C$. These substitutions give

$$\Lambda_{\text{soln}} = (1 - \alpha)[\Lambda_m^0 - S_m(2 + \alpha)^{1/2}C^{1/2}] + \alpha[\Lambda_D^0 - S_D(2 + \alpha)^{1/2}C^{1/2}] \quad (\text{VII})$$

Λ_D^0 is larger than Λ_m^0 , but the Onsager term S_D is larger than S_m . If the formation of dimers is to explain the observed concentration dependence, then the dimer term on the right of eq VII must decrease more rapidly with concentration than the monomer term. It follows if this does occur, that there is a concentration C_E , at which the two terms on the right are equal to each other. Above this concentration, dimerization will result in a larger contribution to the conductance than that caused by the monomer alone, and below C_E , dimerization will result in a smaller conductance. At C_E

$$\Lambda_m^0 - S_m(2 + \alpha)^{1/2}C_E^{1/2} =$$

$$[\Lambda_D^0 - S_D(2 + \alpha)^{1/2}C_E^{1/2}] \frac{\alpha}{1 - \alpha} \quad (\text{VIII})$$

and solving for $C_E^{1/2}$ with $Q = \alpha/(1 - \alpha)$ and $P = (2 + \alpha)^{1/2}$ gives

$$C_E^{1/2} = (\Lambda_D^0 Q - \Lambda_m^0) / (S_D Q - S_m) P$$

For Bu_4NBr^9 and DiBuBr_2 , $\Lambda_m^0 = 97.5$, $S_m = 58.2$, $\Lambda_D^0 = 104.6$, and $S_D = 90.1$. Assigning α the value 0.1 gives $C = 1.5 M$. At $\alpha = 0.01$, $C = 1.41$ and as α approaches zero, C approaches $1.40 M$.

This result shows that in the concentration range 10^{-3} to $10^{-2} M$ in which the larger tetraalkylammonium salts were studied, the formation of cation-cation pairs will only lead to an increase in conductance instead of the decrease observed. This indicates that previous explanations based on cation-cation pairing should be reexamined. However, the magnitude of the deviations from expected behavior, even in dilute solutions and for many different types of measurements, imply that some type of ionic aggregation does take place.

Most of the discussion concerning the tetraalkylammonium solutions have focused attention on the role of the cation, and most of the explanations have emphasized the unique structural properties of water. However, the deviation from ideality in conductance measurements were shown to be independent of tempera-

(18) F. Perrin, *J. Phys. Radium*, **7**, 1 (1936).

(19) The cross terms necessary to describe exactly a tertiary salt solution have been ignored in this approximate calculation.

ture, whereas properties dependent upon structural effects have been found to change with temperature. Furthermore, the magnitude of the deviations from ideality as determined from a number of physical measurements^{4,9,20} is extremely sensitive to the nature of the anion, and any satisfactory explanation must account for this. It is this aspect of the problem that we wish to discuss in some detail.

Studies of other hydrogen bonding solvents, such as the alcohols²¹⁻²³ and amides,²⁴ suggest that some of the features which heretofore have been ascribed to the unique properties of aqueous solutions may in fact be more general properties of hydrogen bonded solvents. In solvents of lower dielectric constant, such as ethanol (ϵ 24.33),²² propanol (ϵ 20.45),²² and butanol (ϵ 17.45),²³ association constants for the tetraalkylammonium salts can be determined with some assurance, and it is found that for a given cation, K_A increases with increasing anionic size as can be seen in Table IV. As the di-

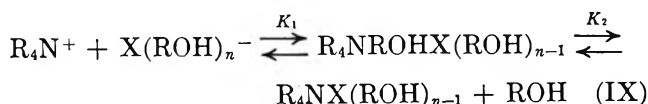
Table IV: Association Constants for the Tetraalkylammonium Salts in the Alcohols

Salt	MeOH ^a	EtOH ^b	PrOH ^b	BuOH ^c
Bu ₄ NCl	..	39	149	640
Bu ₄ NBr	3	75	266	860
Bu ₄ NI	16	123	415	1180
Bu ₄ NCIO ₄			770	2200

^a See ref 21. ^b See ref 22. ^c See ref 23.

electric constant increases, K_A decreases as expected. However, the dependence of K_A upon size remains opposite to that predicted by coulombic theory²⁵ and to that observed in solvents^{14a} where hydrogen bonding is not a predominant factor. For the larger anions, K_A is larger than can be accounted for by simple coulombic theory.

An explanation consistent with these facts is one based on a multiple-step association process involving desolvation of the anion in the second step.²³



Since neither of the ion pairs contributes to the conductance, the total association constant, K_A , is equal to

$$K_A = K_1(1 + K_2) \quad (\text{X})$$

The equilibrium constant for the first step, K_1 , can be calculated²⁶ from

$$K_1 = 2.524 \times 10^{-3} (a^3 e^{e^2/aekT}) \quad (\text{XI})$$

which gives K_1 values of 13, 25, 40, and 65 in methanol, ethanol, propanol, and butanol,²³ respectively. Values of $\log K_2$ appear to vary linearly with $1/\epsilon$.²⁷

As the dielectric constant becomes still larger ($\epsilon > 50$), reliable values of K_A can no longer be obtained. In this case, deviations from ideality can best be studied by using a rearranged form of eq I

$$\Lambda' = \Lambda - \Lambda_0 + S\sqrt{c} - Ec \log c = (J - F\Lambda_0)c \quad (\text{XII})$$

A plot of Λ' vs. c should give a straight line of slope $(J - F\Lambda_0)$ for nonassociated electrolytes. J is a function of the ion-size parameter, δ , which should increase with increasing ionic size; however, its magnitude cannot be calculated *a priori*. $F\Lambda_0$ corrects for the effect of the electrolyte on the viscosity of the solution. The corresponding equation for associated electrolytes is

$$\Lambda' = \Lambda - \Lambda_0 + S\sqrt{c\gamma} - Ec\gamma \log c\gamma = (J\gamma - F\Lambda_0\gamma - K_A\gamma f^2\Lambda)c \quad (\text{XIII})$$

However, when K_A is small and γ close to unity, $K_A\gamma f^2\Lambda$ becomes essentially linear in c and cannot be separated from J . Comparison of eq XII and XIII shows that when an associated electrolyte is analyzed by eq XII, the slope of the line in a Λ' plot will be smaller the larger the value of K_A .

In formamide, a hydrogen bonding solvent of high dielectric constant (ϵ 109), plots for the tetrabutylammonium and tetrapropylammonium halides give slopes which are smallest for the iodides and largest for the chlorides.²⁴ This is the same pattern observed when conductance data for methanol solutions are analyzed by eq XII; however, the deviations are greater than those with formamide and allow association constants to be explicitly evaluated.

The same type of Λ' plots were found for the tetraalkylammonium halides in aqueous solution,⁹ but the deviations from ideality did not increase at lower temperature in D₂O solution, a result that strongly indicates that water structural factors are not involved. It is reasonable to assume that cation-anion pairing of the type given in eq XI can quantitatively account for the concentration dependence of conductance in dilute solution.²⁷ As a consequence, at least part of the peculiar concentration dependence of the tetraalkylammonium salts in aqueous solution is not the result of water structure effects, but rather a general feature of hydrogen bonding solvents.

(20) R. H. Wood, H. L. Anderson, J. D. Beck, J. R. France, W. E. de Urg, and L. J. Soltzberg, *J. Phys. Chem.*, **71**, 2149 (1967).

(21) R. L. Kay, C. Zawoyski, and D. F. Evans, *ibid.*, **69**, 4208 (1965).

(22) D. F. Evans and P. Gardam, *ibid.*, **72**, 3281 (1968).

(23) D. F. Evans and P. Gardam, *ibid.*, **73**, 158 (1969).

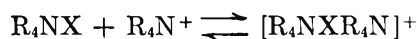
(24) D. F. Evans and J. Thomas, to be published.

(25) R. M. Fuoss, *J. Amer. Chem. Soc.*, **80**, 5059 (1958).

(26) G. G. Hammes and J. I. Steinfeld, *ibid.*, **84**, 4639 (1962).

(27) R. L. Kay, D. F. Evans and G. P. Cunningham, *J. Phys. Chem.*, **73**, 3322 (1969).

However, a number of measurements in more concentrated solutions including partial molar volumes,^{5,12} heats of mixing,²⁰ and volumes of mixing¹⁰ provide strong evidence for some kind of higher aggregation. Furthermore, the similarities in behavior in water and the alcohols do not extend to higher concentrations; in water \bar{V}_2 for Bu_4NEr decreases with concentration while in methanol¹⁷ and ethanol²⁸ it increases. We believe that an explanation that is applicable to the more concentrated solutions and which is compatible with the results for dilute solutions is one that involves a reaction of the ion pairs (either the solvent separated or contact ion pairs of eq IX) with another cation to give a triple ion.



Unlike the triplicates found in media of low dielectric constant where stabilization is entirely coulombic in nature,²⁹ part of the stabilization of this entity in aqueous solution must be attributed to a hydrophobic effect.

Acknowledgment. This work was supported by Contract No. 14-01-001-1281 with the Office of Saline Water, U. S. Department of the Interior.

(28) W. Y. Wen, in "1966 Saline Water Conversion Report," U. S. Department of the Interior, Washington, D. C., 1966, p 13.

(29) H. S. Young and C. A. Kraus, *J. Amer. Chem. Soc.*, **73**, 4752 (1951).

Cooperativity and Composition of the Linear Amylose-Iodine-Iodide Complex^{1a,b}

by Charles L. Cronan and Friedemann W. Schneider^{1c}

Department of Chemistry, University of Southern California, Los Angeles, California 90007
(Received August 13, 1968)

Adsorption isotherms of iodine-iodide in the helical cavity of amylose (D.P. = 800) have been determined by spectrophotometric measurements of titration curves at various iodide concentrations (10^{-6} to 2.5×10^{-2} M KI) and temperatures. A new description of the stoichiometry of the bound species is given in terms of two limiting models: At very low iodide concentrations the predominantly bound species is considered to be I_2 whereas at high iodide the bound species is I_3^- (the theoretical Ising lattice treatment predicts I_4^{2-}). Both models apply in the intermediate transition region where competition for binding sites occurs between I_2 and I_3^- . The over-all composition of the bound species can be expressed approximately as $\text{I}_2 \cdot b \text{I}_3^-$ where b varies between zero and unity. Statistical analysis of the isotherms using the exact one-dimensional Ising model ($n = 15$) with first nearest neighbor interactions (between -1.6 and -3.0 kcal/mol) shows that the degree of cooperativity is moderate. The main source of the stability of the complex originates from the intrinsic binding of a species by one turn of the amylose helix. The enthalpy and entropy of binding have been determined at 10^{-4} M KI. Factors affecting the position of λ_{max} of the blue band are attributed to the aggregation of partially or completely filled amylose helices.

Introduction

Although the blue amylose-iodine-iodide (AI) complex has been known for over 150 years, its detailed structure and composition are not yet completely understood. Basic to the understanding of its over-all stability is an insight into the role played by cooperative interactions between bound species which for many years have been suspected to be important.² In previous work a quantitative model treatment of cooperativity in the linear AI complex at 10^{-2} M KI and 20.0° has been given for the first time.³ Complex formation was treated as a one-dimensional adsorption process of iodine species into the helical cavity of amylose, and it was shown that cooperativity in the linear complex is surprisingly moderate, the over-all stability being due

mainly to the intrinsic binding of an iodine species to a helical turn of ca. eight anhydroglucose units. This work complements the previous equilibrium dialysis measurements and presents spectrophotometric titration studies which cast new light on the stoichiometry and thermodynamics of the complex. The degree of

(1) (a) Presented at the Pacific Conference on Chemistry and Spectroscopy, Anaheim, Calif., Oct 1967. (b) Abstracted in part from the M.S. Thesis of C. L. Cronan, University of Southern California, 1968. (c) To whom correspondence should be addressed.

(2) (a) For a general review of the complex, see H. Morawetz, "Macromolecules in Solution," Interscience, New York, N. Y., 1965; (b) R. L. Whistler and E. F. Paschall, Ed., "Starch: Chemistry and Technology," Vol. 1, Academic Press, New York, N. Y., 1965, Chapter 1; (c) J. Szejtli and S. Augustat, *Stärke*, **18**, 38 (1966).

(3) F. W. Schneider, C. L. Cronan, and S. K. Podder, *J. Phys. Chem.*, **72**, 4563 (1968).

cooperativity is determined over the widest possible range of KI concentrations. It is known from X-ray studies⁴ that the complex is helical in the solid state with the iodine species trapped inside the helical cavity of amylose. Flow dichroism⁵ studies lead to the conclusion that the helical configuration also prevails in solution. Evidence from viscosity,^{6-8a} osmotic pressure, optical rotation,^{7,8} oxidation,⁹ and mechanochemical¹⁰ degradation studies indicate that the helices are deformed resulting in short helical segments of 15 helical turns each for an amylose D.P. (degree of polymerization) ≈ 900 as used in this work. This model of a kinked helical structure in aqueous solution is further supported by Paulson's electric dichroism¹¹ studies which indicate that the hydrodynamic length of the complex is less than that expected for a rigid, rodlike helix.

No clear picture exists with regard to the stoichiometry of the complex. While potentiometric titration studies by Gilbert and Marriott¹² lead to a 2:3 ratio¹³ of bound I^- to I_2 at low percentage adsorption at 10^{-3} and 10^{-4} M KI, spectrophotometric studies by Kontos¹⁴ are used as evidence that the above ratio is 1:1 due to the fact that the intensity of the blue color is highest when the ratio of $I_{2\text{ total}}/I^-_{\text{total}}$ is unity. Kuge and Ono¹⁵ give a titration curve at 10^{-2} M KI at 15.0° and report an enthalpy of formation of -15.5 kcal/mol at 15.0° independent of chain length, a value which is comparable in magnitude with previously reported values between -11 and -20 kcal/mol.² Richter and Szejtli¹⁶ compare continuous photometric titration with amperometric titration and give an adsorption isotherm for which the amylose and presumably the KI concentration are not held constant. Bersohn and Isenberg¹⁷ have considered the iodine chain as a one-dimensional metal in which iodine atoms and ions are equivalent. On the other hand, Peticolas¹⁸ and Paulson found the conductivity of solid AI samples to be dependent on adsorbed water, a fact which was ascribed by Paulson¹¹ to an ionic conduction mechanism in the wet solid.

A theoretical model to explain the optical spectrum of the complex in the solid state has been postulated by Robin.¹⁹ It is based on the linear polytriiodide model which successfully describes the related triiodide-benzamide complex. In the latter complex the chromophoric group has been shown to be an infinite triiodide chain in which the individual triiodide ions are strongly coupled with each other, the excitation energy resonating between them. An optical spectrum is obtained which is quite similar to that of the AI complex. In earlier theoretical work, Murakami²⁰ assumed I_3^{2-} ions to be the basic units in the linear chain.

The foregoing discussion is not considered to be a review, but it is intended to show that the linear description of the blue complex and the assumption of ionic species occupying the voids of the segmented helix seem to be justified.

Experimental Section

Unbranched potato amylose was obtained from K & K Laboratories, Lot No. 59690X. Its approximate molecular weight is 150,000, corresponding to a D.P. between 800 and 1000. Potassium iodide and iodine were of commercially available reagent grade. Spectrophotometric measurements were made on a Beckman DK-2A recording spectrophotometer with constant-temperature attachment. Temperatures were held constant within 0.05° with a Forma-Temp Jr. constant-temperature bath.

Amylose Solutions. Solutions of slightly soluble amylose can be made according to various procedures: (a) solution in concentrated NaOH or KOH and subsequent neutralization with acid; (b) solution in DMSO; (c) solution in boiling water. Methods a and b produce solutions including unwanted ions and solvents, while method c was considered as possibly too drastic. In the present work saturated amylose solutions were prepared by constant stirring (24 hr) of a mixture of excess amylose in water at room temperature. Each mixture was allowed to settle, and the semiclear liquid was filtered through a $5\text{-}\mu$ millipore filter. The resulting stock solutions (ca. 0.50 mg/ml of amylose) were of extreme clarity, indispensable for spectrophotometric measurements. Aliquots of these solutions were analyzed for amylose by a standard enzymatic degradation method²¹ and used for titrations within 1 to 2 days.

Titration. A 100-ml solution of amylose-KI (4.5 mg of amylose/100 ml) was thermostated and titrated under constant stirring with a 0.0005 M I_2 solution containing identical concentrations of amylose and KI. Aliquots were withdrawn after each addition of titrant.

- (4) R. E. Rundle and F. C. Edwards, *J. Amer. Chem. Soc.*, **65**, 2200 (1943), and references therein.
- (5) R. E. Rundle and R. R. Baldwin, *ibid.*, **65**, 554 (1943).
- (6) J. Holló and J. Szejtli, *Stärke*, **10**, 49 (1958).
- (7) T. Kuge, *Bull. Univ. Osaka Prefect., Ser. B*, **11**, 121 (1961).
- (8) (a) T. Kuge and S. Ono, *Bull. Chem. Soc. Jap.*, **34**, 1264 (1961); (b) *ibid.*, **33**, 1269 (1960).
- (9) S. R. Erlander, H. L. Griffin, and F. R. Senti, *Stärke*, **17**, 151 (1965).
- (10) J. Szejtli, M. Richter, and S. Augustat, *Biopolymers*, **5**, 5 (1967), and references therein.
- (11) C. M. Paulson, Ph.D. Thesis, University of California at Berkeley, 1965.
- (12) G. A. Gilbert and J. V. R. Marriott, *Trans. Faraday Soc.*, **44**, 84 (1948).
- (13) See also D. L. Mould, *Biochem. J.*, **58**, 593 (1954).
- (14) E. Kontos, Ph.D. Thesis, Columbia University, New York, N. Y., 1959.
- (15) T. Kuge and S. Ono, *Bull. Chem. Soc. Jap.*, **33**, 1273 (1960).
- (16) M. Richter and J. Szejtli, *Stärke*, **18**, 95 (1966).
- (17) R. Bersohn and I. Isenberg, *J. Chem. Phys.*, **35**, 1640 (1961).
- (18) W. L. Peticolas, *Nature*, **197**, 898 (1963).
- (19) M. B. Robin, *J. Chem. Phys.*, **40**, 3369 (1964).
- (20) H. Murakami, *ibid.*, **22**, 367 (1954).
- (21) S. Meites and N. Bohman, *Amer. J. Med. Technol.*, **29**, 327 (1963).

Table I: Titration Data and Calculated Isotherm at $2.5 \times 10^{-2} M$ KI, 20.0°

OD ₆₄₀ m μ	OD ₃₅₃ m μ	[I ₂] _T $\times 10^6$	λ_{\max} , m μ	θ	[I ₂] _F $\times 10^6$	[I ₂] _F $\times 10^6$	$\epsilon_{353}^I \times 10^{-2}$
0.008	0.008	0.0497	...	0.006	0.0276	0.00128	3.39
0.022	0.017	0.0993	...	0.016	0.0403	0.00186	11.1
0.049	0.027	0.1938	602	0.037	0.0636	0.00294	8.02
0.076	0.036	0.2839	602	0.057	0.0827	0.00382	7.18
0.109	0.046	0.3715	602	0.081	0.0845	0.00390	8.37
0.138	0.055	0.4580	602	0.103	0.0952	0.00440	8.33
0.167	0.065	0.5374	602	0.125	0.0991	0.00458	8.96
0.193	0.075	0.6159	602	0.144	0.109	0.00506	9.19
0.233	0.086	0.7300	602	0.174	0.119	0.00550	9.01
0.272	0.098	0.8359	602	0.203	0.127	0.00572	9.25
0.331	0.116	1.003	602	0.247	0.137	0.00633	9.28
0.389	0.134	1.116	602	0.290	0.101	0.00465	10.6
0.448	0.154	1.327	602	0.334	0.156	0.00722	9.69
0.517	0.175	1.508	602	0.386	0.158	0.00730	9.93
0.578	0.193	1.672	602	0.431	0.163	0.00756	9.98
0.639	0.213	1.842	602	0.477	0.174	0.00803	10.1
0.699	0.229	1.994	602	0.522	0.171	0.00790	10.1
0.758	0.248	2.150	602	0.566	0.173	0.00800	10.3
0.836	0.276	2.348	602	0.624	0.169	0.00780	10.7

Table II: Titration Data and Calculated Isotherm at $1.0 \times 10^{-2} M$ KI, 20.0°

OD ₆₄₀ m μ	OD ₃₅₃ m μ	[I ₂] _T $\times 10^6$	λ_{\max} , m μ	θ	[I ₂] _F $\times 10^6$	[I ₂] _F $\times 10^6$	$\epsilon_{353}^I \times 10^{-11}$
0.067	0.037	0.2752	...	0.080	0.0886	0.0102	7.71
0.140	0.062	0.4981	...	0.105	0.116	0.0134	8.50
0.221	0.085	0.7337	607	0.166	0.136	0.0157	8.42
0.313	0.114	0.9913	607	0.236	0.150	0.0174	9.02
0.401	0.140	1.232	607	0.302	0.158	0.0183	9.31
0.535	0.180	1.607	607	0.402	0.179	0.0207	9.43
0.655	0.215	1.940	607	0.492	0.194	0.0224	9.51
0.811	0.259	2.368	607	0.610	0.210	0.0243	9.54
0.974	0.314	2.816	607	0.733	0.227	0.0263	9.91
1.081	0.347	3.137	607	0.813	0.262	0.0304	9.77
1.155	0.390	3.423	608	0.869	0.343	0.0398	9.85
1.215	0.449	3.735	610	0.914	0.482	0.0559	10.1
1.253	0.519	4.091	612	0.943	0.711	0.0824	10.0
1.285	0.614	4.532	615	0.966	1.03	0.120	10.1
1.303	0.713	4.986	617	0.980	1.39	0.162	10.0
...	0.812	5.395	...	1.00	2.11	0.246	10.4
1.334	0.922	5.871	619				
...	1.032	6.375	...				
1.360	1.162	6.939	619				
1.373	1.290	7.490	620				
1.386	1.505	8.368	621				
1.410	1.904	10.09	622				
1.621	...	50.03	648				

Spectrophotometric measurements were done in a 1-cm cell with water as the reference solution. The aliquot was then returned to the mixture to avoid any loss of material. Throughout the titration the amylose and KI concentrations were kept constant; no other ions were present. The pH was approximately 6 for all titrations. To ensure equilibration of the stirred solutions we allowed at least 15 min between each spectrophotometric measurement. There was no sign of any slow reaction in the *stirred* solutions. Further evidence of equilibration was shown by the fact that their

absorption spectra were identical before and after a heating cycle to $\sim 50^\circ$. All of our data refer to forward titrations, *i.e.*, to forward equilibrium paths at a constant over-all KI concentration. For this reason no hysteresis behavior was observed. Titrations were performed at 20.0° at the following KI concentrations: 2.5×10^{-2} , 10^{-2} , 5×10^{-3} , 10^{-3} , 10^{-4} , and $1.07 \times 10^{-5} M$ KI (Tables I-V, VII). Isotherms were measured at 13.0 , 20.0 , and 30.0° for $10^{-4} M$ KI (Tables VI-VIII). Tables I through VIII give the observed optical densities at 640 and 353 m μ , the total concentration of I₂

Table III: Titration Data and Calculated Isotherm at $5.0 \times 10^{-3} M$ KI, 20.0°

OD ₆₄₀ mμ	OD ₃₅₃ mμ	[I ₂] _T × 10 ⁶	λ _{max} , mμ	θ	[I ₃ ⁻] _F × 10 ⁶	[I ₂] _F × 10 ⁶	ε ₃₅₃ ^I × 10 ⁻³
0.055	0.033	0.2396	600	0.041	0.0786	0.0182	8.58
0.129	0.057	0.4720	605	0.096	0.111	0.0257	8.25
0.218	0.084	0.7168	606	0.162	0.122	0.0283	9.13
0.347	0.120	1.075	607	0.257	0.141	0.0326	9.19
0.486	0.159	1.451	608	0.360	0.153	0.0355	9.39
0.631	0.202	1.836	608	0.467	0.160	0.0371	9.75
0.777	0.242	2.219	609	0.575	0.163	0.0379	9.85
0.909	0.284	2.592	609	0.674	0.187	0.0435	9.93
1.078	0.335	3.052	609	0.799	0.205	0.0476	10.0
1.198	0.394	3.490	610	0.887	0.307	0.0715	10.1
1.248	0.431	3.715	610	0.924	0.384	0.0894	10.2
1.294	0.508	4.141	612	0.960	0.633	0.147	10.1
1.319	0.586	4.551	614	0.976	0.913	0.213	10.1
1.346	0.711	5.173	616	0.996	1.36	0.317	10.1
1.364	0.833	5.762	618				
1.377	0.958	6.344	618				
1.396	1.149	7.280	618				
1.410	1.382	8.456	618				
1.428	1.772	10.01	618				
1.628	...	50.02	633				

Table IV: Titration Data and Calculated Isotherm at $1.0 \times 10^{-3} M$ KI, 20.0°

OD ₆₄₀ mμ	OD ₃₅₃ mμ	[I ₂] _T × 10 ⁶	λ _{max} , mμ	θ	[I ₃ ⁻] _F × 10 ⁶	[I ₂] _F × 10 ⁶	ε ₃₅₃ ^I × 10 ⁻³
0.059	0.032	0.357	610	0.043	0.0936	0.108	4.69
0.098	0.043	0.494	610	0.072	0.110	0.127	5.43
0.177	0.065	0.728	610	0.130	0.122	0.141	7.05
0.262	0.088	0.979	610	0.193	0.134	0.156	7.62
0.343	0.112	1.223	613	0.252	0.148	0.172	8.07
0.426	0.135	1.455	616	0.314	0.154	0.180	8.41
0.510	0.158	1.689	616	0.375	0.160	0.187	8.62
0.672	0.203	2.138	616	0.492	0.170	0.199	8.94
0.836	0.250	2.605	618	0.615	0.186	0.219	9.13
0.908	0.272	2.828	618	0.668	0.201	0.237	9.16
0.985	0.293	3.058	618	0.725	0.214	0.252	9.12
1.040	0.314	3.268	619	0.765	0.244	0.288	9.12
1.157	0.364	3.709	619	0.850	0.304	0.360	9.32
1.205	0.384	2.918	619	0.886	0.342	0.405	9.26
1.236	0.404	4.134	619	0.908	0.403	0.478	9.15
1.264	0.423	4.339	619	0.930	0.463	0.550	9.04
1.302	0.470	7.747	619	0.957	0.603	0.718	9.07
1.326	0.510	5.153	619	0.974	0.758	0.905	8.87
1.343	0.550	5.551	619	0.989	0.919	1.10	8.69
1.356	0.609	6.135	619	0.996	1.17	1.40	8.42
1.376	0.692	6.898	619				
1.386	0.770	7.621	619				
1.398	0.849	8.327	619				
1.410	0.962	9.342	619				
1.413	1.002	9.992	619				
1.616	...	49.96	630				

added, and λ_{max}, the wavelength of maximum absorption for each addition of titrant. Selected titration curves are shown at three wavelengths (Figures 1-6): 640 mμ, representing the blue amylose-iodine-iodide complex; 353 mμ, due to the absorption of free I₃⁻ plus the complex; and 288 mμ, the free I₃⁻ absorption band. In all titrations except at 10⁻⁴ M KI the amylose con-

centration was held constant at 2.75 × 10⁻⁴ N anhydroglucose residues, where N = equivalents/liter.

Test of Linearity of Amylose Sample. The following observations support the linearity of our dissolved amylose. Addition of butanol gives a fine white precipitate of amylose, whereas branched amylopectin solutions will remain clear.^{2b} Our amylose adsorbs 200

Table V: Titration Data and Calculated Isotherm at $1.07 \times 10^{-5} M$ KI, 20.0°

OD _{640 mμ}	OD _{583 mμ}	[I ₂] _T × 10 ⁶	λ _{max} , mμ	ϵ	[I ₂ ⁻] _F × 10 ⁶	[I ₂] _F × 10 ⁶	ε ₅₈₃ ^I × 10 ⁻³
0.000	0.002	0.484	...	0.000	0.00443	0.480	...
0.010	0.008	0.989	...	0.008	0.00875	0.954	...
0.038	0.017	1.484	615	0.031	0.0124	1.36	12.4
0.071	0.028	1.945	620	0.057	0.0155	1.73	11.6
0.126	0.043	2.402	620	0.102	0.0178	2.02	10.5
0.231	0.079	3.050	620	0.186	0.0202	2.37	11.0
0.353	0.113	3.701	620	0.285	0.0219	2.67	10.6
0.465	0.148	4.335	620	0.375	0.0236	2.98	10.6
0.568	0.180	4.952	620	0.458	0.0252	3.30	10.6
0.660	0.209	5.753	620	0.532	0.0283	3.84	10.6
0.790	0.250	6.706	620	0.637	0.0311	4.42	10.6
0.879	0.278	7.623	620	0.709	0.0345	5.08	10.6
0.968	0.303	8.842	620	0.781	0.0394	6.04	10.5
1.028	0.328	9.994	620	0.828	0.0444	7.01	10.7
1.087	0.349	11.52	620	0.875	0.0513	8.36	10.7
1.135	0.364	12.95	620	0.915	0.0575	9.65	10.7
1.177	0.382	15.27	621	0.948	0.0682	11.8	10.7
1.326	0.461	49.97	621				

Table VI: Titration Data and Calculated Isotherm at $1.0 \times 10^{-4} M$ KI, 13.0°

OD _{640 mμ}	OD _{583 mμ}	[I ₂] _T × 10 ⁶	λ _{max} , mμ	ϵ	[I ₂ ⁻] _F × 10 ⁶	[I ₂] _F × 10 ⁶	ε ₅₈₃ ^I × 10 ⁻³
0.073	0.026	0.495	620	0.047	0.0281	0.275	9.65
0.237	0.069	0.980	621	0.153	0.0325	0.324	9.68
0.409	0.117	1.466	621	0.264	0.0349	0.354	10.0
0.550	0.157	1.923	622	0.357	0.0420	0.433	10.1
0.721	0.200	2.381	622	0.468	0.0419	0.442	9.95
0.881	0.244	2.830	622	0.573	0.0436	0.468	10.0
1.022	0.281	3.271	622	0.664	0.0488	0.533	9.97
1.169	0.323	3.734	622	0.752	0.0542	0.603	10.0
1.347	0.380	4.546	622	0.875	0.0807	0.920	10.1
1.428	0.416	5.357	622	0.926	0.127	1.47	10.2
1.462	0.438	6.140	622	0.951	0.181	2.11	10.1
1.501	0.478	7.627	622	0.974	0.285	3.39	10.2
1.529	0.528	10.00	622	0.992	0.452	5.52	10.1
1.621	1.148	50.00	622				

Table VII: Titration Data and Adsorption Isotherm at $1.0 \times 10^{-4} M$ KI, 20.0°

OD _{640 mμ}	OD _{583 mμ}	[I ₂] _T × 10 ⁶	λ _{max} , mμ	ϵ	[I ₂ ⁻] _F × 10 ⁶	[I ₂] _F × 10 ⁶	ε ₅₈₃ ^I × 10 ⁻³
0.038	0.018	0.4950	620	0.026	0.0313	0.364	9.68
0.142	0.051	0.9948	620	0.098	0.0486	0.573	10.2
0.280	0.090	1.456	620	0.193	0.0555	0.664	10.2
0.431	0.132	1.923	620	0.297	0.0599	0.729	10.2
0.560	0.170	2.376	620	0.386	0.0676	0.835	10.3
0.716	0.212	2.830	620	0.494	0.0696	0.876	10.3
0.859	0.253	3.271	620	0.592	0.0732	0.937	10.3
0.962	0.284	3.699	620	0.664	0.0836	1.08	10.3
1.161	0.347	4.545	620	0.808	0.104	1.39	10.4
1.278	0.389	5.357	620	0.881	0.137	1.86	10.5
1.334	0.414	6.140	620	0.920	0.179	2.45	10.4
1.382	0.450	7.616	620	0.954	0.266	3.71	10.4
1.420	0.497	9.994	620	0.980	0.410	5.85	10.4
1.560	1.069	50.00	622				

mg of I₂/g in very good agreement with literature data.^{2b} There is no spectrophotometric evidence of any branched contaminant, since none of our blue so-

lutions have a λ_{max} lower than 600 mμ. We observe the same shift in λ_{max} with KI as reported in the literature.^{8b} A comparison at 15.0° shows that our titration curve

Table VIII: Titration Data and Adsorption Isotherm at $1.0 \times 10^{-4} M$ KI, 30.0°

OD _{640 mμ}	OD _{353 mμ}	[I ₂] _T × 10 ⁵	λ _{max} , mμ	θ	[I ₂] _F × 10 ⁵	[I ₂] _F × 10 ⁵	ε ₃₅₃ ^I × 10 ⁻³
0.003	0.007	0.4950	...	0.002	0.0315	0.456	...
0.028	0.020	0.9852	...	0.020	0.0587	0.853	5.92
0.080	0.039	1.461	612	0.058	0.0799	1.17	8.41
0.141	0.057	1.918	612	0.103	0.0981	1.45	8.31
0.224	0.085	2.376	612	0.163	0.112	1.67	9.34
0.317	0.116	2.830	612	0.232	0.124	1.87	9.94
0.423	0.150	3.275	612	0.308	0.133	2.03	10.3
0.529	0.183	3.704	612	0.386	0.140	2.17	10.5
0.638	0.216	4.128	613	0.466	0.147	2.30	10.5
0.845	0.278	4.955	613	0.616	0.160	2.57	10.6
0.994	0.327	5.752	613	0.725	0.180	2.96	10.7
1.111	0.373	6.893	613	0.812	0.224	3.74	10.7
1.162	0.398	7.627	613	0.849	0.255	4.31	10.8
1.215	0.423	8.678	613	0.887	0.302	5.18	10.7
1.252	0.449	10.00	613	0.914	0.366	6.34	10.7
1.508	0.951	50.00	620				

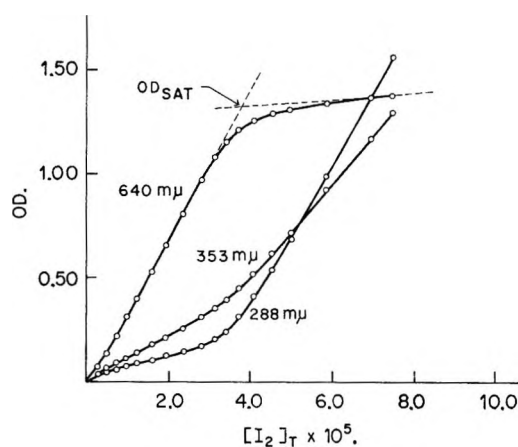


Figure 1. Titration curve at $1.0 \times 10^{-2} M$ KI, 20.0° ; optical density as a function of I_{2T} concentration.

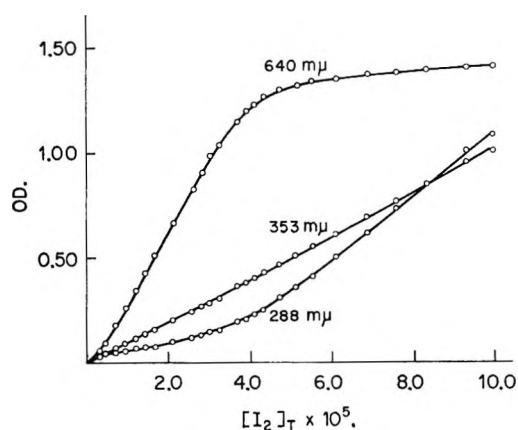


Figure 2. Titration curve at $1.0 \times 10^{-3} M$ KI, 20.0° ; optical density as a function of I_{2T} concentration.

for $10^{-2} M$ KI is virtually identical with that of Kuge and Ono¹⁵ who dissolved their potato amylose in concentrated KOH. Our (unpublished) dichroism studies in electric fields are in agreement with Paulson's¹¹ work

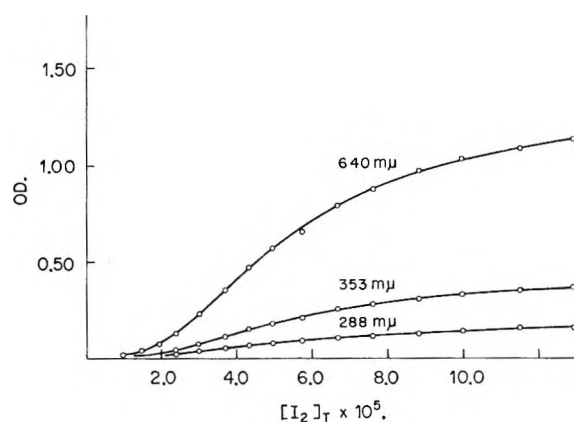


Figure 3. Titration curve at $1.07 \times 10^{-5} M$ KI, 20.0° ; optical density as a function of I_{2T} concentration.

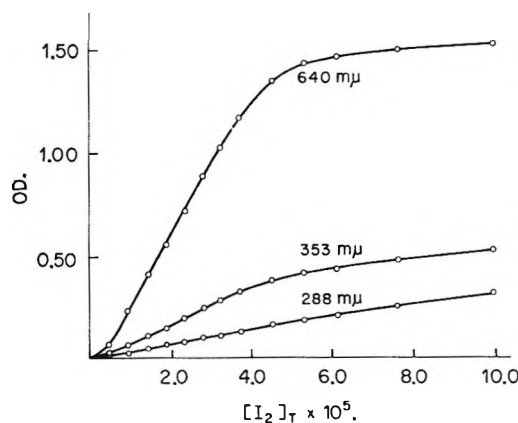


Figure 4. Titration curve at $1.0 \times 10^{-4} M$ KI, 13.0° ; optical density as a function of I_{2T} concentration.

on the amylose complex. Branched amylose would not orient in the same manner in an electric field.

Degree of Polymerization of the Amylose Sample. Our mild extraction procedure is expected to preferentially dissolve lower molecular weight amylose^{2b} whose D.P.

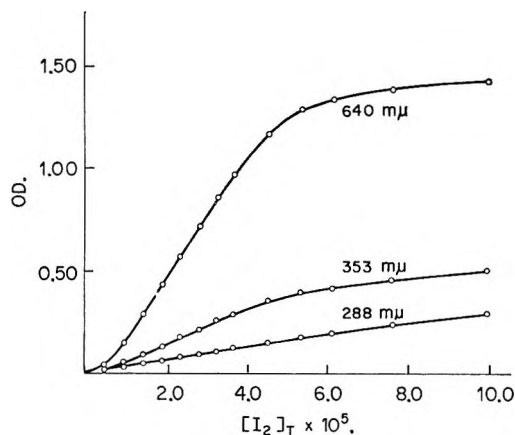


Figure 5. Titration curve at $1.0 \times 10^{-4} M$ KI, 20.0° ; optical density as a function of I_{2T} concentration.

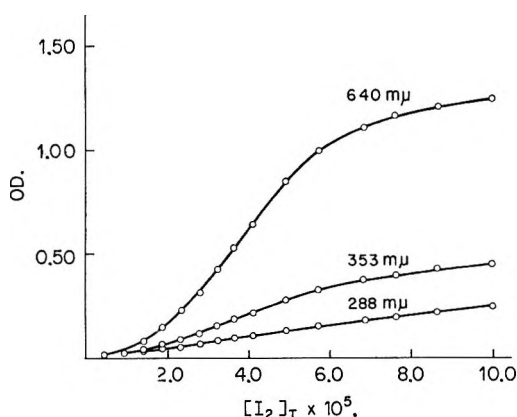


Figure 6. Titration curve at $1.0 \times 10^{-4} M$ KI, 30.0° ; optical density as a function of I_{2T} concentration.

we estimate to be approximately 800. Attempts at molecular weight determinations by viscosity measurements were not successful due to the low amylose concentrations in the saturated solutions. Even if our amylose chains would have a D.P. of only 120 in the extreme case, our conclusions in the present binding study are not affected, since we are using indeed an effective length of 15 helical turns in our theoretical calculations (see Introduction, etc.).

Treatment of Data

The method used for calculating the concentrations of free and bound species is similar to that of Kuge and Ono.¹⁵ In addition, we have introduced the possibility that a variable amount of I^- may be bound together with I_2 resulting in the bound species I_2 and I_3^- whose over-all average contribution to the bound state can be expressed as $I_2 \cdot I_b^-$, where b varies between zero and 1 (or 2 for the one-dimensional model). The following five equations comprise the model. (a) absorption at $640 m\mu$ due to bound species only

$$OD_{640} = \epsilon_{640}[I_2 \cdot I_b^-] \quad (1)$$

(b) absorption at $353 m\mu$ representing the sum of con-

tributions of bound as well as of the free species I_{2F} and I_{3F}^-

$$OD_{353} = \epsilon_{353}^I[I_2 \cdot I_b^-] + \epsilon_{353}^{II}[I_2]_F + \epsilon_{353}^{III}[I_3^-]_F \quad (2)$$

where ϵ_{640} , ϵ_{353}^I , ϵ_{353}^{II} , and ϵ_{353}^{III} are the molar extinction coefficients of bound species at $640 m\mu$, bound species at $353 m\mu$, free I_2 , and free I_3^- at $353 m\mu$, respectively; (c) the triiodide equilibrium relating the free species to each other

$$\frac{[I_3^-]_F}{[I_2]_F[I^-]_F} = K_F \quad (3)$$

and finally, two mass conservation relations

$$[I^-]_T = [I^-]_F + [I_3^-]_F + b[I_2]_B \quad (4)$$

and

$$[I_2]_T = [I_2]_F + [I_3^-]_F + [I_2]_B \quad (5)$$

The latter five equations contain 14 parameters of which the following seven are known: ϵ_{353}^{II} (18)²² ϵ_{353}^{III} (26,400)²² $K_F = 866$ at 20.0° ,²³ $[I^-]_T$, $[I_2]_T$, OD_{640} , and OD_{353} . Unknown parameters are ϵ_{640} , b , ϵ_{353}^I , I_{2F} , I_{3F}^- , I_{F^-} , and I_{2B} .

The degree of saturation θ is defined as

$$\theta = \frac{[I_2 \cdot I_b^-]}{[I_2 \cdot I_b^-]_{sat}}$$

where $[I_2 \cdot I_b^-]_{sat}$ is the calculated value of bound I_2 at saturation. Since ϵ_{640} is constant, the relationship

$$\theta = \frac{OD_{640}}{OD_{640,sat}}$$

holds, where $OD_{640,sat}$ refers to the saturated polymer. Experimentally at high I^- , an increase of OD_{640} beyond OD_{sat} is observed which indicates, along with a shift in λ_{max} , that a second process takes place after or near saturation of the helix, which makes it somewhat difficult to determine OD_{sat} exactly. A possible way to obtain OD_{sat} is to determine the point of intersection of two tangents, one being the tangent to the titration curve at high total I_2 concentration and the second representing the tangent to the steep rise of the isotherm as seen in Figure 1. This method cannot be applied to the isotherm at $1.07 \times 10^{-5} M$ KI where an extrapolated value for OD_{sat} is used. It is fairly certain that the "second process" at the latter iodide concentration is negligible. The present model measures "chromophoric" iodine adsorption, and it neglects any I^- which might be bound to amylose itself but not to I_2 . Viscosity and other measurements^{2b} have not been able to show I^- binding to amylose alone.

(22) A. D. Awtrey and R. E. Connick, *J. Amer. Chem. Soc.*, **73**, 1842 (1951).

(23) M. Davies and E. Gwynne, *ibid.*, **74**, 2748 (1952).

Table IX: Isotherm Parameters

$[I^-]_T$	$T, ^\circ C$	b	$\epsilon_{640} \text{ m}\mu$	OD_{sat}	$[I_2]_{Bound} \times 10^6$
2.50×10^{-2}	20.0	~ 1.0	38,500	(1.34) ^a	(3.48) ^a
1.00×10^{-2}	20.0	~ 1.0	38,000	1.33	3.50
5.00×10^{-3}	20.0	~ 1.0	38,500	1.35	3.50
1.00×10^{-3}	20.0	$\sim 0.7^b$	38,000	1.36	3.58
1.07×10^{-3}	20.0	0.1-0.3	35,000	1.24 ^c	3.54
1.00×10^{-4}	13.0	~ 0.6	38,000	1.54 ^d	4.05 ^d
1.00×10^{-4}	20.0	~ 0.5	38,000	1.45 ^d	3.82 ^d
1.00×10^{-4}	30.0	~ 0.4	38,000	1.37 ^d	3.61 ^d

^a Assigned value on the basis of other results at high I^- . ^b See ref 12. ^c Extrapolated. ^d Amylose concentration is $2.96 \times 10^{-4} N$ in this case, whereas for all other titrations it is $2.75 \times 10^{-4} N$.

Results

In applying the mathematical model the values of two parameters b and ϵ_{640} are chosen. From equilibrium dialysis measurements³ a value of ϵ_{640} has been obtained (38,500) at $10^{-2} M$ KI. Nevertheless, ϵ_{640} was allowed to vary between 35,000 and 44,500 in intervals of 500. For the known parameters above and at each value of ϵ_{640} sets of isotherms were calculated on a Honeywell 800 computer for b increasing from zero to beyond unity in intervals of 0.1. The criterion for selecting the "correct" isotherm is the requirement that ϵ_{353}^I be constant over the titration range. Conversely, b and ϵ_{353}^I could have been chosen and ϵ_{640} calculated. The latter method turned out to be less accurate^{1b} than the former.

Values of the parameters b , ϵ_{640} , and OD_{sat} determined for use in the calculated isotherms are listed in Table IX. The amount of bound I_2 at OD_{sat} (approximately $3.5 \times 10^{-5} M$, or 20 mg of $I_2/100$ mg of amylose) compares well with previously reported values determined by potentiometric titrations,^{2b} *i.e.*, between 18 and 20 mg of $I_2/100$ mg of amylose. The latter quantity of bound I_2 corresponds to one I_2 molecule per eight anhydroglucose units. The calculated isotherms including values for ϵ_{353}^I are also given in Tables I-VIII, some of which appear in Figures 7-12.

$2.5 \times 10^{-2} M$ KI. Higher KI concentrations than $2.5 \times 10^{-2} M$ could not be attained owing to precipitation of the blue complex. Even at $2.5 \times 10^{-2} M$ KI onset of a slow precipitation prevented measurement beyond $\theta \simeq 0.6$ when stirring was terminated. OD_{sat} could not be measured, and it was assumed that it is similar to that at $10^{-2} M$ KI. This follows from the general result that OD_{sat} was similar for all isotherms at high KI. A value of ϵ_{640} 38,500 was found to fit the data well. There was no obvious shift in λ_{max} (602 m μ) (Table I) indicating that similar species are adsorbed over the low θ range studied. The calculated isotherms were insensitive to b since the maximum amount of bound iodide is only a negligible fraction of I_T^- . The best values of ϵ_{353}^I show moderate constancy and tend to increase mildly with θ .

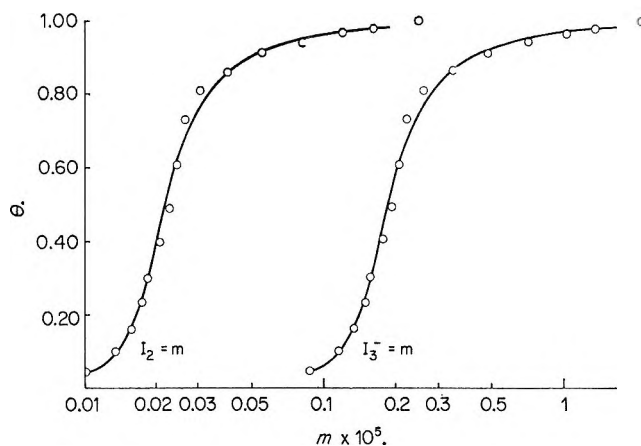


Figure 7. Calculated isotherm at $1.0 \times 10^{-2} M$ KI, 20.0° ; θ as a function of m , where m is I_{2F} and I_{3F}^- , respectively: full lines, theoretical calculation; points, experimental.

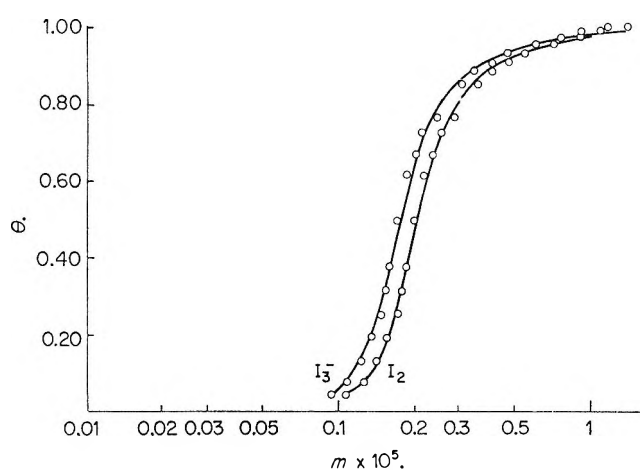


Figure 8. Calculated isotherm at $1.0 \times 10^{-2} M$ KI, 20.0° ; θ as a function of m , where m is I_{2F} and I_{3F}^- , respectively: full lines theoretical calculations; points, experimental.

$10^{-2} M$ KI. The value of ϵ_{640} (38,500) obtained from equilibrium dialysis³ as well as Kuge and Ono's¹⁵ estimated ϵ_{640} (36,300) at $10^{-2} M$ KI compare well with the present one of 38,000. At this concentration of I^- any b values chosen had no effect on the calculated I_{2F} and

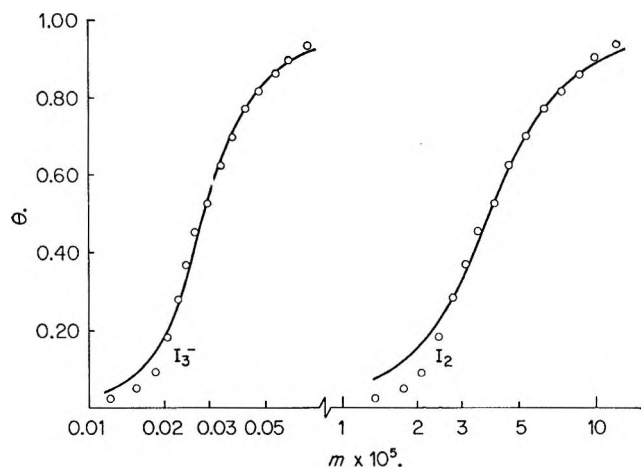


Figure 9. Calculated isotherm at $1.07 \times 10^{-5} M$ KI, 20.0° ; θ as a function of m , where m is I_{2F} and I_{3F}^- , respectively: full lines, theoretical calculation; points, experimental.

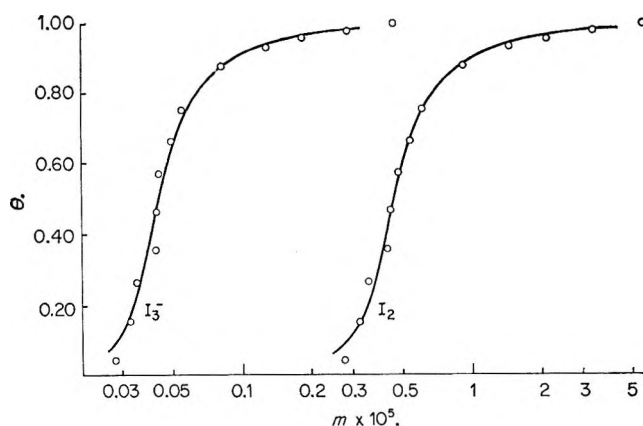


Figure 10. Calculated isotherm at $1.0 \times 10^{-4} M$ KI, 13.0° ; θ as a function of m , where m is I_{2F} and I_{3F}^- , respectively: full lines, theoretical calculation; points, experimental.

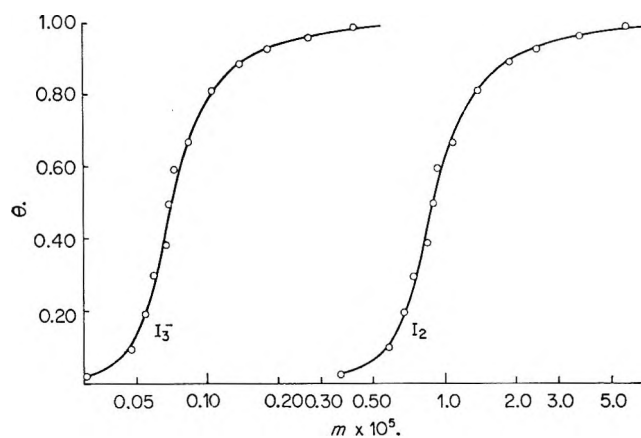


Figure 11. Calculated isotherm at $1.0 \times 10^{-4} M$ KI, 20.0° ; θ as a function of m , where m is I_{2F} and I_{3F}^- , respectively: full lines, theoretical calculation; points, experimental.

I_{3F}^- . While λ_{max} is quite constant up to $\theta \simeq 0.8$ (Figure 16c), a strong increase occurs beyond $\theta = 0.8$ due to a "second process" to be discussed later. The

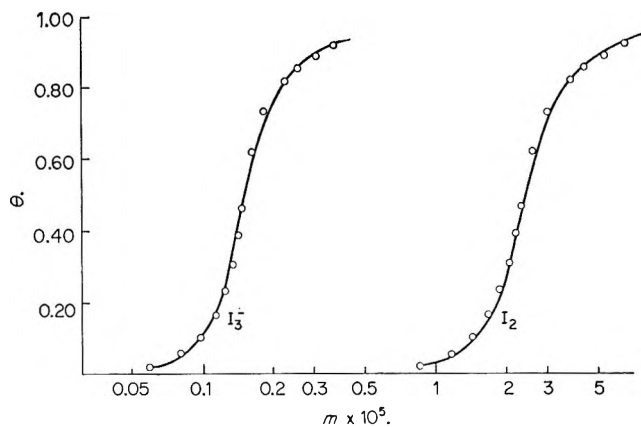


Figure 12. Calculated isotherm at $1.0 \times 10^{-4} M$ KI, 30.0° ; θ as a function of m , where m is I_{2F} and I_{3F}^- , respectively: full lines, theoretical calculation; points, experimental.

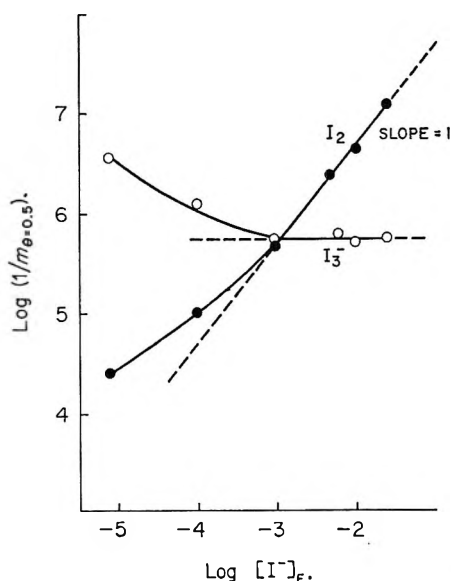


Figure 13. Apparent binding constant $1/m$ vs. free $[I^-]_F$ at $\theta = 0.5$, where m refers to $[I_2]_F$ and $[I_3^-]_F$, respectively.

gradual sigmoid shape of the isotherm (Figure 7) indicates only a "moderate" degree of cooperativity. Over-all binding with respect to I_3^- is quite high: $[1/I_3^-]_F \simeq 6.3 \times 10^5$ at $\theta = 0.5$ (Figure 13).

$5 \times 10^{-3} M$ KI. Values for the individual parameters are found to be similar to the ones at $10^{-2} M$ KI, as seen in Tables III and IX.

$10^{-3} M$ KI. Similarities with all previously discussed isotherms exist (Table IV, Figure 8). At $\theta = 0.5$ values for I_{3F}^- are almost identical for all isotherms discussed so far, indicating that a similar species may be responsible for binding. The maximum amount of I^- which can be bound as I_3^- is less than $\sim 4\%$ of the total iodide concentration. Thus b cannot be determined spectrophotometrically at $10^{-3} M$ KI. Potentiometric titration studies indicate,¹² however, that $b \simeq 0.7$ at low θ , a value adopted in the present study.

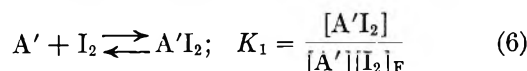
$10^{-4} M$ KI. A change in the composition of the

bound species is indicated due to a lower value of $b \approx 0.5 \pm 0.1$. The latter value was determined on the basis of those calculated values of ϵ_{353}^I per isotherm which showed the least variation over the titration range (Table VII). A slight difference in isotherm shape is found when the free species is taken to be I_3^- in one case and I_{2F} in the other (Figure 11).

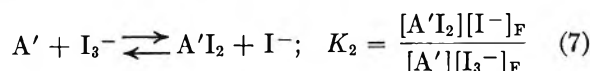
$1.07 \times 10^{-5} M KI$. The nature of the bound species at this lowest I^- of our study is found to be markedly different from that at high I^- . Values of b cannot be larger than 0.2 for $1.07 \times 10^{-5} M KI$ owing to the fact that for $b \geq 0.2$ negative I_{3F}^- are calculated (Table V, Figures 3 and 9). Contributions of I^- from the hydrolysis of I_2 ($K_{hyd} = 4.3 \times 10^{-13}$ at 20.0°) may be as high as 20% for the highest I_2 concentrations used in the titration. The possible production of I^- by processes other than hydrolysis such as reduction of I_2 in the presence of amylose would tend to increase b somewhat. A visual comparison with the titration curve at $10^{-4} M KI$ (Figure 5) shows immediately that $[I^-]_T$ for the present curve must be substantially lower than $10^{-4} M$. Therefore the b value for this curve must be smaller than the previous $b = 0.5$ (at $10^{-4} M KI$). Assuming, in the extreme case, that $[I^-]_T$ were twice as large, *i.e.*, $2 \times 10^{-5} M$, our calculations have shown that b might be as high as 0.3 but certainly not higher for the present titration curve. Thus it has been unequivocally shown that the bound species cannot be I_3^- at this low iodide concentration, since there is not enough I^- available for their formation. This result invalidates the assumption¹⁴ that I_3^- is the binding species at any concentration of KI. The value of b has no effect on the calculated I_{2F} but does have a large effect on the calculated I_{3F}^- which is higher for lower b values. The value of ϵ_{640} is found to be lower than 38,000, probably due to the drastically different composition of the bound species. The extrapolated value of OD_{sat} appears to be somewhat lower than the one at the higher I^- concentrations (Table IX).

Nature of the Bound Species

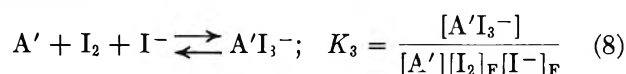
The reciprocal free species concentration at constant θ ($1/m_\theta$) can be used as a measure of binding strength at various total I^- concentrations. This I^- dependence²⁵ of $1/m_\theta$ is shown in the following to lead to the postulate of two limiting binding models for either of the two binding species, I_2 and I_3^- . At very low iodide concentrations the bound species is postulated to be I_2 ; *i.e.*, $b = 0$ for $I_2 \cdot I_b^-$, according to the equilibrium



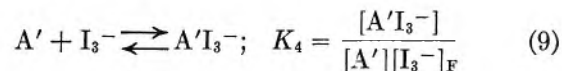
where A' represents an empty site having one nearest neighbor. For I_3^- as the free species, at low I^-



At high iodide concentrations the bound species is postulated to be I_3^- ; *i.e.*, $b = 1$. For I_2 as free species



Alternately, for I_3^- as free species



For the limiting model of I_2 binding to hold (equilibria 6 and 7), the apparent binding constant K_1 as well as $K_2/[I^-]_F$ should be independent of I^- . It is seen from Figure 13 that the $[I_{2F}^-]$ curve could gradually approach a constant value below $10^{-5} M KI$. This behavior is also reflected in the $[I_3^-]_F^{-1}$ curve whose slope could approach a limiting value of -1 below $10^{-5} M KI$. Thus it can be inferred that the limiting model of I_2 binding is likely to be realized at somewhat lower I^- concentrations than that attained in this study. Further experimental lowering of the KI concentration is complicated by interference of I_2 hydrolysis and reduction.

At high iodide concentrations the formal predictions of equilibria 8 and 9 are borne out. For I_2 and I_3^- as the free species, $K_3[I^-]_F$ and K_4 are found to be constant, respectively, above $10^{-3} M KI$, indicating that the bound species is likely to be I_3^- . However, further uptake of I^- to form I_4^{2-} cannot be entirely ruled out. Since, at high $[I^-]_T$, the equivalent concentration of the complex is negligible with respect to $[I^-]_T$, a distinction between I_3^- and I_4^{2-} as the bound species is not possible by use of the $1/m_\theta$ relationship alone. A later one-dimensional model calculation shows that I_4^{2-} binding cannot be entirely excluded.

At intermediate iodide concentrations both limiting models contribute according to $I_2 \cdot I_b^-$ where b varies from zero to 1 (or ~ 2 on the basis of the one-dimensional model) with increasing iodide concentration. To express the average composition of $I_2 \cdot I_b^-$ in terms of bound I_2 and bound I_3^- , one could define a quasi one-dimensional equilibrium constant K_B such as

$$K_B = \frac{[I_3^-]_B}{[I_2]_B[I^-]_F} = \frac{b}{[I^-]_F(1-b)} \text{ at } \theta \approx 0.50 \quad (10)$$

which approximately describes the composition of the bound species as a function of the free iodide concentration. However, due to the cooperativity and competitive nature of the adsorption process, one would not expect K_B to be constant at all iodide concentrations used.

Theoretical Model for Adsorption

The theoretical isotherms are calculated from a statistical model³ which postulates equilibrium between species in their free and bound state. The bound state

(24) M. Eigen and K. Kustin, *J. Amer. Chem. Soc.*, **84**, 1355 (1962).

(25) J. A. Thoma and D. French, *J. Phys. Chem.*, **65**, 1825 (1961).

Table X: Values of K_0 and K_{st} obtained by a Nonlinear Least-Squares Calculation

$[I]_T$	$T, ^\circ C$	I_3^-				I_2			
		K_0	$-\Delta F_0^a$	K_{st}	$-w^a$	K_0	$-\Delta F_0^a$	K_{st}	$-w^a$
2.50×10^{-2}	20.0	2.20×10^4	5.83	30.9	2.00	4.85×10^6	7.63	30.4	1.99
1.0×10^{-2}	20.0	1.10×10^4	5.42	57.3	2.36	9.52×10^4	6.68	57.2	2.36
5.0×10^{-3}	20.0	4.72×10^3	4.93	166	2.98	2.10×10^4	5.80	160	2.95
1.0×10^{-3}	20.0	8.59×10^3	5.28	81.1	2.56	8.18×10^3	5.25	72.2	2.49
1.07×10^{-5}	20.0	1.06×10^6	6.74	38.9	2.13	2.00×10^3	4.43	15.0	1.57
1.0×10^{-4}	13.0	3.90×10^4	6.01	71.4	2.43	5.23×10^3	4.87	49.6	2.22
1.0×10^{-4}	20.0	2.43×10^4	5.88	69.7	2.47	2.96×10^3	4.66	44.8	2.21
1.0×10^{-4}	30.0	1.06×10^4	5.59	75.3	2.60	1.06×10^3	4.20	47.2	2.32

^a ΔF_0 and w are in kilocalories per mole.

is represented by the occupied one-dimensional Ising lattice of finite length. The model assumes all binding sites to be equivalent and all bound species to be "localized." First nearest neighbor interactions are considered between bound adsorbate molecules which leads to a quantitative description of cooperativity in terms of the stacking coefficient.

The degree of saturation, θ , is calculated as a function of the free adsorbate concentration, m , at a given chain length, n , cooperative energy of interaction, w , and intrinsic association constant, K_0 , according to³

$$\theta = D \left(\frac{1 + R^{n+1} - \frac{2R(1 - R^n)}{n(1 - R)}}{1 + \left(\frac{D}{1 - D}\right)R^{n+1}} \right) \quad (11)$$

where

$$D = \frac{\lambda_0 - 1}{\lambda_0 - \lambda_1}$$

$$R = \frac{\lambda_1}{\lambda_0}$$

$$\lambda_{0,1} = 0.5(1 + K_{st}K_0m) \pm$$

$$\sqrt{(1 - K_{st}K_0m)^2 + 4K_0m}$$

where K_{st} is the "stacking coefficient" ($K_{st} = \exp(-w/RT)$).

K_{st} is obtained by curve fitting of the experimental isotherm to a theoretical isotherm curve of θ vs. $\log K_0m$ at a given n . The value of K_0 is calculated from

$$K_0 = \frac{(mK_0)_{\text{theor}}}{(m)_{\text{exptl}}} \text{ at any } \theta$$

A short-chain isotherm model, $n = 15$, was adopted³ mainly on the basis of the previously mentioned mechanochemical degradation studies of amylose done by Szejtli, *et al.*¹⁰

The nonsymmetric shape of the experimental isotherms immediately suggests that n should be substantially smaller than the highest possible value of 120–150. It is believed for the present amylose sample that

$n = 15$ represents a lower limit, and it is assumed to be independent of KI and temperature. A lowering of n tends to increase K_{st} for the same experimental isotherm shape. Therefore the reported values of K_{st} represent maximum values. This is to say that the "true" degree of cooperativity may be even somewhat less than that reported in this work. A good theoretical fit was obtained at all iodide concentrations as shown in Figures 7–12 for some representative isotherms. Values for K_{st} and K_0 have also been determined by a second method: a nonlinear least-squares fit³ calculated on a Honeywell 800 computer. The latter method can be used to refine the less accurate results of the former. Table X summarizes values of K_{st} and K_0 determined by the nonlinear least-squares calculation for either I_2 or I_3^- as the free species.

Intrinsic Association Constant

At any given iodide concentration we may define two intrinsic binding constants: one with respect to I_2 and the other with respect to I_3^- as the free species. The dependence of K_{0I_2} on I_T^- reflects the behavior of $[I_2]_F^{-1}$ (Figure 13) at low values of I_T^- ; K_0 eventually approaches a constant value as expected for the proposed limiting I_2 binding model (Figure 14). At high I_T^- , however, a somewhat stronger dependence on I_T^- is observed than that of $[I_2]_F^{-1}$: a slope of ~ 1.7 is found at $2.5 \times 10^{-2} M$ KI. Thus the bound species is predicted to approach I_4^{2-} (for a slope of 2) at very high I_T^- , rather than I_3^- as predicted by the $[I_2]_T^{-1}$ curve. A similar conclusion is reached upon inspection of the $K_{0I_3^-}$ curve: K_0 declines with I_T^- in a manner indicating limiting I_2 binding at low I_T^- , then it passes through a horizontal region expected for I_3^- binding and finally it increases with I_T^- indicating that further I^- is taken up into the complex (Figure 15). The latter behavior again predicts the species I_4^{2-} for a slope of $+1$, which is not quite attained yet at $2.5 \times 10^{-2} M$ KI. Thus the K_0 plots predict I_4^{2-} as the limiting bound species at high KI whereas the experimental $1/m$ plots (Figure 13) lead to I_3^- as the bound species.

Stacking Coefficient

Two types of stacking coefficients can be defined; one

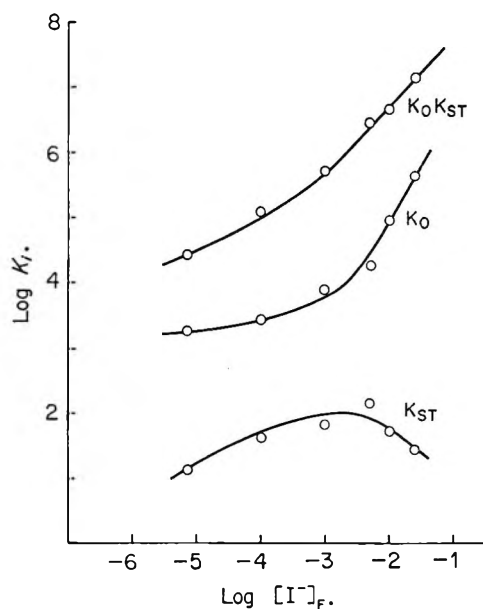


Figure 14. Calculated values of K_0 , K_{st} , K_0K_{st} as a function of free $[I^-]_f$. Free species is taken as I_{2F} at $\theta = 0.5$.

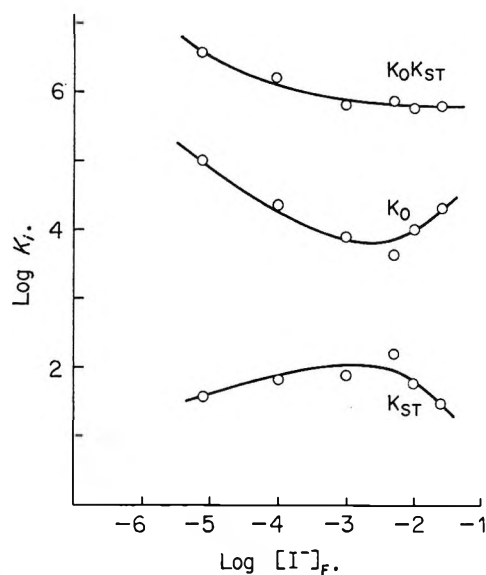


Figure 15. Calculated values of K_0 , K_{st} , K_0K_{st} as a function of free $[I^-]_f$. Free species is taken as I_{3F} at $\theta = 0.5$.

with respect to I_{2F} , the other with respect to I_{3F} as the free species. At sufficiently high I_T^- , where b does not affect I_T^- , the two types of K_{st} should be identical. At low I_T^- , however, where the concentration of bound I^- becomes comparable with I_T^- the two types of K_{st} should be different as seen from Table X and Figures 14 and 15. Interestingly, a slight maximum in K_{st} is found as a function of I_T^- for both K_{st} . This maximum occurs approximately at $I_T^- \simeq 2 \times 10^{-3}$ for a $K_{st(\max)} \simeq 120$. What is the composition of the bound species at the maximum? First, at 1.07×10^{-5} M KI, where $b \approx 0.1-0.3$, the bound species consist mostly of I_2 which would not be expected to interact very strongly

with each other. Support for this argument comes from the fact that even for saturated solutions of I_2 in water no aggregation has been reported. Thus the cooperative energy of interaction w , is approximately -1.57 kcal/mol, corresponding to $K_{st} \approx 15.0$ for I_2 as the free species. As more I^- is bound into the complex the cooperative energy of interaction is found to increase; *i.e.*, $w = -2.47$ kcal/mol for $K_{st} = 69.7$ at 10^{-4} M KI. At $K_{st(\max)}$ the bound species can be calculated from K_B to be approximately $I_2 \cdot 2I_3^-$ ($b = 2/3$) for the limiting I_3^- model, whereas for the limiting I_4^{2-} model the bound species are approximately I_3^- at this particular KI concentration. In any case addition of I^- to the polyiodine chain increases the cooperative energy of interaction between bound species to a certain value at the maximum. The formation of higher I_3^- aggregates occurs in aqueous solution to a small extent.²³ If an analogy to bound I_3^- is permissible, then a relatively moderate interaction in the bound state as exemplified by $K_{st(\max)}$ is conceivable. As I_T^- increases beyond 2×10^{-3} M, K_{st} is observed to decline almost linearly with I_T^- . At 2.5×10^{-2} M KI, $w = -2.0$ kcal/mol for $K_{st} = 30.9$ (relative to I_{3F}). Thus further uptake of I^- is seen to increase the electrostatic repulsion between bound species as evidenced by the decreasing value of w . From the behavior of K_{st} the binding species is again predicted to be I_4^{2-} at very high iodide concentration.

Extrapolation to very high KI concentrations, which are experimentally not attainable owing to precipitation, predicts that eventually repulsive interactions should take over and w should become positive.

Thermodynamic Parameters

For a cooperative system the isosteric heat of binding, ΔH_θ , is expected to be a function of θ as well as of temperature. In this work, due to the moderate degree of cooperativity, variations of ΔH_θ with θ and T were within experimental uncertainty.

Best results were obtained at 10^{-4} M KI to which the following calculations apply. Use of the Clausius-Clapeyron-type equation

$$\log \left(\frac{m_1}{m_2} \right)_\theta = - \frac{\Delta H_\theta}{2.303R} \left(\frac{1}{T_1} - \frac{1}{T_2} \right)$$

leads to an enthalpy of binding, $\Delta H_{0.5}$, at $\theta = 0.5$, of -16.6 ± 0.5 and -12.8 ± 0.5 kcal/mol for I_2 and I_3^- as the free species, respectively. The difference (-3.8 kcal/mol) between the two values is probably due to the enthalpy of formation of free I_3^- which has been reported to show a mild dependence on temperature.²³ Previously given values for ΔH of binding in the amylose-iodine-iodide system range from -11 to -20 kcal/mol of bound I_2 .^{12,15,26} Using $\Delta F_\theta = -RT \ln (1/m_\theta)$ for the over-all free-energy change, the over-all entropy

(26) J. Holl6 and J. Szejtli, *Staerke*, **9**, 109 (1957).

of binding at $\theta = 0.5$ is calculated as -33.7 and -15.6 eu for I_2 and I_3^- as the free species, respectively. The difference ($\Delta(\Delta S_\theta) = -18.1$ eu) between the latter two values is noteworthy, since it cannot be due to the free triiodide whose ΔS of formation is calculated to be approximately $+0.5$ eu at 20.0° from Davies and Gwynne's data.²³ It is likely that this difference is partially due to the particular composition of the bound species which on the average is approximately $I_2 \cdot I_{-0.5}$ at $10^{-4} M$ KI, whereas the free species is taken to be I_2 and I_3^- , respectively. Furthermore, hydration effects may have to be considered as seen from the fact that the above discrepancy is found in ΔS_θ only. Thermodynamic parameters obtained from the one-dimensional model compare satisfactorily with the above: ΔH_θ due to intrinsic binding with one helical turn (K_0) is -16.3 and -13.3 kcal/mol for I_2 and I_3^- , respectively. The good constancy of w over the temperature range suggests that it might be regarded as an enthalpy rather than a free energy: for I_2 , $w = -2.25$ kcal/mol; for I_3^- , $w = -2.50$ kcal/mol at $10^{-4} M$ KI. The product $K_0 K_{st}$ is an exact measure of over-all binding at the point of inflection of the nonsymmetric isotherm which occurs at $\theta \approx 0.28$. Here $K_0 K_{st} = 1/m_{\text{exptl}}$. ΔH_θ for $K_0 K_{st}$ at $\theta \approx 0.28$ is -18.5 and -15.7 kcal/mol for I_2 and I_3^- , respectively, in satisfactory agreement with the "experimental" ΔH_θ . It is evident that practically all of the over-all entropy loss occurs when the species gets "trapped" into one helical turn. The difference in ΔS_θ between I_2 and I_3^- binding is similar to the above $\Delta(\Delta S_\theta)$ which again suggests that hydration effects may play an important role in binding. Importantly, such hydration effects seem to be associated almost exclusively with intrinsic binding rather than with cooperative interaction.

The temperature dependence of the isotherms at $10^{-2} M$ KI has been measured at 13.4 , 20.0 , and 30.0° .^{1b} Since the results show greater scatter, we do not report them here. However, it appears that values for ΔH_θ are somewhat less negative than those at $10^{-4} M$ KI.

λ_{max} and the "Second Adsorption"

A difficulty in determining values of OD_{sat} was mentioned earlier with regard to a "second adsorption process" which was suggested by Higginbotham²⁷ to explain the continuous shift of λ_{max} toward longer wavelengths when iodine is added after apparent saturation. Figure 16a shows the relationship between λ_{max} and the total I^- concentration at a total I_2 concentration of $50 \times 10^{-5} M$, more than ten times the concentration needed for saturation. If λ_{max} is characteristic of the degree of the "second adsorption," then this process is facilitated by a saturated helix at high I_2 and I^- . Alternative explanations for the "second adsorption phenomenon" have been given:¹¹ association of helices by intermolecular hydrogen bonding and the displacement of counterions (K^+) from nonhelical regions by additional I_3^-

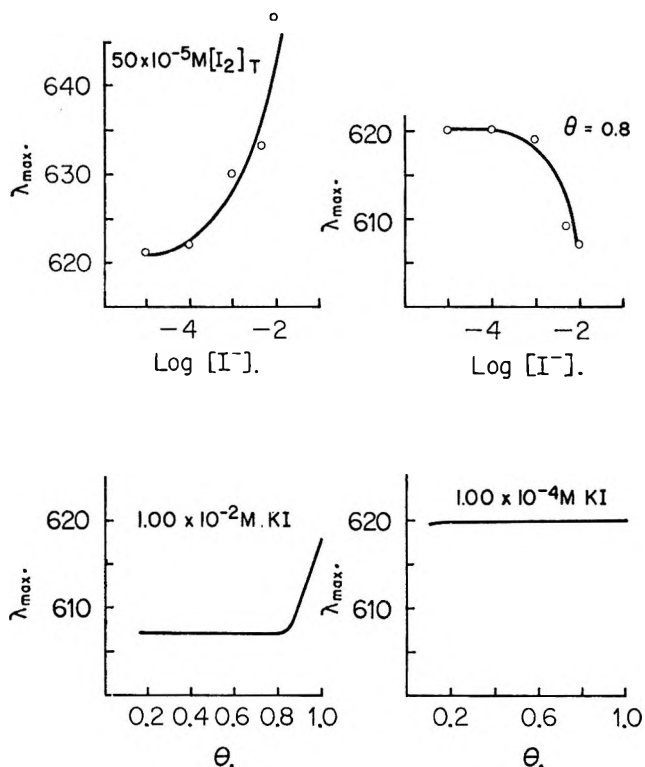


Figure 16. λ_{max} relationships.

binding. We believe the aggregation of partially or completely filled helices to be the most likely process to explain the "second adsorption" phenomenon. Thus aggregation seems to be promoted by increasing KI concentration, *i.e.*, increasing ionic strength. Interhelix interaction would be expected to add a third dimension to the largely one-dimensional species-species interaction within one helix thus increasing λ_{max} due to a greater delocalization of the resonance energy between bound I_2 - I_3^- species.

At lower degrees of saturation, $\theta = 0.8$, λ_{max} decreases with I^- (Figure 16b), indicating that the adsorbed species do indeed change in nature as a function of KI in support of the findings of this work. At a constant KI concentration of $10^{-4} M$, λ_{max} is found to be constant ($\sim 620 \mu\mu$) over the isotherm range (Figure 16d) lending support to the assumption that the nature of the bound species does not change appreciably at a constant KI concentration. At $10^{-2} M$ KI, λ_{max} ($\sim 607 \mu\mu$) is constant up to $\theta \approx 0.8$ beyond which it increases probably due to increased aggregation of amylose helices (Figure 16c). The tables may be consulted for listings of λ_{max} for all points measured.

Discussion

This work shows convincingly that the main stability of the complex originates from the *intrinsic* binding as seen from the high values of K_0 (Table X). Thus one helical turn which has a pitch of $\sim 8 \text{ \AA}$ in the solid is

(27) R. S. Higginbotham, *J. Textile Inst. Trans.*, **40**, 783 (1949).

capable of trapping either the I_2 or I_3^- species rather strongly with a substantial loss in entropy. It is certain from entropy considerations that internal solvation effects must be important here. The channel diameter inside the helix is approximately $6-7 \text{ \AA}^4$ (outer diameter of the helix is $\sim 13 \text{ \AA}$) which is large enough to accommodate species such as other anions or H_2O molecules together with the iodine-iodide chain. Strong intrinsic binding as found in this work makes the existence of a chain of bound species possible, and it therefore is indirectly responsible for *chain* stability. Qualitative evidence for cooperativity has been cited earlier.^{2, 13, 28-30} Rundle, *et al.*,³¹ observed that if only half of the iodine needed for saturation is present in an amylose solution and the complex is precipitated with excess KI, the iodine is found entirely in the precipitate with half of the amylose still in solution. It should be kept in mind, however, that a heterogeneous phase change is involved in the latter process. Statistical calculations using the present parameters of K_{st} and K_0 show³² that for the moderate degree of cooperativity found in this work the often cited "all or nothing" is not important. Instead, for present magnitudes of K_{st} there is a *gradual* increase in the average chain length of bound species from a value of 2-4 to the maximum value of 15 as Θ increases from 0.1 to 1.0, respectively. This is to say that the probability of finding *short* chain lengths of *bound species* is appreciable even at relatively high Θ . Thus we do not consider the binding reaction for the present amylose sample as highly cooperative, although it might be argued from an energetic standpoint that first nearest neighbor interaction energies of -1.6 to -3.0 kcal/mol represent relatively strong interactions for the case of mutual iodine species interactions. The use of a higher effective chain length in the calculations would lead to an even lower degree of cooperativity in this study in which an effective chain length of 15 helical turns has been employed.

An independent determination of w by equilibrium dialysis³ at $10^{-2} M$ KI and 20.0° is in general agreement with the spectrophotometric results. The value of $\epsilon_{640} \sim 38,500$ obtained by equilibrium dialysis at $10^{-2} M$ KI is used in the spectrophotometric isotherm calculations. Surprisingly, this value is found to be a good measure of ϵ_{640} over the KI range from 2.5×10^{-2} to $1 \times 10^{-4} M$ despite the finding that the composition of the bound species changes to some extent. At $1.07 \times 10^{-5} M$ KI, ϵ_{640} has decreased by $\sim 8\%$ to a value of 35,000, whereas the limiting concentration of bound species expressed in terms of I_2 has remained practically constant over the total KI range for a constant amylose concentration of $2.75 \times 10^{-4} N$. Therefore, in the present KI range, ϵ_{640} (unlike λ_{max}) is not very sensitive to the amount of I^- bound in the complex although it is known that ϵ_{640} will eventually approach zero at zero iodide concentration. The expected drastic drop in ϵ_{640} seems to occur at even lower I^- concentrations

than attained in this study. Pure I_2 binding as predicted in the limit of zero KI concentration will therefore not show a blue band at $640 m\mu$; it is likely to have a λ_{max} around $460 m\mu$ similar to free I_2 in aqueous solution. Spectra at low KI show already a pronounced shoulder at $460 m\mu$, which is higher than that expected for free I_2 present at equilibrium. The values for ϵ_{355}^I range in the neighborhood of 10,000 with good constancy for the isotherms at low KI concentrations. Inspection of a large number of machine calculations shows that there is a latitude in the choice of b . At the lowest KI concentration ($1.07 \times 10^{-5} M$), it is required that $b = 0.1$ to 0.3 . The latter b range has been calculated from the consideration of additional production of I^- by hydrolysis and reduction of I_2 at the very low KI level used. If $[I^-]_T \approx 2 \times 10^{-5}$ instead of $1.07 \times 10^{-5} M$, then b is ~ 0.3 . Thus there is convincing proof that the composition of the bound species is drastically different from that at high KI. The value of b is understood to be an average approximate value over the isotherm, and it should reflect conditions well at $\theta = 0.5$, where most of our conclusions are drawn. A more refined model would use a variable b as a function of Θ . The apparent change of b from 0 to 1 with KI leads to the postulate of the quasi-one-dimensional binding constant K_B which is the analog to K_F of the free triiodide equilibrium. The value of K_B will depend on KI, since K_{st} is found to change as a function of KI. However, K_B shows in a qualitative fashion that a competition exists between the I_2 and I_3^- species for a binding site. The average over-all composition of the sum of the bound I_2 and I_3^- species is expressed formally in terms of $I_2 \cdot I_b$, whereas it is the I_2 and I_3^- species that are considered to bind. This is to say that at low KI the equilibrium in the bound state is shifted toward I_{2b} , in the direction of the limiting model. The extrapolated binding constant for limiting I_2 binding is predicted to be approximately $10^3 M^{-1}$ or less from Figure 13. At high KI the limiting $1/m$ model leads to I_3^- , whereas predictions based on the one-dimensional Ising model lead to I_4^{2-} as the binding species. Robin's¹⁹ polytriiodide as well as Murakami's²⁰ I_4^{2-} model (in the solid state) seem to be formally supported, although data obtained in homogeneous solution should be applied only with care to the solid complex, since the two systems are separated by a heterogeneous phase change. Thus in aqueous solution the polyelectrolyte character of the AI complex is enhanced as KI increases where K^+ is the counterion.

(28) F. L. Bates, D. French, and R. E. Rundle, *J. Amer. Chem. Soc.*, **65**, 142 (1943).

(29) R. R. Baldwin, R. S. Bear, and R. E. Rundle, *ibid.*, **66**, 111 (1944).

(30) R. S. Stein and R. E. Rundle, *J. Chem. Phys.*, **16**, 195 (1948).

(31) R. E. Rundle, J. F. Foster, and R. R. Baldwin, *J. Amer. Chem. Soc.*, **66**, 2116 (1944).

(32) P. K. Rawlings and F. W. Schneider, *J. Chem. Phys.*, **50**, 3707 (1969).

Up to the present time the main proof that I_3^- is the binding species at *all* KI concentrations has been the work of Kontos.¹⁴ However, if the triiodide equilibrium and the amount of bound I_2 are taken into account a recalculation of Kontos' data assuming I_3^- binding predicts his spectrophotometric results with unsatisfactory accuracy.^{1b} We therefore conclude that Kontos' often cited work does not strictly support I_3^- binding at very low KI in accordance with our work; for a quantitative discussion see ref 1b. In the closely related benzamide-triiodide solid complex which is used as a model of the AI complex³³ the triiodide ion chains in the crystal are slightly nonlinear with a normal 2.92-Å interval distance per triiodide and a distance of separation between adjacent triiodide ions of only 3.80 Å, which is considerably shorter than the van der Waals distance of 4.7 Å. The Coulomb repulsion between the similarly charged I_3^- ions is evidently overcome by attractive forces. According to Robin⁹ the latter are largely due to dispersion forces as seen from a calculation of the second-order mixing term in the exciton coupled triiodide chain. As more I^- ions are taken up in the AI complex the attractive interactions are more and more compensated by increasing repulsion as seen from the decrease of K_{st} beyond the maximum. On the other hand, this decrease might be artifact of the model which does not consider higher order interactions (which might be important, especially at low ionic strengths) nor parallel aggregation of helices which is likely to occur at higher KI. The latter would tend to decrease the nearest neighbor interactions per nearest neighbor pair, while intrinsic binding to the matrix might then increase. As seen from the existence of the blue benzamide-triiodide complex, it is not necessary that the matrix be of helical configuration in order for the iodine species to bind. For example, a solid water structure provides the rigid matrix in the case of frozen I_3^- solutions¹⁴ such that the trapped I_3^- species can interact with each other to give the blue color. Thus the interaction with the "rigid-preformed" lattice seems to be rather unspecific.¹⁹

As concluded earlier³ there seems to be no experimental evidence that a helix coil transition occurs in the temperature range employed for the present neutral aqueous solutions. Our early kinetic measurements by the temperature jump method^{1a} show an electric field and Θ -dependent dichroism in the microsecond region which is caused by the parallel alignment of the AI helices¹¹ while the condenser discharges into the solu-

tion (ionic strength of 10^{-2}). This transient dichroic effect may obscure any relaxation time which could be due to the rapid portion of the binding process. Concentration-dependent relaxation times which were measured in the millisecond region were attributed to the contributions of the slower portion of the cooperative binding equilibrium.^{1a} According to Rao and Foster³⁴ a partial breakdown of the already deformed helical structure occurs above pH 12. Hence, the temperature dependence of the blue band in this study is due to the temperature dependence of the binding equilibrium in which the helical backbone remains essentially intact. Some additional experiments have shown that the experimental adsorption isotherms are independent of amylose concentration.

The proposed model for I_2/I_3^- binding in this study describes the stoichiometry and cooperativity of the AI complex to a good approximation, and it unifies a large body of literature data.² It is likely that the limitation of the spectrophotometric method and the oversimplification of the one-dimensional model do not warrant better agreement than that actually found. Refinements such as higher order nearest neighbor interactions^{35,36} might be introduced for the long-range electrostatic interactions. A more realistic statistical description of the complex is to treat adsorption and mutual interactions of limiting species as a competitive process for which exact model calculations are presently being made. Recent ruby laser studies³⁷ have shown an interesting optical property of the AI complex in aqueous solution; it represents a novel class of optically saturable absorbers capable of passive Q switching. This Q switch action has been shown to produce giant laser pulses in a ruby laser.³⁷

Acknowledgment. We thank Miss Maymie Chenoweth of the Department of Biological Sciences for the enzymatic analysis of amylose solutions, and Mr. P. K. Rawlings for performing the nonlinear least-squares calculations on a Honeywell 800 computer. F. W. S. gratefully acknowledges a Frederick Gardner Cottrell grant administered by the Research Corporation.

(33) J. M. Reddy, K. Knox, and M. B. Robin, *J. Chem. Phys.*, **40**, 1082 (1964).

(34) V. S. Rao and J. F. Foster, *Biopolymers*, **1**, 527 (1963), and references therein.

(35) M. E. Baur and L. H. Nosanow, *J. Chem. Phys.*, **37**, 153 (1962).

(36) S. Lifson, *ibid.*, **40**, 3705 (1964).

(37) L. Huff, L. G. DeShazer, and F. W. Schneider, *Photochem. Photobiol.*, in press.

The Hydration of Propionaldehyde, Isobutyraldehyde, and Pivalaldehyde. Thermodynamic Parameters, Buffer Catalysis, and Transition State Characterization¹

by Y. Pocker² and D. G. Dickerson³

Department of Chemistry, University of Washington, Seattle, Washington 98105 (Received February 18, 1969)

Values of the thermodynamic parameters ΔG° , ΔH° , and ΔS° for the reversible hydrations of propionaldehyde, isobutyraldehyde, and pivalaldehyde were determined using a spectrophotometric method. Short extrapolations of absorbancy to time zero allow the accurate determination of the molar extinction coefficient for the $n-\pi^*$ absorption of the unhydrated aldehydes in water solvent. Kinetic data on the hydronium ion, acetic acid, acetate ion, dihydrogen phosphate ion, monohydrogen phosphate ion, diethylmalonate dianion, hydroxide ion, and water catalysis are presented for all three aldehydes. The data are shown to be consistent with a concerted mechanism of hydration-dehydration.

Introduction

Although the zinc metalloenzyme erythrocyte carbonic anhydrase was once thought to catalyze only one reaction—the reversible hydration of carbon dioxide—it has been shown in these laboratories that the enzyme very efficiently catalyzes the addition of the elements of water to a great variety of carbonyl systems.⁴⁻⁹ We have recently shown that the reversible hydrations of aliphatic aldehydes are useful reactions for delineating the steric requirements of this enzyme.¹⁰ These reactions proceed at an appreciable rate in the absence of enzyme and are furthermore susceptible to general acid-base catalysis. Consequently, as a prerequisite to the study of enzymatic catalysis, it was necessary to characterize thermodynamically and kinetically the nonenzymatic hydrations of propionaldehyde, isobutyraldehyde, and pivalaldehyde.

The first part of the present paper reports the thermodynamic parameters associated with the reversible hydrations of these aldehydes and compares them with the results of previous studies on related compounds.¹¹⁻¹⁶ The second part of the present paper examines the catalytic coefficients at 0.0° for water, hydronium ion, hydroxide ion, diethylmalonate dianion, acetic acid, acetate ion, monohydrogen phosphate, and dihydrogen phosphate ions for the hydration of each aldehyde and for the dehydration of the corresponding hydrate. Earlier studies from our laboratory have kinetically characterized the catalytic coefficients at 0.0° for these buffer components with respect to the hydration of acetaldehyde¹⁷ and 2- and 4-pyridine aldehydes^{18,19} both in H₂O and D₂O.

For proton transfer reactions, the Brønsted catalysis law has often been interpreted on the basis of free energy curves.²⁰ The interpretation is apparently

valid when curves cross on the reasonably straight part of the energy walls.^{21,22} However, as Brønsted himself suggested,²³ one could not expect the law to

(1) This work was supported by U. S. Public Health Service grants from the National Institutes of Health.

(2) Author to whom correspondence should be addressed.

(3) (a) National Science Foundation Fellow, Summer 1966; Chevron Research Company Fellow, 1966-1967. (b) Taken in part from the Ph.D. Thesis of D. G. Dickerson, University of Washington, 1967.

(4) (a) Y. Pocker and J. E. Meany, "Abstracts of the Sixth International Congress of Biochemistry," Vol. IV, 132, New York, N. Y., 1964, p 327; (b) Y. Pocker and J. E. Meany, *J. Amer. Chem. Soc.*, **87**, 1809 (1965).

(5) Y. Pocker, J. E. Meany, D. G. Dickerson, and J. T. Stone, *Science*, **150**, 382 (1965).

(6) Y. Pocker and J. E. Meany, *Biochemistry*, **4**, 2535 (1965).

(7) Y. Pocker and J. E. Meany, *ibid.*, **6**, 239 (1967).

(8) Y. Pocker and J. T. Stone, *ibid.*, **6**, 668 (1967).

(9) Y. Pocker and D. R. Storm, *ibid.*, **7**, 1202 (1968).

(10) Y. Pocker and D. G. Dickerson, *ibid.*, **7**, 1995 (1969).

(11) E. Lombardi and P. B. Sogo, *J. Chem. Phys.*, **32**, 635 (1960).

(12) (a) R. P. Bell, *Advan. Phys. Org. Chem.*, **4**, 1 (1966), and references quoted therein; (b) R. P. Bell and P. G. Evans, *Proc. Roy. Soc.*, **A291**, 297 (1966).

(13) L. C. Gruen and P. T. McTigue, *J. Chem. Soc.*, 5217 (1963).

(14) (a) J. Hine, J. G. Houston, and J. H. Jensen, *J. Org. Chem.*, **30**, 1184 (1965); (b) J. Hine and J. G. Houston, *ibid.*, **30**, 1328 (1965).

(15) G. E. Leinhard and W. P. Jencks, *J. Amer. Chem. Soc.*, **88**, 3982 (1966).

(16) (a) P. Greenzaid, Z. Luz, and D. Samuel, *J. Amer. Chem. Soc.*, **89**, 749 (1967); (b) P. Greenzaid, Z. Rappoport, and D. Samuel, *Trans. Faraday Soc.*, **63**, 2131 (1967).

(17) Y. Pocker and J. E. Meany, *J. Phys. Chem.*, **71**, 3113 (1967).

(18) Y. Pocker and J. E. Meany, *ibid.*, **72**, 655 (1968).

(19) Y. Pocker and J. E. Meany, *ibid.*, **73**, 1857 (1969).

(20) See, for example, R. P. Bell, "The Proton in Chemistry," Cornell University Press, Ithaca, N. Y., 1959, p 168.

(21) J. E. Leffler and E. Grunwald, "Rates and Equilibria of Organic Reactions," John Wiley and Sons, Inc., New York, N. Y., 1963, p 157.

(22) R. A. Marcus, *J. Phys. Chem.*, **72**, 891 (1968).

(23) J. N. Brønsted and K. J. Pedersen, *Z. Phys. Chem.*, **108**, 185 (1924).

hold over wide values of the acid dissociation constant K . Paradoxically, it is the proton transfer reactions which obey the Brønsted catalysis law over *too* wide a range of pK that are now in need of explanation.^{12b,17,24} The observations reported in the present study are discussed in terms of possible mechanistic pathways for both general acid and general base catalysis.

Experimental Section

Materials. Propionaldehyde, isobutyraldehyde, and pivalaldehyde (J. T. Baker) were fractionally distilled under nitrogen. An electrically heated 20-cm column of Heli-Pak was used for this purpose. In this manner, the small amounts of carboxylic acids usually present in these aldehydes were removed. After purification, the acid content was shown to be less than 0.05 mol % as determined titrimetrically. The acid content remained below 0.20% for several weeks provided full vials of the aldehydes were stored in the dark at -5° in nitrogen-flushed containers.

Sodium salts of the mono- and dianion of diethylmalonic acid, prepared by previously described procedures, were employed as buffers in the pH range 6.3–8.2. Phosphate and acetate buffers were prepared from commercially available analytical grade reagents and were titrated with standard hydrochloric acid or sodium hydroxide in order to verify concentrations.

Reaction rates were determined with a Beckman Model DU ultraviolet spectrophotometer. A specially constructed cell compartment containing a motor-driven stirring device and calibrated thermometer was filled with a methanol–water mixture. The contents of this compartment were maintained at 0.0° by circulating a coolant (ethylene glycol–water) at a precisely regulated temperature through a coil in the compartment. The coolant was supplied by a Forma-Temp Jr. Model 2095-1 refrigeration unit which contained, in addition to the thermostating mechanism, a pump to circulate the coolant. The low temperature used in these studies made the frequent change of desiccant in the phototube housing imperative.

All pH determinations were made with a Beckman Model H2 glass-electrode pH meter. The pH of reaction solutions was determined directly without dilution. Standardization was accomplished with Beckman standard buffer solutions.

Method. Aqueous solutions of all reactants except aldehyde were pipetted into the silica cells which were then placed in the cell compartment and allowed to equilibrate thermally. The differences in absorbancy between the various reactant cells and the reference cell were recorded. Aldehyde was withdrawn from a stoppered glass serum vial with a calibrated Hamilton microliter syringe and injected into the cell to initiate the run. It was necessary to shake the contents to ensure that all material was in solution. The rate of diminution of absorbance (propionaldehyde; λ_{\max} 277.5

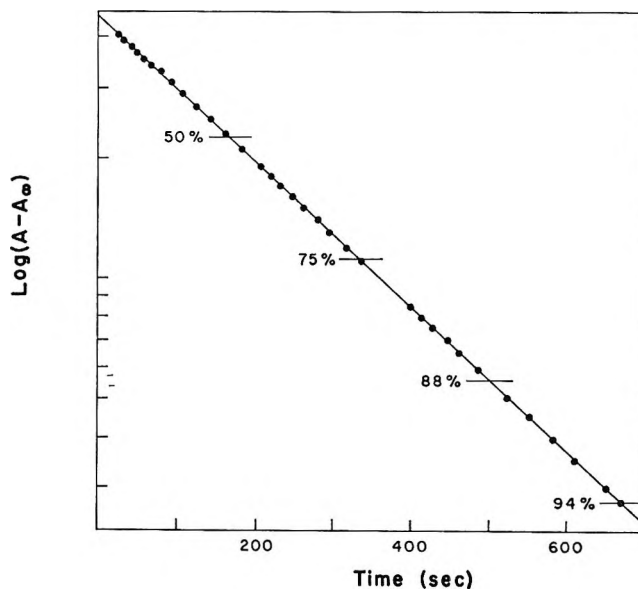


Figure 1. Semilog plot of kinetic data from typical run; [propionaldehyde] = 0.0433 M . Kinetics followed at 277.5 $m\mu$; 0.0° .

$m\mu$; isobutyraldehyde; λ_{\max} 284 $m\mu$; pivalaldehyde; λ_{\max} 285.5 $m\mu$) was taken as a measure of the rate of approach to equilibrium. The absolute value of the slope of a plot of $\ln(A_t - A_\infty)$ vs. time (with A_t representing the absorbance at any time t during the course of the reaction and A_∞ representing the absorbance at equilibrium) is numerically equal to the pseudo-first-order rate constant, k_{obsd} . Because the rate of approach to equilibrium is determined, $k_{\text{obsd}} = k_f + k_r$, where k_f is the rate constant for hydration and k_r that for dehydration. These kinetic plots were linear for a minimum of three half-lives, as shown in Figure 1. The rates were such that half-lives ranged from 0.5 to 25 min. Data for the faster reactions were recorded on tape for subsequent playback and analysis.

The equilibrium extinction coefficients at the wavelength of maximal absorbance, ϵ_∞ , were determined by two methods. The first of these involved weighing various amounts of aldehyde into buffers and determining equilibrium absorbance. The second technique involved calculating the molar extinction coefficients at equilibrium from runs in which the aldehyde was introduced *via* calibrated Hamilton microliter syringes. The two techniques furnished virtually the same value for ϵ_∞ . The spectra of the aldehydes prior to hydration and following equilibration at 0.0° are depicted in Figure 2.

Results

Short extrapolations of the kinetic plots to $t = 0$ furnished an intercept, $A_0 - A_\infty$, and, with knowledge of the equilibrium absorbance A_∞ , it was possible to

(24) M. Eigen, *Discussions Faraday Soc.*, **39**, 7 (1965).

Table I: Thermodynamic Parameters for Aldehyde Hydration

Aldehyde	ϵ_0 (λ_{\max}) ^{a,b}	K_{eq} ^{b,c}	ΔH° ^d	ΔS° ^e
CH ₃ CH ₂ CHO	18.7 ± 0.2, <i>n</i> = 110 (277.5)	1.98 ± 0.02, <i>n</i> = 149	-5.4 ± 0.2	-18.3 ± 0.6
(CH ₃) ₂ CHCHO	22.7 ± 0.2, <i>n</i> = 88 (284)	1.58 ± 0.017, <i>n</i> = 110	-5.8 ± 0.2	-20.4 ± 0.7
(CH ₃) ₃ CCHO	18.7 ± 0.4, <i>n</i> = 25 (285.5)	0.47 ± 0.007, <i>n</i> = 23	-4.4 ± 0.2	-17.6 ± 0.8

^a M⁻¹ cm⁻¹ (m μ). ^b \pm refer to 99% confidence limits based on *n* observations. ^c 0.0°. ^d kcal mol⁻¹. ^e cal mol⁻¹ deg⁻¹.

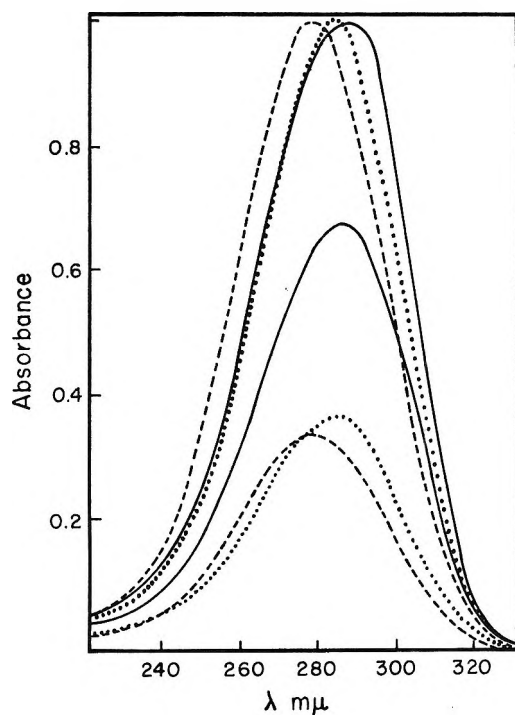


Figure 2. Ultraviolet spectra in aqueous solution at 0.0°. Upper three curves prior to hydration: ---, 0.0547 *M* propionaldehyde; ··· 0.0449 *M* isobutyraldehyde; —, 0.0544 *M* pivalaldehyde. Lower three curves: same solution following equilibration.

calculate the molar extinction coefficients, ϵ_0 , of the unhydrated aldehydes in aqueous solution and equilibrium constants, K_{eq} , as defined by eq 1.

$$K_{\text{eq}} = \frac{(a_{\text{Hydr}})_{\text{eq}}}{(a_{\text{Alid}})_{\text{eq}}} = \frac{[\text{Hydrate}] f_{\text{H}}}{[\text{Aldehyde}] f_{\text{A}}} = \frac{(A_0 - A_\infty) f_{\text{H}}}{A_\infty f_{\text{A}}} \quad (1)$$

The ratio of activity coefficients of hydrate and aldehyde, ($f_{\text{H}}/f_{\text{A}}$), was considered to be unity except for certain special experiments in which very large concentrations of salt were specifically utilized to study this ratio. Presented in Table I are the experimentally observed values of ϵ_0 and K_{eq} as determined at 0.0° for each of the aldehydes studied.

It is interesting to compare values of K_{eq} obtained in this work with the results of previous workers, but most of these older data were obtained either at an unspecified temperature or a temperature other than 0.0°. Gruen and McTigue pointed out that the values of K_{eq} for the hydration of propionaldehyde and isobutyral-

dehyde are very sensitive to temperature.¹³ In order to permit such a comparison, then, it was necessary to vary the temperature of equilibrated solutions of the aldehydes and observe the corresponding changes in absorbancy. A few kinetic runs at 25° established that ϵ_0 is, as expected, temperature invariant over the range 0–25°. Utilization of the kinetic method to determine ϵ_0 at even higher temperatures was not considered to be sufficiently accurate due to the greatly enhanced rate of reaction at these higher temperatures. Thus, these studies furnished values of K_{eq} as a function of temperature, as presented in Table II. The values

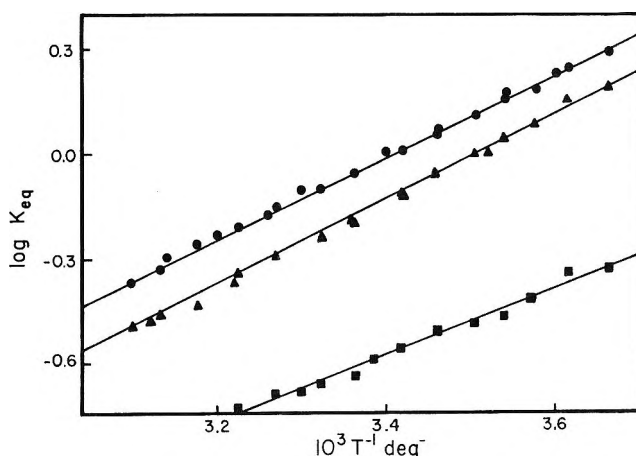


Figure 3. Logarithms of equilibrium constants as functions of reciprocal absolute temperature: ●, propionaldehyde; ▲, isobutyraldehyde; ■, pivalaldehyde.

of ΔH° and ΔS° obtained from Figure 3 are presented in Table I. The values of K_{eq} reported by earlier workers are presented in Table III together with values of the present study at the same temperature as determined from Figure 3. The agreement is generally poor with respect to those workers who utilized spectral methods to measure the equilibrated solutions and various indirect methods to estimate the spectral characteristics of the same solutions prior to hydration. None of these workers utilized a kinetic technique which permits virtually direct observation of the aldehyde solutions prior to hydration, $t = 0$. However, agreement is excellent with those studies in which K_{eq} was determined by examining the integrated nmr spectra of aqueous aldehyde solutions. This latter technique, which provides information on both com-

Table II: Hydration Equilibria at Various Temperatures

$T, ^\circ\text{K}$	K_{eq}^a	$T, ^\circ\text{K}$	K_{eq}^a	$T, ^\circ\text{K}$	K_{eq}^a
Propionaldehyde					
273.0	1.98	289.2	1.14	307.0	0.67
276.7	1.78	293.0	1.04	310.0	0.61
278.0	1.70	294.2	1.02	313.3	0.58
280.1	1.54	297.5	0.87	315.5	0.55
282.5	1.46	298.0	0.89	319.0	0.51
282.7	1.44	301.5	0.785	319.3	0.465
285.4	1.29	303.8	0.785	322.8	0.425
289.0	1.18	306.0	0.70		
Isobutyraldehyde					
273.0	1.58	289.5	0.88	310.2	0.45
276.7	1.43	292.6	0.76	311.0	0.42
280.1	1.22	297.9	0.63	314.8	0.37
282.7	1.11	298.0	0.64	319.3	0.34
284.3	1.005	301.0	0.58	321.0	0.33
285.4	0.99	305.9	0.50	322.6	0.32
Pivalaldehyde					
273.0	0.47	285.4	0.33	297.5	0.235
276.7	0.45	289.0	0.31	301.0	0.22
280.1	0.39	292.6	0.28	303.8	0.21
282.7	0.345	295.5	0.26	305.9	0.205

^a K_{eq} as defined in eq 1.

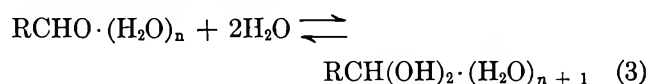
ponents of the equilibrium, is expected to be more reliable than the other methods previously employed.

As first pointed out by Gruen and McTigue, changes in water activity induced by high salt concentrations will disrupt the equilibrium ratio of [Hydrate]/[Aldehyde].¹³ This feature was examined in the present study also since the results obtained by Gruen and McTigue in the absence of salts were not in agreement with those obtained in this work and by Hine.¹⁴ The presence of large quantities of salt lowers the equilibrium ratio of the hydrate to aldehyde, and it is concluded from (1) that the ratio $f_{\text{H}}/f_{\text{A}}$ is therefore increasing. Gruen and McTigue pointed out a method for correlating changes in $f_{\text{H}}/f_{\text{A}}$ with changing salt concentration.¹³ This method, developed by Robinson and Stokes²⁵ and subsequently modified by Gluekauf,²⁶ takes the form of eq 2

$$\log (f_{\text{H}}/f_{\text{A}}) = (h' + 1) \{ [0.018m_1(r_1 + h_1 - 2)/2.3(1 + 0.018m_1r_1)] - \log a_{\omega} \} \quad (2)$$

Equation 2 relates the ratio of activity coefficients of the hydrate and aldehyde to the salt molality, m_1 , in terms of the difference in hydration number of the hydrate and aldehyde, h' , the ratio of the partial molar volume of the electrolyte to that of water, r_1 , hydration number of the electrolyte, h_1 , and water activity, a_{ω} . This equation for 1:1 electrolytes ($\nu = 2$), although disregarding electronic factors, is expected to furnish reasonably accurate estimates of the parameter h' . The ratio [Hydrate]/[Aldehyde] was determined in the presence of varying quantities of NaCl; these ratios,

in conjunction with the values obtained in very dilute buffers ($5\text{--}10 \times 10^{-3} M$), provided values of $f_{\text{H}}/f_{\text{A}}$, which as evidenced by Figure 4, are most consistent with $(h' + 1) = 2$ for all aldehydes. This would indicate the equilibrium to be best expressed by



where n is either zero or an integral value. In view of the different ultraviolet spectra obtained in water and nonaqueous solvents, it is likely that n is not zero. Also, n is not likely to be greater than 1, so the aldehyde is most probably hydrogen bonded to one water molecule and the hydrate to two.

The rate of hydration of each of the aldehydes was studied as a function of pH in each of three buffers: acetate, diethylmalonate, and phosphate. The reactions are general acid-general base catalyzed; hence, k_{obsd} may be expressed by the sum of terms

$$k_{\text{obsd}} = k_0 + k_{\text{H}_3\text{O}^+}[\text{H}_3\text{O}^+] + k_{\text{OH}^-}[\text{OH}^-] + k_{\text{HA}}[\text{HA}] + k_{\text{A}^-}[\text{A}^-] \quad (4)$$

The values of the catalytic coefficients for hydronium ions, $k_{\text{H}_3\text{O}^+}$, hydroxide ions, k_{OH^-} , the protonated constituent of the buffer, k_{HA} , and for its conjugate base, k_{A^-} , as well as the spontaneous term k_0 , were deter-

(25) R. H. Robinson and R. A. Stokes, *Trans. Faraday Soc.*, **53**, 301 (1957).

(26) E. Gluekauf, "The Structure of Electrolytic Solutions," W. J. Hamer, Ed., John Wiley and Sons, Inc., New York, N. Y., 1959, p 97; cf. also, E. Gluekauf, *Trans. Faraday Soc.*, **51**, 1235 (1955).

Table III: Comparison of Thermodynamic Parameters for Aldehyde Hydration

	$\epsilon_0, M^{-1} \text{ cm}^{-1}$		K_{eq}^a	$\Delta H^\circ, \text{ kcal/mol}^{-1}$	$\Delta S^\circ, \text{ cal mol}^{-1} \text{ deg}^{-1}$
$\text{CH}_3\text{CH}_2\text{CHO}$	18.3, ^b 17.7 ^c	25°:	0.87, ^b 0.69 ^c	-5.4, ^b -6.5 ^c	-18.3, ^b -22.5 ^c
$(\text{CH}_3)_2\text{CHCHO}$	22.3, ^b 17.7 ^c	25°:	0.66, ^b 0.61, ^d 0.44 ^c	-5.8, ^b -7.3, ^c -6.5 ^d	-20.4, ^b -26, ^c -26.9 ^d
		35°:	0.43, ^b 0.47 ^c		
$(\text{CH}_3)_3\text{CCHO}$	18.4, ^b 18.5 ^o	25°:	0.24, ^b 0.24, ^e 0.1, ^f 0.24 ^o	-4.4, ^b -4.4 ^o	-17.6, ^b -18 ^o
		14.5°:	0.32, ^b 0.24 ^o		
		4°:	0.42, ^b 0.33 ^o		

^a As defined by eq 1. ^b Present work. ^c Reference 13. ^d Reference 14. ^e Reference 16a. ^f Reference 15. ^o Reference 16b.

Table IV: Comparison of Catalytic Coefficients for Aldehyde Hydrations at 0.0°^a

	CH_3CHO	$\text{CH}_3\text{CH}_2\text{CHO}$	$(\text{CH}_3)_2\text{CHCHO}$	$(\text{CH}_3)_3\text{CCHO}$
$k_{\text{H}_2\text{O}}^b$	0.0011/55.5	0.000931/55.5	0.000515/55.5	0.000125/55.5
$k_{\text{H}_3\text{O}^+}^c$	130	121	97.5	31.4
$k_{\text{OH}^-}^c$	7.91×10^3	2.35×10^3	1.77×10^3	6.30×10^3
$k_{\text{A}^-}^c, d$	0.035	0.040	0.0245	0.0016
k_{HOAc}^c	0.0805	0.0751	0.049	0.0157
$k_{\text{OAc}^-}^c$	0.0154	0.0146	0.098	0.00256
$k_{\text{H}_2\text{PO}_4^-}^c$	0.189	0.146	0.123	0.032
$k_{\text{HPO}_4^{2-}}^c$	0.42	0.312	0.202	0.045

^a Coefficients utilized to calculate rate constants, k_{calcd} , for comparison with k_{obsd} as per Table V. ^b $k_{\text{H}_2\text{O}} = k_0/55.5$; k_0 in sec^{-1} ; $k_{\text{H}_2\text{O}}$ in $M^{-1} \text{ sec}^{-1}$. ^c $M^{-1} \text{ sec}^{-1}$. ^d Catalytic coefficient for diethylmalonate dianion.

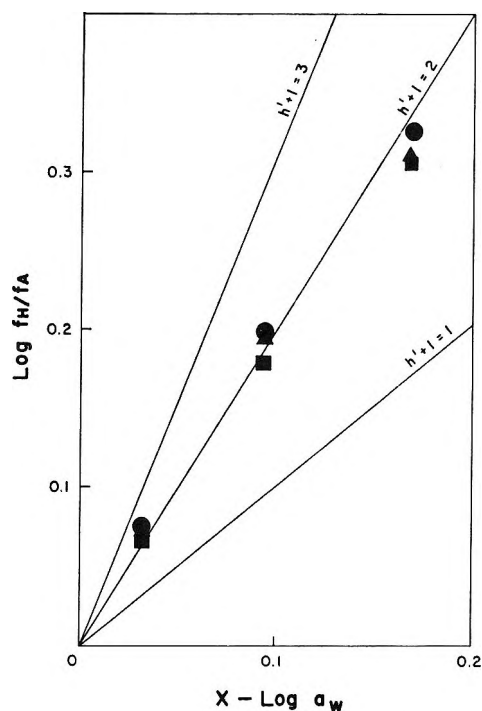


Figure 4. Solvation number of *gem* diols relative to unhydrated aldehydes in aqueous solution: ●, propionaldehyde; ▲, isobutyraldehyde; ■, pivalaldehyde.

mined in the following manner. Plotting the rates obtained in 0.0100 *M* acetate buffer as a function of hydrogen ion concentration furnished a linear relationship, the slope of which was considered a reasonable

first approximation to $k_{\text{H}_3\text{O}^+}$. The data obtained in 0.0100 *M* diethylmalonic acid was plotted as a function of hydroxide ion concentration to furnish a relationship which was linear over a substantial pH range. The slope of the linear portion was taken as a reasonable approximation to k_{OH^-} and the extrapolated intercept was taken as the first approximation to k_0 . With these values as a starting point, all coefficients were evaluated by a series of successive approximations continued until further extension of the procedure did not alter the parameters. The values so obtained, summarized in Table IV, reproduce the observed rate constants to within the limits of experimental uncertainty (Table V). This comparison refers to 0.01–0.1 *M* buffers. Previous workers have concluded that, with reference to aldehyde hydration reactions, catalytic coefficients for various bases show poor correlation with their relative strengths as bases in terms of the Brønsted relationship. A recent investigation of glucose mutarotation in our laboratory, however, shows excellent accord, excepting diethylmalonate dianion which was 0.8 log unit below a line correlating 11 other bases.²⁷ Furthermore, as indicated by Figure 4, the present study furnished a linear relationship over 17 p*K* units for all three aldehydes examined, and the slopes of these three plots were virtually identical (Table V). Again, it was noted that the dianion of diethylmalonic

(27) Y. Pocker, J. W. Long, D. Dahlberg, and T. C. Lacalli, unpublished observations.

Table V: Comparison of Calculated and Observed Rate Constants^a

	Propionaldehyde			Isobutyraldehyde			Pivalaldehyde		
	pH	10 ³ <i>k</i> _{calcd}	10 ³ <i>k</i> _{obsd}	pH	10 ³ <i>k</i> _{calcd}	10 ³ <i>k</i> _{obsd}	pH	10 ³ <i>k</i> _{calcd}	10 ³ <i>k</i> _{obsd}
0.0100 <i>M</i> Diethylmalonic acid	5.38	2.23	2.26	6.12	1.01	1.02	6.12	0.478	0.457
	6.32	1.57	1.57	6.36	1.00	0.98	6.21	0.464	0.480
	6.62	1.59	1.61	6.63	0.98	0.99	6.46	0.441	0.435
	6.90	1.67	1.66	7.14	1.08	1.04	6.80	0.437	0.486
	7.17	1.77	1.77	7.19	1.10	1.10	6.97	0.444	0.480
	7.20	1.78	1.79	7.21	1.11	1.09	7.39	0.488	0.502
	7.45	1.92	1.94	7.46	1.20	1.21	7.77	0.584	0.566
	7.56	2.00	2.05	7.61	1.28	1.22	7.89	0.645	0.647
	7.81	2.19	2.18	7.79	1.39	1.41	8.10	0.765	0.738
	8.00	2.40	2.40	8.05	1.62	1.61	8.30	0.964	0.976
	8.13	2.58	2.56	8.23	1.86	1.85			
8.20	2.71	2.70							
0.0100 <i>M</i> Acetic acid	4.28	11.70	12.28	4.14	13.45	13.57	4.20	7.18	7.20
	4.38	10.20	10.27	4.22	11.58	11.50	4.30	5.88	5.85
	4.44	9.27	9.20	4.40	8.10	8.23	4.50	3.97	4.00
	4.49	8.65	8.43	4.56	6.01	5.96	4.72	2.64	2.59
	4.61	7.07	6.83	4.73	4.48	4.28	4.92	1.88	1.90
	4.63	6.42	6.17	5.04	2.78	2.84	5.24	1.19	1.21
	4.84	4.70	4.85	5.31	1.98	2.17	5.61	0.78	0.75
	4.90	4.29	4.37	5.50	1.65	1.76			
	4.99	3.77	3.92						
	5.22	3.19	3.04						
	5.52	2.44	2.26						
	5.81	2.09	2.01						
	5.92	1.94	1.93						
0.100 <i>M</i> Acetic acid	4.17	24.9	24.7				4.17	11.6	11.7
	4.59	14.7	14.6	4.20	18.8	18.3	4.33	9.13	9.2
	5.00	9.25	9.14	4.32	16.0	16.3	4.73	5.25	5.42
	5.34	6.61	6.64	4.72	9.47	9.53	5.19	2.91	3.05
				5.19	5.50	5.74	5.50	2.08	2.16
0.00500 <i>M</i> Phosphate	6.01	2.75	2.77	5.96	2.03	2.04	6.01	0.99	1.01
	6.60	2.77	2.76	6.63	2.01	2.14	7.12	1.01	1.01
	7.16	3.08	3.12	7.11	2.15	2.10	7.58	1.11	1.14
	7.61	3.51	3.47	7.60	2.40	2.36	7.71	1.16	1.16
	7.81	3.72	3.75	7.71	2.49	2.51			

^a Calculated and observed rate constants are reported in sec⁻¹.

acid was 0.8–1.4 log units below these lines defined by H₂O, OH⁻, CH₃CO₂⁻, and HPO₄²⁻.²⁸

Discussion

In the past, many workers have attempted to measure the equilibrium composition of aqueous solutions of the presently investigated series of aliphatic aldehydes. The most commonly employed technique has been the measurement of the intensity of the n-π* carbonyl absorption band around 280 mμ which diminishes on hydration. These studies have always suffered from the fact that accurate values were only available for equilibrated solutions; the main uncertainty in these measurements lies in the value to be ascribed to ε₀, the maximum extinction coefficient of the unhydrated carbonyl compound. It has been the custom to equate ε₀ in H₂O with that in a nonhydroxylic solvent such as hexane, but this is not strictly valid since the intensities of n-π* transitions and the shape of the bands vary

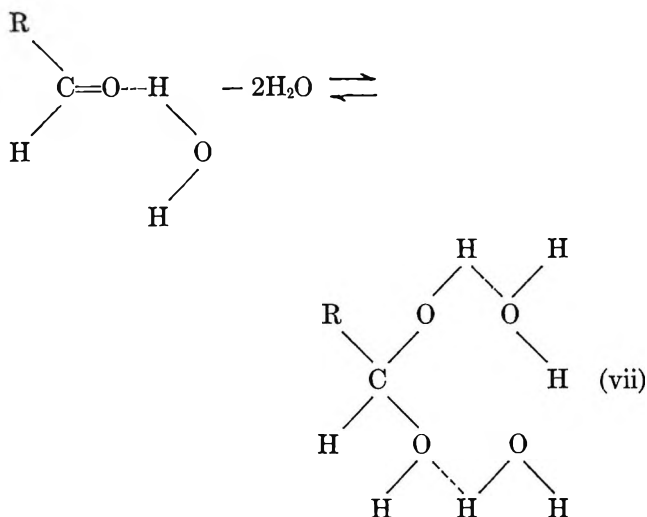
somewhat with solvent. More recently, nmr measurements have permitted estimation of the concentration of both components, but at higher aldehyde concentrations which in turn led to a decrease in water activity.^{29,30} The technique described in this paper has permitted virtually direct observation of the intensity of the n-π* transitions of aldehyde solutions prior to hydration, as well as following equilibration, and, therefore, provides very accurate values of *K*_{eq} over a sufficiently wide

(28) For all three hydrations, the HPO₄²⁻ anion is *ca.* nine times more active as a catalyst than imidazole. Similarly, the catalytic constants for OH⁻ and H₂O are *ca.* eight times as great as those predicted from a line drawn through monofunctional basic catalysts (pyridine, imidazole, C₆Cl₅O⁻, SO₃²⁻, CO₃²⁻, and H₂BO₃⁻).²⁷ It is attractive to suggest that H₂O, CH₃CO₂⁻, HPO₄²⁻ and OH⁻ operate as bifunctional catalysts when hydrogen bonded to one or more water molecules.¹⁷

(29) Interpretation of *K*_{eq} values from nmr data on concentrated solutions of aldehydes may be vitiated by the presence of dimers such as (RCHOH)₂O.³⁰

(30) M. L. Ahrens and H. Strehlow, *Discussions Faraday Soc.*, **39**, 112 (1965).

whereas in (vi) (shown for general base catalysis) the ring is composed (formally) only of water molecules and aldehyde. Similarly, water molecules could be incorporated as bridges in (ii) and (iv). The advantage of utilizing water bridges, in either a cyclic or acyclic mechanism, is that acids and bases would be expected to show good correlation as observed with the Brønsted relation—regardless of the structural type of the acid or base. Transition states similar to (v) or (vi) may well possess one advantage not immediately apparent in (ii) or (iv). The salt effects, as analyzed in the preceding section, could be presented as in (vii).



Inasmuch as the type of solvation depicted in (vii) stabilizes the aldehyde and hydrate, it would be attractive to invoke similar stabilization of the activated complex leading to this product. The similarity between product vii and transition state vi is immediately apparent.

It is interesting to compare the relative values of catalytic constants for hydration and dehydration within the series of aldehydes which has been examined. In general, the values of the catalytic coefficients, relative to acetaldehyde as 100, are approximately 85 (propionaldehyde), 60 (isobutyraldehyde), and 20 (pivalaldehyde); the relative values of the coefficients for dehydration are then approximately 43.5 (acetaldehyde hydrate), 43 (propionaldehyde hydrate), 38 (isobutyraldehyde hydrate), and 21 (pivalaldehyde hydrate). The inductive effect of the three methyl groups would tend to neutralize the dipolar character of the carbonyl group of pivalaldehyde and it would be expected to hydrate slower than, say, acetaldehyde. The transition state is probably more polar than the hydrate, so

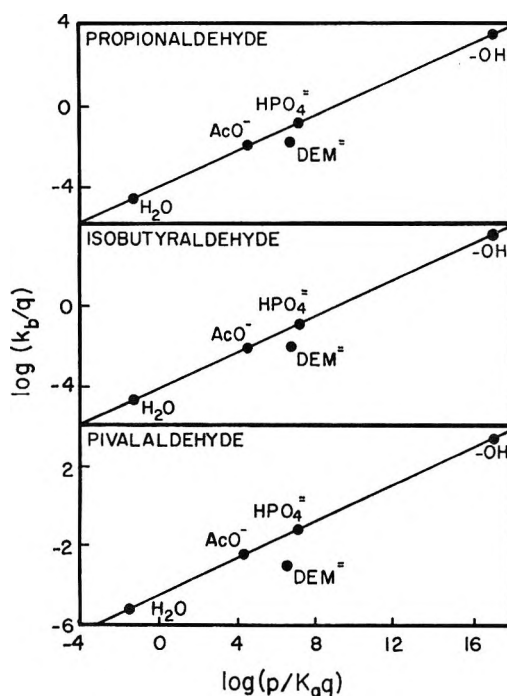


Figure 5. Brønsted plots of $\log k_b/q$ vs. $\log (p/K_aq)$ for propionaldehyde, isobutyraldehyde, and pivalaldehyde. (Values of pK_a taken at 0.0°).

this same inductive effect would tend to enhance the rate of dehydration of pivalaldehyde relative to aldehydes with fewer methyl substituents. The transition state is also more sterically crowded than the aldehyde so that large aldehydes would be expected to hydrate more slowly. In terms of the addition model discussed by Karabatsos,³¹ this steric effect would be most pronounced in going from isobutyraldehyde to pivalaldehyde, because no amount of rotation of the latter would relieve the unfavorable eclipsing by a methyl substituent of the incoming nucleophile. Indeed, the greatest drop in relative hydration coefficients is observed at this point in the series. It is difficult to predict the exact effect of steric factors in the dehydration, since the precise geometry of the transition state is unknown. Additional methyl substituents could result in either slight steric acceleration or slight steric inhibition, depending on the values of the bond angles relative to the distance between the leaving group and the rest of the molecule. At any rate, steric effects should not retard dehydration nearly so much as hydration. These suggestions are all in accord with the observed trends.

(31) G. J. Karabatsos and N. Hsi, *J. Amer. Chem. Soc.*, **87**, 2864 (1965).

NOTES

A Dechlorination Reaction in the Radiolysis of Aqueous Monochloroacetic Acid Solutions in the Presence of Nitrous Oxide

by Akira Yokohata, Takuichi Ohmura, and Satoru Tsuda

Department of Chemistry Faculty of Engineering, Hiroshima University, Senda-machi, Hiroshima, Japan (Received February 20, 1969)

It is well known¹ that the formation of inorganic chloride on irradiation of a deaerated solution of monochloroacetic acid is a result of the reaction of the reducing species with the solute. In general, the reaction of OH radicals is believed to result in dehydrogenation rather than dechlorination. However, during the course of our recent investigation on the effect of electron scavengers such as N₂O, the authors found that the reaction of dechlorination caused by OH radicals should be considered and the degree of its contribution can be expressed as $1/5 G(\text{OH})$.

The present work deals with this interesting reaction.

Experimental Section

Irradiation was carried out using a 260-Ci ⁶⁰Co source. The dose rate (1.59×10^{17} eV g⁻¹ min⁻¹) was determined by the Fricke dosimeter, taking $G(\text{Fe}^{3+}) = 15.5$. The water used was triply distilled. The pH of the sample solution was adjusted with NaOH. All chemicals used were of reagent grade. N₂O (99.0%) was purified by several distillations on a vacuum line, prior to introduction into the irradiation vessel containing the degassed solution. The amount of N₂O in the solutions was determined by measurement of the

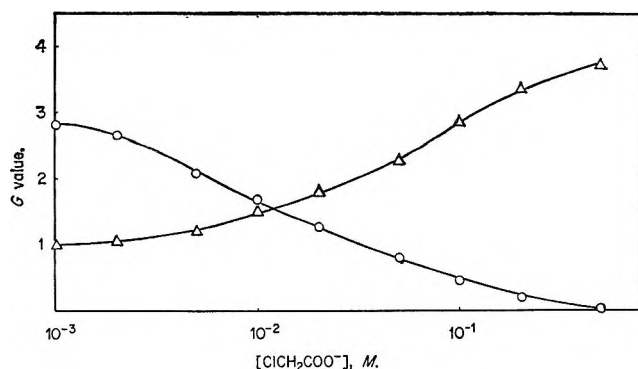
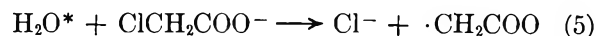
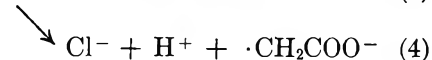
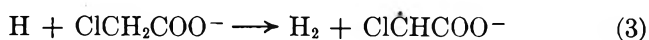
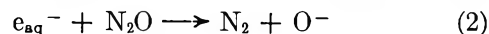
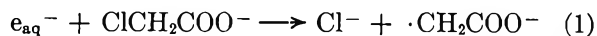


Figure 1. Relation of $G(\text{N}_2)$ and $G(\text{Cl}^-)$ to $[\text{ClCH}_2\text{COO}^-]$. $[\text{N}_2\text{O}]_0 = 8 \times 10^{-3} M$, pH 6.5; Δ , $G(\text{Cl}^-)$; \circ , $G(\text{N}_2)$.

pressure drop after the solution stands for about 24 hr at room temperature. Irradiations were performed in sealed ampoules. Microquantities of chloride were determined by the turbidimetric method.² The turbidity was measured spectrophotometrically at 350 m μ . The gaseous products H₂ and N₂ were measured with the mass spectrometer.

Results and Discussion

Figure 1 shows the relations of $G(\text{N}_2)$ and $G(\text{Cl}^-)$ to $[\text{ClCH}_2\text{COO}^-]$, where $[\text{ClCH}_2\text{COO}^-]$ was changed in the range from $1 \times 10^{-3} M$ to $5 \times 10^{-1} M$ under the condition of $\text{N}_2\text{O} = 8.0 \times 10^{-3} M$ and pH = 6.5. The reactions to be considered are



The occurrence of reaction 5 is suggested by Sworski³ to be important only at concentrations of ClCH₂COO⁻ higher than 0.1 M.

A value of $G(\text{N}_2) = 2.8$ obtained at $[\text{ClCH}_2\text{COO}^-] = 10^{-3} M$ shows clearly that most e_{aq}^- is scavenged by N₂O. On the other hand, the rate of H abstraction by H atoms is known to be faster by a factor of 11 than the rate of dechlorination.⁴ Therefore, $G(\text{Cl}^-)$ should be expected to be <0.04. Contrary to our expectation, however, $G(\text{Cl}^-) = 1.0 \pm 0.05$ was obtained. This finding is noteworthy in suggesting the possibility of dechlorination due to an unknown reaction. Thus, a more detailed experiment was undertaken.

Possibility of Dechlorination Due to OH Radical. Figure 2 shows the effect of additive CH₃OH on $G(\text{N}_2)$, $G(\text{H}_2)$ and $G(\text{Cl}^-)$ in the system of $1 \times 10^{-3} M$ ClCH₂COO⁻ - $2.3 \times 10^{-2} M$ N₂O, where a suppressive effect of CH₃OH on $G(\text{Cl}^-)$ was found. No dependence of $G(\text{N}_2)$ value (2.8 ± 0.1) on CH₃OH shows no influence of CH₃OH on the reaction 2.⁵ The $G(\text{H}_2)$ value (0.95 ± 0.05) obtained is consistent with $G(\text{H}_2)$ estimated from G_{H} and G_{H} , so that most of the H atoms must disappear via the reactions with CH₃OH to yield H₂. Thus, these

(1) E. Hayon and A. O. Allen, *J. Phys. Chem.*, **65**, 2180 (1961).

(2) E. N. Luce, E. C. Denice, and F. E. Akerlund, *Ind. Eng. Chem. Anal. Ed.*, **15**, 365 (1943).

(3) T. J. Sworski in "Solvated Electron," R. F. Gould, Ed., American Chemical Society, Washington, D. C., 1965, p 263.

(4) J. Jortner and J. Rabani, *J. Phys. Chem.*, **66**, 2078, 2081 (1962).

findings force us to take into consideration the possibility of the contribution of OH radicals to dechlorination. If the reactions 6, 7, and 8 are assumed, simple competition of these reactions leads to eq 9.

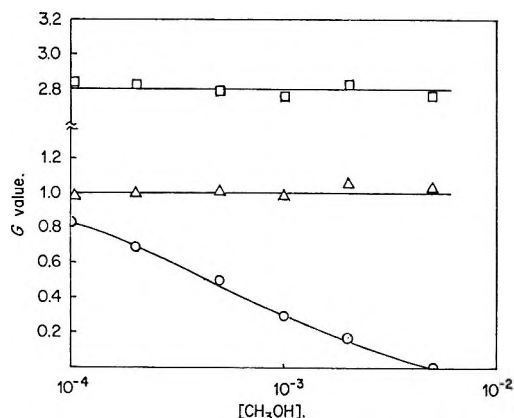


Figure 2. Effect of additive CH_3OH on $G(\text{N}_2)$, $G(\text{H}_2)$, and $G(\text{Cl}^-)$ in the system of $1 \times 10^{-3} \text{ M ClCH}_2\text{COO}^-$ – $2.3 \times 10^{-2} \text{ M N}_2\text{O}$. \circ , $G(\text{Cl}^-)$; \triangle , $G(\text{H}_2)$; \square , $G(\text{N}_2)$.

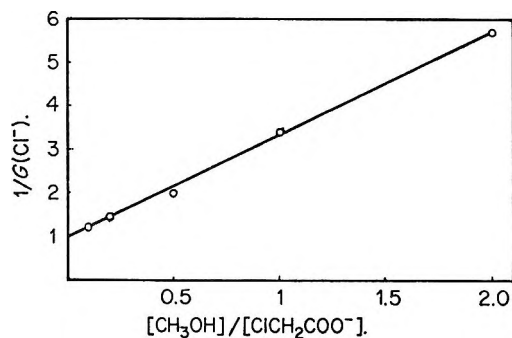
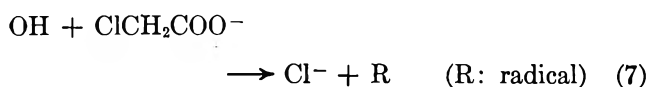
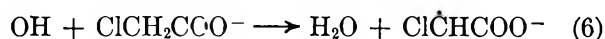


Figure 3. A plot of $1/G(\text{Cl}^-)$ against $[\text{CH}_3\text{OH}]/[\text{ClCH}_2\text{COO}^-]$.



$$\frac{1}{G(\text{Cl}^-)} = \frac{1}{G(\text{OH})} \left(1 + \frac{k_6}{k_7} + \frac{k_8[\text{CH}_3\text{OH}]}{k_7[\text{ClCH}_2\text{COO}^-]} \right) \quad (9)$$

Figure 3 shows a plot of $1/G(\text{Cl}^-)$ against $[\text{CH}_3\text{OH}]/[\text{ClCH}_2\text{COO}^-]$. A straight line supports the validity of the simple competition mentioned above. Since O^- produced *via* reaction 2 is considered to show the same behavior as OH radicals, $G(\text{OH})$ of eq 9 should be taken to be 5.0 ($G_{\text{e,aq}}^- = 2.8$, $G_{\text{OH}} = 2.2^6$). Then, Figure 3 leads to $k_6/k_7 \simeq 4.0$ and $k_8/k_7 \simeq 12$. In other words, it may be concluded that the degree of the contribution

of dechlorination caused by OH radicals is expressed as $1/5 G_{\text{OH}}$.

(5) The solvated electron does not react with CH_3OH in the presence of high N_2O concentration, because of $k_{\text{e,aq}}^- + \text{N}_2\text{O} \gg k_{\text{e,aq}}^- + \text{CH}_3\text{OH}$.

(6) T. Balkas, F. S. Dainton, J. K. Dishman, and D. Smithies, *Trans. Faraday Soc.*, **62**, 81 (1966).

3d Transition Metal Complexes in Molten Potassium Thiocyanate Solution

by H. C. Egghart

Energy Conversion Research Division, U. S. Army Mobility Equipment Research and Development Center, Fort Belvoir, Virginia 22060
(Received November 12, 1968)

Since 1956 adsorption spectroscopy has been used as a technique to study transition metal complexes in molten salts such as molten alkali halides and to a lesser extent low-melting alkali nitrate mixtures.¹⁻⁵ Only one investigation on transition metal species in molten potassium thiocyanate solution was carried out.⁶ In that study results of preliminary character on Cr(III), Co(II), and Ni(II) were obtained. Very low molar absorbances were reported which do not agree well in every case with the tentatively proposed structures of the complexes. The low molar absorbance (ϵ 15) reported for Cr(III), its spectrum indicating octahedral coordination, was not too surprising since d-d transitions in a system having a center of symmetry are Laporte-forbidden and gain some intensity only by distortion from a regular octahedral symmetry or by a vibronic mechanism. A tetrahedral field has no center of symmetry and d, p, and ligand orbitals can become mixed together to some extent. In this way forbidden transitions become allowed to a certain degree.⁷ Therefore, tetrahedral complexes show much higher molar absorbances than octahedral complexes. In view of this, particularly the molar absorbance of 86 reported for the maximum of the spectrum of Co(II) solutions in molten potassium thiocyanate seemed too small for a tetrahedral species.

The present investigation was carried out (i) to resolve these questions concerning the molar absorbances,

- (1) D. M. Gruen, *Nature*, **178**, 1181 (1956).
- (2) D. M. Gruen, *J. Inorg. Nucl. Chem.*, **4**, 74 (1957).
- (3) D. M. Gruen, "Fused Salts," B. R. Sundheim, Ed., McGraw-Hill Book Co., Inc., New York, N. Y., 1964, Chapter 5, p 301.
- (4) G. P. Smith, "Molten Salt Chemistry," M. Blander, Ed., Interscience Publishers, New York, N. Y., 1964, p 427.
- (5) D. M. Gruen, *Quart. Rev.*, **19**, 349 (1965).
- (6) G. Harrington and B. R. Sundheim, *Ann. N. Y. Acad. Sci.*, **79**, 950 (1960).
- (7) C. J. Ballhausen and A. D. Liehr, *J. Mol. Spectrosc.*, **2**, 342 (1958).

(ii) to measure the absorptions also in the near-infrared region which should permit the interpretation of the Ni(II) spectrum, and (iii) to study the spectra of other first row transition metal ions in molten potassium thiocyanate solution. This melt itself aroused interest because it has a considerably higher ligand field than the more widely studied alkali halide and nitrate melts.

Experimental Section

Certified reagent grade potassium thiocyanate was dried at 110° overnight and subsequently subjected to a thermal shock drying technique, described in detail in ref 8. The dried potassium thiocyanate samples were weighed and then melted under vacuum, and known quantities of water-free transition metal thiocyanates, chlorides, or sulfates were added. Part of these solutions were then transferred into quartz cells which were held at temperatures above the melting point of potassium thiocyanate, usually 185°, in a temperature-controlled sample cell holder. The absorptions of the solutions were compared with the absorptions of the pure solvent melt, using a Cary 14 recording spectrophotometer equipped with a water-cooled sample compartment. For the calculation of the molar absorbance it was necessary to know the volumes of the melts. These were determined from the weight of the melt using a value of 1.60 for the density of the potassium thiocyanate melt at 185°. This value for the density was measured with a pycnometer.

Results and Discussion

Molten potassium thiocyanate is a useful medium for studies in the near-infrared, visible, and near-ultraviolet region of the spectrum. Its range of transparency in the near-infrared is far greater than that of water. Only very weak absorptions occur at wavelengths shorter than 2300 m μ . Work at wavelengths below 320 m μ is not possible because of strong absorption by the melt which is due to an internal transition in the thiocyanate ion.⁹ The intense absorptions beginning with Ni(II) and VO²⁺(IV) near 500 m μ and with Co(II) and Cr(III) near 400 m μ , shown on Figure 1, are charge-transfer bands. The same results were obtained when transition metal ions were added as thiocyanates, chlorides, or sulfates. This is understandable in view of the relatively high coordinating power of the thiocyanate group and the large excess in which this group was present.

The results of the spectrophotometric work can be seen in Figure 1 and Table I. The absorption in the near-infrared region expected for octahedral Ni(II) complexes was found and had a maximum at 1170 m μ (8547 cm⁻¹) having a molar absorbance ϵ of 13. Taking the ligand field strength parameter Dq as 854.7, the second band can be predicted to be at the wavelength where it actually occurs. The first band of

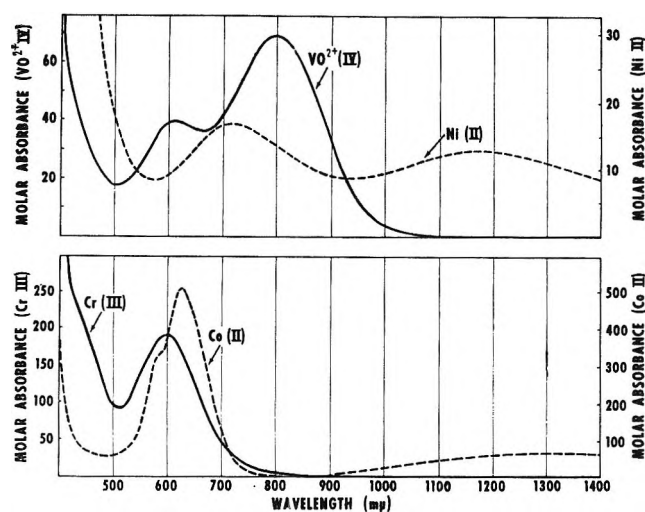


Figure 1. Absorption spectra of Ni(II), Co(II), Cr(III), and VO²⁺(IV) in molten potassium thiocyanate solution.

Cr(III) was found at 597.4 m μ (16.739 cm⁻¹) (ϵ 191). With $Dq = 1673.9$ the second band can be predicted to be where the slight shoulder in the blue part of the spectrum can be seen. The good agreement between the observed spectra and the predictions of theory^{10,11} as well as their similarity with the spectra of Ni(II) and Cr(III) substituted in octahedral sites of host lattices^{12,13} leaves no doubt that these ions are octahedrally coordinated in molten potassium thiocyanate solution. Although Ni(II) was found to be tetrahedrally coordinated in alkali halide melts,¹⁴ this would not be likely in potassium thiocyanate melts because the thiocyanate group exerts a considerably stronger ligand field than the chloride group and ligand field stabilizations in octahedral fields are particularly large for d³ and d⁸ systems.

The spectra found when Cr(III) and Cr(II) salts were dissolved in molten potassium thiocyanate were identical. Since the spectrum of Cr(II), a d⁴ system, should be entirely different, one must conclude the Cr(II) was oxidized to Cr(III). This conclusion gains support from the observation that Cr(VI) is reduced to Cr(III) in molten potassium thiocyanate.¹⁵

Solutions of Co(II) in molten potassium thiocyanate showed an intense band with a maximum at 625 m μ (ϵ 510), a shoulder around 585 m μ and an absorption in the

(8) E. Rhodes and A. R. Ubbelohde, *Proc. Roy. Soc.*, **A251**, 156 (1959).

(9) C. K. Jørgensen, "Absorption Spectra and Chemical Bonding in Complexes," Pergamon Press, Oxford, 1962, p 196.

(10) A. D. Liehr and C. J. Ballhausen, *Ann. Phys. (N. Y.)*, **6**, 134 (1959).

(11) L. E. Orgel, *J. Chem. Phys.*, **23**, 1004 (1955).

(12) W. Low, *Phys. Rev.*, **109**, 247 (1958); **105**, 801 (1957).

(13) More references can be found in C. J. Ballhausen, "Introduction to Ligand Field Theory," McGraw-Hill Book Co., Inc., New York, N. Y., 1962, p 238.

(14) D. M. Gruen and R. L. McBeth, *J. Phys. Chem.*, **63**, 393 (1959).

(15) D. H. Kerridge and M. Mosley, *Chem. Commun.*, 505 (1965).

Table I: Observed Absorption Maxima of Ni(II), Cr(III), Co(II), and VO²⁺(IV) in Molten Potassium Thiocyanate Solution, Their Molar Absorbance ϵ , and Some Assignments^a

Ni(II)	1170 m μ (8547 cm ⁻¹), ϵ 13, ² A _{2g} → ³ T _{2g} (F)	710 m μ (14,084 cm ⁻¹), ϵ 17, ³ A _{2g} → ³ T _{1g} (F)
Cr(III)	5974 m μ (16,739 cm ⁻¹), ϵ 191, ⁴ A _{2g} → ⁴ T _{2g} (F)	shoulder ~430 m μ (23,255 cm ⁻¹), ⁴ A _{2g} → ⁴ T _{1g} (F)
Co(II)	625 m μ (16,000 cm ⁻¹), ϵ 510 13,000 m μ (7692 cm ⁻¹), ϵ 64	shoulder ~585 m μ (17,094 cm ⁻¹)
VO ²⁺ (IV)	800 m μ (12,500 cm ⁻¹), ϵ 69	613 m μ (16,313 cm ⁻¹), ϵ 43

^a See ref 10, 11, 13, and 29.

near-infrared region. This spectrum was observed also with a number of Co(II) solutions in nonaqueous solvents containing an excess of thiocyanate ions.^{16,17} This invariance of the spectrum in different solvents as well as other data indicated the formation of a tetrahedral Co(II) thiocyanate species in organic solvents. A very similar spectrum was also found in investigations of solid K₂[Co(NCS)₄] and [(CH₃)₄N]₂[Co(NCS)₄] and the acetone solution of the latter.¹⁸ X-Ray structure determinations showed that the lattice of K₂[Co(NCS)₄] consists of [Co(NCS)₄]²⁻ tetrahedrons in which the thiocyanate groups are coordinated to cobalt *via* nitrogen.¹⁹ The great similarity of all these spectra with the spectrum of Co(II) in molten potassium thiocyanate as well as the high molar absorbance indicates that in potassium thiocyanate melt solution Co(II) is also tetrahedrally coordinated by four N-coordinated thiocyanate groups.

In addition to Ni(II), Co(II), and Cr(III) also VO²⁺(IV) salts dissolved well in molten potassium thiocyanate and gave stable solutions. The first absorption band was found at 800 m μ (ϵ 69) and the second at 613 m μ (ϵ 43). Similar spectra were observed with many other vanadyl complexes in solution and in the solid state.²⁰⁻²³ In their scheme for [VO(H₂O)₅]²⁺ and related complexes, Ballhausen and Gray assigned the first band to the transition ²B₂ → ²E(I) and the second to the transition ²B₂ → ²B₁.²⁴ The energy of the second band is 10Dq. This scheme is no more generally accepted since it was found that at low temperatures the first band splits into four narrow bands.²⁵⁻²⁷ However, the second band was never found to split and using the energy of this band ligands could be properly ranked according to their ligand field strengths.²⁸

The N-coordinated thiocyanate group generally causes a greater ligand field splitting than water. Consequently the -NCS group is ranked above the aquo group in the spectrochemical series.²⁹ Therefore it

was interesting to note that in molten potassium thiocyanate the ligand field strength of the -NCS group is about the same [observed with Ni(II) and VO²⁺(IV)] or slightly less [observed with Cr(III)] than the ligand field strength of H₂O in aqueous solution. This observation led to a comparison of thiocyanate complexes in different media. In several investigations on solution and solid state spectra of [VO(NCS)₅]³⁻ complexes having organic cations the maximum of the second vanadyl band was found around 580 m μ (17,241 cm⁻¹).^{20-22,28} In molten potassium thiocyanate solution it is at 613 m μ (16,313 cm⁻¹). Cr(III) is known to be octahedrally coordinated at all temperatures, and the positions of the absorption peaks in, for instance, molten alkali halide solution change very little when the temperature is raised from 400 to 800°. However, between the ⁴A_{2g} → ⁴T_{2g}(F) transition (= 10Dq) of [Cr(NCS)₆]³⁻ in ordinary solutions³¹ and molten potassium thiocyanate solution there is a difference of about 1000 wave numbers as was found for [VO(NCS)₅]³⁻. In studies on solids it was shown that the ligand field strengths in octahedral sites is influenced by cations in the second sphere environment.³² In the potassium thiocyanate melt potassium ions form the second sphere environment and their interaction with the thiocyanate group may cause the smaller ligand field strength of this group in the melt.

Acknowledgment. The author wishes to thank Dr. J. R. Huff, Chief of the Energy Conversion Research Division, for his interest in this work.

- (16) V. Gutmann and O. Bohunovsky, *Monatsh. Chem.*, **99**, 751 (1968).
 (17) R. Lundquist, G. D. Markle, and D. F. Boltz, *Anal. Chem.*, **27**, 1731 (1955).
 (18) F. A. Cotton, D. M. L. Goodgame, M. Goodgame, and A. Sacco, *J. Amer. Chem. Soc.*, **83**, 4157 (1961).
 (19) G. S. Zhdanov and A. V. Zvonkova, *Zh. Fiz. Khim.*, **24**, 1339 (1950).
 (20) J. Selbin, *Chem. Rev.*, **65**, 153 (1965).
 (21) V. Gutmann and H. Laussegger, *Monatsh. Chem.*, **99**, 947 (1968).
 (22) V. Gutmann and H. Laussegger, *ibid.*, **99**, 963 (1968).
 (23) V. Gutmann and H. Laussegger, *ibid.*, **98**, 439 (1967).
 (24) C. J. Ballhausen and H. B. Gray, *Inorg. Chem.*, **1**, 111 (1962).
 (25) J. Selbin, T. R. Ortolano, and F. J. Smith, *ibid.*, **2**, 1315 (1963).
 (26) T. R. Ortolano, J. Selbin, and S. P. McGlynn, *J. Chem. Phys.*, **41**, 262 (1964).
 (27) J. Selbin, *Coord. Chem. Rev.*, **1**, 293 (1966).
 (28) O. Piovesana and J. Selbin, *J. Inorg. Nucl. Chem.*, **31**, 433 (1969).
 (29) See, for example, T. M. Dunn, "Modern Coordination Chemistry," J. Lewis and R. G. Wilkins, Ed., Interscience Publishers Inc., New York, N. Y., 1964, p 266.
 (30) D. M. Gruen and R. L. McBeth, *Pure Appl. Chem.*, **6**, 23 (1963).
 (31) C. K. Jørgensen, "Absorption Spectra and Chemical Bonding in Complexes," Pergamon Press, Oxford, 1962, p 291, and references therein.
 (32) D. Reinen, "Proceedings of the Ninth International Conference on Coordination Chemistry, St. Moritz-Bad, Sept. 1966," W. Schneider, Ed., Verlag Helvetica Chimica Acta, Basel, 1966, p 139.

Electron Spin Resonance Studies on Trapped Electrons and Free Radicals in γ -Irradiated Isobutyl Vinyl Ether Glasses¹

by Kozo Tsuji²

Department of Polymer Chemistry, Kyoto University, Kyoto, Japan

and Ffrancon Williams³

Department of Chemistry, University of Tennessee, Knoxville, Tennessee 37916 (Received February 20, 1969)

Trapped electrons have been identified by optical and electron spin resonance (esr) studies on several γ -irradiated and photoionized organic glasses, including alcohols, ethers, amines, and hydrocarbons.⁴ Thermal decay of the trapped electron is arrested by an increase in the viscosity^{4b} and polarity⁵ of the glass, and since γ -irradiated and photoionized glasses behave similarly in this respect,⁶ it has been concluded that the post-irradiation decay is controlled by the mobility of the electron rather than by transfer of positive charge.^{5,6} This note describes related studies on γ -irradiated glasses of isobutyl vinyl ether (IBVE) and mixtures of IBVE and 3-methylpentane (3-MP). IBVE is known to undergo radiation-induced cationic polymerization in the liquid state,⁷ so this was another reason for undertaking the present work.

Experimental Section and Results

IBVE and 3-MP were purified by fractional distillation and dried over sodium-potassium alloy on the vacuum line. The general technique of sample preparation has been described.⁴ Samples were γ -irradiated in a cobalt-60 source at a dose rate of 6×10^5 rads/hr. The uv and visible light sources were provided by a high-pressure mercury lamp (400 W) and a tungsten lamp (150 W), both obtained from the Toshiba Electric Co., Ltd.

A conventional X-band esr spectrometer was used with 100-kHz field modulation. The incident microwave power was adjusted to be less than 1mW. All γ irradiations and also the initial esr measurements on each sample were carried out in the dark at -196° . Subsequently, additional esr spectra were recorded after the γ -irradiated sample had been photolyzed or raised to a higher temperature. The latter operation was carried out by the usual type of variable-temperature accessory.

Figure 1 shows the esr spectra obtained after a sample of pure IBVE had been shock-cooled to -196° and γ -irradiated at the same temperature in the dark. The first spectrum (a) reveals the presence of a sharp line (width 4 G) in the center as denoted by the arrow mark \downarrow and two lines on either side marked by dashed arrows $\downarrow \uparrow$ as well as a set of broader lines extending

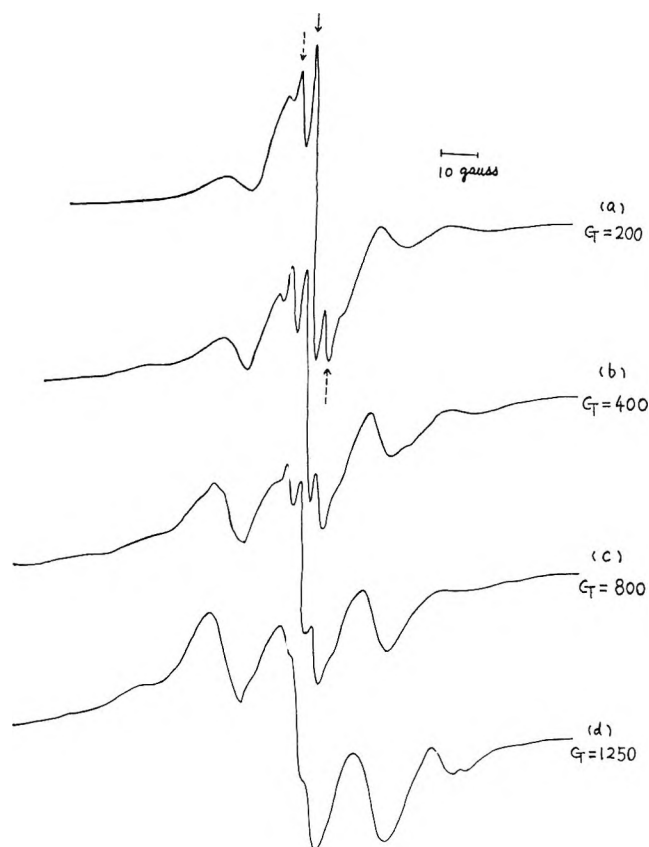


Figure 1. ESR spectra of γ -irradiated isobutyl vinyl ether at -196° before and during photobleaching; dose, 6×10^{18} eV g^{-1} : (a) Immediately after γ -irradiation; (b), (c), and (d) were recorded after 6 sec, 26 sec, and 3 min exposure, respectively, to visible light from a tungsten lamp. G represents an amplifier gain setting.

into the wings. At higher microwave power, the center line saturated rather easily relative to the rest of the spectrum. Moreover, when methyl iodide was introduced into the samples before irradiation, this center line did not appear under the same conditions of γ -irradiation and esr measurement, and methyl

(1) This research was carried out at the Osaka Laboratories of the Japanese Association for Radiation Research on Polymers. This organization is now known as the Osaka Laboratories for Radiation Chemistry, Japan Atomic Energy Research Institute, and the address is 508, Mii, Neyagawa, Osaka, Japan.

(2) Central Research Laboratory, Sumitomo Chemical Co. Ltd., Takatsuki, Osaka, Japan.

(3) Visiting Scientist to Kyoto University, 1965-1966, under National Science Foundation Grant GF-216.

(4) (a) The subject of trapped electrons has been reviewed by J. E. Willard in "Fundamental Processes in Radiation Chemistry," P. Ausloos, Ed., Interscience Publishers, New York, N. Y., 1968, Chapter 9, p 599; (b) for a recent study, see J. Lin, K. Tsuji, and F. Williams, *J. Amer. Chem. Soc.*, **90**, 2766 (1968).

(5) M. A. Bonin, J. Lin, J. Tsuji, and F. Williams, *Advances in Chemistry Series*, No. 82, American Chemical Society, Washington, D. C., 1968, p 269.

(6) J. Lin, K. Tsuji, and F. Williams, *Chem. Phys. Letters*, **1**, 66 (1967).

(7) (a) F. Williams, *Discussions Faraday Soc.*, **36**, 259 (1963); (b) M. A. Bonin, M. L. Calvert, W. L. Miller, and F. Williams, *J. Polymer Sci., B*, **2**, 143 (1964); (c) K. Ueno, K. Hiyashi, and S. Okamura, *J. Macromol. Sci.-Chem.*, **A**, **2**, 209 (1968).

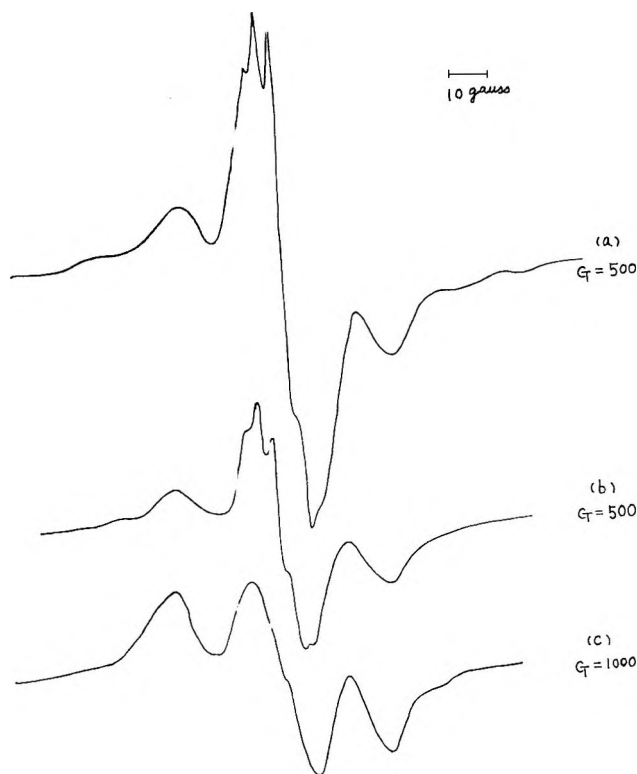


Figure 2. ESR spectra of γ -irradiated isobutyl vinyl ether as recorded during warm-up from -196° ; dose 6×10^{18} eV g^{-1} : (a) -166° , (b) -149° , (c) -147° . G represents an amplifier gain setting.

radicals were produced instead. These experiments characterize the center line as a singlet spectrum due to a trapped electron, and this assignment was confirmed by the effect of progressive photobleaching with visible light, as shown in spectra (b), (c), and (d). The (e^-) singlet disappeared at a slightly faster rate than the neighboring components although the paramagnetic species responsible for the latter features is also photosensitive to visible light. The residual spectrum in (d) is probably derived from a double 1:2:1 triplet structure but the overlap and distortion in the center results in only five lines with approximate intensity ratios of 1:2:2:2:1 and a hyperfine splitting of ca. 20 G. This description closely resembles that of the isobutyl radical in solid matrices^{8,9} and the spectrum may be tenta-

tively assigned to the radical $\cdot\text{CH}_2-\overset{\text{CH}_3}{\underset{|}{\text{C}}}-\text{CH}-\text{CH}_2-\text{O}-\text{CH}=\text{CH}_2$. There are some additional weak lines in the spectrum (d) which probably belong to other radicals, but no assignment can be made.

On warming the γ -irradiated sample in the dark, there was a marked change in the ESR spectrum. As shown in Figure 2, the narrow singlet disappeared at -149° and there was also a change in the underlying spectrum. At -147° , a triplet with a hyperfine splitting of 20 G was observed. It seems likely that this spectrum is characteristic of a "propagating" free

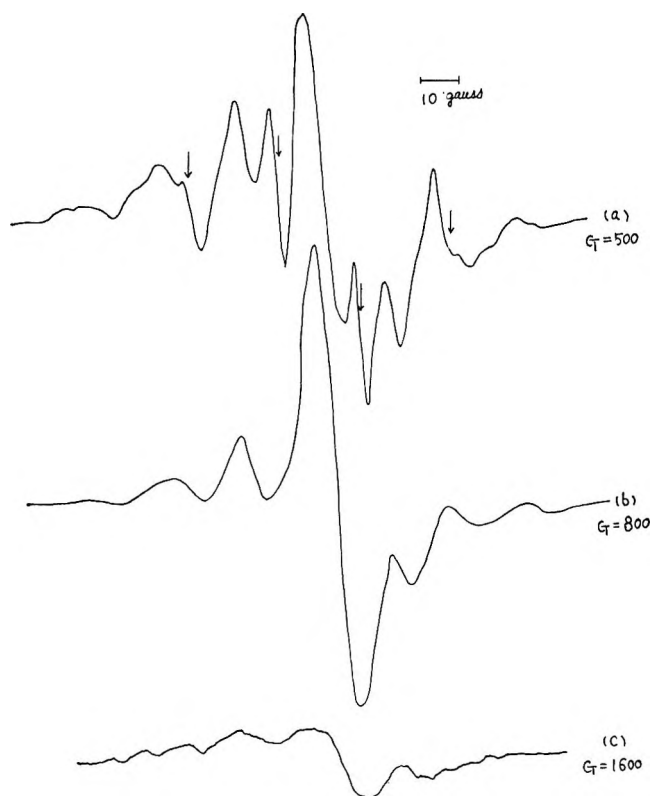


Figure 3. Effect of uv light on γ -irradiated isobutyl vinyl ether. Spectra (a), (b), and (c) were recorded with sample at -196° , -159° , and -143° , respectively, after exposure to uv light for for 30 min.

radical $\sim\text{CH}_2-\dot{\text{C}}\text{H}-\text{OR}$ since very similar spectra have been assigned to propagating radicals in ESR studies on other γ -irradiated solid monomers such as acrylamide,¹⁰ acrylic acid,¹¹ and vinylpyridine zinc complexes.¹²

The effect of uv irradiation on γ -irradiated IBVE is shown in Figure 3. After photolysis of the sample at -196° , the complex ESR spectrum (a) shows four lines (arrow marks \downarrow) attributable to methyl radicals. These lines disappeared when the sample was warmed to -159° , and a seven-line structure is indicated by spectrum (b). However, the abnormal intensity of the center line strongly suggests that more than one radical contributes to this spectrum. One possibility is that the composite spectrum consists of a singlet and a septet attributable to $\text{RO}\cdot$ and $\text{CH}_3\dot{\text{C}}\text{HCH}_2\text{OCH}=\text{CH}_2$, respectively. The radicals decayed out rapidly at -147° .

Similar results to those described above were obtained with samples of IBVE which had been prepared

(8) P. B. Ayscough and C. Thomson, *Trans. Faraday Soc.*, **58**, 1477 (1962).

(9) J. Lin and F. Williams, *J. Phys. Chem.*, **72**, 3707 (1968).

(10) G. Adler, D. S. Ballantine, and B. Baysal, *J. Polymer Sci.*, **48**, 195 (1960).

(11) Y. Shioji, S. Ohnishi, and I. Nitta, *ibid.*, **A**, **1**, 3373 (1963).

(12) K. Tsuji, S. Tazuke, K. Hayashi, and S. Okamura, submitted for publication.

by gradual cooling to -196° . These samples appeared to be polycrystalline in character.

Binary mixtures of 3-MP and IBVE were examined in the glassy state at -196° . It is well established that the trapped electron is thermally unstable in pure 3-MP at this temperature, and the time for half-decay is typically 5 min when the observation is made by esr using narrow (3–4 mm i.d.) sample tubes.^{4,13} With increasing concentration of IBVE in 3-MP, the trapped electron showed greater thermal stability at -196° as indicated by the data of Table I. At

Table I: Thermal Decay of Esr Signal from Trapped Electrons in γ -Irradiated 3-MP-IBVE Glasses at -196° ^a

Composition, Volume % IBVE	Signal intensity as a function of time				
	0 hr	2 hr	7 hr	34 hr	144 hr
4	100	77	50	40	6
13	100		70	58	17
20	100			68	47
100	100			98	95

^a Dose 1.25×10^{19} eV g⁻¹.

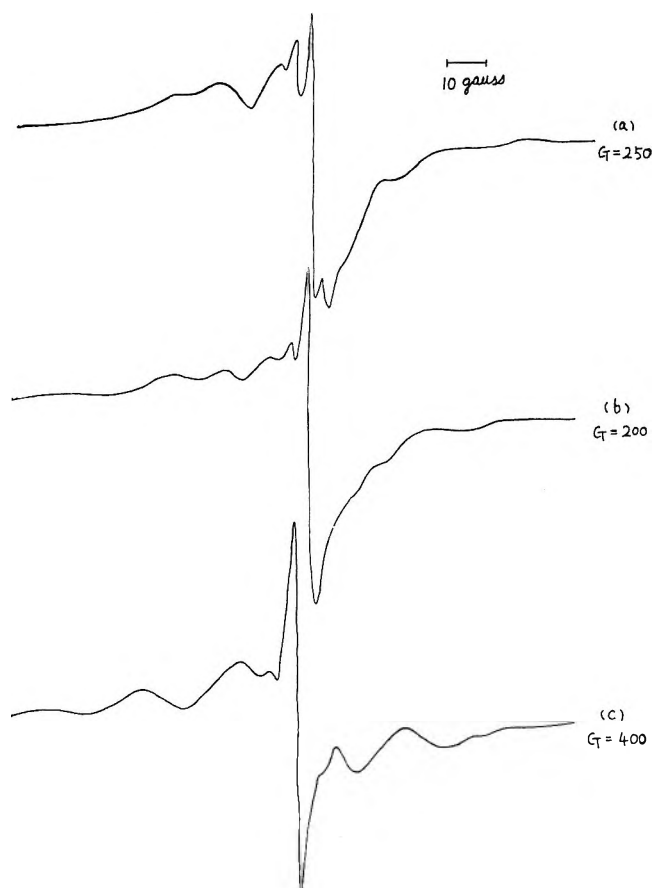


Figure 4. ESR spectra of γ -irradiated 3-methylpentane-isobutyl vinyl ether glasses after γ irradiation at -196° ; dose, 3×10^{18} eV g⁻¹: (a) 70 volume % IBVE; (b) 20 volume % IBVE; (c) 4 volume % IBVE.

constant matrix composition, the intensity of the esr signal increased linearly with dose up to 6×10^{18} eV g⁻¹, and the relative height of the (e⁻) singlet with respect to the remainder of the spectrum hardly altered in this range of dose. As shown in Figure 4, the singlet is more prominently displayed in the spectrum of γ -irradiated 3-MP containing 4 volume % IBVE than in the corresponding spectra of samples richer in IBVE. At the higher IBVE concentrations, the center part of the spectrum is similar to that obtained with pure IBVE and includes the two components that are bleachable with visible light.

Discussion

The present work shows that trapped electrons are produced by γ irradiation of pure IBVE, and that the presence of IBVE contributes to increased thermal stability of trapped electrons in a 3-MP glass. This effect of IBVE as an additive is similar to that observed for 3-MP glasses containing amines⁵ and olefins,^{14–16} and a common mechanism is indicated. Although it has been widely suggested that positive charge transfer to additive could be responsible for the effect by immobilizing the positive ion, the generality of this mechanism is open to question on the basis of previous studies^{5,6} showing that electron decay in γ -irradiated and photoionized glasses is almost independent of the nature of the cations present and is similarly affected by incorporation of polar additives into the matrix. Thus it seems more reasonable to conclude that the diffusive motion of the electron governs the rate of thermal decay, and that the mo-

bility is reduced by charge-dipole forces in polar (including olefinic) matrices.

Since the evidence from this and other work^{5,15,16} indicates that the yield of trapped electrons in 3-MP increases upon addition of amines, ethers, and olefins, it is convenient to suppose that the number of trapping sites in the matrix is increased by the presence of these materials. Then it could be argued that an increase in trap density might also affect the detailed mechanism of electron decay but further consideration must be deferred until more definitive experimental evidence is available to distinguish between various alternative mechanisms.

The present esr studies shed some light on the photochemical and thermal reactions of the paramagnetic intermediates formed by the γ irradiation of pure IBVE. Both the (e⁻) singlet and the two other lines in the center of the spectrum disappear on photobleach-

(13) K. Tsuji, K. Hayashi, and H. Yoshida, *J. Chem. Phys.*, **46**, 810 (1967).

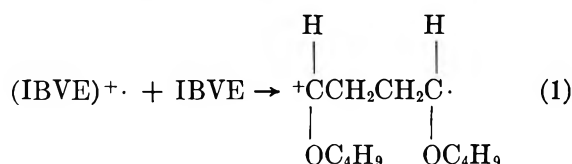
(14) K. Tsuji, H. Yoshida, K. Hayashi, and S. Okamura, *J. Polymer Sci., B*, **5**, 313 (1967).

(15) M. Irie, K. Hayashi, S. Okamura, and H. Yoshida, *J. Chem. Phys.*, **48**, 922 (1968).

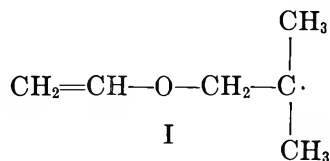
(16) D. R. Smith and J. J. Picconi, *Can. J. Chem.*, **45**, 2723 (1967).

ing, so it is conceivable that the reaction corresponds to the neutralization of a cation radical from IBVE and that the two hyperfine components arise from the latter species. However, since there is little information available on the hyperfine structure of authentic cation radicals derived from simple vinyl monomers, this assignment of the sharp doublet must be regarded as tentative. The radical present after photobleaching is almost surely of the isobutyl type, so it would appear that a hydrogen atom is eliminated from a $-\text{CH}_3$ group in the processes occurring during γ irradiation.

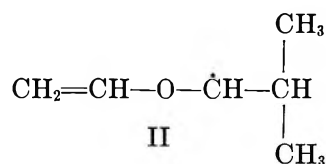
The formation of a "propagating" free radical on warming the sample is somewhat unexpected in this system because IBVE does not ordinarily polymerize by a free radical mechanism. The most likely reaction which can be postulated¹⁴ is the addition of the cation radical to the monomer according to eq 1.



The possibility of proton transfer processes from $(\text{IBVE})^{+\cdot}$ to IBVE seems to be excluded in view of the failure to observe the anticipated free radical products

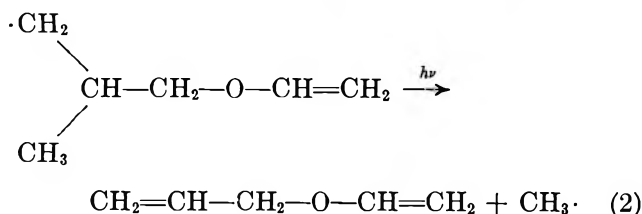


or



Radical I would be expected to give more than three lines in the esr spectrum whereas II should give rise to a well-separated couple doublet if the β -hydrogen makes a small dihedral angle with the axis of the p orbital containing the unpaired electron, as is usually the case for radicals of this general structure.⁹

It is likely that the formation of methyl radicals by uv photolysis of γ -irradiated IBVE is caused by the intramolecular dissociation of a free radical, as in reaction 2, since methyl radicals were not produced



from unirradiated IBVE under the same conditions of photolysis.

Acknowledgment. Our thanks are due to Professor I. Sakurada and Professor S. Okamura for the use of experimental facilities in their laboratories, and to Professor K. Hayashi and Dr. H. Yoshida for helpful discussions.

Temperature-Dependence Nuclear Magnetic Resonance Studies of a Very Strongly Coupled Spin System. Ethylene Sulfit

by Harold Finegold

United States Department of Agriculture, Agricultural Research Service, Human Nutrition Research Division, Beltsville, Maryland 20705 (Received April 25, 1969)

Studies of the temperature dependence of nuclear resonance parameters have heretofore emphasized those systems whose spins are weakly or moderately coupled, since instruments and accessories lacked sufficient stability to afford the high order of reliability demanded for the determination of multiple slight changes in the complex line patterns of strongly coupled systems. We now report sufficiently accurate temperature dependence measurements of all 24 lines in a very strongly coupled spin system, the AA'BB' spectrum of the cyclic glycol thioester, ethylene sulfit, to permit reliable calculations and definitive assessment of trends in the temperature dependence of all the spin coupling constants and the chemical shift difference. Comparison of these results with those recently reported for medium and dielectric constant dependence of the parameters in solution systems of this molecule¹ permit further structure elucidation in terms of possible conformational mobility.

Measurements were made from -70 to $+200^\circ$ using an externally locked Varian 60-MHz spectrometer with a variable-temperature accessory system especially modified to obtain both the long temperature time constant and the high resolution required at the very slow sweep rates necessarily employed for these experiments. Adequate long-term stability could not, however, be maintained at the lower temperatures even though there was sufficient short-term stability to give sharp high-resolution spectra and moderately precise, though probably inaccurate, data. Calculations from the spectral measurements at each temperature were made as described previously.¹ Figure 1 illustrates the positive sign in the curve direction obtained for the temperature dependence of the chemical shift difference

(1) H. Finegold, *J. Phys. Chem.*, **72**, 3244 (1968).

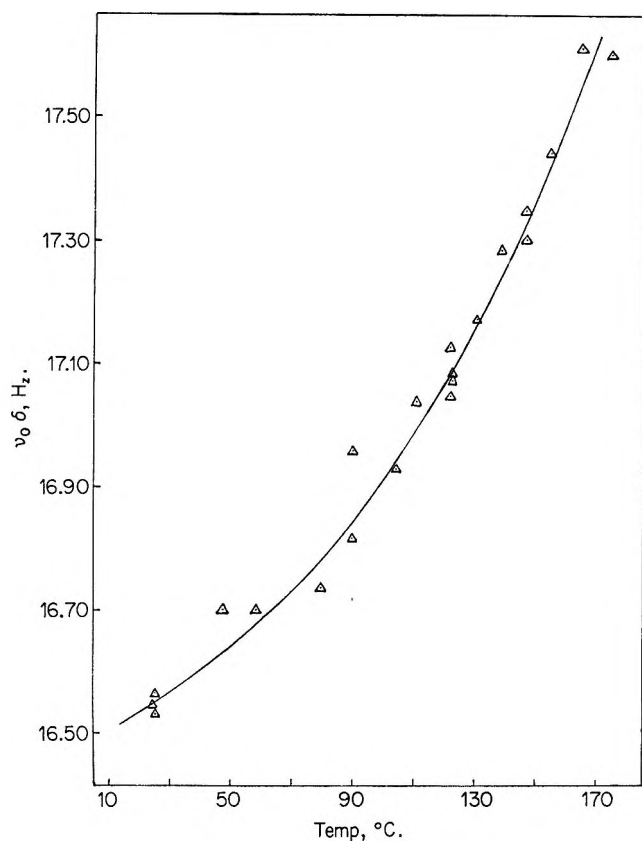


Figure 1. The temperature dependence of the proton chemical shift difference of $\text{OCH}_2\text{CH}_2\text{OSO}$ at 60 MHz.

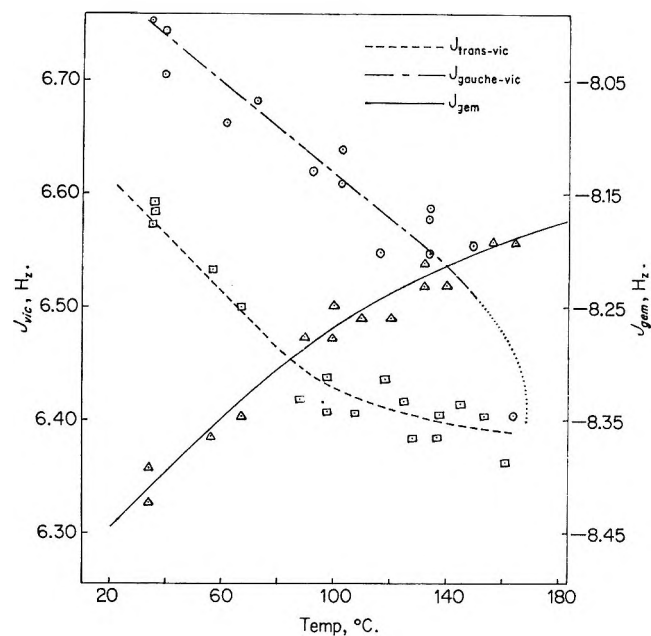


Figure 2. The temperature dependence of all spin-coupling constants of $\text{OCH}_2\text{CH}_2\text{OSO}$ at 60 MHz.

between the proton pairs on each side of the ring, and the solid curve in Figure 2 also shows a positive variation of the geminal spin coupling temperature dependence. The standard error (rms) of the spectral parameters from these curves is ± 0.03 Hz. Both can be compared with the similarly positive dependence on the reciprocal dielectric constant of these same parameters as determined from a study of the medium effects,¹ and both can thus be said to correspond in the sign of the first derivatives of their functions with respect to temperature and reciprocal dielectric constant. However, opposite signs obtain for the first derivatives involving the *gauche* vicinal coupling corresponding functions, as can be inferred from Figure 2 and the previously noted study of medium effects. The *trans*

vicinal coupling varies with temperature as does the *gauche* vicinal coupling, but significance cannot be attached to this in the present context since the first derivative of the *trans* vicinal coupling with respect to reciprocal dielectric constant is very close to vanishing. (See Table I.)

It is well established that a temperature dependence of the chemical shift and coupling parameters in the nuclear magnetic resonance spectrum can be a reflection of time-averaging changes due to temperature-sensitive conformational equilibria. It has also become widely recognized that changes in medium dielectric can similarly affect time-averaging of spectra.^{2,3} In the particular case of ethylene sulfite, cogent evidence has been found in closely related systems pertaining to the probable conformational immobility of this and related structures.⁴ On the other hand, thermochemical and kinetic studies of some other saturated, five-membered heterocyclics have indicated the existence of sufficient ring strain to give rise to considerable structural instability and at least the possibility of temperature dependent conformational equilibration.⁵

If the presently determined temperature dependence of the spectral parameters is to be interpreted as proof of a conformational mobility in ethylene sulfite, then it should be possible to obtain a value for the conformational equilibrium constant which will not only be a "best fit" to all the temperature dependent spectral functions, but which can also, with the appropriate

Table I: Curve Directions for Reciprocal Dielectric and Temperature Functions of Nuclear Parameters in Ethylene Sulfite Systems

	Dielectric function curvature	Temperature function curvature
$\nu_0\delta$	+	+
J_{gem}	+	+
$J_{gauche-vic}$	+	-
$J_{trans-vic}$	(0)	-

(2) R. J. Abraham, L. Cavalli, and K. G. R. Pachler, *Mol. Phys.*, **11**, 471 (1967).

(3) H. Finegold, *J. Chem. Phys.*, **41**, 1808 (1964).

(4) J. Tillett, *Quart. Rep. Sulfur Chem.*, **2**, 227 (1967).

(5) F. H. Westheimer, *Accounts Chem. Res.*, **1**, 70 (1968).

TdH/dT correction factors,² be fitted into the previously determined dielectric constant dependent functions,¹ should these changes also originate in conformational equilibration. However, the "best fit" value of the temperature dependent functions as evaluated by a least-squares method cannot be fitted to the dielectric-dependent functions because of the opposite signs of the curve directions discussed above. This method, therefore, affords a new criterion for the validity of free energy values determined by computer fittings to temperature-dependent functions, since the corresponding curve directions for all spectral functions in the temperature dependent *vs.* dielectric constant dependent functions must be related, pairwise, in sign if the spectral changes are due primarily to changes in the conformational free energy.

It has not been widely appreciated, though it is very well established, that temperature dependence in spectral changes of the magnitude described above can be exclusively ascribed to vibrational effects.^{6,7} Since

the curves in Figures 1 and 2 cannot be accounted for in terms of an equilibrium constant compatible with the corresponding dielectric functions, it is probable that the effect of temperature on the population of methylene group torsional vibration levels makes the major contribution to the spectral changes observed here. The implications regarding conformational stability in ethylene sulfite would thus be consistent with the closely related observations that each of the separable geometrical isomers of a simple 4-substituted methyl analog of ethylene sulfite shows no chromatographically detectable inversion over long periods of time, and that the methyl and methylene resonance lines of the *gem*-dimethyl analog, which are excellent probes of time averaging, indicate no conformational mobility.⁸

(6) L. Petrakis and C. H. Sederholm, *J. Chem. Phys.*, **35**, 1174 (1961).

(7) K. C. Ramey and W. S. Brey, Jr., *ibid.*, **40**, 2349 (1964).

(8) J. G. Pritchard and P. C. Lauterbur, *J. Amer. Chem. Soc.*, **83**, 2105 (1961).

COMMUNICATIONS TO THE EDITOR

Comments on the Paper "Activity Coefficients for Ionic Melts"¹

Sir: Haase² has proposed that an ideal ionic melt be defined as one in which the chemical potential of any ion j is taken as

$$\mu_j = \mu_{0j} + RT \ln x_j \quad (1)$$

where μ_{0j} is the chemical potential of the pure liquid ion and x_j is the ion fraction defined as the number of ions of j divided by the total number of species in the melt. For an ideal melt all of these species would be fully ionized.

The proposal was made without reference to any statistical model, but in fact it corresponds to one for which in an ideal melt all ions mix randomly with each other regardless of charge. This can be shown from Haase's eq 4, here slightly rearranged as

$$\frac{x_a}{x_a^0} = \frac{\nu_1(1-x)}{\nu_1(1-x) + \nu_2x} \quad (2)$$

In a mixture of salts A and B of stoichiometric mole fractions $(1-x)$ and x , a is an ion found only in A. ν_1 and ν_2 are the numbers of particles produced by the complete ionization of 1 formula weight of A and B; if A is $\text{Ca}_2(\text{SO}_4)_3$, ν_1 is $5N$. The denominator thus con-

tains all the particles in the melt. x_a^0 , the fraction of a in pure A, would be ν_a/ν_1 , ν_a being the number of a ions in 1 formula weight of A. (x_a^0 is used to normalize x_a which would otherwise not equal 1 at $x = 0$.) Ion fractions as in (2) will be referred to as the "total ion fraction" in this paper. The ion fractions for the other ions are defined in a similar fashion. Haase then derives expressions for the ideal activities of the component salts which are the products of the total ion fractions of the constituent ions.

Basing the ion activities on the total ion fractions seems to have been proposed first by Herasymenko and Speight in 1950,³ and then again by Bradley in 1962.⁴ While such a treatment is quite reasonable for a mixture of uncharged species it does not take into account the very strong Coulombic forces that tend to alternate ions of opposite charge. The Coulombic ordering has been observed experimentally⁵ and predicted from a general theoretical model.⁶ In 1945, long before this

(1) Research sponsored by the U. S. Atomic Energy Commission under contract with Union Carbide Corporation.

(2) R. Haase, *J. Phys. Chem.*, **73**, 1160 (1969).

(3) P. Herasymenko and G. E. Speight, *J. Iron Steel Inst.* (London), **166**, 169 (1950).

(4) R. S. Bradley, *Amer. J. Sci.*, **260**, 374 (1962).

(5) See, for example, M. Blander, Ed., "Molten Salt Chemistry," Interscience Publishers, New York, N. Y., 1964, Chapter 2.

(6) Reference 5, Chapter 3.

evidence was available, Temkin⁷ proposed that in an ideal salt mixture the anions and cations should mix freely with themselves but not with each other; thus for a salt $A_m Y_p$ the activity should be

$$\left(\frac{n_A}{\sum n_{\text{cations}}}\right)^m \left(\frac{n_Y}{\sum n_{\text{anions}}}\right)^p \quad (3)$$

where n_i is the number of particles i . This treatment is based on the assumption of charge alternation but does not require the use of any specific liquid model. A discussion of the Temkin and Herasymenko approaches may be found in ref 8.

Although component activity coefficients are often given as

$$\gamma_1 = \frac{a_1}{1-x}; \quad \gamma_2 = \frac{a_2}{x} \quad (4)$$

expressions for these activity coefficients may be derived from the Temkin equations. Haase refers to the system (AgNO_3 , K_2SO_4) which we abbreviate as (AY , B_2Z). The Temkin ion fractions are

$$x_A = \frac{1-x}{1+x}; \quad x_B = \frac{2x}{1+x} \quad (5)$$

$$x_Y = 1-x; \quad x_Z = x$$

so that the ideal activities are

$$a_{\text{AY}} = x_A x_Y = \frac{(1-x)^2}{1+x}; \quad a_{\text{B}_2\text{Z}} = x_B^2 x_Z = \frac{4x^3}{(1+x)^2} \quad (6)$$

Haase's expressions are

$$a_{\text{AY}} = \left[\frac{2(1-x)}{2+x}\right]^2; \quad a_{\text{B}_2\text{Z}} = \left[\frac{3x}{2+x}\right]^3 \quad (7)$$

In fact, the values predicted by these two sets of expressions are quite close. For example, at $x = 0.5$

$$a_{\text{AY}} = 0.167; \quad a_{\text{B}_2\text{Z}} = 0.222 \text{ (Temkin)}$$

$$a_{\text{AY}} = 0.160; \quad a_{\text{B}_2\text{Z}} = 0.216 \text{ (total ion fraction)}$$

so that either would fit the data as well despite the very different assumptions used in their derivation.

However, it should also be noted that Watt and Blander⁹ have shown that when small amounts of K_2SO_4 are added to dilute solutions of AgNO_3 in KNO_3 the activity of AgNO_3 drops more than would be predicted by the dilution. They explain the deviation from the ideal (Temkin) activity with the use of the asymmetric approximation to nonrandom mixing, indicating association of the Ag^+ and SO_4^{2-} ions; thus it is doubtful that this system can be regarded as ideal from any point of view.

The ideal fused salt mixture can be defined to be consistent with the Temkin picture. Admittedly it is not settled whether modifications should be made for mixtures of ions of different charge, such as adding vacancies to the lattice, but in any case the principle

of independent mixing, based on charge alternation, is widely maintained. This principle is not compatible with Haase's formulation of the ideal solution. It seems to me that the main reason for talking about ideal solutions at all is to provide some insight into what is really happening, and that therefore one should avoid using a definition of an ideal solution which is in contradiction to what is thought to be physical reality.

Acknowledgment. I wish to thank Drs. J. Braunstein and G. D. Robbins for helpful discussions of this subject.

(7) M. Temkin, *Acta Physicochem. URSS*, **20**, 411 (1945).

(8) P. Gray and T. Førlund, *Discussions Faraday Soc.*, **32**, 163 (1961).

(9) W. J. Watt and M. Blander, *J. Phys. Chem.*, **64**, 729 (1960).

REACTOR CHEMISTRY DIVISION

DAVID M. MOULTON

OAK RIDGE NATIONAL LABORATORY

OAK RIDGE, TENNESSEE 37830

RECEIVED JUNE 9, 1969

Reply to the Comments on the Paper

"Activity Coefficients for Ionic Melts"

Sir: Moulton¹ has critically examined my proposal² of a redefinition of activity coefficients for binary ionic melts. In particular, he compares my definition of an ideal ionic melt with that given by Temkin.

First of all, I should like to stress that the purpose of my paper was to develop a useful definition of activity coefficients. I did not discuss any statistical theory at all. In particular, I did not mention the Temkin model. Indeed the statistical interpretation of thermodynamic properties of ionic melts is an involved matter subject to continuous discussion. Thus the Temkin model and its extensions to melts containing ions of different charge numbers are still debated, but the practical question of a convention about activity coefficients cannot be postponed until agreement is eventually reached with respect to the statistical model to be used for ionic melts. That is the reason why I wrote the paper without any reference to molecular models.

In order to proceed in a logical way, let us briefly discuss the following problems: (a) the meaning of the word "ideal ionic melt"; (b) the definition of activity coefficients for any ionic melt; (c) the analytical representation of activity coefficients; and (d) the interpretation of activity coefficients.

As far as I am aware, there are the following definitions of an *ideal ionic melt* in the literature: (1) a melt ideal with respect to the components, that is to say a

(1) D. M. Moulton, *J. Phys. Chem.*, **73**, 4022 (1969).

(2) R. Haase, *ibid.*, **73**, 1160 (1969).

melt for which the chemical potential μ_i of any component i has the form

$$\mu_i = \mu_{0i} + RT \ln x_i \quad (1)$$

μ_{0i} denoting the chemical potential of the pure liquid component i at the given values of temperature and pressure, R the gas constant, T the thermodynamic temperature, and x_i the stoichiometric mole fraction of component i ; (2) a melt ideal with respect to the particles actually present in the liquid mixture, that is to say a melt for which the chemical potential μ_i of any (molecular or ionic) species i is given by eq 1, μ_{0i} now referring to a fictitious state and x_i denoting the true mole fraction of species i ; (2a) a completely dissociated melt, again ideal with respect to the particles present, that is to say a special case of (2) where all the particles are ions; (3) a melt ideal in the sense of the Temkin model.

It is important to note that for simple ionic melts such as NaCl + KCl the three definitions (1), (2a), and (3) give the same result. Thus, in the case where the Temkin model certainly applies, there is no difference between the various kinds of description. In more complicated cases, however, the definitions no longer coincide. As long as the statistical theory of complex ionic melts has not been further developed it is very difficult to decide what should be called an "ideal ionic melt" in the sense of molecular physics. I adopted definition 2a and called this type of mixture a "completely dissociated ideal melt."³

As far as the system $\text{AgNO}_3 + \text{K}_2\text{SO}_4$ is concerned, I only pointed out that it is more nearly an ideal melt in the sense of definition 2a than it is in the sense of definition 1. It does not seem appropriate to apply¹ the Temkin model to this complicated salt melt and to quote¹ results for the even more complex system $\text{KNO}_3 + \text{AgNO}_3 + \text{K}_2\text{SO}_4$.

The usual definition of activity coefficients for ionic melts starts from type 1 as a reference system. My definition is based on type 2a as a reference system. The advantages of this redefinition have been clearly indicated in several papers.^{2,4,5} This procedure is a question of usefulness and has nothing to do with the ignorance of the Temkin model or of any other model of statistical mechanics. Type 3 is never used as a reference system for the simple reason that quantities like the activity coefficients should be measured and tabulated; thus they should not be defined on the basis of a standard mixture that cannot be unambiguously described in terms of macroscopic variables.

The analytical representation of activity coefficients is simple only if these quantities are appropriately defined. As has been shown elsewhere,⁴ the logarithms of the activity coefficients based on reference system 2a can be expressed as power series in the independent mole fractions. This is not true, in general, for the activity coefficients as usually defined.

The interpretation of activity coefficients is only possible if an adequate statistical model is available. Then, of course, any set of activity coefficients may be considered, but on a careful inspection of a great deal of experimental data, it is again obvious that thermodynamic "excess functions" based on the convention which I suggested behave in a particularly simple manner.⁶

(3) An early thermodynamic treatment of ionic melts based on the true mole fractions is due to P. H. J. Hoenen, *Z. Phys. Chem.*, **83**, 513 (1913). Hoenen belonged to the Schreinemakers school.

(4) R. Haase, *Z. Phys. Chem.* (Frankfurt am Main), **63**, 95 (1969).

(5) J. Richter, *Z. Naturforsch.*, **24a**, 447 (1969).

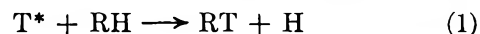
(6) J. Richter, *ibid.*, **24a**, 835 (1969).

INSTITUT FÜR PHYSIKALISCHE CHEMIE R. HAASE
RHEINISCH-WESTFÄLISCHE TECHNISCHE HOCHSCHULE
AACHEN, GERMANY

RECEIVED JUNE 30, 1969

Electron Density and Electronegativity Effects in the Substitution for Hydrogen Atoms by Energetic Tritium Atoms from Nuclear Recoil

Sir: The substitution of energetic tritium atoms for hydrogen atoms in various C-H positions, as in (1), has been the subject of numerous mechanistic studies,



many of them intended to identify the factors controlling the magnitude of the yields of this reaction.^{1,2} In our view, the most serious difficulty in the interpretation of such experiments has been the variable, often substantial, secondary decomposition of excited RT^* molecules formed in the primary substitution event.³⁻¹⁰ We have now studied a sufficient number of such secondary decompositions to permit useful estimates of the yield of reaction 1, for comparison with various possible controlling parameters. The results of a series of such estimates are given in Table I, together with brief descriptions of the data and calculations on which they are based.

The most interesting observation arising from these data is the striking importance of electron density-electronegativity effects, as shown by the correlation of

(1) F. Schmidt-Bleek and F. S. Rowland, *Angew. Chem. Intern. ed.*, **3**, 769 (1964).

(2) R. Wolfgang, *Progr. Reaction Kinetics*, **3**, 97 (1965).

(3) J. K. Lee, B. Musgrave, and F. S. Rowland, *Can. J. Chem.*, **38**, 1756 (1960).

(4) E. K. C. Lee and F. S. Rowland, *J. Amer. Chem. Soc.*, **85**, 897 (1963).

(5) Y.-N. Tang, E. K. C. Lee and F. S. Rowland, *ibid.*, **86**, 1280 (1964).

(6) Y.-N. Tang and F. S. Rowland, *ibid.*, **89**, 6420 (1967).

(7) Y.-N. Tang and F. S. Rowland, *ibid.*, **90**, 574 (1958).

(8) C. T. Ting and F. S. Rowland, *J. Phys. Chem.*, **72**, 763 (1968).

(9) A. J. Johnston, D. Malcolm-Lawes, D. S. Urch, and M. J. Welch, *Chem. Commun.*, 187 (1966).

(10) R. Cipollini and G. Stöcklin, *Radiochim. Acta*, **9**, 105 (1968).

Table I: Relative Yields from the T-for-H Substitution Reaction, per C-H Bond, for Recoil Tritium Reactions in Competitive Systems, Corrected for Secondary Decomposition

Molecule, RH	Yield of Product, RT, in Liquid Phase (vs. CH ₃ Cl)	Corrected Yield
CH ₄	85 ± 3	100 ± 4 ^a
CH ₃ F	68 ± 2	~70 ^b
CH ₃ Cl	(63)	75 ± 3 ^c
CH ₃ Br	80 ± 6	85 ± 6 ^d
CH ₂ F ₂	53 ± 2	64 ± 3 ^e
CH ₂ Cl ₂	46 ± 5	63 ± 5 ^f
CHF ₃	47 ± 3	52 ± 3 ^g
Alkanes	84 ± 3	90-95 ^h

^a Gas-phase yield vs. *c*-C₄H₈, normalized to CH₂TCl yield (gas: 40) vs. *c*-C₄H₈, ref 4, 5. Corrected for decomposition with data of D. Seewald and R. Wolfgang, *J. Chem. Phys.*, **47**, 143 (1967).

^b Can be irradiated at room temperature in mixtures with CH₃Cl, but not alone. High-pressure gas experiments show CHTFI/CH₂TF ~ 0.1. ^c Reference 5. An estimated yield of ≤ 3 units of CH₂T radicals has been attributed to the decomposition of CH₃T* and subtracted from the 78 listed in ref. 5. ^d Measurements of CH₂TI/CH₂TBr in I₂-scavenged CH₃Br show a ratio ~ 0.02. Gas-liquid comparisons suggest that brominated species are competing as scavengers, so that measured CH₂TBr yields in the liquid may include some rescavenged CH₂T radicals from CH₂TBr* decomposition. ^e Reference 6. The ratio of yields of CTF/CHTF₂ in the liquid phase is 0.10 ± 0.03. Correction factor includes an equal yield of CHF + TF from the other isotopic decomposition path. No nmr data are available for CH₂F₂. ^f Reference 7. The ratio of CHTClBr/CHTCl₂ in Br₂-scavenged CH₂Cl₂ is 0.37. ^g Decomposition (to CF₂ + TF) cannot be measured. Assumed to be the same fractional decomposition as for CHTF₂ in footnote e. ^h Experiments show small yields of scavengeable alkyl-*t* radicals, in the order of ~0.1 times the parent yield.

primary RT yields with the nmr proton shifts of the hydrogen atom being replaced, as shown in Figure 1.¹¹ Clearly, the successful replacement of an H atom by a T atom with high kinetic energy is facilitated by the presence of *higher* electron density in the C-H bond under attack. Since the "hot" RT yields are correlated with the nmr proton shifts of the molecules under non-reacting conditions, the electron density in bond-forming regions during the actual process of T-for-H replacement must be a systematic function of the electron density in the unperturbed, isolated molecules.

The major previous explanation for variations in yield for the substitution reaction (1) has been the hypothesis of steric hindrance to such substitution by larger substituent groups.^{2,12-15} This hypothesis was originally proposed as an alkyl-hindrance of major magnitude to the T-for-H reaction, *e.g.*, 45% per alkyl substituent on the carbon atom at which hydrogen replacement occurs,^{12,13} and the concept was later extended to include hindrance to T-for-H substitution by halogen atoms in the halomethanes.¹⁵ The major experimental support for the original hypothesis in alkanes was the observation of large differences in the measured HT/RT ratios, *i.e.*, the relative reaction

yields of HT from abstraction, and RT from substitution, as in (1), from an extended series of alkanes.^{12,13} However, subsequent experiments have failed to support the critical hypothesis of an HT yield independent of the nature of the C-H bond involved, and have actually shown that the major source of changes in the HT/RT ratios was the very high sensitivity of the yield of reaction (2) to the chemical environment of the abstracted atom.¹⁶⁻²¹

The basic experimental evidence for steric hindrance to the T-for-H reaction by halogen atoms in halomethanes has been the decrease in substitution yield at one atmosphere pressure for sequences such as that with CH₃X, for which the yields fell in the order CH₄ > CH₃F > CH₃Cl ≈ CH₃Br.¹⁵ However, these trends in yields in the gas phase near one atmosphere pressure primarily reflect alterations in the activation energy and mechanism of the secondary reactions, and consequently, in the fractional depletion of the primary yields.^{5-7,10}

It is important to note that the variation in substitution yields shown in Figure 1 is much smaller than the variations in gas-phase yields caused by secondary decomposition. Thus, few tests have been made which would disclose whether steric hindrance (or other parameters) are also operative during T-for-H substitution. One such potentially accurate type of measurement is the determination of the intramolecular distribution of tritium in molecules such as isobutane, thereby permitting direct comparison of the efficiency of replacement of H in primary and tertiary positions.¹⁴ Recent gas-phase measurements have shown that replacement in the tertiary position of isobutane is 0.87 ± 0.02 times as likely as in the primary position, per C-H bond.^{22,23} Even this small 13% difference, however, is

(11) Proton shifts nmr are taken from J. W. Emsley, J. Feeney, and L. H. Sutcliffe, "High Resolution Nuclear Magnetic Resonance," Pergamon Press, Ltd., London, 1966; and C. J. Creswell and A. L. Allred, *J. Amer. Chem. Soc.*, **85**, 1723 (1963).

(12) M. Henchman, D. Urch, and R. Wolfgang, *Can. J. Chem.*, **38**, 1722 (1960).

(13) D. Urch and R. Wolfgang, *J. Amer. Chem. Soc.*, **83**, 2982 (1961).

(14) A. Odell, A. Rosenberg, R. D. Fink, and R. Wolfgang, *J. Chem. Phys.*, **40**, 3730 (1964).

(15) R. A. Odum and R. Wolfgang, *J. Amer. Chem. Soc.*, **85**, 1050 (1963).

(16) J. W. Root and F. S. Rowland, *ibid.*, **84**, 3027 (1962).

(17) W. Breckenridge, J. W. Root, and F. S. Rowland, *J. Chem. Phys.*, **39**, 2374 (1963).

(18) J. W. Root, W. Breckenridge, and F. S. Rowland, *ibid.*, **43**, 3694 (1965).

(19) E. Tachikawa and F. S. Rowland, *J. Amer. Chem. Soc.*, **90**, 4767 (1968).

(20) E. Tachikawa, Y.-N. Tang, and F. S. Rowland, *ibid.*, **90**, 3584 (1968).

(21) E. Tachikawa and F. S. Rowland, *ibid.*, **91**, 559 (1969).

(22) T. Smal and F. S. Rowland, *J. Phys. Chem.*, **72**, 1845 (1968); T. Smal and F. S. Rowland, *ibid.*, in press.

(23) Reference 22 also reports that the comparable ratio, per C-D bond, is 0.96 ± 0.02 for *i*-C₄D₁₀.

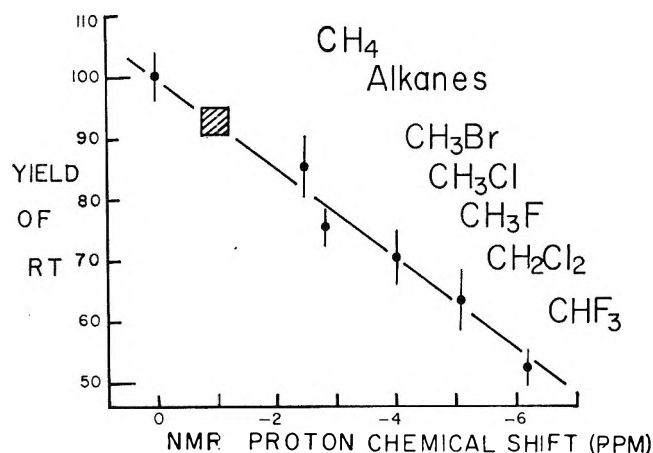


Figure 1. Yield of T-for-H vs. nmr shift.

not a direct measurement of the importance of steric hindrance to T-for-H substitution in isobutane, since the nmr proton shifts, together with Figure 1, would suggest that the tertiary position should be perhaps 5–10% lower in substitution yield per bond for electron density reasons alone. At the present time, we conclude that steric effects for small alkyl or for halogen atom substituents have not been positively demonstrated and are probably less than 4% per alkyl group in the former case.

Additional evidence supporting the importance of electron density/electronegativity effects in substitution reactions can be obtained from competitive studies of the reactivities of alkanes and methyl silanes toward the substitution of T-for-H. Competitive studies in binary mixtures indicate that replacement of H by T is more probable in the higher electron density CH_3 groups of $(\text{CH}_3)_4\text{Si}$ than in $(\text{CH}_3)_4\text{C}$ by a factor of 1.18 ± 0.06 ,^{24,25} in comparison with a predicted ± 1.1 from the nmr proton shifts and Figure 1.

(24) Unpublished experiments by S. H. Daniel and Y.-N. Tang.

(25) Unpublished experiments by T. Tominaga, A. Hosaka, and F. S. Rowland; see also T. Tominaga, A. Hosaka, and F. S. Rowland, *J. Phys. Chem.*, **73**, 465 (1969).

(26) This research was supported by A.E.C. Contract No. AT-(11)-34, Agreement No. 12c.

DEPARTMENT OF CHEMISTRY²⁶
UNIVERSITY OF CALIFORNIA
IRVINE, CALIFORNIA 92664

F. S. ROWLAND
E. K. C. LEE

DEPARTMENT OF CHEMISTRY
TEXAS A & M UNIVERSITY
COLLEGE STATION, TEXAS 77843

Y.-N. TANG

RECEIVED AUGUST 6, 1969

Effect of Water on the Kinetics of the Solid Lithium-Lithium Ion Reaction in Propylene Carbonate

Sir: Lithium metal is known to be stable in electrolytes based on propylene carbonate¹ and shows reversible

Nernstian behavior.² Recently several attempts have been made to measure the electron transfer kinetics of the Li-Li^+ reaction³⁻⁵ but all have used metal surfaces exposed to the electrolyte for as much as a half hour before measurements were made. We wish to report the first measurements of exchange current on clean lithium surfaces within one second after exposure to $\text{LiClO}_4\text{-PC}$ electrolyte, and the influence of small amounts of water.

Experiments were conducted using an improved version of an apparatus described in detail elsewhere.³ A 0.5-in. diameter lithium rod was sliced by a steel guillotine blade which contained in its upper portion a Teflon washer filled with electrolyte, so that an assembled cell was obtained within 1 sec after exposing a fresh lithium surface. This cell consisted of two plane parallel 0.32-cm² lithium electrodes separated by a 0.3-mm electrolyte layer. Kinetics were measured by applying a 12-msec galvanostatic pulse with rise time less than 1 μsec and observing the potential across the cell on an oscilloscope. The potential was constant after 3 msec. Direct feedback ohmic compensation was employed, and the current trace was displayed simultaneously with the voltage trace. Clear separation of ohmic and activation overpotential was obtained, and no mass-transfer polarization was evident. The apparent exchange current I_a^0 was calculated from each trace assuming that the Tafel equation was obeyed for both the anodic and cathodic reaction,³⁻⁶ and that the cathodic transfer coefficient α was 0.72.

$$I_a^0/I = [\exp(\alpha f E_c) - \exp(-(1 - \alpha)f E_c)]^{-1}$$

where

$$E_c = \frac{1}{f} \ln \left\{ \frac{1 + \exp((1 - \alpha)f E)}{1 + \exp(\alpha f E)} \right\}$$

and $f = F/RT$, I is the measured current density, E is the total activation overpotential, and E_c is the cathodic portion of E . I_a^0 obtained in this way varied by less than 10% as I varied from 0.15 to 2.5 mA/cm² ($t = 1$ hr, dry electrolyte), verifying the assumptions. Reversal of the applied current made no difference in I_a^0 and confirmed reversibility of the reaction mechanism. Some experimental results are given in Table I.⁷ Note that the addition of even a small amount of water causes a dramatic decrease in exchange current with

(1) R. J. Jasinski, "High Energy Batteries," Plenum Press, New York, N. Y., 1967; J. N. Butler, *Advan. Electrochem. Electrochem. Eng.*, **7**, 77 (1969).

(2) B. W. Burrows and R. J. Jasinski, *J. Electrochem. Soc.*, **115**, 365 (1968); M. Salomon, *J. Phys. Chem.*, **73**, 3299 (1969).

(3) D. R. Cogley and J. N. Butler, "Kinetics of Deposition and Dissolution of Alkali Metals in Nonaqueous Solvents," Final Report, Contract No. AF-19(628)-5525 (1968). AD 681453.

(4) R. Scarr, Abstract No. 161, Electrochemical Society, New York, N. Y., May 1969.

(5) S. G. Meibuhr, Abstract No. 204, Electrochemical Society, New York, N. Y., May 1969.

(6) D. R. Cogley and James N. Butler, *J. Phys. Chem.*, **72**, 4568 (1968).

Table I

Electrolyte ^a (in propylene carbonate)	I_a^0 (mA/cm ²) at time indicated—					
	$t = 0$	1 sec	10 sec	1 min	10 min	1 hr
0.257 <i>m</i> LiClO ₄ ⁻ <0.001 <i>m</i> H ₂ O	>12	10.2	7.8	5.4	2.8	1.6
0.229 <i>m</i> LiClO ₄ ⁻ 0.02 <i>m</i> H ₂ O	>10	8	3.1	1.5	0.30	0.026
0.257 <i>m</i> LiClO ₄ ⁻ 0.54 <i>m</i> H ₂ O	>5	~3	~1	~0.1

time. Values previously reported^{3,4,5} are consistent with our measurements after 10 min to 1 hr. Our values at $t = 0$ were obtained by extrapolation on a $t^{1/2}$ scale.

In the dry (<0.001 *m* H₂O) electrolyte, the double-layer capacity (obtained from the initial portion of the potential-time trace) is approximately 45 $\mu\text{F}/\text{cm}^2$, a reasonable value for a rough solid metal surface. In the presence of 0.54 *m* H₂O, the capacity drops to as low as 0.3 $\mu\text{F}/\text{cm}^2$, indicating the formation of a dielectric film (possibly LiOH) on the metallic surface. It is not possible at this time to distinguish between the effects of recrystallization of the cold-worked surface and the effect of trace water in dry electrolyte, but future experiments with ultradry electrolyte should make this distinction clear.⁸

(7) Propylene carbonate was purified by distillation and analyzed by gas chromatography as described by R. J. Jasinski and S. Kirkland, *Anal. Chem.*, **39**, 1663 (1967); first two solutions analyzed by infrared absorbance at 1.9 μ . (See R. J. Jasinski and S. Carroll, *ibid.*, **40**, 1908 (1968)); third solution prepared by weight.

(8) This work was supported by the U. S. Air Force Cambridge Research Laboratories under Contracts AF-19(628)-5525 and F-19628-68-0052.

TYCO LABORATORIES, INC.
WALTHAM, MASSACHUSETTS 02154

JAMES N. BUTLER
DAVID R. COGLEY
JOHN C. SYNNOTT

RECEIVED AUGUST 18, 1969

Temperature Dependence of the Molar Absorptivity of the OH Stretching Vibration

Sir: Several workers¹⁻³ have reported the temperature dependence of the molar absorptivity for the fundamental OH stretching vibration of various monomeric molecules in dilute solution; corrections for this temperature dependence have been made by Hamaker, *et al.*,⁴ for solutions of methanol, *t*-butyl alcohol, and di-*t*-butyl carbinol in carbon tetrachloride. Finch and Lippincott⁵ have suggested that a true temperature dependence should exist for hydrogen-bonded complexes. Thus, if the solute should hydrogen bond to the solvent, a temperature dependence would be expected. However, Fletcher and Heller⁶ argue that the molar absorptivity should not change with temperature, and therefore consider any temperature adjust-

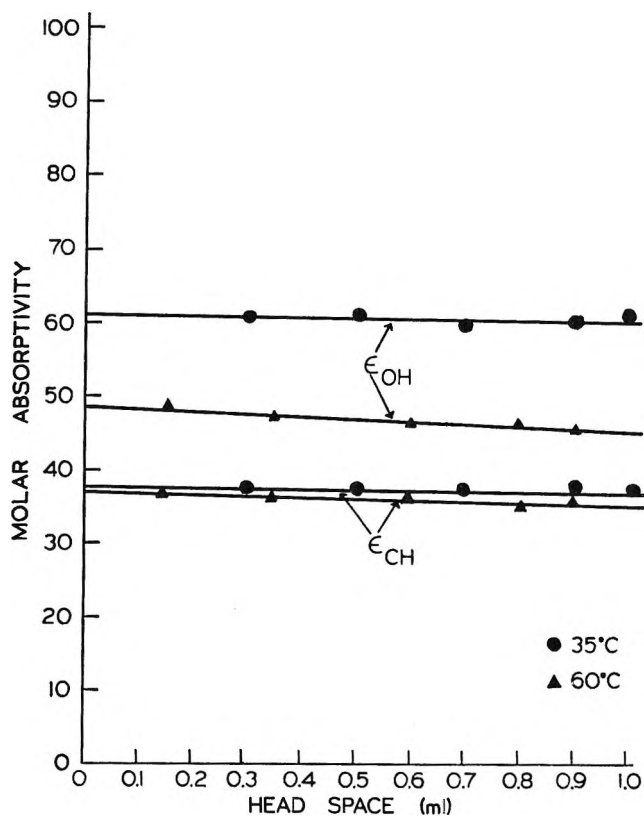


Figure 1. Change in the molar absorptivity for the OH and CH stretch of methanol in carbon tetrachloride at 35 and 60° as a function of the head space over the solution. The solution concentration was 0.0048 *M* at 35°.

ment incorrect. Swenson,⁷ in an attempt to determine the cause of this temperature dependence for methanol in carbon tetrachloride solution, has ascribed the decrease of the molar absorptivity with increasing temperature to reduced concentration of the methanol in solution due to evaporation of the methanol into the head space above the solution. Thus Swenson concludes that a true temperature dependence of the molar absorptivity does not exist. Because of the relative importance of the temperature dependence of the molar absorptivity to the interpretation of spectral data, it seemed that some of our preliminary results in this area should be reported.

The change in the molar absorptivity as a function of increasing head space over a solution of methanol in carbon tetrachloride has been studied. The molar absorptivity for the CH and OH stretching modes of methanol was monitored with some of the results given in Figure 1. The plots of the molar absorptivity

- (1) I. Motoyama and C. H. Jarboe, *J. Phys. Chem.*, **70**, 3226 (1966).
- (2) U. Liddel and E. D. Becker, *J. Chem. Phys.*, **25**, 173 (1956).
- (3) R. H. Hughes, R. J. Martin, and N. D. Coggeshall, *ibid.*, **24**, 489 (1956).
- (4) R. M. Hamaker, R. M. Clagg, L. K. Patterson, P. E. Rider, and S. L. Rock, *J. Phys. Chem.*, **72**, 1837 (1968).
- (5) J. N. Finch and E. R. Lippincott, *ibid.*, **61**, 894 (1957).
- (6) A. N. Fletcher and C. A. Heller, *ibid.*, **72**, 1839 (1968).
- (7) C. A. Swenson, *ibid.*, **71**, 3108 (1967).

Table I: Change in Molar Absorptivity with Temperature for the Fundamental OH and CH Stretch of Methanol in Carbon Tetrachloride^a

$\epsilon(\text{OH})^b$ l. mol ⁻¹ cm ⁻¹	$\epsilon(\text{CH})^b$ l. mol ⁻¹ cm ⁻¹	T, °C	$\Delta\epsilon(\text{OH})\%$ ^c	$\Delta\epsilon(\text{CH})\%$ ^c
61.0 ± 0.8	40.7 ± 0.6	30
55.8 ± 1.1	39.3 ± 0.7	40	8.5	3.7
52.8 ± 0.6	39.9 ± 0.7	50	13.4	2.0
50.5 ± 0.8	39.8 ± 0.7	60	17.2	2.2

^a All spectra were recorded on the Beckman DK-2A spectrophotometer equipped with the Beckman temperature regulated cell holder. One-cm Teflon stoppered cells with CCl₄ serving as the reference were used. The cells were considered adequately sealed since recycling of the temperature gave identical results. The solutions were prepared in a drybox. The molar absorptivities have been corrected for changes in concentration with temperature. ^b The molar absorptivities were obtained by extrapolation of a plot of ϵ vs. concentration to infinite dilution. The errors reported are the errors in the intercept as calculated by least-squares analysis. The concentration range was 0.005 to 0.02 M. ^c $\Delta\epsilon = (\epsilon_{30} - \epsilon_T)/\epsilon_{30}$

against head space for the OH stretch at 35 and 60° do not converge at zero head space as they should if evaporation of the methanol into the head space is the cause of the reduction of the molar absorptivity. Conversely, the molar absorptivity for the CH stretch is only slightly different at the two temperatures. The slope of the OH and CH absorptivity curves for 60° indicates that some evaporation of methanol does occur. We find for head spaces in excess of 1 ml and temperatures around 60° sufficient evaporation of methanol from solution could occur to reduce the solution concentration substantially. At a head space of 0.5 ml or less, evaporation of methanol would cause only a 4–5% reduction in the molar absorptivity from the value at zero head space at 60°. At temperatures lower than 35°, evaporation is negligible even for head spaces considerably greater than 1 ml.

We have also estimated the Henry's law constants for methanol in carbon tetrachloride solution at 35° and 55° from the data of ref 8. Calculations using these constants also indicate that for head spaces of the order used in this work (0.5 ml) evaporation of the methanol would account for only about 2% of the observed decrease in the molar absorptivity in changing the temperature from 35 to 55°.

The temperature dependence of the molar absorptivity for the CH stretch of methanol in carbon tetrachloride has also been determined with the results given in Table I. In agreement with earlier workers,^{2,3} we find slight variation of the molar absorptivity for the CH stretch while the molar absorptivity for the OH stretch changes significantly. The relative constancy of the CH molar absorptivity indicates that any evaporation is not sufficient to account for the observed decrease in the OH molar absorptivity.

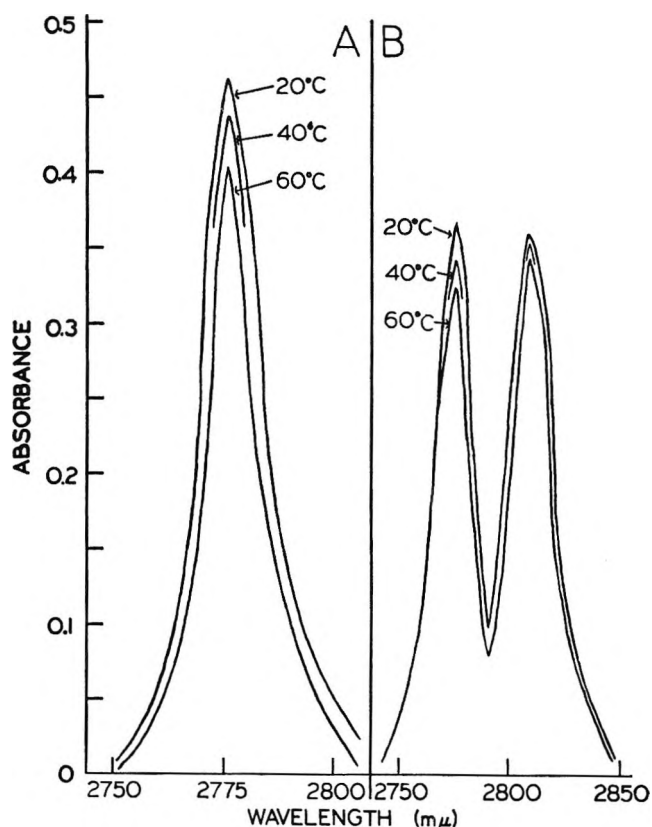


Figure 2. Temperature dependence of the spectra of phenol and catechol in carbon tetrachloride solution. A, phenol in CCl₄ (0.00212 M at 25°); B, catechol in CCl₄ (0.00182 M at 25°). The spectra have been corrected for changes in concentration with temperature.

If evaporation of the methanol were the cause of the decrease of the molar absorptivity with temperature, any temperature dependence of the molar absorptivity for other nonassociated species in carbon tetrachloride solution should also be liable to the same interpretation. Since phenols are relatively nonvolatile, the temperature dependence of the molar absorptivity of these compounds, previously reported,³ cannot easily be ascribed to evaporation. We investigated the temperature dependence of the molar absorptivity of phenol and catechol in carbon tetrachloride with the results given in Table II and Figure 2. For catechol, the molar absorptivity for the OH involved in intramolecular hydrogen bonding is seen to decrease 2.5% while that for the OH not involved directly in the intramolecular bonding decreases 11.3% with increasing temperature. The free OH and the intramolecular hydrogen-bonded OH peaks for catechol would be expected to behave similarly if evaporation solely were responsible for the decrease of the peak height.

The results of our studies indicate that a temperature dependence of the molar absorptivity for the free OH stretch of nonassociated species in carbon tetrachloride

(8) G. Scatchard, S. E. Wood, and J. M. Mochel, *J. Amer. Chem. Soc.*, **68**, 1960 (1946).

Table II: Change in Molar Absorptivity with Temperature for the Fundamental OH Stretch of Phenol and Catechol in Carbon Tetrachloride

	Wavelength, m μ	$\Delta\epsilon\%$ ^a
Phenol	2777	11.0 ^b
Catechol	2772	11.3 ^b
	2806	2.5 ^b

^a $\Delta\epsilon = (\epsilon_{20^\circ} - \epsilon_{60^\circ})/\epsilon_{20^\circ} \times 100$. The temperature range was 20 to 60° in all cases. ^b Average of three samples.

solution does indeed exist. Evaporation of the solute in question may occur but not to such an extent to account for the observed change in the molar absorptivity provided small head spaces are used. We explain this temperature dependence in the manner of Finch and Lippincott,⁵ *i.e.*, the solute-free OH forms a weak hydrogen bond with the carbon tetrachloride. Some support for this can be derived from the work of Fumio and Katsuhiko,⁹ who have isolated complexes of certain diols and carbon tetrachloride, and from Fletcher,¹⁰ who has presented evidence for the existence of a 1:1 complex between carbon tetrachloride and 1-octanol.

Acknowledgment. The authors wish to acknowledge Lebanon Valley College for partial financial support for this research.

(9) T. Fumio and A. Katsuhiko, *Tetrahedron Lett.*, **33**, 3695 (1968).

(10) A. N. Fletcher, *J. Phys. Chem.*, **73**, 2217 (1969).

(11) To whom correspondence should be addressed.

DEPARTMENT OF CHEMISTRY
LEBANON VALLEY COLLEGE
ANNVILLE, PENNSYLVANIA 17003

G. P. HOOVER
E. A. ROBINSON
R. S. McQUATE
H. D. SCHREIBER
J. N. SPENCER¹¹

RECEIVED AUGUST 20, 1969

The Homoconjugation Constant of Picric Acid in Acetonitrile

Sir: In a recent paper, D'Aprano and Fuoss¹ reported that the homoconjugation constant, $K_{\text{HPi}_2^-}^f = [\text{HPi}_2^-]/[\text{HPi}][\text{Pi}^-]$, of picric acid in acetonitrile (AN) is of the order 2×10^2 , a value some one hundred times greater than that reported previously by us.² In the notation of Fuoss, $K = K_{\text{HPi}_2^-}^f - [\text{S}]$, where [S] denotes the molarity of pure AN, *i.e.*, 18.9 M. The method used by these authors is subject to unusually large errors. In brief, they added successive portions of solid picric acid to very dilute solutions of tetramethylammonium or tetrabutylammonium picrate. From the difference in electrical conductance of the mixtures after correction for basic impurities in the solvent and

that of the picrate solution without acid, they arrived at the large value of $K_{\text{HPi}_2^-}^f$ and the mobility of the HPi_2^- ion ranging from 40 to 63 taking $\lambda_{\text{O}^-} = 77.3$.³ The correction to be applied for basic impurities was rather large as compared to the difference between the conductivity of the picrate solution with and without picric acid.

From our work on the effect of picric acid on the solubility of potassium picrate in AN² we arrived at the value of $K_{\text{HPi}_2^-}^f$ of the order of 2. Also, paH measurements in dilute mixtures of picric acid and tetrabutylammonium picrate indicated that $K_{\text{HPi}_2^-}^f$ must be very small. In order to substantiate our previous value we have measured the paH in mixtures of tetrabutylammonium picrate containing a large excess of picric acid. The equation used in the calculation of $K_{\text{HPi}_2^-}^f$ from the experimental paH data had been derived previously.² Also, we have estimated $\lambda_{\text{OHPi}_2^-}$ by determining the effect of a large excess of picric acid on the conductance of dilute tetraethylammonium picrate solutions in AN.

Acetonitrile was purified and dispensed as described previously.⁴ The water content as found from Karl Fischer titration was $1-2 \times 10^{-3}$ M. Picric acid² and tetrabutylammonium picrate² were products used previously. Tetraethylammonium picrate was prepared in this laboratory by H. Smagowski. Conductometric measurements and potentiometric paH techniques with the glass electrode have been described elsewhere.^{2,4}

The following paH values were found in mixtures 3.53×10^{-3} M in tetrabutylammonium picrate and 0.226, 0.439, and 0.835 M in picric acid: 8.92, 8.51, and 8.10, respectively, from which an average value of $K_{\text{HPi}_2^-}^f = 2.4 \pm 0.5$ was obtained. This value is in good agreement with that of 2.0 reported previously from solubility data of potassium picrate in presence of picric acid.²

Conductivity data of mixtures of picric acid and tetraethylammonium picrate are entered in Table I. Even after correction for viscosity, an appreciable decrease in conductivity was observed with increasing picric acid concentration at a given salt concentration as observed by Fuoss.¹ The specific conductivity of 0.91 M picric acid alone was 1.5×10^{-6} ohm⁻¹ cm⁻¹, corresponding to $c_{\text{BH}^+} = 1.1 \times 10^{-5}$ M. Since this value is less than 1% of the concentration of salt taken in the mixtures, c_{BH^+} can be neglected as compared to $c_{\text{E}_4\text{N}^+}$. Values of $[\text{Pi}_n^-]$, the subscript referring to the simple ion in the solvent, and $[\text{HPi}_2^-]$ in columns 5 and 6 in Table I were calculated using $K_{\text{HPi}_2^-}^f = 2.0$ and

(1) D. D'Aprano and R. M. Fuoss, *J. Phys. Chem.*, **73**, 223 (1969).

(2) I. M. Kolthoff and M. K. Chantooni, Jr., *J. Amer. Chem. Soc.*, **87**, 4428 (1965).

(3) J. F. Coetzee and G. P. Cunningham, *ibid.*, **87**, 2529 (1965).

(4) I. M. Kolthoff, S. Bruckenstein, and M. K. Chantooni, Jr., *ibid.*, **83**, 3927 (1961).

Table I: Estimation of $\lambda_{\text{HPI}_2^-}$ from Conductivity of Picric Acid-Tetraethylammonium Picrate Solutions

c_{HPI}, M	$c_{\text{Et}_4\text{NPI}}, M \times 10^3$	Specific conduct., ^a $\text{ohm}^{-1} \text{cm}^{-1} \times 10^4$	Viscosity, cP	$[\text{Pi}_5^-], M \times 10^3$	$[\text{HPI}_2^-], M \times 10^3$	$\lambda_{\text{HPI}_2^-}$ ^c
0.95	0	0.015	0.53	0.003	0.006	...
0.302	3.59	4.93	0.396	2.24	1.35	50
0.645	3.49	4.64	0.455	1.53	1.96	48.5
0.968	3.37	4.42	0.531	1.15	2.22	49
						Av 49

^a Values corrected for viscosity; viscosity of solvent is 0.345 cP. ^b Calculated using $K^f_{\text{HPI}_2^-} = 2.0$ (see text). ^c Uncorrected for ion atmosphere effects.

letting $x = [\text{HPI}_2^-]$ and $[\text{Pi}_5^-] = [\text{Et}_4\text{N}^+] - x$. Since picric acid is in very large excess, its analytical and equilibrium concentrations are practically equal.

In the calculation of $\lambda_{\text{HPI}_2^-}$ from the specific conductance, L , of the picric acid-picrate mixtures the following relation was used in which the ionic mobilities at infinite dilution of the tetraethylammonium and picrate ions were taken as 85⁵ and 77,³ respectively.

$$10^3 L = \lambda_{\text{Et}_4\text{N}^+}[\text{Et}_4\text{N}^+] + \lambda_{\text{Pi}_5^-}[\text{Pi}_5^-] + \lambda_{\text{HPI}_2^-}[\text{HPI}_2^-]$$

From the data in Table I, an average value of $\lambda_{\text{HPI}_2^-}$ equal to 57 was obtained. It is perhaps fortuitous that this value lies within the range reported by Fuoss.¹ Due to the instability of the HPI_2^- homoconjugate, large uncertainties are involved in the estimation of $\lambda_{\text{HPI}_2^-}$. Nevertheless, considering that picric acid has

approximately the same molecular size as the mono- and dinitrophenols studied previously, the $\lambda_{\text{OHA}_1^-}$ values of which varied from 58 to 73,⁶ the value of 57 for $\lambda_{\text{HPI}_2^-}$ seems reasonable.

Acknowledgment. This work has been supported by Air Force AFOSR Grant 1223-67.

(5) D. S. Berns and R. M. Fuoss, *J. Amer. Chem. Soc.*, **82**, 5585 (1960).

(6) I. M. Kolthoff, M. K. Chantooni, Jr., and S. Bhowmik, *ibid.*, **88**, 5430 (1966).

SCHOOL OF CHEMISTRY
UNIVERSITY OF MINNESOTA
MINNEAPOLIS, MINNESOTA 55455

I. M. KOLTHOFF
M. K. CHANTOONI, JR.

RECEIVED AUGUST 25, 1969